Calix[4]pyrrolato Tin Complexes: Augmented Reactivity of Structurally Constrained Sn(II) and Sn(IV) Centers

Synthetic Chemistry of Calix[4]pyrrolato *p*-Block Complexes,
Structurally Constrained Sn(II) Nucleophiles
and Sn(IV) Lewis Acids

INAUGURAL
DISSERTATION

to obtain the Academic Degree
Doctor Rerum Naturalium (Dr. rer. nat.)

of the Combined Faculty of Mathematics, Engineering,
and Natural Sciences of Heidelberg University

by
Heiko Ruppert, M. Sc.
born in Heidelberg

2024

The experimental and computational work presented within this dissertation was carried out from December 2019 to March 2024 under the supervision of PROF. DR. LUTZ GREB at the *Institute of Inorganic Chemistry* at *Ruprecht-Karls-Universität Heidelberg*. Some of the results described here were obtained by JULIETTE SCHLEICHER, PAUL JANßEN, ARNE MEISTER, ANDRÉ FARIA VIEIRA, RONJA PFRETZSCHNER, and TILL SCHREYER as part of their research internships under my supervision. Essential parts of this dissertation have already been published in scientific articles and presented at international conferences.

First referee and advisor	*Prof. Dr. Lutz Greb*
Second referee	*Prof Dr. Lutz H. Gade*
Date of disputation	*August 8, 2024*

List of Publications

7) H. Ruppert, T. Schreyer, M. C. Dietl, M. Rudolph, A. S. K. Hashmi, L. Greb, "*Dynamic Coordination Behavior of a Structurally Constrained, Nucleophilic Sn(II) Towards Gold(I)*", *Z. Anorg. Allg. Chem.* **2024**, e202400081.

6) H. Ruppert, A. Meister, P. Janßen, L. Greb, "*Conformational and Substitution Effects on the Donor and Reducing Strength of Tin(II) Porphyrinogens*", Chem. Eur. J. **2024**, e202401685.

5) H. Ruppert, A. Meister, R. Pfretzschner, A. Faria Vieira, L. Greb, "*Concatenating Structural Constraint Effects at Tin for the Sequential Generation, Stabilization, and Transfer of Acyclic Aminocarbenes*", *J. Am. Chem. Soc.* **2024**, *146*, *16*, 11515-11522.

4) H. Ruppert, L. Greb, "*Calix[4]pyrrolato Stannate(II): A Tetraamido Tin(II) Dianion and Strong Metal-Centered σ-Donor*", *Angew. Chem. Int. Ed.* **2022**, *61*, e20211661.

3) H. Ruppert[+], L. M. Sigmund[+], L. Greb, "*Calix[4]pyrroles as ligands: recent progress with a focus on the emerging p-block element chemistry*", *Chem. Commun.* **2021**, *57*, 11751-11763, [+]: equal contributions.

2) H. Ruppert, L. Greb, "*Bis(alizarinato)silane: In Silico Design and Synthesis of a Powerful Chromogenic Lewis Acid as a Dual-Gated Fluoride Ion Probe*", *Organometallics* **2020**, *39*, *23*, 4340–4349.

1) E. Regulska, H. Ruppert, F. Rominger, C. Romero-Nieto, "*Synthesis of Blue-Luminescent Seven-Membered Phosphorus Heterocycles*", *J. Org. Chem.* **2020**, *85*, 1247-1252.

The rights to adapt the content of some of the above listed publications were obtained through RightsLink®.

List of Presentations

3) Talk on "*Geometrically Constrained Tin Calix[4]pyrroles: One Platform for Strong Tin(II) Nucleophiles and Tin(IV) Lewis Acids*", 17th International Conference of the Coordination and Organometallic Chemistry of Germanium, Tin, and Lead (ICCOC-GTL17), Victoria University in Wellington, New Zealand, **2023**.

2) Talk on "*The Carbene Chemistry of Tin Calix[4]pyrroles*", Skilizium Seminar, Andermatt/Hospental, Switzerland, **2023**.

1) Poster on "*Increasing the Donor Strength of Sn(II) and Lewis Acidity of Sn(IV) by Geometrical Constraint*", Gordon Research Seminar and Conference on Inorganic Chemistry, Salve Regina University in Newport, United States of America, **2022**.

In Gedenken an meine Eltern.

Abstract

Structural constraint represents a viable tool to influence the reactivity of *p*-block centers in molecular compounds. This dissertation for the first time reveals the influence of structural constraint on the *nucleophilicity and donor strength of Sn(II)* and the *Lewis acidity of Sn(IV) center*s based on e*xperimental* and *quantum chemical data*.

The macrocyclic, tetraanionic *meso*-octaalkylcalix[4]pyrrolato ligand delivered the *first tetraamido stannate(II) dianion* $\mathbf{[2^{Et}]^{2-}}$. Coordination of four nitrogen π-donors constrained into a square-pyramidal environment pushed the energetically buried electron lone pair at Sn(II) to an *extreme σ-donor capacity* surpassing those of electron-rich carbene and phosphine ligands. The *increased nucleophilicity* of $\mathbf{[2^{Et}]^{2-}}$ even allowed the direct substitution of hydride from benzaldehyde (**Section 3.1**). Investigation of *meso*-substituent and ligand conformation effects on the electronic structure of $\mathbf{[2^{R}]^{2-}}$ (R = Me, Et) enabled the fine tuning of their donor and reducing strengths (**Section 3.2**).

The *flexible and dynamic coordination chemistry* of $\mathbf{[2^{Et}]^{2-}}$ was explored in bimetallic complexes with Ni(0), W(0), and Ru(II) centers featuring either a η^1-coordination *via* Sn(II) or a η^5-coordination *via* a pyrrolato unit, depending on the electronic structure of the transition metal fragment (**Section 3.1**). With Au(I) centers a novel, dynamic μ_2-coordination of all four pyrrolato N-atoms was discovered (**Section 3.3**).

Application of the augmented nucleophilicity of $\mathbf{[2^{Et}]^{2-}}$ granted access to elusive *low-substituted acyclic aminocarbenes* by the *umpolung reaction* with chloroiminium salts. The newly formed carbenes were bound in the coordination sphere of the *in situ* generated, square-planar Sn(IV) Lewis acid $\mathbf{2^{Et}}$ delivering ambient-air-stable adducts. Eventually, cooperativity of the calix[4]pyrrole ligand backbone completed the reaction sequence and facilitated the *selective transmetalation of the acyclic carbenes onto copper(I) halides* accessing novel carbene complexes (**Section 3.4**).

Lastly, the chemistry of *anti-van't Hoff-Le Bel Sn(IV) Lewis acids* $\mathbf{2^{R}}$ (R = Me, Et) was explored. In the absence of Lewis bases, ambiphilic $\mathbf{2^{R}}$ exist as dimers and showed marked differences compared to their Si and Ge counterparts. $\mathbf{2^{R}}$ enabled the *element-ligand cooperative* activation of Lewis basic substrates, which was limited by their dimerization. Synthesis of the novel, sterically demanding *meso*-octa(*ortho*-phenylene)calix[4]pyrrole $\mathbf{H_4[1^{\textit{o}Phen}]}$ and its Sn(IV) complexes were explored as the first steps towards a monomeric, truly square-planar Sn(IV) Lewis acid (**Section 3.5**).

Kurzzusammenfassung

Strukturelle Verzerrung ist ein wertvolles Werkzeug um die Reaktivität von *p*-Block-Zentren zu beeinflussen. In dieser Dissertation wird zum ersten Mal der Einfluss struktureller Verzerrung auf die *Nukleophilie und Donorstärke von Sn(II)-* und die *Lewis-Azidität von Sn(IV)-Zentren* auf Basis *experimenteller* und *quantenchemischer Daten* aufgezeigt.

Der makrozyklische, tetraanionische *meso*-Oktaalkylcalix[4]pyrrolatoligand lieferte das erste *Tetraamidostannat(II)-dianion* $\mathbf{[2^{Et}]^{2-}}$. Die Koordination von vier Stickstoff π-Donoren in einer quadratisch-pyramidalen Umgebung verlieh dem freien Elektronenpaar des Sn(II) eine *extreme σ-Donorkapazität*, welche die elektronenreicher Carben- und Phosphinliganden übertrifft. Die *erhöhte Nukleophilie* von $\mathbf{[2^{Et}]^{2-}}$ ermöglichte die direkte Substitution eines Hydrids am Benzaldehyd (**Abschnitt 3.1**). Der Einfluss von *meso*-Substituenten und Ligandenkonformation auf die elektronische Struktur von $\mathbf{[2^{R}]^{2-}}$ (R = Me, Et) erlaubte die Feinabstimmung ihrer Donor- und Reduktionsstärke (**Abschnitt 3.2**).

Die *flexible und dynamische Koordinationschemie* von $\mathbf{[2^{Et}]^{2-}}$ wurde in bimetallischen Ni(0)-, W(0)- und Ru(II)-Komplexen erforscht. Je nach Übergangsmetallfragment zeigte $\mathbf{[2^{Et}]^{2-}}$ entweder eine η^1-Koordination des Sn(II)-Zentrums oder eine η^5-Koordination einer Pyrrolatoeinheit (**Abschnitt 3.1**). Mit Au(I)-Fragmenten wurde eine neuartige, dynamische μ_2-Koordination aller vier Pyrrolato-N-Atome beobachtet (**Abschnitt 3.3**).

Die erhöhte Nukleophilie von $\mathbf{[2^{Et}]^{2-}}$ ermöglichte die *Umpolung* von Chloriminiumsalzen zu *azyklischen Aminocarbenen mit geringem sterischem Anspruch*. Die neu gebildeten Carbene wurden in der Koordinationssphäre der *in situ* erzeugten, quadratisch-planaren Sn(IV)-Lewis-Säure $\mathbf{2^{Et}}$ gebunden und lieferten an Luft stabile Addukte. Die Kooperativität des Calix[4]pyrrolato-Ligandengerüsts vermittelte anschließend die selektive *Transmetallierung der azyklischen Carbene auf Kupfer(I)-halogenide*, wodurch bisher schwer zugängliche Komplexe entstanden (**Abschnitt 3.4**).

Letztlich wurde die Chemie der *anti-van't Hoff-Le Bel Sn(IV)-Lewis-Säuren* $\mathbf{2^{R}}$ (R = Me, Et) untersucht. In Abwesenheit von Lewis-Basen liegen die ambiphilen $\mathbf{2^{R}}$ als Dimere vor und zeigten deutliche Unterschiede zu ihren Si- und Ge-Pendants. $\mathbf{2^{R}}$ ermöglichte die *Ligand-kooperative Aktivierung* von Lewis-basischen Substraten. Die Synthese des neuartigen, sterisch anspruchsvollen *meso*-Okta(*ortho*-phenylen)calix[4]pyrrols $\mathbf{H_4[1^{o^{Phen}}]}$ und seiner Sn(IV)-Komplexe wurden als erster Schritte auf dem Weg zu einer monomeren, quadratisch-planaren Sn(IV)-Lewis-Säure untersucht (**Abschnitt 3.5**).

CONTENTS

1 Introduction 1

1.1 Preface 1

1.2 Lewis Acidity: Definition and Scaling Methods 4

1.3 The Theory Behind Square Planar-Coordinated *p*-Block Atoms 8

1.4 Calix[4]pyrrole Chemistry 10

1.5 Amplifying the Lewis Acidity of Tin Lewis Acids 25

1.6 Structurally Constrained *p*-Block and Tin(II) Nucleophiles 29

1.7 Generation of Carbenes with *p*-Block Nucleophiles 34

2 Motivation and Objectives 39

3 Results and Discussion 41

3.1 Calix[4]pyrrolato Stannate(II): A Tetraamido Tin(II) Dianion and Strong Metal-Centered σ-Donor 43

3.2 Conformational and Substitution Effects on the Donor and Reducing Strength of Tin(II) Porphyrinogens 135

3.3 Dynamic Coordination Behavior of a Structurally Constrained, Nucleophilic Sn(II) Towards Gold(I) 229

3.4 Concatenating Structural Constraint Effects at Tin for the Sequential Generation, Stabilization, and Transfer of Acyclic Aminocarbenes 281

3.5 Chemistry of Anti-van't Hoff-Le Bel Calix[4]pyrrolato Stannanes 437

4 Reflection and Summary 473

5 Methods 481

5.1 General Remarks on Experimental Work 481

5.2 Supplementary Details on Quantum Chemical Simulations 485

5.3 Synthetic Procedures and Characterization Data 488

6 References 505

7 Appendix 519

7.1 List of Abbreviations 519

7.2 NMR Spectra 522

7.3 Crystallographic Data 539

7.4 Quantum Chemical Data 554

8 Acknowledgements 561

9 Affidavit 563

1 INTRODUCTION

1.1 Preface

The installation of suitable substituents or ligands at *main-group element centers* is at the center of modern main-group chemistry. Tuning the steric and electronic properties of such ligands allowed chemists to stabilize main-group elements in unusual oxidation states or distorted structures, thereby equipping them with properties previously only associated with transition metals, *e.g.* partaking in reversible bond activations.[1–3] The beginning of substituted main-group element compounds can be dated back to the work of ROBERT BUNSEN and EDWARD FRANKLAND in the middle of the 19th century. Inspired by BUNSEN,[4] FRANKLAND attempted the isolation of the ethyl "radical" *via* the reaction of ethyl iodide with elemental zinc[a] leading to the first synthesis of diethylzinc (Et_2Zn) and ethylzinc iodide (EtZnI).[6] FRANKLAND quickly realized the generalizability of this synthetic approach and also accessed other main-group organometallics including *diethyltin diiodide* (Et_2SnI_2) and *tetraethyltin* (Et_4Sn) starting from ethyl iodide and tin metal. His systematic research on various organometallic compounds eventually led to the initial concept of valency: "*It was evident that the atoms of zinc, tin, arsenic, antimony, etc. had only room, so to speak, for the attachment of a fixed and definite number of the atoms of other elements, or, as I should now express it, of the bonds to other elements.*"[7,8] Thus, together with Et_2Zn and EtZnI, *organometallic tin compounds* not only belong to the first ever reported main-group organometallics, but also played an important role for the formulation of an early concept of valency. Later, this concept would evolve into the *octet rule*[b] for main-group elements by the contributions of ABEGG, KOSSEL, LEWIS, and LANGMUIR.[9–12]

The *p*-block element tin (Sn) belongs to Group 14 of the periodic table. As for the other elements of the *carbon group* or *tetrels* (C, Si, Ge, and Pb), tin can exist in the oxidation state IV fulfilling the octet rule (*vide supra*). For the heavier *p*-block elements in the 4th, 5th and 6th period, however, increasing nuclear charges and occupation of diffuse *d*-

[a] Owing to their completely filled *d*-orbitals and consequent chemical properties the Group 12 elements zinc, cadmium, and mercury have sometimes also been classified as main-group elements.[5]

[b] According to the octet rule elements of the *s*- and *p*-block strive to attain eight electrons in their valence shell thereby obtaining the electron configuration of a noble gas.

and *f*-orbitals in their core shell result in the stabilization of their valence *s*-orbitals (*inert-pair effect*).[13–15] Accordingly, these elements more readily deviate from the octet rule and exist in low-valent oxidation states with a valence electron count below eight. For tin, the inert-pair effect is pronounced enough to allow both oxidation states II (*stannous*) and IV (*stannic*) to be particularly stable and therefore to readily change between both states during the course of a chemical reaction.[16]

As for other tetravalent *p*-block atoms in their highest oxidation state, Sn(IV) compounds (*stannanes*) prefer a *tetrahedral* arrangement of their substituents. This fundamental principle was introduced independently by VAN'T HOFF and LE BEL already in 1874 and based on their observations with tetrasubstituted carbon compounds.[17,18] Thus, the so-called *van't Hoff-Le Bel principle* can be seen as an extension of the early theory of valency (*vide supra*) into the three-dimensional space. Owing to their reduced valency and stereochemically active electron lone pair, the van't Hoff-Le Bel principle cannot be applied to Sn(II) compounds (*stannylenes*). If the electron lone pair is regarded as a phantom substituent, their structure is best described as distorted *trigonal-planar* and can be predicted using the *Valence Shell Electron Pair Repulsion* (VSEPR) theory based on the repulsion of the substituents.[19,20]

Both stannylenes and stannanes can act as electron pair acceptors, *i.e. Lewis acids*, and form hypercoordinated systems with additional neutral or anionic electron pair donors **D**, *i.e. Lewis bases* (Figure 1 A and B).[21,22] The formation of these so-called *Lewis adducts* depends on steric and electronic aspects of both Lewis acid and base. Thus, predicting the stability of donor-acceptor bonds in Lewis adducts represents a multidimensional problem and requires a thorough understanding of the intermolecular interactions between acid and base (**Section 1.2**).[23]

Structural constraint has evolved as a viable handle to influence the reactivity of *p*-block compounds including their Lewis acidic or nucleophilic properties (Figure 1 C).[24–26] As an example, forcing high-valent, tetracoordinated *p*-block elements into a *square-planar anti-van't Hoff-Le Bel configuration* drastically increases their Lewis acidity (**Section 1.3**).[27,28] *Meso-octaalkylcalix[4]pyrroles* are a class of *macrocyclic, tetradentate ligands* closely related to porphyrins. They are actively researched as hosts for anion binding and recognition and ligands in transition metal coordination chemistry and were recently introduced into *p*-block element chemistry covering complexes with Al(III), Ga(III), Si(IV), Ge(IV), and Sb(III/V) centers (**Section 1.4**).[29] The calix[4]pyrrolato ligand backbone serves two purposes in these complexes: i) its structurally constrained coordination

environment grants unusually high Lewis acidities to the *p*-block element centers and ii) the electron-rich ligand backbone can act as a nucleophilic reaction site allowing for the *element-ligand cooperative* bond activation of various small molecules.[30,31]

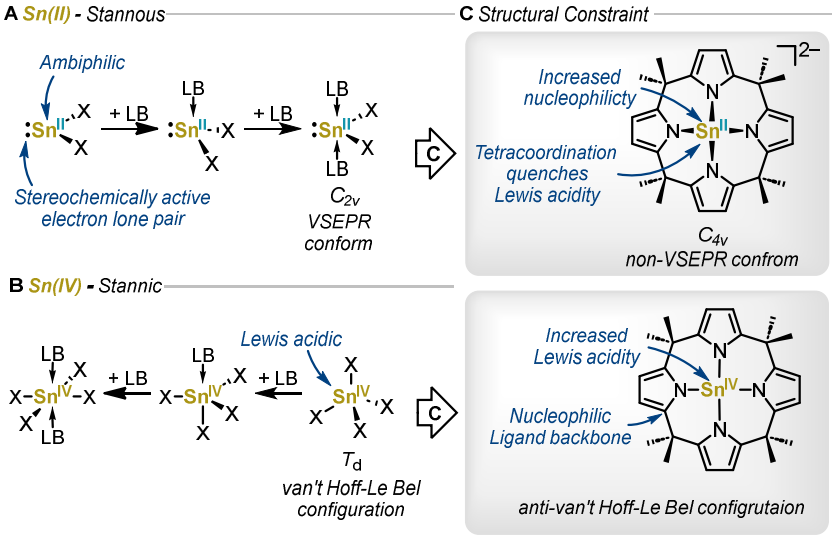


Figure 1. Lewis acid character of **A)** stannylenes and **B)** stannanes forming hypercoordinated tin compounds with Lewis bases (LB). **C)** The effect of the structurally constrained *meso*-octaalkylcalix[4]pyrrolato ligand backbone on Sn(II) and Sn(IV) centers causing deviations from their VSEPR or van't Hoff-Le Bel configuration, respectively.

Up to the work presented within this dissertation a systematic investigation of structural constraint effects on the Lewis acidity of Sn(IV) compounds was still missing (**Section 1.5**). Furthermore, calix[4]pyrrolato complexes of low-valent *p*-block element centers were formerly not reported. Even though tetracoordinated Sn(II) complexes of some porphyrinogens were known since 1970, the effect of their distorted coordination environment on the nucleophilicity of the Sn(II) center remained unexplored (**Section 1.6**).[32] This dissertation will introduce both of these aspects for the first time and describe the detailed influence of structural constraint on the reactivity of Sn(IV) and Sn(II) centers and their application in bond activation reactions.

1.2 Lewis Acidity: Definition and Scaling Methods

According to their eponymous name giver *Lewis acids* such as tin tetrachloride (**$SnCl_4$**) are defined as electron pair acceptors whereas *Lewis bases* act as electron pair donors.[33] By accepting an electron pair from Lewis bases, such as diethyl ether (**Et_2O**), **$SnCl_4$** forms the respective Lewis adduct (Figure 2).[34] This process can be split into two hypothetical steps: i) an energetically uphill deformation step which pre-organizes both the Lewis acid and base from their lowest energy structures into the structures they are adopting in the respective adduct, and ii) an association step forming a new dative bond between the Lewis acidic and basic centers. If the association energy (AE) released during step ii) over-compensates the deformation energy (DE) needed in step i), as well as the loss of entropy associated with the adduct formation, a Lewis adduct is formed with a respective reaction enthalpy ΔH.[35] Since the *International Union of Pure and Applied Chemistry* (IUPAC) defines *Lewis acidity* as "the thermodynamic tendency of a substrate to act as a Lewis acid", the enthalpy difference ΔH can be used to scale the Lewis acidity of the acid against the respective Lewis base.[36]

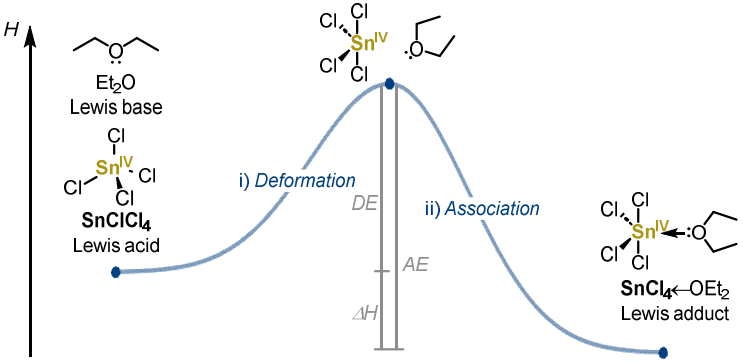


Figure 2. Potential energy diagram of a Lewis adduct formation reaction between the Lewis acid tin tetrachloride (**$SnCl_4$**) and the Lewis base diethyl ether (**Et_2O**). The reaction sequence is split into a deformation step i) requiring a deformation energy (DE) and a subsequent association step ii) releasing an association energy (AE). The energy difference between DE and AE gives the reaction enthalpy ΔH for the formation of the new Lewis adduct.

Owing to the complexity of the interaction between Lewis acids and bases, several scales for the quantification of Lewis acidity have been developed. They can be characterized as being *intrinsic*, *effective*, or *global* in nature.[23] *Intrinsic* scales such as the global electrophilicity index (GEI) ω,[37,38] parameters derived from ^{29}Si nuclear magnetic

resonance (NMR) spectroscopy for the scaling of cationic silylium Lewis acids,[39] and redox potentials obtained by cyclic voltammetry[40] can be advantageous since they are not referenced against a certain Lewis base and can be directly derived from the Lewis acid alone. However, these methods do not account for the deformation energy or the repulsion between acid and base. Two effects which can have a large influence on the Lewis adduct formation and therefore the Lewis acidity.[35,41,42]

In contrast, e*ffective* scales aim to quantify Lewis acidity in respect to specific reference bases which can be probed spectroscopically. Therefore, these methods deliver data containing information about the whole adduct formation process. The most prominent methods rely on changes in NMR shifts for ^{31}P in triethylphosphine oxide (*Gutmann-Beckett method*) [43,44] and ^{1}H in *E*-crotonaldehyde (*Childs method*) upon coordination to a Lewis acid[45] and further approaches towards using IR[46] and fluorescence spectroscopy[47] have been made.

Lastly, *global* scales use the enthalpies of the adduct formation reaction with a reference base to measure Lewis acidity. Therefore, they are the most accurate depiction according to the IUPAC definition given above and contain information about the whole process including the deformation energy. However, to obtain meaningful global Lewis acidities the choice of an appropriate reference base is crucial.[48]

One of the most prominent global Lewis acidity scales is the *fluoride ion affinity* (FIA), *i.e.* the negative reaction enthalpy for the addition of a fluoride anion to a Lewis acid.[49–51] As for global scaling methods in general, the exact determination of experimental affinities can represent a challenging task.[23] With the ongoing development of quantum chemical methods, high-performance computing resources, and recent machine learning approaches, computationally simulated Lewis base affinities became a reliable, easier accessible alternative.[52,53] Standard procedures for the calculation of FIAs use the isodesmic reaction between a given Lewis acid (**[LA]^{n}**) with the charge n and the anchoring system fluorotrimethylsilane (**TMSF**) forming the respective fluoride adduct **[LA-F]$^{n-1}$** and the trimethylsilylium cation (**[TMS]$^{+}$**, Figure 3). Using this approach, the difficult computational treatment of the naked fluoride anion in vacuum can be avoided.[23,54] Furthermore, the related hydride (HIA) and chloride ion affinities (CIA) can be obtained *via* a respective reaction scheme employing trimethylsilane (**TMSH**) and chlorotrimethylsilane (**TMSCl**) and used to obtain a multidimensional scale for Lewis acidity.[48] In the research work presented within this dissertation FIA, HIA, and CIA values computed on the

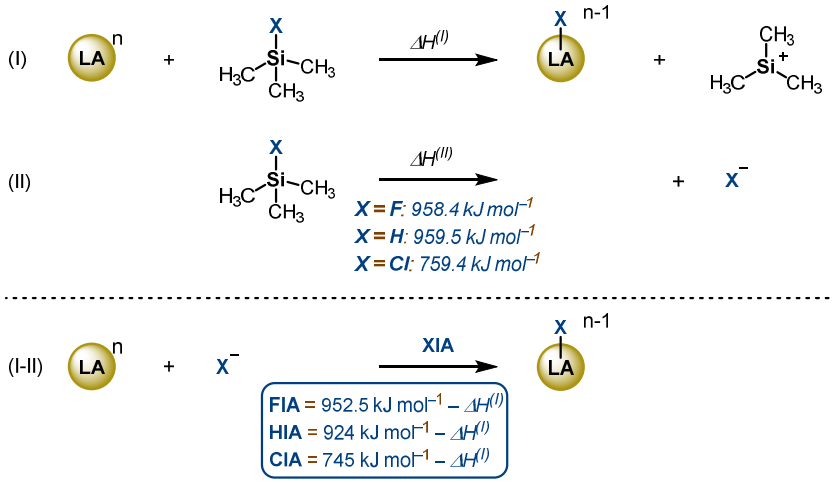
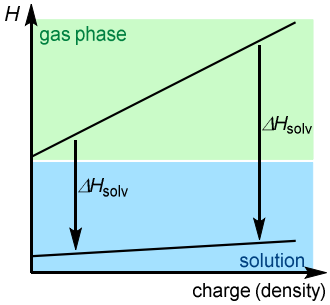


Figure 3. Trimethylsilane anchoring systems for the calculation of the fluoride (FIA), hydride (HIA), and chloride ion affinity (CIA) of a given Lewis acid (**[LA]^n**) with the charge n in the gas phase. $\Delta H^{(II)}$ was calculated at the CCSD(T)/CBS level of theory.[48,54]

accurate DSD-BLYP-D3(BJ)/def2-QZVPP//B97M-D4/def2-TZVPP// CREST/GFN2-xTB level of theory have been used.

In contrast to neutral Lewis acids (n = 0), which preserve the overall charge during the adduct formation with an anion **X**$^-$, cationic Lewis acids (n = +1, +2,...) experience a charge cancellation which causes misleading ion affinities (XIA) in vacuum.[23] To allow the comparison of Lewis acids regardless of their charge on a unified metric, it is necessary to account for these charge effects. Besides the inclusion of counter anions into the computational model or the application of neutral reference Lewis bases, the application of a solvation correction model showed to deliver the most reliable data.[55] Single point calculations of the Lewis acid **[LA]^n**, the free anion **X**$^-$, and the respective adduct **[X-LA]$^{n-1}$** using a solvation model of choice (COSMO-RS, CPCM, SMD) deliver the solvation enthalpies ΔH_{solv}, which can be used to obtain the solvation-corrected ion affinities XIA_{solv} *via* the scheme shown in Figure 4. The damping of the XIA is much more pronounced for charged (cationic) than for neutral Lewis acids and also strongly depends on the polarity of the solvent used for the model environment. Therefore, methylene chloride (CH_2Cl_2) has been established as a standard solvent for the calculation of ion affinities and the BP86/TZP COSMO-RS(DCM) solvation correction will be used throughout the work presented in this dissertation.



$$\mathbf{XIA_{solv}} = \mathrm{XIA} - [\Delta H_{solv}(\mathbf{[X\text{-}LA]^{n-1}}) - \Delta H_{solv}(\mathbf{[LA]^{n}}) - \Delta H_{solv}(\mathbf{X^{-1}})]$$

Figure 4. General scheme for the calculation of solvation-corrected ion affinities (XIA_{solv}).

1.3 The Theory Behind Square Planar-Coordinated *p*-Block Atoms

The *Valence Shell Electron Pair Repulsion* (VSEPR) theory is based on steric and electronic effects and states that the most stable three-dimensional structure for a molecule is the one in which valence and free electron pairs are as far apart as possible.[19,20,56,57] Therefore, the VSEPR theory dictates *e.g.* the trigonal planar, tetrahedral, and trigonal bipyramidal arrangement of three, four, and five substituents, respectively, around a *p*-block element. During recent years, the application of structural constraint to force *p*-block compounds into non-VSEPR conform structures evolved into an effective tool to stir their activity in bond activations and catalysis without the need of unusual oxidation or valence states.[24–26] Besides the well-investigated trigonal group 15,[58–67] and pyramidalized group 13 compounds,[68–70] the planarization of tetrahedrons experienced much less interest and potential applications remained largely unexplored.[71–73] In their minimum energy structure, tetracoordinated *p*-block elements adopt the tetrahedral, so-called *van't Hoff-Le Bel* configuration. The square-planar, D_{4h}-symmetric arrangement only represents a transition structure for stereoinversion on their potential energy surface (PES).[17,18] Early theoretical work by SCHLEYER disclosed an energetic lowering of the LUMO and its p_z-type character at the central element upon planarization as shown in the Walsh diagram in Figure 5.[74] At the same time the triple degeneration of the $1t_2$ highest occupied molecular orbital (HOMO) is lifted and the new $1b_2$ state experiences an energetic destabilization. This ultimately results in i) an increased Lewis acidity of the central element owing to the low-energy lowest unoccupied molecular orbital (LUMO), ii) a decreased HOMO-LUMO gap between the element-centered p_z-orbital and the substituent-centered HOMO, and iii) a destabilization of the D_{4h} structure owing to the high-energy HOMO.

More recent theoretical work by the GREB group focused on the stereoinversion of such tetrahedral *p*-block element compounds and identified several key aspects which influence the stability of their respective square-planar transition structures.[27,28] Employing the *Second-Order Jahn-Teller Effect* (SOJTE) they could correlate the stability of the square-planar transition structures with their HOMO-LUMO gap. Thus, a small frontier molecular orbital (FMO) gap in the D_{4h} structure causes its destabilization and a preferred relaxation into the T_d structure. Since more electropositive central elements result in a higher-lying LUMO and more electronegative substituents result in a lower-lying, ligand-centered HOMO, a large electronegativity difference between central element and

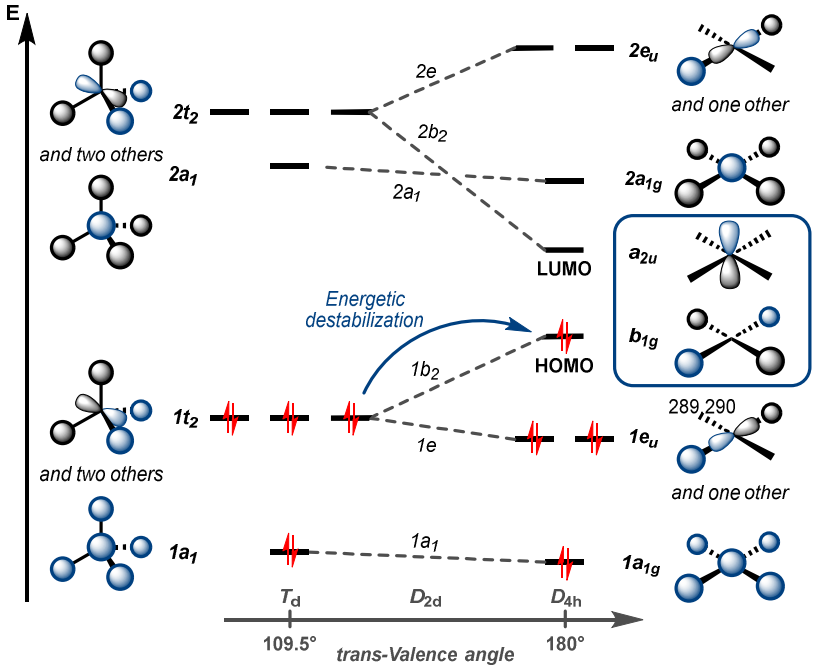


Figure 5. Schematic Walsh diagram for the distortion of tetracoordinated *p*-block element centers from the T_d- to the D_{4h}-symmetric state. This representation is most valid for group 14 central elements other than carbon, bearing pure σ-donor ligands such as hydrogen atoms. For CH_4 the increased electronegativity of the central element carbon results in a stabilization of the a_{2u} orbital and an inversion of the energetic orbital order.

the substituents stabilizes the D_{4h} structure *via* an increased HOMO-LUMO gap. However, this effect only has a large contribution for systems with pure σ-donor substituents such as hydrogen atoms and nearly vanishes for π-donor and σ-acceptor substituents such as fluorine. In addition, even in the D_{4h} structures π-donor substituents remain a high degree of covalency to the central element owing to π-back bonding interactions with the vacant p_z-type orbital. Therefore, π-donor/σ-acceptor ligands like the pyrrole units in calix[4]pyrroles should effectively lower the barrier for the planarization of tetracoordinated *p*-block compounds. Recent work reporting on the square planar anti-van't Hoff–Le-Bel cases of aluminium(III), silicon(IV), and germanium(IV) using the macrocyclic calix[4]pyrrolato ligand will be discussed in the following chapter.

1.4 Calix[4]pyrrole Chemistry

Porphyrinogens are macrocyclic compounds consisting of four pyrrole units linked at their α-position by sp^3-hybridized carbon atoms and occur as important intermediates in the biosynthesis of porphyrin-containing biomolecules.[75] They can readily be synthesized *via* on step in the acid-catalyzed condensation reaction of pyrrole and carbonyl compounds in equimolar ratios (Figure 6 A). This straightforward synthetic approach enables a fast modification of the *meso*-substituents R simply by employing different ketones as staring material. In the absence of hydrogen atoms bound to the *meso*-carbons (R ≠ H) the otherwise occurring oxidation towards porphyrins is prevented yielding the *meso*-octa-substituted macrocycles **$H_4[1^R]$** as stable, crystallin solids.[76] Already in 1886 VON BAEYER reported on the synthesis of the octamethyl derivative **$H_4[1^{Me}]$** from pyrrole and acetone forming the first fully *meso*-substituted porphyrinogen followed by the determination of its molecular structure by CHELINTZEV and TRONOV in 1916.[77,78] Owing to their capability of binding anions over their four NH groups and the cup-like structure of these host-guest complexes (see Figure 6 B), SESSLER and coworkers termed them *calix[4]pyrroles* which is now widely used in literature.[79,80] In the following decades intensive research focused on the functionalization of these ligand systems and the introduction of secondary binding sites linked to the *meso*-positions to control their complexation of neutral and anionic guest molecules as well as ion pairs.[81–83] Their anion binding ability also inspired the investigation of calix[4]pyrroles as drug delivery systems[84] and ion transporters with potential applications as anticancer drugs.[85–88] Besides the thermodynamically favored calix[4]pyrroles, also less stable smaller (n = 3)[89,90] and larger calix[n]pyrroles (n = 5, 6, 8) are known.[91–94]

Even though a large variety of symmetrically and asymmetrically *meso*-substituted calix[4]pyrroles have been reported so far, there are limitation regarding the steric and electronic demand of the substituents R.[95] Furthermore, water can influence the equilibrium of the condensation reaction shown in Figure 6 A.[96] Some of these aspects will be addressed in **Section 3.5.2**.

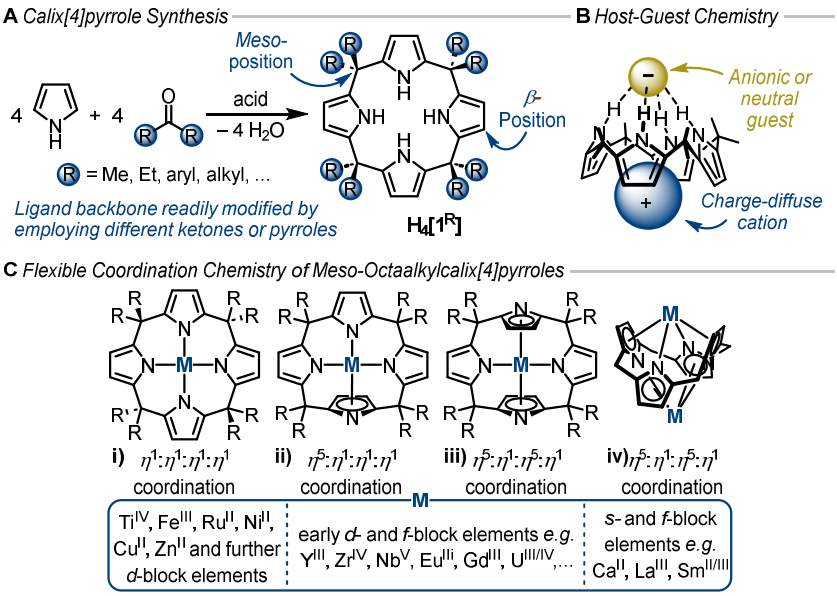


Figure 6. A) Synthesis of *meso*-octa-substituted calix[4]pyrrole $\mathbf{H_4[1^R]}$ *via* the acid-catalyzed condensation of ketones and pyrroles. **B)** Host-guest chemistry of calix[4]pyrrole as anion or ion pair receptor. **C)** Flexible coordination chemistry of *meso*-octaalkylcalix[4]pyrrolate $\mathbf{[1^R]^{4-}}$ showing various binding modes with *s*-, *d*-, and *f*-block metal centers **M**. For coordination mode iv) the *meso*-substituents R have been omitted for clarity.

Pioneered by the research group around FLORIANI in the early 1990s, calix[4]pyrroles were extensively used as ligands in *s*-, *d*-, and *f*-block chemistry.[97,98] Their sp^3-carbon linkers deliver a conformationally highly flexible ligand system which offers multiple η^1, η^3, and η^5 binding sites. These features yielded a plethora of complexes featuring the deprotonated calix[4]pyrrolato ligand $\mathbf{[1^R]^{4-}}$ and metal ions spanning nearly the entire periodic table (Figure 6 C).[29,99,100] They can be classified regarding their number of pyrrolate anions coordinating the central metal **M** *via* either a η^1 σ-coordination of the N atom or a η^5 coordination of the pyrrole π-surface. For high-valent metal centers with small ionic radii, *i.e. 3d*- and *4d*-transition metal ions, the all-η^1 mode i) displays the preferred way of coordination. However, larger, more charge diffuse metal cations from the *f*-block as well as early *4d*-transition metals, prefer the η^5 coordination of the pyrrolate π-faces resulting in the η^5:η^1:η^1:η^1 and η^5:η^1:η^5:η^1 binding modes ii) and iii), respectively. The latter represents the characteristic coordination mode for lanthanide calix[4]pyrrolato complexes. Coordination mode iii) can further be described as a metallocene-like sandwich complex formed by two *trans*-standing pyrrolates and the metal center **M** being

additionally coordinated by the N atoms of the remaining pyrrolates. Finally, the binding of a second metal ion yields the special coordination mode iv). For some *d*- and *f*-block complexes this flexibility enabled the macrocycle to change its coordination during a chemical reaction. Examples are the change from $\eta^5{:}\eta^1{:}\eta^5{:}\eta^1$ mode iii) to the $\eta^5{:}\eta^1{:}\eta^5{:}\eta^1$ mode ii) reported for some complexes containing Yb(IV), Nd(IV),[101] and Zr(IV).[102] In contrast to the *d*- and *f*-metals and owing to the low-charge of the metal cations, the *s*-block complexes of calix[4]pyrroles form di- and tetranuclear as well as polymeric structures in the solid state. They are not included in Figure 6 C and can be found in a review by SESSLER[103] and chapters of the *The Porphyrin Handbook* written by FLORIANI .[99,100,104–106] More recently, a partially deprotonated calix[4]pyrrolate *s*-block salt was reported. The tri-anionic calix[4]pyrrolate still contained one protonated pyrrole unit and coordinated three potassium counter cations.[101] These salts could act as novel starting materials for the synthesis of calix[4]pyrrole metal complexes with new stoichiometries.

In addition to the parent tetraanionic ligand systems **[1]**$^{4-}$, calix[4]pyrrolates can exist in two oxidized states. The twofold de-electronation of **[1^{R}]**$^{4-}$ yields the dianionic delta form **[Δ1^{R}]**$^{2-}$ whereas the overall quadruple de-electronation delivers the neutral double-delta form ΔΔ**1^{R}** (Figure 7). Each de-electronation step removes two electrons from the electron-rich π-system of the pyrrole units causing the formation of a C-C single bond between two neighboring α-carbon atoms and the dearomatization of the respective pyrrole rings.[107] Both, the strain stored in the concomitantly formed cyclopropane ring as well as the loss of aromaticity destabilize the oxidized forms of calix[4]pyrroles enabling the reversible interconversion between the parent tetraanionic and delta forms *via* chemical and electrochemical methods.[100,108–111] Thus, in addition to their ion binding properties and flexible coordination chemistry, calix[4]pyrroles can also act as redox-active ligands further extending their diverse application.

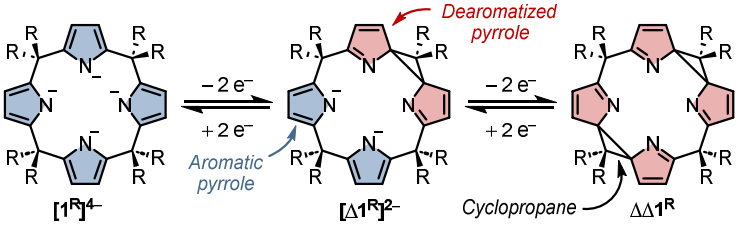


Figure 7. Redox chemistry of calix[4]pyrrolates showing the reversible dearomatization/aromatization of the pyrrole rings and the formation of cyclopropane rings.*p*-Block Calix[4]pyrroles as Structurally Constrained Lewis Acids

The first mention of *p*-block calix[4]pyrroles in literature can be traced back to a research communication of the FLORIANI group from 1999 and chapter 24 of the *Porphyrin Handbook Vol. 3* written by FLORIANI and FLORIANI-MORO and published in 2000.[99,112] They briefly reported on the aluminium(III) and tin(IV) complexes of the *meso*-octaethylcalix[4]pyrrolato ligand **[1^{Et}]$^{4-}$** and the usage of tin(IV) complex **2^{Et}-(thf)$_2$** for the oxidative dealkylation of the ligand backbone delivering ligands **H$_3$[3^{Et}]** and **H$_2$[4^{Et}]** (Figure 8). However, thereafter no immediate follow-up chemistry on this class of compounds has been conducted. In 2018, after lying dormant for nearly two decades, this research field was revived by the GREB group with a focus on *structurally constrained p-block Lewis acids*. The following chapter will summarize their contribution to the *p*-block element chemistry of calix[4]pyrrolato ligands covering eleven research papers,[113–123] a review article,[29] and parts of a book chapter,[24] all published between 2018 and 2023.

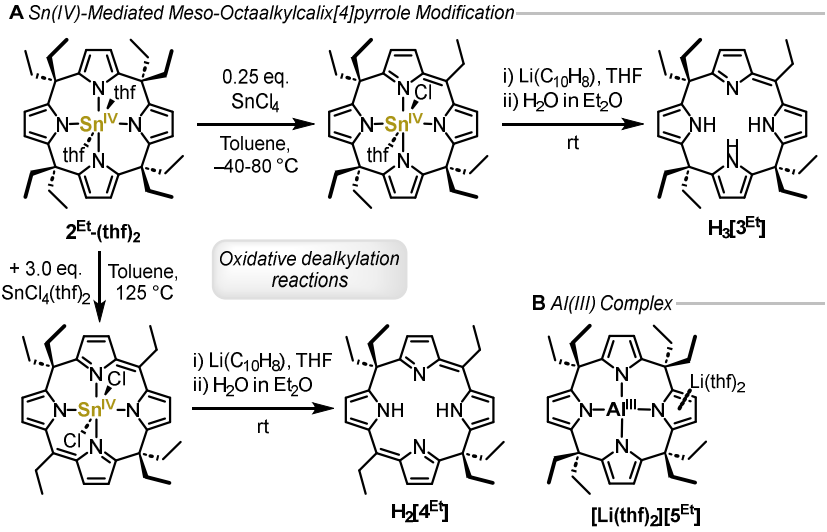


Figure 8. Early examples of *p*-block *meso*-octaalkylcalix[4]pyrrolato complexes reported by the FLORIANI group.

1.4.1 Group 13 Calix[4]pyrrolato Complexes

Owing to their straightforward synthesis and remarkable stability *meso*-octaalkylcalix[4]pyrrolato aluminates **[5^{R}]$^{-}$** (R = Me, Et, C6) represent the most investigated group of *p*-block calix[4]pyrroles (Figure 9 A). They can be obtained directly from the respective protonated calix[4]pyrroles by treatment with two equivalents of lithium aluminium hydride ($LiAlH_4$) in 1,2-dimethoxyethane (DME). $LiAlH_4$ acts as both a base and aluminium(III) precursor. After the initial formation of lithium hydridoaluminate **[Li$_2$(dme)$_4$][H-5^{R}]** salt exchange with tetraphenylphosphonium chloride in CH_2Cl_2 causes the precipitation of LiCl and LiH and the formation of the free aluminates as PPh_4^+ salts in 30% (R = C6) to >90% (R = Et) yield on a multi-gram scale.[116,117] The solid-state molecular structures of the anions **[5^{R}]$^{-}$** feature an essentially square planar, tetracoordinated aluminium(III) center with N-Al-N *trans*-valence angels very close to 180° and show only small deviations depending on the substituents R. Their overall D_{2d} symmetric structure with four equatorial (Me_{eq}) and four axial (Me_{ax}) residues also persists in solution exhibiting two sets of signals for the methyl groups in NMR spectroscopy at room temperature. The *anti-van't Hoff-Le Bel* structure of **[5^{R}]$^{-}$** causes reduced HOMO-LUMO energy gaps, low-energy p_z-type LUMOs essentially localized at the Al(III) center, and π-type HOMOs exclusively localized on the calix[4]pyrrole backbone (exemplarily shown for **[5^{Me}]$^{-}$** in Figure 9 C). This unique electronic structure well aligns with the theoretical predictions

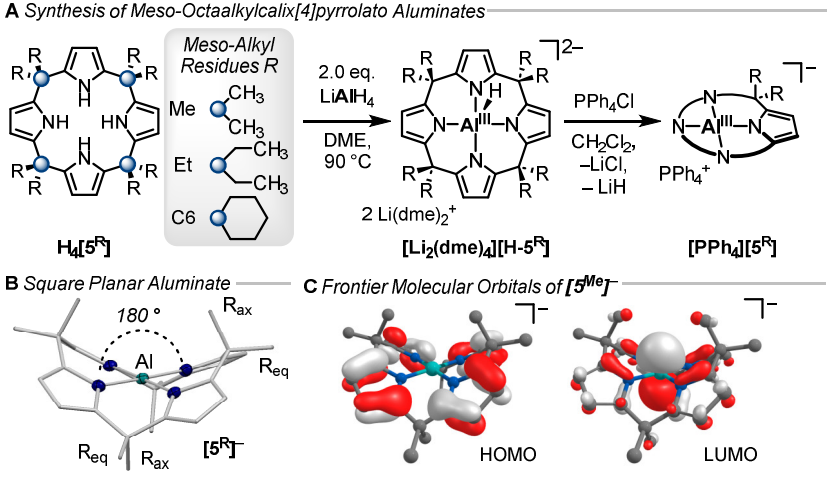


Figure 9. A) Synthesis and **B)** solid-state molecular structure of D_{2d} symmetric square-planar calix[4]pyrrolato aluminates **[5^{R}]$^{-}$**. **C)** Exemplary frontier molecular orbitals of *meso*-octamethylcalix[4]pyrrolato aluminate **[5^{Me}]$^{-}$**.[29]

discussed in the previous **Section 1.3** and yields Lewis acidic compounds despite their negative charge.

All aluminates $[\mathbf{5^{R}}]^-$ form adducts with neutral Lewis bases such as THF and even hydride and fluoride anions despite their negative charge.[116] Changing the *meso*-substituents R enabled the subtle control of these Lewis base binding reactions. When dissolved in THF $[\mathbf{5^{Et}}]^-$ forms a hexacoordinated bis(thf) adduct $[\mathbf{5^{Et}\text{-}(thf)_2}]^-$ while $[\mathbf{5^{Me}}]^-$ only binds one THF donor and $[\mathbf{5^{C6}}]^-$ can be recovered as the free square planar Lewis acid. Detailed computational analysis showed that increased dispersion interactions between the *meso*-ethyl residues and a reduced deformation energy cause the strengthened THF binding of $[\mathbf{5^{Et}}]^-$.[117]

The combination of Lewis acidic Al(III) centers with the electron-rich calix[4]pyrrole ligand backbone further allowed the element-ligand cooperative (ELC) activation of C=O bonds in aldehydes, ketones, and CO_2 and O-H bonds in alcohols (Figure 10).[31,118] In the initial step the carbonyl substrate enters the coordination sphere of the electron-deficient Al(III) center forming a classical Lewis or *σ-adduct*. Polarization of the C=O bond then allows the nucleophilic attack of the basic α-carbon atom at the 2-position in the pyrrole delivering the so-called *1,2-adduct*. The newly formed C-C bond causes the dearomatization of the respective pyrrole ring (red). Latter plays an important role for the reversibility of this process. Rearomatization of the pyrrole unit upon C-C bond cleavage stabilizes the σ-adduct eventually enabling a rapid and highly reversible self-exchange of substrates.[115] These equilibria showed to be highly sensitive to various substituents and external stimuli: i) electron-withdrawing groups (EWG) at the substrates facilitate the nucleophilic attack of the pyrrole α-carbon stabilizing the 1,2-adduct; ii) *vice versa* electron donating groups (EDG) at the carbonyls stabilized the σ-adduct; iii) even though the inductive effect of ethyl substituents showed to increase the basicity of the α-carbon in $[\mathbf{5^{Et}}]^-$, the increased allylic strain between the ethyl residues and the pyrrole backbone disfavors the formation of 1,2-adducts; iv) lithium cations bind to the C=O oxygen atoms acting as a second Lewis acid thereby stabilizing the 1,2-adduct; and v) owing to their increased steric demand, ketones favor the formation of σ-adducts. In addition, these stimuli showed to enable the substrate discrimination in hydroboration catalysis favoring the conversion of less reactive C=O bonds.[115,117]

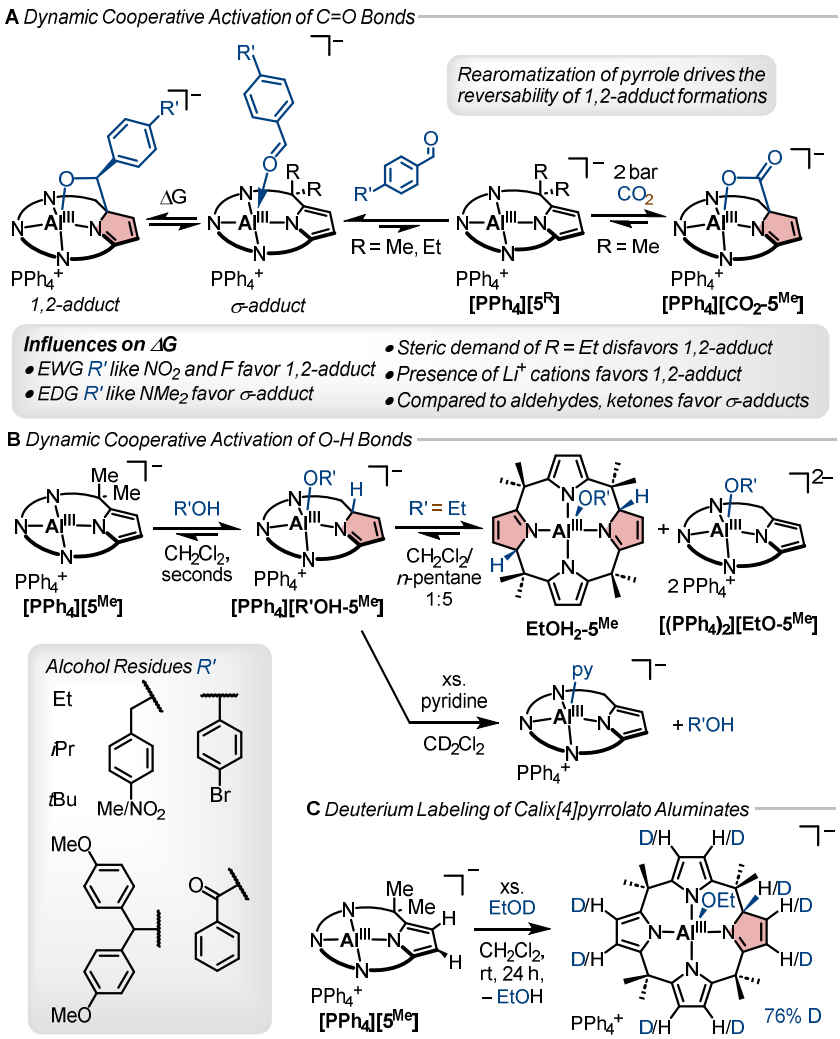


Figure 10. Dynamic cooperative activation of **A)** carbonyls and **B)** alcohols with *meso*-octaalkyl-calix[4]pyrrolato aluminates. For some adducts the *meso*-substituents R are omitted for clarity. **C)** Deuterium labeling of $[\mathbf{5^{Me}}]^-$ with ethanol-d_1.

The ELC properties of *meso*-octaalkylcalix[4]pyrrolato aluminates also enable their application as catalysts for the P-B dehydrocoupling of phenylphosphine borane adducts.[123] The cooperative activation of the P-H bond accessed the transition metal-free

synthesis of high-molecular mass polyphosphinoboranes thereby avoiding the problem of residual *d*-block metal impurities in the resulting material.

A large variety of OH acidic compounds R'OH spanning primary, secondary, and tertiary alkyl and benzylic alcohols, as well as *para*-bromophenol and benzoic acid, selectively react with **[5^{Me}]$^-$**.[118] In analogy to the activation of carbonyls (*vide supra*) binding of the alcohol oxygen atom to the Lewis acidic Al(III) center acidifies the O-H bond and enables a subsequent low-barrier deprotonation *via* the basic pyrrole α-carbon. This reaction forms the activation products **[R'OH-5^{Me}]$^-$** within seconds at room temperature and showed to be highly reversible. Computations revealed the non-VSEPR structure of **[5^{Me}]$^-$** and the concatenation of the four pyrrole units into the calix[4]pyrrole macrocycle to be key factors for the activation of these alcohols and the high stability of the respective products. For R' = *t*Bu the equilibrium could be monitored by variable temperature NMR spectroscopy unveiling that the reaction completely reversed under vacuum conditions in high-boiling solvents. However, for less sterically demanding residues R' even at low temperatures the equilibrium lay completely on the product site. Eventually, addition of a strong Lewis base such as pyridine reverses the alcohol binding delivering free R'OH and the pyridine adduct of **[5^{Me}]$^-$**. The products **[R'OH-5^{Me}]$^-$** possess an amphoteric character and can either be deprotonated at the α-C-H or take up a second proton at a second basic pyrrole α-carbon. For R' = Et this autoprotolysis equilibrium between **[PPh$_4$][EtOH-5^{Me}]** on one side and **EtOH$_2$-5^{Me}** and **[(PPh$_4$)$_2$][EtO-5^{Me}]** on the other side was studied. It could be influenced by the solvent polarity with non-polar solvents causing the precipitation of the salt **[(PPh$_4$)$_2$][EtO-5^{Me}]**. Finally, reaction with an excess ethanol-d_1 (EtOD) revealed an additional dynamic behavior. After the activation of the O-D bond in EtOD a series of [1,5]H/D sigmatropic rearrangements allowed the deuteration of up to 76% of the β-positions in the ligand backbone within 24 hours.

As described in **Section 1.4**, calix[4]pyrroles can act as electron reservoirs showing a reversible, multi-electron redox chemistry. Combination of these properties with the Lewis acidity of the square-planar Al(III) center in **[PPh$_4$][5^R]** (R = Me, Et) leveraged the irreversible, cooperative activation of triplet dioxygen [119] Both aluminates react with $^3O_2$ (1 bar) delivering orange CD_2Cl_2 solutions within seconds (Figure 11). Single crystal X-ray diffraction (sc-XRD) confirmed the formation of an alkylperoxide aluminate **[PPh$_4$][OO-5^R]** showing the cooperative bonding of dioxygen *via* the mode discussed for carbonyls and alcohols (*vide supra*). Time-dependent density functional theory (TD-DFT) calculations revealed the color of **[PPh$_4$][OO-5^R]** originating from low-energy electronic

excitations from the aromatic pyrrole units (HOMO) to the dearomatized (red) pyrrole unit (LUMO). Detailed computations employing density functional theory (DFT) and multireference methods enclosed the mechanism of the formally spin-forbidden activation of $^3O_2$. After an end-on coordination of the weak Lewis base $^3O_2$ to the non-VSEPR Al(III) center, the electron-donating properties of the calix[4]pyrrole ligand backbone allow for an inner-sphere one-electron reduction step forming a triplet intermediate. The formation of this superoxide aluminate then enables spin-vibronic coupling to facilitate intersystem crossing (ISC) onto the singlet potential energy surface delivering **[PPh$_4$][OO-5^R]**. The alkylperoxide aluminates possess a remarkable stability against nucleophilic and electrophilic substrates but degraded into a new discrete species within 24 hours at room temperature in solution. Detailed spectroscopic and computational analysis confirmed the cleavage of the α-C-C bond in the dearomatized pyrrole followed by a multi-step rearrangement ultimately forming compound **[PPh$_4$][6^R]**. While the metal-centered binding of dioxygen in these porphyrinogen aluminates shows a structural analogy to iron porphyrins in heme, they lack the electronic properties of an open-shell d^6 transition metal center. However, redox-activity of the calix[4]pyrrole enabled to bypass the spin barrier by a mechanism similar to the proton coupled electron transfer (PCET) operative in flavin-dependent enzymes.

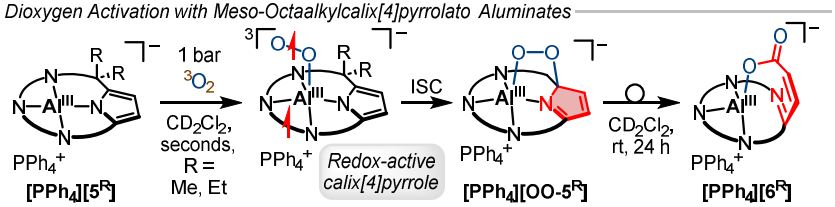


Figure 11. Cooperative activation of dioxygen with **[PPh$_4$][5^R]** (R = Me, Et) and oxidative α-cleavage of a pyrrole unit forming the rearranged product **[PPh$_4$][6^R]**. For some adducts the *meso*-substituents R are omitted for clarity.

Application of the calix[4]pyrrolato ligand framework could also be extended to obtain structurally constrained gallium(III) centers. Deprotonation of methyl-and ethyl-substituted **H$_4$[1^R]** with sodium bis(trimethylsilyl)amide (NaHMDS) formed the respective sodium salts as THF solvates. Subsequent treatment with tetraphenylphosphonium tetrachlorogallate [PPh$_4$][GaCl$_4$] delivered the free, square-planar coordinated gallate salts in fair yields of up to 69% (Figure 12 A).[120] The anions **[7^R]$^-$** (R = Me, Et) showed to possess similar structural characteristics as their aluminium congeners featuring N-Ga-N *trans*-valence angles of 178.6° and 178.7°, respectively. In comparison to **[5^R]$^-$**, the gallates

showed slightly reduced Lewis acidities on the FIA scale. This allowed their initial isolation even in the presence of the Lewis base THF whereas the related aluminates(III) form stable mono- and bis-adducts (*vide supra*). The reduced Lewis acidity is also reflected in the reactivity of **[7^{R}]**$^{-}$ with CO_2 and *iso*-propanol (Figure 12 B). Cooperative 1,2-addition of CO_2 required higher pressures as for the aluminates and for **[7^{Et}]**$^{-}$ only 33% conversion could be observed under five bar CO_2. This allowed to completely reverse the addition of CO_2 under vacuum conditions. For *i*PrOH no reaction could be observed under the standard conditions reported for the aluminate. However, the Brønsted basicity of the α-carbon in the calix[4]pyrrolato ligand backbone allowed its selective protonation with bis(trifluoromethanesulfonic)amid ($HNTf_2$) in the presence of donor solvents such as Et_2O. The neutral gallane **H[7^{Me}]** showed a boosted Lewis acidity with a FIA_{solv} of 191 kJ mol^{-1} *vs.* 149 kJ mol^{-1} for the gallate **[7^{Me}]**$^{-}$. Eventually, this enabled the gallium-ligand cooperative activation of the O-H bond in *i*PrOH forming the neutral product ***i*PrOH$_2$-7^{Me}** and introduced a new handle to influence the Lewis acidities of these compounds by second-sphere ligand protonation.

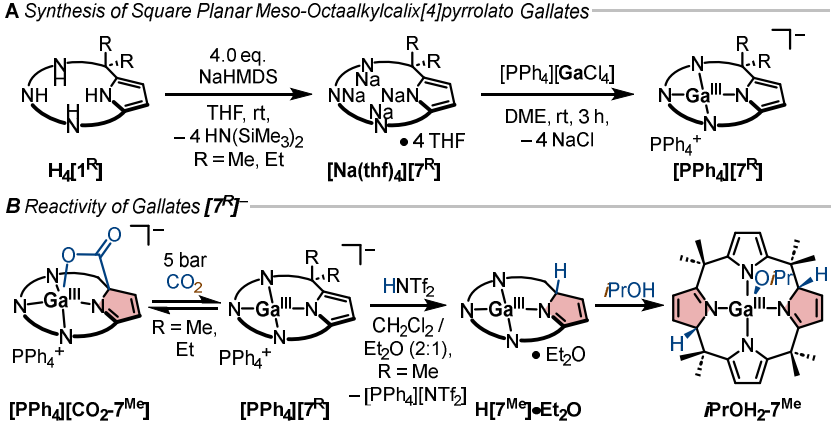


Figure 12. A) Synthesis of square planar *meso*-octaalkylcalix[4]pyrrolato gallates **[PPh$_4$][7^{R}]** (R = Me, Et) and **B)** their reactivity with CO_2 and *i*PrOH. For some adducts the *meso*-substituents R are omitted for clarity.

1.4.2 Group 14 Calix[4]pyrrolato Complexes

In the context of group 14 chemistry the calix[4]pyrrolato silane **8^{Et}** and germane **9^{Et}** have been reported.[113,122] *In situ* deprotonation of **H$_4$[1^{Et}]** with *n*-butyl lithium (*n*BuLi) in *n*-hexane delivered the donor-free lithium salt **[Li$_4$][1^{Et}]**. Subsequent reaction with silicon tetrachloride ($SiCl_4$) in DME enabled the isolation of lithium *meso*-octaethylcalix[4]pyrrolato chloridosilicate **[Li(dme)][Cl-8^{Et}]** in 40% yield. To ensure the complete removal of the donor solvent DME, Li^+ was exchanged for the weakly interacting PPh_4^+ cation delivering **[PPh$_4$][Cl-8^{Et}]** in near quantitative yield. $^1H,^{29}Si$ heteronuclear multiple bond correlation (HMBC) NMR represented a spectroscopical probe for the coordination number of the Si(IV) center. A shift of −129.0 ppm attested a pentacoordinated, hypervalent silicon which ultimately was confirmed by sc-XRD analysis. Subsequent abstraction of the chloride anion was achieved by sodium tetrakis(pentafluorophenyl)borate (Na[BAr^{F20}]). First, salt metathesis formed a tetrameric sodium chloridosilicate **[Na]$_4$[Cl-8^{Et}]$_4$** macrocycle which could be identified *via* sc-XRD analysis. Driven by the lattice energy of sodium chloride and its precipitation in non-polar solvents like *n*-hexane, **[Na]$_4$[Cl-8^{Et}]$_4$** slowly dissociated releasing the free Lewis acid **8^{Et}** which could be isolated on a mg scale (Figure 13 A). A ^{29}Si NMR shift of −55.6 ppm indicated a tetracoordinated silicon center. Eventually, sc-XRD confirmed the synthesis of the first square-planar coordinated silicon(IV) center. Owing to its anti-van't Hoff-Le Bel conformation, **8^{Et}** possesses remarkable features usually associated with transition metal complexes: i) the solid-state molecular structure of **8^{Et}** revealed agostic-type interactions between the ethyl substituents and the central silicon atom; ii) UV-vis measurements and TD-DFT calculations identified a ligand to element charge transfer (CT) band as the origin of its yellow color in solution; iii) the lowered energy of the vacant p_z-type orbital at Si(IV) allowed its mild reduction forming a transient silicon-centered radical anion; iv) **8^{Et}** shows a silicon-ligand cooperative activation of the non-polar C-C triple bond in phenylacetylene; and v) planarization causes drastically increased FIA_{solv} and HIA_{solv} values compared to archetypical, tetrahedral silanes (Figure 13 B).[113] Furthermore, latter enabled the synthesis of the PPh_4^+ salt of *meso*-octamethylcalix[4]pyrrolato hydridosilicate **[PPh$_4$][H-8^{Me}]** and resulted in its remarkable stability even under ambient conditions (Figure 13 C).[114]

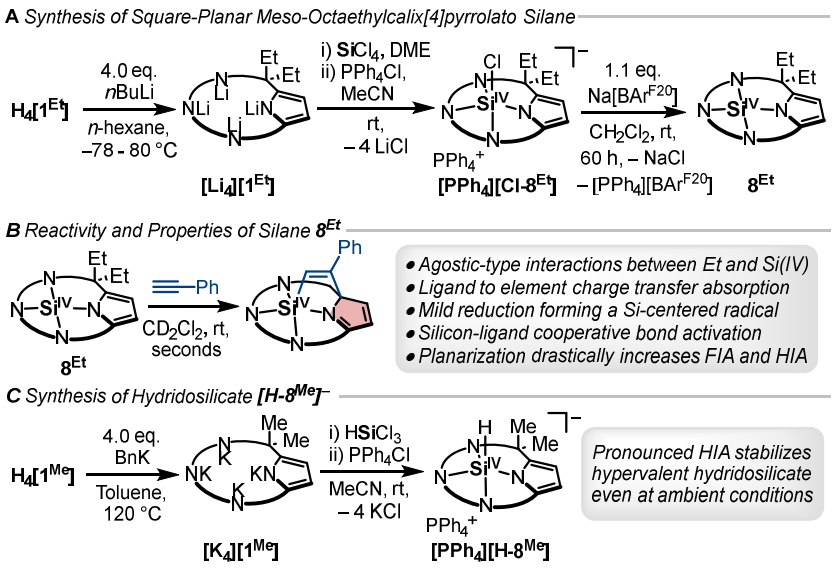


Figure 13. A) Synthesis of square planar *meso*-octaethylcalix[4]pyrrolato silane **8^{Et}** and **B)** its reactivity and properties as a result of its anti-van't Hoff-Le Bel configuration. **C)** Synthesis of the PPh_4^+ salt of *meso*-octamethylcalix[4]pyrrolato hydridosilicate **[PPh$_4$][H-8^{Me}]**. For some adducts the *meso*-substituents R are omitted for clarity.

Incorporation of germanium(IV) was achieved *via* the calix[4]pyrrolato potassium salt **[K$_4$][1^{Et}]** in combination with germanium tetraiodide GeI_4 in THF.[122] However, the square-planar *meso*-octaethylcalix[4]pyrrolato germane could only be isolated as the bis(thf) adduct **9^{Et}-(thf)$_2$** (Figure 14 A). Attempts to remove the THF donors at elevated temperature and reduced pressure caused the decomposition of the potential free Lewis acid **9^{Et}** indicating their vital role in the stabilization of this germane. Furthermore, the abstraction of THF with other Lewis acids or the chloride anion form chloridogermanate **[Cl-9^{Et}]$^-$** using Na[BAr^{F20}], in analogy to the synthesis of silane **8^{Et}**, did not deliver the free Lewis acid **9^{Et}**. NMR spectroscopy of **9^{Et}-(thf)$_2$** in solution revealed an overall D_{4h} symmetry with broadened signals owing to the labile, dynamic coordination of THF. As a result, **9^{Et}-(thf)$_2$** could be used as a surrogate for the respective free square-planar germane allowing to access its pronounced Lewis acidity and ELC bond activations (Figure 14 B). Reactions with several sources of Lewis basic anions (X^- = F^-, H^-, Cl^-, and N_3^-) delivered the respective pentacoordinated germanate salts **[Y][X-9^{Et}]**. In analogy to the aluminate **[5^{Et}]$^-$**, **9^{Et}-(thf)$_2$** also reacted with O-H bonds and the C=O bond in *para*-nitro benzaldehyde. However, a previously unreported reaction with acetonitrile (MeCN) could be

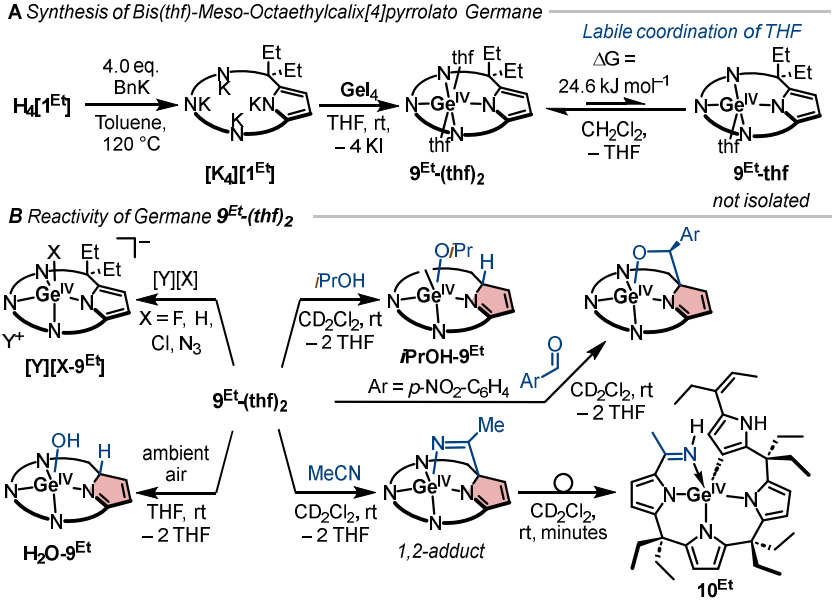


Figure 14. A) Synthesis of the bis(thf) adduct of square planar *meso*-octaethylcalix[4]pyrrolato germane $\mathbf{9^{Et}\text{-}(thf)_2}$ and its labile coordination of THF in solution and **B)** its reactivity acting as a surrogate for the free germane in its anti-van't Hoff-Le Bel configuration. As anion sources [Y][X] $[PPh_4][Cl]$ in CH_2Cl_2, Tetrabutylammonium difluorotriphenylsilicate (TBAT) $[NBu_4][F_2SiPh_3]$ in CH_2Cl_2, $[NBu_4][N_3]$ in CH_2Cl_2, and $NaBHEt_3$ in toluene followed by a salt exchange with PPh_4Cl in CH_2Cl_2 have been used. Latter to obtain the reaction product with the formal salt $[PPh_4][H]$. For some adducts the *meso*-substituents R are omitted for clarity.

observed. After the formation of a short-lived 1,2-adduct of the C-N triplet bond, re-aromatization of the pyrrole unit triggers a C-C bond cleavage in the calix[4]pyrrole backbone forming the rearranged compound $\mathbf{10^{Et}}$ within hours.

The bis(thf) adduct of *meso*-octaethylcalix[4]pyrrolato stannane $\mathbf{2^{Et}\text{-}(thf)_2}$ has already been reported 25 years ago (*vide supra*). However, a detailed investigation of this class of structurally constrained tin(IV) complexes and the attempt to isolate the respective free, square-planar Lewis acids were still missing. **Section 3.5** will describe the contributions to this field made within the work presented in this dissertation.

1.4.3 Electromerism of Antimony(III/IV) Calix[4]pyrrolato Complexes

The combination of structural constraint with the redox-flexibility of pnictogen center has emerged as a viable tool for the design of *p*-block redox catalysts.[124] Extending this principle by employing a redox-active ligand backbone as present in calix[4]pyrroles, furthermore introduces the potential of electromerism. A concept well-known for transition metal chemistry but only scarcely investigated in combination with *p*-block element centers.[125–130] Reaction of the lithium salt **[Li$_4$(thf)$_3$][1^{Et}]** with antimony trichloride ($SbCl_3$) in THF at −78 °C followed by the salt metathesis with PPh_4Cl enabled the multigram scale synthesis of the antimonite **[11^{Et}]$^-$** in good yields.[121] NMR spectroscopy in solution indicated the formation of a square-pyramidal *meso*-octaethylcalix[4]pyrrolato complex with overall C_{4v} symmetry and "*doming*" pyrrole units. In contrast, sc-XRD analysis of **[PPh$_4$][11^{Et}]** revealed a "*ruffling*" conformation with an averaged C_{2v} symmetry evidencing a fast conformational change at room temperature in solution associated with a highly flexible calix[4]pyrrole ligand backbone. Subsequent oxidation with ferrocenium salts [Fc][X] ([X]$^-$ = $[SbF_6]^-$, $[PF_6]^-$) delivered the stibenium(III) cation **[Δ11^{Et}]$^+$** containing the two-electron oxidized delta form of *meso*-octaethylcalix[4]pyrrolato ligand (Figure 15 A). The computed FIA$_{solv}$ value (124 kJ mol^{-1}) and the stability of **[Δ11^{Et}]$^+$** against fluoride containing anions like $[SbF_6]^-$, $[PF_6]^-$, and even $[BF_4]^-$ attested its only marginal Lewis acidity. **[Δ11^{Et}]$^+$** can be seen as an electrometric form of the square-planar coordinated calix[4]pyrrolato stibenium(IV) cation **[11^{Et}]$^+$** containing a fully oxidized antimony center and a reduced ligand backbone (Figure 15 B). Since quantum mechanical calculations showed that the Δ-form is stabilized by 229 kJ mol^{-1}, an external stimulus is needed to facilitate its transformation into **[11^{Et}]$^+$**. Indeed, experimental findings indicated the desired electromerism initiated by the addition of neutral Lewis bases which stabilize the Sb(IV) center in **[11^{Et}]$^+$**. Excess pyridine causes the immediate abstraction of F^- from $[SbF_6]^-$, $[PF_6]^-$, and $[BF_4]^-$ *via* the intermediately formed pyridine adduct **[11^{Et}-py]$^+$**. In comparison to the stibenium(III) cation **[Δ11^{Et}]$^+$**, **[11^{Et}-py]$^+$** shows a significantly increased Lewis acidity as evidenced by i) a LUMO with p_z-character located at the Sb(IV) center, ii) a reduced LUMO energy, iii) a more positively charged Sb atom, and iv) an increased FIA$_{solv}$ of 203 kJ mol^{-1}. Thus, Lewis base coordination to **[Δ11^{Et}]$^+$** does not lead to the saturation of the acceptor element, but induces a significant reactivity increase mediated by electromerism.

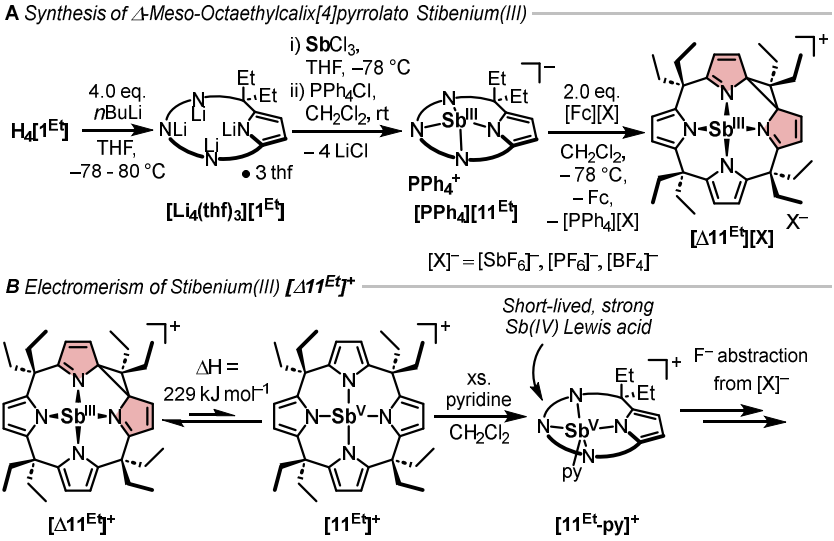


Figure 15. A) Synthesis of the Δ-*meso*-octaethylcalix[4]pyrrolato stibenium(III) **[Δ11^{Et}]$^+$** and **B)** its electromerism forming the Lewis superacidic stibenium(V) **[11^{Et}]$^+$**.

1.5 Amplifying the Lewis Acidity of Tin Lewis Acids

Tin compounds have been used as substrates and catalysts in a plethora of chemical transformations with their chemistry being dominated by the electropositive nature of tin.[131] The highly polarized Sn-C bonds in organotin compounds allowed their application as the source of nucleophilic alkyl, allyl, or aryl residues in different electrophilic substitutions and in the transmetalation step of the *Stille cross-coupling reaction*.[132,133] Furthermore, the intermediate formation of stannylene acetals and stannyl ethers from dibutyltin oxide (**DBTO**) has been extensively used for the direction of electrophilic *O*-functionalization reactions in carbohydrates and other diols and polyols.[134] Some of the most important industrial applications of tin catalysts are based on their *Lewis acidic* properties.[135] As an example, dibutyltin dilaurate (**DBTL**) is widely employed as a Lewis acid catalysts for transesterifications, the ring-opening polymerization (ROP) of lactones, and the synthesis of polyurethanes.[136]

The activity of Lewis acid catalysts can be correlated with their Lewis acidity.[137] Thus, the following section will discuss strategies to increase the Lewis acidic character of tin compounds. To allow a quantitative comparison between Lewis acids, the solvation-corrected (CH_2Cl_2) fluoride ion affinity scale discussed in **Section 1.2** will be employed. In comparison to its lighter homologs tetramethylsilane (**SiMe$_4$**) and tetramethylgermane (**GeMe$_4$**), **SnMe$_4$** exhibits a positive FIA_{solv} value of 7 kJ mol^{-1} (Figure 16 A). Thus, it should weakly bind a fluoride anion in solution. In the series **SiMe$_4$**, **GeMe$_4$**, **SnMe$_4$** the decrease in electronegativities and increased ionic radii for the heavier *p*-block elements lead to an accumulation of positive charge at the central atom and a more flexible substituent shell around the *p*-block elements. Both effects mutually result in increased Lewis acidities.[35,54,138,139] The deviation of the FIA_{solv} for **SiMe$_4$** can be explained by the exceptional stability of the Si-F bond.[138,140,141]

Presumably, the most intuitive approach to increase the electron pair-accepting character of an element is the installation of electron-withdrawing substituents (Figure 16 B). As evidenced by their FIA_{solv} values, the exchange of methyl substituents with fluorides (**SnF$_4$**), chlorides (**SnCl$_4$**), pyrrolates (**12**), or carboxylates (**DBTL**) results in a significant increase in Lewis acidity. Correspondingly, **SnF$_4$** acts as a strong Lewis acid towards the fluoride of neighboring **SnF$_4$** molecules forming oligomeric, planar layers of octahedrally coordinated tin centers in its solid state.[142]

Stannylenes are ambiphilic in nature possessing both Lewis basic and acidic properties. Their reduced valency bearing only two substituents results in a readily accessible

vacant p_z-orbital. Both characteristics drastically decrease the deformation energy needed upon coordination of a Lewis base therefore increasing their Lewis acidity (Figure 16 C).[143] Stannous chloride **$SnCl_2$** and other tin(II) compounds are used as efficient Lewis acid catalysts for the synthesis of poly(lactic acid).[144,145] In contrast to the stannic halides SnX_4, stannous fluoride SnF_2 shows a smaller FIA_{solv} than its chloride homolog. This trend might be explained by the tendency of fluoride substituents to undergo π-back bonding

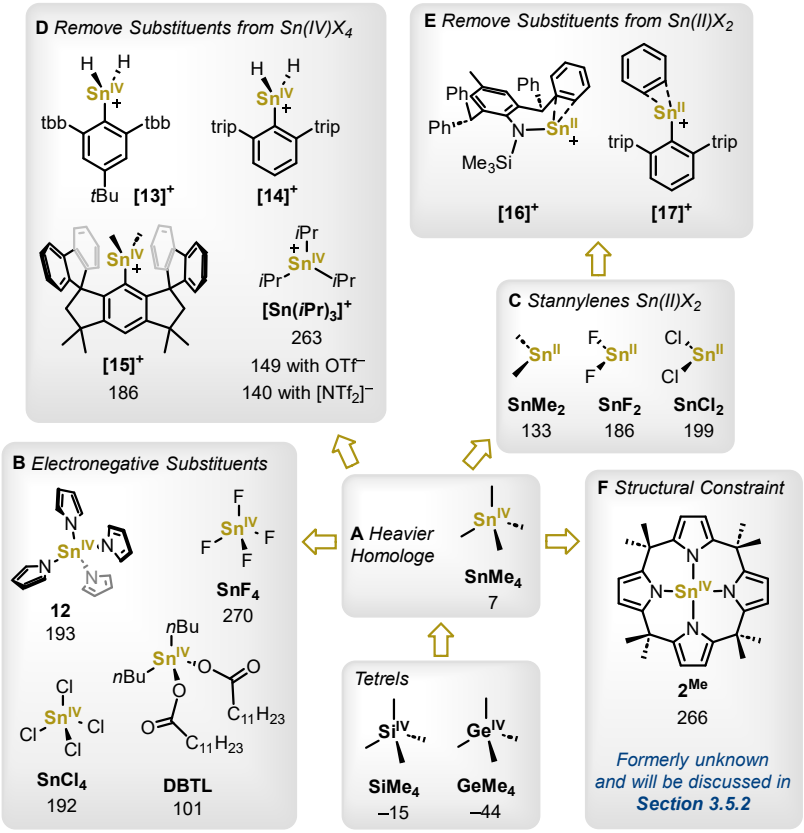


Figure 16. Literature known approaches to increase the Lewis acidity of tin Lewis acids. To allow a quantitative comparison of their Lewis acid strengths, the solvation-corrected fluoride ion affinities (FIA_{solv}, DSD-BLYP-D3(BJ)/def2-QZVPP//BP86/TZP COSMO-RS(DCM)//B97M-D3(BJ)/def2-TZVPP)) are given in kJ mol^{-1} for some compounds. FIA_{solv} values for **[15]**+[146] and **[Sn(*i*Pr)$_3$]**+[55] where taken from the respective publications and calculated for **2^{Me}** within the work of this dissertation. The remaining FIA_{solv} values were generated using the FIA-GNN (graph neural network) machine learning approach reported by SIGMUND *et al.*[52]

thereby lowering the electron-accepting character of the vacant p_z-orbital at Sn(II). However, recent work on the Lewis acidity trend in boron trihalides casted doubt on this explanation and a more complex combination of orbital and electrostatic interactions most likely explains such trends.[147,148]

An additional strategy to decrease the deformation energy of tin(IV) compounds and also increase their electron deficiency is the removal of anionic substituents X from tetravalent SnX_4 molecules (Figure 16 D). The first free, tricoordinated stannylium cations $[SnX_3]^+$ were reported independently in 2003 by the groups around MÜLLER[149] and SEKIGUCHI.[150] Both used sterically demanding substituents such as *2,4,6*-triisopropylphenyl or di(*tert*-butyl)methylsilyl to stabilize the reactive tin center and accessed these cations either *via* the electrophilic abstraction of an allyl residue or the oxidation of a stable stannyl radical. The WESEMANN group used hydride abstraction from parent monoarylstannanes $ArSnH_3$ to obtain the respective stannylium cations **[13]**$^+$ and **[14]**$^+$.[151,152] While the $ArSnH_3$ compounds can be handled in donor solvents like Et_2O and THF, the stannylium cations form bis(thf) adducts possessing trigonal-bipyramidal coordinated Sn(IV) centers. The aryldimethylstannylium cation **[15]**$^+$ could be synthesized by either hydride or chloride abstraction from the respective organotin precursors.[146] BECKMANN and coworkers also computed its FIA_{solv} value as 186 kJ mol^{-1} which lies in the range of **$SnCl_4$** even in the absence of electron-withdrawing substituents. Recent theoretical work by ERDMANN *et al.* reported a FIA_{solv} value of 263 kJ mol^{-1} for the tris(*iso*-propyl)stannylium cation **[Sn(*i*Pr)$_3$]**$^+$ and analyzed the damping of co-anions on its Lewis acidity.[55] While non-coordinating anions like tetrakis(pentafluorophenyl)borate $[BAr^{F20}]^-$ and the perfluoroalkoxyaluminate $[Al(OC(CF_3)_3)_4]^-$ only show a marginal effect on the FIA_{solv} of **[Sn(*i*Pr)$_3$]**$^+$, bis(trifluoromethanesulfonyl)imide $[NTf_2]^-$ and triflate OTf^- (Tf = CF_3SO_2) caused a significant reduction by around 120 kJ mol^{-1} owing to their coordination to the Sn(IV) center. Interestingly, the latter compounds still proved to be excellent Lewis acids in *Frustrated Lewis Pairs* (FLP) with 2,4,6-collidine which could be employed for the direct hydrogenation of imines, ketones, and even esters. Besides stabilizing the active Lewis acid **[Sn(*i*Pr)$_3$]**$^+$ in its resting state, interaction of OTf^- and $[NTf_2]^-$ with the Sn(IV) center also showed to lower the transition state energy for the splitting of dihydrogen by the **[Sn(*i*Pr)$_3$]**$^+$-collidine FLP thereby increasing the activity of the catalytic systems.[153,154]

Abstraction of anionic substituents can also be used to increase the reactivity of stannylenes (Figure 16 E). Owing to their enhanced Lewis acidities, the stannylenium

cations **[16]**$^+$ and **[17]**$^+$ even show weak η^2-arene interactions of their Sn(II) center with an internal phenyl residue or benzene.[151,155]

Beyond the strategies discussed above, structural constraint was developed as an expedient concept to increase the Lewis acidity of *p*-block element compounds.[156–158] As described in **Section 1.3**, the square-planar anti-van't Hoff-Le Bel structure effectively lowers the LUMO energy in tetracoordinated *p*-block element complexes thereby increasing their Lewis acidity. Employing the *meso*-octaalkylcalix[4]pyrrole ligand system (**Section 1.4**) the GREB group reported a variety of square-planar coordinated *p*-block element compounds containing Al, Ga, Si, Ge, and Sb central atoms and investigated their chemistry as structurally constrained Lewis acid and in element-ligand cooperative bond activations (**Section 0**). However, up to the work presented within this dissertation a systematic investigation of structural constraint effects on the Lewis acidity of Sn(IV) compounds was still missing (Figure 16 F). Early computations delivered a significantly increased FIA_{solv} value of 266 kJ mol^{-1} for the square-planar *meso*-octamethylcalix[4]pyrrolato stannane **2^{Me}** if compared with the unconstrained reference compound **12**. The synthesis and chemistry of these tin(IV) Lewis acids will be presented in detail in **Section 3.5.2**.

1.6 Structurally Constrained *p*-Block and Tin(II) Nucleophiles

Non-classical, VSEPR non-compliant molecules generate frontier molecular orbital manifolds which distinctively differ from classical systems. These geometric and electronic structures are mutually connected and constraining them can enable new modes of stoichiometric or catalytic reactivity. In the context of *p*-block chemistry, this concept has been the topic of various review articles.[24–26] The following section focuses on the effect of structural constraint on the nucleophilic and donor properties of *p*-block elements in low oxidation states (I, II, III). Thus, it will not cover high-valent, constrained Lewis acids and ambiphilic *p*-block compounds featuring for example P(III/IV)[62–66] and Bi(I/III) centers.[58,61]

SU and KONG reported on the two-electron reduction of the boronium dication **[18]**$^{2+}$ delivering the respective T-shaped borylene **18** (Figure 17 A).[159] In contrast to the Lewis superacidic properties of **[18]**$^{2+}$, structural constraint grants Brønsted superbasic properties to **18**. *In silico* comparison with an unconstrained reference borylene revealed an increased HOMO energy with a large contribution of the electron lone-pair in the p_z-type orbital at the B(I) center. Thus, **18** even surpassed the basicity of the *Verkade*[160] and *Schwesinger* bases.[161] The nucleophilicity of **18** was further confirmed by the reaction with methyl triflate delivering the methylated boronium salt. Owing to its redox-active dihydroacridine backbone, the T-shaped germanate(II) **[19]**$^-$ reported by WANG and coworkers can exist in the two mesomeric forms **[19A]**$^-$ and **[19B]**$^-$.[162] Sc-XRD analysis and quantum mechanical calculations revealed a partial double bonding character for the C-N bonds and the presence of two electron lone-pairs at the germanium center contributing to the HOMO and HOMO-2 of **[19]**$^-$. In analogy to borylene **18**, the comparison of **[19]**$^-$ to a non-constrained, pyramidal tris(amido)germanate(II) anion, revealed an increased HOMO and LUMO energy. Eventually, its reactivity with methyl iodide (MeI), and elemental sulfur and selenium evidenced the nucleophilicity of **[19]**$^-$ forming the respective methylgermane and germane chalcogenides possessing formal Ge(IV) centers. In accordance with its energetically high-lying LUMO, **[19]**$^-$ did show no reaction with a variety of nucleophiles including triethylphosphine, KO*t*Bu, and methyl lithium. Very recently, the same group extended this chemistry onto silicon isolating **[20]**$^-$ as its potassium salt.[163] According to the VSEPR principle, silyl anions adapt a trigonal-pyramidal structure and predominantly act as nucleophiles. Structural constraint imparted by the triamido pincer ligand in **[20]**$^-$ crafted the first T-shaped planar silyl anion. Its electronic

structure resembles that of a singlet silylene rather than a silyl anion, showing an electron lone-pair with high *s*-character (HOMO) and a vacant p_z-orbital (LUMO) at the Si center. *In silico* comparison with trigonal-pyramidal silyl anions revealed a significantly increased HOMO energy and decreased HOMO-LUMO gap for **[20]**$^-$. The Si-centered, high-energy electron lone-pair enabled the application of **[20]**$^-$ as an anionic donor ligand in complexes with $[AuPPh_3]^+$ and $[W(CO)_5]$ fragments. In the potassium salt **[K(Et$_2$O)$_2$][20]** the ambiphilic Si center is stabilized by an interaction with the counter cation. However, complexation of K^+ by 18-crown-6 leveraged the ambiphilic reactivity of **[20]**$^-$ causing the intramolecular insertion into the C(sp^3)-H bond of one of the Dip substituents. Subsequently, the decreased HOMO-LUMO gap in **[20]**$^-$ enabled the oxidative addition of the C(sp^2)-H bond in C_6F_5H and the H-H bond in dihydrogen (1 atm) as well as the activation of CO_2 (1 atm) and isonitirles under room temperature conditions.

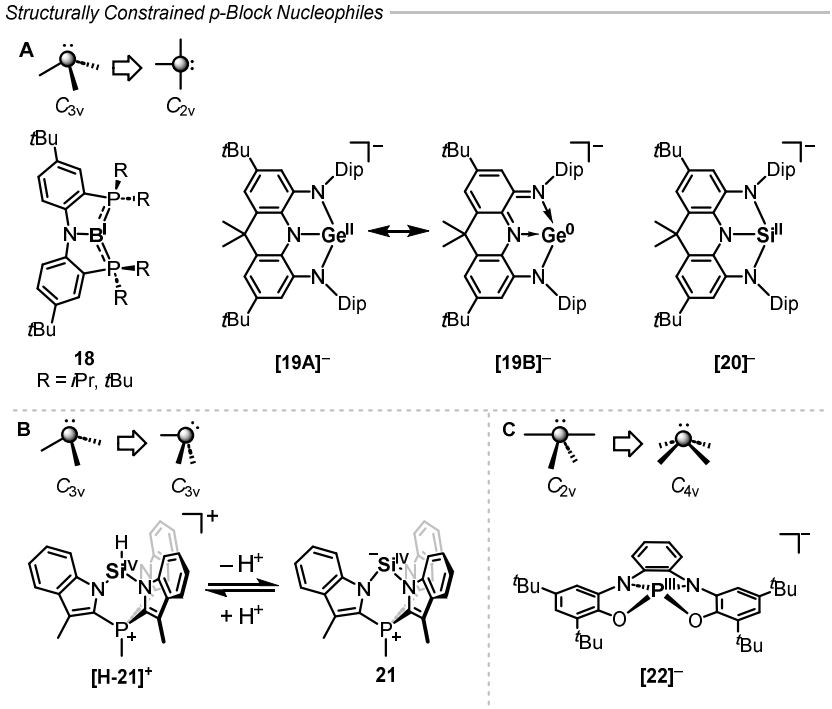


Figure 17. Selected examples of structurally constrained *p*-block nucleophiles according to the change in structure imparted by the ligand backbone.

Structural constraint effects can also increase the acidity of *p*-block element hydrogen bonds despite their often hydridic character. For the cationic silane **[H-21]**$^+$, deprotonation results in the release of strain in the resulting zwitterionic silanide **21** contributing to the unprecedent acidity of **[H-21]**$^+$ (Figure 17 B).[164] The tridentate *tris*(2-skatyl)methyl-phosphonium ligand in **[H-21]**$^+$ prefers N-Si-N valence angles close to 90° which are widened upon quaternization of the silicon(IV) center. Combination of this buildup of strain upon quaternization with the zwitterionic character of **21** also reduces its nucleophilicity and donicity**.** Thus, IR spectroscopy of the respective iron pentacarbonyl adduct **[Fe(21)(CO)$_5$]** placed the donor strength of **21** in the vicinity of neutral silylenes and P(NMe$_2$)$_3$ rather than other silanides.

The DOBROVETSKY research group reported the square-pyramidal phosphoranide anion **[22]**$^-$ (Figure 17 C).[165] Coordinative saturation of the P(III) center by a fourth anionic donor quenches the ambiphilic character usually related with tricoordinated phosphorus(III). While acting as a nucleophile in the reaction with MeI, the rigid, tetradentate ligand backbone also enabled single-electron transfer processes which are unprecedented for phosphoranides in their VSEPR structure.

In contrast to lighter tetrylenes such as carbenes and silylenes, the donor ability of stannylenes drops significantly owing to the high *s*-character and increased radial expansion of the tin-centered electron lone pair.[13,166–169] As a result only the lower-lying HOMO-2 (−5.94 eV, B97M-D3(BJ)/def2-TZVPP CPCM SMD(THF)//B97M-D3(BJ)/def2-TZVPP) of *N*-heterocyclic stannylene **23** shows a contribution of the Sn(II) electron lone pair while the HOMO (−4.26 eV) is delocalized over the π-backbone of the stannylene (Figure 18 A).[166,170] The pronounced ambiphilic nature of heavier tetrylenes allows the coordination of additional ligands to the vacant p_z-orbital.[171–174] As shown for the amidinato stannylene **24**, this increases the σ-donor strength of the Sn(II) center. Recently, LIU and coworkers reported on the cationic, nucleophilic tin(II) complex **[25]**$^+$ bearing a *tris*(carbene)borate ligand.[175] Owing to the predominantly dative bonding between the carbene units and Sn(II) and its overall cationic charge the solvation-corrected HOMO energy of **[25]**$^+$ is significantly reduced (−6.04 eV). However, threefold coordination of the tin(II)-center effectively quenches its Lewis acidic character and enabled its application as a σ-donor ligand with only weak π-acceptor properties in various coinage metal complexes. Additional coordination of anionic ligands to neutral Sn(II) compounds may lead to an even more significant increase in σ-donicity, as attested for the well-known class of

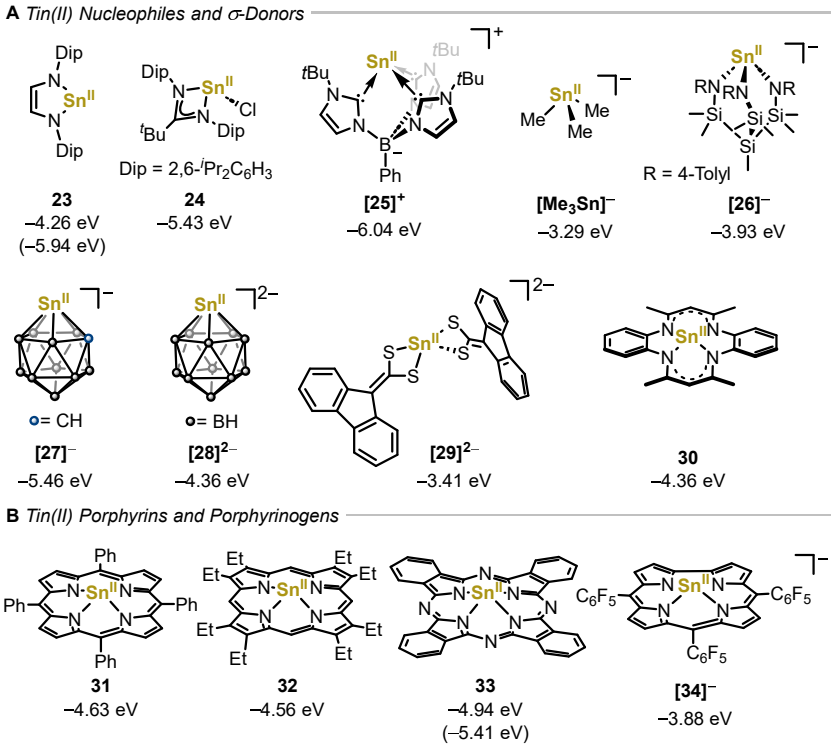


Figure 18. A) Solvation-corrected HOMO energy levels for selected, literature known cationic, neutral, and anionic tin(II) compounds and **B)** porphyrin(ogen) tin(II) complexes computed at the B97M-D3(BJ)/def2-TZVPP CPCM SMD(THF)//B97M-D3(BJ)/def2-TZVPP level of theory. For the *N*-heterocyclic stannylene **23** the HOMO and HOMO-1 are ligand-centered and the energy of the HOMO-2 showing a contribution of the tin-centered electron lone pair is given in parentheses. For the phthalocyanine tin(II) complex **33** the HOMO is ligand-centered and the energy of the tin-centered HOMO-1 is given in parentheses.

nucleophilic stannate(II) anions **[R$_3$Sn]**$^-$ (R = Me, *n*Bu, Ph,...).[176–179] With a HOMO energy of –3.29 eV for **[Me$_3$Sn]**$^-$, these stannate anions surpass all other compounds in Figure 18 A. However, the application of **[R$_3$Sn]**$^-$ anions as organolithium or -magnesium compounds with highly covalent tin-metal bonds effectively lowers their nucleophilicity. In contrast, the tridentate amido ligand in GADE's amido stannate(II) anion **[26]**$^-$ binds alkali metal counter cations *via* the nitrogen atoms or arene units in the ligand backbone retaining the free electron lone pair at the Sn(II) center.[180–182] **[26]**$^-$ showed an increased HOMO energy (–3.93 eV) if compared to the neutral, tricoordinated stannylene **24**. Accordingly, this class of compounds proved to be effective ligands in a range of transition

metal complexes.[183–187] The WESEMANN group extensively investigated the nucleophilic behavior of the 1,2-carbastannaborate anion **[27]**$^-$ and stannaborate dianion **[28]**$^{2-}$ and their application as ligands in transition metal chemistry.[188–192] Based on the computed HOMO energies and experimental findings, the dianion **[28]**$^{2-}$ shows an increased nucleophilic reactivity compared to its monoanionic relative **[27]**$^-$.[193] Even though the negative charge in these compounds is highly delocalized over the carborate backbone, their comparison clearly shows the effect negative charge accumulation can have on the nucleophilic properties of Sn(II) compounds. However, Sn(II)-based dianions are scarce in literature, and only two additional tetracoordinated stannate(II) dianions of the type **[29]**$^{2-}$ featuring weakly coordinating 1,1-dithiolato ligands have been known prior to the work reported in this dissertation.[194]

The detailed investigation of structural constraint effects on the nucleophilicity and σ-donor strength of tin(II) centers represented an essentially unexplored field. In 1999, tin(II) complex **30** (HOMO energy of −4.36 eV) was reported to undergo a nucleophilic substitution reaction with primary alkyl iodides forming cationic, pentacoordinated allylstannane complexes.[195] Although **30** clearly possesses a C_{4v}-symmetric, VSEPR non-compliant coordination environment around the tin(II) center, its effect on the nucleophilicity of Sn(II) has not been discussed. Correspondingly, structural constraint effects were not assumed in the tin(II) porphyrins **31**[196] and **32**,[197,198] the phthalocyanine complex **33**,[32,199] and the tin(II) corrole anion **[34]**.$^-$[200] These compounds showed an expedient application as σ-donor ligands in transition metal chemistry and tin nucleophile in S_N2 reactions (Figure 18 B). **Sections 3.1** and **3.2** of the Results und Discussion chapter will describe the first detailed investigation of structural constraint effects on the donor strength and nucleophilicity of tetracoordinated tin(II) centers. Therefore, this work will shed light on aspects which have been overseen in all previously reported tin(II) porphyrinogens.

1.7 Generation of Carbenes with *p*-Block Nucleophiles

Since the first synthesis of a hetero-atom stabilized carbene complex by *Fischer* and *Maasböl* in the 60s this class of carbenes has evolved into one of the most prominent tools in chemistry.[201,202] Particularly, the development of *N*-heterocyclic carbenes (NHCs)[203–205] and their advancement into cyclic alkyl(amino)carbenes (*c*AACs)[206] boosted their application in various fields such as ligands in transition metal catalysis,[207–209] in the stabilization of reactive *p*-block element centers,[3,210,211] as organocatalysts,[212–215] or in medicine[216] and material sciences.[217–220] In contrast to their cyclic analogues, acyclic diamino (ADCs), aryl- (*a*ArAC), and alkyl(amino)carbenes (*a*AAC) have received much less attention owing to their pronounced fragility as free carbenes and their tendency to dimerize in the absence of bulky substituents.[221,222] However, the increased σ-donor strengths and valence bond angles of acyclic carbenes showed to improve the catalytic selectivity and activity of their transition metal complexes compared to cyclic analogues.[223,224] Thus, to extend the bibliography of this ligand class and thereby gain a better understanding of their effects on catalysis there is a need for a more modular synthetic protocol accessing a wide range of carbene complexes. Figure 19 summarizes the synthetic routes to ADCs, *a*ArACs, *a*AACs, and their complexes known to date. Despite their instability, many synthetic approaches proceed *via* the generation of free transient carbenes by the deprotonation of iminium cations (Route A).[222,225] However, the weak acidity of the iminium proton requires the use of strong bases. In the case of *a*AACs this limits the scope to quaternary C-atoms bound to the carbene C and does not tolerate NHR groups.[226–228] Furthermore, bulky substituents and low temperature are required to hinder the dimerization of the free carbenes.[229,230] A promising approach to circumvent such side reactions is to prevent the formation of free carbenes in the first place. In a few cases precursors with internal alkoxide bases showed to deliver ADC complexes even at room temperature.[231] Treating amides with oxalyl chloride readily produces chloroiminium salts which also have been used as carbene synthons. Oxidative addition of the C(sp^2)-Cl bond to various low-valent and nucleophilic transition metal precursors produced a variety of complexes while avoiding the formation of free carbenes (Route B, top).[232–235] Thus, it was possible to introduce carbenes even with little steric protection. To extend the scope for chloroiminium synthons, *Hong* and co-workers reported the prior lithiation at low temperatures to form ADC adducts of Rh(I), Ir(I), and Pd(II) (Route B, bottom).[236,237] Furthermore, the group of *Bertrand* employed the chloronium ion abstraction from chloroamidinium salts with $Hg(SiMe_3)_2$ for the generation of free ADCs alongside elemental mercury. However, as for Route **A**, smaller substituents (Y = aryl, Cl, H) yielded the dimerization products of

the respective carbenes (Route **C**).[238] Modification of carbonyl or isocyanide ligands in the coordination sphere of transition metals displays one of the earliest approaches to obtain metal carbene complexes.[239–241] The multi-step synthesis of FISCHER carbenes coordinated to chromium and tungsten carbonyls allowed for subsequent transmetalation of *a*ArACs onto palladium(II), copper(I), and gold(I) (Route D, top).[241–243] Metal-promoted addition of amines to palladium[244–246] and gold isocyanides[247] directly delivered ADC complexes which catalyzed a variety of coupling reactions.[223] Both strategies require an electrophilic metal to activate isocyanides for the nucleophilic attack of amines and so far, are limited to ADC complexes (Route D, bottom). It should be noted here, that in a similar approach the BITTNER group activated isocyanides *via* their coordination to the Lewis acid BPh_3, obtaining the first NHC-borane complex.[248]

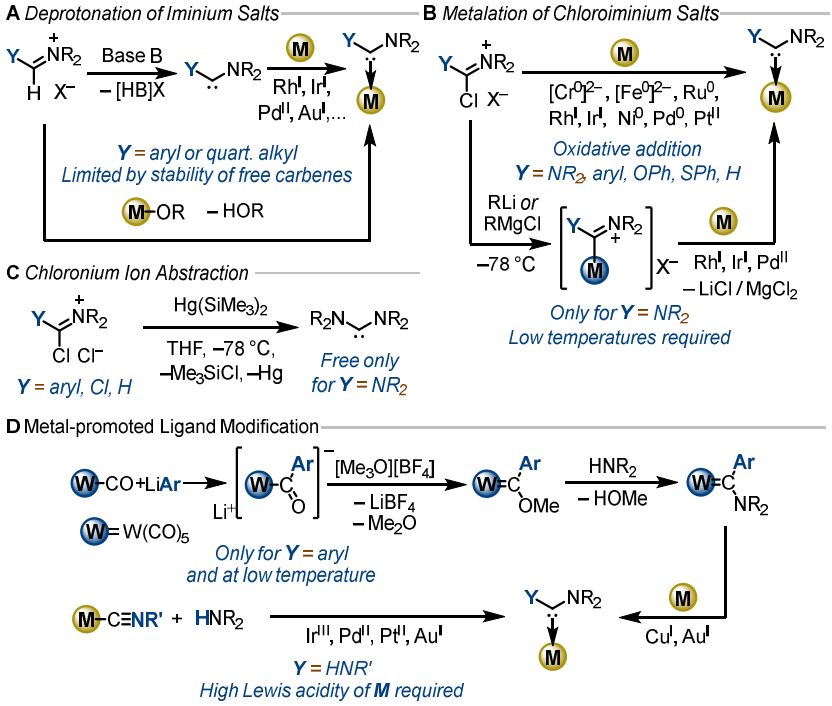


Figure 19. Literature known synthetic routes towards acyclic aminocarbenes and their transition metal complexes starting from **A)** iminium salts), **B)** and **C)** chloroiminium salts, and **D)** *via* the modification of carbonyls and isocyanides at transition metal centers.

In the realm of main-group chemistry, NHCs and *c*AACs have effectively stabilized low-valent *p*-block centers in different open- and closed-shell oxidation states.[249–252] This chemistry has been reviewed on numerous occasions with synthetic methods typically centered on the initial reactions of free carbenes with Lewis acidic *p*-block precursors.[211,253] Conversely, the generation and stabilization of carbenes *via p*-block element compounds remain far less explored. Chloroamidinium salt **35** reacts with Ph_2PH and $Ph_2As(SiMe_3)$ *via* the nucleophilic substitution of Cl^- with Ph_2P^- or Ph_2As^-, eliminating HCl or Me_3SiCl, respectively (Figure 20 A). ALCARAZO and coworkers employed this reactivity for the generation of a variety of α-cationic phosphine and arsine ligands **36a** and **36b** which could be interpreted as carbene adducts of the respective low-valent cations Ph_2E^+.[254–257] Notably, harnessing the potential of bulky, more electron-rich tris(guadinato)-substituted phosphines **37**, the DIELMANN group was able to generate free NHCs *via* the abstraction of chloronium ions from chloroamidinium cations at ambient conditions (Figure 20 B).[258] The *Röschenthaler* group employed several nucleophilic *p*-block halides for the synthesis of cyclic and acyclic (amino)carbene complexes of $SiCl_4$ **38**,[259] PF_5 **39**,[260–262] $[GeF_5]^-$ **[40]**$^-$, and $[SnF_5]^-$ **[41]**$^-$.[260] (Figure 20 C and D). In particular, the oxidative addition of C-F bonds in (*gem*-difluoro)dimethylamines to PF_3 at –196 °C allowed the generation and stabilization of reactive, sterically nonprotected carbenes (Y = NMe_2, *t*Bu, Ph, H) as their formal PF_5 adducts **38**. However, a subsequent transmetalation chemistry has not been reported so far. Besides the oxidative addition of C-F bonds to SnF_2, there is no report of tin(II) nucleophiles for the generation of carbenes.

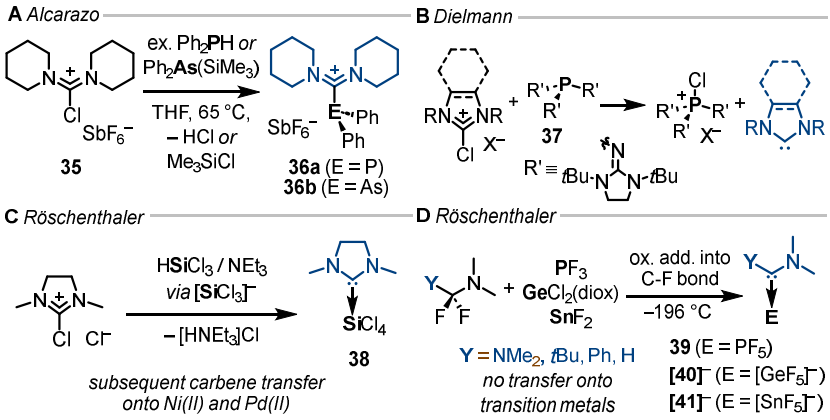


Figure 20. Literature known reactions of *p*-block element nucleophiles for the generation of carbenes (blue) from chloro-amidinium and -iminium salts (**A**, **B**, and **C**) and **D)** (*gem*-difluoro)dimethylamines.

Furthermore, the application of structural constraint approaches to tune the nucleophilic properties of tin(II) for such applications has not been explored so far. Both aspects will be discussed in **Section 3.4**.

2 MOTIVATION AND OBJECTIVES

The main objective of the work described herein was to investigate the *influence of structural constraint effects on the reactivity of tetracoordinated Sn(II) and Sn(IV) centers*. Figure 21 shows the influence of structural constraint on the electronic structure of the reference compounds tetrahydridostannate(II) **[SnH_4]$^{2-}$** and stannane **SnH_4** and how both structural motives can be realized employing the *calix[4]pyrrolato* ligand system.

Objective A focused on the synthesis of *electron-rich, nucleophilic stannate(II) dianions* **[2^R]$^{2-}$** (Figure 21 A). Stannylenes usually possess diminished donor strengths owing to the high *s*-character, increased radial expansion, and low energy of the tin-centered electron lone pair.[13,166–169] Their ambiphilic nature allows for the coordination of additional ligands involving the vacant p_z-orbital at tin ultimately increasing their donor strength.[171–174] Even though neutral and monoanionic Sn(II) complexes of macrocyclic tetraamido ligands are known to act as tin-centered donors and nucleophiles, no dianionic tetraamido Sn(II) complexes have been reported prior to this work. Furthermore, the influence of structural constraint imparted by the ligand backbone on their donor strength and nucleophilicity has never been considered (see **Section 1.6**). Combination of the flexible *meso*-octaalkylcalix[4]pyrrolato ligand system with Sn(II) centers delivered structurally constrained, electron-rich stannate(II) dianions which were employed as tin-centered σ-donors in transition metal coordination chemistry and nucleophiles for challenging chemical transformations owing to their enhanced nucleophilicity and reducing power.

The Lewis acidity of tin(IV) compounds can be employed in a variety of fields ranging from industrial applications as catalysts in transesterifications, the ring-opening polymerization (ROP) of lactones, and the synthesis of polyurethanes to tin-based FLPs for dihydrogen activation in fundamental research. [135,136,153,154,263] While the approaches to increase the Lewis acidity of these stannanes mainly focused on the installation of *electronegative substituents* or the generation of *tricoordinated stannylium cations*, the application of *structural constraint effects* was essentially unexplored (see **Section 1.5**). Furthermore, the most achievements in this area are based on the deformation of group 13[42,68,72,264–266] and 15 elements,[61,64,66,156–158,165,267–270] and only a few structurally constrained tetrels have been reported so far.[113,114,122] The *square-planar anti-van't Hoff-Le*

Bel structure of *meso*-octaalkylcalix[4]pyrrolato *p*-block compounds effectively lowers their LUMO energy resulting in increased Lewis acidities (Figure 21 B). In combination with a ligand-centered HOMO, reduced HOMO-LUMO gaps, and the nucleophilic calix[4]pyrrole ligand backbone these planarized main group compounds have been employed in a variety of element-ligand cooperative bond activations (see **Section 0**).[115–121,123] However, up to the work presented within this dissertation no attempt on the synthesis of a free, *square-planar coordinated calix[4]pyrrolato stannane* $\mathbf{2^R}$ has been reported. Filling this knowledge gap was the aim of **Objective B**.

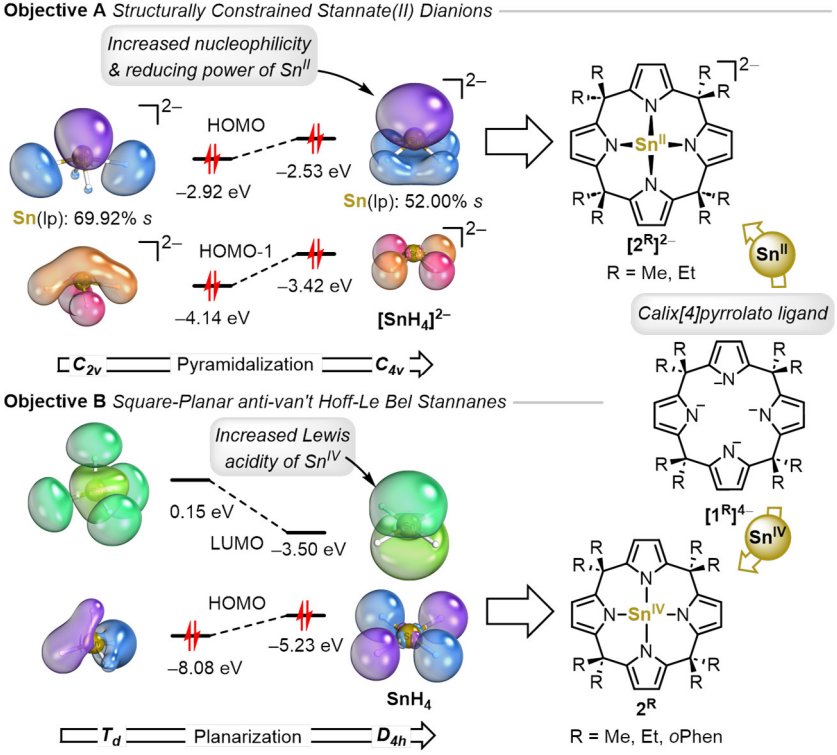


Figure 21. Objectives of the work presented within this dissertation. Influence of structural constraint on the frontier molecular orbital energies of the reference compounds **A)** tetrahydridostannate(II) $\mathbf{[SnH_4]^{2-}}$ and **B)** stannane $\mathbf{SnH_4}$ computed on the B97M-D4/def2-TVZPP CPCM SMD(THF)//PBEh-3c level of theory. NBO calculations yielded the orbital contributions to the electron lone pair at Sn(II) and were performed on the PBE0/def2-TZVPP//PBEh-3c level of theory. Experimental realization of structurally constrained tin centers employing the calix[4]pyrrolato ligand (right).

3 Results and Discussion

First, the chemistry of *meso*-octaalkylcalix[4]pyrrolato stannate(II) dianions $[\mathbf{2^R}]^{2-}$ and the effect of ligand modification and conformation on their nucleophilicity, donor, and reducing strengths will be discussed in the publications in **Section 3.1** and **3.2.**

The work presented in **Section 3.3** extended the coordination chemistry of these compounds onto mono- and dinuclear gold(I) complexes revealing a new coordination mode in calix[4]pyrrole chemistry.

The paper in **Section 3.4** connected the nucleophilicity of the stannate(II) dianions with the Lewis acidity of the respective Sn(IV) complexes to allow the generation, stabilization, and transmetalation of acyclic aminocarbenes in one reaction sequence.

Eventually, the unpublished work described in **Section 3.5** will discuss the *in silico* comparison of group 14 calix[4]pyrroles bearing Si, Ge, and Sn centers followed by the synthesis of structurally constrained Sn(IV) calix[4]pyrrole complexes $\mathbf{2^R}$ and their tin-ligand cooperative reactivity. Furthermore, modification of the *meso*-residues in the ligand periphery will be introduced as an approach towards the isolation of a square-planar, tetracoordinated Sn(IV) Lewis acid.

The rights to adapt the content of the publications in **Section 3.1 - 3.4** were obtained through RightsLink®.

3.1 Calix[4]pyrrolato Stannate(II): A Tetraamido Tin(II) Dianion and Strong Metal-Centered σ-Donor

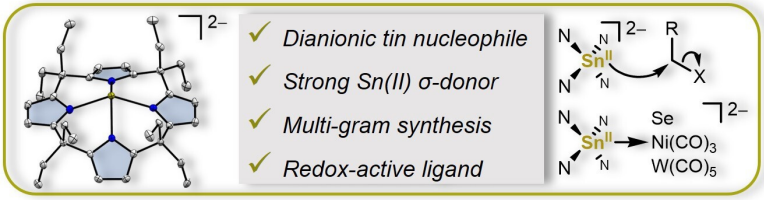


Figure 22. Table of contents graphic of the publication presented in this chapter.

The article and supplementary information (SI) presented within this section were previously published and can be found under: H. Ruppert, L. Greb, *Angew. Chem. Int. Ed.* **2022**, *61*, e20211661, https://doi.org/10.1002/anie.202116615.

According to the CRediT scheme[271] the authors contributed to this publication as followed:

H. Ruppert – Conceptualization (*lead*), Methodology (*lead*), Validation (*lead*), Formal analysis (*lead*), Investigation (*lead*), Data curation (*lead*), Writing – Original Draft Preparation (*lead*), Writing – Review & Editing (*equal*), Visualization (*lead*), Supervision (*equal*), Project Administration (*equal*), Funding acquisition (*equal*);

L. Greb –Resources (*lead*), Writing – Review & Editing (*equal*), Supervision (*equal*), Project Administration (*equal*), Funding acquisition (*equal*).

How to cite: *Angew. Chem. Int. Ed.* **2022**, *61*, e202116615
International Edition: doi.org/10.1002/anie.202116615
German Edition: doi.org/10.1002/ange.202116615

Low-Valent Complexes

Calix[4]pyrrolato Stannate(II): A Tetraamido Tin(II) Dianion and Strong Metal-Centered σ-Donor

*Heiko Ruppert and Lutz Greb**

Abstract: Anionic, metal-centered nucleophiles are emerging compounds with unique reactivities. Here, we describe the isolation and full characterization of the first tetraamido tin(II) dianion, its behavior as ligand towards transition metals, and its reactivity as a tin-centered nucleophile. Experimental values such as the Tolman electronic parameter (TEP) and computations attest tin-located σ-donor ability exceeding that of carbenes or electron-rich phosphines. Against transition metals, the stannate(II) can act as η^1- or η^5-type ligand. With aldehydes, it reacts by hydride substitution to give valuable acyl stannates. The reductive dehalogenation of iodobenzene indicates facile redox pathways mediated by halogen bond interaction. Calix[4]pyrrolato stannate-(II) represents the first example of this macrocyclic ligand in low-valent *p*-block element chemistry.

Introduction

N-Heterocyclic carbenes (NHCs; e.g. **A** in Figure 1) and cyclic alkyl amino carbenes (CAACs, e.g. **B**) became indispensable tools in transition metal catalysis or for the stabilization of reactive *p*-block element centers.[1] Their pronounced σ-donor ability is of most vital impact, usually expressed by the energy of the carbon-centered, highest occupied molecular orbital (HOMO, **A** = −5.74 eV, **B** = −5.04 eV, all values in Figure 1 computed at a consistent, solvation corrected level of theory).[2] In contrast to the lighter tetrylenes, the donor ability of stannylenes drops significantly by the high *s*-character of the Sn-centered electron lone pair.[3] Accordingly, the HOMO of *N*-heterocyclic stannylene **C** shows delocalized π-character, but only the lower-lying HOMO−2 (−5.94 eV) is of Sn^{II} lone pair type.[3e,4] Among the strategies to raise the σ-donor strength of tetrylenes,[5] the coordination of additional ligands to SnR_2 appears particularly effective (e.g. amidinato stannylene **D** in Figure 1).[4,6] Coordination of anionic ligands to Sn^{II} may lead to an even more pronounced increase of the σ-donicity, as attested in the class of nucleophilic anionic stannates(II), R_3Sn^-.[7] For instance, the tridentate amido ligand in Gade's amido stannate(II) **[E]**$^-$ causes a solvation-corrected HOMO energy of −3.93 eV. Accordingly, this[8] and related compounds proved expedient ligands in a range

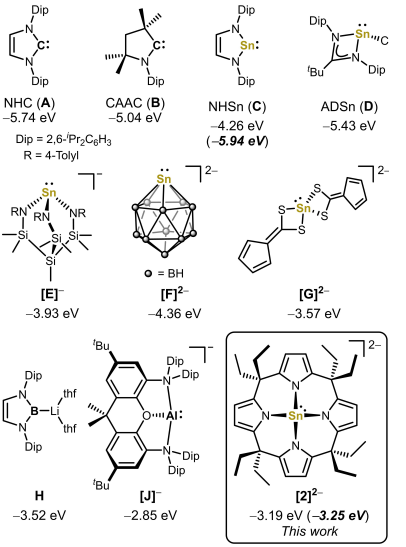


Figure 1. Solvation-corrected HOMO energy levels for the NHC (**A**), CAAC (**B**), the *N*-heterocyclic stannylene (NHSn) (**C**), the amidinato stannylene (ADSn) (**D**), the anionic stannate(II) **[E]**$^-$, the dianionic stannates(II) **[F]**$^{2-}$, and **[G]**$^{2-}$, boryl **H** and the aluminyl anion **[J]**$^-$, and **[2]**$^{2-}$ (B97M-D3(BJ)/def2-TZVPP CPCM(THF)//B97M-D3(BJ)/def2-TZVPP). For **C** and **[2]**$^{2-}$ the HOMO and HOMO−1 are ligand-centered and the energies of their tin electron lone pairs centered HOMO−2 are given in parentheses.

[*] L. Greb
Department of Chemistry and Biochemistry - Inorganic Chemistry
Freie Universität Berlin
Fabeckstr. 34/36, 14195 Berlin (Germany)
E-mail: lutz.greb@fu-berlin.de
H. Ruppert, L. Greb
Anorganisch-Chemisches Institut
Ruprecht-Karls-Universität Heidelberg
Im Neuenheimer Feld 270, 69120 Heidelberg (Germany)

© 2022 The Authors. Angewandte Chemie International Edition published by Wiley-VCH GmbH. This is an open access article under the terms of the Creative Commons Attribution Non-Commercial License, which permits use, distribution and reproduction in any medium, provided the original work is properly cited and is not used for commercial purposes.

© 2022 The Authors. Angewandte Chemie International Edition published by Wiley-VCH GmbH

15213773, 2022, 13, Downloaded from https://onlinelibrary.wiley.com/doi/10.1002/anie.202116615 by

of transition metal complexes.[9] We surmised that the coordination of a fourth anionic ligand to Sn^{II} might push the σ-donor strength even farther. Sn^{II}-based dianions are scarce,[10] and molecular compounds are limited to $[\mathbf{F}]^{2-}$[11] and $[\mathbf{G}]^{2-}$,[12] which are stabilized by charge delocalization into the carborate ($[\mathbf{F}]^{2-}$) or the fluorenyl moiety ($[\mathbf{G}]^{2-}$). Given the substantial π-donor ability of nitrogen and the unique role of amido substituents in low valent tin chemistry,[13] the formation of a yet elusive tetraamido Sn^{II} dianion, $[Sn(NR_2)_4]^{2-}$, appeared of particular relevance. However, a strong Pauli- and Coulomb repulsion between the anionic, electron-rich $[Sn(NR_2)_3]^-$ and NR_2^- fragments renders the formation of such high-energy species highly challenging. Thus, a macrocyclic strategy was sought. The *meso*-octaalkyl calix[4]pyrroles have been intensively investigated as macrocyclic ligands in transition and rare-earth metal chemistry.[14] Owing to their flexible coordination behavior, these ligands enabled the isolation of many *d*- and *f*-block metal complexes.[14d,15]

More recently, the calix[4]pyrrole ligand enabled the synthesis of planar, tetracoordinated Al^{III}[16] and Si^{IV}[17] complexes and transferred concepts like element ligand cooperativity, ligand-to-metal-charge-transfer and C–H agostic interactions into the *p*-block.[18] However, no complexes of calix[4]pyrroles with low-valent *p*-block elements have been described so far. Herein we present the synthesis of calix[4]pyrrolato stannate(II) $[\mathbf{2}]^{2-}$ as the first dianionic, tetraamido Sn^{II}, and its chemistry as a nucleophile and strong σ-donor. Compared to previous carbenes, stannylenes, and (di)anionic stannates, $[\mathbf{2}]^{2-}$ possess a drastically increased tin-centered electron lone pair energy (Figure 1). Strikingly, these hallmarks are approaching that of seminal (semi)metal-centered σ-donors such as boryl (e.g. **H** in Figure 1)[19] or aluminyl anions (e.g. $[\mathbf{J}]^-$ in Figure 1).[20]

Results and Discussion

Reaction of the lithium salt of *meso*-octaethylcalix-[4]pyrrolate **[Li$_4$(thf)$_3$][1]** with one equivalent tin(II) chloride in tetrahydrofuran (THF) at room temperature completed within minutes, forming a clear, colorless reaction solution. Workup yielded the lithium salt of the dianionic stannate(II) **[Li$_2$(thf)$_x$][2]** with varying THF content in excellent yields and at a multigram scale (e.g. 80 % yield at a 2.0 g scale) (Figure 2A). ^{1}H, ^{13}C, ^{119}Sn NMR spectroscopy revealed the incorporation of a tin(II) center into a C_{4v} symmetric calix[4]pyrrole species. In THF-*d*8, $[\mathbf{2}]^{2-}$ exhibits two diastereotopic sets of ethyl residues (*syn* and *anti* to the Sn^{II} center) and one singlet for the pyrrolyl β-hydrogen atoms at 5.85 ppm. One sharp ^{7}Li NMR resonance at −2.12 ppm indicated solvated lithium cations. The comparatively high-field shifted ^{119}Sn NMR resonance at −481.3 ppm disclosed a highly coordinated tin(II) atom with increased electron density compared to related species.[21] Even though **[Li$_2$(thf)$_x$][2]** can be seen as a lithium salt of a dianion, it rendered surprisingly soluble in non-polar organic solvents such as Et_2O, benzene and toluene. Interestingly, NMR spectroscopy in C_6D_6 showed symmetry lowering for $[\mathbf{2}]^{2-}$ and the appearance of shifted resonances in the ^{7}Li NMR spectrum indicating the coordination of lithium cations to the complex $[\mathbf{2}]^{2-}$ (Figure S4). This picture was confirmed by SCXRD of **[Li$_2$(thf)$_x$][2]** (Figure S43), resembling the structure of other anionic calix[4]pyrrolato complex–alkali metal salts in non-polar media.[14b,c,22]

Metathesis of **[Li$_2$(thf)$_x$][2]** with two equivalents of the respecting phosphonium and ammonium chlorides yielded the PPh_4^+ and NBu_4^+ salts of $[\mathbf{2}]^{2-}$ in up to 92 % yield (Figure 2B). Whereas the NBu_4^+ salt is soluble in less polar solvents such as 1,2-*ortho*-difluorobenzene (*o*DFB), the PPh_4^+ salt only dissolves in solvent mixtures containing MeCN. NMR spectroscopy and elemental analysis confirmed the bulk purity of both salts. The Li^+ and PPh_4^+ salts of $[\mathbf{2}]^{2-}$ possess comparable ^{119}Sn NMR shifts in THF-d_8 at −481.32 ppm and −486.17 ppm, respectively, but the NBu_4^+ salt exhibits a significantly more high-field shifted ^{119}Sn NMR resonance at −517.83 ppm. The ^{119}Sn shift of free $[\mathbf{2}]^{2-}$ was DFT-computed at −509.38 ppm (PBE0/SO-ZORA-TZ2P), supporting the "naked" dianion character in THF. Indeed, the solid-state molecular structure of **[(NBu$_4$)$_2$][2]** contains a free tin(II) calix[4]pyrrolato dianion with two independent NBu_4^+ cations in the asymmetric unit (Figure 2C). The absence of associated cations results in a highly symmetric, calix[4]pyrrolato stannate(II) dianion possessing a nearly perfect square-pyramidal coordination geometry and only minor differences between the Sn–N bond lengths ($Sn–N_{avg} = 231$ pm), comparable to previously reported N_4-coordinated, neutral tin(II) complexes.[23] In contrast, the solid-state molecular structure of **[(PPh$_4$)$_2$(*o*DFB)$_{0.5}$][2]** shows a saddle-shaped calix-[4]pyrrolato ligand with alternating orientations of the bridging *meso*-carbon atoms, highlighting the structural flexibility of the calix[4]pyrrolato ligand backbone in the coordination sphere of tin (Figure S45). All salts of $[\mathbf{2}]^{2-}$ are stable under inert gas at room temperature for several months, but decompose under oxygen atmosphere or with traces of humidity. Their temperature stability in aprotic solvents depends on the respective counter cation, e.g., with **[Li$_2$(thf)$_x$][2]** being stable in THF at 80 °C for several hours.

The electronic structure of $[\mathbf{2}]^{2-}$ was analyzed by DFT calculations and bonding analysis tools. $[\mathbf{2}]^{2-}$ possess an energetically high lying HOMO−2 with a major contribution of the tin-centered lone pair (Figure 2D and S55, B97M-D3(BJ)/def2-TVZPP CPCM(THF)). NBO calculation revealed a diminished positive charge at the tin (+1.13) compared to trisamido stannate $[\mathbf{E}]^-$ (+1.23), and a decreased *s*-character of the tin-centered lone pair (79 %) compared to all other stannylenes (>88 %, Figure S51 and Table S12). To elucidate the influence of structure and electronics imparted by the calix[4]pyrrolato ligand, $[\mathbf{2}]^{2-}$ was compared with hypothetical bis(pyrrolato)stannylene **K** and tetrakis(pyrrolato)stannate(II) $[\mathbf{L}]^{2-}$ (Figure 2E and S52). The coordination of two additional anionic pyrrolato ligands to the neutral bis(pyrrolato)stannylene **K** (step i) raises the energy of the lone pair containing HOMO by 3.10 eV and decreases the positive charge located at the tin(II) center from +1.41 to +1.15. The tethering of four pyrrolato ligands into a macrocyclic ligand and the concom-

© 2022 The Authors. Angewandte Chemie International Edition published by Wiley-VCH GmbH

Online Library on [12/04/2024]. See the Terms and Conditions (https://onlinelibrary.wiley.com/terms-and-conditions) on Wiley Online Library for rules of use; OA articles are governed by the applicable Creative Commons License

1521-3773, 2022, 13, Downloaded from https://onlinelibrary.wiley.com/doi/10.1002/anie.202116615 by Heidelberg University Universitätsbibliothek, Wiley Online Library on [12/04/2024]. See the Terms and Conditions (https://onlinelibrary.wiley.com/terms-and-conditions) on Wiley Online Library for rules of use; OA articles are governed by the applicable Creative Commons License

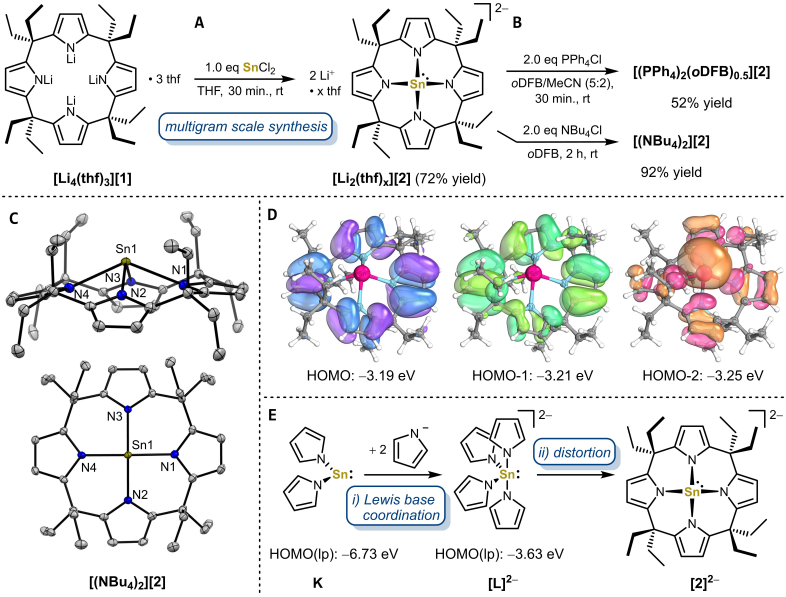


Figure 2. A) Synthesis of the dianionic calix[4]pyrrolato stannate(II) as the lithium salt **[Li_2(thf)$_x$][2]** and B) subsequent salt exchange reactions with PPh_4Cl and NBu_4Cl forming the phosphonium salt **[(PPh_4)$_2$(*o*DFB)$_{0.5}$][2]** and the ammonium salt **[(NBu_4)$_2$][2]**. C) Solid-state molecular structure of **[(NBu_4)$_2$][2]**. Displacement ellipsoids are drawn at 50% probability level. Hydrogens and NBu_4^+ counter cations are omitted for clarity. Selected bond lengths [pm] and angels [°]: Sn1–N1 232.27(16), Sn1–N2 230.61(15), Sn1–N3 230.73(15), Sn1–N4 232.11(15), Sn1–N_4-plane 95.8, N1–Sn1–N4 133.23(5), N2–Sn1–N3 129.10(5), *cis*–N–Sn–N between 79.64(5) and 80.85(5). D) Occupied frontier molecular orbitals calculated at the B97M-D3(BJ)/def2-TZVPP CPCM(THF)//B97M-D3(BJ)/def2-TZVPP level of theory. E) Effects of Lewis base coordination (i) and distortion into the calix[4]pyrrole coordination geometry (ii) on the energy of the lone pair (lp) containing orbital at tin(II) for the hypothetical bis(pyrrolato)-stannylene **K**, tetrakis(pyrrolato)stannate(II) **[L]$^{2-}$**, and **[2]$^{2-}$**.

itant distortion of the coordination geometry around tin(II) in **[2]$^{2-}$** raises the lone pair containing HOMO by an additional 0.38 eV and decreases the atomic charge at tin to +1.13 (step ii, an additional effect might result from the pyrrole alkyl substitution). ETS-NOCV bonding analysis showed that the nearly coplanar arrangement of the four pyrrolato units in the calix[4]pyrrole backbone of **[2]$^{2-}$** enables the ligand to act as both a σ-donor towards the Sn(5*s*,*p*) orbital and as π-donor towards the Sn($5p_z$) orbital. Especially, interaction of these latter orbitals contributes to the high lying HOMO−2, and constitutes the highly directional and high-energy lone pair at the tin(II) center. Overall, these theoretical considerations strongly suggested that **[2]$^{2-}$** should act as a tin-centered σ-donor that was thus probed experimentally.

The Tolman electronic parameter (TEP)[24] and ^{77}Se-{^{1}H} NMR spectroscopy[25] have become standard techniques to evaluate the electronic properties of a variety of ligands. Thus, to gain experimental insights into the coordination chemistry and scale the electron donor and acceptor properties of **[2]$^{2-}$**, metal carbonyl complexes and its selenium adduct were synthesized. Reaction of **[(PPh_4)$_2$(*o*DFB)$_{0.5}$][2]** with $W(CO)_5$(thf) at room temperature over 36 hours, and subsequent workup yielded the tungsten complex **[(PPh_4)$_2$][W(η^1-2)(CO)$_5$]** in acceptable yield (Figure 3B). The respective $Ni(CO)_3$ adduct **[(NBu_4)$_2$][Ni(η^1-2)(CO)$_3$]** was accessed via the reaction of **[(NBu_4)$_2$][2]** with $Ni(COD)_2$ (COD = 1,5-cyclooctadiene) and carbon monoxide at room temperature. ^{1}H NMR spectroscopy revealed C_{4v} symmetry for both compounds at room temperature in solution, indicative for symmetrical η^1-coordinations of the tin(II) lone pair to the transition metal carbonyl fragments. The coordination of tin(II) to W and Ni causes coordination chemical shifts $\Delta\delta(^{119}Sn) = \delta(^{119}Sn)_{coord.} - \delta(^{119}Sn)_{free}$ compared to free **[2]$^{2-}$** which are more pronounced for **[(NBu_4)$_2$][Ni(η^1-2)(CO)$_3$]** ($\Delta\delta(^{119}Sn) = 183$ ppm) than for **[(PPh_4)$_2$][W(η^1-2)(CO)$_5$]** ($\Delta\delta(^{119}Sn) = 35$ ppm) being in line with previous observations.[26,27] The solid-state molecular

© 2022 The Authors. Angewandte Chemie International Edition published by Wiley-VCH GmbH

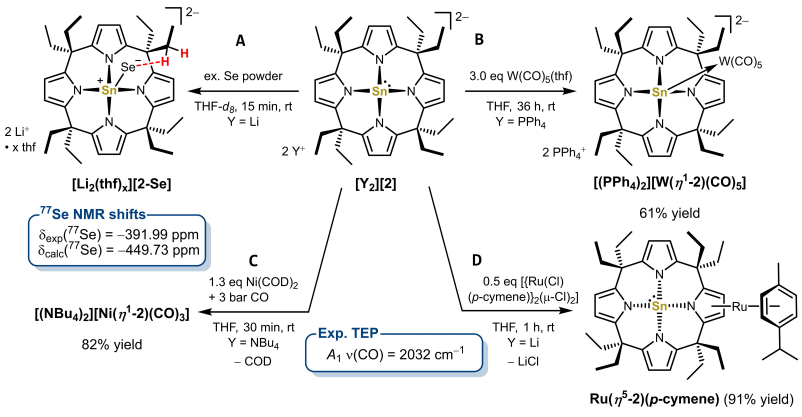


Figure 3. Synthesis of A) the lithium stanna(II) selenido complex **[Li$_2$(thf)$_x$][2-Se]**, the η^1-coordinated metal carbonyl complexes **[(PPh$_4$)$_2$][W(η^1-2)(CO)$_5$]** (B) and **[(NBu$_4$)$_2$][Ni(η^1-2)(CO)$_3$]** (C) and the η^5-coordinated ruthenium(II) sandwich complex **Ru(η^5-2)(*p*-cymene)** (D).

structure of **[(PPh$_4$)$_2$][W(η^1-2)(CO)$_5$]** verifies **[2]$^{2-}$** acting as a η^1 σ-donor ligand via the tin(II) electron lone pair (Figure 4A). Coordination of the tin(II) to tungsten causes a shortening of the Sn–N bonds and a decreased pyramidalization of **[2]$^{2-}$** as shown by increased *trans*-N–Sn–N valence angles compared to free **[2]$^{2-}$** (cf. Figure 2C). Both effects align well with the transfer of electron density from tin(II) to the Lewis acidic W(CO)$_5$ fragment. Interestingly, the Sn1–W1 bond is slightly longer than the W–Sn bonds found for a variety of tin(II) ligands (283.44(6) ppm vs. an average of 274.2 ppm).[21] As can be seen by the bending of the tungsten bound carbonyl ligands, this bond lengthening can be attributed to the steric pressure imparted by the *meso*-octaethylcalix[4]pyrrolato backbone. Indeed, a solution ATIR spectrum of **[(NBu$_4$)$_2$][Ni(η^1-2)(CO)$_3$]** in THF delivered a TEP (A_1 symmetrical C–O stretching band) of 2032 cm^{-1} (Figure S49). Remarkably, this value lies below that of all hitherto described carbenes (including CAACs)[2b] and the most electron-rich phosphine ligands,[28] corroborating the σ-donor and weak π-acceptor properties of **[2]$^{2-}$**.

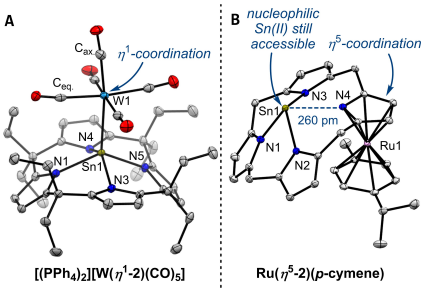


Figure 4. Solid-state molecular structure of A) the η^1-complex **[(PPh$_4$)$_2$][W(η^1-2)(CO)$_5$]** and B) the η^5-complex **Ru(η^5-2)(*p*-cymene)**. Displacement ellipsoids are drawn at 50% probability level. Hydrogens, counter cations, solvent molecules, and *meso*-ethyl residues in B) are omitted for clarity. Selected bond lengths [pm] and angles [°] for **[(PPh$_4$)$_2$][W(η^1-2)(CO)$_5$]**: Sn1–N1 222.3(2), Sn1–N3 225.7(2), Sn1–N4 224.6(2), Sn1–N5 222.5(2), W1–Sn1 283.44(6), W1–C$_{ax.}$ 196.9(3), W1–C$_{eq.}$ between 202.0(3) and 204.4(3), Sn1–N$_4$-plane 83.2, N1–Sn1–N4 133.41(9), N3–Sn1–N4 139.25(9), *cis*–N–Sn–N between 81.54(8) and 82.53(8); and **Ru(η^5-2)(*p*-cymene)**: Sn1–N1 219.80(11), Sn1–N2 232.01(11), Sn1–N3 233.01(12), Sn1–N4 259.95(12), Sn1–N$_4$-plane 103.3, Ru1-pyrrole 183.7, Ru1-cymene 171.8, N1–Sn1–N4 126.45(4), N2–Sn1–N3 128.10(4), *cis*–N–Sn–N between 74.76(4) and 83.13(4).

Reaction of **[Li$_2$(thf)$_x$][2]** with excess selenium powder in THF-d_8 at room temperature completed within minutes, quantitatively forming the lithium salt of the stanna(II) selenido complex **[Li$_2$(thf)$_x$][2-Se]** (Figure 3A). Depending on the π-accepting properties of stannylenes, the tin-selenium bond can be described via two resonance forms: i) as a Sn=Se double bond (strong π-acceptor, deshielded selenium, downfield shift) and ii) as a Sn$^+$–Se$^-$ single bond with partial charges (weak π-acceptor, shielded selenium, upfield shift). **[Li$_2$(thf)$_x$][2-Se]** shows a ^{77}Se NMR shift of −391.99 ppm, lying in a range comparable to a tetracoordinated but neutral, bis amidinato stanna(II) selenido complex —thus no notable strong upfield shift.[29] An explanation for this seemingly contrasting result with the TEP number was required. In 2020, Bertrand and co-workers reported carbene selenide adducts with stronger than expected downfield ^{77}Se NMR chemical shifts caused by C(sp^3)H–Se non-classical hydrogen bonding.[30] Indeed, as indicated by ^{1}H

© 2022 The Authors. Angewandte Chemie International Edition published by Wiley-VCH GmbH

15213773, 2022, 13, Downloaded from https://onlinelibrary.wiley.com/doi/10.1002/anie.202116615 by ... Online Library on [12/04/2024]. See the Terms and Conditions (https://onlinelibrary.wiley.com/terms-and-conditions) on Wiley Online Library for rules of use; OA articles are governed by the applicable Creative Commons License

1521373, 2022, 13, Downloaded from https://onlinelibrary.wiley.com/doi/10.1002/anie.202116615 by Heidelberg University Universitätsbibliothek, Wiley Online Library on [12/04/2024]. See the Terms and Conditions (https://onlinelibrary.wiley.com/terms-and-conditions) on Wiley Online Library for rules of use; OA articles are governed by the applicable Creative Commons License

and 2D ^{77}Se,^{1}H-HMBC NMR spectroscopy (Figure S16) and evidenced by NBO and ETS-NOCV calculations (Table S11, S12 and Figure S56) on **[2-Se]$^{2-}$**, significant interactions exist between the selenium and the methylene hydrogen atoms of the *meso*-ethyl residues in **[2-Se]$^{2-}$**, shifting the ^{77}Se NMR signals potentially downfield (cf. Figure 3A). To correct the experimental ^{77}Se NMR shifts for these secondary interactions, we calculated the ^{77}Se NMR chemical shifts of **[2-Se]$^{2-}$** and of the hypothetical *meso*-unsubstituted derivative **[2^{H}-Se]$^{2-}$** (PBE0/SO-ZORA-TZ2P COSMO(THF)//B97M-D3(BJ)/def2-TZVPP). The computed ^{77}Se shift for **[2-Se]$^{2-}$** lies at −449.37 ppm. Notably, the absence of *meso*-alkyl residues in **[2^{H}-Se]$^{2-}$** induces a ^{77}Se NMR resonance strongly upfield shifted to −638.57 ppm. NBO calculations revealed that the removal of the *meso*-substituents do not change the direct Sn(lp)→Se(p_x) bonding interactions, supporting the ^{77}Se NMR shift of **[2^{H}-Se]$^{2-}$** as a meaningful, value corrected for the absence of C(sp^3)H–Se hydrogen bonding. Hence, a notably negative selenium shift in comparison with ^{77}Se NMR shifts of other literature-known stanna(II) selenido complexes[29,31] additionally confirms **[2]$^{2-}$** as a strong σ-donor ligand with weak π-acceptor properties (Table S13 and Figure S57). The absent π-acceptor property is further illustrated by ETS-NOCV and NBO calculations of **[2-Se]$^{2-}$**, showing negligible contributions of a Se(lp)→π*(Sn–N) back donation to the total orbital interaction between **[2]$^{2-}$** and Se (Table S11, S12 and Figure S56).

Next, alternative coordination modes of **[2]$^{2-}$** against transition metals were probed. A rapid reaction of **[Li$_2$(thf)$_x$][2]** with 0.5 equivalents [{Ru(Cl)(*p*-cymene)}$_2$(μ-Cl)$_2$] at room temperature provided neutral **Ru(η^5-2)(*p*-cymene)** at excellent yield and bulk purity (Figure 3D). The structure of **Ru(η^5-2)(*p*-cymene)** was confirmed by SCXRD (Figure 4B). η^5-coordination to a ruthenium(II) *p*-cymene fragment decreases the electron density in one of the pyrrolato units in **[2]$^{2-}$**, causing an elongated Sn1-N4 bond in contrast to the other Sn–N bonds. However, ^{119}Sn NMR spectroscopy still shows a high-field resonance at −424.83 ppm as expected for a tetra-coordinated tin(II) atom. Owing to the energetically nearly degenerated HOMO, HOMO−1 and HOMO−2 (Figure 2D), **[2]$^{2-}$** can either act as a η^1-coordinating 2e$^-$ donor with 16 VE fragments like W(CO)$_5$ and Ni(CO)$_3$ or as a η^5-coordinating 6e$^-$ donor with the 12 VE fragment [Ru(*p*-cymene)]$^{2+}$. Interestingly, dianionic calix[4]pyrrole complexes of Ni^{II} and Cu^{II} were shown to act as η^5-coordinating 6e$^-$ donors solely via their pyrrolato units forming polymetallic sandwich-type complexes in their second coordination sphere, whereas the σ-donor mode is unique for **[2]$^{2-}$**.[14d,32]

Oxidative addition across carbon-halogen bonds displays a common reactivity mode for low-valent main group element species, including classical stannylenes.[33] However, since the tin(II) center in **[2]$^{2-}$** possesses a high-energy lone pair but no π-accepting character at tin, a reactivity closer to R$_3$Sn$^-$ nucleophiles should be expected.[7a,34] Indeed, in toluene-d_8 the lithium salt **[Li$_2$(thf)$_x$][2]** readily substitutes the chloride in benzoyl chloride forming acyl stannate(IV) **[Li(thf)$_2$][3-COPh]** (Figure 5A) as shown by NMR spectroscopy and high-resolution ESI(−) MS. Cooling of the reaction solution to −30 °C yielded single crystals suitable for X-ray diffractometry, validating the nucleophilic substitution at the carbonyl C atom (Figure 5C). Compared to free **[2]$^{2-}$** and the η^1-complex **[W(η^1-2)(CO)$_5$]$^{2-}$**, the acyl stannate(IV) **[3-COPh]$^-$** possess significantly shortened Sn-N bond lengths and increased *trans*–N–Sn–N valence angles, being in line with formal oxidation of the tin(II) center to a tin(IV). It represents a rare example of an acyl stannate characterized in the solid-state and, to the best of our knowledge, the first example with a pentacoordinated tin. To our surprise, the respective acyl stannates(IV) were also obtained upon reacting **[Li$_2$(thf)$_x$][2]** with 4-CF$_3$-benzaldehyde and benzaldehyde, alongside the precipitation of lithium hydride. Whereas for benzaldehyde, the product could only be detected by HRMS ESI(−) measurements, the more reactive 4-CF$_3$-benzaldehyde yielded **[3-COC$_6$H$_4$-(CF$_3$)]$^-$** at around 45 % yield. In contrast to monoanionic tin nucleophiles such as ^{n}Bu$_3$SnMgBr and ^{n}Bu$_3$SnLi, which need specialized oxidants as hydride acceptors to form neutral acyl stannates(IV) from the alcoholato stage, the dianionic nucleophile **[2]$^{2-}$** enables a direct hydride substitution.[35] Possibly, the missing π-acceptor ability and the high electron richness of **[2]$^{2-}$** destabilizes the tetrahedral alcoholato intermediate to an extend that hydride expulsion becomes a viable process. Noteworthily, the corresponding dianionic calix[4]pyrrole complexes of Ni^{II} react both with acyl chlorides or aldehydes by nucleophilic attack of the pyrrole-backbone, once again underscoring the unique metal-centered nucleophilicity of **[2]$^{2-}$**.[36] In the reaction of **[(NBu$_4$)$_2$][2]** with benzoyl chloride, CH_2Cl_2 or benzyl chloride, ^{1}H, ^{13}C and ^{119}Sn NMR spectroscopy showed near quantitative conversion of the starting materials into new species, which were identified as the nucleophilic substitution products **[NBu$_4$][3-R]** (R=CH_2Cl, CH_2Ph, COPh; Figure 5B). No reaction was observed with benzaldehydes, rendering the precipitation of lithium hydride as an additional factor for the hydride substitution.

Besides being a nucleophile, **[2]$^{2-}$** also rendered as reductant, showing two irreversible one-electron oxidations at −0.42 V and 0.04 V and quasi-reversible two-electron oxidation at 0.55 V (*vs.* AgCl/Ag/KCl, Figure S54). Since electron donors can engage in radical-nucleophilic aromatic substitutions,[37] **[(NBu$_4$)$_2$][2]** was reacted with one equivalent iodobenzene. Mixing for 48 hours at room temperature in THF-d_8, the near quantitative reduction of iodobenzene to benzene could be observed alongside the clean formation of the tin(IV) bis-(thf) complex **3-(thf)$_2$**.[38] Following literature reports, the NBu$_4^+$ cation was assumed as the proton source.[39] Interestingly, the reduction potential of **[(NBu$_4$)$_2$][2]** should not allow a direct reduction of iodobenzene (≈ −2.24 V *vs.* AgCl/Ag/KCl).[40] Instead, computations revealed the exergonic formation of a precursor complex via Sn→I σ-hole halogen bond interaction, potentially reducing the activation barrier of an inner sphere electron transfer (Figure S53). Generally, this observation adds a promising facet to the features of **[2]$^{2-}$**, such as selective reductant or for the participation in frustrated radical pair chemistry.[41]

© 2022 The Authors. Angewandte Chemie International Edition published by Wiley-VCH GmbH

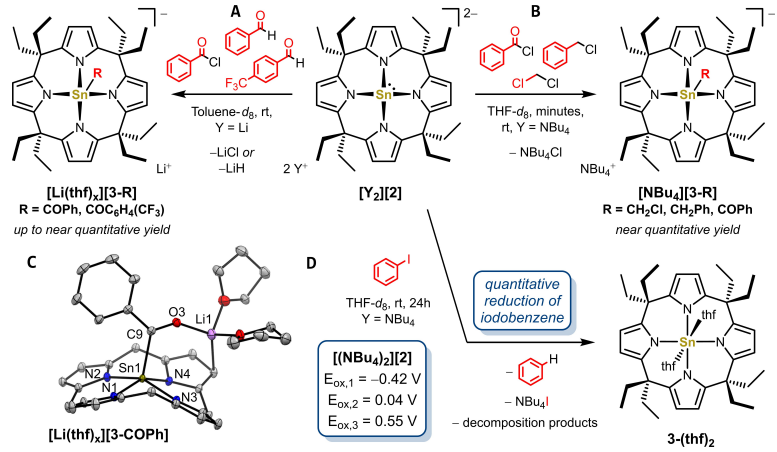


Figure 5. Reactivity of A) **[Li_2(thf)$_x$][2]** and B) **[$(NBu_4)_2$][2]** with electrophiles and **D)** reaction of **[$(NBu_4)_2$][2]** with iodobenzene. Yields where determined by NMR spectroscopy. Oxidation potentials were determined by cyclic voltammetry of **[$(NBu_4)_2$][2]** (10^{-3} M) and Bu_4NPF_6 (0.01 M) in 1,2-difluorobenzene at a scan rate of 0.05 V s^{-1}. C) Solid state molecular structure of **[Li(thf)$_x$][3-COPh]**. Displacement ellipsoids are drawn at 50% probability level. Hydrogens and toluene solvent molecules are omitted for clarity. Selected bond lengths [pm] and angles [°]: Sn1–N1 208.11(10), Sn1–N2 210.25(10), Sn1–N3 211.02(12), Sn1–N4 211.31(11), Sn1–N_4-plane 49.4, Sn1–C9 220.94(13), C9–O3 123.20(14), N1–Sn1–N4 152.56(4), N2–Sn1–N3 153.09(4), *cis*–N–Sn–N between 84.37(4) and 89.43(4).

Conclusion

Amido ligands hold a unique role in the chemistry of low-valent *p*-block element compounds.[13] With the present work, we extend this substance class by the first tetraamido tetrylene dianion, **[2]$^{2-}$**. The substantial repulsion that usually would prohibit the formation of such high-energy species is surpassed by taking advantage of the macrocyclic effect of the calix[4]pyrrole ligand. Consequently, by coordinating four anionic nitrogen π-donors, the energetically buried tin(II) electron lone pair is pushed to extreme σ-donor capacity. A TEP value of 2032 cm^{-1} attests donor strength exceeding that of all previously described carbene or phosphine ligands, offering potential as an electron-rich ligand in transition metal catalysis (Figure 6).[42]

The coordinative properties of **[2]$^{2-}$** are exemplified in structurally diverse complexes with tungsten and ruthenium. The η^5-coordination behavior suggests the possibility of placing a transition metal center near a nucleophilic tin(II) atom, expedient for cooperative activation modes.[43] Spontaneous hydride substitution reaction with benzaldehydes and the straightforward reaction of **[2]$^{2-}$** with acyl chlorides grants access to the yet underexplored class of acyl metalloids, e.g., of interest as visible-light photoinitiators.[44] Of note, **[2]$^{2-}$** represents the first foray of low-valent *p*-block element chemistry with the versatile calix[4]pyrrole ligand.

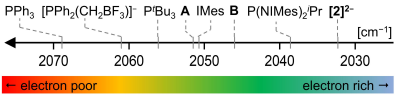


Figure 6. Comparison between the TEP values of **[2]$^{2-}$** and other literature-known carbene and phosphine ligands. Absolute values and references are given in Table S9.

Acknowledgements

We thank Prof. H.-J. Himmel for his constant support. Financial support was provided by the European Research Council (ERC) under the European Union's Horizon 2020 research and innovation program (grant agreement No948708) and the Foundation of German Business (sdw, H.R.). The BWFor/BWUniCluster, funded by the DFG, are acknowledged for computational resources. Open Access funding enabled and organized by Projekt DEAL.

Conflict of Interest

The authors declare no conflict of interest.

© 2022 The Authors. Angewandte Chemie International Edition published by Wiley-VCH GmbH

15213773, 2022, 13, Downloaded from https://onlinelibrary.wiley.com/doi/10.1002/anie.202116615 by Bibliothek, Wiley Online Library on [12/04/2024]. See the Terms and Conditions (https://onlinelibrary.wiley.com/terms-and-conditions) on Wiley Online Library for rules of use; OA articles are governed by the applicable Creative Commons License

15213773, 2022, 13, Downloaded from https://onlinelibrary.wiley.com/doi/10.1002/anie.202116615 by Heidelberg University Universitätsbibliothek, Wiley Online Library on [12/04/2024]. See the Terms and Conditions (https://onlinelibrary.wiley.com/terms-and-conditions) on Wiley Online Library for rules of use; OA articles are governed by the applicable Creative Commons License

Data Availability Statement

The data that support the findings of this study are available in the supplementary material of this article.

Keywords: Calix[4]Pyrrole · Dianions · Low-Valent · Tin · σ-Donor

[1] a) A. Doddi, M. Peters, M. Tamm, *Chem. Rev.* **2019**, *119*, 6994–7112; b) M. N. Hopkinson, C. Richter, M. Schedler, F. Glorius, *Nature* **2014**, *510*, 485–496; c) V. Nesterov, D. Reiter, P. Bag, P. Frisch, R. Holzner, A. Porzelt, S. Inoue, *Chem. Rev.* **2018**, *118*, 9678–9842; d) P. Bellotti, M. Koy, M. N. Hopkinson, F. Glorius, *Nat. Chem. Rev.* **2021**, *5*, 711–725; e) M. Melaimi, R. Jazzar, M. Soleilhavoup, G. Bertrand, *Angew. Chem. Int. Ed.* **2017**, *56*, 10046–10068; *Angew. Chem.* **2017**, *129*, 10180–10203; f) R. Jazzar, M. Soleilhavoup, G. Bertrand, *Chem. Rev.* **2020**, *120*, 4141–4168.

[2] a) D. J. Nelson, S. P. Nolan, *Chem. Soc. Rev.* **2013**, *42*, 6723–6753; b) H. V. Huynh, *Chem. Rev.* **2018**, *118*, 9457–9492.

[3] a) L. Álvarez-Rodríguez, J. A. Cabeza, P. García-Álvarez, D. Polo, *Coord. Chem. Rev.* **2015**, *300*, 1–28; b) N. Parvin, S. Pal, V. C. Rojisha, S. De, P. Parameswaran, S. Khan, *ChemistrySelect* **2016**, *1*, 1991–1995; c) C.-W. So, H. W. Roesky, J. Magull, R. B. Oswald, *Angew. Chem. Int. Ed.* **2006**, *45*, 3948–3950; *Angew. Chem.* **2006**, *118*, 4052–4054; d) H. Arp, J. Baumgartner, C. Marschner, P. Zark, T. Müller, *J. Am. Chem. Soc.* **2012**, *134*, 10864–10875; e) T. A. N. Nguyen, G. Frenking, *Chem. Eur. J.* **2012**, *18*, 12733–12748; f) W. Kutzelnigg, *Angew. Chem. Int. Ed. Engl.* **1984**, *23*, 272–295; *Angew. Chem.* **1984**, *96*, 262–286; g) M. S. Nechaev, *Organometallics* **2021**, *40*, 3408–3423.

[4] F. E. Hahn, A. V. Zabula, T. Pape, A. Hepp, R. Tonner, R. Haunschild, G. Frenking, *Chem. Eur. J.* **2008**, *14*, 10716–10721.

[5] a) C. Mohapatra, L. T. Scharf, T. Scherpf, B. Mallick, K.-S. Feichtner, C. Schwarz, V. H. Gessner, *Angew. Chem. Int. Ed.* **2019**, *58*, 7459–7463; *Angew. Chem.* **2019**, *131*, 7537–7541; b) S. Takahashi, J. Sekiguchi, A. Ishii, N. Nakata, *Angew. Chem. Int. Ed.* **2021**, *60*, 4055–4059; *Angew. Chem.* **2021**, *133*, 4101–4105.

[6] a) K. Angermund, K. Jonas, C. Krüger, J. L. Latten, Y.-H. Tsay, *J. Organomet. Chem.* **1988**, *353*, 17–25; b) C. Drost, P. B. Hitchcock, M. F. Lappert, *Angew. Chem. Int. Ed.* **1999**, *38*, 1113–1116; *Angew. Chem.* **1999**, *111*, 1185–1187; c) M. Wagner, K. Dorogov, M. Schürmann, K. Jurkschat, *Dalton Trans.* **2011**, *40*, 8839–8848; d) J. A. Cabeza, P. Garcia-Alvarez, D. Polo, *Eur. J. Inorg. Chem.* **2016**, 10–22.

[7] a) A. Capperucci, A. Degl'Innocenti, C. Faggi, G. Reginato, A. Ricci, P. Dembech, G. Seconi, *J. Org. Chem.* **1989**, *54*, 2966–2968; b) P. Riviere, A. Castel, M. Riviere-Baudet, in *The Chemistry of Organic Germanium, Tin and Lead Compounds, Vol. 2* (Ed.: Z. Rappoport), Wiley, Hoboken, **2002**, pp. 653–748; c) V. Y. Lee, A. Sekiguchi, in *Organometallic Compounds of Low-Coordinate Si, Ge, Sn and Pb: From Phantom Species to Stable Compounds*, Wiley, Hoboken, **2010**, pp. 89–138; d) D.-Y. Wang, C. Wang, M. Uchiyama, *J. Am. Chem. Soc.* **2015**, *137*, 10488–10491; e) A. G. Davies, in *Organotin Chemistry*, 2nd ed., Wiley, Hoboken, **2004**, pp. 311–332.

[8] a) H. Memmler, U. Kauper, L. H. Gade, D. Stalke, J. W. Lauher, *Organometallics* **1996**, *15*, 3637–3639; b) M. Kilian, H. Wadepohl, L. H. Gade, *Dalton Trans.* **2008**, 582–584.

[9] a) L. H. Gade, *Eur. J. Inorg. Chem.* **2002**, 1257–1268; b) M. Lutz, M. Haukka, T. A. Pakkanen, L. H. Gade, *Inorg. Chem.* **2003**, *42*, 2798–2804; c) M. Kilian, H. Wadepohl, L. H. Gade, *Organometallics* **2007**, *26*, 3076–3078; d) M. Kilian, H. Wadepohl, L. H. Gade, *Eur. J. Inorg. Chem.* **2008**, 1892–1900.

[10] a) R. C. Elder, M. J. Heeg, E. Deutsch, *Inorg. Chem.* **1978**, *17*, 427–431; b) B. Schiemenz, G. Huttner, *Angew. Chem. Int. Ed. Engl.* **1993**, *32*, 297–298; *Angew. Chem.* **1993**, *105*, 295–296; c) G. Renner, P. Kircher, G. Huttner, P. Rutsch, K. Heinze, *Eur. J. Inorg. Chem.* **2001**, 973–980; d) P. Kircher, G. Huttner, L. Zsolnai, A. Driess, *Angew. Chem. Int. Ed.* **1998**, *37*, 1666–1668; *Angew. Chem.* **1998**, *110*, 1756–1758.

[11] a) L. Wesemann, *Z. Anorg. Allg. Chem.* **2004**, *630*, 1349–1356; b) R. W. Chapman, J. G. Kester, K. Folting, W. E. Streib, L. J. Todd, *Inorg. Chem.* **1992**, *31*, 979–983.

[12] T. Vollgraff, N. Michel, J. Sundermeyer, *Eur. J. Inorg. Chem.* **2021**, 3852–3860.

[13] a) M. F. Lappert, P. P. Power, A. R. Sanger, R. C. Srivastava, *Metal and Metalloid Amides: Synthesis, Structures, and Physical and Chemical Properties*, Ellis Horwood-Wiley, Chichester, **1980**; b) M. F. Lappert, P. P. Power, A. Protchenko, A. Seeber *Metal Amide Chemistry*, Wiley, Hoboken,, **2009**; c) M. Veith, *Angew. Chem. Int. Ed. Engl.* **1987**, *26*, 1–14; *Angew. Chem.* **1987**, *99*, 1–14; d) Y. Mizuhata, T. Sasamori, N. Tokitoh, *Chem. Rev.* **2009**, *109*, 3479–3511; e) M. Asay, C. Jones, M. Driess, *Chem. Rev.* **2011**, *111*, 354–396.

[14] a) D. Jacoby, C. Floriani, A. Chiesi-Villa, C. Rizzoli, *J. Chem. Soc. Chem. Commun.* **1991**, 220–222; b) C. Floriani, R. Floriani-Moro, in *The Porphyrin Handbook, Vol. 3* (Eds.: K. M. Kadish, K. M. Smith, R. Guilard), Academic Press, San Diego, **2000**, pp. 405–420; c) C. Floriani, R. Floriani-Moro, in *The Porphyrin Handbook, Vol. 3* (Eds.: K. M. Kadish, K. M. Smith, R. Guilard), Academic Press, San Diego, **2000**, pp. 385–402; d) L. Cuesta, J. L. Sessler, *Chem. Soc. Rev.* **2009**, *38*, 2716–2729; e) J. Bachmann, D. G. Nocera, *J. Am. Chem. Soc.* **2004**, *126*, 2829–2837; f) J. Bachmann, D. G. Nocera, *J. Am. Chem. Soc.* **2005**, *127*, 4730–4743; g) P. Buranaprasertsuk, Y. Tangsakol, W. Chavasiri, *Catal. Commun.* **2007**, *8*, 310–314; h) S. Mohebbi, S. Rayati, *Transition Met. Chem.* **2007**, *32*, 1035–1038.

[15] a) G. B. Deacon, Z. Guo, P. C. Junk, J. Wang, *Angew. Chem. Int. Ed.* **2017**, *56*, 8486–8489; *Angew. Chem.* **2017**, *129*, 8606–8609; b) N. F. M. Mukthar, N. D. Schley, G. Ung, *Dalton Trans.* **2020**, *49*, 16059–16061.

[16] a) F. Ebner, H. Wadepohl, L. Greb, *J. Am. Chem. Soc.* **2019**, *141*, 18009–18012; b) F. Ebner, L. M. Sigmund, L. Greb, *Angew. Chem. Int. Ed.* **2020**, *59*, 17118–17124; *Angew. Chem.* **2020**, *132*, 17266–17272; c) L. M. Sigmund, L. Greb, *Chem. Sci.* **2020**, *11*, 9611–9616; d) F. Ebner, P. Mainik, L. Greb, *Chem. Eur. J.* **2021**, *27*, 5120–5124; e) L. M. Sigmund, C. Ehlert, M. Enders, J. Graf, G. Gryn'ova, L. Greb, *Angew. Chem. Int. Ed.* **2021**, *60*, 15632–15640; *Angew. Chem.* **2021**, *133*, 15761–15769.

[17] a) F. Ebner, L. Greb, *J. Am. Chem. Soc.* **2018**, *140*, 17409–17412; b) F. Ebner, L. Greb, *Chem* **2021**, *7*, 2151–2159.

[18] H. Ruppert, L. M. Sigmund, L. Greb, *Chem. Commun.* **2021**, *57*, 11751–11763.

[19] a) Y. Segawa, M. Yamashita, K. Nozaki, *Science* **2006**, *314*, 113–115; b) Y. Segawa, Y. Suzuki, M. Yamashita, K. Nozaki, *J. Am. Chem. Soc.* **2008**, *130*, 16069–16079; c) L. Weber, *Eur. J. Inorg. Chem.* **2017**, 3461–3488; d) A. V. Protchenko, P. Vasko, M. Á. Fuentes, J. Hicks, D. Vidovic, S. Aldridge, *Angew. Chem. Int. Ed.* **2021**, *60*, 2064–2068; *Angew. Chem.* **2021**, *133*, 2092–2096.

[20] a) J. Hicks, P. Vasko, J. M. Goicoechea, S. Aldridge, *Nature* **2018**, *557*, 92–95; b) Y. Liu, J. Li, X. Ma, Z. Yang, H. W. Roesky, *Coord. Chem. Rev.* **2018**, *374*, 387–415; c) J. Hicks, P. Vasko, J. M. Goicoechea, S. Aldridge, *J. Am. Chem. Soc.* **2019**, *141*, 11000–11003; d) J. Hicks, P. Vasko, J. M. Goicoechea, S. Aldridge, *Angew. Chem. Int. Ed.* **2021**, *60*, 1702–1713; *Angew. Chem.* **2021**, *133*, 1726–1737.

[21] D. Agustin, M. Ehses, *C. R. Chim.* **2009**, *12*, 1189–1227.

© 2022 The Authors. Angewandte Chemie International Edition published by Wiley-VCH GmbH

[22] Deposition numbers 2125915, 2125916, 2125917, 2125918, 2125919 and 2125920 contain the supplementary crystallographic data for this paper. These data are provided free of charge by the joint Cambridge Crystallographic Data Centre and Fachinformationszentrum Karlsruhe Access Structures service.

[23] a) D. A. Atwood, V. O. Atwood, A. H. Cowley, J. L. Atwood, E. Roman, *Inorg. Chem.* **1992**, *31*, 3871–3872; b) S. B. Kim, P. Sinsermsuksakul, A. S. Hock, R. D. Pike, R. G. Gordon, *Chem. Mater.* **2014**, *26*, 3065–3073; c) T. Ungpittagul, P. Wongmahasirikun, K. Phomphrai, *Dalton Trans.* **2020**, *49*, 8460–8471; d) R. Samii, D. Zanders, A. Fransson, G. Bacic, S. T. Barry, L. Ojamae, V. Kessler, H. Pedersen, N. J. O'Brien, *Inorg. Chem.* **2021**, *60*, 12759–12765.

[24] C. A. Tolman, *Chem. Rev.* **1977**, *77*, 313–348.

[25] A. Liske, K. Verlinden, H. Buhl, K. Schaper, C. Ganter, *Organometallics* **2013**, *32*, 5269–5272.

[26] W.-W. D. Mont, H.-J. Kroth, *Z. Naturforsch. B* **1980**, *35*, 700–702.

[27] Even via prolonged ^{119}Sn NMR measurements of [$(PPh_3)_2$][W-(η^1-2)$(CO)_5$] no $^1J_{Sn\text{-}W}$ coupling constant could be obtained, which might be related to the structural flexibility of the calix[4]pyrrole ligand causing broadened ^{119}Sn resonances.

[28] M. L. Kelty, A. J. McNeece, A. S. Filatov, J. Anderson, *ChemRxiv.* **2021**, https://doi.org/10.33774/chemrxiv-2021-4jd82-v2. This content is a preprint and has not been peer-reviewed.

[29] I. Y. Ahmet, J. R. Thompson, A. L. Johnson, *Eur. J. Inorg. Chem.* **2018**, 1670–1678.

[30] G. P. Junor, J. Lorkowski, C. M. Weinstein, R. Jazzar, C. Pietraszuk, G. Bertrand, *Angew. Chem. Int. Ed.* **2020**, *59*, 22028–22033; *Angew. Chem.* **2020**, *132*, 22212–22217.

[31] a) W.-P. Leung, W.-H. Kwok, Z.-Y. Zhou, T. C. W. Mak, *Organometallics* **2000**, *19*, 296–303; b) B. Mairychová, L. Dostál, A. Růžička, M. Fulem, K. Růžička, A. Lyčka, R. Jambor, *Organometallics* **2011**, *30*, 5904–5910; c) M. Saito, N. Tokitoh, R. Okazaki, *J. Am. Chem. Soc.* **2004**, *126*, 15572–15582; d) J.-H. Park, S. G. Kang, Y. K. Lee, T.-M. Chung, B. K. Park, C. G. Kim, *Inorg. Chem.* **2020**, *59*, 3513–3517.

[32] a) L. Bonomo, E. Solari, G. Martin, R. Scopelliti, C. Floriani, *Chem. Commun.* **1999**, 2319–2320; b) L. Bonomo, E. Solari, M. Latronico, R. Scopelliti, C. Floriani, *Chem. Eur. J.* **1999**, *5*, 2040–2047; c) L. Cuesta, D. Gross, V. M. Lynch, Z. Ou, W. Kajonkijya, K. Ohkubo, S. Fukuzumi, K. M. Kadish, J. L. Sessler, *J. Am. Chem. Soc.* **2007**, *129*, 11696–11697.

[33] a) T. Chu, G. I. Nikonov, *Chem. Rev.* **2018**, *118*, 3608–3680; b) M. F. Lappert, M. C. Misra, M. Onyszchuk, R. S. Rowe, P. P. Power, M. J. Slade, *J. Organomet. Chem.* **1987**, *330*, 31–46.

[34] H. J. Reich, J. P. Borst, R. R. Dykstra, *Organometallics* **1994**, *13*, 1–3.

[35] a) J. A. Marshall, in *Organometallics in Synthesis: A Manual*, 2nd ed. (Ed.: M. Schlosser), Wiley, Hoboken, **2001**, pp. 353–464; b) J. A. Marshall, G. S. Welmaker, B. W. Gung, *J. Am. Chem. Soc.* **1991**, *113*, 647–656.

[36] L. Bonomo, E. Solari, C. Floriani, A. Chiesi-Villa, C. Rizzoli, *J. Am. Chem. Soc.* **1998**, *120*, 12972–12973.

[37] a) J. F. Bunnett, J. K. Kim, *J. Am. Chem. Soc.* **1970**, *92*, 7463–7464; b) R. A. Rossi, J. F. Guastavino, M. E. Budén, in *Arene Chemistry: Reaction Mechanisms and Methods for Aromatic Compounds* (Ed.: J. Mortier), Wiley, Hoboken, **2015**, pp. 243–268.

[38] a) J.-M. Benech, L. Bonomo, E. Solari, R. Scopelliti, C. Floriani, *Angew. Chem. Int. Ed.* **1999**, *38*, 1957–1959; *Angew. Chem.* **1999**, *111*, 2107–2109; b) G. R. Fulmer, A. J. M. Miller, N. H. Sherden, H. E. Gottlieb, A. Nudelman, B. M. Stoltz, J. E. Bercaw, K. I. Goldberg, *Organometallics* **2010**, *29*, 2176–2179.

[39] R. Alvarado de la Torre, J. W. Sease, *J. Am. Chem. Soc.* **1979**, *101*, 1687–1690.

[40] L. Pause, M. Robert, J.-M. Savéant, *J. Am. Chem. Soc.* **1999**, *121*, 7158–7159.

[41] a) L. L. Liu, D. W. Stephan, *Chem. Soc. Rev.* **2019**, *48*, 3454–3463; b) F. Holtrop, A. R. Jupp, B. J. Kooij, N. P. Van Leest, B. De Bruin, J. C. Slootweg, *Angew. Chem. Int. Ed.* **2020**, *59*, 22210–22216; *Angew. Chem.* **2020**, *132*, 22394–22400.

[42] M. A. Wünsche, P. Mehlmann, T. Witteler, F. Buß, P. Rathmann, F. Dielmann, *Angew. Chem. Int. Ed.* **2015**, *54*, 11857–11860; *Angew. Chem.* **2015**, *127*, 12024–12027.

[43] R. J. Somerville, J. Campos, *Eur. J. Inorg. Chem.* **2021**, 3488–3498.

[44] a) A. Eibel, J. Radebner, M. Haas, D. E. Fast, H. Freißmuth, E. Stadler, P. Faschauner, A. Torvisco, I. Lamparth, N. Moszner, H. Stueger, G. Gescheidt, *Polym. Chem.* **2018**, *9*, 38–47; b) J. Radebner, A. Eibel, M. Leypold, N. Jungwirth, T. Pickl, A. Torvisco, R. Fischer, U. K. Fischer, N. Moszner, G. Gescheidt, H. Stueger, M. Haas, *Chem. Eur. J.* **2018**, *24*, 8281–8285; c) S. D. Püschmann, P. Frühwirt, M. Pillinger, A. Knöchl, M. Mikusch, J. Radebner, A. Torvisco, R. C. Fischer, N. Moszner, G. Gescheidt, M. Haas, *Chem. Eur. J.* **2021**, *27*, 3338–3347; d) A. Holownia, C. N. Apte, A. K. Yudin, *Chem. Sci.* **2021**, *12*, 5346–5360.

Manuscript received: December 6, 2021
Accepted manuscript online: January 12, 2022
Version of record online: February 7, 2022

© 2022 The Authors. Angewandte Chemie International Edition published by Wiley-VCH GmbH

15213773, 2022, 13, Downloaded from https://onlinelibrary.wiley.com/doi/10.1002/anie.202116615 by ... Bibliothek, Wiley Online Library on [12/04/2024]. See the Terms and Conditions (https://onlinelibrary.wiley.com/terms-and-conditions) on Wiley Online Library for rules of use; OA articles are governed by the applicable Creative Commons License

Angewandte Chemie
Eine Zeitschrift der Gesellschaft Deutscher Chemiker

Supporting Information

3.1SI

Calix[4]pyrrolato Stannate(II): A Tetraamido Tin(II) Dianion and Strong Metal-Centered σ-Donor

*H. Ruppert, L. Greb**

Supporting Information

Table of Contents

1 Experimental Details 3
2 Computational Details 5
3 Synthesis 6
3.1 Lithium tin(II) *meso*-octaethylcalix[4]pyrrolate $[Li_2(thf)_x][2]$ 6
3.2 Tetrabutylammonium tin(II) *meso*-octaethylcalix[4]pyrrolate $[(NBu_4)_2][2]$ 7
3.3 Tetraphenylphosphonium tin(II) *meso*-octaethylcalix[4]pyrrolate $[(PPh_4)_2(o\text{DFB})_{0.5}][2]$ 8
3.4 Lithium tin(II) *meso*-octaethylcalix[4]pyrrolato selenide $[Li_2(thf)_x][2\text{-Se}]$ 9
3.5 Tetraphenylphosphonium $^1\eta$-(tin(II) *meso*-octaethylcalix[4]pyrrolate) pentacarbonyl tungsten(0) $[(PPh_4)_2][W(^1\eta\text{-}2)(CO)_5]$ 10
3.6 Tetrabutylammonium $^1\eta$-(tin(II) *meso*-octaethylcalix[4]pyrrolate) triscarbonyl nickel(0) $[(NBu_4)_2][Ni(^1\eta\text{-}2)(CO)_3]$ 11
3.7 Ruthenium(II) $^5\eta$-(tin(II) *meso*-octaethylcalix[4]pyrrolate) *para*-cymene $Ru(^5\eta\text{-}2)$(*p*-cymene) 12
3.8 Reaction of $[Li_2(thf)_x][2]$ with Electrophiles 13
3.8.1 Entry 3 (Benzoyl Chloride) 13
3.8.2 Entry 4 (Benzaldehyde) 13
3.8.3 Entry 5 (4-CF_3-Benzaldehyde) 14
3.9 Reaction of $[(NBu_4)_2][2]$ with Electrophiles 14
3.9.1 Entry 1 (Methylene Chloride) 15
3.9.2 Entry 2 (Benzyl chloride) 15
3.9.3 Entry 3 (Benzoyl chloride) 16
3.9.4 fEntry 6 (Iodobenzene) 16
4 NMR Spectra 17
4.1 $[Li_2(thf)_x][2]$ 17
4.2 $[(NBu_4)_2][2]$ 20
4.3 $[(PPh_4)_2(o\text{DFB})_{0.5}][2]$ 21
4.4 $[Li_2(thf)_x][2\text{-Se}]$ 23
4.5 $[(PPh_4)_2][W(^2\eta\text{-}2)(CO)_5]$ 25
4.6 $[(NBu_4)_2][Ni(^1\eta\text{-}2)(CO)_3]$ 26

4.7 Ru(^{5}η-2)(cymene) 28
4.8 Reaction of [$Li_2(thf)_x$][2] with Benzoyl chloride 29
4.9 Reaction of [$Li_2(thf)_x$][2] with 4-CF_3-Benzaldehyde 31
4.10 Reaction of [$(NBu_4)_2$][2] with Methylene Chloride 32
4.11 Reaction of [$(NBu_4)_2$][2] with Benzyl Chloride 34
4.12 Reaction of [$(NBu_4)_2$][2] with Benzoyl Chloride 35
4.13 Reaction of [$(NBu_4)_2$][2] with Iodobenzene 37
5 Crystallographic Data 38
5.1 [$Li_2(thf)_x$][2] 38
5.2 [$(NBu_4)_2$][2] 39
5.3 [$(PPh_4)_2$(*o*DFB)$_{0.5}$][2] 40
5.4 [$(PPh_4)_2$][W(^{2}η-2)$(CO)_5$] 41
5.5 Ru(^{5}η-2)(cymene) 42
5.6 [Li$(thf)_2$][3-COPh] 43
6 Infrared Spectroscopy 44
7 Comparative TEP Scale 44
8 DFT Calculations 45
9 Cyclic Voltammetry 48
10 ETS-NOCV Results 48
11 NBO Results 51
12 ^{77}Se and ^{119}Sn NMR Shift Calculation Results 53
13 Optimized Molecular Geometries 53
14 Literature 81

1 Experimental Details

All manipulations were carried out under a dry argon atmosphere by using standard Schlenk techniques to prevent oxidation and hydrolysis of the sensitive compounds. *meso*-Octamethylcali[4]pyrrole as well as the deprotonated *tris*-(thf) *tetra*-lithium *meso*-octamethylcalix[4]pyrrolate have been synthesized by literature known procedures.[1] The commercially available chemicals were used as received. All solvents and liquid chemicals were rigorously dried by applying standard procedures, freshly degassed and stored over activated molecular sieve (3 Å resp. 4 Å) prior to use. All glassware, syringes, magnetic stirring bars, and needles were thoroughly dried. All air sensitive compounds were stored in a glove box (MBraun LABmaster dp, MB-20-G, SylaTech Y05G) under N_2 atmosphere. Analytical data of literature known compounds were compared to data of the respective reference and were found to be consistent in all cases. Purity and identity of novel compounds were confirmed by high resolution multinuclear NMR-spectroscopy, mass spectrometry, elemental analysis and if possible, X-ray diffraction analysis.

^{1}H, ^{13}C, ^{19}F, ^{31}P, ^{77}Se and ^{119}Sn NMR spectra were collected with a Bruker (DPX) 200, a Bruker Advance II 400 or a Bruker 2 Advance III 600 NMR spectrometer and referenced to tetramethylsilane (^{1}H, ^{13}C), tetramethylstannane (^{119}Sn), or dimethyl selenide (^{77}Se). Chemical shifts are reported as dimensionless δ values in ppm, coupling constants J are given in hertz (Hz).

High-resolution electrospray ionization mass spectra (HRMS-ESI) were obtained with a Bruker ApexQe FT-ICR instrument.

Fourier-transform infrared (FTIR) spectra at 298 K were obtained with an Agilent Cary 630 FTIR spectrometer, which was operated with the MicroLab PC software, and processed with BioRad Merlin and OriginPro 2020 64Bit.

Cyclic voltammetry was done inside a dry nitrogen-filled glove box at room temperature with a EmStat3+blue device from PalmSens, which was operated with the PSTrace 5.7 software. A glassy carbon electrode (working area of 0.07 cm^2) was used as a working electrode, a platinum wire as a counter electrode, and a silver wire as a quasi-reference electrode. The scan rate was set to 0.05 V s^{-1}. As solvent, 1,2-difluorobezene (*o*DFB), as supporting electrolyte, [NnBu$_4$][PF$_6$] was used. The analyte concentration was approximately c = 10^{-3} mol L^{-1}, the supporting electrolyte concentration c_{supp} = 0.1 mol L^{-1}. The acquired data was externally referenced against the decamethyl-ferrocene/decamethylferrocenium (dmfc/dmfc$^+$) redox couple and then transferred to the Ag/AgCl/KCl reference. Under the same conditions as described fc/fc$^+$ has a redox potential of 532 mV and dmfc/dmfc$^+$ a redox potential of 30 mV against the Ag/AgCl/KCl redox couple.[2] The dmfc/dmfc$^+$ reference measurement was carried out under the same conditions as described.

Elemental analysis for the determination of the C-,H- and N-content was carried out by the microanalysis laboratory of the Institute of Inorganic Chemistry at Heidelberg University using a vario MICRO cube of Elementar Analysensysteme.

Suitable crystals of the compounds were taken directly out of the mother liquor, immersed in perfluorinated polyether oil, and fixed on top of a cryo loop. Measurements were made on Bruker D8 Venture CCD diffractometer with a low-temperature unit using (100 K) Mo-Kα radiation chromated by mirror optics. The data collected were processed using standard Bruker APEX3 software. Structures were solved by intrinsic phasing using the SHELXT program[3] and refined with the SHELXL.[4] Graphical handling

of the structural data during solution and refinement was performed with shelXLe.[5] Atomic coordinates and anisotropic thermal parameters of non-hydrogen atoms were refined by full-matrix least-squares calculations[6] and displacement ellipsoids are displayed with 50 % probability. Hydrogen atoms were included using a riding model. Crystallographic data for the structures reported in this article are deposited within the Cambridge Crystallographic Data Centre as supplementary publication no. 2125915-2125920 and can be obtained free of charge. Crystal data and structure are summarized in the tables under the crystallographic figures.

2 Computational Details

All computations employing the Orca 4.2.1[7] software or the Amsterdam Modelling Suite AMS2021.102[8] were carried out with the computational resources available on the bwFor Cluster JUSTUS2 located at Ulm University within the Baden Württemberg High Performance Computing program.

All structures were optimized with the Orca 4.2.1 software at the B97M-D3(BJ)[9]/def2-TVZPP[10] level of theory. Minima structures were obtained with the following ORCA input line:

```
! RKS B97M-D3BJ def2-TZVPP Grid5 NoFinalGrid Opt NumFreq TightSCF
```

All calculated geometries have been confirmed as energetic minima on the potential energy surface by numerical calculation of harmonic frequencies at the B97M-D3(BJ)/def2-TVZPP level, revealing only positive values.

Subsequent single point calculations employing the Conductor-like Polarizable Continuum Model (C-PCM)[11] were performed with the following ORCA input line:

```
! RKS B97M-D3BJ def2-TZVPP CPCM(THF) Grid5 NoFinalGrid SP NumFreq
TightSCF
```

Natural Bond Orbital (NBO) calculations were conducted on the PBE0[12]/def2-TZVPP[10] level of theory including a C-PCM solvation model using NBO6.0.18a[13] as included in Orca 4.2.1 *via* the following ORCA input line:

```
! RKS PBE0 def2-TZVPP CPCM(THF) NBO TightSCF Grid5 NoFinalGrid
```

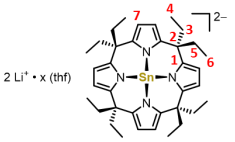
Calculations employing the Extended Transition State (ETS) method for energy decomposition analysis (EDA)[14] combined with the natural orbitals for chemical valence (NOCV)[15] calculations were performed on the BP86-G3[16] /TZ2P level of theory as implemented in the AMS2021.201 software.

Computational ^{77}Se and ^{119}Sn NMR absolute chemical shieldings (σ) were calculated with AMS2021.201 software at the PBE0[12]/TZ2P level of theory, chemical shifts were obtained by referencing to the computed value of $SeMe_2$ and $SnMe_4$ respectively. NMR chemical shift computations were carried out without the frozen core approximation and with the scalar relativistic spin-orbit ZORA approximation[17] to address correct treatment of heavy elements.

Isosurface plots were created using the IboView software v20150427.

3 Synthesis

3.1 Lithium tin(II) *meso*-octaethylcalix[4]pyrrolate [$Li_2(thf)_x$][2]



In a 200 mL Schlenk tube, *tris*-(thf) *tetra*-lithium *meso*-octamethylcalix[4]pyrrolate **[$Li_4(thf)_3$][1]** (1.0 eq, 2.82 mmol, 2.2 g) was dissolved in 55 mL THF. While stirring at room temperature tin(II) chloride (1.0 eq, 2.82 mmol, 545 mg) was added in portions. After turning slightly yellow for 5 minutes the clear, colorless solution was stirred at room temperature for 30 minutes before the solvent was evaporated at reduced pressure. The obtained crude was extracted with 200 mL Et_2O and the extract filtered over a low porosity frit to remove surplus lithium chloride. After evaporation of Et_2O the obtained crude was redissolved in 20 mL THF and the product precipitated by adding of 85 mL pentane. Isolation of the precipitant by filtration over a low porosity frit and drying at reduced pressure yielded **[$Li_2(thf)_x$][2]** as a colorless solid (2.237 g, 2.26 mmol (x=4.2), 80% yield). Cooling of a concentrated toluene solution of **[$Li_2(thf)_x$][2]** to −30 °C yielded single crystals suitable for X-ray diffraction.

3.1SI

^{1}H NMR [^{1}H, ^{1}H,^{1}H-COSY] (600.13 MHz, THF-d_8, 295 K): δ [ppm] = 5.85 (*s*, ^{117}Sn-satelites $^4J_{Sn,H}$ = 156.41 Hz, ^{119}Sn-satelites $^4J_{Sn,H}$ = 162.29 Hz, H_7, 8H), 3.62 (*m*, H_{thf}, 16.8H), 1.88 (*q*, $^3J_{H,H}$ = 7.3 Hz, H_3, 8H), 1.78 (*m*, H_{thf}, 16.8H), 1.76 (*q*, $^3J_{H,H}$ = 7.3 Hz, H_5, 8H, overlapped with thf), 0.79 (*t*, $^3J_{H,H}$ = 7.3 Hz, H_4, 12H), 0.50 (*t*, $^3J_{H,H}$ = 7.3 Hz, H_6, 12H).
^{1}H NMR [^{1}H, ^{1}H,^{1}H-COSY] (600.13 MHz, C_6D_6, 295 K): δ [ppm] = δ [ppm] = 6.44 (*s*, H_7, 8H), 3.38 (*m*, H_{thf}, 16.8H), 2.22 (*q*, $^3J_{H,H}$ = 7.3 Hz, H_3, 8H), 2.13 (*q*, $^3J_{H,H}$ = 7.3 Hz, H_3, 6H), 2.01 (*q*, $^3J_{H,H}$ = 7.3 Hz, H_3, 2H), 1.27 (*m*, H_{thf}, 16.8H), 1.08 (*t*, $^3J_{H,H}$ = 7.3 Hz, H_4, 8H), 0.90 (*t*, $^3J_{H,H}$ = 7.3 Hz, H_6, 16H).

^{7}Li NMR (233.25 MHz, THF-d_8, 295 K): δ [ppm] = −2.12 (*s*).
^{7}Li NMR (233.25 MHz, C_6D_6, 295 K): δ [ppm] = −1.40 (*s*, broad), −3.01 (*s*), −4.30 (*s*, broad).

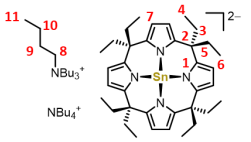
^{13}C NMR [^{13}C{^{1}H}, ^{13}C-DEPT135, ^{1}H,^{13}C-HSQC, ^{1}H,^{13}C-HMBC] (150.92 MHz, THF-d_8, 295 K): δ [ppm] = 144.05 (*s*, C_1), 106.56 (*s*, C_7H), 68.02 (*s*, $C_{thf}H_2$), 46.33 (*s*, C_2), 45.94 (*s*, C_2), 39.47 (*s*, $^{117/119}$Sn-satelites $^4J_{Sn,C}$ = 16 Hz, C_5H_2), 33.69 (*s*, C_3H_2), 26.15 (*s*, $C_{thf}H_2$), 10.47 (*s*, C_4H_3), 10.22 (*s*, C_6H_3).
^{13}C NMR [^{13}C$^{[18]}$, ^{13}C-DEPT135, ^{1}H,^{13}C-HSQC, ^{1}H,^{13}C-HMBC] (150.92 MHz, C_6D_6, 295 K): δ [ppm] = 143.92 (*s*, C_1), 105.14 (*s*, C_7H), 67.79 (*s*, $C_{thf}H_2$), 46.63 (*s*, C_2), 37.86 (*s*, C_5H_2), 36.50 (*s*, C_5H_2), 32.72 (*s*, C_3H_2), 25.06 (*s*, $C_{thf}H_2$), 9.99 (*s*, C_4H_3), 9.76 (*s*, C_6H_3), 9.69 (*s*, C_6H_3).

^{119}Sn NMR [^{119}Sn,^{1}H-HMBC] (223.81 MHz, THF-d_8, 295 K): δ [ppm] = −481.32.
^{119}Sn NMR [^{119}Sn,^{1}H-HMBC] (223.81 MHz, C_6D_6, 295 K): δ [ppm] = −618.90.

HR-MS (ESI, negative, THF): calcd. for $[C_{32}H_{48}Li_2N_4Sn+Cl]^-$ (Cl^- from ESI atmosphere) m/z = 705.2918, found m/z = 705.2929.

EA: Due to loss of THF upon isolation, a correct elemental analysis could not be obtained.

3.2 Tetrabutylammonium tin(II) *meso*-octaethylcalix[4]pyrrolate [(NBu$_4$)$_2$][2]



In a 50 mL Schlenk tube, **[Li$_2$(thf)$_x$][2]** (1.0 eq, x = 4.2, 522 µmol, 500 mg) and tetrabutylammonium chloride (2.0 eq, 1.044 mmol, 296 mg) where dissolved in 30 mL 1,2-difluorobenzene (*o*DFB) and stirred at room temperature for 2 hours. The colorless suspension was filtered over a PTFE syringe filter (pore size 0.22 µm) and the filtrate evaporated at reduced pressure to obtain **[(NBu$_4$)$_2$][2]** as a colorless solid (550 mg, 482 µmol, 92% yield). Gas phase diffusion of pentane into a concentrated solution of **[(NBu$_4$)$_2$][2]** in *o*DFB at −30 °C yielded single crystals suitable for X-ray diffraction.

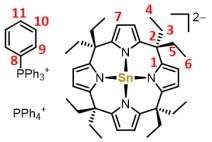
^{1}H NMR [^{1}H, ^{1}H,^{1}H-COSY] (600.18 MHz, THF-d_8, 295 K): δ [ppm] = 5.68 (*s*, ^{119}Sn-satellites $^4J_{Sn,H}$ = 12 Hz, H_7, 8H), 2.60 – 2.89 (*m*, H_8, 16), 2.08 (*q*, $^3J_{H,H}$ = 8.0 Hz, H_3, 8H), 1.95 (*q*, $^3J_{H,H}$ = 9.0 Hz, H_5, 8H), 1.34 (*m*, H_9, 16H), 1.24 (*q*, $^3J_{H,H}$ = 4.0 Hz, H_{10}, 16H), 1.18 (*t*, $^3J_{H,H}$ = 7.3 Hz, H_4, 12H), 0.89 (*t*, $^3J_{H,H}$ = 9.0 Hz, H_{11}, 24H), 0.39 (*t*, $^3J_{H,H}$ = 6.0 Hz, H_6, 12H).

^{13}C NMR [^{13}C{^{1}H}, ^{13}C-DEPT135, ^{1}H,^{13}C-HSQC, ^{1}H,^{13}C-HMBC] (150.92 MHz, THF-d_8, 295 K): δ [ppm] = 144.05 (*s*, C_1), 101.96 (*s*, C_7H), 59.15 (*s*, C_8H$_2$), 46.37 (*s*, C_2), 41.36 (*s*, C_5H$_2$), 29.40 (*s*, C_3H$_2$), 25.02 (*s*, C_9H$_2$), 21.00 (*s*, C_{10}H$_2$), 14.41 (*s*, C_{11}H$_3$), 12.02 (*s*, C_4H$_3$), 10.25 (*s*, C_6H$_3$).

^{119}Sn NMR [^{119}Sn,^{1}H-HMBC] (223.81 MHz, THF-d_8, 295 K): δ [ppm] = −517.83 (*s*).

EA: calcd. for $C_{68}H_{120}N_6Sn$: C, 71.62; H, 10.61; N, 7.37. Found: C, 71.41; H, 10.91; N, 7.69.

3.3 Tetraphenylphosphonium tin(II) *meso*-octaethylcalix[4]pyrrolate [$(PPh_4)_2$(*o*DFB)$_{0.5}$][2]



In a 50 mL Schlenk tube, **[Li_2(thf)$_x$][2]** (x = 4.2, 1.0 eq, 514 µmol, 500 mg) was dissolved in 15 mL *o*DFB and tetraphenylphosphonium chloride (2.0 eq, 1.028 mmol, 386 mg) was added while stirring at room temperature. The clear colorless solution immediately turned orange and a colorless solid precipitated. After stirring for 30 minutes precipitation of an orange solid occurred which could be redissolved by adding 6 mL acetonitrile. Filtration of the reaction mixture over a PTFE syringe filter (pore size 0.22 µm) to remove the lithium chloride formed during the reaction yielded an orange clear solution. To remove residue lithium chloride, the solvent was evaporated at reduced pressure and the remaining was redissolved in 9 mL *o*DFB/MeCN (2:1) and kept at −30 °C over night. Filtration over a PTFE syringe filter and subsequent addition of three times the volume of pentane at −30 °C caused the slow precipitation of **[$(PPh_4)_2$(*o*DFB)$_{0.5}$][2]** as a dark red solid (372 mg, 267 µmol, 52% yield). Gas phase diffusion of pentane into a concentrated solution of **[$(PPh_4)_2$(*o*DFB)$_{0.5}$][2]** in *o*DFB and CH_3CN at −30 °C yielded single crystals suitable for X-ray diffraction.

^{1}H NMR [^{1}H, ^{1}H,^{1}H-COSY] (399.89 MHz, THF-d_8/CD_3CN, 295 K): δ [ppm] = 7.78 (*m*, H_{11}, 8H), 7.58 – 7.68 (*m*, $H_{9,10}$, 32H), 7.20 – 7.30 (*m*, H_{oDFB}, 1H), 7.10 – 7.17 (*m*, H_{oDFB}, 1H), 5.66 (*s*, H_7, 8H), 1.79 – 1.94 (*m*, $H_{3,5}$, overlayed with CD_3CN, 16H), 0.72 (*t*, $^3J_{H,H}$ = 9.0 Hz, H_4, 12H), 0.58 (*t*, $^3J_{H,H}$ = 9.0 Hz, H_6, 12H).

^{13}C NMR [^{13}C{^{1}H}, ^{13}C-DEPT135, ^{1}H,^{13}C-HSQC, ^{1}H,^{13}C-HMBC] (100.55 MHz, THF-d_8/CD_3CN, 295 K): δ [ppm] = 143.45 (*s*, C_1), 137.20 (*d*, $^4J_{P,C}$ = 3.0 Hz, CH_{11}), 136.00 (*d*, $^2J_{P,C}$ = 10.4 Hz, CH_9), 131.93 (*d*, $^3J_{P,C}$ = 13.07 Hz, CH_{10}), 119.18 (*d*, $^1J_{P,C}$ = 89.49 Hz, C_8), 102.92 (*s*, C_7H), 47.06 (*s*, C_2), 39.69 (*s*, C_5H_2), 35.75 (*s*, C_3H_2), 11.99 (*s*, C_4H_3), 11.46 (*s*, C_6H_3).

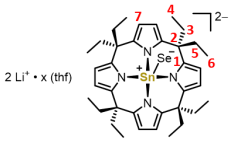
^{19}F NMR (376.27 MHz, THF-d_8/CD_3CN, 295 K): δ [ppm] = −140.36 - −140.29 (*m*, *o*DFB).

^{31}P{^{1}H} NMR (161.88 MHz, THF-d_8/CD_3CN, 295 K): δ [ppm] = 22.82 (*s*, PPh_4^+).

^{119}Sn NMR [^{119}Sn,^{1}H-HMBC] (223.81 MHz, THF-d_8/CD_3CN, 295 K): δ [ppm] = −485.98.

EA: calcd. for $C_{87}H_{90}FN_4P_2Sn$: C, 75.10; H, 6.52; N, 4.03. Found: C, 75.09; H, 6.57; N, 4.25.

3.4 Lithium tin(II) *meso*-octaethylcalix[4]pyrrolato selenide [$Li_2(thf)_x$][2-Se]



0.5 mL THF-d_8 were added to **[$Li_2(thf)_x$][2]** (x = 4.2, 1.0 eq, 20.56 µmol, 20 mg) and selenium powder (3.0 eq, 61.67 µmol, 4.9 mg) in a Young NMR tube and mixed at room temperature for 30 minutes. The dark red reaction solution was filtered over a PTFE syringe filter (pore size 0.22 µm) to remove surplus selenium and the selenium adduct was characterized *via* NMR spectroscopy and HR-MS ESI(−) measurements. No yield was determined.

^{1}H NMR [^{1}H, ^{1}H,^{1}H-COSY] (399.89 MHz, THF-d_8/CD_3CN, 295 K): δ [ppm] = 5.88 (*s*, H_7, 8H), 3.69 – 3.59 (m, thf, 13H), 2.13 (*q*, $^3J_{H,H}$ = 7.3 Hz, H_5, 6H), 2.02 – 1.91 (*m*, H_5, 2H), 1.85 (*q*, $^3J_{H,H}$ = 7.1 Hz, H_3, 8H), 1.81 – 1.74 (*m*, thf, 13H), 0.69 (*t*, $^3J_{H,H}$ = 7.4 Hz, H_6, 12H), 0.62 (*t*, $^3J_{H,H}$ = 7.1 Hz, H_4, 12H).

^{13}C NMR [^{13}C{^{1}H}, ^{13}C-DEPT135, ^{1}H,^{13}C-HSQC, ^{1}H,^{13}C-HMBC] (100.55 MHz, THF-d_8, 295 K): δ [ppm] = 143.64 (*s*, C_1), 104.13 (*s*, C_7H), 67.39 (*s*, thf), 45.43 (*s*, C_2), 38.13 (*s*, C_5H_2), 36.01 (*s*, C_3H_2), 25.53 (*s*, thf), 9.74 (*s*, C_4H_3), 9.65 (*s*, C_6H_3).

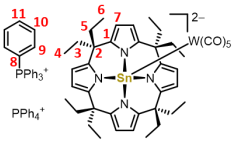
^{7}Li NMR (155.41 MHz, THF-d_8/CD_3CN, 295 K): δ [ppm] = −0.29 (*s*).

^{77}Se NMR [^{77}Se{^{1}H}, ^{1}H,^{77}Se-HMBC] (114.46 MHz, THF-d_8, 295 K): δ [ppm] = −391.99 (*s*).

^{119}Sn NMR [^{119}Sn,^{1}H-HMBC] (149.12 MHz, THF-d_8, 295 K): δ [ppm] = −560.18 (*s*).

HR-MS (ESI, negative, THF): calcd. for $[C_{36}H_{48}N_4SnSe+H]^-$($H^+$ from ESI atmosphere) m/z = 735.2225, found m/z =735.2225.

3.5 Tetraphenylphosphonium $^{1}\eta$-(tin(II) *meso*-octaethylcalix[4]pyrrolate) pentacarbonyl tungsten(0) [$(PPh_4)_2$][$W(^{1}\eta\text{-}2)(CO)_5$]



Tungsten hexacarbonyl (3.0 eq, 107.7 µmol, 38 mg) was suspended in 1.0 mL THF in a quartz glass flask and irradiated with a Hg-lamp for 4 hours until gas evolution stopped and solid got dissolved into a clear yellow solution. **[$(PPh_4)_2$(*o*DFB)$_{0.5}$][2]** (1.0 eq, 35.9 µmol, 50 mg) was added to the solution and stirred for 36 hours at room temperature. The solvent was removed at reduced pressure. Crystallization from a concentrated solution in acetonitrile (MeCN) layered with pentane at −30 °C yielded **[$(PPh_4)_2$][$W(^{1}\eta\text{-}2)(CO)_5$]** as a yellow-orange crystalline solid (35 mg, 21.9 µmol, 61% yield). Storing a concentrated solution of **[$(PPh_4)_2$][$W(^{1}\eta\text{-}2)(CO)_5$]** in MeCN at room temperature yielded single crystals suitable for X-ray diffraction.

^{1}H NMR [^{1}H, ^{1}H,^{1}H-COSY] (600.18 MHz, CD_3CN, 295 K): δ [ppm] = 7.92 – 7.87 (*m*, H_{11}, 8H), 7.74 – 7.70 (*m*, H_{10}, 16H), 7.68 – 7.63 (*m*, H_9, 16H), 5.77 (*s*, H_7, 8H), 1.92 (*q*, $^{3}J_{H,H}$ = 7.4 Hz, 8H), 1.86 (q, $^{3}J_{H,H}$ = 7.1 Hz, 8H), 0.65 (t, $^{3}J_{H,H}$ = 7.1 Hz, 12H), 0.50 (t, $^{3}J_{H,H}$ = 7.4 Hz, 12H).

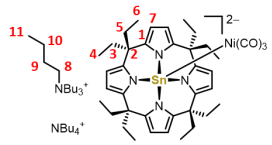
^{13}C NMR [^{13}C{^{1}H}, ^{13}C-DEPT135, ^{1}H,^{13}C-HSQC, ^{1}H,^{13}C-HMBC] (150.92 MHz, CD_3CN, 295 K): δ [ppm] = 202.48 (*s*, *C*O), 143.90 (*s*, C_1), 136.39 (*d*, $^{4}J_{P,C}$ = 3.0 Hz, CH_{11}), 135.68 (*d*, $^{2}J_{P,C}$ = 10.5 Hz, CH_9), 131.31 (*d*, $^{3}J_{P,C}$ = 13.07 Hz, CH_{10}), 118.89 (*d*, $^{1}J_{P,C}$ = 90.6 Hz, C_8), 105.07 (*s*, C_7H), 46.28 (*s*, C_2), 42.25 (*s*, C_5H_2), 34.10 (*s*, C_3H_2), 10.90 (*s*, C_4H_3), 10.50 (*s*, C_6H_3).

^{31}P{^{1}H} NMR (161.88 MHz, CD_3CN, 295 K): δ [ppm] = 22.92 (*s*, *P*Ph_4^+).

^{119}Sn NMR [^{119}Sn,^{1}H-HMBC] (223.81 MHz, CD_3CN, 295 K): δ [ppm] = −482.78.

EA: calcd. for $C_{89}H_{88}N_4O_5P_2SnW$: C, 64.47; H, 5.35; N, 3.38; O, 4.82; P, 3.74; Sn, 7.16; W, 11.09. Found: C, 63.10; H, 5.38; N, 3.43. Low carbon content might be related to metal carbide formation during combustion.[19]

3.6 Tetrabutylammonium $^{1}\eta$-(tin(II) *meso*-octaethylcalix[4]pyrrolate) triscarbonyl nickel(0) $[(NBu_4)_2][Ni(^{1}\eta\text{-}2)(CO)_3]$



Bis(cyclooctadiene)nickel(0) (1.3 eq, 57.0 µmol, 15.7 mg) and **[(NBu$_4$)$_2$][2]** (1.0 eq, 43.85 µmol, 50 mg) were dissolved in 0.5 mL THF-d_8 in a NMR pressure tube yielding a yellow clear solution. Addition of 3 atm CO gas and mixing at room temperature for 30 minutes caused the discoloration of the solution. Evaporation of the solvent at reduced pressure and washing of the crude with 5 mL pentane yielded **[(NBu$_4$)$_2$][Ni($^{1}\eta$-2)(CO)$_3$]** as an off-white crystalline solid (45 mg, 35.9 µmol, 82% yield).

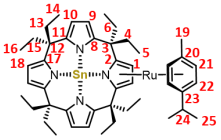
^{1}H NMR [^{1}H, ^{1}H,^{1}H-COSY] (600.18 MHz, THF-d_8, 295 K): δ [ppm] = 5.72 (*s*, H_7, 8H), 2.94 – 2.74 (m, H_8, 16H), 2.09 (*q*, $^{3}J_{H,H}$ = 6.3 Hz, H_3, 8H), 2.05 (*q*, $^{3}J_{H,H}$ = 6.1 Hz, H_5, 8H), 1.45 – 1.34 (m, H_9, 16H), 1.34 – 1.29 (m, 7H), 1.29 – 1.22 (*m*, H_{10}, 16H), 1.16 (*t*, $^{3}J_{H,H}$ = 7.2 Hz, H_4, 12H), 0.92 (*t*, $^{3}J_{H,H}$ = 7.3 Hz, H_{11}, 24H), 0.40 (*t*, $^{3}J_{H,H}$ = 7.3 Hz, H_6, 12H).

^{13}C NMR [^{13}C{^{1}H}, ^{13}C-DEPT135, ^{1}H,^{13}C-HSQC, ^{1}H,^{13}C-HMBC] (150.92 MHz, THF-d_8, 295 K): δ [ppm] = 198.46 (*s*, *C*O), 141.89 (*s*, C_1), 99.89 (*s*, C_7H), 56.14 (*s*, C_8H_2), 42.74 (*s*, C_2), 38.65 (*s*, C_5H_2), 26.37 (*s*, C_3H_2), 23.55 (*s*, C_9H_2), 20.38 (*s*, $C_{10}H_2$), 11.39 (*s*, $C_{11}H_3$), 9.02 (*s*, C_4H_3), 7.04 (*s*, C_6H_3).

^{119}Sn NMR [^{119}Sn,^{1}H-HMBC] (223.81 MHz, THF-d_8, 295 K): δ [ppm] = −335.24 (*s*).

EA: calcd. for $C_{71}H_{120}N_6O_3NiSn$: C, 66.42; H, 9.43; N, 6.55; O, 3.74; Ni, 4.52; Sn, 9.35. Found: C, 66.01; H, 9.73; N, 6.44.

3.7 Ruthenium(II) $^{5}\eta$-(tin(II) *meso*-octaethylcalix[4]pyrrolate) *para*-cymene Ru($^{5}\eta$-2)(*p*-cymene)



[Li$_2$(thf)$_x$][2] (x = 4.2, 1.0 eq, 102.85 µmol, 100 mg) and [{Ru(Cl)(*p*-cymene)}$_2$(μ-Cl)$_2$] (0.5 eq, 51.43 µmol, 31.5 mg) were dissolved in 4 mL THF and stirred at room temperature for 1 hour. The solvent was evaporated at reduced pressure and the remaining extracted with 6 mL *o*DFB. Filtration of the extract over a PTFE syringe filter (pore size 0.22 µm) to remove the lithium chloride formed during the reaction followed by the evaporation of the *o*DFB at reduced pressure yielded **Ru($^{5}\eta$-2)(*p*-cymene)** as an orange solid (83.5 mg, 93.58 µmol, 91% yield). Keeping a concentrated solution of **Ru($^{5}\eta$-2)(*p*-cymene)** in benzene for 12 hours at room temperature yielded single crystals suitable for X-ray diffraction.

^{1}H NMR [^{1}H, ^{1}H,^{1}H-COSY] (399.89 MHz, THF-d_8, 295 K): δ [ppm] = 5.99 (*d*, $^{3}J_{H,H}$ = 3.20 Hz, $H_{9,10}$, 2H), 5.93 (*d*, $^{3}J_{H,H}$ = 3.20 Hz, $H_{9,10}$, 2H), 5.91 (*s*, $H_{1,18}$, 2H), 5.76 (*s*, $H_{1,18}$, 2H), 5.46 (*d*, $^{3}J_{H,H}$ = 6.20 Hz, H_{22}, 2H), 5.06 (*d*, $^{3}J_{H,H}$ = 6.10 Hz, H_{21}, 2H), 2.71 (*hept*, $^{3}J_{H,H}$ = 6.90 Hz, H_{24}, 1H), 2.21 – 2.09 (*m*, $H_{4,6,13,15}$, 10H), 2.08 – 1.98 (*m*, $H_{4,15}$, 2H), 1.87 – 1.80 (*m*, $H_{4,15}$, 4H), 1.23 (*t*, $^{3}J_{H,H}$ = 7.3 Hz, $H_{9,14}$, 6H), 1.14 (*d*, $^{3}J_{H,H}$ = 6.9 Hz, H_{25}, 6H), 1.09 (*t*, $^{3}J_{H,H}$ = 7.2 Hz, $H_{9,14}$, 6H), 0.96 (*s*, H_{19}, 3H), 0.56 (*t*, $^{3}J_{H,H}$ = 7.3 Hz, $H_{5,16}$, 6H), 0.50 (*t*, $^{3}J_{H,H}$ = 7.3 Hz, $H_{5,16}$, 6H).

^{13}C NMR [^{13}C{^{1}H}, ^{13}C-DEPT135, ^{1}H,^{13}C-HSQC, ^{1}H,^{13}C-HMBC] (150.92 MHz, C_6D_6, 295 K): δ [ppm] = 146.05 (*s*, $C_{8,11}$), 142.32 (*s*, $C_{2,17}$), 136.13 (*s*, $C_{8,11}$), 134.27 (*s*, $C_{2,17}$), 110.68 (*s*, C_{20}), 110.53 (*s*, C_{23}), 105.49 (*s*, $C_{9,10,18}$H), 105.26 (*s*, $C_{9,10,18}$H), 105.00 (*s*, $C_{9,10,18}$H), 103.57 (*s*, C_1H), 89.82 (*s*, $C_{21,22}$H), 76.72 (*s*, $C_{21,22}$H), 46.40 (*s*, $C_{3,12}$), 43.42 (*s*, $C_{3,12}$), 34.44 (*s*, C_{24}H) 31.13 (*s*, $C_{6,15}H_2$), 29.54 (*s*, $C_{6,15}H_2$), 28.65 (*s*, $C_{4,13}H_2$), 27.07 (*s*, $C_{4,13}H_2$), 17.29 (*s*, $C_{19}H_3$), 11.41 (*s*, $C_{25}H_3$), 10.26 (*s*, $C_{4,13}H_3$), 10.02 (*s*, $C_{4,13}H_3$), 9.44 (*s*, $C_{6,15}H_3$), 8.18 (*s*, $C_{6,15}H_3$).

^{119}Sn NMR [^{119}Sn,^{1}H-HMBC] (149.12 MHz, THF-d_8, 295 K): δ [ppm] = −424.83 (*s*).

EA: calcd. for $C_{46}H_{62}N_4RuSn$: C, 61.86; H, 7.00; N, 6.28; Ru, 11.42; Sn, 13.44. Found: C, 61.78; H, 7.03; N, 6.24.

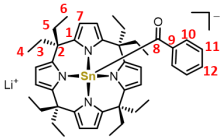
3.8 Reaction of [$Li_2(thf)_x$][2] with Electrophiles

[$Li_2(thf)_x$][2] (x = 4.2, 1.0 eq, 17.54 µmol, 17.0 mg) was dissolved in 0.45 mL toluene-d_8 and one equivalent of the respective electrophile was added in one portion at room temperature. The reaction conditions for each electrophile are summarized in Table S1 below. The reaction products were characterized by ^{1}H, ^{13}C, ^{119}Sn as well as 2D-NMR methods and HRMS ESI(−) measurements. For Entry 3 storing of the reaction solution at −30 °C after removal of the precipitated lithium chloride yielded single crystals suitable for X-ray diffraction.

Table S1: Reaction conditions for the reaction of **[$Li_2(thf)_x$][2]** with electrophiles.

Entry	Electrophile	Reaction Conditions
1	Methylene chloride	No reaction
2	Benzyl chloride	Unselective reaction forming mixture of compounds
3	Benzoyl chloride	Reaction completed at rt within minutes
4	Benzaldehyde	Reacted at rt over 20 hours, formation of side products
5	4-CF_3-Benzaldehyde	Reacted at rt over 20 hours, formation of side products

3.8.1 Entry 3 (Benzoyl Chloride)



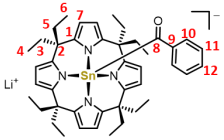
^{1}H NMR [^{1}H, ^{1}H,^{1}H-COSY] (600.15 MHz, Toluene-d_8, 295 K): δ [ppm] = 7.26 – 7.21 (*m*, H_{10}, 2H), 7.00 – 6.98 (*m*, $H_{11'}$ 2H), 6.94 (*d*, $^{3}J_{H,H}$ = 7.3 Hz, H_{12}, 1H), 6.29 (*s*, H_7, 8H), 2.04 (*q*, $^{3}J_{H,H}$ = 7.2 Hz, H_3, 8H), 1.95 (*q*, $^{3}J_{H,H}$ = 7.3 Hz, H_5, 8H), 0.91 (*t*, $^{3}J_{H,H}$ = 7.2 Hz, H_4, 13H), 0.86 (*t*, $^{3}J_{H,H}$ = 7.3 Hz, H_6, 13H).

^{13}C NMR [$^{13}C\{^{1}H\}$, ^{13}C-DEPT135, ^{1}H,^{13}C-HSQC, ^{1}H,^{13}C-HMBC] (150.92 MHz, Toluene.-d_8, 295 K): δ [ppm] = 143.93 (*s*, C_1), 134.91 (*s*, $C_{12}H$), 131.40 (*s*, C_9), 129.15 (*s*, $C_{10}H$), 128.22 (*s*, $C_{11}H$), 125.38 (*s*, C_8), 106.57 (*s*, $^{117/119}Sn$-satelites $^{3}J_{Sn,C}$ = 30 Hz, C_7H), 67.86 (*s*, $C_{thf}H_2$), 45.60 (*s*, $^{117/119}Sn$-satelites $^{3}J_{Sn,C}$ = 7.5 Hz, C_2), 40.42 (C_5H_2), 34.89 (*s*, C_3H_2), 25.67 (*s*, $C_{thf}H_2$), 10.14 (*s*, C_4H_3), 10.02 (*s*, C_6H_3).

^{119}Sn NMR [^{119}Sn,^{1}H-HMBC] (149.12 MHz, Toluene-d_8, 295 K): δ [ppm] = −487.99.

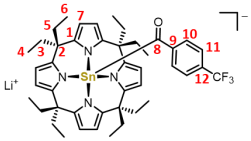
HR-MS (ESI, negative, THF): calcd. for $C_{43}H_{53}N_4OSn^-$ m/z = 761.3267, found m/z = 761.3283.

3.8.2 Entry 4 (Benzaldehyde)



HR-MS (ESI, negative, THF): calcd. for $C_{43}H_{53}N_4OSn^-$ m/z = 761.3267, found m/z = 761.3243.

3.8.3 Entry 5 (4-CF_3-Benzaldehyde)



^{1}H NMR [^{1}H, ^{1}H,^{1}H-COSY] (399.89 MHz, Toluene-d_8, 295 K): δ [ppm] = 7.41 (*d*, $^{3}J_{H,H}$ = 7.8 Hz, H_{10}, 2H), 6.98 (*d*, $^{3}J_{H,H}$ = 7.8 Hz, H_{11}, 2H), 6.34 (*s*, H_7, 8H), 1.94 (*q*, $^{3}J_{H,H}$ = 7.3 Hz, H_3, 8H), 1.75 (*q*, $^{3}J_{H,H}$ = 7.3 Hz, H_5, 8H), 0.76 (t, $^{3}J_{H,H}$ = 7.1 Hz, H_4, 12H), 0.73 (t, $^{3}J_{H,H}$ = 7.1 Hz, H_6, 12H).

^{13}C NMR [^{13}C{^{1}H}, ^{13}C-DEPT135, ^{1}H,^{13}C-HSQC, ^{1}H,^{13}C-HMBC] (100.55 MHz, Toluene-d_8, 295 K): δ [ppm] = 145.40 (*s*, C_1), 136.11 (*s*, C_{12}), 129.16 (*s*, C_9), 127.82 (*s*, C_{10}H), 126.35 (*s*, C_{11}H), 126.31 (*s*, C_8), 106.64 (*m*, CF_3), 105.45 (*s*, C_7H), 47.20 (*s*, C_2), 35.61 (C_5H_2), 35.04 (*s*, C_3H_2), 10.02 (*s*, C_4H_3), 9.71 (*s*, C_6H_3).

^{19}F NMR (149.12 MHz, THF-d_8, 295 K): δ [ppm] = −62.36.

^{119}Sn NMR [^{119}Sn,^{1}H-HMBC] (149.12 MHz, THF-d_8, 295 K): δ [ppm] = −750.37.

HR-MS (ESI, negative, THF): calcd. for $C_{44}H_{52}N_4OF_3Sn^-$ m/z = −829.3141, found m/z = −829.3159.

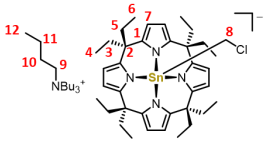
3.9 Reaction of [(NBu$_4$)$_2$][2] with Electrophiles

[(NBu$_4$)$_2$][2] (1.0 eq, 17.54 µmol, 20.0 mg) was dissolved in 0.45 mL THF-d_8 and one equivalent of the respective electrophile was added in one portion at room temperature. The reaction conditions for each electrophile are summarized in Table S2 below. The products were characterized by ^{1}H, ^{13}C, ^{119}Sn as well as 2D-NMR methods and HRMS ESI(−) measurements.

Table S2: Reaction conditions for the reaction of **[(NBu$_4$)$_2$][2]** with electrophiles. The yield was determined by NMR spectroscopy.

Entry	Electrophile	Reaction Conditions
1	Methylene chloride	Near quantitative yield after mixed at rt for 24h
2	Benzyl chloride	Near quantitative yield at rt within minutes
3	Benzoyl chloride	Near quantitative yield at rt within minutes
4	Benzaldehyde	No reaction
5	4-CF_3-Benzaldehyde	No reaction
6	Iodobenzene	Quantitative reduction of iodobenzene to benzene at rt, 48h

3.9.1 Entry 1 (Methylene Chloride)



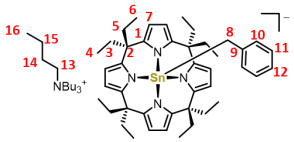
^{1}H NMR [^{1}H, ^{1}H,^{1}H-COSY] (399.89 MHz, THF-d_8, 295 K): δ [ppm] = 5.90 (*s*, $^{117/119}$Sn-satellites $^{4}J_{Sn,H}$ = 8.0 Hz, H_7, 8H), 3.56 – 3.35 (*m*, H_{13}, 16H), 2.67 (*s*, $^{117/119}$Sn-satellites $^{2}J_{Sn,H}$ = 36.0 Hz, H_8, 2H), 1.90 (*q*, $^{3}J_{H,H}$ = 7.2 Hz, H_5, 8H), 1.86 (*q*, $^{3}J_{H,H}$ = 7.2 Hz, H_3, 8H), 1.78 – 1.68 (*m*, H_{14} 16H, overlayed with THF-d_8), 1.46 – 1.35 (*m*, H_{15}, 16H), 0.99 (*t*, $^{3}J_{H,H}$ = 7.4 Hz, H_{16}, 24H), 0.75 (*t*, $^{3}J_{H,H}$ = 7.2 Hz, H_4, 12H), 0.62 (*t*, $^{3}J_{H,H}$ = 7.3 Hz, H_6, 12H).

^{13}C NMR [^{13}C{^{1}H}, ^{13}C-DEPT135, ^{1}H,^{13}C-HSQC, ^{1}H,^{13}C-HMBC] (100.55 MHz, THF-d_8, 295 K): δ [ppm] = 143.56 (*s*, $^{117/119}$Sn-satellites $^{3}J_{Sn,C}$ = 8.0 Hz,C_1), 106.22 (*s*, $^{117/119}$Sn-satellites $^{3}J_{Sn,C}$ = 23.1 Hz, C_7H), 59.64 (*s*, C_9H_2), 46.49 (*s*, C_2), 40.26 (*s*, $C_{3,5}H_2$), 38.74 (*s*, C_8H_2), 36.05 (*s*, $C_{3,5}H_2$), 25.15 (*s*, $C_{10}H_2$), 20.90 (*s*, $C_{11}H_2$), 14.28 (*s*, $C_{12}H_3$), 10.92 (*s*, $C_{4,6}$H), 10.52 (*s*, $C_{4,6}$H).

^{119}Sn NMR [^{119}S n{^{1}H}, ^{119}Sn,^{1}H-HMBC] (149.12 MHz, THF-d_8, 295 K): δ [ppm] = −477.52.

HR-MS (ESI, negative, THF): calcd. for $C_{37}H_{50}N_4SnCl^-$ m/z = 747.3448, found m/z = 747.3456.

3.9.2 Entry 2 (Benzyl chloride)



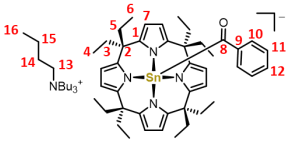
^{1}H NMR [^{1}H, ^{1}H,^{1}H-COSY] (399.89 MHz, THF-d_8, 295 K): δ [ppm] = 6.78 – 6.69 (*m*, H_{11}, 2H), 6.67 – 6.60 (*m*, H_{12}, 1H), 6.33 – 6.25 (m, H_{10}, 2H), 5.95 (*s*, $^{117/119}$Sn-satellites $^{4}J_{Sn,H}$ = 8.0 Hz, H_7, 8H), 3.55 – 3.42 (*m*, H_{13}, 16H), 2.20 (*s*, ^{119}Sn-satellites $^{2}J_{Sn,H}$ = 116.6 Hz, ^{117}Sn-satellites $^{2}J_{Sn,H}$ = 111.2 Hz, H_8, 2H), 1.83 – 1.68 (*m*, $H_{3,5,14}$ 32H), 1.46 – 1.35 (*m*, H_{15}, 16H), 0.99 (*t*, $^{3}J_{H,H}$ = 7.4 Hz, H_{16}, 24H), 0.60 (*t*, $^{3}J_{H,H}$ = 7.1 Hz, $H_{4,6}$, 24H).

^{13}C NMR [^{13}C{^{1}H}, ^{13}C-DEPT135, ^{1}H,^{13}C-HSQC, ^{1}H,^{13}C-HMBC] (100.55 MHz, THF-d_8, 295 K): δ [ppm] = 143.91 (*s*, $^{117/119}$Sn-satellites $^{3}J_{Sn,C}$ = 8.0 Hz, C_1), 141.46 (*s*, C_9), 130.74 (*s*, C_{10}H), 128.02 (*s*, C_{11}H), 123.69 (*s*, C_{12}H), 106.90 (*s*, $^{117/119}$Sn-satellites $^{3}J_{Sn,C}$ = 23.1 Hz, C_7H), 59.64 (*s*, $C_{13}H_2$), 46.65 (*s*, C_2), 39.41 (*s*, $C_{3,5}H_2$), 39.37 (*s*, $C_{3,5}H_2$), 31.76 (*s*, C_8H_2), 25.14 (*s*, $C_{14}H_2$), 20.89 (*s*, $C_{15}H_2$), 14.27 (*s*, $C_{16}H_3$), 10.68 (*s*, $C_{4,6}$H), 10.62 (*s*, $C_{4,6}$H).

^{119}Sn NMR [^{119}Sn{^{1}H}, ^{119}Sn,^{1}H-HMBC] (149.12 MHz, THF-d_8, 295 K): δ [ppm] = −409.19 (*s*).

HR-MS (ESI, negative, THF): calcd. for $C_{43}H_{55}N_4Sn^-$ m/z = 747.3448, found m/z = 747.3456.

3.9.3 Entry 3 (Benzoyl chloride)



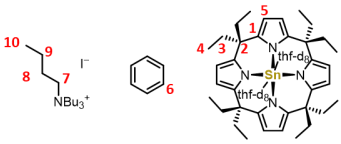
^{1}H NMR [^{1}H, ^{1}H,^{1}H-COSY] (399.89 MHz, THF-d_8, 295 K): δ [ppm] = 7.20 – 7.13 (*m*, H_{12}, 1H), 7.11 – 7.00 (*m*, $H_{10,11}$, 4H), 5.89 (*s*, $^{117/119}$Sn-satellites $^{4}J_{Sn,H}$ = 12.0 Hz, H_7, 8H), 3.54 – 3.44 (*m*, H_{13}, 16H), 1.83 – 1.68 (*m*, $H_{3,5,14}$ overlayed, 32H), 1.35 – 1.46 (*m*, H_{15}, 16H), 0.99 (*t*, $^{3}J_{H,H}$ = 7.4 Hz, H_{16}, 24H), 0.66 (*t*, $^{3}J_{H,H}$ = 7.1 Hz, $H_{4,6}$, 12H), 0.64 (*t*, $^{3}J_{H,H}$ = 7.1 Hz, $H_{4,6}$, 12H).

^{13}C NMR [^{13}C{^{1}H}, ^{13}C-DEPT135, ^{1}H,^{13}C-HSQC, ^{1}H,^{13}C-HMBC] (100.55 MHz, THF-d_8, 295 K): δ [ppm] = 235.44 (*s*, C_8), 143.23 (*s*, $^{117/119}$Sn-satellites $^{3}J_{Sn,C}$ = 9.0 Hz, C_1), 143.07 (*s*, C_9), 135.49, 132.20 (*s*, C_{12}H), 131.37, 129.98, 129.39 (*s*, $C_{10,11}$H), 128.93 (*s*, $C_{10,11}$H), 106.03 (*s*, $^{117/119}$Sn-satellites $^{3}J_{Sn,C}$ = 26.1 Hz, C_7H), 59.63 (*s*, $C_{13}H_2$), 45.96 (*s*, C_2), 39.07 (*s*, $C_{3,5}H_2$), 37.60 (*s*, $C_{3,5}H_2$), 25.15 (*s*, $C_{14}H_2$), 20.89 (*s*, $C_{15}H_2$), 14.30 (*s*, $C_{16}H_3$), 10.82 (*s*, $C_{4,6}$H), 10.54 (*s*, $C_{4,6}$H).

^{119}Sn NMR [^{119}Sn{^{1}H}, ^{119}Sn,^{1}H-HMBC] (149.12 MHz, THF-d_8, 295 K): δ [ppm] = −542.67.

HR-MS (ESI, negative, THF): calcd. for $C_{43}H_{53}N_4OSn^-$ m/z = 761.3267, found m/z = 761.3256.

3.9.4 Entry 6 (Iodobenzene)



^{1}H NMR [^{1}H, ^{1}H,^{1}H-COSY] (399.89 MHz, THF-d_8, 295 K): δ [ppm] = 7.30 (s, H_6, 5H), 6.11 (*s*, $^{117/119}$Sn-satellites $^{4}J_{Sn,H}$ = 16.0 Hz, H_5, 8H), 3.47 – 3.37 (*m*, H_7, 16H), 1.84 (*q*, $^{3}J_{H,H}$ = 7.3 Hz, H_3, 16H), 1.79 – 1.68 (*m*, H_7 overlayed, 21H), 1.50 – 1.37 (*m*, H_8 overlayed, 25H), 1.36 – 1.25 (*m*, H_9 overlayed, 9H), 1.00 (*t*, $^{3}J_{H,H}$ = 7.3 Hz, H_{10} overlayed, 28H), 0.65 (*t*, $^{3}J_{H,H}$ = 7.3 Hz, H_4, 24H).

^{13}C NMR [^{13}C{^{1}H}, ^{13}C-DEPT135, ^{1}H,^{13}C-HSQC, ^{1}H,^{13}C-HMBC] (100.55 MHz, THF-d_8, 295 K): δ [ppm] = 143.14 (*s*, $^{117/119}$Sn-satellites $^{2}J_{Sn,C}$ = 7.0 Hz, C_1), 129.20 (*s*, C_6), 109.26 (*s*, $^{117/119}$Sn-satellites $^{2}J_{Sn,C}$ = 42.2 Hz, C_5H), 59.76 (*s*, C_7H_2), 46.78 (*s*, C_2), 30.93 (*s*, C_3H_2), 25.29 (*s*, overlayed with THF-d_8, C_9H_2), 20.83 (*s*, C_9H_2), 14.33 (*s*, $C_{10zz}H_3$), 10.22 (*s*, C_4H_3).

^{119}Sn NMR [^{119}Sn{^{1}H}, ^{119}Sn,^{1}H-HMBC] (149.12 MHz, THF-d_8, 295 K): δ [ppm] = −560.83.

4 NMR Spectra

4.1 [Li$_2$(thf)$_x$][2]

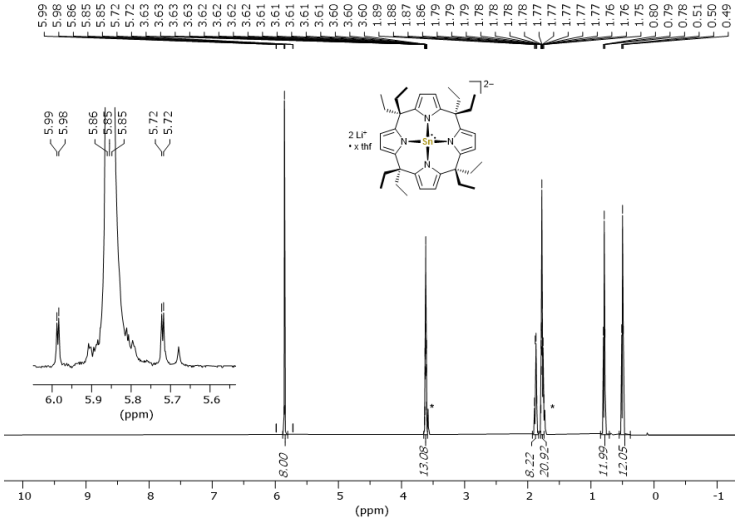


Figure S1. ^{1}H NMR spectrum of **[Li$_2$(thf)$_x$][2]** (600.18 MHz, THF-d_8, 295 K). Solvent resonances are indicated by an asterisk (*).

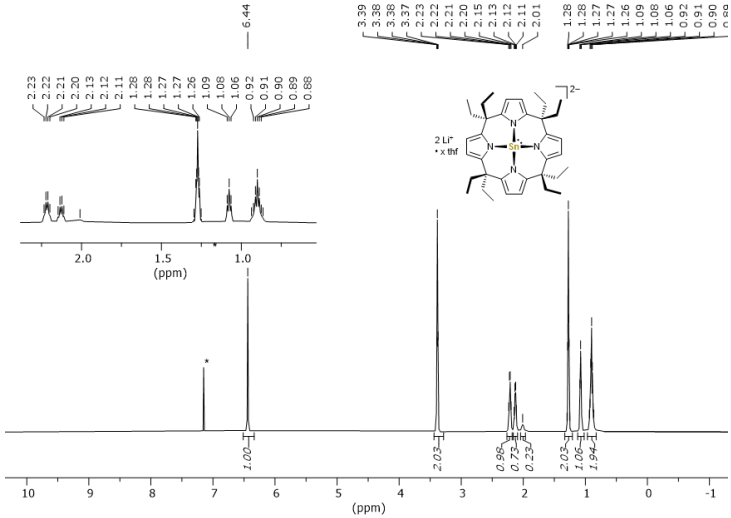


Figure S2. ^{1}H NMR spectrum of **[Li$_2$(thf)$_x$][2]** (600.18 MHz, C_6D_6, 295 K). Solvent resonances are indicated by an asterisk (*).

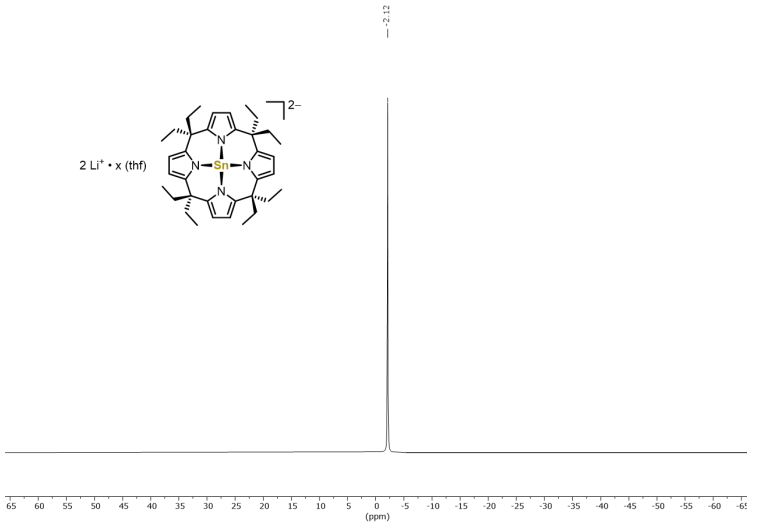


Figure S3. ^{7}Li NMR spectrum of **[Li$_2$(thf)$_x$][2]** (233.24 MHz, THF-d_8, 295 K).

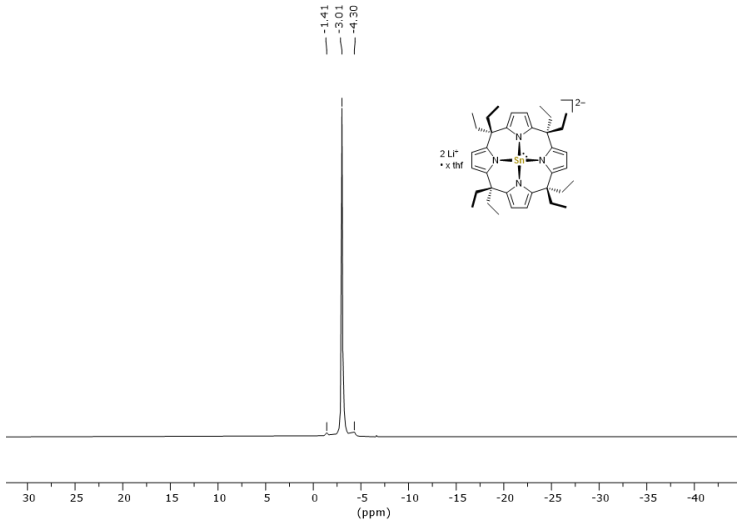


Figure S4. ^{7}Li NMR spectrum of **[Li$_2$(thf)$_x$][2]** (233.24 MHz, C_6D_6, 295 K).

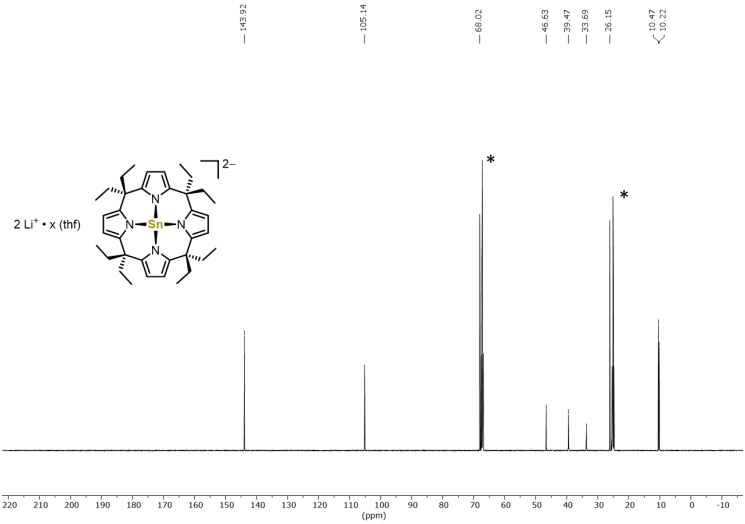


Figure S5. ^{13}C NMR spectrum of **[Li$_2$(thf)$_x$][2]** (150.92 MHz, THF-d_8, 295 K). Solvent resonances are indicated by an asterisk (*).

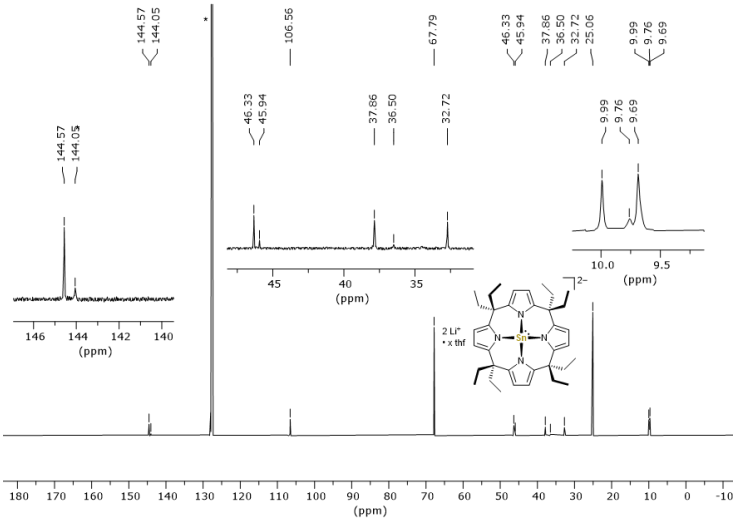


Figure S6. ^{13}C NMR spectrum of **[Li$_2$(thf)$_x$][2]** (150.92 MHz, C_6D_6, 295 K). Solvent resonances are indicated by an asterisk (*).

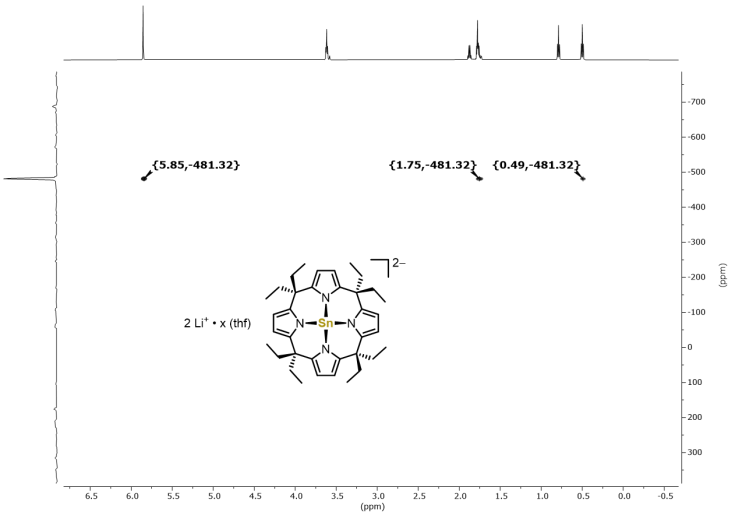


Figure S7. ^{119}Sn-^{1}H HMBC NMR spectrum of **[Li_2(thf)$_x$][2]** (THF-d_8, 295 K).

4.2 [(NBu_4)$_2$][2]

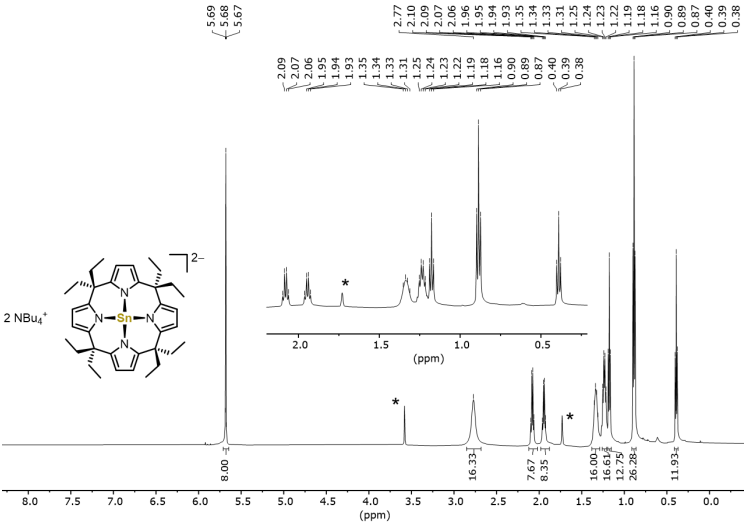


Figure S8. ^{1}H NMR spectrum of **[(NBu_4)$_2$][2]** (600.18 MHz, THF-d8, 295 K). Solvent resonances are indicated by an asterisk (*).

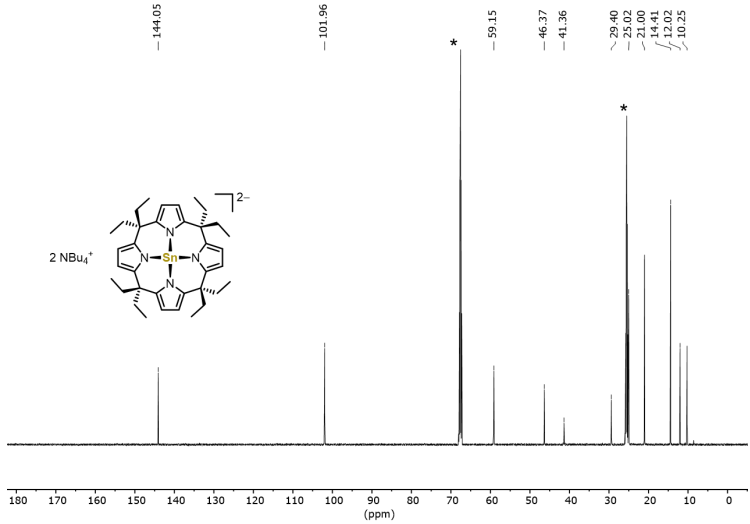


Figure S9. ^{13}C NMR spectrum of **[(NBu$_4$)$_2$][2]** (150.92 MHz, THF-d_8, 295 K). Solvent resonances are indicated by an asterisk (*).

4.3 [(PPh$_4$)$_2$(oDFB)$_{0.5}$][2]

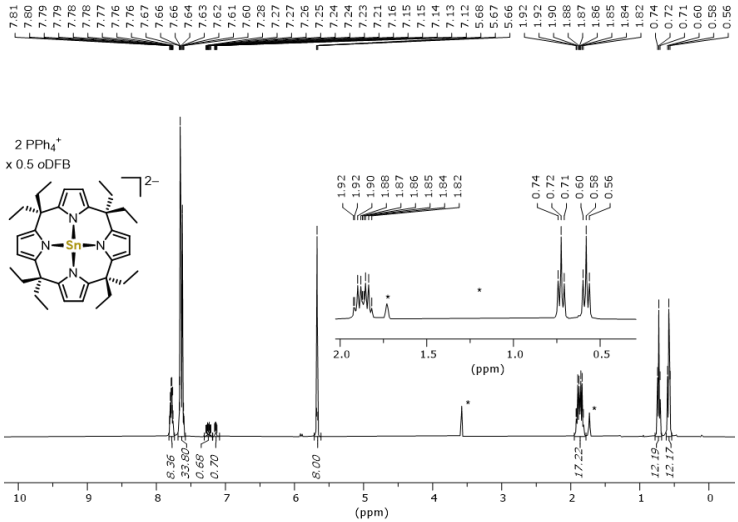


Figure S10. ^{1}H NMR spectrum of **[(PPh$_4$)$_2$(*o*DFB)$_{0.5}$][2]** (399.89 MHz, THF-d_8/CD$_3$CN, 295 K). Solvent resonances are indicated by an asterisk (*).

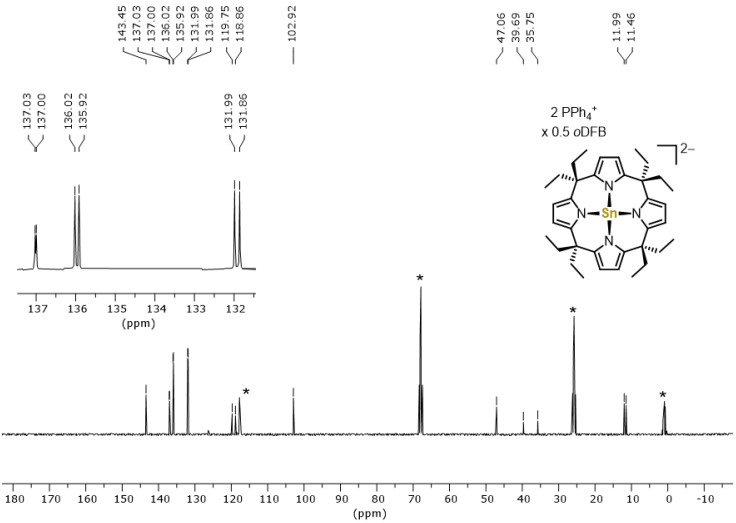


Figure S11. ^{13}C NMR spectrum of **[(PPh$_4$)$_2$(*o*DFB)$_{0.5}$][2]** (100.55 MHz, THF-d_8/CD_3CN, 295 K). Solvent resonances are indicated by an asterisk (*).

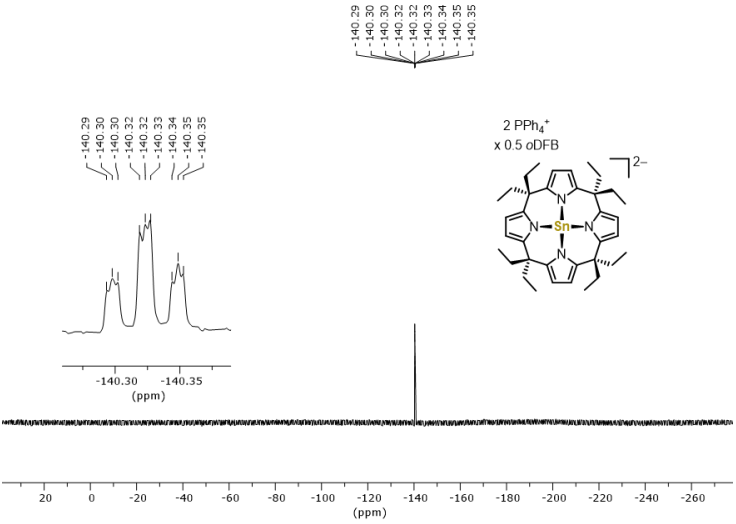


Figure S12. ^{19}F NMR spectrum of **[(PPh$_4$)$_2$(*o*DFB)$_{0.5}$][2]** (376.27 MHz, THF-d_8/CD_3CN, 295 K).

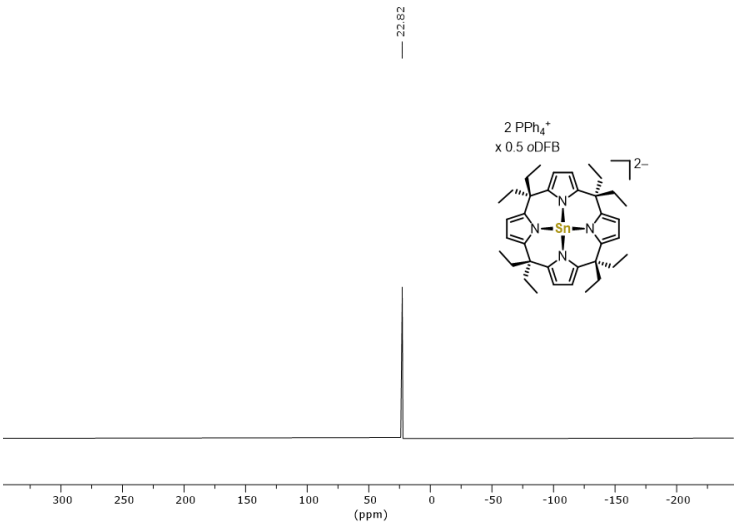


Figure S13. $^{31}P\{^{1}H\}$ NMR spectrum of **[(PPh$_4$)$_2$(*o*DFB)$_{0.5}$][2]** (161.88 MHz, THF-d_8/CD_3CN, 295 K).

4.4 [Li$_2$(thf)$_x$][2-Se]

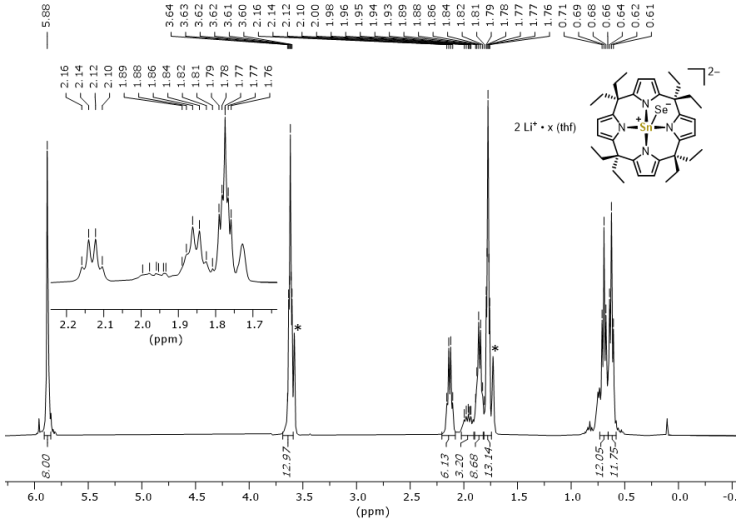


Figure S14. ^{1}H NMR spectrum of **[Li$_2$(thf)$_x$][2-Se]** (399.89 MHz, THF-d_8, 295 K). Solvent resonances are indicated by an asterisk (*).

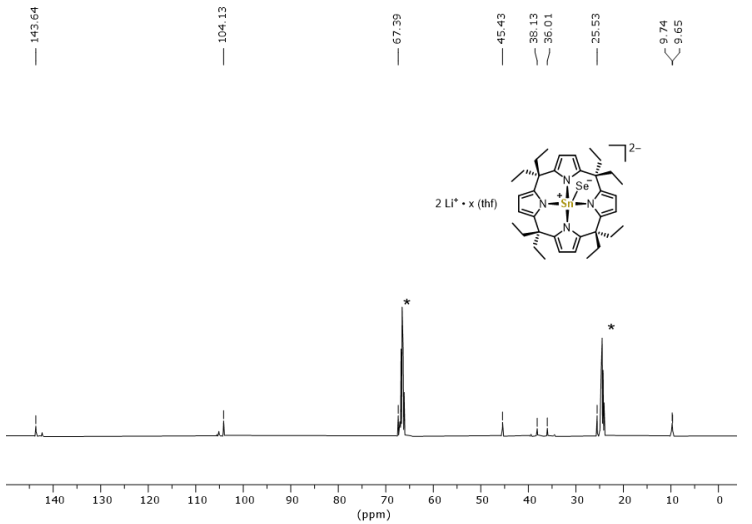


Figure S15. ^{13}C NMR spectrum of **[Li$_2$(thf)$_x$][2-Se]** (100.55 MHz, THF-d_8, 295 K). Solvent resonances are indicated by an asterisk (*).

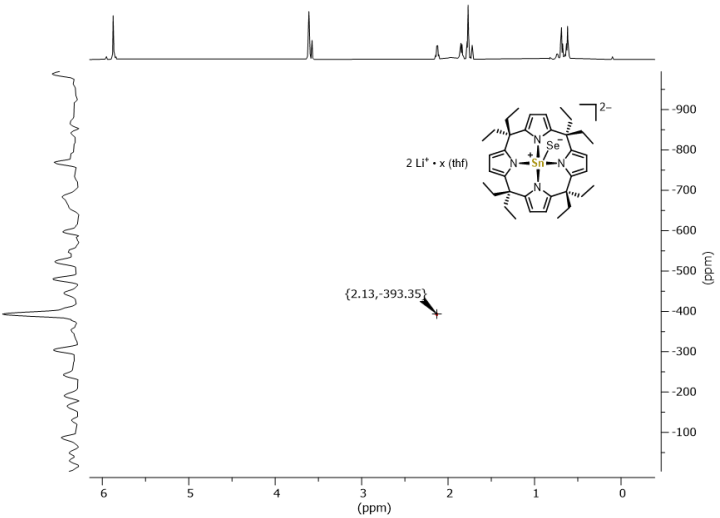


Figure S16. ^{77}Se-^{1}H HMBC NMR spectrum of **[Li$_2$(thf)$_x$][2]** (THF-d_8, 295 K).

4.5 [(PPh$_4$)$_2$][W(^{2}η-2)(CO)$_5$]

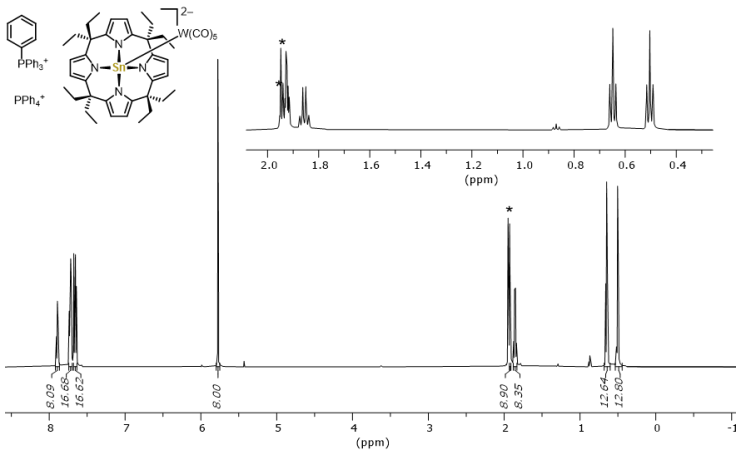


Figure S17. ^{1}H NMR spectrum of **[(PPh$_4$)$_2$][W(^{1}η-2)(CO)$_5$]** (600.15 MHz, MeCN-d_3, 295 K). Solvent resonances are indicated by an asterisk (*).

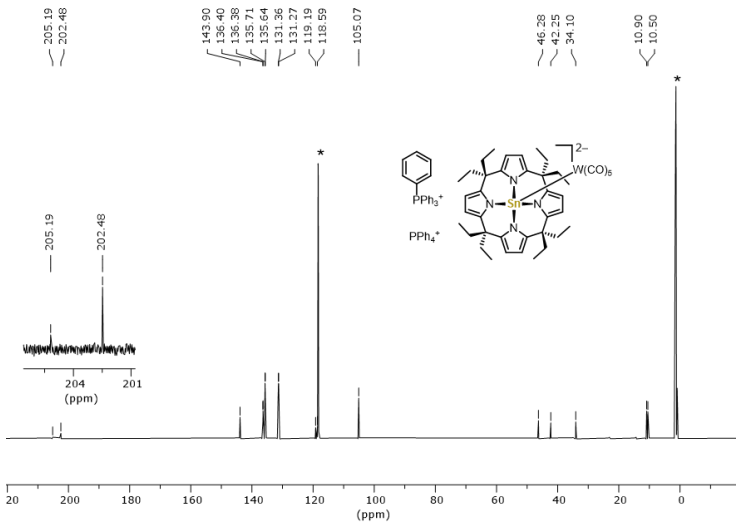


Figure S18. ^{13}C NMR spectrum of **[(PPh$_4$)$_2$][W(^{1}η-2)(CO)$_5$]** (150.92 MHz, MeCN-d_3, 295 K). Solvent resonances are indicated by an asterisk (*).

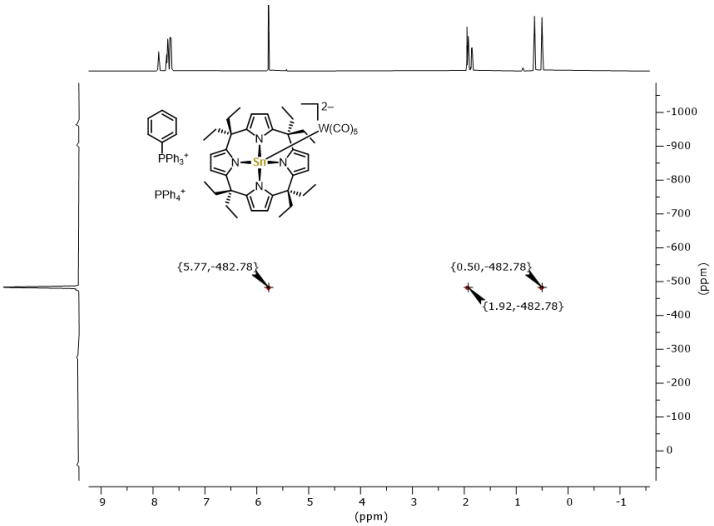


Figure S19. ^{119}Sn-^{1}H HMBC NMR spectrum of **[(PPh$_4$)$_2$][W(^{1}η-2)(CO)$_5$]** (MeCN-*d*$_3$, 295 K).

4.6 [(NBu$_4$)$_2$][Ni(^{1}η-2)(CO)$_3$]

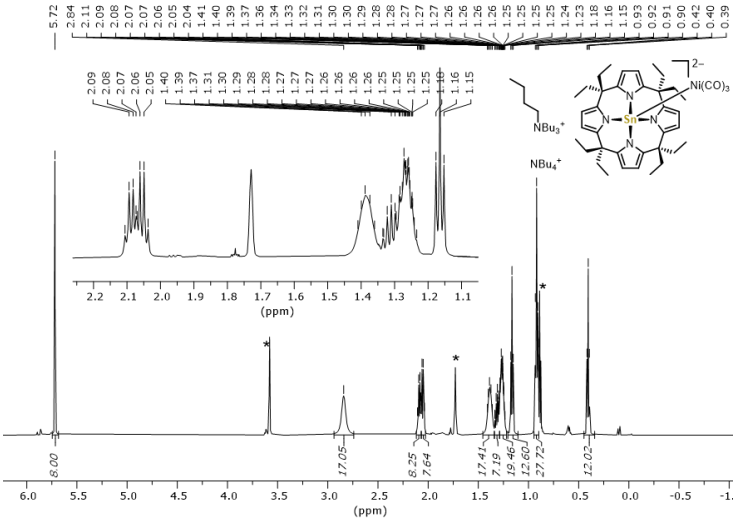


Figure S20. ^{1}H NMR spectrum of **[(NBu$_4$)$_2$][Ni(^{1}η-2)(CO)$_3$]** (600.15 MHz, THF-*d*$_8$, 295 K). Solvent resonances and resonances of residue pentane are indicated by an asterisk (*).

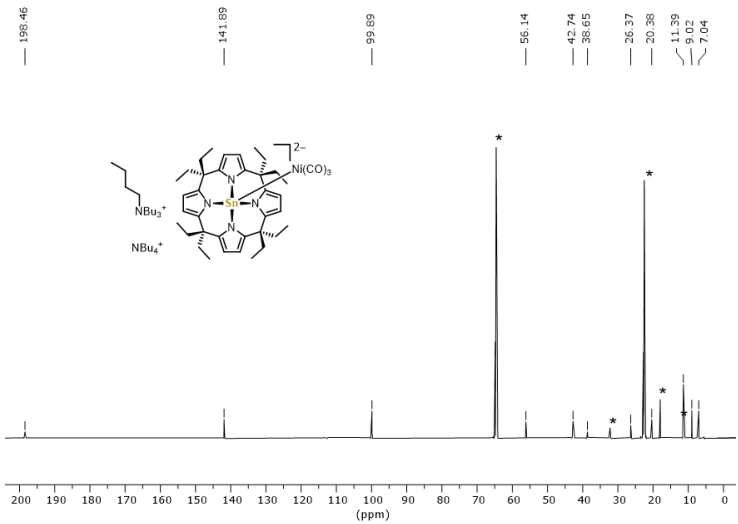


Figure S21. ^{13}C NMR spectrum of **[(NBu$_4$)$_2$][Ni(^{1}η-2)(CO)$_3$]** (150.92 MHz, THF-d_8, 295 K). Solvent resonances and resonances of residue pentane are indicated by an asterisk (*).

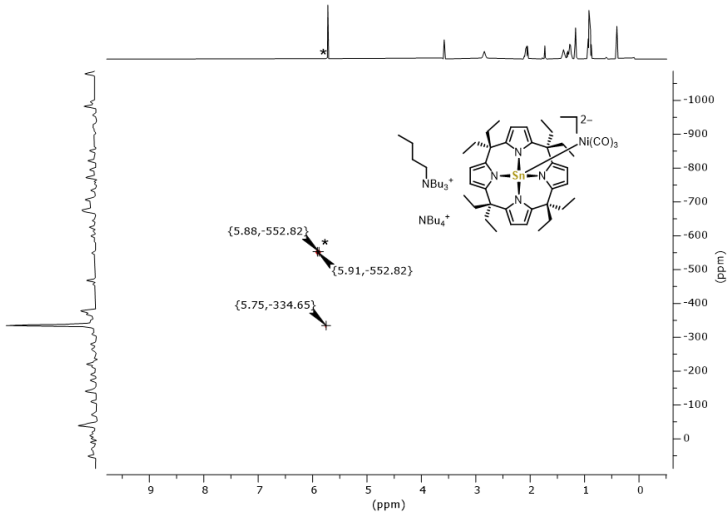


Figure S22. ^{119}Sn-^{1}H HMBC NMR spectrum of **[(NBu$_4$)$_2$][Ni(^{1}η-2)(CO)$_3$]** (THF-d_8, 295 K). Traces of free stannate(II) dianion formed by decomposition are indicated by an asterisk (*).

4.7 Ru(5η-2)(cymene)

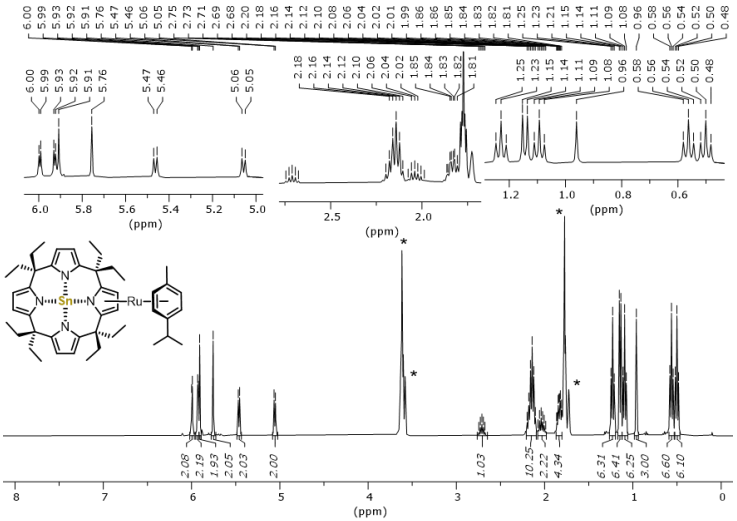


Figure S23. ^{1}H NMR spectrum of **Ru(5η-2)(cymene)** (400 MHz, THF-d_8, 295 K). Solvent resonances and resonances of residue pentane are indicated by an asterisk (*).

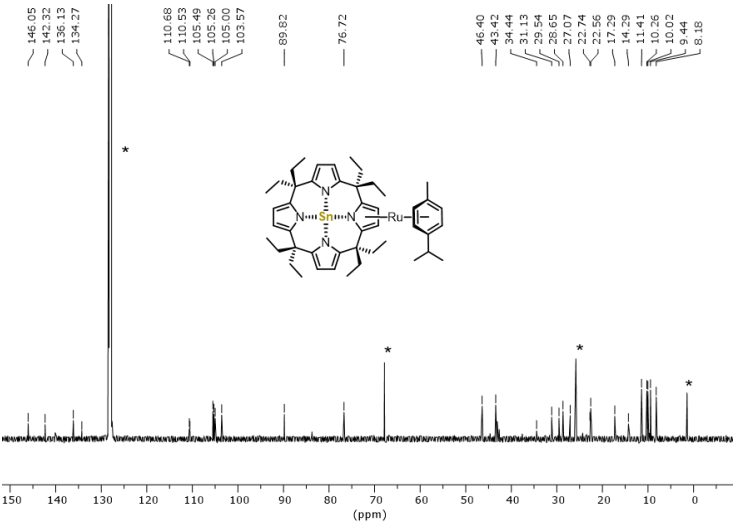


Figure S24. ^{13}C NMR spectrum of **Ru(5η-2)(cymene)** (150.29 MHz, C_6D_6, 295 K). Solvent resonances and resonances of residue pentane are indicated by an asterisk (*).

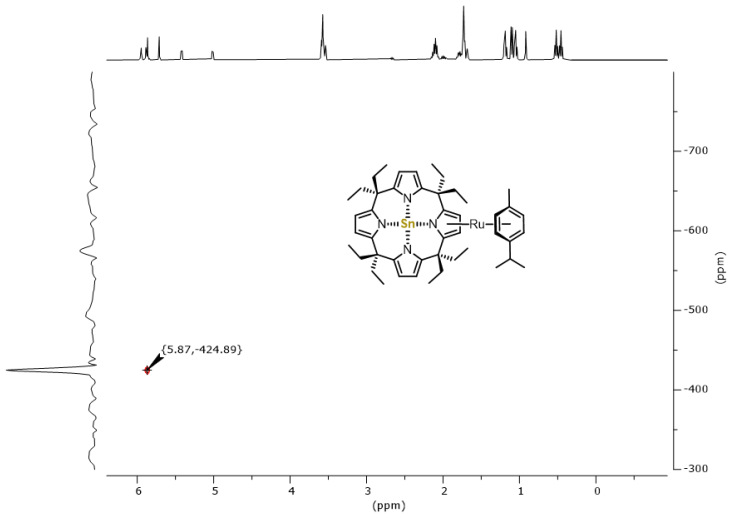


Figure S25. ^{119}Sn-^{1}H HMBC NMR spectrum of **Ru(^{5}η-2)(cymene)** (THF-d_8, 295 K).

4.8 Reaction of [Li$_2$(thf)$_x$][2] with Benzoyl chloride

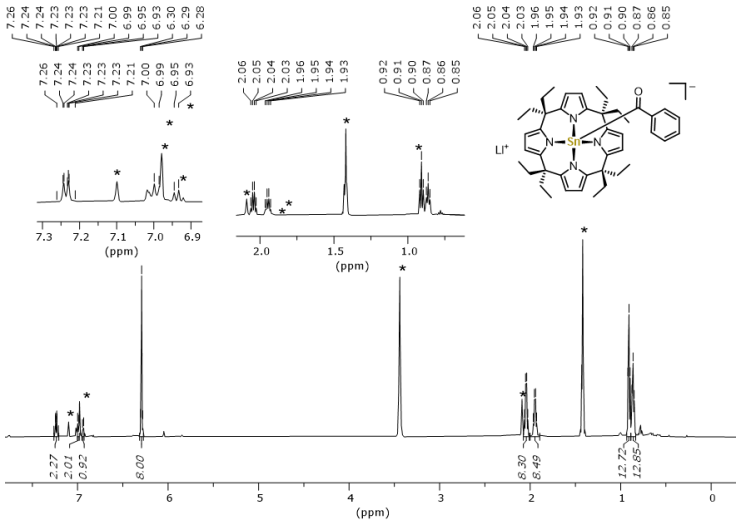


Figure S26. ^{1}H NMR spectrum of the reaction of **[Li$_2$(thf)$_x$][2]** with benzoyl chloride (600.15 MHz, Toluene-d8, 295 K). Solvent resonances and resonances of THF from starting material are indicated by an asterisk (*).

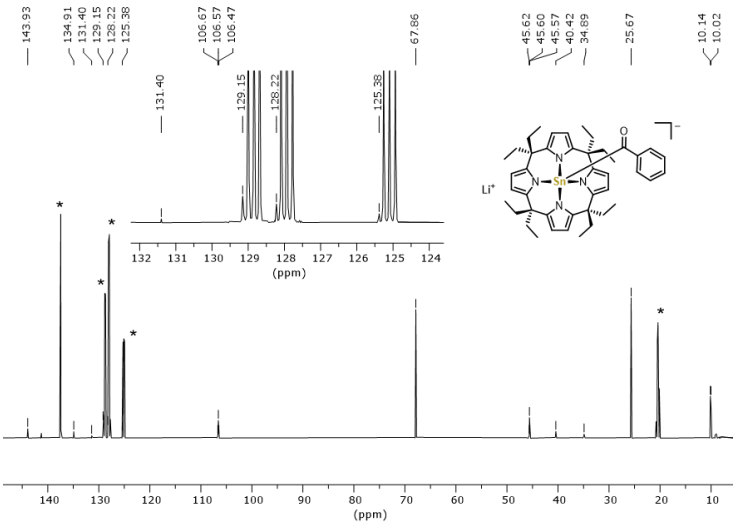


Figure S27. ^{13}C NMR spectrum of the reaction of **[Li$_2$(thf)$_x$][2]** with benzoyl chloride (155.29 MHz, Toluene-d8, 295 K). Solvent resonances and resonances are indicated by an asterisk (*).

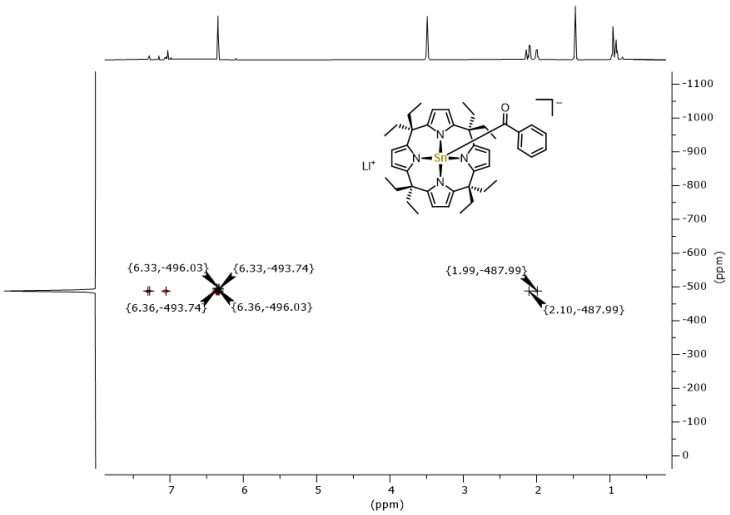


Figure S28. ^{129}Sn-^{1}H HMBC spectrum of the reaction of **[Li$_2$(thf)$_x$][2]** with benzoyl chloride (399.89 MHz, Toluene-d_8, 295 K).

4.9 Reaction of $[Li_2(thf)_x]$[2] with 4-CF_3-Benzaldehyde

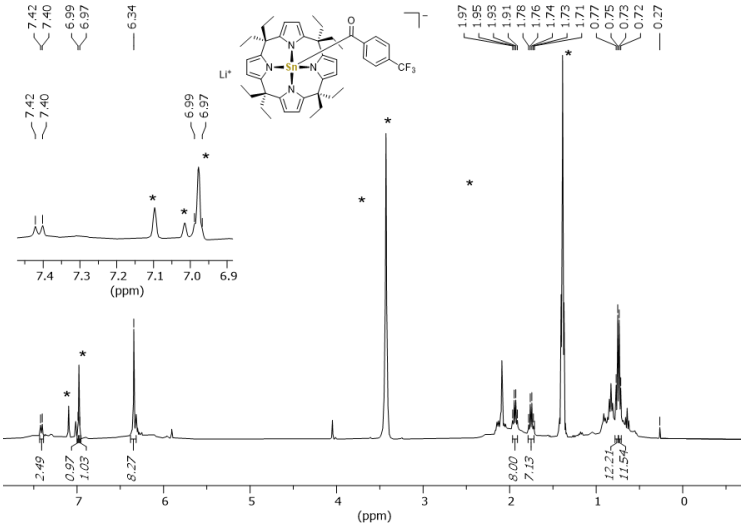


Figure S29. ^{1}H NMR spectrum of the reaction of **$[Li_2(thf)_x]$[2]** with 4-CF_3-benzaldehyde (399.89 MHz, Toluene-d_8, 295 K). Solvent resonances and resonances of THF from starting material are indicated by an asterisk (*).

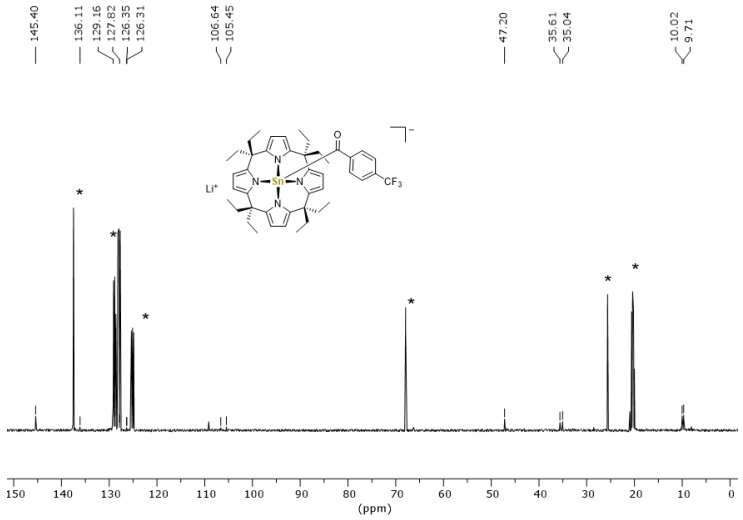


Figure S30. ^{13}C NMR spectrum of the reaction of **$[Li_2(thf)_x]$[2]** with 4-CF_3-benzaldehyde (100.55 MHz, Toluene-d_8, 295 K). Solvent resonances and resonances of THF from starting material are indicated by an asterisk (*).

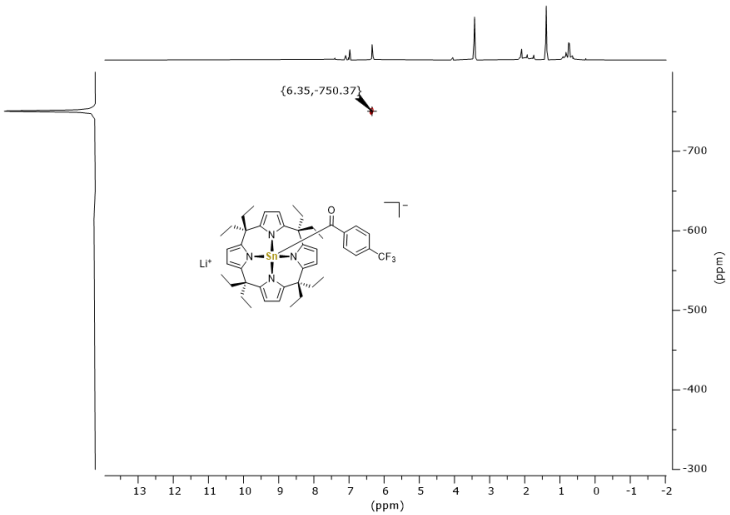


Figure S31. ^{119}Sn-^{1}H HMBC spectrum of the reaction of **[Li$_2$(thf)$_x$][2]** with 4-(CF$_3$)-benzaldehyde (Toluene-d$_8$, 295 K).

4.10 Reaction of [(NBu$_4$)$_2$][2] with Methylene Chloride

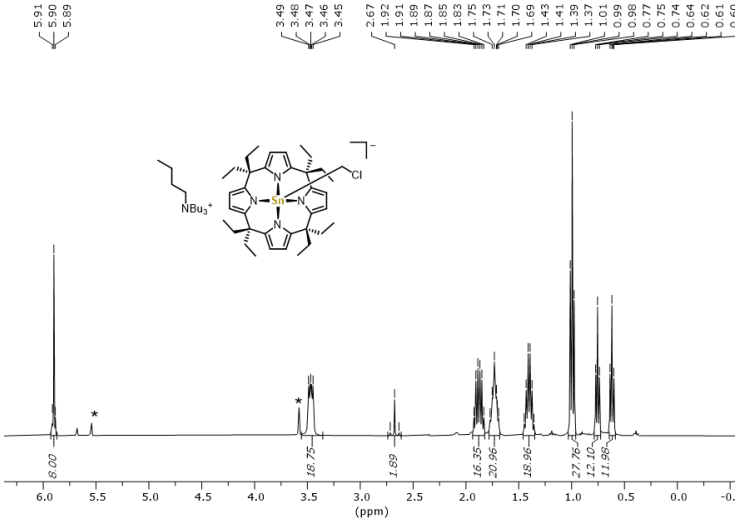


Figure S32. ^{1}H NMR spectrum of the reaction of **[(NBu$_4$)$_2$][2]** with methylene chloride (399.89 MHz, THF-d$_8$, 295 K). Solvent and residual methylene chloride resonances are indicated by an asterisk (*).

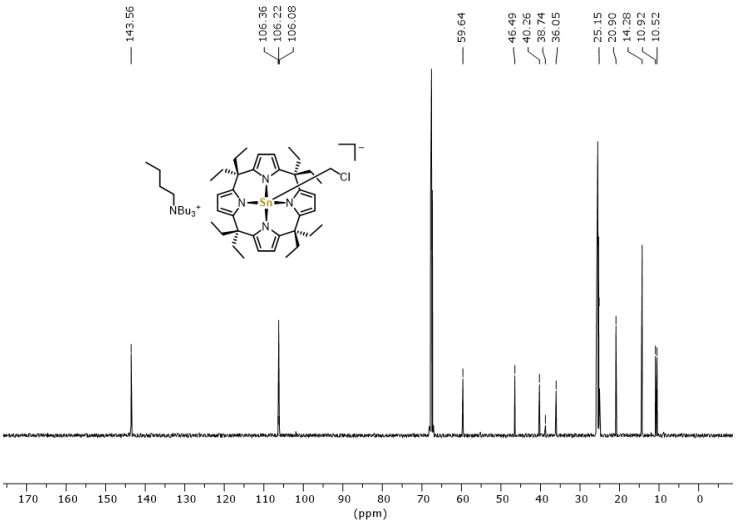


Figure S33. ^{13}C NMR spectrum of the reaction of **[(NBu$_4$)$_2$][2]** with methylene chloride (100.55 MHz, THF-d$_8$, 295 K). Solvent resonances are indicated by an asterisk (*).

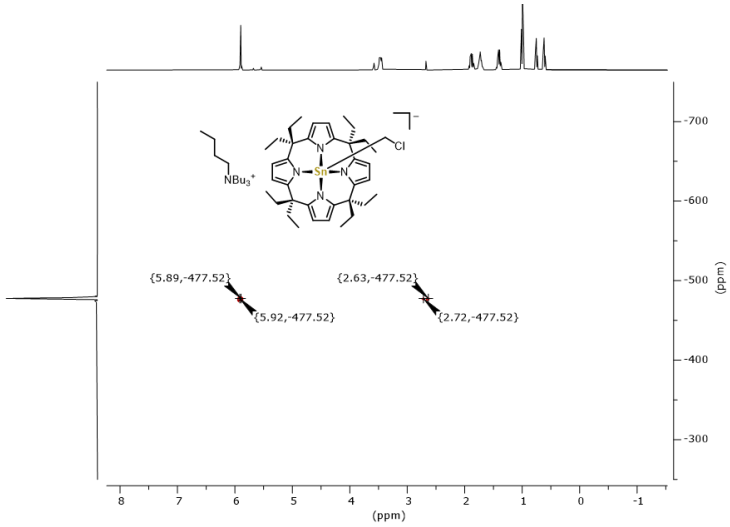


Figure S34. ^{119}Sn-^{1}H HMBC spectrum of the reaction of **[(NBu$_4$)$_2$][2]** with methylene chloride (THF-d8, 295 K).

4.11 Reaction of [(NBu$_4$)$_2$][2] with Benzyl Chloride

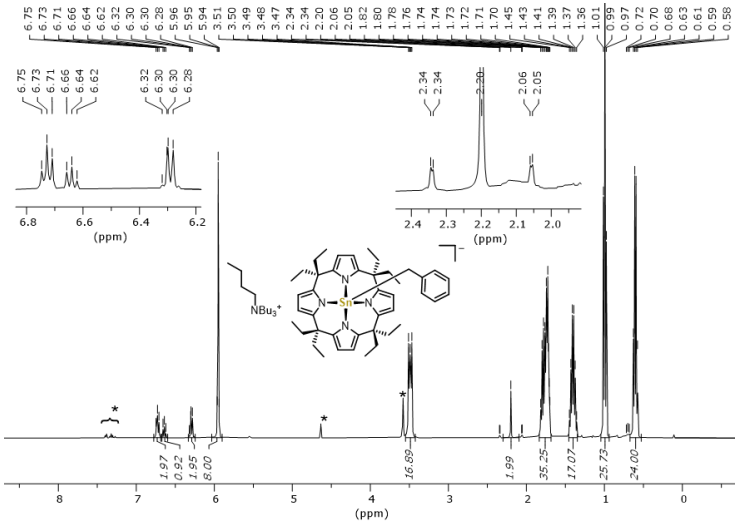


Figure S35. ^{1}H NMR spectrum of the reaction of **[(NBu$_4$)$_2$][2]** with benzyl chloride (399.89 MHz, THF-d8, 295 K). Solvent resonances are indicated by an asterisk (*).

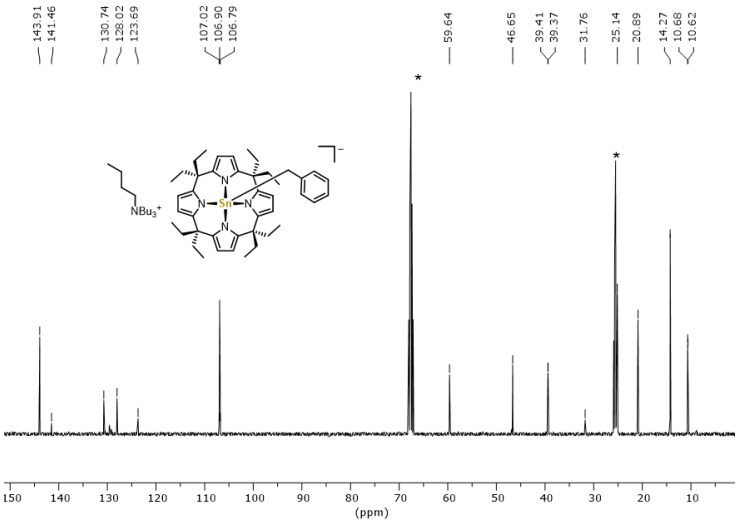


Figure S36. ^{13}C NMR spectrum of the reaction of **[(NBu$_4$)$_2$][2]** with benzyl chloride (100.55 MHz, THF-d8, 295 K). Solvent resonances are indicated by an asterisk (*).

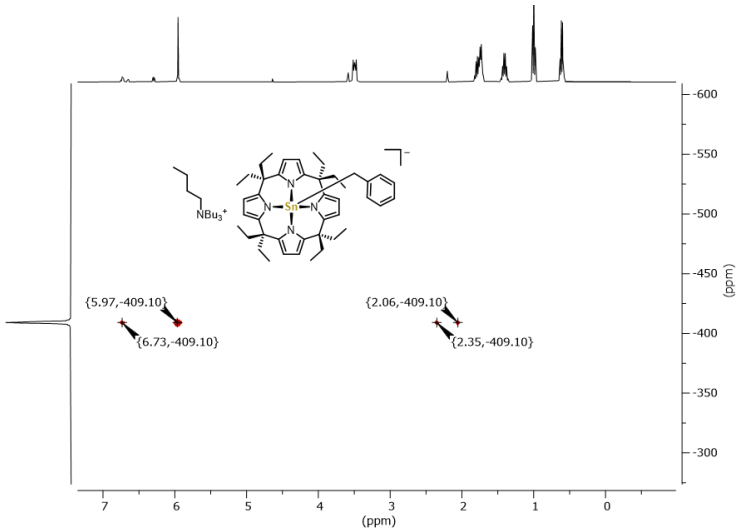


Figure S37. ^{119}Sn-^{1}H HMBC spectrum of the reaction of **[(NBu$_4$)$_2$][2]** with benzyl chloride (THF-d8, 295 K).

4.12 Reaction of [(NBu$_4$)$_2$][2] with Benzoyl Chloride

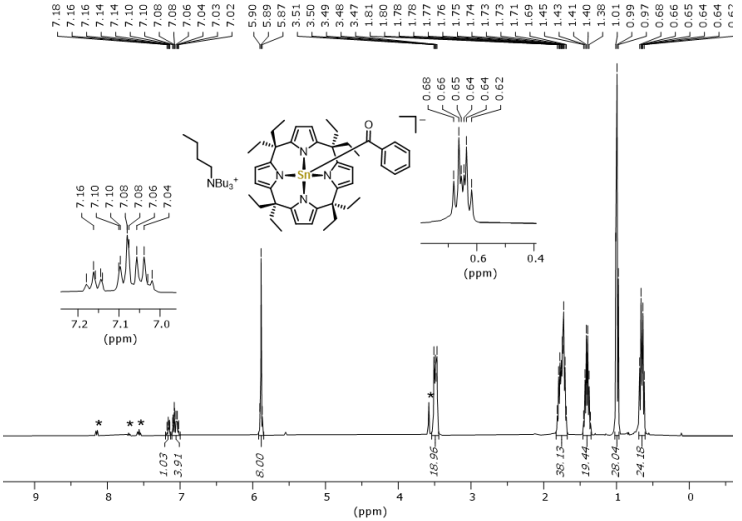


Figure S38. ^{1}H NMR spectrum of the reaction of **[(NBu$_4$)$_2$][2]** with benzoyl chloride (399.89 MHz, THF-d8, 295 K). Solvent and residue benzoyl chloride (slight excess) resonances are indicated by an asterisk (*).

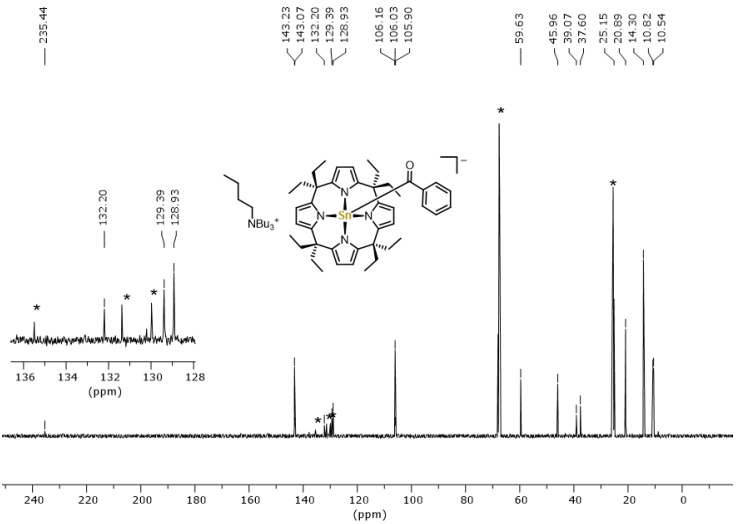


Figure S39. ^{13}C NMR spectrum of the reaction of **[(NBu$_4$)$_2$][2]** with benzoyl chloride (100.55 MHz, THF-d8, 295 K). Solvent and residue benzoyl chloride (slight excess) resonances are indicated by an asterisk (*).

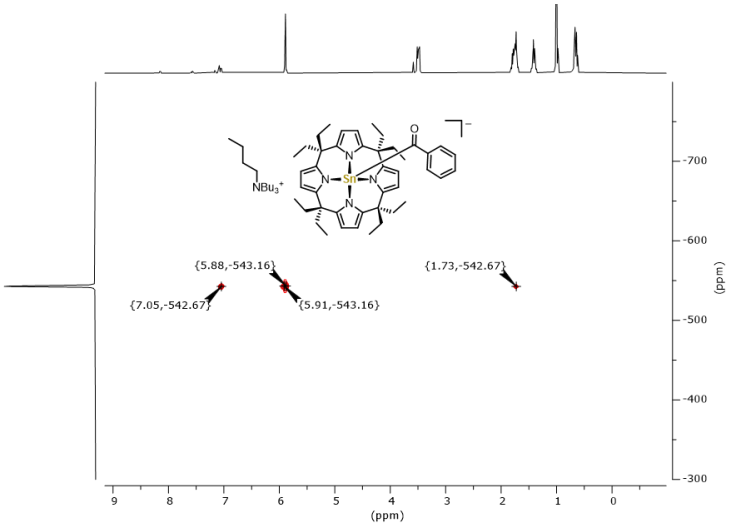


Figure S40. ^{119}Sn-^{1}H HMBC spectrum of the reaction of **[(NBu$_4$)$_2$][2]** with benzoyl chloride (THF-d8, 295 K).

4.13 Reaction of [(NBu$_4$)$_2$][2] with Iodobenzene

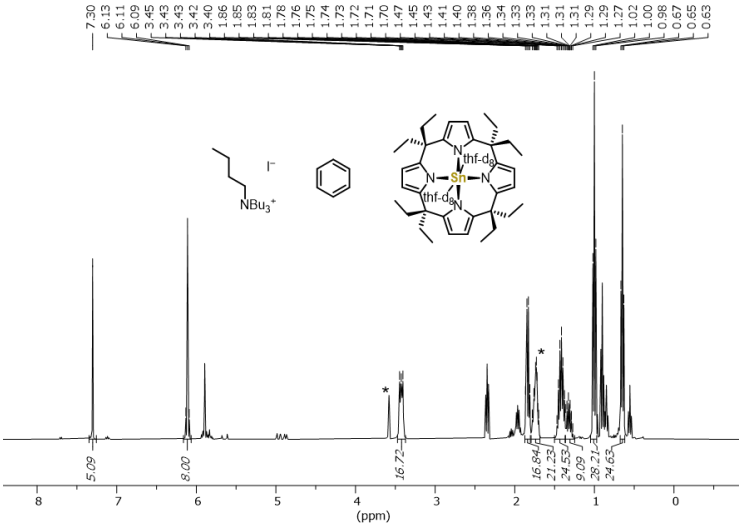


Figure S41. ^{1}H NMR spectrum of the reaction of **[(NBu$_4$)$_2$][2]** with iodobenzene (399.89 MHz, THF-d8, 295 K). Solvent resonances are indicated by an asterisk (*).

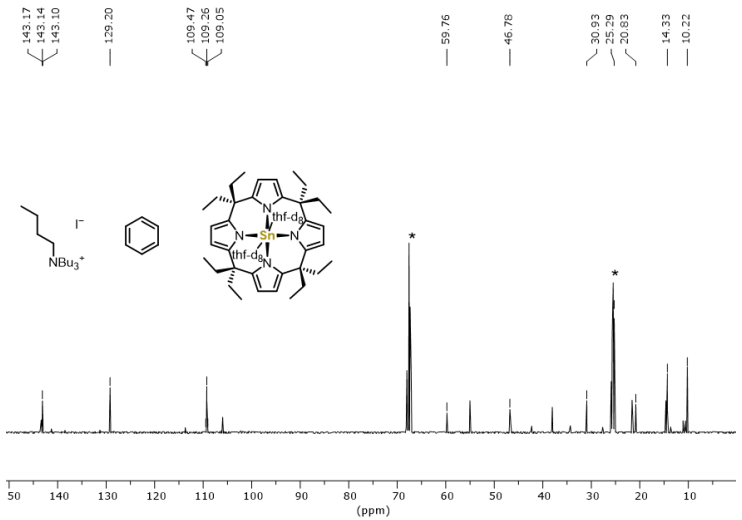


Figure S42. ^{13}C NMR spectrum of the reaction of **[(NBu$_4$)$_2$][2]** with iodobenzene (100.55 MHz, THF-d8, 295 K). Solvent resonances are indicated by an asterisk (*).

5 Crystallographic Data

5.1 [Li$_2$(thf)$_x$][2]

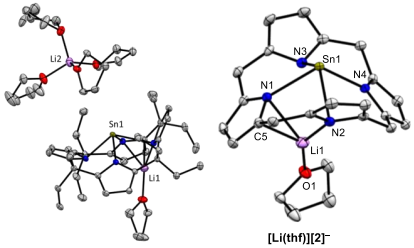


Figure S43: Solid state molecular structure of **[Li$_2$(thf)$_x$][2]** (left) and the isolated **[Li(thf)][2]**$^-$ anion (left, *meso*-ethyl residues and solvated lithium counter cation are omitted for clarity). Ellipsoids are drawn with a probability of 50%. Hydrogen atoms are omitted for clarity.

Table S3: Crystal data for **[Li$_2$(thf)$_x$][2]**.

CCDC number	2125920
Identification code	mo_hr283_0ma
Empirical formula	$C_{56}H_{88}Li_2N_4O_5Sn$
Formula weight	1029.87
Temperature/K	100
Crystal system	monoclinic
Space group	$P2_1/c$
a/Å	17.0606(16)
b/Å	16.1225(14)
c/Å	19.5523(18)
α/°	90
β/°	90.037(4)
γ/°	90
Volume/Å^3	5378.0(8)
Z	4
ρ_{calc}/g cm^{-3}	1.272
μ/mm^{-1}	0.525
F(000)	2192.0
Crystal size/mm^3	0.221 × 0.164 × 0.044
Radiation	MoKα (λ = 0.71073)
2Θ range for data collection/°	4.052 to 52
Index ranges	-21 ≤ h ≤ 21, -19 ≤ k ≤ 19, -24 ≤ l ≤ 24
Reflections collected	236904
Independent reflections	10548 [R_{int} = 0.0979, R_{sigma} = 0.0272]
Data/restraints/parameters	10548/0/650
Goodness-of-fit in F^2	1.081
Final R indexes [I>=2σ(I)]	R_1 = 0.0293, wR_2 = 0.0591
Final R indexes [all data]	R_1 = 0.0415, wR_2 = 0.0632
Largest diff. peak/hole/eÅ^{-3}	0.47/-0.50

5.2 [(NBu$_4$)$_2$][2]

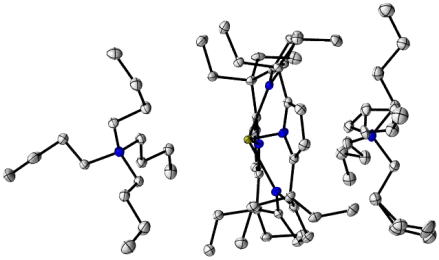


Figure S44: Solid state molecular structure of **[(NBu$_4$)$_2$][2]**. Ellipsoids are drawn with a probability of 50%. Hydrogen atoms are omitted for clarity.

Table S4: Crystal data for **[(NBu$_4$)$_2$][2]**.

CCDC number	2125918
Identification code	mo_hr342_2_0ma
Empirical formula	$C_{68}H_{120}N_6Sn$
Formula weight	1140.38
Temperature/K	100.0
Crystal system	orthorhombic
Space group	$Pbca$ (61)
a/Å	18.9095(7)
b/Å	18.6657(5)
c/Å	35.9481(10)
α/°	90
β/°	90
γ/°	90
Volume/Å^3	12688.2(7)
Z	8
ρ_{calc}/g cm^{-3}	1.194
μ/mm^{-1}	0.447
F(000)	4960
Crystal size/mm^3	0.349×0.342×0.263
Radiation	MoK_α (λ=0.71073 Å)
2Θ range for data collection/°	4.31 to 51.00 (0.83 Å)
Index ranges	-22 ≤ h ≤ 22, -22 ≤ k ≤ 22, -43 ≤ l ≤ 43
Reflections collected	83712
Independent reflections	11805 [R_{int} = 0.0486, R_{sigma} = 0.0294]
Data/restraints/parameters	11805/0/731
Goodness-of-fit in F^2	1.045
Final R indexes [I>=2σ(I)]	R_1 = 0.0298, wR_2 = 0.0658
Final R indexes [all data]	R_1 = 0.0354, wR_2 = 0.0685
Largest diff. peak/hole/eÅ^{-3}	0.32/-0.53

5.3 [(PPh$_4$)$_2$(*o*DFB)$_{0.5}$][2]

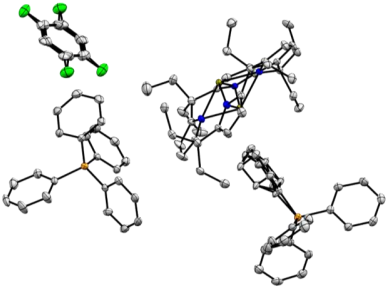


Figure S45: Solid state molecular structure of **[(PPh$_4$)$_2$(*o*DFB)$_{0.5}$][2].** Ellipsoids are drawn with a probability of 50%. Hydrogen atoms are omitted for clarity.

Table S5: Crystal data for **[(PPh$_4$)$_2$(*o*DFB)$_{0.5}$][2]**.

CCDC nmuber	2125916
Identification code	mo_hr308_0ma
Empirical formula	$C_{87}H_{90}FN_4P_2Sn$
Formula weight	1391.25
Temperature/K	100(2)
Crystal system	triclinic
Space group	$P\overline{1}$ (2)
a/Å	12.227(4)
b/Å	12.276(5)
c/Å	23.438(10)
α/°	87.397(10)
β/°	84.496(11)
γ/°	80.754(10)
Volume/Å^3	3455(2)
Z	2
ρ_{calc}/g cm^{-3}	1.337
μ/mm^{-1}	0.470
F(000)	1458
Crystal size/mm^3	0.169×0.084×0.030
Radiation	MoK_α (λ=0.71073 Å)
2Θ range for data collection/°	3.95 to 50.00 (0.84 Å)
Index ranges	-14 ≤ h ≤ 14, -14 ≤ k ≤ 14, -27 ≤ l ≤ 27
Reflections collected	75371
Independent reflections	12169 [R_{int} = 0.1052, R_{sigma} = 0.0634]
Data/restraints/parameters	12169/1209/935
Goodness-of-fit in F^2	1.041
Final R indexes [I>=2σ(I)]	R_1 = 0.0440, wR_2 = 0.0853
Final R indexes [all data]	R_1 = 0.0672, wR_2 = 0.0929
Largest diff. peak/hole/eÅ^{-3}	0.50/-0.54

5.4 [(PPh$_4$)$_2$][W(^{2}η-2)(CO)$_5$]

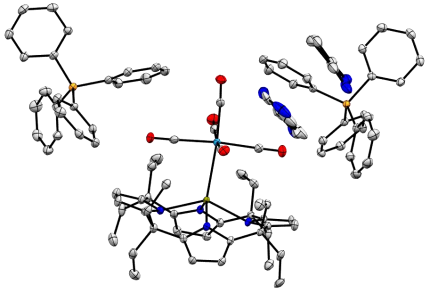


Figure S46: Solid state molecular structure of **[(PPh$_4$)$_2$][2-W(CO)$_5$].** Ellipsoids are drawn with a probability of 50%. Hydrogen atoms are omitted for clarity.

Table S6: Crystal data for **[(PPh$_4$)$_2$][2-W(CO)$_5$].**

CCDC nmuber	2125915
Identification code	mo_hr313_2_2
Empirical formula	$C_{93}H_{94}N_6O_5P_2SnW$
Formula weight	1740.22
Temperature/K	100(2)
Crystal system	triclinic
Space group	$P\overline{1}$ (2)
a/Å	13.510(2)
b/Å	13.587(2)
c/Å	25.095(4)
α/°	81.048(6)
β/°	84.270(7)
γ/°	60.976(5)
Volume/Å^3	3977.3(12)
Z	2
ρ_{calc}/g cm^{-3}	1.453
μ/mm^{-1}	1.857
F(000)	1776
Crystal size/mm^3	0.107×0.103×0.044
Radiation	MoK_α (λ=0.71073 Å)
2Θ range for data collection/°	3.78 to 56.02 (0.76 Å)
Index ranges	-17 ≤ h ≤ 17, -17 ≤ k ≤ 17, -33 ≤ l ≤ 33
Reflections collected	193114
Independent reflections	19158 [R_{int} = 0.1119, R_{sigma} = 0.0560]
Data/restraints/parameters	19158/2225/1011
Goodness-of-fit in F^2	1.017
Final R indexes [I>=2σ(I)]	R_1 = 0.0316, wR_2 = 0.0665
Final R indexes [all data]	R_1 = 0.0430, wR_2 = 0.0720
Largest diff. peak/hole/eÅ^{-3}	1.00/-1.01

5.5 Ru(^{5}η-2)(cymene)

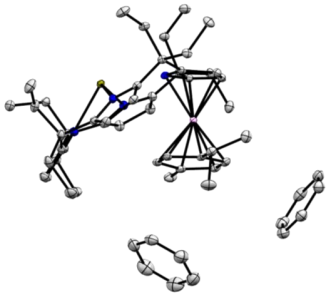


Figure S47: Solid state molecular structure of **Ru(^{5}η-2)(cymene)**. Ellipsoids are drawn with a probability of 50%. Hydrogen atoms are omitted for clarity.

Table S7: Crystal data for **Ru(^{5}η-2)(cymene)**.

CCDC number	2125917
Identification code	mo_hr372_0ma
Empirical formula	$C_{58}H_{74}N_4RuSn$
Formula weight	1046.97
Temperature/K	100(2)
Crystal system	triclinic
Space group	$P\overline{1}$ (2)
a/Å	11.465(3)
b/Å	12.8505(17)
c/Å	19.451(4)
α/°	97.710(8)
β/°	101.873(10)
γ/°	114.506(5)
Volume/Å^3	2473.0(9)
Z	2
ρ_{calc}/g cm^{-3}	1.406
μ/mm^{-1}	0.853
F(000)	1088
Crystal size/mm^3	0.123×0.106×0.074
Radiation	MoK_α (λ=0.71073 Å)
2Θ range for data collection/°	4.02 to 57.46 (0.74 Å)
Index ranges	-15 ≤ h ≤ 15, -17 ≤ k ≤ 17, -26 ≤ l ≤ 26
Reflections collected	155733
Independent reflections	12835 [R_{int} = 0.0390, R_{sigma} = 0.0165]
Data/restraints/parameters	12835/282/588
Goodness-of-fit in F^2	1.089
Final R indexes [I>=2σ(I)]	R_1 = 0.0180, wR_2 = 0.0476
Final R indexes [all data]	R_1 = 0.0207, wR_2 = 0.0485
Largest diff. peak/hole/eÅ^{-3}	0.46/-0.57

5.6 [Li(thf)$_2$][3-COPh]

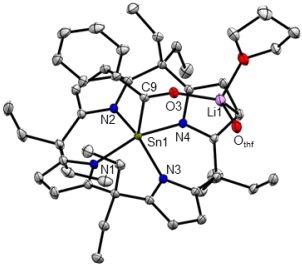


Figure S48: Solid state molecular structure of **[Li(thf)$_2$][3-COPh]**. Displacement ellipsoids are drawn at 50% probability level. Hydrogens and toluene solvent molecules are omitted for clarity.

Table S8: Crystal data for **[Li(thf)$_2$][3-COPh]**.

CCDC nmuber	2125919
Identification code	mo_hr389c_0m_a
Empirical formula	$C_{58}H_{77}LiN_4O_3Sn$
Formula weight	1003.86
Temperature/K	101(2)
Crystal system	triclinic
Space group	$P\overline{1}$ (2)
a/Å	10.618(3)
b/Å	11.653(3)
c/Å	21.103(5)
α/°	99.542(11)
β/°	93.042(8)
γ/°	92.079(12)
Volume/Å^3	2568.7(12)
Z	2
ρ_{calc}/g cm^{-3}	1.298
μ/mm^{-1}	0.545
F(000)	1060
Crystal size/mm^3	0.339×0.313×0.207
Radiation	MoK_α (λ=0.71073 Å)
2Θ range for data collection/°	3.92 to 61.11 (0.70 Å)
Index ranges	-15 ≤ h ≤ 15, -16 ≤ k ≤ 16, -30 ≤ l ≤ 30
Reflections collected	101029
Independent reflections	15729 [R_{int} = 0.0476, R_{sigma} = 0.0311]
Data/restraints/parameters	15729/831/734
Goodness-of-fit in F^2	1.037
Final R indexes [I>=2σ(I)]	R_1 = 0.0242, wR_2 = 0.0560
Final R indexes [all data]	R_1 = 0.0263, wR_2 = 0.0572
Largest diff. peak/hole/eÅ^{-3}	0.49/-0.56

6 Infrared Spectroscopy

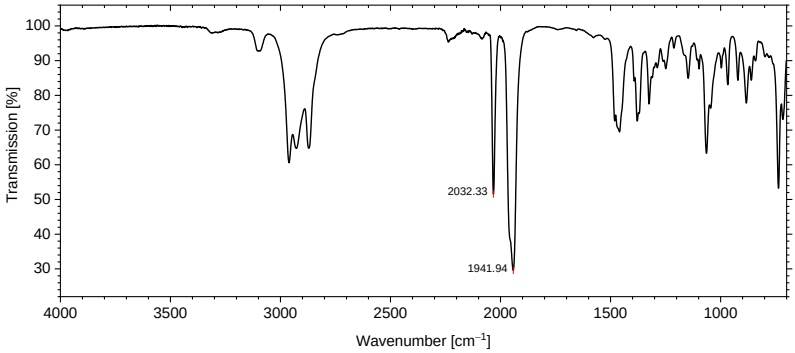


Figure S49: FTIR spectrum of **[(NBu$_4$)$_2$][Ni($^2\eta$-2)(CO)$_3$]** in THF-d_8.

7 Comparative TEP Scale

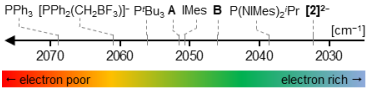


Figure S50. Comparison between TEP values of **[2]$^{2-}$** and other literature known carbene and phosphine ligands.

Table S9. TEP values of **[2]$^{2-}$** and other literature known carbene and phosphine ligands.

Compound	TEP [cm^{-1}]	Solvent	Reference
[2]$^{2-}$	2032.3	THF	This work
P(NIMes)$_2$iPr	2038.6	DCM	[20]
B	2046	DCM	[21]
IMes	2050.7	DCM	[22]
IPr (**A**)	2051.5	DCM	[20]
P^{t}Bu$_3$	2056.1	DCM	[20]
[PPh$_2$(CH$_2$BF$_3$)]$^-$	2061	DCM	[23]
PPh$_3$	2068.9	DCM	[20]

8 DFT Calculations

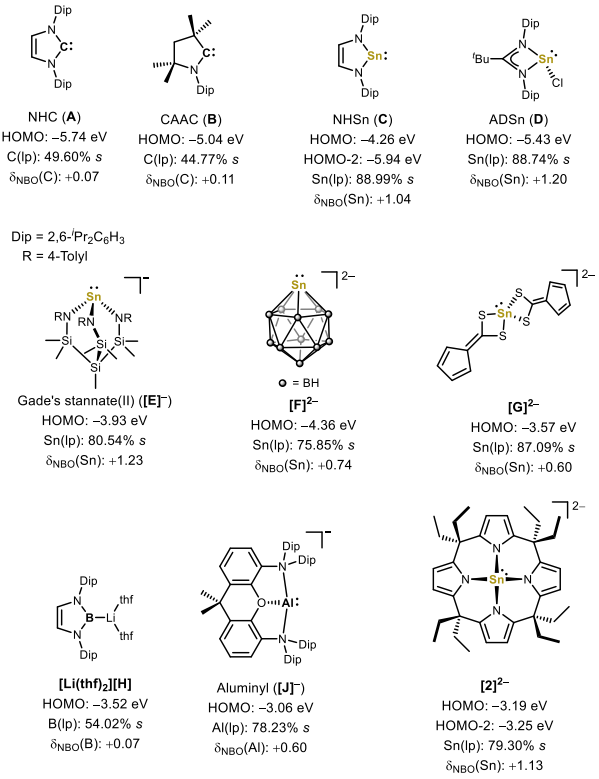


Figure S51. HOMO energy levels, *s*-character of the lone pair (lp), and NBO atomic charges δ_{NBO} of the central atom for the NHC **A**, the CAAC **B**, the NHSn **C**, ADSn **D**, the anionic stannate(II) **[E]**$^{-}$, the dianionc stannates(II) **[F]**$^{2-}$, and **[G]**$^{2-}$, the boryl **H**, the aluminyl anion **[J]**$^{-}$, and **[2]**$^{2-}$. HOMO energies were calculated at the B97M-D3(BJ)/def2-TZVPP CPCM(THF)//B97M-D3(BJ)/def2-TZVPP and NBO analysis at the PBE0/def2-TZVPP CPCM(THF)//B97M-D3(BJ)/def2-TZVPP level of theory. For **C** and **[2]**$^{2-}$ the HOMO and HOMO-1 are mainly ligand-centered and the energies of their HOMO-2 containing a mayor contribution of their tin-centered lone pairs are given as well.

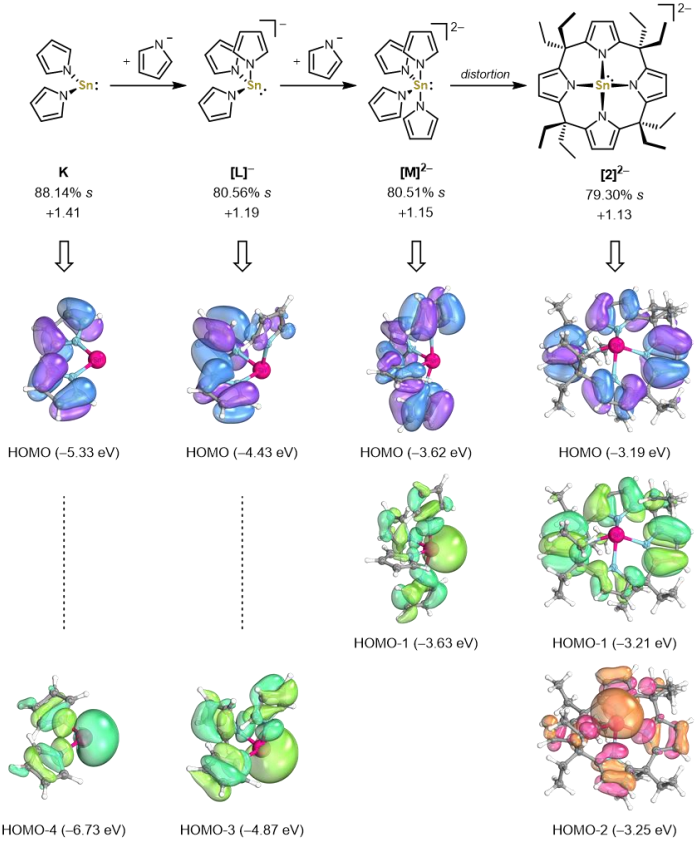


Figure S52. Frontier molecular orbital energies for the hypothetical pyrrolato stannanes **K**, **[M]**$^{-}$, and **[L]**$^{2-}$,and **[2]**$^{2-}$ at the B97M-D3(BJ)/def2-TVZPP CPCM(THF)//B97M-D3(BJ)/def2-TVZPP level of theory and *s*-character of the lone pair and NBO atomic charges at the central atom calculated on the PBE0/def2-TZVPP CPCM(THF)//B97M-D3(BJ)/def2-TZVPP level of theory. Isosurfaces sampled at a value of 0.03.

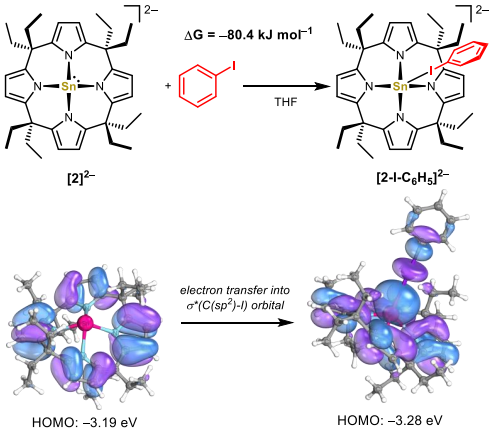


Figure S53. Free reaction enthalpy for the *σ*-hole adduction formation between **[2]**$^{2-}$ and iodobenzene and frontier molecular orbitals calculated on the B97M-D3(BJ)/def2-TVZPP CPCM(THF)//B97M-D3(BJ)/def2-TVZPP level of theory. Isosurfaces sampled at a value of 0.03.

9 Cyclic Voltammetry

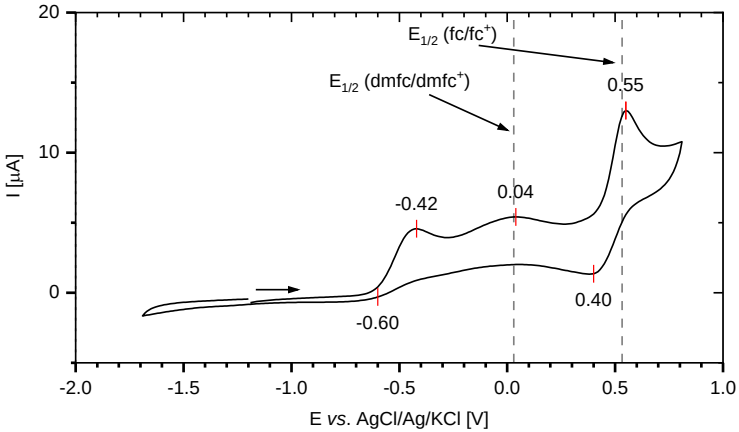


Figure S54: Cyclic voltammogram of **[(NBu$_4$)$_2$][2]** and [NBu$_4$][PF$_6$] in *o*DFB.

10 ETS-NOCV Results

Table S11: Bonding energy decomposition terms calculated on the BP86-D3/TZ2P COSMO(THF)//B97M-D3(BJ)/def2-TVZPP level of theory.

Compound	Total Pauli Repulsion (ΔE_{Pauli}) [Eh]	Total Electrostatic Interaction (ΔV_{elst}) [Eh]	Total Orbital Interaction ($\Delta E_{oi,tot}$) [Eh]	Total Dispersion Energy (E_{disp}) [Eh]	Solvation Energy (E_{solv}) [Eh]	Residue [Eh]	Total Bonding Energy (ΔE) [Eh]
[2]$^{2-}$	0.477164845	-1.340814347	-0.573479385	-0.010706268	-0.173999447	0.004544433	-0.169455015
[Sn(pyr)$_4$]$^{2-}$	0.463414466	-1.446258898	-0.535590216	-0.006556682	-0.20239567	0.00298029	-0.19941538
[2-Se]$^{2-}$	0.350999376	-0.236227689	-0.294142204	-0.012874307	-0.189065305	0.004530776	-0.184534529
[2^{H}-Se]$^{2-}$	0.331996112	-0.228345683	-0.292003221	-0.009634874	-0.216411735	0.003181708	-0.213230027

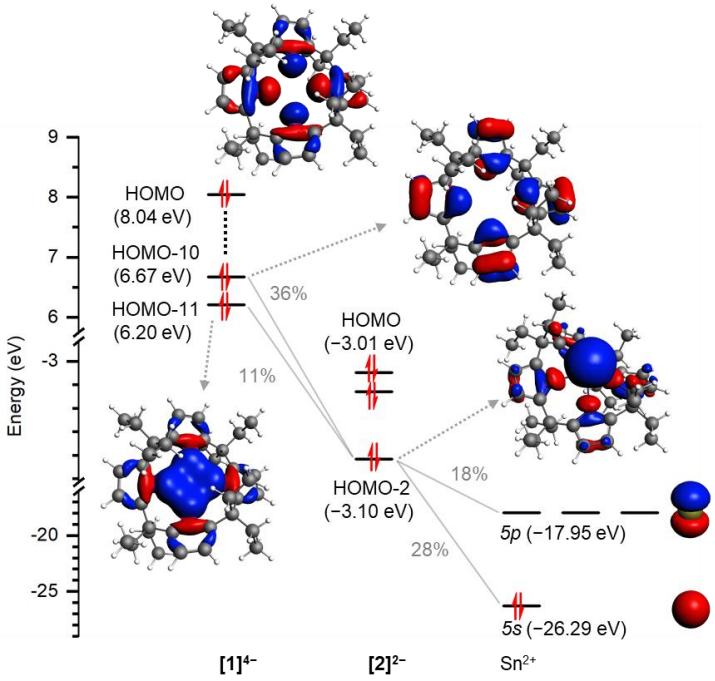
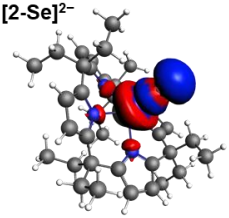
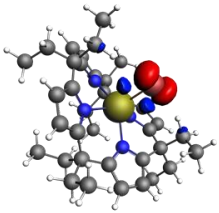


Figure S55. ETS-NOCV bond analysis of **[2]**$^{2-}$ on the BP86-D3/TZ2P COSMO(THF)//B97M-D3(BJ)/def2-TVZPP level of theory. Isosurfaces sampled at a value of 0.03.

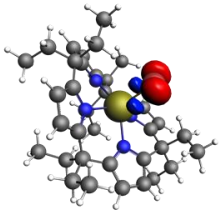
[2-Se]$^{2-}$



Sn→Se σ donation
$\Delta E_{oi}(\sigma)$ = −658.18 kJ mol^{-1}
(85.23% of $\Delta E_{oi,tot}$)

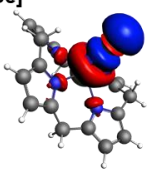


Se→π*(Sn-N) back donation
+ Se→σ*(C-H) donation
$\Delta E_{oi}(\pi_1)$ = −57.04 kJ mol^{-1}
(7.39% of $\Delta E_{oi,tot}$)

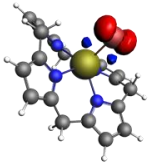


Se→π*(Sn-N) back donation
$\Delta E_{oi}(\pi_2)$ = −40.88 kJ mol^{-1}
(5.29% of $\Delta E_{oi,tot}$)

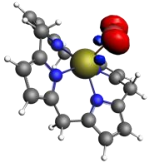
[2^{H}-Se]$^{2-}$



Sn→Se σ donation
$\Delta E_{oi}(\sigma)$ = −681.40 kJ mol^{-1}
(88.89% of $\Delta E_{oi,tot}$)



Se→π*(Sn-N) back donation
+ Se→ σ*(C-H) donation
$\Delta E_{oi}(\pi_1)$ = −44.28 kJ mol^{-1}
(5.78% of $\Delta E_{oi,tot}$)



Se→π*(Sn-N) back donation
$\Delta E_{oi}(\pi_2)$ = −35.64 kJ mol^{-1}
(4.65% of $\Delta E_{oi,tot}$)

Figure S56. ETS-NOCV bond analysis of **[2-Se]$^{2-}$** and the *meso*-unsubstituted derivative **[2^{H}-Se]$^{2-}$** on the BP86-D3/TZ2P COSMO(THF)//B97M-D3(BJ)/def2-TVZPP level of theory. The Se fragment was considered in its closed shell ^{1}D excited state with doubly occupied p_x and p_y orbitals and an empty p_z orbital directed towards the Sn(II) lone pair of a singlet tin(II) calix[4]pyrrolato fragment. NOCV deformation densities sampled at a value of 0.003. The color code of the charge flow is red to blue.

11 NBO Results

Table S12: NBO analysis results calculated on PBE0/def2-TZVPP CPCM(THF)//B97M-D3(BJ)/def2-TVZPP level of theory. NBO and second order perturbation theory stabilization energies $\Delta E^{(2)}$ for selected bonding interactions are given in kJ mol^{-1}. Additionally, Lewis density parameters $\%\rho_L$ and single point energies are given for each system.

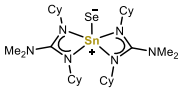
NHC (**A**) (single point energy = −1159.062799534277 Eh, $\%\rho_L$ = 97.91)	
s-Character of lp(1) at C2	49.60%
Natural charge at C2	0.073
CAAC (**B**) (single point energy = −874.060935133861 Eh, $\%\rho_L$ = 98.32)	
s-Character of lp(1) at C2	41.18%
Natural charge at C2	0.127
NHB Li THF Adduct (**H**) (single point energy = −1617.970242201778 Eh, $\%\rho_L$ = 99.32)	
s-Character of lp(1) at B1	54.02%
Natural charge at B1	0.072
NHSn (**C**) (single point energy = −1335.373499564167 Eh, $\%\rho_L$ = 98.13)	
s-Character of lp(1) at Sn2	88.99%
Natural charge at Sn2	1.040
ADSn (**D**) (single point energy = −1913.919385348876 Eh, $\%\rho_L$ = 99.98)	
s-Character of lp(1) at Sn2	88.74%
Natural charge at Sn2	1.203
Bis dithiolato stannate(II) **[G]**$^{2-}$ (single point energy = −2268.592659566669 Eh, $\%\rho_L$ = 98.23)	
s-Character of lp(1) at Sn1	87.09
Natural charge at Sn1	0.600
Stanna dodecaborate **[F]**$^{2-}$ (single point energy = −494.486522724303 Eh, $\%\rho_L$ = 98.31)	
s-Character of lp(1) at Sn5	75.85%
Natural charge at Sn5	0.741
Gade's stannate (II) (**[E]**$^{-}$) (single point energy = −2627.689403573425 Eh, $\%\rho_L$ = 98.29)	
s-Character of lp(1) at Sn78	80.54%
Natural charge at Sn78	1.232
Aldridge's Aluminyl Anion (**[J]**$^{-}$) (single point energy = −2293.177232006270 Eh, $\%\rho_L$ = 97.85)	
s-Character of lp(1) at Al29	78.34%
Natural charge at Al29	0.603
[2]$^{2-}$ (single point energy = −1832.964212044182 Eh, $\%\rho_L$ = 98.14)	
s-Character of lp(1) at Sn89	79.30%
Natural charge at Sn89	1.129
[2-Se]$^{2-}$ (single point energy = −4234.292224 Eh, $\%\rho_L$ = 98.40)	
NBO175 $\sigma_{Sn89\text{-}Se90}$ (occupation = 1.94116)	−925.49
$\Delta E^{(2)}$ $lp(2)_{Se90} \rightarrow \pi^*_{N1\text{-}Sn89}$	6.31
$\Delta E^{(2)}$ $lp(2)_{Se90} \rightarrow \pi^*_{N27\text{-}Sn89}$	14.83
$\Delta E^{(2)}$ $lp(2)_{Se90} \rightarrow \pi^*_{N61\text{-}Sn89}$	14.78
$\Delta E^{(2)}$ $lp(2)_{Se90} \rightarrow \pi^*_{N71\text{-}Sn89}$	6.26
$\Delta E^{(2)}$ $lp(3)_{Se90} \rightarrow \sigma^*_{C16\text{-}H17}$ (**C(sp^3)H-Se interaction**)	21.88
$\Delta E^{(2)}$ $lp(3)_{Se90} \rightarrow \sigma^*_{C78\text{-}H80}$ (**C(sp^3)H-Se interaction**)	21.67
$\Delta E^{(2)}$ $lp(3)_{Se90} \rightarrow \pi^*_{N1\text{-}Sn89}$	14.30
$\Delta E^{(2)}$ $lp(3)_{Se90} \rightarrow \pi^*_{N27\text{-}Sn89}$	4.86

$\Delta E^{(2)}$ lp(3)$_{Se90}\rightarrow\pi^*_{N61\text{-}Sn89}$	4.86
$\Delta E^{(2)}$ lp(3)$_{Se90}\rightarrow\pi^*_{N71\text{-}Sn89}$	14.25
[2^{H}-Se]$^{2-}$ (single point energy = −3605.895922 Eh, %ρ_L = 98.06)	
NBO111 $\sigma_{Sn33\text{-}Se34}$ (occupation = 1.94806)	−953.08
$\Delta E^{(2)}$ lp(2)$_{Se34}\rightarrow\pi^*_{N1\text{-}Sn33}$	8.79
$\Delta E^{(2)}$ lp(2)$_{Se34}\rightarrow\pi^*_{N13\text{-}Sn33}$	9.25
$\Delta E^{(2)}$ lp(2)$_{Se34}\rightarrow\pi^*_{N19\text{-}Sn33}$	9.25
$\Delta E^{(2)}$ lp(2)$_{Se34}\rightarrow\pi^*_{N29\text{-}Sn33}$	8.74
$\Delta E^{(2)}$ lp(3)$_{Se34}\rightarrow\sigma^*_{C32\text{-}H40}$ (**C(sp^3)H-Se interaction**)	4.14
$\Delta E^{(2)}$ lp(3)$_{Se34}\rightarrow\sigma^*_{C8\text{-}H36}$ (**C(sp^3)H-Se interaction**)	4.06
$\Delta E^{(2)}$ lp(3)$_{Se34}\rightarrow\pi^*_{N1\text{-}Sn33}$	9.29
$\Delta E^{(2)}$ lp(3)$_{Se34}\rightarrow\pi^*_{N13\text{-}Sn33}$	8.74
$\Delta E^{(2)}$ lp(3)$_{Se34}\rightarrow\pi^*_{N19\text{-}Sn33}$	8.74
$\Delta E^{(2)}$ lp(3)$_{Se34}\rightarrow\pi^*_{N29\text{-}Sn33}$	9.29

12 ^{77}Se and ^{119}Sn NMR Shift Calculation Results

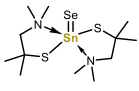
Table S13: ^{77}Se and ^{119}Sn NMR shifts calculated on the PBE0/SO-ZORA-TZ2P COSMO(THF)//B97M-D3(BJ)/def2-TZVPP level of theory and referenced against $SeMe_2$ and $SnMe_4$, respectively.

Compound	Total ^{119}Sn NMR isotropic shielding tensor [ppm]	^{119}Sn NMR chemical shift against $SnMe_4$ [ppm]	Total ^{77}Se NMR isotropic shielding tensor [ppm]	^{77}Se NMR chemical shift against $SeMe_2$ [ppm]
$SnMe_4$	3004.14	0.00	-	-
$SeMe_4$	-	-	1978.08	0.00
[2]$^{2-}$	3513.52	-509.38	-	-
[2-Se]$^{2-}$	3575.747	-571.606	2427.45	-449.37
[2^{H}-Se]$^{2-}$	3562.074	-557.933	2616.62	-638.54



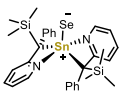
Ahmet *et al. J. Inorg. Chem.* **2018**, 2018, 1670-1678.

$\delta(^{77}Se, C_6D_6) = -476.01$ ppm
$\delta(^{119}Sn, C_6D_6) = -566.30$ ppm



Park *et al. Inorg. Chem.* **2020,** 59, 3513-3517.

$\delta(^{77}Se, C_6D_6) = -218.13$ ppm
$\delta(^{119}Sn, C_6D_6) = -264.50$ ppm



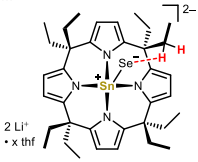
Leung *et al.* Organometallics **2000**, 19, 296-303.

$\delta(^{77}Se, THF/C_6D_6) = -531.95$ ppm
$\delta(^{119}Sn, THF/C_6D_6) = -179.18$ ppm



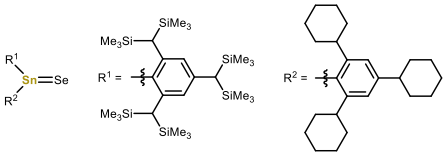
Leung *et al.* Organometallics **2000**, 19, 296-303.

$\delta(^{77}Se, THF/C_6D_6) = -734.8$ ppm
$\delta(^{119}Sn, THF/C_6D_6) = -111.55$ ppm



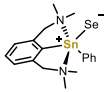
[Li_2(thf)$_x$][2-Se]

$\delta(^{77}Se, THF\text{-}d_8) = -391.99$ ppm
$\delta(^{119}Sn, THF\text{-}d_8) = -560.18$ ppm



Saito *et al.* J. Am. Chem. Soc. **2004**, 126, 15572-15582.

$\delta(^{77}Se, CDCl_{36}) = 839$ ppm
$\delta(^{119}Sn, CDCl_3) = 556$ ppm



Mairychová *et al.* Organometallics **2011**,30, 5904-5910.

$\delta(^{77}Se, CDCl_{36}) = -570.90$ ppm
$\delta(^{119}Sn, CDCl_3) = -4.70$ ppm

Figure S57. Experimental ^{77}Se and ^{119}Sn NMR data for **[Li_2(thf)$_x$][2-Se]** and other literature-known, monomeric stanna(II) selenido complexes.

13 Optimized Molecular Geometries

aldrdige_aluminyl_anion_B97M_D3_TZVPP_optfreq

Total correction: 2823.8826 kJ/mol
Single point energy: -6032185.6891 kJ/mol

Total enthalpy: -6029359.3278 kJ/mol
Final entropy term: 343.6942 kJ/mol
Total gibbs free enthalpy: -6029703.022 kJ/mol
Method and Basis: B97M-D3BJ / def2-TZVPP

xyz, charge: -1, multiplicity: 1

C	0.561060	0.112350	0.399967
C	0.916841	-0.035129	3.089450
C	0.346933	-1.126870	0.988810
C	0.845545	1.279366	1.059714
C	1.042116	1.192620	2.433955
C	0.567449	-1.174009	2.375185
H	1.277005	2.078148	2.995806
H	0.416692	-2.111941	2.874651
C	0.861701	2.549502	0.214672
C	0.789340	3.797524	1.070399
H	1.645420	3.850361	1.734980
H	-0.113815	3.817783	1.670766
H	0.806764	4.685072	0.446653
C	2.158465	2.584780	-0.604001
H	3.018769	2.618430	0.059136
H	2.173501	3.464888	-1.241176
H	2.244960	1.707188	-1.232328
C	-0.326497	2.442259	-0.734196
C	-2.599602	1.865423	-2.255763
C	-1.241714	3.447182	-1.036875
C	-0.558094	1.206001	-1.275472
C	-1.722106	0.815326	-1.928653
C	-2.359114	3.164342	-1.826754
H	-1.094427	4.438921	-0.649754
H	-3.497742	1.620601	-2.789335
O	0.295261	0.150420	-0.963631
N	-1.895535	-0.517053	-2.118486
N	-0.100671	-2.117793	0.167679
Al	-0.344549	-1.771904	-1.802808
C	-0.121092	-3.428693	0.643364
C	-0.308078	-6.097913	1.437613
C	1.035426	-4.113464	1.050111
C	-1.330147	-4.122286	0.600890
C	-1.446271	-5.446557	0.985165
C	0.905710	-5.434008	1.456146
H	-2.198546	-3.587052	0.257772
H	1.788074	-5.971975	1.766777
H	-0.358154	-7.128017	1.753806
C	-3.061293	-0.904287	-2.805385
C	-5.368831	-1.590132	-4.155772
C	-3.081067	-0.858887	-4.205297

C	-4.190220	-1.331622	-2.076843
C	-5.363731	-1.652311	-2.768765
C	-4.246853	-1.215205	-4.861267
H	-4.282082	-1.184498	-5.939046
H	-6.277070	-1.837428	-4.684069
C	-1.882358	-0.422156	-5.004808
H	-1.082617	-0.201765	-4.307624
C	-4.078494	-1.362063	-0.568095
H	-3.014381	-1.387676	-0.361330
C	2.407149	-3.503271	0.926035
H	2.291657	-2.449400	0.710939
C	-2.771574	-6.151498	0.900784
H	-3.503649	-5.418979	0.566911
C	-1.394256	-1.539879	-5.913183
H	-0.514705	-1.223022	-6.468631
H	-2.158827	-1.826151	-6.632498
H	-1.126709	-2.412403	-5.327058
C	-2.178408	0.839172	-5.803934
H	-1.293126	1.167367	-6.342975
H	-2.495597	1.647531	-5.152914
H	-2.965608	0.665880	-6.534730
C	-4.602345	-0.075150	0.058498
H	-5.664991	0.054061	-0.135086
H	-4.081817	0.788659	-0.337331
H	-4.460440	-0.091251	1.136551
C	-4.680671	-2.580177	0.121061
H	-4.496749	-3.489989	-0.442128
H	-5.749265	-2.493194	0.276877
H	-4.224900	-2.700893	1.099651
C	-2.730286	-7.275011	-0.124657
H	-2.012664	-8.035795	0.171734
H	-2.432274	-6.901488	-1.098288
H	-3.702460	-7.752945	-0.221550
C	-3.220682	-6.679385	2.254597
H	-3.274582	-5.881535	2.988226
H	-2.523920	-7.424774	2.628748
H	-4.199706	-7.147531	2.184843
C	3.228110	-3.626897	2.198664
H	2.719025	-3.166745	3.039242
H	4.190980	-3.136672	2.080415
H	3.420348	-4.666624	2.451258
C	3.137937	-4.125500	-0.257148
H	4.117289	-3.670202	-0.388540
H	2.569501	-3.986198	-1.171037
H	3.279079	-5.193371	-0.105220
C	-6.647024	-2.040552	-2.097547
H	-6.626827	-3.059145	-1.721152

H	-7.465392	-1.973646	-2.807066
H	-6.886993	-1.399217	-1.257275
C	1.164038	-0.084983	4.590832
C	0.892726	-1.457251	5.187077
H	1.074186	-1.429010	6.258229
H	1.539544	-2.217323	4.762168
H	-0.135622	-1.765817	5.029513
C	0.260255	0.917743	5.304938
H	0.430627	0.881365	6.379048
H	-0.784719	0.690534	5.117618
H	0.442448	1.933139	4.972514
C	-3.315010	4.298516	-2.169101
C	-2.566642	5.366429	-2.964293
H	-1.730678	5.766206	-2.401032
H	-3.231637	6.190199	-3.217167
H	-2.174777	4.948921	-3.886927
C	-3.861062	4.921323	-0.886026
H	-3.067075	5.323180	-0.266811
H	-4.395200	4.179908	-0.299631
H	-4.548346	5.732002	-1.120274
C	-4.498670	3.836500	-3.004630
H	-4.179305	3.399234	-3.945142
H	-5.136668	4.686831	-3.230715
H	-5.098411	3.100302	-2.479492
C	2.623458	0.270964	4.867523
H	2.828770	0.244497	5.936178
H	2.862871	1.262901	4.499803
H	3.286265	-0.434124	4.374782

dipp_caac_B97M_D3_TZVPP_optfreq

Total correction:	1298.8758 kJ/mol
Single point energy:	-2196405.6075 kJ/mol
Total enthalpy:	-2195104.2527 kJ/mol
Final entropy term:	184.9048 kJ/mol
Total gibbs free enthalpy:	-2195289.1576 kJ/mol
Method and Basis:	B97M-D3BJ / def2-TZVPP

xyz, charge: 0, multiplicity: 1

C	-0.712336	-0.492345	1.640589
C	0.569440	0.167547	2.086035
N	0.217252	1.188984	2.810161
C	-1.266664	1.449481	3.024701
C	-1.846254	0.485437	1.999896
H	-2.146951	1.036216	1.113201
H	-2.728181	-0.018459	2.381398

C	-0.662492	-0.775778	0.150085
H	0.158473	-1.444516	-0.083339
H	-0.517760	0.139856	-0.415856
H	-1.590434	-1.234675	-0.182802
C	-0.824183	-1.810924	2.399474
H	0.032747	-2.441540	2.190759
H	-1.725320	-2.338828	2.098648
H	-0.867557	-1.657117	3.472964
C	-1.629361	2.894463	2.755940
H	-1.430673	3.178770	1.731265
H	-1.090181	3.567984	3.413602
H	-2.690316	3.032134	2.937899
C	-1.657892	1.112956	4.451586
H	-1.506142	0.066213	4.680326
H	-2.709482	1.337726	4.596584
H	-1.091108	1.706984	5.160311
C	1.187904	2.036291	3.437881
C	2.982327	3.729344	4.670848
C	1.694007	1.691119	4.692160
C	1.635012	3.167969	2.753131
C	2.529208	4.011139	3.397517
C	2.585661	2.566195	5.298465
H	2.890109	4.887115	2.886627
H	2.991078	2.319199	6.264477
H	3.670736	4.398197	5.159373
C	1.294947	3.412365	1.306474
H	0.460430	2.776867	1.040103
C	0.906173	4.851250	1.015656
H	0.085406	5.179703	1.645046
H	0.602023	4.956137	-0.021323
H	1.737553	5.530341	1.175686
C	2.472223	2.976338	0.441823
H	3.355475	3.565089	0.673736
H	2.243893	3.111089	-0.611793
H	2.704274	1.931099	0.614071
C	1.427582	0.351160	5.325284
H	0.590195	-0.105965	4.817167
C	1.093261	0.438311	6.804212
H	1.933966	0.806666	7.383587
H	0.844046	-0.545143	7.190649
H	0.250989	1.097143	6.989697
C	2.632203	-0.553128	5.090835
H	3.518590	-0.140228	5.564729
H	2.827234	-0.656780	4.029397
H	2.455398	-1.540477	5.508327

dipp_cnc_sncl_B97M_D3_TZVPP_optfreq

Total correction:	1855.0072 kJ/mol
Single point energy:	-5032447.3356 kJ/mol
Total enthalpy:	-5030589.8495 kJ/mol
Final entropy term:	263.0695 kJ/mol
Total gibbs free enthalpy:	-5030852.919 kJ/mol
Method and Basis:	B97M-D3BJ / def2-TZVPP

xyz, charge: 0, multiplicity: 1

N	0.770739	1.251775	2.266860
Sn	2.017439	-0.540098	2.784476
C	-0.171313	1.027986	3.176781
N	0.130326	-0.055932	3.892699
C	-1.351615	1.948444	3.486895
C	-1.406844	3.187413	2.604593
H	-0.487684	3.757007	2.638084
H	-2.206073	3.821036	2.975675
H	-1.621113	2.957295	1.570154
C	-2.694726	1.232800	3.369524
H	-2.786294	0.410540	4.063025
H	-2.867982	0.863462	2.364789
H	-3.480592	1.947653	3.593738
C	-1.169563	2.422957	4.930016
H	-0.196775	2.882225	5.073094
H	-1.274240	1.610791	5.632839
H	-1.930578	3.163847	5.153414
C	-0.634860	-0.765766	4.834823
C	-2.061164	-2.285985	6.673837
C	-1.577175	-1.707844	4.384980
C	-0.354956	-0.646097	6.203271
C	-1.090882	-1.404601	7.103142
C	-2.285569	-2.445202	5.319773
H	-0.887427	-1.310711	8.156187
H	-3.016450	-3.160771	4.984629
H	-2.624525	-2.863143	7.387301
C	0.800825	2.082596	1.135002
C	1.060265	3.575707	-1.192563
C	1.705283	3.149093	1.092200
C	0.021290	1.763080	0.010356
C	0.166454	2.522268	-1.138779
C	1.817500	3.881320	-0.081348
H	-0.426871	2.288568	-2.005724
H	2.511271	4.704498	-0.119479
H	1.161737	4.153183	-2.095679
C	-0.938872	0.604074	0.037804
H	-1.224694	0.439496	1.069168

C	-0.263516	-0.669111	-0.451839
H	0.051732	-0.555938	-1.485197
H	-0.941211	-1.516608	-0.393820
H	0.618895	-0.905492	0.135175
C	-2.220738	0.855611	-0.736427
H	-2.044785	0.905124	-1.806158
H	-2.693569	1.784488	-0.433722
H	-2.923532	0.045933	-0.564549
C	2.554031	3.516158	2.278713
H	2.267538	2.878485	3.106081
C	4.025119	3.259806	1.986295
H	4.630277	3.457415	2.865050
H	4.374389	3.899091	1.179504
H	4.196724	2.229084	1.696368
C	2.343585	4.962466	2.702645
H	2.926050	5.181825	3.592202
H	1.301062	5.168834	2.924093
H	2.657542	5.654028	1.926273
C	0.784277	0.200463	6.702527
H	1.103132	0.848868	5.895076
C	1.956432	-0.708116	7.053593
H	2.827115	-0.123838	7.332077
H	2.238268	-1.333360	6.213650
H	1.693700	-1.359263	7.883473
C	0.422895	1.065384	7.898961
H	1.261106	1.703199	8.161031
H	0.191669	0.463696	8.772683
H	-0.433017	1.700884	7.699188
C	-1.761284	-1.985870	2.916174
H	-1.407435	-1.123483	2.364565
C	-3.204136	-2.230614	2.509540
H	-3.857966	-1.432019	2.841810
H	-3.583104	-3.162656	2.916447
H	-3.278462	-2.301841	1.428404
C	-0.896324	-3.173987	2.511582
H	0.149932	-3.004871	2.747283
H	-0.973416	-3.367989	1.445572
H	-1.211111	-4.066993	3.044044
Cl	3.452451	0.671793	4.277701

gade_tol_sn_B97M_D3_TZVPP_optfreq

Total correction:	1793.2969 kJ/mol
Single point energy:	-6907356.5888 kJ/mol
Total enthalpy:	-6905560.8128 kJ/mol
Final entropy term:	310.1679 kJ/mol

Total gibbs free enthalpy: -6905870.9808 kJ/mol
Method and Basis: B97M-D3BJ / def2-TZVPP

xyz, charge: -1, multiplicity: 1

C	1.438848	2.552618	0.497423
C	1.343245	3.638034	-0.387741
H	1.372284	4.636327	0.018316
C	1.245169	3.453600	-1.753509
H	1.177881	4.318649	-2.397166
C	1.250598	2.186658	-2.320313
C	1.355117	1.105039	-1.454083
H	1.358511	0.103567	-1.860257
C	1.437174	1.276673	-0.086494
H	1.482674	0.413954	0.557916
C	1.112094	1.992328	-3.795517
H	0.071615	1.864467	-4.094559
H	1.648909	1.110486	-4.134822
H	1.496345	2.847020	-4.345073
C	1.652466	0.339370	3.662367
H	0.755159	0.647900	4.188394
H	2.305207	-0.163397	4.373279
H	1.363523	-0.387260	2.905315
C	4.022888	1.190882	1.987430
H	3.788321	0.429054	1.250127
H	4.728148	0.763763	2.697089
H	4.521666	2.006941	1.472751
C	4.796897	2.940452	5.389722
H	5.611923	2.730228	4.703226
H	4.654792	2.064791	6.016431
H	5.104251	3.762121	6.030202
C	-1.133987	2.791569	4.947591
C	-1.790601	3.013431	6.166945
H	-1.356181	3.706158	6.869110
C	-2.989395	2.396235	6.468100
H	-3.462946	2.599974	7.417910
C	-3.614223	1.538849	5.571901
C	-2.980879	1.323627	4.354731
H	-3.437946	0.664560	3.630882
C	-1.773571	1.920376	4.050294
H	-1.293668	1.709663	3.108075
C	-4.901081	0.858031	5.909101
H	-4.748013	-0.174198	6.223935
H	-5.575181	0.829760	5.056721
H	-5.414448	1.366130	6.720275
C	1.327062	2.336825	7.066630
H	0.484691	2.416785	7.747038
H	2.239719	2.406493	7.654550

H	1.296016	1.348992	6.616265
C	1.272180	5.324147	6.601039
H	1.250399	6.130401	5.875452
H	2.147868	5.461449	7.232400
H	0.390235	5.417995	7.231894
C	1.121195	6.992468	3.063088
C	-0.089354	7.305912	3.699272
H	-0.617913	6.520824	4.215685
C	-0.601710	8.589920	3.691842
H	-1.539459	8.784084	4.191640
C	0.063998	9.636829	3.071558
C	1.266623	9.338329	2.440298
H	1.803959	10.125986	1.931247
C	1.779091	8.057218	2.426474
H	2.692375	7.853071	1.891726
C	-0.474877	11.030562	3.093855
H	0.058404	11.664932	3.801603
H	-1.522290	11.041611	3.379660
H	-0.392878	11.508974	2.120571
C	4.161437	6.613479	4.223592
H	4.260155	7.560401	3.701545
H	5.160900	6.263034	4.471924
H	3.633860	6.801951	5.154006
C	4.184448	5.128475	1.591761
H	3.698293	4.395563	0.956679
H	5.208102	4.801296	1.763325
H	4.224024	6.069965	1.047028
N	1.505903	2.755440	1.857997
N	0.051732	3.405381	4.610186
N	1.596903	5.700140	3.046478
Si	2.506749	1.824836	2.901499
Si	1.328630	3.662924	5.733347
Si	3.262330	5.305950	3.214681
Si	3.208303	3.369801	4.448491
Sn	0.085188	4.213961	2.599105

iPr_NHC_B97M_D3_TZVPP_optfreq

Total correction:	1592.3559 kJ/mol
Single point energy:	-3049451.8114 kJ/mol
Total enthalpy:	-3047856.9764 kJ/mol
Final entropy term:	222.8927 kJ/mol
Total gibbs free enthalpy:	-3048079.869 kJ/mol
Method and Basis:	B97M-D3BJ / def2-TZVPP

xyz, charge: 0, multiplicity: 1

N	-0.698174	0.842655	1.111872
C	0.509529	1.213088	1.619677
N	0.133009	1.910611	2.726631
C	-1.238845	1.967178	2.898740
C	-1.769893	1.290497	1.863992
H	-1.693008	2.473412	3.723974
H	-2.784635	1.087606	1.594367
C	-0.853213	0.095849	-0.090058
C	-1.168622	-1.343728	-2.404256
C	-0.752951	0.760662	-1.308370
C	-1.107094	-1.273379	0.002293
C	-1.267861	-1.979750	-1.180066
C	-0.909119	0.009881	-2.466730
H	-1.465248	-3.036288	-1.147038
H	-0.826507	0.493037	-3.425109
H	-1.292492	-1.909016	-3.312672
C	1.053561	2.497757	3.639830
C	2.817960	3.635595	5.406305
C	1.673823	1.682749	4.581692
C	1.292333	3.870386	3.557643
C	2.183859	4.424460	4.463592
C	2.568790	2.279727	5.460721
H	2.391877	5.478939	4.429632
H	3.072959	1.673859	6.193937
H	3.510819	4.082671	6.099304
C	-0.432389	2.228926	-1.389895
H	-0.567225	2.658915	-0.402637
C	-1.347801	2.973135	-2.348483
H	-2.393364	2.827034	-2.096842
H	-1.204295	2.648486	-3.374460
H	-1.136764	4.037593	-2.315196
C	1.028545	2.413743	-1.777619
H	1.678550	1.929525	-1.057815
H	1.284648	3.468302	-1.819932
H	1.218456	1.980945	-2.756392
C	-1.116391	-1.963521	1.341348
H	-1.501478	-1.261994	2.076160
C	-1.994245	-3.200424	1.384273
H	-3.003509	-2.993060	1.043072
H	-2.050916	-3.578175	2.400014
H	-1.590848	-3.999842	0.770219
C	0.313881	-2.308305	1.742880
H	0.945196	-1.427760	1.739599
H	0.733580	-3.027643	1.044501
H	0.338131	-2.748950	2.735927
C	0.666701	4.694057	2.462378
H	-0.309978	4.272046	2.242825

C	1.511139	4.576613	1.197914
H	2.495723	5.004997	1.366261
H	1.046822	5.112231	0.374250
H	1.640077	3.540567	0.908111
C	0.462680	6.150741	2.834904
H	1.407927	6.674923	2.937781
H	-0.082298	6.257608	3.767437
H	-0.097865	6.656362	2.055297
C	1.436395	0.197340	4.630578
H	0.570882	-0.026422	4.015575
C	1.145308	-0.297688	6.038172
H	0.309750	0.233319	6.482840
H	2.002965	-0.174778	6.692377
H	0.903144	-1.355889	6.019378
C	2.629154	-0.534704	4.030735
H	2.795495	-0.219287	3.007028
H	2.464810	-1.608202	4.038663
H	3.529195	-0.327177	4.603603

iPr_NHSn_B97M_D3_TZVPP_optfreq

Total correction:	1577.514 kJ/mol
Single point energy:	-3512414.6779 kJ/mol
Total enthalpy:	-3510834.6849 kJ/mol
Final entropy term:	239.2382 kJ/mol
Total gibbs free enthalpy:	-3511073.9231 kJ/mol
Method and Basis:	B97M-D3BJ / def2-TZVPP

xyz, charge: 0, multiplicity: 1

N	-0.304608	0.590122	0.755046
Sn	1.693699	0.896444	1.266522
N	0.660511	1.845190	2.809855
C	-0.699951	1.784512	2.705151
C	-1.204936	1.127469	1.630097
H	-1.311026	2.250824	3.458340
H	-2.258690	1.017631	1.441042
C	-0.773076	-0.064861	-0.408381
C	-1.552912	-1.361345	-2.724478
C	-0.975087	0.678329	-1.577030
C	-0.982453	-1.447876	-0.383798
C	-1.367491	-2.078475	-1.558803
C	-1.361090	0.006488	-2.728335
H	-1.520128	-3.144649	-1.561298
H	-1.508161	0.560895	-3.640004
H	-1.848625	-1.867372	-3.628035
C	1.242193	2.566401	3.879312

C	2.508033	3.954885	5.909974
C	1.600761	1.892753	5.051786
C	1.489251	3.935482	3.725432
C	2.129597	4.610833	4.754805
C	2.240997	2.607630	6.054675
H	2.339500	5.661842	4.647756
H	2.536367	2.102001	6.958559
H	3.008136	4.493599	6.697164
C	-0.739712	2.165780	-1.613973
H	-0.641223	2.511976	-0.590626
C	-1.898600	2.919313	-2.247078
H	-2.836259	2.690650	-1.751643
H	-2.010117	2.672776	-3.298620
H	-1.732404	3.990341	-2.181438
C	0.562319	2.478472	-2.339187
H	1.405466	1.983756	-1.865497
H	0.757500	3.547152	-2.344266
H	0.518408	2.138680	-3.370388
C	-0.756963	-2.253861	0.868212
H	-0.668709	-1.559026	1.696541
C	-1.914729	-3.191711	1.170633
H	-2.854876	-2.653313	1.227372
H	-1.754324	-3.694961	2.119321
H	-2.017667	-3.959965	0.410305
C	0.549636	-3.029707	0.768716
H	1.391067	-2.363297	0.601331
H	0.516295	-3.731487	-0.060275
H	0.739350	-3.591613	1.678864
C	1.118114	4.664399	2.460361
H	0.467643	4.017082	1.882114
C	2.360708	4.942161	1.624857
H	3.051989	5.582352	2.166205
H	2.100017	5.438214	0.694174
H	2.885273	4.022538	1.381715
C	0.360297	5.953125	2.736385
H	0.980020	6.679302	3.253662
H	-0.517954	5.771866	3.346926
H	0.037908	6.407879	1.804578
C	1.344238	0.418189	5.218780
H	0.654605	0.113238	4.438794
C	0.705903	0.087318	6.558390
H	-0.203818	0.657301	6.714628
H	1.376534	0.299295	7.385554
H	0.457253	-0.968524	6.606465
C	2.635639	-0.367046	5.033206
H	3.073947	-0.179342	4.057105
H	2.458774	-1.435034	5.124144

H	3.368291	-0.080968	5.783036

boryl_li_thf2_B97M_D3_TZVPP_optfreq

Total correction:	2260.2654 kJ/mol
Single point energy:	-4256791.2991 kJ/mol
Total enthalpy:	-4254528.5546 kJ/mol
Final entropy term:	296.8922 kJ/mol
Total gibbs free enthalpy:	-4254825.4467 kJ/mol
Method and Basis:	B97M-D3BJ / def2-TZVPP

xyz, charge: 0, multiplicity: 1

B	1.027853	1.956075	3.435961
N	1.088029	3.419834	3.517284
C	2.395416	3.888038	3.472468
H	2.632863	4.933140	3.511733
C	3.222467	2.834204	3.355835
H	4.292553	2.817909	3.291192
N	2.457819	1.673390	3.311364
Li	-0.839844	0.753407	3.602372
C	0.013001	4.301311	3.737422
C	-0.161607	4.870195	5.005244
C	-1.226731	5.739075	5.202188
H	-1.377699	6.185593	6.169422
C	-2.105170	6.030301	4.176495
H	-2.926215	6.707340	4.344984
C	-1.932420	5.448130	2.935057
H	-2.624706	5.679389	2.144332
C	-0.879370	4.576936	2.692865
C	0.723338	4.459487	6.154780
H	1.705780	4.232252	5.755978
C	0.890612	5.533752	7.213504
H	1.212132	6.477000	6.783195
H	1.634083	5.223283	7.940916
H	-0.031684	5.712715	7.758970
C	0.180738	3.178230	6.778667
H	-0.809324	3.351734	7.195165
H	0.828116	2.836161	7.581793
H	0.110874	2.388160	6.037369
C	-0.665309	3.962856	1.334744
H	-0.278878	2.961591	1.504716
C	0.395066	4.739594	0.564421
H	0.068308	5.762716	0.393829
H	0.582021	4.280194	-0.402535
H	1.330678	4.767996	1.110455
C	-1.935413	3.838763	0.515563

H	-2.719872	3.327955	1.068094
H	-1.738774	3.272237	-0.389396
H	-2.322398	4.806397	0.208005
C	3.083201	0.412464	3.364986
C	3.245647	-0.338898	2.193138
C	3.860628	-1.579504	2.284621
H	3.995003	-2.174594	1.398108
C	4.313683	-2.064718	3.498713
H	4.791676	-3.028984	3.548508
C	4.148714	-1.312636	4.643743
H	4.490537	-1.699322	5.589889
C	3.529275	-0.070193	4.597875
C	2.797402	0.221982	0.868079
H	1.881822	0.778544	1.055389
C	3.829540	1.207339	0.330395
H	3.990557	2.026365	1.018944
H	3.501953	1.624071	-0.618197
H	4.779482	0.704214	0.167191
C	2.512689	-0.836613	-0.181616
H	2.063226	-0.377942	-1.056531
H	1.835966	-1.604767	0.179529
H	3.423174	-1.328569	-0.512497
C	3.300267	0.700162	5.871960
H	2.883237	1.664554	5.607882
C	4.594310	0.940454	6.632512
H	5.047984	0.007576	6.955566
H	4.407674	1.538369	7.519859
H	5.317996	1.465385	6.017524
C	2.280315	-0.016184	6.745031
H	1.333966	-0.111599	6.221665
H	2.101858	0.535801	7.663397
H	2.623408	-1.012388	7.012751
O	-1.034180	-1.133846	3.272463
C	-0.233488	-1.623650	2.172238
H	0.466912	-0.839133	1.903532
H	-0.898603	-1.817357	1.338111
C	0.477216	-2.849036	2.694760
H	-0.145038	-3.733560	2.585623
H	1.417694	-3.020607	2.187363
C	0.658098	-2.492860	4.160203
H	0.858984	-3.347860	4.794139
H	1.470335	-1.783127	4.267844
C	-0.659142	-1.830993	4.476073
H	-1.436459	-2.555529	4.713726
H	-0.604281	-1.104468	5.281585
O	-2.570381	1.175814	4.256931
C	-3.766925	0.490253	3.895685

H	-4.265330	0.138859	4.800968
H	-3.485948	-0.361492	3.292001
C	-4.587485	1.544336	3.187803
H	-5.647866	1.321748	3.195878
H	-4.269762	1.618894	2.152889
C	-4.235878	2.826879	3.953272
H	-4.032147	3.649526	3.280727
H	-5.039817	3.133411	4.612143
C	-2.989270	2.455819	4.755326
H	-2.162729	3.137546	4.628693
H	-3.209425	2.354071	5.816314

sn2_cxet_C2_sym_B97M_D3_TZVPP_opt_freq

Total correction:	2137.4583 kJ/mol
Single point energy:	-4821002.9493 kJ/mol
Total enthalpy:	-4818863.0121 kJ/mol
Final entropy term:	282.2566 kJ/mol
Total gibbs free enthalpy:	-4819145.2687 kJ/mol
Method and Basis:	B97M-D3BJ / def2-TZVPP

xyz, charge: -2, multiplicity: 1

N	-0.124733	0.339902	0.321157
C	0.821571	-0.652542	0.286980
C	0.313432	-1.782488	0.901857
C	-0.988584	-1.459847	1.343478
C	-1.229801	-0.151528	0.964979
H	0.821783	-2.718132	1.049424
H	-1.636466	-2.094931	1.919190
C	2.165924	-0.497418	-0.379633
C	3.171917	-1.429218	0.321539
H	4.124010	-1.357686	-0.197193
H	2.828684	-2.452148	0.174928
C	3.387571	-1.176302	1.801180
H	3.729610	-0.162754	1.973068
H	4.133365	-1.861703	2.204322
H	2.465300	-1.313313	2.353331
C	2.030952	-0.997081	-1.846672
H	1.179158	-0.495159	-2.294938
H	1.770763	-2.055723	-1.804167
C	3.239330	-0.778991	-2.734545
H	3.481077	0.276247	-2.798548
H	3.043530	-1.147002	-3.740598
H	4.125001	-1.290903	-2.365561
C	2.693909	0.913328	-0.345603
C	4.006533	1.316688	-0.174640

C	4.024090	2.722721	-0.285580
C	2.722564	3.122547	-0.535831
N	1.914542	2.020794	-0.567235
H	4.854877	0.684490	0.012527
H	4.882424	3.358640	-0.168243
C	2.167188	4.520258	-0.500934
C	1.625470	4.719684	0.945219
H	0.979009	3.872703	1.153556
H	2.472369	4.640886	1.628622
C	0.850964	5.998898	1.189192
H	0.532159	6.056715	2.228531
H	-0.032498	6.036829	0.561654
H	1.442232	6.887013	0.977492
C	3.294010	5.529716	-0.743070
H	2.887231	6.530402	-0.624220
H	4.028875	5.404755	0.050747
C	3.984277	5.427576	-2.091632
H	4.462209	4.462588	-2.209745
H	4.744597	6.201573	-2.198415
H	3.272360	5.539055	-2.900735
C	-2.304969	0.777393	1.452588
C	-1.642916	1.728566	2.492570
H	-2.434779	2.333883	2.936375
H	-1.009974	2.409106	1.931358
C	-3.410093	-0.018740	2.154260
H	-4.082313	0.693870	2.629756
H	-2.959285	-0.592976	2.959205
C	-4.210320	-0.951262	1.262392
H	-4.723607	-0.397424	0.485584
H	-4.954306	-1.498731	1.841470
H	-3.563979	-1.671612	0.775244
C	-0.810237	1.056700	3.565466
H	0.019199	0.515713	3.123702
H	-1.388235	0.347564	4.153911
H	-0.405113	1.798926	4.251147
C	-2.912433	1.677307	0.411156
N	-2.151199	2.335257	-0.513633
C	-2.950060	3.251456	-1.150353
C	-4.228259	3.171516	-0.626347
C	-4.202848	2.177419	0.373980
H	-5.081490	3.755307	-0.919008
H	-5.024406	1.888601	1.003677
C	1.022918	4.790285	-1.435914
C	0.764452	5.934097	-2.169341
C	-0.579625	5.854622	-2.595464
C	-1.093063	4.674118	-2.089746
N	-0.111088	4.022918	-1.387442

H	1.432098	6.759676	-2.334166
H	-1.108650	6.591405	-3.172409
C	-2.479572	4.115467	-2.291450
C	-3.459545	5.289513	-2.474135
H	-4.446320	4.883719	-2.680567
H	-3.163421	5.825487	-3.374416
C	-2.481984	3.312120	-3.623912
H	-2.276550	4.020047	-4.428242
H	-1.641120	2.625890	-3.604590
C	-3.740871	2.521006	-3.915813
H	-4.624482	3.152006	-3.975881
H	-3.921201	1.789549	-3.135811
H	-3.648273	1.994322	-4.864513
C	-3.549956	6.263263	-1.315008
H	-3.852097	5.755644	-0.406866
H	-4.277124	7.047471	-1.526596
H	-2.589847	6.730551	-1.130285
Sn	-0.161069	1.773153	-1.413187

se_me2_B97M_TZVPP_optfreq

Total correction:	210.9131 kJ/mol
Single point energy:	-6514382.6723 kJ/mol
Total enthalpy:	-6514169.2802 kJ/mol
Final entropy term:	90.8452 kJ/mol
Total gibbs free enthalpy:	-6514260.1254 kJ/mol
Method and Basis:	B97M-D3BJ / def2-TZVPP

xyz, charge: 0, multiplicity: 1

Se	0.212154	-0.948711	0.849987
C	1.765040	-0.005770	1.519983
H	2.610990	-0.161371	0.863089
H	1.992476	-0.410668	2.497021
H	1.551744	1.051257	1.612318
C	0.097787	-0.005328	-0.837178
H	0.999770	-0.159013	-1.415232
H	-0.062407	1.051409	-0.666828
H	-0.746382	-0.411804	-1.377963

sn2_py2_B97M_D3_TZVPP_optfreq

Total correction:	406.6968 kJ/mol
Single point energy:	-1664672.2335 kJ/mol
Total enthalpy:	-1664263.0576 kJ/mol
Final entropy term:	127.4968 kJ/mol
Total gibbs free enthalpy:	-1664390.5544 kJ/mol

Method and Basis: B97M-D3BJ / def2-TZVPP

xyz, charge: 0, multiplicity: 1

Sn	0.424245	0.435842	1.616764
N	-0.509415	0.807483	3.435964
C	-0.635345	1.949560	4.196907
C	-1.212032	1.628679	5.393137
C	-1.457952	0.229352	5.383259
C	-1.010873	-0.243136	4.184281
H	-0.279289	2.889329	3.829051
H	-1.425777	2.310474	6.192737
H	-1.907998	-0.349852	6.165052
H	-1.013536	-1.240522	3.787392
N	0.279346	2.380097	0.896043
C	1.080986	2.786860	-0.156271
C	0.713807	4.041873	-0.544822
C	-0.371339	4.430240	0.285804
C	-0.611892	3.399915	1.150262
H	1.855478	2.143995	-0.529454
H	1.162501	4.620059	-1.328141
H	-0.913892	5.354045	0.239879
H	-1.357051	3.293279	1.910936

sn2_py3_B97M_D3_TZVPP_optfreq

Total correction: 606.1873 kJ/mol
Single point energy: -2215822.5461 kJ/mol
Total enthalpy: -2215213.8797 kJ/mol
Final entropy term: 156.8635 kJ/mol
Total gibbs free enthalpy: -2215370.7432 kJ/mol
Method and Basis: B97M-D3BJ / def2-TZVPP

xyz, charge: -1, multiplicity: 1

Sn	-0.512397	0.317129	0.827212
N	1.617228	0.011173	0.780088
C	2.312285	-0.309422	-0.352065
C	3.660348	-0.327656	-0.077265
C	3.794362	-0.004225	1.293896
C	2.523679	0.197067	1.784238
H	4.449454	-0.547060	-0.772377
H	4.708294	0.069221	1.853594
H	2.190300	0.463221	2.767868
N	-0.445998	0.650399	2.951733
C	-0.136636	1.799055	3.622199
C	-0.112322	1.544544	4.975017
C	-0.420315	0.173446	5.141854

C	-0.619370	-0.337712	3.880052
H	0.046613	2.705773	3.080179
H	0.097628	2.258078	5.750108
H	-0.489462	-0.368280	6.066924
H	-0.863182	-1.337444	3.571172
N	-0.244228	2.420182	0.457415
C	0.918450	3.135737	0.430421
C	0.628482	4.469561	0.250382
C	-0.779901	4.576901	0.163871
C	-1.276858	3.300383	0.292951
H	1.860567	2.637202	0.546345
H	1.342378	5.269584	0.185291
H	-1.354847	5.473383	0.023149
H	-2.293197	2.952029	0.289739
H	1.793998	-0.490837	-1.275555

sn2_py4_B97M_D3_TZVPP_optfreq

Total correction:	801.6555 kJ/mol
Single point energy:	-2766550.168 kJ/mol
Total enthalpy:	-2765746.0335 kJ/mol
Final entropy term:	186.8122 kJ/mol
Total gibbs free enthalpy:	-2765932.8457 kJ/mol
Method and Basis:	B97M-D3BJ / def2-TZVPP

xyz, charge: -2, multiplicity: 1

Sn	-0.403203	-0.069244	1.036870
N	1.760954	0.050065	0.714290
C	2.434020	1.106262	0.170182
C	3.758782	0.768320	-0.010827
C	3.900692	-0.566297	0.441490
C	2.655023	-0.970196	0.873580
H	4.527420	1.407833	-0.409560
H	4.800293	-1.157236	0.459225
H	2.339253	-1.903195	1.294506
N	-0.190572	0.613543	3.097949
C	0.959346	0.926161	3.750008
C	0.668529	1.307297	5.046099
C	-0.736858	1.220118	5.186742
C	-1.219616	0.790625	3.966229
H	1.900297	0.852387	3.240842
H	1.378975	1.609283	5.795599
H	-1.319728	1.442839	6.063469
H	-2.230371	0.598396	3.655669
N	-0.421796	2.262370	0.628996
C	-0.095724	3.342788	1.383363

C	-0.211205	4.503153	0.635917
C	-0.634213	4.103960	-0.654265
C	-0.750869	2.725283	-0.604660
H	0.201868	3.212240	2.407018
H	-0.021997	5.508206	0.975584
H	-0.831699	4.739074	-1.502123
H	-1.041554	2.035484	-1.378858
N	0.029986	-2.164093	2.052295
C	0.459719	-2.531500	3.286447
C	0.599312	-3.907913	3.356515
C	0.230688	-4.409524	2.085568
C	-0.112020	-3.303415	1.326840
H	0.641798	-1.784343	4.036182
H	0.918144	-4.478847	4.213076
H	0.214035	-5.439754	1.769939
H	-0.441902	-3.252567	0.302958
H	1.922153	2.025139	-0.033171

sn2_se_cxet_B97M_TZVPP_optfreq

Total correction:	2150.8152 kJ/mol
Single point energy:	-11125702.2397 kJ/mol
Total enthalpy:	-11123548.9454 kJ/mol
Final entropy term:	291.002 kJ/mol
Total gibbs free enthalpy:	-11123839.9473 kJ/mol
Method and Basis:	B97M-D3BJ / def2-TZVPP

xyz, charge: -2, multiplicity: 1

N	-0.125903	0.306799	0.262673
C	0.836076	-0.679961	0.257106
C	0.327174	-1.795188	0.886477
C	-0.981346	-1.479939	1.308298
C	-1.236054	-0.187296	0.908199
H	0.844054	-2.720743	1.056397
H	-1.629329	-2.109938	1.887314
C	2.210547	-0.540612	-0.338271
C	3.190352	-1.347627	0.544318
H	4.171366	-1.319330	0.078786
H	2.878178	-2.388339	0.505652
C	3.298341	-0.906990	1.990180
H	3.626969	0.123417	2.058745
H	4.010953	-1.528790	2.531654
H	2.337208	-0.985418	2.486343
C	2.205594	-1.216043	-1.736928
H	1.337891	-0.865594	-2.281981
H	2.061188	-2.284489	-1.568931

C	3.430088	-0.972459	-2.592436
H	3.508352	0.077323	-2.851233
H	3.354675	-1.538258	-3.519056
H	4.358233	-1.260490	-2.101596
C	2.697171	0.881203	-0.399991
C	4.003364	1.301165	-0.259223
C	4.013402	2.703438	-0.385636
C	2.712760	3.098929	-0.614065
N	1.905374	1.989090	-0.621846
H	4.855610	0.675418	-0.076308
H	4.869200	3.344702	-0.292843
C	2.165627	4.493587	-0.571186
C	1.641679	4.700596	0.882004
H	1.002532	3.852954	1.112352
H	2.498983	4.629380	1.552455
C	0.865876	5.978084	1.128612
H	0.566023	6.043817	2.172754
H	-0.029022	6.008327	0.517112
H	1.449775	6.865709	0.898177
C	3.292911	5.499905	-0.826856
H	2.889699	6.500488	-0.698291
H	4.036000	5.371462	-0.041815
C	3.965130	5.400649	-2.184265
H	4.439887	4.436132	-2.314337
H	4.724757	6.173903	-2.295865
H	3.245042	5.515236	-2.985041
C	-2.315077	0.731544	1.386929
C	-1.672314	1.689283	2.435143
H	-2.476708	2.279926	2.875130
H	-1.046834	2.387025	1.885619
C	-3.420868	-0.072062	2.079835
H	-4.104938	0.637105	2.542617
H	-2.972693	-0.633056	2.895088
C	-4.199548	-1.021257	1.187017
H	-4.719138	-0.482481	0.404487
H	-4.935559	-1.578408	1.766061
H	-3.539985	-1.731989	0.704512
C	-0.836202	1.026695	3.510576
H	0.008375	0.505087	3.074299
H	-1.405687	0.302204	4.087428
H	-0.453108	1.771710	4.205307
C	-2.915077	1.617606	0.337813
N	-2.151125	2.301731	-0.574313
C	-2.963275	3.214296	-1.215426
C	-4.239164	3.094657	-0.705279
C	-4.208190	2.091901	0.282556
H	-5.097299	3.667978	-0.998994

H	-5.030679	1.778218	0.896806
C	1.020089	4.760743	-1.495430
C	0.752125	5.908265	-2.207655
C	-0.596138	5.838458	-2.616047
C	-1.113443	4.658788	-2.126449
N	-0.119708	3.991722	-1.443437
H	1.421019	6.731914	-2.369539
H	-1.130163	6.583622	-3.174863
C	-2.525434	4.167139	-2.293692
C	-3.459438	5.398869	-2.253855
H	-4.473402	5.065152	-2.455370
H	-3.189619	6.036962	-3.091654
C	-2.660863	3.546907	-3.711638
H	-2.553975	4.366335	-4.424226
H	-1.823177	2.880135	-3.874267
C	-3.935773	2.775220	-3.975168
H	-4.835159	3.359372	-3.787660
H	-3.980869	1.893507	-3.346133
H	-3.963249	2.445421	-5.012015
C	-3.431671	6.209286	-0.973679
H	-3.711631	5.600215	-0.122158
H	-4.122006	7.050451	-1.032805
H	-2.436917	6.601331	-0.791978
Sn	-0.155365	1.829301	-1.282064
Se	-0.257363	0.833204	-3.452635

sn2_se_cxh_B97M_TZVPP_optfreq

Total correction:	892.4403 kJ/mol
Single point energy:	-9472035.7851 kJ/mol
Total enthalpy:	-9471140.8659 kJ/mol
Final entropy term:	180.7943 kJ/mol
Total gibbs free enthalpy:	-9471321.6601 kJ/mol
Method and Basis:	B97M-D3BJ / def2-TZVPP

xyz, charge: -2, multiplicity: 1

N	-0.251770	0.338792	0.223980
C	0.703399	-0.642017	0.265509
C	0.293814	-1.630907	1.130210
C	-0.973680	-1.235604	1.633497
C	-1.276602	-0.021922	1.054909
H	0.839159	-2.529343	1.361665
H	-1.579387	-1.752429	2.358209
C	1.923452	-0.534055	-0.583397
C	2.600006	0.790481	-0.488086
C	3.925715	1.112341	-0.308386

C	4.011623	2.529059	-0.343575
C	2.733503	3.005895	-0.540524
N	1.874960	1.944458	-0.625186
H	4.730996	0.410478	-0.177806
H	4.891697	3.134028	-0.206748
C	2.251370	4.410942	-0.457460
C	-2.389693	0.906378	1.390530
C	-2.930038	1.771179	0.307313
N	-2.121128	2.364965	-0.622219
C	-2.875822	3.243874	-1.353005
C	-4.170352	3.218674	-0.887195
C	-4.205625	2.275773	0.173694
H	-4.988648	3.801700	-1.272697
H	-5.048716	2.018862	0.792096
C	1.080800	4.799733	-1.289297
C	0.780977	6.037829	-1.815488
C	-0.537522	5.959459	-2.336509
C	-0.979202	4.676539	-2.107559
N	0.005489	3.973141	-1.465860
H	1.424113	6.900971	-1.791813
H	-1.095436	6.738536	-2.826352
C	-2.258926	4.006882	-2.474756
Sn	-0.157518	1.831923	-1.323413
Se	-0.264344	0.835084	-3.492476
H	3.079926	5.077150	-0.691929
H	1.646945	-0.717177	-1.627494
H	2.625751	-1.313299	-0.297625
H	-3.208341	0.327176	1.814362
H	-2.050665	1.560206	2.207493
H	-2.074147	3.322636	-3.310092
H	-2.964646	4.755919	-2.825494
H	2.004839	4.622235	0.593455

sn_dodecaborate_B97M_D3_TZVPP_optfreq

Total correction:	423.165 kJ/mol
Single point energy:	-1300280.5692 kJ/mol
Total enthalpy:	-1299854.9251 kJ/mol
Final entropy term:	112.0966 kJ/mol
Total gibbs free enthalpy:	-1299967.0217 kJ/mol
Method and Basis:	B97M-D3BJ / def2-TZVPP

xyz, charge: -2, multiplicity: 1

B	0.917182	1.081397	-0.867889
B	-0.566166	0.409403	-1.527349
B	0.857031	-0.617081	-1.313820

B	1.666439	-0.205375	0.189691
Sn	1.030560	1.706066	1.386465
B	-0.713478	1.511461	-0.167240
B	-0.749726	-1.244866	-0.940020
B	0.606151	-1.603808	0.131083
B	0.497740	-0.569975	1.548570
B	-0.971501	0.490528	1.328454
B	-1.695175	0.056565	-0.214038
B	-0.971557	-1.188616	0.809295
H	1.561802	1.831817	-1.553949
H	-0.952664	0.726464	-2.619566
H	1.480457	-1.028308	-2.254593
H	2.853264	-0.388858	0.273544
H	-1.252944	2.573184	-0.342616
H	-1.263743	-2.097058	-1.611557
H	1.052882	-2.715817	0.216447
H	0.839785	-1.022678	2.610134
H	-1.705881	0.811806	2.226682
H	-2.884003	0.124447	-0.373467
H	-1.645996	-2.005596	1.375594

sn_me4_PBEh3c_optfreq

Total correction:	418.198 kJ/mol
Single point energy:	-980942.3411 kJ/mol
Total enthalpy:	-980521.6641 kJ/mol
Final entropy term:	125.3206 kJ/mol
Total gibbs free enthalpy:	-980646.9847 kJ/mol
Method and Basis:	PBEh-3c / def2-mSVP

xyz, charge: 0, multiplicity: 1

Sn	0.000012	-0.000000	0.999958
C	-1.018761	-1.764587	1.720326
H	-0.523849	-2.669890	1.370424
H	-2.050208	-1.788687	1.370360
H	-1.032696	-1.788648	2.809440
C	2.037553	-0.000004	1.720379
H	2.574141	0.881232	1.370467
H	2.574141	-0.881235	1.370457
H	2.065323	-0.000010	2.809492
C	-1.018761	1.764579	1.720346
H	-0.523850	2.669886	1.370453
H	-1.032696	1.788628	2.809460
H	-2.050209	1.788683	1.370380
C	-0.000023	0.000012	-1.161196
H	0.508741	-0.881220	-1.550463

H	0.508741	0.881249	-1.550454
H	-1.017596	0.000014	-1.550410

sn_dithiolate_B97M_D3_TZVPP_optfreq

Total correction:	468.1406 kJ/mol
Single point energy:	-5959619.6617 kJ/mol
Total enthalpy:	-5959149.0422 kJ/mol
Final entropy term:	168.4528 kJ/mol
Total gibbs free enthalpy:	-5959317.495 kJ/mol
Method and Basis:	B97M-D3BJ / def2-TZVPP

xyz, charge: -2, multiplicity: 1

Sn	5.190364	-0.265657	4.791056
S	6.712104	0.768042	6.787963
S	7.191583	1.000637	3.921334
S	3.790052	0.251249	2.528635
S	3.381020	1.460964	5.148614
C	7.835667	1.059616	5.531643
C	9.190406	1.321073	5.756760
C	9.840576	1.423202	7.028232
H	9.339103	1.310469	7.971261
C	11.174433	1.678814	6.813467
H	11.927972	1.805753	7.574592
C	11.398492	1.746828	5.400370
H	12.348071	1.931415	4.923649
C	10.199480	1.532223	4.762289
H	10.020056	1.509745	3.703514
C	2.731912	1.081906	3.585206
C	1.424769	1.437410	3.239724
C	0.784488	1.211951	1.979220
H	1.257316	0.735599	1.140735
C	-0.498113	1.702282	2.051042
H	-1.232108	1.680391	1.261102
C	-0.698486	2.250270	3.359136
H	-1.608652	2.705497	3.716041
C	0.463924	2.091391	4.076591
H	0.647446	2.386164	5.093062

phi_B97M_D3_TZVPP_opt_freq

Total correction:	254.7123 kJ/mol
Single point energy:	-1390798.861 kJ/mol
Total enthalpy:	-1390541.6697 kJ/mol
Final entropy term:	100.8168 kJ/mol

Total gibbs free enthalpy: -1390642.4865 kJ/mol
Method and Basis: B97M-D3BJ / def2-TZVPP

xyz, charge: 0, multiplicity: 1

H	-0.000001	-0.005664	-0.005601
C	0.000003	-0.001131	1.069467
C	0.000002	-0.003106	3.842451
C	0.000005	-1.193260	1.772803
C	0.000002	1.194219	1.768733
C	0.000001	1.197165	3.152968
C	0.000004	-1.206350	3.156892
H	-0.000003	2.123510	1.224718
H	-0.000004	2.129041	3.691223
H	0.000000	-2.139652	3.690524
H	-0.000003	-0.009485	4.919231
I	-0.000007	-3.000151	0.729836

phi_sn2_cxet_B97M_D3_TZVPP_TightOpt_opt_freq

Total correction: 2400.345 kJ/mol
Single point energy: -6211860.6354 kJ/mol
Total enthalpy: -6209457.8114 kJ/mol
Final entropy term: 328.8666 kJ/mol
Total gibbs free enthalpy: -6209786.678 kJ/mol
Method and Basis: B97M-D3BJ / def2-TZVPP

xyz, charge: -2, multiplicity: 1

N	-0.007564	0.522737	0.198932
C	1.014985	-0.396697	0.173938
C	0.584847	-1.562443	0.776036
C	-0.743097	-1.345131	1.198593
C	-1.081401	-0.059369	0.826742
H	1.158839	-2.458988	0.918237
H	-1.349370	-2.030975	1.759865
C	2.338646	-0.160722	-0.502889
C	3.399771	-1.066145	0.151761
H	4.329378	-0.952066	-0.399698
H	3.088939	-2.096917	-0.004592
C	3.654558	-0.834726	1.628275
H	3.984272	0.180971	1.810742
H	4.422313	-1.514391	1.997335
H	2.751267	-0.998836	2.204230
C	2.192612	-0.630972	-1.974956
H	1.261161	-0.241440	-2.361310
H	2.070213	-1.714312	-1.955941
C	3.307325	-0.235769	-2.918583

H	3.376398	0.843038	-3.000998
H	3.118312	-0.637586	-3.911837
H	4.278211	-0.598527	-2.588739
C	2.804991	1.267779	-0.426193
C	4.105893	1.713252	-0.298073
C	4.063764	3.122102	-0.275406
C	2.738477	3.489235	-0.407249
N	1.969703	2.357969	-0.499971
H	4.985849	1.103738	-0.213748
H	4.902130	3.779596	-0.141436
C	2.130897	4.840011	-0.159807
C	1.618084	4.800732	1.311510
H	1.023591	3.897802	1.412001
H	2.487207	4.670904	1.957905
C	0.786506	5.986503	1.755291
H	0.507135	5.881266	2.802001
H	-0.121867	6.060425	1.168034
H	1.319917	6.928330	1.650903
C	3.211517	5.920667	-0.267869
H	2.776921	6.870620	0.030863
H	3.978679	5.694711	0.470425
C	3.851536	6.072129	-1.636073
H	4.326682	5.149758	-1.947334
H	4.606419	6.857994	-1.625344
H	3.111512	6.324546	-2.385826
C	-2.230382	0.764935	1.323984
C	-1.676194	1.695109	2.444901
H	-2.527014	2.208000	2.895517
H	-1.082710	2.459367	1.952419
C	-3.303846	-0.143500	1.932101
H	-4.051404	0.495034	2.399161
H	-2.852111	-0.716316	2.737209
C	-3.980736	-1.093856	0.960960
H	-4.480662	-0.549537	0.169050
H	-4.720805	-1.708740	1.472533
H	-3.257722	-1.752363	0.494973
C	-0.827142	1.022883	3.504030
H	0.061968	0.585812	3.063620
H	-1.361001	0.227522	4.018784
H	-0.514394	1.747437	4.253646
C	-2.857398	1.683590	0.315197
N	-2.103073	2.506536	-0.480396
C	-2.946529	3.418134	-1.071293
C	-4.238255	3.162510	-0.655229
C	-4.181477	2.069124	0.232583
H	-5.121169	3.703283	-0.939698
H	-5.008811	1.644826	0.769764

C	0.960037	5.194248	-1.025993
C	0.618711	6.439113	-1.515538
C	-0.722852	6.361791	-1.944262
C	-1.157374	5.076590	-1.687579
N	-0.124748	4.358774	-1.130919
H	1.233067	7.319751	-1.512879
H	-1.302188	7.160604	-2.368180
C	-2.497670	4.484964	-2.032620
C	-3.548437	5.611830	-2.051024
H	-4.491620	5.189838	-2.388379
H	-3.250664	6.320887	-2.820448
C	-2.402305	3.936950	-3.482104
H	-2.303608	4.796749	-4.145491
H	-1.473815	3.391137	-3.575883
C	-3.534734	3.040882	-3.933605
H	-4.504624	3.526447	-3.853602
H	-3.574447	2.139871	-3.331974
H	-3.390205	2.746339	-4.970944
C	-3.761289	6.347657	-0.742632
H	-4.080930	5.667750	0.037774
H	-4.521727	7.120125	-0.855104
H	-2.843252	6.821093	-0.414558
Sn	-0.081312	2.143830	-1.321338
I	-0.135856	1.074528	-4.381717
C	-0.164523	0.342539	-6.450274
C	-0.195893	-0.588703	-9.080630
C	0.997275	-0.125283	-7.046350
C	-1.342338	0.339280	-7.182769
C	-1.360125	-0.123752	-8.489277
C	0.984048	-0.587086	-8.353251
H	1.917209	-0.126971	-6.482390
H	-2.250428	0.701355	-6.726055
H	-2.284091	-0.121093	-9.048559
H	1.896064	-0.947577	-8.805741
H	-0.207952	-0.948517	-10.097335

14 Literature

[1] D. Jacoby, C. Floriani, A. Chiesi-Villa, C. Rizzoli, *Journal of the American Chemical Society* **1993**, *115*, 3595-3602.

[2] D. Geiß, M. I. Arz, M. Straßmann, G. Schnakenburg, A. C. Filippou, *Angewandte Chemie International Edition* **2015**, *54*, 2739-2744.

[3] G. Sheldrick, *Acta Crystallogr. A* **2015**, *71*, 3-8.

[4] G. Sheldrick, *Acta Crystallographica Section C* **2015**, *71*, 3-8.

[5] C. B. Hubschle, G. M. Sheldrick, B. Dittrich, *Journal of Applied Crystallography* **2011**, *44*, 1281-1284.

[6] G. Sheldrick, *Acta Crystallographica Section A* **2008**, *64*, 112-122.

[7] aF. Neese, *WIREs Computational Molecular Science* **2012**, *2*, 73-78; bF. Neese, *WIREs Computational Molecular Science* **2018**, *8*, e1327.

[8] aT. Z. E.J. Baerends, A.J. Atkins, J. Autschbach, O. Baseggio, D. Bashford, A. Bérces, F.M. Bickelhaupt, C. Bo, P.M. Boerrigter, L. Cavallo, C. Daul, D.P. Chong, D.V. Chulhai, L. Deng, R.M. Dickson, J.M. Dieterich, D.E. Ellis, M. van Faassen, L. Fan, T.H. Fischer, A. Förster, C. Fonseca Guerra, M. Franchini, A. Ghysels, A. Giammona, S.J.A. van Gisbergen, A. Goez, A.W. Götz, J.A. Groeneveld, O.V. Gritsenko, M. Grüning, S. Gusarov, F.E. Harris, P. van den Hoek, Z. Hu, C.R. Jacob, H. Jacobsen, L. Jensen, L. Joubert, J.W. Kaminski, G. van Kessel, C. König, F. Kootstra, A. Kovalenko, M.V. Krykunov, E. van Lenthe, D.A. McCormack, A. Michalak, M. Mitoraj, S.M. Morton, J. Neugebauer, V.P. Nicu, L. Noodleman, V.P. Osinga, S. Patchkovskii, M. Pavanello, C.A. Peeples, P.H.T. Philipsen, D. Post, C.C. Pye, H. Ramanantoanina, P. Ramos, W. Ravenek, M. Reimann, J.I. Rodríguez, P. Ros, R. Rüger, P.R.T. Schipper, D. Schlüns, H. van Schoot, G. Schreckenbach, J.S. Seldenthuis, M. Seth, J.G. Snijders, M. Solà, M. Stener, M. Swart, D. Swerhone, V. Tognetti, G. te Velde, P. Vernooijs, L. Versluis, L. Visscher, O. Visser, F. Wang, T.A. Wesolowski, E.M. van Wezenbeek, G. Wiesenekker, S.K. Wolff, T.K. Woo, A.L. Yakovlev*, Vol. 2020*, Theoretical Chemistry, Vrije Universiteit, Amsterdam, The Netherlands, **2019**; bG. te Velde, F. M. Bickelhaupt, E. J. Baerends, C. Fonseca Guerra, S. J. A. van Gisbergen, J. G. Snijders, T. Ziegler, *Journal of Computational Chemistry* **2001**, *22*, 931-967.

[9] A. Najibi, L. Goerigk, *Journal of Chemical Theory and Computation* **2018**, *14*, 5725-5738.

[10] F. Weigend, R. Ahlrichs, *Physical Chemistry Chemical Physics* **2005**, *7*, 3297-3305.

[11] V. Barone, M. Cossi, *The Journal of Physical Chemistry A* **1998**, *102*, 1995-2001.

[12] C. Adamo, V. Barone, *Journal of Chemical Physics* **1999**, *110*, 6158--6170.

[13] E. Glendening, J. Badenhoop, A. Reed, J. Carpenter, J. Bohmann, C. Morales, C. Landis, F. Weinhold, in *Google Scholar There is no corresponding record for this reference*, Theoretical Chemistry Institute,

University of Wisconsin: Madison, WI, **2013**.

[14] F. M. Bickelhaupt, E. J. Baerends, in *Reviews in Computational Chemistry*, **2000**, pp. 1-86.

[15] M. P. Mitoraj, A. Michalak, T. Ziegler, *Journal of Chemical Theory and Computation* **2009**, *5*, 962-975.

[16] aJ. P. Perdew, *Physical Review B* **1986**, *33*, 8822-8824; bA. D. Becke, *Physical Review A* **1988**, *38*, 3098-3100; cS. Grimme, J. Antony, S. Ehrlich, H. Krieg, *The Journal of Chemical Physics* **2010**, *132*, 154104.

[17] S. K. Wolff, T. Ziegler, E. v. Lenthe, E. J. Baerends, *The Journal of Chemical Physics* **1999**, *110*, 7689-7698.

[18] K. Anjali, M. Ahmed, J. Christopher, A. Sakthivel, *Dalton Transactions* **2018**, *47*, 12353-12361.

[19] R. F. Culmo, C. Shelton, *Application note. Waltham, MA: Perkin Elmer* **2013**.

[20] M. A. Wünsche, P. Mehlmann, T. Witteler, F. Buß, P. Rathmann, F. Dielmann, *Angewandte Chemie International Edition* **2015**, *54*, 11857-11860.

[21] U. S. D. Paul, U. Radius, *European Journal of Inorganic Chemistry* **2017**, *2017*, 3362-3375.

[22] R. A. Kelly Iii, H. Clavier, S. Giudice, N. M. Scott, E. D. Stevens, J. Bordner, I. Samardjiev, C. D. Hoff, L. Cavallo, S. P. Nolan, *Organometallics* **2008**, *27*, 202-210.

[23] M. L. Kelty, A. J. McNeece, A. S. Filatov, J. Anderson, *ChemRxiv* **2021**.

3.2 Conformational and Substitution Effects on the Donor and Reducing Strength of Tin(II) Porphyrinogens

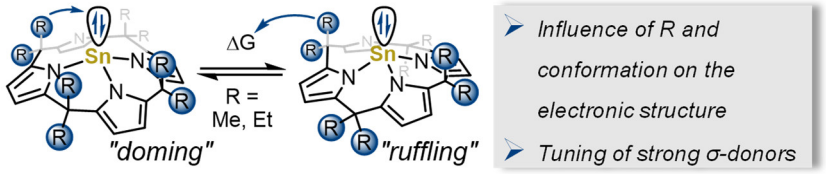


Figure 23. Table of contents graphic of the publication presented in this chapter.

The article and supplementary information (SI) presented within this section were previously published and can be found under: H. Ruppert, A. Meister, P. Janßen, L. Greb, *Chem. Eur. J.* **2024**, e202401685, https://doi.org/10.1002/chem.202401685.

According to the CRediT scheme[271] the authors contributed to this publication as followed:

H. Ruppert – Conceptualization (*lead*), Methodology (*lead*), Validation (*lead*), Formal analysis (*lead*), Investigation (*lead*), Data curation (*lead*), Writing – Original Draft Preparation (*lead*), Writing – Review & Editing (*equal*), Visualization (*lead*), Supervision (*equal*), Project Administration (*equal*), Funding acquisition (*equal*);

A. Meister – Formal analysis (*supporting*), Investigation (*supporting*), Data curation (*supporting*);

P. Janßen – Formal analysis (*supporting*), Investigation (*supporting*), Data curation (*supporting*);

L. Greb –Resources (*lead*), Writing – Review & Editing (*equal*), Supervision (*equal*), Project Administration (*equal*), Funding acquisition (*equal*).

Check for updates

Chemistry
A European
Journal

Chemistry Europe
European Chemical Societies Publishing

Accepted Article

Title: Conformational and Substitution Effects on the Donor and Reducing Strength of Tin(II) Porphyrinogens

Authors: Heiko Ruppert, Arne Meister, Paul Janßen, and Lutz Greb

This manuscript has been accepted after peer review and appears as an Accepted Article online prior to editing, proofing, and formal publication of the final Version of Record (VoR). The VoR will be published online in Early View as soon as possible and may be different to this Accepted Article as a result of editing. Readers should obtain the VoR from the journal website shown below when it is published to ensure accuracy of information. The authors are responsible for the content of this Accepted Article.

To be cited as: *Chem. Eur. J.* **2024**, e202401685

Link to VoR: https://doi.org/10.1002/chem.202401685

WILEY VCH

10.1002/chem.202401685

WILEY-VCH

RESEARCH ARTICLE

Conformational and Substitution Effects on the Donor and Reducing Strength of Tin(II) Porphyrinogens

Heiko Ruppert,[a] Arne Meister,[a] Paul Janßen,[a] and Lutz Greb*[a]

Dedicated to Ian Manners

[a] Heiko Ruppert, Arne Meister, Paul Janßen, Prof. Dr. Lutz Greb
Anorganisch-Chemisches Institut
Ruprecht-Karls-Universität Heidelberg
Im Neuenheimer Feld 275, 69120 Heidelberg (Germany)
E-mail: greb@uni-heidelberg.de

Supporting information for this article is given via a link at the end of the document.

Abstract: *Meso*-octaalkylcalix[4]pyrrolates are a class of redox-active porphyrinogen ligands. They have been well established in *d*- and *f*-block chemistry for over three decades but have only recently been introduced as ligands for *p*-block elements. Here, we present a study on the influence of *meso*-substituents on the redox chemistry of calix[4]pyrrolato stannate(II) dianions **[2^{R}]$^{2-}$** (R = Me, Et). Expansion of the normal-mode structural decomposition (NSD) method, well known for porphyrin chemistry, provides insights into the ligand conformation of a calix[4]pyrrolato *p*-block complex. Combined with the results of spectroscopic donor scaling, electrochemical studies, and quantum mechanical bond analysis tools, subtle but significant substitution and conformational effects on the electronic structure are revealed. Exploiting this knowledge rationalizes the role of this class of tin(II) dianions to act as potent reducing agents, but can also be expanded for other central elements. Photoexcitation boosts this reactivity further, allowing for the reduction of even challenging chlorobenzene.

Introduction

Molecular, low-valent main group element compounds find widespread application as selective reducing agents,[1,2] ambiphiles for the activation of small molecules,[3–5] or strong σ-donor ligands in transition metal chemistry.[6–8] In each field, modifications of the ligand backbone enabled chemists to tune the properties of these complexes by influencing the electronic structure around the main group element center.[2,9–11]

We recently reported the tetracoordinated, structurally constrained *meso*-octaethylcalix[4]-pyrrolato stannate(II) dianion **[2^{Et}]$^{2-}$** and explored its chemistry as a strong tin-centered σ-donor and nucleophile as well as reducing agent (Figure 1A).[12,13] The calix[4]pyrrolato ligand acts as a macrocyclic, tetradentate scaffold which imparts a structurally constrained coordination environment around the tin(II) center, leveraging its reducing and nucleophilic properties. Beneficially, the straightforward synthesis of the calix[4]pyrrole ligand system **H$_4$[1^{R}]** *via* the acid-catalyzed condensation of pyrrole with ketones allows its fast modification simply by employing different ketones or pyrroles as starting material (Figure 1 B).[14–17] Even though the redox-chemistry of calix[4]pyrrolato **[1^{R}]$^{4-}$** complexes of transition metals have been studied over three decades, a comparative work on the influence of the *meso*-substituents on their redox-properties is missing.[18–22] Moreover, it is well known that the conformation of porphyrins, e.g., ruffling and doming, strongly affects their chemical and optical properties,[23–27] while corresponding insights for calix[4]pyrrolato complexes are lacking.

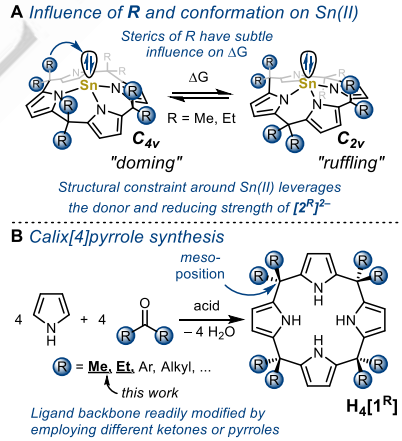


Figure 1. A) Different conformers of structurally constraint *meso*-octaalkylcalix[4]pyrrolato stannate(II) dianion **[2^{R}]$^{2-}$** and **B)** calix[4]pyrrole synthesis *via* the acid-catalyzed condensation of pyrrole and ketones.

This article is protected by copyright. All rights reserved.

15213765, ja, Downloaded from https://chemistry-europe.onlinelibrary.wiley.com/doi/10.1002/chem.202401685 by Heidelberg University, Wiley Online Library on [03/04/2024]. See the Terms and Conditions (https://onlinelibrary.wiley.com/terms-and-conditions) on Wiley Online Library for rules of use; OA articles are governed by the applicable Creative Commons License

Accepted manuscript

10.1002/chem.202401685

In this work we are introducing the *meso*-octamethylcalix[4]-pyrrolato stannate(II) dianion **[2^{Me}]$^{2-}$** and experimentally scale and compare its σ-donor and reducing strength with its homologue **[2^{Et}]$^{2-}$**. Experimental and computational analyses, including bond analysis tools (NBO, ETS-NOCV, and QTAIM), identify the key influence of the *meso*-substituents R as well as the conformation of the calix[4]pyrrole backbone on the electronic structure of these stannate(II) dianions, which allow for a more rational tuning of properties for future applications.

Results and Discussion

Synthesis of [2^{Me}]$^{2-}$ Salts

In analogy to its ethyl congener, reaction of the lithium salt of *meso*-octamethylcalix[4]pyrrolate **[Li$_4$(thf)$_x$][1^{Me}]** with one equivalent tin(II) chloride in tetrahydrofuran (THF) at room temperature yielded the lithium salt of the dianionic stannate(II) **[Li$_2$(thf)$_x$][2^{Me}]** in excellent yields of 92% and varying THF contents x (Figure 2A). Heteronuclear NMR spectroscopy in THF-d_8 indicated characteristics in solution which are in agreement with the respective *meso*-octaethylcalix[4]pyrrolato stannate(II) **[Li$_2$(thf)$_x$][2^{Et}]**: i) a C_{4v} symmetric complex with two diastereotopic sets of methyl residues and one sharp singlet with $^{117/119}$Sn satellites ($^4J_{Sn,H}$ = 162.8 Hz) for the β-hydrogen atoms of the pyrroles at 5.85 ppm, ii) a sharp ^{7}Li NMR resonance at −0.79 ppm for solvated lithium cations, and iii) a relatively high-field shifted ^{119}Sn NMR resonance at −495.9 ppm indicating a highly coordinated tin(II) center (*cf.* −481.3 ppm for R = Et).[12] Cooling of a concentrated solution of the crude material in 1,2-difluorobenzene (*o*DFB) at −30 °C yielded single crystals (sc) suitable for X-ray diffraction (XRD). The molecular solid-state structure shows the coordination of tin(II) by the *tetra*-dentate calix[4]pyrrolate forming a square pyramidal C_{4v} symmetric complex. In this structure, two **[2^{Me}]$^{2-}$** are bridged by four lithium cations forming a cage-like complex that captures a chloride anion in its center (Figure S28). Similar structural motifs have already been reported for the lithium salts of anionic nickel(II) complexes of calix[4]pyrrolate.[28] Redissolving the crude in THF and its subsequent precipitation with excess *n*-pentane allowed the removal of excess LiCl, delivering **[Li$_2$(thf)$_x$][2^{Me}]** (x = 4.0) in bulk purity as confirmed by elemental analysis. Salt metathesis with PPh_4Cl or NBu_4Cl yielded the respective phosphonium and ammonium salts of **[2^{Me}]$^{2-}$** in satisfying yields (Figure 2B).

Recrystallization of crude **[(PPh$_4$)$_2$(*o*DFB$_{0.5}$)][2^{Me}]** from *o*DFB yielded single crystals suitable for X-ray diffraction (co-crystallized with 0.5 *o*DFB, one THF, and one MeCN molecule in the asymmetric unit, Figure 2C). The solid-state molecular structure shows a C_{2v} symmetric conformation of **[2^{Me}]$^{2-}$** with two axial methyl residues (Me_{ax}) pointing upward *syn* to the Sn(II), two Me_{ax} pointing downward *anti* to the Sn(II), and four equatorial methyl groups (Me_{eq}). A similar sc-XRD structure could also be observed for the respective **[(PPh$_4$)$_2$(*o*DFB$_{0.5}$)][2^{Et}]** salt.[12]

Experimental Scaling of [2^{Me}]$^{2-}$ and Comparison with [2^{Et}]$^{2-}$

The high σ-donor and reducing strength of *meso*-octaethylcalix[4]pyrrolato stannate(II) **[2^{Et}]$^{2-}$** has been evidenced on different experimental scales consisting of i) the ^{77}Se NMR shift of the respective tin(II) selenide **[Li$_2$(thf)$_x$][2^{Et}-Se]**,[29] ii) the Tolman Electronic Parameter (TEP) recorded for its σ-adduct with Ni(CO)$_3$ **[(NBu$_4$)$_2$][Ni(η^1-2^{Et})(CO)$_3$]**,[30] and iii) cyclic voltammetry of **[(NBu$_4$)$_2$][2^{Et}]**.[12] In analogy, we synthesized the respective selenium and Ni(CO)$_3$ adducts of **[2^{Me}]$^{2-}$**. **[Li$_2$(thf)$_x$][2^{Me}-Se]** delivered a down-field shifted ^{77}Se NMR shift in comparison to the

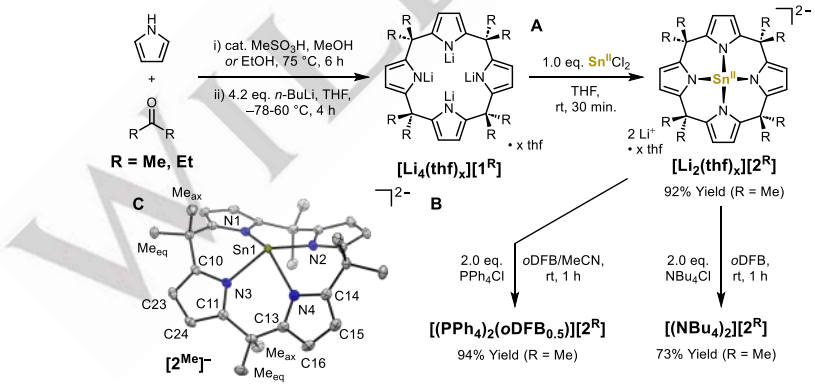


Figure 2. A) Synthesis of the lithium salts of *meso*-octaalkylcalix[4]pyrrolato stannates(II) **[2^R]$^{2-}$** (R = Me, Et) and **B)** their subsequent salt exchange forming the respective NBu_4^+ and PPh_4^+ salts. A mixture of *o*DFB with traces of MeCN has been used to increase the solubility of **[(PPh$_4$)$_2$(*o*DFB)$_{0.5}$][2^{Me}]** and allow its quantitative extraction. **C)** Solid-state molecular structure of **[(PPh$_4$)$_2$(*o*DFB)$_{0.5}$][2^{Me}]**. Displacement ellipsoids are drawn at 50% probability level. Hydrogens, PPh_4^+ counter cations, displaced Sn(II), and solvent molecules are omitted for clarity. Selected bond lengths [pm] and angels [°]: Sn1-N1 226.0(2), Sn1-N2 222.7(2), Sn1-N3 222.82(19), Sn1-N4 225.3(2), N1-Sn1-N4 128.98(7), N2-Sn1-N3 126.33(7), *cis*-N-Sn-N between 76.02(7) and 81.29(7), Sn1-N3-C11-C24 153.71(16), Sn1-N3-C10-C23 −157.28(15), Sn1-N4-C13-C16 −172.27(15), Sn1-N4-C14-C15 173.33(15).

This article is protected by copyright. All rights reserved.

15213765, ja, Downloaded from https://chemistry-europe.onlinelibrary.wiley.com/doi/10.1002/chem.202401685 by Heidelberg University Hochschulrech, Wiley Online Library on [14/06/2024]. See the Terms and Conditions (https://onlinelibrary.wiley.com/terms-and-conditions) on Wiley Online Library for rules of use; OA articles are governed by the applicable Creative Commons License

Accepted Manuscript

10.1002/chem.202401685
WILEY-VCH

RESEARCH ARTICLE

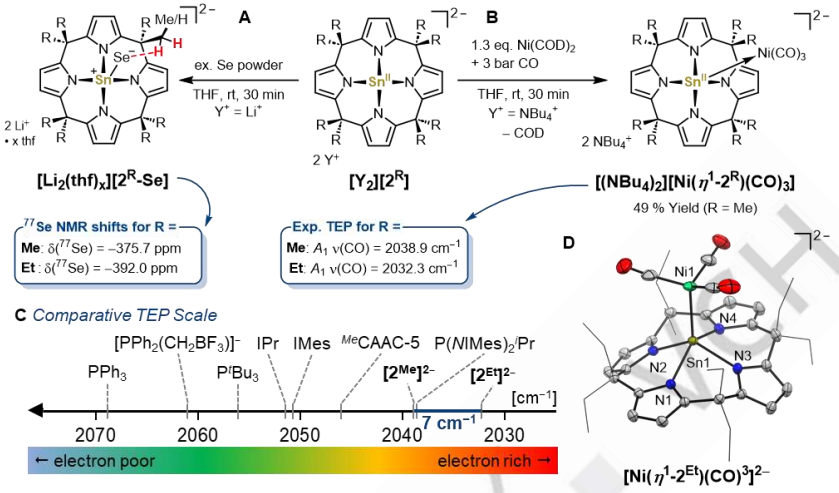


Figure 3. Synthesis of **A)** the tin(II) selenides $[2^{R}\text{-Se}]^{2-}$ and **B)** $[(Ni(\eta^1\text{-}2^{R})(CO)_3]^{2-}$ complexes with their respective ^{77}Se NMR shifts and TEP values for R = Me, Et.[12] **C)** TEP scale comparing $[2^{Me}]^{2-}$ and $[2^{Et}]^{2-}$ with literature known phosphine and carbene ligands. **D)** Solid-state molecular structure of $[(NBu_4)_2][Ni(\eta^1\text{-}2^{R})(CO)_3]$. Displacement ellipsoids are drawn at 50% probability level. Hydrogens and NBu_4^+ counter cations are omitted for clarity. R_{int} = 15.5%

ethyl-substituted analogue (δ(^{77}Se) = −375.7 ppm for R = Me *vs.* −392.0 ppm for R = Et, Figure 3A). As for $[2^{Et}\text{-Se}]^{2-}$ ^{1}H,^{77}Se HMBC NMR spectroscopy aided by NBO and ETS-NOCV calculations evidenced non-classical hydrogen bonding interactions between methyl hydrogen atoms and selenium in $[2^{Me}\text{-Se}]^{2-}$ potentially causing a downfield shift of the ^{77}Se resonance.[31] However, since for both $[2^{R}\text{-Se}]^{2-}$ (R = Me, Et) these secondary interactions are in a similar energy range (~2% to the total orbital interaction energy $\Delta E_{oi,tot}$ between the Se atom and $[2^{R}]^{2-}$), the main influence on the ^{77}Se chemical shift can be expected to stem from the Sn→Se σ-donor interaction contributing to ~85% of $\Delta E_{oi,tot}$ (Table S4 and S5 and Figure S37).The observed downfield shift could further be reproduced by quantum chemical calculations of the ^{77}Se-NMR-shifts (PBE0 / SO-ZORA-TZ2P (COSMO(THF)) // B97M-D3(BJ) / def2-TZVPP, Table S6). Hence, the ^{77}Se-NMR-shift scale attested stronger donicity to the *meso*-ethyl-substituted derivative. IR spectra of $[(NBu_4)_2][Ni(\eta^1\text{-}2^{Me})(CO)_3]$ in THF yielded an A_1 ν(CO) stretching frequency which is red shift by ~7 cm^{-1} (TEP = 2038.9 cm^{-1} for R = Me *vs.* 2032.3 cm^{-1} for R = Et, Figure 3 B). Accordingly, also this scale indicates a reduced σ-donor strength of the Sn(II) center when going from the ethyl- to the methyl-substituted calix[4]pyrrolato stannate(II) dianion. Still, comparison of these TEP values with those of other literature known σ-donor ligands demonstrates their remarkable donor strengths surpassing that of neutral and anionic phosphines, *N*-heterocyclic carbenes (NHC), and even cyclic alkyl(amino)carbenes (CAAC) and lying in the range of highly electron-rich phosphines (Figure 3 C).[32,33] Supplementing the previously reported synthesis of $[(NBu_4)_2][Ni(\eta^1\text{-}2^{Et})(CO)_3]$ we were now able to obtain its solid-state molecular structure, clearly evidencing the η^1 coordination of the Sn(II) to the Ni(CO)$_3$ fragment (Figure 3 D).

The influence of the *meso*-substituents R was further probed by the redox behavior of the stannate(II) dianions via cyclic voltammetry. $[(NBu_4)_2][2^{Me}]$ possesses two irreversible one-electron oxidations at −0.85 V and −0.36 V and one irreversible two-electron oxidation at 0.02 V (*vs.* Fc$^+$/Fc, Figure S35). Whereas the first two oxidation waves are shifted to higher potentials, the third oxidation wave stays unchanged at 0.02 V (*cf* −0.95 V, −0.49 V, and 0.02 V observed for $[(NBu_4)_2][2^{Et}]$). These findings are in line with the first two one-electron oxidations taking place at the calix[4]pyrrole ligand backbone followed by a two-electron oxidation of the Sn(II) center. Thus, the *meso*-substituents strongly influence the oxidation of the ligand backbone, while having a neglectable effect on the oxidation of the Sn(II) center.

Conformational Analysis and Computation

Owing to their structural relationship with metalloporphyrins, calix[4]pyrrole complexes can be characterized based on the normal-coordinate structural decomposition method (NSD) developed by *Jentzen* and *Shelnutt*.[34,35] Whereas the solid-state molecular structures of $[(PPh_4)_2(oDFB_{0.5})][2^{Me}]$ and $[(PPh_4)_2(oDFB_{0.5})][2^{Et}]$ contain C_{2v} symmetric Sn(II) dianions $[2^{R}]^{2-}$, the lithium salt of $[2^{Me}]^{2-}$ and the ammonium salt, W(CO)$_5$

This article is protected by copyright. All rights reserved.

15213765, ja, Downloaded from https://chemistry-europe.onlinelibrary.wiley.com/doi/10.1002/chem.202401685 by Heidelberg University, Universitaetsbibliothek, Wiley Online Library on [date]. See the Terms and Conditions (https://onlinelibrary.wiley.com/terms-and-conditions) on Wiley Online Library for rules of use; OA articles are governed by the applicable Creative Commons License

Accepted manuscript

10.1002/chem.202401685

and Ni(CO)$_3$ complexes of **[2^{Et}]$^{2-}$** show a C_{4v} symmetric conformer of the respective calix[4]pyrrolato stannate(II).[12] Using the *PorphyStruct* tool developed by the group around *Bröring*, the C_{2v} conformer could be characterized as doming, while the C_{4v} form resembles a ruffling displacement of the pyrrole rings from a perfectly planar arrangement.[36] However, for all cases ^{1}H NMR spectroscopy showed C_{4v} symmetric (doming) species in solution, indicating a highly flexible calix[4]pyrrole backbone around Sn(II) which shows a fast conformational ring flip at room temperature. For **[2^{Me}]$^{2-}$**, computations (DSD-BLYP/def2-QZVPP COSMO-RS(THF)// B97M-D3(BJ)/def2-TZVPP// CREST/GFN2-xTB level of theory) revealed only a 0.2 kJ mol^{-1} energy difference between the C_{2v} and C_{4v} conformers, whereas for **[2^{Et}]$^{2-}$** a slight stabilization of −12.4 kJ mol^{-1} favoring the C_{2v} symmetric (ruffling) conformer could be observed (Figure 4A *vs*. B). For **[2^{Me}]$^{2-}$**, a flipping mechanism consisting of two independent ring inversions with low transition energies ($\Delta G^{\ddagger}$ = 14.5 and 16.7 kJ mol^{-1}) converting the C_{2v} into the respective C_{4v} forms were identified (Figure S36). The orbital energies and the influence of the conformation was studied next. Investigation of the frontier molecular orbital (FMO) energies of **[2^{R}]$^{2-}$** confirmed the experimental trends. The energies of the highest occupied molecular orbitals (HOMO) correlate with the experimental reducing power of **[2^{R}]$^{2-}$** (−3.00 eV for R = Me *vs*. −2.79 eV for R = Et), and the energies of the tin-centered HOMO-4 are in agreement with the observed trend in σ-donor strengths (−3.37 eV for R = Me *vs*. −3.26 eV for R = Et), rendering **[2^{Et}]$^{2-}$** the stronger σ-donor and reducing agent (Figure 6). Interestingly, this comparison also revealed a significant impact of the conformers for each stannate(II). As shown in Figure 4C for **[2^{Me}]$^{2-}$**, the respective orbitals of both conformers show similar shape and localization. However, the C_{4v} stannates(II) possess a higher-lying HOMO being centered on the calix[4]pyrrole backbone, while the respective C_{2v} conformers showed significantly increased energies for their HOMO-4 possessing a large contribution of the electron lone-pair (lp) at Sn(II) and *vice versa* (Figure 4A and B). ETS-NOCV bonding analysis (BP86-D3/TZ2P COSMO-RS(THF)) of the interaction between the tetraanionic calix[4]pyrrolato ligand orbitals with the Sn^{2+} revealed the origin for the strong influence of the conformation in **[2^{R}]$^{2-}$**. Whereas the doming conformers show a predominant mixing of ligand-centered σ-donor orbitals into the tin-centered HOMO-4, the ruffling conformers show a more effective admixing of higher-lying

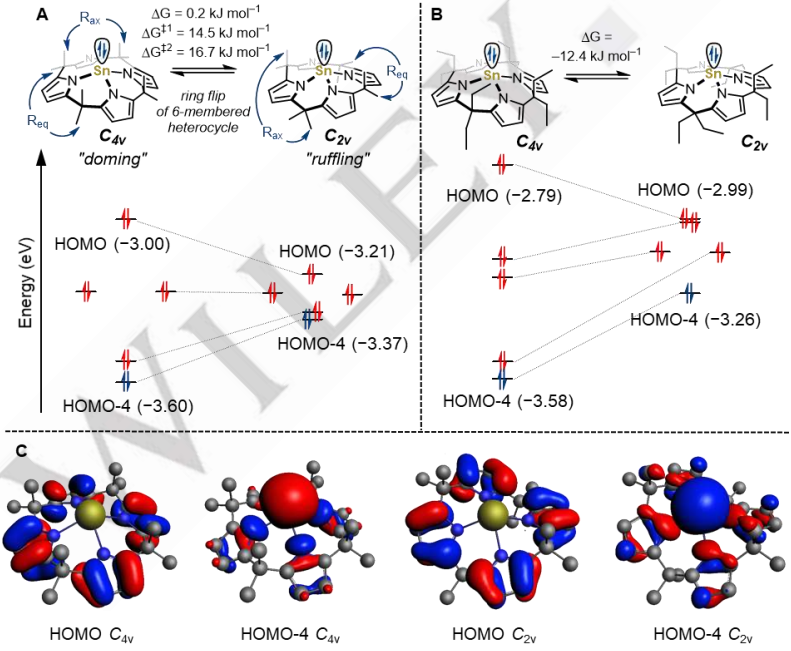


Figure 4. Thermodynamics computed on the DSD-BLYP/def2-QZVPP COSMO-RS(THF)//B97M-D3(BJ)/def2-TZVPP// CREST/GFN2-xTB and energies of occupied molecular orbitals computed on the BP86-D3/TZ2P COSMO-RS(THF)//B97M-D3(BJ)/def2-TZVPP// CREST/GFN2-xTB level of theory for the C_{2v} (ruffling) and C_{4v} (doming) conformers of **A) [2^{Me}]$^{2-}$** and **B) [2^{Et}]$^{2-}$**. **C)** MO isosurface plots for the ligand-centered HOMO and tin-centered HOMO-4 for the different conformers of **[2^{Me}]$^{2-}$** computed on the BP86-D3/TZ2P COSMO(THF)//B97M-D3(BJ)/def2-TVZPP// CREST/GFN2-xTB level of theory and sampled at a value of 0.03.

This article is protected by copyright. All rights reserved.

15213765, ja, Downloaded from https://chemistry-europe.onlinelibrary.wiley.com/doi/10.1002/chem.202401685 by Heidelberg University Universitaetsbibliothek, Wiley Online Library on [14/06/2024]. See the Terms and Conditions (https://onlinelibrary.wiley.com/terms-and-conditions) on Wiley Online Library for rules of use; OA articles are governed by the applicable Creative Commons License

Accepted Manuscript

3.2

π-donor orbitals (Figure S42 – S47). Furthermore, the ruffling conformers show increased total orbital interaction $\Delta E_{oi,tot}$ and Pauli repulsion energies ΔE_{Pauli} indicating an increased bonding between the calix[4]pyrrole and the Sn(II) center (Table S7). In other words, in the C_{2v} form the calix[4]pyrrolate ligand backbone can transfer more of its π-electron density to the Sn(II) center resulting in increased HOMO-4 and decreased, ligand-centered HOMO energies. This picture is supported by the orientation of the pyrrole units in the computed and sc-XRD structures of **[2^{R}]$^{2-}$**. Whereas in their C_{4v} form all pyrrole units point directly towards the Sn(II) acting as σ-donors (Sn-N-C=C dihedral angles between 158° and 174°), the C_{2v} conformers show a tilting of the pyrrole π-faces towards the Sn(II) center enabling a more efficient π-donation (Sn-N-C=C dihedral angles between 144° and 165°, Figure 2C). Eventually, these influences make the C_{2v} conformers stronger tin-centered σ-donors whereas the C_{4v} conformers represent stronger reducing agents. These findings are in close relationship to metalloporphyrins whose electronic structure is highly sensitive to the out-of-plane deformation of the pyrrole units and which can also show only small differences in energy between their conformers.[26,37–39] Even though, the isolation of the doming and ruffling conformers of **[2^{R}]$^{2-}$** is not possible owing to their low-energy barrier interconversion, these findings introduce a linchpin of influencing the electronic properties of *p*-block calix[4]pyrroles by enforcing different conformations in these already structurally constrained complexes.

Further bonding analysis revealed the inductive influence of the *meso*-substituents R on the electronic structure of **[2^{R}]$^{2-}$**. According to ETS-NOCV, QTAIM (PBE0-D3(BJ)/ZORA-TZ2P /COSMO-RS(THF), Table S8) and NBO calculations (PBE0/def2-TZVPP, Table S9) the Sn-N bonds in **[2^{R}]$^{2-}$** are highly polar in nature and are best described as electron donation of the lone pairs at nitrogen into the vacant *p*-orbitals at Sn(II) (Figure S49). Changing R in the sequence H, Me, Et causes an increased charge density at the N atoms in **[2^{R}]$^{2-}$** while both the α-C atoms and the Sn(II) center experience a decrease in charge density (NBO and QTAIM, Figure S48 and Table S8). In addition, ETS-NOCV calculations of the sequence of **[2^{R}]$^{2-}$** (R = H, Me, Et) show a consistent increase in energy for the calix[4]pyrrole-centered orbitals contributing to the final HOMO and HOMO-4. We therefore presume that the *meso*-residues, in addition to the conformational influence described above, further act on the reducing and donor properties of **[2^{R}]$^{2-}$** *via* their inductive influence.

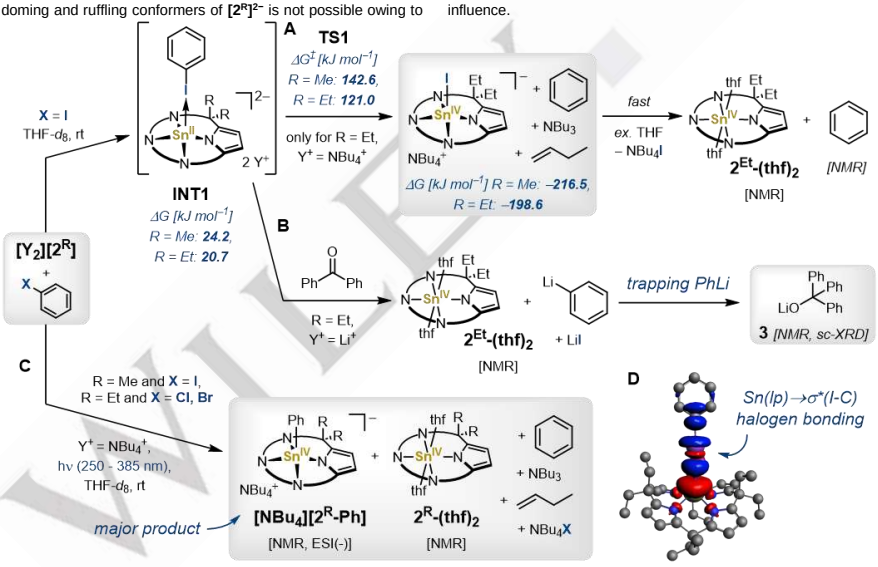


Figure 5. A) Reduction of iodobenzene PhI with **[(NBu$_4$)$_2$][2^{Et}]** in THF-*d*$_8$ *via* a proposed halogen bond precursor complex. Thermodynamics computed on the DSD-BLYP/def2-QZVPP COSMO-RS(THF)//B97M-D3(BJ)/def2-TZVPP// CREST/GFN2-xTB level of theory. Quaternary (alkyl)ammonium cations are known to act as a proton source during the electrochemical reduction of iodobenzene[40] and undergo *Hofmann* degradation under basic conditions (Ph^{-} anion) forming tertiary (alkyl)amines and the respective alkene.[41] This reaction was also presumed for the calculation of free reaction enthalpies. **B)** PhLi trapping experiment with benzophenone on THF-*d*$_8$ forming lithium triphenylmethanolate **3**. **C)** Photoreduction of halobenzenes PhX (X = Cl, Br, I) with different ammonium stannates(II) **[(NBu$_4$)$_2$][2^{R}]** R = Me, Et) in THF-*d*$_8$ forming phenylstannates(IV) **[NBu$_4$][2^{R}-Ph]** as the main product. **D)** ETS-NOCV deformation density for the main interaction between **[2^{Et}]$^{2-}$** and PhI sampled at a value of 0.001 and computed on the BP86-D3/TZ2P COSMO-RS(THF)//B97M-D3(BJ)/def2-TVZPP level of theory. The color code of the charge flow is red to blue.

This article is protected by copyright. All rights reserved.

15213765, ja, Downloaded from https://chemistry-europe.onlinelibrary.wiley.com/doi/10.1002/chem.202401685 by Heidelberg University, Universitaetsbibliothek, Wiley Online Library on [03/04/2024]. See the Terms and Conditions (https://onlinelibrary.wiley.com/terms-and-conditions) on Wiley Online Library for rules of use; OA articles are governed by the applicable Creative Commons License

10.1002/chem.202401685

15213765, ja, Downloaded from https://chemistry-europe.onlinelibrary.wiley.com/doi/10.1002/chem.202401685 by Heidelberg University Kirchhoff Institut, Wiley Online Library on [14/08/2024]. See the Terms and Conditions (https://onlinelibrary.wiley.com/terms-and-conditions) on Wiley Online Library for rules of use; OA articles are governed by the applicable Creative Commons License

Accepted Manuscript

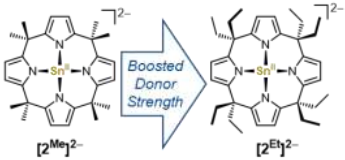
(Photo-)reduction of Aryl Halides

Next, we investigated the influence of R in $[2^{R}]^{2-}$ on their ability to act as a reducing agent. The ammonium salt of $[2^{Et}]^{2-}$ is known to reduce iodobenzene to benzene in THF at room temperature concomitantly forming the oxidized *bis*-(thf)-adduct of *meso*-octaethylcalix[4]pyrrolato stannane 2^{Et}-$(thf)_2$ (Figure 5A).[12] In our previous study, the NBu_4^+ cations were proposed to act as a proton source for intermediate phenyl anions, further details were not available. To confirm the intermediate formation of phenyl anions during the reduction of PhI, we reacted the lithium salt of $[2^{Et}]^{2-}$ with PhI in the presence of benzophenone (Figure 5B). In the absence of NBu_4^+ acting as a proton source, the intermediately formed phenyl lithium should react with benzophenone forming lithium triphenylmethanolate **3**. Indeed, after six hours at room temperature in THF-d_8, ^{1}H NMR spectroscopy confirmed the complete consumption of the starting material and the formation of a new aromatic species. Crystallization attempts at −30 °C yielded single crystals. Despite their quality, the obtained solid-state molecular structure confirmed the formation of **3** (Figure S31). Interestingly, $[(NBu_4)_2][2^{Me}]$ did not reduce PhI under the same conditions, in line with its lower reducing power. Hence, the process was investigated computationally. Optimization of possible encounter complexes before reduction revealed slightly endergonic but exothermic halogen bonding interactions between the electron lone-pair at Sn(II) in $[2^{R}]^{2-}$ and the σ*(I-C) in PhI (**INT1**, Figure 5D and Table S10). The reduction of PhI by $[(NBu_4)_2][2^{R}]$ (R = Me, Et) is calculated to be exergonic with ΔG of −216.5 and −198.6 kJ mol^{-1}, respectively. However, for R = Et a slight stabilization of the encounter complex **INT1** and a reduced transition state energy $\Delta G^{\ddagger}$ for the reduction could be obtained, being in agreement with the increased reactivity of $[(NBu_4)_2][2^{Et}]$.

For the weaker halogen bond donors PhBr and PhCl, adducts as **INT1** could not be optimized and all starting structures dissociated. In addition, no reactions for $[(NBu_4)_2][2^{R}]$ were observed experimentally for these substrates. Photoexcitation represents a prominent way of generating highly reducing excited species.[42][43,44] Hence, we presumed that irradiation of $[2^{R}]^{2-}$ might facilitate its reducing chemistry. Indeed, irradiating a solution of $[(NBu_4)_2][2^{Me}]$ and PhI in THF-d_8 at room temperature for 30 minutes with UV light (250 – 385 nm) resulted in the reduction of PhI. Besides the formation of the *bis*-(thf)-adduct 2^{Me}-$(thf)_2$ and minor, unidentified decomposition products, NMR spectroscopy and ESI(−)-MS revealed the predominant formation of the calix[4]pyrrolato phenylstannate(IV) $[2^{Me}\text{-}Ph]^-$. Encouraged by the photo-enhanced reducing power, we finally attempted the reduction of the more challenging bromo- and chlorobenzene. Indeed, upon irradiating $[(NBu_4)_2][2^{Et}]$ in the presence of PhBr and PhCl, the formation of $[2^{Et}\text{-}Ph]^-$ and 2^{Et}-$(thf)_2$ was observed (Figure 5C). The changed product selectivity favoring the phenyl-stannate(IV) under UV irradiation is in agreement with a proposed single electron transfer (SET) mechanism intermediately forming a calix[4]pyrrolato tin radical anion and a phenyl radical which eventually recombine forming the respective phenyl stannate(IV). The transient formation of phenyl radicals with photo-reductants is known in literature and for some cases their transfer onto substrates could also be achieved.[44–46] In this context, the reactions reported herein only serve as a proof of principle study, and investigations focusing on reaction optimization and substrate scope are required for future studies.

Conclusion

In porphyrin chemistry, the influence of the ligand conformation and substitution on chemical and optoelectronic properties is well understood.[23–27] With this work we introduced the handle of conformational control into the field of calix[4]pyrrole chemistry. It represents the first comparative study on the influence of *meso*-substituents on the conformation and electronic structure of calix[4]pyrrole complexes. Synthesis of *meso*-octamethylcalix[4]-pyrrolato stannate(II) $[2^{Me}]^{2-}$ and comparison with its ethyl analog $[2^{Et}]^{2-}$ revealed substantial differences: i) inductive influences increase the electronic richness of the calix[4]pyrrolato ligand backbone when exchanging methyl for ethyl substituents, ultimately making $[2^{Et}]^{2-}$ a stronger σ-donor and reducing agent on several experimental and theoretical scales (Figure 6); ii) owing to differences in the orbital interactions between ligand and Sn(II) center for ruffling and doming systems, the conformation of the calix[4]pyrrole backbone has a significant effect on the electronic properties of $[2^{R}]^{2-}$; iii) even though inductive effects are subtle for R = Me, Et, the *meso*-substituents steer the preferred conformation of these flexible calix[4]pyrrolato tin(II) complexes, thereby controlling the electronics beyond pure induction. Latter findings highlight the strong influence out-of-plane displacements of the pyrrole units can have in calix[4]pyrrole chemistry, revealing a formerly unknown relationship with metalloporphyrins. This opens up new approaches to influence the electronic properties of structurally constrained complexes such as $[2^{R}]^{2-}$ *via* their conformer distribution and the introduction of *e.g.* highly substituted *ansa*-calix[4]pyrroles.[47] Finally, first experiments showed that the reducing strength of $[2^{R}]^{2-}$ can be boosted by photoexcitation.



R	Me		Et
HOMO (C_{4v}) [eV]	−3.00	↗	−2.79
HOMO-4 (lp, C_{2v}) [eV]	−3.37	↗	−3.26
^{77}Se NMR shift [ppm]	−392.0	↗	−375.7
TEP [cm^{-1}]	2039	↘	2032
$E_{ox,1}$ / $E_{ox,2}$ (Fc/Fc$^+$) [V]	−0.85 / −0.36	↘	−0.95 / −0.49
Reduces PhI at rt	✗		✓

Figure 6. Summary of experimental and theoretical values for the comparison of the σ-donor strength and reducing power of $[2^{Me}]^{2-}$ and $[2^{Et}]^{2-}$. MO energies computed on the BP86-D3/TZ2P COSMO(THF)//B97M-D3(BJ)/def2-TVZPP//CREST/GFN2-xTB level of theory.

This article is protected by copyright. All rights reserved.

WILEY-VCH

RESEARCH ARTICLE

Author Contributions

H.R.: Conceptualization (lead), Investigation (lead), Project Administration (equal), Supervision (equal), Visualization (lead), Writing – Original Draft Preparation (lead), Writing – Review & Editing (equal); **A.M.**: Investigation (supporting); **P.J.**: Investigation (supporting); **L.G.**: Project Administration (equal), Resources (lead), Supervision (equal), Writing – Review & Editing (equal).

Acknowledgements

Financial support for this project was provided by the European Research Council (ERC) under the European Union's Horizon 2020 research and innovation program (grant agreement no 948708). We acknowledge support by the state of Baden-Württemberg through bwHPC and the German Research Foundation (DFG) through Grant INST 40/575-1 FUGG (JUSTUS 2 cluster). H.R. acknowledges the Foundation of German Business (sdw) for funding. We acknowledge M. Schmitt for his support with X-ray crystal structure refinement.

Keywords: Calix[4]pyrrole • Porphyrinogen • Dianion • Conformers • Tin

[1] J. T. Boronski, A. E. Crumpton, L. L. Wales, S. Aldridge, *Science* **2023**, *380*, 1147–1149.
[2] C. Jones, *Nat. Rev. Chem.* **2017**, *1*, 1–9.
[3] C. Weetman, in *Encycl. Inorg. Bioinorg. Chem.*, John Wiley & Sons, Ltd, **2021**, pp. 1–27.
[4] P. P. Power, *Nature* **2010**, *463*, 171–177.
[5] C. Weetman, S. Inoue, *ChemCatChem* **2018**, *10*, 4213–4228.
[6] A. Doddi, M. Peters, M. Tamm, *Chem. Rev.* **2019**, *119*, 6994–7112.
[7] J. Hicks, A. Mansikkamäki, P. Vasko, J. M. Goicoechea, S. Aldridge, *Nat. Chem.* **2019**, *11*, 237–241.
[8] J. Hicks, P. Vasko, J. M. Goicoechea, S. Aldridge, *Angew. Chem. Int. Ed.* **2021**, *60*, 1702–1713.
[9] J. Yu, Y. Qin, G. Tan, H. Wang, H. Cheng, W. Wang, A. Li, *Inorg. Chem.* **2019**, *58*, 5688–5694.
[10] C. Chen, S. M. Bellows, P. L. Holland, *Dalton Trans.* **2015**, *44*, 16654–16670.
[11] S. P. Green, C. Jones, A. Stasch, *Science* **2007**, *318*, 1754–1757.
[12] H. Ruppert, L. Greb, *Angew. Chem. Int. Ed.* **2022**, *61*, e202116615.
[13] H. Ruppert, A. Meister, R. Pfretzschner, A. F. Vieira, L. Greb, *J. Am. Chem. Soc.* **2024**, DOI 10.1021/jacs.4c02446.
[14] A. Baeyer, *Berichte Dtsch. Chem. Ges.* **1886**, *19*, 2184–2185.
[15] B. Turner, A. Shterenberg, M. Kapon, K. Suwinska, Y. Eichen, *Chem. Commun.* **2002**, 404–405.
[16] V. V. Chelintzev, B. V. Tronov, *J Russ Phys Chem Soc* **1916**, 105–155.
[17] P. A. Gale, J. L. Sessler, V. Král, V. Lynch, *J. Am. Chem. Soc.* **1996**, *118*, 5140–5141.
[18] M. Schorpp, R. Yadav, D. Roth, L. Greb, *Angew. Chem.* **2022**, *134*, e202207963.
[19] J. Jubb, C. Floriani, A. Chiesi-Villa, C. Rizzoli, *J. Am. Chem. Soc.* **1992**, *114*, 6571–6573.
[20] J. Bachmann, D. G. Nocera, *J. Am. Chem. Soc.* **2004**, *126*, 2829--2837.
[21] J. Bachmann, D. G. Nocera, *J. Am. Chem. Soc.* **2005**, *127*, 4730–4743.
[22] H. Ruppert, L. M. Sigmund, L. Greb, *Chem. Commun.* **2021**, *57*, 11751–11763.
[23] M. Ravikumar, A. Kathiravan, A. Neels, E. M. Mothi, *Eur. J. Inorg. Chem.* **2018**, *2018*, 3868–3877.
[24] A. B. J. Parusel, T. Wondimagegn, A. Ghosh, *J. Am. Chem. Soc.* **2000**, *122*, 6371–6374.
[25] S. G. DiMagno, A. K. Wertsching, C. R. I. Ross, *J. Am. Chem. Soc.* **1995**, *117*, 8279–8280.
[26] A. Y. Lebedev, M. A. Filatov, A. V. Cheprakov, S. A. Vinogradov, *J. Phys. Chem. A* **2008**, *112*, 7723–7733.
[27] O. A. Dmitrieva, N. V. Chizhova, N. Z. Mamardashvili, *Inorganica Chim. Acta* **2021**, *528*, 120620.
[28] L. Bonomo, E. Solari, M. Latronico, R. Scopelliti, C. Floriani, *Chem. – Eur. J.* **1999**, *5*, 2040–2047.
[29] A. Liske, K. Verlinden, H. Buhl, K. Schaper, C. Ganter, *Organometallics* **2013**, *32*, 5269–5272.
[30] C. A. Tolman, *Chem. Rev.* **1977**, *77*, 313–348.
[31] G. P. Junor, J. Lorkowski, C. M. Weinstein, R. Jazzar, C. Pietraszuk, G. Bertrand, *Angew. Chem.* **2020**, *132*, 22212–22217.
[32] M. A. Wünsche, P. Mehlmann, T. Witteler, F. Buß, P. Rathmann, F. Dielmann, *Angew. Chem. Int. Ed.* **2015**, *54*, 11857–11860.
[33] H. V. Huynh, *Chem. Rev.* **2018**, *118*, 9457–9492.
[34] J. A. Shelnutt, *J. Porphyr. Phthalocyanines* **2001**, *05*, 300–311.
[35] W. Jentzen, X.-Z. Song, J. A. Shelnutt, *J. Phys. Chem. B* **1997**, *101*, 1684–1699.
[36] J. Krumsieck, M. Bröring, *Chem. – Eur. J.* **2021**, *27*, 11580–11588.
[37] J. Conradie, A. Ghosh, *ACS Omega* **2017**, *2*, 6708–6714.
[38] M. P. Austeria, P. D. Pancharatna, M. M. Balakrishnarajan, *Eur. J. Inorg. Chem.* **2014**, *2014*, 3200–3207.
[39] C. J. Kingsbury, M. O. Senge, *Coord. Chem. Rev.* **2021**, *431*, 213760.
[40] R. Alvarado de la Torre, J. W. Sease, *J. Am. Chem. Soc.* **1979**, *101*, 1687–1690.
[41] P. A. S. Smith, S. Frank, *J. Am. Chem. Soc.* **1952**, *74*, 509–513.
[42] N. A. Romero, D. A. Nicewicz, *Chem. Rev.* **2016**, *116*, 10075–10166.
[43] K. Liu, J. Xu, Y. Sun, Y. Guo, S. Jiang, S. Shao, *Spectrochim. Acta. A. Mol. Biomol. Spectrosc.* **2008**, *69*, 1201–1206.
[44] F. Glaser, C. B. Larsen, C. Kerzig, O. S. Wenger, *Photochem. Photobiol. Sci.* **2020**, *19*, 1035–1041.
[45] I. A. MacKenzie, L. Wang, N. P. R. Onuska, O. F. Williams, K. Begam, A. M. Moran, B. D. Dunietz, D. A. Nicewicz, *Nature* **2020**, *580*, 76–80.
[46] F. Weick, N. Hagmeyer, M. Giraud, B. Dietzek-Ivanšić, H.-A. Wagenknecht, *Chem. – Eur. J.* **2023**, *29*, e202302347.
[47] I. A. Rather, R. Ali, A. Ali, *Org. Chem. Front.* **2022**, *9*, 6416–6440.

This article is protected by copyright. All rights reserved.

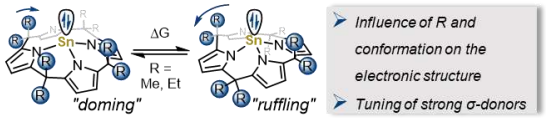
15213765, ja, Downloaded from https://chemistry-europe.onlinelibrary.wiley.com/doi/10.1002/chem.202401685 by Friedrich-Alexander-Universitaet Erlangen-Nuernberg, Wiley Online Library on [03/04/2024]. See the Terms and Conditions (https://onlinelibrary.wiley.com/terms-and-conditions) on Wiley Online Library for rules of use; OA articles are governed by the applicable Creative Commons License

10.1002/chem.202401685

WILEY VCH

RESEARCH ARTICLE

Entry for the Table of Contents



This work presents the first study on the influence of *meso*-substituents on the electronic structure of a calix[4]pyrrolato complex. Expansion of NSD method from porphyrin chemistry provides insights on the ligand conformation of a calix[4]pyrrolato *p*-block complex. Experimental donor strength scaling methods and detailed bond analysis reveal subtle but significant substitution and conformational effects.

Institute and/or researcher Twitter usernames: @GrebGroup

3.2

WILEY · VCH

Accepted Manuscript

15213765, ja, Downloaded from https://chemistry-europe.onlinelibrary.wiley.com/doi/10.1002/chem.202401685 by Heidelberg University Universitaetsbibliothek, Wiley Online Library on [14/08/2024]. See the Terms and Conditions (https://onlinelibrary.wiley.com/terms-and-conditions) on Wiley Online Library for rules of use; OA articles are governed by the applicable Creative Commons License

This article is protected by copyright. All rights reserved.

Supporting Information for

Conformational and Substitution Effects on the Donor and Reducing Strength of Tin(II) Porphyrinogens

*Heiko Ruppert, Arne Meister, Paul Janßen, and Lutz Greb**

Table of Contents

1 Experimental Details 3
2 Computational Details 5
3 Synthesis. 7
3.1 Lithium tin(II) *meso*-octamethylcalix[4]pyrrolate $[Li_2(thf)_x][2^{Me}]$ 7
3.2 Tetrabutylammonium tin(II) *meso*-octamethylcalix[4]pyrrolate $[(NBu_4)_2][2^{Me}]$ 7
3.3 Tetraphenylphosphonium tin(II) *meso*-octamethylcalix[4]pyrrolate $[(PPh_4)_2][2^{Me}]$ 8
3.4 Lithium tin(II) *meso*-octamethylcalix[4]pyrrolato selenide $[Li_2(thf)_x][2^{Me}$-Se] 9
3.5 Tetrabutylammonium η^1-(*meso*-octamethylcalix[4]pyrrolato stannate(II)) triscarbonyl nickel(0) $[(NBu_4)_2][Ni(\eta^1\text{-}2^{Me})(CO)_3]$ 9
3.6 Tetrabutylammonium η^1-(*meso*-octaethylcalix[4]pyrrolato stannate(II)) triscarbonyl nickel(0) $[(NBu_4)_2][Ni(\eta^1\text{-}2^{Et})(CO)_3]$ 10
3.7 Reactions of *meso*-ocataalkylcalix[4]pyrrolato stannates(II) with halobenzenes 10
3.7.1 $[(NBu_4)_2][2^{Me}]$ + PhI after irradiation with UV light 10
3.7.2 $[(NBu_4)_2][2^{Et}]$ + PhBr after irradiation with UV light 11
3.7.3 $[(NBu_4)_2][2^{Et}]$ + PhCl after irradiation with UV light 11
3.7.4 $[Li_2(thf)_x][2^{Et}]$ + PhI + benzophenone 12
4 NMR Spectra 13
4.1 $[Li_2(thf)_x][2^{Me}]$ 13
4.2 $[(NBu_4)_2][2^{Me}]$ 15
4.3 $[(PPh_4)_2(oDFB)_{0.5}][2^{Me}]$ 16
4.4 $[Li_2(thf)_x][2^{Me}$-Se] 18
4.5 $[(NBu_4)_2][Ni(\eta^1\text{-}2^{Me})(CO)_3]$ 20
4.6 $[(NBu_4)_2][2^{Me}]$ + PhI after irradiation with UV light 22
4.7 $[(NBu_4)_2][2^{Et}]$ + PhBr after irradiation with UV light 23
4.8 $[(NBu_4)_2][2^{Et}]$ + PhCl after irradiation with UV light 24
4.9 $[Li_2(thf)_x][2^{Et}]$ + PhI in the presence of benzophenone 25
5 Crystallographic Data 26

5.1 $[Li_2(thf)_2][2^{Me}]$ x 0.5 LiCl 26
5.2 $[(PPh_4)_2][2^{Me}]$ 28
5.3 $[(NBu_4)_2][Ni(\eta^1\text{-}2^{Et})(CO)_3]$ 30
5.4 $[3 \text{ x } LiCl]_2$ 31
6 Elemental Analysis 32
7 Infrared Spectroscopy 33
8 Cyclic Voltammetry 33
9 DFT Calculations 34
10 ETS-NOCV Analysis of $[2^R\text{-Se}]^{2-}$ 36
11 NBO Analysis of $[2^R\text{-Se}]^{2-}$ 38
12 ^{77}Se and ^{119}Sn NMR Shift Calculation Results 38
13 ETS-NOCV Analysis of C_{2v} and C_{4v} $[2^R]^{2-}$ 39
14 QTAIM Analysis of C_{4v} $[2^R]^{2-}$ 48
15 NBO Analysis of C_{4v} $[2^R]^{2-}$ 49
16 ETS-NOCV Analysis of PhI Halogen Bonding with C_{4v} $[2^R]^{2-}$ 50
17 Literature 51
18 Optimized Molecular Geometries 52

1 Experimental Details

All manipulations were carried out under a dry argon atmosphere by using standard Schlenk techniques to prevent oxidation and hydrolysis of the sensitive compounds. *Meso*-octamethylcalix[4]pyrrole **H_4[1]**[1] and its lithium salt **[Li_4(thf)x][1]**[2] where prepared according to literature known procedures and their purity confirmed by NMR spectroscopy before use. Commercially available chemicals were used as received. All solvents and liquid chemicals were rigorously dried by applying standard procedures, freshly degassed, and stored over activated molecular sieve (3 Å resp. 4 Å) prior to use. All glassware, syringes, magnetic stirring bars, and needles were thoroughly dried. All air sensitive compounds were stored in a glove box (MBraun LABmaster dp, MB-20-G, SylaTech Y05G) under N_2 atmosphere. Analytical data of literature known compounds were compared to data of the respective reference and were found to be consistent in all cases. The purity and identity of novel compounds were confirmed by high resolution multinuclear NMR-spectroscopy, mass spectrometry, elemental analysis and if possible, X-ray diffraction analysis.

^{1}H, ^{7}Li, ^{13}C, ^{31}P, ^{77}Se, and ^{119}Sn NMR spectra were collected with a Bruker (DPX) 200, a Bruker Advance II 400 or a Bruker 2 Advance III 600 NMR spectrometer and referenced to tetramethylsilane (^{1}H, ^{13}C), tetramethylstannane (^{119}Sn). If not stated otherwise, ^{1}H and ^{13}C chemical shifts were taken from one-dimensional NMR spectra. To assist the correct peak assignment additional two-dimensional NMR spectra such as ^{1}H,^{1}H-COSY, ^{1}H,^{13}C-HSQC and HMBC, and broadband ^{1}H-decoupled ^{13}C-DEPT135 were recorded (only selected spectra were depicted in the supplementary information). ^{119}Sn chemical shifts were obtained from two-dimensional ^{1}H,^{119}Sn HMBC measurements. ^{77}Se chemical shifts were obtained from two-dimensional ^{1}H,^{77}Se HMBC measurements. Chemical shifts are reported as dimensionless δ values in ppm, coupling constants J are given in hertz (Hz). Peak multiplicities are given as singlet (*s*), doublet (*d*), triplet (*t*), quartet (*q*), quintet (*quint*), sextet (*sext*), and septet (*sept*).

High-resolution electrospray ionization mass spectra (HRMS-ESI) were obtained with a Bruker ApexQe FT-ICR instrument.

Fourier-transform infrared (FTIR) spectra at 298 K were obtained with an Agilent Cary 630 FTIR spectrometer, which was operated with the MicroLab PC software, and processed with BioRad Merlin and OriginPro 2020 64Bit.

Cyclic voltammetry was done inside a dry nitrogen-filled glove box at room temperature with a EmStat3+blue device from PalmSens, which was operated with the PSTrace 5.7 software. A glassy carbon electrode (working area of 0.07 cm^2) was used as a working electrode, a platinum wire as a counter electrode, and a silver wire as a quasi-reference electrode. The scan rate was set to 0.05 V s^{-1}. As solvent, 1,2-difluorobezene (*o*DFB), as supporting electrolyte, [NBu_4][PF_6] was used. The analyte concentration was approximately c = 10^{-3} mol L^{-1}, the supporting electrolyte concentration c_{supp} = 0.1 mol L^{-1}. The acquired data was externally referenced against the decamethyl-ferrocene/decamethylferrocenium ($dmfc^+$/dmfc) redox couple and then transferred to the fc^+/fc reference. Under the same conditions as described fc^+/fc has a redox potential of 532 mV and dmfc/$dmfc^+$ a redox potential of 30 mV against the AgCl/Ag/KCl redox couple.[3] The $dmfc^+$/dmfc reference measurement was carried out under the same conditions as described.

Elemental analysis for the determination of the C-, H- and N-content was carried out by the microanalysis laboratory of the Institute of Inorganic Chemistry at Heidelberg University using a vario MICRO cube of

Elementar Analysensysteme.

UV irradiation experiemnts were carried out in borosilicate Boro 5.1 Young NMR tubes and a ASAHI SPECTRA MAX-303 Xenon Light Source with an 250 – 385 nm filter.

Suitable crystals of the compounds were taken directly out of the mother liquor, immersed in perfluorinated polyether oil, and fixed on top of a cryo loop. Measurements were made on Bruker D8 Venture CCD diffractometer with a low-temperature unit using (100 or 120 K) Mo-Kα radiation chromated by mirror optics. The data collected were processed using standard Bruker APEX3 software. Structures were solved by intrinsic phasing using the SHELXT program[4] and refined with the SHELXL.[5] Graphical handling of the structural data during solution and refinement was performed with shelXLe.[6] Atomic coordinates and anisotropic thermal parameters of non-hydrogen atoms were refined by full-matrix least-squares calculations[7] and displacement ellipsoids are displayed with 50 % probability. Hydrogen atoms were included using a riding model. Crystallographic data for the structures reported in this article are deposited within the Cambridge Crystallographic Data Centre as supplementary publication no. 2351852-2351854 which can be obtained free of charge. Crystal data and structure are summarized in the tables under the crystallographic figures. Figures depicting solid state molecular structures and distances and angles between planes spanned by atoms have been calculated and generated by Mercury 2023.3.0 without a standard deviation.

.

2 Computational Details

All computations employing the Orca 5.0.3[8] software or the Amsterdam Modelling Suite AMS2021.102[9,10] were carried out with the computational resources available on the bwFor Cluster JUSTUS2 located at Ulm University within the Baden Württemberg High Performance Computing program.

All structures were optimized with the Orca 5.0.3 software at the B97M[11]-D4[12]/def2-TVZPP[13] level of theory employing a def2/J auxiliary basis set.[14] Minima structures were obtained with the following ORCA input line:

```
! RKS B97M-D4 def2-TZVPP defGrid2 NoPop Opt NumFreq TightSCF
```

Conformational spaces, especially to find the lowest energy orientations of the ethyl residues of the calix[4]pyrrole ligand, were initially explored with the conformer-rotamer ensemble sampling tool (CREST)[15] for the xtb program package[16] using the following command line input. The lowest-energy conformer was then reoptimized as described below.

```
crest [file_name].xyz --alpb THF --chrg [charge] --noreftopo > [file_name].out
```

All calculated geometries have been confirmed as energetic minima on the potential energy surface by numerical calculation of harmonic frequencies at the B97M-D4/def2-TVZPP level, revealing only positive values.

Subsequent single point calculations employing the Conductor-like Polarizable Continuum Model Based on Solute Electron Density (C-PCM SMD)[17] were performed with the following ORCA input line:

```
! RKS B97M-D4 def2-TZVPP defGrid2 TightSCF

CPCM SMD TRUE
      SMDSOLVENT "THF"
END
```

High-level thermodynamic data was obtained by subsequent single point calculations employing the double-hybrid density functional DSD-BLYP[18] and def2-QZVPP basis set[13] combined with the D3(BJ) dispersion correction[19] and the resolution-of-identity approximation[20] with automatically generated auxiliary basis sets:[21]

```
! RI-DSD-BLYP D3BJ def2-QZVPP RIJCOSX AutoAux defGrid3 TightSCF
```

Transition structures were optimized toward a single negative Hessian matrix eigenvalue using the `OptTS` keyword. It was ensured that the correct first-order saddle point on the potential energy surface was located by animation of the imaginary frequency in Chemcraft software version 1.8.[22]

Natural Bond Orbital (NBO) calculations were conducted on the PBE0[23]/def2-TZVPP[13] level of theory using NBO6.0.18a[24] as included in Orca 5.0.3 *via* the following ORCA input line:

```
! RKS PBE0 def2-TZVPP NBO TightSCF defGrid2
```

Furthermore the $CHOOSE keylist was used to specify meaningful Lewis structure for the NBO search.

Calculations employing the Extended Transition State (ETS) method for energy decomposition analysis (EDA)[25–27] combined with the natural orbitals for chemical valence (NOCV)[28] calculations were performed on the BP86-D3(BJ)[29–31]/TZ2P level of theory with COSMO(THF) solvation correction as implemented in the AMS2021.201 software.[9,10]

QTAIM analyses were performed on the PBE0-D3(BJ)/ZORA-TZ2P/COSMO(THF) electron densities,[32–34] as implemented in the AMS2021.201 software.[9,10] QTAIM charges of atoms were calculated using the grid-based method implemented in AMS.[35,36] The Numerical Quality Good keyword was used in the calculations to increase the numerical quality of the results in order to avoid numerical artefacts in the atomic charges.

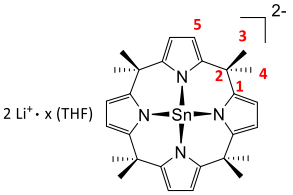
Normal-mode structural decomposition (NSD) analysis on computed structutres was performed using the *PorphyStruct* tool.[37]

Optimized geometries were visualized using Chemcraft version 1.8.

Isosurface plots were created using the IboView software v20150427.[38]

3 Synthesis.

3.1 Lithium tin(II) *meso*-octamethylcalix[4]pyrrolate [$Li_2(thf)_x$][2^{Me}]



Under N_2-atmosphere **[$Li_4(thf)_x$][1^{Me}]** (x = 3.65) (1.00 eq, 698.9 mmol, 500.0 mg) was dissolved in THF (10 ml). $SnCl_2$ (1.00 eq, 698.9 mmol, 135.2 mg) was added in small portions to the reaction mixture while stirring at room temperature. The resulting pale-yellow solution was stirred at room temperature for 1h. The solvent was removed under reduced pressure and the crude product was dried for 90 min. The obtained solid was crushed with a spatula and extracted with oDFB (40 ml). The solution was filtered over a PTFE syringe filter (pore size 0.22 µm) to remove surplus lithium chloride. The solvent was removed *in vacuo*. The crude solid was dissolved in THF (1.5 ml) and precipitated with *n*-pentane (20ml). The precipitate was filtered of and dried in vacuo. **[$Li_2(thf)_x$][2^{Me}]** was obtained as off-white solid with varying THF content (449.5 mg, 640 µmol (x = 2.0), 92% yield).

^{1}H NMR [^{1}H, ^{1}H,^{1}H-COSY] (399.89 MHz, THF-d_8, 295 K): δ [ppm] = 5.74 (*s*, $^{117/119}$Sn-satellites $^4J_{Sn,H}$ = 156.85 Hz, $^{117/119}$Sn-satellites $^4J_{Sn,H}$ = 162.8 Hz, H_5, 8H), 3.63 – 3.60 (*m*, H_{thf}, 8H), 1.79 – 1.76 (*m*, H_{thf}, 8H), 1.53 (*s*, H_4, 12H), 1.51 (*s*, H_3, 12H).

^{13}C NMR [^{13}C, ^{13}C-DEPT135, ^{1}H,^{13}C-HSQC, ^{1}H,^{13}C-HMBC] (150.91 MHz, CD_3CN, 295 K): δ [ppm] = 147.3 (*s*, C_1), 101.5 (*s*, C_5H), 68.32 (*s*, thf), 38.11 (*s*, C_2), 34.99 (*s*, C_4H_3) 33.56 (*s*, C_3H_3), 26.22 (*s*, thf).

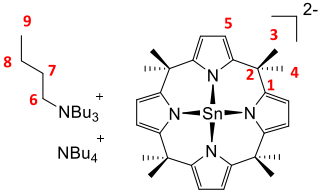
^{119}Sn NMR [^{1}H,^{119}Sn-HMBC] (149.04 MHz, THF-d_8, 295 K): δ [ppm] = −465.9 (*s*).

^{7}Li NMR (155.41 MHz, THF-d_8, 295 K): δ [ppm] = −0.79 (*s*).

HR-MS (ESI$^-$, CD_3CN): *m/z* = 575.1833 [M+OCH_3]$^-$. Calculated for [$C_{29}H_{35}N_4OSn$]$^-$: 575.1833 (MeOH from ESI atmosphere).

Anal. calc. for $C_{28}H_{32}N_4SnLi_2$ x 4 THF: C: 60.51, H: 7.39, N: 6.42; found: C: 60.61, H: 7.32, N: 6.46.

3.2 Tetrabutylammonium tin(II) *meso*-octamethylcalix[4]pyrrolate [(NBu_4)$_2$][2^{Me}]



Under N_2-atmosphere **[$Li_2(thf)_x$][2^{Me}]** (x = 3.58) (1.00 eq, 618.5 µmol, 500.0 mg) and NBu_4Cl (1.60 eq,

989.6 µmol, 275.0 mg) were dissolved in oDFB (20 ml). The reaction mixture was stirred at room temperature for 90 min which resulted in the formation of white precipitate. The solution was filtered over a PTFE syringe filter (pore size 0.22 µm). The solvent was removed under reduced pressure and dried for 30 min. The resulting crude product was again dissolved in oDFB (15 ml) and filtered through a PTFE syringe filter (pore size 0.22 µm). After removing the solvent under reduced pressure $[NBu_4]_2[SnCx^{Me}]$ was obtained as off-white solid (467.0 mg, 618.6 µmol, 73% yield).

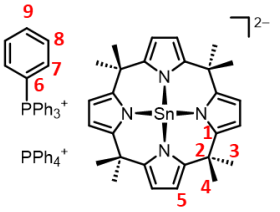
^{1}H NMR [^{1}H, ^{1}H,^{1}H-COSY] (600.18 MHz, THF-*d*$_8$, 295 K): = 5.57 (*s,* ^{117}Sn-satellites $^4J_{Sn,H}$ = 156.40 Hz, ^{119}Sn-satellites $^4J_{Sn,H}$ = 161.99 Hz, *H*$_5$, 8H), 2.75 (*s*, *H*$_6$, 16H), 1.65 (*s*, *H*$_4$, 12H), 1.54 (*s*, *H*$_3$, 12H), 1.37 (*s*, *H*$_7$, 16H), 1.19 – 1.15 (*m*, *H*$_8$, 16H), 0.87 (*t*, $^3J_{H,H}$ = 7.18 Hz, *H*$_9$, 24H).

^{13}C NMR [^{13}C$^{[1]}$, ^{13}C-DEPT135, ^{1}H,^{13}C-HSQC, ^{1}H,^{13}C-HMBC] (100.56 MHz, THF-*d*$_8$, 295 K): δ [ppm] = 146.7 (*s*, *C*$_1$), 98.27 (*s*, *C*$_5$H), 58.82 (*s*, *C*$_6$H$_2$), 38.96 (*s*, *C*$_2$), 38.18 (*s*, *C*$_3$H$_3$), 28.38 (s, *C*$_4$H$_3$), 24.75 (*s*, *C*$_7$H$_2$) 20.68 (*s*, *C*$_8$H$_2$), 14.11 (*s*, *C*$_9$H$_3$).

^{119}Sn NMR [^{1}H,^{119}Sn-HMBC] (223.81 MHz, THF-*d*$_8$, 295 K): δ [ppm] = −473.4 (*s*).

EA calcd. for $C_{60}H_{104}N_6Sn$: C, 70.09; H, 10.20; N, 8.17. Found: C, 69.69; H, 10.35; N, 7.88

3.3 Tetraphenylphosphonium tin(II) *meso*-octamethylcalix[4]pyrrolate [$(PPh_4)_2$][2^{Me}]



In a nitrogen-filled glovebox **[Li$_2$(thf)$_x$][2^{Me}]** (1.00 eq, 220.3 mg, 240.1 mmol) and tetraphenylphosphonium chloride (2.00 eq, 180 mg, 480.2 mmol) were dissolved in oDFB (5 ml) plus some drops MeCN in a 10 ml *Schlenk* flask. Wihtout MeCN a quantitative precipitation of **[$(PPh_4)_2$(*o*DFB)$_{0.5}$][2^{Me}]** was observed during the salt exchange. The solution was stirred at room temperature for 1 h. The solution was filtrated through a syringe filter. The solvent of the filtrate was removed *in vacuo* over night yielding **[$(PPh_4)_2$(*o*DFB)$_{0.5}$][2^{Me}]** as a deep orange solid (267.3 mg, 94% yield).

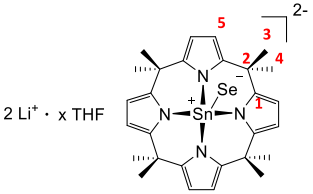
^{1}H NMR [^{1}H, ^{1}H,^{1}H-COSY] (600 MHz, 295 K, THF-*d*8/MeCN): δ [ppm] = 7.86 – 7.83 (*m*, *H*$_9$, 8H), 7.70 – 7.63 (*m*, *H*$_{7,8}$, 32H), 7.28 – 7.21 (*m*, *o*DFB, 1H), 7.17 – 7.12 (*m*, *o*DFB, 1H), 5.65 (*s*, *H*$_5$, 8H), 1.66 (*s*, ^{117}Sn-satellites $^4J_{Sn,H}$ = 156.0 Hz, ^{119}Sn-satellites $^4J_{Sn,H}$ = 168.0 Hz, *H*$_4$, 12H), 1.60 (*s*, *H*$_3$, 12H).

^{13}C NMR [^{13}C{^{1}H}, ^{13}C-DEPT135, ^{1}H,^{13}C-HSQC, ^{1}H,^{13}C-HMBC] (101 MHz, 295 K, THF-*d*8/MeCN): δ [ppm] = 146.9 (*s*, *C*$_1$), 136.5 (*d*, $^4J_{PC}$ = 2.0 Hz, *C*$_9$H), 134.7 (*d*, $^3J_{PC}$ = 6.1 Hz, *C*$_8$H), 131.5 (*d*, $^2J_{PC}$ = 9.1 Hz, *C*$_7$H), 119.0 (*d*, $^1J_{PC}$ = 59.6 Hz, *C*$_6$), 100.1 (*C*$_5$H), 38.2 (*s*, *C*$_2$), 35.8 (*s*, *C*$_5$H$_3$), 33.6 (*s*, *C*$_3$H$_3$).

^{31}P{^{1}H} NMR (242 MHz, 295 K, THF-d8): δ [ppm] = 21.01 (*s*, *P*PH_4^+).

^{119}Sn NMR [^{1}H,^{119}Sn-HMBC] (223 MHz, 298 K, THF-d8): δ [ppm] = −474.4.

3.4 Lithium tin(II) *meso*-octamethylcalix[4]pyrrolato selenide [Li$_2$(thf)$_x$][2^{Me}-Se]



Under N_2 atmosphere **[Li$_2$(thf)$_x$][2^{Me}]** (x = 2) (1.00 eq, 21.39 µmol, 15.0 mg) and selenium powder (3.00 eq, 64.16 µmol, 5.07 mg) were stirred in THF-d_8 (0.5 ml) at room temperature for 30 min to give a dark red reaction mixture. Unreacted selenium powder was removed by filtration over a PTFE syringe filter (pore size 0.22 µm). The resulting solution was analysed *via* NMR spectroscopy.

^{1}H NMR [^{1}H, ^{1}H,^{1}H-COSY] (399.89 MHz, THF-d_8, 295 K): δ [ppm] = 5.85 (*s*, $^{117/119}$Sn-satellites $^{4}J_{Sn,H}$ = 159.14 Hz, ^{119}Sn-satellites $^{4}J_{Sn,H}$ = 165.55 Hz, H_5, 8H), 3.63 – 3.60 (*m*, thf, 8H), 1.81 (*s*, H_4, 12H), 1.79 – 1.76 (*m*, thf, 8H), 1.48 (*s*, H_3, 12H).

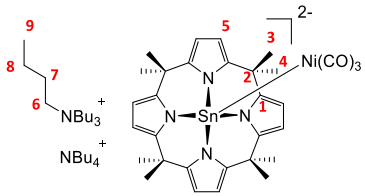
^{13}C NMR [^{13}C, ^{13}C-DEPT135, ^{1}H,^{13}C-HSQC, ^{1}H,^{13}C-HMBC] (100.56 MHz, THF-d_8, 295 K): δ [ppm] = 148.25 (*s*, C_1), 102.07 (*s*, C_5H), 68.03 (*s*, thf), 37.47 (*s*, C_3H_3), 37.23 (*s*, C_2), 31.85 (*s*, C_4H_3), 26.18 (*s*, thf).

^{7}Li NMR (155.41 MHz, THF-d_8, 295 K): δ [ppm] = −0.62 (*s*).

^{119}Sn NMR [^{1}H,^{119}Sn-HMBC] (149.04 MHz, THF-d_8, 295 K): δ [ppm] = −522.9 (*s*).

^{77}Se NMR [^{1}H,^{77}Se-HMBC] (76.24 MHz, THF-d_8, 295 K) = −375.7 (*s*).

3.5 Tetrabutylammonium η^1-(*meso*-octamethylcalix[4]pyrrolato stannate(II)) triscarbonyl nickel(0) [(NBu$_4$)$_2$][Ni(η^1-2^{Me})(CO)$_3$]



Under N_2 atmosphere **[(NBu$_4$)$_2$][2^{Me}]** (1.00 eq, 38.90 µmol, 40.0 mg) and *bis*(cyclooctadiene)nickel(0) (1.30 eq, 50.57 µmol, 13.91 mg) were dissolved in THF-d_8 (0.5 ml) inside a pressure NMR tube. 3 atm of CO gas were added to the tube and the reactants mixed for 24 h at room temperature. The solvent was removed *in vacuo* and the resulting crude solid was suspended in hexane (3 ml) and stirred for 30 min. The solid was separated *via* centrifugation and again washed with hexane and subsequently dried under reduced pressure to yield the target compound as an off-white solid (13.00 mg, 18.95 µmol, 48.7% yield).

^{1}H NMR [^{1}H, ^{1}H,^{1}H-COSY] (399.89 MHz, THF-d_8, 295 K): δ [ppm] = 5.62 (*s*, H_5, 8H), 2.56 (*s*, H_6, 16H), 1.65 (*s*, H_3, 12H), 1.63 (*s*, H_4, 12H), 1.35-1.15 (*m*, H_7/H_8, 32H), 0.90 (*t*, $^{3}J_{H,H}$ = 7.20 Hz, H_9, 24H).

^{13}C NMR [^{13}C{^{1}H}, ^{13}C-DEPT135, ^{1}H,^{13}C-HSQC, ^{1}H,^{13}C-HMBC] (100.56 MHz, THF-d_8, 295 K): δ [ppm] = 201.90 (*s*, *C*O), 148.18 (s, C_1), 99.40 (s, C_5H), 58.94 (s, C_6H_2), 39.36 (s, C_3H_3), 37.78 (s, C_2), 29.38 (*s*, C_4H_3), 24.94 (s, C_7H_2), 21.04 (s, C_8H_2), 14.44 (s, C_9H_3).

^{119}Sn NMR [^{1}H,^{119}Sn-HMBC] (149.04 MHz, THF-d_8, 295 K): δ [ppm] = −325.9 (*s*).

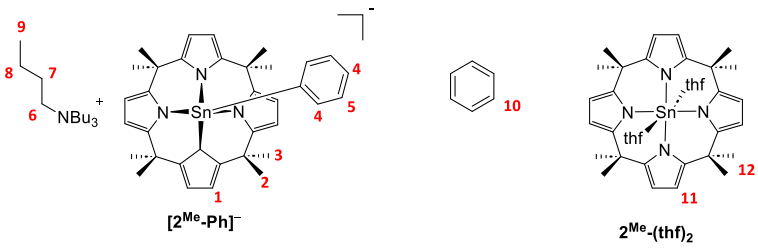
3.6 Tetrabutylammonium η^1-(*meso*-octaethylcalix[4]pyrrolato stannate(II)) triscarbonyl nickel(0) [$(NBu_4)_2$][Ni(η^1-2^{Et})$(CO)_3$]

[$(NBu_4)_2$][Ni(η^1-2^{Et})$(CO)_3$] has been synthesized according to a literature known procedure and its purity confirmed by NMR spectroscopy.[39] Recrystallization from a concentrated solution in THF by gas phase diffusion of *n*-pentane at −30 °C over the course of one week yielded single crystalls suitable for X-ray diffraction.

3.7 Reactions of *meso*-ocataalkylcalix[4]pyrrolato stannates(II) with halobenzenes

Meso-octaalkylcalix[4]pyrrolato stannate(II) **[Y_2][2^R]** (1.00 eq.; R = Me, Et; Y = Li, NBu_4) was dissolved in THF-d_8 (0.45 mL) under N_2 atmosphere in a Young NMR tube and halobenzene PhX (1.00 eq.; X = Cl, Br, I) was added to the solution. The reaction progress was monitored *via* ^{1}H and ^{1}H,^{119}Sn HMBC NMR spectroscopy. If no reaction at room temperature could be observed within 24 h the reaction mixture inside the Young NMR tube was irradiated with UV light (250 – 385 nm) for 30 minutes. Reaction products were only analayzed *in situ via* NMR spectroscopy and ESI(-) MS and no subsequent isolation and purification were performed.

3.7.1 [$(NBu_4)_2$][2^{Me}] + PhI after irradiation with UV light

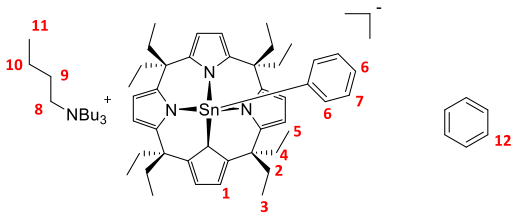


[2^{Me}-Ph]$^-$ 2^{Me}-$(thf)_2$

^{1}H NMR [^{1}H, ^{1}H,^{1}H-COSY] (399.89 MHz, THF-d_8, 295 K) δ [ppm] = 7.30 (*s*, H_{10}, 4.6H), 7.02 – 6.88 (*m*, H_4, 3H), 6.87 – 6.79 (*m*, H_5, 2H), 6.08 (*s*, $^{117/119}$Sn-satellites $^{4}J_{Sn,H}$ = 18.21 Hz, H_{11}, 3H), 5.87 (*s*, $^{117/119}$Sn-satellites $^{4}J_{Sn,H}$ = 11.42 Hz,0 H_1, 8H), 3.27 – 3.25 (*m*, H_6, 33H), 1.69 – 1.59 (*m*, H_7 overlayed, 48H), 1.56 (*s*, H_{12} overlayed, 16H), 1.53 (*s*, H_3 overlayed, 15H), 1.36 (*h*, $^{3}J_{H,H}$ = 7.4 Hz, H_8 overlayed, 39H), 1.24 (*s*, H_2, 9H), 0.97 (*t*, $^{3}J_{H,H}$ = 7.3 Hz, H_9, 49H).

^{119}Sn NMR [^{119}Sn,^{1}H-HMBC] (149.04 MHz, THF-d_8, 295 K): δ [ppm] = −425.3 (*s*, **[2^{Me}-Ph]$^-$**), −555.7 (*s*, **2^{Me}-(thf)$_2$**), −569.9 (*s*, *unidentified side product*).

3.7.2 $[(NBu_4)_2][2^{Et}]$ + PhBr after irradiation with UV light

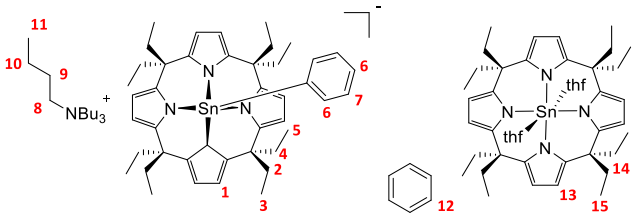


^{1}H NMR [^{1}H, ^{1}H,^{1}H-COSY] (200.18 MHz, THF-d_8, 295 K) δ [ppm] = 7.30 (*s*, H_{12}, 11H), 6.92 – 6.76 (*m*, H_6, 3H), 6.50 (*d*, $^{3}J_{H,H}$ = 6.0 Hz, H_7, 2H), 5.93 (*s*, H_1, 8H), 3.53 – 3.38 (*m*, H_8, 58H), 1.73 (*s*, H_9 overlayed, 94H), 1.41 (*h*, $^{3}J_{H,H}$ = 7.3 Hz, H_{10}, 71H), 0.99 (*t*, $^{3}J_{H,H}$ = 7.3 Hz, H_{11}, 93H).

^{119}Sn NMR [^{119}Sn,^{1}H-HMBC] (149.04 MHz, THF-d_8, 295 K): δ [ppm] = −441.0 (*s*, **[2^{Et}-Ph]$^-$**), −574.7 (*s*, *unidentified side product*).

HR-MS (ESI, negative, THF): **[2^{Et}-Ph]$^-$** calcd. for $[C_{42}H_{53}N_4Sn]^-$ m/z = −733.3292, found m/z = −733.3294

3.7.3 $[(NBu_4)_2][2^{Et}]$ + PhCl after irradiation with UV light

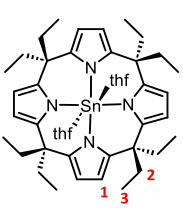


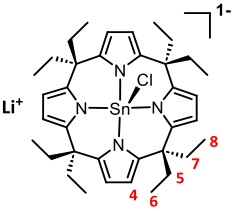
^{1}H NMR [^{1}H, ^{1}H,^{1}H-COSY] (399.89 MHz, THF-d_8, 295 K) δ [ppm] = 7.30 (*s*, H_{12}, 5H), 6.93 – 6.77 (*m*, H_6, 2H,), 6.51 – 6.47 (*m*, H_7, 1H), 6.11 (*s*, H_{13}, 3H), 5.93 (*s*, H_1, 8H), 3.55 – 3.45 (*m*, H_8, 41H), , 1.84 (*qd*, $^{3}J_{H,H}$ = 7.6, 1.8 Hz, H_4/H_{14} overlayed, 20H), 1.79 – 1.66 (*m*, H_9, 56H), 1.58 (*q*, $^{3}J_{H,H}$ = 7.3 Hz, H_2, 7H), 1.40 (*h*, $^{3}J_{H,H}$ = 7.4 Hz, H_{10}, 44H), 0.99 (*t*, $^{3}J_{H,H}$ = 7.4 Hz, H_{11}, 63H), 0.70 (*t*, $^{3}J_{H,H}$ = 7.3 Hz, H_5 overlayed, 14H), 0.64 (*td*, *J* = 7.3, 4.3 Hz, H_{15} overlayed, 23H), 0.50 (*t*, *J* = 7.3 Hz, H_3, 10H).

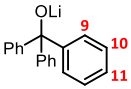
^{119}Sn NMR [^{119}Sn,^{1}H-HMBC] (149.04 MHz, THF-d_8, 295 K): δ [ppm] = −441.0 (*s*, **[2^{Et}-Ph]$^-$**), −560.8 (*s*, **2^{Et}-(thf)$_2$**).

HR-MS (ESI, negative, THF): **[2^{Et}-Ph]$^-$** calcd. for $[C_{42}H_{53}N_4Sn]^-$ m/z = −733.3292, found m/z = −733.3337

3.7.4 $[Li_2(thf)_x][2^{Et}]$ + PhI + benzophenone







3

Lithium *meso*-octaethylcalix[4]pyrrolato stannate(II) **$[Li_2(thf)_x][2^{Et}]$** (1.00 eq.) and benzophenone (1.00 eq.) were dissolved in THF-d_8 (0.45 mL) under N_2 atmosphere in a Young NMR tube and iodobenzene (1.00 eq.) was added to the solution. The reaction progress was monitored *via* ^{1}H NMR spectroscopy. After 24 hours at room temperature ^{1}H NMR spectroscopy revealed the complete consumption of the starting material and the formation of **3**. Gas phase diffusion of *n*-pentane into the crude reaction solution at −30 °C yielded single crystall suitable for X-ray diffraction. Despite their low quality the unrefined solid-state molecular structure of **3** clearly shows the addition of PhLi across the C=O double bond. The concomitant formation of chlirodstannate(IV) **$[2^{Et}\text{-}Cl]^-$** can be explained by traces of LiCl still present in **$[Li_2(thf)_x][2^{Et}]$**.

^{1}H NMR [^{1}H, ^{1}H,^{1}H-COSY] (600.15 MHz, THF-d_8, 295 K): δ[ppm] = 7.75 – 7.65 (m, $H_{Iodobenzene}$, 1H), 7.33 - 7.27 (*m*, H_9, 8H), 7.15 – 7.09 (*m*, H_{10}, 8H), 7.07 – 6.99 (*m*, H_{11}, 4H), 6.11 (s, H_1, 8H), 5.89 (*s*, H_4, 3H), 1.96 (*t*, $^3J_{H,H}$ = 9.1, 7.3 Hz, $H_{5,7}$, 6H), 1.84 (*q*, $^3J_{H,H}$ = 7.3 Hz, H_2, 16H), 0.85 (*t*, $^3J_{H,H}$ = 7.1 Hz, H_8, 4H), 0.65 (*t*, $^3J_{H,H}$ = 7.3 Hz, H_3, 24H), 0.54 (*t*, $^3J_{H,H}$ = 7.4 Hz, H_6, 4H).

^{119}Sn NMR [^{119}Sn,^{1}H-HMBC] (149.12 MHz, THF-d_8, 295 K) δ[ppm] = −561.17 (*s*, **$2^{Et}\text{-}(thf)_2$**), −575.79 (*s*, **$[2^{Et}\text{-}Cl]^-$**).

HR-MS (ESI, negative, THF): calcd. for $C_{36}H_{48}ClN_4Sn$ m/z = −691.2589, found m/z = −691.2597

4 NMR Spectra

4.1 [Li$_2$(thf)$_x$][2^{Me}]

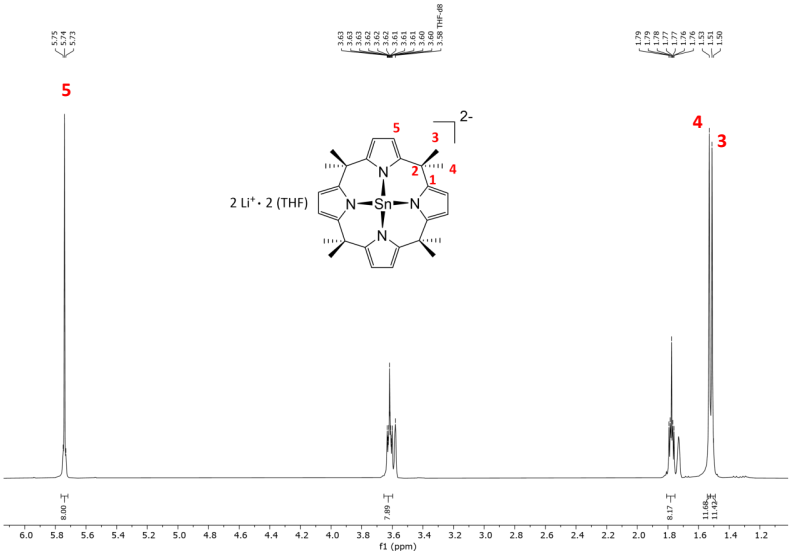


Figure S1. ^{1}H NMR spectrum of **[Li$_2$(thf)$_x$][2^{Me}]** (x = 2) (399.98 MHz, THF-d_8, 295 K).

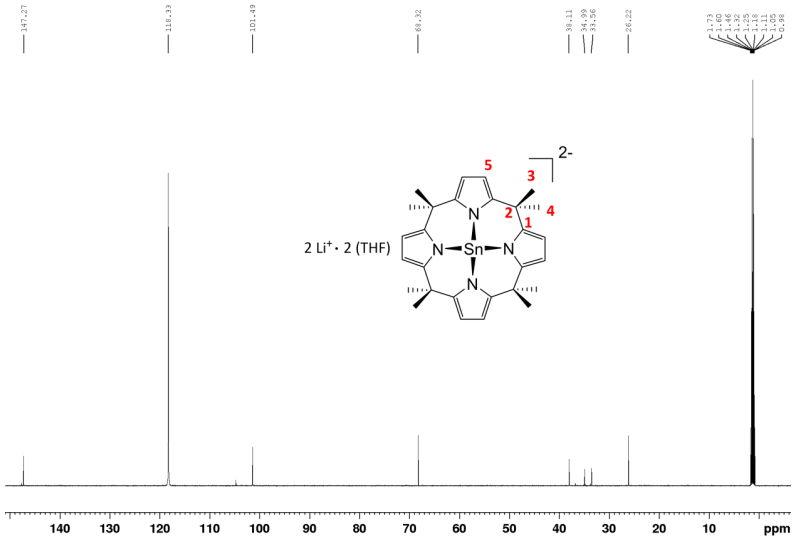


Figure S2. ^{13}C NMR spectrum of **[Li$_2$(thf)$_x$][2^{Me}]** (x = 2) (150.91 MHz, THF-d_8, 295 K).

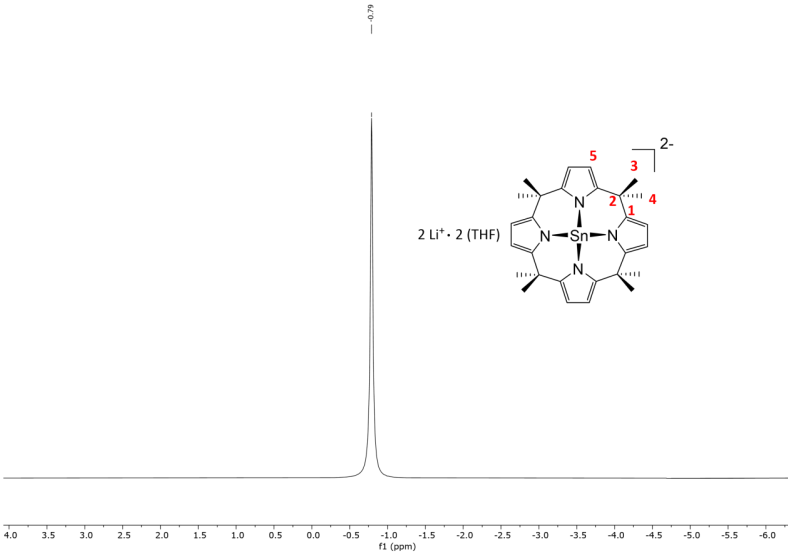


Figure S3. ^{7}Li NMR spectrum of **[Li$_2$(thf)$_x$][2^{Me}]** (x = 2) (155.41 MHz, THF-d_8, 295 K).

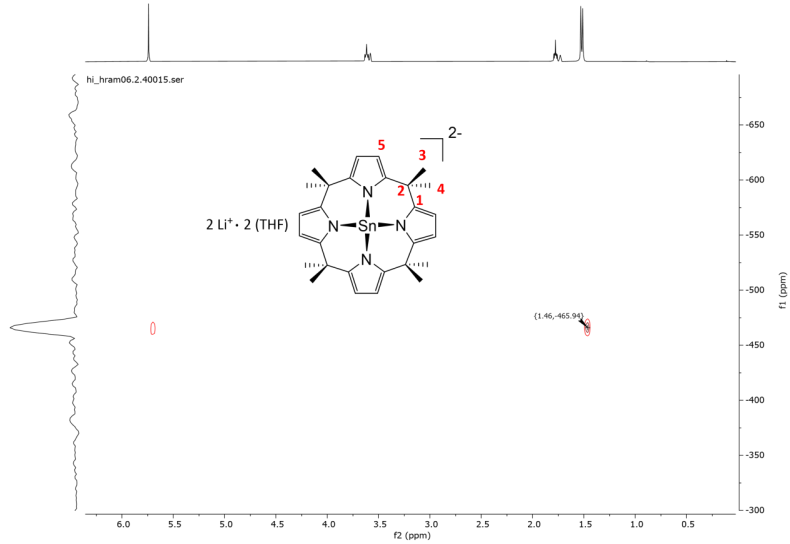


Figure S4. ^{1}H,^{119}Sn HMBC NMR spectrum of **[Li$_2$(thf)$_x$][2^{Me}]** (x = 2) (THF-d_8, 295 K).

4.2 $[(NBu_4)_2][2^{Me}]$

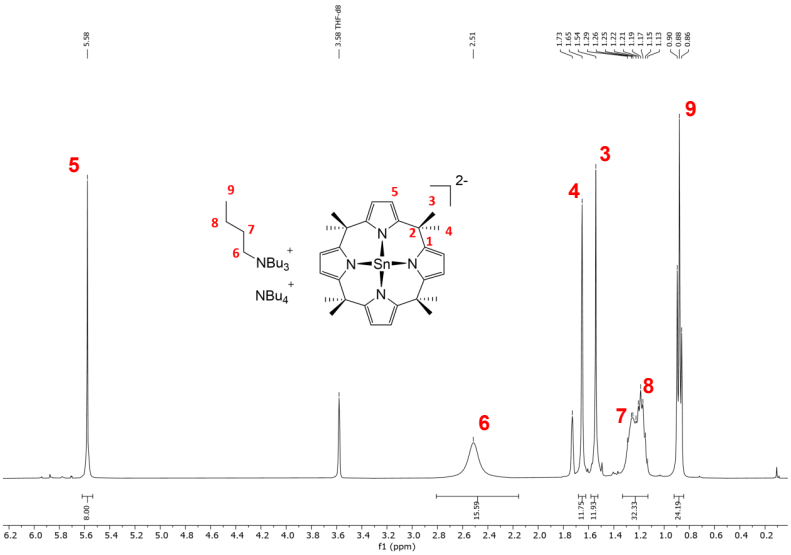


Figure S5. ^{1}H NMR spectrum of **$[(NBu_4)_2][2^{Me}]$** (600.18 MHz, THF-d_8, 295 K).

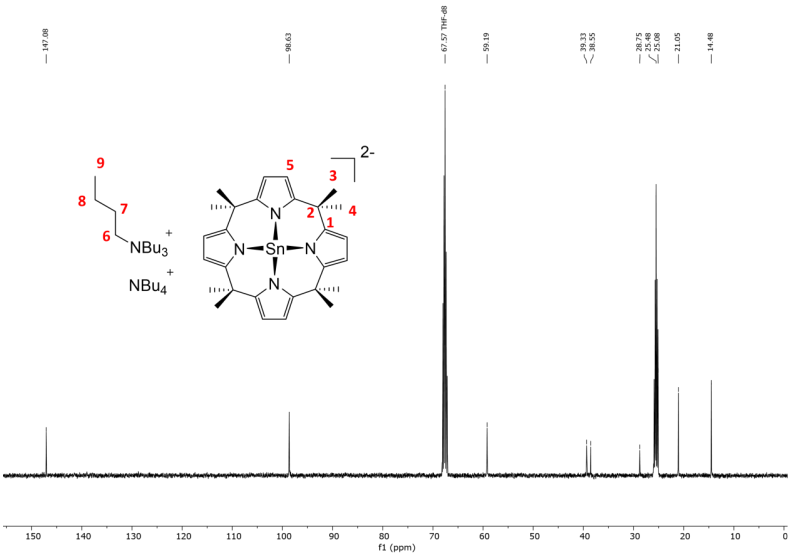


Figure S6. ^{13}C NMR spectrum of **$[(NBu_4)_2][2^{Me}]$** (100.56 MHz, THF-d_8, 295 K).

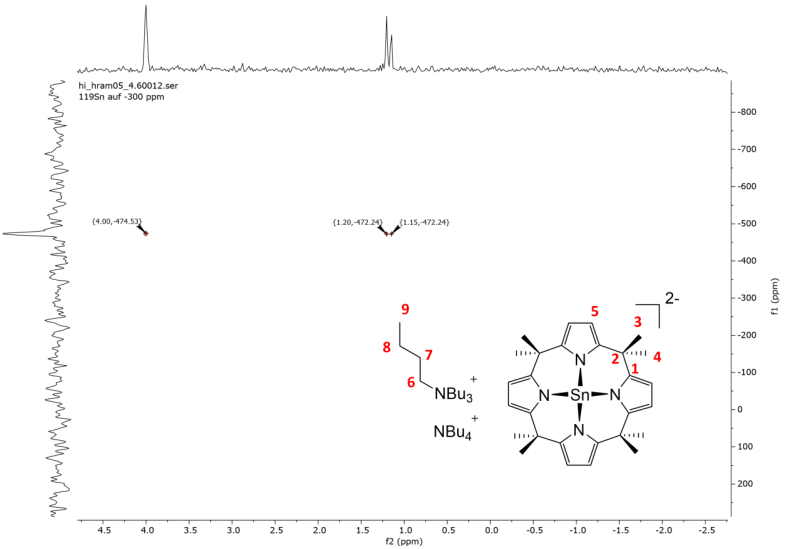


Figure S7. $^{1}H,^{119}Sn$ HMBC NMR spectrum of **[(NBu$_4$)$_2$][2^{Me}]** (x = 2) (THF-d_8, 295 K).

4.3 [(PPh$_4$)$_2$(*o*DFB)$_{0.5}$][2^{Me}]

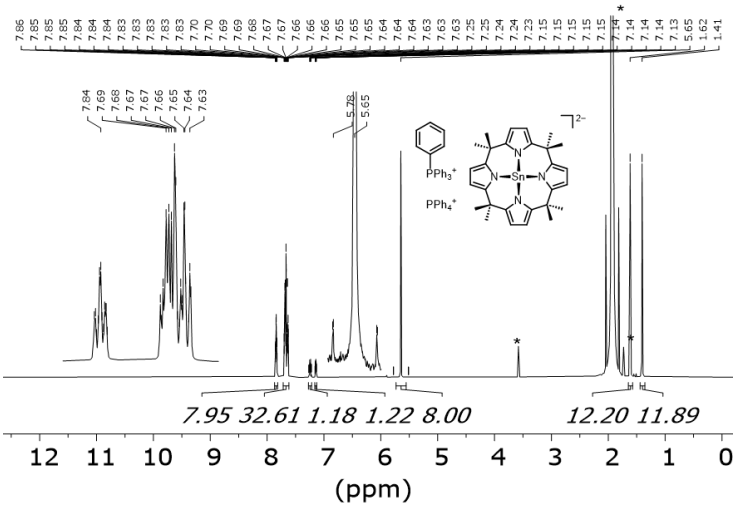


Figure S8. ^{1}H NMR spectrum of **[(PPh$_4$)$_2$][2^{Me}]**. Solvent resonances of THF-d_8 and MeCN are indicated by an asterisk (*). (600.18 MHz, THF-d_8, 295 K).

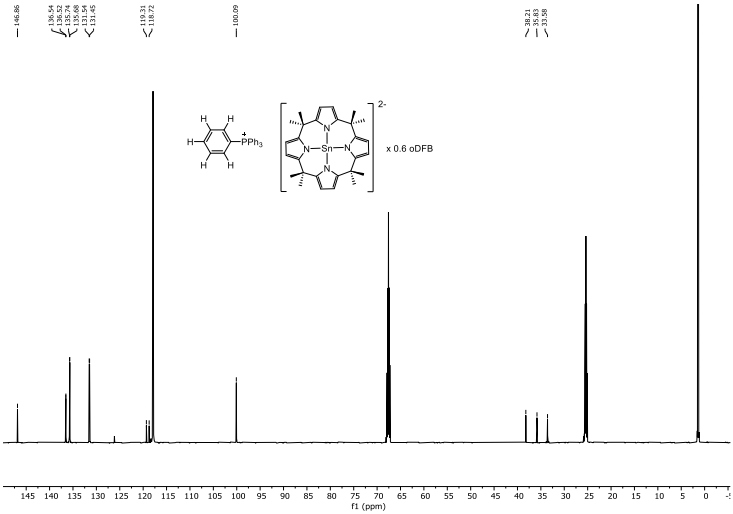


Figure S10. ^{13}C NMR spectrum of **[(PPh$_4$)$_2$][2^{Me}]** (100.56 MHz, THF-d_8, 295 K).

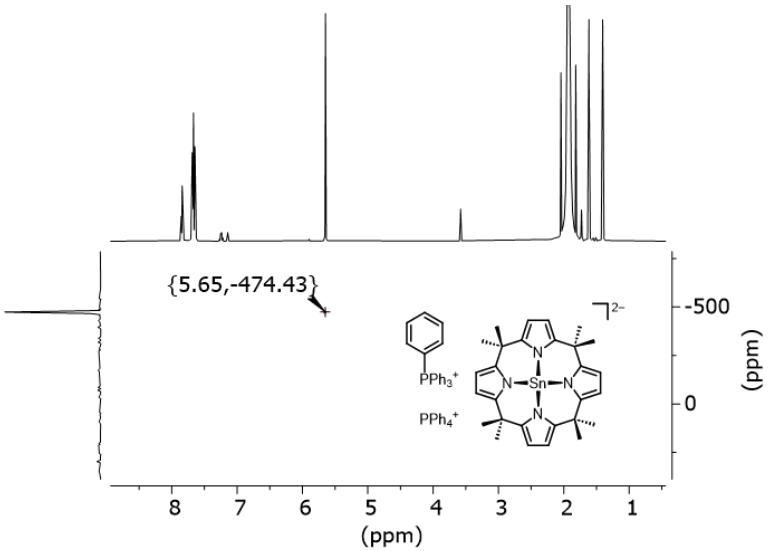


Figure S11. ^{1}H,^{119}Sn HMBC NMR spectrum of **[(PPh$_4$)$_2$][2^{Me}]** (THF-d_8, 295 K).

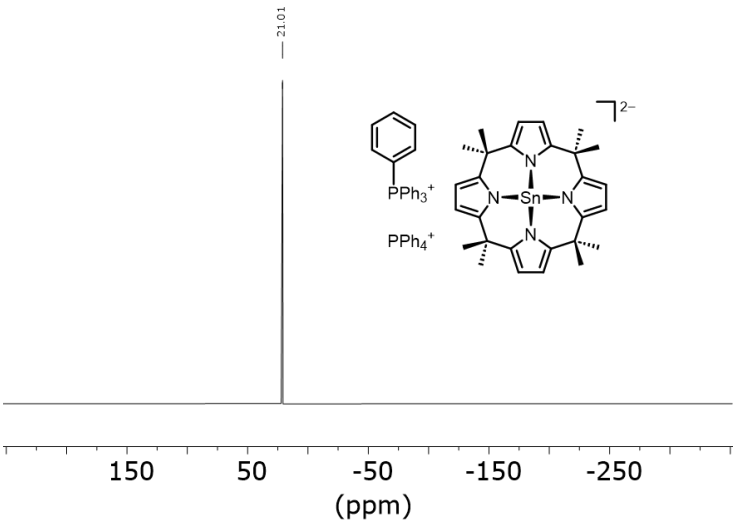


Figure S12. $^{31}P\{^{1}H\}$ NMR spectrum of **[(PPh$_4$)$_2$][2^{Me}]** (242.95 MHz, THF-d_8, 295 K).

4.4 [Li$_2$(thf)$_x$][2^{Me}-Se]

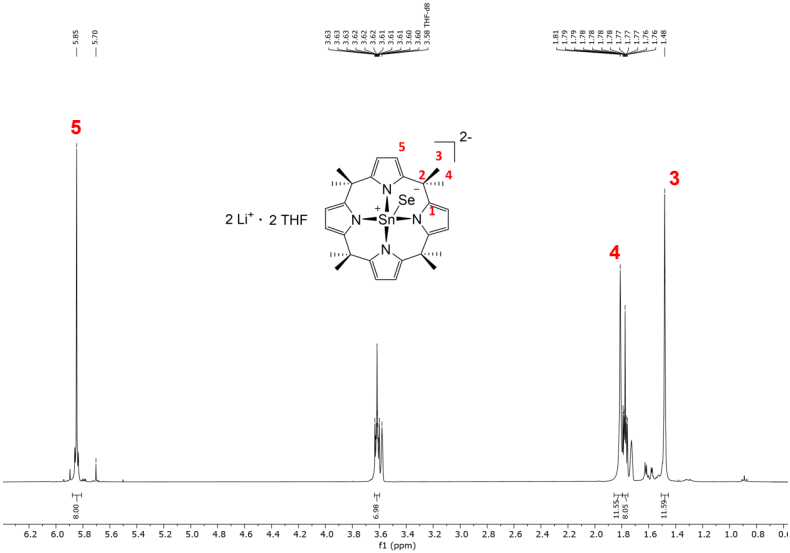


Figure S14. ^{1}H NMR spectrum of **[Li$_2$(thf)$_x$][2^{Me}-Se]** (399.89 MHz, THF-d_8, 295 K).

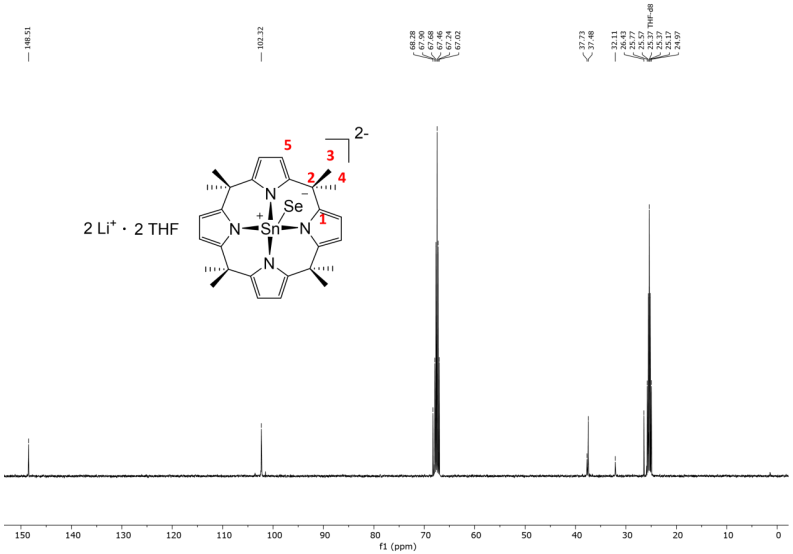


Figure S15. ^{13}C NMR spectrum of **[Li$_2$(thf)$_x$][2^{Me}-Se]** (100.56 MHz, THF-d_8, 295 K).

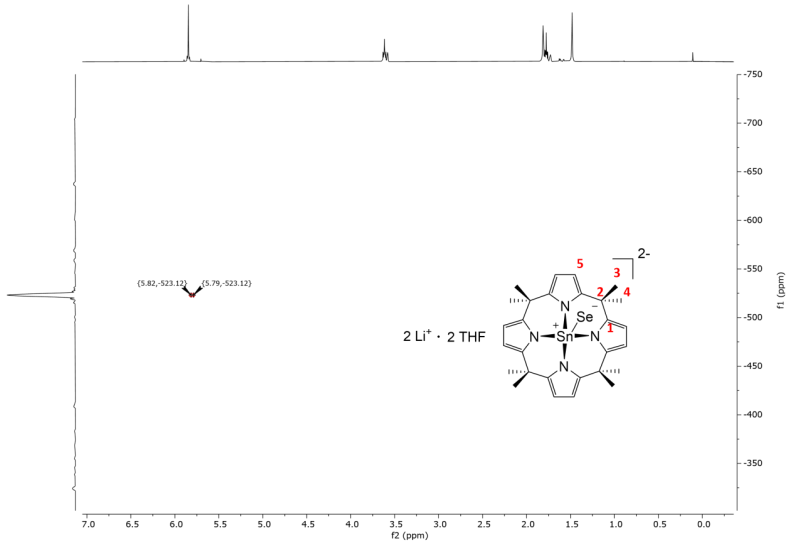


Figure S16. ^{1}H,^{119}Sn HMBC NMR spectrum of **[Li$_2$(thf)$_x$][2^{Me}-Se]** (THF-d_8, 295 K).

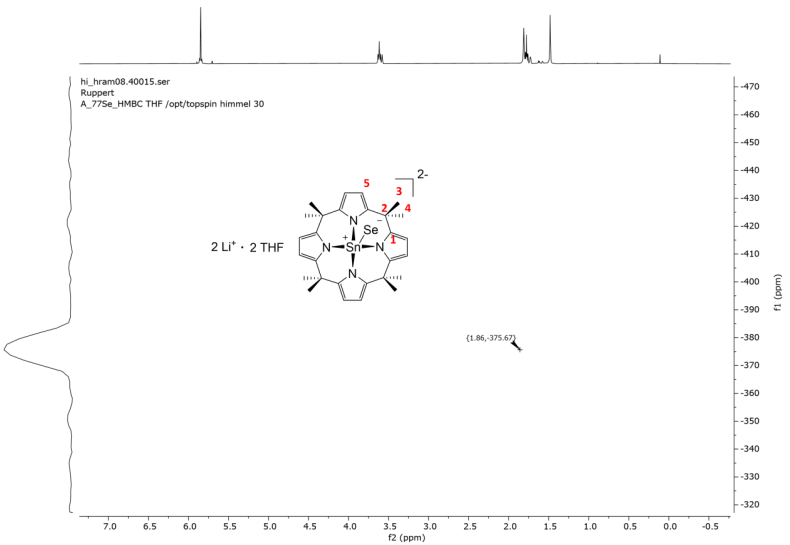


Figure S17. ^{1}H,^{77}Se HMBC NMR spectrum of **[Li$_2$(thf)$_x$][2^{Me}-Se]** (THF-d_8, 295 K).

4.5 [(NBu$_4$)$_2$][Ni(η^1-2^{Me})(CO)$_3$]

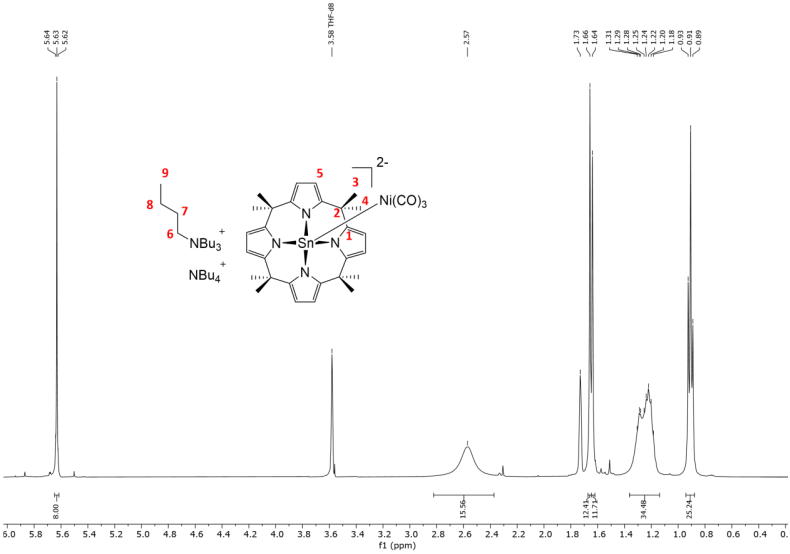


Figure S18. ^{1}H NMR spectrum of **[(NBu$_4$)$_2$][Ni(η^1-2^{Me})(CO)$_3$]** (399.89 MHz, THF-d_8, 295 K).

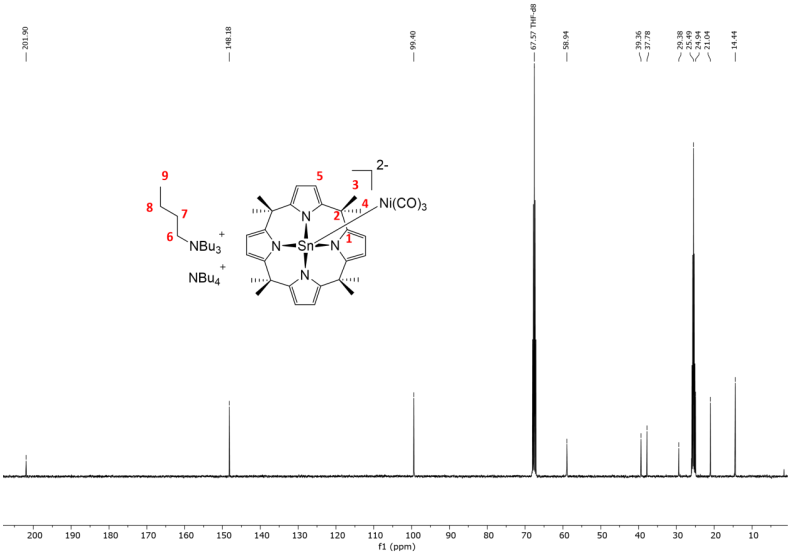


Figure S19. ^{13}C NMR spectrum of **[(NBu$_4$)$_2$][Ni(η^1-2^{Me})(CO)$_3$]** (100.56 MHz, THF-d_8, 295 K).

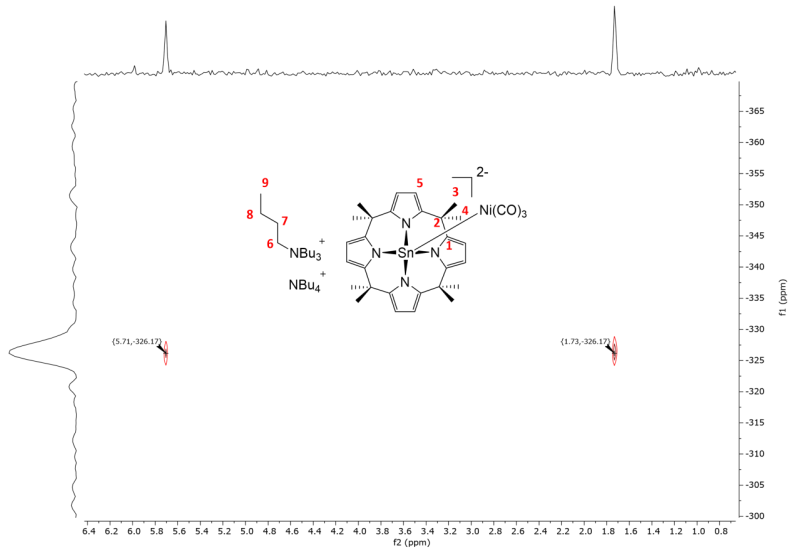


Figure S20. ^{1}H,^{119}Sn HMBC NMR spectrum of **[(NBu$_4$)$_2$][Ni(η^1-2^{Me})(CO)$_3$]** (THF-d_8, 295 K).

4.6 [(NBu$_4$)$_2$][2^{Me}] + PhI after irradiation with UV light

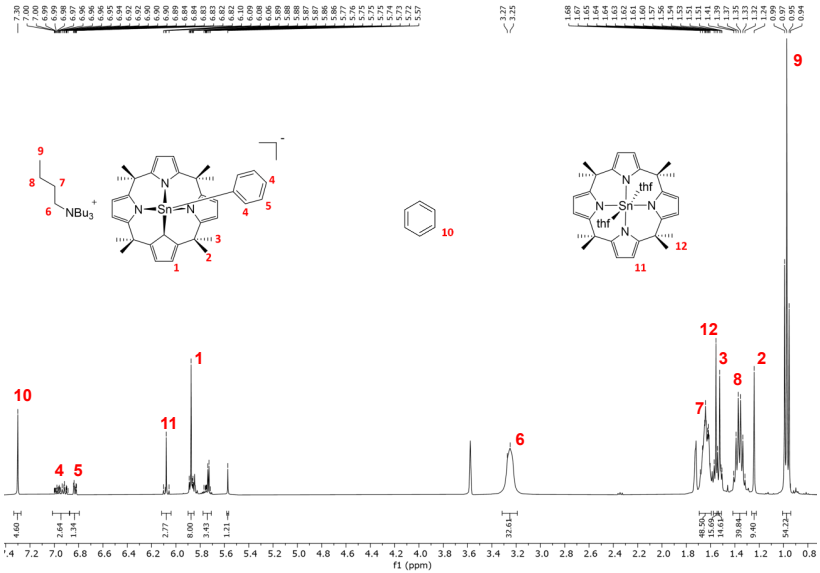


Figure S21. ^{1}H NMR spectrum of the reaction of **[(NBu$_4$)$_2$][2^{Me}]** with PhI after UV irradiation (399.89 MHz, THF-d_8, 295 K).

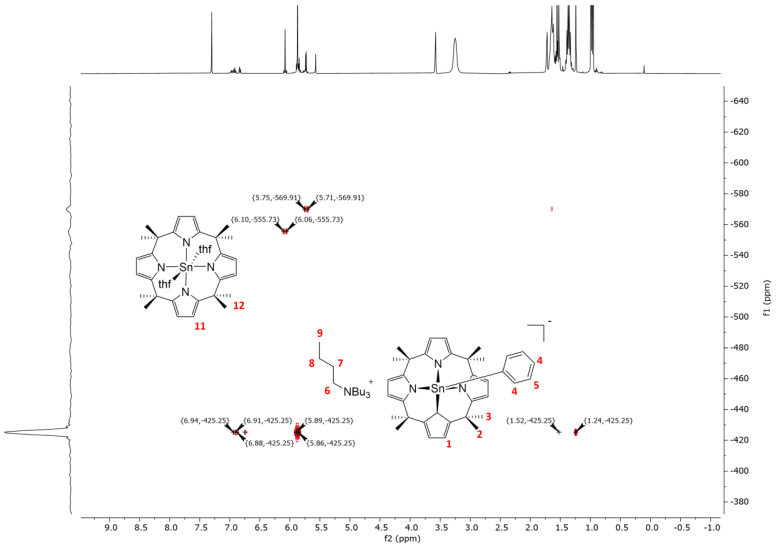


Figure S22. ^{1}H,^{119}Sn HMBC NMR spectrum of the reaction of **[(NBu$_4$)$_2$][2^{Me}]** with PhI after UV irradiation (THF-d_8, 295 K).

4.7 [(NBu$_4$)$_2$][2^{Et}] + PhBr after irradiation with UV light

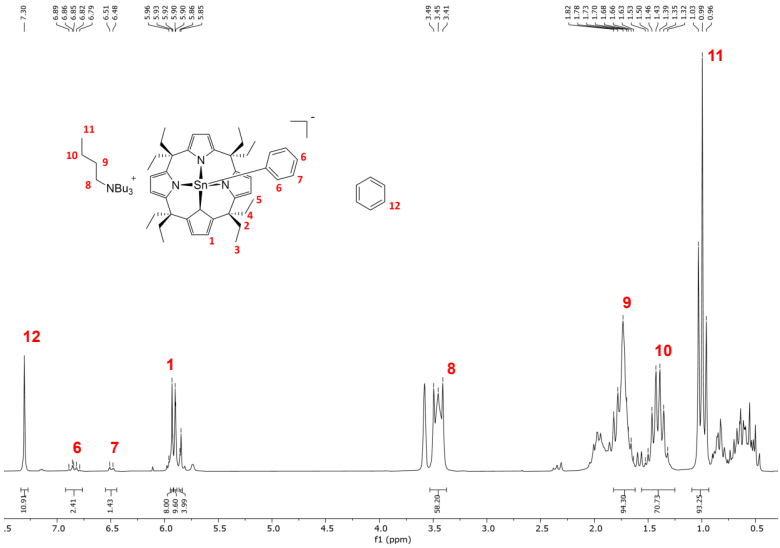


Figure S23. ^{1}H NMR spectrum of the reaction of **[(NBu$_4$)$_2$][2^{Et}]** with PhBr after UV irradiation (200.18 MHz, THF-d_8, 295 K).

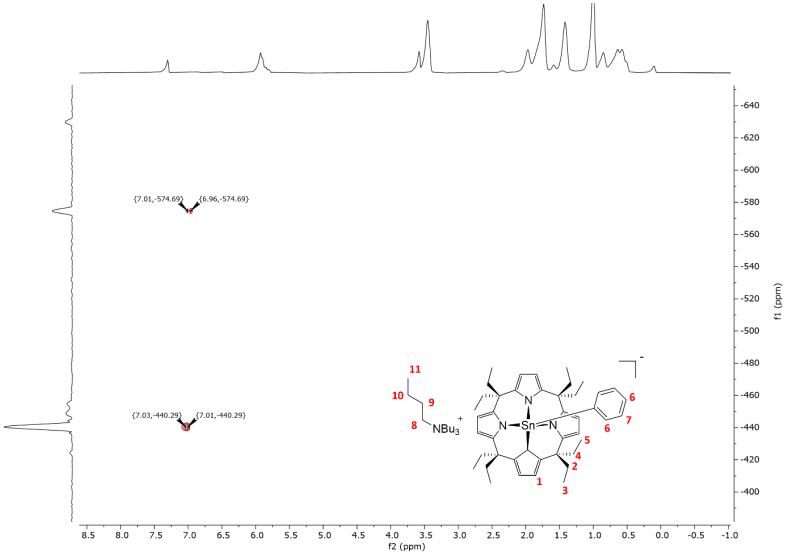


Figure S24. ^{1}H,^{119}Sn HMBC NMR spectrum of the reaction of **[(NBu$_4$)$_2$][2^{Et}]** with PhBr after UV irradiation (THF-d_8, 295 K).

4.8 [(NBu$_4$)$_2$][2^{Et}] + PhCl after irradiation with UV light

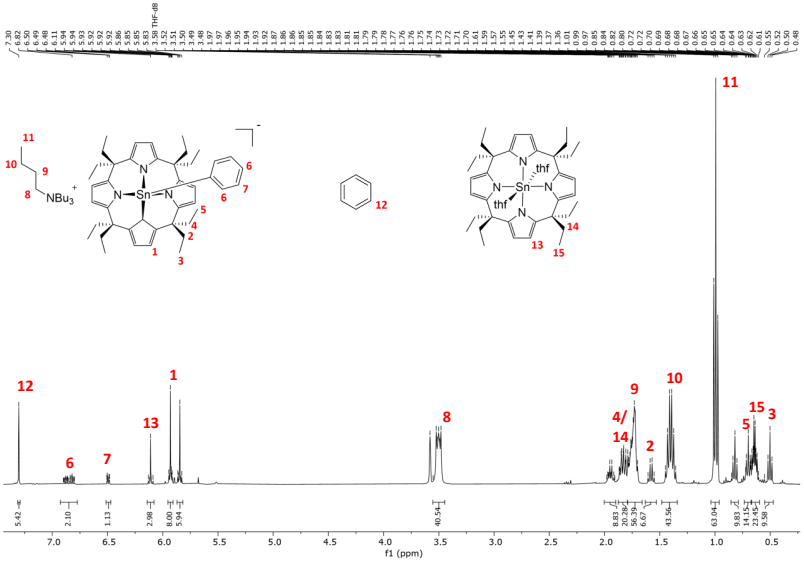


Figure S25. ^{1}H NMR spectrum of the reaction of **[(NBu$_4$)$_2$][2^{Et}]** with PhCl after UV irradiation (399.89 MHz, THF-d_8, 295 K).

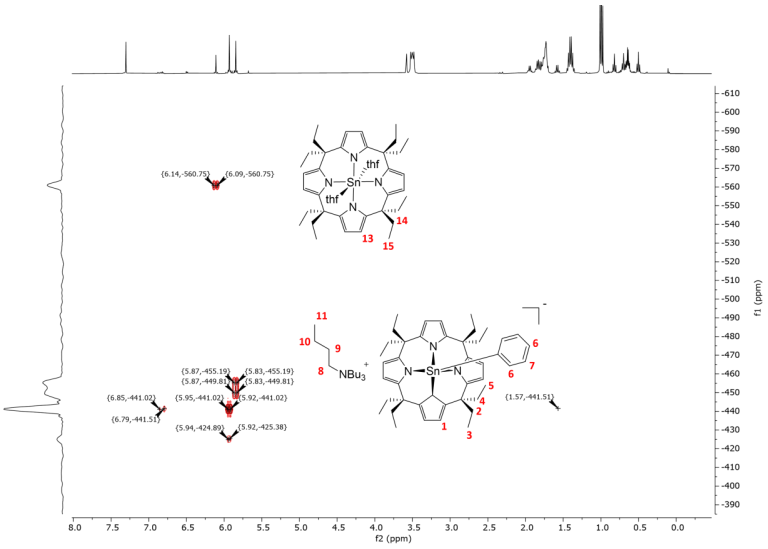


Figure S26. ^{1}H,^{119}Sn HMBC NMR spectrum of the reaction of **[(NBu$_4$)$_2$][2^{Et}]** with PhCl after UV irradiation (THF-d_8, 295 K).

4.9 $[Li_2(thf)_x][2^{Et}]$ + PhI in the presence of benzophenone

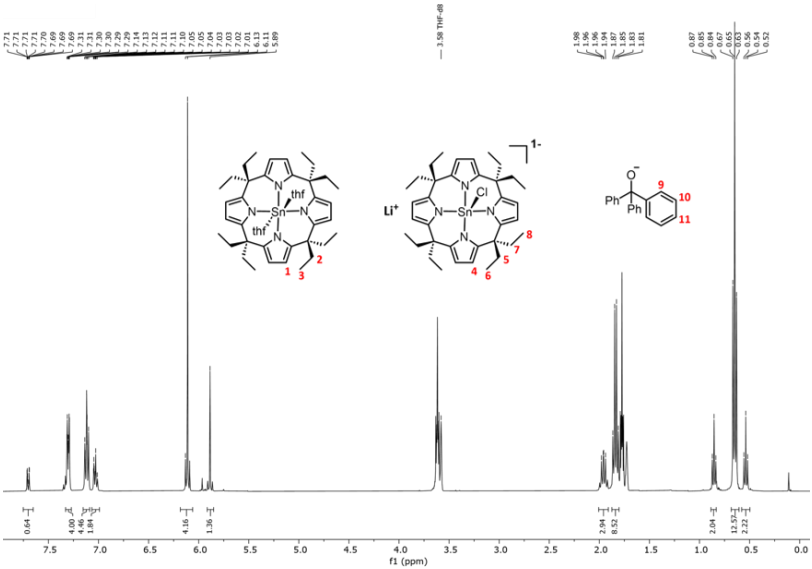


Figure S27. ^{1}H NMR spectrum of the reaction of **$[Li_2(thf)_x][2^{Et}]$** with PhI in the presence of benzophenone (399.89 MHz, THF-d_8, 295 K).

5 Crystallographic Data

5.1 [Li$_2$(thf)$_2$][2^{Me}] x 0.5 LiCl

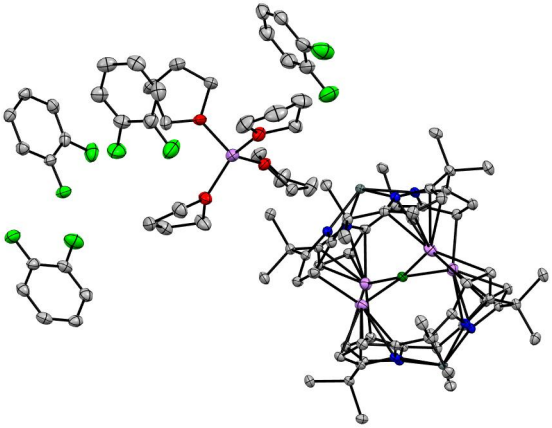


Figure S28. Solid state molecular structure of **[Li$_2$(thf)$_2$][2^{Me}] x 0.5 LiCl**. Ellipsoids are drawn with a probability of 50%. Hydrogen atoms are omitted for clarity. The molecule co-crystallized with four *o*DFB molecules in its asymmetric unit.

Table S1. Crystal data for **[Li$_2$(thf)$_2$][2^{Me}] x 0.5 LiCl**.

CCDC number	2351853
Identification code	mo_hrpj16b_a
Empirical formula	$C_{96}H_{112}ClF_8Li_5N_8O_4Sn_2$
Formula weight	1901.46
Temperature [K]	100(2)
Crystal system	triclinic
Space group (number)	$P\overline{1}$ (2)
a [Å]	13.543(3)
b [Å]	17.999(3)
c [Å]	20.807(3)
α [°]	109.662(8)
β [°]	107.340(6)
γ [°]	92.220(6)
Volume [Å^3]	4504.3(13)
Z	2
ρ_{calc} [gcm^{-3}]	1.402
μ [mm^{-1}]	0.656
F(000)	1960
Crystal size [mm^3]	0.321×0.274×0.195
Crystal colour	colourless

Crystal shape	block
Radiation	MoK_α (λ=0.71073 Å)
2θ range [°]	4.18 to 57.54 (0.74 Å)
Index ranges	−18 ≤ h ≤ 18, −24 ≤ k ≤ 24, −28 ≤ l ≤ 28
Reflections collected	266773
Independent reflections	23341, R_{int} = 0.0376, R_{sigma} = 0.0156
Completeness to θ = 25.242°	99.9 %
Data / Restraints / Parameters	23341/184/1180
Absorption correction Tmin/Tmax (method)	0.6898/0.7458 (multi-scan)
Goodness-of-fit on F^2	1.041
Final R indexes [I≥2σ(I)]	R_1 = 0.0246 wR_2 = 0.0609
Final R indexes [all data]	R_1 = 0.0288 wR_2 = 0.0644
Largest peak/hole [eÅ^{-3}]	0.73/−0.61

5.2 [(PPh$_4$)$_2$][2^{Me}]

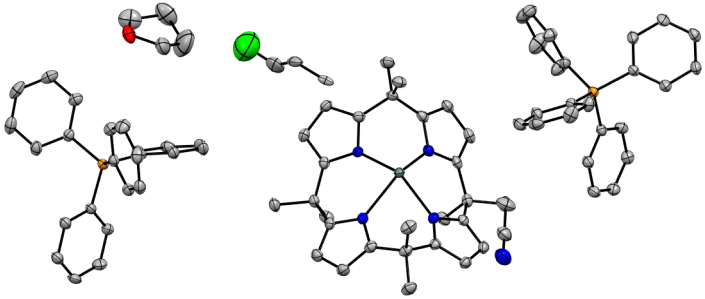


Figure S29. Solid-state molecular structure of **[(PPh$_4$)$_2$][2^{Me}]**. Ellipsoids are drawn with a probability of 50%. Hydrogen atoms are omitted for clarity. The molecule co-crystallized with 0.5 *o*DFB, one THF, and one MeCN molecules in its asymmetric unit.

Table S2. Crystal data for **[(PPh$_4$)$_2$][2^{Me}]**.

CCDC number	2351852
Identification code	mo_hrpj25_a
Empirical formula	$C_{85}H_{85}FN_5OP_2Sn$
Formula weight	1392.20
Temperature [K]	100(2)
Crystal system	triclinic
Space group (number)	$P\overline{1}$ (2)
a [Å]	12.963(5)
b [Å]	14.445(5)
c [Å]	21.214(7)
α [°]	99.16(2)
β [°]	97.306(16)
γ [°]	114.784(18)
Volume [Å^3]	3476(2)
Z	2
ρ_{calc} [gcm^{-3}]	1.330
μ [mm^{-1}]	0.468
F(000)	1454
Crystal size [mm^3]	0.173×0.101×0.046
Crystal colour	yellow
Crystal shape	block
Radiation	MoK_α (λ=0.71073 Å)
2θ range [°]	3.98 to 57.64 (0.74 Å)
Index ranges	−17 ≤ h ≤ 17, −19 ≤ k ≤ 19, −28 ≤ l ≤ 28
Reflections collected	179901
Independent reflections	18071, R_{int} = 0.0779, R_{sigma} = 0.0377
Completeness to θ = 25.242°	99.9 %
Data / Restraints / Parameters	18071/328/957

Absorption correction Tmin/Tmax (method)	0.6398/0.7458 (multi-scan)
Goodness-of-fit on F^2	1.057
Final R indexes [$I \geq 2\sigma(I)$]	R_1 = 0.0403 wR_2 = 0.0946
Final R indexes [all data]	R_1 = 0.0529 wR_2 = 0.1013
Largest peak/hole [eÅ^{-3}]	0.97/−0.92

5.3 [(NBu$_4$)$_2$][Ni(η^1-2^{Et})(CO)$_3$]

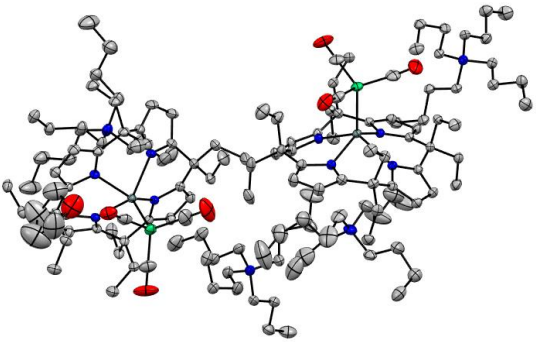


Figure S30. Solid-state molecular structure of **[(NBu$_4$)$_2$][Ni(η^1-2^{Et})(CO)$_3$]**. Ellipsoids are drawn with a probability of 50%. Hydrogen atoms are omitted for clarity. The asymmetric unit contains two **[(NBu$_4$)$_2$][Ni(η^1-2^{Et})(CO)$_3$]** molecules co-crystallized with one THF molecules. The poor quality of the single crystals did only allow to obtain data with an R_{int} of 15.5%.

Table S3. Crystal data for **[(NBu$_4$)$_2$][Ni(η^1-2^{Et})(CO)$_3$]**.

CCDC number	2351854
Identification code	mo_hr406_2_a
Empirical formula	$C_{146}H_{248}N_{12}Ni_2O_7Sn_2$
Formula weight	2638.35
Temperature [K]	100(2)
Crystal system	orthorhombic
Space group (number)	$Pbca$ (61)
a [Å]	26.090(8)
b [Å]	25.612(11)
c [Å]	42.779(17)
α [°]	90
β [°]	90
γ [°]	90
Volume [Å^3]	28586(19)
Z	8
ρ_{calc} [gcm^{-3}]	1.226
μ [mm^{-1}]	0.662
F(000)	11360
Crystal size [mm^3]	0.359×0.102×0.090
Crystal colour	yellow
Crystal shape	block
Radiation	MoK_α (λ=0.71073 Å)
2θ range [°]	3.99 to 57.42 (0.74 Å)
Index ranges	−35 ≤ h ≤ 32, −34 ≤ k ≤ 34, −57 ≤ l ≤ 57
Reflections collected	1005747

Independent reflections	36957, R_{int} = 0.1555, R_{sigma} = 0.0417
Completeness to θ = 25.242°	99.9 %
Data / Restraints / Parameters	36957/1152/1800
Absorption correction Tmin/Tmax (method)	0.6907/0.7458 (multi-scan)
Goodness-of-fit on F^2	1.047
Final *R* indexes [$I \geq 2\sigma(I)$]	R_1 = 0.0392 wR_2 = 0.0814
Final *R* indexes [all data]	R_1 = 0.0772 wR_2 = 0.1001
Largest peak/hole [eÅ^{-3}]	0.93/−0.73

5.4 [3 x LiCl]$_2$

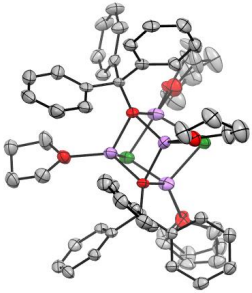


Figure S31. Unrefined solid-state molecular structure of **[3 x LiCl]$_2$**. Ellipsoids are drawn with a probability of 50%. Hydrogen atoms are omitted for clarity. The poor quality of the single crystals did only allow to obtain data with an R_{int} of 15.5%.

6 Elemental Analysis

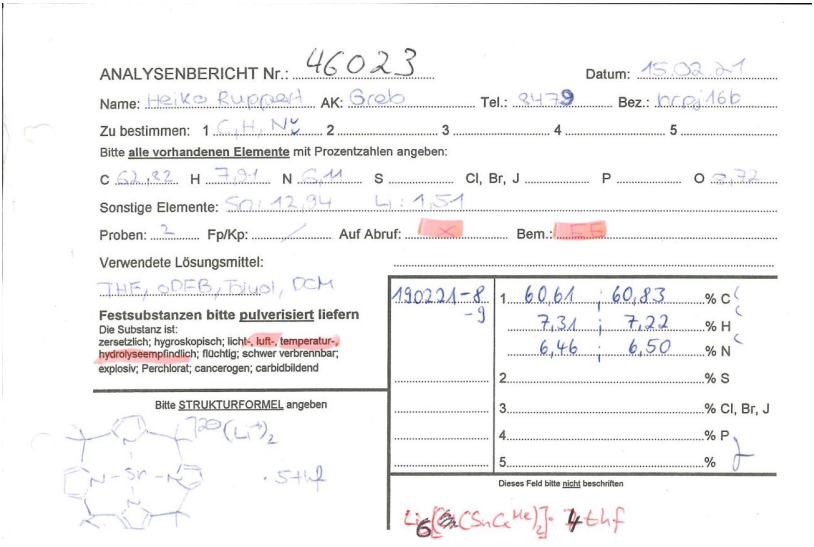


Figure S32. Elemental analysis report for **$[Li_2(thf)_x][2^{Me}]$** (x = 4.0).

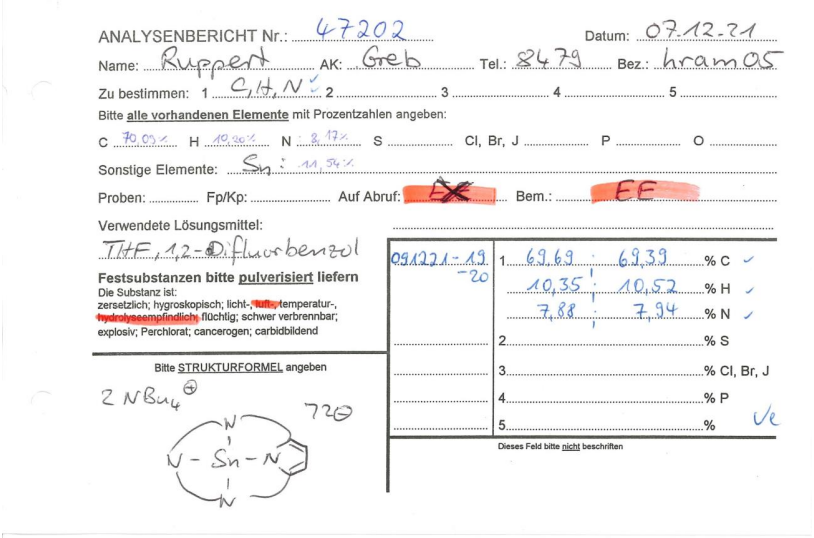


Figure S33. Elemental analysis report for **$[(NBu_4)_2][2^{Me}]$**.

7 Infrared Spectroscopy

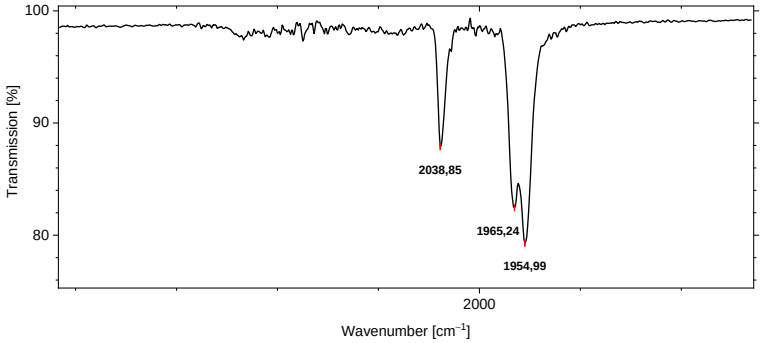


Figure S34. FTIR spectrum of **[(NBu$_4$)$_2$][Ni(η^1-2^{Me})(CO)$_3$]** in THF-d_8.

8 Cyclic Voltammetry

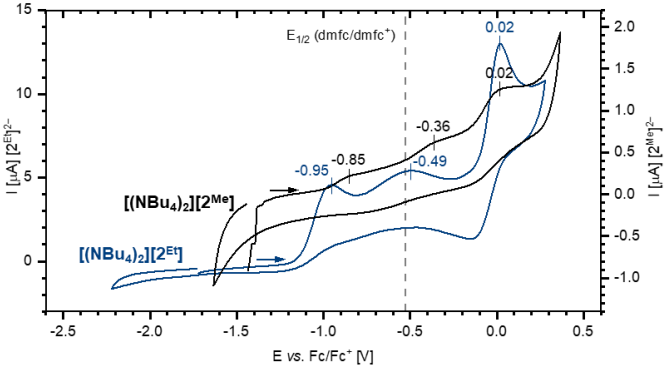


Figure S35. Cyclic voltammogram of **[(NBu$_4$)$_2$][2^{Me}]** (black curve) and **[(NBu$_4$)$_2$][2^{Et}]**[39] (blue curve) in *o*DFB. The scan rate was set to 0.05 V s^{-1}. As supporting electrolyte, [NBu$_4$][PF$_6$] was used. The analyte concentration was approximately c = 10^{-3} mol L^{-1}, the supporting electrolyte concentration c_{supp} = 0.1 mol L^{-1}.

9 NSD Analysis of C_{2v} and C_{4v} Conformers of $[2^R]^{2-}$

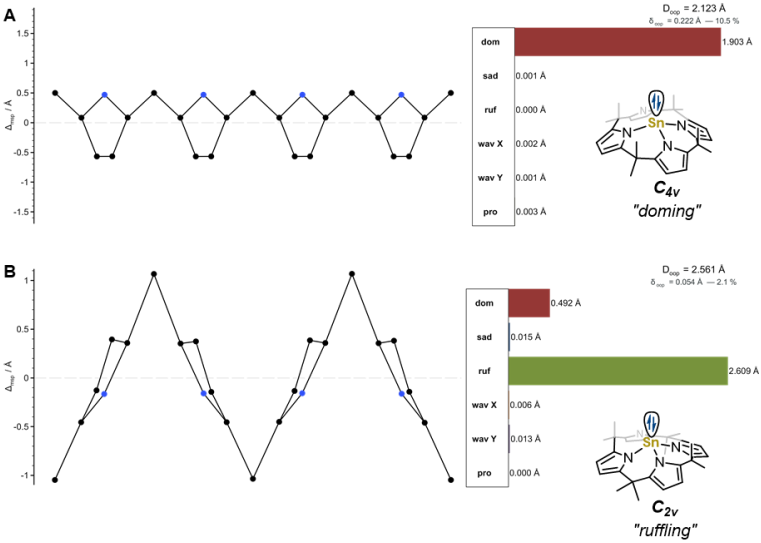


Figure S36. NSD analysis on **A)** the C_{4v} and **B)** the C_{4v} conformer of $[2^{Me}]^{2-}$. Structures were calculated on the B97M-D3(BJ)/def2-TZVPP// CREST/GFN2-xTB level of theory.

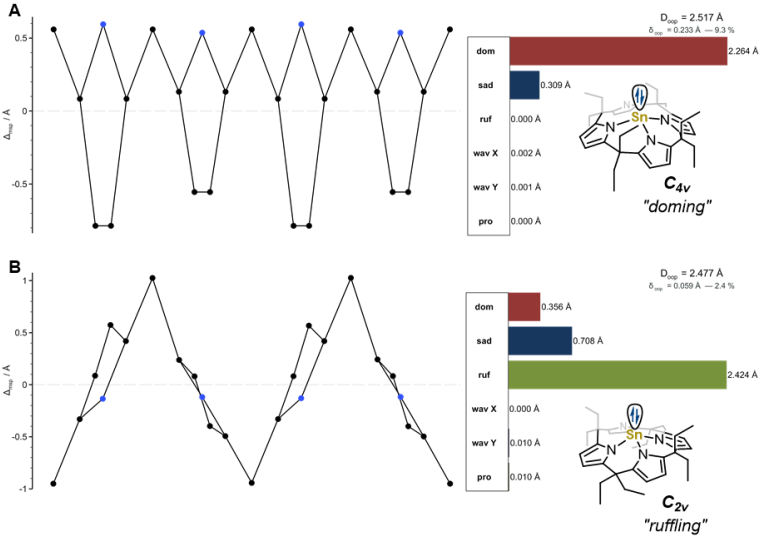


Figure S37. NSD analysis on **A)** the C_{4v} and **B)** the C_{4v} conformer of $[2^{Et}]^{2-}$. Structures were calculated on the B97M-D3(BJ)/def2-TZVPP// CREST/GFN2-xTB level of theory.

10 DFT Calculations

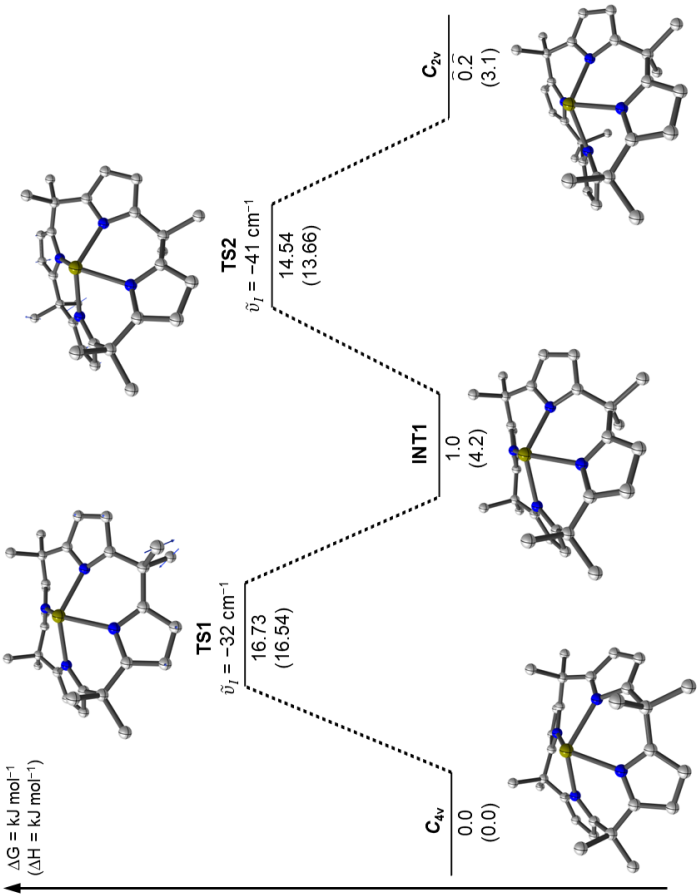


Figure S38. Ring flip mechanism interconverting the C_{4v} and C_{2v} form of $[\mathbf{2}^{Me}]^{2-}$ calculated at the DSD-BLYP/def2-QZVPP COSMO-RS(THF)//B97M-D3(BJ)/def2-TZVPP// CREST/GFN2-xTB level of theory. For **TS1** and **TS2** the scaled displacement vectors of the transition modes are shown as blue arrows.

11 ETS-NOCV Analysis of $[2^{R}\text{-Se}]^{2-}$

Table S4. ETS-NOCV bond analysis of $[2^{R}\text{-Se}]^{2-}$ (R = H, Me, Et) on the BP86-D3/TZ2P COSMO(THF)//B97M-D3(BJ)/def2-TVZPP level of theory. The Se fragment was considered in its closed shell 1D excited state with doubly occupied p_x and p_y orbitals and an empty p_z orbital directed towards the Sn(II) lone pair of a singlet tin(II) calix[4]pyrrolato fragment.

Compound	$[2^{H}\text{-Se}]^{2-}$	$[2^{Me}\text{-Se}]^{2-}$	$[2^{Et}\text{-Se}]^{2-}$
Total Pauli Repulsion (ΔE_{Pauli}) [Eh]	0.331996111878095	0.350339320333676	0.350999376350654
Total Electrostatic Interaction (ΔV_{elst}) [Eh]	-0.228345683224234	-0.236116929972923	-0.236227689437783
Total Orbital Interaction ($\Delta E_{oi,tot}$) [Eh]	-0.292003220768115	-0.293822164014434	-0.294142204425156
Total Dispersion Energy (E_{disp}) [Eh]	-0.009634873943829	-0.011378555454250	-0.012874306980149
Solvation Energy (E_{solv}) [Eh]	-0.213230027047564	-0.201461619539535	-0.184534529258877
Residue [Eh]	-0.000002096350534	0.000001459090166	0.000001863491850
Total Bonding Energy (ΔE) [Eh]	-0.411219789456181	-0.392438489557299	-0.376777490259458

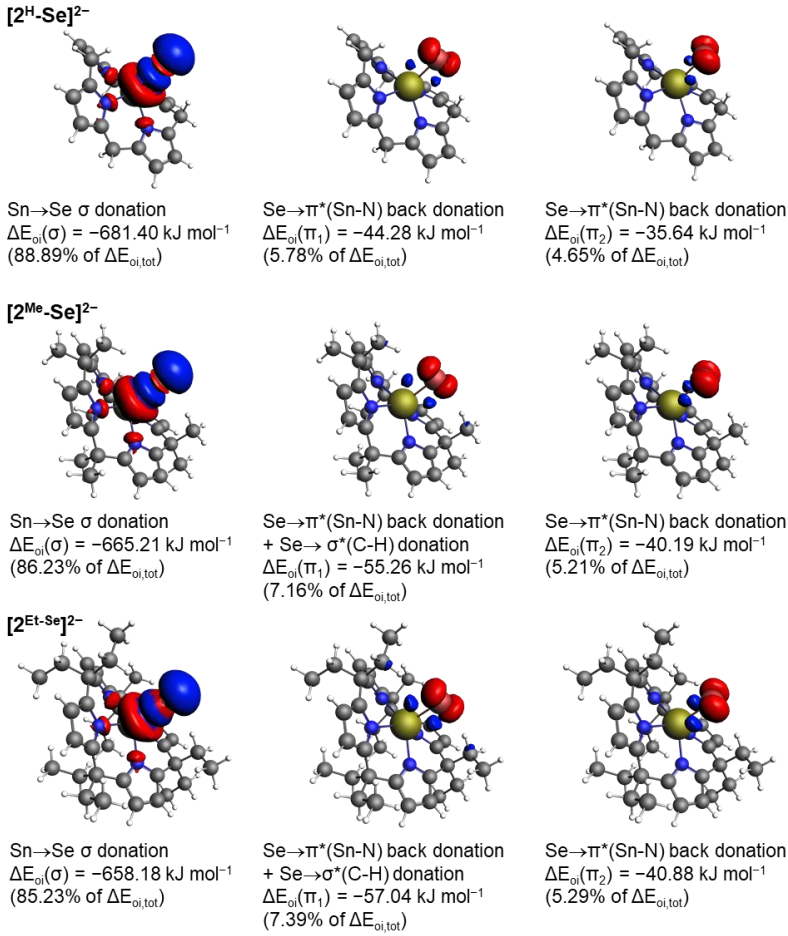


Figure S39. ETS-NOCV bond analysis of **[2^{R}-Se]$^{2-}$** (R = H, Me, Et) on the BP86-D3/TZ2P COSMO(THF)//B97M-D3(BJ)/def2-TVZPP level of theory. The Se fragment was considered in its closed shell 1D excited state with doubly occupied px and py orbitals and an empty p_z orbital directed towards the Sn(II) lone pair of a singlet tin(II) calix[4]pyrrolato fragment. NOCV deformation densities sampled at a value of 0.003. The color code of the charge flow is red to blue.

12 NBO Analysis of $[2^{R}\text{-Se}]^{2-}$

Table S5. NBO analysis results for $[2^{R}\text{-Se}]^{2-}$ (R = H, Me, Et) calculated on PBE0/def2-TZVPP//B97M-D4/def2-TVZPP level of theory. NBO and second order perturbation theory stabilization energies $\Delta E^{(2)}$ for selected bonding interactions are given in kJ mol^{-1}. Additionally, Lewis density parameters %ρ_L and single point energies are given for each system.

$[2^{H}\text{-Se}]^{2-}$ (single point energy = −3605.895922 Eh, %ρ_L = 98.06)	
NBO111 $\sigma_{Sn33\text{-}Se34}$ (occupation = 1.94806)	−953.08
$\Delta E^{(2)}$ $lp(3)_{Se34} \rightarrow \sigma^*_{C32\text{-}H40}$ (**C(sp^3)H-Se interaction**)	4.14
$\Delta E^{(2)}$ $lp(3)_{Se34} \rightarrow \sigma^*_{C8\text{-}H36}$ (**C(sp^3)H-Se interaction**)	4.06
$[2^{Me}\text{-Se}]^{2-}$ (single point energy = −1832.695050950664 Eh, %ρ_L = 98.40)	
NBO143 $\sigma_{Sn57\text{-}Se58}$ (occupation = 1.94615)	−946.36
$\Delta E^{(2)}$ $lp(3)_{Se90} \rightarrow \sigma^*_{C12\text{-}H13}$ (**C(sp^3)H-Se interaction**)	22.72
$\Delta E^{(2)}$ $lp(3)_{Se90} \rightarrow \sigma^*_{C54\text{-}H56}$ (**C(sp^3)H-Se interaction**)	22.84
$[2^{Et}\text{-Se}]^{2-}$ (single point energy = −4234.292224 Eh, %ρ_L = 98.40)	
NBO175 $\sigma_{Sn89\text{-}Se90}$ (occupation = 1.94116)	−925.49
$\Delta E^{(2)}$ $lp(3)_{Se90} \rightarrow \sigma^*_{C16\text{-}H17}$ (**C(sp^3)H-Se interaction**)	21.88
$\Delta E^{(2)}$ $lp(3)_{Se90} \rightarrow \sigma^*_{C78\text{-}H80}$ (**C(sp^3)H-Se interaction**)	21.67

13 ^{77}Se and ^{119}Sn NMR Shift Calculation Results

Table S6. ^{77}Se and ^{119}Sn NMR shifts calculated on the PBE0/SO-ZORA-TZ2P COSMO(THF)//B97M-D3(BJ)/def2-TZVPP level of theory and referenced against $SeMe_2$ and $SnMe_4$, respectively.

Compound	**Total ^{119}Sn NMR isotropic shielding tensor [ppm]**	**^{119}Sn NMR chemical shift against $SnMe_4$ [ppm]**	**Total ^{77}Se NMR isotropic shielding tensor [ppm]**	**^{77}Se NMR chemical shift against $SeMe_2$ [ppm]**
$SnMe_4$	3004.14	0.00	-	-
$SeMe_2$	-	-	1978.08	0.00
$[2^{H}\text{-Se}]^{2-}$	3562.074	-557.933	2616.62	-638.54
$[2^{Me}\text{-Se}]^{2-}$	3560.316	-556.175	2399.702	-421.621
$[2^{Et}\text{-Se}]^{2-}$	3575.747	-571.606	2427.45	-449.37

14 ETS-NOCV Analysis of C_{2v} and C_{4v} $[2^R]^{2-}$

Table S7. ETS-NOCV bond analysis of different conformers of $[2^R]^{2-}$ (R = H, Me, Et) build from a Sn(II) and a *tetra*-anionic calix[4]pyrrolato fragment on the BP86-D3/TZ2P COSMO(THF)//B97M-D3(BJ)/def2-TVZPP//CREST/GFN2-xTB level of theory. To obtain negative orbital energies for the *tetra*-anionic calix[4]pyrrolato fragments and analyze the influence of R on the respective orbital energies COSMO(THF) solvation correction was also used on the fragments. All values given in kJ mol^{-1}.

Compound	C_{2v} $[2^H]^{2-}$	C_{4v} $[2^H]^{2-}$	C_{2v} $[2^{Me}]^{2-}$	C_{4v} $[2^{Me}]^{2-}$	C_{2v} $[2^{Et}]^{2-}$	C_{4v} $[2^{Et}]^{2-}$
Total Pauli Repulsion (ΔE_{Pauli}) [kJ mol−1]	1287.7	1070.4	1272.52	1036.03	1234.27	995.1
Total Electrostatic Interaction (ΔV_{elst}) [kJ mol−1]	-4156.37	-4102.02	-3911.25	-3785.35	-3771.88	-3654.93
Total Orbital Interaction ($\Delta E_{oi,tot}$) [kJ mol^{-1}]	-1171.41	-978.41	-1272.01	-1129.79	-1298.24	-1136.62
Total Dispersion Energy (E_{disp}) [kJ mol−1]	-17.14	-19.11	-23.85	-24.45	-27.84	-28.28
Solvation Energy (E_{solv}) [kJ mol−1]	2697.71	2741.74	2541.27	2565.74	2428.15	2488.41
Residue [kJ mol−1]	0	0	0	0.01	0	-0.01
Total Bonding Energy (ΔE) [kJ mol−1]	-1359.51	-1287.39	-1393.32	-1337.82	-1435.53	-1336.33
NOCV 1 [kJ mol-1]	-440.17	-372.38	-423.06	-380.70	-397.37	-364.32
NOCV 2 [kJ mol-1]	-189.84	-171.35	-205.32	-188.26	-213.76	-191.74
NOCV 3 [kJ mol-1]	-185.61	-170.85	-201.88	-188.26	-200.88	-188.42

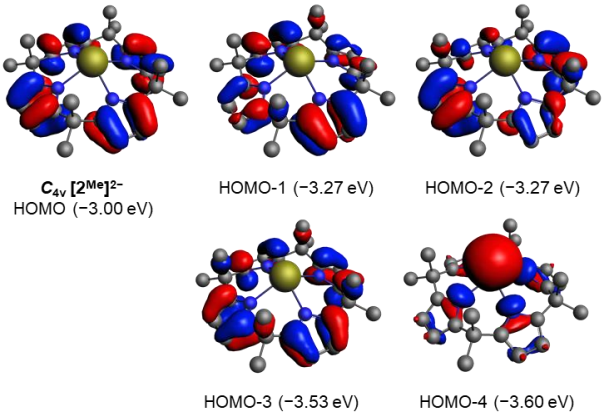


Figure S40. FMO of C_{4v} [2^{Me}]$^{2-}$ computetd on the BP86-D3/TZ2P COSMO(THF)//B97M-D3(BJ)/def2-TVZPP// CREST/GFN2-xTB level of theory. Isosurface plots sampled at a value of 0.03. HOMO-1, -2, and -3 show direct orbital contributions of the Me residues at the *meso*-carbons.

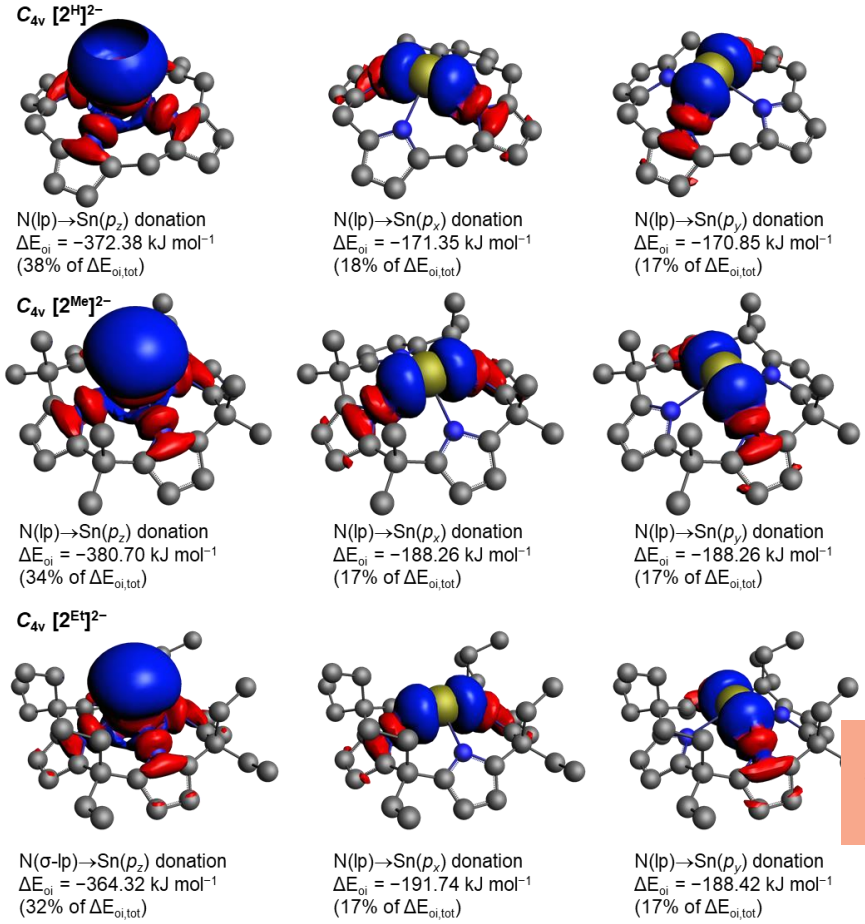


Figure S41. ETS-NOCV bond analysis of **[2^{R}]$^{2-}$** (R = H, Me, Et) build from a Sn(II) and a *tetra*-anionic calix[4]pyrrolato fragment on the BP86-D3/TZ2P COSMO(THF)//B97M-D3(BJ)/def2-TVZPP level of theory. NOCV deformation densities sampled at a value of 0.001. The color code of the charge flow is red to blue.

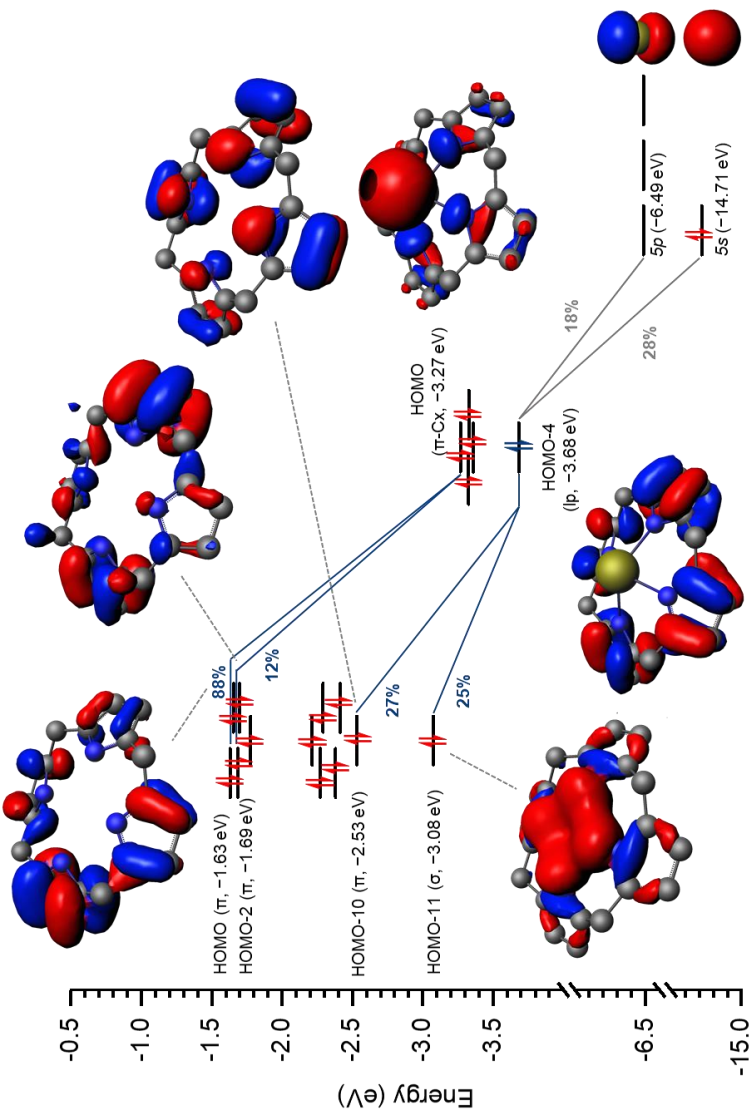


Figure S42. ETS-NOCV bond analysis of C_{4v} $[2^{H}]^{2-}$ build from a Sn(II) and a *tetra*-anionic calix[4]pyrrolato fragment C_{4v} $[1^{H}]^{4-}$ on the BP86-D3/TZ2P COSMO(THF)//B97M-D3(BJ)/def2-TVZPP//CREST/GFN2-xTB level of theory. Isosurfaces sampled at a value of 0.03.

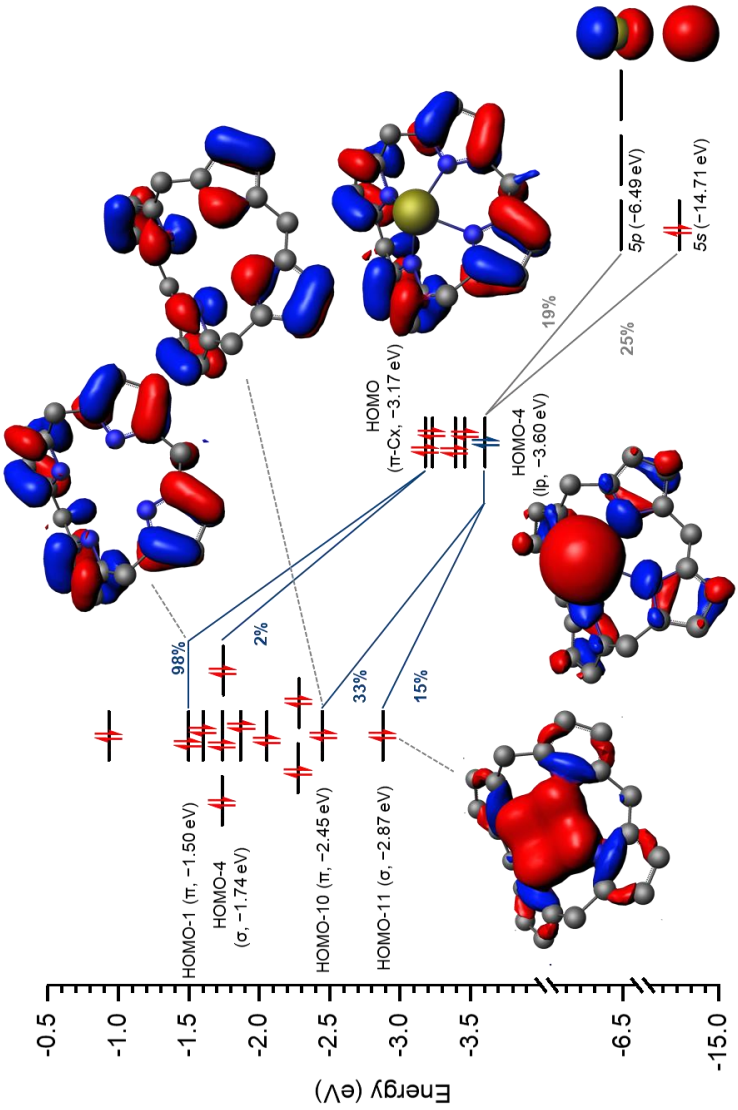


Figure S43. ETS-NOCV bond analysis of C_{2v} $[2^{H}]^{2-}$ build from a Sn(II) and a *tetra*-anionic calix[4]pyrrolato fragment C_{2v} $[1^{H}]^{4-}$ on the BP86-D3/TZ2P COSMO(THF)//B97M-D3(BJ)/def2-TVZPP//CREST/GFN2-xTB level of theory. Isosurfaces sampled at a value of 0.03.

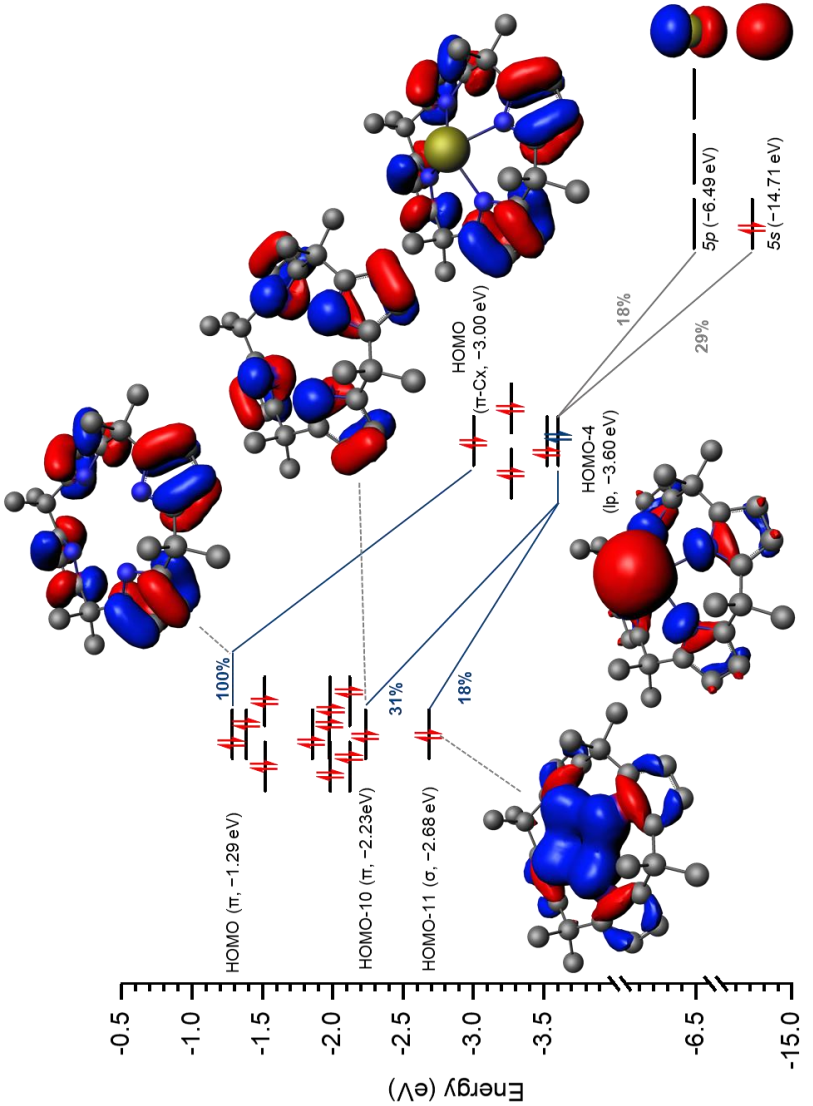


Figure S44. ETS-NOCV bond analysis of C_{4v} $[\mathbf{2}^{Me}]^{2-}$ build from a Sn(II) and a *tetra*-anionic calix[4]pyrrolato fragment C_{4v} $[\mathbf{1}^{Me}]^{4-}$ on the BP86-D3/TZ2P COSMO(THF)//B97M-D3(BJ)/def2-TVZPP//CREST/GFN2-xTB level of theory. Isosurfaces sampled at a value of 0.03.

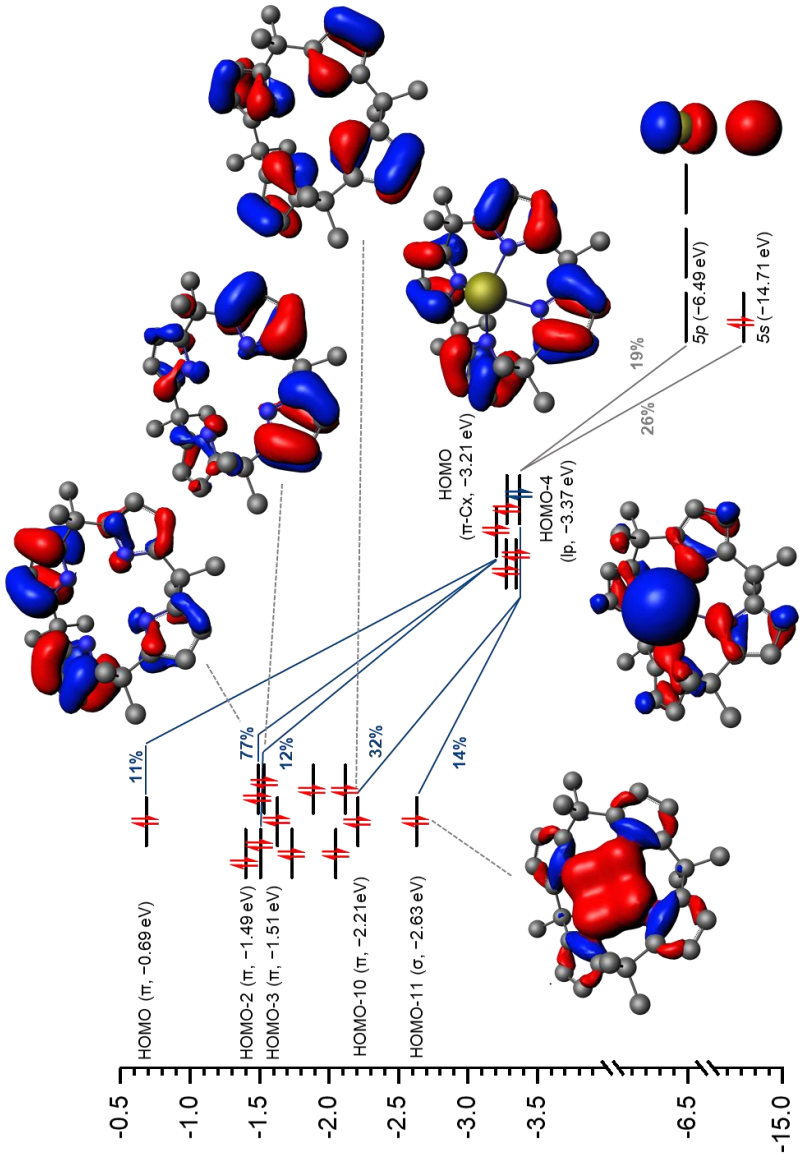


Figure S45. ETS-NOCV bond analysis of C_{2v} $[2^{Me}]^{2-}$ build from a Sn(II) and a *tetra*-anionic calix[4]pyrrolato fragment C_{2v} $[1^{Me}]^{4-}$ on the BP86-D3/TZ2P COSMO(THF)//B97M-D3(BJ)/def2-TVZPP//CREST/GFN2-xTB level of theory. Isosurfaces sampled at a value of 0.03.

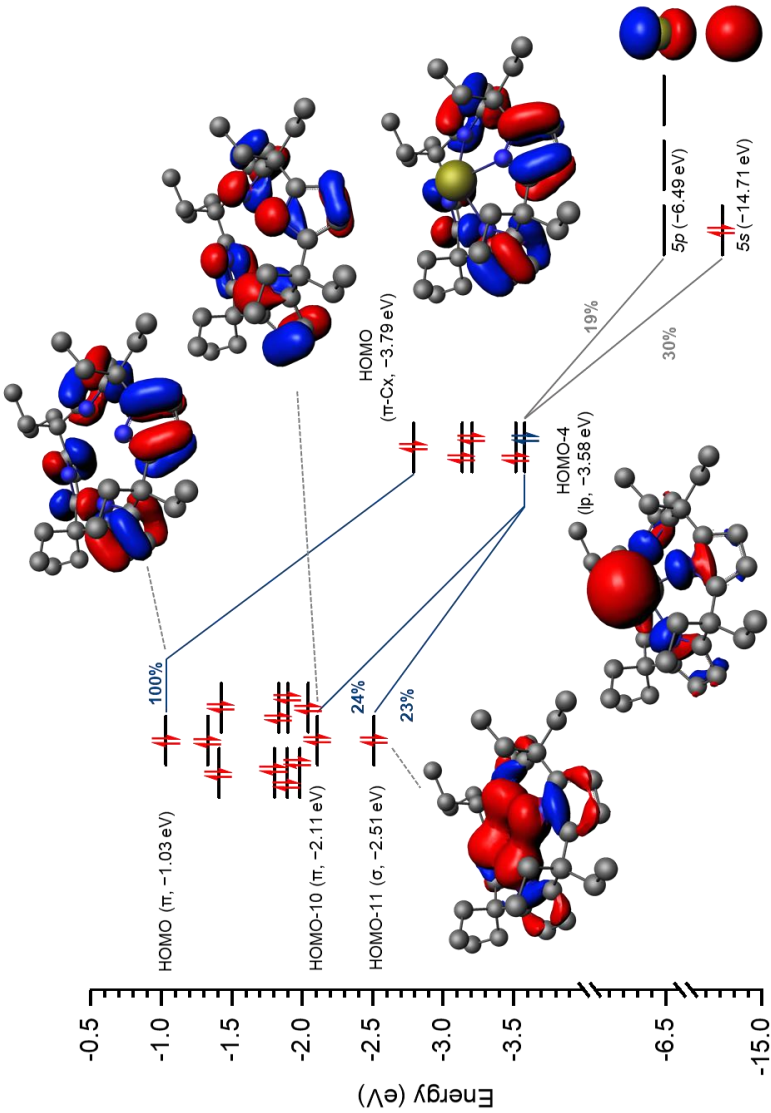


Figure S46. ETS-NOCV bond analysis of C_{4v} $[\mathbf{2}^{Et}]^{2-}$ build from a Sn(II) and a *tetra*-anionic calix[4]pyrrolato fragment C_{4v} $[\mathbf{1}^{Et}]^{4-}$ on the BP86-D3/TZ2P COSMO(THF)//B97M-D3(BJ)/def2-TVZPP//CREST/GFN2-xTB level of theory. Isosurfaces sampled at a value of 0.03.

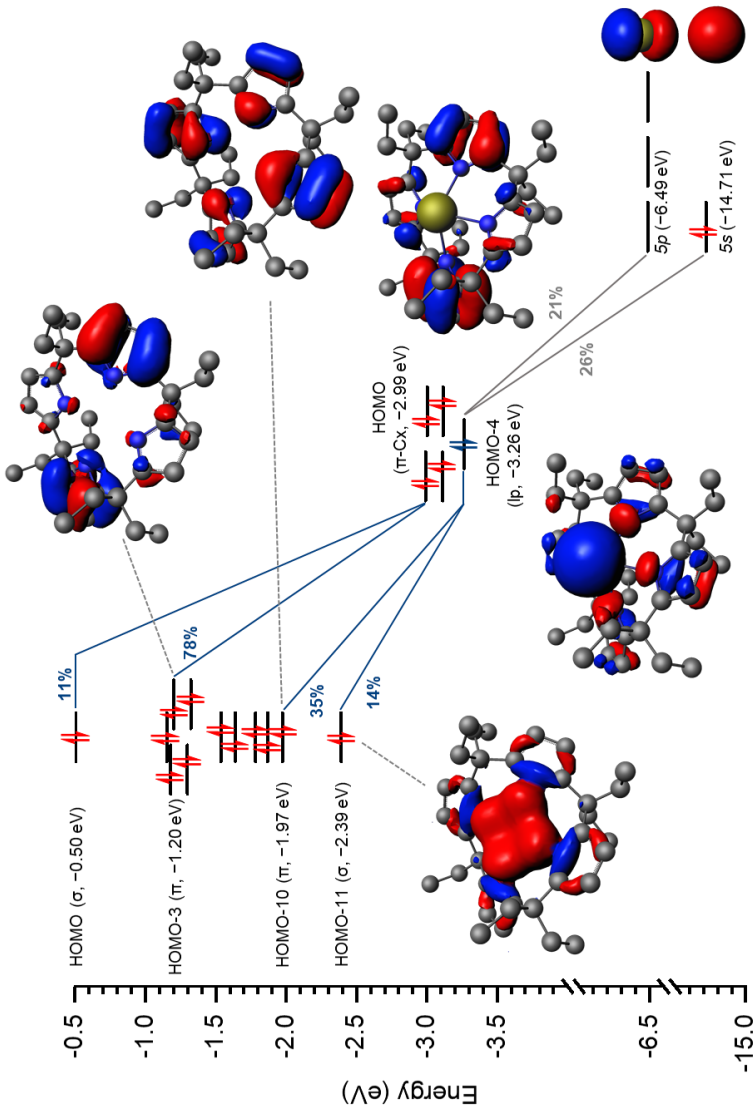


Figure S47. ETS-NOCV bond analysis of C_{2v} $[\mathbf{2}^{Et}]^{2-}$ build from a Sn(II) and a *tetra*-anionic calix[4]pyrrolato fragment C_{2v} $[\mathbf{1}^{Et}]^{4-}$ on the BP86-D3/TZ2P COSMO(THF)//B97M-D3(BJ)/def2-TVZPP//CREST/GFN2-xTB level of theory. Isosurfaces sampled at a value of 0.03.

15 QTAIM Analysis of C_{4v} $[2^R]^{2-}$

Table S8. QTAIM analysis results for C_{4v} $[2^R]^{2-}$ (R = H, Me, Et) calculated on PBE0-D3(BJ)/ZORA-TZ2P/COSMO(THF)//B97M-D4/def2-TVZPP//CREST/GFN2-xTB level of theory.

C_{4v} $[2^R]^{2-}$	R = H	R = Me	R = Et
Total bonding energy [Eh]	−12.531204889841167	−18.355259477322939	−24.165177701101349
QTAIM charge at Sn(II)	1.178	1.202	1.193
average QTAIM charge at N atoms	−1.224	−1.219	−1.215
average QTAIM charge at α-C atoms	0.341	0.344	0.346
average $\rho(r_{BCP})$ at Sn-N BCP's	0.0613	0.0612	0.0590
average $\nabla^2\rho(r_{BCP})$ at Sn-N BCP's	0.1444	0.1433	0.1340
average $H_b(r_{BCP})$ at Sn-N BCP's	−0.0153	−0.0154	−0.0145
average $G_b(r_{BCP})$ at Sn-N BCP's	0.0514	0.0512	0.0480
$G_b(r_{BCP})/\rho(r_{BCP})$ at Sn-N BCP's	0.8385	0.8366	0.8136
average ellipticity at Sn-N BCP's $\varepsilon = (\lambda_1/\lambda_2)-1$	0.1324	0.1306	0.1307
average DI between Sn and N	0.4656	0.4472	0.4406
average $\rho(r_{BCP})$ at C_α-N BCP's	0.3226	0.3206	0.3204
average $\rho(r_{BCP})$ at C_{meso}-C_α BCP's	0.2660	0.2607	0.2593

A variety of descriptors have been used in the context of Bader's theory of AIM, to describe and compare the nature of chemical bonds.[40–43] The main components considered are the electron density, $\rho(r_{BCP})$, and the Laplacian of the density, $\nabla^2\rho(r_{BCP})$ at the bond critical points (bcp's). Low $\rho(r_{BCP})$ and positive Laplacians, as found at the bcp's the Sn-N bonds suggest closed shell (ionic) interactions, whereas the opposite would indicate shared (covalent) interactions. The total electronic energy density $H_b(r_{BCP})$ serves as a criterion for the bond classification, with negative values for shared-type (covalent) atomic interactions (typical covalent single bonds ≈ -0.35) and positive values in closed-shell bonds.[44] At the bcp's the Sn-N bonds $H_b(r_{BCP})$ were only slightly negative. In addition, the ratio of $G_b(r_{BCP})/\rho(r_{BCP})$ (Lagrangian kinetic energy per electron) indicates the kind of interatomic interactions, with a value <1 for shared interaction and >1 for closed-shell (ionic) bonding.[45,46] For the Sn-N bonds values <1 could be obtained which, however, are close to 1. The ellipticity ($\varepsilon=\lambda_1/\lambda_2$-1) of a bond quantifies the anisotropy of the electron density, with deviations from a cylindrical distribution leading to values larger than zero. The delocalization index DI is yet another indicator for covalent bonding. In conclusion these results indicate a predominantly polar (closed-shell) interactions between the Sn center and the N-atoms of the calix[4]pyrrole ligand.

16 NBO Analysis of C_{4v} $[2^R]^{2-}$

Table S9. NBO analysis results for different conformers of $[2^R]^{2-}$ (R = H, Me, Et) calculated on PBE0/def2-TZVPP//B97M-D4/def2-TZVPP//CREST/GFN2-xTB level of theory. NBO and second order perturbation theory stabilization energies $\Delta E^{(2)}$ for selected bonding interactions are given in kJ mol^{-1}. Additionally, Lewis density parameters $\%\rho_L$ and single point energies are given for each system.

C_{4v} $[2^H]^{2-}$ (single point energy = −1204.352002595777 Eh, $\%\rho_L$ = 98.12)	
p-Character of NBO42 (Sn(II) lp)	16.38%
Energy of NBO42 (Sn(II) lp) [eV]	−0.07510
Average energy of σ-lp at N [eV]	−0.11451
Average energy of π-lp at N [eV]	0.03870
Energy of NBO95 (Sn(II) p_z) [eV]	0.23098
Energy of NBO96 (Sn(II) p_x) [eV]	0.27767
Energy of NBO97 (Sn(II) p_y) [eV]	0.27767
average WBI for Sn-N bond	0.3578
d(Sn-N) [pm]	234.79
C_{4v} $[2^{Me}]^{2-}$ (single point energy = −1518.574067920755 Eh, $\%\rho_L$ = 98.15)	
p-Character of NBO50 (Sn(II) lp)	15.68%
Energy of NBO50 (Sn(II) lp) [eV]	−0.08281
Average energy of NBO42, 44, 46, 48 (σ-lp at N) [eV]	−0.12030
Average energy of NBO43, 45, 47, 49 (π-lp at N) [eV]	0.02914
Energy of NBO127 (Sn(II) p_z) [eV]	0.23375
Energy of NBO128 (Sn(II) p_x) [eV]	0.28458
Energy of NBO129 (Sn(II) p_y) [eV]	0.28457
Average WBI for Sn-N bond	0.3396
d(Sn-N) [pm]	234.93
C_{4v} $[2^{Et}]^{2-}$ (single point energy = −1832.780799640192 Eh, $\%\rho_L$ = 98.18)	
p-Character of NBO58 (Sn(II) lp)	14.16%
Energy of NBO58 (Sn(II) lp) [eV]	−0.09299
Average energy of NBO50, 52, 54, 56 (σ-lp at N) [eV]	−0.12465
Average energy of NBO51, 53, 55, 57 (π-lp at N) [eV]	0.02167
Energy of NBO159 (Sn(II) p_z) [eV]	0.22588
Energy of NBO160 (Sn(II) p_x) [eV]	0.28874
Energy of NBO161 (Sn(II) p_y) [eV]	0.28309
Average WBI for Sn-N bond	0.3255
d(Sn-N) [pm]	237.04

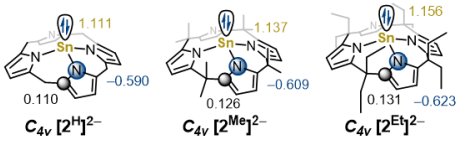


Figure S48. NBO charges of C_{4v} $[2^R]^{2-}$ (R = H, Me, Et) calculated on PBE0/def2-TZVPP//B97M-D4/def2-TZVPP//CREST/GFN2-xTB level of theory.

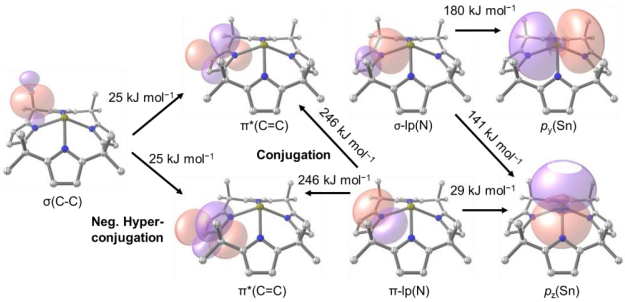


Figure S49. Exemplary pre-orthogonal NBOs and second order perturbation theory stabilization energies $\Delta E^{(2)}$ for selected bonding interactions in C_{4v} $[2^{Me}]^{2-}$ calculated on PBE0/def2-TZVPP//B97M-D4/def2-TVZPP//CREST/GFN2-xTB level of theory.

17 ETS-NOCV Analysis of PhI Halogen Bonding with C_{4v} $[2^{R}]^{2-}$

Table S10. ETS-NOCV bond analysis of halogen bonding adducts of PhI with $[2^{R}]^{2-}$ (R = Me, Et) on the BP86-D3/TZ2P COSMO(THF)//B97M-D3(BJ)/def2-TVZPP//CREST/GFN2-xTB level of theory. All values given in kJ mol^{-1}.

Compound	C_{4v} $[2^{Me}$-PhI$]^{2-}$	C_{2v} $[2^{Et}$-PhI$]^{2-}$
Total Pauli Repulsion (ΔE_{Pauli}) [kJ mol^{-1}]	193.52	144.68
Total Electrostatic Interaction (ΔV_{elst}) [kJ mol^{-1}]	-125.27	-87.76
Total Orbital Interaction ($\Delta E_{oi,tot}$) [kJ mol^{-1}]	-96.89	-76.41
Total Dispersion Energy (E_{disp}) [kJ mol^{-1}]	-26.69	-32.80
Solvation Energy (E_{solv}) [kJ mol^{-1}]	-483.22	-424.77
Residue [kJ mol^{-1}]	0	0
Total Bonding Energy (ΔE) [kJ mol^{-1}]	-538.56	-477.05
NOCV 1 [kJ mol^{-1}]	-101.34	-69.66

18 Literature

[1] L. M. Sigmund, E. Engels, N. Richert, L. Greb, *Chem. Sci.* **2022**, *13*, 11215–11220.
[2] S. De Angelis, E. Solari, C. Floriani, A. Chiesi-Villa, C. Rizzoli, *Journal of the Chemical Society, Dalton Transactions* **1994**, 2467–2469.
[3] D. Geiß, M. I. Arz, M. Straßmann, G. Schnakenburg, A. C. Filippou, *Angewandte Chemie* **2015**, *127*, 2777–2782.
[4] G. Sheldrick, *Acta Crystalogr. A* **2015**, *71*, 3–8.
[5] G. Sheldrick, *Acta Crystalogr. C* **2015**, *71*, 3–8.
[6] C. B. Hübschle, G. M. Sheldrick, B. Dittrich, *J. Appl. Crystalogr.* **2011**, *44*, 1281–1284.
[7] G. Sheldrick, *Acta Crystalogr. A* **2008**, *64*, 112–122.
[8] F. Neese, *WIREs Comput. Mol. Sci.* **2022**, e1606.
[9] R. Rüger, M. Franchini, T. Trnka, A. Yakovlev, E. van Lenthe, P. Philipsen, T. van Vuren, B. Klumpers, T. Soini, *AMS 2021.102, SCM* **2021**.
[10] G. te Velde, F. M. Bickelhaupt, E. J. Baerends, C. Fonseca Guerra, S. J. A. van Gisbergen, J. G. Snijders, T. Ziegler, *J. Comput. Chem.* **2001**, *22*, 931–967.
[11] N. Mardirossian, M. Head-Gordon, *J. Chem. Phys.* **2015**, *142*, 074111.
[12] E. Caldeweyher, C. Bannwarth, S. Grimme, *J. Chem. Phys.* **2017**, *147*, 034112.
[13] F. Weigend, R. Ahlrichs, *Phys. Chem. Chem. Phys.* **2005**, *7*, 3297–3305.
[14] F. Weigend, *Phys. Chem. Chem. Phys.* **2006**, *8*, 1057–1065.
[15] P. Pracht, F. Bohle, S. Grimme, *Phys. Chem. Chem. Phys.* **2020**, *22*, 7169–7192.
[16] C. Bannwarth, E. Caldeweyher, S. Ehlert, A. Hansen, P. Pracht, J. Seibert, S. Spicher, S. Grimme, *WIREs Comput. Mol. Sci.* **2021**, *11*, e1493.
[17] A. V. Marenich, C. J. Cramer, D. G. Truhlar, *J. Phys. Chem. B* **2009**, *113*, 6378–6396.
[18] S. Kozuch, D. Gruzman, J. M. L. Martin, *J. Phys. Chem. C* **2010**, *114*, 20801–20808.
[19] S. Grimme, J. Antony, S. Ehrlich, H. Krieg, *J. Chem. Phys.* **2010**, *132*, 154104.
[20] X. Ren, P. Rinke, V. Blum, J. Wieferink, A. Tkatchenko, A. Sanfilippo, K. Reuter, M. Scheffler, *New J. Phys.* **2012**, *14*, 053020.
[21] G. L. Stoychev, A. A. Auer, F. Neese, *J. Chem. Theory Comput.* **2017**, *13*, 554–562.
[22] G. Zhurko, **2005**.
[23] C. Adamo, V. Barone, *J. Chem. Phys.* **1999**, *110*, 6158–6170.
[24] E. D. Glendening, J. K. Badenhoop, A. E. Reed, J. E. Carpenter, J. A. Bohmann, C. M. Morales, C. R. Landis, F. Weinhold, “NBO 6.0,” **2013**.
[25] T. Ziegler, A. Rauk, *Theoret. Chim. Acta* **1977**, *46*, 1–10.
[26] T. Ziegler, A. Rauk, *Inorg. Chem.* **1979**, *18*, 1755–1759.
[27] T. Ziegler, A. Rauk, *Inorg. Chem.* **1979**, *18*, 1558–1565.
[28] M. P. Mitoraj, A. Michalak, T. Ziegler, *J. Chem. Theory Comput.* **2009**, *5*, 962–975.
[29] S. Grimme, S. Ehrlich, L. Goerigk, *J. Comput. Chem.* **2011**, *32*, 1456–1465.
[30] A. D. Becke, *Phys. Rev. A* **1988**, *38*, 3098–3100.
[31] J. P. Perdew, *Phys. Rev. B* **1986**, *33*, 8822–8824.
[32] J. D. Rolfes, F. Neese, D. A. Pantazis, *J Comput Chem* **2020**, *41*, 1842–1849.
[33] S. Grimme, *J Comput Chem* **2004**, *25*, 1463–1473.
[34] M. Ernzerhof, G. E. Scuseria, *The Journal of Chemical Physics* **1999**, *110*, 5029–5036.
[35] J. I. Rodríguez, R. F. W. Bader, P. W. Ayers, C. Michel, A. W. Götz, C. Bo, *Chemical Physics Letters* **2009**, *472*, 149–152.
[36] J. I. Rodríguez, A. M. Köster, P. W. Ayers, A. Santos-Valle, A. Vela, G. Merino, *Journal of Computational Chemistry* **2009**, *30*, 1082–1092.
[37] J. Krumsieck, M. Bröring, *Chemistry – A European Journal* **2021**, *27*, 11580–11588.
[38] G. Knizia, J. E. M. N. Klein, *Angew. Chem. Int. Ed.* **2015**, *54*, 5518–5522.
[39] H. Ruppert, L. Greb, *Angew. Chem. Int. Ed.* **2022**, *61*, e202116615.
[40] D. Stalke, *Chemistry A European J* **2011**, *17*, 9264–9278.
[41] R. F. W. Bader, *Chem. Rev.* **1991**, *91*, 893–928.

[42]R. F. W. Bader, H. Essén, *The Journal of Chemical Physics* **1984**, *80*, 1943–1960.
[43]F. Cortesguzman, R. Bader, *Coordination Chemistry Reviews* **2005**, *249*, 633–662.
[44]D. Cremer, E. Kraka, *Angew. Chem. Int. Ed. Engl.* **1984**, *23*, 627–628.
[45]R. F. W. Bader, *J. Phys. Chem. A* **1998**, *102*, 7314–7323.
[46]D. Leusser, J. Henn, N. Kocher, B. Engels, D. Stalke, *J. Am. Chem. Soc.* **2004**, *126*, 1781–1793.

19 Optimized Molecular Geometries

41
Coordinates from ORCA-job sn2_cxh_c2v_cmp_Compound_1

N	-0.17846746190976	0.28414599548954	0.15775909191393
C	0.82345108114772	-0.63704580534648	0.24405649726762
C	0.49479071128080	-1.60218117728063	1.17260587307183
C	-0.77977563196571	-1.24999212629591	1.67713603933988
C	-1.15446455477279	-0.08652311880715	1.03263131013563
H	1.10314103145570	-2.44642563617821	1.45173059032096
H	-1.33933929202668	-1.74546551149748	2.45390290850260
C	2.04825336622818	-0.49846660206736	-0.59668679591848
C	2.65642637609241	0.86287196833808	-0.54428603574684
C	3.96476545490897	1.23654762297394	-0.32001525121292
C	3.98817656763746	2.65074372569675	-0.37180998979794
C	2.69175482554248	3.06054928493207	-0.61814749924315
N	1.88209285865623	1.97062078227668	-0.72647015310490
H	4.79194657109357	0.57073412252830	-0.13767463583342
H	4.83088434270786	3.29987181775596	-0.19733010494002
C	2.15605749208504	4.44872787032643	-0.53187918018193
C	-2.29988540989064	0.80257898652971	1.37836586175673
C	-2.89220630326733	1.66011684413114	0.31258752117879
N	-2.13684822456232	2.25155606617556	-0.65429044987444
C	-2.93422995632499	3.13986248945712	-1.31394792955986
C	-4.20328290914943	3.12143663323109	-0.77476965277157
C	-4.17731857191721	2.16619289627494	0.26925742847741
H	-5.03591912655876	3.72582326123146	-1.09452388360199
H	-4.97614149977086	1.91288142007171	0.94722029131291
C	0.95424766261803	4.80606761290164	-1.33777591563292
C	0.59083294947242	6.06443482864387	-1.77790411175179
C	-0.73345295513557	5.95801386805032	-2.26578507700085
C	-1.10107495828554	4.63893899167385	-2.10223127801317
N	-0.07581785712065	3.93786531076942	-1.53901340397837
H	1.19203646556234	6.95566864882135	-1.69894387998595
H	-1.34785799523977	6.74069798388793	-2.67895367434631
C	-2.38570467989787	3.95707626391674	-2.43545132656358
Sn	-0.17483266396919	1.68128878143536	-1.61872960666621
H	2.78652612477266	-1.22668388875904	-0.26613382617687
H	1.81399755534960	-0.76066004194416	-1.63880909385462
H	-2.25024757544233	3.32377699751346	-3.32438885228359
H	-3.12117723485645	4.70877258116551	-2.71569619991850
H	-3.09175275358217	0.19580805802253	1.81856445239374

H	-1.97101037738348	1.46553480725756	2.19303771164685
H	1.91778909770749	4.64662577151583	0.52419136771507
H	2.95780745871053	5.14791161518053	-0.77088913707376

41

Coordinates from ORCA-job sn2_cxh_c2v_cmp_Compound_1

N	-2.10080611353578	-0.37436798199244	0.02111167429780
C	-2.63954676264092	-1.58078234505189	0.36688707947998
C	-3.87569085855202	-1.40730544011114	0.94925092216153
C	-4.12316550951892	-0.01630776616146	0.94891740768194
C	-3.02271693614766	0.57253819252365	0.36637670123569
H	-4.51053746996767	-2.19560533543631	1.31846033621125
H	-4.99132957826787	0.50527583928686	1.31630016942161
C	-1.99651515129423	-2.86187556554999	-0.00328918995044
C	-0.57236681044678	-3.02249730741154	0.36781979455095
C	0.01702848358596	-4.12272867419714	0.95022818606383
C	1.40805485406598	-3.87540579359506	0.94891117054581
C	1.58099421052780	-2.63955770602372	0.36577548056201
N	0.37426346129764	-2.10085263689516	0.02107480937486
H	-0.50422551378424	-4.99074047825559	1.31844011567458
H	2.19668419644105	-4.51012923973038	1.31762409409032
C	2.86164531002626	-1.99639948367761	-0.00569062019642
C	-2.86169052243574	1.99638555737643	-0.00571714925980
C	-1.58104588568504	2.63952519833337	0.36580045843076
N	-0.37430900343313	2.10083949541756	0.02109137691622
C	0.57231274171326	3.02247266726510	0.36788688736730
C	-0.01709395256412	4.12268267918278	0.95032389359578
C	-1.40811800833229	3.87534533038257	0.94899885119961
H	0.50415191998670	4.99068553294293	1.31856883025822
H	-2.19675384107933	4.51004966742706	1.31773183358667
C	3.02265101163018	-0.57256364115414	0.36645522151572
C	4.12306058499987	0.01626755533024	0.94908428625843
C	3.87557010473650	1.40726272350062	0.94946944003753
C	2.63948230601973	1.58075672176166	0.36699223881716
N	2.10076927503727	0.37435264181949	0.02113909086684
H	4.99120555188815	-0.50532447412104	1.31649947484431
H	4.51038268102492	2.19555167997667	1.31876065259290
C	1.99646883264443	2.86185560106955	-0.00319526847185
Sn	-0.00002091211747	-0.00000392721848	-0.95826880767590
H	2.09246927417309	3.00084435741922	-1.09157934755704
H	2.56470281793700	3.67506817702393	0.44499122724396
H	-3.67548409189648	2.56496212696360	0.44096750943221
H	-2.99917494753630	2.09153080369845	-1.09435972387639
H	-2.09249330027669	-3.00086251286102	-1.09167620678225
H	-2.56475739213914	-3.67509214220797	0.44488010821578
H	3.67543165081852	-2.56498645709345	0.44099419697103
H	2.99915550459752	-2.09150476365624	-1.09433307383250

65
Coordinates from ORCA-job sn2_cxme_c2v_cmp_Compound_1

N	-0.14011420403024	0.30880947963929	0.22122741898796
C	0.83685077754636	-0.64528386716527	0.28733476528528
C	0.42238343426487	-1.66597427751871	1.12235940678560
C	-0.85758266315585	-1.31181461591418	1.59364010821418
C	-1.16931004544838	-0.09267575641480	1.02183439941780
H	0.97482689243438	-2.54801182076666	1.38949741319635
H	-1.44983742561143	-1.86183951120133	2.30187264120294
C	2.14267847819395	-0.54343214705771	-0.46430519567143
C	3.17037127595680	-1.43517874698372	0.23173059434241
C	1.99393640402586	-1.10578415583617	-1.89251190799982
C	2.68080729977814	0.86733000039950	-0.49747204782642
C	4.00027753464877	1.26738590189114	-0.39752353584255
C	4.00577240326612	2.67444690604867	-0.47493283719187
C	2.68973358396216	3.07035665276162	-0.62299601880084
N	1.88464844341814	1.96926088873538	-0.64343470080198
H	4.85833823094112	0.63561609835185	-0.25889426366359
H	4.86520712187383	3.31309841533123	-0.38319612156409
C	2.12551248332384	4.45411163521020	-0.45131879280441
C	1.62355618375122	4.55605648690686	1.00545484206961
C	3.23137188177854	5.48557289794804	-0.62583093387243
C	-2.26626718803047	0.85408856221883	1.42630484701662
C	-3.34376394558811	0.09605789104044	2.18830167928427
C	-2.89342854425086	1.64445971291019	0.31057243480905
N	-2.13466594737786	2.30601646537975	-0.61001721079545
C	-2.95509507307186	3.16557665272815	-1.28648843943462
C	-4.24453727383650	3.04114894329774	-0.80433918232030
C	-4.20465962056698	2.07169413648171	0.21776706566380
H	-5.10939624611765	3.59312068898724	-1.12356052461981
H	-5.02803064569590	1.76405352572036	0.83617368995832
C	0.96287471078785	4.80157871195711	-1.34032679329079
C	0.64975703273225	6.03991651016433	-1.86843011806972
C	-0.67469890018397	5.95615435938335	-2.34261452589433
C	-1.11249034981758	4.67195532724775	-2.07826839487638
N	-0.10828126990137	3.96734715401073	-1.47436563906594
H	1.27378815721074	6.91481252710583	-1.87418223847351
H	-1.24017143603467	6.75073439529444	-2.79375036402001
C	-2.46685133968219	4.07866947844106	-2.38543299380050
C	-3.46972913531882	5.21989061673782	-2.54783483147757
C	-2.44463422621415	3.34033422980848	-3.73869686952596
Sn	-0.16790985654303	1.71217397846293	-1.54502292860347
H	1.27224081470402	-0.54472519738573	-2.47418746485099
H	1.65784971741089	-2.14125327837648	-1.84885512068642
H	2.95155060540116	-1.06137329619928	-2.40996941080243
H	-2.14000647657830	4.02470019403187	-4.52987502704287
H	-3.43623852634246	2.95013855089738	-3.96560606111740
H	-1.75089943715642	2.50828845380777	-3.73109973092808

H	-3.82862653771918	-0.64162510207771	1.55557106668654
H	-4.09985763485154	0.78175319542987	2.55874238703690
H	-2.91311500541833	-0.41480336631445	3.04421361855375
H	-3.16111991355530	5.88209338530630	-3.35140792926764
H	-3.55542657580034	5.79874870427349	-1.63446114426833
H	-4.44957899757629	4.82645779852598	-2.80237961385885
C	-1.63977982505257	1.87461007875336	2.40153057496264
H	-0.86364187703461	2.43928807470122	1.89922355618837
H	-1.19299626939350	1.36204231368032	3.25248256431314
H	-2.39565169439006	2.57420263233501	2.75594651537322
H	1.23542149890258	5.55417603058651	1.20457930413391
H	2.43159389596002	4.33488395753010	1.70138494106103
H	0.82592738604729	3.84263846337307	1.17329931647319
H	4.11525092794434	-1.41220138959363	-0.30332605606258
H	2.82683327491259	-2.46535560419973	0.24849309490358
H	3.34108336363136	-1.10924151177380	1.25208647093679
H	3.62842833687982	5.47108440434541	-1.63665888287506
H	4.04493720127527	5.29071243325418	0.06642875797531
H	2.85402475438251	6.48254574334539	-0.41904962276413

65

Coordinates from ORCA-job sn2_cxme_c4v_cmp_Compound_1

N	0.14817568647089	-2.13534087835170	-0.06501150327354
C	-0.89550463663984	-2.93216431765461	-0.44903088838101
C	-0.42370008140137	-4.05130897640594	-1.10090665768929
C	0.98108479942427	-3.95248995648293	-1.10232157342226
C	1.29284440862433	-2.77830916156019	-0.45133666480649
H	-1.01268169885858	-4.84725983322679	-1.51730007045489
H	1.67484236006409	-4.65756434362334	-1.52111871253536
C	-2.30465234712999	-2.64948399782729	-0.03449801303718
C	-3.22919056397747	-3.71341526994636	-0.60957337772536
C	-2.40243587324715	-2.75710541723396	1.49916847136491
C	-2.77841971624283	-1.29289177223864	-0.45106127383242
C	-3.95284161616232	-0.98114735347105	-1.10162051314916
C	-4.05168051163587	0.42363251404837	-1.10016625624476
C	-2.93227472751909	0.89545577011152	-0.44875047658296
N	-2.13530264006289	-0.14821412101838	-0.06500378192667
H	-4.65805022214722	-1.67491457074514	-1.52017483954915
H	-4.84777155288340	1.01260333425961	-1.51630612545493
C	-2.64942813907078	2.30463796165367	-0.03444355526700
C	-3.71337101615043	3.22918850562720	-0.60947700863247
C	-2.75681015978788	2.40262572581100	1.49922492009761
C	2.64942061286441	-2.30470312631244	-0.03454313034982
C	3.71335077926273	-3.22924896298272	-0.60960874499573
C	2.75684160295102	-2.40269987276721	1.49912211824840
C	2.93225810232679	-0.89551753220333	-0.44884332609592
N	2.13529251507321	0.14814810233358	-0.06507159801727
C	2.77840433472460	1.29283044891938	-0.45112462619038

C	3.95280368907808	0.98109281247125	-1.10172790921884
C	4.05166634139242	-0.42368507968070	-1.10024891681908
H	4.65799449691060	1.67486412919709	-1.52030528188211
H	4.84776114961092	-1.01265014799631	-1.51638948342783
C	-1.29286341837356	2.77824543107575	-0.45127193792659
C	-0.98112305615996	3.95242269835139	-1.10227210957998
C	0.42366138507497	4.05124542269531	-1.10089181202313
C	0.89548526205666	2.93209818404371	-0.44903463806180
N	-0.14818371032489	2.13527582153721	-0.06498166444951
H	-1.67489340950796	4.65749507973196	-1.52105178454191
H	1.01263160594014	4.84719809228151	-1.51729811790383
C	2.30464497974018	2.64942011952465	-0.03454225983269
C	3.22916213535270	3.71335670354836	-0.60964136409345
C	2.40247112975394	2.75703991613261	1.49912265191806
Sn	0.00001191457908	-0.00003886775493	0.90329569575365
H	3.54223073099622	-4.24869528993368	-0.27653590387262
H	4.69889028971465	-2.92082169362504	-0.27318231761260
H	3.70246923863802	-3.21665508043717	-1.69498977362107
H	2.02533152255719	-1.76720383210741	1.98453787544952
H	3.74692315384764	-2.08904598160512	1.82813056918677
H	2.57874872303841	-3.42751912533828	1.82267989274788
H	-1.76695100943057	-2.02559132808475	1.98459216642985
H	-2.08864168201289	-3.74719302455503	1.82802689959294
H	-3.42723438663664	-2.57915236588566	1.82286685909993
H	-3.21679790774714	-3.70234319490695	-1.69495490265338
H	-4.24859802841589	-3.54246998703449	-0.27629194024364
H	-2.92058548690391	-4.69897599685787	-0.27337248082899
H	-3.54223988733044	4.24863294577411	-0.27640356712874
H	-4.69890267462468	2.92076156501202	-0.27302745653107
H	-3.70251698669734	3.21660064470760	-1.69485840683389
H	-3.74688467497111	2.08897372143526	1.82825649217838
H	-2.57870565498150	3.42744242826324	1.82278504389075
H	-2.02529083515159	1.76712439794792	1.98461925488916
H	3.42727996091576	2.57909078118493	1.82279023160552
H	1.76700435857135	2.02552082277858	1.98456203529548
H	2.08868167071109	3.74712552691583	1.82799175953973
H	2.92056122351234	4.69891532648545	-0.27343008634230
H	3.21673920566759	3.70228623758864	-1.69502267210896
H	4.24857964684090	3.54241740660668	-0.27638795243656

89

Coordinates from ORCA-job sn2_cxet_c2v_cmp_Compound_1

N	-0.12029088801206	0.31764022808646	0.24712855443514
C	0.82911552874747	-0.66736716540943	0.24211617993391
C	0.33330914612257	-1.78319191434318	0.88851581191248
C	-0.96291394166932	-1.45789323689994	1.32823316840104
C	-1.21149758708402	-0.16372593083578	0.91574196413345
H	0.85192951428910	-2.70755678874103	1.06680402883486

H	-1.60274825086442	-2.07782276008804	1.92876786898373
C	2.19175601324422	-0.51845486472078	-0.38891846064144
C	3.18609062350485	-1.40090448406861	0.39297360888355
H	4.15702408227519	-1.33884004760092	-0.09121519213011
H	2.86782936694304	-2.43676200633879	0.27991529878531
C	3.34647110396870	-1.08163483775096	1.86786546613970
H	3.65597508598844	-0.05268180064589	2.00937211775807
H	4.09961468495047	-1.72742702083674	2.32030302025555
H	2.41401648961868	-1.22430451875311	2.40146618655574
C	2.11802051822978	-1.08330735883211	-1.83491231205875
H	1.31070179588455	-0.57410968780206	-2.35346354810317
H	1.81372098946923	-2.12846225007621	-1.75885178001361
C	3.38073033193573	-0.95855900970841	-2.66545762784972
H	3.70367135054468	0.07575199215583	-2.72066922167585
H	3.20715723577246	-1.31706121840720	-3.67886244826445
H	4.20683224014862	-1.53486241226624	-2.25490589889701
C	2.69727077061792	0.90124047099583	-0.39299682828700
C	4.00033807417785	1.31856591434038	-0.19590491503523
C	4.00255177414167	2.71921492065014	-0.30744367747300
C	2.70278321076704	3.09920077875088	-0.58374376804857
N	1.90752310496722	1.99216857443892	-0.63828775877102
H	4.85106120149383	0.69772259824281	0.01654229256836
H	4.84770556075189	3.36774035786686	-0.16648240557210
C	2.13524754264857	4.49063546467004	-0.52914671856732
C	1.58620635715148	4.65612081445391	0.92016730354793
H	0.92960095953983	3.81149821509340	1.10426249127403
H	2.42912026331357	4.54812022914520	1.60516374917578
C	0.82691265388542	5.93670156618544	1.20717032226767
H	0.49007004981975	5.95176149596797	2.24252096843738
H	-0.04569030910187	6.02169551436487	0.56881083026903
H	1.43580142726608	6.82490088013729	1.05060855808012
C	3.25265019717330	5.51781215106479	-0.73902769278253
H	2.83242129645322	6.51160023263956	-0.60642690747646
H	3.97759321698293	5.39241489211076	0.06469138789925
C	3.96766252537350	5.45839897366170	-2.07715348410158
H	4.46688033611433	4.50610591676519	-2.21263397978993
H	4.71578496882990	6.24843310626667	-2.14879397952957
H	3.26949281274490	5.57978493845198	-2.89729031959128
C	-2.28033330604461	0.77093098693814	1.40462412958371
C	-1.60225050915575	1.74387777058078	2.41577496067426
H	-2.38692006674261	2.36430980873219	2.85281989099317
H	-0.97167064566918	2.41076683679810	1.83567264658026
C	-3.37124648191405	-0.00821203094457	2.14602761341449
H	-4.03090084430249	0.71663790529190	2.62165957905001
H	-2.90487544149544	-0.56434641705365	2.95544361046372
C	-4.19656337001796	-0.96091233114624	1.29996405439282
H	-4.73059437674144	-0.42800499186871	0.52194148972917
H	-4.92723883819855	-1.48782703147085	1.91434886465888

H	-3.56684837543123	-1.69948336940098	0.81753072146895
C	-0.76159609279716	1.10387228084396	3.50323355743201
H	0.06279683183543	0.54179491054362	3.07769335414635
H	-1.33532173718924	0.42115165615566	4.12690159501221
H	-0.34539167328528	1.86949350024485	4.15618770250768
C	-2.90293023272620	1.65380155557585	0.35829769364479
N	-2.15728487326390	2.29613133386200	-0.58604794399913
C	-2.96281144591481	3.22303510981276	-1.19102171199976
C	-4.22781122909260	3.15627861310307	-0.63816530146789
C	-4.18766170337019	2.16373397454647	0.35578544749252
H	-5.07944942403680	3.75500307416707	-0.90342286644687
H	-4.99245750809576	1.88500761084548	1.01109527238688
C	0.99345890198792	4.76570108875972	-1.46473939642509
C	0.73066459351058	5.92689950088268	-2.16437530572215
C	-0.60647523559022	5.84878024781786	-2.59525748715867
C	-1.10961540724332	4.65119260252937	-2.12518746400604
N	-0.12764291485576	3.98334881591946	-1.44538826653086
H	1.39097596382979	6.76401848834266	-2.29732486671762
H	-1.14323337302751	6.60065490858123	-3.14466384541319
C	-2.51054032356230	4.12200956351604	-2.31231448552085
C	-3.47178306796714	5.32360057521300	-2.41060896388897
H	-4.47494475147447	4.95015704266688	-2.59906209462989
H	-3.19884109690651	5.89194661640196	-3.29908575321436
C	-2.56817008598237	3.37546919160529	-3.67452652629238
H	-2.31080384961794	4.09679701989576	-4.45186184240454
H	-1.77619673322100	2.63232072172269	-3.68238026191171
C	-3.87901768938691	2.68646992012546	-4.00024763620309
H	-4.70711637081473	3.38638993464286	-4.08613110114741
H	-4.13930782867503	1.97290185308449	-3.22562557804727
H	-3.80426032335563	2.15229959021532	-4.94613178705383
C	-3.50888787862862	6.25346316413924	-1.21152565926652
H	-3.81320382303088	5.72325267237102	-0.31672997433151
H	-4.21487059751907	7.06736728057872	-1.37974490264117
H	-2.53357430413334	6.68735491697262	-1.02367668459797
Sn	-0.16798288980593	1.72356461547694	-1.52232873046549

89

Coordinates from ORCA-job sn2_cxet_c4v_cmp_Compound_1

N	0.00146046114751	-2.15945774880615	0.23256607836606
C	1.10051938770565	-2.87007272665649	0.63725678316802
C	0.70707951466465	-3.99778914936894	1.32378225080030
C	-0.70171641850068	-3.99877563109081	1.32369078934678
C	-1.09665107842253	-2.87161459531045	0.63710081868456
H	1.34380470272526	-4.74031854976150	1.76670075798291
H	-1.33745370283250	-4.74219831053081	1.76652396332030
C	2.48211559839732	-2.47773747783230	0.20990923323699
C	3.49095258739107	-3.48819468963652	0.77202933261455
H	3.10991791368380	-4.48911938661615	0.59187795302189

H	3.51613502859803	-3.36971253206526	1.85221415594434
C	4.89852081836474	-3.40368160741175	0.20566095080779
H	4.94173632658559	-3.77502639214329	-0.81549954929264
H	5.58646791191150	-4.00870746425827	0.79472822519802
H	5.26803081637831	-2.38493271438773	0.20133406946914
C	2.54914589773037	-2.50189157784444	-1.33678912474883
H	3.53631033259941	-2.16394357347475	-1.64954460514981
H	1.85621168014447	-1.76190311608036	-1.72074676528210
C	2.22227308552039	-3.84362890679154	-1.96031261441181
H	2.94580158431085	-4.61079617737143	-1.69176240730752
H	2.20932004168384	-3.77435397878671	-3.04642927840483
H	1.24739673934866	-4.19135209720460	-1.63291046610452
C	2.81850033746619	-1.09677827729822	0.68532035448528
C	3.81113901540427	-0.70214925899446	1.55509178609203
C	3.81021752458071	0.70744148735632	1.55496524291548
C	2.81701290404084	1.10061179964041	0.68518640719173
N	2.18205761888478	0.00145338580555	0.17457447415856
H	4.48259544460428	-1.33933716382265	2.10009076334345
H	4.48083529507424	1.34562020622477	2.09984533907635
C	2.47875674320791	2.48106121730229	0.20966364835422
C	3.48624478847994	3.49290354725565	0.77171191956447
H	3.10396048636425	4.49330711866491	0.59133032687721
H	3.51147504137460	3.37465006072714	1.85191880680293
C	4.89396361114561	3.41009330141921	0.20549541396801
H	5.58105495408682	4.01618161324332	0.79446997057464
H	4.93677157217528	3.78126664673932	-0.81574325577850
H	5.26484244672536	2.39183135459143	0.20143229200785
C	2.54574622052770	2.50519277047786	-1.33703356891877
H	3.53342914249160	2.16874763672526	-1.64977840107389
H	1.85399122723298	1.76408179248450	-1.72095455125617
C	2.21684726758554	3.84639341852258	-1.96065162604034
H	1.24151606261132	4.19274817194279	-1.63315428025716
H	2.20385971687748	3.77700496857285	-3.04675986205493
H	2.93929378484526	4.61463560502304	-1.69225743760175
C	-2.47875957054999	-2.48111942008758	0.20970613972200
C	-3.48625788177375	-3.49293922466167	0.77177645659421
H	-3.51146569728488	-3.37468095367016	1.85198326192239
H	-3.10400039930723	-4.49335184824493	0.59139098881632
C	-2.54574610827870	-2.50528135268650	-1.33699088635447
H	-1.85399331731110	-1.76417513660901	-1.72092547419335
H	-3.53342969756821	-2.16884563303377	-1.64974415345597
C	-2.21684072081353	-3.84649301239378	-1.96058184314530
H	-2.93928647393180	-4.61473190846219	-1.69217694769290
H	-1.24151013111349	-4.19283918923970	-1.63307331808452
H	-2.20384788055576	-3.77712476114911	-3.04669128728104
C	-4.89398637744303	-3.41009501081510	0.20559021615922
H	-4.93682604574921	-3.78126619421479	-0.81564765809895
H	-5.26484042383191	-2.39182314105170	0.20153667284690

H	-5.58107956675141	-4.01616638760786	0.79457993232723
C	-2.81701561621648	-1.10066037056898	0.68519641220716
N	-2.18205832921331	-0.00151412751994	0.17456133655218
C	-2.81850461363941	1.09672942563747	0.68527814900457
C	-3.81113433615690	0.70212034067238	1.55506899159513
C	-3.81023984049497	-0.70747028472910	1.55494361450533
H	-4.48258075606175	1.33932135303071	2.10006464758137
H	-4.48087431987757	-1.34563625207074	2.09981883174684
C	1.09664679676033	2.87156220715606	0.63704516337957
C	0.70170817072235	3.99874368539667	1.32359897187702
C	-0.70708768293925	3.99774647904022	1.32369999121822
C	-1.10052321221156	2.87002054522945	0.63718808127150
N	-0.00146211645405	2.15939694209807	0.23251828348839
H	1.33744345207391	4.74218173474762	1.76640978808336
H	-1.34381606779932	4.74028173251499	1.76660464819610
C	-2.48211724982832	2.47767960234103	0.20984039447030
C	-3.49095059699381	3.48815228883901	0.77193776595192
H	-3.10989634601945	4.48907072023090	0.59179079544085
H	-3.51615579990110	3.36967411454741	1.85212266109606
C	-2.54914519271008	2.50181071913241	-1.33685893830621
H	-1.85620639768312	1.76182142632844	-1.72080501185885
H	-3.53630746013828	2.16385235397531	-1.64961005908027
C	-2.22228108217756	3.84354121804735	-1.96040133076513
H	-1.24740809382613	4.19127561163648	-1.63300167408366
H	-2.94581607910251	4.61070703362681	-1.69186361556243
H	-2.20932502372491	3.77425098326358	-3.04651701226361
C	-4.89850816711868	3.40366141534296	0.20553930636864
H	-5.58645751888924	4.00870116247217	0.79458973890425
H	-5.26803542725029	2.38491937835206	0.20120695175761
H	-4.94169555116043	3.77500431920642	-0.81562330234565
Sn	0.00000249327322	-0.00004102112298	-0.74809663750263

65

Coordinates from ORCA-job sn2_cxme_flip_TS1

N	-0.11801459460355	0.34779021133127	0.25985185249892
C	0.93706024576745	-0.51009525423774	0.44376812292244
C	0.64185986622886	-1.38706041246485	1.46880635824616
C	-0.64103894887797	-1.05321662863159	1.92932290077129
C	-1.07908341969895	0.01639110888849	1.16878900057081
H	1.27611687287801	-2.16153081432250	1.85750954401864
H	-1.17167139528471	-1.51551527357638	2.74293153496837
C	2.19397656312036	-0.48281140542280	-0.38904950133379
C	3.25189569772732	-1.34822199258834	0.29283462324053
C	1.95000679466500	-1.12757588490321	-1.76758716118042
C	2.74208642632839	0.91320502188884	-0.53189894502342
C	4.06565489659643	1.30965622274946	-0.52063726278293
C	4.06728396092800	2.71372769753458	-0.64429611765730
C	2.74551372075558	3.10518074460221	-0.72960689118320

N	1.93613419749910	2.00798699618080	-0.66858506591676
H	4.92807402669921	0.67922029282743	-0.40417438806804
H	4.92868842890500	3.35617288627426	-0.62506271665726
C	2.18756990368791	4.49287076148698	-0.60072684313407
C	1.68507156761288	4.64962767066419	0.85001668622393
C	3.29100678386896	5.51763179763910	-0.81711073372286
C	-2.39490302626463	0.71245516975389	1.40694991638993
C	-3.51681470649086	-0.33497946396185	1.25125138483395
C	-2.75856628832292	1.89368233641971	0.54536509931851
N	-2.13329484613890	2.30567900969743	-0.59488300264867
C	-2.85189197867532	3.35938625294220	-1.09909841353996
C	-3.93524243612277	3.61224863223484	-0.28311110771324
C	-3.87538354370468	2.68059856495040	0.76553766092447
H	-4.66970699140155	4.38590242458847	-0.40818464767253
H	-4.57302376431359	2.59028485084689	1.57934838329821
C	1.02944516713428	4.79162490466447	-1.50749279258805
C	0.76667842846471	5.96053126036515	-2.19441547701179
C	-0.56679440778306	5.87302499294644	-2.64582306309065
C	-1.05284975803228	4.65695933017297	-2.20787783052876
N	-0.07633807824110	3.99144134529639	-1.52220208516232
H	1.42870102222053	6.79858701472471	-2.31589543794569
H	-1.10985815357967	6.62741433424717	-3.18555105889074
C	-2.45118265830734	4.10912565493967	-2.34161505383091
C	-3.40972984930251	5.28004729769780	-2.54463691533784
C	-2.59914160470068	3.22061380409195	-3.59035125293952
Sn	-0.15477954859716	1.71445702952745	-1.53313613711272
H	1.20679946093010	-0.58907877059003	-2.34309357623701
H	1.60038301982003	-2.15203271961211	-1.64200321058270
H	2.87585002954512	-1.13523054918837	-2.34193692293032
H	-2.32219530254829	3.78334950638020	-4.48110368026843
H	-3.63118518771220	2.88485464073825	-3.68792724831666
H	-1.96523729662105	2.34380725417285	-3.54189149413943
H	-3.55632851313821	-0.68506032611678	0.22439373959670
H	-4.48200851214174	0.10170327096609	1.49759373912350
H	-3.34093426175519	-1.19442663024788	1.89474883434206
H	-3.16346508833458	5.81173754068729	-3.45926418562476
H	-3.35568541758512	5.98025770274521	-1.71812105140359
H	-4.43205659593613	4.92068354923735	-2.63119647735608
C	-2.40605429507716	1.18138071429594	2.87577536957582
H	-1.62054371359866	1.91204471951456	3.03751298573929
H	-2.23339610347304	0.34423021449410	3.54656760322345
H	-3.35610440530842	1.64148073243884	3.13442046664391
H	1.29098547165908	5.65278015324507	1.00921217341638
H	2.49765325870870	4.46558966946635	1.55163385947376
H	0.89377362011460	3.93741272987111	1.04856589436401
H	4.16131701794740	-1.36414506863351	-0.30023953276751
H	2.90056108125003	-2.37178838782299	0.38813777619781
H	3.48998831174495	-0.96792093781667	1.28034679518619

H	3.68804685327886	5.46430474752722	-1.82681723356269
H	4.10542503219338	5.34989524607722	-0.11858382171118
H	2.91033496339380	6.52127150610431	-0.65057196753523

65

Coordinates from ORCA-job sn2_cxme_flip_INT1_Compound_1

N	-0.15205672662529	0.30905453810986	0.36715713143949
C	0.99791242214524	-0.32095826187470	0.75875203252557
C	0.84411206745478	-0.82132241368669	2.03394157465786
C	-0.46547827791992	-0.49387968284466	2.44094742896949
C	-1.04635234070255	0.19125458083038	1.39326292094751
H	1.57893851583945	-1.35569140997739	2.60728560287867
H	-0.92633341604440	-0.74753646847082	3.37772118239994
C	2.18265981390859	-0.45882615734727	-0.15261628773668
C	3.26997120588194	-1.26158064773716	0.55602703119502
C	1.79240614365786	-1.26438724782604	-1.40430744347908
C	2.73919296475091	0.88828430147709	-0.52657848771513
C	4.05943058243111	1.22658267511339	-0.74402872597942
C	4.08443540931407	2.61555402884515	-0.98266560427969
C	2.77758029140789	3.05343258970887	-0.90372697497774
N	1.94935454989152	1.99937309738831	-0.63514644314656
H	4.90872590865955	0.56935313215947	-0.69620339802411
H	4.95779800620876	3.22197399147837	-1.13918923683408
C	2.28973540017645	4.46850055284504	-0.80564454609697
C	1.92979791486191	4.72667393008175	0.67168923190596
C	3.40979055243299	5.42808860418024	-1.17903398574880
C	-2.49457467113929	0.54448922883835	1.22385446614955
C	-3.10297186549334	-0.46723475736069	0.23077515326662
C	-2.75841323306639	1.91749696433884	0.67908173783791
N	-2.18273283554125	2.35394497713620	-0.48049279317728
C	-2.81701497496741	3.51336591375824	-0.83615114610204
C	-3.77762681371276	3.82509846467302	0.10199388147573
C	-3.74095500551070	2.80308172785443	1.07254283373094
H	-4.43049945036120	4.67832455580313	0.09564934315349
H	-4.37133039718763	2.72049418916654	1.93856174365257
C	1.06780856433769	4.76965865708931	-1.62158679851950
C	0.80421918054607	5.90677819498618	-2.35882554572517
C	-0.56666847710325	5.86728327740342	-2.68462713546896
C	-1.07066102693792	4.71049601844286	-2.12550952831806
N	-0.07304428043069	4.02937551864412	-1.48494429389545
H	1.49500864244617	6.69622966318706	-2.59230490854669
H	-1.11914413972448	6.61534973384399	-3.22375589117910
C	-2.49945374683474	4.23925501338670	-2.11119314163823
C	-3.41851038023802	5.45057401273595	-2.23900992386359
C	-2.80152985786915	3.33630074130077	-3.32066844875969
Sn	-0.19588297589005	1.72559790828440	-1.44206785320224
H	1.01537236472230	-0.76914966732254	-1.97413414757595
H	1.42394211403290	-2.24984294472829	-1.12030431895757

H	2.65950728432127	-1.38078285641753	-2.05306144532447
H	-2.60038136747383	3.87689884307785	-4.24469949389288
H	-3.84667269791430	3.02806433118295	-3.30819177489676
H	-2.19046590593698	2.44138857633880	-3.32053779008223
H	-2.61695900070054	-0.38260033793880	-0.73452515069132
H	-4.16631858978820	-0.27202670522926	0.09639710893045
H	-2.96498471842735	-1.48483399167944	0.59447671481322
H	-3.23477118909298	5.96729033244179	-3.17639214660136
H	-3.25594987506315	6.15161380691073	-1.42732373449923
H	-4.45906050401313	5.13560548336310	-2.22398629272940
C	-3.22170865105868	0.37011854751627	2.54949742551221
H	-2.83668237715349	1.05136449329261	3.30232764370107
H	-3.10042331766813	-0.64598847136188	2.91243174501354
H	-4.28350977974575	0.55963205555161	2.42530854639248
H	1.59340236714264	5.75420760923647	0.80514703127772
H	2.79524558071011	4.54509488302329	1.30787107660570
H	1.13240933133022	4.06320657151508	0.98172447805429
H	4.11907739815100	-1.40974796448462	-0.10439198807586
H	2.88901385843468	-2.23869016648117	0.84260221428647
H	3.61718936726174	-0.74730738735404	1.44566971057059
H	3.71622051114939	5.29733946565173	-2.21306020332567
H	4.27356648689573	5.26338948420897	-0.54179974835471
H	3.08473506683199	6.45547827372025	-1.04458221392241

65

Coordinates from ORCA-job sn2_cxme_flip_TS2

N	-0.21886034136893	0.32306978717701	0.47120199851054
C	0.92090319532656	-0.20184658385499	1.01241265658800
C	0.66134265393255	-0.68755647808595	2.27598237591788
C	-0.71207414284236	-0.47239279126237	2.51407070001914
C	-1.21802581808515	0.13419561082300	1.38337906835401
H	1.36209239411558	-1.15805522004135	2.94078437767460
H	-1.26107574563562	-0.75386425553724	3.39371196128342
C	2.16612540695515	-0.36172311066911	0.19828499868270
C	3.22511776894559	-1.07546185608753	1.03417116941389
C	1.86171652263896	-1.27684072604033	-1.00442978373644
C	2.71987936520692	0.94841136163168	-0.28194903623270
C	4.03955031041741	1.21428072463600	-0.58368356109127
C	4.08785458779428	2.54572500234005	-1.02219026119647
C	2.79646135632847	3.03553014744304	-0.96204002711680
N	1.94852542315369	2.05790341835884	-0.51529728791944
H	4.87174033708145	0.54207907010462	-0.48078104948020
H	4.97171614285469	3.10391251420564	-1.27680627320023
C	2.46544208788455	4.49104103182540	-1.12636676801962
C	3.15474179793785	5.24479327508291	0.02780193963082
C	3.09227356909440	4.98593301156905	-2.44493344016338
C	-2.65541937655899	0.32098988700963	1.00776173613019
C	-2.97937224287960	-0.69118864366033	-0.11076278036193

C	-2.99463584687938	1.68849166836721	0.50092879363958
N	-2.26339311048514	2.31498370254734	-0.47101564841955
C	-2.97219124600186	3.42423333613464	-0.84284033390546
C	-4.13132337948266	3.51684147805756	-0.10303040855609
C	-4.14576614111588	2.40381081571195	0.75883341597768
H	-4.86922391260162	4.29547827158659	-0.15975412819524
H	-4.90832412592172	2.15600430990974	1.47353475740253
C	1.01671915466489	4.88550861988996	-1.14905101827865
C	0.59601274415998	6.20202026669319	-1.12421145655702
C	-0.77603061516006	6.19958528468941	-1.41806667031602
C	-1.13389387336655	4.88109690691663	-1.59878627609937
N	-0.04500968281678	4.06763041203856	-1.42672512388236
H	1.21351411779751	7.06748658343069	-0.96309029829200
H	-1.42416783764620	7.05397712251873	-1.47516749236595
C	-2.49784213456877	4.35064409223030	-1.92012179343109
C	-3.47493025541308	5.51179367060314	-2.05238910316423
C	-2.49338787578281	3.63648574260929	-3.28193485317223
Sn	-0.18613844085879	1.74807403689997	-1.35980737565423
H	1.11367330811277	-0.83400673165750	-1.65171881265583
H	1.48412567538409	-2.24081815457547	-0.66446102844382
H	2.76610591784993	-1.43170771420697	-1.59122050901196
H	-2.18401483333274	4.32837283938940	-4.06460061065554
H	-3.49097017438530	3.26314856204407	-3.51048907657043
H	-1.81224730680044	2.79431957535772	-3.29895078188814
H	-2.37698780691036	-0.49260949998550	-0.99004766463094
H	-4.02922809072129	-0.61666477460667	-0.39170117853600
H	-2.76561402489323	-1.70617183251518	0.22286506118169
H	-3.14741516446646	6.18794524669019	-2.83729025026226
H	-3.55379747799803	6.07272508978572	-1.12728609938121
H	-4.46245602045773	5.13838627943857	-2.30905448393386
C	-3.54404426018407	-0.02380999017174	2.19460497977358
H	-3.37659633668120	0.65756971029122	3.02332483881422
H	-3.33857623501304	-1.03475515720245	2.53383870732792
H	-4.59070392059112	0.03197439614806	1.91171641366896
H	2.99444834502617	6.31791251983442	-0.04266885103929
H	4.22426082952385	5.05237045085900	0.01697073914653
H	2.75778578222872	4.90503350947005	0.97855720841464
H	4.11566304236833	-1.26167230319702	0.44212190610462
H	2.84570804628070	-2.03328908229244	1.38100698911602
H	3.50935930325856	-0.48114981507481	1.89654426232114
H	2.61170209919580	4.49946092585253	-3.28800205127434
H	4.15661908938476	4.76486695643248	-2.48886075715330
H	2.95199542300279	6.05910449608969	-2.54739665084941

42

Coordinates from ORCA-job se_sn2_cxh_cmp_Compound_1

N	0.00002124512806	-2.06808264986408	0.35564158867502
C	1.12489613477353	-2.84723824760848	0.34223020813758

C	0.88913209669317	-4.03000896654033	0.99707843713627
C	-0.45465021919135	-3.98602280599158	1.42991191786506
C	-0.97007799535135	-2.78168584052111	1.01086213911120
H	1.61006021810635	-4.81421191358704	1.14857140810762
H	-1.00981188037502	-4.75195281263563	1.94396645683459
C	2.36753322047350	-2.36222156755865	-0.29787736710022
C	2.85641307690739	-1.11182523543600	0.32386593762982
C	4.04690655651966	-0.86521732722128	0.96039384178698
C	4.00473679859125	0.48342120386897	1.37819496042887
C	2.79368350520641	0.99072554769630	0.96884990392749
N	2.07423114438212	0.01101019091236	0.33465350026956
H	4.83527220898996	-1.58205535016116	1.10964971952770
H	4.77590291901714	1.04676102919493	1.87523912303561
C	2.42018230987283	2.42218212540239	0.93184289059262
C	-2.40289554438370	-2.41239260201149	0.98663352505813
C	-2.77441261169135	-0.98101841002574	1.04274684062636
N	-2.07443076754371	0.00199434836570	0.39198853092788
C	-2.85594362655923	1.12513728046338	0.41229957467588
C	-4.02633329127127	0.87527091978672	1.08397959616380
C	-3.97199905490629	-0.47578234198319	1.49231524317325
H	-4.80873733476726	1.59178494185674	1.26321919365055
H	-4.72777693932476	-1.04150786945490	2.00988658895621
C	0.98869753321710	2.79097444783395	1.00116645319856
C	0.48592011828033	3.99271356084039	1.44231309156296
C	-0.86984632751864	4.03932115678522	1.04874937366987
C	-1.12472077163882	2.86052576271832	0.39388089981453
N	-0.00014410517452	2.08123255009415	0.37015050888766
H	1.05580022594517	4.75571924564606	1.94447394459608
H	-1.58598368541835	4.82237520832488	1.22662818569601
C	-2.38509736677340	2.38008425312261	-0.21404070008717
Sn	-0.00965702931202	0.00917623371035	-0.39740488388950
Se	-0.04401732174402	0.01903052539308	-2.82248501250759
H	-2.91131104473597	-2.93650113647468	1.79469450148335
H	-2.83326941375909	-2.82696188980450	0.06352546515742
H	3.13507519674546	-3.12713523754714	-0.21300379265830
H	2.19111446148937	-2.19748460676634	-1.36572098211752
H	2.82172703424983	2.84174110767466	-0.00195254593774
H	2.95312080773047	2.94226382215380	1.72658074157155
H	-2.23961693272917	2.22385097610077	-1.28780522504139
H	-3.14982354814979	3.14414037324754	-0.10067378259666

66

Coordinates from ORCA-job se_sn2_cxme_cmp_Compound_1

N	0.00992873439177	-2.10244705414874	0.32778883036146
C	1.11436743483997	-2.84695615426845	0.67191745427988
C	0.71934227285415	-4.01706090055707	1.27163089749157
C	-0.68754430919736	-4.01797526039755	1.27859643585997
C	-1.09004790289665	-2.84841338165042	0.68278287795917

H	1.36352540531557	-4.79141974524513	1.64101325814019
H	-1.32702474692026	-4.79318474867963	1.65431810258854
C	2.49495028693402	-2.47735944746588	0.24915439450719
C	3.49115960703909	-3.47007755683731	0.83305543787352
C	2.59808525742519	-2.58450844712200	-1.28378784663771
C	2.86321968750156	-1.09496376977572	0.66701071040168
C	4.03413871681621	-0.69610060686795	1.26257836628602
C	4.03306190390448	0.71083692561322	1.26446089256295
C	2.86153680585726	1.10951074613653	0.66995762778750
N	2.11632864000217	0.00716860195626	0.32069613469052
H	4.81032011344783	-1.33780355198459	1.63246329841925
H	4.80828951443951	1.35272003485587	1.63603051206327
C	2.49129433094600	2.49242702066178	0.25558152080562
C	3.48599022404336	3.48510912804489	0.84212929791354
C	2.59451113552770	2.60355938057319	-1.27707576892159
C	-2.47505478260308	-2.48120700362336	0.27266785529862
C	-3.46416886192620	-3.47528758055253	0.86625813041176
C	-2.59199382496933	-2.58954064844233	-1.25922209904350
C	-2.84174018745981	-1.09917721320711	0.69312734441563
N	-2.09953814374648	0.00405675792297	0.34018228078265
C	-2.84334654381995	1.10526083147185	0.69600350306823
C	-4.00897792938373	0.70484464566713	1.30083913283360
C	-4.00796012632883	-0.70204823915869	1.29898482130504
H	-4.78179528135204	1.34556701680336	1.67936270150640
H	-4.77984953422370	-1.34489592587673	1.67579344756104
C	1.11013849307087	2.85895044336905	0.67910355663174
C	0.71337057883125	4.02692519455069	1.28181640987482
C	-0.69351005897217	4.02572126371109	1.28877919971561
C	-1.09426015560272	2.85710964324024	0.68992457893424
N	0.00683036828740	2.11368252932748	0.33301032741314
H	1.35637352742449	4.80128332952641	1.65325580058715
H	-1.33413382177578	4.79902258230218	1.66648296983702
C	-2.47875940613202	2.48888012832250	0.27901263129782
C	-3.46930878406026	3.47996549247575	0.87522060339434
C	-2.59607291475536	2.60087399106856	-1.25258945248820
Sn	0.00497649697599	0.00643749573567	-0.39247832521089
Se	-0.00632597035642	0.00956572292182	-2.82889878464178
H	4.48913893275142	3.24878365512069	0.50185937930222
H	3.47601840606985	3.46959127276336	1.92780710621517
H	3.24699311880485	4.48976271668037	0.50821356603211
H	-3.23466112882841	4.48509570430250	0.53968058631630
H	-3.44947075822075	3.46383089594217	1.96075816229372
H	-4.47522955653915	3.24260750233076	0.54393749677748
H	-1.92149893475316	1.92558181492071	-1.76538680479508
H	-2.35875530763769	3.61608458381978	-1.56728356523840
H	-3.61197295541675	2.36111585793062	-1.56321762030271
H	1.91584504447800	1.92746332489577	-1.78337531924911
H	3.60778021005014	2.36437558535176	-1.59656165904513

H	2.35363158576403	3.61842166626759	-1.59021755883479
H	-1.91857604892336	-1.91176733790142	-1.77026916423392
H	-3.60828571781133	-2.35082759795627	-1.56937787662685
H	-2.35282564497013	-3.60354109187755	-1.57639952593013
H	-3.22803219748185	-4.47921434927813	0.52816816425474
H	-4.47041585898566	-3.23855952225363	0.53552446365655
H	-3.44441208625783	-3.46190498944827	1.95183335357662
H	1.91849179013469	-1.90803496909936	-1.78833849159079
H	2.35844643443543	-3.59890535008545	-1.59936664391167
H	3.61100053223422	-2.34325865684295	-1.60285516788980
H	4.49391948985730	-3.23152576718195	0.49318935599676
H	3.25349745795271	-4.47423417201869	0.49670964560266
H	3.48136694389969	-3.45725244677973	1.91876904970699

90

Coordinates from ORCA-job se_sn2_cxet_cmp_Compound_1

N	0.00260111919871	-2.11921889544896	0.26887979091825
C	1.10700992683719	-2.85582751251870	0.63690338508953
C	0.70791806959831	-4.00670699871560	1.26863944593170
C	-0.69915339616301	-4.00818252075872	1.26842391498867
C	-1.10023970125607	-2.85798260355167	0.63671661472451
H	1.34437793952977	-4.77366786047170	1.66442017525802
H	-1.33430391795932	-4.77619514596858	1.66421969131251
C	2.48610453577298	-2.46830907305405	0.21906760071386
C	3.49144000676850	-3.48197643915410	0.78287111138479
H	3.10794871371359	-4.47964392047389	0.59412383014895
H	3.51779290275623	-3.37080580355062	1.86423908959813
C	4.89863129206206	-3.40860543163396	0.21283553636735
H	4.93450509807998	-3.78777558079094	-0.80464001526392
H	5.58191198164599	-4.01476790244866	0.80581008767712
H	5.27918861648127	-2.39449402951603	0.19646788501025
C	2.56955196177179	-2.46892987252495	-1.32611238006495
H	3.56648983315535	-2.14078926814763	-1.61640299326348
H	1.89731787162382	-1.71889326423157	-1.72304062246280
C	2.23676831439677	-3.79556706212517	-1.97515291209928
H	2.94605227465649	-4.58071238021583	-1.71682147005783
H	2.23335296998138	-3.69433570012975	-3.05743042047008
H	1.25152207553563	-4.13658339795881	-1.67295212006365
C	2.80169464100466	-1.09685485547341	0.71620949074931
C	3.82730330641551	-0.69774583990471	1.53531670200493
C	3.82617522043788	0.71141508699400	1.53725272825544
C	2.79997869774519	1.11113440363482	0.71918798282521
N	2.12983882610727	0.00725876832207	0.24285283828254
H	4.52928420362469	-1.33553085187991	2.03653335918707
H	4.52720493093009	1.34896000157902	2.04010259371712
C	2.48245974304485	2.48341866202226	0.22559375846199
C	3.48626589263708	3.49708869010898	0.79206728950616
H	3.10129974075832	4.49466158640293	0.60582614041711

H	3.51277378612815	3.38320349724666	1.87314998088701
C	4.89355440187369	3.42734162917254	0.22182206053741
H	5.57589481564383	4.03309475354772	0.81629714919803
H	4.92876106830831	3.80911445186544	-0.79469970902400
H	5.27576632858760	2.41389287924059	0.20286352497268
C	2.56602706949507	2.48812974661831	-1.31954350782973
H	3.56333122610081	2.16182754607516	-1.61066683100774
H	1.89461866635931	1.73840093227940	-1.71840805521831
C	2.23188185893290	3.81604859646126	-1.96529851314323
H	1.24638067077660	4.15548025410962	-1.66212484771958
H	2.22836800637220	3.71741092269086	-3.04781389223424
H	2.94049506203419	4.60122576730596	-1.70522351342418
C	-2.47991332741061	-2.47188634549046	0.21938108780680
C	-3.48405382952081	-3.48685496863190	0.78297935458203
H	-3.50987865176643	-3.37648337683327	1.86442888129449
H	-3.09958324722709	-4.48398369947552	0.59345580263474
C	-2.56351591321690	-2.47179427063529	-1.32575152494246
H	-1.89210293089970	-1.72082889536664	-1.72236180868622
H	-3.56085318161723	-2.14471117884468	-1.61587631675778
C	-2.22915462611139	-3.79771085983393	-1.97544467226747
H	-2.93626007315290	-4.58434506646187	-1.71570136249897
H	-1.24261799302759	-4.13664427801935	-1.67516430825197
H	-2.22808185121959	-3.69654784431576	-3.05773712744506
C	-4.89152817907665	-3.41407890304133	0.21368019011638
H	-4.92768261387187	-3.79283001599006	-0.80393998053875
H	-5.27234644195465	-2.40002947292608	0.19788539730012
H	-5.57443424647354	-4.02059396798639	0.80669891278477
C	-2.79682809919252	-1.10102968174672	0.71723584580446
N	-2.12637312048302	0.00408119014093	0.24433151893722
C	-2.79836987881059	1.10692933756061	0.72031222126604
C	-3.82401234460614	0.70572527817555	1.53832648574397
C	-3.82303550273611	-0.70353981396484	1.53636051319115
H	-4.52634212950732	1.34229428050963	2.04057188301365
H	-4.52439919439633	-1.34244836225026	2.03698876399368
C	1.10278073183730	2.86788486871074	0.64429032052566
C	0.70199354767148	4.01659586058648	1.27890697042892
C	-0.70507630860278	4.01594536180109	1.27878052744954
C	-1.10445133803711	2.86669449517068	0.64426764775274
N	-0.00052780021512	2.13051782714669	0.27447861819834
H	1.33732498245730	4.78351905057932	1.67657183400723
H	-1.34136974967209	4.78202049695905	1.67649451871176
C	-2.48355997724219	2.47956692658418	0.22603810461526
C	-3.48924157625850	3.49152253118777	0.79227465931637
H	-3.10633842425755	4.48973354933133	0.60528788618287
H	-3.51484509130315	3.37834261657247	1.87344201393845
C	-2.56724734940770	2.48323293351963	-1.31905973817566
H	-1.89463105622470	1.73434635047464	-1.71752931161648
H	-3.56406535249274	2.15526282694524	-1.60996520920958

C	-2.23501221479689	3.81127295846622	-1.96552635532664
H	-1.24887605102738	4.15089398917370	-1.66469930858272
H	-2.94319291296523	4.59622007106741	-1.70362528147459
H	-2.23410200283163	3.71279844692503	-3.04806655659354
C	-4.89664219123862	3.41795833304410	0.22285328154452
H	-5.58059215976363	4.02151392730602	0.81768032170024
H	-5.27563702047114	2.40327691034597	0.20417322150125
H	-4.93351014271148	3.79952985780418	-0.79368431491193
Sn	0.00106512175517	0.00649059559873	-0.46162135883371
Se	0.00207506057179	0.00975416509732	-2.90329420300774

9
Coordinates from ORCA-job se_me2_B97M_TZVPP_optfreq

Se	0.21215374492911	-0.94871109518445	0.84998677312896
C	1.76503958981499	-0.00576980156571	1.51998269235465
H	2.61099032717270	-0.16137140971226	0.86308919424650
H	1.99247566015477	-0.41066789388217	2.49702132691470
H	1.55174409270890	1.05125726314782	1.61231820984622
C	0.09778724997415	-0.00532831500629	-0.83717804027789
H	0.99977049130256	-0.15901255093149	-1.41523182696258
H	-0.06240674875624	1.05140911548423	-0.66682795616140
H	-0.74638240730095	-0.41180431234967	-1.37796337308916

17
Coordinates from ORCA-job sn_me4_B97M_TZVPP_optfreq
Sn 0.000012 -0.000000 0.999958
C -1.018761 -1.764587 1.720326
H -0.523849 -2.669890 1.370424
H -2.050208 -1.788687 1.370360
H -1.032696 -1.788648 2.809440
C 2.037553 -0.000004 1.720379
H 2.574141 0.881232 1.370467
H 2.574141 -0.881235 1.370457
H 2.065323 -0.000010 2.809492
C -1.018761 1.764579 1.720346
H -0.523850 2.669886 1.370453
H -1.032696 1.788628 2.809460
H -2.050209 1.788683 1.370380
C -0.000023 0.000012 -1.161196
H 0.508741 -0.881220 -1.550463
H 0.508741 0.881249 -1.550454
H -1.017596 0.000014 -1.550410

12
Coordinates from ORCA-job phi_cmp_Compound_1

C	-3.49004053581845	2.47840886132043	-0.03535085814386
C	-2.11441037841538	2.51867837550289	-0.19294986805762
C	-4.12033314130146	1.30054998489108	0.32841385612841

C	-1.37597309372813	1.36604225214344	0.01774817935213
C	-3.36999923922724	0.15554598008821	0.53556207429005
C	-1.99355735969912	0.18095352538120	0.38164595013789
I	0.70278103431489	1.41658817655421	-0.21584283186180
H	-1.62588173614625	3.43416027125593	-0.47468515636389
H	-4.06585756134573	3.37373328895686	-0.19823645178756
H	-5.18947575464546	1.27542786060367	0.44990333783877
H	-3.85216010389925	-0.76508103409219	0.81781412521520
H	-1.41183213008840	-0.70891754260575	0.54251764325228

12

Coordinates from ORCA-job phbr_cmp_Compound_1

C	-3.47348393121219	2.47909144996200	-0.03704171278574
C	-2.09804864723960	2.52043737454183	-0.19426380428197
C	-4.10372091034090	1.30083909361952	0.32618174000275
C	-1.36527464059125	1.36669900226792	0.01730614062166
C	-3.35333799640878	0.15578267920527	0.53393982986027
C	-1.97708345329366	0.18074903323266	0.38081623361002
Br	0.51427314860396	1.41048114473895	-0.19687094011397
H	-1.60283991487693	3.43208115517741	-0.47575697612434
H	-4.04979562448267	3.37389557022656	-0.20011973577897
H	-5.17290848314556	1.27540087416949	0.44663926797088
H	-3.83580204131041	-0.76465595658235	0.81575398304216
H	-1.38871750570198	-0.70471142055928	0.53995597397724

12

Coordinates from ORCA-job phcl_cmp_Compound_1

C	-3.46067638150299	2.47927312781469	-0.03858759365045
C	-2.08585365771185	2.52029469656224	-0.19606431812420
C	-4.09138508891813	1.30120746921460	0.32503005800030
C	-1.35184007066966	1.36679636760970	0.01533208948102
C	-3.34060063337900	0.15613447629224	0.53235062706533
C	-1.96493718803782	0.18103729439531	0.37890635800538
Cl	0.36814058164045	1.40780370653850	-0.17895408406250
H	-1.58611976855043	3.42962405899235	-0.47754067281754
H	-4.03718235236013	3.37395603293238	-0.20136734608974
H	-5.16048023354266	1.27597701934519	0.44612503883436
H	-3.82340559307325	-0.76401052205120	0.81438196810968
H	-1.37239961389449	-0.70200372764603	0.53692787524837

77

Coordinates from ORCA-job phi_sn2_cxme_cmp_Compound_1

Sn	19.42678841678958	13.74842388512667	22.06440960261775
I	19.25119709764083	10.49878733401919	21.50602699572356
N	17.84876733876106	14.90273284244128	20.86398213039940
C	16.60273894491858	15.27576758006737	21.29807261477139
N	18.10368652785520	14.40151884903982	23.81967548739926
C	16.00592394264308	16.09286380637007	20.36574632062296

N	20.84168239675018	14.79329402746989	20.58984578486902
C	16.91153488670395	16.21327649614082	19.29418474043795
N	21.09557036739642	14.28525116350897	23.54478187574923
C	18.01704445246569	15.46389233939845	19.62450726920547
C	15.97770836180799	14.68578916703718	22.51991334421530
C	16.81412965194452	14.86101045854036	23.74538445658620
C	16.40305386964375	15.30771773294908	24.98015552169551
C	17.47609168647496	15.09286524226049	25.86640334811412
C	18.48992870883511	14.52557413538234	25.12949928018799
C	19.17396888540526	15.11701622334655	18.74543285215132
C	20.49361890264693	15.37333591762231	19.39728338952630
C	22.17079835051203	15.06655843460616	20.78603380206386
C	22.64819640558378	15.84182329285898	19.75439830971183
C	21.57415684654829	16.03822392823698	18.86516920991767
C	22.38073885609802	14.64722087733470	23.23312086149852
C	23.04325987894695	15.05135176037802	24.36933283872735
C	22.13707614530788	14.91066271406995	25.43804567465891
C	20.96561059012674	14.42773310522401	24.90194499307501
C	14.60596480756554	15.30639678597122	22.74370465829018
C	15.75416052341181	13.17966175440197	22.28352547989529
C	19.76381617817345	13.93572575450385	25.64029378388027
C	19.91271242265028	14.24252874890679	27.12377628774598
C	19.08755138117781	13.62514138836523	18.37110749657819
C	19.08267533127372	15.90365615701573	17.44561022114036
C	22.96221224966959	14.42009487312135	21.87570264478726
C	23.02103515552696	12.90341829519688	21.61204587845443
C	19.68891585730233	12.40294213426732	25.50619826478345
C	24.39564854081219	14.93066616404501	21.84007809385261
H	15.44284226358391	15.72234142883737	25.22226768522485
H	17.49558509418227	15.31098354533866	26.91741498247352
H	21.59651311744904	16.58442118160968	17.94124095157060
H	23.65124120486199	16.20743819156445	19.64126196480754
H	22.32606460953221	15.12176031818538	26.47355460560918
H	24.06012044577614	15.39031969827101	24.42955406907896
H	16.76333628725331	16.76792300835463	18.38704046681869
H	15.03082840140657	16.53645116620715	20.43588000558656
C	19.13850791189242	8.32974593377106	21.12236189344241
C	20.09940465763723	7.70333528546795	20.34105547698856
C	18.10747552477941	7.56796897114587	21.65403174731826
C	18.03706378465110	6.20483115758675	21.40966773422429
C	20.03219842485240	6.34059034717196	20.09456884664574
C	18.99973146120630	5.58483543392158	20.62818158380890
H	18.94582145588560	4.52470189224649	20.43712250031914
H	17.22865598271095	5.62456545837808	21.82952680183658
H	20.90557401813630	8.28589438173998	19.92289935807698
H	20.78687723247458	5.86745325215321	19.48384608163146
H	17.35451191850477	8.04323232105692	22.26337969485565
H	19.89762481391782	15.62603740476673	16.78427500499063

H	19.13494648119651	16.97301356849130	17.62479224390791
H	18.14621298736892	15.68543073674685	16.94126529424168
H	19.89751052913477	13.36249935623778	17.69266259892735
H	18.13437968115804	13.41107947525228	17.89105514388417
H	19.17019587064601	12.98797831768929	19.24322139128212
H	15.12221375813519	13.02766076410399	21.41025915096100
H	15.27788544989241	12.72992615041658	23.15305762887267
H	16.68861456011875	12.65968127782864	22.11030472271108
H	13.97640101785163	15.14240796315891	21.87468935253355
H	14.67895318664872	16.37526473727248	22.91846519499133
H	14.12494201743611	14.85018183385664	23.60338379039967
H	19.57012913550455	12.09717624367502	24.47380254384542
H	18.83761141980212	12.01934284217241	26.06592870329652
H	20.60178947036291	11.94654519688882	25.88475577569828
H	19.97071834796340	15.31140198296261	27.30393641538772
H	20.81446526998950	13.77887633695152	27.51178895933463
H	19.06402547348721	13.84724701201183	27.67346256275369
H	24.84244258267739	14.72210564181883	20.87277114315646
H	24.98835579585561	14.43313348528713	22.60146397731508
H	24.43992405303461	16.00103600641191	22.01561175481958
H	23.45550000960444	12.70845182735061	20.63303456343822
H	22.03413083203828	12.45676846973488	21.63164497945240
H	23.62305950002406	12.41361702667706	22.37554714014331

101

Coordinates from ORCA-job phi_sn2_cxet_c2v_cmp_Compound_1

N	0.13181408723715	0.57698115436191	0.09324499494956
C	1.15787420372372	-0.32658460981759	-0.01098510225298
C	0.69704872770338	-1.57738990134092	0.34302269654189
C	-0.65751020858646	-1.43262268516102	0.69461241641336
C	-0.97700261507168	-0.10218983540362	0.52503996885423
H	1.27150118053910	-2.48453884289042	0.38405558061806
H	-1.29643948319727	-2.20450976996804	1.08080709967622
C	2.55328226390897	0.02510320251826	-0.46363772136905
C	3.54558560246271	-0.90263213472012	0.26417438455135
H	4.54731261428505	-0.68353236828875	-0.09421141859319
H	3.33649617515244	-1.92266818748450	-0.05559505955727
C	3.53252675644911	-0.83202181149391	1.77908545841648
H	3.74396645347055	0.17476028188082	2.12106226323004
H	4.28460908550317	-1.49802483251539	2.20183211459085
H	2.56503684526637	-1.11919011329533	2.17485826533655
C	2.65644398805989	-0.28688848650975	-1.98179258289970
H	1.89622323724247	0.29377518675732	-2.49061347058001
H	2.37507196487319	-1.33096348621303	-2.12094575642682
C	3.99307860103030	-0.00631801623827	-2.63950408930936
H	4.30330169082217	1.01839993788473	-2.46264938145924
H	3.92234578469824	-0.15893673031588	-3.71452230925215
H	4.78386794340372	-0.65585442584318	-2.27081750165803

C	2.93170728729271	1.45800313009638	-0.19989017957214
C	4.17599600948663	1.93092290620399	0.16441122923279
C	4.08502751595483	3.33156713107131	0.21953818073341
C	2.79060575846280	3.66384053024623	-0.12611356591186
N	2.08412694657592	2.52231061839622	-0.37984895593843
H	5.05107334089866	1.34263282030087	0.36733501483736
H	4.86712513370705	4.00975829530204	0.50600868507248
C	2.13552547573526	5.00749852819214	0.02984258509467
C	1.51204718428364	5.00225917924808	1.45827523280573
H	0.92120956050240	4.09472611826468	1.54151566337975
H	2.33173181725223	4.90266078658538	2.17174248221867
C	0.63944105769359	6.19027930127086	1.81157371198511
H	0.28387687753173	6.10592333182449	2.83712667299146
H	-0.22475483447502	6.24729178361068	1.15886889172450
H	1.17364608853469	7.13399251864266	1.72767264306781
C	3.20137265045916	6.10835402047537	-0.02989622507551
H	2.72299787568852	7.06171018841500	0.17876281868311
H	3.89992155500026	5.94177938007565	0.78866897902247
C	3.96868889649531	6.20794676329897	-1.33590711741445
H	4.50708851286977	5.28969090530191	-1.53954251257976
H	4.68968682709597	7.02460182512023	-1.30123437248220
H	3.29923680006800	6.38506985283045	-2.16967348896112
C	-2.16806170663312	0.63851369671792	1.05947363952899
C	-1.68425745881079	1.43170263859962	2.31042854000813
H	-2.55964147999311	1.90425176273763	2.75876006919927
H	-1.05366970032638	2.23722976992029	1.94542220942188
C	-3.25081774256131	-0.35264246993966	1.50085315884239
H	-4.01476672066547	0.20790482524391	2.03801208826301
H	-2.81567897543833	-1.03328794120640	2.22801253626296
C	-3.90165855217502	-1.15767763586286	0.39007942753900
H	-4.40058917003447	-0.50906296871218	-0.32004649449019
H	-4.63934123417790	-1.84948727006001	0.79646188975941
H	-3.16634353493516	-1.73400238900535	-0.15917054348620
C	-0.91439316413458	0.63743110107002	3.34748505973925
H	-0.00807648413924	0.21982324877012	2.92263855311766
H	-1.49770573597432	-0.18738913536475	3.75068891590701
H	-0.63293497873904	1.27716755589475	4.18202378009008
C	-2.76749317621624	1.66576011703567	0.13981722961462
N	-2.00391191061156	2.52178982416682	-0.60174277492166
C	-2.83447261321177	3.48157896411993	-1.12165741994235
C	-4.12652324677875	3.22817256339980	-0.70766683617072
C	-4.08366298675778	2.07997283828821	0.10043385872653
H	-5.00248030164526	3.79896387456496	-0.95270965569253
H	-4.91437414496091	1.63228194705439	0.61356624610476
C	1.02484138465097	5.31393706982765	-0.93191896139957
C	0.71591842116450	6.53256927828806	-1.49866164731367
C	-0.59597911797827	6.43330254450426	-1.99623957182514
C	-1.04406818024212	5.16300811474710	-1.69960234878126

N	-0.04996944268908	4.47213055785534	-1.05647442995899
H	1.32967976048502	7.41378562868323	-1.50323120478383
H	-1.15521985340892	7.21283134479328	-2.47991208380427
C	-2.38518513729919	4.57472632778211	-2.05494172025372
C	-3.43323782293082	5.70629705694722	-2.03882200183004
H	-4.38775240041343	5.29329756475204	-2.35415823906012
H	-3.15341507991392	6.42288335239996	-2.80878745825658
C	-2.29788364005594	4.05773819944447	-3.51846564576153
H	-2.14427734422607	4.92837673410877	-4.15749716037510
H	-1.39740102606025	3.46281245235517	-3.61652581614825
C	-3.47348593681239	3.23897357884912	-4.01115802391969
H	-4.41220668725776	3.78531675506274	-3.95286828033544
H	-3.58854354132065	2.33568501450118	-3.42270340548140
H	-3.32251825049500	2.94849457755047	-5.04920046791327
C	-3.60993799206770	6.43045089016322	-0.71777695590696
H	-3.87998398436842	5.73842846224792	0.07136381078291
H	-4.39456158982533	7.18331299373902	-0.79210515090991
H	-2.69211054797092	6.92703717779162	-0.42405101275814
Sn	0.08352223656322	2.26149506585868	-1.36322812771237
I	-0.29127234842512	0.83226817398737	-4.49296691942071
C	-0.65533782572615	-0.07152875824646	-6.42760376329945
C	-1.12986118228461	-1.20231797831157	-8.93278568549086
C	0.28818223181250	-0.90342068970045	-7.01418552887983
C	-1.83934090662533	0.18859911573698	-7.10413403686077
C	-2.07521117428226	-0.37359627571353	-8.34868031126077
C	0.05283006444793	-1.46511130002308	-8.25943948952220
H	1.20964665592818	-1.11217472910392	-6.49471232206705
H	-2.57769137762584	0.83214978900982	-6.65322204296129
H	-3.00027035050551	-0.16289514170720	-8.86372477378050
H	0.79587663232431	-2.10926544934969	-8.70508981935910
H	-1.31404386373545	-1.63903585694140	-9.90147610354677

77

Coordinates from ORCA-job phi_reduction_sn2_cxme_v2_TS

Sn	19.45272914201854	14.33143512096562	22.14946415280017
I	19.29846914090476	11.61114043752089	21.66968494835217
N	17.85550013116241	15.19592556720697	20.93241311657542
C	16.60510427885565	15.56721021575708	21.38738621220307
N	18.13583648050338	14.65361081998300	23.86578907345888
C	16.01178581554796	16.39198888053277	20.47005786114961
N	20.83259874730728	15.07144442465402	20.62429446342344
C	16.90733898502271	16.52713885232113	19.39221741151258
N	21.11165897608076	14.53758417771379	23.55857155988324
C	18.01474178270621	15.78008613911956	19.69086074302301
C	15.97990675454783	14.96557881281418	22.59860298787781
C	16.83518892953127	15.11535948029968	23.80952195997675
C	16.44489724828478	15.53494477004658	25.05264297986355
C	17.52633263469620	15.31065267686669	25.92538824250595

C	18.53737214013552	14.76224236319050	25.18323884862833
C	19.14958852549837	15.44492391924262	18.78530147589361
C	20.47260977013836	15.67087519329601	19.43275898706911
C	22.17679760644703	15.33188378830044	20.80777927434722
C	22.63790843653397	16.10294558946044	19.77494223681968
C	21.55531737003438	16.31822174874257	18.90152346828962
C	22.40435674949038	14.90159037386125	23.23399123601720
C	23.06764721251873	15.28987227147418	24.36667921207673
C	22.17213411426639	15.14450858968271	25.44312055980217
C	20.99478761733847	14.67299018568455	24.92832765036589
C	14.62542484732816	15.61446428980090	22.84803348945747
C	15.72219542124917	13.46984777674277	22.34393372099638
C	19.81194427825469	14.17763219625430	25.68695242631814
C	19.97748116317776	14.51101120249563	27.16340835716439
C	19.03939710965793	13.96992446294144	18.36074450462537
C	19.05368818991570	16.28118124208808	17.51679329699267
C	22.98422107949833	14.68317222903551	21.87871931234000
C	23.06882091570581	13.17111367785000	21.60570738796692
C	19.74473741386793	12.64418207410066	25.57763329738823
C	24.40773689190534	15.22170890080683	21.84035061558380
H	15.48320303185033	15.93080640260324	25.31253832065907
H	17.54875741973851	15.50217415747981	26.97987232190302
H	21.57665988709475	16.86012968277028	17.97694132557424
H	23.64412112149417	16.44888168918934	19.64478188426209
H	22.37830071489609	15.33365661588853	26.47792379349979
H	24.08853319134966	15.61202317527576	24.42223914583685
H	16.74476549420748	17.08306094758082	18.49017193410888
H	15.03398313844832	16.82432729254509	20.54818242057548
C	19.07782440033751	6.61232977675097	20.82771200319261
C	20.19822020690472	5.80220687362719	20.58548560170360
C	17.86592501388400	5.90408947314027	20.82480844500360
C	17.76422665418167	4.53239684143329	20.60472457100489
C	20.13448302532154	4.42880438964395	20.36163594403597
C	18.90712684004392	3.78048315807857	20.36979350878721
H	18.84317708044398	2.71484752368796	20.19725876177132
H	16.79411969903188	4.04339972983889	20.61523160087670
H	21.18853760171405	6.25263157135364	20.56719894490234
H	21.04079939310813	3.85766799212757	20.18043041003566
H	16.93538669646858	6.43876506325643	21.00377000888316
H	19.85344123327590	16.01224164083922	16.83542409557994
H	19.12348580935379	17.34298404260623	17.73013193758531
H	18.11070970557174	16.09010113271534	17.01593976830423
H	19.84878635561612	13.71759081675664	17.68011956474950
H	18.08862687338519	13.79485471836139	17.86331834424936
H	19.09819347234128	13.29880312127773	19.20639012728717
H	15.08066874472686	13.34571790870636	21.47498418681732
H	15.23941056066431	13.02324421308750	23.20965319702873
H	16.63858459245413	12.92643616516473	22.15905334463829

H	13.98197788780426	15.47142823495965	21.98677928597493
H	14.71961567794622	16.67910059862012	23.03654999533764
H	14.14480632435036	15.15349399184009	23.70406144506009
H	19.61964141617107	12.31540738958148	24.55544919114652
H	18.90293651247676	12.26714664298233	26.15313310203881
H	20.66245056181149	12.20228314995082	25.95779662801782
H	20.03216121437075	15.58206659968541	27.32941207637886
H	20.88346676681868	14.05448221138908	27.54699707603470
H	19.14053034860401	14.11587090492718	27.72882399472446
H	24.85353499391223	15.02304219354680	20.87172416456171
H	25.01205806553553	14.72628716978242	22.59237358429637
H	24.43753555580211	16.29122804921926	22.02225152436688
H	23.50243394819741	12.99256918978982	20.62482624581808
H	22.09605547180924	12.69937157992570	21.62769343494453
H	23.68682939634722	12.69175452715895	22.36100666769188

101

Coordinates from ORCA-job phi_reduction_c2v_sn2_cxet_TS

N	0.10938403855513	0.60954049767831	0.53721024412253
C	1.15668233802440	-0.17271838048566	0.08501914767970
C	0.69932025887414	-1.43380081261962	-0.18511608823277
C	-0.67806611014370	-1.45034595069635	0.11586926752160
C	-1.01517086812467	-0.19688607739951	0.55483362424675
H	1.28804782438900	-2.26436285131025	-0.52645591811146
H	-1.33028642928150	-2.30003059998997	0.05218369899818
C	2.58250298189657	0.28892246265288	0.11130394788558
C	3.31572316507801	-0.55731861837941	1.17104430872219
H	4.35044147588005	-0.22982420062399	1.23849890329183
H	3.34323281226369	-1.58244531642723	0.80421337829522
C	2.67807544169026	-0.52797445942537	2.54548940733162
H	2.60024943087532	0.48886512293439	2.91517281664237
H	3.26259658424035	-1.10487088560265	3.25938918790996
H	1.67629000197933	-0.94411485510288	2.51763588247341
C	3.20935883326296	0.02059877267453	-1.27921977696402
H	2.65574047493476	0.60519810305716	-2.00676562422391
H	3.02788544827372	-1.02182610011453	-1.53470580368171
C	4.68817213858946	0.32584638735703	-1.40748133880340
H	4.90645143939068	1.34521170679760	-1.10605420739104
H	5.00778656913652	0.20498117880713	-2.43880963109686
H	5.29966871114404	-0.33611731645191	-0.79889106648582
C	2.72250187738225	1.74196774517691	0.43596415808488
C	3.70626350617040	2.36298592766233	1.16385915097293
C	3.54876680846194	3.75077386654414	0.98133946423258
C	2.47722996797176	3.93210122145036	0.14082828320561
N	1.96191719905650	2.70320191013623	-0.19055120040774
H	4.47060012314814	1.87879332514452	1.74080675734384
H	4.18613037514124	4.52209679542900	1.37078849531299
C	2.11385185450708	5.20664657331128	-0.56265556738107

C	1.99970551006440	6.31676361572770	0.51230684844707
H	1.18091523345186	6.03594543633738	1.16976076330689
H	2.90266590826451	6.29259386262875	1.11935813528247
C	1.78245016391127	7.72736946195898	0.00347879678007
H	1.66557843063153	8.41454505075758	0.83841354806486
H	0.89277308942113	7.79604312667159	-0.61296528951854
H	2.62234536943563	8.08038298608520	-0.58918446341376
C	3.26713489207590	5.53600964696653	-1.53202175653650
H	3.02662021085631	6.43843150104644	-2.08977807343907
H	4.14478232684963	5.77225843731899	-0.93057257076566
C	3.59331031652132	4.41097727631060	-2.49311310630927
H	3.96676643631510	3.54234235065052	-1.96135132989131
H	4.34988327941822	4.71695297827702	-3.21130182728229
H	2.71242939201565	4.09985129389543	-3.04478160177492
C	-2.25576952682223	0.23791836837083	1.26539971964351
C	-2.02864055108781	0.06042145859639	2.78913162652039
H	-2.90945104566053	0.43735478951345	3.30602265135356
H	-1.20643146536846	0.71591808324766	3.06445335734560
C	-3.44496718362662	-0.63291189693918	0.81445688158303
H	-4.27701855668970	-0.42973101087729	1.48828181903045
H	-3.19234360572949	-1.68247326488888	0.94702062884698
C	-3.87326400525341	-0.38745472590574	-0.61814573951089
H	-4.25221629984375	0.62142062847452	-0.74238456396441
H	-4.65659484963378	-1.07991293930206	-0.91643243488299
H	-3.03871810773464	-0.50949679165452	-1.30030654050866
C	-1.73323187480789	-1.34855157471415	3.26279599619594
H	-0.86115594441179	-1.75714198221034	2.76413836682537
H	-2.56464032006250	-2.02343397843765	3.07698575941125
H	-1.54346208933447	-1.35551998511200	4.33381215497249
C	-2.63097344099342	1.67140148752941	1.02979406056971
N	-2.14263166226788	2.43465325384807	-0.00185076932341
C	-2.89221704377241	3.58784851844204	-0.06723374277155
C	-3.84275172839515	3.55237767953930	0.92218795356282
C	-3.67464118471163	2.34075834462869	1.62075323045438
H	-4.59549525408270	4.29423257292350	1.10788647815860
H	-4.28601619217560	1.97587180053655	2.42473169252200
C	0.82471193151568	5.14813739653791	-1.31717370702698
C	0.44510275615253	5.88698875030589	-2.40726112257968
C	-0.94395199675898	5.71153131596477	-2.57150481330931
C	-1.36618693695561	4.87523399065175	-1.57429396809256
N	-0.28552261244723	4.51073242346280	-0.79115111146023
H	1.07865528259332	6.51739560138490	-3.00088942973571
H	-1.56324706459648	6.17784933900013	-3.31439436574678
C	-2.78243510191628	4.53885958866414	-1.21627022919145
C	-3.48934358777208	5.86289163471963	-0.86550932834092
H	-4.51374708728170	5.65419794313029	-0.56688567456069
H	-3.55251109273851	6.45013266574553	-1.78063931794367
C	-3.46209760423366	3.91023534400451	-2.45867561589624

H	-3.31544314715689	4.58600670576380	-3.29939650123566
H	-2.91744958775300	3.00514420899210	-2.70780567632031
C	-4.93485309313013	3.58612443955262	-2.31376890968917
H	-5.54270226315728	4.47794204265594	-2.18136683195355
H	-5.11156737178280	2.93949877514736	-1.46040070563606
H	-5.29581911966104	3.07566948269410	-3.20231876799078
C	-2.79701418628466	6.67458396422529	0.21072678733848
H	-2.68707181734278	6.09725898448422	1.12232805590517
H	-3.36138733363281	7.57515134649537	0.44421572198374
H	-1.80434210340399	6.97366066015646	-0.10967222813186
Sn	-0.10435469504707	2.37508293716462	-0.66944949848245
I	-0.15250924440189	1.48839456628926	-3.25324369588147
C	-0.12093640032252	-0.10281100815852	-7.79850470744181
C	0.01966872551038	-1.09198750064003	-10.49618823616639
C	1.08307351474836	-0.45271093245516	-8.43167337898051
C	-1.24932059715647	-0.28514670459107	-8.61458182471956
C	-1.20067476327447	-0.76272629731995	-9.92224238985333
C	1.17050373954395	-0.93268929636579	-9.73633745212017
H	2.01979939075183	-0.34966327204141	-7.88784539929035
H	-2.23549177509504	-0.04481326946210	-8.22186146455643
H	-2.11316994112364	-0.88123509536655	-10.50036159422015
H	2.13565242943100	-1.18453758254013	-10.16747753802498
H	0.07259185464559	-1.46296418067854	-11.51068164112628

66

Coordinates from ORCA-job i_sn4_cxme_CREST_cmp_Compound_1

N	-1.49937787063825	1.28674318477163	0.84880656852803
C	-2.79627089524830	1.20112769382502	0.37448450130154
C	-3.32595096156136	2.46006612568372	0.29547569310821
C	-2.34130157446199	3.36264238421356	0.74578399836942
C	-1.23928875630761	2.62431626060207	1.07635013821373
H	-4.32630246181525	2.70521992258701	-0.00485883164823
H	-2.44963590789102	4.42326354512763	0.85765277044508
C	-3.51623909832233	-0.08899489789340	0.11825388766534
C	-4.91091158477044	0.00932309442397	0.73929165357845
H	-5.45290433042325	0.84501863098333	0.31310660047102
H	-4.85135024110082	0.15359372697278	1.81238366823304
C	-3.71101941900884	-0.31695826331805	-1.39162467498225
H	-4.22254724673876	0.53400249618769	-1.83402352410277
H	-4.30577658492787	-1.21202960148770	-1.55643352045731
C	-2.81030218430242	-1.27195719415985	0.69470794027436
C	-3.36406185709391	-2.33485843430124	1.35458860399017
C	-2.37377939529049	-3.33474297425260	1.45284768914115
C	-1.24625703808262	-2.84862542223531	0.85179655053661
N	-1.49271523461124	-1.56910193458911	0.39137409502700
H	-4.37829654273429	-2.41097755687542	1.69199580070803
H	-2.49059217312186	-4.30910251499352	1.88381758267581
C	-0.00101840282797	-3.58339812179702	0.48499838221829

C	-0.00134240440760	-4.95595117267055	1.13894694494087
H	-0.00102194828259	-4.87991252976215	2.22131059202753
H	-0.87867701729318	-5.51568622670830	0.83389238284624
C	-0.00145547247777	-3.78620594714068	-1.04375314751152
H	-0.88823647431540	-4.33632282827536	-1.34803008979047
H	-0.00121595955856	-2.83443494098672	-1.56136848730520
C	0.00140015574728	3.06492140304399	1.77931432831152
C	0.00115276330244	2.46387590890443	3.19718432836877
H	-0.88497707671039	2.78347930640621	3.73960190905698
H	0.88744112487786	2.78294067326900	3.73965846206834
C	0.00188250937478	4.57906928969732	1.91465430619076
H	0.00211409521375	5.06265533657513	0.94351197454420
H	0.88004319561759	4.90583193641306	2.46104505233154
C	1.24186002097112	2.62348754196945	1.07644964736360
N	1.50078024917386	1.28582333815792	0.84814744630304
C	2.79775026771603	1.19928344225558	0.37420500174320
C	3.32864616691583	2.45777961710251	0.29621336804494
C	2.34468915809703	3.36098457405998	0.74674265970490
H	4.32929567402288	2.70220609556843	-0.00370270171325
H	2.45397295714302	4.42143314807493	0.85930801832380
C	1.24490070174888	-2.84948446229721	0.85121389928870
C	2.37236804871158	-3.33642128258049	1.45169954347657
C	3.36330747642781	-2.33723023248795	1.35302393151131
C	2.80997840381929	-1.27390190903660	0.69347395893322
N	1.49203171864405	-1.57010200813973	0.39074889273637
H	2.48869165493456	-4.31089094184036	1.88255154885566
H	4.37764261477880	-2.41407136970785	1.68996246329599
C	3.51642834626819	-0.09133300074529	0.11684414927649
C	4.91173321863410	0.00551131482644	0.73664250251624
H	5.48169082804168	-0.89594889513801	0.53399982159079
H	4.85329816046954	0.14947053574732	1.80983807068766
C	3.70966529442327	-0.31887372993042	-1.39330628871404
H	4.22186677257045	0.53166780042524	-1.83573236428493
H	4.30317540058967	-1.21460350594051	-1.55903480707085
Sn	0.00012076431631	-0.06840743846732	0.16186658874768
I	-0.00065719611336	0.49500154555884	-2.52586766758169
H	2.76327645248934	-0.43978796755717	-1.90194381220863
H	5.45412291933538	0.84084238866131	0.31024572128007
H	0.00082091409703	1.38116337995602	3.16181442122549
H	-0.87615673509309	4.90637866631189	2.46091614998986
H	0.87540671873412	-5.51634002020247	0.83341031171372
H	0.88475096648420	-4.33700987004016	-1.34846153070036
H	-2.76519906582965	-0.43929368968740	-1.90099546599502
H	-5.48188752862928	-0.89168198201746	0.53748448548511

90

Coordinates from ORCA-job i_sn4_cxet_CREST_cmp_Compound_1

N	-2.06004326747361	-0.58856243933824	0.63434081542266

C	-2.55013931846033	-1.87255643296827	0.79574197360498
C	-3.82165477719301	-1.79596819077150	1.30189782684442
C	-4.13662332327648	-0.43780138068736	1.46313425189210
C	-3.05395062784783	0.28404584540264	1.04008888924249
H	-4.47748494881245	-2.62411268658149	1.47820401192422
H	-5.05540568917060	-0.04005958484416	1.84226577514082
C	-1.89489070605529	-3.13395631845991	0.32509317185024
C	-1.65024386548209	-4.12066491206053	1.50907166147159
H	-0.90750161717519	-3.65875838094966	2.15444159562441
H	-1.16926776371904	-4.99520019537907	1.07457077655601
C	-2.82715275748269	-4.57142941652139	2.35185165023438
H	-2.50323806460141	-5.34953539178955	3.03904333310997
H	-3.63070843277574	-4.98973286627228	1.75165549185863
H	-3.23725046886382	-3.76133179806144	2.94163242784686
C	-2.81587999039209	-3.80061281358277	-0.71102893330429
H	-3.76274561576441	-4.02926629486625	-0.23116124714405
H	-2.38223986275943	-4.75829509826992	-0.99607546265631
C	-3.07035449805733	-2.94880641658259	-1.93747708402774
H	-3.72807097664401	-3.45791960215133	-2.63747285351884
H	-2.14643183919458	-2.71023155070063	-2.45246645184838
H	-3.54090580765076	-2.01080267672812	-1.65980535666847
C	-0.53215811830255	-2.95349969582625	-0.25807765803042
C	0.11389666679182	-3.80383052097509	-1.11031972975589
C	1.49798344101053	-3.54923772807781	-0.99473793141161
C	1.64919425331939	-2.54763882152800	-0.07975657570498
N	0.40506783547575	-2.14764452414967	0.37882777544124
H	-0.33871877564556	-4.57866053011450	-1.69794999594969
H	2.28411316875955	-4.07247042820135	-1.50196251437753
C	2.88515546141355	-1.99015035291722	0.54663303136114
C	2.77305363083282	-2.17299607623675	2.08016194168314
H	3.64928300207026	-1.72576933467581	2.54385195372112
H	1.92646932768791	-1.58995337727996	2.42403574668013
C	2.60655491895031	-3.61020740813859	2.52751072653298
H	2.49849506352573	-3.66714693969858	3.60725309309021
H	3.45935230705383	-4.22589002130725	2.25366347167407
H	1.72473582169422	-4.05777072384406	2.07987944691399
C	4.10763144835830	-2.74110970760183	0.00737087775995
H	3.88109737067791	-3.80301321109220	0.00871693562450
H	4.23680976148223	-2.46563403343229	-1.03607484404251
C	5.40353052564785	-2.52690550631276	0.77000069398641
H	5.38563475366483	-3.02297603584394	1.73579353286237
H	5.60461132247700	-1.47768242780307	0.94892976727349
H	6.24239422137347	-2.93760549321720	0.21424862594928
C	-2.92473287933988	1.76772253168033	0.91170886036595
C	-4.10219222176047	2.47222710725690	1.60321229871317
H	-3.82469957716511	3.50903164940398	1.76218212622486
H	-4.22113578760290	2.03914262326771	2.59285206336821
C	-2.90633651165089	2.13603918265082	-0.59317012173188

H	-3.84504931803288	1.80944297295936	-1.03298730081042
H	-2.14127839781957	1.54963109104036	-1.08553989617128
C	-2.65839476684150	3.60163732456630	-0.88027062847686
H	-1.69764161099540	3.91447908473104	-0.48565778734592
H	-3.41735810463044	4.24224093310563	-0.43864622348652
H	-2.65426889498241	3.78607989069991	-1.95079916509711
C	-5.42944419483024	2.45870713766842	0.86159678691684
H	-5.69097175444745	1.47677902775722	0.48772493358990
H	-5.41543070811246	3.13475128255045	0.01211554540477
H	-6.22947757591553	2.78914712260045	1.51908026595087
C	-1.64545434367607	2.23665012097083	1.52296402795327
N	-0.43999258618710	1.89267167162222	0.94293435579078
C	0.54063311031147	2.66879066639376	1.53549200878497
C	-0.03549336033687	3.43545481809255	2.51126074921584
C	-1.42185636668996	3.16627192142990	2.50034242354362
H	0.46057585071391	4.17375716575892	3.11022921230649
H	-2.16470903725188	3.63810405583469	3.11184930683424
C	2.99951369155653	-0.52966276164651	0.25239434815603
C	4.00988216784048	0.16132493441498	-0.35648364458218
C	3.67520573295951	1.52897563525140	-0.29509398264420
C	2.47627256727528	1.62489733741593	0.35369369893603
N	2.03289136679641	0.35887653265956	0.69290452442360
H	4.90272936787592	-0.25547603192446	-0.77793679618063
H	4.28261260515964	2.35027830549645	-0.62526797232241
C	1.85350418478705	2.88403090854911	0.86281590340489
C	2.84557455129272	3.54227431743681	1.83876915153615
H	2.40848653582246	4.45354544014341	2.23889652744443
H	3.71638827907630	3.85017547679392	1.26264907102970
C	1.62329951384133	3.81619807793314	-0.35702440191301
H	2.56772928966458	3.89998426260645	-0.89138895436959
H	0.94260823361316	3.29974666227934	-1.02863032387560
C	1.09077310438997	5.20199936382986	-0.05554222768220
H	0.91966482001013	5.74744810701333	-0.97991522618385
H	1.78710998196288	5.78641743259336	0.53978783988908
H	0.15135695219085	5.16054526971148	0.48467473355226
C	3.27740047475293	2.63851327457468	2.97492061202839
H	2.41916823529223	2.29184825422862	3.54100656703452
H	3.94424105305088	3.15923133925763	3.65754021988718
H	3.79778224653003	1.76429691226054	2.59770973860629
Sn	-0.02509404673939	-0.06298566974340	0.20755939484470
I	0.12219890697480	0.21157029896074	-2.51454248840065

53

Coordinates from ORCA-job nbu4_cmp_Compound_1

N	-1.85422832580712	0.12255540303397	-0.12487782563500
C	-0.55953230914834	-0.42350325080307	-0.68389784383490
C	-2.57598693141251	0.77455326278596	-1.28061643471753
C	0.38058878780110	-1.06662944552857	0.30189891354600

H	-0.07749592845091	0.40809323366867	-1.18123579963758
H	-0.84657320616619	-1.12849070451906	-1.45276496785815
H	-1.90790416095567	1.54069313307239	-1.65150769483836
C	-3.93272251528503	1.35677669832088	-0.98249398682221
H	-2.64656989657028	0.01700996540604	-2.05029040087885
C	-1.59207547130737	1.11648183589818	0.98257770040076
H	-1.11026269177946	0.55398346612972	1.77148885721384
H	-2.56535238708381	1.41044747171939	1.35264293067154
C	-0.77530339270029	2.32849059128586	0.61849799303551
C	-2.68978951585050	-0.98123431388938	0.48404494540496
H	-2.11275525548652	-1.36450072791920	1.31502149153735
C	-3.10288610197234	-2.09875445731971	-0.43781859194045
H	-3.56114061640015	-0.49342053146582	0.90112323521949
H	-3.87549848172519	2.09686136718612	-0.18833763993851
H	-4.62210177816416	0.58600175706153	-0.64771668142228
C	-4.49733309498531	2.01698684108941	-2.23219587962378
H	0.18659920199523	2.04381209697630	0.19981170255503
C	-0.53875540823315	3.18156942806158	1.85695045794504
H	-1.28243055125896	2.92892160485201	-0.13223917177538
H	0.70770979184386	-0.35005291796608	1.05064042746897
C	1.60107471991620	-1.60950792766486	-0.42739008532979
H	-0.10386247095228	-1.88160255616921	0.83375748288313
H	-2.23512475546536	-2.62084397439497	-0.83194903371535
H	-3.65915705288286	-1.71696468797001	-1.28965153149999
C	-3.97755586093337	-3.09227127988248	0.31439707735627
H	-3.42789752079757	-3.47833868698323	1.17079149705165
C	-4.42888883646789	-4.23467828303307	-0.57143141750315
H	-4.84353155647773	-2.57110567414132	0.71871724445973
H	2.08486515151898	-0.79882841883525	-0.96941654971934
H	1.27972133435231	-2.32709704437006	-1.18022494219907
C	2.58828917720765	-2.26056400905463	0.51851860745861
H	-0.02793498711510	2.58345299525993	2.60950555069172
H	-1.49756242064029	3.45930490743831	2.29113675879561
C	0.26861477054387	4.42499239986966	1.54818884515778
H	-3.81202357235741	2.79269011220336	-2.56945227108827
C	-5.87014588737247	2.61008964822983	-1.99309203776170
H	-4.54374229528580	1.28413393980388	-3.03586509618809
H	-5.84265554706955	3.36000206098490	-1.20823330934339
H	-6.58271955796619	1.84689544356488	-1.69565008704079
H	-6.25243528388652	3.08638207581340	-2.88769863057105
H	-3.58087849560795	-4.79050000641201	-0.95978570355073
H	-5.00062773986739	-3.86993404982693	-1.41946075013265
H	-5.05605366872680	-4.93059313869822	-0.02773811549263
H	2.94629711363176	-1.55471583050959	1.26189651049075
H	3.45080682765958	-2.63958616915244	-0.01600834754397
H	2.13669353913438	-3.09469537170173	1.04708628281700
H	1.24272316213568	4.17095232972421	1.14117751243788
H	0.43004836987236	5.01863133839280	2.43973243570861

H	-0.23844641699711	5.05315805037774	0.82211636729569

11
Coordinates from ORCA-job ph_anion_cmp_Compound_1

C	-0.00000000357649	-0.00254739585030	1.11429283367882
C	-0.00000000938947	0.02540548013620	3.85123382834084
C	0.00000001976626	-1.27500780575422	1.72556257787800
C	-0.00000000371380	1.21589308185083	1.78914372526688
C	0.00000000899065	1.23923582537524	3.17737777810000
C	0.00000000006158	-1.16815425251947	3.13325348111205
H	0.00000000117517	-2.08087790538016	3.73196218908133
H	-0.00000001188753	0.01797916127837	4.93876014624546
H	0.00000001039618	2.17601776742670	3.71772642845463
H	-0.00000000016049	2.15417705526804	1.23928721261779
H	-0.00000001166207	0.05937898816878	0.02446679922419

40
Coordinates from ORCA-job nbu3_cmp_Compound_1

N	-1.65786713574102	0.36070416785571	-0.30178749787270
C	-0.42127604815262	-0.20689286593577	-0.80532948484034
C	-2.40444749059993	0.96076677672914	-1.39150658013481
C	0.36962740051030	-0.98496253123620	0.22244152241769
H	0.22911305097459	0.55503647486135	-1.26204638073651
H	-0.69437911129017	-0.88172025323569	-1.61534671454915
H	-1.83590553374634	1.75890921181757	-1.89410237639188
C	-3.76297514000370	1.49495956825232	-0.99591200882258
H	-2.54183612086948	0.18298369102319	-2.14168168637996
C	-1.47611480136345	1.24183427640740	0.84152857082962
H	-1.00997267010296	0.66421993741178	1.63459269136978
H	-2.46003888118409	1.50434305586603	1.21981823091148
C	-0.67338901107558	2.51456430797520	0.61568768884494
H	-3.65794273880469	2.38697192703330	-0.38021552798967
H	-4.27021770603242	0.75282798356939	-0.38027016523364
C	-4.61600675414214	1.83414214521786	-2.20276077094812
H	0.32050723492632	2.26953696432091	0.24238439129956
C	-0.54205574427518	3.33232805436359	1.88463547304265
H	-1.14412824207662	3.12226498167642	-0.15663038583786
H	0.79434824764234	-0.31477846414436	0.96823019058540
C	1.49399352490737	-1.78418547090395	-0.40724733093369
H	-0.30647316439789	-1.65247822456300	0.75566602892934
H	2.15009832193892	-1.11040086873743	-0.95770566440540
H	1.07810312299979	-2.46763171806211	-1.14675725949593
C	2.29932774980540	-2.56185012246991	0.61342240603701
H	-0.06794953840978	2.72375139050285	2.65464218254749
H	-1.53623092474443	3.56866457469966	2.26399771509377
C	0.24640807918436	4.61075238142679	1.68494948788403
H	-4.08203403449558	2.54397648213724	-2.83410888519263
C	-5.96647954846058	2.40556539823453	-1.82135039429011

H	-4.75248584160596	0.93888867010049	-2.80824954055940
H	-5.85464068904183	3.31833842982815	-1.24214021201726
H	-6.52900449316813	1.70220263140396	-1.21313951174633
H	-6.56696251210463	2.64026534623670	-2.69430911860473
H	2.75022973914913	-1.89734092767104	1.34584588811174
H	3.09848508766894	-3.13160785370395	0.15018279765312
H	1.66863169484399	-3.26160855137351	1.15536273370342
H	1.25055698001357	4.39789242122563	1.32769546809756
H	0.33844804443854	5.17928616718370	2.60499802141569
H	-0.22996440311434	5.25162043467601	0.94768600820845

12

Coordinates from ORCA-job c6h6_cmp_Compound_1

C	-6.53134742942791	-0.50240795995019	0.70443085344638
C	-5.42076823898285	-1.17066752141684	0.21489717959299
C	-6.65378044380997	0.86527488038585	0.52018306347006
C	-4.43259817012351	-0.47145463361150	-0.45897784409455
C	-4.55503089821816	0.89622739986415	-0.64322577184535
H	-3.56939432742832	-0.99141731010444	-0.83930596471180
C	-5.66561019071417	1.56448801433635	-0.15369224579896
H	-3.78742538228926	1.44034588955225	-1.16749843631784
H	-7.29895283113632	-1.04652715746313	1.22870323876101
H	-5.32587230859731	-2.23393152429262	0.35839627140765
H	-7.51698504090423	1.38523732394341	0.90051215695434
H	-5.76050473836799	2.62775259875670	-0.29719250086393

12

Coordinates from ORCA-job but-1-ene_cmp_Compound_1

C	-6.47268510639985	-0.34048465752838	0.25062756769286
C	-5.04273570710407	0.13023900422001	0.02824820044254
H	-6.98928322180625	0.28996235171299	0.96728001752083
H	-6.49207686185440	-1.36008327858275	0.62279821244740
H	-7.03868700446679	-0.32011357247043	-0.67660584856301
H	-4.49043230204081	0.11225726724692	0.96530517747150
H	-5.06150011735257	1.16981099186725	-0.30105161486120
C	-4.32917370992070	-0.69276931863752	-0.98533659039239
C	-3.22291748368178	-1.38516809186929	-0.76736677934120
H	-4.78384151030701	-0.72341404361908	-1.96801361812151
H	-2.74367093668347	-1.38219966807250	0.19970737118346
H	-2.75676603838228	-1.97379698426721	-1.53899209547927

3.3 Dynamic Coordination Behavior of a Structurally Constrained, Nucleophilic Sn(II) Towards Gold(I)

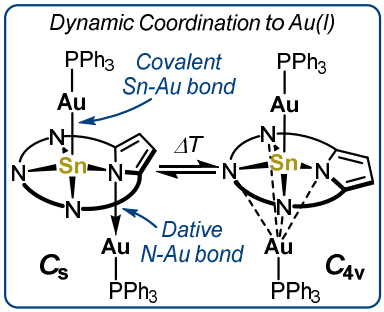


Figure 24. Table of contents graphic of the publication presented in this chapter.

The article and supplementary information (SI) presented within this section were previously published and can be found under: H. Ruppert, T. Schreyer, M. C. Dietl, M. Rudolph, A. S. K. Hashmi, L. Greb, *Z. Anorg. Allg. Chem.* **2024**, e202400081, https://doi.org/10.1002/zaac.202400081.

According to the CRediT scheme[271] the authors contributed to this publication as followed:

H. Ruppert – Conceptualization (*lead*), Methodology (*lead*), Validation (*lead*), Formal analysis (*lead*), Investigation (*lead*), Data curation (*lead*), Writing – Original Draft Preparation (*lead*), Writing – Review & Editing (*equal*), Visualization (*lead*), Supervision (*equal*), Project Administration (*equal*), Funding acquisition (*equal*);

T. Schreyer – Formal analysis (*supporting*), Investigation (*supporting*), Data curation (*supporting*);

M. C. Dietl – Investigation (*supporting*);

M. Rudolf – Writing – Review & Editing (*equal*);

A. S. K. Hashmi – Writing – Review & Editing (*equal*), Resources (*supporting*),

L. Greb –Resources (*lead*), Writing – Review & Editing (*equal*), Supervision (*equal*), Project Administration (*equal*), Funding acquisition (*equal*).

Check for updates

Journal of Inorganic and General Chemistry

ZAAC

Zeitschrift für anorganische und allgemeine Chemie

Accepted Article

Title: Dynamic Coordination Behavior of a Structurally Constrained, Nucleophilic Sn(II) Towards Gold(I)

Authors: Heiko Ruppert, Till Schreyer, Martin C. Dietl, Matthias Rudolph, Stephen K. Hashmi, and Lutz Greb

This manuscript has been accepted after peer review and appears as an Accepted Article online prior to editing, proofing, and formal publication of the final Version of Record (VoR). The VoR will be published online in Early View as soon as possible and may be different to this Accepted Article as a result of editing. Readers should obtain the VoR from the journal website shown below when it is published to ensure accuracy of information. The authors are responsible for the content of this Accepted Article.

To be cited as: *Z. anorg. allg. Chem.* **2024**, e202400081

Link to VoR: https://doi.org/10.1002/zaac.202400081

WILEY VCH

www.zaac.wiley-vch.de

10.1002/zaac.202400081

15213749, ja, Downloaded from https://onlinelibrary.wiley.com/doi/10.1002/zaac.202400081 by Heidelberg University Universitätsbibliothek, Wiley Online Library on [14/06/2024]. See the Terms and Conditions (https://onlinelibrary.wiley.com/terms-and-conditions) on Wiley Online Library for rules of use; OA articles are governed by the applicable Creative Commons License

Dynamic Coordination Behavior of a Structurally Constrained, Nucleophilic Sn(II) Towards Gold(I)

Heiko Ruppert[a], Till Schreyer[a], Martin C. Dietl[b], Matthias Rudolph[b], A. Stephen K. Hashmi[b], and Lutz Greb*[a]

[a] Anorganisch-Chemisches Institut
Ruprecht-Karls-Universität Heidelberg
Im Neuenheimer Feld 270, 69120 Heidelberg (Germany)
E-mail: greb@uni-heidelberg.de

[b] Organisch-Chemisches Institut
Ruprecht-Karls-Universität Heidelberg
Im Neuenheimer Feld 270, 69120 Heidelberg (Germany)

Abstract

Tetradentate *meso*-octaalkylcalix[4]pyrroles are well-established ligands in *d*- and *f*-block chemistry. In contrast to the related porphyrins, the sp^3-hybridized *meso*-carbon atoms linking the four pyrrole units result in highly divers coordination modes. We previously reported on the combination of this ligand system with Sn(II) centers yielding tetracoordinated stannate(II) anions which could be employed as electron-rich, strong σ-donor ligands in transition metal chemistry. With this work we are extending the coordination chemistry of *meso*-octaethylcalix[4]pyrrolato stannate(II) **[1]$^{2-}$** onto gold(I). Synthesis of mono- and dinuclear gold complexes reveal a new dynamic binding mode involving μ_2-bridging coordination of a pyrrole nitrogen atom to both Sn and Au. Single-crystal X-ray diffraction and variable temperature NMR spectroscopy combined with quantum mechanical computations and bond analysis tools shed light on the involved intermediates.

Introduction

Meso-octaalkylcalix[4]pyrroles are known as ligands in transition metal chemistry for more than 30 years.[1,2] In contrast to their related, conjugated porphyrin macrocycles, the C(sp^3) atoms linking the four pyrrole units in calix[4]pyrroles yield a highly flexible ligand framework with each pyrrole unit offering multiple η^1, η^3, and η^5 coordination sites. This conformational flexibility resulted in the isolation of a plethora of complexes with metal centers spanning nearly the whole periodic table (Figure 1 A).[2–7] Whereas the all-η^1 coordination mode (i) can predominantly be found for high-valent transition metal centers, the η^3- and η^5-coordination involving the π-surfaces of pyrroles are limited to early transition metals, as well as *s*- and *f*-block elements (ii-iv).[3] More recently, calix[4]pyrroles have been established as ligands in the field of *p*-block chemistry enabling the isolation of structurally constrained high- and low-valent *p*-block compounds. For high-valent *p*-block elements, these constrained, so-called "anti-van't Hoff-Le Bel" structures, resulted in elevated Lewis acidities at the central elements and transferred concepts like agostic interactions, ligand-to-metal charge transfer, and element-ligand cooperative bond activations into the *p*-block.[4,5,8–11] For low-valent *p*-block centers such as Sn(II), the tetradentate calix[4]pyrrolate ligand backbone drastically increased tin's nucleophilicity and σ-donor strength (TEP of 2032 cm^{-1}) delivering electron-rich stannate(II) dianions **[1]$^{2-}$** (Figure 1 B).[7] Besides being a strong tin-centered nucleophile and reducing agent, **[1]$^{2-}$** itself could also be employed as a ligand in transition metal chemistry. Against 16 valence electron (VE) fragments such as $[Ni^0(CO)_3]$ and $[W^0(CO)_5]$, **[1]$^{2-}$** acted as a η^1 two-electron donor *via* the electron lone-pair of the Sn(II) center. With the 12 VE fragment $[Ru^{II}(p\text{-cymene})]^{2+}$, a Ru^{II} sandwich complex employing an anionic pyrrolate unit of the calix[4]pyrrole backbone as a η^5 six-electron π-donor was formed.[7]

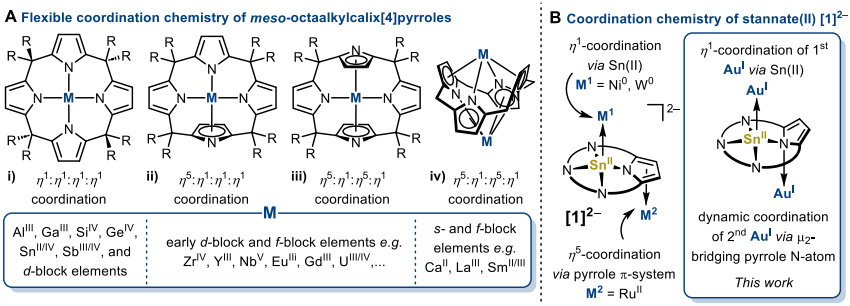


Figure 1. A) Different coordination modes of *meso*-octaalkylcalix[4]pyrroles. **B)** Coordination chemistry of *meso*-octaethylcalix[4]pyrrolato stannate(II) **[1]$^{2-}$** acting as both a η^1- and η^5-ligand (left) and coordination chemistry of **[1]$^{2-}$** with Au(I) reported in this work (right).

This article is protected by copyright. All rights reserved.

10.1002/zaac.202400081

15213749, ja, Downloaded from https://onlinelibrary.wiley.com/doi/10.1002/zaac.202400081 by Heidelberg University Hochschulbibliothek, Wiley Online Library on [14/06/2024]. See the Terms and Conditions (https://onlinelibrary.wiley.com/terms-and-conditions) on Wiley Online Library for rules of use; OA articles are governed by the applicable Creative Commons License

Accepted Manuscript

Advances in gold(I) chemistry were often guided by employing soft P- or C-centered donors such as phosphines and carbenes owing to their excellent σ-donating ability and a varying π-accepting capacity.[12] In contrast, the coordination chemistry of gold(I) and strongly σ-donating tin-centered ligands is by far less developed. *Gade* and co-workers reported the gold(I) complex **A** coordinated by a tripodal tris(amido)-stannate(II) anion (Figure 2).[13,14] The *Wesemann* group employed mono- and dianionic 1,2-carba-stannaborate **[B]**$^-$ and stannaborate **[C]**$^{2-}$ to reduce AuCl(PPh$_3$) forming tin-bridged di- and tetranuclear gold(0) clusters.[15,16] Pushing the electron-donating capacity even further, the *Aldridge* group showed that aluminyl anions can act as strongly electron-donating metal-centered ligands towards Au(I). Complex **D** showed Au-centered nucleophilic behavior resembling that of a formal Au(-I).[17]

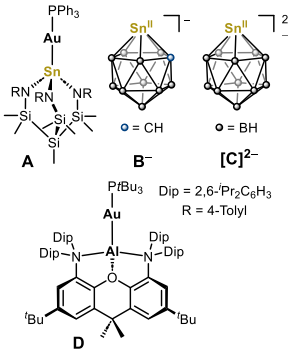


Figure 2. Gold(I) complex of the stannate(II) anion reported by the *Gade* group **A**,[13] 1,2-carba-stannaborate **[B]**$^-$ and stannaborate **[C]**$^{2-}$ used for the reductive generation of multinuclear Au(0) complexes,[15,16] and aluminyl gold complex **D** reported by the *Aldridge* group.[17]

With this work we describe the strong σ-donor character as well as the diverse coordination modes of *meso*-octaethyl-calix[4]pyrrolato stannate(II) **[1]**$^{2-}$ in gold(I) chemistry (Figure 1 B). It further introduces a new dynamic coordination mode of **[1]**$^{2-}$ involving the tin-bound pyrrole N-atoms as secondary coordination sites. Experimental work supported by DFT calculations and bond analysis tools (NBO, QTAIM, and ETS-NOCV) elucidates the nature of the Sn- and N-Au bonds.

Results and Discussion

Reacting **[Li$_2$(thf)$_x$][1]** with one equivalent of AuCl(PPh$_3$) in toluene at room temperature resulted in fast dissolution of the starting materials accompanied by the precipitation of LiCl (Figure 3 A). Removal of the precipitate and evaporation of the solvent yielded a crude material consisting of **[Li(thf)$_x$][1-AuPPh$_3$]** and a minor side product as evidenced by ^{1}H and ^{31}P{^{1}H} NMR spectroscopy. Exposure towards vacuum to remove excess THF and subsequent washing with small amounts of toluene afforded **[Li(thf)$_x$][1-AuPPh$_3$]** as an off-white solid in bulk purity and acceptable yield (47%). ^{1}H in THF-d_8 indicate a C_{4v} symmetry in solution with two diastereotopic sets of ethyl residues and one sharp singlet with $^{117/119}$Sn satellites ($^4J_{Sn,H}$ = 156.0 Hz) for the β-hydrogen atoms of the pyrroles at 5.90 ppm. A ^{31}P NMR shift at 41.77 ppm is in agreement with the PPh$_3$ ligand still coordinated to Au(I).[13] ^{1}H,^{119}Sn HMBC NMR spectroscopy showed a doublet at −70.3 ppm (*cf.* −481.3 ppm for **[Li$_2$(thf)$_x$][1]**). In combination with the symmetry in solution, the $^2J_{Sn,P}$ coupling constant of 3431.0 Hz and the significant coordination chemical shift $\Delta\delta(^{119}Sn) = \delta(^{119}Sn)_{coord.} - \delta(^{119}Sn)_{free}$ of 411 ppm indicate the coordination of tin(II) to the gold(I) center.[7,18] Eventually, single crystal X-ray diffraction (sc-XRD) evidenced the η^1 coordination of **[1]**$^{2-}$ to the [AuPPh$_3$]$^+$ fragment acting as a σ-donor (Figure 4 A, **[Li(thf)$_2$][1-AuPPh$_3$]** co-crystallized with one toluene molecule). The Sn-N bond lengths in **[Li(thf)$_2$][1-AuPPh$_3$]** are significantly shortened (~216 pm) compared to the parent stannate(II) **[1]**$^{2-}$ (~231 pm),[7] owing to a significant charge transfer from Sn(II) to Au(I). A similar trend in Sn-N bond length and comparable Sn-Au bond length were reported for the tris(amido)stannate(II) gold(I) complex **A** (256.51(13) pm *vs* 255.68(5) pm for **[Li(thf)$_2$][1-AuPPh$_3$]**).[13,19] Figure 3 A shows the additional coordination of a [Li(thf)$_2$]$^+$ cation by the calix[4]pyrrole ligand backbone forming an overall neutral complex. Such a coordination mode is also known for the lithium salt of the parent stannate(II) and results in a moderate solubility of **[Li(thf)$_x$][1-AuPPh$_3$]** in solvents such as THF, toluene, benzene, and 1,2-difluorobenzene (*o*DFB) depending on the content of THF. To decrease the solubility of **[1-AuPPh$_3$]**$^-$ in non-polar solvents and thereby improve the yield after the washing step we aimed to exchange Li$^+$ for the weakly interacting NBu$_4^+$ cation. *In situ* treatment of the crude product directly after evaporating the reaction solution with one equivalent of NBu$_4$Cl in *o*DFB caused the precipitation of a second equivalent LiCl. Filtration followed by precipitation of **[NBu$_4$][1-AuPPh$_3$]** *via* the addition of *n*-hexane delivered the ammonium salt in bulk purity and an improved yield of 85%. NMR spectroscopy in THF-d_8 showed comparable characteristics as found for **[Li(thf)$_x$][1-AuPPh$_3$]** indicating an intact **[1-AuPPh$_3$]**$^-$ anion and the absence of lithium *via* ^{7}Li NMR.

The side product observed during the synthesis of **[Li(thf)$_x$][1-AuPPh$_3$]** showed comparable ^{1}H NMR characteristics as observed for the target compound but two chemically inequivalent ^{31}P centers ($\delta(^{31}P)$ = 44.87 and 30.98 ppm). Aldridge and co-workers reported the selective reaction of their aluminyl anion with two equivalents AuI(PPh$_3$) forming a dinuclear Au(0) complex featuring an Au-Au interaction.[17] We hypothesized that the side product we observed could be the result of **[1]**$^{2-}$ reacting with two equivalents AuCl(PPh$_3$). Indeed, stoichiometric treatment of **[Li$_2$(thf)$_x$][1]** with two equivalents AuCl(PPh$_3$) in toluene at room temperature formed a clear yellow reaction solution accompanied by the precipitation of LiCl. Subsequent workup yielded the dinuclear complex **[1-(AuPPh$_3$)$_2$] x tol** as a yellow solid in 55% yield and bulk purity. Its ^{1}H and ^{13}C NMR spectra in Tol-d_8 and THF-d_8 at room temperature indicated C_{4v} symmetry. In contrast to **[Li(thf)$_x$][1-AuPPh$_3$]** the resonances for the CH$_2$ groups of the *meso*-ethyl residues were significantly broadened indicating a dynamic rearrangement of the ligand backbone.[6] Even though $^{117/119}$Sn-satellites in the ^{1}H spectra evidence the presence of tin, the dynamic behavior of **[1-(AuPPh$_3$)$_2$]** did not allow to obtain its ^{119}Sn chemical shift *via* ^{1}H,^{119}Sn HMBC NMR spectroscopy at room temperature. Thus, we turned to NMR measurements at elevated temperature.

This article is protected by copyright. All rights reserved.

10.1002/zaac.202400081

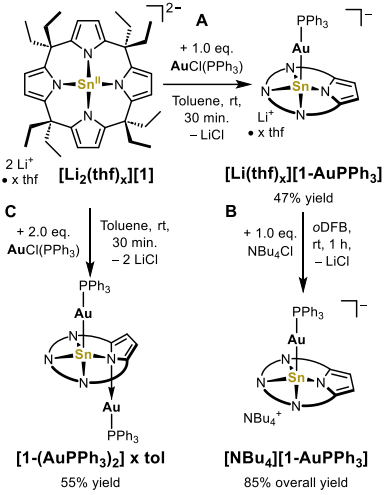


Figure 3. Synthetic route towards A) $[Li(thf)_x][1\text{-}AuPPh_3]$, B) $[NBu_4][1\text{-}AuPPh_3]$, and C) $[1\text{-}(AuPPh_3)_2]$.

At 50 °C, a sharpening of the resonances for the CH_2 groups could be observed now resolving the $^2J_{H,H}$ coupling to their neighboring CH_3 protons (Figure S13). Furthermore, ^1H,^{119}Sn HMBC NMR spectroscopy delivered a doublet at 39.7 ppm with a $^2J_{Sn,P}$ coupling constant of 3446.7 Hz indicating a change in the coordination environment of the Sn-center ($\Delta\delta(^{119}Sn)$ = 521 ppm) while maintaining the communication with the phosphorus in PPh_3 (Figure S14). Recrystallization from a concentrated toluene solution at −30 °C gave single crystals suitable for XRD (Figure 4 B). In contrast to the NMR observations the solid-state molecular structure of **[1-(AuPPh$_3$)$_2$] x tol** shows a decreased C_s symmetry. The coordination of a second $[AuPPh_3]^+$ fragment *via* the μ_2-bridging N4 atom results in a tilting of the respective pyrrole ring towards Au1 of the tin-bound $[AuPPh_3]^+$. While the Sn1-Au1 bond length in **[1-(AuPPh$_3$)$_2$]** is close to the one observed in **[Li(thf)$_2$][1-AuPPh$_3$]**, coordination of Au2 by the N4 causes a significant elongation of the Sn1-N4 bond (258.6(3) pm *vs*. previous ~216 pm). In fact, Wiberg bond indices (WBI) obtained by natural bond orbital (NBO) calculations (PBE0/def2-TZVP) revealed a significantly decreased population of the Sn1-N4 bond (Table S3, WBI of 0.1413 *vs* 0.3411 for the remaining Sn-N bonds). The Au-P bond lengths are markedly different, with elongated Au1-P1 bond (231.59(10) pm) *vs*. 223.29(10) for Au2-P2, indicating differences in the interactions. NBO, QTAIM (Table S4, PBE0-D3(BJ)/ZORA-TZ2P/COSMO (Toluene)), and ETS-NOCV analysis (Table S5 and S6, Figure S22, BP86-D3/TZ2P COSMO(Toluene)) revealed that the Sn-Au interactions in **[1-AuPPh$_3$]$^-$** and **[1-(AuPPh$_3$)$_2$]** are best described as covalent electron-sharing bonds whereas the N-Au bond in **[1-(AuPPh$_3$)$_2$]** is predominantly dative in nature. This results in a significant buildup of negative charge at Au1 (QTAIM charge of −0.28 and −0.20) while Au2 remains positively charged (0.14) (Figure 4 C). Very different are also the computed free reaction enthalpies for the $[AuPPh_3]^+$ coordination reactions lying at −234.7 for the Sn- and −188.1 kJ mol^{-1} for the N-binding (B97M-D3(BJ)/def2-TZVPP(COSMO-RS(THF))). Owing to these computed ΔG values, we envisioned that the effective C_{4v} symmetry of **[1-(AuPPh$_3$)$_2$]** in solution is caused by a fast migration of the second $[AuPPh_3]^+$ fragment between the N atoms of the calix[4]pyrrole backbone rather than a dissociation of a $[AuPPh_3]^+$.

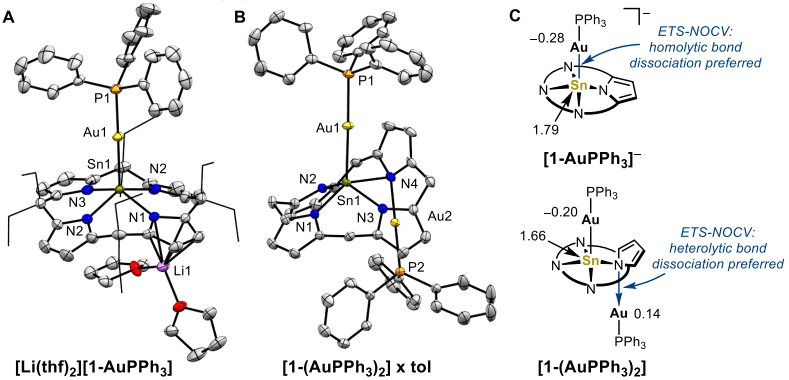


Figure 4. Solid-state molecular structure of **A) [Li(thf)$_2$][1-AuPPh$_3$]** and **B) [1-(AuPPh$_3$)$_2$] x tol**. Displacement ellipsoids are drawn at 50% probability level. Hydrogens, solvent molecules and *meso*-ethyl residues of [1-$(AuPPh_3)_2$] x tol are omitted for clarity. Selected bond lengths [pm] and angels [deg] for **[Li(thf)$_2$][1-AuPPh$_3$]**: Sn1-N1 213.7(3), Sn1-N2 217.9(3), Sn1-N3 216.5(3), Au1-Sn1 255.68(5), Au1-P1 229.59(10), N1-Sn1-N4 144.34(11), N2-Sn1-N3 142.02(11), P1-Au1-Sn1 179.23(2); and **[1-(AuPPh$_3$)$_2$] x tol**: Sn1-N1 225.5(3), Sn1-N2 218.9(2), Sn1-N3 218.1(3), Sn1-N4 258.6(3), Au1-Sn1 257.49(6), Au1-P1 231.59(10), Au2-N4 208.2(3), Au2-P2 223.29(10), N1-Sn1-N4 144.82(10), N2-Sn1-N3 132.89(11), P1-Au1-Sn1 177.36(3), P2-Au2-N4 179.78(10). **C)** Differences in bonding between Au1 and Au2 and QTAIM charges for selected atoms computed at the PBE0-D3(BJ)/ZORA-TZ2P/COSMO(Toluene)//B97M-D4/def2-TVZPP//CREST/GFN2-xTB level of theory.

This article is protected by copyright. All rights reserved.

15213749, ja, Downloaded from https://onlinelibrary.wiley.com/doi/10.1002/zaac.202400081 by Heidelberg University Universitätsbibliothek, Wiley Online Library on [14/06/2024]. See the Terms and Conditions (https://onlinelibrary.wiley.com/terms-and-conditions) on Wiley Online Library for rules of use; OA articles are governed by the applicable Creative Commons License

10.1002/zaac.202400081

15213749, ja, Downloaded from https://onlinelibrary.wiley.com/doi/10.1002/zaac.202400081 by Heidelberg University, Universitatsbibliothek, Wiley Online Library on [14/06/2024]. See the Terms and Conditions (https://onlinelibrary.wiley.com/terms-and-conditions) on Wiley Online Library for rules of use; OA articles are governed by the applicable Creative Commons License

Accepted Manuscript

Variable temperature (VT) NMR spectroscopy in Tol-d_8 revealed a lowering of its symmetry below −20 °C (Figure 5 A, see Figure S15 for NMR spectra at additional temperatures). At −50 °C four resonances for the pyrrole hydrogens and six resonances for the CH_2 group of the *meso*-ethyl residues could be observed being consistent with the C_s symmetry in the solid state. The additional splitting of the CH_2 resonances is assumed to be caused by hindered rotations around the C_{meso}-CH_2 bond at −50 °C.[6] For a reference system **[1*-(AuPMe$_3$)$_2$]**, where the *meso*-ethyl and phenyl residues were substituted by methyl groups, a migration mechanism of $[AuPMe_3]^+$ consisting of two low-energy transition structures and an intermediate could be obtained (Figure 5 B, DSD-BLYP/def2-QZVPP(COSMO-RS(Toluene))//B97M-D3(BJ)/def2-TZVPP). The ring flip of pyrrole 1 (blue) forms **INT1** with a free transition enthalpy $\Delta G^{\ddagger,1}$ of 49.9 kJ mol^{-1} and an endergonic free reaction enthalpy ΔG of 43.1 kJ mol^{-1}. The inclined orientation of the two neighboring pyrrolates in **INT1** then allows the low-barrier migration of the $[AuPMe_3]^+$ *via* **TS2** ($\Delta G^{\ddagger,2}$ = 75.8 kJ mol^{-1}) forming **INT1'**. The magnitude of $\Delta G^{\ddagger,2}$ is in accordance with the slow migration of $[AuPPh_3]^+$ at diminished temperature in solution as observed by ^{1}H NMR. Ring flip of pyrrole 2 (red) formerly bound to gold *via* **TS1'** finalizes the migration mechanism. Calix[4]pyrrole complexes bearing multiple metal centers are well known, however they are usually involving η^5 coordination of the pyrrole π-surfaces strongly binding additional metal centers (*cf.* Figure 1).[3,7,20] To the best of our knowledge this represents the first example of a multi-metallic calix[4]pyrrole complex showing this dynamic μ_2-bridging coordination mode.

Inspired by the reactivity of the aluminyl gold complex **D** we tested our complexes in the activation of CO_2.[17] The Li^+ and NBu_4^+ salt of **[1-AuPPh$_3$]$^-$** showed to undergo decomposition under 2.0 atm CO_2 at room temperature (Li^+) or elevated temperatures (NBu_4^+) in Tol-d_8 over 24 hours. Interestingly the decomposition showed the concomitant formation of **[1-(AuPPh$_3$)$_2$]** from released $[AuPPh_3]^+$ and remaining **[1-AuPPh$_3$]$^-$**

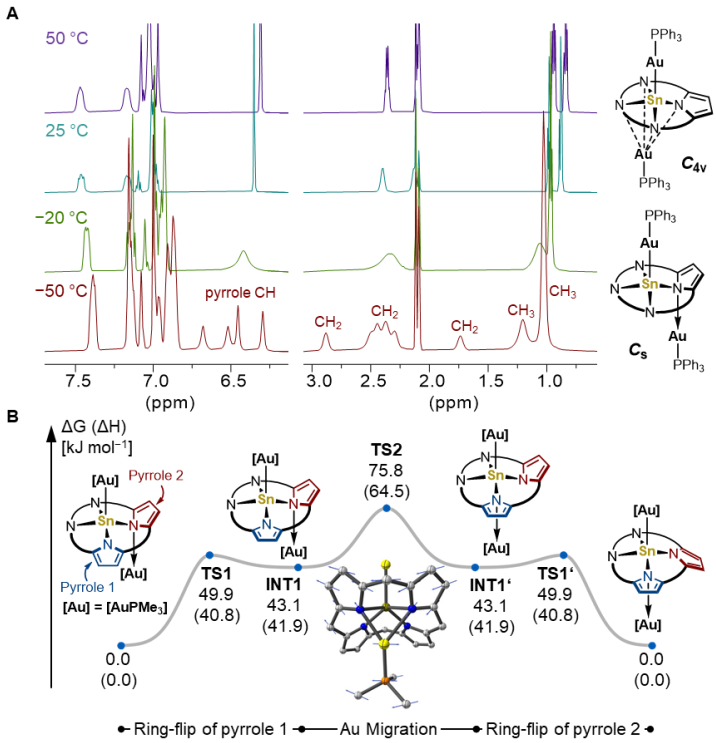


Figure 5. A) Variable temperature NMR spectra of **[1-(AuPPh$_3$)$_2$] x tol** in Tol-d_8 and **B)** reaction mechanism for the migration of gold between the nitrogen atoms of the calix[4]pyrrolato ligand backbone for the reference system **[1*-(AuPMe$_3$)$_2$]** computed at the DSD-BLYP/def2-QZVPP COSMO-RS(Toluene)//B97M-D3(BJ)/def2-TZVPP level of theory. For the transition structure of **TS2** the *meso*-methyl substituents and the PMe_3 bound to the upper gold atom are omitted for clarity.

This article is protected by copyright. All rights reserved.

besides unidentified decomposition products. No reaction could be observed for the dinuclear complex **[1-(AuPPh$_3$)$_2$]** toward CO_2, being stable in toluene at 80 °C for over 24 hours. Computational studies for aluminyl gold complex **D** revealed the importance of the electrophilic aluminum center for the activation of CO_2 and SO_2.[21–23] Owing to the high coordination number of tin in **[1-AuPPh$_3$]$^-$**, such an electrophilic assisting cannot occur. Eventually, the coordination of a second gold(I) phosphine not only stabilizes **[1-AuPPh$_3$]$^-$** at elevated temperatures in solution but also allowed **[1-(AuPPh$_3$)$_2$] x tol** to be stable in the solid state under ambient conditions for up to 48 hours.

Conclusion

Structural constraint and tetracoordination furnish a highly σ-donating tin(II) center which can form dative bonds. In this work we presented its reaction with AuCl(PPh$_3$) yielding the two bimetallic complexes **[1-AuPPh$_3$]$^-$** and **[1-(AuPPh$_3$)$_2$]** which could be fully characterized by sc-XRD, spectroscopy methods and quantum mechanical bond analysis tools. **[1-AuPPh$_3$]$^-$** is best described containing a covalent Sn-Au bond owing to a significant charge transfer from tin(II) to gold(I) upon coordination. Reaction of **[1]$^{2-}$** with two equivalents AuCl(PPh$_3$) delivered the dinuclear complex **[1-(AuPPh$_3$)$_2$]** showing a formerly unknown coordination mode in calix[4]pyrrole chemistry, *i.e.* the dynamic μ_2-coordination of the second triphenylphosphine gold(I) fragment *via* the four nitrogen atoms of the calix[4]pyrrole ligand. Combination of sc-XRD structure, variable temperature NMR measurements, and computations led to the mechanism for the migration of the second [AuPPh$_3$]$^+$ between the pyrrole units. Further studies extending this coordination mode to other bimetallic complexes and employing them in catalytic transformations are under current investigations in our labs.

Author Contributions

H.R.: Conceptualization (lead), Investigation (lead), Project Administration (equal), Supervision (equal), Visualization (lead), Writing – Original Draft Preparation (lead), Writing – Review & Editing (equal); **T.S.**: Investigation (supporting); **M.D.**: Investigation (supporting); **M.R.**: Writing – Review & Editing (equal); **A.S.H.**: Writing – Review & Editing (equal); Resources (supporting); **L.G.**: Project Administration (equal), Resources (lead), Supervision (equal), Writing – Review & Editing (equal).

Acknowledgements

We acknowledge support by the state of Baden-Württemberg through bwHPC and the German Research Foundation (DFG) through Grant INST 40/575-1 FUGG (JUSTUS 2 cluster). H.R. acknowledges the Foundation of German Business (sdw) for funding. We acknowledge M. Schmitt for his support with X-ray crystal structure refinement.

[1] D. Jacoby, C. Floriani, A. Chiesi-Villa, C. Rizzoli, *J. Chem. Soc. Chem. Commun.* **1991**, 220–222.
[2] C. Floriani, R. Floriani-Moro, in *Porphyr. Handb.*, **2000**.
[3] H. Ruppert, L. M. Sigmund, L. Greb, *Chem. Commun.* **2021**, *57*, 11751–11763.
[4] R. Yadav, P. Janßen, M. Schorpp, L. Greb, *J. Am. Chem. Soc.* **2023**, *145*, 17746–17754.
[5] M. Schorpp, R. Yadav, D. Roth, L. Greb, *Angew. Chem.* **2022**, *134*, e202207963.
[6] H. Ruppert, A. Meister, R. Pfretzschner, A. F. Vieira, L. Greb, *J. Am. Chem. Soc.* **2024**, DOI 10.1021/jacs.4c02446.
[7] H. Ruppert, L. Greb, *Angew. Chem. Int. Ed.* **2022**, *61*, e202116615.
[8] F. Ebner, L. Greb, *Chem* **2021**, *7*, 2151–2159.
[9] L. M. Sigmund, E. Engels, N. Richert, L. Greb, *Chem. Sci.* **2022**, *13*, 11215–11220.
[10] F. Ebner, L. M. Sigmund, L. Greb, *Angew. Chem. Int. Ed.* **2020**, *59*, 17118–17124.
[11] L. M. Sigmund, C. Ehlert, M. Enders, J. Graf, G. Gryn'ova, L. Greb, *Angew. Chem. Int. Ed.* **2021**, *60*, 15632–15640.
[12] H. G. Raubenheimer, H. Schmidbaur, *J. Chem. Educ.* **2014**, *91*, 2024–2036.
[13] B. Findeis, M. Contel, L. H. Gade, M. Laguna, M. C. Gimeno, I. J. Scowen, M. McPartlin, *Inorg. Chem.* **1997**, *36*, 2386–2390.
[14] M. Contel, K. W. Hellmann, L. H. Gade, I. J. Scowen, M. McPartlin, M. Laguna, *Inorg. Chem.* **1996**, *35*, 3713–3715.
[15] D. Joosten, I. Weissinger, M. Kirchmann, C. Maichle-Mössmer, F. M. Schappacher, R. Pöttgen, L. Wesemann, *Organometallics* **2007**, *26*, 5696–5701.
[16] S. Hagen, I. Pantenburg, F. Weigend, C. Wickleder, L. Wesemann, *Angew. Chem. Int. Ed.* **2003**, *42*, 1501–1505.
[17] J. Hicks, A. Mansikkamäki, P. Vasko, J. M. Goicoechea, S. Aldridge, *Nat. Chem.* **2019**, *11*, 237–241.
[18] D. Agustin, M. Ehses, *Comptes Rendus Chim.* **2009**, *12*, 1189–1227.
[19] M. Kilian, H. Wadepohl, L. H. Gade, *Organometallics* **2008**, *27*, 524–533.
[20] L. Cuesta, J. L. Sessler, *Chem. Soc. Rev.* **2009**, *38*, 2716–2729.
[21] D. Sorbelli, L. Belpassi, P. Belanzoni, *J. Am. Chem. Soc.* **2021**, *143*, 14433–14437.
[22] D. Sorbelli, L. Belpassi, P. Belanzoni, *Chem. – Eur. J.* **2023**, *29*, e202203584.
[23] I. F. Leach, D. Sorbelli, L. Belpassi, P. Belanzoni, R. W. A. Havenith, J. E. M. N. Klein, *Dalton Trans.* **2022**, *52*, 11–15.

This article is protected by copyright. All rights reserved.

15213749, ja, Downloaded from https://onlinelibrary.wiley.com/doi/10.1002/zaac.202400081 by Heidelberg University, Universitätsbibliothek, Wiley Online Library on [14/06/2024]. See the Terms and Conditions (https://onlinelibrary.wiley.com/terms-and-conditions) on Wiley Online Library for rules of use; OA articles are governed by the applicable Creative Commons License

Supporting Information for

Dynamic Coordination Behavior of a Structurally Constrained, Nucleophilic Sn(II) Towards Gold(I)

Table of Contents

1 Experimental Details 2
2 Computational Details 3
3 Synthesis. 5
3.1 Lithium (*meso*-octaethylcalix[4]pyrrolato stannate(II))(triphenylphosphine)aurate(I) [Li(thf)$_x$][1-AuPPh$_3$] 5
3.2 Tetrabutylammonium (*meso*-octaethylcalix[4]pyrrolato stannate(II))(triphenyl-phosphine) aurate(I) [NBu$_4$][1-AuPPh$_3$] 6
3.3 *Meso*-octaethylcalix[4]pyrrolato stannate(II) *bis*-(triphenylphosphine gold(I)) [1-(AuPPh$_3$)$_2$] 7
4 NMR Spectra 8
4.1 [Li(thf)$_x$][1-AuPPh$_3$] x 0.5 tol 8
4.2 [NBu$_4$][1-AuPPh$_3$] 11
4.3 [1-(AuPPh$_3$)$_2$] x tol 13
5 Crystallographic Data 17
5.1 [Li(thf)$_2$][1-AuPPh$_3$] 17
5.2 [NBu$_4$][1-AuPPh$_3$] 19
5.3 [1-(AuPPh$_3$)$_2$] x tol 20
6 Elemental Analysis 22
7 NBO Analysis of [1-(AuPPh$_3$)$_2$] 23
8 QTAIM Analysis 24
9 ETS-NOCV Analysis of [1-AuPPh$_3$]$^-$ 25
10 ETS-NOCV Analysis of [1-(AuPPh$_3$)$_2$] 25
11 Optimized Molecular Geometries 26
12 Literature 44

1 Experimental Details

All manipulations were carried out under a dry argon atmosphere by using standard Schlenk techniques to prevent oxidation and hydrolysis of the sensitive compounds. The lithium salt of *meso*-octaethylcalix[4]pyrrolato stannate(II) **[Li_2(thf)$_x$][1]**[1] and chloro(triphenylphosphine)gold(I)[2] were prepared according to literature known procedures and their purity confirmed by NMR spectroscopy before use. Commercially available chemicals were used as received. All solvents and liquid chemicals were rigorously dried by applying standard procedures, freshly degassed, and stored over activated molecular sieve (3 Å resp. 4 Å) prior to use. All glassware, syringes, magnetic stirring bars, and needles were thoroughly dried. All air sensitive compounds were stored in a glove box (MBraun LABmaster dp, MB-20-G, SylaTech Y05G) under N_2 atmosphere. Analytical data of literature known compounds were compared to data of the respective reference and were found to be consistent in all cases. The purity and identity of novel compounds were confirmed by high resolution multinuclear NMR-spectroscopy, mass spectrometry, elemental analysis and if possible, X-ray diffraction analysis.

^{1}H, ^{7}Li, ^{13}C, ^{31}P, and ^{119}Sn NMR spectra were collected with a Bruker (DPX) 200, a Bruker Advance II 400 or a Bruker 2 Advance III 600 NMR spectrometer and referenced to tetramethylsilane (^{1}H, ^{13}C), tetramethylstannane (^{119}Sn). If not stated otherwise, ^{1}H and ^{13}C chemical shifts were taken from one-dimensional NMR spectra. To assist the correct peak assignment additional two-dimensional NMR spectra such as ^{1}H,^{1}H-COSY, ^{1}H,^{13}C-HSQC and HMBC, and broadband ^{1}H-decoupled ^{13}C-DEPT135 were recorded (only selected spectra were depicted in the supplementary information). ^{119}Sn chemical shifts were obtained from two-dimensional ^{1}H,^{119}Sn HMBC measurements. ^{77}Se chemical shifts were obtained from two-dimensional ^{1}H,^{77}Se HMBC measurements. Chemical shifts are reported as dimensionless δ values in ppm, coupling constants J are given in hertz (Hz). Peak multiplicities are given as singlet (*s*), doublet (*d*), triplet (*t*), quartet (*q*), quintet (*quint*), sextet (*sext*), and septet (*sept*).

High-resolution electrospray ionization mass spectra (HRMS-ESI) were obtained with a Bruker ApexQe FT-ICR instrument.

Elemental analysis for the determination of the C-, H- and N-content was carried out by the microanalysis laboratory of the Institute of Inorganic Chemistry at Heidelberg University using a vario MICRO cube of Elementar Analysensysteme.

Suitable crystals of the compounds were taken directly out of the mother liquor, immersed in perfluorinated polyether oil, and fixed on top of a cryo loop. Measurements were made on Bruker D8 Venture CCD diffractometer with a low-temperature unit using (100 or 120 K) Mo-Kα radiation chromated by mirror optics. The data collected were processed using standard Bruker APEX3 software. Structures were solved by intrinsic phasing using the SHELXT program[3] and refined with the SHELXL.[4] Graphical handling of the structural data during solution and refinement was performed with shelXLe.[5] Atomic coordinates and anisotropic thermal parameters of non-hydrogen atoms were refined by full-matrix least-squares calculations[6] and displacement ellipsoids are displayed with 50 % probability. Hydrogen atoms were included using a riding model. Crystallographic data for the structures reported in this article are deposited within the Cambridge Crystallographic Data Centre as supplementary publication no. 2358521-2358522 which can be obtained free of charge. Crystal data and structure are summarized in the tables under the crystallographic figures. Figures depicting solid state molecular structures and distances and angles between planes spanned by atoms have been calculated and generated by Mercury 2023.3.0 without a standard deviation..

2 Computational Details

All computations employing the Orca 5.0.3[7] software or the Amsterdam Modelling Suite AMS2021.102[8,9] were carried out with the computational resources available on the bwFor Cluster JUSTUS2 located at Ulm University within the Baden Württemberg High Performance Computing program.

All structures were optimized with the Orca 5.0.3 software at the B97M[10]-D4[11]/def2-TVZPP[12] level of theory employing a def2/J auxiliary basis set.[13] Minima structures were obtained with the following ORCA input line:

```
! RKS B97M-D4 def2-TZVPP defGrid2 NoPop Opt NumFreq TightSCF
```

Conformational spaces, especially to find the lowest energy orientations of the ethyl residues of the calix[4]pyrrole ligand, were initially explored with the conformer-rotamer ensemble sampling tool (CREST)[14] for the xtb program package[15] using the following command line input. The lowest-energy conformer was then reoptimized as described below.

```
crest [file_name].xyz --alpb Toluene --chrg [charge] --noreftopo >
[file_name].out
```

All calculated geometries have been confirmed as energetic minima on the potential energy surface by numerical calculation of harmonic frequencies at the B97M-D4/def2-TVZPP level, revealing only positive values.

Subsequent single point calculations employing the Conductor-like Polarizable Continuum Model Based on Solute Electron Density (C-PCM SMD)[16] were performed with the following ORCA input line:

```
! RKS B97M-D4 def2-TZVPP defGrid2 TightSCF

CPCM SMD TRUE
     SMDSOLVENT "Toluene"
END
```

High-level thermodynamic data was obtained by subsequent single point calculations employing the double-hybrid density functional DSD-BLYP[17] and def2-QZVPP basis set[12] combined with the D3(BJ) dispersion correction[18] and the resolution-of-identity approximation[19] with automatically generated auxiliary basis sets:[20]

```
! RI-DSD-BLYP D3BJ def2-QZVPP RIJCOSX AutoAux defGrid3 TightSCF
```

Transition structures were optimized toward a single negative Hessian matrix eigenvalue using the `OptTS` keyword. It was ensured that the correct first-order saddle point on the potential energy surface was located by animation of the imaginary frequency in Chemcraft software version 1.8.[21]

Natural Bond Orbital (NBO) calculations were conducted on the PBE0[22]/def2-TZVP[12] level of theory (def2-TZVPP basis set for Au atoms) using NBO6.0.18a[23] as included in Orca 5.0.3 *via* the following ORCA

input line:

```
! RKS PBE0 def2-TZVP NBO TightSCF defGrid2

%basis
      newgto Au "def2-TZVPP" end
end
```

Furthermore the $CHOOSE keylist was used to specify meaningful Lewis structure for the NBO search.

Calculations employing the Extended Transition State (ETS) method for energy decomposition analysis (EDA)[24–26] combined with the natural orbitals for chemical valence (NOCV)[27] calculations were performed on the BP86-D3(BJ)[28–30]/TZ2P level of theory with COSMO(THF) solvation correction as implemented in the AMS2021.201 software.[8,9]

QTAIM analyses were performed on the PBE0-D3(BJ)/ZORA-TZ2P/COSMO(THF) electron densities,[31–33] as implemented in the AMS2021.201 software.[8,9] QTAIM charges of atoms were calculated using the grid-based method implemented in AMS.[34,35] The Numerical Quality Good keyword was used in the calculations to increase the numerical quality of the results in order to avoid numerical artefacts in the atomic charges.

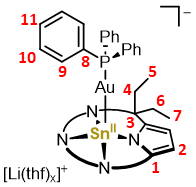
Optimized geometries were visualized using Chemcraft version 1.8.

The potential energy surface path for the migration mechanism shown in Figure 5 B was generated using the EveRplot web-based application.[36,37]

Isosurface plots were created using the IboView software v20150427.[38]

3 Synthesis.

3.1 Lithium (*meso*-octaethylcalix[4]pyrrolato stannate(II))(triphenylphosphine)aurate(I) [Li(thf)$_x$][1-AuPPh$_3$]



Inside a N2 filled glovebox, **[Li$_2$(thf)$_x$][1]** (1.00 eq., 200 mg, 240 µmol) was dissolved in toluene (3.5 mL) and AuCl(PPh3) (1.00 eq., 119 mg, 240 µmol) was added in portions to the solution over the course of five minutes. The reaction mixture was stirred at room temperature for 30 minutes, filtered over a PTFE syringe filter (pore size 0.22 µm), the solvent removed in vacuo, and the residue dried at reduced pressure for > 12 hours. Toluene (~0.5 mL) was added dropwise to the solid residue until the substance was barely covered with solvent. The suspension was treated with *n*-hexane (3 mL) and centrifuged. The supernatant was removed *via* pipette, the solid was washed with *n*-hexane (1.5 mL) and centrifuged. The supernatant was removed *via* pipette and the washing step was repeated twice more. The solid residue was dried under reduced pressure to afford **[Li(thf)$_x$][1-AuPPh$_3$] x 0.5 tol** as an off-white solid (138 mg, 114 µmol, 47% yield). Extensive drying over days afforded a toluene-free compound which was used for elemental analysis. Single crystals suitable for X-ray diffraction could be obtained from the crude reaction solution by gas phase diffusion of *n*-pentane at −30 °C.

^{1}H NMR [^{1}H, ^{1}H,^{1}H-COSY] (600.16 MHz, THF-d_8, 295 K): δ[ppm] = 7.45 – 7.33 (*m*, $H_{9,10,11}$, 15H), 7.21 – 7.05 (*m*, tol, 2.5H), 5.90 (*s*, $^{117/119}$Sn-satellites $^4J_{H,Sn}$ = 156.0 Hz, H_2, 8H), 2.31 (*s*, tol, 1.5H), 1.95 (*q*, $^3J_{H,H}$ = 7.2 Hz, H_4, 8H), 1.90 (*q*, $^3J_{H,H}$ = 7.1 Hz, H_6, 8H), 0.79 (*t*, $^3J_{H,H}$ = 7.2 Hz, H_5, 12H), 0.55 (*t*, $^3J_{H,H}$ = 7.3 Hz, H_7, 12H).

^{7}Li NMR (233.25 MHz, THF-d_8, 295 K): δ[ppm] = −2.70 (*s*)

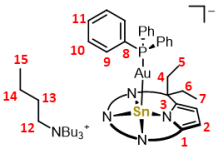
^{13}C NMR [^{13}C, ^{13}C-DEPT135, ^{1}H,^{13}C-HSQC, ^{1}H,^{13}C-HMBC] (150.91 MHz, THF-d_8, 295 K): δ [ppm] = 143.81 (*s*, C_1), 138.60 (*s*, *C* tol), 135.48 (*d*, $^3J_{P,C}$ = 15.1 Hz, C_{10}H), 131.73 (*s*, broad, C_{11}H), 129.83 (*s*,*C*H tol), 129.73 (*d*, $^2J_{P,C}$ = 10.6 Hz, C_9H), 129.07 (*s*, *C*H tol), 126.20 (*s*, *C*H tol), 125.0 (*s*, C_8, only in HMBC), 105.37 (*s*, C_2H), 46.79 (*s*, C_3), 42.52 (*s*, C_4H_2), 36.31 (*s*, C_6H_2), 21.65 (*s*, CH_3 tol), 11.23 (*s*, $C_{5,7}H_3$), 11.21 (*s*, $C_{5,7}H_3$).

^{31}P NMR (242.96 MHz, THF-d_8, 295 K): δ[ppm] = 41.77 (*s*)

^{119}Sn NMR [^{1}H,^{119}Sn-HMBC] (223.81 MHz, THF-d_8, 295 K): δ [ppm] = −70.3 (*d*, $^2J_{Sn,P}$ = 3431.0 Hz).

Anal. calc. for $C_{54}H_{63}AuLiN_4PSn$: C, 57.74; H, 5.66; N, 4.99. Found: C, 57.86; H, 5.58; N, 5.11.

3.2 Tetrabutylammonium (*meso*-octaethylcalix[4]pyrrolato stannate(II))(triphenylphosphine) aurate(I) [NBu_4][1-$AuPPh_3$]



Inside a N2 filled glovebox, **[$Li_2(thf)_x$][1]** (1.00 eq., 100 mg, 120 µmol) was dissolved in toluene (2.0 mL) and AuCl(PPh3) (1.00 eq., 60 mg, 120 µmol) was added in portions to the solution over the course of five minutes. The reaction mixture was stirred at room temperature for 30 minutes, filtered over a PTFE syringe filter (pore size 0.22 µm), the solvent removed in vacuo. The residue and NBu_4Cl (1.00 eq., 33.4 mg, 120 µmol) were dissolved in 2 mL *o*DFB and stirred at room temperature for one hour. After second filtration over a syringe filter (pore size 0.22 µm) a part of the solvent was removed in vacuo until a precipitation occurred. Addition of excess *n*-hexane (~3 mL) caused the precipitation of a solid. Centrifugation and washing with ~1.5 mL *n*-hexane followed by drying at reduced pressure over night afforded **[NBu_4][1-$AuPPh_3$]** as an off-white solid (138.4 mg, 102 µmol, 85% yield). Low-quality single crystals suitable for X-ray diffraction could be obtained from a *o*DFB solution by gas phase diffusion of *n*-pentane at −30 °C.

^{1}H NMR [^{1}H, ^{1}H,^{1}H-COSY] (600.16 MHz, THF-d_8, 295 K): δ[ppm] = 7.48 – 7.37 (*m*, $H_{9,10,11}$, 15H), 5.88 (s, H_2, 8H), 2.64 – 2.57 (*m*, H_{12}, 8H), 2.09 (*q*, $^2J_{H,H}$ = 7.2 Hz, H_6, 8H), 2.01 (*q*, $^2J_{H,H}$ = 7.2 Hz, H_4, 8H), 1.30 – 1.24 (*m*, H_{13}, 8H), 1.23 – 1.16 (*m*, H_{14}, 8H), 0.98 (*t*, $^2J_{H,H}$ = 7.2 Hz, H_5, 12H), 0.84 (*t*, $^2J_{H,H}$ = 7.2 Hz, H_7, 12H), 0.44 (*t*, $^2J_{H,H}$ = 7.3 Hz, H_{15}, 12H).

^{13}C NMR [^{13}C, ^{13}C-DEPT135, ^{1}H,^{13}C-HSQC, ^{1}H,^{13}C-HMBC] (150.91 MHz, THF-d_8, 295 K): δ [ppm] = 144.43 (*s*, C_1), 135.34 (*d*, $^3J_{P,C}$ = 15.1 Hz, C_{10}H), 132.02 (*s*, $^4J_{P,C}$ = 3.0 Hz, C_{11}H), 129.93 (*d*, $^2J_{P,C}$ = 10.6 Hz, C_9H), 125.98 (*s*, broad, C_8), 104.90 (*s*, C_2H), 58.46 (*s*, $C_{12}H_2$), 46.15 (*s*, C_3), 42.56 (*s*, C_6H_2), 32.75 (*s*, C_4H_2), 24.92 (*s*, $C_{13}H_2$), 20.85 (*s*, $C_{14}H_2$), 14.42 (*s*, C_7H_3), 11.32 (*s*, C_5H_3), 10.64 (*s*, $C_{15}H_3$).

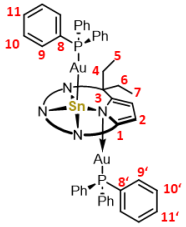
^{31}P NMR (242.96 MHz, THF-d_8, 295 K): δ[ppm] = 43.18 (*s*)

^{119}Sn NMR [^{1}H,^{119}Sn-HMBC] (223.81 MHz, THF-d_8, 295 K): δ [ppm] = −75.4 (*d*, $^2J_{Sn,P}$ = 3166.9 Hz)

Anal. calc. for $C_{70}H_{99}AuN_5PSn$: C, 61.87; H, 7.35; N, 5.16. Found: C, 61.51; H, 7.32; N, 4.86.

MS (ESI(-), THF): calcd. for $C_{54}H_{63}AuN_4PSn$ **[1-$AuPPh_3$]**$^-$: 1115.350 *m/z*. Found: 1115.327 *m/z*.

3.3 *Meso*-octaethylcalix[4]pyrrolato stannate(II) *bis*-(triphenylphosphine gold(I)) [1-(AuPPh$_3$)$_2$]



Inside a N2 filled glovebox, **[Li$_2$(thf)$_x$][1]** (1.00 eq., 200 mg, 240 µmol) was dissolved in toluene (3.5 mL) and AuCl(PPh3) (1.95 eq., 232 mg, 469 µmol) was added in portions to the solution over the course of five minutes. The reaction mixture truned yellow and a colorless precipitant (LiCl) occurred. The solution was stirred at room temperature for 30 minutes, filtered over a PTFE syringe filter (pore size 0.22 µm), the solvent removed in vacuo, and the residue dried at reduced pressure for > 12 hours. The residue was over layered with toluene (2 mL) and the supernatant removed *via* pipette and stored at −30 °C for crystallization. The solid residue was collected and dried under reduced pressure to afford the first product fraction (172 mg, 103 µmol, 43% yield). The second product fraction was collected from the recrystallized supernatant after three days (47 mg, 28 µmol, 12% yield). Both fractions were combined to afford **[1-(AuPPh$_3$)$_2$] x tol** (219 mg, 131 mmol, 55% yield) as a yellow solid. Single crystals suitable for X-ray diffraction could be obtained from the recrystallization mixture at −30 °C.

^{1}H NMR [^{1}H, ^{1}H,^{1}H-COSY] (600.16 MHz, Tol-d_8, 295 K): δ[ppm] = 7.50 – 7.43 (*m*, PPh$_3$, 6H), 7.21 – 7.13 (*m*, PPh$_3$, 6H), 7.12 – 7.07 (*m*, tol, 3H), 7.04 – 6.95 (*m*, PPh$_3$, overlayed with tol and Tol-d_8, 22H), 6.36 (*s*, H_2, ^{117}Sn-satellites $^4J_{H,Sn}$ = 162.0 Hz, ^{119}Sn-satellites $^4J_{H,Sn}$ = 168.0 Hz, 8H), 2.40 (*s*, broad, H_4, 8H), 2.13 (*s*, broad, H_6 overlayed with tol and Tol-d_8, 10H), 0.98 (*t*, $^2J_{H,H}$ = 7.3 Hz, H_5, 12H), 0.89 (t, $^2J_{H,H}$ = 7.3 Hz, H_7, 12H).

^{13}C NMR [^{13}C, ^{13}C-DEPT135, ^{1}H,^{13}C-HSQC, ^{1}H,^{13}C-HMBC] (150.91 MHz, THF-d_8, 295 K): δ [ppm] = 146.64 (*s*, C_1), 138.61 (*s*, *C* tol), 135.34 (*d*, $^3J_{P,C}$ = 13.6 Hz, C_{10}H C_{11}H or C_{10}H'), 135.25 135.34 (*d*, $^3J_{P,C}$ = 15.1 Hz, C_{10}H C_{11}H or C_{10}H'), 130.17 (*s*, $^4J_{P,C}$ = 10.6 Hz, C_{11}H and C_{11}H'), 129.67 (*d*, $^2J_{P,C}$ = 12.1 Hz, C_9H and C_9H'), 129.84 (*s*,*C*H tol), 129.08 (*s*, *C*H tol), 126.21 (*s*, *C*H tol), 132.57 (*s*, broad, C_8), 131.74 (*s*, broad, C_8'), 108.99 (*s*, broad, C_2H), 46.94 (*s*, C_3), 39.7 (*s*, only in HSQC C_6H_2), 33.7 (*s*, only in HSQC C_4H_2), 21.66 (*C*H$_3$, tol), 10.65 (*s*, C_7H_3), 10.59 (*s*, C_5H_3).

^{31}P NMR (242.96 MHz, Tol-d_8, 295 K): δ[ppm] = 44.87 (*s*, $^{117/119}$Sn-satellites $^2J_{Sn,P}$ = 3328.6 Hz, Sn-Au-*P*), 30.98 (*s*¸ N-Au-*P*).

^{119}Sn NMR [^{1}H,^{119}Sn-HMBC] (223.81 MHz, Tol-d_8, 295 K): δ [ppm] = not observed.

^{1}H NMR [^{1}H, ^{1}H,^{1}H-COSY] (600.16 MHz, Tol-d_8, 323 K): δ[ppm] = 7.50 – 7.36 (*m*, PPh$_3$, 6H), 7.22 – 7.09 (*m*, PPh$_3$, 6H), 7.08 – 7.03 (*m*, tol, 5H), 7.03 – 6.97 (*m*, PPh$_3$, 18H), 6.29 (*s*, $^{117/119}$Sn-satellites $^4J_{H,Sn}$ = 168.0 Hz, 8H), 2.34 (*q*, $^2J_{H,H}$ = 7.2 Hz, H_4, 8H), 2.11 – 2.04 (*m*, overlayed with tol and Tol-d_8, 15H), 0.92 (*t*, $^2J_{H,H}$ = 7.2 Hz, H_5, 12H), 0.82 (t, $^2J_{H,H}$ = 7.2 Hz, H_7, 12H).

^{119}Sn NMR [^{1}H,^{119}Sn-HMBC] (223.81 MHz, Tol-d_8, 323 K): δ [ppm] = 39.7 (d, $^{2}J_{Sn,P}$ = 3446.7 Hz).

Anal. calc. for $C_{82.5}H_{90}Au_2N_4P_2Sn$ (x 1.5 tol): C, 57.81; H, 5.30; N, 3.27. Found: C, 57.72; H, 5.42; N, 3.37.

4 NMR Spectra

4.1 [Li(thf)$_x$][1-AuPPh$_3$] x 0.5 tol

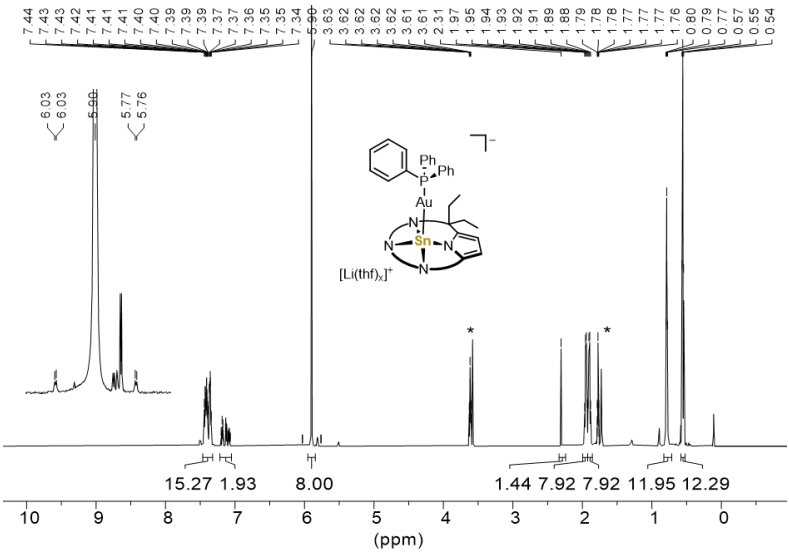


Figure S1. ^{1}H NMR spectrum of **[Li(thf)$_x$][1-AuPPh$_3$] x 0.5 tol** (600.15 MHz, THF-d_8, 295 K). Solvent resonances are indicated by an asterisk (*).

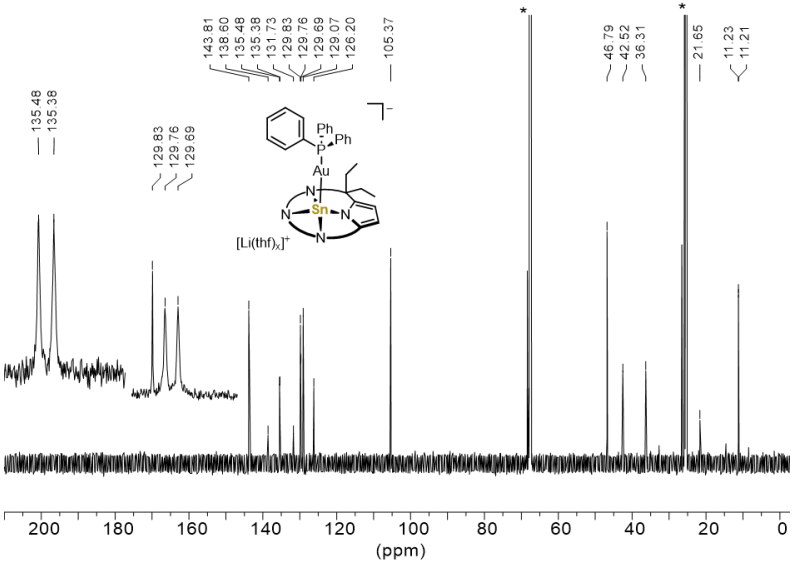


Figure S2. ^{13}C NMR spectrum of **[Li(thf)$_x$][1-AuPPh$_3$] x 0.5 tol** (150.91 MHz, THF-d_8, 295 K). Solvent resonances are indicated by an asterisk (*).

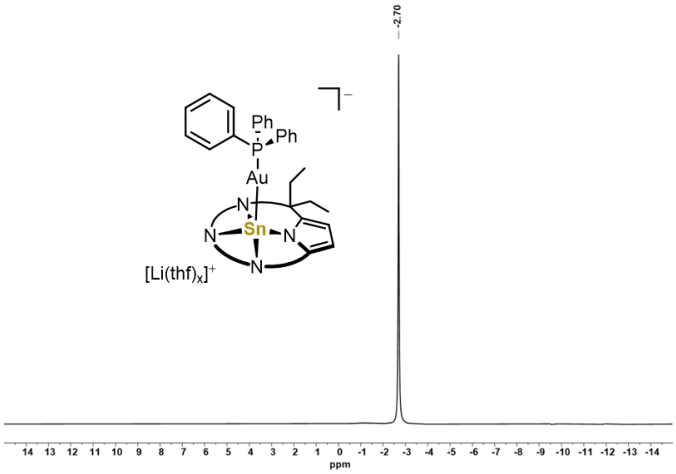


Figure S3. ^{7}Li NMR spectrum of **[Li(thf)$_x$][1-AuPPh$_3$] x 0.5 tol** (233.25 MHz, THF-d_8, 295 K).

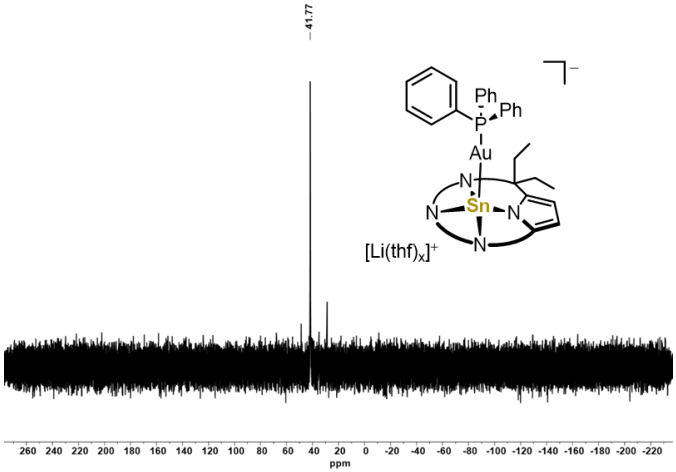


Figure S4. $^{31}P\{^{1}H\}$ NMR spectrum of **[Li(thf)$_x$][1-AuPPh$_3$] x 0.5 tol** (242.96 MHz, THF-d_8, 295 K).

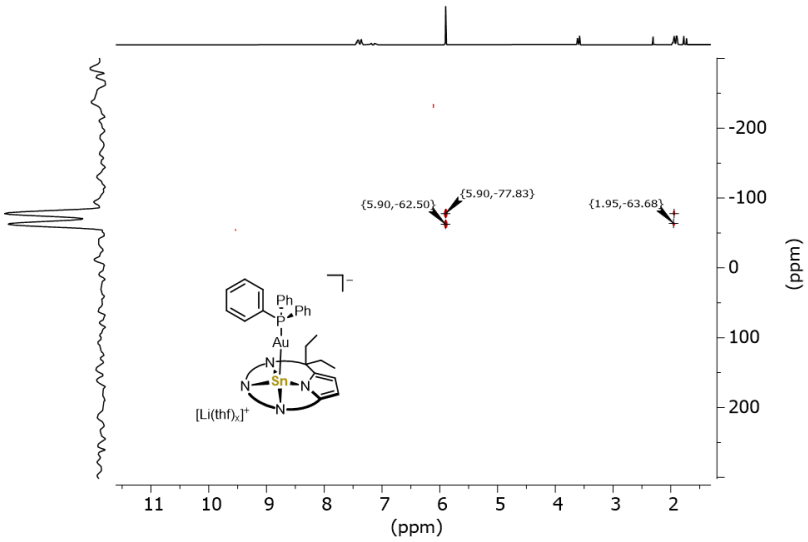


Figure S5. $^{1}H,^{119}Sn$ HMBC NMR spectrum of **[Li(thf)$_x$][1-AuPPh$_3$] x 0.5 tol** (THF-d_8, 295 K).

4.2 [NBu$_4$][1-AuPPh$_3$]

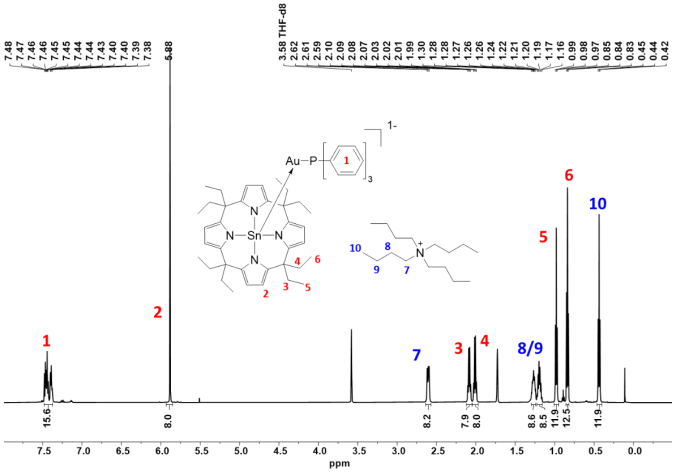


Figure S6. ^{1}H NMR spectrum of **[NBu$_4$][1-AuPPh$_3$]** (600.15 MHz, THF-d_8, 295 K).

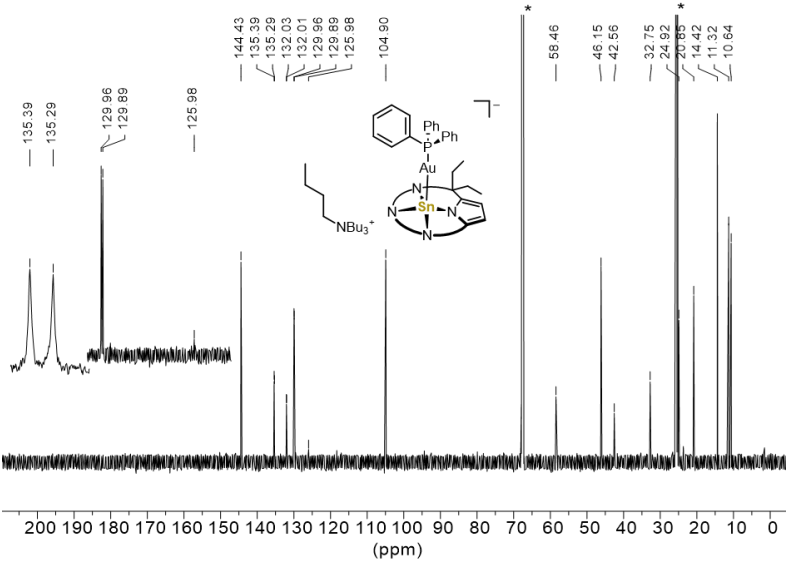


Figure S7. ^{13}C NMR spectrum of **[NBu$_4$][1-AuPPh$_3$]** (150.91 MHz, THF-d_8, 295 K). Solvent resonances are indicated by an asterisk (*).

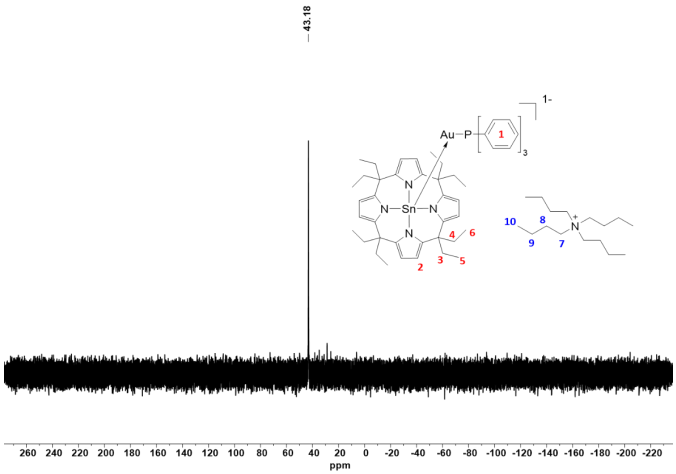


Figure S8. $^{31}P\{^{1}H\}$ NMR spectrum of **[NBu$_4$][1-AuPPh$_3$]** (242.96 MHz, THF-d_8, 295 K).

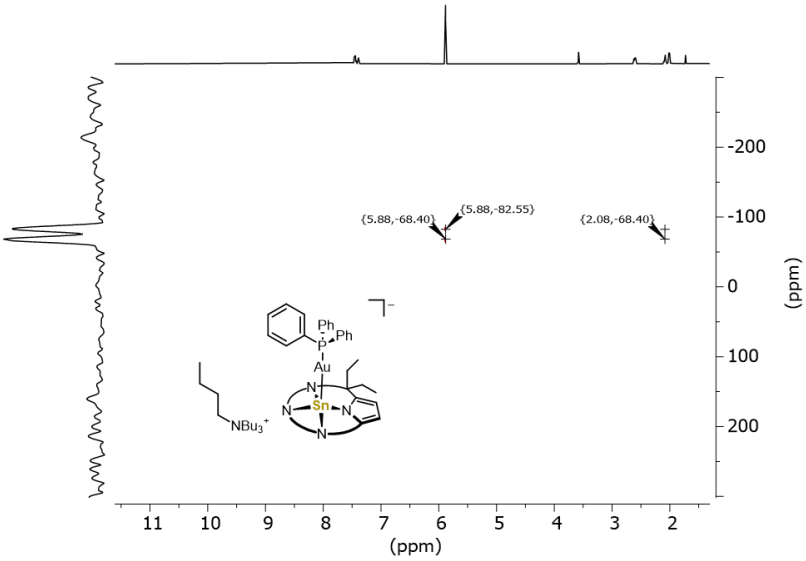


Figure S9. $^{1}H,^{119}Sn$ HMBC NMR spectrum of **[NBu$_4$][1-AuPPh$_3$]** (THF-d_8, 295 K).

4.3 [1-(AuPPh$_3$)$_2$] x tol

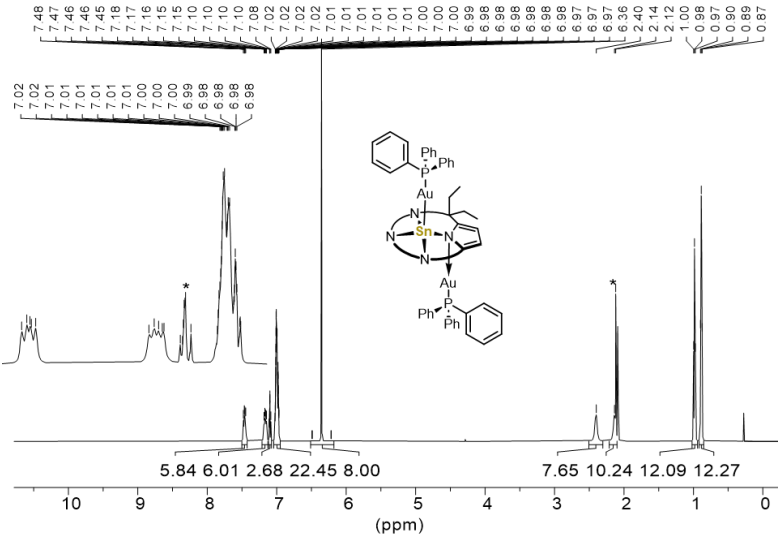


Figure S10. ^{1}H NMR spectrum of **[1-(AuPPh$_3$)$_2$] x tol** (600.15 MHz, Tol-d_8, 295 K). Solvent signals are indicated by an asterisk (*).

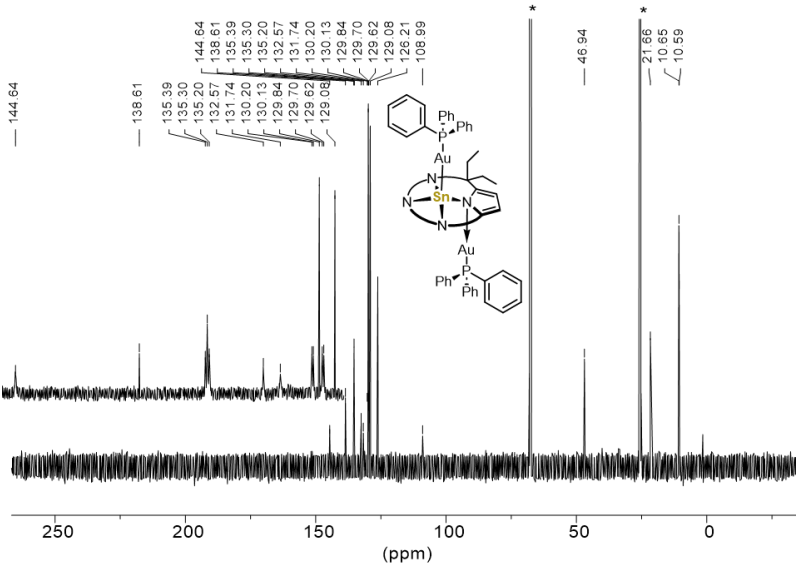


Figure S11. ^{13}C NMR spectrum of **[1-(AuPPh$_3$)$_2$] x tol** (150.91 MHz, THF-d_8, 295 K). Solvent resonances are indicated by an asterisk (*).

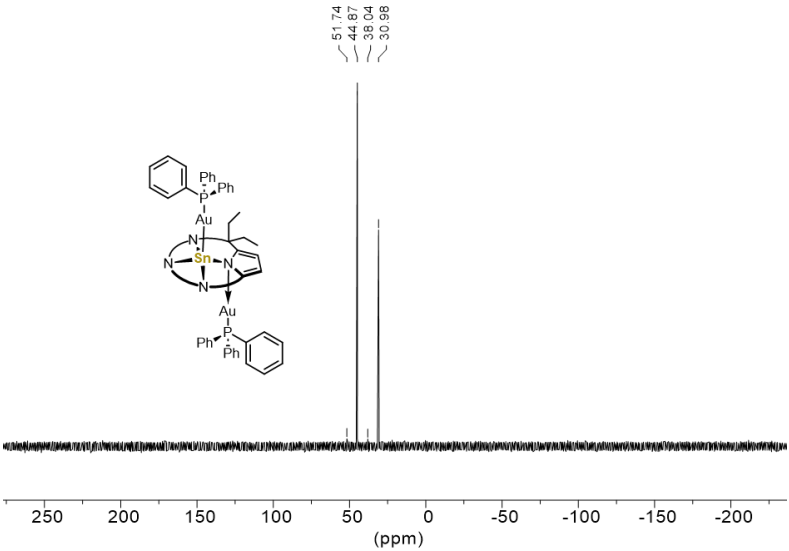


Figure S12. $^{31}P\{^{1}H\}$ NMR spectrum of **[1-(AuPPh$_3$)$_2$] x tol** (242.96 MHz, Tol-d_8, 295 K).

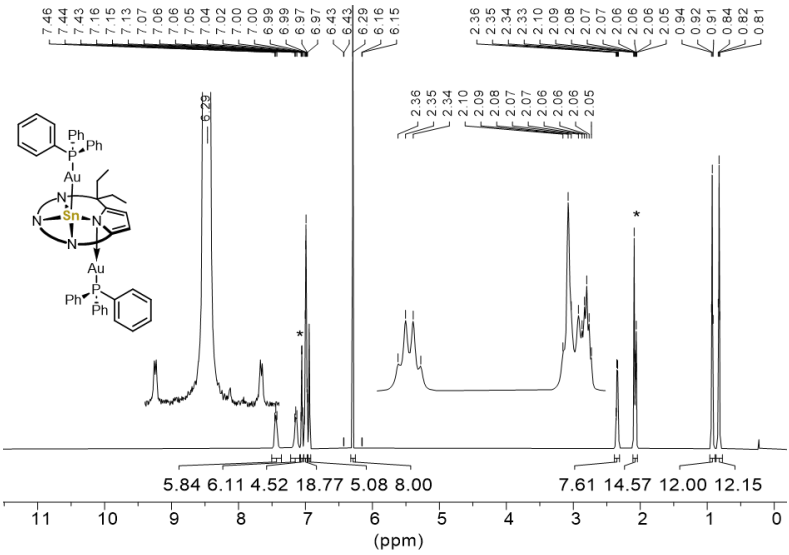


Figure S13. ^{1}H NMR spectrum of **[1-(AuPPh$_3$)$_2$] x tol** (600.15 MHz, Tol-d_8, 323 K). Solvent signals are indicated by an asterisk (*).

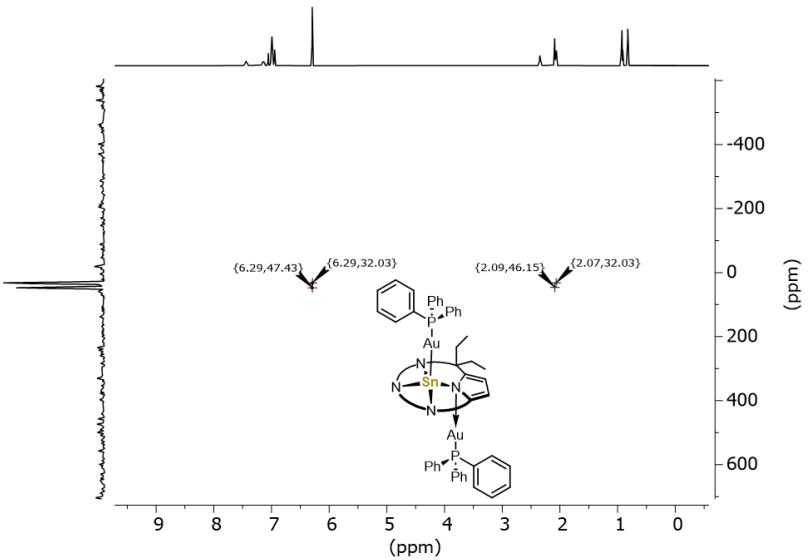


Figure S14. $^{1}H,^{119}Sn$ HMBC NMR spectrum of **[1-(AuPPh$_3$)$_2$] x tol** (Tol-d_8, 323 K).

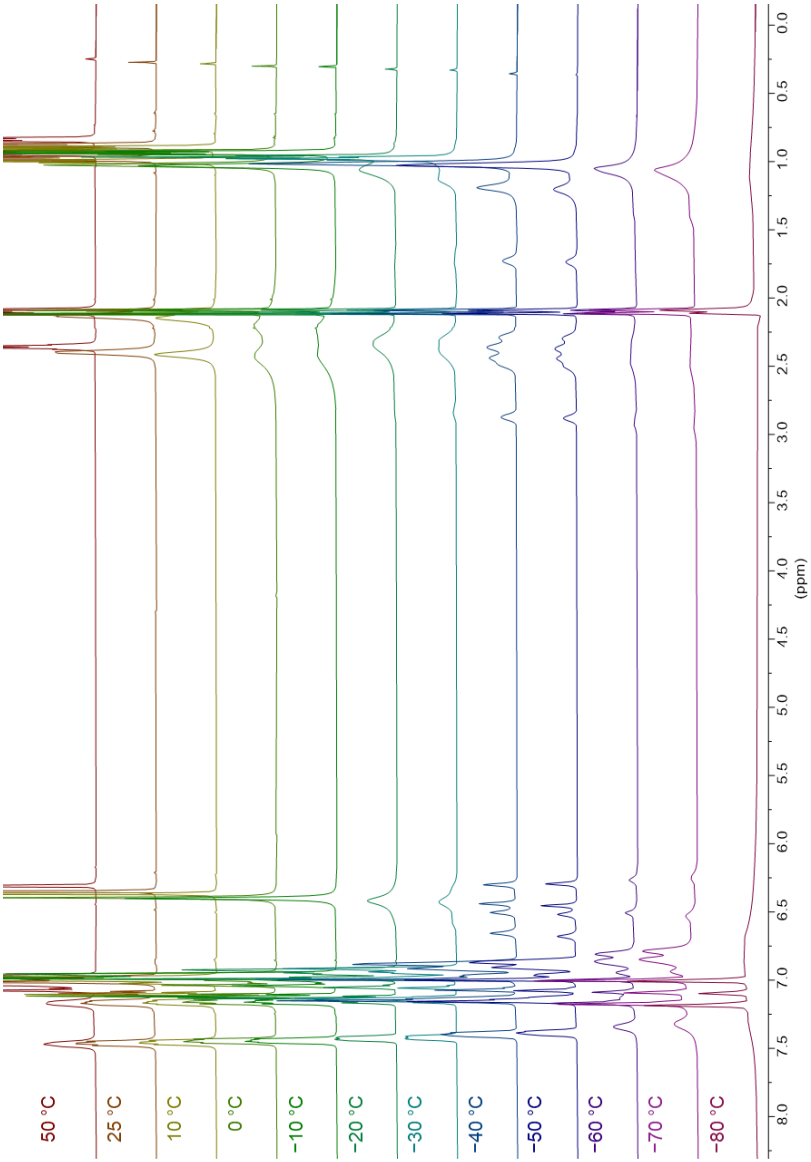


Figure S15. ^{1}H NMR spectrum of **[1-(AuPPh$_3$)$_2$] x tol** at different temperatures between −80 and 50 °C (600.15 MHz, Tol-d_8).

5 Crystallographic Data

5.1 [Li(thf)$_2$][1-AuPPh$_3$]

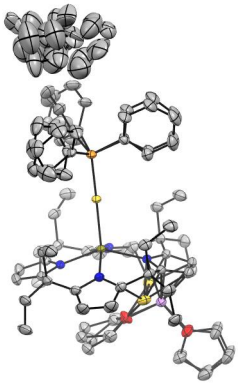


Figure S16: Solid-state molecular structure of **[Li(thf)$_2$][1-AuPPh$_3$]**. Ellipsoids are drawn with a probability of 50%. Hydrogen atoms are omitted for clarity. The molecule co-crystallized with one toluene molecule in its asymmetric unit and 3% of a dinuclear species containing a second Au atom bound by the calix[4]pyrrole ligand backbone.

Table S1: Crystal data for **[Li(thf)$_2$][1-AuPPh$_3$]**.

CCDC number	2358521
Identification code	mo_hr686a
Empirical formula	$C_{69}H_{87}Au_{1.03}Li_{0.98}N_4O_2PSn$
Formula weight	1363.87
Temperature [K]	100(2)
Crystal system	monoclinic
Space group (number)	$P2_1/m$ (11)
a [Å]	13.367(4)
b [Å]	15.364(5)
c [Å]	14.823(5)
α [°]	90
β [°]	92.549(11)
γ [°]	90
Volume [Å^3]	3041.3(16)
Z	2
ρ_{calc} [gcm^{-3}]	1.489
μ [mm^{-1}]	2.967
F(000)	1389
Crystal size [mm^3]	0.232×0.177×0.127
Crystal colour	colourless
Crystal shape	block
Radiation	MoK_α (λ=0.71073 Å)
2θ range [°]	3.82 to 67.46 (0.64 Å)

Index ranges	−20 ≤ h ≤ 20, −24 ≤ k ≤ 24, −23 ≤ l ≤ 23
Reflections collected	169538
Independent reflections	12515, R_{int} = 0.1017, R_{sigma} = 0.0456
Completeness to θ = 25.242°	99.9 %
Data / Restraints / Parameters	12515/989/609
Absorption correction Tmin/Tmax (method)	0.6093/0.7026 (multi-scan)
Goodness-of-fit on F^2	1.085
Final *R* indexes [$I \geq 2\sigma(I)$]	R_1 = 0.0353 wR_2 = 0.0805
Final *R* indexes [all data]	R_1 = 0.0450 wR_2 = 0.0866
Largest peak/hole [eÅ^{-3}]	1.75/−1.10

5.2 [NBu$_4$][1-AuPPh$_3$]

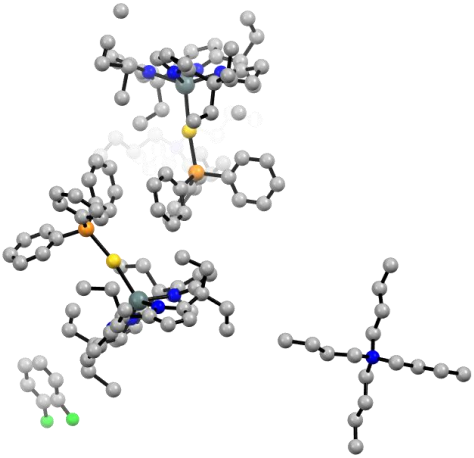


Figure S17: Unrefined solid-state molecular structure of **[NBu$_4$][1-AuPPh$_3$]**. The asymmetric unit contains two **[NBu$_4$][1-AuPPh$_3$]** co-crystallized with one *o*DFB solvent molecule.

5.3 [1-(AuPPh$_3$)$_2$] x tol

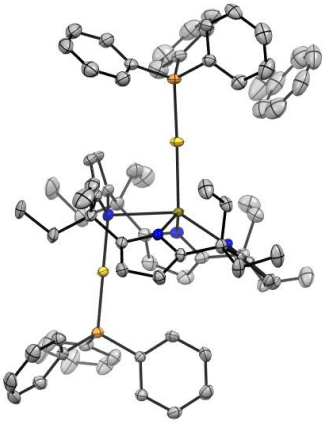


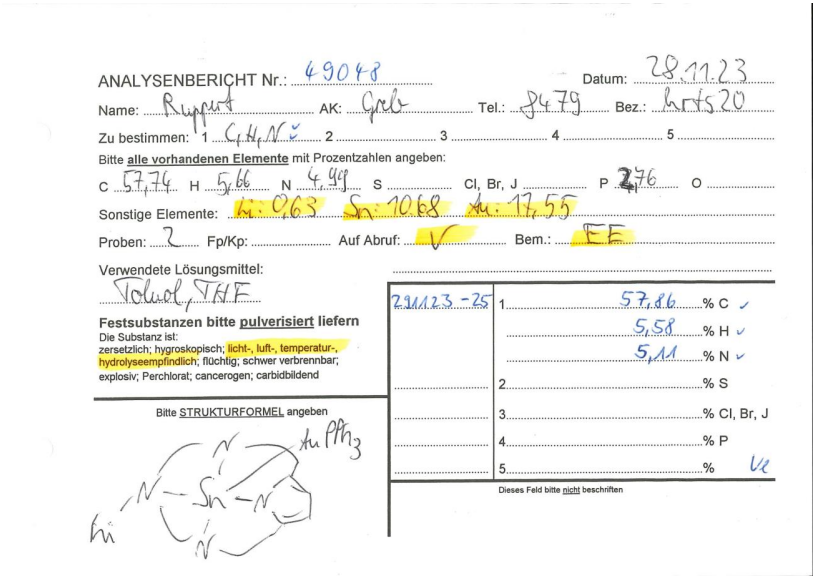
Figure S18: Solid state molecular structure of **[1-(AuPPh$_3$)$_2$] x tol**. Ellipsoids are drawn with a probability of 50%. Hydrogen atoms are omitted for clarity. The molecule co-crystallized with one toluene molecule in its asymmetric unit.

Table S2: Crystal data for **[1-(AuPPh$_3$)$_2$] x tol**.

CCDC number	2358522
Identification code	mo_hrts08_a
Empirical formula	$C_{79}H_{86}Au_2N_4P_2Sn$
Formula weight	1666.08
Temperature [K]	120(2)
Crystal system	monoclinic
Space group (number)	$P2_1/n$ (14)
a [Å]	13.716(4)
b [Å]	19.633(3)
c [Å]	25.253(5)
α [°]	90
β [°]	94.485(13)
γ [°]	90
Volume [Å^3]	6779(2)
Z	4
ρ_{calc} [gcm^{-3}]	1.632
μ [mm^{-1}]	4.778
F(000)	3304
Crystal size [mm^3]	0.132×0.116×0.091
Crystal colour	yellow
Crystal shape	block
Radiation	MoK_α (λ=0.71073 Å)
2θ range [°]	3.88 to 57.00 (0.74 Å)
Index ranges	−18 ≤ h ≤ 18, −26 ≤ k ≤ 26, −33 ≤ l ≤ 33

Reflections collected	189246
Independent reflections	17171, R_{int} = 0.0678, R_{sigma} = 0.0351
Completeness to θ = 25.242°	99.9 %
Data / Restraints / Parameters	17171/122/803
Absorption correction Tmin/Tmax (method)	0.6506/0.7459 (multi-scan)
Goodness-of-fit on F^2	1.102
Final *R* indexes [$I \geq 2\sigma(I)$]	R_1 = 0.0330 wR_2 = 0.0775
Final *R* indexes [all data]	R_1 = 0.0379 wR_2 = 0.0811
Largest peak/hole [eÅ^{-3}]	3.29/−1.12

6 Elemental Analysis



ANALYSENBERICHT Nr.: 49048 Datum: 28.11.23

Name: Ruppert AK: Greb Tel.: 8479 Bez.: Inst 20

Zu bestimmen: 1 $C_4H_4N_2$ 2 3 4 5

Bitte **alle vorhandenen Elemente** mit Prozentzahlen angeben:

C 57,74 H 5,66 N 4,99 S Cl, Br, J P 2,76 O

Sonstige Elemente: Li: 0,63 Sn: 10,68 Au: 17,55

Proben: 2 Fp/Kp: Auf Abruf: ✓ Bem.: EE

Verwendete Lösungsmittel:

Toluol, THF

Festsubstanzen bitte pulverisiert liefern

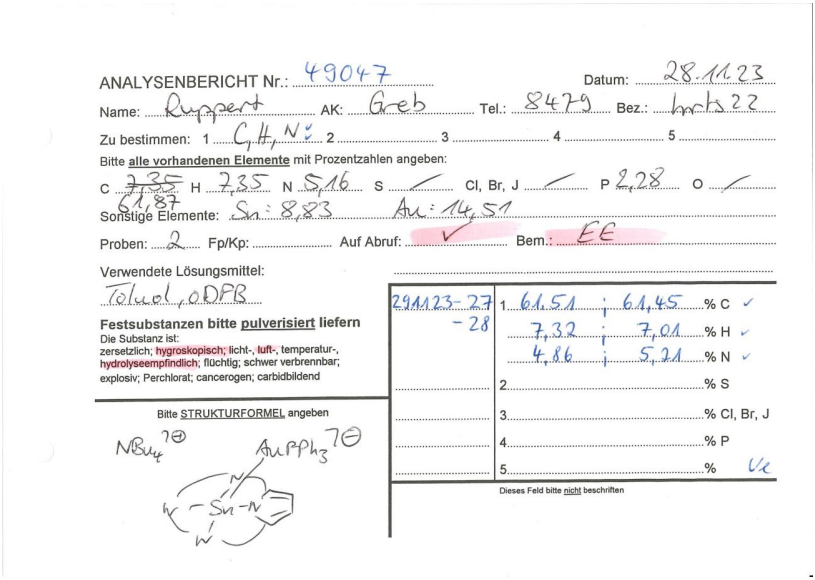
Die Substanz ist:
zersetzlich; hygroskopisch; licht-, luft-, temperatur-, hydrolyseempfindlich; flüchtig; schwer verbrennbar; explosiv; Perchlorat; cancerogen; carbidbildend

Bitte STRUKTURFORMEL angeben

291123-25	1	57,86	% C ✓
		5,58	% H ✓
		5,11	% N ✓
	2		% S
	3		% Cl, Br, J
	4		% P
	5		% Ue

Dieses Feld bitte nicht beschriften

Figure S19. Elemental analysis report for **[Li][1-AuPPh$_3$]**.



ANALYSENBERICHT Nr.: 49047 Datum: 28.11.23

Name: Ruppert AK: Greb Tel.: 8479 Bez.: Inst 22

Zu bestimmen: 1 $C_4H_4N_2$ 2 3 4 5

Bitte **alle vorhandenen Elemente** mit Prozentzahlen angeben:

C 7,35 51,87 H 2,35 N 5,16 S ✓ Cl, Br, J ✓ P 2,28 O ✓

Sonstige Elemente: Sn: 8,83 Au: 14,51

Proben: 2 Fp/Kp: Auf Abruf: ✓ Bem.: EE

Verwendete Lösungsmittel:

Toluol, oDFB

Festsubstanzen bitte pulverisiert liefern

Die Substanz ist:
zersetzlich; hygroskopisch; licht-, luft-, temperatur-, hydrolyseempfindlich; flüchtig; schwer verbrennbar; explosiv; Perchlorat; cancerogen; carbidbildend

Bitte STRUKTURFORMEL angeben

291123-27 -28	1	61,51 ; 61,45	% C ✓
		7,32 ; 7,01	% H ✓
		4,86 ; 5,21	% N ✓
	2		% S
	3		% Cl, Br, J
	4		% P
	5		% Ue

Dieses Feld bitte nicht beschriften

Figure S20. Elemental analysis report for **[NBu$_4$][1-AuPPh$_3$]**.

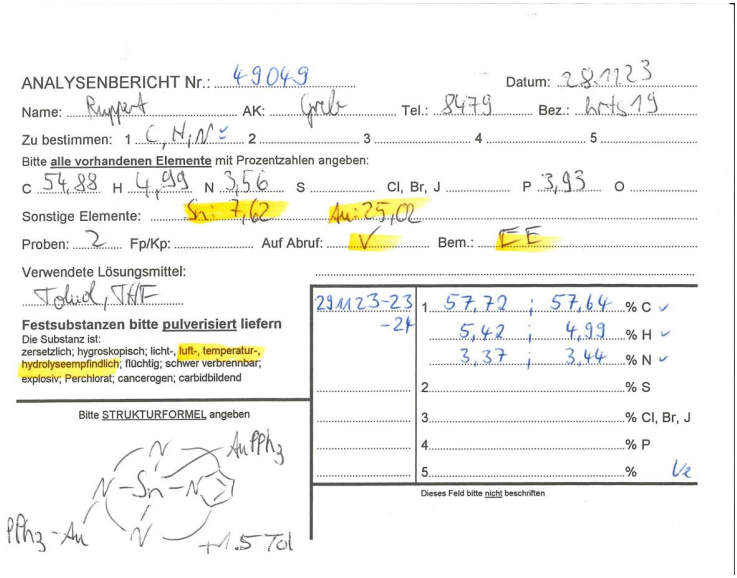


Figure S21. Elemental analysis report for **1-(AuPPh$_3$)$_2$ x 1.5 tol**.

7 NBO Analysis of [1-(AuPPh$_3$)$_2$]

Table S3: NBO analysis results for **[1-(AuPPh$_3$)$_2$]** calculated on PBE0/def2-TZVP//B97M-D4/def2-TVZPP//CREST/GFN2-xTB level of theory (def2-TZVPP for Au atoms). NBO and second order perturbation theory stabilization energies $\Delta E^{(2)}$ for selected bonding interactions are given in kJ mol^{-1}. Additionally, Lewis density parameters $\%\rho_L$ and single point energies are given for each system.

[1-(AuPPh$_3$)$_2$] (single point energy = −4175.515602807946 Eh, $\%\rho_L$ = 98.25)	
d(Sn-Au) [pm]	261.91
WBI for Au1-Sn3 bond	0.5934
WBI for Au1-P4 bond	0.4062
$\Delta E^{(2)}$ P4(σ-lp) (NBO114) → σ*(Au1-Sn3) (NBO318)	613.54
d(N-Au) [pm]	211.97
WBI for Au2-N12 bond	0.2520
WBI for Au2-P5 bond	0.6455
WBI for Sn3-N12 bond	0.1413
Average WBI for residue Sn3-N bonds	0.3411
$\Delta E^{(2)}$ N12(σ-lp) (NBO121) → σ*(Au2-P5) (NBO319)	264.05
$\Delta E^{(2)}$ N12(π-lp) (NBO122) → *p*-orbital Sn3 (NBO315)	38.15
$\Delta E^{(2)}$ N12(π-lp) (NBO122) → *p*-orbital Sn3 (NBO317)	30.79

8 QTAIM Analysis

Table S4: QTAIM analysis results calculated on PBE0-D3(BJ)/ZORA-TZ2P/COSMO(Toluene)//B97M-D4/def2-TVZPP//CREST/GFN2-xTB level of theory.

Compound	**[1-AuPPh$_3$]$^{-1}$**	**[1-(AuPPh$_3$)$_2$]**
Total bonding energy [Eh]	-34.065206566553812	-43.972280605059261
QTAIM charge at Sn	1.794	1.657
Average charge at N	-1.219	-1.222
Sn-Au bond		
QTAIM charge at tin-bound Au	-0.279	-0.199
$\rho(r_{BCP})$ at Sn-Au BCP	0.0757	0.0735
$\nabla^2\rho(r_{BCP})$ at Sn-Au BCP	0.0360	0.0427
$H_b(r_{BCP})$ at Sn-Au BCP	-0.0359	-0.0335
$G_b(r_{BCP})$ at Sn-Au BCP	0.0449	0.0442
$G_b(r_{BCP})/\rho(r_{BCP})$ at Sn-Au BCP	0.6592	0.6014
ellipticity at Sn-Au BCP $\varepsilon = (\lambda_1/\lambda_2)-1$	0.0108	0.0139
DI between Sn and Au	0.8470	0.8347
N-Au bond		
QTAIM charge at N-bound Au	-	0.142
QTAIM charge at N bound to Au	-	-1.200
$\rho(r_{BCP})$ at N-Au BCP	-	0.0105
$\nabla^2\rho(r_{BCP})$ at N-Au BCP	-	0.0323
$H_b(r_{BCP})$ at N-Au BCP	-	-0.0403
$G_b(r_{BCP})$ at N-Au BCP	-	0.0121
$G_b(r_{BCP})/\rho(r_{BCP})$ at N-Au BCP	-	1.1524
ellipticity at N-Au BCP $\varepsilon = (\lambda_1/\lambda_2)-1$	-	0.0615
DI between N and Au	-	0.6679

A variety of descriptors have been used in the context of Bader's theory of AIM, to describe and compare the nature of chemical bonds.[39–42] The main components considered are the electron density, $\rho(r_{BCP})$, and the Laplacian of the density, $\nabla^2\rho(r_{BCP})$ at the bond critical points (bcp's). Low $\rho(r_{BCP})$ and positive Laplacians, as found at the bcp's of the Sn-Au and N-Au bonds suggest closed shell (ionic) interactions, whereas the opposite would indicate shared (covalent) interactions. It should be noted that the $\rho(r_{BCP})$ at the N-Au bond is significantly lower than at the Sn-Au bonds. The total electronic energy density $H_b(r_{BCP})$ serves as a criterion for the bond classification, with negative values for shared-type (covalent) atomic interactions (typical covalent single bonds ≈ -0.35) and positive values in closed-shell bonds.[43] At the bcp's $H_b(r_{BCP})$ values are only slightly negative. In addition, the ratio of $G_b(r_{BCP})/\rho(r_{BCP})$ (Lagrangian kinetic energy per electron) indicates the kind of interatomic interactions, with a value <1 for shared interaction and >1 for closed-shell (ionic) bonding.[44,45] For the Sn-Au bond values <1 could be obtained indicating covalent bonding whereas for the N-Au bond a value >1 could be obtained indicating ionic bonding. The ellipticity ($\varepsilon=\lambda_1/\lambda_2-1$) of a bond quantifies the anisotropy of the electron density, with deviations from a cylindrical distribution leading to values larger than zero. The delocalization index DI is yet another indicator for covalent bonding. In conclusion these results indicate a predominantly shared (covalent) interaction between Sn and Au and a polar (closed-shell) interactios between N and Au.

9 ETS-NOCV Analysis of $[1\text{-}AuPPh_3]^-$

Table S5: ETS-NOCV bond analysis of **$[1\text{-}AuPPh_3]^-$** on the BP86-D3/TZ2P COSMO(Toluene)//B97M-D3(BJ)/def2-TVZPP//CREST/GFN2-xTB level of theory. All values given in kJ mol^{-1}.

Compound	Heterolytic Sn-Au bond cleavage into stannate(II) and gold(I)	Homolytic Sn-Au bond cleavage (preferred)	Heterolytic Sn-Au bond cleavage into stannane and gold(-I)
Total Pauli Repulsion (ΔE_{Pauli}) [kJ mol^{-1}]	719.35	719.73	1339.52
Total Electrostatic Interaction (ΔV_{elst}) [kJ mol^{-1}]	-1104.69	-625.79	-981.40
Total Orbital Interaction ($\Delta E_{oi,tot}$) [kJ mol^{-1}]	-441.73	-311.32	-1253.62
Total Dispersion Energy (E_{disp}) [kJ mol^{-1}]	-99.16	-99.16	-99.16
Solvation Energy (E_{solv}) [kJ mol^{-1}]	-83.96	-85.56	-85.56
Residue [kJ mol^{-1}]	-0.00	0.00	0.00
Total Bonding Energy (ΔE) [kJ mol^{-1}]	-1010.20	-402.11	-1080.22
NOCV 1 [kJ mol^{-1}]	-316.28	-157.63	-1127.64

10 ETS-NOCV Analysis of $[1\text{-}(AuPPh_3)_2]$

Table S6: ETS-NOCV bond analysis of **$[1\text{-}(AuPPh_3)_2]$** on the BP86-D3/TZ2P COSMO(Toluene)//B97M-D3(BJ)/def2-TVZPP//CREST/GFN2-xTB level of theory. All values given in kJ mol^{-1}.

Compound	Heterolytic N-Au bond cleavage (preferred)	Homolytic N-Au bond cleavage
Total Pauli Repulsion (ΔE_{Pauli}) [kJ mol^{-1}]	636.02	1174.61
Total Electrostatic Interaction (ΔV_{elst}) [kJ mol^{-1}]	-782.45	-759.38
Total Orbital Interaction ($\Delta E_{oi,tot}$) [kJ mol^{-1}]	-353.72	-655.98
Total Dispersion Energy (E_{disp}) [kJ mol^{-1}]	-163.68	-163.68
Solvation Energy (E_{solv}) [kJ mol^{-1}]	-16.30	-16.30
Residue [kJ mol^{-1}]	0.00	-0.00
Total Bonding Energy (ΔE) [kJ mol^{-1}]	-680.13	-420.73
NOCV 1 [kJ mol^{-1}]	-163.80	-553.53

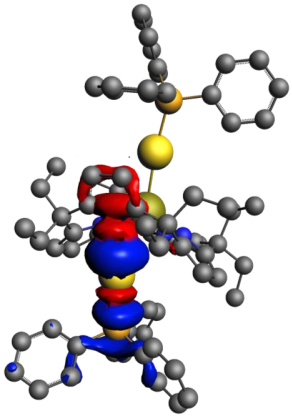


Figure S22. ETS-NOCV deformation density for the preferred dissociation of **1-(AuPPh$_3$)$_2$** into **[1-AuPPh$_3$]$^-$** and **[AuPPh$_3$]$^+$** computed on the BP86-D3/TZ2P COSMO(Toluene)//B97M-D3(BJ)/def2-TVZPP level of theory and sampled at a value of 0.001. The color code of the charge flow is red to blue.

11 Optimized Molecular Geometries

35

Coordinates from ORCA-job au_pph3_cmp_Compound_1

Au	-0.41010480935917	1.18969709254471	-3.42765953956065
P	0.33141885595711	0.37410905807853	-5.41181058451364
C	1.96205961978390	1.01061998725624	-5.75148958070638
C	0.39188098294394	-1.40648888311762	-5.33533612976200
C	-0.78031526159104	0.87549363266764	-6.71285325525573
C	1.51348561789445	-2.09837177644978	-5.78269943152581
C	-0.72070436125234	-2.10272459457331	-4.86523737747553
C	2.93350493992084	0.96052895104968	-4.75299822764108
C	2.28018961439754	1.50303760841235	-7.01397864445786
C	-1.13347703838153	2.22019307517698	-6.81795058127185
C	-1.25198922406635	-0.04698706538353	-7.64202468385110
C	-2.06710991553912	0.38125548409874	-8.67514183504777
C	-1.94304439156807	2.63802422548533	-7.85360643154750
C	-2.41147049284637	1.71774264453687	-8.78124864492802
H	-2.21619192359653	3.67514866578298	-7.93530141909473
H	-3.04930156772025	2.04533147533395	-9.58334753644034
H	-0.77643338156055	2.93155631790650	-6.09125493142710
H	-0.98251035817015	-1.08472344266836	-7.56259663608534
H	-2.43154650821802	-0.33049598745189	-9.39460232971886
C	4.21633699331875	1.39154818845512	-5.02132565809367
C	3.56865728847424	1.93634478711327	-7.27224560701915
C	4.53300104603939	1.88185594994100	-6.28053306188031
H	3.81544223496016	2.31811161422633	-8.24715440947809

H	5.53138245950905	2.22715899019390	-6.48426806723132
H	1.53314394248912	1.54203842658635	-7.78615673144671
H	2.68326995928479	0.58829116585683	-3.77303617668147
H	4.96556482031195	1.35654883946515	-4.25036100838256
C	1.51291024420765	-3.48206475532427	-5.76518170972824
C	-0.71326056031232	-3.48216201780900	-4.85543945456317
C	0.40476846241677	-4.17167873013234	-5.30395419412822
H	0.41155851858481	-5.24740383738316	-5.28722996053505
H	2.37882006276924	-4.01833816192432	-6.11109053628174
H	-1.58345902855745	-1.56474466318162	-4.50772895972549
H	-1.57075644685139	-4.01990825941670	-4.49152371167226
H	2.37398960632691	-1.56376400535257	-6.14284295284090

89

Coordinates from ORCA-job sn2_cxet_CREST_cmp_Compound_1

N	0.00146046114751	-2.15945774880615	0.23256607836606
C	1.10051938770565	-2.87007272665649	0.63725678316802
C	0.70707951466465	-3.99778914936894	1.32378225080030
C	-0.70171641850068	-3.99877563109081	1.32369078934678
C	-1.09665107842253	-2.87161459531045	0.63710081868456
H	1.34380470272526	-4.74031854976150	1.76670075798291
H	-1.33745370283250	-4.74219831053081	1.76652396332030
C	2.48211559839732	-2.47773747783230	0.20990923323699
C	3.49095258739107	-3.48819468963652	0.77202933261455
H	3.10991791368380	-4.48911938661615	0.59187795302189
H	3.51613502859803	-3.36971253206526	1.85221415594434
C	4.89852081836474	-3.40368160741175	0.20566095080779
H	4.94173632658559	-3.77502639214329	-0.81549954929264
H	5.58646791191150	-4.00870746425827	0.79472822519802
H	5.26803081637831	-2.38493271438773	0.20133406946914
C	2.54914589773037	-2.50189157784444	-1.33678912474883
H	3.53631033259941	-2.16394357347475	-1.64954460514981
H	1.85621168014447	-1.76190311608036	-1.72074676528210
C	2.22227308552039	-3.84362890679154	-1.96031261441181
H	2.94580158431085	-4.61079617737143	-1.69176240730752
H	2.20932004168384	-3.77435397878671	-3.04642927840483
H	1.24739673934866	-4.19135209720460	-1.63291046610452
C	2.81850033746619	-1.09677827729822	0.68532035448528
C	3.81113901540427	-0.70214925899446	1.55509178609203
C	3.81021752458071	0.70744148735632	1.55496524291548
C	2.81701290404084	1.10061179964041	0.68518640719173
N	2.18205761888478	0.00145338580555	0.17457447415856
H	4.48259544460428	-1.33933716382265	2.10009076334345
H	4.48083529507424	1.34562020622477	2.09984533907635
C	2.47875674320791	2.48106121730229	0.20966364835422
C	3.48624478847994	3.49290354725565	0.77171191956447
H	3.10396048636425	4.49330711866491	0.59133032687721

H	3.51147504137460	3.37465006072714	1.85191880680293
C	4.89396361114561	3.41009330141921	0.20549541396801
H	5.58105495408682	4.01618161324332	0.79446997057464
H	4.93677157217528	3.78126664673932	-0.81574325577850
H	5.26484244672536	2.39183135459143	0.20143229200785
C	2.54574622052770	2.50519277047786	-1.33703356891877
H	3.53342914249160	2.16874763672526	-1.64977840107389
H	1.85399122723298	1.76408179248450	-1.72095455125617
C	2.21684726758554	3.84639341852258	-1.96065162604034
H	1.24151606261132	4.19274817194279	-1.63315428025716
H	2.20385971687748	3.77700496857285	-3.04675986205493
H	2.93929378484526	4.61463560502304	-1.69225743760175
C	-2.47875957054999	-2.48111942008758	0.20970613972200
C	-3.48625788177375	-3.49293922466167	0.77177645659421
H	-3.51146569728488	-3.37468095367016	1.85198326192239
H	-3.10400039930723	-4.49335184824493	0.59139098881632
C	-2.54574610827870	-2.50528135268650	-1.33699088635447
H	-1.85399331731110	-1.76417513660901	-1.72092547419335
H	-3.53342969756821	-2.16884563303377	-1.64974415345597
C	-2.21684072081353	-3.84649301239378	-1.96058184314530
H	-2.93928647393180	-4.61473190846219	-1.69217694769290
H	-1.24151013111349	-4.19283918923970	-1.63307331808452
H	-2.20384788055576	-3.77712476114911	-3.04669128728104
C	-4.89398637744303	-3.41009501081510	0.20559021615922
H	-4.93682604574921	-3.78126619421479	-0.81564765809895
H	-5.26484042383191	-2.39182314105170	0.20153667284690
H	-5.58107956675141	-4.01616638760786	0.79457993232723
C	-2.81701561621648	-1.10066037056898	0.68519641220716
N	-2.18205832921331	-0.00151412751994	0.17456133655218
C	-2.81850461363941	1.09672942563747	0.68527814900457
C	-3.81113433615690	0.70212034067238	1.55506899159513
C	-3.81023984049497	-0.70747028472910	1.55494361450533
H	-4.48258075606175	1.33932135303071	2.10006464758137
H	-4.48087431987757	-1.34563625207074	2.09981883174684
C	1.09664679676033	2.87156220715606	0.63704516337957
C	0.70170817072235	3.99874368539667	1.32359897187702
C	-0.70708768293925	3.99774647904022	1.32369999121822
C	-1.10052321221156	2.87002054522945	0.63718808127150
N	-0.00146211645405	2.15939694209807	0.23251828348839
H	1.33744345207391	4.74218173474762	1.76640978808336
H	-1.34381606779932	4.74028173251499	1.76660464819610
C	-2.48211724982832	2.47767960234103	0.20984039447030
C	-3.49095059699381	3.48815228883901	0.77193776595192
H	-3.10989634601945	4.48907072023090	0.59179079544085
H	-3.51615579990110	3.36967411454741	1.85212266109606
C	-2.54914519271008	2.50181071913241	-1.33685893830621
H	-1.85620639768312	1.76182142632844	-1.72080501185885

H	-3.53630746013828	2.16385235397531	-1.64961005908027
C	-2.22228108217756	3.84354121804735	-1.96040133076513
H	-1.24740809382613	4.19127561163648	-1.63300167408366
H	-2.94581607910251	4.61070703362681	-1.69186361556243
H	-2.20932502372491	3.77425098326358	-3.04651701226361
C	-4.89850816711868	3.40366141534296	0.20553930636864
H	-5.58645751888924	4.00870116247217	0.79458973890425
H	-5.26803542725029	2.38491937835206	0.20120695175761
H	-4.94169555116043	3.77500431920642	-0.81562330234565
Sn	0.00000249327322	-0.00004102112298	-0.74809663750263

124

Coordinates from ORCA-job sn2_cxet_au_pph3_cmp_Compound_1

N	0.24578412762100	0.63036583158428	-0.19438763892561
C	1.31930888437327	-0.17413962353621	-0.49670307175367
C	0.87988439654947	-1.46654091027149	-0.66084550449001
C	-0.51102545260010	-1.46271563146202	-0.43700653749878
C	-0.87530780882160	-0.16434647849700	-0.16699866771773
H	1.49159249759444	-2.32728392977492	-0.85688090760841
H	-1.15064475800786	-2.32384386064197	-0.40386805472587
C	2.74955404551714	0.29599057063373	-0.52656977600112
C	3.57954379856787	-0.69880297651442	0.31201415846560
H	4.62104836385308	-0.39336149634210	0.29023316104429
H	3.54363562767998	-1.66393220937106	-0.19074384283813
C	3.13005251696438	-0.85638625304421	1.75013814761574
H	3.14274833114179	0.09697852847477	2.26586256526671
H	3.78458516865068	-1.54047892147211	2.28536675607797
H	2.12066180044296	-1.24939434482216	1.80045197169532
C	3.25918718549154	0.22029216120316	-1.99294865218655
H	2.64982692522194	0.90423182313610	-2.57997959243908
H	3.03437059426250	-0.77928699357378	-2.36676848115630
C	4.72038315617657	0.55207850280822	-2.21841161131985
H	4.96737386494558	1.52082309033488	-1.79805101713530
H	4.94537806056260	0.58299196052040	-3.28270715870109
H	5.38338917680170	-0.18277105138999	-1.77134652995395
C	2.94995257265684	1.68312130112417	0.01309905000956
C	4.05107676085785	2.14873845789432	0.69334062453328
C	3.89024695977505	3.53437447645042	0.85529749179144
C	2.69852904988711	3.87781051093374	0.26156237564376
N	2.11362736184747	2.74836955078122	-0.24743508715981
H	4.88636369327917	1.56565207082638	1.02880322785405
H	4.56748574145898	4.20118264318404	1.35319803541331
C	2.03410951361633	5.22334231697578	0.30547207815985
C	1.25622146909940	5.28630548607982	1.65408006743618
H	0.65990614605838	4.38060760329315	1.72857224993617
H	1.99296358251970	5.23364769057276	2.45538187590391
C	0.34916399551292	6.48651782213380	1.83933495177569

H	-0.10146222773411	6.47099261050302	2.82874756644687
H	-0.45034095226237	6.48742543320343	1.10669650683542
H	0.88562407080880	7.42593493311187	1.73971225014430
C	3.10756074690916	6.31974779013400	0.31137578336749
H	2.61181432569165	7.28190861318704	0.40472307981705
H	3.69710974143085	6.20190074824739	1.21788409716139
C	4.03089049837716	6.33991165622319	-0.89207916895730
H	4.59765976097763	5.41875300934065	-0.96384637995468
H	4.73632927488116	7.16537297573596	-0.82291451265816
H	3.47436187305489	6.45328228055353	-1.81521992519184
C	-2.15388412985894	0.35068969613445	0.41859399364043
C	-1.87058240592811	0.71193699169170	1.90533526666792
H	-2.81836290520472	1.00824722896759	2.35341982561877
H	-1.24100138687594	1.59773540677756	1.90687602435385
C	-3.23056511982395	-0.74352646882446	0.37550958579564
H	-4.07359900091420	-0.40041195034983	0.97142090435033
H	-2.84750986469468	-1.62324845003205	0.88473949605975
C	-3.72382434668954	-1.12997103478979	-1.00670287582105
H	-4.17207034622628	-0.28132841218321	-1.50963890853490
H	-4.47028322170967	-1.91899301200684	-0.94343062884404
H	-2.91507281231268	-1.48901878456382	-1.63358304823592
C	-1.20278370997734	-0.36585601635755	2.73560577549318
H	-0.23480180324763	-0.63038670773058	2.32453428053295
H	-1.79744110717687	-1.27363204982448	2.78988538601586
H	-1.04933079213015	-0.01792411341463	3.75404141671147
C	-2.69037229238520	1.59530778049368	-0.22949159582867
N	-1.91541908753759	2.53775128715869	-0.84996942038944
C	-2.73275468266661	3.58388672774835	-1.21813712142943
C	-4.01645050667202	3.30072958967867	-0.81310369672113
C	-3.98926194428166	2.04646440685776	-0.18197519529821
H	-4.88381235052803	3.91147400078646	-0.97088055645529
H	-4.82454599951994	1.53316987543761	0.25454498068284
C	1.04324690549614	5.48008055081185	-0.78728577445142
C	0.80979487818279	6.64240914868381	-1.48009590054787
C	-0.45038210239289	6.51519576132930	-2.09770907135719
C	-0.95357556781466	5.28646911803087	-1.74716907361374
N	-0.03672120461425	4.64168414733783	-0.94857147914519
H	1.43442191323746	7.51427406655646	-1.49330216227714
H	-0.94997826685470	7.26322596982314	-2.68378628916871
C	-2.29717381409947	4.71400680883773	-2.10647738426373
C	-3.33402700398074	5.85295625685512	-2.02716019476916
H	-4.30179647896863	5.46597962319237	-2.33338625646486
H	-3.06225323032311	6.59424808671867	-2.77565945325632
C	-2.24344285221158	4.23470052032456	-3.58565513056682
H	-2.07756979998237	5.11620052059776	-4.20578999587829
H	-1.35463391350500	3.61884451803702	-3.70590565324388
C	-3.44462040761914	3.45359189276125	-4.07726204029894

H -4.36959136958974 4.01402829270647 -3.97675157514483
H -3.56486199336496 2.53326339258591 -3.51688676738184
H -3.33002348490071 3.19666822757976 -5.12775352672835
C -3.46161185408258 6.52807495075986 -0.67572113730850
H -3.70911540431048 5.81248991513940 0.09953716828496
H -4.24195437458034 7.28579816300244 -0.69725579522706
H -2.53284771407529 7.01234064360505 -0.39566980509106
Sn 0.21005138812765 2.53618964545138 -1.23048869767438
Au 0.43329157001627 1.65688629651220 -3.68884949232719
P 0.46638126810103 0.34930810643002 -5.64947784587321
C 2.00786000055266 0.38412850912241 -6.59341284584025
C 0.27054830988691 -1.39489949261145 -5.22184055235868
C -0.82751123876233 0.74012452106427 -6.85039104935448
C 0.70770609117648 -2.41162664690361 -6.06810417459267
C -0.31281478755042 -1.72170599657002 -4.00177459026661
C 3.18407500323349 0.15205769653043 -5.88223741105087
C 2.07640778496564 0.65692747989045 -7.95321821455434
C -1.21115569274415 2.07279678412644 -6.96669706188360
C -1.44040889212520 -0.21701020844736 -7.65091957254839
C -2.41285565490973 0.15685759550912 -8.56159971045295
C -2.17697055265235 2.44524405026255 -7.88371026179142
C -2.77884508494771 1.48757209223490 -8.68278841095233
H -2.47146328006323 3.47810941979027 -7.95837396564838
H -3.54161684493747 1.77494584004428 -9.38691415300901
H -0.76426980644153 2.81121420408951 -6.32137769063474
H -1.16610961987836 -1.25300232669217 -7.55388936499188
H -2.88820581761442 -0.59184299656284 -9.17318579095100
C 4.40446784056239 0.17544109377778 -6.52676590482630
C 3.30453564880814 0.68794839011906 -8.59480831867418
C 4.46788149256290 0.44439684544823 -7.88625617405523
H 3.34896271400775 0.90234199476155 -9.64973393056099
H 5.42119695576005 0.47221109933208 -8.38677767114392
H 1.17519539695047 0.84706220936473 -8.51002959303872
H 3.13777828902532 -0.03827983912070 -4.82249628067925
H 5.30614512150050 -0.00309978813342 -5.96558233804048
C 0.53700229777635 -3.73537220822491 -5.71052266041474
C -0.48013441880147 -3.04899679528539 -3.64751465790552
C -0.06304489137333 -4.05442200285190 -4.50092292832869
H -0.18678112582122 -5.08685129703346 -4.21867318904831
H 0.87936713159880 -4.51708819948354 -6.36826392607989
H -0.60998017792524 -0.94908561169856 -3.31160461626982
H -0.91441501913393 -3.28177612970415 -2.69122301726757
H 1.19243109609229 -2.16350866994277 -6.99774648139601

159
Coordinates from ORCA-job dinuclear_sn2_cxet_au_pph3_cmp_Compound_1
Au 8.30895800430331 8.72140553153531 3.38233346642125

Au	10.43192214920322	13.03144818327604	6.07824380499666
Sn	9.90634821593337	10.78748231826767	3.58116873562184
P	6.56256379959948	7.15565391116500	3.38799099153748
P	11.60978967841157	14.95309710230982	6.02397062443810
N	8.49672750530049	12.46937555995849	3.54364038372092
N	11.89005970118948	10.47267886268578	4.40635193355698
N	10.87774531182944	11.72182373190685	1.93951190213984
C	8.06888433990234	11.00041766334978	6.03967705556217
C	8.58362154953038	13.45069614134114	2.58026043562656
C	9.98273726069927	9.98457454546743	6.55806286786807
N	9.44322744053620	11.15654565475829	6.05922204968709
C	8.97169147910115	9.09516621742068	6.79506104531804
H	9.07973812232257	8.09565916537742	7.16512394382789
C	12.07202467120836	11.28074113045470	1.41189580513828
C	11.43726100575869	9.87914872241421	6.84214751293101
C	7.82427485573250	13.00839494755359	4.62503208428100
C	10.25425047436691	12.48359008838088	0.97465388560984
C	6.92893129599117	5.48769279462688	2.80690979016722
C	7.75809884131926	9.73757578038266	6.46724422867602
H	6.77749683728804	9.31547991988546	6.54873824122425
C	13.02847630423016	10.62183938890419	3.63871559479502
C	6.87187403273378	12.97526212385875	6.92126211565089
H	6.31718500111584	13.86072953066175	6.62559459983203
H	7.82395621327865	13.33017601811537	7.31178926412189
C	7.18113451561299	12.13512132042654	5.66461295027652
C	8.90189877940366	13.09131576555925	1.16056272579319
C	11.82181372000640	8.39336384447156	7.01338188867048
H	12.83247947639846	8.36947344194219	7.41479916300734
H	11.18179293605262	7.94684401674929	7.77039643499768
C	12.79095601016060	15.06745269285476	7.38461154613486
C	4.09723444592344	6.80883331942213	2.11918138759936
H	4.19069163970425	5.76504945255044	2.36528335994341
C	12.27891762302846	10.44937629000116	5.73202786057465
C	4.79833214812408	7.54163096810062	5.52621478250320
H	4.14408777950530	8.03171632434796	4.82719529138705
C	7.54840806993013	14.32811290032553	4.35968850381399
H	7.00498723994748	15.00512389755610	4.98805408164433
C	8.02267003621053	14.60626049037731	3.06452070460576
H	7.90840882567858	15.53167131658699	2.53741699477348
C	11.76393964371186	10.61751547893067	8.16236693028855
H	12.82738966592338	10.50239806119728	8.35906091367382
H	11.60282269848258	11.68146679178529	8.00302076216976
C	5.98311889807896	6.96676796728291	5.08524740978429
C	13.64430795436825	13.98250900979873	7.57472888123087
H	13.56681671761482	13.11992324560558	6.93149216744595
C	2.84054616837460	8.60498373709594	1.14554036082218
H	1.95902765431236	8.95566014304493	0.63639279312511

C	10.97437746629341	10.17537704294440	9.37644461312488
H	9.90698627626278	10.28392944065329	9.21533668632959
H	11.24489079156388	10.77672658101862	10.23914103580347
H	11.16163687631464	9.13812276686540	9.63628335110309
C	5.11405189990028	7.69722176729247	2.45469144074763
C	11.77172407515896	7.56942816658691	5.74439329872567
H	12.52345786215255	7.89901133850055	5.03894481893081
H	10.80692659734076	7.64916879409995	5.25220478568514
H	11.95289980856406	6.52004452463123	5.95896772373331
C	13.64003669480648	10.62315956739966	5.79332600413115
H	14.24007827351919	10.58039176758810	6.68183605950694
C	13.02425673672099	10.39664665596419	2.15393728462636
C	12.59356677640959	8.92300396909318	1.88279070131900
H	12.45035559951746	8.82339160943929	0.80864677290030
H	11.61400559689834	8.76443356227488	2.33077279713710
C	2.96723701480612	7.26176572830526	1.46443811471949
H	2.18617189759627	6.56835053998056	1.20297028183854
C	7.83787283007713	5.34645461559275	1.76299948641187
H	8.33197253596761	6.21936906577985	1.36907825495404
C	10.59876841357148	16.44489629312845	6.10506800787482
C	7.49742078279808	2.97386762923448	1.77307365832457
H	7.72026097997752	1.99854335291088	1.37529264253095
C	4.98820591518497	9.04044169415296	2.11825063017923
H	5.78077078097964	9.72848305805066	2.35971316581419
C	12.10500446142325	14.57000351934647	3.35093285648032
H	11.14736589748966	14.07868433541458	3.33987880466998
C	14.11362562794239	10.72400750797553	4.47360140373062
H	15.13780052872521	10.82251645939353	4.17601895357188
C	12.60867553149128	15.09544322471889	4.53520818006700
C	8.74381117228389	14.32084383410271	0.25468980181057
H	7.74336175597021	14.71378849427962	0.40511781862229
H	8.77298238585882	13.97864333165503	-0.77770287735821
C	5.88311496955347	11.54390252410971	5.06651197661356
H	6.17453300581077	10.99121879047070	4.17654471201631
H	5.48148477024333	10.80617176819548	5.75619753907692
C	6.40770285405078	12.35447562747171	0.96483150435649
H	6.11477740306690	13.30286428647031	0.52720936025919
H	6.20112408344170	12.40665110134502	2.02883649963722
H	5.76885656559130	11.59018344745235	0.53134480098220
C	3.85077892532741	9.49276832354199	1.47232601328268
H	3.76176914465590	10.53541355198411	1.22133052014242
C	7.86212517916204	12.02531129781136	0.70181335035287
H	8.02839690876538	11.85701498990620	-0.36070240622966
H	8.10389253019497	11.08261935962441	1.19074170011572
C	11.03397902305994	12.49919005931091	-0.15225215454492
H	10.82083388178595	13.02813981285936	-1.06054829110062
C	6.82888964295784	6.35117390154874	6.00467850379465

S33

H 7.76193788329462 5.92534953120607 5.67423350216405
C 6.11310885935211 12.25321630863905 8.01421938572285
H 5.11849755475628 11.95944631047256 7.69106075238927
H 5.99191243059507 12.89660405644043 8.88028655232290
H 6.63374891103431 11.35758025386405 8.33448596068453
C 6.31565424250146 4.35742008213279 3.33741114871037
H 5.62600000595686 4.45528921554362 4.15814775452827
C 8.11562913515353 4.09519782517572 1.24454771938579
H 8.82081899962134 3.99571529621625 0.43741771847331
C 12.18312240952225 11.73513687988735 0.12347148064496
H 13.01405337378355 11.57362795482964 -0.53410376565981
C 4.46270408497218 7.49758353980895 6.86941731142826
H 3.54609007073830 7.95321923830680 7.20297807544122
C 6.60152036452696 3.10594237213704 2.82149440168078
H 6.12484501602010 2.23488123493537 3.23789932939051
C 6.48622712151673 6.30136688646608 7.34092847934041
H 7.14748811070232 5.82601372593374 8.04497037481859
C 14.58260708672960 14.01173335571364 8.58705179975675
H 15.23984865719979 13.17040474001092 8.72738515375701
C 12.88169410183646 16.17091497530258 8.22088203429172
H 12.22275139819423 17.01000660392831 8.08082423838496
C 12.83493223560580 14.66841591031621 2.18248575705594
H 12.44843826888344 14.22229787218415 1.28420497964160
C 14.67134289644579 15.11515346752154 9.42309208328447
H 15.39979050972718 15.13271658002548 10.21605325974921
C 4.79556022205792 12.53595782726290 4.71862266182585
H 5.14724609815809 13.28900286447836 4.02274644992922
H 4.41846864654416 13.05148952974569 5.59772627451384
H 3.95333777421020 12.02374698069337 4.26169849818953
C 13.54825180511201 7.85567780894186 2.38140715949053
H 13.06776754403343 6.88194456777648 2.38899539454413
H 13.88623488915860 8.06701010768461 3.39052471644024
H 14.42804623242219 7.77615299111295 1.75138406876385
C 5.30361804693517 6.87918030936216 7.77745038012805
H 5.04468849751566 6.85193566412891 8.82190209077642
C 11.02630106385572 17.64463953954711 5.54775596174476
H 11.96699516707762 17.68960216080940 5.02652598754217
C 13.82030613087266 16.19078197174838 9.24057358693826
H 13.88555961780192 17.04734341099073 9.88994685528698
C 14.44245821018859 10.56921282447917 1.58793596555977
H 15.10013074615195 9.90376049530424 2.13660867597063
H 14.43619030888106 10.19190085808813 0.56668209335748
C 15.02645196558343 11.96848762583750 1.60599295772826
H 16.08079416324049 11.93785549541247 1.34354988456867
H 14.93921592384484 12.42797646839996 2.58272671586839
H 14.52825890403333 12.62073921126017 0.90127954796760
C 9.36993047679163 16.38971743938736 6.75235243905474

C 10.23760680515553 18.77660578080729 5.64855976159328
C 13.84920970857771 15.72478305874353 4.54148243788831
C 14.06443897428039 15.30451776238210 2.19026790919150
C 9.75408803530506 15.43911910713230 0.43774844653988
H 10.72444494365244 15.17024757307416 0.04110528332872
H 9.89280284607600 15.69376899524644 1.48156591186061
H 9.42411130098938 16.33490233500004 -0.08134574247777
C 9.01946702733156 18.71833689657221 6.30611249744425
C 14.57068869249872 15.83329328123532 3.36636675431010
H 14.63976239684498 15.37047124891973 1.28226029899580
H 15.53248292083145 16.31791411137000 3.37268412692327
H 14.25331259776163 16.11616077715924 5.45933572954307
H 10.56953618791211 19.70095792977922 5.20728460608551
C 8.58659011346474 17.52409539621078 6.85775748448176
H 8.40457965029730 19.59930080026746 6.37993728398822
H 9.02531293428068 15.45184183566766 7.15345734626218
H 7.63431123292376 17.47201715043259 7.35748956664553

93
Coordinates from ORCA-job dinuc_sn2_cxme_au_pme3_opt
Au 8.23361455791634 8.75906384515333 3.45292451158401
Au 10.41302185241619 12.93225408618721 6.01239057602231
Sn 9.74027788971430 10.90109049685481 3.59504685056879
P 6.82000190249046 6.90286423841195 3.50359178852889
P 11.75182701139955 14.64907545478552 5.44026872845237
N 8.38693320626180 12.64951525070528 3.57752354166172
N 11.67331525830181 10.39912611305696 4.54264400918131
N 10.83170839041624 11.82413658457741 2.02296060237484
C 7.82484234357673 11.16680172587569 6.05094357385839
C 8.53874900440019 13.64050879031285 2.63399862651716
C 9.61152186914424 9.96183221147883 6.58166429589090
N 9.19298217224929 11.20774392441497 6.17766416009893
C 8.52351251573107 9.13415864835872 6.68704358097786
H 8.54074546481124 8.10346163220169 6.98208595186927
C 12.15918995331312 11.60860583970238 1.72076739642119
C 11.04442645366318 9.71785594134591 6.89605045352697
C 7.76236348023670 13.22283375360948 4.67026473160562
C 10.38624431434626 12.84021865201402 1.20497791764539
C 7.18751349361137 5.52495856023939 2.38552329928152
C 7.38396735435471 9.90199936785334 6.34825171284720
H 6.36388131816752 9.56982134391539 6.33824642506061
C 12.85616640122409 10.66826681431240 3.89016096168624
C 6.85823251637649 13.21890139428914 6.99255483861098
C 7.06396055237991 12.39955172359356 5.71479444920115
C 8.97349547609693 13.31750034988875 1.23803428488496
C 11.32182373300509 8.21118499179075 6.87010925521479
C 13.36458572876040 14.67463139701587 6.25478097381995

C	11.95573726248239	10.37268392076496	5.89669573275371
C	7.57445764660905	14.56076808495553	4.42901177571557
H	7.06501700814255	15.25357848579730	5.07017542218049
C	8.06557369555147	14.82694370855316	3.13320753679765
H	8.01556455114896	15.76188267975260	2.61074428266019
C	11.33742067246498	10.23773963310003	8.30657440971421
C	6.77194497402415	6.12719372609386	5.13947004530519
C	5.08019626503281	7.27711390042326	3.16279965051623
C	13.28250895911119	10.66908095884907	6.08415439111051
H	13.80296317300878	10.66519051600939	7.02211330061183
C	12.96032101729643	10.55055873761124	2.40121723529889
C	12.45932076385466	9.16073609950644	1.97062544697456
C	11.05224157884783	16.29608956191991	5.69568217668846
C	13.85648264339966	10.85518353322601	4.80907663658644
H	14.89082748545489	11.03724424933032	4.59365739665788
C	12.12775751667891	14.58793265915903	3.68110425345824
C	8.83125099049482	14.55168084539605	0.36040611056224
C	5.68776192676837	12.01224549818656	5.16222265909792
C	8.04639590808950	12.23232234209156	0.66113916607799
C	11.41527023597451	13.25717420842950	0.40524689606457
H	11.36972169121452	14.03383955070535	-0.33150378277560
C	12.54172056303454	12.47470038965838	0.73289937838939
H	13.51679751152714	12.53979064046306	0.29359482587920
C	14.41735205956751	10.66131256512725	1.97927682448834
H	11.16241295938840	11.30703161504778	8.36776323469044
H	12.36666513046558	10.04523376115943	8.59235019943238
H	10.68931043234929	9.74368698629609	9.02312069878742
H	11.12892046814061	7.80592461261040	5.88233984861718
H	10.69788723906103	7.68661730342519	7.58909334257447
H	12.35988877254548	8.02480355286715	7.12036347444201
H	12.56417951644339	9.04875238052656	0.89553673187498
H	11.41449964091391	9.00637128603194	2.21935504286618
H	13.03193100896343	8.38226698556614	2.46696466829877
H	9.11104779989880	14.31983656863680	-0.66086615040565
H	9.46323944840133	15.36170038879518	0.70824422028307
H	7.80281750427404	14.89494905035692	0.36004884576948
H	8.32298467914595	12.02263720332067	-0.36795852689988
H	7.01205229220350	12.56343404302700	0.69132109295286
H	8.10810525544607	11.30210751228136	1.21692123899759
H	14.50761161489585	10.53682190139449	0.90607387256994
H	15.00612749546869	9.88828403480444	2.46023684452285
H	14.83584690406843	11.62615707917699	2.24394065841256
H	5.79572567718949	11.43364617827298	4.25051779273339
H	5.11753598763938	12.90598236661540	4.93586060974511
H	5.12730860802350	11.42339564963185	5.88391462623821
H	6.26360374147528	14.10633569746440	6.80066964461195
H	7.81032428638534	13.52993811500508	7.41034228676105

H 6.34141912058122 12.61796827178722 7.73357967767300
H 13.85440288514210 13.72457961919241 6.07144427435125
H 13.24295008242770 14.79651100989388 7.32450962313913
H 13.97889581779307 15.48213316796469 5.86707738423718
H 11.20651410355823 14.66309583841170 3.11437444484315
H 12.58964749946949 13.63938147955289 3.43041017029173
H 12.79322176170030 15.40021969869896 3.40239307461062
H 10.10815683207896 16.34943682318789 5.16500186787922
H 11.72291700898588 17.06464144011922 5.32273086745452
H 10.86338684201775 16.46383502699348 6.74930042955557
H 7.14371523004124 5.86685310985136 1.35830316022230
H 6.48007093521698 4.71198614887417 2.52158404538663
H 8.18990247810157 5.15997134053104 2.57525098597573
H 4.97704750103001 7.64634771686303 2.14934291404370
H 4.73823392450549 8.05237266216533 3.83832539582552
H 4.45967706028637 6.39424940768991 3.28665518800648
H 6.06685876991953 5.30129549197173 5.16035169710233
H 6.48514124782968 6.86561971174436 5.87864432535151
H 7.75918412237974 5.76321813513367 5.39829690796561

93
Coordinates from ORCA-job ring_flip_sn2_cxme_pme3_TS
Au 8.52698152053870 8.53368390507000 3.72819004472293
Au 9.94810099835791 13.24206988267011 5.77171241105330
Sn 9.51130755889923 10.96459923274926 3.69607612212942
P 8.56257007649923 6.23268794826710 4.05986849521799
P 11.70933360215338 14.60390980681482 5.39758545134396
N 8.49779637101078 12.84536456205499 3.12242379661875
N 11.13543702042925 10.18793741185718 5.09040497137799
N 11.11564545037801 11.52705514486485 2.41648525159326
C 7.20818685575918 11.73409413196964 5.50847797435391
C 9.00442156216257 13.71222726267384 2.17958958772212
C 8.64395106555869 10.49958619944156 6.68518669860369
N 8.51529928269275 11.67849324314365 5.96910588677471
C 7.45544309396199 9.81832234328918 6.62976961117093
H 7.24531249143657 8.87485589133808 7.09186951974446
C 12.41603435795773 11.09194510950279 2.56960288092488
C 9.91405303419162 10.06646937393594 7.34185947398632
C 7.65675799226153 13.58732747784843 3.93356776070117
C 11.14395423082180 12.63605685068665 1.60156443543589
C 9.83559721888036 5.43927226086012 3.04632968967244
C 6.54865478149875 10.59816002410389 5.88227461403118
H 5.52500224881616 10.36111953645312 5.67289128003155
C 12.21353817377710 9.53205652784703 4.53120454616882
C 6.26749370346896 13.95074132221040 5.96141211296408
H 5.80410854533989 14.83852483991162 5.54288134927093
H 7.13279151301054 14.25922005640890 6.53950783364377

C	6.66768985983468	12.95921688845539	4.86315167674997
C	9.88436062355609	13.23779650918612	1.07196205596494
C	9.58513261250676	8.91018922738900	8.28650368010523
H	10.46540478719323	8.61311963607427	8.84240081967293
H	8.82670905791923	9.21717482513448	8.99887639240956
C	13.20832350184955	13.63201112067440	5.15572601003903
C	10.92623020014479	9.60678003487633	6.32768066746268
C	7.65780532571217	14.89329904234685	3.51223205434137
H	7.05790813480614	15.68535205961111	3.91560541075927
C	8.50609410317537	14.97026937369733	2.39181474064096
H	8.70714121202154	15.84017030952801	1.79861078119652
C	10.51905631948478	11.16877339125077	8.22670739964078
H	11.34127765530656	10.75301195452052	8.80063104549817
H	10.91903460056722	11.98676850829726	7.63899489770336
C	9.08368867932343	5.86335187603121	5.75099682171040
H	9.77826952825336	11.57131906725309	8.91314884880352
C	7.09282718642050	5.20279646245115	3.80626847061678
H	9.22412500468712	8.04311652574382	7.74774874381236
C	11.86032734329042	8.62110867460064	6.53851828757347
H	11.97855406453228	8.03801500998241	7.43072933283387
C	12.73409829411734	9.75107477353982	3.14050501375290
C	12.13772487973915	8.68191447475980	2.20094184547799
H	12.50616610202873	8.81416200549474	1.18709176366602
H	11.05385483976917	8.73723212456020	2.17472642824670
C	12.11152271833308	15.75665208152552	6.73472942940806
C	12.67565305501891	8.57144283739499	5.39858616337805
H	13.51599299432547	7.92380835655698	5.24447185458731
C	11.59731703999680	15.63462486398058	3.92580406264631
C	10.21970193124336	14.39236172341156	0.14151081067680
H	9.31143370286034	14.83165825113788	-0.25485065456216
H	10.81651454896483	14.03704059378663	-0.69090381327207
C	5.41582789823017	12.60214722230492	4.05516747019543
H	5.65762466725446	11.89108149994321	3.27267045047612
H	4.64513617982499	12.17068174733414	4.68744368018621
H	8.23011472833443	12.60893880583238	-0.17888784739675
C	9.13363665241655	12.17991802323333	0.24449340376450
H	9.76521316210818	11.81689611823377	-0.56108193543676
H	8.83971617379374	11.32591206478080	0.84548971258498
C	12.44293801767778	12.92384268760647	1.27821007623923
H	12.77573590939018	13.71402689763765	0.63510880640703
H	5.55601804830404	13.48252170085437	6.63318108995763
C	13.25038710302749	11.94186285285726	1.89114747210962
H	14.31373219395781	11.84757630962996	1.80085969448461
H	5.01456099073203	13.49608933816579	3.59141348687758
H	10.77917538628407	15.17146435168186	0.64897125306880
H	12.41269728451765	7.69078313413388	2.55168291036224
H	14.50876731915548	8.57010897635191	3.49474718345970

H 14.63800121263410 9.64923815146434 2.12556986275595
H 14.74066161731353 10.28787018686315 3.76588690642120
C 14.24872856134677 9.55679863960421 3.13371716737149
H 11.49667956427136 14.99053125833110 3.05998816791169
H 12.49307338746606 16.24105115969754 3.82561595676609
H 10.72191471011747 16.26916418964065 3.97967246524062
H 13.08797741087833 13.00271848527175 4.27935505078954
H 13.37397331561898 12.98941912618494 6.01227498897321
H 14.06794089433862 14.28104575144841 5.01376440669308
H 11.28230460324839 16.43445693648675 6.89890326338001
H 12.99876618375590 16.33192558204713 6.48695144782248
H 12.28882538525696 15.20727276476905 7.65171999976887
H 9.59219217475037 5.54006352819095 1.99547411771763
H 9.92958087667363 4.38599943271279 3.29493076665889
H 10.78223755061412 5.93685161106046 3.22301297439965
H 9.26706611340537 4.80036770983134 5.87970166500426
H 8.31568307701946 6.18087746924954 6.44647466889754
H 9.98776076960375 6.42292325435334 5.97074909049945
H 6.76234430242936 5.28196637059033 2.77731813622549
H 6.28976572049660 5.54855233136625 4.44624327285801
H 7.30566419690651 4.16180140102792 4.03253287570505

93
Coordinates from ORCA-job dinuc_sn2_cxme_au_pme3_INT1_opt
Au 8.64764406536626 8.50611338881873 3.65508768679571
Au 10.28478066637347 12.95153653687267 5.90086211265392
Sn 9.99479255720211 10.76268609205380 3.65857584416896
P 7.39447839892857 6.57491547695925 4.03525721063568
P 11.64503580538939 14.70040754466128 5.47808400042649
N 8.67280403632110 12.50482992074551 3.26003615171435
N 11.75710828099744 10.23143410693749 4.94244407726176
N 11.39327381350643 11.61914992314587 2.31351972418193
C 7.67641601681277 11.30763652735252 5.78660542751277
C 8.89909874888542 13.35112201014925 2.19795851176234
C 9.25346844380490 10.04971969904272 6.72738478237631
N 9.02841079260213 11.24829975295195 6.07267988712459
C 8.06683167597121 9.37175521562663 6.83327817323581
H 7.92632391190989 8.41508370978057 7.29612280666951
C 12.75736105500601 11.58354268018637 2.49977596280452
C 10.61669949481296 9.56112934670802 7.10342646728316
C 7.85316767610256 13.18682479137772 4.14495319180888
C 11.11727935907892 12.65209219591937 1.44950344952393
C 8.17148761894356 5.48663844725052 5.25673632805509
C 7.06873251210388 10.16620418644245 6.23174092892794
H 6.02299031680947 9.94193302207685 6.16527855820102
C 12.61536572139423 9.61297605758065 4.03713970012739
C 6.76957795265932 13.51606582241612 6.36450616657252

H	6.26096661437348	14.40427428478620	6.00487242616232
H	7.69650009868426	13.82457712433311	6.83756311154398
C	7.03840011142006	12.52774937333742	5.22175356435584
C	9.71825932361071	12.93823290238447	1.01691920772081
C	10.46589016697176	8.28993642222560	7.93063308344184
H	11.43827868274525	7.93907588613176	8.25593040947853
H	9.86101183442167	8.48347815417906	8.80976877559301
C	13.38277871338815	14.24171390236447	5.32575644986205
C	11.42949927230199	9.25947420719923	5.87500012696031
C	7.59994877980043	14.44212424789642	3.64524118158087
H	6.94279051708228	15.17028405789338	4.07989533209705
C	8.25329420273019	14.54222347045524	2.40501389444678
H	8.23840276812092	15.37976328718274	1.73643024964625
C	11.37006261939879	10.57056912474805	7.97913493602325
H	12.31166109691369	10.13762916482077	8.30358326555529
H	11.60094444556496	11.48005108827675	7.43695781271117
C	5.76921583333526	6.91976806026596	4.75598466946588
H	10.78269392127086	10.83243848148219	8.85524976551043
C	7.01767694140485	5.46899572907094	2.64903949586063
H	9.99823324808872	7.49530644841990	7.35960626946869
C	12.02971378092161	8.07305044046589	5.54643765752922
H	11.98492046007401	7.15825626981511	6.10395115031843
C	13.45833120548887	10.40245758701426	3.08989458315872
C	13.91128767762580	9.50458958299232	1.93196440094076
H	14.56408263556596	10.05936212713619	1.26748183382667
H	13.05742054460404	9.15777831785805	1.35974830904782
C	11.61609414587005	16.02303769995891	6.71422697012745
C	12.77736256152889	8.29515442248999	4.37242427295172
H	13.41879062586683	7.58610053996958	3.88685748718161
C	11.26592192174301	15.51532925063387	3.92020044902292
C	9.72409395285067	14.04650865180358	-0.02386861459327
H	8.71267412798079	14.26047084565299	-0.35101652521384
H	10.30442921468715	13.74151429956838	-0.88785779857850
C	5.68609225228890	12.14612600876557	4.60460988120169
H	5.82281797226983	11.44255215052666	3.79002913264211
H	5.02539987306955	11.69938208776159	5.34213053793573
H	8.09575880401897	11.91447649585757	0.01644849497065
C	9.10201084623009	11.69333257338523	0.36016370005774
H	9.70440036985792	11.37695586428968	-0.48624765095019
H	9.03020038488425	10.85251511912614	1.04244398178504
C	12.28731366294274	13.27728033792623	1.10721803560192
H	12.38991207547123	14.10452085209970	0.43324472438958
H	6.14364047227380	13.04622332572060	7.11622029452505
C	13.32808121091160	12.60260406563006	1.78106971408176
H	14.37981762405305	12.78938654914958	1.67996788326842
H	5.20285368677411	13.03260697012882	4.21111777778133
H	10.15478744636605	14.96151529892657	0.36728959659404

H 14.45483596941802 8.63809243034481 2.29533490083076
H 15.26381201910256 9.99861023325730 4.20194339123698
H 15.35579462539318 11.46487102770690 3.23299255417064
H 14.42077687310623 11.44556087497574 4.72726622763930
C 14.70371962580972 10.86228757028297 3.85842078339301
H 11.44195770827812 14.82084082702036 3.10486677601824
H 11.89626804419655 16.39049420957747 3.78966422827161
H 10.22057966602147 15.79673832661775 3.89503632781337
H 13.48218595835094 13.56884762933134 4.48025491475704
H 13.71942114338048 13.73028022159177 6.21934736997912
H 13.99710741522941 15.12165981151854 5.15754831570197
H 10.61088528113444 16.41901907665099 6.79704082507461
H 12.29245119294823 16.82397684749704 6.43084888025117
H 11.90851758391312 15.63319816837491 7.68195712202155
H 9.14261269518741 5.16651337724035 4.89897174646743
H 7.55264094114038 4.61604160982517 5.45427140718293
H 8.32113529177163 6.03768328410266 6.17793860608312
H 5.24994080075944 5.99840773946259 5.00369896318557
H 5.17113104588076 7.49088152206165 4.05588900199443
H 5.89780339566701 7.51638168813730 5.65075029921321
H 7.93718331461203 5.13208261225261 2.18579374264756
H 6.44162838792160 6.00419536627842 1.90341029771363
H 6.44989337194214 4.60662593872285 2.98655186143640

93
Coordinates from ORCA-job au_migration_sn2_cxme_pme3_TS
Au 8.61044158832901 8.43669293587998 3.69044793784175
Au 11.05296090166448 12.51468030357527 5.76283801566642
Sn 9.69968724333040 10.83272345357085 3.73031555051399
P 7.72256302228124 6.29603603259315 3.89336962094500
P 11.89003239517631 14.56070925855484 5.33458495008887
N 8.67640946456978 12.65750894136641 3.20511957706087
N 11.50524566419162 10.18689536240282 5.18202804763254
N 11.27463182056525 11.52610076788036 2.42876649473269
C 7.68547637499095 11.78265960839671 5.79955341494524
C 8.82848042977407 13.26257922511765 1.97568654868621
C 8.88152448221563 10.09169605554504 6.60455393817015
N 8.98970409689256 11.32678701945676 5.98115816002576
C 7.56360401612521 9.76244303044607 6.75699482053965
H 7.17835667257933 8.87836535690523 7.22553809286889
C 12.62338534708957 11.57558213825235 2.70800355783007
C 10.08065160184498 9.32453107398048 7.05525659387970
C 7.89946651821453 13.49078956322467 3.97818703329401
C 11.03267327030506 12.41999043897443 1.41081869650528
C 8.95659203223474 5.05713907227609 4.36248420090644
C 6.80503952534479 10.83345830499068 6.24008900594636
H 5.73651912561805 10.90559125174818 6.23248282156958

C	12.43924458258443	9.65995871864728	4.30084963470877
C	7.89511272261135	14.17319956413777	6.37890989656285
H	7.66062527447971	15.18769505269366	6.07000786558402
H	8.96943267335197	14.08727823560743	6.48837063695734
C	7.36466976002080	13.16738841998423	5.34432488188432
C	9.65166760899579	12.65005113301167	0.88599231334385
C	9.64816342132491	7.97611958853588	7.60950084124408
H	10.50888516054059	7.42093662466066	7.96511070157572
H	8.96775298403909	8.10803519331313	8.44306104377594
C	13.66558836176585	14.68702225883087	5.02259418337074
C	11.02821675333923	9.11872882567443	5.92104123930877
C	7.58531007202134	14.61005515755026	3.24766373953991
H	6.97100367174067	15.42434482988436	3.58097715878794
C	8.16944882222022	14.46370723800079	1.97693770779591
H	8.11000046565502	15.15361832950698	1.15920736615612
C	10.78921831214976	10.07972023328282	8.19212737602779
H	11.65943890618055	9.52272777918307	8.52669566069360
H	11.12914919457450	11.06006661764207	7.87096845089482
C	6.46669665577214	6.16215509598062	5.19091358035391
H	10.11319904990800	10.22121084506683	9.03049243895858
C	6.91952267938698	5.57375724765221	2.43814637760886
H	9.14961743931193	7.38229061370134	6.84840831469696
C	11.59915192943313	7.95564316346750	5.48211967734117
H	11.43431779561556	6.97327897918869	5.87963564891768
C	13.34944719165048	10.53310730864097	3.50727706821484
C	14.14534195100980	9.66898214011704	2.52267448552304
H	14.83092967480683	10.29134322589131	1.96062163919194
H	13.48294619612580	9.17623757357119	1.81911017494489
C	11.57933313343802	15.82558922560079	6.59348755228945
C	12.49289938061908	8.30045513339121	4.44420213581481
H	13.12786274542337	7.62673475204694	3.90476160241163
C	11.13907929283874	15.19556315516247	3.82974477678169
C	9.70783764880106	13.59557735083438	-0.30396375117789
H	8.71079999145602	13.76246231630204	-0.69657044295924
H	10.31738715711788	13.16771067144702	-1.09255853998457
C	5.84192095407575	13.33276551939617	5.30355632459104
H	5.39430954400084	12.65592542266777	4.58428439011896
H	5.40660788151052	13.14458091940335	6.28025902231981
H	8.02567412694991	11.52296871031098	0.01326690047761
C	9.02803263187326	11.33782276752567	0.38752528457824
H	9.63300020643720	10.91610392706639	-0.40996072650692
H	8.94707003255064	10.57975600808170	1.15998564032588
C	12.20561877366625	13.03704040234596	1.05883005747478
H	12.32833656303975	13.76785721703115	0.28445327690523
H	7.44227730738733	13.98894705035396	7.34929349552979
C	13.21269268684458	12.50674382086848	1.88916763019102
H	14.26537917477295	12.71010887907595	1.82742309038126

H	5.58654039929092	14.34347405269719	5.01164767996630
H	10.12830341338603	14.55645947731990	-0.03108059656439
H	14.72483875685761	8.91272875806214	3.04414664261684
H	14.94217022120055	10.42183904613472	4.96402928565727
H	15.02485203985203	11.85001502763923	3.93760980218265
H	13.83290298377774	11.75856105271613	5.23122495962641
C	14.34968769063070	11.18603527100212	4.47002129214356
H	11.40568149956612	14.54325841535834	3.00487301006024
H	11.49432608030762	16.20142941192320	3.62247953541860
H	10.05838281119505	15.19656551489036	3.91964300661203
H	13.89880537343874	14.07298652304208	4.16075769276410
H	14.23193276489734	14.32440760351329	5.87185760431676
H	13.94000734090251	15.71813720044617	4.81880191217034
H	10.51371109652284	15.90496036136582	6.77110236840375
H	11.95977790825881	16.78893117633074	6.26611357325571
H	12.06140272170469	15.55228895949188	7.52489349538823
H	9.72880209533465	5.00677418889854	3.60417851797353
H	8.50280431628223	4.07771010675057	4.48260761271158
H	9.42534291063361	5.35435088637332	5.29314940087404
H	6.10016030879069	5.14334985379551	5.27697102106306
H	5.63923911175757	6.82576362432641	4.97026682793663
H	6.89665812301706	6.47066093934370	6.13660251627870
H	7.62964889276196	5.51705064563672	1.62170076330710
H	6.09649477141021	6.20427793614001	2.12347834100528
H	6.54399223146527	4.57779252932608	2.65496383165509

12 Literature

[1] H. Ruppert, L. Greb, *Angew. Chem. Int. Ed.* **2022**, *61*, e202116615.
[2] T. Tamai, K. Fujiwara, S. Higashimae, A. Nomoto, A. Ogawa, *Org. Lett.* **2016**, *18*, 2114–2117.
[3] G. Sheldrick, *Acta Crystalogr. A* **2015**, *71*, 3–8.
[4] G. Sheldrick, *Acta Crystalogr. C* **2015**, *71*, 3–8.
[5] C. B. Hübschle, G. M. Sheldrick, B. Dittrich, *J. Appl. Crystalogr.* **2011**, *44*, 1281–1284.
[6] G. Sheldrick, *Acta Crystalogr. A* **2008**, *64*, 112–122.
[7] F. Neese, *WIREs Comput. Mol. Sci.* **2022**, e1606.
[8] R. Rüger, M. Franchini, T. Trnka, A. Yakovlev, E. van Lenthe, P. Philipsen, T. van Vuren, B. Klumpers, T. Soini, *AMS 2021.102, SCM* **2021**.
[9] G. te Velde, F. M. Bickelhaupt, E. J. Baerends, C. Fonseca Guerra, S. J. A. van Gisbergen, J. G. Snijders, T. Ziegler, *J. Comput. Chem.* **2001**, *22*, 931–967.
[10] N. Mardirossian, M. Head-Gordon, *J. Chem. Phys.* **2015**, *142*, 074111.
[11] E. Caldeweyher, C. Bannwarth, S. Grimme, *J. Chem. Phys.* **2017**, *147*, 034112.
[12] F. Weigend, R. Ahlrichs, *Phys. Chem. Chem. Phys.* **2005**, *7*, 3297–3305.
[13] F. Weigend, *Phys. Chem. Chem. Phys.* **2006**, *8*, 1057–1065.
[14] P. Pracht, F. Bohle, S. Grimme, *Phys. Chem. Chem. Phys.* **2020**, *22*, 7169–7192.
[15] C. Bannwarth, E. Caldeweyher, S. Ehlert, A. Hansen, P. Pracht, J. Seibert, S. Spicher, S. Grimme, *WIREs Comput. Mol. Sci.* **2021**, *11*, e1493.
[16] A. V. Marenich, C. J. Cramer, D. G. Truhlar, *J. Phys. Chem. B* **2009**, *113*, 6378–6396.
[17] S. Kozuch, D. Gruzman, J. M. L. Martin, *J. Phys. Chem. C* **2010**, *114*, 20801–20808.
[18] S. Grimme, J. Antony, S. Ehrlich, H. Krieg, *J. Chem. Phys.* **2010**, *132*, 154104.
[19] X. Ren, P. Rinke, V. Blum, J. Wieferink, A. Tkatchenko, A. Sanfilippo, K. Reuter, M. Scheffler, *New J. Phys.* **2012**, *14*, 053020.
[20] G. L. Stoychev, A. A. Auer, F. Neese, *J. Chem. Theory Comput.* **2017**, *13*, 554–562.
[21] G. Zhurko, **2005**.
[22] C. Adamo, V. Barone, *J. Chem. Phys.* **1999**, *110*, 6158–6170.
[23] E. D. Glendening, J. K. Badenhoop, A. E. Reed, J. E. Carpenter, J. A. Bohmann, C. M. Morales, C. R. Landis, F. Weinhold, "NBO 6.0," **2013**.
[24] T. Ziegler, A. Rauk, *Theoret. Chim. Acta* **1977**, *46*, 1–10.
[25] T. Ziegler, A. Rauk, *Inorg. Chem.* **1979**, *18*, 1755–1759.
[26] T. Ziegler, A. Rauk, *Inorg. Chem.* **1979**, *18*, 1558–1565.
[27] M. P. Mitoraj, A. Michalak, T. Ziegler, *J. Chem. Theory Comput.* **2009**, *5*, 962–975.
[28] S. Grimme, S. Ehrlich, L. Goerigk, *J. Comput. Chem.* **2011**, *32*, 1456–1465.
[29] A. D. Becke, *Phys. Rev. A* **1988**, *38*, 3098–3100.
[30] J. P. Perdew, *Phys. Rev. B* **1986**, *33*, 8822–8824.
[31] J. D. Rolfes, F. Neese, D. A. Pantazis, *J Comput Chem* **2020**, *41*, 1842–1849.
[32] S. Grimme, *J Comput Chem* **2004**, *25*, 1463–1473.
[33] M. Ernzerhof, G. E. Scuseria, *The Journal of Chemical Physics* **1999**, *110*, 5029–5036.
[34] J. I. Rodríguez, R. F. W. Bader, P. W. Ayers, C. Michel, A. W. Götz, C. Bo, *Chemical Physics Letters* **2009**, *472*, 149–152.
[35] J. I. Rodríguez, A. M. Köster, P. W. Ayers, A. Santos-Valle, A. Vela, G. Merino, *Journal of Computational Chemistry* **2009**, *30*, 1082–1092.
[36] M. K. Bogdos, B. Morandi, *J. Chem. Educ.* **2023**, *100*, 3641–3644.
[37] "EveRplot," can be found under http://mor-vm-shiny.ethz.ch:3838/, **n.d.**
[38] G. Knizia, J. E. M. N. Klein, *Angew. Chem. Int. Ed.* **2015**, *54*, 5518–5522.
[39] D. Stalke, *Chemistry A European J* **2011**, *17*, 9264–9278.
[40] R. F. W. Bader, *Chem. Rev.* **1991**, *91*, 893–928.
[41] R. F. W. Bader, H. Essén, *The Journal of Chemical Physics* **1984**, *80*, 1943–1960.
[42] F. Cortesguzman, R. Bader, *Coordination Chemistry Reviews* **2005**, *249*, 633–662.

[43] D. Cremer, E. Kraka, *Angew. Chem. Int. Ed. Engl.* **1984**, *23*, 627–628.
[44] R. F. W. Bader, *J. Phys. Chem. A* **1998**, *102*, 7314–7323.
[45] D. Leusser, J. Henn, N. Kocher, B. Engels, D. Stalke, *J. Am. Chem. Soc.* **2004**, *126*, 1781–1793.

3.4 Concatenating Structural Constraint Effects at Tin for the Sequential Generation, Stabilization, and Transfer of Acyclic Aminocarbenes

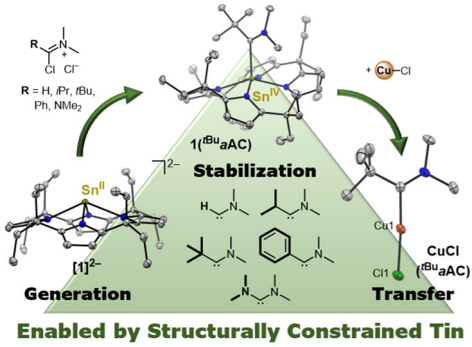


Figure 25. Table of contents graphic of the publication presented in this chapter.

The article and supplementary information (SI) presented within this section were previously published and can be found under: H. Ruppert, A. Meister, R. Pfretzschner, A. F. Vieira, L. Greb, *J. Am. Chem. Soc.* **2024**, *146*, *16*, 11515-11522, https://doi.org/10.1021/jacs.4c02446.

According to the CRediT scheme[271] the authors contributed to this publication as followed:

H. Ruppert – Conceptualization (*lead*), Methodology (*lead*), Validation (*lead*), Formal analysis (*lead*), Investigation (*lead*), Data curation (*lead*), Writing – Original Draft Preparation (*lead*), Writing – Review & Editing (*equal*), Visualization (*lead*), Supervision (*equal*), Project Administration (*equal*), Funding acquisition (*equal*);

A. Meister – Formal analysis (*supporting*), Investigation (*supporting*), Data curation (*supporting*);

R. Pfretzschner – Formal analysis (*supporting*), Investigation (*supporting*), Data curation (*supporting*);

A. F. Vieira – Formal analysis (*supporting*), Investigation (*supporting*), Data curation (*supporting*);

L. Greb –Resources (*lead*), Writing – Review & Editing (*equal*), Supervision (*equal*), Project Administration (*equal*), Funding acquisition (*equal*).

JACS
JOURNAL OF THE AMERICAN CHEMICAL SOCIETY
pubs.acs.org/JACS
Article

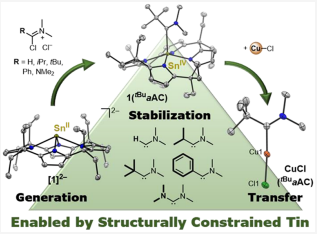
Concatenating Structural Constraint Effects at Tin for the Sequential Generation, Stabilization, and Transfer of Acyclic Aminocarbenes

Heiko Ruppert, Arne Meister, Ronja Pfretzschner, André Faria Vieira, and Lutz Greb*

Cite This: J. Am. Chem. Soc. 2024, 146, 11515−11522
Read Online

ACCESS | Metrics & More | Article Recommendations | Supporting Information

ABSTRACT: Structural constraint approaches have been employed toward different ends in recent years, from augmenting the nucleophilicity in pyramidalized low-valent p-block compounds to enhancing the Lewis acidities at planarized tetravalent p-block elements. While previous studies exploited these effects separately, this work introduces a strategy to concatenate structural constraint approaches at individual stages of a reaction sequence in a row to unlock a synthetic path unattainable by conventional methodologies. The boosted nucleophilicity resulting from the constrained tetracoordinated calix[4]-pyrrolato stannate(II) dianion enables the reductive formation of sterically unprotected acyclic aminocarbenes. These amino carbenes are stabilized at the concomitantly formed square-planar stannane(IV) as air-stable adducts. Transfer of the carbenes onto copper(I) by cooperativity of the calix[4]pyrrole ligand finalizes this protocol to hitherto unreported yet prototypical carbene complexes. Detailed spectroscopic and quantum theoretical analyses establish the synergy of structural constraints and element−ligand cooperation as the linchpin to this reaction path and its selectivity.



INTRODUCTION

Incorporating p-block element centers into structurally constrained ligand frameworks has emerged as a promising approach to enhance reactivity.[1−4] For example, by distortion of low-valent tetracoordinated p-block compounds from their VSEPR-conform C_{2v} symmetric structure, their reducing power and nucleophilicity can be significantly increased (Figure 1A).[5−7] As an illustration, the Dobrovetsky research group reported the square-pyramidal phosphoranide anion $[\mathbf{1}]^-$, in which the rigid, tetradentate ligand backbone enabled single-electron transfer processes which are unprecedented for phosphoranides in their VSEPR structure.[8] In our group, we explored the structurally constrained *meso*-octaethylcalix[4]-pyrrolato stannate(II) dianion $[\mathbf{1}]^{2-}$.[9] The effect of pyramidalization on a Sn(II) center can be described through the Walsh diagram of $[\mathbf{SnH_4}]^{2-}$ (Figure 1A). Distortion toward the non-VESPR square-pyramidal structure significantly increases the HOMO and HOMO−1 energies. NBO calculations indicate mixing of the p_z(Sn) orbital into the electron lone pair (lp), increasing the tin-centered lp's directionality. In $[\mathbf{1}]^{2-}$, both effects are amplified by the π-donor influence of the calix[4]pyrrole ligand.[10] By consequence, $[\mathbf{1}]^{2-}$ has demonstrated its capacity as a strong tin-centered σ-donor and nucleophile, facilitating the nucleophilic substitution of chlorides at C_{sp2}−Cl bonds in acyl chlorides and C_{sp3}−Cl bonds in alkyl chlorides. The combination of a rigid tetradentate ligand backbone with σ-acceptor and π-donor properties makes calix[4]pyrroles also ideal for the planarization of high-valent p-block elements.[11] This is exemplified by the first reported square-planar Al(III),[12] Ga(III),[13] and Si(IV)[14] complexes **II** as well as the Ge(IV) complex as a weak donor adduct (Figure 1B).[15] These compounds exhibit substantially increased Lewis acidities owing to the lower LUMO energy in their anti-van't-Hoff−Le-Bel configuration. The same effect is predicted for the yet hypothetical calix[4]pyrrolato stannane **1**, as depicted in the Walsh diagram of $\mathbf{SnH_4}$ (Figure 1B). Beyond structural constraints, the calix[4]pyrrole ligand system introduces a third advantage: the strong propensity for element−ligand cooperativity. Accordingly, the decreased HOMO−LUMO gap in **II** combined with the pronounced nucleophilicity of the ligand backbone enabled element−ligand cooperative bond activations in various small molecules (Figure 1 C).[16−19] Finally, the pyrrolato units in calix[4]pyrrole can serve as excellent π-donors toward transition metal centers forming polymetallic complexes **III**.[20,21] As an example, the Ru(II) sandwich complex $\mathbf{Ru(\eta^5\text{-}1)(\textit{p}\text{-}cymene)}$ contains the dianionic calix[4]pyrrolato stannate(II) $[\mathbf{1}]^{2-}$ (Figure 1 C).[9]

The present study revolved around the synergistic combination of these properties to facilitate a particularly

Received: February 19, 2024
Revised: March 22, 2024
Accepted: March 25, 2024
Published: April 11, 2024



Downloaded via UNIV HEIDELBERG on May 29, 2024 at 19:58:49 (UTC).
See https://pubs.acs.org/sharingguidelines for options on how to legitimately share published articles.

© 2024 The Authors. Published by American Chemical Society

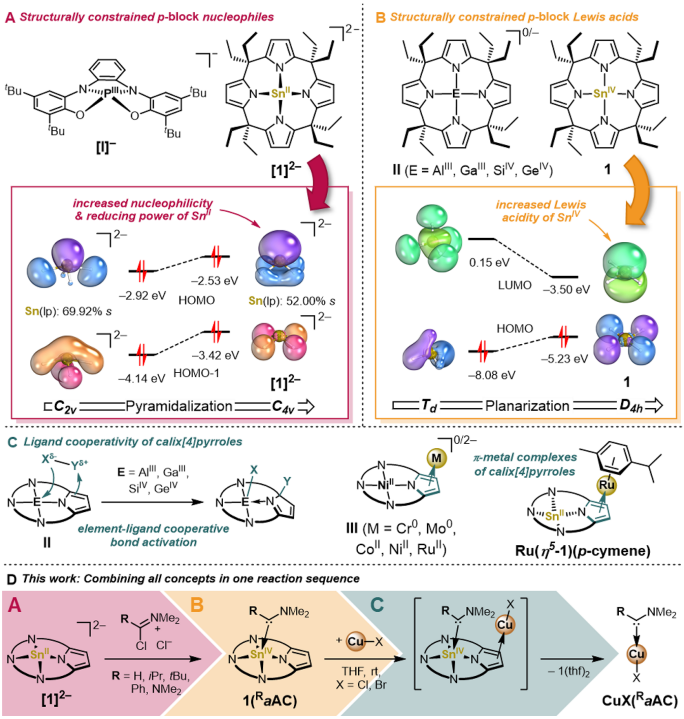


Figure 1. (A) Selected examples of structurally constrained p-block nucleophiles (top) and Walsh diagram showing the effect of pyramidalization on $[\mathbf{SnH_4}]^{2-}$ computed at the B97M-D4/def2-TVZPP CPCM(THF)//PBEh-3c level of theory. NBO calculations to obtain the orbital contributions to the electron lone pair at Sn(II) were done on the PBE0/def2-TZVPP//PBEh-3c level of theory. (B) Selected examples of anti-van't-Hoff−Le-Bel main group calix[4]pyrroles **II** and the hypothetical free square-planar stannane **1** (top) and Walsh diagram showing the effect of structural constraint on $\mathbf{SnH_4}$ computed on the B97M-D4/def2-TVZPP CPCM(THF)//PBEh-3c level of theory. (C) Element−ligand cooperative activation of small molecules by square-planar p-block calix[4]pyrroles (left) and π-metal complexes of calix[4]pyrrole nickelates(II) **III** and $[\mathbf{1}]^{2-}$ (right). (D) This work: combining all concepts (A−C) into a reaction sequence for the synthesis of copper(I) halide complexes of reactive acyclic aminocarbenes with low steric bulk **CuX(**$^{\mathrm{R}}$***a*****AC)**.

challenging reaction sequence (as depicted in Figure 1D): (i) generating acyclic aminocarbenes ($^{\mathrm{R}}$***a*****AC**) by utilizing the strong nucleophilic character of the constrained stannate(II) dianion $[\mathbf{1}]^{2-}$. (ii) Preserving the $^{\mathrm{R}}$***a*****AC** by capitalizing on the Lewis acidity of the anti-van't-Hoff−Le-Bel calix[4]pyrrolato stannane(IV). (iii) Transferring the $^{\mathrm{R}}$***a*****AC** onto transition metal centers by leveraging the element−ligand cooperative interactions and π-donor capabilities inherent to the calix[4]-pyrrole ligand. As we will demonstrate, it is the interplay between structural constraints and element−ligand cooperativity that is pivotal in enabling this reaction sequence.

In the realm of main group chemistry, carbenes have effectively stabilized low-valent main group element centers in different oxidation states.[22−24] This chemistry has been the subject of numerous reviews, with synthetic methods typically centered on the reaction of free carbenes with Lewis acidic p-block precursors.[25,26] Conversely, the generation and stabilization of carbenes via main group element compounds remain comparatively less explored. Notably, the Dielmann group harnessed the potential of an electron-rich tris-guanidinato-substituted phosphine **IV** to liberate free N-heterocyclic carbenes (NHCs) through the abstraction of chloronium ions from chloroamidinium cations under ambient conditions (see Figure 2A).[27] The Röschenthaler group employed nucleophilic p-block halides for the synthesis of cyclic and acyclic aminocarbene complexes of $SiCl_4$ **V**,[28] PF_5 **VIa**,[29−31] $[GeF_5]^-$ **VIb**, and $[SnF_5]^-$ **VIc**.[29] (Figure 2B,C). The oxidative addition of C−F bonds in (*gem*-difluoro)-dimethylamines to PF_3 at −196 °C allowed the generation and stabilization of reactive, sterically nonprotected carbenes (R = NMe_2, *t*Bu, Ph,

https://doi.org/10.1021/jacs.4c02446
J. Am. Chem. Soc. 2024, 146, 11515−11522

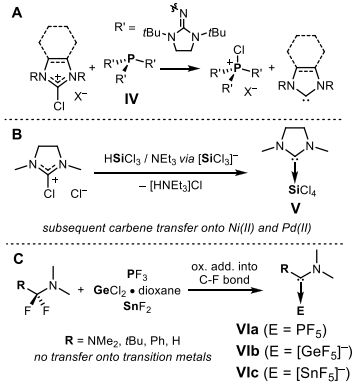


Figure 2. Literature of known reactions of p-block nucleophiles with chloroamidinium and -iminium salts (A, B) and (*gem*-difluoro)-dimethylamines (C) as precursors for aminocarbenes.

H). Subsequent transmetalation chemistry has not been reported.

RESULTS AND DISCUSSION

Synthesis of Carbene Adducts 1(^R*a*AC). Treatment of amides **2^R** with oxalyl chloride in methyl *tert*-butyl ether (MTBE) readily produces chloroiminium salts **3^R** in good to excellent yields (Figure 3A).[32] Subsequent reaction of **3^R** (R = *t*Bu, Ph, and NMe_2) with the lithium salt of $[\mathbf{1}]^{2-}$ in 1,2-difluorobenzene (*o*DFB) at −30 °C formed intensely colored reaction solutions within minutes accompanied by the precipitation of lithium chloride. Filtration over silica yielded the carbene adducts **1(^R*a*AC)** as yellow to dark red solids in bulk purity and yields of up to 85%. ^{1}H NMR spectroscopy revealed decreased symmetries of the calix[4]pyrrolato units compared to $[\mathbf{1}]^{2-}$ caused by a hindered rotation around the newly formed Sn−C bond at room temperature. For all adducts, two singlets for the NMe_2 groups at the carbenes indicate a partial double bond character for the C−N bond. Solutions of **1(^tBu*a*AC)**, **1(^Ph*a*AC)**, and **1(^NMe2*a*AC)** in CD_2Cl_2 showed ^{119}Sn NMR resonances between −451 and −475 ppm, all lying in the range of previously reported hypervalent calix[4]pyrrolato stannate(IV) complexes containing Sn−C bonds.[9] Corresponding cross signals in ^{1}H, ^{119}Sn-HMBC NMR experiments and $^{117/119}$Sn-satellites disclosed proximity of the NMe_2 groups ($^4J_{Sn,H}$ between 6 and 11 Hz) and the residues R with the tin center. The presence of carbenoid C atoms was confirmed by ^{13}C NMR chemical shifts at 234.1 ppm (R = *t*Bu), 220.2 ppm (R = Ph), and 195.8 ppm (R = NMe_2), respectively. Cooling of concentrated solutions in toluene or acetonitrile (MeCN) yielded single crystals (sc) suitable for X-ray diffraction (XRD) for all adducts **1(^R*a*AC)**, confirming their proposed molecular structures (for structures, see Figure 3B and Supporting Information section 5, where **1(^NMe2*a*AC)** crystallized with one MeCN molecule in the asymmetric unit, Figure S60). The Sn−N bond lengths in **1(^tBu*a*AC)**, **1(^Ph*a*AC)**, and **1(^NMe2*a*AC)** are significantly shortened (∼210 pm) compared to the stannate(II) $[\mathbf{1}]^{2-}$ (∼231 pm),[9] indicating the oxidation of Sn(II) to Sn(IV). With values between 224 and 228 pm, the Sn−C_{carb} bond lengths in **1(^R*a*AC)** are comparable to those of previously reported hypervalent Sn(IV)-NHC adducts.[29] With 129 pm, the C_{carb}−N bonds in **1(^tBu*a*AC)** and **1(^Ph*a*AC)** are close to a C=N double bond, in line with the hindered rotation around the C−N bond observed by ^{1}H NMR spectroscopy. Having established the synthesis and isolation of these acyclic alkyl, aryl, and diamino carbene Sn(IV) complexes, we were interested if this approach might allow us to generate and stabilize also carbenes bearing *α*-hydrogen atoms (R = *i*Pr) or even monosubstituted aminocarbenes (R = H). Dropwise addition of a solution of $[\mathbf{1}]^{2-}$ in THF to a suspension of the respective iminium salts **3^R** in THF at −78 °C immediately formed clear yellow reaction solutions. Workup yielded the expected carbene adducts **1(^iPr*a*AC)** (41% yield) and **1(^H*a*AC)(thf)** (57% yield) as elemental pure yellow solids. Whereas **1(^iPr*a*AC)** shows comparably high stability, NMR characteristics (δ ^{119}Sn = −458.0 ppm, δ ^{1C}C = 232.4 ppm, $^{117/119}$Sn-satellites of the NMe_2 group with $^4J_{Sn,H}$ = 9.0 Hz) and solid-state molecular structure as the previous adducts,

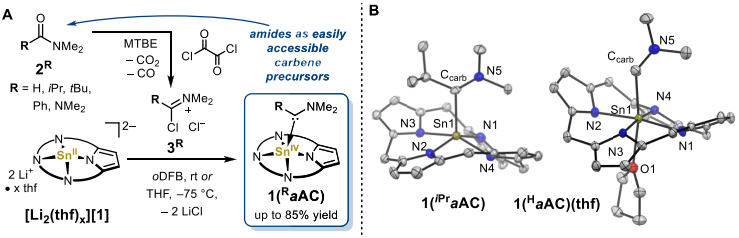
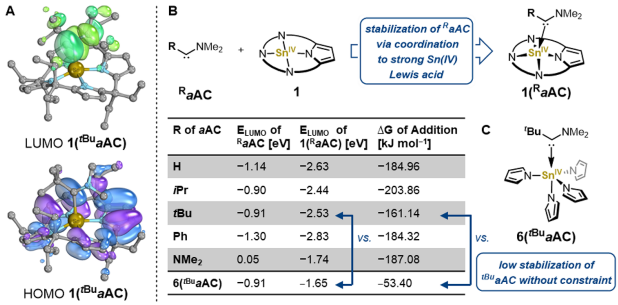


Figure 3. (A) Protocol for the synthesis of tin(IV) calix[4]pyrrole carbene adducts **1(^R*a*AC)**. (B) Solid state molecular structures of **1(^iPr*a*AC)** and **1(^H*a*AC)(thf)**. Displacement ellipsoids are drawn at the 50% probability level. Hydrogens and *meso*-ethyl residues of the calix[4]pyrrolato ligand are omitted for clarity. Selected bond lengths [pm] and angles [deg]: **1(^iPr*a*AC)**: Sn1−C_{carb} = 223.9(4), Sn1−N_{avg} = 209.7(9), C_{carb}−N5 = 129.5(6), Sn1−C_{carb}−N5 = 122.1(3), C−C_{carb}−N5 = 123.7(4), N1−Sn1−N2 = 153.44(15), N3−Sn1−N4 = 155.64(14); and **1(^H*a*AC)(thf)**: Sn1−C_{carb} = 225.2(3), Sn1−O1 = 228.6(2), Sn1−N_{avg} = 210.7(8), C_{carb}−N5 = 126.7(4), Sn1−C_{carb}−N5 = 134.4(3), N1−Sn1−N2 = 172.51(10), and N3−Sn1−N4 = 171.40(10).

https://doi.org/10.1021/jacs.4c02446
J. Am. Chem. Soc. 2024, 146, 11515−11522



R of aAC	E_{LUMO} of RaAC [eV]	E_{LUMO} of 1(RaAC) [eV]	ΔG of Addition [kJ mol⁻¹]
H	−1.14	−2.63	−184.96
*i*Pr	−0.90	−2.44	−203.86
*t*Bu	−0.91	−2.53	−161.14
Ph	−1.30	−2.83	−184.32
NMe_2	0.05	−1.74	−187.08
6(tBuaAC)	−0.91	−1.65	−53.40

Figure 4. A Frontier molecular orbitals of **1**(*^{tBu}aAC**)** computed at the B97M-D4/def2-TVZPP SMD(DCM) level of theory. Isosurfaces were sampled at a value of 0.03. Hydrogen atoms are omitted for clarity. (B) Hypothetical adduct formation reaction of the free acyclic aminocarbenes *^{R}aAC with the *meso*-octaethylcalix[4]pyrrolato stannane **1**. E_{LUMO} of the free aminocarbenes *^{R}aAC, their respective adducts **1**(*^{R}aAC**)**, and the reference system **6**(*^{tBu}aAC**)** (C) in eV computed at the B97M-D4/def2-TVZPP SMD(DCM) level of theory. Free reaction enthalpies Δ*G* were computed at the DSD-BLYP-D3(BJ)/def2-QZVPP COSMO-RS(DCM)//B97M-D4/def2-TZVPP//CREST/GFN2-xTB level of theory.

1(*^{H}aAC**)(thf)** could only be handled in THF and aromatic solvents. Furthermore, ^{1}H NMR spectroscopy of **1**(*^{H}aAC**)(thf)** in THF-d_8 attested a pseudo-C_{4v} symmetry, indicating a free rotation around the Sn−C bond at room temperature enabled by the primary carbene carbon. The solid-state molecular structure of **1**(*^{H}aAC**)(thf)** shows the additional coordination of THF forming a hexacoordinated Sn(IV) center, causing a ^{119}Sn NMR resonance at −576.4 ppm, which is high-field-shifted compared to the other carbene adducts. In addition to the $^{117/119}$Sn-satellites for the NMe_2 group ($^{4}J_{Sn,H}$ = 6.0 Hz) a $^{2}J_{Sn,H}$ coupling of 84.9 Hz to the hydrogen atom directly bound to the carbene center supports the direct coordination of the carbene to the tin(IV) center. Prolonged drying of **1**(*^{H}aAC**)(thf)** at reduced pressure did not allow for the removal of thf. Both **1**(*^{iPr}aAC**)** and **1**(*^{H}aAC**)(thf)** possess Sn−C_{carb} and C_{carb}−N bond lengths comparable to those of the other adducts (Figure 3 B). The adducts **1**(*^{R}aAC**)** showed excellent solubilities in dry and degassed organic solvents (DCM, THF, MeCN, toluene, and C_6H_6) being stable in solution at room temperature for several days and tolerating even elevated temperatures for several hours (except **1**(*^{H}aAC**)(thf)**). Furthermore, they showed stability in the solid state at room temperature and could even be kept under ambient-air conditions for over 24 h without any sign of decomposition.

Computational Evaluation of the Structural Constraint Effects for the Generation and Stabilization of the Acyclic Carbenes. The fast formation of the carbene adducts **1**(*^{R}aAC**)** at low temperatures can be explained by the superior nucleophilicity of $[\mathbf{1}]^{2-}$ (for a more detailed computational discussion please see ref 9). The exemplarily computed reaction mechanism for the formation of **1**(*^{tBu}aAC**)** from $[\mathbf{1}]^{2-}$ and **3**^{tBu} in THF (DSD-BLYP-D3(BJ)/def2-QZVPP COSMO-RS(THF)// B97M-D4/def2-TZVPP//CREST/GFN2-xTB level of theory, Figure S71) shows the nucleophilic Sn(II) center in $[\mathbf{1}]^{2-}$ readily attacking the carbocation center in **3**^{tBu}. The following elimination of a chloride anion forms the carbene carbon center coordinated to the oxidized Sn(IV). The overall reaction free enthalpy is strongly exergonic (Δ*G* = −143 kJ mol^{-1}). In comparison, a dipyrrolato coordinated reference stannylene, a tricoordinated Sn(II) anion and a tetracoordinated Sn(II) dianion show drastically reduced tendencies to attack the carbocation in **3**^{tBu} highlighting the importance of structural constraint in $[\mathbf{1}]^{2-}$ (Figure S71). The electronic structures of carbene adducts **1**(*^{R}aAC**)** were analyzed by DFT calculations and bonding analysis tools. The HOMOs in **1**(*^{R}aAC**)** reside on the calix[4]pyrrole backbone (shown exemplarily for **1**(*^{tBu}aAC**)**, Figure 4A), while the LUMOs in **1**(*^{R}aAC**)** possess the π-character of a vacant p-orbital at the C_{carb}. Compared to the free carbenes, the LUMO energies are drastically decreased by 1.5−1.8 eV (Figure 4B, B97M-D4/def2-TVZPP SMD-(DCM)). ETS-NOCV and NBO calculations indicated that the Sn−C bonds in **1**(*^{R}aAC**)** are best described as dative covalent bonds of the carbene electron lone pair and a vacant p_z-orbital at the Sn(IV) center (Figure S73). This picture is also assisted by the calculated Δ*G* values for the hypothetical adduct formation reactions between free carbenes *^{R}aAC and the Lewis acid **1** (Figure 4 B), lying in the range of strong dative bonds (−161 and −203 kJ mol^{-1}).[33−36] For R = H, Ph, and NMe_2 the computed Δ*G* values are lying in a close range around −180 kJ mol^{-1}. However, the *t*Bu- and *i*Pr-substituted carbene adducts show significantly increased and decreased Δ*G* values, respectively. For **1**(*^{tBu}aAC**)** the weakened carbene coordination results from the increased steric demand of the *t*Bu-substituent. In comparison to the other carbene adducts, the solid-state molecular structure of **1**(*^{tBu}aAC**)** shows an increased Sn−C_{carb} bond length and decreased *trans*-N−Sn−N bond angles, indicating a significant repulsion between the *t*Bu substituent and the calix[4]pyrrole ligand backbone (Figure S55). In contrast, for **1**(*^{iPr}aAC**)** the relatively strong coordination can be explained by the perfect fit of the *i*Pr substituent (Figure 3B). Furthermore, computations with and without dispersion correction revealed an increased London attraction between *^{iPr}aAC and **1** (15.27 kJ mol^{-1}) compared to the respective monosubstituted carbene adduct **1**(*^{H}aAC**)** (8.0 kJ mol^{-1}).

To understand the specific role of structural constraint at Sn(IV) for the stabilization of the carbenes, we compared the calculated Δ*G* values for **1**(*^{tBu}aAC**)** with that for a hypo-

https://doi.org/10.1021/jacs.4c02446
J. Am. Chem. Soc. 2024, 146, 11515−11522

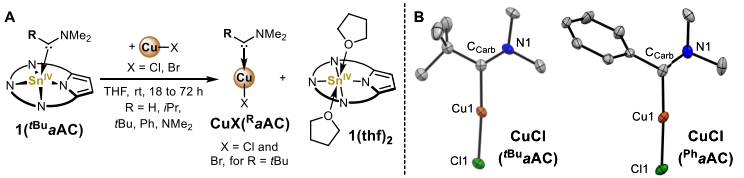


Figure 5. (A) Carbene transfers onto CuBr and CuCl fragments in THF at room temperature. (B) Solid state molecular structures of **CuCl(**^{tBu}***a*****AC)** and **CuCl(**^{Ph}***a*****AC)**. Displacement ellipsoids are drawn at 50% probability level. Hydrogen atoms are omitted for clarity. Selected bond lengths (pm) and angles [deg]: **CuCl(**^{tBu}***a*****AC)**: Cu1−C_{carb} = 189.8(5), Cu1−Cl1 = 211.31(15), C_{carb}−N1 = 129.6(7), Cl1−Cu1−C_{Carb} = 176.07(17); **CuCl(**^{Ph}***a*****AC)**: Cu1−C_{carb} = 188.2(6), Cu1−Cl1 = 211.26(18), C_{carb}−N1 = 130.3(8), and Cl1−Cu1−C_{Carb} = 176.21(19).

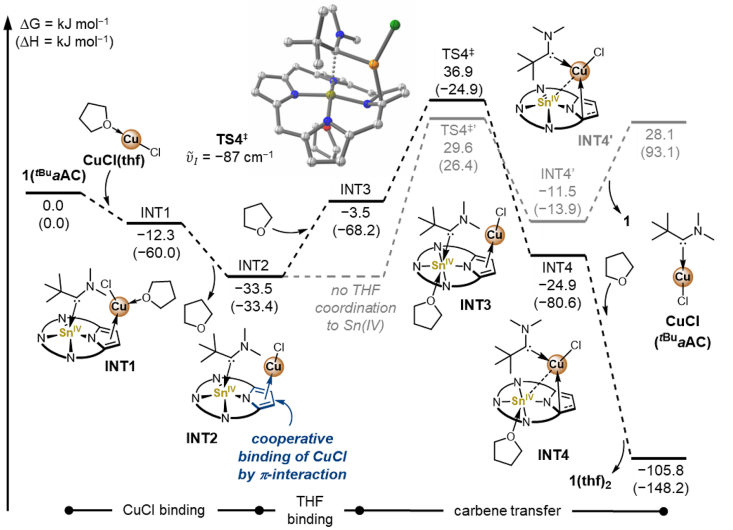


Figure 6. Mechanism of the carbene transfer reaction between **1(**^{tBu}***a*****AC)** and CuCl in THF at 298.15 K computed at the DSD-BLYP-D3(BJ)/def2-QZVPP COSMO-RS(THF)//B97M-D4/def2-TZVPP//CREST/GFN2-xTB level of theory with coordination of THF to Sn(IV) (black path) and without coordination of THF to Sn(IV) (gray path). *Meso*-ethyl residues and hydrogen atoms of the transition structure **TS4**‡ are omitted for clarity.

thetical adduct of ^{tBu}***a*****AC** with unconstrained (VSEPR conform) *tetra*-pyrrolato stannane **6**, forming **6(**^{tBu}***a*****AC)** (Figure 4 C). Tethering the four pyrrolato units decreases the Δ*G* by around 107 kJ mol^{-1}. These findings align with the increased Lewis acidities of square-planar coordinated p-block compounds in their anti-van't-Hoff−Le-Bel configuration, as shown in the Walsh diagram in Figure 1 B.[14,37,11] The effect of planarization on the Lewis acidity of **1** can further be seen by the calculated hydride (HIA), fluoride (FIA), and chloride ion affinities (CIA) (Tables S10 and S11). Thus, the structural constraint imparted by the calix[4]pyrrole ligand backbone serves two roles up to this point in the reaction sequence: (i) it enables the formation of **1(**^{R}***a*****AC)** through increased nucleophilicity of Sn(II) in [**1**]$^{2-}$ and (ii) plays a key role in the stabilization of the formed carbenes at the Lewis acidic Sn(IV). To the best of our knowledge, this situation represents the first example of a structural-constraint-enabled umpolung strategy for the generation and stabilization of otherwise inaccessible species.

Transmetalation Chemistry of 1(^{R}***a*****AC).** Next, we tested the carbene adducts **1(**^{R}***a*****AC)** as transfer agents of acyclic aminocarbenes. Treatment with elemental selenium, *trans*- and *cis*-hex-3-ene, as well as 2 atm of H_2 in CD_2Cl_2 or THF-d_8, respectively, did not show reactivity even at elevated temperatures over prolonged reaction times. The strong binding of the carbene fragments in **1(**^{R}***a*****AC)** does not allow the characteristic reactivity expected for free, ambiphilic carbenes. Thus, we tested **1(**^{R}***a*****AC)** as a carbene transfer

https://doi.org/10.1021/jacs.4c02446
J. Am. Chem. Soc. 2024, 146, 11515−11522

agent to transition metals. Coinage metal carbene complexes often act as an entry point and allow a wide range of applications.[38,39] Especially, the previous use of Cu(I) carbene complexes as catalysts for various transformations[40] and their photophysical properties[41−43] made these complexes ideal targets. Copper(I) halide complexes of acyclic aminocarbenes are underrepresented in literature with only a few examples of acyclic diaminocarbenes complexes been isolated,[44,45] aryl-(amino)carbene complexes being characterized *in situ*,[46] and alkyl(amino)carbene adducts even being unknown in literature. No solid-state molecular structure of such complexes has been reported so far. More detrimentally, NHCs bearing only small substituents are known to form bis(carbene) copper(I) dihalide cuprate(I) salts, tricoordinated copper(I) complexes bearing two carbene ligands, or dimeric and oligomeric bridged structures.[47−50] Thus, the selective synthesis of linear monocoordinated, monomeric copper(I) halide carbene complexes bearing small carbene ligands is an ambitious task. The reaction of **1(*^t^*^Bu^*a*AC)** with (dms)CuBr (dms = dimethyl sulfide) in THF at room temperature showed the consumption of the starting material and the clean formation of a new carbene species within 24 h. Workup yielded single crystals suitable for X-ray diffraction, confirming the formation of the respective acyclic alkyl(amino)carbene Cu(I)Br adduct **CuBr-(*^t^*^Bu^*a*AC)** (Figure S61). To the best of our knowledge, this presents the first example of a copper(I) halide complex of an acyclic alkyl(amino)carbene characterized in the solid state. Solvent screenings revealed that excess THF is necessary to enable fast transmetalation. This observation is in line with the concomitant formation of the bis-(thf)-adduct of *meso*-octaethylcalix[4]pyrrolato stannane **1(thf)$_2$**, which was identified NMR spectroscopically.[51] The full range of **1(*^R^*aAC)** derivatives also reacted with CuCl under the same conditions to quantitatively form the respective CuCl carbene adducts **CuCl(*^R^*aAC)** which were followed by NMR spectroscopy (Figure 5A). Besides **CuCl(*^H^*aAC)** all CuCl adducts are stable in dry THF and DCM at room temperature over several days. The unprotected **CuCl(*^H^*aAC)** slowly degrades in THF during the transmetalation reaction which only allowed its transient characterization by ^{1}H and ^{13}C NMR spectroscopy. They show NMR properties similar to those of their parent Sn(IV) complexes **1(*^R^*aAC)**. Except for R = NMe$_2$ a hindered rotation of the C$_{carb}$−N bond resulting in chemically inequivalent N-bound methyl groups can be observed at room temperature being in line with literature known acyclic diaminocarbene copper(I) complexes.[45] The characteristic ^{13}C NMR shifts between 211.3 ppm for **CuCl(*^NMe2^*aAC)** and 251.0 ppm for **CuCl(*^t^*^Bu^*a*AC)** are in the range of literature known Cu(I) *c*AAC complexes indicating the intact carbene fragments.[52] The absence of any $^{117/119}$Sn satellites and ^{1}H, ^{119}Sn-HMBC cross signals evidenced the successful transfer of the carbene units from Sn(IV) to Cu(I). Workup afforded the Cu(I)Cl carbene complexes in yields of around 50%. Single crystal X-ray diffraction confirmed the solid-state molecular structures for R = *t*Bu, Ph, and NMe$_2$. Despite the small steric hindrance at the acyclic carbenes they selectively form linear mono-carbene CuCl complexes which possess similar bonding parameters as related Cu(I) cAAC complexes (Figures 5B and S64).[52]

To gain insight into the carbene transfer between **1(*^R^*aAC)** and CuCl, we computed a possible reaction mechanism for R = *t*Bu at the DSD-BLYP-D3(BJ)/def2-QZVPP COSMO-RS-(THF)//B97M-D4/def2-TZVPP//CREST/GFN2-xTB level of theory (black path, Figure 6). As indicated by the bound THF in the solid-state molecular structure of **1(*^H^*aAC)(thf)** (Figure 3B), the Sn(IV) center in **1(*^R^*aAC)** still possesses Lewis acidic character, suggesting a nucleophile assisted pathway. However, the ^{119}Sn resonance of **1(*^t^*^Bu^*a*AC)** in THF-d_8 and CD_2Cl_2 show nearly identical shifts (−476.0 ppm vs −474.7 ppm) significantly differing from the ^{119}Sn resonance of **1(*^H^*aAC)(thf)** (−576.39 ppm), indicating the absence of THF coordination even in excess THF. Indeed, THF coordination to the Sn(IV) center in **1(*^t^*^Bu^*a*AC)** was computed endergonic (ΔG = 29.0 kJ mol^{-1}), rendering a nucleophile assisted pathway unlikely. We therefore proposed the reaction to be initiated by the binding of CuCl(thf) to the π-basic calix[4]pyrrolato ligand in **1(*^t^*^Bu^*a*AC)**. Indeed, this binding mode is exergonic, forming **INT1** followed by a release of THF and **INT2** with a ΔG of −33.5 kJ mol^{-1}. In the following step, THF can coordinate the Sn(IV) center with a ΔG of −3.5 kJ mol^{-1} forming **INT3**. Using THF as a solvent additionally favors THF coordination at this step. The proximity of the carbene and the CuCl in **INT3** allows a transfer step via the low energy transition state **TS4**‡ ($\Delta G^‡$ = 36.9 kJ mol^{-1}), forming the intermediate **INT4**. The transition structure **TS4**‡ shows one imaginary mode at −87 cm^{-1} with major contributions of the Sn, Cu, and C$_{carb}$ atoms. NBO calculations revealed a significantly decreased population of the Sn−C$_{Carb}$ bond (WBI of 0.2206 vs. 0.4897 for **1(*^t^*^Bu^*a*AC)**) for **INT4** which can best be described as a tricoordinated Cu(I) complex showing a week back-donation from Cu(I) to the Sn(IV) center (see Table S13). Finally, the addition of another THF causes the release of the carbene complex **CuCl(*^t^*^Bu^*a*AC)** accompanied by the formation of **1(thf)$_2$** and an overall ΔG of −105.8 kJ mol^{-1}. To evaluate the role of THF in this reaction sequence we calculated **TS4**$^{‡\prime}$ and **INT4′** without THF-coordination to the Sn(IV) center (gray path, Figure 6). The transition state **TS4**$^{‡\prime}$ is kinetically favored lying around 7 kJ mol^{-1} lower in energy than **TS4**, but the corresponding carbene transfer intermediate **INT4′** is destabilized by around 13 kJ mol^{-1}. In contrast to the formation of **1(thf)$_2$**, the dissociation of **CuCl(*^t^*^Bu^*a*AC)** and free Lewis acid **1** shows an overall positive ΔG of 28.1 kJ mol^{-1}. Thus, THF binding in **INT4** and to the free Lewis acid **1** acts as a thermodynamic driving force of the transmetalation reaction. It should be noted that THF could also bind to Sn(IV) in **INT4′** after the carbene transfer onto Cu(I). This would yield **INT4** (ΔG of −13.4 kJ mol^{-1}), subsequently releasing **1(thf)$_2$** and Cu(I) carbene. However, owing to the excess THF present as the solvent, the earlier THF binding forming **INT3** prior to the carbene transfer might be favored.

Finally, the reason for the selectivity leading to the mono(carbene) CuCl as the sole product was studied. The computed energies for binding of primary product **CuCl-(*^t^*^Bu^*a*AC)** by the calix[4]pyrrole backbone of **1(*^t^*^Bu^*a*AC)** (**INT5**, **INT6**, and **INT7** in Figure S72) lie around 50 kJ mol^{-1} above the coordination of CuCl(thf), thereby disfavoring the synthesis of bis(carbene) copper(I) complexes. In contrast to putative pathways via free carbenes, the unique ligand-cooperative transfer not only leverages a low barrier pathway but also enables selectivity to linear CuCl complexes bearing only one carbene ligand.

CONCLUSIONS

In previous studies, the application of structural constraint on p-block elements has been restricted to enhancing specific

https://doi.org/10.1021/jacs.4c02446
J. Am. Chem. Soc. 2024, 146, 11515−11522

isolated attributes such as Lewis acidity, reducing strength, or nucleophilicity. In this work, we strategically concatenate these steps to facilitate a complex reaction sequence (i–iii): (i) The augmented nucleophilicity of the tetracoordinated, constrained stannate(II) dianion $[\mathbf{1}]^{2-}$ enables a umpolung reaction, yielding low-substituted acyclic aminocarbenes ^{R}*a*AC (R = H, *i*Pr, *t*Bu, Ph, NMe_2) from easily accessible chloroiminium salts. (ii) The newly formed carbenes find stability within the coordination sphere of the square-planar stannane(IV) **1**. Thanks to its marked Lewis acidity induced by its anti-van't-Hoff–Le-Bel configuration, these compounds are stable even under ambient air. (iii) The cooperativity of the calix[4]-pyrrolato ligand backbone within **1**(^{R}*a*AC) facilitates the smooth and selective transmetalation of the acyclic carbenes onto copper(I) halides at room temperature, offering convenient access to previously elusive complexes of high potential for catalysis or emissive materials.[53] Hence, this study serves as a demonstration of how the strategic combination of structural constraint effects can enable reaction sequences that would remain beyond the reach of conventional approaches or individual reagents. We believe that this finding can serve as a blueprint for even more challenging processes, such as the generation, stabilization, and transfer of elusive oxycarbenes, phosphinidenes, or nitrenes.

■ ASSOCIATED CONTENT

Supporting Information

The Supporting Information is available free of charge at https://pubs.acs.org/doi/10.1021/jacs.4c02446.

Experimental procedures, NMR spectra, crystallographic data, and computational details (PDF)

Accession Codes

CCDC 2303620–2303625 and 2333350–2333352 contain the supplementary crystallographic data for this paper. These data can be obtained free of charge via www.ccdc.cam.ac.uk/data_request/cif, or by emailing data_request@ccdc.cam.ac.uk, or by contacting The Cambridge Crystallographic Data Centre, 12 Union Road, Cambridge CB2 1EZ, UK; fax: +44 1223 336033.

■ AUTHOR INFORMATION

Corresponding Author

Lutz Greb – *Anorganisch-Chemisches Institut, Ruprecht-Karls-Universität Heidelberg, Heidelberg 69120, Germany;* orcid.org/0000-0002-5253-419X; Email: greb@uni-heidelberg.de

Authors

Heiko Ruppert – *Anorganisch-Chemisches Institut, Ruprecht-Karls-Universität Heidelberg, Heidelberg 69120, Germany*

Arne Meister – *Anorganisch-Chemisches Institut, Ruprecht-Karls-Universität Heidelberg, Heidelberg 69120, Germany*

Ronja Pfretzschner – *Anorganisch-Chemisches Institut, Ruprecht-Karls-Universität Heidelberg, Heidelberg 69120, Germany*

André Faria Vieira – *Anorganisch-Chemisches Institut, Ruprecht-Karls-Universität Heidelberg, Heidelberg 69120, Germany*

Complete contact information is available at: https://pubs.acs.org/10.1021/jacs.4c02446

Funding

Financial support for this project was provided by the European Research Council (ERC) under the European Union's Horizon 2020 research and innovation program (Grant Agreement 948708).

Notes

The authors declare no competing financial interest.

■ ACKNOWLEDGMENTS

We acknowledge support by the state of Baden-Württemberg through bwHPC and the German Research Foundation (DFG) through Grant INST 40/575-1 FUGG (JUSTUS 2 cluster). H.R. acknowledges the Foundation of German Business (sdw) for funding. We acknowledge M. Schmitt for his support with X-ray crystal structure refinement.

■ REFERENCES

(1) Maiti, A.; Yadav, R.; Greb, L. Structural Constraint Effects on P-Block Elements: Recent Advances. *Adv. Inorg. Chem.* **2023**, *82*, 261.

(2) Ruppert, H.; Sigmund, L. M.; Greb, L. Calix[4]Pyrroles as Ligands: Recent Progress with a Focus on the Emerging p-Block Element Chemistry. *Chem. Commun.* **2021**, *57* (89), 11751–11763.

(3) Hannah, T.; Chitnis, S. Ligand-Enforced Geometries and Associated Reactivity in P-Block Compounds. *ChemRxiv* **2024**, *53*, 764.

(4) Abbenseth, J.; Goicoechea, J. M. Recent Developments in the Chemistry of Non-Trigonal Pnictogen Pincer Compounds: From Bonding to Catalysis. *Chem. Sci.* **2020**, *11* (36), 9728–9740.

(5) Sidgwick, N. V.; Powell, H. M. Bakerian Lecture: Stereochemical Types and Valency Groups. *Proc. R. Soc. London, Ser. A* **1940**, *176* (965), 153–180.

(6) Gillespie, R. J. Fifty Years of the VSEPR Model. *Coord. Chem. Rev.* **2008**, *252* (12), 1315–1327.

(7) Gillespie, R. J.; Nyholm, R. S. Inorganic Stereochemistry. *Q. Rev. Chem. Soc.* **1957**, *11* (4), 339–380.

(8) Volodarsky, S.; Malahov, I.; Bawari, D.; Diab, M.; Malik, N.; Tumanskii, B.; Dobrovetsky, R. Geometrically Constrained Square Pyramidal Phosphoranide. *Chem. Sci.* **2022**, *13* (20), 5957–5963.

(9) Ruppert, H.; Greb, L. Calix[4]Pyrrolato Stannate(II): A Tetraamido Tin(II) Dianion and Strong Metal-Centered σ-Donor. *Angew. Chem., Int. Ed.* **2022**, *61* (13), e202116615.

(10) For a more detailed discussion of the electronic structure of $[\mathbf{1}]^{2-}$ see ref 9 and the corresponding Supporting Information.

(11) Sigmund, L. M.; Maier, R.; Greb, L. The Inversion of Tetrahedral P-Block Element Compounds: General Trends and the Relation to the Second-Order Jahn-Teller Effect. *Chem. Sci.* **2022**, *13* (2), 510–521.

(12) Ebner, F.; Wadepohl, H.; Greb, L. Calix[4]Pyrrole Aluminate: A Planar Tetracoordinate Aluminum(III) Anion and Its Unusual Lewis Acidity. *J. Am. Chem. Soc.* **2019**, *141* (45), 18009–18012.

(13) Sigmund, L. M.; Engels, E.; Richert, N.; Greb, L. Calix[4]-Pyrrolato Gallate: Square Planar-Coordinated Gallium(III) and Its Metal-Ligand Cooperative Reactivity with CO2 and Alcohols. *Chem. Sci.* **2022**, *13* (37), 11215–11220.

(14) Ebner, F.; Greb, L. An Isolable, Crystalline Complex of Square-Planar Silicon(IV). *Chem* **2021**, *7* (8), 2151–2159.

(15) Yadav, R.; Janßen, P.; Schorpp, M.; Greb, L. Calix[4]Pyrrolato-Germane-(Thf)2: Unlocking the Anti-van't Hoff-Le Bel Reactivity of Germanium(IV) by Ligand Dissociation. *J. Am. Chem. Soc.* **2023**, *145* (32), 17746–17754.

(16) Ebner, F.; Sigmund, L. M.; Greb, L. Metal-Ligand Cooperativity of the Calix[4]Pyrrolato Aluminate: Triggerable C-C Bond Formation and Rate Control in Catalysis. *Angew. Chem., Int. Ed.* **2020**, *59* (39), 17118–17124.

(17) Ruppert, H.; Sigmund, L. M.; Greb, L. Calix[4]Pyrroles as Ligands: Recent Progress with a Focus on the Emerging p-Block Element Chemistry. *Chem. Commun.* **2021**, *57* (89), 11751–11763.

(18) Sigmund, L. M.; Greb, L. Reversible OH-Bond Activation and Amphoterism by Metal-Ligand Cooperativity of Calix[4]Pyrrolato Aluminate. *Chem. Sci.* **2020**, *11* (35), 9611−9616.
(19) Sigmund, L. M.; Ehlert, C.; Enders, M.; Graf, J.; Gryn'ova, G.; Greb, L. Dioxygen Activation and Pyrrole α-Cleavage with Calix[4]-Pyrrolato Aluminates: Enzyme Model by Structural Constraint. *Angew. Chem., Int. Ed.* **2021**, *60* (28), 15632−15640.
(20) Cuesta, L.; Sessler, J. L. π-Metal Complexes of Tetrapyrrolic Systems. A Novel Coordination Mode in "Porphyrin-like" Chemistry. *Chem. Soc. Rev.* **2009**, *38* (9), 2716−2729.
(21) Bonomo, L.; Solari, E.; Latronico, M.; Scopelliti, R.; Floriani, C. Meso-Octaethylporphyrinogen Displaying Site Selectivity in the Stepwise Synthesis of Polymetallic Aggregates with Interesting Redox Properties: The π-Binding Ability of Metalla-Porphyrinogens. *Chem. - Eur. J.* **1999**, *5* (7), 2040−2047.
(22) Jędrzkiewicz, D.; Mai, J.; Langer, J.; Mathe, Z.; Patel, N.; DeBeer, S.; Harder, S. Access to a Labile Monomeric Magnesium Radical by Ball-Milling. *Angew. Chem., Int. Ed.* **2022**, *61* (15), e202200511.
(23) Mondal, K. C.; Roesky, H. W.; Schwarzer, M. C.; Frenking, G.; Niepötter, B.; Wolf, H.; Herbst-Irmer, R.; Stalke, D. A Stable Singlet Biradicaloid Siladicarbene: (L:)2Si. *Angew. Chem., Int. Ed.* **2013**, *52* (10), 2963−2967.
(24) Jones, C.; Sidiropoulos, A.; Holzmann, N.; Frenking, G.; Stasch, A. An N-Heterocyclic Carbene Adduct of Diatomic Tin, :SnSn. *Chem. Commun.* **2012**, *48* (79), 9855−9857.
(25) Wang, Y.; Robinson, G. H. Counterintuitive Chemistry: Carbene Stabilization of Zero-Oxidation State Main Group Species. *J. Am. Chem. Soc.* **2023**, *145*, 5592.
(26) Nesterov, V.; Reiter, D.; Bag, P.; Frisch, P.; Holzner, R.; Porzelt, A.; Inoue, S. NHCs in Main Group Chemistry. *Chem. Rev.* **2018**, *118* (19), 9678−9842.
(27) Böhme, M. D.; Eder, T.; Röthel, M. B.; Dutschke, P. D.; Wilm, L. F. B.; Hahn, F. E.; Dielmann, F. Synthesis of N-Heterocyclic Carbenes and Their Complexes by Chloronium Ion Abstraction from 2-Chloroazolium Salts Using Electron-Rich Phosphines. *Angew. Chem., Int. Ed.* **2022**, *61* (28), e202202190.
(28) Böttcher, T.; Bassil, B. S.; Zhechkov, L.; Heine, T.; Röschenthaler, G.-V. (NHCMe)SiCl4: A Versatile Carbene Transfer Reagent - Synthesis from Silicochloroform. *Chem. Sci.* **2013**, *4* (1), 77−83.
(29) Böttcher, T.; Bassil, B. S.; Röschenthaler, G.-V. Complexes of Ge(IV)- and Sn(IV)-Fluorides with Cyclic and Acyclic Carbenes: Bis(Dialkylamino)-Difluoromethylenes as Carbene Sources. *Inorg. Chem.* **2012**, *51* (2), 763−765.
(30) Böttcher, T.; Bassil, B. S.; Zhechkov, L.; Röschenthaler, G.-V. Phosphorus(V) Complexes with Acyclic Monoaminocarbene Ligands via Oxidative Addition. *Inorg. Chem.* **2013**, *52* (10), 5651−5653.
(31) Böttcher, T.; Röschenthaler, G.-V. Highly Reactive Carbenes as Ligands for Main Group Element Fluorides. Syntheses and Applications. *J. Fluor. Chem.* **2015**, *171*, 4−11.
(32) Ebenbeck, W. D.; Hilgers, P. D.; Marhold, A. D.; Barten, J. A. D.; Kolomeitsev, A. D.; Röschenthaler, G.-V. P. D. Fluorierungsreagenzien Und Verfahren Zu Deren Herstellung. Patent DE10300112A1, July 15, 2004. https://patents.google.com/patent/DE10300112A1/de (accessed Nov 9, 2022).
(33) Haaland, A. Covalent versus Dative Bonds to Main Group Metals, a Useful Distinction. *Angew. Chem., Int. Ed. Engl.* **1989**, *28* (8), 992−1007.
(34) Himmel, D.; Krossing, I.; Schnepf, A. Dative or Not Dative? *Angew. Chem., Int. Ed.* **2014**, *53* (24), 6047−6048.
(35) Himmel, D.; Krossing, I.; Schnepf, A. Dative Bonds in Main-Group Compounds: A Case for Fewer Arrows! *Angew. Chem., Int. Ed.* **2014**, *53* (2), 370−374.
(36) Frenking, G. Dative Bonds in Main-Group Compounds: A Case for More Arrows! *Angew. Chem., Int. Ed.* **2014**, *53* (24), 6040−6046.
(37) Sigmund, L. M.; Ehlert, C.; Gryn'ova, G.; Greb, L. Stereoinversion of Tetrahedral P-Block Element Hydrides. *J. Chem. Phys.* **2022**, *156* (19), 194113.
(38) Lin, J. C. Y.; Huang, R. T. W.; Lee, C. S.; Bhattacharyya, A.; Hwang, W. S.; Lin, I. J. B. Coinage Metal-N-Heterocyclic Carbene Complexes. *Chem. Rev.* **2009**, *109* (8), 3561−3598.
(39) Furst, M. R. L.; Cazin, C. S. J. Copper N-Heterocyclic Carbene (NHC) Complexes as Carbene Transfer Reagents. *Chem. Commun.* **2010**, *46* (37), 6924−6925.
(40) Egbert, J. D.; Cazin, C. S. J.; Nolan, S. P. Copper N-Heterocyclic Carbene Complexes in Catalysis. *Catal. Sci. Technol.* **2013**, *3* (4), 912−926.
(41) Li, J.; Wang, L.; Zhao, Z.; Li, X.; Yu, X.; Huo, P.; Jin, Q.; Liu, Z.; Bian, Z.; Huang, C. Two-Coordinate Copper(I)/NHC Complexes: Dual Emission Properties and Ultralong Room-Temperature Phosphorescence. *Angew. Chem., Int. Ed.* **2020**, *59* (21), 8210−8217.
(42) Hossain, J.; Akhtar, R.; Khan, S. Luminescent Coinage Metal Complexes of Carbenes. *Polyhedron* **2021**, *201*, 115151.
(43) Amouri, H. Luminescent Complexes of Platinum, Iridium, and Coinage Metals Containing N-Heterocyclic Carbene Ligands: Design, Structural Diversity, and Photophysical Properties. *Chem. Rev.* **2023**, *123* (1), 230−270.
(44) Hirsch-Weil, D.; Snead, D. R.; Inagaki, S.; Seo, H.; Abboud, K. A.; Hong, S. In Situ Generation of Novel Acyclic Diaminocarbene-Copper Complex. *Chem. Commun.* **2009**, No. 18, 2475−2477.
(45) Coyle, J. P.; Sirianni, E. R.; Korobkov, I.; Yap, G. P. A.; Dey, G.; Barry, S. T. Study of Monomeric Copper Complexes Supported by N-Heterocyclic and Acyclic Diamino Carbenes. *Organometallics* **2017**, *36* (15), 2800−2810.
(46) Toledo, A.; Salamanca, V.; Pérez-Moro, T.; Albéniz, A. C. Transmetalation of Acyclic Tungsten Carbenes to Coinage Metals: Distinct Behavior of Silver toward Carbene Transfer and Hydrolysis. *Organometallics* **2021**, *40* (1), 38−47.
(47) Kuehn, L.; Eichhorn, A. F.; Marder, T. B.; Radius, U. Copper(I) Complexes of N-Alkyl-Substituted N-Heterocyclic Carbenes. *J. Organomet. Chem.* **2019**, *881*, 25−33.
(48) Lake, B. R. M.; Bullough, E. K.; Williams, T. J.; Whitwood, A. C.; Little, M. A.; Willans, C. E. Simple and Versatile Selective Synthesis of Neutral and Cationic Copper(I) N-Heterocyclic Carbene Complexes Using an Electrochemical Procedure. *Chem. Commun.* **2012**, *48* (40), 4887−4889.
(49) Lake, B. R. M.; Willans, C. E. Structural Diversity of Copper(I)-N-Heterocyclic Carbene Complexes; Ligand Tuning Facilitates Isolation of the First Structurally Characterised Copper(I)-NHC Containing a Copper(I)-Alkene Interaction. *Chem. - Eur. J.* **2013**, *19* (49), 16780−16790.
(50) Williams, T. J.; Bray, J. T. W.; Lake, B. R. M.; Willans, C. E.; Rajabi, N. A.; Ariafard, A.; Manzini, C.; Bellina, F.; Whitwood, A. C.; Fairlamb, I. J. S. Mechanistic Elucidation of the Arylation of Non-Spectator N-Heterocyclic Carbenes at Copper Using a Combined Experimental and Computational Approach. *Organometallics* **2015**, *34* (14), 3497−3507.
(51) Benech, J.-M.; Bonomo, L.; Solari, E.; Scopelliti, R.; Floriani, C. Porphomethenes and Porphodimethenes Synthesized by the Two- and Four-Electron Oxidation of the Meso-Octaethylporphyrinogen. *Angew. Chem., Int. Ed.* **1999**, *38* (13−14), 1957−1959.
(52) Lorkowski, J.; Serrato, M. R.; Gembicki, M.; Mauduit, M.; Bertrand, G.; Jazzar, R. A Straightforward Access to Cyclic (Alkyl)(Amino)Carbene Copper (I) Complexes. *Eur. J. Inorg. Chem.* **2023**, *26*, e202300074.
(53) Kumar Kushvaha, S.; Mishra, A.; Roesky, H. W.; Chandra Mondal, K. Recent Advances in the Domain of Cyclic (Alkyl)-(Amino) Carbenes. *Chem. - Asian J.* **2022**, *17* (7), e202101301.

Supporting Information for

Concatenating Structural Constraint Effects at Tin for the Sequential Generation, Stabilization, and Transfer of Acyclic Aminocarbenes

Heiko Ruppert, Arne Meister, Ronja Pfretzschner, André Faria Vieira, Lutz Greb*

AUTHOR ADDRESS: Anorganisch-Chemisches Institut, Ruprecht-Karls-Universität Heidelberg, Heidelberg 69120, Germany.

Table of Contents

1 Experimental Details 3
2 Computational Details 4
3 Synthesis. 6
3.1 *N*,*N*-Dimethylpivalamide [2^{tBu}] 6
3.2 1-Chloro-*N*,*N*-dimethylmethaniminium chloride [3^{H}] 6
3.3 *N*,*N*-Dimethyl(1-chloroisobutyl)iminium chloride [3^{iPr}] 6
3.4 *N*,*N*-Dimethyl(1-chloroneopentyl)iminium chloride [3^{tBu}] 7
3.5 *N*,*N*-Dimethyl(1-chlorobenzyl)iminium chloride [3^{Ph}] 7
3.6 2-Chlor-*N*,*N*,*N*',*N*'-tetramethylformamidinium chloride [3^{NMe2}] 8
3.7 Stannane *N*,*N*-dimetyhlamino-*N*-methan-1-ylidene adduct 1(^{H}*a*AC)(thf) 8
3.8 Stannane *N*,*N*-dimetyhlamino-*N*-isobutan-1-ylidene adduct 1(^{iPr}*a*AC) 9
3.9 Stannane *N*,*N*-dimetyhlamino-*N*-neopentan-1-ylidene adduct [4^{tBu}] 10
3.10 Stannane *N*,*N*-dimetyhlamino-*N*-benzyl-1-ylidene adduct 1(^{Ph}*a*AC) 11
3.11 Stannane bis(*N*,*N*-dimetyhlamino)-*N*-methan-1-ylidene adduct 1(^{NMe2}*a*AC) 12
3.12 Copper(I) bromide *N*,*N*-dimetyhlamino-*N*-neopentan-1-ylidene adduct CuBr(^{tBu}*a*AC) 12
3.13 General procedure for the generation of CuCl(^{R}*a*AC) 14
3.13.1 CuCl(^{H}*a*AC) (*in situ*) 14
3.13.2 CuCl(^{iPr}*a*AC) 15
3.13.3 CuCl(^{tBu}*a*AC) 15
3.13.4 CuCl(^{Ph}*a*AC) 15
3.13.5 CuCl(^{NMe2}*a*AC) 15
4 NMR Spectra 16
4.1 3^{H} 16
4.2 3^{tBu} 17
4.3 3^{Ph} 18

4.4 1(^{H}*a*AC)(thf) 19
4.5 1(^{iPr}*a*AC) 20
4.6 1(^{tBu}*a*AC) 24
4.7 1(^{Ph}*a*AC) 26
4.8 1(^{NMe2}*a*AC) 29
4.9 Reaction of 1(^{H}*a*AC)(thf) with CuCl 31
4.10 Reaction of 1(^{iPr}*a*AC) with CuCl 32
4.11 Reaction of 1(^{tBu}*a*AC) with CuCl 34
4.12 Reaction of 1(^{Ph}*a*AC) with CuCl 37
4.13 Reaction of 1(^{NMe2}*a*AC) with CuCl 39
4.14 Reaction of 1(^{tBu}*a*AC) with (dms)CuBr 42

5 Crystallographic Data 44
5.1 Solid state molecular structures of adducts 1(^{tBu}*a*AC), 1(^{Ph}*a*AC), and 1(^{NMe2}*a*AC) 44
5.2 1(^{H}*a*AC)(thf) 45
5.3 1(^{iPr}*a*AC) 47
5.4 1(^{tBu}*a*AC) 49
5.5 1(^{Ph}*a*AC) 51
5.6 1(^{NMe2}*a*AC) 53
5.7 CuBr(^{tBu}*a*AC) 55
5.8 CuCl(^{tBu}*a*AC) 57
5.9 CuCl(^{Ph}*a*AC) 59
5.10 CuCl(^{NMe2}*a*AC) 61

6 Elemental Analysis 63
7 DFT Calculations 66
8 Bonding Analysis Results 70
9 Optimized Molecular Geometries 73
10 Literature 145

1 Experimental Details

All manipulations were carried out under a dry argon atmosphere by using standard Schlenk techniques to prevent oxidation and hydrolysis of the sensitive compounds. Lithium tin(II) *meso*-octaethylcalix[4]pyrrolate[1] and the respective chloroiminium salts **3**^{R2,3} and **3**^{NMe24} where prepared by literature-known procedures and their purity confirmed by NMR spectroscopy before use. Commercially available chemicals were used as received. All solvents and liquid chemicals were rigorously dried by applying standard procedures, freshly degassed, and stored over activated molecular sieve (3 Å resp. 4 Å) prior to use. All glassware, syringes, magnetic stirring bars, and needles were thoroughly dried. All air sensitive compounds were stored in a glove box (MBraun LABmaster dp, MB-20-G, SylaTech Y05G) under N_2 atmosphere. Analytical data of literature known compounds were compared to data of the respective reference and were found to be consistent in all cases. The purity and identity of novel compounds were confirmed by high resolution multinuclear NMR-spectroscopy, mass spectrometry, elemental analysis and if possible, X-ray diffraction analysis.

^{1}H, ^{13}C, and ^{119}Sn NMR spectra were collected with a Bruker (DPX) 200, a Bruker Advance II 400 or a Bruker 2 Advance III 600 NMR spectrometer and referenced to tetramethylsilane (^{1}H, ^{13}C) or tetramethylstannane (^{119}Sn). If not stated otherwise, ^{1}H and ^{13}C chemical shifts were taken from one-dimensional NMR spectra. To assist the correct peak assignment additional two-dimensional NMR spectra such as ^{1}H,^{1}H-COSY, ^{1}H,^{13}C-HSQC and HMBC, and broadband ^{1}H-decoupled ^{13}C-DEPT135 were recorded (only selected spectra were depicted in the supplementary information). ^{119}Sn chemical shifts were obtained from two-dimensional ^{1}H,^{119}Sn HMBC measurements. Chemical shifts are reported as dimensionless δ values in ppm, coupling constants J are given in hertz (Hz). Peak multiplicities are given as singlet (*s*), doublet (*d*), triplet (*t*), quartet (*q*), quintet (*quint*), sextet (*sext*), and septet (*sept*).

Elemental analysis for the determination of the C-,H- and N-content was carried out by the microanalysis laboratory of the Institute of Inorganic Chemistry at Heidelberg University using a vario MICRO cube of Elementar Analysensysteme.

Suitable crystals of the compounds were taken directly out of the mother liquor, immersed in perfluorinated polyether oil, and fixed on top of a cryo loop. Measurements were made on Bruker D8 Venture CCD diffractometer with a low-temperature unit using (100 or 120 K) Mo-Kα radiation chromated by mirror optics. The data collected were processed using standard Bruker APEX3 software. Structures were solved by intrinsic phasing using the SHELXT program[5] and refined with the SHELXL.[6] Graphical handling of the structural data during solution and refinement was performed with shelXLe.[7] Atomic coordinates and anisotropic thermal parameters of non-hydrogen atoms were refined by full-matrix least-squares calculations[8] and displacement ellipsoids are displayed with 50 % probability. Hydrogen atoms were included using a riding model. Crystallographic data for the structures reported in this article are deposited within the Cambridge Crystallographic Data Centre as supplementary publication no. 2303620-2303625 and 2333350-2333352 which can be obtained free of charge. Crystal data and structure are summarized in the tables under the crystallographic figures. Figures depicting solid state molecular structures and distances and angles between planes spanned by atoms have been calculated and generated by Mercury 4.2.0 without a standard deviation.

2 Computational Details

All computations employing the Orca 5.0.3[9] software or the Amsterdam Modelling Suite AMS2021.102[10,11] were carried out with the computational resources available on the bwFor Cluster JUSTUS2 located at Ulm University within the Baden Württemberg High Performance Computing program.

All structures were optimized with the Orca 5.0.3 software at the B97M[12]-D4[13]/def2-TVZPP[14] level of theory employing a def2/J auxiliary basis set.[15] Minima structures were obtained with the following ORCA input line:

```
! RKS B97M-D4 def2-TZVPP defGrid2 NoPop Opt NumFreq TightSCF
```

Conformational spaces, especially to find the lowest energy orientations of the ethyl residues of the calix[4]pyrrole ligand, were initially explored with the conformer-rotamer ensemble sampling tool (CREST)[16] for the xtb program package[17] using the following command line input. The lowest-energy conformer was then reoptimized as described below.

```
crest [file_name].xyz --alpb CH2Cl2 --chrg [charge] --noreftopo >
[file_name].out
```

```
crest [file_name].xyz --alpb THF --chrg [charge] --noreftopo >
[file_name].out
```

All calculated geometries have been confirmed as energetic minima on the potential energy surface by numerical calculation of harmonic frequencies at the B97M-D4/def2-TVZPP level, revealing only positive values.

Subsequent single point calculations employing the Conductor-like Polarizable Continuum Model Based on Solute Electron Density (C-PCM SMD)[18] were performed with the following ORCA input line:

```
! RKS B97M-D4 def2-TZVPP defGrid2 TightSCF

CPCM SMD TRUE
      SMDSOLVENT "dichloromethane"
END
```

or

```
! RKS B97M-D4 def2-TZVPP defGrid2 TightSCF

CPCM SMD TRUE
      SMDSOLVENT "THF"
END
```

High-level thermodynamic data was obtained by subsequent single point calculations employing the double-hybrid density functional DSD-BLYP[19] and def2-QZVPP basis set[14] combined with the D3(BJ)

dispersion correction[20] and the resolution-of-identity approximation[21] with automatically generated auxiliary basis sets:[22]

```
! RI-DSD-BLYP D3BJ def2-QZVPP RIJCOSX AutoAux defGrid3 TightSCF
```

Transition structures were optimized toward a single negative Hessian matrix eigenvalue using the `OptTS` keyword. It was ensured that the correct first-order saddle point on the potential energy surface was located by animation of the imaginary frequency in Chemcraft software version 1.8.[23]

Natural Bond Orbital (NBO) calculations were conducted on the PBE0[24]/def2-TZVPP[14] level of theory including a C-PCM solvation model using NBO6.0.18a[25] as included in Orca 5.0.3 *via* the following ORCA input line:

```
! RKS PBE0 def2-TZVPP NBO TightSCF defGrid2

CPCM SMD TRUE
      SMDSOLVENT "dichloromethane"
END
```

Calculations employing the Extended Transition State (ETS) method for energy decomposition analysis (EDA)[26–28] combined with the natural orbitals for chemical valence (NOCV)[29] calculations were performed on the BP86-D3(BJ)[30–32]/TZ2P level of theory as implemented in the AMS2021.201 software.[10,11]

Optimized geometries were visualized using Chemcraft version 1.8.

Isosurface plots were created using the IboView software v20150427.[33]

3 Synthesis.

3.1 *N*,*N*-Dimethylpivalamide [2^{tBu}]



According to a literature-known procedure,[34] a solution of dimethylammonium chloride (3.72 g, 45.6 mmol, 1.1 eq.) and triethylamine (6.37 g, 63.7 mmol, 1.02 eq.) was dissolved in DCM and cooled down to 0 °C. Under stirring, pivaloyl chloride (5.00 g, 5.11 mL, 41.5 mmol, 1.0 eq.) was added dropwise at 0 °C. The reaction mixture was allowed to reach room temperature and stirred overnight. The reaction mixture was diluted with 125 mL DCM, washed with 400 mL 1 M HCl, and the combined organic phases dried over $MgSO_4$. Removal of the solvent at reduced pressure yielded **2^{tBu}** as a yellowish liquid, which was used without further purification (2.87 g, 76%).

^{1}H NMR [^{1}H, ^{1}H,^{1}H-COSY] (200 MHz, $CDCl_3$, 295 K): δ [ppm] = 3.03 (*s*, $H_{2,3}$, 6H), 1.27 (*s*, H_5, 9H). In accordance with literature.[34]

3.2 1-Chloro-*N*,*N*-dimethylmethaniminium chloride [3^H]



In a 250 mL Schlenk tube under inert gas atmosphere *N*,*N*-dimethylformamide (3.02 g, 3.20 mL, 41.3 mmol, 1.00 eq.) was dissolved in MTBE (20 mL). Under vigorous stirring oxalyl chloride (5.55 g, 3.8 mL, 43.71 mmol, 1.06 eq.) was slowly added dropwise. The reaction mixture was stirred for 1 h at room temperature until the formation of gas had subsided. To ensure completeness of the reaction, the reaction mixture was heated for 1 h at 40 °C. After the mixture was cooled to room temperature, the precipitate was filtered off and washed with *n*-hexane (1 × 20 mL). The product was used without further purification. **2^H** was obtained as a pale-yellow, flaky solid in 95% yield.

^{1}H NMR [^{1}H, ^{1}H,^{1}H-COSY] (399.98 MHz, CD_3CN, 295 K): δ [ppm] = 11.10 – 11.20 (*m*, H_1, 1H), 3.75 (*s*, $H_{2,3}$, 6H).

^{13}C NMR [^{13}C{^{1}H}, ^{13}C-DEPT135, ^{1}H,^{13}C-HSQC, ^{1}H,^{13}C-HMBC] (100.55 MHz, CD_3CN, 295 K): δ [ppm] = 166.99 (*s*, C_1H), 46.42 (*s*, $C_{2,3}H_3$).

3.3 *N*,*N*-Dimethyl(1-chloroisobutyl)iminium chloride [3^{iPr}]



In a 50 mL Schlenk tube under inert gas atmosphere *N*,*N*-dimethyl isobutyramide (206 mg, 0.23 mL, 1.88 mmol, 1.00 eq.) was diluted in MTBE (10 mL). Under vigorous stirring oxalyl chloride (238 mg, 0.16 mL, 1.05 eq.) was slowly added. The reaction mixture was stirred at room temperature for 6 h until the formation of gas had subsided. The precipitate was filtered off, washed with Et_2O (1 × 20 mL) and dried in vacuo. **2^{iPr}** was obtained as colorless flaky solid in 69% yield and used without further purification.

^{1}H NMR [^{1}H, ^{1}H,^{1}H-COSY] (399.89 MHz, CD_2Cl_2, 295 K): δ [ppm] = 4.02 (*s*, $H_{2,3}$, 3H), 3.92 (*s*, $H_{2,3}$, 3H), 2.99 (*hept*, $^{3}J_{H,H}$ = 6.5 Hz, H_4, 1H), 1.43 (*d*, $^{3}J_{H,H}$ = 6.5 Hz, H_5, 6H).

^{13}C NMR [^{13}C{^{1}H}, ^{1}H,^{13}C-HSQC] (100.55 MHz, CD_2Cl_2, 295 K): δ [ppm] = 185.54 (*s*, C_1), 44.48 (*s*, $C_{2,3}H_3$), 37.43 (*s*, C_4H), 19.75 (*s*, C_5H_3).

3.4 *N*,*N*-Dimethyl(1-chloroneopentyl)iminium chloride [3^{tBu}]

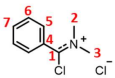


Under an inert atmosphere, in a 200 mL Schlenk tube N,N-dimethylpivalamide (3.00 g, 3.45 mL, 23.2 mmol) was dissolved in 20 mL methyl tert-butyl ether (MTBE). Under stirring, oxalyl chloride (2.10 mL, 3.15 g, 24.4, 1.05 eq.) was added dropwise at room temperature. After addition of the reagent, the solution turned cloudy and colorless precipitant was observed. The reaction mixture was stirred at 40 °C for 1 h. Subsequently, the suspension was filtered, washed with hexane (30 mL) and dried under vacuum to obtain **2^{tBu}** as colorless fluffy crystals (2.87 g, 67%) which where used without further purification.

^{1}H NMR [^{1}H, ^{1}H,^{1}H-COSY] (200 MHz, CD_3CN, 295 K): δ [ppm] = 3.84 (*s*, $H_{2,3}$, 6H), 1.55 (*s*, H_5, 9H).

^{13}C NMR [^{13}C{^{1}H}, ^{1}H,^{13}C-HSQC] (100.55 MHz, CD_3CN, 295 K): δ [ppm] = 187.79 (*s*, C_1), 51.26 (*s*, $C_{2,3}H_3$), 45.64 (*s*, C_4), 29.34 (*s*, C_5H_3).

3.5 *N*,*N*-Dimethyl(1-chlorobenzyl)iminium chloride [3^{Ph}]



In a 250 mL Schlenk flask under inert gas atmosphere *N*,*N*-dimethyl benzamide (2.02 g, 13.5 mmol, 1.00 eq.) was suspended in MTBE (80 mL). Oxalyl chloride (1.20 mL, 1.8 g, 14.2 mmol, 1.05 eq.) was added dropwise under vigorous stirring and the reaction mixture was stirred for 1 h at room temperature. The reaction mixture was heated to 40°C and stirred for an additional 4.5 h until the formation of gas had subsided. After cooling to room temperature, the precipitate was filtered off, washed with Et_2O (1 × 20 mL) and dried in vacuo. **2^{Ph}** was obtained as white flaky solid in 82% yield and used without further purification. ^{1}H-NMR spectra where in accordance with literature.[2]

^{1}H NMR [^{1}H, ^{1}H,^{1}H-COSY] (399.89 MHz, CD_2Cl_2, 295 K): δ [ppm] = : 8.04 – 8.10 (*m*, H_5, 2H), 7.65 – 7.75 (*m*, H_7, 1H), 7.56 – 7.63 (*m*, H_6, 2H), 4.08 (*s*, $H_{2,3}$, 6H).

^{13}C NMR [^{13}C{^{1}H}, ^{13}C-DEPT135, ^{1}H,^{13}C-HSQC, ^{1}H,^{13}C-HMBC] (100.55 MHz, CD_2Cl_2, 295 K): δ [ppm] = 173.33 (*s*, C_1), 134.79 (*s*, C_7H) , 131.29 (*s*, C_4), 129.70 (*s*, C_5H), 129.63 (*s*, C_6H), 49.77 (*s*, $C_{2,3}H_3$).

3.6 2-Chlor-*N*,*N*,*N*',*N*'-tetramethylformamidinium chloride [3^{NMe2}]



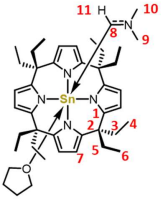
In a 50 mL Schlenk tube 15 mL $CHCl_3$, 0.96 ml (929.3 mg, 8.00 mmol) *N*,*N*,*N*',*N*'-tetramethyl urea and 3.43 ml (5072.2 mg, 40.00 mg) oxalyl chloride are refluxed for 16 hours. Volatile compounds are removed in vacuo and the residue is washed with 5 x 5 ml diethyl ether. After removal of the solvent, the product was obtained as a colorless solid (1297.3 mg, 7.58 mmol, 92% yield).

^{1}H NMR [^{1}H, ^{1}H,^{1}H-COSY] (399.89 MHz, CD_3CN, 295 K): δ [ppm] 3.30 (*s*, $H_{2,3}$, 12H).

^{13}C NMR [^{13}C{^{1}H}, ^{13}C-DEPT135, ^{1}H,^{13}C-HSQC, ^{1}H,^{13}C-HMBC] (100.55 MHz, CD_3CN, 295 K): δ [ppm] = 160.37 (*s*, C_1), 44.86 (*s*, $C_{2,3}H_3$).

Both in accordance with literatue.[4]

3.7 Stannane *N*,*N*-dimetyhlamino-*N*-methan-1-ylidene adduct 1(^{H}*a*AC)(thf)



In a 50 mL Schlenk tube under an inert gas atmosphere **3^H** (1.00 eq., 180.7 mmol, 22.6 mg) was suspended in 3 mL THF and cooled to −78°C. Separately **[Li$_2$(thf)$_x$][1]** (1.00 eq., 179.6 mmol, 150 mg) was dissolved in 2 mL THF. Under stirring the solution of **[Li$_2$(thf)$_x$][1]** was added dropwise to the suspension of **3^H** and the resulting yellow reaction mixture was stirred at −78°C for 30 min. Subsequently, the mixture was allowed to reach room temperature and stirred for another 30 min. The solvent was removed in vacuo. The obtained solid was suspended in hexane and extracted until the extract became colorless. The combined hexane phases were stored at −30°C for several days to facilitate the crystallization **1(^{H}*a*AC)(thf)** as yellow/orange crystals (74.0 mg, 103.8 µmol, 57 % yield). Cooling of a concentrated hexane solution at −30°C also yielded single crystals suitable for X-ray diffraction.

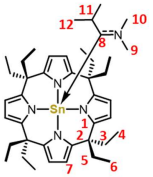
^{1}H NMR [^{1}H, ^{1}H,^{1}H-COSY] (399.89 MHz, THF-*d*$_8$, 295 K): δ [ppm] = 7.42 (*s*, ^{117,119}Sn-satellites $^2J_{Sn,H}$ = 84.88 Hz , H_{11}, 1H), 6.07 (*s*, ^{117,119}Sn-satellites $^4J_{Sn,H}$ = 13.0 Hz, H_7, 8H), 3.60 – 3.63 (*m*, H_{thf}, 2H), 3.27 (*d*, $^4J_{H,H}$ = 1.1 Hz, H_{10}, 3H), 2.63 (*s*, ^{117,119}Sn-satellites $^4J_{Sn,H}$ = 6.0 Hz, H_9 ,3H), 1.85 (*q*, $^3J_{H,H}$ = 7.3 Hz, $H_{3,5}$, 8H), 1.77 (*q*, $^3J_{H,H}$ = 7.3 Hz, $H_{3,5}$, 8H overlapped with THF), 1.75 – 1.81 (*m*, H_{thf}, 2H), 0.66 (*t*, $^3J_{H,H}$ = 7.3 Hz, $H_{4,6}$, 12H overlapped with H_8), 0.63 (*t*, $^3J_{H,H}$ = 7.3 Hz, $H_{4,6}$, 12H).

^{13}C NMR [^{13}C{^{1}H}, ^{13}C-DEPT135, ^{1}H,^{13}C-HSQC, ^{1}H,^{13}C-HMBC] (100.55 MHz, THF-*d*$_8$, 295 K): δ [ppm] = 225.31 (*s*, C_8H), 143.06 (*s*, C_1), 109.01 (*s*, ^{117,119}Sn-satellites $^3J_{Sn,C}$ = 35.2 Hz, C_7H), 68.39 (*s*, $C_{thf}H_2$), 53.52 (*s*, $C_{10}H_3$), 47.35 (*s*, C_9H_3), 46.98 (*s*, ^{117,119}Sn-satellites $^3J_{Sn,C}$ = 11.1 Hz, C_2), 38.31 (*s*, $C_{3,5}H_2$), 38.25 (*s*, $C_{3,5}H_2$), 26.56 (.*s*, $C_{thf}H_2$), 10.40 (*s*, $C_{4,6}H_3$), 10.36 (*s*, $C_{4,6}H_3$).

^{119}Sn NMR [^{1}H,^{119}Sn-HMBC] (149.04 MHz, THF-d_8, 295 K): δ[ppm] = −576.4.

EA: calcd. for $C_{43}H_{63}N_5OSn$: C, 65.82; H, 8.09; N, 8.92. Found: C, 65.61; H, 7.92; N, 8.87.

3.8 Stannane *N*,*N*-dimetyhlamino-*N*-isobutan-1-ylidene adduct 1(*i*Pr*a*AC)



In a 50 mL Schlenk tube under inert gas atmosphere **3**^{iPr} (96.8 mg, 569 µmol, 1.00 eq.) was suspended in 8 mL THF. After cooling the mixture to −78°C, a solution of **[Li$_2$(thf)$_x$][1]** (500 mg, 569 µmol, 1.00 eq.) in 4 mL THF was added dropwise while stirring vigorously. The reaction mixture turned orange and was stirred for an additional 30 minutes at −78°C before being allowed to reach room temperature. At room temperature, the reaction mixture was stirred for 30 minutes before the solvent was removed at reduced pressure. The crude product was extracted with 10 mL DCM, filtered over a syringe filter to remove the LiCl formed during the reaction, and subsequently purified over a short silica plug. Evaporation of the eluate yielded **4**^{iPr} as an orange solid (175.0 mg, 232 µmol, 41 % yield) was obtained as an orange crystalline solid. Gas phase diffusion of pentane into a concentrated solution of **1(**^{iPr}***a*AC)** at −30°C yielded single crystals suitable for X-ray diffraction.

^{1}H NMR [^{1}H, ^{1}H,^{1}H-COSY] (600.18 MHz, CD_2Cl_2, 295 K): δ [ppm] = 6.13 (*s*, ^{117,119}Sn-satellites $^{4}J_{Sn,H}$ = 16.8 Hz, H_7, 8H), 3.23 (*s*, ^{117,119}Sn-satellites $^{4}J_{Sn,H}$ = 9.0 Hz, H_{10},3H), 2.72 (*s*, ^{117,119}Sn-satellites $^{4}J_{Sn,H}$ = 9.0 Hz, H_9, 3H), 2.22 (*sept*, $^{3}J_{H,H}$ = 7.1 Hz, H_{11}, 1H), 1.90 – 1.81 (*m*, H_5, 8H), 1.79 (*q*, $^{3}J_{H,H}$ = 7.2 Hz, H_3, 8H), 0.87 (*t*, $^{3}J_{H,H}$ = 7.4 Hz, H_6, 12H), 0.63 (*d*, $^{3}J_{H,H}$ = 7.1 Hz, H_{12}, 6H), 0.56 (*t*, $^{3}J_{H,H}$ = 7.2 Hz, H_4, 12H).

^{1}H NMR [^{1}H, ^{1}H,^{1}H-COSY] (600.18 MHz, CD_2Cl_2, 323 K): δ [ppm] = 6.16 (*s*, ^{117,119}Sn-satellites $^{4}J_{Sn,H}$ = 12.0 Hz, H_7, 8H), 3.23 (*s*, H_{10},3H), 2.73 (*s*, H_9, 3H), 2.31 (*sept*, $^{3}J_{H,H}$ = 7.1 Hz, H_{11}, 1H), 1.90 (*q*, $^{3}J_{H,H}$ = 7.2 Hz, H_5, 8H), 1.83 (*q*, $^{3}J_{H,H}$ = 7.2 Hz, H_3, 8H), 0.92 (*t*, $^{3}J_{H,H}$ = 7.2 Hz, H_6, 12H), 0.67 (*d*, $^{3}J_{H,H}$ = 7.1 Hz, H_{12}, 6H), 0.60 (*t*, $^{3}J_{H,H}$ = 7.1 Hz, H_4, 12H).

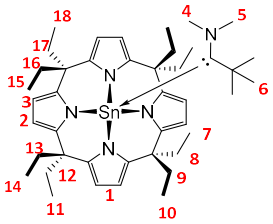
^{13}C NMR [^{13}C{^{1}H}, ^{13}C-DEPT135, ^{1}H,^{13}C-HSQC, ^{1}H,^{13}C-HMBC] (150.92 MHz, CD_2Cl_2, 295 K): δ [ppm] = 232.43 (*s*, C_8), 143.13 (*s*, C_1), 107.97 (*s*, C_7H), 49.67 (*s*, ^{117,119}Sn-satellites $^{3}J_{Sn,C}$ = 34.7 Hz, C_9H_3), 47.14 (*s*, ^{117,119}Sn-satellites $^{3}J_{Sn,C}$ = 42.3 Hz, $C_{10}H_3$), 45.27 (*s*, ^{117,119}Sn-satellites $^{3}J_{Sn,C}$ = 10.6 Hz, C_2), 40.60 (*s*, *broad,* C_3H_2), 36.0 (*s*, *broad and overlayed with* C_{11}H), coupling in ^{1}H,^{13}C-HSQC, C_5H_2), 35.84 (*s*, ^{117,119}Sn-satellites $^{2}J_{Sn,C}$ = 52.8 Hz, C_{11}H), 19.30 (*s*, ^{117,119}Sn-satellites $^{2}J_{Sn,C}$ = 16.6 Hz, $C_{12}H_3$), 10.21 (*s*, C_6H_3), 9.89 (*s*, C_4H_3).

^{13}C NMR [^{13}C{^{1}H}, ^{13}C-DEPT135, ^{1}H,^{13}C-HSQC, ^{1}H,^{13}C-HMBC] (150.92 MHz, CD_2Cl_2, 323 K): δ [ppm] = not measured (*s*, C_8), 143.65 (*s*, C_1), 108.40 (*s*, ^{117,119}Sn-satellites $^{3}J_{Sn,C}$ = 36.2 Hz, C_7H), 50.20 (*s*, ^{117,119}Sn-satellites $^{3}J_{Sn,C}$ = 33.2 Hz, C_9H_3), 47.23 (*s*, ^{117,119}Sn-satellites $^{3}J_{Sn,C}$ = 40.8 Hz, $C_{10}H_3$), 45.75 (*s*, ^{117,119}Sn-satellites $^{3}J_{Sn,C}$ = 4.5 Hz, C_2), 41.07 (*s*, *broad,* C_3H_2), 36.26 (*s*, ^{117,119}Sn-satellites $^{2}J_{Sn,C}$ = 52.8 Hz, C_{11}H) 35.89 (*s*, *broad*, C_5H_2), 19.53 (*s*, ^{117,119}Sn-satellites $^{2}J_{Sn,C}$ = 16.6 Hz, $C_{12}H_3$), 10.44 (*s*, C_6H_3), 10.01 (*s*, C_4H_3).

^{119}Sn NMR [^{1}H,^{119}Sn-HMBC] (223.81 MHz, CD_2Cl_2, 295 K): δ[ppm] = −458.0.

EA: calcd. for $C_{42}H_{61}N_5Sn$: C, 66.84; H, 8.15; N, 9.28. Found: C, 66.37; H, 8.17; N, 9.33.

3.9 Stannane *N*,*N*-dimetyhlamino-*N*-neopentan-1-ylidene adduct [4^{tBu}]



In a 50 mL Schlenk tube **[Li$_2$(thf)$_x$][1]** (1.00 eq., 598.6 µmol, 500 mg) and **3^{tBu}** (1.00 eq., 598.6 µmol, 110.2 mg) were combined and cooled to −30°C. The solids were dissolved in 10 mL *o*DFB precooled to −30°C under stirring to give an intensely red colored suspension that was subsequently stirred for 20 minutes. LiCl formed during the reaction was removed by filtration over a PTFE syringe filter. The crude oDFB solution was transferred onto a 2 cm thick silica plug and eluted with DCM. Evaporation of the solvent from the eluate and subsequent drying at vacuum yielded **1(*^{tBu}*aAC)** as a red solid (355 mg, 462 µmol, 85 % yield). Cooling of a concentrated solution of **1(*^{tBu}*aAC)** in toluene to −30°C yielded single crystals suitable for X-ray diffraction.

^{1}H NMR [^{1}H, ^{1}H,^{1}H-COSY] (600.16 MHz, CD_2Cl_2, 295 K) δ[ppm] = 6.13 (*d*, $^{3}J_{H,H}$ = 3.3 Hz, H_2, 2H), 6.11 (*s*, ^{117,119}Sn-satellites $^{4}J_{Sn,H}$ = 24.0 Hz, H_1, 4H), 6.07 (*d*, $^{3}J_{H,H}$ = 3.3 Hz, H_3, 2H), 3.38 (*s*, H_5, 3H), 2.69 (*s*, ^{117,119}Sn-satellites $^{3}J_{Sn,H}$ = 10.6 Hz, H_4, 3H), 2.13 (*q*, $^{3}J_{H,H}$ = 6.9 Hz, H_{12}, 4H), 2.03 – 1.95 (*m*, H_8 and H_{17} overlapped, 4H), 1.60 – 1.67 (m, H_9, H_{16}, and ½ H_{13} overlapped, 6H), 1.56 (*m*, ½ H_{13}, 2H), 1.13 (*t*, $^{3}J_{H,H}$ = 7.2 Hz, H_{11}, 3H), 0.96 (t, $^{3}J_{H,H}$ = 7.2 Hz, H_{11}, 3H), 0.90 (*t*, $^{3}J_{H,H}$ = 7.3 Hz, H_{14}, 6H), 0.86 (s, H_6, 9H), 0.56 (t, $^{3}J_{H,H}$ = 7.2 Hz, H_{18}, 6H overlapped with H_{15}), 0.55 (*t*, $^{3}J_{H,H}$ = 7.2 Hz, H_{15}, 3H overlapped with H_{10}), 0.50 (*t*, $^{3}J_{H,H}$ = 7.4 Hz, H_{10}, 3H).

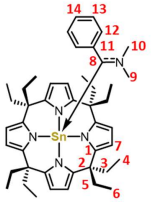
^{13}C NMR [^{13}C{^{1}H}, ^{13}C-DEPT135, ^{1}H,^{13}C-HSQC, ^{1}H,^{13}C-HMBC] (100.55 MHz, CD_2Cl_2, 295 K): δ [ppm] = 234.14 (*s*, C_{carb}), 145.00 (*s*, α-$C_{pyrrole}$), 143.72 (*s*, α-$C_{pyrrole}$), 141.23 (*s*, α-$C_{pyrrole}$), 140.85 (*s*, α-$C_{pyrrole}$), 108.53 (*s*, $C_{2,3}$H), 108.45 (*s*, C_1H), 107.78 (*s*, $C_{2,3}$H), 107.16 (*s*, C_1H), 50.63 (*s*, C_4H$_3$), 49.84 (*s*, C_5H$_3$), 45.47 (*s*, CH_2), 45.05 (*s*, $C(C_6H_3)_3$), 44.89 (*s*, $C(C_{12}H_2)(C_{13}H_2)$), 44.83 (*s*, CEt_2), 44.76 (*s*, CEt_2), 41.79 (*s*, C_{17}H$_3$), 35.37 (*s*, $C_{12,16}$H$_3$), 30.28 (*s*, 3x CH_2), 30.16 (*s*, C_6H$_3$), 28.63 (*s*, CH_2), 28.38 (*s*, CH_2), 10.52 (*s*, CH_3), 10.45 (*s*, CH_3), 9.88 (*s*, CH_3), 9.80 (*s*, CH_3), 9.56 (*s*, CH_3), 8.03 (*s*, CH_3).

^{119}Sn NMR [^{1}H-^{119}Sn-HMBC] (223.81 MHz, CD_2Cl_2, 295 K): δ[ppm] = −474.7.

^{119}Sn NMR [^{1}H-^{119}Sn-HMBC] (149.04 MHz, THF-d_8, 295 K): δ[ppm] = −476.0

EA: calcd. for $C_{43}H_{63}N_5Sn$: C, 67.10; H, 8.38; N, 9.10. Found: C, 66.68; H, 8.64; N, 9.02.

3.10 Stannane *N*,*N*-dimetyhlamino-*N*-benzyl-1-ylidene adduct 1(^Ph*a*AC)



In a 50 mL Schlenk tube **[Li$_2$(thf)$_x$][1]** (1.00 eq., 598.6 µmol, 500 mg) and **3^{Ph}** (1.00 eq., 598.6 µmol, 122.0 mg) were combined and cooled to −30°C. The solids were dissolved in 10 mL oDFB precooled to −30°C under stirring to give an intensely red colored suspension that was subsequently stirred for 20 minutes. LiCl formed during the reaction was removed by filtration over a PTFE syringe filter. The crude oDFB solution was transferred onto a 2 cm thick silica plug and eluted with ~4 mL DCM. Evaporation of the solvent from the eluate and subsequent drying at vacuum yielded **1(^Ph*a*AC)** as a red solid (376 mg, 477 µmol, 80 % yield). Cooling of a concentrated solution of **1(^Ph*a*AC)** in toluene to −30°C yielded single crystals suitable for X-ray diffraction.

^{1}H NMR [^{1}H, ^{1}H,^{1}H-COSY] (399.89 MHz, CD_2Cl_2, 295 K) δ[ppm] = 7.29 – 7.23 (*m*, ^{117,119}Sn-satellites $^6J_{Sn,H}$ = 3.2 Hz, H_{14}, 1H), 7.12 – 7.09 (*m*, ^{117,119}Sn-satellites $^5J_{Sn,H}$ = 3.6 Hz, H_{13}, 2H), 6.06 (*s*, *broad*, H_7, 8H), 5.99 – 5.95 (*m*, H_{12}, 2H), 3.17 (*s*, ^{117,119}Sn-satellites $^4J_{Sn,H}$ = 6.4 Hz, H_{10}, 3H), 2.75 (*s*, ^{117,119}Sn-satellites $^4J_{Sn,H}$ = 8.4 Hz, H_9, 3H), 1.88 (*q*, *broad*, H_5, 8H), 1.79 (*q*, b*road*, $^3J_{H,H}$ = 7.2 Hz, H_3, 8H), 0.87 (*t*, *broad*, $^3J_{H,H}$ = 7.6 Hz, H_6, 12H), 0.55 (*t*, $^3J_{H,H}$ = 7.2 Hz, H_4, 12H).

^{1}H NMR [^{1}H, ^{1}H,^{1}H-COSY] (399.89 MHz, CD_2Cl_2, 323 K) δ[ppm] = 7.29 – 7.22 (*m*, H_{14}, 1H), 7.14 – 7.08 (*m*, H_{13}, 2H), 6.06 (*s*, ^{117,119}Sn-satellites $^4J_{Sn,H}$ = 18.0 Hz,z H_7, 8H), 6.06 – 6.02 (*m*, H_{12}, 2H), 3.17 (*s*, H_{10}, 3H), 2.77 (*s*, H_9, 3H), 1.93 (*q*, $^3J_{H,H}$ = 7.5 Hz, H_5, 8H), 1.83 (*q*, $^3J_{H,H}$ = 7.4 Hz, H_3, 8H), 0.91 (*t*, $^3J_{H,H}$ = 7.4 Hz, H_6, 12H), 0.58 (*t*, $^3J_{H,H}$ = 7.2 Hz, H_4, 12H).

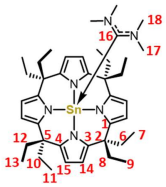
^{13}C NMR [^{13}C{^{1}H}, ^{13}C-DEPT135, ^{1}H,^{13}C-HSQC, ^{1}H,^{13}C-HMBC] (150.93 MHz, CD_2Cl_2, 295 K): δ [ppm] = 220.19 (*s*, C_8), 143.29 (*s*, C_1), 134.29 (*s*, ^{117,119}Sn-satellites $^2J_{Sn,C}$ = 43.8 Hz, C_{11}), 131.79 (*s*, ^{117,119}Sn-satellites $^5J_{Sn,C}$ = 6.0 Hz, C_{14}H), 128.93 (*s*, ^{117,119}Sn-satellites $^4J_{Sn,C}$ = 3.0 Hz, C_{13}H), 128.81 (*s*, ^{117,119}Sn-satellites $^3J_{Sn,C}$ = 13.6 Hz, C_{12}H), 107.63 (*s*, *broad*, C_7H), 48.8 (*s*, ^{117,119}Sn-satellites $^3J_{Sn,C}$ = 24.1 Hz, C_9H_3), 47.66 (*s*, ^{117,119}Sn-satellites $^3J_{Sn,C}$ = 30.2 Hz, $C_{10}H_3$), 45.13 (*s*, *broad*, C_2), *not observed* (*s*, C_5H_2), *not observed* (*s*, *broad*, C_3H_2), 10.41 (*s*, C_6H_3), 9.79 (*s*, C_4H_3).

^{13}C NMR [^{13}C{^{1}H}, ^{13}C-DEPT135, ^{1}H,^{13}C-HSQC, ^{1}H,^{13}C-HMBC] (150.93 MHz, CD_2Cl_2, 323 K): δ [ppm] = *not measured* (*s*, C_8), 143.74 (*s*, C_1), 134.83 (*s*, C_{11}), 131.93 (*s*, C_{14}H), 129.15 (*s*, C_{13}H), 128.92 (*s*, C_{12}H), 108.09 (*s*, ^{117,119}Sn-satellites $^3J_{Sn,C}$ = 36.2 Hz, C_7H), 48.79 (*s*, ^{117,119}Sn-satellites $^3J_{Sn,C}$ = 25.7 Hz, C_9H_3), 48.14 (*s*, ^{117,119}Sn-satellites $^3J_{Sn,C}$ = 28.7 Hz, $C_{10}H_3$), 45.60 (*s*, ^{117,119}Sn-satellites $^3J_{Sn,C}$ = 9.1 Hz, C_2), 41.24 (*s*, *broad* C_5H_2), 35.22 (*s*, *broad*, C_3H_2), 10.41 (*s*, C_6H_3), 9.79 (*s*, C_4H_3).

^{119}Sn NMR [^{1}H,^{119}Sn-HMBC] (149.12 MHz, CD_2Cl_2, 295 K): δ[ppm] = −451.3.

EA: calcd. for $C_{45}H_{59}N_5Sn$: C, 68.44; H, 7.66; N, 8.87. Found: C, 68.71; H, 7.44; N, 8.92.

3.11 Stannane bis(*N*,*N*-dimetyhlamino)-*N*-methan-1-ylidene adduct 1(^NMe2*a*AC)



In a 50 mL Schlenk tube **[Li$_2$(thf)$_x$][1]** (1.00 eq., 598.6 µmol, 500 mg) and **3^{NMe2}** (1.00 eq., 598.6 µmol, 102.4 mg) were combined and cooled to −30°C. The solids were dissolved in 10 mL *o*DFB precooled to −30°C under stirring to give a pale orange colored suspension that was subsequently stirred for 20 minutes. LiCl formed during the reaction was removed by filtration over a PTFE syringe filter. The crude oDFB solution was transferred onto a 2 cm thick silica plug and eluted with ~4 mL DCM. Evaporation of the solvent from the eluate and subsequent drying at vacuum yielded **1(^NMe2*a*AC)** as a red solid (340 mg, 450 µmol, 75 % yield). Cooling of a concentrated solution of **1(^NMe2*a*AC)** in toluene to −30°C yielded single crystals suitable for X-ray diffraction.

^{1}H NMR [^{1}H, ^{1}H,^{1}H-COSY] (600.15 MHz, CD_2Cl_2, 295 K) δ[ppm] = 6.10 (*d*, $^3J_{H,H}$ = 3.0 Hz, ^{117,119}Sn-satellites $^6J_{Sn,H}$ = 18.6 Hz, $H_{14;15}$, 4H), 6.06 (*d*, $^3J_{H,H}$ = 3.0 Hz, ^{117,119}Sn-satellites $^6J_{Sn,H}$ = 18.6 Hz, $H_{14;15}$, 4H), 2.78 (*s*, H_{18}, 6H), 2.12 (*q*, $^3J_{H,H}$ = 7.2 Hz, H_8, 4H), 2.03 (*s*, H_{17}, 6H), 2.00 (*q*, $^3J_{H,H}$ = 7.1 Hz, H_{12}, 4H), 1.67 (*q*, $^3J_{H,H}$ = 7.3 Hz, H_{10}, 4H), 1.53 (*q*, $^3J_{H,H}$ = 7.4 Hz, H_6, 4H), 1.02 (*t*, $^3J_{H,H}$ = 7.2 Hz, H_9, 6H), 0.80 (*t*, $^3J_{H,H}$ = 7.4 Hz, H_7, 6H), 0.61 (*t*, $^3J_{H,H}$ = 7.1 Hz, H_{13}, 6H), 0.54 (*t*, $^3J_{H,H}$ = 7.4 Hz, H_{11}, 6H).

^{13}C NMR [^{13}C{^{1}H}, ^{13}C-DEPT135, ^{1}H,^{13}C-HSQC, ^{1}H,^{13}C-HMBC] (100.55 MHz, CD_2Cl_2, 295 K): δ [ppm] = 195.75 (*s*, C_{16}), 143.88 (*s*, C_4), 141.42 (*s*, C_1), 108.01 (*s*, $CH_{14;15}$), 106.98 (*s*, $CH_{14;15}$), 46.69 (*s*, $C_{18}H_3$), 45.40 (*s*, C_5), 44.84 (*s*, C_2), 44.57 (*s*, $C_{10}H_2$), 40.99 (*s*, $C_{17}H_3$), 39.82 (*s*, C_6H_2), 35.29 (*s*, $C_{12}H_2$), 29.32 (*s*, C_8H_2), 10.44 (*s*, C_9H_3), 10.31 (*s*, C_7H_3), 9.98 (*s*, $C_{13}H_3$), 9.78 (*s*, $C_{11}H_3$).

^{119}Sn NMR [^{1}H,^{119}Sn-HMBC] (149.12 MHz, CD_2Cl_2, 295 K): δ[ppm] = −462.7.

EA: calcd. for $C_{41}H_{60}N_6Sn$: C, 65.17; H, 8.00; N, 11.12. Found: C, 65.63; H, 8.01; N, 11.72

3.12 Copper(I) bromide *N*,*N*-dimetyhlamino-*N*-neopentan-1-ylidene adduct CuBr(^tBu*a*AC)



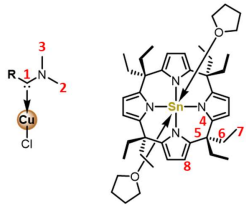
In a Young NMR tube **1(^tBu*a*AC)** (1.00 eq., 32.5 µmol, 25.0 mg) and (dms)CuBr (1.00 eq.,32.5 µmol, 6.7 mg) where dissolved in 0.45 mL THF-d_8. The reaction mixture was mixed at room temperature for 24 hours and the reaction monitored by NMR spectroscopy. The formation of **CuBr(^tBu*a*AC)** and **1(thf$_2$)** (characteristic ^{1H,119Sn}-HMBC signal at −560.8 ppm and intense singlet in ^{1}H NMR at 6.11 ppm with ^{117,119}Sn-satellites for H_8) were evidenced by ^{1}H, ^{13}C, and ^{119}Sn NMR spectroscopy. Evaporation of the solvent yielded an orange residue which was redissolved in DCM. PPh_4Br (1.1 eq., 35.8 µmol, 136. mg) was added and the solution was mixed for 1 hour until all solids were dissolved. Evaporation of the

solvent afforded an orange solid which was dried at reduced pressure. Recrystallization from *n*-hexane yielded single crystals of **CuBr(^{tBu}aAC)** suitable for X-ray diffraction.

^{1}H NMR [^{1}H, ^{1}H,^{1}H-COSY] (600.15 MHz, THF-d_8, 295 K) δ[ppm] = 3.87 (*s*, $H_{2,3}$, 3H), 3.39 (s, $H_{2,3}$, 3H), 1.32 (*s*, H_5, 9H).

^{13}C NMR [^{13}C{^{1}H}, ^{13}C-DEPT135, ^{1}H,^{13}C-HSQC, ^{1}H,^{13}C-HMBC] (150.92 MHz, THF-d_8, 295 K): δ [ppm] = 251.41 (*s*, C_1), 52.65 (*s*, $C_{2,3}H_3$), 39.94 (*s*, $C_{2,3}H_3$), 25.26 (*s*, C_5H_3).

3.13 General procedure for the generation of CuCl(RaAC)



In a Young NMR tube **1(R*a*AC)** (1.00 eq., ~40 µmol) and CuCl (1.50 eq.) where dissolved in 0.40 mL THF and 0.05 mL C_6D_6 to follow the completeness of the reaction *via* ^{1}H NMR spectroscopy. The reaction mixture was mixed at room temperature for 18 to 60 hours depending on the adduct **1(R*a*AC)** (R = Ph, t = 18 h; R = NMe_2, t = 60 h; R = *t*Bu, t = 18 h; R = *i*Pr, t = 72). The complete consumption of **1(R*a*AC)** and the formation of **CuCl(R*a*AC)** and **1(thf$_2$)** (characteristic ^{1}H,^{119}Sn-HMBC signal at −560.8 ppm and intense singlet in ^{1}H NMR at 6.11 ppm with ^{117,119}Sn-satellites for H_8) were evidenced by ^{1}H, ^{13}C, and ^{1}H,^{119}Sn-HMBC NMR spectroscopy. **1(H*a*AC)** decomposed at room temperature in THF and was only transiently analyzed *via* a test reaction in pure THF-d_8.

^{1}H NMR of **1(thf$_2$)** [^{1}H, ^{1}H,^{1}H-COSY] (600.15 MHz, THF-d_8, 295 K) δ[ppm] = 6.11 (*s*, ^{117,119}Sn-satellites $^4J_{Sn,H}$ = 17.1 Hz, H_8, 8H), 1.84 (*q*, $^3J_{H,H}$ = 7.3 Hz, H_6, 16H), 0.65 (*t*, $^3J_{H,H}$ = 7.3 Hz, H_7, 24H).

General workup procedure:
The residue CuCl was removed *via* filtration over a PTFE syringe filter and the solvent of the filtrate removed at vacuum. The residue was washed four times with 4-5 mL *n*-hexane to remove the **1(thf$_2$)** formed during the reaction. For each washing step the crude was stirred in *n*-hexane for about 30 minutes and the supernatant removed by centrifugation. After drying the residue at reduced pressure recrystallization from THF and excess *n*-hexane at −30 °C yielded the carbene adducts **CuCl(RAC)** as off-white to orange solids (R = *i*Pr, 5.9 mg, 29.8 µmol, 60% yield; R = *t*Bu, 5.0 mg, 23.6 µmol, 50% yield; R = Ph, 5.3 mg, 23.0 µmol, 52% yield; R = NMe_2, 5.3 mg, 26.6 µmol, 51% yield). Singel crystals suitable for X-ray diffraction for R = *t*Bu, Ph, and NMe_2 could be obtained from the recrystallization mother liquor.

3.13.1 CuCl(H*a*AC) (*in situ*)

^{1}H NMR [^{1}H, ^{1}H,^{1}H-COSY] (600.15 MHz, THF-d_8, 295 K) δ[ppm] = 8.80 (*s*, C_1H, 1H), 3.73 (*s*, $H_{2,3}$, 3H), 3.52 (s, $H_{2,3}$, 3H).

^{13}C NMR [^{13}C{^{1}H}, ^{13}C-DEPT135, ^{1}H,^{13}C-HSQC, ^{1}H,^{13}C-HMBC] (150.92 MHz, THF-d_8, 295 K): δ [ppm] = 231.5 (*s*, C_1H, only observed in ^{1}H,^{13}C-HMBC), 52.7 (*s*, $C_{2,3}H_3$, only observed in ^{1}H,^{13}C-HMBC).

3.13.2 CuCl(*iPr*aAC)

^{1}H NMR [^{1}H, ^{1}H,^{1}H-COSY] (600.15 MHz, THF-d_8, 295 K) δ[ppm] = 3.78 (*s*, $H_{2,3}$, 3H), 3.28 (*s*, $H_{2,3}$, 3H), 2.64 (*hept*, $^3J_{H,H}$ = 6.6 Hz, C*H*$(CH_3)_2$, 1H), 1.15 (*d*, $^3J_{H,H}$ = 6.5 Hz, CH(CH_3)$_2$, 6H).

^{13}C NMR [^{13}C{^{1}H}, ^{13}C-DEPT135, ^{1}H,^{13}C-HSQC, ^{1}H,^{13}C-HMBC] (150.92 MHz, THF-d_8, 295 K): δ [ppm] = 248.03 (*s*, C_1), 55.73 (*s*, $C_{2,3}H_3$), 39.74 (*s*, $C_{2,3}H_3$), 38.34 (*s*, *C*H$(CH_3)_2$), 20.81 (*s*, CH(*C*H_3)$_2$).

HR-MS (ESI, positive, THF): calcd. for [M-Cl = $C_6H_{13}CuN]^+$ m/z = 162.0444, found m/z = 162.0439.

3.13.3 CuCl(*tBu*aAC)

^{1}H NMR [^{1}H, ^{1}H,^{1}H-COSY] (600.15 MHz, THF-d_8, 295 K) δ[ppm] = 3.87 (*s*, $H_{2,3}$, 3H), 3.39(*s*, $H_{2,3}$, 3H), 1.32 (*s*, C(*C*H_3)$_3$, 9H).

^{13}C NMR [^{13}C{^{1}H}, ^{13}C-DEPT135, ^{1}H,^{13}C-HSQC, ^{1}H,^{13}C-HMBC] (150.92 MHz, THF-d_8, 295 K): δ [ppm] = 253.9 (*s*, C_1, only observed *in situ*), 57.57 (*s*, $C_{2,3}H_3$), 42.63 (*s*, $C_{2,3}H_3$), 41.92 (*s*, *C*$(CH_3)_3$), 28.32 (*s*, C(*C*H_3)$_3$).

HR-MS (ESI, positive, THF): calcd. for [M-Cl = $C_7H_{15}CuN]^+$ m/z = 176.0600, found m/z = 176.0594.

3.13.4 CuCl(*Ph*aAC)

^{1}H NMR [^{1}H, ^{1}H,^{1}H-COSY] (600.15 MHz, THF-d_8, 295 K) δ[ppm] = 7.37 – 7.42 (*m*, *meta*-H_{Ph}, 2H), 7.27 – 7.30 (*m*, *para*-H_{Ph}, 1H), 7.08 – 7.12 (*m*, *ortho*-H_{Ph}, 2H), 3.92 (*s*, $H_{2,3}$, 3H), 3.18 (s, $H_{2,3}$, 3H).

^{13}C NMR [^{13}C{^{1}H}, ^{13}C-DEPT135, ^{1}H,^{13}C-HSQC, ^{1}H,^{13}C-HMBC] (150.92 MHz, THF-d_8, 295 K): δ [ppm] = 239.61 (*s*, C_1), 145.23 (*s*, *ipso*-C_{Ph}), 129.67 (*s*, *meta*-CH_{Ph}), 128.92 (*s*, *para*-CH_{Ph}), 124.76 (*s*, *ortho*-CH_{Ph}), 54.74 (*s*, $C_{2,3}H_3$), 42.28 (*s*, $C_{2,3}H_3$).

HR-MS (ESI, positive, THF): calcd. for [M-Cl = $C_9H_{11}CuN]^+$ m/z = 196.0287, found m/z = 196.0967.

3.13.5 CuCl(*NMe2*aAC)

^{1}H NMR [^{1}H, ^{1}H,^{1}H-COSY] (600.15 MHz, THF-d_8, 295 K) δ[ppm] = 3.22 (*s*, N(CH_3)$_2$, 12 H).

^{13}C NMR [^{13}C{^{1}H}, ^{13}C-DEPT135, ^{1}H,^{13}C-HSQC, ^{1}H,^{13}C-HMBC] (150.92 MHz, THF-d_8, 295 K): δ [ppm] = 212.3 (*s*, C_1, only observed in ^{1}H,^{13}C-HMBC), 45.10 (*s*, N(*C*H_3)$_2$).

HR-MS (ESI, positive, THF): calcd. for [M-Cl = $C_5H_{12}CuN_2]^+$ m/z = 163.0396, found m/z = 163.0349.

4 NMR Spectra

4.1 3^H

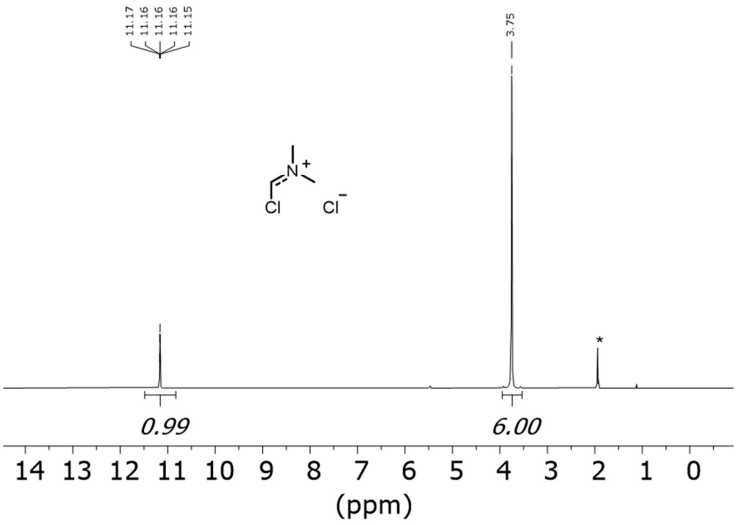


Figure S1. ^{1}H NMR spectrum of **3^H** (399.98 MHz, CD_3CN, 295 K). Solvent resonances are indicated by an asterisk (*).

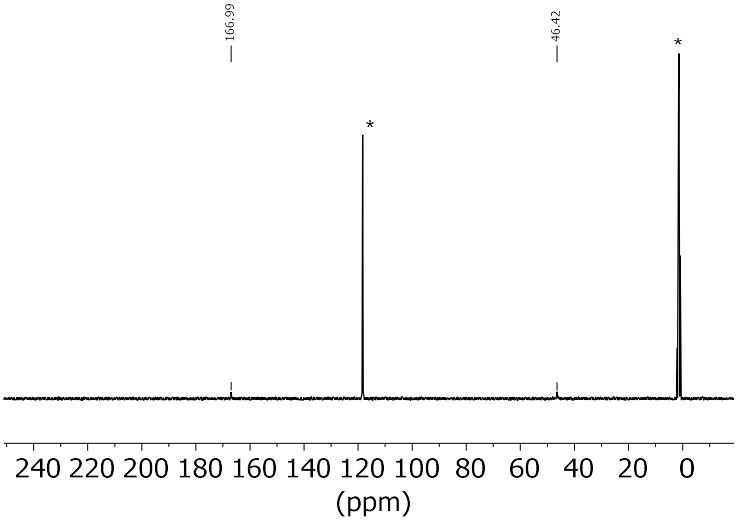


Figure S2. ^{13}C NMR spectrum of **3^H** (100.55 MHz, CD_3CN, 295 K). Solvent resonances are indicated by an asterisk (*).

4.2 3^{tBu}

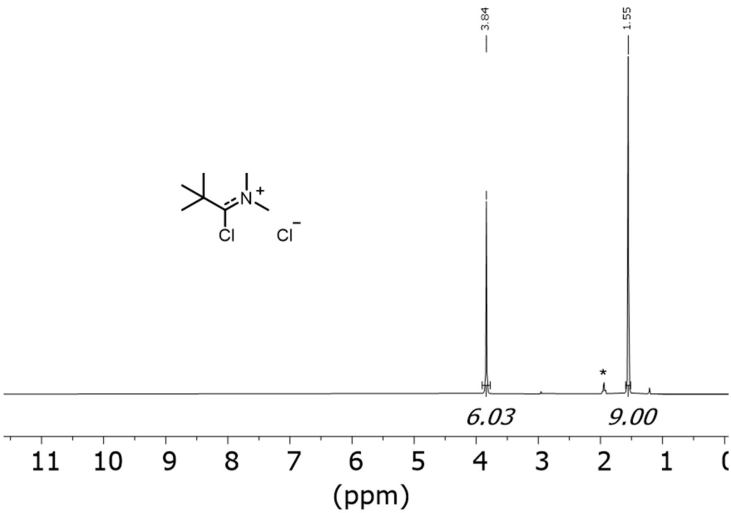


Figure S3. ^{1}H NMR spectrum of $\mathbf{3}^{tBu}$ (200 MHz, CD_3CN, 295 K). Solvent resonances are indicated by an asterisk (*).

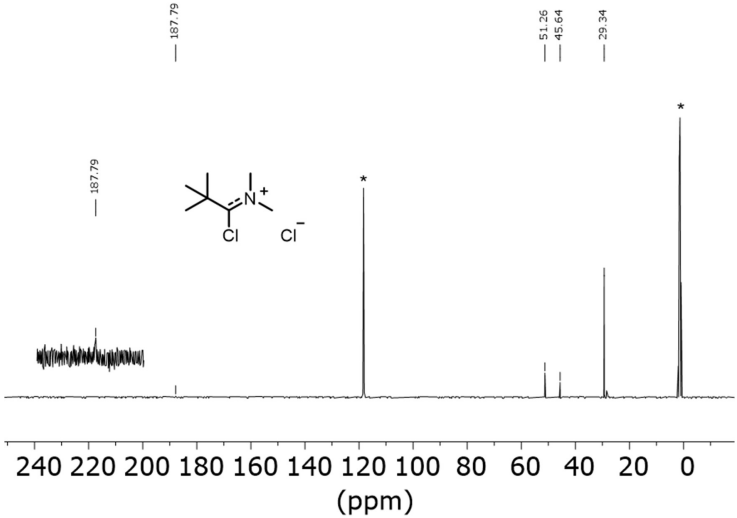


Figure S4. ^{13}C NMR spectrum of $\mathbf{3}^{tBu}$ (100.55 MHz, CD_3CN, 295 K). Solvent resonances are indicated by an asterisk (*).

4.3 3^{Ph}

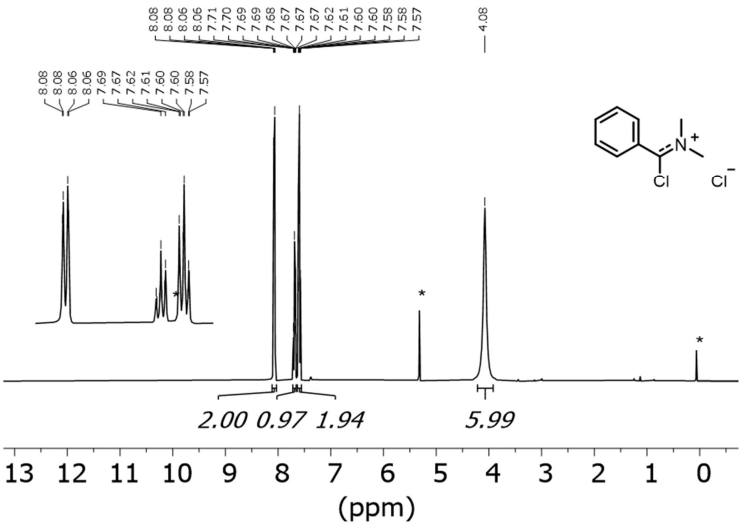


Figure S5. ^{1}H NMR spectrum of $\mathbf{3^{Ph}}$ (399.89 MHz, CD_2Cl_2, 295 K). Solvent and residue silicon grease resonances are indicated by an asterisk (*).

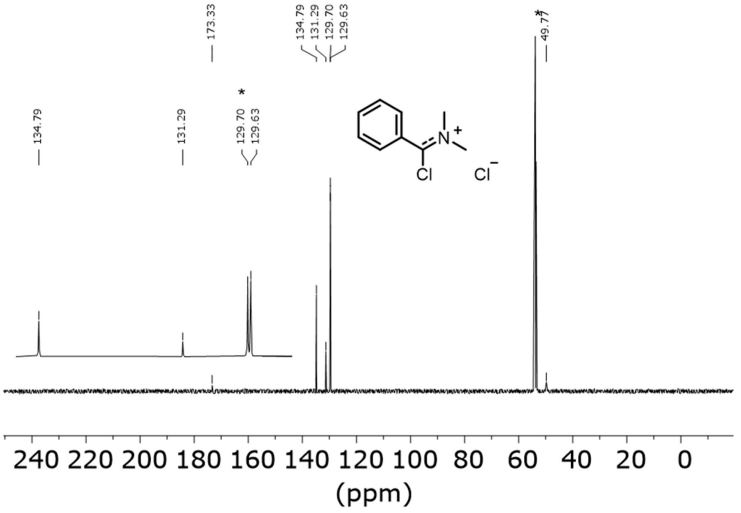


Figure S6. ^{13}C NMR spectrum of $\mathbf{3^{Ph}}$ (100.55 MHz, CD_2Cl_2, 295 K). Solvent resonances are indicated by an asterisk (*).

4.4 1(HaAC)(thf)

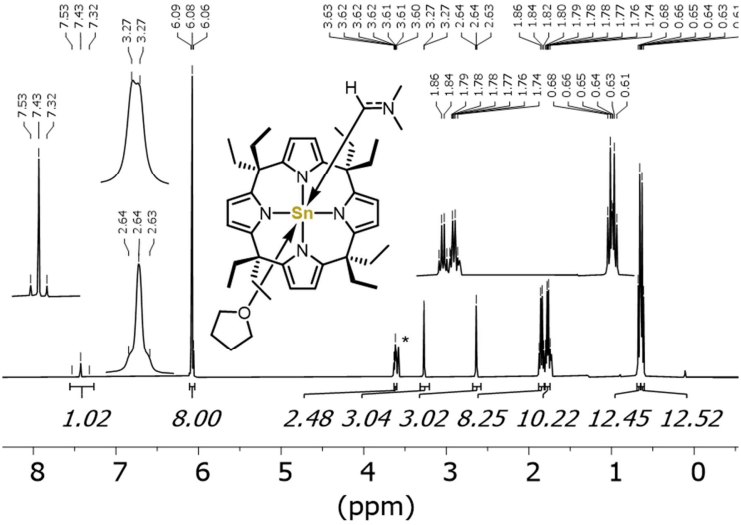


Figure S7. ^{1}H NMR spectrum of **1(H*a*AC)(thf)** (399.89 MHz, THF-d_8, 295 K). Solvent resonances are indicated by an asterisk (*).

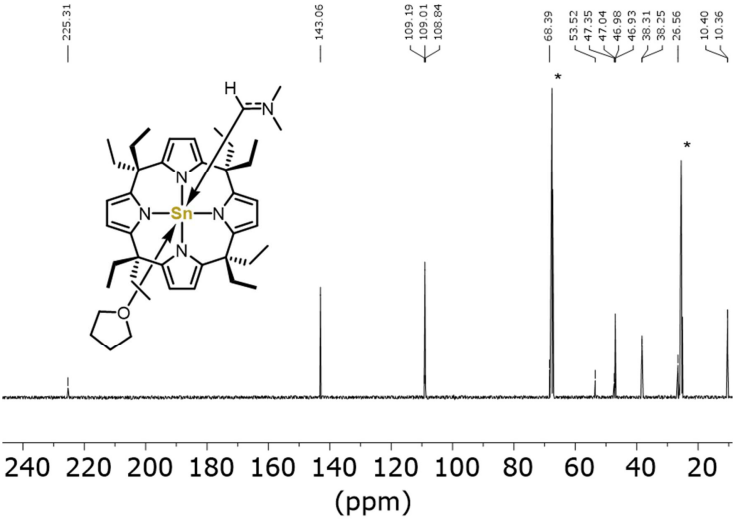


Figure S8. ^{13}C NMR spectrum of **1(H*a*AC)(thf)** (100.55 MHz, THF-d_8, 295 K). Solvent resonances are indicated by an asterisk (*).

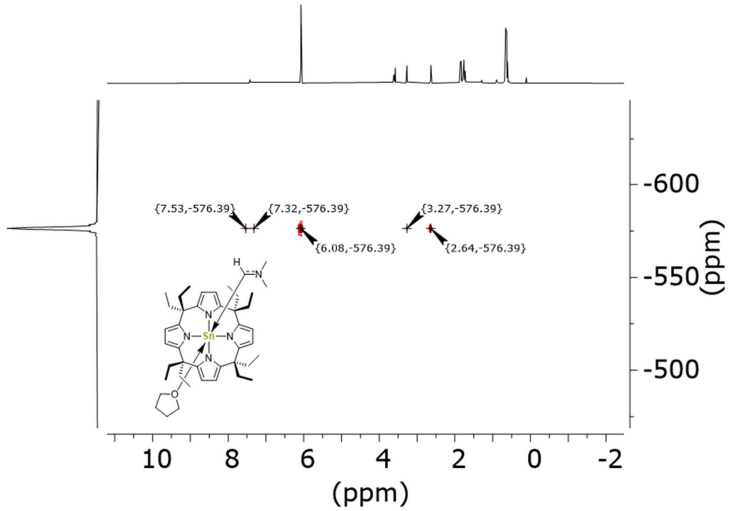


Figure S9. ^{1}H,^{119}Sn-HMBC NMR spectrum of **1(**^{H}***a*AC)(thf)** (THF-d_8, 295 K).

4.5 1(*^{iPr}*aAC)

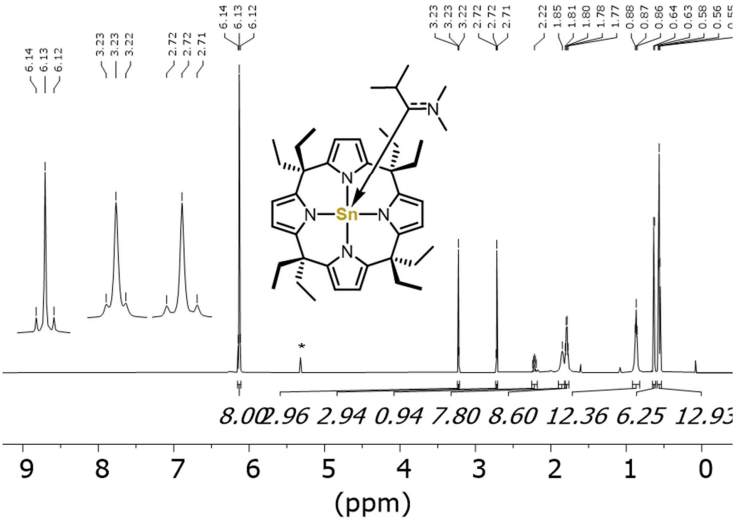


Figure S10. ^{1}H NMR spectrum of **1(***^{iPr}a*AC)** (600.15 MHz, CD_2Cl_2, 295 K). Solvent resonances are indicated by an asterisk (*).

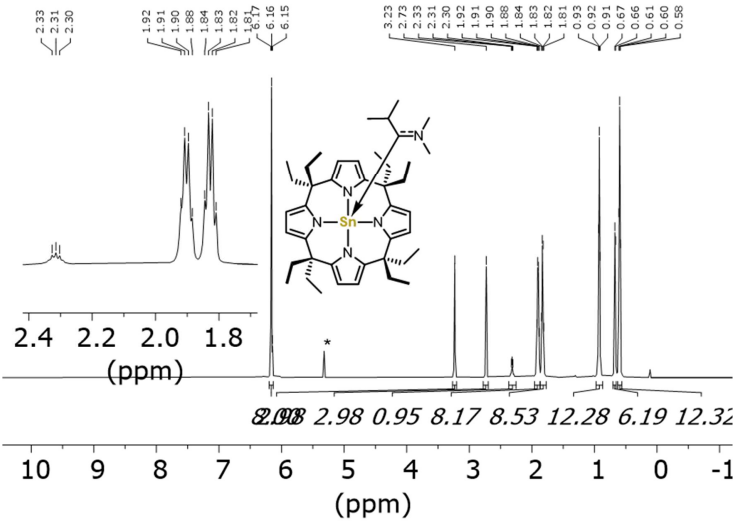


Figure S11. ^{1}H NMR spectrum of **1(*^{iPr}aAC)** (600.15 MHz, CD_2Cl_2, 323 K). Solvent resonances are indicated by an asterisk (*).

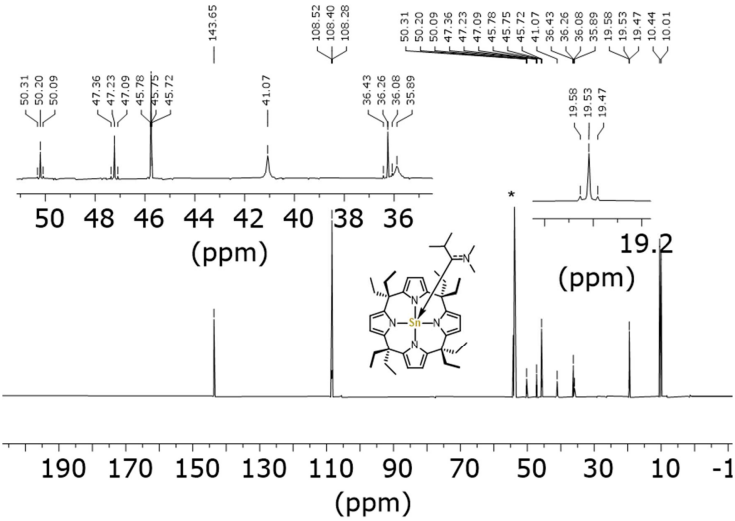


Figure S12. ^{13}C NMR spectrum of **1(*^{iPr}aAC)** (150.39 MHz, CD_2Cl_2, 323 K). Solvent resonances are indicated by an asterisk (*).

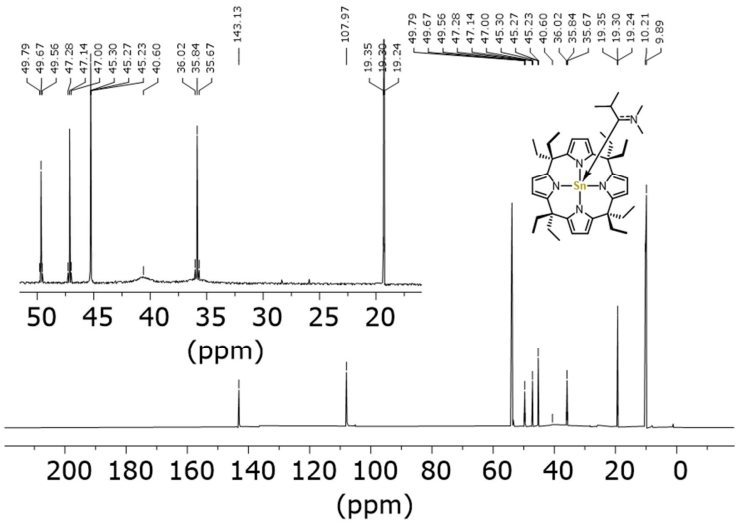


Figure S13. ^{13}C NMR spectrum of **1(*i*Pr*a*AC)** (150.92 MHz, CD_2Cl_2, 295 K). Solvent resonances are indicated by an asterisk (*).

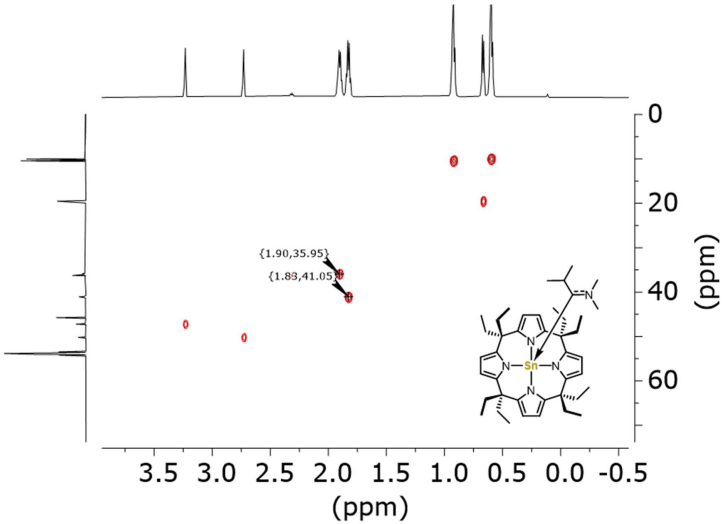


Figure S14. $^{1}H,^{13}C$-HSQC NMR spectrum of **1(*i*Pr*a*AC)** (CD_2Cl_2, 323 K). Cross peaks for CH_2 groups are indicated.

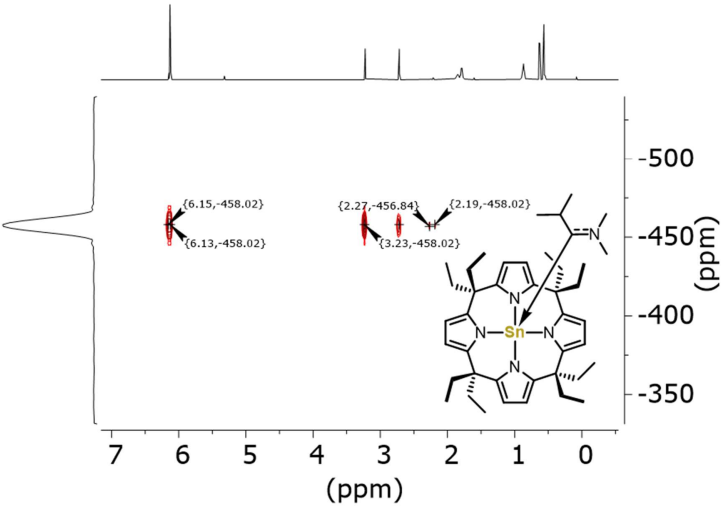


Figure S15. $^{1}H,^{119}Sn$-HMBC NMR spectrum of **1(*i*Pr*α*AC)** (CD_2Cl_2, 295 K).

4.6 1(*t*BU*a*AC)

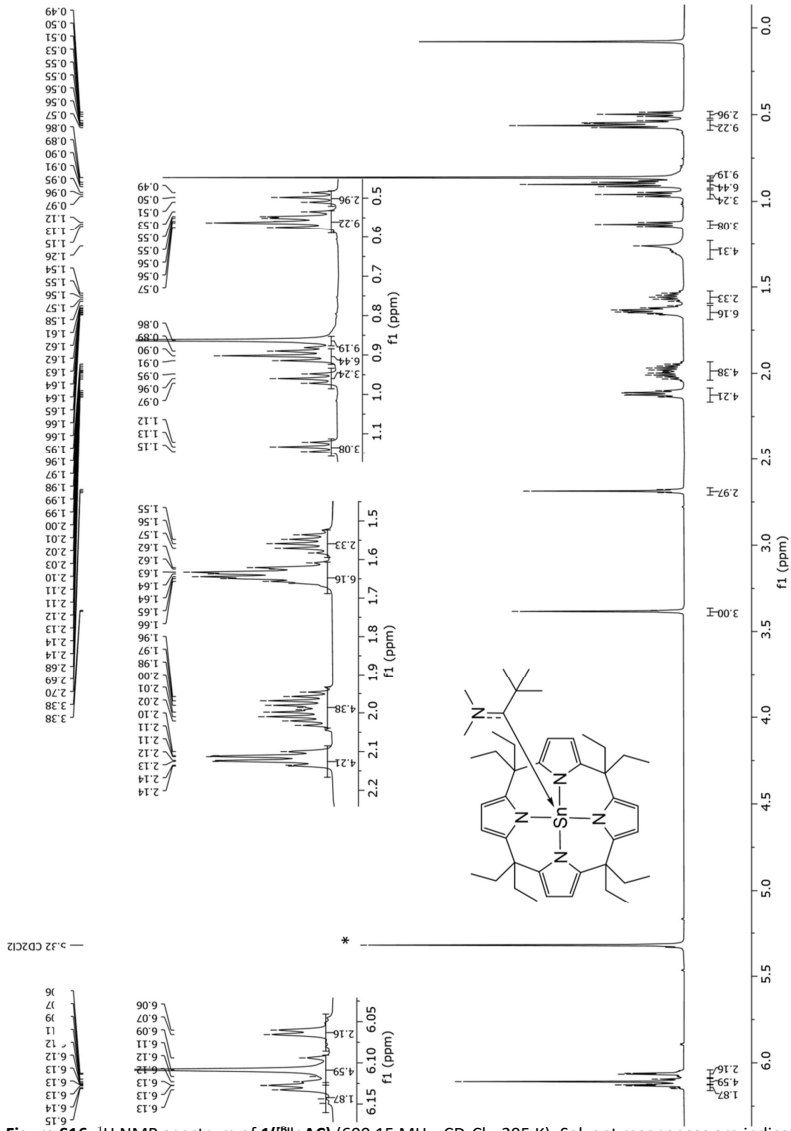


Figure S16. ^{1}H NMR spectrum of **1(*t*BU*a*AC)** (600.15 MHz, CD_2Cl_2, 295 K). Solvent resonances are indicated by an asterisk (*).

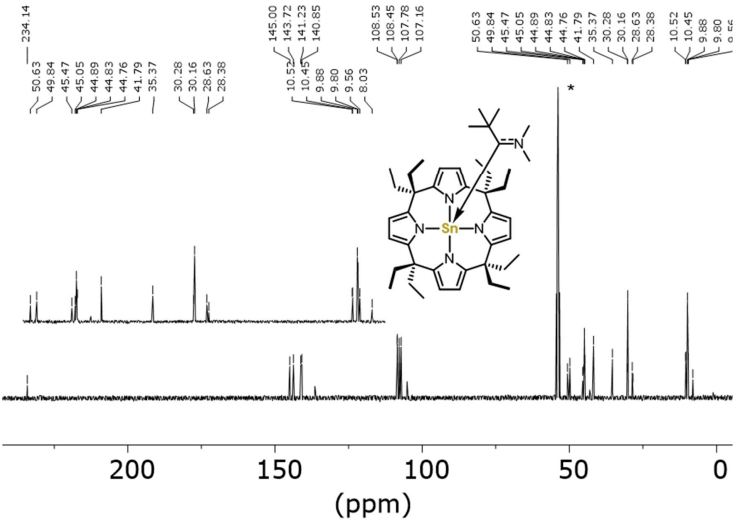


Figure S17. ^{13}C NMR spectrum of **1(*t*Bu*a*AC)** (150.92 MHz, CD_2Cl_2, 295 K). Solvent resonances are indicated by an asterisk (*).

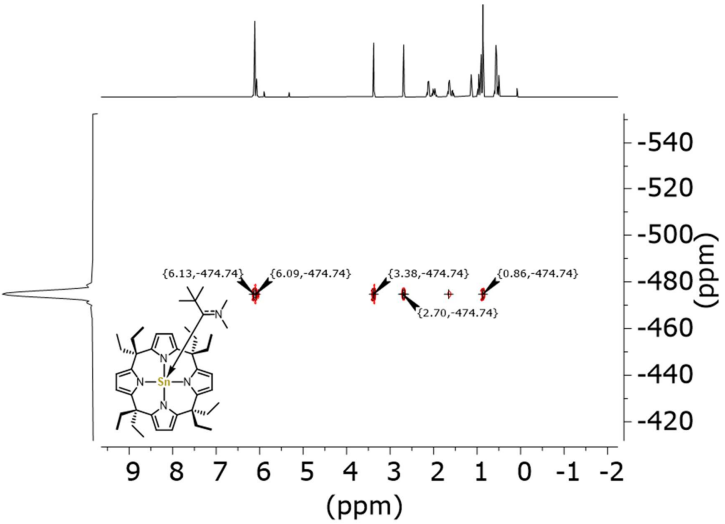


Figure S18. ^{1}H,^{119}Sn-HMBC NMR spectrum of **1(*t*Bu*a*AC)** (CD_2Cl_2, 295 K).

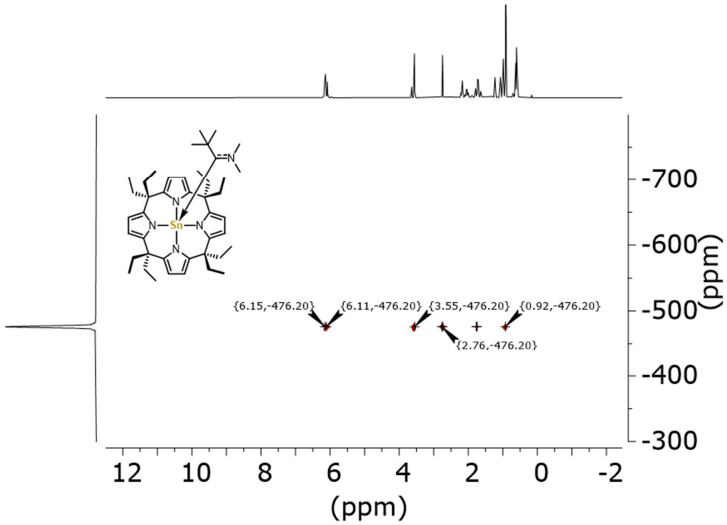


Figure S19. ^{1}H,^{119}Sn-HMBC NMR spectrum of **1(*t*Bu*a*AC)** (THF-d_8, 295 K).

4.7 1(Pha AC)

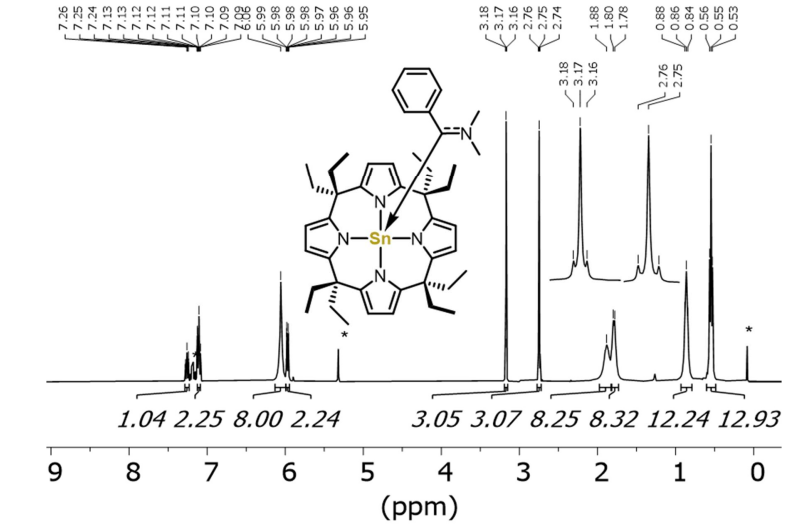


Figure S20. ^{1}H NMR spectrum of **1(Pha AC)** (399.89 MHz, CD_2Cl_2, 295 K). Solvent and silicon grease resonances are indicated by an asterisk (*).

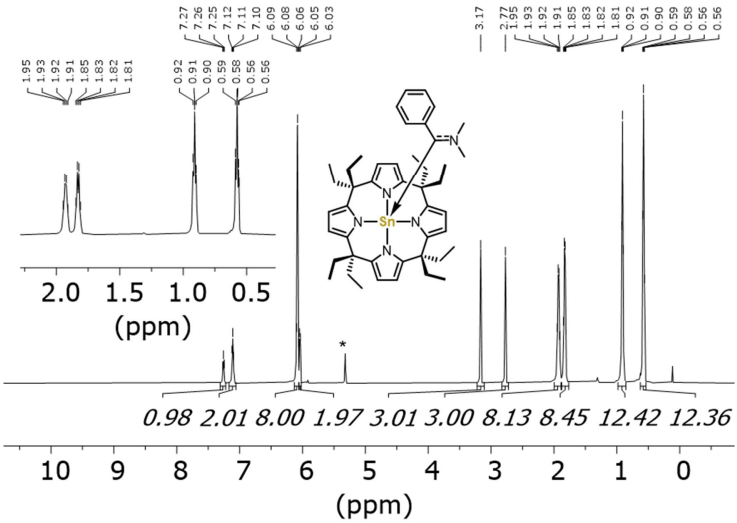


Figure S21. ^{1}H NMR spectrum of **1(**^{Ph}***a*****AC)** (399.89 MHz, CD_2Cl_2, 323 K). Solvent resonances are indicated by an asterisk (*).

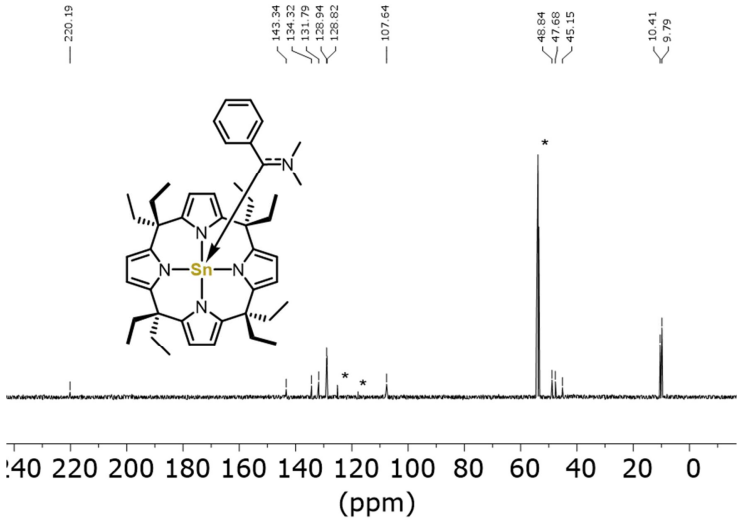


Figure S22. ^{13}C NMR spectrum of **1(**^{Ph}***a*****AC)** (150.39 MHz, CD_2Cl_2, 295 K). Solvent resonances are indicated by an asterisk (*).

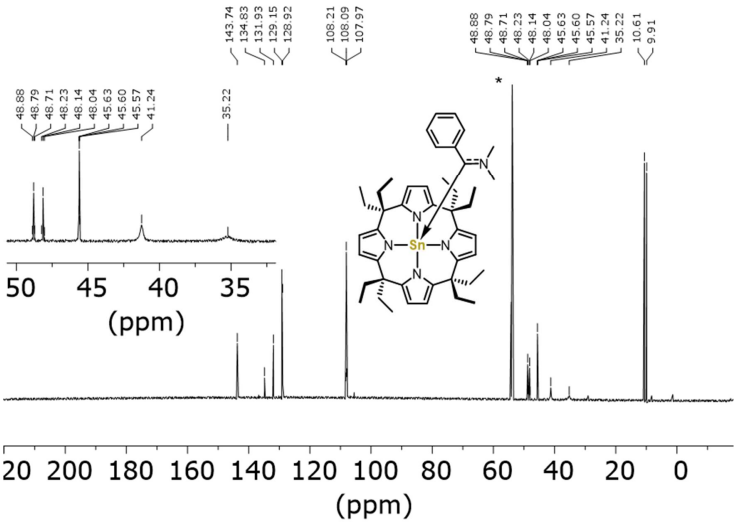


Figure S23. ^{13}C NMR spectrum of **1(**^{Ph}***a*****AC)** (150.39 MHz, CD_2Cl_2, 323 K). Solvent resonances are indicated by an asterisk (*).

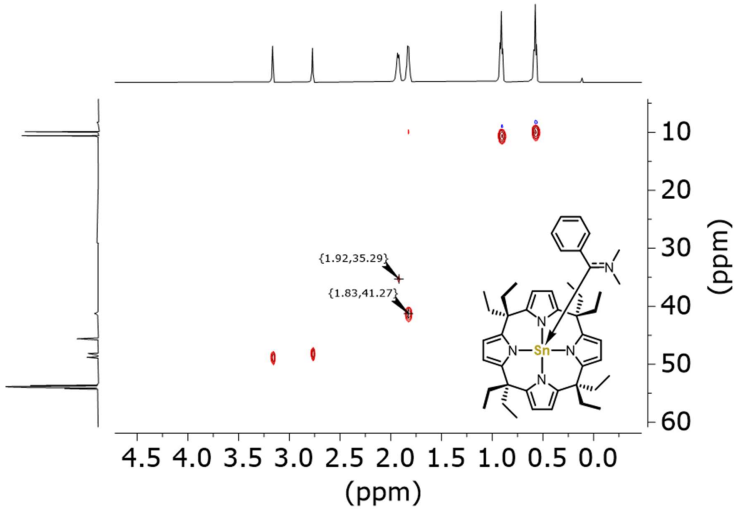


Figure S24. ^{1}H,^{13}C-HSQC NMR spectrum of **1(**^{Ph}***a*****AC)** (CD_2Cl_2, 323 K). Cross peaks of CH_2 groups are indicated.

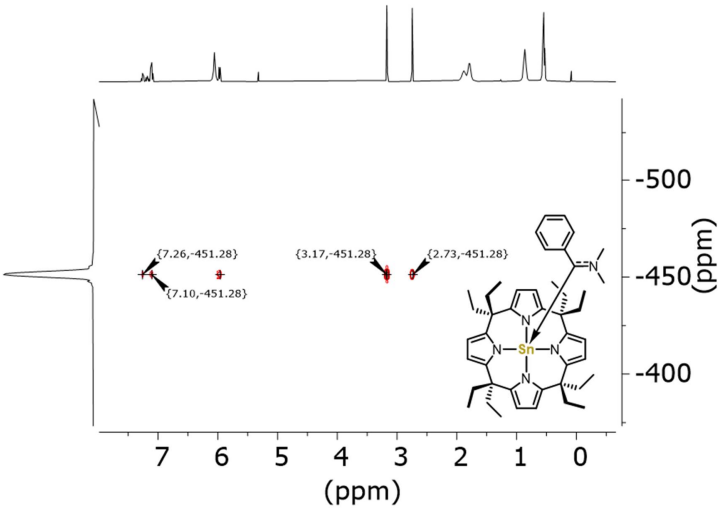


Figure S25. $^{1}H,^{119}Sn$-HMBC NMR spectrum of **1(^Ph*a*AC)** (CD_2Cl_2, 295 K).

4.8 1(^NMe2*a*AC)

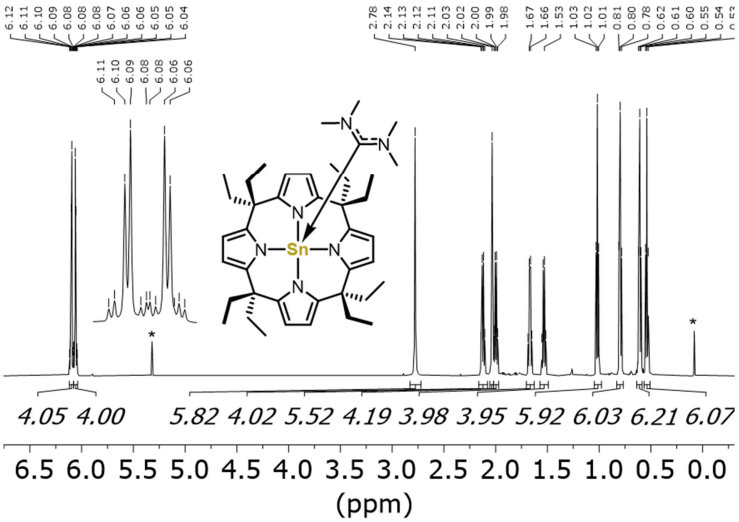


Figure S26. ^{1}H NMR spectrum of **1(^NMe2*a*AC)** (600.15 MHz, CD_2Cl_2, 295 K). Solvent and silicon grease resonances are indicated by an asterisk (*).

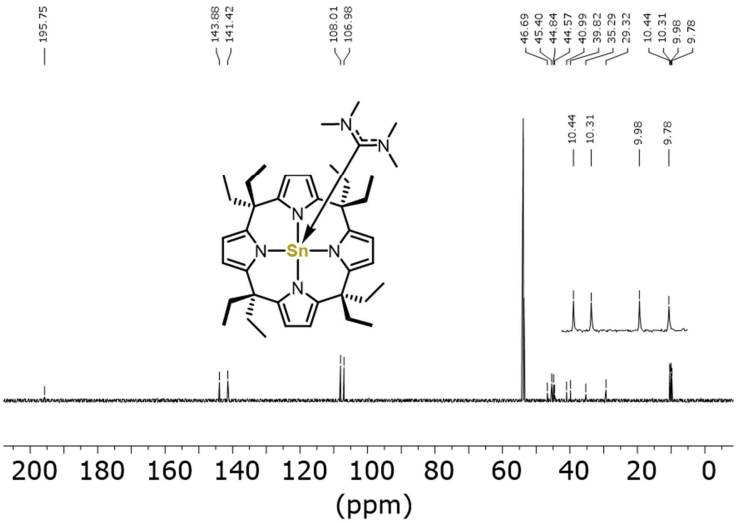


Figure S27. ^{13}C NMR spectrum of **1(**^{NMe2}***a*****AC)** (150.92 MHz, CD_2Cl_2, 295 K). Solvent resonances are indicated by an asterisk (*).

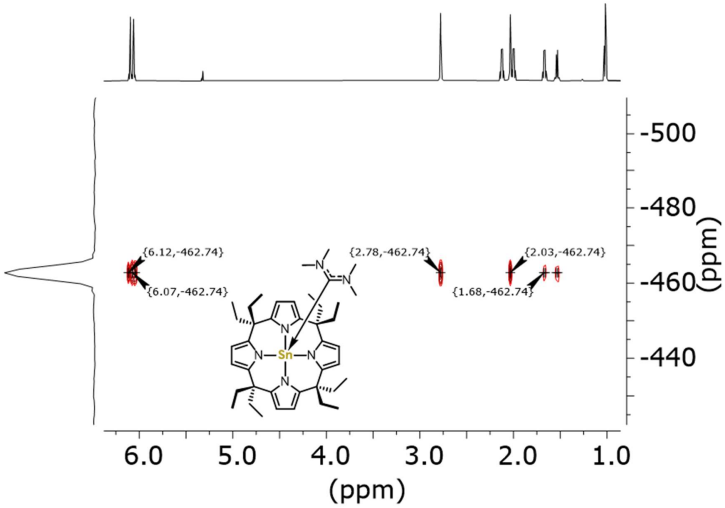


Figure S28. ^{1}H,^{119}Sn-HMBC NMR spectrum of **1(**^{NMe2}***a*****AC)** (CD_2Cl_2, 295 K).

4.9 Reaction of 1(HaAC)(thf) with CuCl

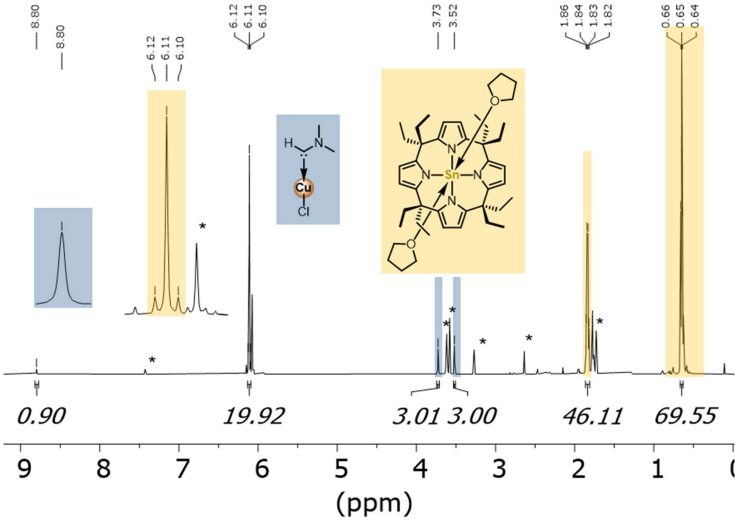


Figure S29. ^{1}H NMR spectrum of the reaction of **1(H*a*AC)(thf)** with CuCl (600.15 MHz, THF-d_8, 295 K). Solvent resonances and unconsumed **1(H*a*AC)(thf)** are indicated by an asterisk (*).

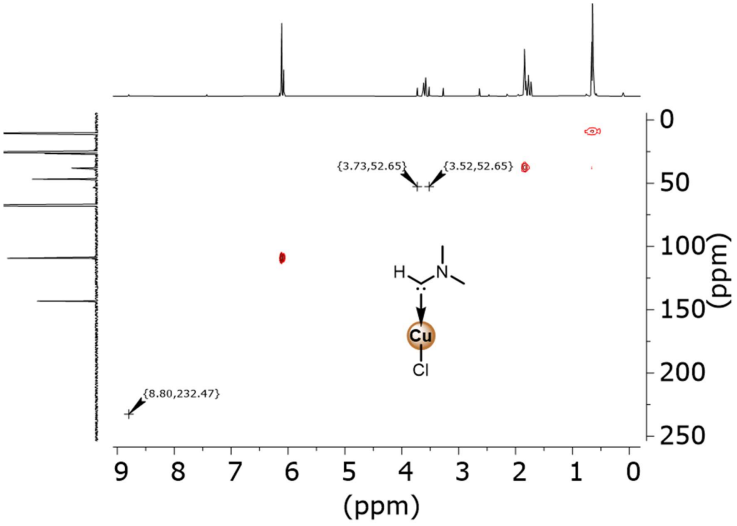


Figure S30. ^{1}H,^{13}C-HSQC NMR spectrum of the reaction of **1(H*a*AC)(thf)** with CuCl (THF-d_8, 295 K).

4.10 Reaction of 1(*i*Pr*a*AC) with CuCl

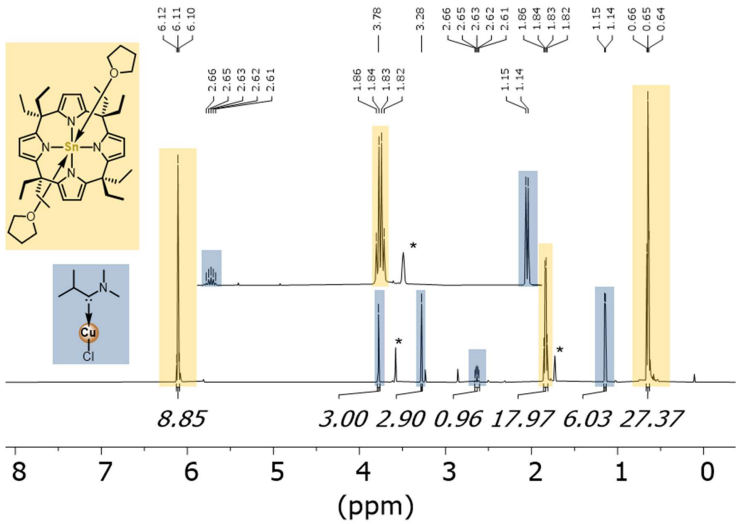


Figure S31. ^{1}H NMR spectrum of the reaction of **1(*i*Pr*a*AC)** with CuCl (600.15 MHz, THF-d_8, 295 K). Solvent resonances are indicated by an asterisk (*).

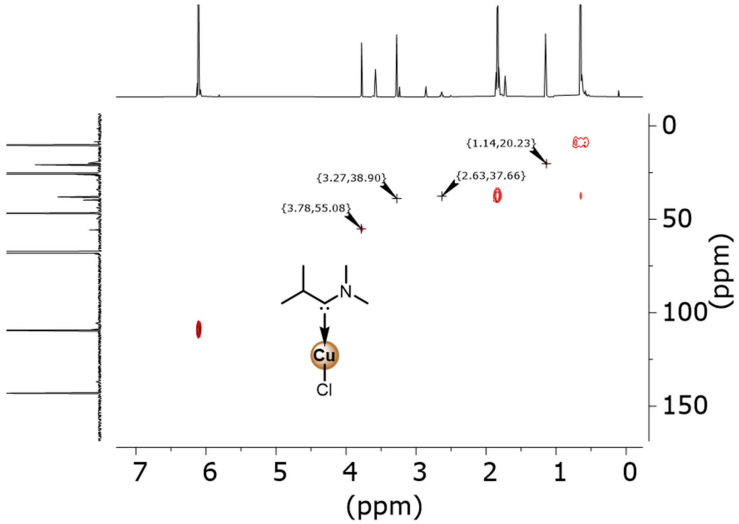


Figure S32. ^{1}H,^{13}C-HSQC NMR spectrum of the reaction of **1(*i*Pr*a*AC)** with CuCl (THF-d_8, 295 K).

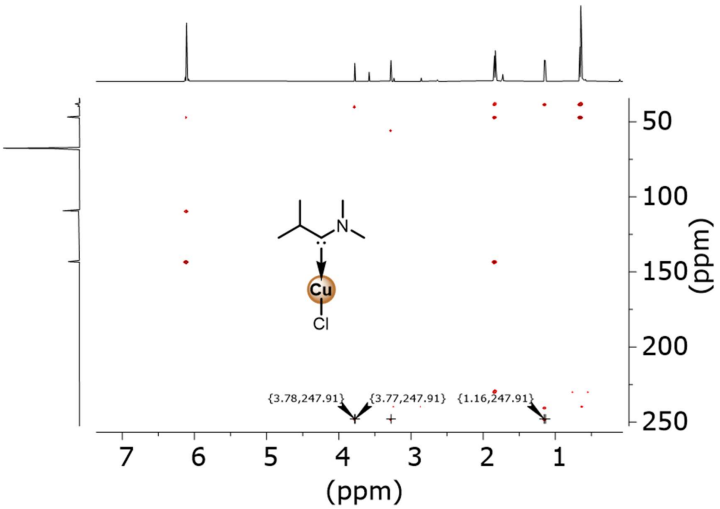


Figure S33. $^{1}H,^{13}C$-HMBC NMR spectrum of the reaction of **1(*i*Pr*a*AC)** with CuCl (THF-d_8, 295 K).

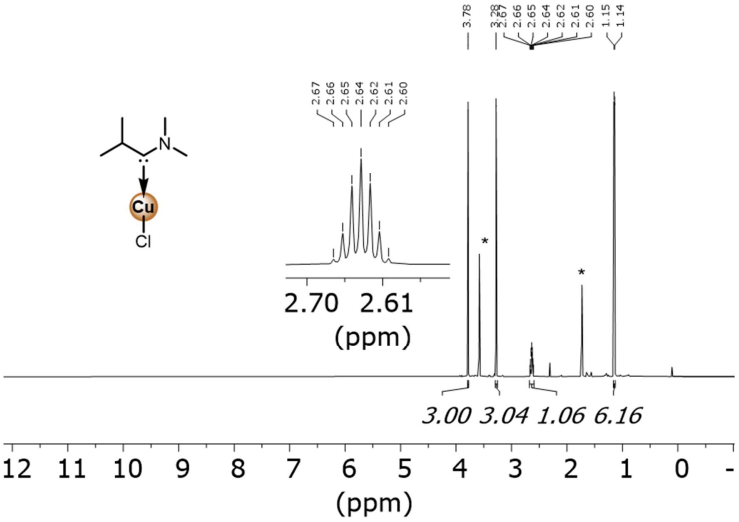


Figure S34. ^{1}H NMR spectrum of **CuCl(*i*Pr*a*AC)** (600.15 MHz, THF-d_8, 295 K). Solvent resonances are indicated by an asterisk (*).

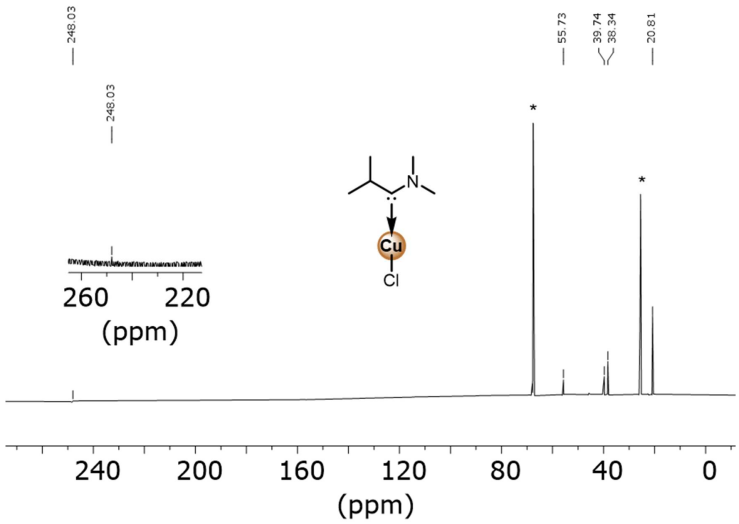


Figure S35. ^{13}C NMR spectrum of **CuCl(*^{iPr}aAC*)** (150.92 MHz, THF-d_8, 295 K). Solvent resonances are indicated by an asterisk (*).

4.11 Reaction of 1(*^{tBu}aAC*) with CuCl

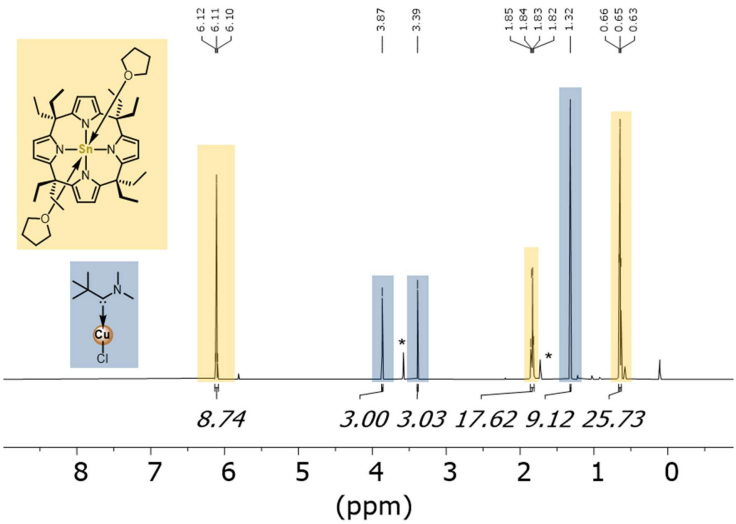


Figure S36. ^{1}H NMR spectrum of the reaction of **1(*^{tBu}aAC*)** with CuCl (600.15 MHz, THF-d_8, 295 K). Solvent resonances are indicated by an asterisk (*).

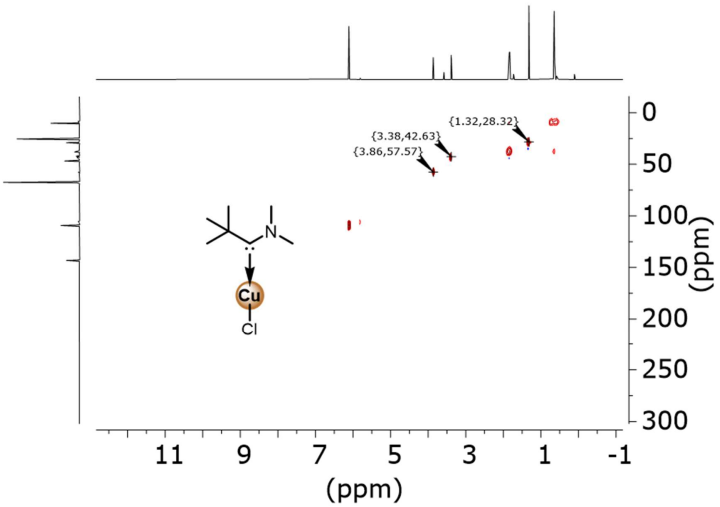


Figure S37. $^{1}H,^{13}C$-HSQC NMR spectrum of the reaction of **1(*t*Bu*a*AC)** with CuCl (THF-d_8, 295 K).

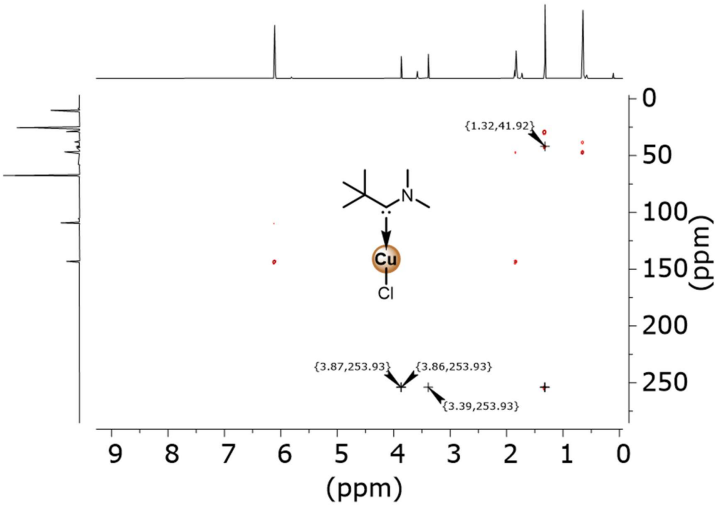


Figure S38. $^{1}H,^{13}C$-HMBC NMR spectrum of the reaction of **1(*t*Bu*a*AC)** with CuCl (THF-d_8, 295 K).

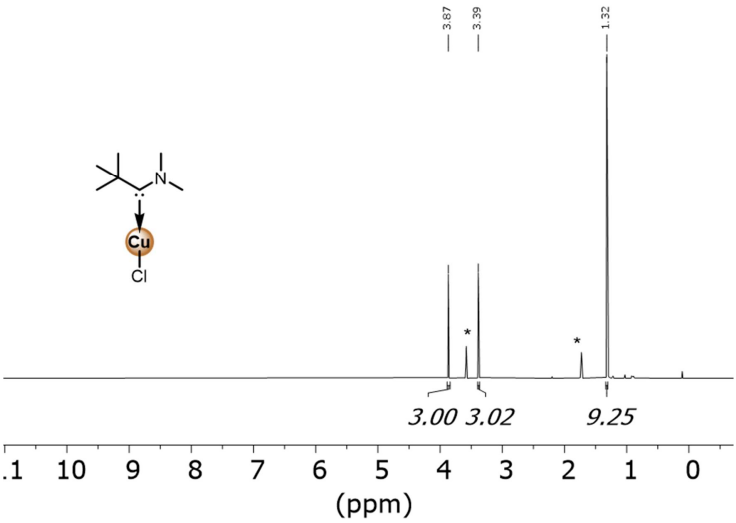


Figure S39. ^{1}H NMR spectrum of **CuCl(*$^{t\text{Bu}}$*AC)** (600.15 MHz, THF-d_8, 295 K). Solvent resonances are indicated by an asterisk (*).

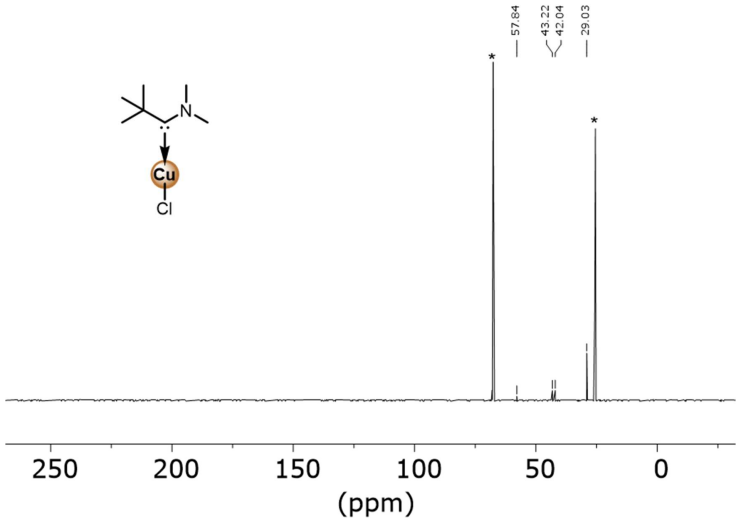


Figure S40. ^{13}C NMR spectrum of **CuCl(*$^{t\text{Bu}}$*AC)** (150.92 MHz, THF-d_8, 295 K). Solvent resonances are indicated by an asterisk (*).

4.12 Reaction of 1(Ph*a*AC) with CuCl

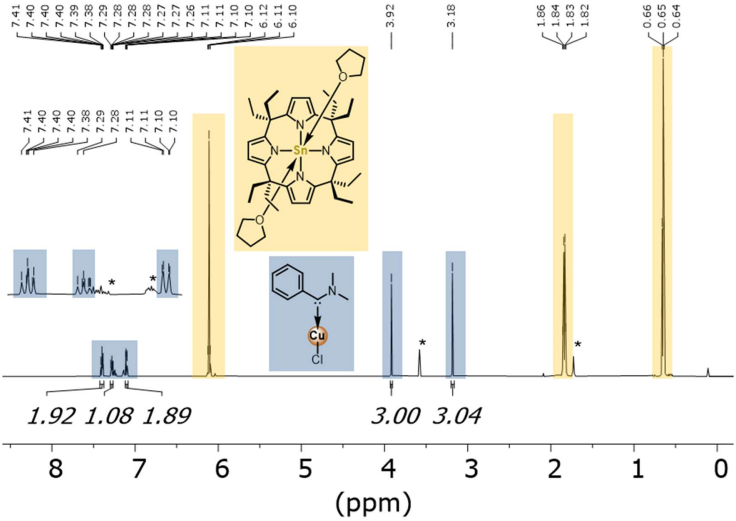


Figure S41. ^{1}H NMR spectrum of the reaction of **1(Ph*a*AC)** with CuCl (600.15 MHz, THF-d_8, 295 K). Solvent resonances and residual *o*DFB resonances from the starting material are indicated by an asterisk (*).

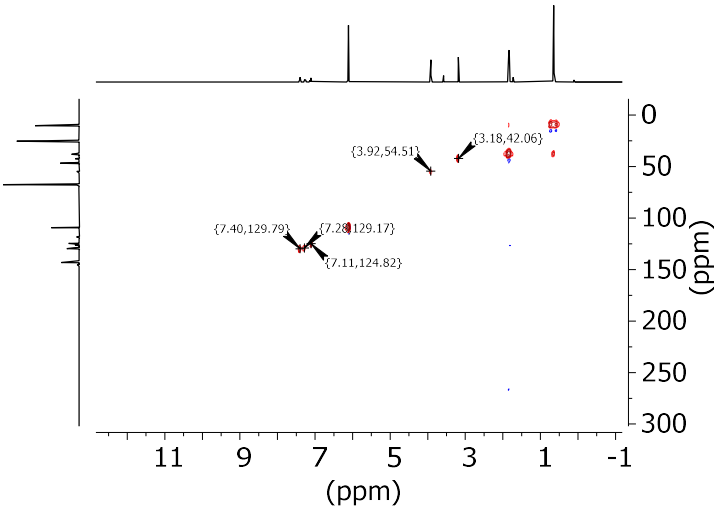


Figure S42. ^{1}H,^{13}C-HSQC NMR spectrum of the reaction of **1(Ph*a*AC)** with CuCl (THF-d_8, 295 K).

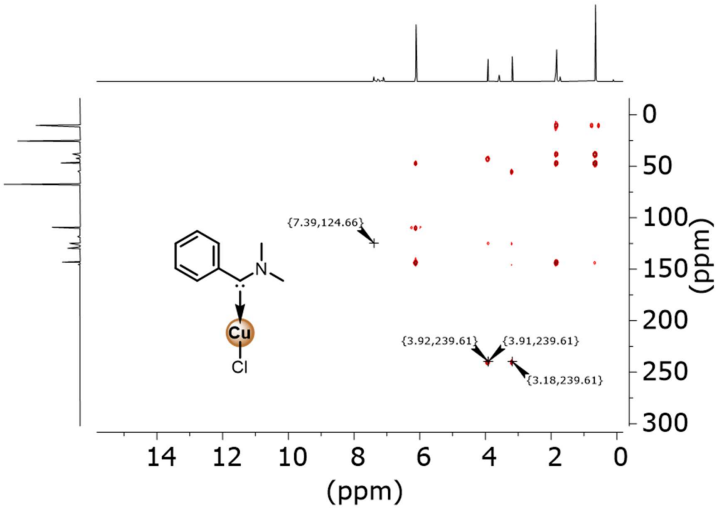


Figure S43. ^{1}H,^{13}C-HMBC NMR spectrum of the reaction of **1(**^{Ph}***a*****AC)** with CuCl (THF-d_8, 295 K).

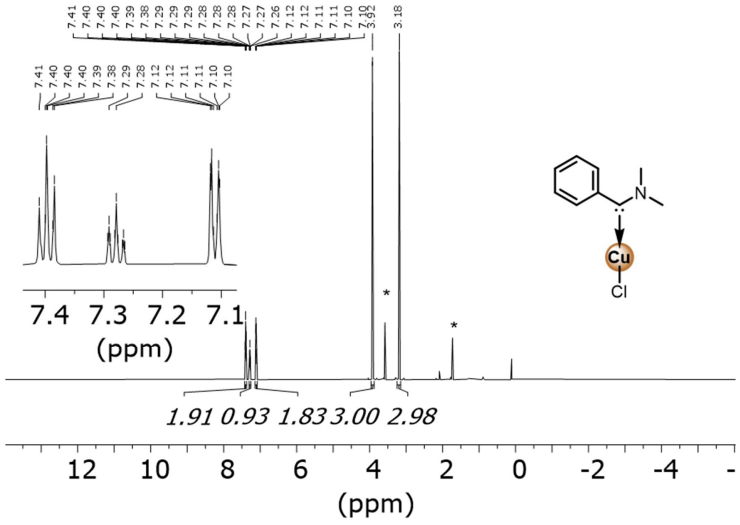


Figure S44. ^{1}H NMR spectrum of **CuCl(**^{Ph}***a*****AC)** (600.15 MHz, THF-d_8, 295 K). Solvent resonances are indicated by an asterisk (*).

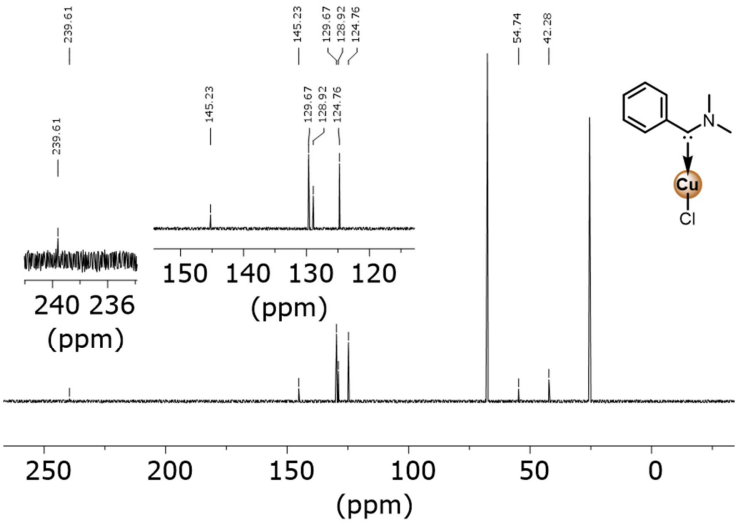


Figure S45. ^{13}C NMR spectrum of **CuCl(**^{Ph}***a*AC)** (150.92 MHz, THF-d_8, 295 K). Solvent resonances are indicated by an asterisk (*).

4.13 Reaction of 1(^NMe2*a*AC) with CuCl

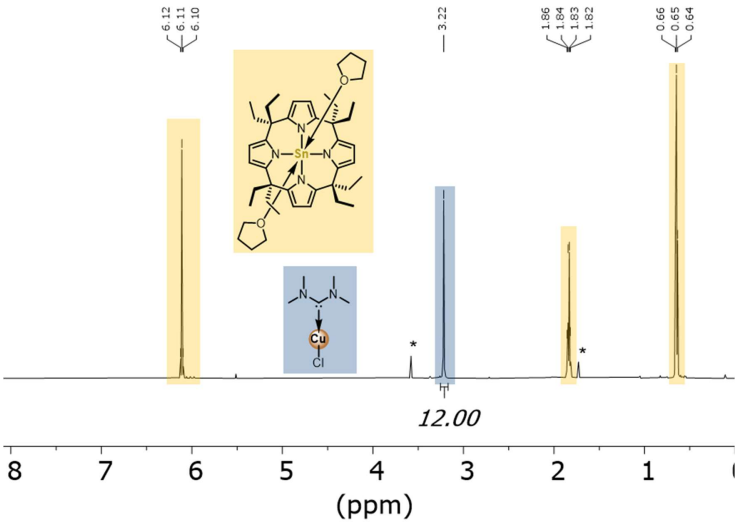


Figure S46. ^{1}H NMR spectrum of the reaction of **1(**^{NMe2}***a*AC)** with CuCl (600.15 MHz, THF-d_8, 295 K). Solvent resonances are indicated by an asterisk (*).

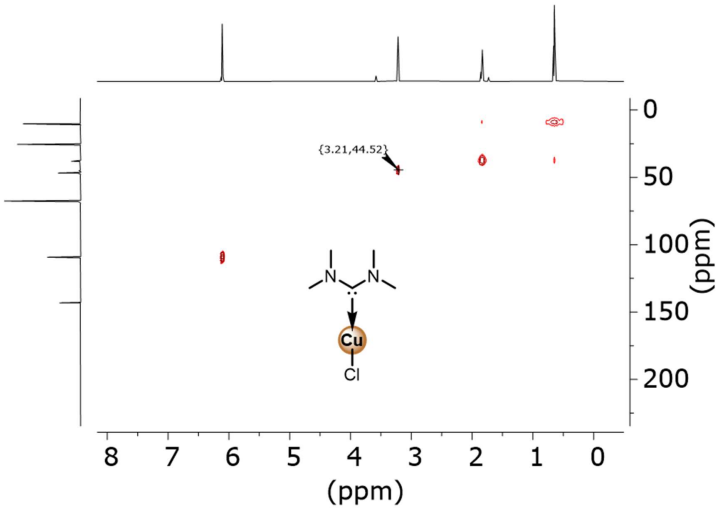


Figure S47. ^{1}H,^{13}C-HSQC NMR spectrum of the reaction of **1(**^{NMe2}***a*****AC)** with CuCl (THF-d_8, 295 K).

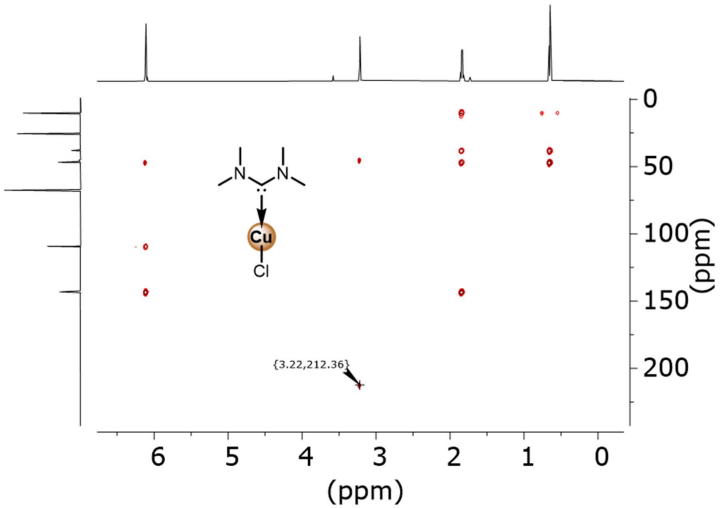


Figure S48. ^{1}H,^{13}C-HMBC NMR spectrum of the reaction of **1(**^{NMe2}***a*****AC)** with CuCl (THF-d_8, 295 K).

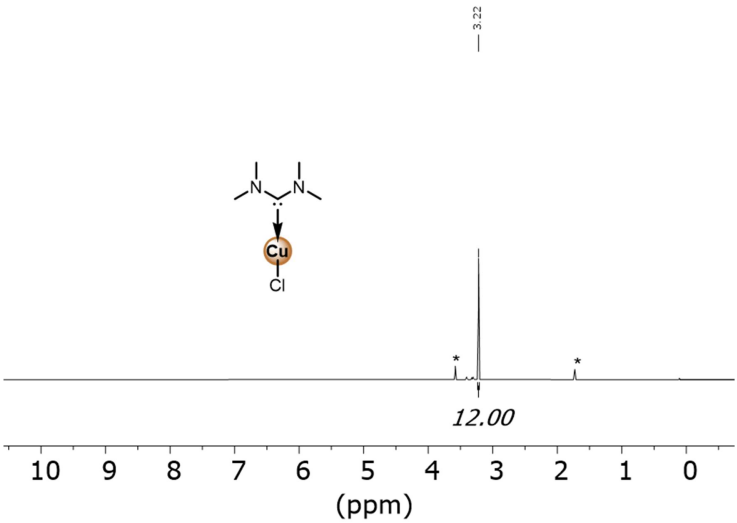


Figure S49. ^{1}H NMR spectrum of **CuCl(^{NMe2}*a*AC)** (600.15 MHz, THF-d_8, 295 K). Solvent resonances are indicated by an asterisk (*).

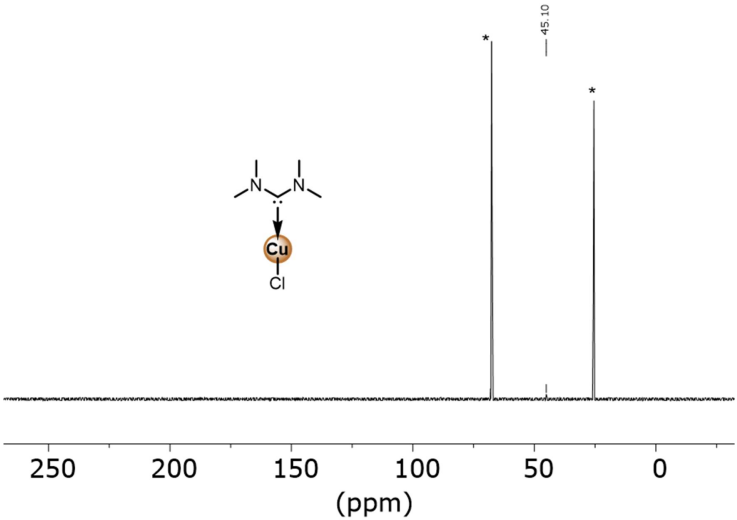


Figure S50. ^{13}C NMR spectrum of **CuCl(^{NMe2}*a*AC)** (150.92 MHz, THF-d_8, 295 K). Solvent resonances are indicated by an asterisk (*).

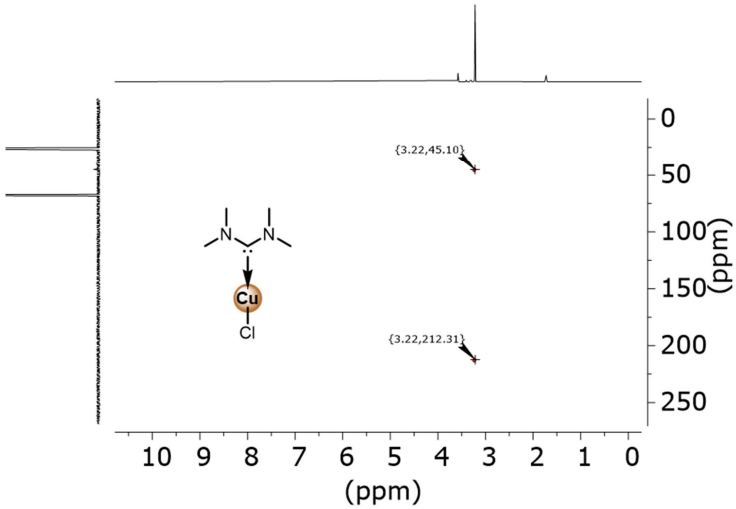


Figure S51. ^{1}H,^{13}C-HMBC NMR spectrum of **CuCl(NMe2*a*AC)** (THF-d_8, 295 K).

4.14 Reaction of 1(*t*Bu*a*AC) with (dms)CuBr

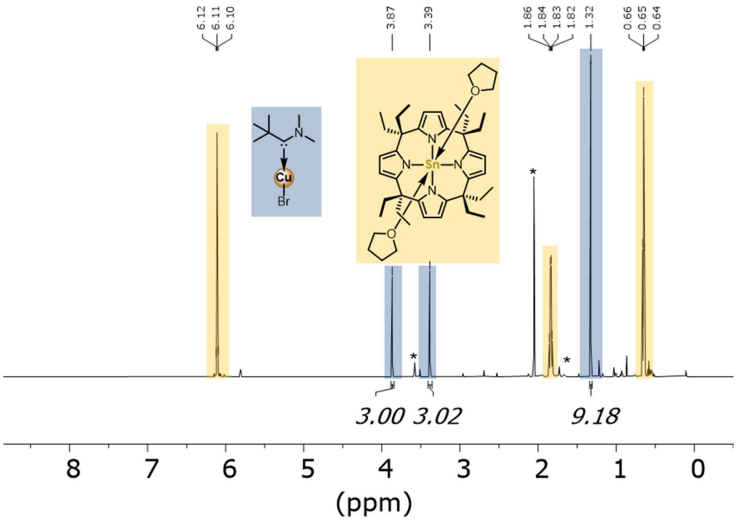


Figure S52. ^{1}H NMR spectrum of the reaction of **1(*t*Bu*a*AC)** with (dms)CuBr (600.15 MHz, THF-d_8, 295 K). Solvent and dms resonances are indicated by an asterisk (*).

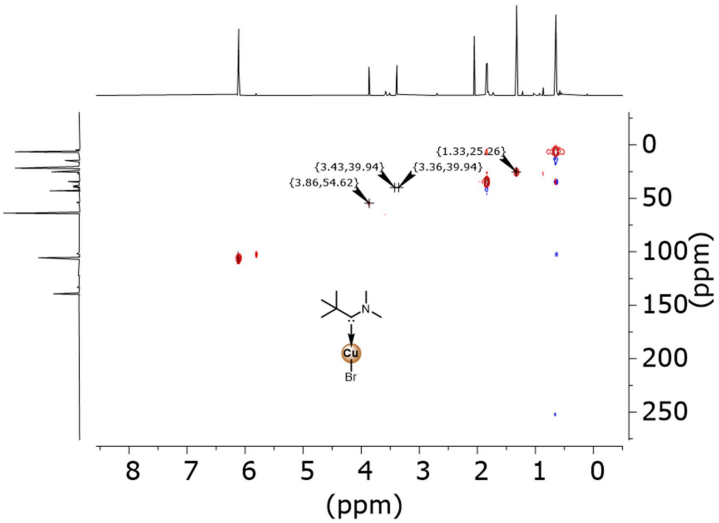


Figure S53. $^{1}H,^{13}C$-HSQC NMR spectrum of the reaction of **1(*^{tBu}aAC)** with (dms)CuBr.

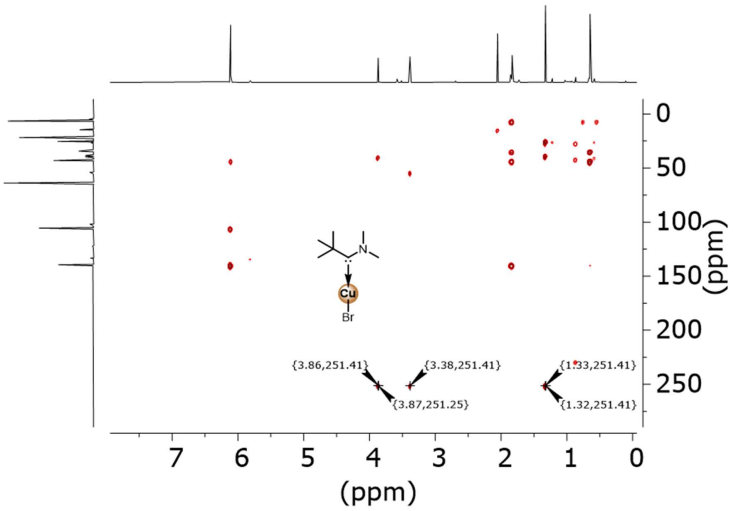


Figure S54. $^{1}H,^{13}C$-HMBC NMR spectrum of the reaction of **1(*^{tBu}aAC)** with (dms)CuBr.

5 Crystallographic Data

5.1 Solid state molecular structures of adducts 1(*t*Bu*a*AC), 1(Ph*a*AC), and 1(NMe2*a*AC)

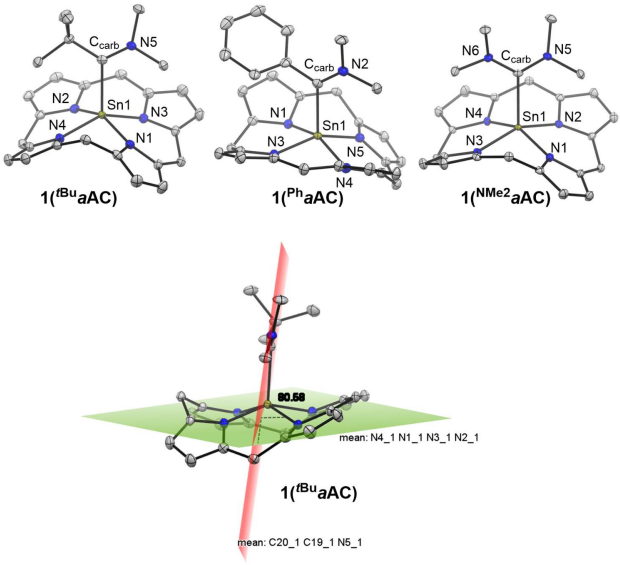


Figure S55: Top: Solid state molecular structures of **1(R*a*AC)** (R = *t*Bu, Ph, NMe2) . Displacement ellipsoids drawn at 50% probability level. Hydrogens, *meso*-ethyl residues of the calix[4]pyrrolato ligand and solvent molecules are omitted for clarity. Selected bond lengths [pm] and angles [°] for **1(*t*Bu*a*AC)**: Sn1-C_{carb} = 227.3(2), Sn1-N_{avg} = 210.3(14), Sn1-N_4 plane = 53.7, C_{carb}-N5 = 129.8(2), Sn1-C_{carb}-N5 = 116.90(11), C-C_{carb}-N5 = 121.07(14), N1-Sn1-N2 = 152.32(5), N3-Sn1-N4 = 148.40(5); **1(Ph*a*AC)**: Sn1-C_{carb} = 224.4(2), Sn1-N_{avg} = 210.4(8), Sn1-N_4 plane = 45.1, C_{carb}-N2 = 129.4(2), Sn1-C_{carb}-N2 = 123.38(13), C-C_{carb}-N2 = 118.86(16), N1-Sn1-N4 = 154.69(6), N3-Sn1-N5 = 155.60(6); and **1(NMe2*a*AC)**: Sn1-C_{carb} = 226.2(2), Sn1-N_{avg} = 210.0(7), Sn1-N_4 plane = 49.4, C_{carb}-N5 = 133.3(2), C_{carb}-N6 = 133.9(2), Sn1-C_{carb}-N5 = 119.48(13), Sn1-C_{carb}-N6 = 120.52(13), N5-C_{carb}-N6 = 119.92(16)), N1-Sn1-N4 = 150.85(6), N2-Sn1-N3 = 154.76(6). Bottom: Solid state molecular structure of **1(*t*Bu*a*AC)** with inclination (80.58°) between the plane spanned by C20, C_{Carb}, and N5 of the carbene unit (red) and the plane spanned by the four calix[4]pyrrole N-atoms (green) determined by Mercury without a standard uncertainty.

5.2 1(HaAC)(thf)

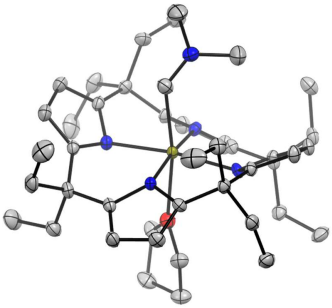


Figure S56: Solid state molecular structure of **1(HaAC)(thf)**. Ellipsoids are drawn with a probability of 50%. Hydrogen atoms are omitted for clarity. This structure was refined as an inversion twin with a Flack x (BASF parameter) of 0.398(16).

Table S1: Crystal data for **1(HaAC)(thf)**.

CCDC number	2303624
Identification code	mo_hram148_0m_a
Empirical formula	$C_{43}H_{63}N_5OSn$
Formula weight	784.67
Temperature [K]	120(2)
Crystal system	orthorhombic
Space group (number)	$P2_12_12_1$ (19)
a [Å]	11.6830(19)
b [Å]	18.325(4)
c [Å]	18.707(4)
α [°]	90
β [°]	90
γ [°]	90
Volume [Å^3]	4037(5)
Z	4
ρ_{calc} [gcm^{-3}]	1.301
μ [mm^{-1}]	0.677
F(000)	1656
Crystal size [mm^3]	0.111×0.090×0.059
Crystal colour	yellow
Crystal shape	block
Radiation	MoK_α (λ=0.71073 Å)
2θ range [°]	4.11 to 67.74 (0.64 Å)
Index ranges	−18 ≤ h ≤ 17, −28 ≤ k ≤ 28, −28 ≤ l ≤ 29
Reflections collected	179750

Independent reflections	16051, R_{int} = 0.0729, R_{sigma} = 0.0401
Completeness to θ = 25.098°	100.0 %
Data / Restraints / Parameters	16051/0/462
Absorption correction Tmin/Tmax (method)	0.6832/0.7467 (multi-scan)
Goodness-of-fit on F^2	1.048
Final *R* indexes [$I \geq 2\sigma(I)$]	R_1 = 0.0341 wR_2 = 0.0711
Final *R* indexes [all data]	R_1 = 0.0430 wR_2 = 0.0767
Largest peak/hole [eÅ^{-3}]	1.26/-1.27
Flack X parameter	0.398(16)

5.3 1(*iPr*aAC)

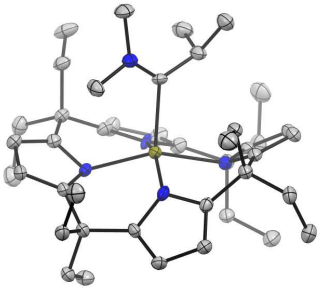


Figure S57: Solid state molecular structure of **1(*iPr*aAC)**. Ellipsoids are drawn with a probability of 50%. Hydrogen atoms are omitted for clarity.

Table S2: Crystal data for **1(*iPr*aAC)**.

CCDC number	2303621
Identification code	mo_hrrp26_0ma
Empirical formula	$C_{42}H_{61}N_5Sn$
Formula weight	754.64
Temperature [K]	100(2)
Crystal system	monoclinic
Space group (number)	$P2_1/n$ (14)
a [Å]	11.5048(8)
b [Å]	19.7861(13)
c [Å]	16.5080(11)
α [°]	90
β [°]	90.382(3)
γ [°]	90
Volume [Å^3]	3757.7(4)
Z	4
ρ_{calc} [gcm^{-3}]	1.334
μ [mm^{-1}]	0.716
F(000)	1592
Crystal size [mm^3]	0.083×0.059×0.044
Crystal colour	yellow
Crystal shape	block
Radiation	MoK_α (λ=0.71073 Å)
2θ range [°]	4.10 to 50.20 (0.84 Å)
Index ranges	−13 ≤ h ≤ 13, −23 ≤ k ≤ 23, −19 ≤ l ≤ 19
Reflections collected	75138
Independent reflections	6669, R_{int} = 0.0947, R_{sigma} = 0.0376
Completeness to θ = 25.098°	99.7 %
Data / Restraints / Parameters	6669/0/445

Absorption correction Tmin/Tmax (method)	0.6141/0.7452 (multi-scan)
Goodness-of-fit on F^2	1.103
Final *R* indexes [$I \geq 2\sigma(I)$]	R_1 = 0.0461 wR_2 = 0.1148
Final *R* indexes [all data]	R_1 = 0.0616 wR_2 = 0.1271
Largest peak/hole [eÅ^{-3}]	1.66/-0.84

5.4 1(*t*Bu*a*AC)

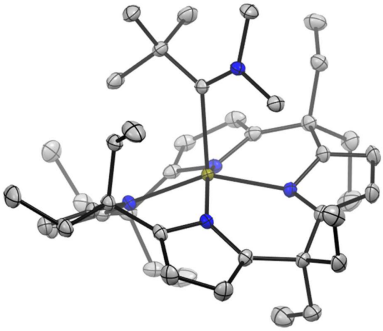


Figure S58: Solid state molecular structure of **1(*t*Bu*a*AC)**. Ellipsoids are drawn with a probability of 50%. Hydrogen atoms are omitted for clarity.

Table S3: Crystal data for **1(*t*Bu*a*AC)**.

CCDC number	2303625
Identification code	mo_hr528_0ma
Empirical formula	$C_{43}H_{63}N_5Sn$
Formula weight	768.67
Temperature [K]	100(2)
Crystal system	monoclinic
Space group (number)	$P2_1/n$ (14)
a [Å]	11.9091(17)
b [Å]	21.890(5)
c [Å]	15.608(3)
α [°]	90
β [°]	103.804(13)
γ [°]	90
Volume [Å^3]	3951.2(14)
Z	4
ρ_{calc} [gcm^{-3}]	1.292
μ [mm^{-1}]	0.683
F(000)	1624
Crystal size [mm^3]	0.197×0.115×0.072
Crystal colour	orange
Crystal shape	block
Radiation	MoK_α (λ=0.71073 Å)
2θ range [°]	3.89 to 72.74 (0.60 Å)
Index ranges	−18 ≤ h ≤ 18, −34 ≤ k ≤ 36, −25 ≤ l ≤ 24
Reflections collected	278974
Independent reflections	18431, R_{int} = 0.0555, R_{sigma} = 0.0321
Completeness to θ = 25.098°	100.0 %

Data / Restraints / Parameters	18431/0/455
Absorption correction Tmin/Tmax (method)	0.6941/0.7458 (multi-scan)
Goodness-of-fit on F^2	1.031
Final *R* indexes [$I \geq 2\sigma(I)$]	R_1 = 0.0287 wR_2 = 0.0598
Final *R* indexes [all data]	R_1 = 0.0386 wR_2 = 0.0632
Largest peak/hole [eÅ^{-3}]	1.08/-0.69

5.5 1(Ph*a*AC)

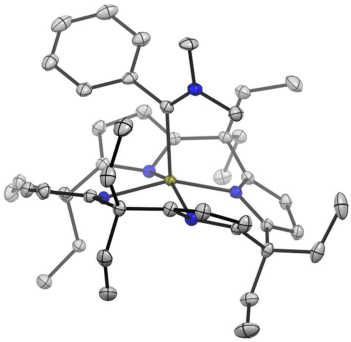


Figure S59: Solid state molecular structure of **1(Ph*a*AC)**. Ellipsoids are drawn with a probability of 50%. Hydrogen atoms are omitted for clarity.

Table S4: Crystal data for **1(Ph*a*AC)**.

CCDC number	2303622
Identification code	mo_hrrp20b_3_0ma
Empirical formula	$C_{45}H_{59}Cl_0N_5Sn$
Formula weight	788.66
Temperature [K]	100(2)
Crystal system	triclinic
Space group (number)	$P\overline{1}$ (2)
a [Å]	8.6770(13)
b [Å]	13.3223(19)
c [Å]	17.276(3)
α [°]	86.584(7)
β [°]	85.727(7)
γ [°]	82.392(6)
Volume [Å^3]	1971.5(5)
Z	2
ρ_{calc} [gcm^{-3}]	1.329
μ [mm^{-1}]	0.686
F(000)	828
Crystal size [mm^3]	0.178×0.042×0.037
Crystal colour	orange
Crystal shape	block
Radiation	MoK_α (λ=0.71073 Å)
2θ range [°]	3.80 to 61.21 (0.70 Å)
Index ranges	−12 ≤ h ≤ 12, −19 ≤ k ≤ 19, −24 ≤ l ≤ 24
Reflections collected	78068
Independent reflections	12091, R_{int} = 0.0644, R_{sigma} = 0.0424
Completeness to θ = 25.098°	100.0 %

Data / Restraints / Parameters	12091/0/470
Absorption correction Tmin/Tmax (method)	0.7071/0.7459 (multi-scan)
Goodness-of-fit on F^2	1.037
Final R indexes [$I \geq 2\sigma(I)$]	R_1 = 0.0310 wR_2 = 0.0698
Final R indexes [all data]	R_1 = 0.0460 wR_2 = 0.0761
Largest peak/hole [eÅ^{-3}]	0.56/-0.74

5.6 1(NMe2aAC)

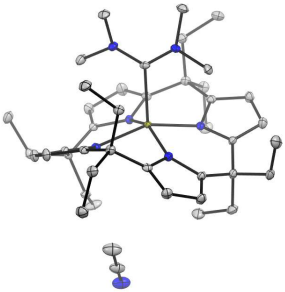


Figure S60: Solid state molecular structure of **1(NMe2aAC)**. Ellipsoids are drawn with a probability of 50%. Hydrogen atoms are omitted for clarity. **1(NMe2aAC)** crystallized with one MeCN molecule in the asymmetric unit.

Table S5: Crystal data for **1(NMe2aAC)**.

CCDC number	2303623
Identification code	mo_hr523_0ma
Empirical formula	$C_{43}H_{63}N_7Sn$
Formula weight	796.69
Temperature [K]	100(2)
Crystal system	monoclinic
Space group (number)	$P2_1/c$ (14)
a [Å]	12.700(2)
b [Å]	12.0235(16)
c [Å]	25.990(3)
α [°]	90
β [°]	90.075(5)
γ [°]	90
Volume [Å^3]	3968.6(10)
Z	4
ρ_{calc} [gcm^{-3}]	1.333
μ [mm^{-1}]	0.683
F(000)	1680
Crystal size [mm^3]	0.156×0.151×0.068
Crystal colour	colorless
Crystal shape	block
Radiation	MoK_α (λ=0.71073 Å)
2θ range [°]	4.48 to 57.47 (0.74 Å)
Index ranges	−16 ≤ h ≤ 16, −15 ≤ k ≤ 15, −33 ≤ l ≤ 33
Reflections collected	213717
Independent reflections	8658, R_{int} = 0.0480, R_{sigma} = 0.0142
Completeness to θ = 25.098°	99.9 %
Data / Restraints / Parameters	8658/0/473

Absorption correction Tmin/Tmax (method)	0.7019/0.7458 (multi-scan)
Goodness-of-fit on F^2	1.174
Final *R* indexes [$I \geq 2\sigma(I)$]	R_1 = 0.0295 wR_2 = 0.0617
Final *R* indexes [all data]	R_1 = 0.0307 wR_2 = 0.0623
Largest peak/hole [eÅ^{-3}]	0.71/-1.32

5.7 CuBr(tBuaAC)

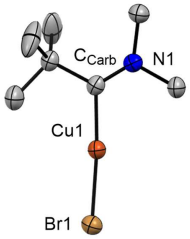


Figure S61: Solid state molecular structure of **CuBr(tBuaAC)**. Ellipsoids are drawn with a probability of 50%. Hydrogen atoms are omitted for clarity. Selected bond lengths [pm] and angles [°]: Cu1-C_{carb} = 189.5(5), Cu1-Br1 = 222.94(9), C_{carb}-N1 = 131.0(7), Br1-Cu1-C_{carb} = 175.27(16).

Table S6: Crystal data for **CuBr(tBuaAC)**.

CCDC number	2303620
Identification code	mo_hr614_0m_a
Empirical formula	$C_7H_{15}BrCuN$
Formula weight	256.65
Temperature [K]	100(2)
Crystal system	orthorhombic
Space group (number)	$Pnma$ (62)
a [Å]	16.465(3)
b [Å]	7.3316(15)
c [Å]	8.3780(16)
α [°]	90
β [°]	90
γ [°]	90
Volume [$Å^3$]	1011.3(4)
Z	4
ρ_{calc} [gcm^{-3}]	1.686
μ [mm^{-1}]	6.047
F(000)	512
Crystal size [mm^3]	0.064×0.042×0.042
Crystal colour	orange
Crystal shape	block
Radiation	MoK_α (λ=0.71073 Å)
2θ range [°]	4.95 to 57.55 (0.74 Å)
Index ranges	−22 ≤ h ≤ 22, −9 ≤ k ≤ 9, −11 ≤ l ≤ 11
Reflections collected	26509
Independent reflections	1409, R_{int} = 0.1009, R_{sigma} = 0.0335
Completeness to θ = 25.098°	100.0 %
Data / Restraints / Parameters	1409/0/60
Absorption correction Tmin/Tmax (method)	0.6345/0.7458 (multi-scan)
Goodness-of-fit on F^2	1.072

Final *R* indexes [*I*≥2σ(*I*)]	R_1 = 0.0386 wR_2 = 0.0862
Final *R* indexes [all data]	R_1 = 0.0602 wR_2 = 0.0966
Largest peak/hole [eÅ^{-3}]	0.71/−0.65

5.8 CuCl(*t*Bu*a*AC)

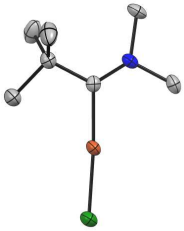


Figure S62: Solid state molecular structure of **CuCl(*t*Bu*a*AC)**. Ellipsoids are drawn with a probability of 50%. Hydrogen atoms are omitted for clarity.

Table S7: Crystal data for **CuCl(*t*Bu*a*AC)**.

CCDC number	2333351
Identification code	mo_hram154b_0m_a
Empirical formula	$C_7H_{15}ClCuN$
Formula weight	212.19
Temperature [K]	100(2)
Crystal system	orthorhombic
Space group (number)	$Pnma$ (62)
a [Å]	16.3296(16)
b [Å]	7.2395(7)
c [Å]	8.1352(7)
α [°]	90
β [°]	90
γ [°]	90
Volume [Å^3]	961.73(16)
Z	4
ρ_{calc} [gcm^{-3}]	1.465
μ [mm^{-1}]	2.482
F(000)	440
Crystal size [mm^3]	0.366×0.068×0.027
Crystal colour	colourless
Crystal shape	needle
Radiation	MoK_α (λ=0.71073 Å)
2θ range [°]	4.99 to 52.00 (0.81 Å)
Index ranges	−20 ≤ h ≤ 20, −8 ≤ k ≤ 8, −10 ≤ l ≤ 10
Reflections collected	32178
Independent reflections	1021, R_{int} = 0.1053, R_{sigma} = 0.0333
Completeness to θ = 25.098°	100.0 %
Data / Restraints / Parameters	1021/0/61
Absorption correction Tmin/Tmax (method)	0.5921/0.7458 (multi-scan)
Goodness-of-fit on F^2	1.057
Final *R* indexes	R_1 = 0.0429

[$I \geq 2\sigma(I)$]	wR_2 = 0.0904
Final *R* indexes [all data]	R_1 = 0.0585 wR_2 = 0.1016
Largest peak/hole [eÅ^{-3}]	0.68/−0.56
Extinction coefficient	0.0037(9)

5.9 CuCl(PhaAC)

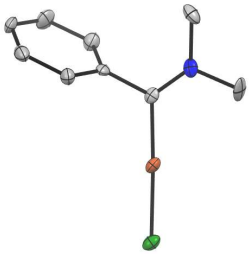


Figure S63: Solid state molecular structure of **CuCl(PhaAC)**. Ellipsoids are drawn with a probability of 50%. Hydrogen atoms are omitted for clarity. This structure was integrated and refined as a 2-component twin with a BASF parameter of 0.06027.

Table S8: Crystal data for **CuCl(PhaAC)**.

CCDC number	2333350
Identification code	mo_hram154a_0m_a
Empirical formula	$C_9H_{11}ClCuN$
Formula weight	232.18
Temperature [K]	100(2)
Crystal system	monoclinic
Space group (number)	P2_1/c (14)
a [Å]	6.780(3)
b [Å]	7.036(2)
c [Å]	21.292(8)
α [°]	90
β [°]	93.133(16)
γ [°]	90
Volume [Å^3]	1014.3(6)
Z	4
ρ_{calc} [gcm^{-3}]	1.520
μ [mm^{-1}]	2.361
F(000)	472
Crystal size [mm^3]	0.200×0.033×0.033
Crystal colour	yellow
Crystal shape	needle
Radiation	MoKα (λ=0.71073 Å)
2θ range [°]	3.83 to 53.14 (0.79 Å)
Index ranges	−8 ≤ h ≤ 8, 0 ≤ k ≤ 8, 0 ≤ l ≤ 26
Reflections collected	2288
Independent reflections	2136, R_{int} = 0.1179, R_{sigma} = 0.0308
Completeness to θ = 25.098°	99.9 %
Data / Restraints / Parameters	2136/0/112
Absorption correction Tmin/Tmax (method)	0.624191/0.745372

	(multi-scan)
Goodness-of-fit on F^2	1.259
Final *R* indexes [$I \geq 2\sigma(I)$]	R_1 = 0.0572 wR_2 = 0.1479
Final *R* indexes [all data]	R_1 = 0.0614 wR_2 = 0.1500
Largest peak/hole [eÅ^{-3}]	1.51/−0.90

5.10 CuCl(NMe2aAC)

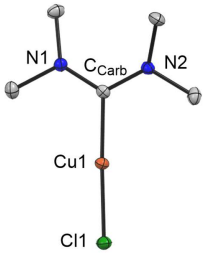


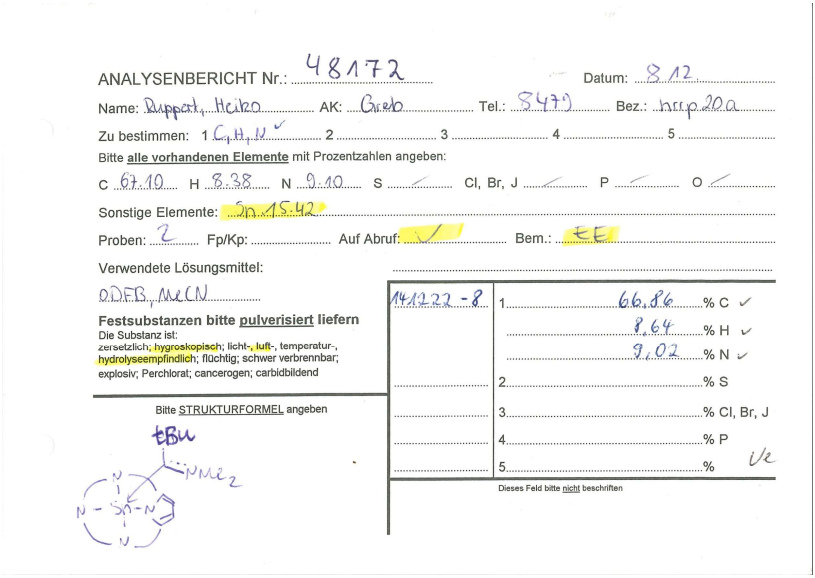
Figure S64: Solid state molecular structure of **CuCl(NMe2*a*AC)**. Ellipsoids are drawn with a probability of 50%. Hydrogen atoms are omitted for clarity. Selected bond lengths [pm] and angles [°]: Cu1-C_{carb} = 190.93(17), Cu1-Cl1 = 211.47(5), C_{carb}-N1 = 134.0(2), C_{carb}-N2 = 134.7(2), Cl1-Cu1-C_{carb} = 176.95(5)

Table S9: Crystal data for **CuCl(NMe2*a*AC)**.

CCDC number	2333352
Identification code	mo_hram154c_0m_a
Empirical formula	$C_5H_{12}ClCuN_2$
Formula weight	199.16
Temperature [K]	100(2)
Crystal system	monoclinic
Space group (number)	$P2_1/n$ (14)
a [Å]	9.1436(5)
b [Å]	9.2443(5)
c [Å]	9.7612(6)
α [°]	90
β [°]	92.512(2)
γ [°]	90
Volume [Å^3]	824.28(8)
Z	4
ρ_{calc} [gcm^{-3}]	1.605
μ [mm^{-1}]	2.893
F(000)	408
Crystal size [mm^3]	0.217×0.054×0.045
Crystal colour	colourless
Crystal shape	block
Radiation	MoK_α (λ=0.71073 Å)
2θ range [°]	5.98 to 61.13 (0.70 Å)
Index ranges	−13 ≤ h ≤ 13, −13 ≤ k ≤ 13, −13 ≤ l ≤ 13
Reflections collected	32832
Independent reflections	2514, R_{int} = 0.0567, R_{sigma} = 0.0275
Completeness to θ = 25.098°	100.0 %
Data / Restraints / Parameters	2514/0/86
Absorption correction Tmin/Tmax (method)	0.5747/0.7461 (multi-scan)
Goodness-of-fit on F^2	1.132

Final *R* indexes [*I*≥2σ(*I*)]	R_1 = 0.0321 wR_2 = 0.0770
Final *R* indexes [all data]	R_1 = 0.0369 wR_2 = 0.0814
Largest peak/hole [eÅ^{-3}]	0.80/−0.53

6 Elemental Analysis



ANALYSENBERICHT Nr.: 48172 Datum: 8.12

Name: Ruppert, Heiko AK: Greb Tel.: 8479 Bez.: hrrp20a

Zu bestimmen: 1 C_4H_4N ✓ 2 3 4 5

Bitte **alle vorhandenen Elemente** mit Prozentzahlen angeben:

C 67.10 H 8.38 N 9.10 S / Cl, Br, J / P / O /

Sonstige Elemente: Sn: 15.42

Proben: 2 Fp/Kp: Auf Abruf: ✓ Bem.: EE

Verwendete Lösungsmittel:

ODFB, MeCN

Festsubstanzen bitte pulverisiert liefern

Die Substanz ist:
zersetzlich; hygroskopisch; licht-, luft-, temperatur-, hydrolyseempfindlich; flüchtig; schwer verbrennbar; explosiv; Perchlorat; cancerogen; carbidbildend

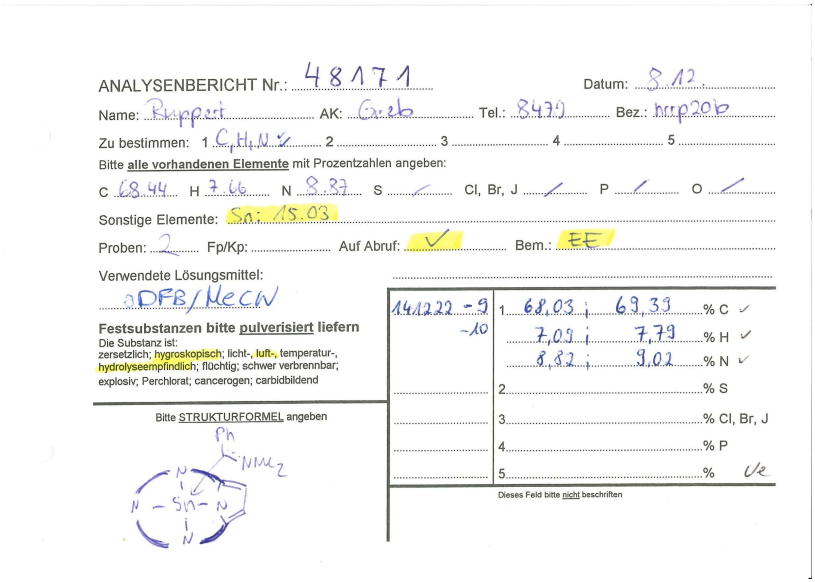
Bitte STRUKTURFORMEL angeben

141222 - 8

1	66.86	% C ✓
	8.64	% H ✓
	9.02	% N ✓
2		% S
3		% Cl, Br, J
4		% P
5		% Ve

Dieses Feld bitte nicht beschriften

Figure S65. Elemental analysis report for **1(*^{tBu}aAC*)**.



ANALYSENBERICHT Nr.: 48171 Datum: 8.12

Name: Ruppert AK: Greb Tel.: 8479 Bez.: hrrp20b

Zu bestimmen: 1 C_4H_4N ✓ 2 3 4 5

Bitte **alle vorhandenen Elemente** mit Prozentzahlen angeben:

C 68.44 H 7.66 N 8.37 S / Cl, Br, J / P / O /

Sonstige Elemente: Sn: 15.03

Proben: 2 Fp/Kp: Auf Abruf: ✓ Bem.: EE

Verwendete Lösungsmittel:

ODFB/MeCN

Festsubstanzen bitte pulverisiert liefern

Die Substanz ist:
zersetzlich; hygroskopisch; licht-, luft-, temperatur-, hydrolyseempfindlich; flüchtig; schwer verbrennbar; explosiv; Perchlorat; cancerogen; carbidbildend

Bitte STRUKTURFORMEL angeben

141222 - 9 / -10

1	68.03 ; 69.39	% C ✓
	7.09 ; 7.79	% H ✓
	8.82 ; 9.02	% N ✓
2		% S
3		% Cl, Br, J
4		% P
5		% Ve

Dieses Feld bitte nicht beschriften

Figure S66. Elemental analysis report for **1(*^{Ph}aAC*)**.

ANALYSENBERICHT Nr.: 47957 Datum: 09.09.22

Name: Ruppert AK: Greb Tel.: 8479 Bez.: braun15_2

Zu bestimmen: 1 C,H,N 2 3 4 5

Bitte **alle vorhandenen Elemente** mit Prozentzahlen angeben:

C 65,17 H 8,00 N 11,12 S Cl, Br, J P O

Sonstige Elemente: Sn: 15,71

Proben: 2 Fp/Kp: Auf Abruf: ✓ Bem.: EE

Verwendete Lösungsmittel:

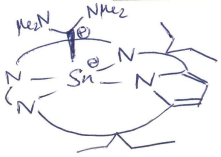
Toluol, MeCN

Festsubstanzen bitte pulverisiert liefern

Die Substanz ist:

zersetzlich; hygroskopisch, licht-, luft-, temperatur-, hydrolyseempfindlich; flüchtig; schwer verbrennbar; explosiv; Perchlorat; cancerogen; carbidbildend

Bitte STRUKTURFORMEL angeben



1409.22-18 -19	1	65,58 ; 65,62	% C ✓
		7,65 ; 8,36	% H ✓
		11,65 ; 11,78	% N ✓
	2		% S
	3		% Cl, Br, J
	4		% P
	5		% Ve

Dieses Feld bitte nicht beschriften

Figure S67. Elemental analysis report for **1(NMe2αAC)**.

ANALYSENBERICHT Nr.: 48949 Datum: 19.09.23

Name: Ruppert AK: Greb Tel.: 8629 Bez.: braun145

Zu bestimmen: 1 C,H,N 2 3 4 5

Bitte **alle vorhandenen Elemente** mit Prozentzahlen angeben:

C 66,84 H 8,15 N 9,28 S Cl, Br, J P O

Sonstige Elemente: Sn = 15,73

Proben: 2 Fp/Kp: Auf Abruf: ✓ Bem.: EE

Verwendete Lösungsmittel:

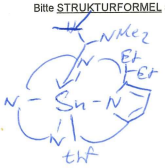
THF, pentan

Festsubstanzen bitte pulverisiert liefern

Die Substanz ist:

zersetzlich; hygroskopisch; licht-, luft-, temperatur-, hydrolyseempfindlich; flüchtig; schwer verbrennbar; explosiv; Perchlorat; cancerogen; carbidbildend

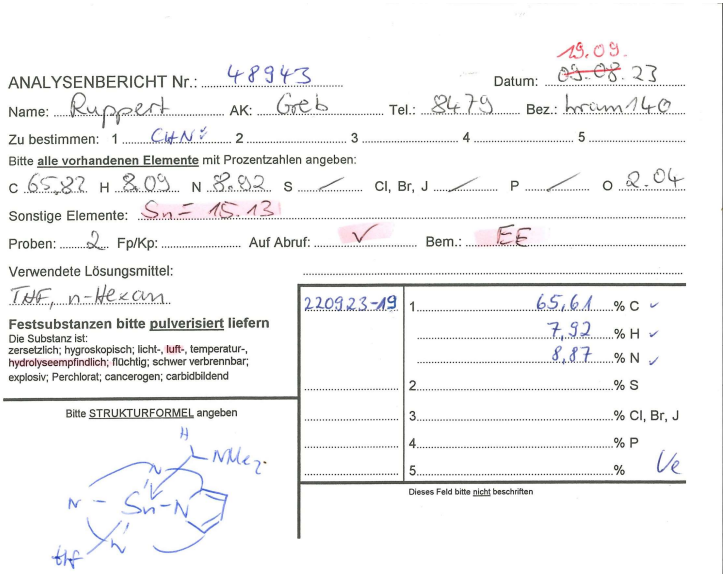
Bitte STRUKTURFORMEL angeben



220923-21 -22	1	66,40 ; 66,37	% C ✓
		7,60 ; 8,17	% H ✓
		9,45 ; 9,33	% N ✓
	2		% S
	3		% Cl, Br, J
	4		% P
	5		% Ve

Dieses Feld bitte nicht beschriften

Figure S68. Elemental analysis report for **1(iPrαAC)**.



ANALYSENBERICHT Nr.: 48943 Datum: 19.09. ~~05.08~~ 23

Name: Ruppert AK: Greb Tel.: 8479 Bez.: bronn140

Zu bestimmen: 1 CHN 2 3 4 5

Bitte **alle vorhandenen Elemente** mit Prozentzahlen angeben:

C 65.87 H 8.09 N 8.92 S / Cl, Br, J / P / O 2.04

Sonstige Elemente: Sn = 15.13

Proben: 2 Fp/Kp: Auf Abruf: ✓ Bem.: EE

Verwendete Lösungsmittel:

THF, n-Hexan

Festsubstanzen bitte pulverisiert liefern

Die Substanz ist:
zersetzlich; hygroskopisch; licht-, luft-, temperatur-, hydrolyseempfindlich; flüchtig; schwer verbrennbar; explosiv; Perchlorat; cancerogen; carbidbildend

Bitte STRUKTURFORMEL angeben

220923-19

1. 65.61 % C ✓
7.92 % H ✓
8.87 % N ✓
2. % S
3. % Cl, Br, J
4. % P
5. % Ve

Dieses Feld bitte nicht beschriften

Figure S69. Elemental analysis report for **1(**^{H}***a*****AC)(thf)**.

7 DFT Calculations

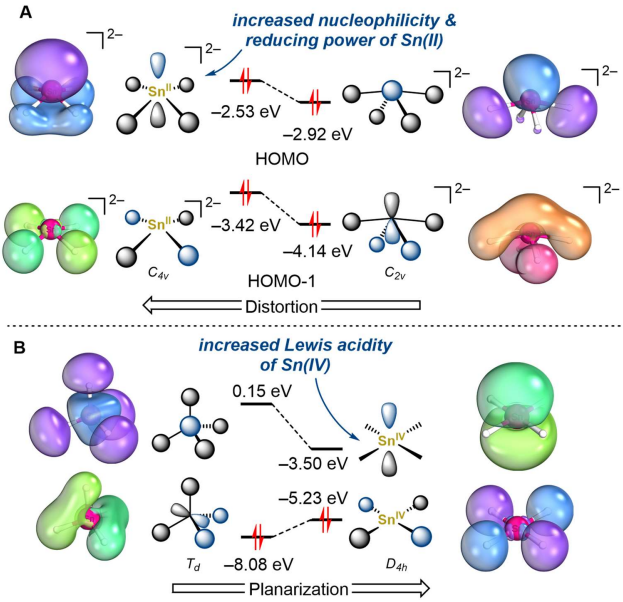


Figure S70. Frontier molecular orbital energies for **A** $[SnH_4]^{2-}$ and **B** SnH_4 at the B97M-D4/def2-TVZPP CPCM(THF)//PBEh-3c level of theory. Isosurfaces sampled at a value of 0.03.

Table S10. Computed reference values for the calculation of isodesmic ion affinities at the DSD-BLYP-D3(BJ)/def2-QZVPP//B97M-D4/def2-TZVPP//CREST/GFN2-xTB level of theory with COSMO-RS (DCM) solvent correction.[35]

Compound	DSD-BLYP-D3(BJ)/def2-QZVPP electronic energy [kJ mol^{-1}]	DSD-BLYP-D3(BJ)/def2-QZVPP Enthalphy with B97M-D4/def2-TZVPP thermal correction [kJ mol^{-1}]	+ COSMO-RS(DCM) enthalpy correction [kJ mol^{-1}]
$SiMe_3^+$	-1073011.45	-1072696.73	-1072696.73
$HSiMe_3$	-1075327.40	-1074991.30	-1075009.35
$FSiMe_3$	-1336053.07	-1335728.47	-1335753.08
$ClSiMe_3$	-2281687.13	-2281364.08	-2281392.30
H^-	-1335.46	-1332.98	-1537.89
F^-	-262071.30	-262068.82	-262411.87
Cl^-	-1207915.21	-1207912.74	-1208217.44

Table S11. Computed isodesmic ion affinities of **1** and the reference compound **6** at the DSD-BLYP-D3(BJ)/def2-QZVPP//B97M-D4/def2-TZVPP//CREST/GFN2-xTB level of theory with COSMO-RS (DCM) solvent correction.[35]

Compound	DSD-BLYP-D3(BJ)/def2-QZVPP electronic energy [kJ mol^{-1}]	DSD-BLYP-D3(BJ)/def2-QZVPP Enthalpy with B97M-D4/def2-TZVPP thermal correction [kJ mol^{-1}]	+ COSMO-RS(DCM) enthalpy correction [kJ mol^{-1}]	Isodesmic ion affinity in the gas phase [kJ mol^{-1}]	Isodesmic ion affinity in solution COSMO-RS(DCM) [kJ mol^{-1}]
1	-4811472.02	-4809317.82	-4809405.84	-	-
[1-H]$^-$ (HIA)	-4813367.11	-4811193.84	-4811390.85	**631.91**	**535.99**
[1-F]$^-$ (FIA)	-5074026.95	-5071866.26	-5072071.45	**567.70**	**341.81**
[1-Cl]$^-$ (CIA)	-6019726.33	-6017567.29	-6017769.35	**427.34**	**236.67**
6	-2761487.63	-2760669.62	-2760737.36	-	-
[6-H]$^-$ (HIA)	-2763279.93	-2762444.83	-2762646.58	**556.13**	**485.24**
[6-F]$^-$ (FIA)	-3023967.19	-3023140.86	-3023346.64	**511.37**	**306.36**
[6-Cl]$^-$ (CIA)	-3969656.55	-3968831.55	-3969036.36	**362.84**	**195.21**
BCF	-5795524.46	-5795036.70	-5795082.43	-	-
[BCF-H]$^-$ (HIA)	-5797387.06	-5796878.29	-5797037.97	**602.44**	**511.49**
SbF_5	-1940876.13	-1940824.96	-1940852.63	-	-
[SbF_6]$^-$ (FIA)	-2203455.26	-2203395.97	-2203611.82	**661.29**	**506.42**

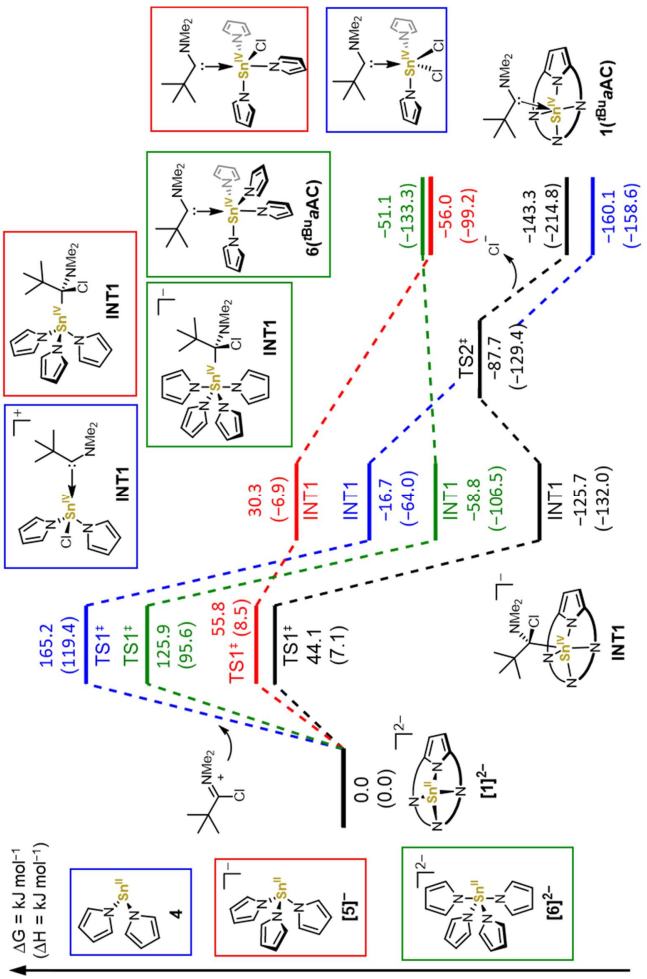


Figure S71. Mechanism for the formation of **1(*t*Bu*α*AC)** from $[\mathbf{1}]^{2-}$ and the respective chloroiminium cation in THF (black) compared to the reactions of the reference tin(II) complexes **4** (blue), $[\mathbf{5}]^{-}$ (red), and $[\mathbf{6}]^{2-}$ (green) with the chloroiminium cation computed at the DSD-BLYP-D3(BJ)/def2-QZVPP COSMO-RS(THF)//B97M-D4/ def2-TZVPP//CREST/GFN2-xTB level of theory.

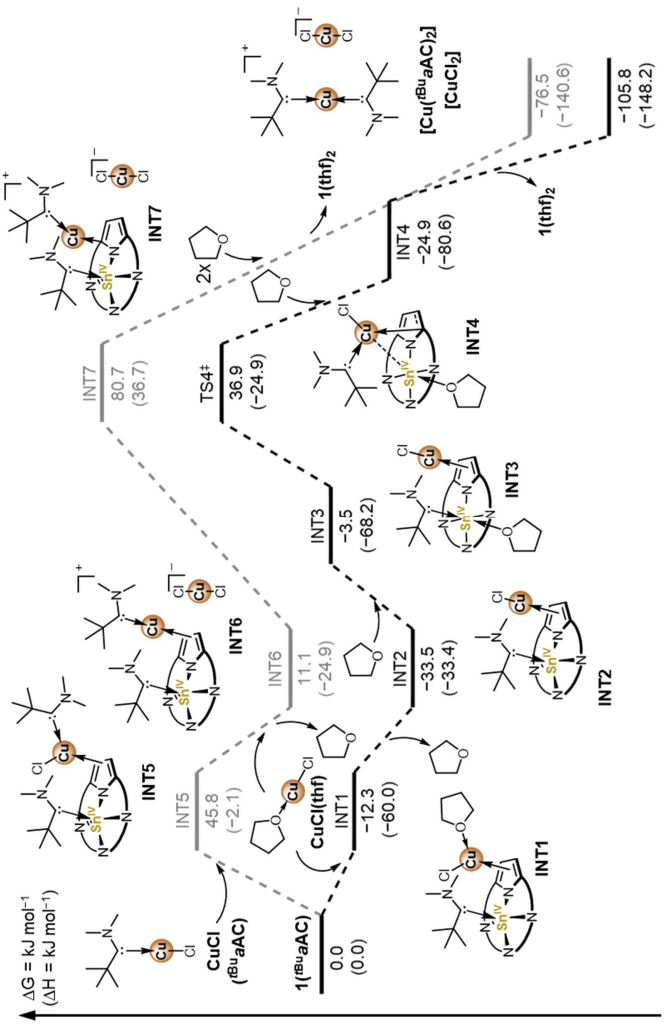


Figure S72. Mechanism of the carbene transfer reaction between **1(*t*Bu*a*AC)** and CuCl in THF at 298.15 K computed at the DSD-BLYP-D3(BJ)/def2-QZVPP COSMO-RS(THF)//B97M-D4/def2-TZVPP//CREST/GFN2-xTB level of theory (black path) and the hypothetical 2nd carbene transfer reaction between **1(*t*Bu*a*AC)** and **CuCl(*t*Bu*a*AC)** forming the ionic compound **[Cu(*t*Bu*a*AC)$_2$][CuCl$_2$]** (grey path).

8 Bonding Analysis Results

Table S12: ETS-NOCV Bonding energy decomposition terms of **1(^{tBu}*a*AC)** calculated on the BP86-D3/TZ2P COSMO(DCM)//B97M-D4/def2-TVZPP level of theory.

Compound	Total Pauli Repulsion (ΔE_{Pauli}) [Eh]	Total Electrostatic Interaction (ΔV_{elst}) [Eh]	Total Orbital Interaction ($\Delta E_{oi,tot}$) [Eh]	Total Dispersion Energy (E_{disp}) [Eh]	Solvation Energy (E_{solv}) [Eh]	Residue [Eh]	Total Bonding Energy (ΔE) [Eh]
1(^{tBu}*a*AC) (homolytical)	0.23396516169 1499	-0.24311173970 4091	-0.20323542019 4188	-0.05199915035 6871	0.00495384535 3640	0.00000005514 0282	-0.27630310758 8261
1(^{tBu}*a*AC) (heterolytical)	0.31656288402 0302	-0.23449913900 5948	-0.15506464988 8844	-0.05199915035 6871	0.00495384535 3640	-0.00000004367 6454	-0.13692210675 7548

Table S13: NBO analysis results calculated on PBE0/def2-TZVPP//B97M-D4/def2-TZVPP level of theory. NBO and second order perturbation theory stabilization energies $\Delta E^{(2)}$ for selected bonding interactions are given in kJ mol^{-1}. Additionally, Lewis density parameters $\%\rho_L$ and single point energies are given for each system.

^{tBu}*a*AC (single point energy = −330.155703002113 Eh, $\%\rho_L$ = 99.18)	
Natural charge at C1	0.11328
Natural charge at N2	−0.36939
1 (single point energy = −1832.695050950664 Eh, $\%\rho_L$ = 98.40)	
Natural charge at Sn1	2.37596
Avararge Sn-N Wiberg bond index	0.4932
1(^{tBu}*a*AC) (single point energy = − 2162.916008875927 Eh, $\%\rho_L$ = 99.08)	
Natural charge at Sn1	2.38001
Natural charge at C_{carb}	0.13686
Natural charge at N47	−0.33376
Avararge Sn-N Wiberg bond index	0.3881
Sn1-C2 Wiberg bond index	0.4897
N3-Sn1-C2 3c-4e Hyperbond	N3-Sn1 :C2 (41.0%) N3: SN1-C2 (59.0%) Occupation: 3.7079
1(^{iPr}*a*AC) (single point energy = − 2123.654940392767 Eh, $\%\rho_L$ = 98.22)	
Sn1-C2 Wiberg bond index	0.4866
$\Delta E^{(2)}$ $\pi_{C53\text{-}C67}\rightarrow\sigma^*_{C100\text{-}H109}$ (H-bonding)	6.53 kJ mol^{-1}
6 (single point energy = −1051.951643526803 Eh, $\%\rho_L$ = 97.67)	
Natural charge at Sn1	2.37496
Avararge Sn-N Wiberg bond index	0.5653
6(^{tBu}*a*AC) (single point energy = −1382.134204196669 Eh, $\%\rho_L$ = 97.56)	
Natural charge at Sn1	2.30556
Natural charge at C_{carb}	0.20023
Natural charge at N15	−0.34953
Avararge Sn-N Wiberg bond index	0.4355
Sn1-C2 Wiberg bond index	0.4749
1(^{tBu}*a*AC)(thf) (single point energy = −2395.184216973770 Eh, $\%\rho_L$ = 98.32)	
Natural charge at Sn1	2.5694
Natural charge at C_{carb}	0.13466
Sn1-C_{carb} Wiberg bond index	0.3864
INT4 (single point energy = −4495.620259722679 Eh, $\%\rho_L$ = 98.35)	
$\Delta E^{(2)}$ $\pi_{C51\text{-}C54}\rightarrow 4s_{Cu126}$ (pyrrole coordination to Cu(I))	60.84 kJ mol^{-1}
$\Delta E^{(2)}$ $4d_{Cu126}\rightarrow\sigma^*_{Sn1\text{-}N48}$ (back donation from Cu(I))	26.11 kJ mol^{-1}
Sn1-C_{carb} Wiberg bond index	0.2206
C_{2v} $[SnH_4]^{2-}$ (single point energy = − 216.783736369459 Eh, $\%\rho_L$ = 99.31)	
s Character of Sn(II) electron lone pair	69.92 %
p Character of Sn(II) electron lone pair	30.08 %
C_{4v} $[SnH_4]^{2-}$ (single point energy = −216.765253130359 Eh, $\%\rho_L$ = 98.90)	
s Character of Sn(II) electron lone pair	52.00 %
p Character of Sn(II) electron lone pair	48.00 %

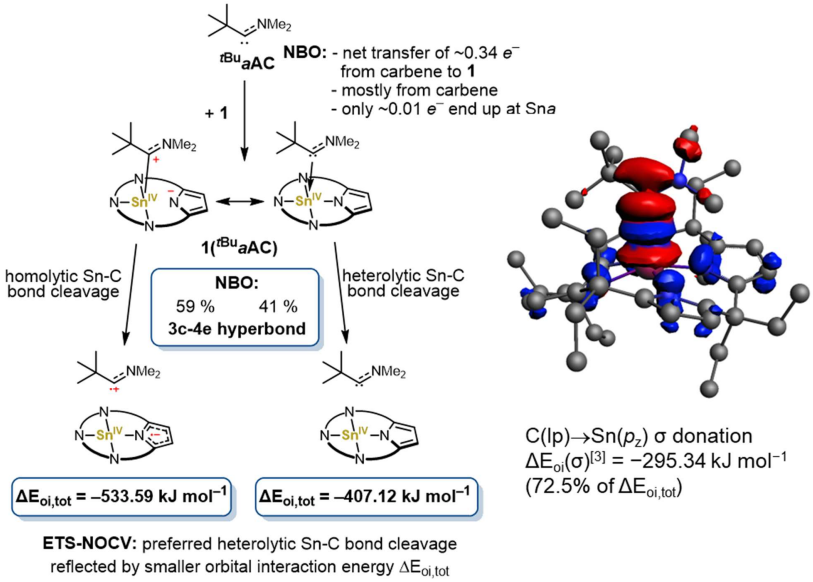


Figure S73. Bond analysis of the AAAC adduct **1(*t*Bu*a*AC)**. NBO results were calculated at the PBE0/def2-TZVPP//B97M-D4/def2-TZVPP level of theory. ETS-NOCV results were calculated on the BP86-D3/TZ2P COSMO(DCM)//B97M-D4/def2-TZVPP level of theory. For the homolytic cleavage of the Sn-C bond in **1(*t*Bu*a*AC)** the fragments where treated as unrestricted open-shell species. NOCV deformation densities (right) for the main orbital interaction of a heterolytic Sn-C bond cleavage sampled at a value of 0.003. Hydrogen atoms were omitted for clarity. The color code of the charge flow is red to blue.

9 Optimized Molecular Geometries

```
5
Coordinates from ORCA-job snh4_PBEh3c_opt
  Sn  -0.51966895853119      1.32259116930336      0.44204037093111
  H   -1.49314993341832      0.09125614884617     -0.20762932362981
  H    1.10065794330976      0.81294421299572      0.45856679111988
  H   -0.66305134053295      2.72120285613039     -0.51142780809901
  H   -1.02248771082730      1.66404561272435      2.02828996967783

5
Coordinates from ORCA-job snh4_sqpl_PBEh3c_opt
  Sn  -3.19479567065265      4.00322247941150     -3.83227617360112
  H   -2.81476084522976      2.75937666619362     -2.63739114834353
  H   -3.39767494095507      5.19520231302535     -2.54297739940494
  H    0.08459085770769      0.05921678396717      0.72279140472271
  H    5.68582059912958     -5.90916824259779      8.28985331662687

5
snh4_dianion_c2v
Sn   -0.617186000000      0.034915000000      0.010463000000
H    -0.152704000000      0.048059000000      2.207191000000
H    -0.273597000000     -0.026392000000     -2.186968000000
H     0.444752000000     -1.416535000000      0.010562000000
H     0.598734000000      1.359954000000     -0.041249000000

5
snh4_dianion_c4v
Sn   -0.453350000000      0.025342000000      0.012144000000
H     0.161967000000      0.024752000000      1.822510000000
H     0.062567000000     -0.037283000000     -1.828538000000
H     0.013335000000     -1.828415000000      0.030639000000
H     0.215481000000      1.815604000000     -0.036755000000

11
Coordinates from ORCA-job h_aaac_cmp_Compound_1
  C   9.84664484291241      6.01422565945455      4.17904222733767
  N   8.59021782432278      6.28693204230930      4.36316883129463
  C   7.46684463299450      5.34773484323170      4.35270189447389
  H   7.83817540206795      4.35319052524408      4.15572439516451
  H   6.75004194532021      5.62834348332871      3.58591187398557
  H   6.95535505789587      5.36347059839410      5.31116044538335
  C   8.16640648972453      7.65761174680595      4.61499207355308
  H   7.66076373933764      7.72225826723691      5.57475872112022
  H   7.47102018713039      7.98116442269445      3.84504902605944
  H   9.04121612427919      8.28782642445518      4.61291742146634
  H   9.90275375401449      4.92391198684503      4.01047309016128

20
Coordinates from ORCA-job ipr_aaac_cmp_Compound_1
```

C	9.85160472144547	5.93422800009356	4.13930242228990
N	8.63675695381975	6.34766133584640	4.35819722414911
C	7.55985403771852	5.36520980920556	4.34819525724169
H	7.98758064360739	4.39945501316061	4.13289531875306
H	6.82243471169751	5.62621071839472	3.59265553862572
H	7.06040500277123	5.34742352014046	5.31416302585684
C	10.91569705859274	7.95398753000100	3.00631180919182
H	11.86766856875357	8.46955455675230	2.91428911744112
H	10.14962059911727	8.71159859744993	3.13179541247834
C	8.10166204811812	7.69080003312349	4.63165653314329
C	10.97660576915244	6.94487487185001	4.15123472241591
C	11.22587129487644	7.58660421090217	5.51471201082162
H	11.23558931362503	6.83139344636638	6.29526284153750
H	10.48504840502607	8.32949606704572	5.78803350151346
H	12.19497799651788	8.07776318529128	5.52229304388682
H	7.60109288218078	7.69321909707539	5.59559086290474
H	7.36926030895336	7.95082945773645	3.87307857437230
H	8.87944897611582	8.42941266876381	4.63719265795263
H	10.72429581941593	7.44952349551201	2.06366954837023
H	11.86555488849461	6.34833438528869	3.95389057705387

23

Coordinates from ORCA-job tbu_aaac_cmp_Compound_1

C	0.62621796483711	-0.25398380116296	0.47363092109644
N	1.44542810893889	0.06515924756870	1.43192718043042
C	2.62302023751484	0.94792795048957	1.46937147623582
H	2.51062477907675	1.66048521079171	2.28078185396257
H	2.75012138112404	1.48334508991309	0.54893340848510
H	3.51334661027728	0.35713527643866	1.66417995284109
C	1.22652670864124	-0.53203738042982	2.74495265836337
H	2.11707870545560	-1.06830845580817	3.06448185129393
H	0.39008588830843	-1.20793559347859	2.67216201866075
H	1.01855176913451	0.24325273879284	3.47867601041836
C	0.81539954498398	0.33271995908444	-0.91395104074910
C	2.15575530027147	-0.05755681426685	-1.54116014097735
H	3.00954939832490	0.45032113251527	-1.11054276674987
H	2.14410663487207	0.17113130638392	-2.60372962049139
H	2.32095903299464	-1.12713591592174	-1.44234656602045
C	-0.28301974429567	-0.29264143035385	-1.77782265547871
H	-0.18773670162835	-1.37333114634575	-1.78927556988902
H	-0.23143157389079	0.07418510630095	-2.80092925013757
H	-1.26181529274944	-0.06057599731283	-1.37178836402026
C	0.59033776430501	1.84607554541192	-0.93054257609401
H	0.49430393613005	2.19079592001069	-1.95689522608453
H	1.38776936512642	2.41711532015562	-0.47081000411262
H	-0.33443881775301	2.09488073122319	-0.41704655098296

21

Coordinates from ORCA-job ph_aaac_cmp_Compound_1

C	9.47880770515106	6.54522681041553	3.27976029141977

N	8.59835011543326	6.37082417902864	4.21511554796840
C	7.43725862047860	5.52802407580293	3.97107536411254
H	7.57599924340525	5.02622491894999	3.02664602282618
H	6.53546661675354	6.13354668595906	3.94129414322213
H	7.33273944836370	4.80123477948214	4.77172160898497
C	8.61983371942491	6.94398106194798	5.57047493349595
C	10.63347177376698	7.35489166181183	3.61997746266816
H	7.60310427643425	7.12760557093005	5.89670193472197
H	9.17540159329174	7.86930935172413	5.56892232461850
H	9.08626989194918	6.25419589242838	6.26557126824098
C	10.78733056225768	8.64165380084261	3.10085882606054
C	11.67027621630316	6.82259676081495	4.39290411499018
C	12.81236261004344	7.55851084262396	4.64481371885756
C	11.92446970121612	9.37889191325565	3.37403373235800
C	12.94522556026798	8.84440420224300	4.14446767329810
H	11.58193522571953	5.81677929826558	4.77132611481784
H	13.83501220445260	9.41712111226701	4.34202514154059
H	13.60025964602766	7.12800747896033	5.24086418649396
H	10.00722578338323	9.05775935481932	2.48514060003198
H	12.01969948587579	10.37312024742675	2.96958498927159

19

Coordinates from ORCA-job nme2_aaac_cmp_Compound_1

C	2.58588923453432	5.00852855951964	3.06197177330743
N	2.02490345272406	4.16029835334015	2.18728392904361
C	1.26302460584515	4.75283694830553	1.11022916129283
C	2.27175765222631	2.73697317129113	1.98854332655801
H	1.20501816977702	5.81725191815936	1.27834476542785
H	0.25586753132568	4.34050459690081	1.07583281487951
H	1.73391826327951	4.56000442694886	0.14567450671007
H	3.19343729924254	2.44069657960425	2.46542308590805
H	2.37603249590283	2.55307522950900	0.92303415222191
H	1.46459838357108	2.10296119557355	2.35118627773583
N	3.17049453918328	4.49724298492221	4.15578369242937
C	3.90343358592561	5.42374435230177	4.98975758775665
C	2.96997270688337	3.20231057455750	4.79528714411207
H	3.94076044899567	6.37913446196198	4.48947646569192
H	4.91850521470220	5.06941189488485	5.16158718961881
H	3.42301849687763	5.53981958302128	5.96202551405641
H	2.06893319222426	2.73186885423789	4.43360299700164
H	2.85248783552553	3.36288655127721	5.86341708862860
H	3.80683689125391	2.51951976368293	4.65938852761937

24

Coordinates from ORCA-job tbu_aaac_cl_cmp_Compound_1

C	0.63963142824146	0.87299193485928	0.49003793490895
C	1.95335081612712	0.07413006251068	0.49247929899018
C	-0.31670044390888	0.14915348333855	1.43810563286589
C	0.08314970565642	0.92684873001916	-0.92194557846467
C	0.80354110519423	2.30093069322417	1.03616430362826

H	1.78359632375112	-0.93975606715649	0.14756467117689
H	2.30440535806712	0.01716749158003	1.51584679787091
H	2.74908488743884	0.50149846511360	-0.09960189523664
H	1.13130555126192	2.22326672100521	2.06581432532855
H	-0.14707525338404	2.82241063477724	1.03377973404423
H	1.52509297817874	2.91191601773729	0.51442998684821
H	-0.48617647172753	-0.87898140960631	1.14530619837821
H	-1.27194619157497	0.65155519105455	1.52098340500632
H	0.13812076267494	0.14164109021595	2.42046192372781
N	0.64064847425246	1.46946651701106	-1.95951477694601
Cl	-1.42495876025953	0.20736727073213	-1.20328998905020
C	1.93700099172965	2.14976680611063	-1.96832187085001
C	0.00198885374964	1.45465628971601	-3.28566772484597
H	-0.15140957654779	0.43544459849597	-3.61249858919683
H	0.65679819906872	1.96265376528205	-3.97450072480589
H	-0.95156163194206	1.96276687425979	-3.24563457011311
H	2.57635654406863	1.64301462129240	-2.68039111703867
H	2.39999803040338	2.15281128226976	-1.00441983433060
H	1.77880831948037	3.16772893615718	-2.30219754189574

89

Coordinates from ORCA-job sn2_cxet_CREST_cmp_Compound_1

N	0.00146046114751	-2.15945774880615	0.23256607836606
C	1.10051938770565	-2.87007272665649	0.63725678316802
C	0.70707951466465	-3.99778914936894	1.32378225080030
C	-0.70171641850068	-3.99877563109081	1.32369078934678
C	-1.09665107842253	-2.87161459531045	0.63710081868456
H	1.34380470272526	-4.74031854976150	1.76670075798291
H	-1.33745370283250	-4.74219831053081	1.76652396332030
C	2.48211559839732	-2.47773747783230	0.20990923323699
C	3.49095258739107	-3.48819468963652	0.77202933261455
H	3.10991791368380	-4.48911938661615	0.59187795302189
H	3.51613502859803	-3.36971253206526	1.85221415594434
C	4.89852081836474	-3.40368160741175	0.20566095080779
H	4.94173632658559	-3.77502639214329	-0.81549954929264
H	5.58646791191150	-4.00870746425827	0.79472822519802
H	5.26803081637831	-2.38493271438773	0.20133406946914
C	2.54914589773037	-2.50189157784444	-1.33678912474883
H	3.53631033259941	-2.16394357347475	-1.64954460514981
H	1.85621168014447	-1.76190311608036	-1.72074676528210
C	2.22227308552039	-3.84362890679154	-1.96031261441181
H	2.94580158431085	-4.61079617737143	-1.69176240730752
H	2.20932004168384	-3.77435397878671	-3.04642927840483
H	1.24739673934866	-4.19135209720460	-1.63291046610452
C	2.81850033746619	-1.09677827729822	0.68532035448528
C	3.81113901540427	-0.70214925899446	1.55509178609203
C	3.81021752458071	0.70744148735632	1.55496524291548
C	2.81701290404084	1.10061179964041	0.68518640719173
N	2.18205761888478	0.00145338580555	0.17457447415856
H	4.48259544460428	-1.33933716382265	2.10009076334345

H	4.48083529507424	1.34562020622477	2.09984533907635
C	2.47875674320791	2.48106121730229	0.20966364835422
C	3.48624478847994	3.49290354725565	0.77171191956447
H	3.10396048636425	4.49330711866491	0.59133032687721
H	3.51147504137460	3.37465006072714	1.85191880680293
C	4.89396361114561	3.41009330141921	0.20549541396801
H	5.58105495408682	4.01618161324332	0.79446997057464
H	4.93677157217528	3.78126664673932	-0.81574325577850
H	5.26484244672536	2.39183135459143	0.20143229200785
C	2.54574622052770	2.50519277047786	-1.33703356891877
H	3.53342914249160	2.16874763672526	-1.64977840107389
H	1.85399122723298	1.76408179248450	-1.72095455125617
C	2.21684726758554	3.84639341852258	-1.96065162604034
H	1.24151606261132	4.19274817194279	-1.63315428025716
H	2.20385971687748	3.77700496857285	-3.04675986205493
H	2.93929378484526	4.61463560502304	-1.69225743760175
C	-2.47875957054999	-2.48111942008758	0.20970613972200
C	-3.48625788177375	-3.49293922466167	0.77177645659421
H	-3.51146569728488	-3.37468095367016	1.85198326192239
H	-3.10400039930723	-4.49335184824493	0.59139098881632
C	-2.54574610827870	-2.50528135268650	-1.33699088635447
H	-1.85399331731110	-1.76417513660901	-1.72092547419335
H	-3.53342969756821	-2.16884563303377	-1.64974415345597
C	-2.21684072081353	-3.84649301239378	-1.96058184314530
H	-2.93928647393180	-4.61473190846219	-1.69217694769290
H	-1.24151013111349	-4.19283918923970	-1.63307331808452
H	-2.20384788055576	-3.77712476114911	-3.04669128728104
C	-4.89398637744303	-3.41009501081510	0.20559021615922
H	-4.93682604574921	-3.78126619421479	-0.81564765809895
H	-5.26484042383191	-2.39182314105170	0.20153667284690
H	-5.58107956675141	-4.01616638760786	0.79457993232723
C	-2.81701561621648	-1.10066037056898	0.68519641220716
N	-2.18205832921331	-0.00151412751994	0.17456133655218
C	-2.81850461363941	1.09672942563747	0.68527814900457
C	-3.81113433615690	0.70212034067238	1.55506899159513
C	-3.81023984049497	-0.70747028472910	1.55494361450533
H	-4.48258075606175	1.33932135303071	2.10006464758137
H	-4.48087431987757	-1.34563625207074	2.09981883174684
C	1.09664679676033	2.87156220715606	0.63704516337957
C	0.70170817072235	3.99874368539667	1.32359897187702
C	-0.70708768293925	3.99774647904022	1.32369999121822
C	-1.10052321221156	2.87002054522945	0.63718808127150
N	-0.00146211645405	2.15939694209807	0.23251828348839
H	1.33744345207391	4.74218173474762	1.76640978808336
H	-1.34381606779932	4.74028173251499	1.76660464819610
C	-2.48211724982832	2.47767960234103	0.20984039447030
C	-3.49095059699381	3.48815228883901	0.77193776595192
H	-3.10989634601945	4.48907072023090	0.59179079544085
H	-3.51615579990110	3.36967411454741	1.85212266109606
C	-2.54914519271008	2.50181071913241	-1.33685893830621

H	-1.85620639768312	1.76182142632844	-1.72080501185885
H	-3.53630746013828	2.16385235397531	-1.64961005908027
C	-2.22228108217756	3.84354121804735	-1.96040133076513
H	-1.24740809382613	4.19127561163648	-1.63300167408366
H	-2.94581607910251	4.61070703362681	-1.69186361556243
H	-2.20932502372491	3.77425098326358	-3.04651701226361
C	-4.89850816711868	3.40366141534296	0.20553930636864
H	-5.58645751888924	4.00870116247217	0.79458973890425
H	-5.26803542725029	2.38491937835206	0.20120695175761
H	-4.94169555116043	3.77500431920642	-0.81562330234565
Sn	0.00000249327322	-0.00004102112298	-0.74809663750263

113

Coordinates from ORCA-job TS1_sn_attack_v2_optTS

Sn	-0.13305980572872	-0.29337421631389	-0.15416319843350
C	-0.56544509143743	0.27832806796100	-3.61041501605508
N	-1.10780388027411	1.57481488020386	0.56338404591677
N	-1.79656126351887	-1.19862616954702	0.97455513861081
C	-3.02345267309433	-0.58823894040423	1.13617011671134
C	-2.46648898394833	1.74669723923386	0.41394425475296
C	-0.54989377941246	2.83040819302925	0.62750937840371
C	-1.86506471907617	-2.41482904580498	1.61551912542359
C	-2.75516847337677	3.09023156071297	0.37464495072258
H	-3.73021750933092	3.53192081561398	0.30782210347409
C	0.89311344998807	3.06155976269452	0.94481635456137
C	-3.84511661724639	-1.40743754426636	1.86850031616823
H	-4.86000002439886	-1.21012250937288	2.14940198173316
C	1.06266749474518	2.73508070088689	2.45899579726467
H	0.43866166549814	3.43910614175018	3.00969810976693
H	0.63575818510171	1.75131255187820	2.62422219512114
C	-3.45621864149973	0.62090364446636	0.37409560147949
C	-1.54032283320494	3.77747327525842	0.53101502357302
H	-1.41759882636451	4.84031931248983	0.60020399731544
C	-3.68025595021709	0.19929090748149	-1.10036941014840
H	-4.17913569832723	1.02753839315732	-1.60328493157459
C	-3.11554653016129	-2.56259885693999	2.16890807596167
H	-3.45847287064660	-3.38934030995273	2.75833386745238
C	1.25813270716244	4.53781777242108	0.73949161546049
H	0.65028074462093	5.12136879708933	1.42847157148722
H	2.28481482820274	4.67446185549179	1.06643979450055
C	-4.80461575779265	1.12462948817922	0.91895279286356
H	-5.14533913882764	1.92170175802725	0.26147421336471
H	-5.53440729104590	0.32750543845146	0.81046548759475
C	-4.81328434143709	1.62091191544503	2.35328163517932
H	-5.81276092880227	1.94529366016715	2.63612194070373
H	-4.14002346954726	2.45969573708283	2.48213472486518
H	-4.50454854101594	0.84628480358316	3.04410239615348
C	1.11405516676166	5.11222730734309	-0.65914194460173
H	1.45373828812322	6.14591423808656	-0.67651559586980
H	0.08634692678649	5.09353113242045	-0.99746008729824

H	1.70121634838769	4.56068190694160	-1.38272687009191
C	-4.44295227932205	-1.08877427465590	-1.33098459561901
H	-4.58787634348226	-1.25287521287836	-2.39659981866412
H	-5.42396585605735	-1.07778299883910	-0.86575408966384
H	-3.90566592991930	-1.93946886359597	-0.92610814441056
C	2.48113035013495	2.74979982500538	2.99094494549889
H	3.09428493444070	2.01020887873209	2.48808111106075
H	2.48600804949812	2.51658274076074	4.05279176919869
H	2.96399377531690	3.71580819104507	2.87123377337371
H	-2.70307681748886	0.10580288006072	-1.56134093755758
N	0.64198067387064	-0.25322194382974	-3.87113107553277
N	1.06625420821433	-1.93023499829963	0.80078506147080
N	1.76223197655554	0.80737685519358	0.33861491597680
C	2.93936995372995	0.29225548393152	-0.14078250607908
C	2.44156243005369	-1.91183371753076	0.91787457827262
C	0.61355356611680	-2.95691814348880	1.59980833736689
C	1.83568978983863	2.17565033241604	0.19377806322895
C	2.84036076897499	-2.89534296849217	1.78821530373164
H	3.84755445395846	-3.12740095096068	2.07252164060241
C	-0.79433229399464	-3.45897284761635	1.65397711716379
C	3.72915199182578	1.30971868021318	-0.62304783649949
H	4.72951076808121	1.21465792945068	-1.00290646037365
C	-0.97386180513120	-4.30352259666084	2.93354409555692
H	-1.94876338991349	-4.78065346184533	2.88359124017221
H	-0.25790893173625	-5.11990992870109	2.89654391137840
C	3.34146806282515	-1.14217884775115	0.00897559947912
C	1.68602491522880	-3.55891170000941	2.21795813365836
H	1.64977221983510	-4.37261830433203	2.91383805008656
C	3.32032126501319	-1.82363011567144	-1.38024664556758
H	2.31065481326913	-1.71608358644626	-1.75397547058985
C	3.03078570763149	2.51188856903870	-0.39718485648688
H	3.40747396901257	3.50153254981973	-0.56575315492081
C	-1.02272492641928	-4.45331048810889	0.48035848430405
H	-0.32039713253513	-5.27751538801295	0.60688252840223
H	-2.02706605551422	-4.86027288451453	0.59624662686305
C	4.78891623376781	-1.17724759320761	0.53784872253258
H	5.10061940088527	-2.21227363251177	0.63759498534825
H	5.42824281938643	-0.74961696121041	-0.23282295466639
C	5.02329847995910	-0.44998022831693	1.84680541002526
H	4.84750348754409	0.61425150014119	1.73951309505558
H	6.04835859468965	-0.58716041351010	2.18393899267593
H	4.36216573737848	-0.81642157466201	2.62352788730196
C	-0.87366335304026	-3.87401321544243	-0.90726848164129
H	-1.54148087079169	-3.02964856811213	-1.05459809208538
H	-1.10887806461356	-4.61608712555959	-1.66630535542722
H	0.14201776849760	-3.53174373230972	-1.07629108503294
C	3.69393479675362	-3.29151128629503	-1.42121537412819
H	4.72527173912123	-3.45997479636292	-1.12619155929129
H	3.57834118619073	-3.68642335719013	-2.42875547216566
H	3.06477060504279	-3.87025800288178	-0.75417266173408

C	-0.83844929096303	-3.55732011638226	4.24541220198299
H	0.13582969076365	-3.09065697885042	4.33187615858614
H	-0.96360229364668	-4.23431150627515	5.08780310871343
H	3.96464966764122	-1.25060902186175	-2.04924323249541
H	-1.58611356412458	-2.77691191812845	4.32753936151088
C	0.78960479507522	-1.69108239467841	-3.81283646008612
H	0.17145833999110	-2.17484986003643	-4.55356368988302
H	0.49184107941680	-2.04688870753434	-2.82133878655952
H	1.82523688617466	-1.94117578520632	-3.98205776425727
C	-0.30939113032396	2.64260650291561	-2.69696466090349
H	-0.37999971955191	3.68139470027539	-3.00598078485443
H	0.71226975908063	2.45255189741138	-2.40709941421828
C	1.83101820429988	0.46430756404118	-3.44612110384825
C	-0.85363692965865	1.76731628345029	-3.82394455250703
C	-2.34865098446397	2.06729448910392	-3.88564866707939
H	-2.85383842108672	1.75522730702817	-2.98521428094261
H	-2.83167762886426	1.61089593872322	-4.74144685611191
H	-2.46141210355346	3.14326103499388	-3.96725599950877
C	-0.28327556557347	2.16737561088543	-5.19576389163305
H	0.79431159238000	2.10751262838573	-5.26131377629278
H	-0.57012907222626	3.19482008882724	-5.39583129473706
H	-0.70325383036230	1.54190375787201	-5.97808483769519
H	1.90626678664475	0.46710206105925	-2.35878076502072
H	1.82837423825931	1.48223811951107	-3.78815430035892
H	2.69558240022915	-0.04192085696351	-3.84796492875105
H	-0.91956989425869	2.52714673824029	-1.81227384438136
Cl	-1.88526761962641	-0.78718094774776	-3.97120224282969

113

Coordinates from ORCA-job INT1_tbu_aaac_cl_sn4cxet_CREST_cmp_Compound_1

Sn	-0.15861971055188	-0.00711216457312	-0.23365742530471
C	-0.14667044421311	-0.08531127843498	-2.54374185670419
N	-1.31920435275451	1.62647654673562	0.51682926686683
N	-1.85579078743909	-1.12350860134412	0.39549566873981
C	-3.15294115734786	-0.75137989578168	0.09268414967608
C	-2.67025759236712	1.75030293400450	0.24393642393505
C	-0.83949122174391	2.89239045483507	0.78993210234820
C	-1.85999921846974	-2.47639741407569	0.66886220691065
C	-3.02086193200422	3.07194117310214	0.35312969495644
H	-4.00779326654600	3.47346439766986	0.23325003414911
C	0.54129170777129	3.13937442630489	1.30547427460675
C	-3.95095768761391	-1.86576856157501	0.16865018140324
H	-5.01306370867577	-1.89252534092726	0.03838350724787
C	0.56186711853992	2.58568657184132	2.76142720137016
H	-0.16645091827107	3.16000896782522	3.33381801359552
H	0.18217183928591	1.56888525031597	2.72443752920220
C	-3.67430369226883	0.65426407706913	0.02710533031051
C	-1.87119343101827	3.78921057127992	0.71115976554284
H	-1.81970059781083	4.83908485200510	0.91760125481637
C	-4.43203028254388	0.99450310920832	-1.28440960260588

H	-4.94166885823888	1.93904158912762	-1.10672927051720
C	-3.14166541833300	-2.94817254485284	0.53075641312662
H	-3.47622594211734	-3.95033999592690	0.70874135202659
C	0.81364393043000	4.64781252920192	1.35361934956914
H	0.07274186772387	5.09343699302955	2.01406340380608
H	1.77090725807541	4.80274644018993	1.84245784502610
C	-4.69350210428736	0.77109810222450	1.20072607453785
H	-5.12888112055614	1.76707030088077	1.16930129889127
H	-5.50499114660227	0.06772553984090	1.03233987196868
C	-4.07773506763171	0.52353533981297	2.56045160875949
H	-4.80560994915589	0.67467750521225	3.35347994254610
H	-3.24665494410867	1.20032566720011	2.73545478326392
H	-3.70488190994246	-0.49277371114867	2.63873264716924
C	0.81610422996711	5.38278671036155	0.02332746178954
H	1.07031263345197	6.43017476969622	0.16991623091686
H	-0.15016449796882	5.33896421236628	-0.46252091885926
H	1.53769687443838	4.95879418128244	-0.66381013268262
C	-5.43454784635448	-0.00725430920914	-1.81678570820651
H	-5.92732935877521	0.40322528769127	-2.69490364383601
H	-6.21112837227503	-0.24506859612521	-1.09447106614917
H	-4.95283577307909	-0.93253286092399	-2.10774061084327
C	1.90602799056526	2.58248204500177	3.45884571899192
H	2.61444774037678	1.94514707832025	2.94188330200928
H	1.80144962358072	2.21070676797023	4.47482258842118
H	2.34378110911553	3.57470954251688	3.51970439422740
H	-3.70035636626617	1.19047055724346	-2.05661126484002
N	0.67072247792018	-1.15206773336152	-2.90572797179701
N	1.07514106677449	-1.66171193716781	0.37920059537108
N	1.60470334314610	1.08743400967489	0.32848058778869
C	2.87204432651003	0.71352989369039	-0.07326619016845
C	2.42525397343671	-1.77536380459894	0.09521575761371
C	0.63706455290295	-2.90103483383912	0.79202885529545
C	1.62595825228159	2.45139780276333	0.54109707809619
C	2.81541790419658	-3.07012845018871	0.33776628989665
H	3.80845886579036	-3.45908830265007	0.23640993824495
C	-0.72616196805544	-3.19207420332308	1.33314926478353
C	3.66656928626855	1.83177607128286	-0.12485610336823
H	4.70784391114694	1.85565865355205	-0.38110320473955
C	-0.73912089297972	-2.84684161306008	2.85305089514366
H	-1.72393551394175	-3.11386358253659	3.23601389946211
H	-0.01585791305848	-3.50720515740021	3.33246349846439
C	3.36856044725280	-0.68235800337446	-0.31132804023149
C	1.69297894889908	-3.77692191568491	0.78077975539299
H	1.66921941177306	-4.80696931453257	1.07391475140191
C	3.77399923022665	-0.78634188277353	-1.80587916691401
H	2.89417455166636	-0.56383207615329	-2.39072909643371
C	2.88424423731507	2.92561324364883	0.27188730241088
H	3.22560686860943	3.93287246966493	0.40128673095724
C	-0.98460366505675	-4.70770729933711	1.25600740061915
H	-0.22653554440650	-5.20641451517954	1.85369576091934

H	-1.92333501334442	-4.90760889103039	1.76595976018794
C	4.65685992970695	-0.84453107552515	0.53936828929217
H	5.09172973567595	-1.81811296030683	0.33896556285231
H	5.38310343074605	-0.11506415879517	0.18918569216591
C	4.44730184789359	-0.68453041801409	2.02914963687504
H	4.06125670004018	0.30180066531162	2.26293967921819
H	5.38192562092628	-0.81406186076875	2.56902652932974
H	3.74115680045989	-1.41908098680359	2.40193633759104
C	-1.01954181454087	-5.31167789256711	-0.13387113505625
H	-1.78623581490994	-4.85012904812798	-0.74490357518029
H	-1.22851401597049	-6.37777880211906	-0.08258324672583
H	-0.07116334145428	-5.18289767892915	-0.64308129693963
C	4.35879716586342	-2.09759249594278	-2.29072501589067
H	5.27309776171340	-2.36774042131778	-1.76948807533337
H	4.60410373334778	-2.02204684436971	-3.34759681541763
H	3.65954220139197	-2.91700295115267	-2.16930530247656
C	-0.42248224323464	-1.41408810785943	3.22523383344579
H	0.56603042569172	-1.12571660646690	2.88294149774954
H	-0.44401183982388	-1.28996558701850	4.30468337295234
H	4.48276898859720	0.01725619218062	-1.99834325881285
H	-1.14328797923524	-0.72217366603846	2.80434028988982
C	0.29881762670693	-2.46223599746419	-2.38606330304582
H	-0.20507016950677	-3.03673173648706	-3.16218284197535
H	-0.39819203301947	-2.38943845980924	-1.57018842422604
H	1.17971446988817	-2.99742532984843	-2.04826308866688
C	1.54529179296039	1.71640136517005	-3.10889450045885
H	1.63305323501065	2.73273793214191	-3.48309735007938
H	2.23494155582023	1.10315978985984	-3.67347939039826
C	1.15728901573446	-1.33352948520944	-4.25848766644122
C	0.08451736042353	1.28615424632526	-3.23908191006698
C	-0.73953756871374	2.36864526596743	-2.54681115767974
H	-0.34411742178733	2.62214323341058	-1.57325305875157
H	-1.77773755431747	2.08724868977624	-2.43613184411284
H	-0.69876507409645	3.27456348749851	-3.14373947300213
C	-0.33369482849670	1.33987294217921	-4.71622689632775
H	0.10867821554337	0.58277413063444	-5.34517945307078
H	-0.03011186481711	2.30771466470271	-5.10721633894346
H	-1.40793184516274	1.26198882998704	-4.81202485301525
H	1.86259308419654	-2.15775395224486	-4.23608513801284
H	1.68082134354835	-0.46792787972417	-4.62725009339413
H	0.35362978134866	-1.59322278709758	-4.95178247961890
H	1.87908733165711	1.72781472119698	-2.08144229201913
Cl	-2.00293013706915	-0.58671681088905	-3.02642918679495

113

Coordinates from ORCA-job TS2_cl_dissociation_CREST_optTS

Sn	-0.16374636419140	-0.01019647093445	-0.16134374546409
C	0.11350416112844	-0.01310688170948	-2.44173166222935
N	-1.31398333599121	1.61632383732940	0.54478288402623
N	-1.83593984941639	-1.14193761972883	0.41754120300875

C	-3.14329933591501	-0.75891059502693	0.17231040681894
C	-2.64767856807050	1.74253483922085	0.19215826780347
C	-0.82711248303018	2.88757388245654	0.79393004308413
C	-1.84126624088442	-2.48403073963311	0.74801607423431
C	-2.98176931158368	3.07078537402595	0.23005095551751
H	-3.95550476621940	3.47839158463171	0.04424203789193
C	0.53533294131283	3.12798402281331	1.35956993514688
C	-3.94823063307200	-1.85545540290831	0.34227807926036
H	-5.01380783081568	-1.87258965581533	0.24517579200756
C	0.51403306834302	2.56451121992799	2.81145731115460
H	-0.21908391515626	3.14544510670051	3.37059515984032
H	0.12069334028103	1.55345198388490	2.76326900495860
C	-3.65203177726251	0.64155039891414	-0.00070127936054
C	-1.84321160640369	3.78859708608234	0.62546615249314
H	-1.79195102148642	4.84486496406906	0.79544874617624
C	-4.33403640122237	0.87354170118794	-1.37200572993255
H	-4.73323575303583	1.88598241583974	-1.35338979997618
C	-3.13552712282002	-2.93488624837907	0.70425369109940
H	-3.47337437351855	-3.92470986040159	0.93678707756295
C	0.80616501356764	4.63668603992130	1.42816572316654
H	0.03074791174374	5.07413404917206	2.05316303759554
H	1.73663252242252	4.79138820547527	1.96691155260500
C	-4.71543304994078	0.84962508710305	1.11784439438359
H	-5.16876408454235	1.82718090718070	0.97048466244130
H	-5.50865584634655	0.12000881671162	0.99028744210441
C	-4.15535493754702	0.74749505683300	2.52015354913487
H	-4.92652244338930	0.93624764144021	3.26275351338173
H	-3.35804652973769	1.46797661060088	2.67656612529261
H	-3.75315328522773	-0.24410216298574	2.70465895222049
C	0.87315931351549	5.38408420817608	0.10652360010105
H	1.01315847856455	6.44798397425284	0.28351700186631
H	-0.03300044936360	5.25904986656987	-0.47154314256884
H	1.69398692154751	5.03994095344214	-0.50976426392393
C	-5.42462239592000	-0.08843534502123	-1.79228815743355
H	-5.86085647823574	0.25442997544519	-2.72652781781502
H	-6.23060471765609	-0.16239268279431	-1.06502247679465
H	-5.01906591259881	-1.07449432244843	-1.97668384386274
C	1.84202003917950	2.53889039729939	3.53931392689397
H	2.55231813103575	1.89100582484966	3.03755198736670
H	1.70837670563353	2.16825647195877	4.55208735061559
H	2.29417267014432	3.52381303382964	3.61055403678313
H	-3.57012657752249	0.84386791309637	-2.13791321731760
N	0.53831236496203	-1.14131874507891	-2.92054352722253
N	1.08798966345966	-1.66176205552767	0.37834940582129
N	1.60422796275645	1.09339432268063	0.34528457245419
C	2.87241441845681	0.72042556643481	-0.05699559636067
C	2.41834046733534	-1.77687027196644	0.01202422638579
C	0.65555864336768	-2.91148629246859	0.76601977339688
C	1.63791227336864	2.44498562065926	0.61768960431499
C	2.80191478927553	-3.08607672663352	0.17547979324071

H	3.78326136244958	-3.48173187757705	0.00821885311565
C	-0.68241030980520	-3.19957252859468	1.36703085216180
C	3.68100630858723	1.82955274716387	-0.04466800221012
H	4.72577447996832	1.85281588336162	-0.28560857766072
C	-0.62680283991309	-2.85189330662297	2.88511673325366
H	-1.57406107488382	-3.16869405366600	3.32009328567323
H	0.15463001247824	-3.47167228449911	3.32581494393763
C	3.35874735952395	-0.66822952811656	-0.35858857534758
C	1.69695926603688	-3.79751007306550	0.65525080061649
H	1.67582476983245	-4.83882073883413	0.90414116558820
C	3.74798215802127	-0.70891727822592	-1.86027224644843
H	2.86913193941411	-0.44505906926521	-2.43082832802147
C	2.90662031224424	2.91368557121681	0.39110377028661
H	3.25729284282581	3.90986239420189	0.56990013012321
C	-0.94636560400762	-4.71463204396504	1.30206707058076
H	-0.15961388210220	-5.21525227906410	1.86055972866731
H	-1.85819741727834	-4.91136132513474	1.85877077071170
C	4.65536448974258	-0.87534833518656	0.47030493011383
H	5.07841902883472	-1.84333857055157	0.22386813319389
H	5.38528722927776	-0.13761958465132	0.14648332944347
C	4.45522365314736	-0.78132667074988	1.96703644614343
H	4.07365240953469	0.19475722090675	2.24701731748756
H	5.39220135979641	-0.93883495716723	2.49455908302291
H	3.74878088127908	-1.53014106970883	2.30983124734605
C	-1.05946492392812	-5.31696085552957	-0.08487653840136
H	-1.85523415739303	-4.85097010154662	-0.65363345398786
H	-1.27112619614414	-6.38166430671255	-0.02249372148157
H	-0.13972102118820	-5.19489154672029	-0.64534174951567
C	4.32109082975384	-1.99795379028601	-2.41396888639493
H	5.23866422526835	-2.29132425197457	-1.91299104112439
H	4.55751935618657	-1.87480741341590	-3.46808692125017
H	3.62152218650362	-2.82121374674831	-2.32243186867307
C	-0.37606635915841	-1.40181914670714	3.23994582091238
H	0.57592713657865	-1.05422181381488	2.85098202204726
H	-0.34936800923806	-1.27500267471489	4.31879317789908
H	4.45660544430200	0.10073671883824	-2.02433357549493
H	-1.15935570633309	-0.75632839137901	2.85724947834924
C	0.16779602209954	-2.42814907344622	-2.34125293312253
H	-0.29136019103283	-2.99811218374989	-3.13915127858954
H	-0.58881359566336	-2.31069896360952	-1.58718073064920
H	1.04416352934561	-2.93534937747314	-1.95486916245049
C	1.58424532947706	1.93002641467620	-3.04029409038490
H	1.56680436017536	2.90375358595896	-3.52226051855099
H	2.36198238465802	1.34319659821126	-3.51665305503175
C	1.13317334441652	-1.33631166275119	-4.23390784911099
C	0.19483803655564	1.30738326017990	-3.20731070907517
C	-0.82201520892844	2.26295805092249	-2.58674322332184
H	-0.57957151736049	2.52068891171080	-1.56573282575487
H	-1.81685474572124	1.84111915316840	-2.62432099215985
H	-0.81939794436546	3.18948750154278	-3.15066875072304

C	-0.15231009289648	1.23132610932144	-4.70282542274411
H	0.66875426112765	0.90312636947078	-5.32636761702835
H	-0.39840619565481	2.23768670734333	-5.02697387313088
H	-1.01512354095186	0.59677673047488	-4.86318650130904
H	1.74779351423384	-2.22559768890583	-4.17539329046329
H	1.75650661032197	-0.50410234894603	-4.50763274947847
H	0.34196512216538	-1.48460328776657	-4.96114308113548
H	1.85781388519944	2.07869360073268	-2.00466771751669
Cl	-2.44753031069375	-0.98301420931373	-3.57824302632141

112

Coordinates from ORCA-job tbu_aaac_sn4_cxet_cmp_Compound_1

Sn	10.36002036224385	3.25919522810630	3.83544078792022
C	10.41507012443304	5.57046025577812	4.00921466553498
N	11.91043200290975	2.86959291803835	5.17450453513607
N	9.12242163314051	2.80834835471900	5.47162790320097
C	9.37517820930687	3.27127517368504	6.75191397391561
C	11.91248898996593	3.41366827573270	6.44715162928063
C	13.21241459141489	2.62519571431638	4.80136389335590
C	7.80897167282837	2.39496145253914	5.41394250876455
C	13.21746473781647	3.50467147854309	6.86302521577893
H	13.55160087356154	3.84328959068115	7.82425224152097
C	13.53215791519805	1.83289695223616	3.56754152165791
C	8.21890599567904	3.14102698719310	7.48281515744619
H	8.10046337561859	3.35967472836970	8.52444161756882
C	12.96827131710029	0.39611666777211	3.76535635297908
H	11.88209755269109	0.46540397956325	3.74663346221531
H	13.24440410596847	-0.18120697766719	2.88487982041614
C	10.70650677563662	3.69502773581407	7.31002144390670
C	14.03299367360558	2.99928005387095	5.83474199282019
H	15.09640796723660	2.88024519155627	5.87627631892829
C	10.71486661581479	5.21042985107541	7.64070809833961
H	11.71206446583992	5.45415454310582	7.99998129290204
C	7.23951049142749	2.58356650466484	6.64509402192650
H	6.24356962353805	2.31706414186538	6.93371803986891
C	15.05324760509921	1.74842091613375	3.38728110658527
H	15.47177251006794	1.29504686386707	4.28013812617947
H	15.24985034672744	1.04357442675660	2.58267489702636
C	10.91969751291703	2.90487492211447	8.62828298135605
H	11.81948759133263	3.28368157453166	9.10695022888286
H	10.10048844556494	3.12276021838424	9.30451708797952
C	11.02443682235325	1.40899389153274	8.43108339696549
H	11.87830163646423	1.15412292069810	7.81239494115462
H	10.13310623671539	1.01975868511868	7.94960553362915
H	11.13934749868795	0.89975534193581	9.38258688785962
C	15.78035790146790	3.05222576747211	3.10608332033528
H	15.44745204584934	3.50885400575298	2.18302137676127
H	16.84862352821628	2.87426312649173	3.02255570612677
H	15.62952285215063	3.77698736971238	3.89683930674071
C	9.69144833609828	5.73754488225608	8.62607061520320

H	8.67700594566250	5.59591377763626	8.27141067190313
H	9.84532931934971	6.80215043797212	8.78068990162215
H	9.77023670438272	5.26278047497757	9.59798211725584
C	13.39276575510973	-0.32097708347665	5.02911943899251
H	14.46669033181144	-0.46895145039584	5.07709507329899
H	12.93024156510592	-1.30199146802049	5.07642892648096
H	13.09621915994770	0.22944266935006	5.91545205281820
H	10.60117132491049	5.74688928047783	6.70538956472854
N	9.32996339860469	6.13623818488977	4.43473533721427
N	8.79303429525757	2.72658635737111	2.55074020087362
N	11.58378262222400	2.74412341150787	2.23638306379440
C	11.27855830650080	3.02215015954233	0.91392014373555
C	8.77414673599420	3.04340770994933	1.20561806778420
C	7.51865607303825	2.34226145059742	2.91936694380215
C	12.90341865989194	2.35696041813018	2.30729001932120
C	7.49537138987695	2.87593236799396	0.74343294833232
H	7.16209977265278	3.02233310932459	-0.26428053296858
C	7.24695492261094	1.67113166076867	4.22853184381335
C	12.40515662341179	2.79515164622358	0.16746773903428
H	12.49011031465532	2.89690370658940	-0.89559679095329
C	7.93228367992276	0.27252682908638	4.20922748452719
H	9.00739709869455	0.42935576448809	4.27478242433931
H	7.65234924569867	-0.23671336209126	5.13029130275345
C	9.95558517151764	3.54473036499926	0.42600444984495
C	6.70915855485934	2.42391557773141	1.81807437457858
H	5.67980995249423	2.13267530019692	1.76596301469765
C	9.91576591067908	5.09877204274261	0.48971318972159
H	8.90866829325654	5.40698692634008	0.21568672094448
C	13.42214656946815	2.36800797437731	1.04033351342990
H	14.41180993421649	2.07192415413182	0.75777045604983
C	5.73652903023070	1.47426822233378	4.41221081836649
H	5.37942996015741	0.84150340171176	3.60600731222654
H	5.59023962174654	0.89695988831417	5.32185274958219
C	9.77552034413910	3.13548796016068	-1.04953367828838
H	8.88425261112288	3.63382980860152	-1.42453558460369
H	10.59762560613110	3.55183990288981	-1.62064241323386
C	9.69004480497647	1.64642148359112	-1.31614286037081
H	8.84059975217607	1.19875261805315	-0.81493062308095
H	10.58293132204280	1.13625949863092	-0.97401816305837
H	9.58740637912996	1.45903150451190	-2.38092139094874
C	4.88338792911876	2.73030465930907	4.46120794040104
H	5.16307276243444	3.38095975427299	5.28057781496963
H	3.83732417661554	2.46820656538959	4.59083208042082
H	4.96836262067489	3.30498183101844	3.54768743838459
C	10.92900219695727	5.83942142118064	-0.35830918366932
H	11.93724377343172	5.47815977411945	-0.18728999582426
H	10.91218786101545	6.90279956878180	-0.13740419554331
H	10.71663388117288	5.73394280468744	-1.41632491059444
C	7.64015394935392	-0.59749597491926	3.00538527302594
H	6.58197531788879	-0.81337011111274	2.89862088806420

H	8.15522141882330	-1.54874711359679	3.09797029743337
H	10.03268600385043	5.38574265133782	1.53445871145212
H	7.97198058540560	-0.12531952905961	2.08733351636845
C	8.03107909402079	5.45502341580578	4.46920863487972
H	7.98973493977154	4.66223860673212	3.74199083329286
H	7.27533320688660	6.18744148061675	4.21529018627949
H	7.83809005276512	5.06968054685805	5.46430180642327
C	11.39127981203976	7.64858970187814	2.95577789231163
H	12.32579309523330	8.00706745511293	2.53957365251231
H	10.97070160267917	8.46080887497460	3.53081569202391
C	9.19281512209945	7.48341953304528	4.99113834744077
C	11.69090154303520	6.37996522217545	3.77173237166443
C	12.68098003607276	5.55235970173609	2.95359675545753
H	13.55087640187411	6.16633962506939	2.74991225071863
H	12.27684562687567	5.22479812010951	2.00647838283640
H	13.02515608602038	4.68995659277006	3.50517743497743
C	12.43268544868297	6.72838975714491	5.06838883355278
H	12.72051346609269	5.82899708932831	5.59866834166147
H	11.88109309987172	7.36151138140411	5.75084489053917
H	13.33879326231410	7.25849554717335	4.79170852341695
H	8.58051861284769	7.39285047360009	5.88029229123413
H	8.68382926467670	8.12456234190945	4.28120387648485
H	10.13985585256104	7.90564384429063	5.25944369450339
H	10.72828989048563	7.44019399032733	2.12360079636787

100

Coordinates from ORCA-job h_aaac_sn4_cxet_CREST_cmp_Compound_1

Sn	0.04086095936894	-0.14886186818737	-0.12369457405510
C	0.05604061413290	0.03056527019555	-2.35091688731806
N	-1.19324915217785	1.47679766597114	0.33427948698939
N	-1.64903834901615	-1.33994359956553	0.06279506733475
C	-2.94359083722390	-0.84974379001407	-0.01723706109340
C	-2.40559555299341	1.60075638612774	-0.31530371109287
C	-0.72343401217779	2.73780016000751	0.62779742821800
C	-1.69745085431203	-2.61089376836893	0.59429878245841
C	-2.69035709560557	2.94040940570483	-0.42920167819211
C	0.49235005266765	2.92265121661098	1.48405479912422
C	-3.79103556404390	-1.82204944521868	0.44307944812863
H	-4.85994207607769	-1.76437353507756	0.48229194807614
C	0.20778161167830	2.27040307352651	2.86712720042689
H	0.16519294156186	1.19194174911069	2.72561913401656
H	1.07880497079316	2.45192222647955	3.49349487881618
C	-3.30800331831913	0.44812541275407	-0.67702535002163
C	-1.64102325757724	3.65415552602053	0.18278059990586
C	-3.28754564118624	0.26648273049841	-2.22044446398057
H	-3.44567860906685	1.24500652293354	-2.67327841688405
C	-3.01013614562957	-2.92417572557535	0.83213902816462
H	-3.37502286834195	-3.84224615840435	1.24686521739358
C	0.76569355317650	4.41790819424181	1.69079760748506
H	-0.13154197607992	4.86796152699144	2.10362335620609

H	1.52283059937753	4.51017978076625	2.46624339440432
C	-4.74459182739521	0.83292611708906	-0.26630518197597
H	-5.05291642116868	1.67403873260379	-0.88404308311442
H	-5.40755846350687	0.01820679896422	-0.53544557578384
C	-4.93581330447032	1.17589449784734	1.19710058383519
H	-4.37040701650311	2.05746129197440	1.47653312982493
H	-4.61838514246023	0.36122547878090	1.83737565997113
H	-5.98303087542413	1.37430434574534	1.40472551354054
C	1.20001370288888	5.20809782985140	0.46833761563780
H	2.15929416748224	4.87635025219644	0.09176781577430
H	1.28679142184743	6.26245945098945	0.71413150743921
H	0.48604603877998	5.12000751416812	-0.34212438419020
C	-4.26410187392558	-0.73997355065475	-2.79223865808600
H	-4.07992917822821	-0.88732956886783	-3.85243698641019
H	-5.29238865002742	-0.41138929750285	-2.69030219106296
H	-4.16992782983450	-1.70084424923462	-2.29816057661309
C	-1.05686038580367	2.72402688943199	3.56562596015572
H	-1.04105432562472	3.78505568237088	3.79259663999150
H	-1.17781552766320	2.19444617508648	4.50541097142338
H	-1.93567291919621	2.52984609774598	2.95991107581654
H	-2.27956614164187	-0.03816890573954	-2.49469960718985
N	0.14179658712051	1.08826881689730	-3.06879867197751
N	1.24517935484472	-1.81210548250218	0.12788351162151
N	1.70860294027928	1.00986853998142	0.34910175789667
C	3.01568682336981	0.60018790796190	0.15108266307158
C	2.58445777315110	-1.85972877728451	-0.21001879439218
C	0.79977732270288	-3.10091140092214	0.34831428190962
C	1.72566795125349	2.25525547648994	0.94223667282852
C	2.97054664738863	-3.17361124135894	-0.22194241271230
C	-0.51008164355889	-3.43671533331530	0.99941340351509
C	3.84159825291893	1.59507640656802	0.60446240245491
C	-0.33976441424872	-3.30062753397173	2.53933395523401
H	-1.24313647745318	-3.69805900867058	2.99859504843632
H	0.48578307222697	-3.94323665401696	2.83918450108292
C	3.39982652096526	-0.65322855417068	-0.58347170348000
C	1.85459208876604	-3.95156228353462	0.13537060672624
C	3.25383191512489	-0.45089578699529	-2.12073933233931
H	3.79257953933365	-1.26323122280848	-2.60455534852483
C	3.03275600618029	2.62933980069944	1.11004422508596
C	-0.83355689518038	-4.91723979375365	0.72720509315284
H	-0.02529178311900	-5.52032510926078	1.13141001396301
H	-1.70805082117332	-5.18067883090417	1.31448781645192
C	4.88642076436979	-0.95620711864758	-0.31284449541416
H	5.16500855843473	-1.79876699127962	-0.94020945187663
H	5.47496873591797	-0.11910498136635	-0.67826784592851
C	5.26207921606744	-1.25711851083552	1.12497681219590
H	4.73084614355901	-2.12539940438952	1.49482869858149
H	5.03340936486722	-0.42836107713213	1.78292561534409
H	6.32653029000854	-1.45959143306150	1.19977272943532
C	-1.07494287058629	-5.26788849571988	-0.72574603661578

H	-0.20393338948876	-5.05108409966978	-1.33420391407925
H	-1.91201051379717	-4.70421382798562	-1.12432571274616
H	-1.30352416701075	-6.32386422195443	-0.83435700641407
C	3.70278443109939	0.88494584388957	-2.67104215434359
H	3.11679825582735	1.70285890241717	-2.26488502960571
H	3.61853569442946	0.90216787174608	-3.75510231116102
H	4.73867932738922	1.09333116999019	-2.42490827311559
C	-0.10691620342380	-1.89456956993422	3.04957601125915
H	-0.04968127570779	-1.88364583257177	4.13336735679198
H	-0.92476660412171	-1.23394512228551	2.77005508101783
H	2.21288510113455	-0.61657336549195	-2.38819019163401
H	0.82341206448921	-1.47681234563111	2.67764193390501
C	0.19572838321714	2.42666736949796	-2.48502745174104
H	-0.81714526986522	2.76466921356755	-2.28555045008243
H	0.68115519294953	3.09331855861481	-3.18333539687114
H	0.74735983444641	2.40703962759750	-1.55788923483626
C	0.08256806339022	1.06438036151495	-4.52336864735379
H	-0.01616367325932	0.04697445961679	-4.87015317496906
H	0.98535559832215	1.50939961217232	-4.92466097017478
H	-0.76964210584703	1.64981472506388	-4.85108481067136
H	-3.59175504372484	3.36266244613388	-0.82873943911934
H	-1.59810532698158	4.71577192317108	0.31787759266118
H	3.37577487058137	3.53623074325131	1.56619116703251
H	4.91228126814964	1.59058600543765	0.57613243426306
H	3.95256838921932	-3.54360000669932	-0.43904770072943
H	1.84436707692102	-5.01576634243012	0.25648161587030
H	-0.03248363722164	-0.88147852819963	-2.93078942227435

109

Coordinates from ORCA-job ipr_aaac_sn4_cxet_CREST_cmp_Compound_1

Sn	-0.05818084755798	-0.04617187732596	-0.04524129514103
C	-0.12788066491035	0.19173404870063	2.17701103920560
N	1.27026788091313	1.54558297102751	-0.34906629270443
N	1.60156222774379	-1.26325192503499	-0.35665700995594
C	2.82022797964006	-1.00029632424878	0.24117387313920
C	2.56048436492683	1.54929273110538	0.14580529432921
C	0.90756891488421	2.84207971463304	-0.63116274030494
C	1.53670108451742	-2.60696927081865	-0.65459976097992
C	3.00081537659995	2.84995812798775	0.16277928793934
H	3.96975738485519	3.18582704207134	0.47642948752919
C	-0.39213076661013	3.14411120591799	-1.32417197981451
C	3.51530256354405	-2.18485871662727	0.30978825527558
H	4.51531609982143	-2.31232924924387	0.67205305640844
C	-0.34297464213959	2.52407141272453	-2.74289880932530
H	-0.24548101135799	1.44717939758502	-2.64496455753745
H	-1.30495034471274	2.68295557927623	-3.22335338488513
C	3.35452366985924	0.35626130996635	0.62038691052178
C	1.96264155856689	3.66340308526410	-0.32895263809766
H	2.00438395842531	4.72426833008133	-0.46925678194144
C	3.48545189591346	0.49963714447164	2.16356989411646

H	3.88665197893228	1.49226578876203	2.35270142288752
C	2.71265595976329	-3.19003450196551	-0.25285225045880
H	2.99246869222767	-4.21584414246118	-0.38163454030262
C	-0.57818416979389	4.66243968072872	-1.40867944325074
H	-0.72175253913748	5.03934710440050	-0.39898593603766
H	0.34834430166222	5.10527791518081	-1.75720064282861
C	4.76923432392567	0.47469883009526	0.00307801165761
H	5.21722512312343	1.40075393178118	0.35447377174200
H	5.38882105502543	-0.32537875227443	0.39390720135810
C	4.78320725871469	0.43139615957068	-1.50926852520419
H	4.19973500556086	1.24430066911565	-1.92816792322842
H	4.36957088939463	-0.50360372827089	-1.87343389388398
H	5.79667157192015	0.51687697065202	-1.88842503506681
C	-1.70399722450853	5.13201326299964	-2.31096894279035
H	-1.46985863081269	4.97056086048268	-3.35825646629341
H	-1.87185976796623	6.19676925112598	-2.18264667344784
H	-2.63722833260414	4.62172975423601	-2.10291153861717
C	4.31328032136980	-0.52301052995946	2.91616719061234
H	4.34727528898405	-0.26346432184954	3.97089777512326
H	5.33957785318236	-0.56062443885932	2.56674986007115
H	3.90440501138523	-1.52361659183346	2.83240363430955
C	0.78302130148104	3.03691018605428	-3.61430978337674
H	0.69749650579657	4.10156532513926	-3.80964356958820
H	0.78204621487090	2.53049372123639	-4.57424078280450
H	1.74779523354875	2.86722752572308	-3.14774384539398
H	2.48334542630769	0.51407184536936	2.58132147705768
N	0.22903669334863	-0.75973397305111	2.97362235253770
N	-1.29805722840787	-1.66110243645047	-0.49609546213218
N	-1.69206300776241	1.16345788332432	-0.54671612427680
C	-2.84143947300345	0.86915947687447	0.16524711553723
C	-2.67754446771260	-1.54082403299171	-0.53929569868328
C	-0.94114884831586	-2.78876718456138	-1.20422471530318
C	-1.54204253434655	2.53226384642909	-0.57569378425785
C	-3.17453980094383	-2.60096836426376	-1.24813255729991
H	-4.20937184489016	-2.81269251559809	-1.42773393212631
C	0.46569504303430	-3.21188889543983	-1.51267791382372
C	-3.40674941387708	2.05007847028863	0.57598151024735
H	-4.34370742003684	2.15739114257727	1.08835498579461
C	0.76537302962988	-2.85748111854259	-2.99688457718955
H	1.77120830567906	-3.20610762226659	-3.22460847325659
H	0.07682718121850	-3.43944997347402	-3.60672260969760
C	-3.43645020539497	-0.51356802718589	0.24540263837570
C	-2.08375746835717	-3.38316568958374	-1.67053009079177
H	-2.13726634040416	-4.28360088544408	-2.24987766396311
C	-3.48457995341564	-0.94261915960929	1.73352632337639
H	-2.45629062669408	-0.98895660716991	2.08888919535798
C	-2.59132707902133	3.10079729443495	0.10366001484181
H	-2.78294768476832	4.14954327289319	0.21503959668180
C	0.54288597579840	-4.74515781343195	-1.40753780770618
H	-0.13966776545378	-5.15990476077882	-2.14320330466589

H	1.53399683516585	-5.05919349709947	-1.72487422118388
C	-4.87975173675721	-0.42145776162548	-0.29048031543079
H	-5.33945111641742	-1.40353312073339	-0.24332543671637
H	-5.44216286565771	0.20403106334021	0.39987444352854
C	-5.00274116920721	0.13330485542958	-1.69486091272226
H	-4.61054539596669	1.14261392838984	-1.75351599535134
H	-6.04336321185798	0.16323333140039	-2.00328640900668
H	-4.46068796759951	-0.47537194471526	-2.40919015559521
C	0.22107972147500	-5.32364528086437	-0.04507021957463
H	-0.78897345362014	-5.06616165036545	0.25704070081913
H	0.90181659239314	-4.95748914238923	0.71606955529434
H	0.29498975552371	-6.40683796261833	-0.05967044181090
C	-4.16525351479436	-2.26331574547492	2.02556625281717
H	-5.22789484974975	-2.22703557644277	1.81163425196077
H	-4.05949075197066	-2.52208830647484	3.07523733780550
H	-3.73594267352141	-3.06631425340218	1.43603408563957
C	0.62838240920367	-1.39531848807875	-3.36374519994623
H	1.35992683663764	-0.77621624305826	-2.85556332440390
H	-0.36726497451129	-1.02522691324028	-3.12913760313228
H	-3.96358762091669	-0.14309871459744	2.29617506089081
H	0.77374107126259	-1.25307256803639	-4.42990232652036
C	0.53097155816033	-2.10795996773833	2.48619021330065
H	1.58726176732615	-2.18966375549740	2.24799290010835
H	-0.05466701587229	-2.33060791429507	1.60820549660313
H	0.27735457497676	-2.81360700363430	3.26601254213345
C	-1.58788727198695	1.56567965843479	3.77303175783524
H	-2.27991988978056	0.73502077271378	3.70768437236207
H	-2.17052437043491	2.47487769411066	3.67877880114221
C	0.45308405246902	-0.62371280595694	4.40947921515314
C	-0.55193654236493	1.55330343190225	2.64678820245469
C	0.61730234893149	2.49229030857857	2.94792187168218
H	1.28235845996845	2.59775469559302	2.10233880032628
H	1.20068503086692	2.17033452504693	3.80529547633927
H	0.20817266072500	3.47092482446632	3.17506980365029
H	-0.35416735123141	-1.09584579888984	4.95840337438225
H	0.53418551526963	0.40916646435773	4.69068758565419
H	1.38013254429731	-1.13202004575754	4.64621620318809
H	-1.14316583236012	1.56868431870921	4.76191268474202
H	-1.04526027555210	1.98995739964117	1.78548755478258

110

Coordinates from ORCA-job ph_aaac_sn4_cxet_CREST_cmp_Compound_1

Sn	0.20107590211293	0.07207221709861	0.16904306505612
C	-0.40667333507837	-0.00380734423032	-1.99790672818048
N	0.99534348623889	1.98966218701381	0.34781066816033
N	-1.52491743618704	0.86702789441096	1.02630186668325
C	-2.02761725833694	1.93356778669427	0.29921136030247
C	0.19651862522586	3.11293128366326	0.47087192946441
C	2.27222470467632	2.31559309483170	0.75174364128404
C	-2.56927082784304	0.02035137904480	1.32509900535501

C	0.97936513580509	4.13926851210650	0.92974955073465
C	3.40606340074227	1.34145499604488	0.91189070765205
C	-3.37903430314533	1.75108017057134	0.15132078321887
H	-4.06432806173011	2.43852232234911	-0.30684769868900
C	3.54064432695354	0.99947088256162	2.42296006741347
H	4.38275195265293	0.31887611815206	2.53611394253895
H	3.80214132325919	1.92427348723724	2.93401583214419
C	-1.22840259740154	3.17702296694295	0.00237329349908
C	2.28205111471086	3.63844798344506	1.10988338756562
C	-1.26134266196195	3.42383180234681	-1.52623841786154
H	-0.72165008000580	2.60377464298959	-1.99620234338417
C	-3.72228656298922	0.54900243383534	0.80333992836991
H	-4.70972303777003	0.14329544241621	0.90062782511169
C	4.71291297905639	2.04789560170409	0.50981825573312
H	4.84655521277441	2.89313708438759	1.17791677304828
H	5.54157043438381	1.37764931132216	0.72307784644034
C	-1.93932621399679	4.34682188377476	0.71509019305573
H	-1.39075628717631	5.26519425443360	0.53143001589677
H	-2.90968956858538	4.47810108053445	0.23996839672315
C	-2.12360922203597	4.15139431409892	2.20576906737218
H	-2.72075873051145	3.26999879467994	2.41351391907070
H	-2.62806973777643	5.00690675832807	2.64433988577804
H	-1.16951564391526	4.03238945721239	2.70674727660881
C	4.78250163726736	2.52784762357539	-0.92517262015617
H	3.96902996175249	3.21242719516329	-1.14287852437416
H	4.72599487325685	1.70246648296819	-1.62670715024754
H	5.71439715208723	3.05343619610427	-1.11060522654386
C	-0.67779323189032	4.73620822972427	-2.00586699103037
H	0.33612309103542	4.87327455434632	-1.64504422901840
H	-1.26500865054477	5.58558033427500	-1.67420746193461
H	-0.65466433633902	4.76827357718752	-3.09154471050275
C	2.30754652520193	0.41088898788628	3.07392173943177
H	1.45957781211391	1.08567199535836	2.98483926622443
H	2.47316143446457	0.24956861893622	4.13438690574554
H	2.04064733564393	-0.54906833061202	2.64375730260907
H	-2.29459926882114	3.33271899198939	-1.85675594981696
N	0.43369454344418	0.24973273553654	-2.95458106447244
N	-0.33453513372216	-1.86382204646701	0.75730439497398
N	2.13257681100221	-0.68971233987040	0.08670792951352
C	2.41386825326769	-1.90154268906457	-0.51514226575878
C	0.18493785539098	-2.98177032220708	0.13036457160547
C	-1.52883023126834	-2.21055825432925	1.34703085835135
C	3.28585740750363	0.05906392476809	0.14084652869122
C	-0.68338309155913	-4.02367349383682	0.34124037066764
C	-2.31291022949476	-1.21077886952584	2.14867579767572
C	3.75041547484870	-1.90476636759003	-0.83781216523189
C	-1.48150223855534	-0.80989081456871	3.39081370377307
H	-0.56270328198494	-0.34099048311800	3.05376401767228
H	-2.01858071987287	-0.03369289272133	3.92954273590845
C	1.45017312257599	-3.04708393990772	-0.69154448583451

C	-1.75884372529653	-3.54034558521975	1.11376949973559
C	1.00224108235863	-3.19443548120811	-2.17503464359511
H	0.35380563901041	-4.06610476830968	-2.22151032810048
C	4.29746395832460	-0.67885285269137	-0.42283789032494
C	-3.64180602517822	-1.84366563009488	2.57290451077323
H	-4.23221745151826	-2.01782815651500	1.67623976019655
H	-3.43618971494974	-2.82568766467254	2.98576617658798
C	2.19429603113230	-4.34376161012779	-0.29435716092979
H	1.54516832626966	-5.18592546324591	-0.52005475314937
H	3.06132593288536	-4.45802063145776	-0.93632033611181
C	2.62612508220974	-4.39713745899416	1.15471148473910
H	3.30426962091678	-3.58344282070337	1.38921276015043
H	3.13919565209239	-5.32942235294339	1.36946040279865
H	1.77259994928511	-4.32524594183856	1.82017851147654
C	-4.44763995560553	-1.05247073565698	3.58524366524867
H	-5.42714391820595	-1.50039439282355	3.72106952038365
H	-4.59276362489467	-0.02319631346047	3.27859368097759
H	-3.96614568639187	-1.03874168124680	4.55774532149909
C	2.08186897531450	-3.31671616261093	-3.23094648404676
H	2.69816929254716	-4.19738850115952	-3.08430227838565
H	2.74383011598978	-2.45786929588234	-3.24148158478460
H	1.63007704073114	-3.40719219548558	-4.21512242470125
C	-1.13284906555801	-1.95859141570466	4.31219015067809
H	-2.01464877439771	-2.42356502066652	4.74237497737883
H	-0.51589833656713	-1.61090371641933	5.13468512507494
H	0.36075793483947	-2.35179910331057	-2.41610161154160
H	-0.58120713817098	-2.73005630384422	3.78483775875872
C	1.80028994281156	0.70634976359702	-2.70007900635031
H	2.13536766308425	1.26665385600237	-3.56226256689384
H	2.45266348721190	-0.14784002307774	-2.54878293323794
H	1.83232756787389	1.34596798538224	-1.83304830164354
C	0.18848367588919	-0.02433161128254	-4.36818172499614
H	1.05199996506754	-0.55736529780334	-4.74890937438932
H	0.08357896281566	0.90325750890918	-4.91950195637570
H	-0.69767174726998	-0.62359904426360	-4.49237790404731
H	0.66321327274430	5.14852564928112	1.10178706751492
H	3.12831266506669	4.19198058909209	1.46548431644936
H	5.32721390262806	-0.39439190057655	-0.50024967432445
H	4.29389125812039	-2.71610201097661	-1.27890502047507
H	-0.55394623558730	-5.03348654724407	0.00459641304179
H	-2.58628706582381	-4.11657705263978	1.47489162706715
C	-1.78896084815829	-0.34026904590274	-2.30627868117801
C	-2.54959596568467	0.48607076524797	-3.13931407685041
C	-2.39406495231707	-1.44531163841472	-1.71143176040731
C	-3.88036605771716	0.21359758617847	-3.36532704647371
C	-3.72069326985451	-1.73159470618129	-1.97377086798553
C	-4.46910066603086	-0.90269439933711	-2.78741935726602
H	-2.10329205630040	1.36664950400622	-3.56721798005937
H	-4.46160693490905	0.87463325202022	-3.98483474593989
H	-5.50897169430615	-1.11607422874867	-2.96668727827325

H	-1.82936991049682	-2.10552207001473	-1.08352926545703
H	-4.16632939457962	-2.59817704996187	-1.51711905602247

108

Coordinates from ORCA-job nme2_aaac_sn4_cxet_CREST_cmp_Compound_1

Sn	-0.00006189112231	-0.00006599997882	-0.00299732547437
C	-0.00008491992196	0.00010424392274	-2.28684939752231
N	1.67437908779339	-1.15284252469152	0.43984126628211
N	1.22602266696517	1.63352034901173	0.42952729681975
C	2.60131160485713	1.63394487190062	0.27201337101353
C	2.89245102152308	-0.84586791549806	-0.13510572436053
C	1.63613515703437	-2.50576658452054	0.69574476873287
C	0.85093565388109	2.82920920793483	1.00364227612167
C	3.60833791816583	-2.01100253183898	-0.25029100559438
H	4.61674198242316	-2.10093590105944	-0.60403725646048
C	0.53501858784091	-3.09830251389303	1.52130516315490
C	3.07687544243710	2.83260600602130	0.73812006708357
H	4.10059219327261	3.14858058334988	0.74388532016506
C	0.60428227577373	-2.45143128058223	2.93579179864304
H	0.27964259879941	-1.41591240334516	2.84304880193179
H	-0.14650710343496	-2.94284708889503	3.55137086391358
C	3.37339689522755	0.55446241367286	-0.43430112077830
N	0.43120601874926	-1.05853543698789	-2.96337793642740
C	2.82470627844920	-3.05198390334443	0.28977958468643
H	3.13030808298495	-4.07215176921437	0.40607798481005
C	3.30695054255869	0.78203861021271	-1.97019438253930
H	3.78590647352290	-0.07104563923560	-2.44927350942083
C	1.97967162351819	3.57989760286497	1.20332462735253
H	2.02048850795899	4.55207604091024	1.65241048359630
C	0.74663191874991	-4.61103766985696	1.65830662506833
H	1.74014720453851	-4.77540388226505	2.06342503061370
H	0.05813384019975	-4.97765001308712	2.41601790395104
C	4.85390767544304	0.64015548344852	-0.00785431485567
H	5.41617847298236	-0.04570662403514	-0.63791667067224
H	5.22627614933072	1.62903107699366	-0.25171697109313
C	5.13168585619954	0.34508420019872	1.45163488857254
H	6.19455377398253	0.42590511246021	1.65909726071525
H	4.81609947578737	-0.65643315084218	1.71998731879210
H	4.61274942936227	1.04195347306744	2.09935743633269
C	0.58154745165744	-5.42718498907598	0.38869286769149
H	0.85414073364578	-6.46364211390340	0.56472466248386
H	1.21283838846217	-5.05339801934503	-0.40940534623732
H	-0.44050776854304	-5.40854820379432	0.03091734522765
C	3.90141847424411	2.07517728929380	-2.49004514517696
H	3.68182931776627	2.19435369465058	-3.54760145893675
H	4.98029107271521	2.10063912434835	-2.38475090031141
H	3.49570961481299	2.93311722974693	-1.96458988201731
C	1.95787031916562	-2.48233953133393	3.61368374109261
H	2.32081522482777	-3.49505899729595	3.75691844452735
H	1.89885129461031	-2.01916220977708	4.59383119764584

H	2.70143287547099	-1.94432189189079	3.03574907874889
H	2.26201571423911	0.74547997515740	-2.26006080780243
N	-0.43130182136684	1.05893212337392	-2.96314017936728
N	-1.67444649903509	1.15268231999381	0.44010621720850
N	-1.22610957012130	-1.63370010772550	0.42946649412243
C	-2.60142054546035	-1.63412858719672	0.27212940755627
C	-2.89256903228341	0.84574210653607	-0.13476305760544
C	-1.63615600751962	2.50559137111187	0.69604506453975
C	-0.85093686182748	-2.82947193165243	1.00338639621353
C	-3.60844158190540	2.01089923656424	-0.24985414330496
H	-4.61688137177803	2.10086717914189	-0.60348825949908
C	-0.53500208597803	3.09807361682400	1.52161787807122
C	-3.07690573561254	-2.83286848960044	0.73810493180290
H	-4.10061521721265	-3.14886726282969	0.74393478246855
C	-0.60425323228369	2.45108858906935	2.93606226052606
H	-0.27964495963955	1.41556871149745	2.84313115176515
H	0.14657398715267	2.94238017603084	3.55168789218885
C	-3.37365567824200	-0.55456156190754	-0.43388694841539
C	-2.82474549488071	3.05184979887173	0.29018403907183
H	-3.13032647614467	4.07201690964161	0.40653947782053
C	-3.30772680769188	-0.78205933124930	-1.96980889305143
H	-3.78675136196738	0.07109808117745	-2.44868695445132
C	-1.97963766406140	-3.58021871146079	1.20305484334961
H	-2.02039198240962	-4.55246453878531	1.65199749198267
C	-0.74652210975925	4.61078726476840	1.65872058807664
H	-1.74005829682203	4.77521739366509	2.06376821092969
H	-0.05806269252880	4.97724690438918	2.41654304546160
C	-4.85403021792120	-0.64021006474763	-0.00696086313485
H	-5.41647834412294	0.04575249631686	-0.63675324759856
H	-5.22654103852062	-1.62904049495988	-0.25079635145148
C	-5.13128623500032	-0.34527865253230	1.45265607963768
H	-4.61242926386850	-1.04244551205058	2.10012090495137
H	-6.19412701960609	-0.42573100737629	1.66040040373692
H	-4.81525128837352	0.65608156891689	1.72107677002100
C	-0.58122588272050	5.42703342744829	0.38919563025713
H	-0.85400404605381	6.46344335132993	0.56523855195127
H	-1.21232241025931	5.05324770216677	-0.40905333057174
H	0.44090691662806	5.40855173516664	0.03163946093006
C	-3.90249636545439	-2.07510538890369	-2.48954560825353
H	-3.68326676310134	-2.19424480064985	-3.54718037099738
H	-4.98133769296250	-2.10046316059133	-2.38389965317385
H	-3.49670575222551	-2.93311598512244	-1.96426835503819
C	-1.95783123996043	2.48194407296172	3.61395613465441
H	-1.89885134518152	2.01878400545627	4.59411218907737
H	-2.70139663803205	1.94396457320764	3.03599181968525
H	-2.26288360433503	-0.74560173897591	-2.25999035314712
H	-2.32078166992349	3.49466575726242	3.75721706776413
C	0.62028862710643	-2.35365289219822	-2.32976576079276
H	-0.05497410203888	-2.48028402734088	-1.49947439176053
H	1.64655851367134	-2.47265995819443	-1.99653715495366

H	0.39098112785141	-3.12084986270942	-3.06037749783069
C	-0.62032708961201	2.35389541672851	-2.32918770818181
H	0.05486349605324	2.48023099169030	-1.49878557066838
H	-1.64661844435972	2.47290665845899	-1.99602629153458
H	-0.39086973044203	3.12127972914068	-3.05955563227977
C	1.05901455586780	-0.96842118826971	-4.27127277299813
H	0.44256308707314	-1.38471740012451	-5.06183625609195
H	1.98266792807272	-1.53478782119502	-4.22416639076105
C	-1.05901984856462	0.96920977636628	-4.27110327614561
H	-1.98265002898075	1.53560720675898	-4.22390736372196
H	-1.30277702373378	-0.05608675668946	-4.50348669838844
H	-0.44248462620806	1.38569518917903	-5.06150297690777
H	1.30274587710959	0.05695065874670	-4.50335290383304

37

Coordinates from ORCA-job sn4_pyrr4_cmp_Compound_1

Sn	-0.26785531275108	-0.04660152887226	1.03253140219899
N	-1.03158298776602	-1.78843796335672	1.69844777519113
C	-0.37981879398547	-2.67528953132462	2.52898288316123
C	-1.27881054864248	-3.61046678120418	2.95445998175211
C	-2.53085454426181	-3.28647977461084	2.37952323810288
C	-2.35443092319596	-2.16424629569289	1.62260864086891
H	0.67007291154059	-2.57531973691205	2.72150290880678
H	-1.06160632833026	-4.44203121287815	3.59482862974783
H	-3.45038763184991	-3.82406652795287	2.49822135034502
H	-3.04790013556369	-1.61114971003442	1.02013291274017
N	1.65212566680367	-0.43925286924212	0.56554139114572
C	2.68986261467400	0.46410814685005	0.63270626533550
C	3.78883559342464	-0.09336466023218	0.04560549440344
C	3.41743550307079	-1.38031847643615	-0.41168115588245
C	2.10413283273012	-1.56579145884565	-0.08787191074482
H	2.55620521138403	1.41442574601053	1.11098071442205
H	4.75488793577936	0.36357041886046	-0.03513814291567
H	4.04578769120037	-2.09285400105400	-0.90794693120566
H	1.45770218583839	-2.40709830890849	-0.24149893722313
N	-0.39860186289481	1.39918619785290	2.43021674084598
C	-0.32099962103615	2.75311398047503	2.18180941149083
C	-0.22410222606642	3.40718457309328	3.37620602201746
C	-0.22976711214402	2.42714907222650	4.39747380680190
C	-0.32984814639594	1.20763391176379	3.79237231738881
H	-0.36743308040383	3.12850322272634	1.17875088613022
H	-0.16998858396062	4.46982768158926	3.50522525145946
H	-0.18032564876385	2.59969780648137	5.45408556818189
H	-0.37782438883135	0.22061522493783	4.20855787429381
N	-1.29115527090702	0.65132546809075	-0.55654662270893
C	-1.01338513963386	0.37336246886416	-1.87657607737406
C	-2.03896287761356	0.84498415588739	-2.64422466368245
C	-2.99040988474927	1.42356412458691	-1.77066119727874
C	-2.51328990783125	1.28654541693228	-0.49882292418298
H	-0.10017710104105	-0.11692210965290	-2.15121805233852

H	-2.09492122617055	0.79411619754154	-3.71329041092855
H	-3.91202215313853	1.89703614549325	-2.04494018578353
H	-2.92282270851713	1.60230498694685	0.44030874541736

60

Coordinates from ORCA-job tbu_aaac_sn4_pyrr4_cmp_Compound_1

Sn	10.25396415278644	3.45337931289542	3.74107018083517
C	10.09190454743431	5.82267156703811	4.04425156438202
N	12.23185300479560	3.27512602930287	4.33458494566282
N	9.21925848060469	3.09993169213217	5.49919240555676
C	9.33933451517144	3.80837073949524	6.66606431473688
C	12.85295560597309	3.83024043964229	5.42073984106829
C	13.20449483568773	2.80517323217220	3.49004159899474
C	8.07981198600906	2.34516354056455	5.58850780917664
C	14.21004859740208	3.70509082464196	5.27488842048907
C	8.29473079868689	3.49477939271779	7.49581235440019
H	8.14551957662088	3.86488656886677	8.49131059289825
C	14.43326537170825	3.05582983347292	4.03993022262150
C	7.48888377920939	2.56095915900360	6.80497809705393
H	6.59809668651471	2.08559304665037	7.16531351698731
N	8.95105282144038	6.25746755209803	4.47908101280089
N	9.11405927050784	3.82354930771084	2.00329810251807
N	10.28283145730490	1.45404953238929	3.14002895093021
C	10.52479582404072	1.01463579566418	1.85912965830790
C	8.96683016391860	5.01400968751766	1.34249848690444
C	7.98324687711728	3.08072914989609	1.75717177549932
C	10.60242665932464	0.42779444461976	3.99036875506636
C	7.77377217220326	5.02208184453016	0.66807475164229
C	10.95736781376844	-0.28354195309313	1.90071436681520
C	7.14303522552323	3.78760687878470	0.93841674417239
C	11.00508713268625	-0.65934442623038	3.26258600795710
C	7.71956325644526	5.45803153731101	4.47544127927804
H	7.77649773108997	4.64878028640552	3.77152806963719
H	6.92210071906647	6.11617013838820	4.15377218721869
H	7.50649590209891	5.09023070151936	5.47158103547560
C	10.74637281102643	8.03563421458452	2.98738154726699
H	11.59889461221745	8.49205843375607	2.49828388556916
H	10.30121377931239	8.79769545192585	3.60952259615592
C	8.65128178497495	7.58844966270965	5.01505193795396
C	11.23540847004023	6.79402350706608	3.75664724296289
C	12.25702589529275	6.10117858442170	2.84808486388687
H	12.98526141242443	6.83265745706764	2.51669776935954
H	11.79224086331695	5.68809717811220	1.95724130348031
H	12.79810768734281	5.31757281294639	3.35403225660910
C	11.97875262545189	7.20811249325864	5.03099485503539
H	12.43726297873750	6.34991523991084	5.50314377683512
H	11.35415945415027	7.70900552115871	5.76043690753725
H	12.77398459329793	7.89361404482105	4.75388064748417
H	8.00397241868524	7.44244445436015	5.87087228003289
H	8.12076474150504	8.17775143004779	4.27656846613089

H	9.53734539809326	8.10217628549440	5.33119763921544
H	10.03132644717116	7.77074840478002	2.21552275452159
H	7.79414009446646	1.69615341448164	4.78484544928663
H	10.16765899657646	4.46963155110546	6.82771341896452
H	7.41767498326205	5.80322238626862	0.02473181254836
H	9.74445256657390	5.74991589644309	1.35042656424649
H	6.19659058089522	3.45037022773797	0.56392095244651
H	7.88182881395260	2.09748859073541	2.16856772155544
H	11.19605114114973	-0.89526089870863	1.05255253548980
H	10.34215285390393	1.65461006729175	1.01986033094671
H	11.28286410880777	-1.61596723749775	3.66012248631271
H	10.51553497897746	0.55314921668961	5.05143397063451
H	12.93754538633603	2.29744682379983	2.58349585214175
H	15.37967532130114	2.77550076294765	3.62148893068077
H	12.28518506572952	4.21084343736730	6.24553950700147
H	14.95080416988514	4.00041472880835	5.99220268861920

89

Coordinates from ORCA-job sn4_cxet_CREST_cmp_Compound_1

N	0.00771735798878	2.00597952526661	-0.18361670846069
C	-1.00823616173050	2.72064860682447	-0.79014254595492
C	-0.59775135561580	4.02286337179243	-0.86485207150152
C	0.68849551716468	4.11033117380519	-0.27902176823393
C	1.05384051009945	2.85646691660698	0.12277156481056
H	-1.14930233135540	4.83494988359607	-1.29431549651899
H	1.25852305792582	5.00754944985663	-0.14527882868273
C	-2.18264829678771	2.03835570996375	-1.44024313774242
C	-3.27407532139980	3.07454174593996	-1.73375835943838
H	-4.06419966574885	2.59057527809227	-2.29912823675034
H	-2.84784439850398	3.81722554129681	-2.40418317059401
C	-3.87451741047274	3.76404020550832	-0.52299168851166
H	-3.12167855470088	4.28251223111294	0.05817755355018
H	-4.36405169976205	3.05756444203406	0.13619069013569
H	-4.61532922010028	4.49392920473442	-0.83474432967056
C	-1.65879369953670	1.47177175501411	-2.79482193124212
H	-0.76689250553262	0.87159512226408	-2.59042004122226
H	-1.30054940383474	2.31549352589320	-3.38089153058037
C	-2.62853984457101	0.63261111798649	-3.59745531996313
H	-2.95101104766026	-0.24318340266327	-3.04591359702145
H	-2.15995232983411	0.29842704723734	-4.51777380641594
H	-3.51667439438293	1.19090486273770	-3.87351123467851
C	-2.75684551820199	0.90121753859912	-0.64348719344438
C	-4.04898176083041	0.46908019870133	-0.53175138218941
C	-4.03622815721028	-0.78019164872732	0.13351173277740
C	-2.73489937555088	-1.10318370578005	0.39950975120977
N	-1.95007326220141	-0.06895523934887	-0.07797280857334
H	-4.91727324485981	0.97760739740518	-0.89990329065959
H	-4.89762862370772	-1.35377456981458	0.41087054021949
C	-2.16844509211674	-2.15211783890543	1.31446316815217
C	-1.82211280724406	-1.46808050186679	2.67328305064578

H	-1.50971402560600	-2.25296446317401	3.35875822220709
H	-0.93072731225403	-0.85073880835474	2.52685466289497
C	-2.90571150505295	-0.61134075902257	3.29001567804639
H	-2.57347454307227	-0.21359373959499	4.24378614730849
H	-3.81253152379180	-1.17726222759628	3.47490268032736
H	-3.16741765417281	0.22380893593171	2.65019295308943
C	-3.21467381482142	-3.24213986973151	1.57247783247221
H	-2.82022981983830	-3.90235531148599	2.34157950007789
H	-4.09091570453962	-2.77510239998401	2.01101665253984
C	-3.63156104289442	-4.05866221523206	0.36354705296809
H	-4.39683803389873	-4.77699356760745	0.64108462367021
H	-2.79713657973777	-4.60812005947740	-0.05468276592135
H	-4.03525112060954	-3.43244883014450	-0.42300572234007
C	2.17685806695850	2.40544260366181	1.01162349431363
C	1.58748427915328	2.14197578016567	2.43146002802389
H	2.42297654238457	1.92477282438160	3.09320052620179
H	1.00835641771050	1.21359942493534	2.39563806765796
C	3.23495070056085	3.50932043842638	1.12191732399695
H	3.94337089293237	3.20977397361655	1.89064986285833
H	2.75067482316931	4.40427458417405	1.49995652472602
C	3.97910816990100	3.83861057642470	-0.15860665083264
H	4.66749027938462	4.66165122279417	0.00658136607896
H	3.30055181507982	4.12838731526956	-0.95187163890518
H	4.55211185903554	2.99169668468781	-0.51583697472282
C	0.71150884886303	3.23465693647027	3.00455301693923
H	1.23709804426960	4.18137306122131	3.06952766001258
H	0.39032663082908	2.97290939884766	4.00784943130802
H	-0.17364691867369	3.39355651765751	2.39899281823244
C	2.83262492609557	1.11977646236664	0.58336959023559
N	2.11407968089717	0.07184916298381	0.03393376674257
C	2.93230322151244	-1.03645316557955	-0.07872255247290
C	4.16645675323875	-0.68445531229498	0.38937325318866
C	4.10131127483070	0.66758794438467	0.81112075574518
H	5.03621405116210	-1.30892726694542	0.41540968526508
H	4.90930902290156	1.23867894738112	1.22339876718533
C	-0.89295830260450	-2.78324002372481	0.82685649477723
C	-0.39808168756903	-4.04004590756191	1.03212080353932
C	0.93194077755264	-4.07308325259189	0.54065207445099
C	1.23078192163181	-2.82944145959811	0.06225014162087
N	0.11089377214755	-2.03768730699516	0.23435573408226
H	-0.92515444552677	-4.85984980380531	1.47777382783816
H	1.57499710109177	-4.92945201735075	0.52568901324131
C	2.41271463480029	-2.30182123109747	-0.70768386911745
C	3.51569572559651	-3.36633399824207	-0.72688845638046
H	3.05859336465706	-4.32731033322600	-0.93670495760029
H	3.91742951658677	-3.44138884010246	0.27989181183003
C	1.95179754333023	-1.98717432254969	-2.15454421021240
H	1.21517330506747	-1.17915066269667	-2.12945736677897
H	2.79252053204829	-1.57115709244637	-2.70165647762709
C	1.34373688538041	-3.15870321824083	-2.89274143048029

H	1.02891666838214	-2.86510787556968	-3.88869683264864
H	0.47963949825282	-3.54722845463098	-2.36512800281629
H	2.05229683045023	-3.97349019543250	-3.00169411520015
C	4.63496218431861	-3.14157113651446	-1.72762014069035
H	5.44910980778531	-3.83442565963016	-1.54145201228854
H	5.03873663309253	-2.13736499286243	-1.68162346153069
H	4.30127985354472	-3.31080905131485	-2.74644304602126
Sn	0.07953471375108	-0.01499954933548	0.00137792564309

90

Coordinates from ORCA-job f_sn4_cxet_CREST_cmp_Compound_1

N	1.12948325844843	-1.72829346674764	0.14720546626368
C	2.42442567879161	-1.83531401150008	-0.31642253405292
C	2.69266119378233	-3.15372388376654	-0.57074634450055
C	1.53859629324368	-3.88857996619309	-0.24622179368031
C	0.58970535157958	-2.99776661785193	0.18703098794820
H	3.62801163309814	-3.55171314039404	-0.91435065963452
H	1.43789484152050	-4.95603643537996	-0.27629551168555
C	3.35817104917305	-0.67208501665501	-0.48092755151767
C	4.77772367040174	-1.12101787268235	-0.09172465849514
H	5.44089390358389	-0.26720440758978	-0.19237946978624
H	5.11092467133402	-1.84181701223040	-0.83642653563978
C	4.93182048627172	-1.72218442533249	1.29334884681251
H	4.53317468837254	-1.06584580127822	2.05807599596703
H	5.98139948541289	-1.89833580634003	1.51771917738559
H	4.40813473717600	-2.66703736809243	1.37171433446164
C	3.36659573630685	-0.26709790706090	-1.98098116449683
H	2.34794205313081	-0.04051702387971	-2.27755993479691
H	3.65606135022185	-1.15043212217301	-2.54905800712998
C	4.26208263012412	0.90226444918286	-2.33771160965528
H	4.02569574253459	1.77470646597606	-1.73751091043903
H	4.13257757657442	1.17274338894178	-3.38202642162055
H	5.31475067763924	0.67810386210172	-2.18978447620304
C	2.96528490317047	0.51553590004838	0.34038059962298
C	3.74704581602329	1.31116055980872	1.13517533561079
C	2.96968680314510	2.42018796136702	1.51800699823535
C	1.73707593828562	2.28295081451375	0.93400477087438
N	1.72460962904511	1.11076830065044	0.20900583015405
H	4.77318298229713	1.13997163246142	1.39220651539254
H	3.29964985087908	3.25525575358288	2.10575860300091
C	0.69046699696524	3.35467607449785	0.87673838542144
C	0.35170122324985	3.80605286848534	2.31669642920822
H	1.27738480117719	4.10124019319293	2.80887012538097
H	-0.26790986591089	4.69845372853085	2.24395026781947
C	-0.35719460203191	2.75583641395531	3.14314666040438
H	0.22668172443304	1.84027337563909	3.18854882854259
H	-1.32593371736294	2.51135114204251	2.72184762011201
H	-0.51038143659087	3.09935992552519	4.16262862077488
C	1.32057535428038	4.56648573113916	0.15331916227894
H	0.59977840485711	5.38140568004554	0.14412922888412

H	2.16019252914089	4.90768070097444	0.75472315026200
C	1.78553626456157	4.26680124836342	-1.25475057378952
H	2.56365002307271	3.51065489525619	-1.25190882380216
H	2.18496363317331	5.15650628356007	-1.73429411620138
H	0.96649793357516	3.89543917971307	-1.86202892526860
C	-0.69052963591272	-3.35506875749508	0.87532737437545
C	-0.35176845193830	-3.80682913125501	2.31517196483598
H	0.26789382348762	-4.69917541793733	2.24219364039760
H	-1.27745415224675	-4.10219360922281	2.80723613349739
C	-1.32056134790922	-4.56670915069085	0.15156750492619
H	-2.16017265424434	-4.90809928863859	0.75286608660697
H	-0.59973213802416	-5.38159925044103	0.14218437804860
C	-1.78550620007079	-4.26667414978717	-1.25643349423198
H	-0.96645932976874	-3.89516981058580	-1.86361257494436
H	-2.56361743723842	-3.51052318647763	-1.25341631070050
H	-2.18493375638088	-5.15626004387310	-1.73619864699413
C	0.35704623481348	-2.75680324938032	3.14193579278728
H	-0.22684976413806	-1.84125978392855	3.18751181186017
H	1.32581568048771	-2.51220190956738	2.72077796820791
H	0.51015227550957	-3.10056926426098	4.16134800428194
C	-1.73719526050471	-2.28341346113349	0.93288346866281
N	-1.72467290222241	-1.11090829395570	0.20841118398542
C	-2.96537084381486	-0.51575749526664	0.33992826060898
C	-3.74719215882463	-1.31173484499285	1.13431057387636
C	-2.96985990732604	-2.42093046973854	1.51670619748942
H	-4.77335034292289	-1.14066416938627	1.39134135977814
H	-3.29986400060754	-3.25626606732899	2.10405441062503
C	-0.58977681704738	2.99764941633574	0.18831434466632
C	-1.53866899213329	3.88865526108728	-0.24453729085976
C	-2.69271319212709	3.15393746986340	-0.56944213470142
C	-2.42447476403808	1.83541153484288	-0.31571790372162
N	-1.12953948603347	1.72818959277584	0.14788805515203
H	-1.43797923079919	4.95612709032156	-0.27410682148200
H	-3.62805945933830	3.55208247161551	-0.91287661060393
C	-3.35819462596773	0.67224676940761	-0.48084767810082
C	-4.77779743207957	1.12094428246390	-0.09154039882904
H	-5.44093953561510	0.26717927679300	-0.19276982596002
H	-5.11093448140509	1.84217738933589	-0.83585146826406
C	-3.36648869408174	0.26799574607295	-1.98110320515475
H	-3.65594367288228	1.15160517755408	-2.54875715516822
H	-2.34780507588550	0.04160016465386	-2.27772204590415
C	-4.26190427660542	-0.90122166332335	-2.33847840743249
H	-4.13239244817816	-1.17110514977853	-3.38294704400521
H	-5.31458624874155	-0.67721171204667	-2.19041879701126
H	-4.02545778469194	-1.77398853428493	-1.73877444987531
C	-4.93205179486347	1.72127154260969	1.29387797436062
H	-4.40840878945726	2.66609366644563	1.37286030621296
H	-4.53344730776484	1.06448436619824	2.05824518053707
H	-5.98165863865810	1.89724492772451	1.51825781730704
Sn	-0.00001627335791	0.00003004439321	-0.23328318390747

S101

F	0.00004265939191	0.00042131197441	-2.16759959025790

38

Coordinates from ORCA-job f_sn4_pyrr4_cmp_Compound_1

Sn	-0.26141083591636	-0.55339019716698	0.59505017008356
N	-1.23844594425098	-1.88911977328948	1.83959641092383
C	-2.27865719674570	-1.61892233904937	2.68976692231760
C	-2.70320769704167	-2.78717881622123	3.26578749006002
C	-1.89101471907644	-3.82226922257731	2.74607986767227
C	-1.01140884373510	-3.23940610712537	1.87248765511066
H	-2.62797017139034	-0.61510279971195	2.82081168576683
H	-3.50553929389844	-2.88384393703941	3.97227384543140
H	-1.94528616244383	-4.86816087761760	2.98135718774711
H	-0.25444788466922	-3.67069996484776	1.25018746399710
N	1.79098916545459	-0.26482964785961	0.68068027395395
C	2.45976601845129	0.68245251396722	1.41516155957936
C	3.80473217225928	0.54769179195108	1.19716538393927
C	3.97481659149648	-0.52598246895517	0.29110449191804
C	2.72577784846205	-1.00129841960804	-0.00527562508744
H	1.93149621464173	1.37718835652137	2.03503288268983
H	4.57392005174780	1.15271123820926	1.63866364563650
H	4.90042477153761	-0.90579270733163	-0.09872332567602
H	2.41000578191956	-1.79848327552665	-0.64415662790576
N	-0.57867010863210	1.05519206262936	1.94691633312531
C	-0.49205821675720	2.37747286391980	1.60085687244878
C	-0.26288444299211	3.13400467323553	2.72167528879133
C	-0.18426566615346	2.23617157961001	3.81014557976666
C	-0.36965129616771	0.97730966736925	3.29829712555933
H	-0.60369390323346	2.68137292278808	0.57939159700081
H	-0.17300200608213	4.20322572459801	2.75378165636893
H	-0.02365210282062	2.48070255627979	4.84298257603624
H	-0.37152275981310	0.02800819851328	3.79526244030398
N	-1.43434235045807	0.34142636014100	-0.85864333597939
C	-1.30331726300036	0.13640984439454	-2.20644056745026
C	-2.29029998269405	0.82219516581791	-2.86386956245953
C	-3.07039441069610	1.46943788704003	-1.87714791282767
C	-2.52053584407165	1.15348617224422	-0.66272092946730
H	-0.52797420398016	-0.50119747650156	-2.57859496049091
H	-2.43501202196850	0.85282065223028	-3.92703339607687
H	-3.93310482155139	2.08842197272798	-2.03463288674457
H	-2.80994743233271	1.44700896924419	0.32564754402653
F	0.10109896660255	-2.03319814300311	-0.65786482008961

90

Coordinates from ORCA-job h_sn4_cxet_CREST_cmp_Compound_1

N	-1.12800611855512	-1.71352837918792	0.00632436389572
C	-0.61731128262825	-2.97200091476023	0.24497327034088
C	-1.59623743366620	-3.89636855156289	-0.03037054668730
C	-2.73560070837185	-3.19376423214886	-0.45732136532932
C	-2.43130803551606	-1.85708984375360	-0.41900747566976

H	-1.52153866481610	-4.95853106491207	0.09421409075310
H	-3.68062553729282	-3.62275187366191	-0.72799375389134
C	0.67810866466224	-3.23792933152193	0.95218963088362
C	0.43071072294841	-3.15462542432247	2.48391236086143
H	1.34449120544081	-3.48505978926456	2.97767193436895
H	-0.35050538554730	-3.87227795037221	2.73281667585549
C	0.05545781145679	-1.78197121377693	2.99270744204104
H	-0.87946206430630	-1.44142125764322	2.56263172151425
H	0.82388199697373	-1.05549618438654	2.74743654133624
H	-0.05798688603511	-1.78388569855682	4.07333788218371
C	1.11036536520767	-4.68942691430529	0.66779547450289
H	0.32481785166297	-5.35274065483817	1.02170393244454
H	1.97402445907535	-4.90687050409598	1.28993156029509
C	1.43841983262211	-4.99390107345693	-0.77866326929084
H	1.74252748747744	-6.03119011796061	-0.89707253361194
H	2.25104361783132	-4.36573356937891	-1.12882816115571
H	0.58179415906727	-4.81950017953851	-1.42002928709801
C	1.82479232092798	-2.33248474804349	0.60761331016910
C	3.14437431938153	-2.58300521626681	0.89534415305245
C	3.88855969052268	-1.47071501217496	0.47092540866979
C	3.00601974267231	-0.56061636137066	-0.05273365313874
N	1.73279256016851	-1.08919318158112	0.02930054044407
H	3.53374729293019	-3.46918434015734	1.35696793625789
H	4.95374392208662	-1.36537478125030	0.52196418906376
C	3.32350385173546	0.70588642870910	-0.78984709177033
C	4.78431446081298	1.10581110589313	-0.51451823329042
H	5.42518981027860	0.28983134071240	-0.83497086247068
H	5.02332916869280	1.93840825814833	-1.17280527708366
C	5.12725961085058	1.48170597569550	0.91523497021168
H	4.88899320847751	0.68104707565604	1.60461451830704
H	4.57992783967120	2.36027121246779	1.23415259592096
H	6.18989674180705	1.69657316778383	1.00489974151967
C	3.18835801542747	0.46761508564417	-2.32153496936640
H	2.13410136597305	0.40852224420068	-2.56998314818092
H	3.55600385339268	1.36455907509762	-2.81927189406398
C	3.88257561529757	-0.76537438260536	-2.86469225266902
H	4.95352874853238	-0.75078558077129	-2.68478797296616
H	3.73429984071793	-0.83928578140599	-3.93905205450824
H	3.49045957512369	-1.66737138021931	-2.40744312128461
C	-3.32333991788419	-0.70629589846901	-0.79096873619848
C	-4.78392308910637	-1.10769321969990	-0.51674141272459
H	-5.02350532956205	-1.93655530385767	-1.17955195962845
H	-5.42485457092187	-0.28977276990234	-0.83214817389193
C	-3.18895041596385	-0.46075786903117	-2.32150244921954
H	-3.55724133824546	-1.35514616104538	-2.82335294114399
H	-2.13482375003287	-0.40084206957693	-2.57027284146343
C	-3.88312082541965	0.77513004680635	-2.85814052929309
H	-4.95389502874014	0.76019690113325	-2.67719516837125
H	-3.73588489546468	0.85416988041486	-3.93227503449924
H	-3.49009638052651	1.67477924430247	-2.39698523116902

C	-5.12614758979279	-1.49175276040602	0.91107104065921
H	-4.88396362360366	-0.69662997849042	1.60544928486572
H	-4.58175024180684	-2.37445972682386	1.22347614432792
H	-6.18946512175715	-1.70322988509874	1.00079327786643
C	-3.00542785217946	0.55686739175365	-0.04831368916100
N	-1.73273842215390	1.08746342136468	0.03041461212548
C	-1.82441742619814	2.32760096084570	0.61541537095494
C	-3.14308597735086	2.57411299124300	0.91062466773274
C	-3.88721138847861	1.46264171293195	0.48396969292740
H	-3.53189323771895	3.45749383925090	1.37811794639501
H	-4.95196736712634	1.35519365695330	0.53919061352405
C	2.43199510435052	1.85551546163199	-0.41281772825935
C	2.73749320081940	3.19205755369561	-0.44663585322584
C	1.59773769594131	3.89440537204444	-0.02069633641832
C	0.61733345602159	2.97019946932024	0.24982210315159
N	1.12756216868323	1.71186615994408	0.00939931296350
H	3.68330319136563	3.62104522250862	-0.71446497897864
H	1.52351588100743	4.95630029351631	0.10650833864611
C	-0.67974008956931	3.23823952918703	0.95331673375426
C	-0.43339573445913	3.16862627493402	2.48567094302767
H	-1.34928602215804	3.49738480633700	2.97659166772483
H	0.34357699930906	3.89246513538438	2.72979264698082
C	-1.11586868443298	4.68606696736436	0.65523126360154
H	-1.98182212399658	4.90635228770627	1.27315358257331
H	-0.33331515410738	5.35538678148705	1.00440980882552
C	-1.44152204137745	4.97529995953300	-0.79479260071212
H	-0.58203586211766	4.79932437577867	-1.43195013061900
H	-1.75070499282299	6.00979373171467	-0.92389510157988
H	-2.25004122941875	4.33961649414504	-1.14113124973015
C	-0.05031181838672	1.80170698498504	3.00380967543629
H	0.88663159287655	1.46385597332846	2.57598283875070
H	-0.81438221337432	1.06937328384786	2.76251442924594
H	0.06254995082144	1.81105030604690	4.08445913267441
Sn	0.00007344561552	-0.00050261984414	-0.51578383865089
H	0.00036661937223	0.00059319294898	-2.23136029866317

38

Coordinates from ORCA-job h_sn4_pyrr4_cmp_Compound_1

Sn	-0.21589156464374	-0.61559625847079	0.54244260211710
N	-1.26582406257988	-1.88678225823308	1.85061481995346
C	-2.30911259518515	-1.59636527679673	2.68541708751660
C	-2.77132186641312	-2.75499562542607	3.25631118458694
C	-1.97775199786721	-3.80880212915537	2.74761500222112
C	-1.07410810751144	-3.24062085498498	1.88669209065624
H	-2.63829231361452	-0.58492809503031	2.81035391173982
H	-3.58624176621116	-2.83369789416229	3.95092856949906
H	-2.05684563585596	-4.85311677592144	2.98367764725640
H	-0.30937841076487	-3.69534585661801	1.28724569876878
N	1.86011131935547	-0.22894920218464	0.70288224355503
C	2.52897508975359	0.71675325389192	1.43100529824335

C	3.87700181669164	0.58503662588857	1.21349566176929
C	4.04811954243352	-0.49021429258329	0.31041308272733
C	2.79430665029803	-0.96272378837975	0.02077139226364
H	1.99811972749421	1.41208543642098	2.04855741130459
H	4.64687521340475	1.19180894052938	1.65248648199334
H	4.97335321289697	-0.87090299069029	-0.08003812697494
H	2.48788587119655	-1.76572176464105	-0.62068603363670
N	-0.52507037832962	0.99880739823516	1.89982674086432
C	-0.45502855511348	2.32189307779989	1.55755895674820
C	-0.24778867751087	3.08100552200722	2.68185461319506
C	-0.16578466549098	2.18248368104540	3.76911988396909
C	-0.32744862038361	0.92177216514990	3.25178427405295
H	-0.56188994508912	2.62609416277140	0.53582091247363
H	-0.17403381647518	4.15155993920663	2.71634267383659
H	-0.01779776865926	2.42690928035756	4.80404190961817
H	-0.32067706352121	-0.02824991186361	3.74706598072411
N	-1.45759930651501	0.34937021901313	-0.85684299937144
C	-1.35688716554526	0.14712419421851	-2.20580198744230
C	-2.36672030504850	0.81802254114764	-2.84672813203622
C	-3.13237254710592	1.45399610263590	-1.84264796534414
C	-2.54875994586798	1.14438813900365	-0.64030776980334
H	-0.57297703936293	-0.46722871020106	-2.60454447304717
H	-2.53276367489773	0.84888329199419	-3.90693627845869
H	-4.00788152195423	2.05984787257755	-1.98118128491675
H	-2.82138137292548	1.43252757238647	0.35449022711662
H	0.15419424691874	-1.92029073093834	-0.56204230773921

90

Coordinates from ORCA-job cl_sn4_cxet_CREST_cmp_Compound_1

N	1.17410822641914	-1.70525051990485	0.11433012780394
C	2.46151070778442	-1.73640298663160	-0.38320930328397
C	2.72546938144612	-2.99236462053393	-0.85844044171793
C	1.57343305705210	-3.77239544437771	-0.64549721157946
C	0.63558093498598	-2.96589466286278	-0.05575951220900
H	3.65992517578050	-3.32645410332357	-1.26804097314726
H	1.46795745598618	-4.82077862191751	-0.84875382410402
C	3.43413215485029	-0.60133623878467	-0.27198376312441
C	4.71503767864471	-1.13680537908517	0.39468401291546
H	5.42459812788888	-0.32029688797476	0.49325270075038
H	5.17115717636168	-1.84645402068019	-0.29329265478352
C	4.50675655492341	-1.80219248771241	1.74058377954511
H	4.00669697782707	-1.13734350591764	2.43605461189142
H	5.45825292357336	-2.09261811002897	2.17940145090286
H	3.89768481296092	-2.69382366649580	1.64117184541510
C	3.77705570508665	-0.12095689534986	-1.70747054305513
H	2.85253809772921	0.20673262420465	-2.17286964695420
H	4.10687968085206	-0.99201909611967	-2.27181039893547
C	4.81339136447486	0.98014854395935	-1.80530440624004
H	4.54003897327476	1.83425486720478	-1.19474646175881
H	4.90676046049328	1.32103845473053	-2.83278698008685

H	5.79713385224299	0.64924788026689	-1.48409556067861
C	2.90901399725388	0.55995636299482	0.50895622857021
C	3.57849239883382	1.36698425925507	1.39043140710574
C	2.76238451771879	2.48659356717575	1.64291547724624
C	1.61863823786702	2.33754178002137	0.90249375899317
N	1.69480628269183	1.14742286233249	0.20864882156456
H	4.56123127667831	1.19700935550782	1.78352863526700
H	3.01521778381252	3.33530266772361	2.24862029692528
C	0.62603173042169	3.41839629592259	0.60618291553730
C	0.24311747356814	4.13954276042886	1.91662619229598
H	1.15434814509453	4.49852209913170	2.39282923277876
H	-0.33469475775421	5.02181658740078	1.64635181369962
C	-0.54541730526836	3.28875203471021	2.88771780130858
H	0.00198990117566	2.38660587058121	3.14447580615506
H	-1.49572154069439	2.98604926035943	2.46205935570914
H	-0.74508698782700	3.83121902784443	3.80803161876071
C	1.32957830689098	4.45369470646184	-0.29993931420151
H	0.63324136242943	5.26621828729024	-0.50097301012796
H	2.14981656765629	4.88282918115126	0.27244723582910
C	1.85243168074804	3.88477973039803	-1.60044170606609
H	2.61886633784910	3.13962926950546	-1.41962160258376
H	2.28547782070784	4.66561406082687	-2.22025010990924
H	1.05817643044765	3.40859569072756	-2.16676068314562
C	-0.62611883779206	-3.41868951012240	0.60481044819194
C	-0.24328463443052	-4.14040126275571	1.91496549956272
H	0.33445811281329	-5.02261145185414	1.64433534415887
H	-1.15454653401010	-4.49950459065848	2.39101407215399
C	-1.32963290147241	-4.45359057206827	-0.30178644198087
H	-2.14988351236561	-4.88299304136690	0.27038407016614
H	-0.63327579897635	-5.26601103986550	-0.50316252976112
C	-1.85246295999390	-3.88411583121194	-1.60205517016849
H	-1.05821015720569	-3.40765285783484	-2.16814245482157
H	-2.61893286503562	-3.13907753020539	-1.42092943061732
H	-2.28546413115292	-4.66469737795936	-2.22221335925771
C	0.54530853481352	-3.29007475556377	2.88641770214450
H	-0.00200656100584	-2.38796538491206	3.14349924866269
H	1.49566626920039	-2.98731839336369	2.46091627113247
H	0.74487210073628	-3.83291890657221	3.80653199154550
C	-1.61871490069400	-2.33793701339388	0.90152667950541
N	-1.69485143833839	-1.14755552264099	0.20812543616181
C	-2.90906918978567	-0.56019997442580	0.50860210023409
C	-3.57858796828530	-1.36755564583267	1.38974561817876
C	-2.76249358629501	-2.48726239654710	1.64184414813419
H	-4.56134339032476	-1.19772249496153	1.78286324083132
H	-3.01535926255397	-3.33620579095186	2.24720631585991
C	-0.63561754334536	2.96585309986436	-0.05465069145526
C	-1.57341141120118	3.77256016363170	-0.64419721546716
C	-2.72542424864973	2.99260062576476	-0.85753527189407
C	-2.46151129844286	1.73647272650095	-0.38271859402294
N	-1.17415721369592	1.70514660599942	0.11493820420838

H	-1.46791527543249	4.82101328432212	-0.84708117670401
H	-3.65983944390671	3.32683694013920	-1.26710869027002
C	-3.43415420429637	0.60138084144226	-0.27193323081085
C	-4.71506441827466	1.13663822341326	0.39490253692740
H	-5.42465784677857	0.32011906390815	0.49314342249114
H	-5.17113456336812	1.84656664317526	-0.29281774036617
C	-3.77704419353129	0.12152371447086	-1.70759955404764
H	-4.10679785095347	0.99280059720357	-2.27164784188148
H	-2.85252124854155	-0.20605196485687	-2.17306912847273
C	-4.81342462407062	-0.97949780258916	-1.80585877120910
H	-4.90680418262897	-1.31999174589045	-2.83347204944782
H	-5.79715583078227	-0.64868456388591	-1.48452669913142
H	-4.54010691100040	-1.83385299745209	-1.19563284710246
C	-4.50678479884669	1.80151445896636	1.74105360325488
H	-3.89766858900608	2.69315308727055	1.64197894810350
H	-4.00677111153138	1.13638477229690	2.43628825528949
H	-5.45827604485474	2.09182568405556	2.17995775384097
Sn	-0.00000964593744	0.00002986193315	-0.29745679303665
Cl	0.00004023629139	0.00048306706806	-2.65931557469111

38

Coordinates from ORCA-job cl_sn4_pyrr4_cmp_Compound_1

Sn	-0.26189941967211	-0.63781550768154	0.51771703932603
N	-1.24016727451731	-1.90914109736419	1.83652906024006
C	-2.35159211734841	-1.58997605001519	2.57223741644985
C	-2.74113002668408	-2.68584488803933	3.29557354765611
C	-1.83012695243649	-3.72459103960678	2.99245223709656
C	-0.93059548534208	-3.21761557924186	2.09282316637378
H	-2.76249375375596	-0.60182605384316	2.53669880853155
H	-3.58232803949872	-2.73413083051155	3.96041906377825
H	-1.83168851872238	-4.72345928885532	3.38514575392091
H	-0.10679817655006	-3.68657757527995	1.59524078585983
N	1.79589245729096	-0.33939806353877	0.62418636496039
C	2.41214282068762	0.62630748135741	1.38623847804053
C	3.76619960323207	0.53129938195899	1.21752590575101
C	4.00091810277586	-0.53325268088768	0.31654468322704
C	2.77982521365821	-1.04453859886383	-0.02748648237895
H	1.84665300301335	1.30651559722700	1.98669630529225
H	4.49901999368779	1.15783484495168	1.68960853259593
H	4.95014150182929	-0.88613196531706	-0.04015244603978
H	2.52531648531431	-1.84953824822893	-0.68188369713015
N	-0.58275044387418	0.96919868489583	1.87342995456250
C	-0.50043901002299	2.29338299714682	1.53389553770972
C	-0.28420938196677	3.04586764577376	2.65979023145254
C	-0.21168132704425	2.14333175933122	3.74535635777039
C	-0.38741504104858	0.88618389951496	3.22647538041595
H	-0.60929412105107	2.60106440724483	0.51349881951239
H	-0.20036482366591	4.11544618949006	2.69730864853621
H	-0.06236585063575	2.38388043915520	4.78086088255700
H	-0.39446519890607	-0.06495724852541	3.71937263658830

N	-1.43061717010046	0.34990229643867	-0.88721898092120
C	-1.23454268604466	0.37436486037156	-2.24177260245013
C	-2.23184786837423	1.10784766839196	-2.82743671832570
C	-3.08615302550353	1.54642425500406	-1.78887266935687
C	-2.56731875991796	1.06612525292245	-0.61587597709081
H	-0.41247586100509	-0.15404590823759	-2.67888196800570
H	-2.33340314970519	1.30559059067901	-3.87744872086273
H	-3.97605748319439	2.13831764297704	-1.88736332072040
H	-2.90390420360548	1.19253385404248	0.39269091593732
Cl	0.04332898870471	-2.49274212483689	-1.04286493086005

13

Coordinates from ORCA-job thf_cmp_Compound_1

C	1.03519672073862	1.03369455439472	1.73874794146331
C	0.60096891701909	0.91278957372452	3.18574494814654
C	-0.88521659107844	1.21510161675272	3.07643865002088
C	-1.23400891890831	0.51901923340766	1.77628933677484
H	1.27889412623611	2.06789955992877	1.48789330230562
H	1.89272329300793	0.41532596491375	1.49079259313971
H	0.75229204989020	-0.10251444646864	3.54372360387844
H	1.13573440815667	1.58663458321294	3.84518756526792
H	-1.04453007506143	2.28689741881550	2.98874483552991
H	-1.46708824995855	0.85489834962268	3.91702045597768
H	-2.06759411151049	0.97398188896924	1.24956404404755
H	-1.47516579476146	-0.53193373647563	1.94751404197260
O	-0.07442377376995	0.60766243920176	0.95342168147499

2

Coordinates from ORCA-job cucl_cmp_Compound_1

Cl	-5.58597197177774	0.44212000000000	0.00000000000000
Cu	-3.51616802822226	0.44212000000000	0.00000000000000

15

Coordinates from ORCA-job thfcucl_cmp_Compound_1

Cu	-3.64391798905931	1.87808602896776	-0.55044344696038
Cl	-3.46649228490893	-0.13606317836778	-1.01447440167603
O	-3.81227071579026	3.73273121518972	-0.10983382512637
C	-2.73066511366545	4.52499690389597	0.43309399776961
C	-5.08493444075940	4.38988735741116	0.11956602219186
H	-5.76108950910500	3.66757494165214	0.55829006068429
H	-5.47012065871793	4.69853998624425	-0.84728957405645
C	-4.76095218674689	5.56241975149332	1.01592239592357
C	-3.33032190868101	5.89601704005216	0.61719834627973
H	-4.80116944429147	5.26603865215621	2.05966396844009
H	-5.44851884748619	6.38631813831758	0.87250916994759
H	-2.80364860421026	6.47637721507643	1.36415980545157
H	-3.31249650959611	6.44710259615991	-0.31827790696524
H	-1.91140211933930	4.47730202195866	-0.27214016214222
H	-2.41831966764239	4.08409132979238	1.37588555023838

125
Coordinates from ORCA-job TS1_thf_add_optTS

Sn	10.45185653695482	3.17899580936251	3.87093779779568
C	10.41700532213289	5.51053937421824	3.97786746900728
N	12.02409360117766	2.91160658512174	5.22091182752005
N	9.20150659232816	2.75982014434918	5.50446274102402
C	9.44823290012346	3.25473730546070	6.77543332283947
C	11.98187636437848	3.50937167901939	6.46923529419343
C	13.34596817272134	2.77804460187473	4.85131778077146
C	7.88368094721824	2.35241890318917	5.45276556518834
C	13.27297276806289	3.73421566162284	6.87648543782214
H	13.57458725148816	4.14658324409053	7.81933687408128
C	13.76090385963729	1.97738046342095	3.65362359737782
C	8.29313053705239	3.13414507382404	7.50843528265690
H	8.17297309532714	3.37772868479443	8.54402390019436
C	13.43586695355363	0.48538739335173	3.94659457714719
H	12.35757403316464	0.38797005551048	3.98854614427093
H	13.75381550343045	-0.08621178582793	3.07484263166865
C	10.76294020447446	3.72874033891871	7.32882422298320
C	14.12912453270243	3.26949804531718	5.86430808928562
H	15.19941917288150	3.25955055284101	5.90034100702026
C	10.71001497433520	5.24542855068907	7.65656764948601
H	11.69802847930803	5.52814305308727	8.01093541084393
C	7.31505066380115	2.56447559365594	6.68018934800005
H	6.31517820943794	2.31367414637745	6.96950893862842
C	15.27645367539063	2.11530031630317	3.44247118310339
H	15.77272878184694	1.78550310656139	4.34886098386959
H	15.56701880462197	1.39768018241636	2.67919161382215
C	11.01269844610908	2.94536395873353	8.64479374368058
H	11.89648077292063	3.36101358504855	9.12299412303648
H	10.18470066658022	3.12082059785652	9.32318505767007
C	11.18557251158293	1.45725918071138	8.43577548707495
H	12.03600779249125	1.24858350050505	7.79505069853222
H	10.30377277336306	1.02657440451681	7.97218913532474
H	11.34796978809651	0.94918594808582	9.38098440381776
C	15.78991398741631	3.49336967618022	3.06800964916814
H	15.36695995787360	3.83657599810873	2.13186224765823
H	16.87050773757183	3.47652583811630	2.95904548718667
H	15.54782513689224	4.22928152027766	3.82551296634913
C	9.67463041933088	5.74104937729987	8.64588197308893
H	8.66369193630539	5.58906729596060	8.28673042583029
H	9.81143915492377	6.80579197939575	8.81469713307457
H	9.75907725614180	5.25436226341647	9.61158096433670
C	14.04297922952831	-0.09675753831407	5.20606447814149
H	15.12790926513660	-0.10876532560317	5.17982826252103
H	13.71522438884511	-1.12395174377434	5.33813724423957
H	13.74126097559960	0.45939549674576	6.08712480987359
H	10.57235795553713	5.77502891544420	6.71950502517282
N	9.31138284676537	6.05185144428305	4.38298420958119
N	8.89951265588040	2.58944550534320	2.58936896908509

N	11.72266388440946	2.70014762092305	2.29226239995312
C	11.40049025756608	2.87303969455963	0.95578463008687
C	8.89808672951520	2.84057954320507	1.22865849818739
C	7.62657108366903	2.18471342351660	2.95032201647227
C	13.04936077653648	2.33543404032014	2.37612741036946
C	7.63647304789906	2.60983377367880	0.74894795824929
H	7.31922454451639	2.70559714465757	-0.26985380700990
C	7.28500449961982	1.61604420981718	4.29345292815372
C	12.51947192600318	2.60084975128230	0.21385373347686
H	12.59389432569067	2.63148091638014	-0.85430198012714
C	7.82938349169326	0.16162069272307	4.39019344798444
H	8.91154140282515	0.21165439214481	4.40152137748998
H	7.52644538467271	-0.22280210386729	5.36311493406362
C	10.07190379039504	3.36071551724012	0.45124982543311
C	6.84095713872321	2.19119920379739	1.82840005642189
H	5.81633651339293	1.88435924849625	1.77309294990926
C	10.00186702461408	4.91509641341152	0.50217084361321
H	8.98881269046134	5.20166902444787	0.22659053613839
C	13.55048883402153	2.25368700019323	1.10358091186312
H	14.54723172892750	1.96909507819816	0.83384802780177
C	5.75783059840520	1.57329731424923	4.45221160734603
H	5.35479965629147	0.94410293320378	3.66631758927061
H	5.53887173232496	1.04881174841757	5.37888247707336
C	9.91240746781057	2.95284243524961	-1.02670105615824
H	9.01925934673014	3.44322771334770	-1.40765397133582
H	10.73484666894009	3.38591277039664	-1.58451285985631
C	9.85012400278214	1.46799257609257	-1.32243803841640
H	8.99259835663972	0.99775976176754	-0.85739264218028
H	10.73950925726291	0.95997712300334	-0.96898995171418
H	9.77924824394985	1.30327263874354	-2.39366022764213
C	5.03141224038768	2.90605856349783	4.43431009391896
H	5.35105000263351	3.55243368977153	5.24349102403946
H	3.96086946074142	2.75452571531598	4.53925771651889
H	5.19691614362502	3.43661456409306	3.50359716821953
C	11.00231096063177	5.66219834426535	-0.35616942230240
H	12.01030280198546	5.28748799378131	-0.21278319593746
H	11.00288356644598	6.72157801905909	-0.11738709952236
H	10.76604530826146	5.57599681731265	-1.41079859263963
C	7.40266036927960	-0.79149090276636	3.29493975130716
H	6.33108212342768	-0.96734887641714	3.28989639544275
H	7.88741936244676	-1.75272303346802	3.43344550150817
H	10.11619073248959	5.21396688662685	1.54265242241760
H	7.68043366997528	-0.42038645168953	2.31485357903894
C	8.03507962688645	5.33219870367491	4.44065682412855
H	8.01674812401035	4.51571386154963	3.74000523949795
H	7.25660205953820	6.03254666042400	4.16544908685871
H	7.85502501879450	4.97481822789056	5.44810138109773
C	11.30341408202331	7.60537635499167	2.87276288538747
H	12.21257745810994	7.96165073838999	2.40227342531526
H	10.89768874401809	8.43166456384966	3.43846254939037

C	9.12383652178049	7.41345643926502	4.88902533022888
C	11.65702949935435	6.37016927936622	3.71952077716661
C	12.68640758652407	5.56936729399012	2.92421775443354
H	13.53834450213762	6.21044570455479	2.72754949246988
H	12.30960948022212	5.21711778348195	1.97540308088569
H	13.05029938452836	4.72559045880792	3.48964098065694
C	12.37779758588471	6.78053446053943	5.00969614157012
H	12.71957028194394	5.90732721974629	5.55127992054476
H	11.78801709674726	7.38511195431526	5.68590119487283
H	13.24900125722002	7.36302376174324	4.72586530171166
H	8.49920243676720	7.33532068421832	5.77058910986916
H	8.60776497746110	8.01363870402643	4.14903343943798
H	10.05224427844640	7.87450244323205	5.15743549437327
H	10.60618568822953	7.36023458238331	2.07935750933310
O	10.57126913590575	-0.65174284493795	3.00494988471760
C	10.63966873972268	-0.37676975629144	1.60672259727071
C	10.99288235763317	-1.99053697063910	3.24877856474583
C	11.41063569976876	-2.56344722456244	1.90488981929535
H	10.15617107549984	-2.54244795152670	3.67778696506009
H	11.80003528716882	-1.98491871015408	3.97745753055390
C	10.58706930729931	-1.72844388502265	0.93606803026338
H	11.57162423086034	0.14096551649820	1.37809396107962
H	9.81568210054859	0.28084727307371	1.36228878249221
H	10.98615871776535	-1.71570870845899	-0.07159757131248
H	9.56301043385355	-2.09161398543375	0.89462147608823
H	11.22726667268257	-3.62931603627435	1.83154406745636
H	12.47024480959721	-2.39276148357960	1.73315582108542

125

Coordinates from ORCA-job thf_tbu_aaac_sn4_cxet_cmp_Compound_1

Sn	10.49698167668887	2.94134730993272	3.69785573053660
C	10.42011252662340	5.37682894110931	3.87134915913366
N	12.10551985830902	2.70853387118475	5.03108814715579
N	9.19760895416810	2.50148635951897	5.30155714056167
C	9.63551753022210	2.39566141406115	6.61215000798463
C	12.04008867996418	3.15252878487099	6.33527351479582
C	13.42837923677937	2.75050969646302	4.62770776302302
C	8.01342923556537	1.79709316444274	5.19144898449324
C	13.30741576587625	3.47834622707280	6.74668341111493
H	13.58745129508918	3.81637335521260	7.72521849247213
C	13.92116274253057	2.07423459153892	3.38170683419486
C	8.72238051554017	1.65086776682378	7.31350696887163
H	8.76127961091687	1.41828422781640	8.35815931029505
C	13.91631554998428	0.53766108469963	3.63312217051131
H	12.89071946955756	0.21386693932025	3.58241084576778
H	14.42301756585932	0.07543578210573	2.78801540184655
C	10.79212138667531	3.16570401585165	7.18049677030183
C	14.18050886988617	3.22361264024371	5.67305504272971
H	15.24739267993067	3.32187214542949	5.69214556578799
C	10.36556867552384	4.64306340124891	7.39292660348478

H	11.21866206389202	5.17585966579179	7.80910280045682
C	7.70693029415534	1.27322480375717	6.42180934071923
H	6.84072494187418	0.68672926782165	6.65750735404969
C	15.38494110612569	2.46862452241955	3.10998919116664
H	15.97775088760132	2.18811208269140	3.97528044971162
H	15.74118259744646	1.83683205767359	2.30152544315782
C	11.16318614182976	2.57668167074368	8.55691499761813
H	11.88498229540401	3.24763431744132	9.01607838422312
H	10.28932946244199	2.60846603799560	9.19910045045944
C	11.72557234695834	1.16946184405943	8.53459474126759
H	12.66173565891656	1.12912464154378	7.98883360557347
H	11.03619375428873	0.47572954484480	8.06670276049921
H	11.91624463765637	0.81844433838998	9.54434957886417
C	15.65873004667684	3.91552671008990	2.76070925760814
H	15.08740938896736	4.22371000195626	1.89170398941656
H	16.71120771348162	4.05284680702585	2.53001326536832
H	15.41206285773894	4.58214654768730	3.57843621786457
C	9.13457973140143	4.87627826223742	8.24545095297072
H	8.27322429680350	4.34743900054662	7.85050867566382
H	8.89547014700832	5.93618078424582	8.28297216206548
H	9.27411974246625	4.54750604972342	9.26972691158439
C	14.51638049434233	0.05483361857848	4.93711130259010
H	15.54963827917514	0.36156289329166	5.06327040567914
H	14.49757963718736	-1.03110081053458	4.97587389605318
H	13.96252960596490	0.42911099974188	5.79140888379203
H	10.19680961739462	5.07409195435021	6.41315181698403
N	9.29961613027417	5.90447230970733	4.25731194229850
N	8.91468015837759	2.55682169299059	2.35626808257750
N	11.80778884597666	2.78017824786847	2.08718720240786
C	11.40345536891165	2.82981788271056	0.76718945208175
C	8.90534907377785	3.17328994291728	1.12366277775092
C	7.59937938258125	2.38170829347115	2.75265924135689
C	13.10551504631045	2.32084496509613	2.13451555832359
C	7.60345969248255	3.39552942909589	0.75300822336912
H	7.27321220839564	3.82029336626872	-0.17460833247384
C	7.20100793991444	1.56658852065389	3.94120520733033
C	12.44667098121800	2.38938083990691	-0.00991901064798
H	12.46016493839638	2.32667679203224	-1.07919579049615
C	7.34127566049706	0.06033895432268	3.57756290046581
H	8.39533735213013	-0.16554208459134	3.56578343970374
H	6.92010673224804	-0.51304139993419	4.40110213807841
C	10.12624448912401	3.46934245552753	0.29347045856208
C	6.78183018456644	2.88658968223691	1.77472373105763
H	5.71066177218580	2.85615923665769	1.76479431346465
C	10.27907316363337	5.01430587042696	0.27131933072485
H	9.32708192384501	5.42976141131425	-0.05319673787479
C	13.51220927704592	2.06840242201490	0.84766683554476
H	14.47607227952526	1.70428150434947	0.55153768391589
C	5.71560209502913	1.81248051154619	4.27215600944360
H	5.12052549655216	1.57093013728154	3.39697733704168

H	5.42913138435295	1.08750707873639	5.02822942869175
C	9.83773560793175	2.99516440118421	-1.14545840037836
H	9.01126978559762	3.58831112162023	-1.52879289334092
H	10.68909275108547	3.24156140257605	-1.77106058764586
C	9.51402604435036	1.52153246433466	-1.28192245877199
H	8.61400482302606	1.26594775904750	-0.73239135635832
H	10.32349567913873	0.90622967577632	-0.90511053525306
H	9.35241625441985	1.25779479520218	-2.32287910072607
C	5.35789080606667	3.19985296109313	4.75932593629438
H	5.90257958082026	3.44541861391229	5.66556928913975
H	4.29810215118760	3.26410940647655	4.98669749719654
H	5.57763291231915	3.95359240843994	4.01168194171389
C	11.40213808789106	5.57698014774183	-0.57288628397184
H	12.35492503241864	5.11910209984930	-0.33073002855167
H	11.49437894787014	6.64823558348974	-0.41625110408326
H	11.22552870997671	5.42214234971263	-1.63217639908824
C	6.72943273972348	-0.38415934340831	2.26553026949361
H	5.66459347914870	-0.18121829215843	2.21065071199840
H	6.85803998284551	-1.45577347691165	2.13889116640953
H	10.39788302489692	5.33440259502780	1.30366940844248
H	7.19586001326371	0.11006195522726	1.42030699630135
C	8.03834912369316	5.17312902012247	4.24813568333449
H	8.05280310535920	4.38562560556905	3.52070982120466
H	7.25303607186605	5.86816639985900	3.97882034061756
H	7.83503312246753	4.77102111660352	5.23256163511830
C	11.33721273917639	7.58100845589387	2.97238721434613
H	12.27912857533855	7.99989707611101	2.63625206790363
H	10.84716495601626	8.34905544905055	3.55135190488951
C	9.07046701959236	7.23664457606688	4.82714840266588
C	11.64764755236306	6.28023070772009	3.73512368779237
C	12.73208340737473	5.57868656012787	2.92786132865809
H	13.58804030201760	6.24061590221137	2.85531262226865
H	12.41558816452678	5.33210024828958	1.92594104610296
H	13.06175545226730	4.68072530307769	3.41903223527549
C	12.27600536908184	6.56583443983368	5.10572707618735
H	12.60762840738193	5.64709422901172	5.57338270637763
H	11.62441466262834	7.07385395378067	5.80515749406738
H	13.14756272628013	7.19399196082959	4.94914102191984
H	8.40748149516199	7.10134640433207	5.67317032627767
H	8.57634630352786	7.86947808763653	4.09942087184148
H	9.97488839105492	7.69861127352694	5.16478068360702
H	10.73784235367475	7.38751337145616	2.08845827353843
O	10.62668185597196	0.56251944523379	3.61287447407629
C	10.64036058725419	-0.19796592794063	2.38555854852624
C	10.72919788489731	-0.29993669040069	4.76715625178652
C	11.09238682206975	-1.66041065667145	4.21239758526919
H	9.77253810466350	-0.29338069162283	5.27957306573992
H	11.47791756387240	0.12274462050014	5.42425365374087
C	10.48714832887438	-1.64174331342059	2.81378176144392
H	11.58038994276093	-0.00644149909485	1.87651415895138

H	9.83097428170065	0.16773010588737	1.76703708747075
H	10.98617236085964	-2.31874518629768	2.13071516233348
H	9.43921495350192	-1.92048162467908	2.85067932509611
H	10.70341043850621	-2.46285103691588	4.82782535379815
H	12.16982000999348	-1.77460370959146	4.15837693578238

140

Coordinates from ORCA-job INT2_thfcucl_tbu_aaac_thf_sncxet_cmp_Compound_1

Sn	10.46972751996790	2.96257921180907	3.71322632565056
C	10.28607452803222	5.33852324669993	3.86684047683665
N	12.11312564357556	2.73720074157987	4.99883346190634
N	9.23610311908060	2.46796671055342	5.34404417762981
C	9.67004736364763	2.46689844222336	6.65809298447247
C	12.07330282363065	3.22413943359207	6.28942414119786
C	13.42031176250511	2.81284884421111	4.55322769315776
C	8.00721145383421	1.84203463806203	5.29708513562323
C	13.34068001451613	3.60584414285898	6.64852205058128
H	13.63979994068024	3.98672706343808	7.60540778516073
C	13.88873766731216	2.11656466798503	3.31171073464232
C	8.71938319976254	1.83544838500864	7.42126532325812
H	8.75285144683256	1.68640214672091	8.48105686839230
C	13.91376420889974	0.58622499268006	3.59639868367000
H	12.89055158357220	0.24751817201226	3.58847400771975
H	14.39814607770574	0.11072734660154	2.74538621361607
C	10.86410856550065	3.21224744927740	7.18672546000841
C	14.18839437199684	3.34414395699238	5.55709965305771
H	15.25077324674218	3.48164878128587	5.53877362335861
C	10.47692490850948	4.68959102090022	7.47189331108635
H	11.36955369991740	5.19544564055437	7.83403900102914
C	7.67841404457368	1.44364909796863	6.56889326921903
H	6.78435453830754	0.92877150632022	6.85951061766273
C	15.33623458255324	2.53494788803515	2.99251809062700
H	15.95416911515060	2.29328365165520	3.85162932677854
H	15.69093680637336	1.88965938264307	2.19406560367863
C	11.29878391172946	2.56689010430246	8.52131298891995
H	12.07103646217470	3.19807143393716	8.95262841406537
H	10.47022119225569	2.60002627728673	9.22036194937091
C	11.80645914027073	1.14510553422926	8.40701606121817
H	12.67437782132331	1.08941461267003	7.75786852161804
H	11.04212954759409	0.48978131531381	8.00391551426178
H	12.09562996042565	0.76013290251088	9.38009948589527
C	15.56336583990161	3.97912025016164	2.59897031142469
H	14.97418659492523	4.24652773224984	1.72863450805171
H	16.60877989153560	4.14121722107852	2.35327508615951
H	15.30386642646125	4.66124783405913	3.39962152136136
C	9.32751890639756	4.92765447349333	8.42964254160317
H	8.42240377496509	4.42703418057125	8.10280018284579
H	9.11608516554026	5.99091771895971	8.50458630906088
H	9.54840992008625	4.57641953717367	9.43182312424443
C	14.56338188383953	0.14305348417098	4.89042446644733

H	15.59514048154623	0.46833256475225	4.97524141553803
H	14.56259502168291	-0.94183982762605	4.95578839054842
H	14.03121903592341	0.52949158015362	5.75314644193475
H	10.24675758900199	5.15331897722680	6.51951193335086
N	9.21403005780500	5.85601264578846	4.37451757413902
N	8.82798354183663	2.53666540931597	2.40233935338169
N	11.71630749544414	2.71874651732394	2.05306500993639
C	11.29613334398799	2.73485599323523	0.73556110562374
C	8.79775862187749	2.92756080513909	1.09412927180132
C	7.53718577425723	2.29338974773166	2.82481913343592
C	13.03587441589941	2.31829788737939	2.08276589659673
C	7.47402920126790	2.95582983731676	0.66536120978071
H	7.14369697057190	3.03969449717941	-0.35185792719028
C	7.17670270772162	1.54979031747497	4.07296996906234
C	12.34511195980884	2.32980894618596	-0.05097151687621
H	12.34577928520097	2.25297516056136	-1.11912852630864
C	7.32316727735292	0.02472413113935	3.78216820040863
H	8.37821702464587	-0.19783391809842	3.77857180170275
H	6.90710475627649	-0.49826740503057	4.64063837758326
C	9.98880049328462	3.30487299783635	0.26204125002022
C	6.67452192208019	2.55732412907080	1.77865296681164
H	5.62478588536491	2.35232788224355	1.75342419132838
C	10.04840540263188	4.85965659044428	0.25218365737674
H	9.07198137669846	5.22605340409772	-0.05524642035000
C	13.43354321291738	2.06535128996683	0.79406420079335
H	14.40677272864291	1.73713327960934	0.48832825767128
C	5.69126580559764	1.79835092946435	4.41061034481942
H	5.08154810138490	1.45393363871890	3.58166962781536
H	5.43907346544532	1.14493978600686	5.23936557956758
C	9.72655496859708	2.83584462016717	-1.18160106922434
H	8.87330760947750	3.39317208678789	-1.56069497866356
H	10.56277377032343	3.14748342639082	-1.79626479147514
C	9.49733850808630	1.34804969696959	-1.35762176223848
H	8.61886521525782	1.01009327105040	-0.81792565050665
H	10.34542009492679	0.77698321971424	-0.99805101766281
H	9.35277680455800	1.10445391838004	-2.40576152954388
C	5.30383043116034	3.21828607399082	4.76153614884783
H	5.87784714119976	3.57947217839600	5.60837370096508
H	4.25358688564014	3.26923745899670	5.03102263949192
H	5.45571163023158	3.89581119283899	3.92728039910890
C	11.12539404631005	5.48461355739005	-0.60730465800543
H	12.10566175064094	5.07200061780891	-0.39493429516431
H	11.16439746789964	6.55568323482720	-0.43439701502225
H	10.93066637423111	5.33924909827444	-1.66464885303423
C	6.70998060270127	-0.50504575802088	2.50209783360354
H	5.65580807922914	-0.26523974632644	2.40886339798062
H	6.79506465254371	-1.58776654759397	2.47342746610441
H	10.15818294278110	5.18807509383850	1.28246943782956
H	7.21038500282285	-0.11327461063720	1.62260736471472
C	8.01379294012231	5.09304063273527	4.69477041511864

H	7.93075396410584	4.22707037822354	4.06990301721847
H	7.16145315379809	5.72629594884289	4.50263504466761
H	8.03687298741438	4.79977248560009	5.73739702387510
C	11.01067819108619	7.49491726193800	2.71708669062745
H	11.65970390629826	7.58923857026563	1.85534518865626
H	11.08698236268460	8.42367136899367	3.27102903713715
C	8.98849638893778	7.24848805565450	4.78210469648830
C	11.45701749693030	6.27039839643057	3.55761306219283
C	12.55277113664499	5.56537302166902	2.77258036949488
H	13.36776278528282	6.26671676753000	2.62946132142597
H	12.23038892652446	5.23145780702307	1.79936639700594
H	12.94846498870478	4.72551611770613	3.31820890684820
C	12.12415712716344	6.66372489330664	4.88813955976135
H	12.51633135141019	5.78388325704784	5.38528234688148
H	11.47122513543200	7.17160376079385	5.58513384331090
H	12.95874875402192	7.32176965647413	4.66829826466013
H	8.61101487529513	7.21693287603072	5.79845855554867
H	8.22836107824296	7.66246003057040	4.13153512631873
H	9.87311027346778	7.84573082730691	4.75017303083598
H	9.99582810420865	7.41189266882197	2.34456369206766
O	10.58609269008335	0.55923480730364	3.65358660603081
C	10.59973363145871	-0.22796969210662	2.44630381546515
C	10.75357901364515	-0.27211704012507	4.82362518461500
C	11.11519975369874	-1.64161251745140	4.28926056013760
H	9.81971411032717	-0.26658184203795	5.37724293288351
H	11.52065023581054	0.17918731816011	5.43883175128469
C	10.46882198227939	-1.66230111560393	2.90921092951427
H	11.53143709803687	-0.03816076736996	1.92101290346140
H	9.77869932183381	0.11064180940957	1.82667083411777
H	10.95244092038350	-2.35204940526444	2.22785121016669
H	9.42394286707189	-1.94618318535305	2.98326548178342
H	10.75525681370348	-2.43422148109099	4.93421685265529
H	12.19183541890137	-1.74486145852967	4.20466572586499
Cu	6.80958152162925	4.72496989150370	1.52616266187255
Cl	6.95761140654733	6.84045994245042	1.93207780622808
O	4.35821432029578	4.55049146706652	1.04768569319475
C	3.64098738133113	5.58267164656359	1.73129371640693
C	4.10779078402170	4.75072963284975	-0.33766843709195
C	4.19266109198454	6.24944154443724	-0.52048964506586
H	3.11612068840463	4.36816568917525	-0.59308482599902
H	4.85005181308795	4.18518982595764	-0.88981473351239
C	3.57965139783055	6.78024833109643	0.77927042133001
H	4.18003087304168	5.79085009608072	2.64670127813703
H	2.64574280581087	5.21384266568512	1.97887884642733
H	4.14940932598780	7.61567236625081	1.16402211992705
H	2.55446963324363	7.10317758547510	0.63270597292011
H	3.67429770124949	6.59534364103400	-1.40763614416999
H	5.23281386313103	6.54852440977670	-0.58790365370894

127

Coordinates from ORCA-job INT3_cucl_tbu_aaac_thf_sncxet_cmp_Compound_1

Sn	10.55717225009614	2.97846500367469	3.71759569538821
C	10.42099867176015	5.35510374208170	3.92120918042396
N	12.14386260353663	2.68386025254410	5.05238553278053
N	9.24846335587488	2.48770260624011	5.28516486906846
C	9.63636245562420	2.44087562053727	6.61319408704806
C	12.06890760170885	3.14853400765834	6.34964744282494
C	13.46756650673555	2.73269837183011	4.65491179349692
C	8.00934027231014	1.89105729177290	5.17738097917683
C	13.33199034394135	3.48922575367969	6.76106808806355
H	13.60679296026119	3.84322765453242	7.73541597702972
C	13.95960460683211	2.04887976121496	3.41614099857428
C	8.64545167864113	1.81065406603632	7.32417259766748
H	8.63814562250768	1.63309253605495	8.37999029942785
C	13.93070792525833	0.51271421742536	3.66649809750402
H	12.89914860797560	0.20466812541491	3.61097043542049
H	14.43333379422336	0.04298965595697	2.82291797516516
C	10.82782126665056	3.14414368149074	7.20287676133921
C	14.21198354205075	3.22416704812140	5.69602925998311
H	15.27755150407992	3.33314065991969	5.71834538361231
C	10.46620463877151	4.62244339182632	7.51509405182887
H	11.35878441105073	5.09665818988647	7.91811791389822
C	7.62695829641292	1.46597495267669	6.42532849081638
H	6.71131807764496	0.96560275158315	6.67056340831312
C	15.42760884546873	2.43316616679690	3.15523779751229
H	16.00842320926130	2.15983333063149	4.03062413264828
H	15.79321833411223	1.79304066449156	2.35768472608325
C	11.20060292440896	2.45414345517959	8.53410740384860
H	11.97192612884691	3.05591296810467	9.00704691870069
H	10.35015821180120	2.48948753509186	9.20649235265143
C	11.67972363535394	1.02412456733719	8.40041555040143
H	12.56127782662322	0.96256092548825	7.77040299448744
H	10.91170072056403	0.39300121774068	7.96689388630702
H	11.93853438741862	0.61288898920081	9.37127229877831
C	15.70548396189555	3.87777423961235	2.79689222617966
H	15.14965966424741	4.17723316038249	1.91503921352934
H	16.76154578544272	4.01572095599575	2.58477941024612
H	15.44114460777810	4.55205254074429	3.60263394589563
C	9.29493670447255	4.86239390305219	8.44561776560561
H	8.39230964558422	4.37812493616977	8.08870549989302
H	9.09496728283886	5.92700046145344	8.53055469437257
H	9.48591994233983	4.49493108424365	9.44812300969802
C	14.51933359557190	0.02221814889008	4.97226063486447
H	15.55594859231896	0.31616177611681	5.10026936786565
H	14.48643474545038	-1.06336607775577	5.01216028150552
H	13.96805539106164	0.40451934920033	5.82463716506548
H	10.27679578686102	5.11819726675492	6.56975967756122
N	9.34575125492653	5.88995495886230	4.40477721737513
N	8.94958061416453	2.63406071742070	2.33122679527404
N	11.85289520620994	2.74539095496342	2.09461164057964

C	11.47904531272215	2.79015258761227	0.76373329827320
C	8.98130595690124	3.06682283261643	1.03623619010121
C	7.63918085229627	2.41204649761809	2.69845845247548
C	13.15616923652725	2.29865230656564	2.16334340306238
C	7.67307161431782	3.14294026917251	0.55735014715837
H	7.37974506320819	3.25903676271939	-0.46786250133369
C	7.21194461763529	1.65449401554461	3.91843035568077
C	12.53986569983384	2.35953582481078	0.00768115994852
H	12.57542544085084	2.29796442421819	-1.06084395988079
C	7.31971029516584	0.13252951031190	3.59684701645174
H	8.36711863216131	-0.12241005810841	3.61577964158437
H	6.86593162092817	-0.39487089220729	4.43280573263327
C	10.21337589128345	3.41784065021348	0.25390329985700
C	6.82359839321548	2.74142228908847	1.63355750130377
H	5.76998229267720	2.56435381973280	1.56746637422923
C	10.33420656905039	4.96930598103690	0.27500888500103
H	9.38894722570979	5.37934190731784	-0.07451053134867
C	13.58880651976564	2.04803185279171	0.88558478234673
H	14.56024238396408	1.69026300364400	0.60883008122399
C	5.72522445182574	1.94401847052498	4.21314978289339
H	5.13476212214549	1.64856606930715	3.35186662106542
H	5.42052391025365	1.27261956664191	5.00924862770513
C	9.98510016662159	2.98607609055073	-1.20702028112563
H	9.16929948894469	3.58381581181837	-1.60624884031118
H	10.85571363444318	3.27536179507015	-1.78348745483582
C	9.70331635434283	1.51233792550135	-1.42054972075881
H	8.79536937567583	1.19942676791523	-0.91553849557156
H	10.51590437734664	0.90006707871469	-1.04744171800735
H	9.58097473816260	1.29624612485283	-2.47728027765950
C	5.37530675080551	3.36415625550358	4.60023096715475
H	5.91366357858291	3.66625441920187	5.49231472311371
H	4.31471902383313	3.44867280734929	4.81426102896675
H	5.60187274681792	4.06843136224231	3.80675400078805
C	11.47203717131456	5.56564063842138	-0.52419371926899
H	12.42535233643196	5.11201232379825	-0.27656218140020
H	11.54358947100288	6.63128005154313	-0.32992966809767
H	11.31871373970869	5.44545792821089	-1.59127825172910
C	6.72320578270791	-0.35101320126861	2.29097604545998
H	5.67838336708022	-0.08008561043082	2.17885575856402
H	6.77802630807274	-1.43469643794708	2.23990280811961
H	10.40860825903474	5.27746729089247	1.31486116242750
H	7.25564691328922	0.04445223937361	1.43216501713666
C	8.11478637128666	5.15627764524121	4.67201789498981
H	8.03376478950878	4.29451066086426	4.04210165424687
H	7.28721604317928	5.81238196321507	4.45048175126881
H	8.08979236750906	4.85599455045476	5.71266214784555
C	11.23445284890162	7.51461949791354	2.84109296765905
H	11.90491128888188	7.60246338735872	1.99525395134752
H	11.32565628347363	8.43148783320529	3.41219411853620
C	9.14046790563684	7.28152919049008	4.82869267255118

C	11.62369023865486	6.26410379092235	3.67221829214693
C	12.73242783613794	5.55076062339494	2.91321464094297
H	13.56316764181110	6.24016506051259	2.80661645182770
H	12.43671038159778	5.23706738444419	1.92514773413245
H	13.09758248166198	4.69608128061091	3.45754434619751
C	12.25277876160817	6.61744829653816	5.03280085700792
H	12.60897747485573	5.71976945294279	5.52526282489658
H	11.58891035163451	7.12676506519969	5.71814863876130
H	13.10842784757695	7.26050974597405	4.85358905170193
H	8.71742702268563	7.24312032527334	5.82650566396741
H	8.42044608563079	7.72916134253347	4.15494249854037
H	10.04210280655559	7.85336760463414	4.84792122646551
H	10.22651966851621	7.47021643681152	2.44413681572372
O	10.60269473246262	0.58161811180769	3.59892774609111
C	10.62394536477141	-0.18278540929022	2.37631220336709
C	10.70106046015346	-0.27753620061068	4.75703138230554
C	11.04452064217497	-1.64492094548464	4.20679411565286
H	9.74719399054766	-0.25550591792042	5.27499201054423
H	11.45761063583272	0.13809722923968	5.40946026018856
C	10.44238070503085	-1.62202673285301	2.80706785309070
H	11.57253368380005	-0.00723561909178	1.87722585779641
H	9.82749227738088	0.19041690551556	1.74435428430283
H	10.92949024544065	-2.31075278866925	2.12731128050676
H	9.38890630353669	-1.88040573853838	2.84261411587428
H	10.64353163792755	-2.44002105493106	4.82377026856277
H	12.12025677974722	-1.77464196263165	4.15434449191838
Cu	7.20523515904638	4.92763137187626	1.42284266865304
Cl	7.08997519920137	6.98901072222819	1.93634407120621

127

Coordinates from ORCA-job TS4_cucl_migration_optTS

Sn	10.53227041264837	2.94266853218986	3.65021065253010
C	10.23917483239800	5.59247941604930	3.83328457229338
N	12.08820566139822	2.74752734179940	5.02942632948134
N	9.18208203346826	2.52230347505422	5.20521133949745
C	9.54676290383629	2.40376676504120	6.53812317918820
C	11.98535171266128	3.11528439539339	6.35514599784716
C	13.42100722442659	2.83359142465701	4.65741084655886
C	7.95994131392211	1.90049431234242	5.03743964363936
C	13.23775864275245	3.43606687940448	6.81051369397928
H	13.49216366236898	3.72790892241026	7.81044203847103
C	13.97616660425812	2.18658260897398	3.42566017211522
C	8.55195779498101	1.72041421697909	7.19062940779963
H	8.52731409949982	1.48567238936835	8.23508800349387
C	14.15161527068291	0.66502002207701	3.71731608448286
H	13.15969662690127	0.23396779954033	3.76259669146169
H	14.63071005802119	0.22762108237678	2.84415599413168
C	10.73227829055715	3.06008201210591	7.18867397186141
C	14.13819642089206	3.25770590414707	5.74655893500846
H	15.20172114729902	3.37504932665305	5.79755988553226

C	10.37766626831612	4.51640765517098	7.58681894613449
H	11.26143811696321	4.94617593260801	8.05426018477539
C	7.56026629916103	1.40387040359038	6.25147719478949
H	6.64620141081420	0.87821034443793	6.44578090909187
C	15.36751133749095	2.77692065593047	3.12145655499679
H	16.01078570187423	2.62721976530749	3.98248426724073
H	15.80658885320139	2.18594323779897	2.32282305714395
C	11.08275402958848	2.29479424526779	8.48564089913129
H	11.84554929347287	2.87091195121103	9.00220734688026
H	10.22177647108794	2.29835505617861	9.14532706371600
C	11.56615320932019	0.87288190465666	8.29855092714511
H	12.44987355650695	0.83762672925334	7.66910917645502
H	10.80115500937255	0.25265479175922	7.84486434908465
H	11.82639463479996	0.42913156223728	9.25467403570657
C	15.36774539790788	4.23866664468566	2.73217458200049
H	14.78489804757166	4.40096349030240	1.83182073179744
H	16.37816282286151	4.58757369538304	2.54238562945619
H	14.94480078727926	4.85503998388568	3.51803136098266
C	9.17721192603010	4.71346208326481	8.48883054851446
H	8.27642481434625	4.28754954531096	8.06021246222782
H	9.00378288606432	5.77300493243018	8.65601747685952
H	9.31786213823809	4.26063422214703	9.46458734394366
C	14.91435238667571	0.27625230347363	4.96624517962162
H	15.91636313807748	0.69221734936305	4.98665522888415
H	15.01641500288807	-0.80459846056087	5.01252870126417
H	14.40794964708589	0.60162171594040	5.86751970453674
H	10.23339323949355	5.06601280879675	6.66753044728226
N	9.30739959374649	5.92214029893630	4.70257987851488
N	8.97511384679230	2.58720277816079	2.23488191324562
N	11.86993646572454	2.79778216143280	2.04714237817986
C	11.48131697455210	2.67226365301425	0.72124494958503
C	9.08680126857142	3.38454849811509	1.08830948627511
C	7.65825731258557	2.55452884694129	2.60185503804980
C	13.14519957246953	2.28214048159442	2.17109663635354
C	7.79666140898432	3.80267530640541	0.74566285260846
H	7.52740324863399	4.34719898048538	-0.13767044620044
C	7.18687223527032	1.71968286343864	3.75125813049973
C	12.50617585570604	2.07983578618716	0.03096261467673
H	12.52224908586500	1.87862442535929	-1.02134768021258
C	7.34086727642889	0.22916999637196	3.33404603718386
H	8.39632556969451	0.05948837054755	3.17487258651456
H	7.05643019757384	-0.37439807229195	4.19237184094015
C	10.24238281931394	3.26120286207928	0.11363201021825
C	6.91023587326046	3.27505370734395	1.69591471952129
H	5.84987698743939	3.41866172910699	1.71207143989250
C	10.52526789655435	4.67047781535012	-0.46827252794680
H	9.60467502796920	5.03206194661388	-0.92212946853499
C	13.54920083058144	1.83762199185299	0.93740796990873
H	14.50126650519267	1.40257749871674	0.70550384204208
C	5.69280196286629	1.97759150062949	4.01853511158316

H	5.15063249068035	1.82790594539839	3.09010629170186
H	5.34348493503126	1.19305957402902	4.68455409391889
C	9.76833622816206	2.38192107788064	-1.06642116772878
H	8.95199277602027	2.91454381181962	-1.54828115967316
H	10.56354018340402	2.32711347670976	-1.80272618222718
C	9.32098862871580	0.98460402840070	-0.70941781883095
H	8.55361282495262	0.99587876493164	0.05806858200702
H	10.15284884842078	0.39171339460518	-0.34855459073624
H	8.90940852751485	0.48073050152846	-1.57812744062716
C	5.32635901937310	3.32579227792394	4.60203374440151
H	5.81944075752574	3.48961039384105	5.55362476711911
H	4.25596021349162	3.38454760601026	4.77195722335876
H	5.59238144690597	4.14082267498253	3.93839088973972
C	11.65916192253190	4.79978924405689	-1.46183382386205
H	12.60791004812199	4.51957245203094	-1.02036510532748
H	11.73528194825844	5.82978115213038	-1.79514796774474
H	11.50897328049016	4.18733230301105	-2.34476735623314
C	6.56163416905405	-0.21115131106865	2.11215426052255
H	5.49161112893357	-0.22019961387093	2.28906297698155
H	6.84705849435107	-1.21965663995693	1.82794276787298
H	10.72731295520416	5.34294965971988	0.36064223123331
H	6.74810366602850	0.43427166714894	1.26040065767102
C	8.01444099617405	5.26435544745347	4.72618049603236
H	7.97399197968483	4.46188841436960	4.01245675084200
H	7.26578297339727	5.99922484744121	4.44817628465611
H	7.81010256003225	4.87925189876130	5.71820930560105
C	11.24706357858932	7.98239424246664	3.60862094067261
H	12.12263801019832	8.41855507384241	3.13863431601311
H	11.13243640615684	8.48171328140936	4.55974470021569
C	9.26270247431462	7.11400726454967	5.54387730287706
C	11.49643851155246	6.46679539031501	3.72116937124221
C	12.25134582216331	6.09274476192770	2.45008376510482
H	13.22740220587497	6.56547648444249	2.46926743139194
H	11.73118170336515	6.46868974096843	1.57703861679977
H	12.40052707818259	5.02946480316318	2.34192453089390
C	12.42368971390847	6.18496092232325	4.90433307887124
H	12.80218012308407	5.17496287562586	4.88954636349526
H	11.96050730347754	6.35263264679149	5.86834583667997
H	13.27724382897578	6.85235951534349	4.82651201715514
H	8.60444138704688	6.90376292278322	6.37615354959676
H	8.85509266656889	7.93816884403595	4.96828522665883
H	10.23354151317470	7.36868324662807	5.92554757883388
H	10.39049116548411	8.20375831925306	2.98578973612415
O	10.70937631608139	0.60211271208927	3.62371704378504
C	10.80087447671426	-0.22516908832162	2.44321963774082
C	10.72976585311135	-0.20426732521543	4.82434992869105
C	11.14305554113038	-1.58160629282255	4.36089540236236
H	9.73540393094549	-0.18569555523827	5.26066078026743
H	11.42388956270296	0.25734745438455	5.51121948518731
C	10.59755582724557	-1.63778868326329	2.94111698110226

H	11.77590441873416	-0.06719699826437	1.99325046915335
H	10.03933485914434	0.10864697930047	1.75490056684275
H	11.10470070947778	-2.36415802896508	2.31761571951327
H	9.54063932824428	-1.88727596482320	2.95456278078693
H	10.74287400771705	-2.35945650148181	4.99990305448084
H	12.22442967566062	-1.67460851909807	4.35650816439595
Cu	9.15655415269227	5.34988601577307	1.99073487444626
Cl	8.25822989057865	7.33176760800278	1.83480097601412

127

Coordinates from ORCA-job INT4_tbu_aaac_cucl_thf_sncxet_cmp_Compound_1

Sn	10.52571404198826	2.72870011522738	3.58916133127506
C	10.19246863764543	6.08037359906576	3.88059813915011
N	12.06673413163765	2.67471842976541	4.98599594824012
N	9.13788784829346	2.40774451546458	5.14982754956938
C	9.54557110724209	2.23789838594788	6.46511374995251
C	11.93244258058474	3.09469947651368	6.29152112256949
C	13.39186753883261	2.83507034524702	4.60702306736057
C	7.98445783892615	1.66918338283155	4.96457226329301
C	13.15821068683308	3.51937174043927	6.73362230435206
H	13.38717282621744	3.87447712623558	7.71942912531099
C	13.99118071764092	2.14092109986988	3.41773329866478
C	8.63639692866129	1.42721712190220	7.09429055439780
H	8.65444808683048	1.13449694560652	8.12443454513315
C	14.21300891714845	0.64524981974783	3.79358372535695
H	13.23619823692522	0.17665076458126	3.82680592983700
H	14.73822303173876	0.18326880502772	2.96023416083540
C	10.66859632673649	3.00159933704100	7.10650792232688
C	14.07288064240563	3.35747806219875	5.67639915455603
H	15.12673485980557	3.54559773273972	5.72251769941804
C	10.19170024221880	4.44773321229959	7.39867632546235
H	11.02139414333315	4.97985804608632	7.86038105050926
C	7.65908376744203	1.06628906833335	6.15152748071793
H	6.79499423345576	0.45620824455842	6.33071070504802
C	15.35983235059953	2.76755866213682	3.09144932676367
H	16.01004762757148	2.67992378350628	3.95685682164456
H	15.81730160857232	2.15986728296243	2.31552096408266
C	11.03763670505587	2.33767092200414	8.44952664537417
H	11.73172738175625	3.00282742669644	8.95652669161524
H	10.15568178459889	2.30002168792725	9.08046207017306
C	11.64755987002919	0.95495261127025	8.35074813992900
H	12.56091811728780	0.96975385048465	7.76495689706906
H	10.96328637164249	0.25146742528933	7.89007842490293
H	11.89535242590006	0.57528604681995	9.33730277491555
C	15.30135964720934	4.21031856056779	2.63797640841974
H	14.68486686073069	4.31438458540485	1.75080412109793
H	16.29329775013116	4.58188493809844	2.39995936535563
H	14.88179706228856	4.84799070766806	3.40822399815824
C	8.94639611703718	4.58628309764397	8.24967155071584
H	8.10634109770760	4.05392478715250	7.81560009070896

H	8.66836974204493	5.63196578872677	8.35130404997347
H	9.08999945154914	4.20304502974614	9.25436766059017
C	14.94564193483834	0.35490283086405	5.08653634996508
H	15.92702970740745	0.81696604473421	5.11826353066894
H	15.09235967004251	-0.71604285150260	5.19642251838314
H	14.39303815267214	0.70702642856956	5.94996252844840
H	10.02925709823312	4.92246561302444	6.44003015704027
N	9.27981458307815	6.38299812346134	4.75994490835443
N	8.96246557053587	2.35601654795209	2.18455483029734
N	11.90904742781252	2.67483377297476	2.01664835398536
C	11.49656705230070	2.48953273856770	0.70866824403282
C	9.15495216992315	3.30726238456840	1.14517286491400
C	7.67383641385173	2.43796324116708	2.58560723690740
C	13.17103626864360	2.14299550714938	2.15464122165925
C	7.90667998233247	3.88183139680776	0.88769981818745
H	7.69598399254761	4.59833589367744	0.12047519029862
C	7.16071146515806	1.58386637263820	3.70244295429955
C	12.49856809156153	1.84284753067180	0.03368839746246
H	12.49993856177277	1.59342705541955	-1.00887808474704
C	7.18615677859026	0.11077639460918	3.21746933184613
H	8.21921425536518	-0.13522021891472	2.99778414224972
H	6.89122010250818	-0.51636727151203	4.05503555875588
C	10.27567947629006	3.14234092073333	0.13044973471208
C	6.98951668722482	3.34222718143699	1.78832648008138
H	5.94977744670267	3.59008724232236	1.85056749400991
C	10.64992193215363	4.55018307360513	-0.39317864181009
H	9.73737755680206	5.07122155146655	-0.66912600371570
C	13.55300918153580	1.62581452329792	0.94203812857837
H	14.49786124056503	1.16966823202596	0.71832345783383
C	5.70626523927721	1.96043158068351	4.04387254891227
H	5.11192616493039	1.92512203295990	3.13513953388388
H	5.31386815072077	1.17282187611752	4.68243458360895
C	9.73558237599527	2.32554255461864	-1.05875392299414
H	8.97441433814887	2.93444713220276	-1.54255867933853
H	10.53341676565076	2.20746406175941	-1.78507456607940
C	9.16702097731274	0.96617694917513	-0.72403509717807
H	8.35008766902154	1.03251569551715	-0.01376904375862
H	9.93118930201232	0.32351518860988	-0.30204257245527
H	8.78688558092764	0.48065079111868	-1.61738386596166
C	5.51035966185534	3.29723892261707	4.72897311451759
H	6.10758003118606	3.36346355544710	5.63228204345781
H	4.47011204112806	3.43222349577478	5.00750450282279
H	5.78288839957010	4.12468938732498	4.08439369190279
C	11.63058519184911	4.61419069655852	-1.54382119398309
H	12.55977327914387	4.10816606979144	-1.30751931871128
H	11.86400424312151	5.65116870030189	-1.76259684670429
H	11.23096827811051	4.17853480329995	-2.45359381470267
C	6.32117412685126	-0.19795369005892	2.01234936106768
H	5.26325602835492	-0.12083910687463	2.23848000691245
H	6.50215617443433	-1.21056929083815	1.66562304293040

H	11.06445584256301	5.10924307143269	0.43947987619489
H	6.53142231536487	0.47329792027228	1.18609989937794
C	7.98367296761306	5.72178215741428	4.72482808536312
H	8.06534258289019	4.77891083337009	4.20674973163489
H	7.27301347003565	6.35322930896896	4.20110003503661
H	7.64037770666597	5.53623090570795	5.73493836309439
C	11.37702942617417	8.33049225690675	3.65731956519337
H	12.33889775524487	8.72948731693079	3.35010561391226
H	11.10182794113703	8.84392350639788	4.56742497027090
C	9.29204779374679	7.48500663937505	5.71671201979745
C	11.52082636183736	6.81050885153935	3.80835200380446
C	12.27532336995723	6.32755488569724	2.57217895921431
H	13.27499647135637	6.74948617685624	2.57304161219307
H	11.77469674787943	6.65212896083921	1.66776321929519
H	12.37640313945747	5.24785883322774	2.55793852351996
C	12.36851537228107	6.42991237130509	5.02196306238523
H	12.58258251726049	5.37008505053669	5.02762669552397
H	11.91694937877298	6.67893801184290	5.97429637869214
H	13.31844175749963	6.95263717545367	4.95830845682046
H	8.75960978893309	7.16879540434048	6.60390703940979
H	8.78429281227952	8.34457707886475	5.29158868932228
H	10.29186212260107	7.75616615034071	5.99480118217834
H	10.65129119973855	8.56697181474679	2.88814085314868
O	10.73446119689118	0.45181601271680	3.61162083080090
C	10.83434183685505	-0.38495190673618	2.43472735475018
C	10.76287699382406	-0.34726521000091	4.82083549587777
C	11.20001042776029	-1.71704459660039	4.36090754307152
H	9.76378179624432	-0.34291172503324	5.24364471186798
H	11.44478622220377	0.13274766745436	5.50859178968823
C	10.63534157549062	-1.79053190767047	2.94942958728573
H	11.81259118980106	-0.22584970889294	1.99274361745618
H	10.07420401719100	-0.05656456219064	1.74181777377818
H	11.13444635778504	-2.52346104052297	2.32717327392185
H	9.57813334111831	-2.03834722208851	2.97972093100601
H	10.82453531598643	-2.49881189483064	5.01003613958637
H	12.28319808976821	-1.78711362799560	4.34059384336778
Cu	9.58773200373725	5.05140693880199	2.36516702451470
Cl	8.79880662973867	7.00793486446085	1.46288488196510

115

Coordinates from ORCA-job thf2_sn4_cxet_CREST_cmp_Compound_1

Sn	-0.00083454008234	-0.00845988037622	0.00083125516421
O	-0.09642637183627	-0.00264563257564	-2.21002059644898
O	0.09668989820246	-0.01503355866280	2.21142301883382
N	-1.44591054796367	1.49446010126110	0.07916327601174
N	-1.50380171315407	-1.45510399241903	0.04888348213453
C	-2.82361029677310	-1.08302095899454	0.24937041571448
C	-2.67128270630851	1.31817839582361	-0.52685060198271
C	-1.08015538364631	2.82231407686767	-0.07376028216780
C	-1.29726970656361	-2.65491470936263	0.69525133637319

C	-3.07874615750426	2.51980586091874	-1.04550043541468
H	-4.01287452711581	2.71156600106449	-1.53692644798525
C	0.07157045059120	3.42210306008851	0.67132406999334
C	-3.43538300918172	-2.05311323892783	0.99860624190043
H	-4.46939865102428	-2.08041292803141	1.27850911565012
C	-0.31581522867353	3.53149907850531	2.17099495816214
H	-0.38187435306210	2.51915625143779	2.55868565690561
H	0.51741357547995	4.00072504569139	2.69090671555019
C	-3.46011081589846	0.03828406753632	-0.51154530335756
C	-0.30474314921866	1.18794872240512	-3.02047099745980
H	0.61068836514273	1.77014314599781	-2.98893483883991
H	-1.11143301463076	1.75273610054004	-2.57513419522021
C	-2.07900114807113	3.46849942322434	-0.75305525622125
H	-2.11625321069001	4.51469272675914	-0.98193459662997
C	-3.64596951265999	-0.41078190102209	-1.98628916022264
H	-4.13566686248086	0.40338361477702	-2.51737484697903
C	1.32265160734787	0.15013852080004	2.97817562483927
H	1.86932800848991	0.97897105827671	2.55116561907069
H	1.90050772750179	-0.76237695352944	2.87231523761424
C	-2.47248318057384	-3.04060685820493	1.28606566152684
H	-2.63960140242743	-3.95390973869452	1.82347624392368
C	0.36161160210556	4.83264383954048	0.12380339991442
H	-0.53823730825050	5.43575161830069	0.19676829851477
H	1.08616677426996	5.29787558497670	0.78752239192029
C	-4.84089636847011	0.35400163890259	0.09489823831552
H	-5.34110741776577	1.04850958473422	-0.57554176995940
H	-5.44563330989520	-0.54767408289461	0.09401348715401
C	0.83911869517999	0.37837828850374	4.38818259395615
H	0.62312783831724	1.43135458750762	4.54356148902706
H	1.57399831738205	0.07138786087271	5.12216329438289
C	-4.79909800619412	0.94329277040474	1.49022984439808
H	-4.25354548693816	1.88131322115038	1.49958210521532
H	-4.31564339737428	0.26984618268308	2.18945876797415
H	-5.80216975626130	1.13911275422002	1.85650485688109
C	0.88798013657520	4.86437128602694	-1.29678756780310
H	1.81983039772612	4.31420058183163	-1.37819329662650
H	1.07644897503883	5.88498281796686	-1.61542065100402
H	0.18004879199364	4.42520256160960	-1.99102148858996
C	-4.40300881030311	-1.70409613041059	-2.20289481465045
H	-3.90828959706956	-2.53873968987951	-1.71847700060546
H	-4.47355984717784	-1.92613632111132	-3.26370298841133
H	-5.41620591409704	-1.65586787701710	-1.81741481000636
C	-1.60335204631564	4.26641769791623	2.47923500943517
H	-1.57874145514419	5.29714440328277	2.14088923185171
H	-1.77941966583200	4.28458328366879	3.55082190352864
H	-2.45509605106512	3.78820476844725	2.00819971893210
C	-0.60547356684331	0.64234298959361	-4.39378561773828
H	-1.66455128403208	0.41927970823314	-4.48386979932488
H	-2.65456267836152	-0.50125060887442	-2.42058290857624
C	0.03863847922266	-1.19029876103325	-3.04038947438758

H	-0.86991634204676	-1.77315877497478	-2.92828962487340
H	0.88231027137424	-1.75603495496954	-2.67114649453078
C	0.21413103254076	-0.63969060198569	-4.43327212927430
H	1.26073053327180	-0.41612407359966	-4.61802716292958
C	-1.05332210676560	-0.19252894489750	3.08531932682309
H	-1.63759865385173	-1.01501472713256	2.69777359007174
H	-1.63744247415713	0.72142370384964	3.04778587920492
C	-0.44217285469780	-0.44161744322819	4.44125917172890
H	-0.21363971364716	-1.49660767259096	4.56064902289531
H	-1.10607796777628	-0.14591012715763	5.24427084463070
N	1.44506686027216	-1.51180371953918	-0.05295136903968
N	1.50023441096032	1.43865683884757	-0.07172860380090
C	2.83286493365771	1.06725747010491	0.00893273322768
C	2.61531513624259	-1.33205989182296	-0.75896440717191
C	1.06735197642369	-2.83890756576649	-0.18191461912105
C	1.35113741847644	2.63627884091267	0.59415805561209
C	2.97720698850843	-2.53081964417879	-1.31657260295464
H	3.86623120210266	-2.71978579609487	-1.88644714495951
C	-0.01843545728085	-3.44446726535267	0.65235799065241
C	3.50834200655458	2.03558719482447	0.70371270648381
H	4.56327697650228	2.06332714375699	0.88978852766337
C	0.49604931902521	-3.57435097164958	2.11162776232739
H	0.60546952996977	-2.56707555586195	2.50309464464622
H	-0.29355858045098	-4.04183900927002	2.69698243875022
C	3.39962956395032	-0.05022491536184	-0.81042113832028
C	2.00526238029104	-3.48114641414758	-0.94647673928513
H	2.02270577502308	-4.52597278417869	-1.18373341514448
C	3.44844912061070	0.40364304133547	-2.29467214019218
H	3.89473437975795	-0.40537965413620	-2.87000364865190
C	2.57404576430220	3.02096863483321	1.07942460251971
H	2.78742300582642	3.93238660714336	1.60347289862174
C	-0.36015795715117	-4.84708828918800	0.11362978441109
H	0.54070637633688	-5.45281951692029	0.09787263820552
H	-1.02442731369004	-5.32018194057779	0.83262301882354
C	4.83080004729449	-0.36447067730382	-0.33467959754690
H	5.26680293383330	-1.05891524606243	-1.04853828660303
H	5.43225693174117	0.53759100071334	-0.39238081899807
C	4.91976584678248	-0.95365624904038	1.05856398734581
H	4.36779213196804	-1.88588862328680	1.12202566172918
H	4.51493446091575	-0.27561615497411	1.80176898394750
H	5.95184168069547	-1.16039505168428	1.32458542258815
C	-1.01026976664568	-4.85744726211947	-1.25500440218450
H	-1.94556500736790	-4.30719912582363	-1.24500944161569
H	-1.22619745486519	-5.87314788389165	-1.57184729607292
H	-0.36625960039222	-4.40640536184994	-2.00196893615959
C	4.17230114561390	1.70370457013848	-2.57526423241305
H	3.71559683885147	2.53361448225133	-2.04737296259605
H	4.14656642816285	1.92734664017665	-3.63778823752387
H	5.21607923042030	1.66405817438985	-2.28124885057815
C	1.79748426896209	-4.32506277527825	2.29957420181992

H	1.73140697171511	-5.35252205754564	1.95684413443260
H	2.06685597486791	-4.35443816375809	3.35131911203656
H	2.60987943048410	-3.85185865770773	1.75911808461531
H	2.42122539154088	0.48648276843422	-2.63723536039166
H	-0.33955262398473	1.34410323144512	-5.17471732632833
H	-0.12158804549494	-1.33864598397469	-5.18942872460952

25

Coordinates from ORCA-job tbu_aaac_cucl_cmp_Compound_1

Cu	4.09204436136008	5.28927887964694	2.32817216389025
Cl	6.10926996913963	4.99776995256317	2.84318968563102
C	2.27487174736945	5.56342722775421	1.85366846567833
N	1.87651240630191	6.71041941894551	1.35859611137578
C	1.28774354937352	4.42003020062282	2.05428993366809
C	0.72950210448225	3.91941984302247	0.71882014281671
H	0.07661090293972	4.61667421321560	0.21133535499573
H	0.16229746498125	3.00956015645192	0.89008284130151
H	1.54167332326195	3.67424311191750	0.04133515196312
C	0.18906356897778	4.78634221830214	3.05681542223891
C	2.05530067977060	3.24679334986095	2.66794112259338
H	-0.49952395794193	5.54820848023193	2.71724777556877
H	0.63258530161950	5.13052408838161	3.98614469781845
H	-0.39344987565693	3.89866052712530	3.28380094823897
H	2.86241518434245	2.91893941444116	2.02061985501627
H	1.38472743289823	2.40648487806889	2.82499487515293
H	2.48996061593575	3.51683186468165	3.62496164989155
C	2.82758676732216	7.80060588823325	1.17437465608654
H	2.89625556687014	8.05101943281316	0.12012550551335
H	3.79924276508747	7.50409049460773	1.54174657775283
H	2.48346651501994	8.67728378063854	1.71456570342862
C	0.54676214473021	7.12951513894708	0.92631926062896
H	0.21171578950484	7.95374708204749	1.54830026373669
H	-0.16895249114119	6.33507550468913	0.97883621350926
H	0.60672816345108	7.48536485278930	-0.09713437849623

137

Coordinates from ORCA-job INT5x_v2_tbu_aaac_cucl_tbu_aaac_sncxet_CREST_cmp_Compound_1

Sn	-1.33904867253109	0.08443075153267	0.16574252862297
C	-0.78678525009471	-0.08047250000427	-2.04558435594532
N	-3.42675936316828	0.05965227042089	0.01495778607945
N	-1.59986823298669	-1.93002311298633	0.69294564719494
C	-2.48729125472435	-2.76420796364051	0.03293217280514
C	-4.04326080941611	-0.90723597038407	-0.75826097117372
C	-4.20272798750356	1.19558577519010	-0.01584092163689
C	-0.72249438892020	-2.71509663141217	1.40594063975765
C	-5.19514813300636	-0.36939609740483	-1.27444014695364
H	-5.91969290584088	-0.88395314297791	-1.87521368728553
C	-3.92862923338118	2.33287008909282	0.91912970502340
C	-2.16968441773176	-4.05985339371599	0.36011598300090

H	-2.69435758456773	-4.93788680708186	0.04338949689343
C	-4.12231302009219	1.81195009190975	2.37347574038211
H	-3.31157461449215	1.11671044435033	2.58360915567008
H	-3.97222744961549	2.65969690145923	3.03948637086591
C	-3.63615655847587	-2.35436496222551	-0.84784430389815
C	-5.30218507806864	0.95003137211419	-0.79737437738517
H	-6.12250070042750	1.61664879938588	-0.97007756647325
C	-3.34214226583699	-2.66273836955367	-2.34027475520650
H	-4.19781290824512	-2.30797860487870	-2.91035743400678
C	-1.06553416165128	-4.02883978136151	1.22548194270984
H	-0.60238928701622	-4.87724711127875	1.68583235960781
C	-4.93445875469941	3.46245885760698	0.66119556123313
H	-5.93139681071247	3.04787927259506	0.77032904252607
H	-4.83481088360088	4.19077156097758	1.46284311321904
C	-4.86900415163375	-3.18853824064387	-0.41462775168532
H	-5.67280015723218	-2.99013465986693	-1.11975402745146
H	-4.63448482996131	-4.24297524335062	-0.51281747521118
C	-5.33696664757300	-2.90766220376325	0.99599558570034
H	-5.63693107397296	-1.87166114166171	1.11000435894044
H	-4.54879257838020	-3.11084572180235	1.71350992266221
H	-6.18853190734240	-3.53067674970285	1.25108255316247
C	-4.83624500117802	4.16402460572777	-0.68249339820547
H	-3.91515987547187	4.72414974273967	-0.78216634553673
H	-5.66268830857504	4.85808015000852	-0.80559310437575
H	-4.87407053090790	3.45808187068011	-1.50352349537413
C	-3.04393667951440	-4.09658623359331	-2.72921124185486
H	-2.15622550695675	-4.47409537253697	-2.23503697593916
H	-2.88122148432556	-4.16104544861890	-3.80158697182784
H	-3.86265406278301	-4.76711034450082	-2.49124581354872
C	-5.44256093380458	1.13136223098633	2.66568190131885
H	-6.28857815214183	1.79548254711478	2.52160965044524
H	-5.47081344745017	0.79106790433683	3.69630896669634
H	-5.58933682255798	0.26804639642268	2.02637570494928
H	-2.51148389374292	-2.03791223301729	-2.64802818606965
N	-0.14518309073492	-1.13336491369548	-2.42590184545993
N	0.50983066707629	0.08225085451596	1.22138251310477
N	-1.40245382817752	2.08887643694192	0.74642247702447
C	-0.29184601430656	2.91102572998479	0.86396754575528
C	1.42412137263523	1.09737638097238	1.17159964962343
C	1.09805828469256	-1.01466067984182	1.82155942524797
C	-2.53086020981204	2.87634668234072	0.85071923425686
C	2.62411333861370	0.63392953364263	1.69450200768632
H	3.44003174473910	1.24782649768320	2.02191792706579
C	0.27415126077582	-2.14084610654343	2.36543562174825
C	-0.73278927745500	4.19337549324118	1.05895580785294
H	-0.11863124659283	5.06049815290427	1.19466983974229
C	-0.55251749884776	-1.57118092282139	3.55823054590821
H	-1.32738927028048	-0.92724294059804	3.14712692232974
H	-1.07799271563849	-2.41222061779462	4.00715858732131
C	1.13719047169758	2.48509374574384	0.67350238716132

C	2.39561632166591	-0.70461114025822	2.11786653020750
H	3.09019617452601	-1.31701097864456	2.65450692699009
C	1.52864610702443	2.54152989007807	-0.82726993503752
H	2.55317836733050	2.19068224144458	-0.91787743569100
C	-2.13676953244056	4.17010073936724	1.05924536950897
H	-2.78256362433523	5.00944426768623	1.21801480672132
C	1.19008849691341	-3.25331512275477	2.88824466129395
H	1.80441933685894	-2.84317952466374	3.68357239081941
H	0.55729876483614	-3.99730650566430	3.36529256461081
C	2.05137980566137	3.46807368297315	1.43180472402167
H	3.08126839999827	3.21187287739893	1.19186914817986
H	1.90125728442251	4.45702716259065	1.01514744185506
C	1.86697466759163	3.53048353747344	2.93494620156787
H	2.05828826189224	2.57411504088411	3.40755429264918
H	0.85765770531670	3.82775693315293	3.19198349482990
H	2.54802315151078	4.25617121025113	3.37008294541003
C	2.08778030221528	-3.92418845128678	1.86397086365239
H	2.76864515897382	-3.21936199652122	1.40398263990324
H	1.51588159345606	-4.38473842714155	1.06830340940232
H	2.68550431449931	-4.69921699806566	2.33490859206258
C	1.39414015114737	3.87976404556803	-1.52056379838076
H	2.11594075201979	4.60105938581250	-1.15104347893696
H	0.40799402959873	4.31233167567130	-1.39404067676807
H	1.57809223736617	3.76312205834710	-2.58437404157336
C	0.21834487693742	-0.79953848501725	4.60822379327304
H	-0.44806438291616	-0.48979796194572	5.40722808699300
H	0.67459320829177	0.09276827700597	4.19317198032509
H	0.94514869774968	1.79151944092054	-1.35418628806864
H	1.00808037917006	-1.39257665289142	5.05801337448983
C	0.39153638767538	-2.14375855283996	-1.50919810396208
H	0.68660127399234	-1.69742608378947	-0.57860871171213
H	1.27962498048357	-2.55257912684341	-1.96284953263434
H	-0.35143753102314	-2.91778853864308	-1.35117422184281
C	-0.09817898773885	1.40401129021258	-3.97630544597661
H	-0.14874903620619	2.47693729875009	-4.11673735581206
H	-0.14987844912913	0.95368841805461	-4.95989713916770
C	0.14678037216263	-1.53326935272363	-3.80247592904831
C	-1.26097907132306	0.96103330482049	-3.05587109045540
C	-1.78632933372158	2.20407034243692	-2.34169149508495
H	-2.10047201762622	2.91773661157684	-3.09499517249104
H	-1.03956497493125	2.68478325013864	-1.72744751674256
H	-2.65256591745410	1.98554906311575	-1.73185419013549
C	-2.45938520197620	0.43038310997132	-3.85871355273304
H	-3.30185512026354	0.23681954421276	-3.20447382331836
H	-2.25905618176359	-0.47107514883094	-4.42288922028085
H	-2.75296489113682	1.20261406158550	-4.56301058962362
H	1.21457418230722	-1.42739430041403	-3.95319966837122
H	-0.39501303263887	-0.95810928495117	-4.52297161905055
H	-0.12765776277385	-2.57794861628932	-3.89348523603561
H	0.87556705481002	1.17471246041365	-3.55641328673297

Cu	3.78571882317573	-0.00531562303695	-0.05887693572933
Cl	2.99759293213407	-0.37496783245843	-2.14808170102274
C	5.74314319113370	-0.05874513201124	-0.06785896728273
N	6.43871549565458	1.01350289816553	-0.36832711827101
C	6.41069690813771	-1.42672457639846	-0.07777185039385
C	5.41120122190022	-2.42310948576214	0.51108460226413
C	7.66395449481461	-1.50856740420986	0.79826465556357
C	6.66764772055817	-1.86393524151775	-1.52375717443137
H	5.17716047132605	-2.17642249156427	1.54154374892339
H	5.82228574140998	-3.42869979504685	0.48886178571740
H	4.48439574003142	-2.42558724755693	-0.05444870248058
H	5.74689414630323	-1.80076439909965	-2.09463884253313
H	7.00730417430526	-2.89596823131607	-1.53317405186031
H	7.41504079818453	-1.26887906659166	-2.03400292122992
H	8.52527958404574	-0.98550307691181	0.40773295949656
H	7.94939469508153	-2.54979746277959	0.91632863434856
H	7.45717564280151	-1.11560979130315	1.79006889169953
C	5.78623122322527	2.31421506347634	-0.36176965137171
C	7.82796383060466	1.14624325089899	-0.80245472958955
H	6.41674760557745	3.03826842850150	0.14669758706903
H	4.83673751195919	2.23802557608227	0.14557336182527
H	5.61899900338433	2.65445313409171	-1.37966683880167
H	8.43235956787562	1.56453970111641	-0.00262215086197
H	7.86246181538689	1.83121835766983	-1.64312349742869
H	8.24566879300972	0.20813795776401	-1.10990467200886

136

Coordinates from ORCA-job INT6x_v2_tbu_aaac_cu_tbu_aaac_sncxet_CREST_cmp_Compound_1

Sn	-1.14333388622574	0.43520862429557	0.35869561467388
C	-1.88271378236499	-0.42713560128940	-1.66132299492449
N	-2.84617986847082	1.02881899609668	1.35799509384830
N	-1.17524215394895	-1.19952785204209	1.64950641686988
C	-2.35336074890290	-1.91747599109762	1.79402269913876
C	-3.80145702648377	0.14880934668088	1.83757036823925
C	-3.29429728472472	2.31565200921351	1.55978205927522
C	-0.12284747890577	-2.03131201439348	1.95952338448949
C	-4.83937253280416	0.88845356823018	2.33782016445510
H	-5.73221791823258	0.50600464038800	2.78915720193400
C	-2.44024069616712	3.52884008413032	1.32608159614342
C	-2.02415897079814	-3.19331073725049	2.17841337702433
H	-2.71356902453284	-3.97586860920378	2.42155545311393
C	-1.52308843104773	3.67277338915805	2.57386513747176
H	-2.17521002422789	3.78006923080967	3.43736255559433
H	-0.99976815097944	2.72875836439039	2.71058102081274
C	-3.73951697715566	-1.34372883059379	1.66846450070833
C	-4.51532533547500	2.24806626396798	2.17358291191673
H	-5.10487135092422	3.08008391082646	2.50149835406079
C	-4.35244018434718	-1.66941736795844	0.27994038658753
H	-5.34185853963787	-1.21893868123664	0.25373816792691

C	-0.62654023436587	-3.26177147139372	2.29491167115825
H	-0.06862903734600	-4.10455728981535	2.64979391532135
C	-3.33056330061105	4.77392372308811	1.21317925845234
H	-3.78831873626599	4.94099137781144	2.18519218034105
H	-2.68620556931716	5.63119203138924	1.04754164477203
C	-4.63328001832903	-1.99944669991292	2.74156420362301
H	-5.64951817483492	-1.64933951862089	2.58001678744719
H	-4.66535846152882	-3.06747958059028	2.55518065371090
C	-4.22061922254453	-1.75610135847403	4.17816865325855
H	-3.22543759348382	-2.14065123649920	4.37268054132262
H	-4.90444270306203	-2.25573864791164	4.85642263394397
H	-4.22153242593577	-0.70098840285010	4.42238289481067
C	-4.41366305196403	4.74532955176094	0.14789886354659
H	-4.89250990115261	5.71663058778814	0.07578928351965
H	-5.18019768566028	4.01537316942193	0.37228780082778
H	-4.01602091499610	4.50382237662491	-0.83082016110727
C	-4.43620083845942	-3.12484069402133	-0.12809837806219
H	-3.46902707093907	-3.61556504474119	-0.08723999492982
H	-4.81914381852962	-3.21335303108881	-1.14128077011237
H	-5.11057322853288	-3.68622147193595	0.50821669512392
C	-0.51284191368472	4.79945261241849	2.52856909462588
H	0.16513829428042	4.69434976867920	1.68760597133159
H	0.08401687563244	4.80549547346662	3.43502030404930
H	-0.98613897670516	5.77212960133542	2.45080326025077
H	-3.76905217088660	-1.12640415182705	-0.45807987206597
N	-1.40424982133639	-1.57192072103941	-2.03840607393624
N	1.04028951450426	0.15321407022725	0.26746083466161
N	-0.61964281087606	2.41902599254237	-0.00007621101744
C	0.13241864587538	2.67028816651289	-1.14172770665503
C	1.86620551090180	1.06700440100566	-0.35502385464958
C	1.77644788950741	-0.53318852292242	1.19650104060431
C	-1.55908189432448	3.42711842024949	0.11869775577485
C	3.13475717912196	0.96912359418922	0.19011833697246
H	3.95537429633204	1.63100743607048	0.00358237759209
C	1.27214999950598	-1.54683964885616	2.17884345463384
C	-0.33414721701767	3.81855555667989	-1.72068022195950
H	0.08905473391128	4.31656203507036	-2.57160024815183
C	1.35886800368844	-0.89878971363628	3.59236132247538
H	1.00908557300941	-1.64092346292088	4.30491085038739
H	2.41151946290128	-0.72578573272560	3.80999971667013
C	1.43162674676025	1.97738963526947	-1.46144856999018
C	3.08193822690938	-0.05495576390537	1.18472716430522
H	3.83208916513531	-0.27611444348084	1.91896843241438
C	1.28157138514414	1.18813962421423	-2.78934697527473
H	0.62815181718397	0.33674138076534	-2.60135109746790
C	-1.38456023058411	4.30395769234810	-0.91892009846308
H	-1.91693031496680	5.21975975889954	-1.07137036616925
C	2.23664215177488	-2.75114508928657	2.19503070853375
H	3.23124648490109	-2.37553971969539	2.41388856309269
H	1.97146746987238	-3.37797584416532	3.04098513193795

C	2.50581323542666	3.06852527030221	-1.66718990225095
H	3.45951987012917	2.58442895754070	-1.85734106835745
H	2.26310184236287	3.59319009104887	-2.58801659785614
C	2.65315595920470	4.07303186579542	-0.54109861348120
H	1.77299719901367	4.69623728210445	-0.44646943883186
H	3.50066579578306	4.72406831878769	-0.72744590730852
H	2.81248513204827	3.59108088856142	0.41677889111197
C	2.28013480473318	-3.58766228548216	0.93340959896933
H	3.08372601271068	-4.31561376802559	0.98116575745319
H	2.46349300174787	-2.96650411094259	0.05984887456873
H	1.35329976418029	-4.12410589228385	0.77067549680035
C	2.56168721516763	0.72468723531417	-3.45257108740399
H	3.12630436110296	1.55550021808717	-3.85825983298352
H	2.34404628251884	0.05367154589253	-4.27831613872211
H	3.21460780932423	0.19692708911132	-2.76106790181565
C	0.59014070927944	0.39221631100508	3.76624140464244
H	0.91716359399863	1.15037574522724	3.05791825653936
H	0.75029942036370	0.79757154805868	4.75907181590697
H	0.74431586172693	1.82904541215711	-3.48144212086477
H	-0.47683379284520	0.24768553746103	3.64346746594204
C	-0.60199122895571	-2.41354538985189	-1.14001140766822
H	0.22207591876658	-1.85308742491154	-0.72698490837141
H	-0.21262999309045	-3.24686840091187	-1.70363340032648
H	-1.22340485635495	-2.79060262790828	-0.33729309676878
C	-3.99538962800295	-0.56149794962663	-3.10905391822223
H	-4.10654016488598	-1.50061103046042	-2.58251174638933
H	-3.86066778142666	-0.77924300399118	-4.16120692686381
C	-1.62263665282635	-2.22978403201290	-3.32926961309371
C	-2.87297970395279	0.33686008932167	-2.53117888455523
C	-2.10539277744964	1.04616883645021	-3.65773104126239
H	-1.49550185140894	0.37713820433047	-4.25438296610903
H	-1.46974000206668	1.82091654191052	-3.24984810209906
H	-2.82991089531730	1.51706048230741	-4.31344345770262
C	-3.55336257243140	1.43367049568395	-1.71551751236958
H	-4.14895153336440	1.03855148736922	-0.90227938130928
H	-4.21585334582161	1.98266914820376	-2.37490154955817
H	-2.84519154159035	2.14581335732456	-1.31973281018288
H	-2.08138609872142	-1.57883221576394	-4.04335773070543
H	-2.23491559346024	-3.11251787276165	-3.18592701243174
H	-0.65393892301894	-2.53876811075384	-3.70257588302418
H	-4.93848679371922	-0.03873384622435	-3.01604898007161
Cu	3.81141451629042	-0.89652800865236	-0.59007100611871
C	4.72804390396092	-2.09246353756004	-1.78057262757095
N	4.09078419315757	-2.85299716885461	-2.63086553966789
C	6.24305141350002	-2.14355159007854	-1.66104337619622
C	6.66490806710394	-3.44528999152648	-0.97212028503691
C	6.67555638371984	-0.99565133147748	-0.74542807378879
C	6.96530825071584	-1.92573792762427	-2.99445525726772
H	6.14276282918198	-3.56303174707783	-0.02758563971115
H	7.72781488613601	-3.40527832127876	-0.75757765582229

H	6.48577666106022	-4.33491335163402	-1.56199421815681
H	6.57760056600620	-1.04673729667738	-3.50085325817317
H	6.90969099441220	-2.75886591483790	-3.67962866793539
H	8.01715160611771	-1.74667688548974	-2.79895690998515
H	6.40850196386745	-0.03170087338424	-1.16869377669432
H	7.75195512205097	-1.01206876845277	-0.61021646013022
H	6.21898148097851	-1.07668180377147	0.23760791813265
C	2.64328626617519	-2.76511145586973	-2.75509621826204
C	4.62226773603446	-3.85382558557852	-3.55822633134575
H	2.18977726736723	-3.69247447965463	-2.41942075632918
H	2.37987477267693	-2.60660381720928	-3.79638501424865
H	2.27262587542478	-1.94202718723174	-2.16169414160911
H	5.59809721036260	-4.19016400016715	-3.26888538569895
H	4.66193110909197	-3.44339973703685	-4.56149731566810
H	3.94955107907389	-4.70276094185241	-3.56353258492948

136

Coordinates from ORCA-job INT7x_cmp_Compound_1

Sn	10.47045534893810	3.22256592986800	3.75167262221825
C	10.25172040349560	5.45517475663437	4.39263744563306
N	12.10300850636297	2.79559668525038	4.96080921863774
N	9.30685145789896	2.34424000967095	5.26645110796339
C	9.62197903532348	2.44133506382870	6.61934424249234
C	12.08981149093602	3.01253475785945	6.33103879308494
C	13.41298481867915	2.84666769586097	4.53174009250990
C	8.01684854629629	1.85314424058077	5.17484447788952
C	13.38333752630747	3.19380498559844	6.74296514094901
H	13.70967533027706	3.33920826421772	7.75332818938447
C	13.79749464892208	2.39318400007139	3.16198028129503
C	8.54809944610517	1.98459952329371	7.33885026216069
H	8.49477947484351	1.89882272582748	8.40394666939997
C	13.49544029357064	0.86704748668662	3.05917788989718
H	12.41383036604222	0.74629841419439	3.05306105574146
H	13.83694642429876	0.53797251949557	2.07924837837146
C	10.89950155865308	2.92781555315301	7.24155691272596
C	14.21484522592143	3.07998048245422	5.61664587522613
H	15.28469776310094	3.10706707710367	5.62031255134522
C	10.71241876220426	4.33549522098855	7.87617148125468
H	11.66709099455940	4.60782281518162	8.31898731072965
C	7.54603868787082	1.61175626738013	6.43522191424457
H	6.59448613255498	1.19181775855388	6.68770116227916
C	15.30010095787245	2.61612908362945	2.94533431913083
H	15.83158307414099	2.04269608877361	3.69692354425219
H	15.56601374687270	2.15993750985164	1.99550195389388
C	11.27437726561391	1.93598544160111	8.37421568936832
H	12.13614196621340	2.33974081804289	8.89757020650973
H	10.47087959933372	1.91115635949102	9.10133667626873
C	11.56936277294319	0.53237599491563	7.89490005462897
H	12.41291042766285	0.51863368612038	7.21272903644378
H	10.71412871838154	0.10820261699969	7.37938433927924

H	11.80849932636387	-0.11683475705952	8.73004080724948
C	15.79404749790750	4.05232901433721	2.98103078165197
H	15.31481193844766	4.66838723764109	2.23023876629124
H	16.86329130849356	4.08350150792136	2.79785606828079
H	15.61384340859617	4.51881047453715	3.94147892512636
C	9.61525935017801	4.52421769483235	8.90307703278605
H	8.63031439173673	4.34078556954879	8.48823711878208
H	9.63659391045814	5.54216223156925	9.28198445309470
H	9.73473487302485	3.86894632701888	9.75843713477233
C	14.08123118036920	-0.00379965238476	4.14887260273511
H	15.16426181187808	0.04207441026777	4.17851852591603
H	13.80849207963155	-1.04069659658871	3.98222012994699
H	13.71178766228879	0.28194957132657	5.12758995533658
H	10.56297769445769	5.03996268858236	7.06527628291252
N	9.18468829020496	5.78829516060891	5.05066955985997
N	8.84359638091595	2.79533960897204	2.40539933558708
N	11.64389340937221	3.09508396763467	2.01006388475588
C	11.27087478360178	3.56334031260212	0.74121382346110
C	8.78649942558546	3.47266923154967	1.18619230775281
C	7.57234519769813	2.47998111091829	2.78600074803566
C	13.02368561493120	3.02894707631128	2.04442164571339
C	7.42092750008198	3.61597600228321	0.86379780757530
H	7.02522404513392	3.92455212999175	-0.08472778183297
C	7.31887660660226	1.51476193923729	3.89577161334361
C	12.42099758799703	3.76153489130361	0.02022982720193
H	12.49244311015145	4.02840865504606	-1.00907727078712
C	7.87419761082413	0.13590670511439	3.42592204349457
H	8.95874984809153	0.21361376143271	3.39804602743166
H	7.64639518705141	-0.57230315012060	4.21827161373646
C	9.90202403033576	3.33667188712276	0.16915312812042
C	6.67604835486918	2.99046284762558	1.87584133501385
H	5.61196419577275	2.88624054025962	1.89621217761248
C	9.51111233562438	4.23866259021457	-1.02837479485079
H	8.59906008566512	3.80246621994303	-1.42421264229845
C	13.51275831785187	3.43308412536992	0.83420138547969
H	14.54012407465556	3.45454916339731	0.53796022505723
C	5.80802368999802	1.38722166014341	4.13560876074381
H	5.34526930159737	1.08503597512852	3.20191885989424
H	5.65179778550190	0.55353807127105	4.81359114658870
C	9.84361023016335	1.87098030618143	-0.38120631303940
H	8.79798755047974	1.63816058382387	-0.57893214819078
H	10.34507552277994	1.88549666267402	-1.34522763420456
C	10.47399272484537	0.78263533451730	0.45662778568939
H	10.07029225097513	0.74889131036157	1.46087920439990
H	11.54734452688081	0.91032176451786	0.53091713668221
H	10.28473283977315	-0.18289663235492	-0.00088855716870
C	5.09495697613340	2.61722173617623	4.67024723166499
H	5.43916214391648	2.88390320384012	5.66091254933669
H	4.02682473891440	2.43610272943548	4.72921612925419
H	5.23984568728356	3.48207456131830	4.03090025020082

C	10.43811938238192	4.45052276747841	-2.21072784096382
H	11.22628522616294	5.16230448570809	-2.00154746191002
H	9.86139683115309	4.84558341805328	-3.04069929738290
H	10.90145413118447	3.53323527502792	-2.55414459316064
C	7.37058855648700	-0.37973711599422	2.09490691425950
H	6.29767131975965	-0.53750552552316	2.09305422593457
H	7.83450616174062	-1.33331888454598	1.86673934005403
H	9.21602386535392	5.22263763082908	-0.66190597023971
H	7.60695192798157	0.29849503302453	1.28148850988497
C	7.96409784212101	4.97999788954044	5.07457154725786
H	7.87809190691486	4.38619358639168	4.18205931364259
H	7.12317987245399	5.65867723785434	5.11457392119678
H	7.94913890330716	4.34540792009673	5.95262149775216
C	10.93336043103208	7.81918641171948	3.82109304341666
H	11.77765814971909	8.36317714940235	3.41291754616559
H	10.53629918042382	8.42299981678436	4.62370415858531
C	9.01183367064805	6.94700567935875	5.93213184044983
C	11.42168238868536	6.42667769283992	4.25278747633929
C	12.36812913086228	5.92325776631830	3.16573991595919
H	13.11684732274156	6.68243386402182	2.97217528533164
H	11.87035660984315	5.69460873257718	2.23142406563484
H	12.89742521706332	5.04201341430941	3.49451892505298
C	12.27430837733668	6.51530347290542	5.52587249191481
H	12.67779150466915	5.54648373820744	5.79263416909187
H	11.75413173501054	6.90957676486218	6.38809892666665
H	13.10895464587952	7.17679191044195	5.31617374416764
H	8.51706618904087	6.58950904863526	6.82671236615789
H	8.37383952202759	7.68121042236436	5.45294855841379
H	9.94789605040612	7.38877832719464	6.20461334409815
H	10.17594401332287	7.74864628416327	3.04854800654674
Cu	8.34401103530256	5.52278540562183	1.41919395443550
C	8.29634766774462	7.46563852884454	1.23456745896652
N	9.24436647771670	8.09300884456683	0.59761100614761
C	7.01799991324652	8.17976229286665	1.64124607295527
C	6.28918187343205	7.27953401039950	2.63951392549543
C	6.11824137190641	8.31443016715568	0.40864425176824
C	7.23218010219330	9.52355977888800	2.34797409058518
C	9.26833674638200	9.48659116484367	0.14142995061058
H	9.74294681005293	10.11423347692594	0.88701950564352
H	8.28065430310023	9.85244993889907	-0.06599994559631
H	9.85390935099151	9.53256962582886	-0.76661773999716
C	10.49950715214928	7.42528954169619	0.26516309662101
H	10.53043570353058	6.43673346261744	0.69585584052067
H	11.32498168208287	8.01071188091835	0.65550992389392
H	10.60489105653721	7.35688963476191	-0.81182902232241
H	5.92074547577928	7.34111180820851	-0.02969065098916
H	6.53693578689129	8.94596937126258	-0.36519387405072
H	5.16584816808721	8.74275910956338	0.70380895892215
H	8.03933680712531	9.46058128328113	3.07368103281504
H	6.33014212361392	9.78189208207857	2.89180557893710

H	7.44204332708282	10.34894864696109	1.68484711754210
H	6.09851335190857	6.29084755030580	2.23125265962074
H	5.33524160543541	7.71817149127898	2.91193518093649
H	6.87415287369556	7.16053908959355	3.54583977481087

3

Coordinates from ORCA-job cucl2_cmp_Compound_1

Cu	-2.98835761377021	1.72037959166091	0.00000007618430
Cl	-0.84956930698364	1.65163701123137	-0.00000003809209
Cl	-5.12715307924615	1.78866339710772	-0.00000003809221

19

Coordinates from ORCA-job sn2_pyrr2_cmp_Compound_1

Sn	0.42260432631074	0.43267357138479	1.61637117074069
N	-0.51346099517067	0.80826697110585	3.44038855059780
C	-0.65095343108273	1.94638376869339	4.20213804348794
C	-1.22200493076097	1.62209937990661	5.39919754546657
C	-1.45301780417002	0.22250262863234	5.39086967615251
C	-1.00233349145796	-0.24373774254978	4.19177005244435
H	-0.30773028564538	2.89217768035846	3.83667543509554
H	-1.44160142751569	2.30358338905374	6.19768047341681
H	-1.89447929132053	-0.36270445908577	6.17317697226453
H	-0.99837874716935	-1.24297547161686	3.79879057168134
N	0.27431418926753	2.38026104082073	0.88703609703013
C	1.07365811613932	2.78441532556666	-0.16567302998019
C	0.71844741515404	4.04284664115156	-0.55145296792558
C	-0.35935337851317	4.43783116118832	0.28177502972873
C	-0.60513690449795	3.40766793980207	1.14333643707155
H	1.84453430046561	2.14011103174040	-0.54457226726471
H	1.17048048725689	4.61836518120293	-1.33491596068628
H	-0.89428869490154	5.36651268671123	0.24132011771898
H	-1.35132845238817	3.31129127593330	1.90486905295922

43

Coordinates from ORCA-job TS1_sn2_pyrr2_attack_optTS

Sn	10.03839880330299	4.19784154190407	2.35456563109349
C	10.00437750978464	5.74899421370307	4.12146876281675
N	8.92372163511638	6.50880063414565	4.19464660826553
N	8.29087233138129	3.81193841186677	1.35532000571317
N	10.82026395269289	2.31885122361033	2.23774948835487
C	10.94153646768313	1.80952184911960	0.93359578256600
C	7.57180804645541	4.81766053348305	0.73586541996390
C	7.37756871863303	2.95341832831023	1.94623322967845
C	11.80423016002705	1.75044521772755	2.99567271348289
C	6.23885863604891	4.56717516901628	0.88277601772048
C	11.94368505159701	0.89357317594220	0.91782457902725
C	6.11538719118785	3.38744295023311	1.65652003950496
C	12.48927468054246	0.84681219697544	2.22674762248759
C	7.58444323076482	5.98616225676441	3.94267885553626
H	7.59737134025966	5.00409133195610	3.49907053434513

H	7.06316567240870	6.66394315123313	3.27917780375568
H	7.04489707899487	5.92316979191595	4.88169075796241
C	11.82162935025663	7.32928957335102	3.51555524598279
H	12.85782122645110	7.58342619300428	3.70428082283734
H	11.24339009720466	8.23505273905945	3.60918184858424
C	8.86332814771819	7.91385973631508	4.59025002565338
C	11.41471287348255	6.20335120152483	4.47276354861055
C	12.44297056432082	5.09037720174309	4.28391566630872
H	13.41984050469722	5.48065148655808	4.54129298557993
H	12.51796338809586	4.76140107702669	3.24861506862909
H	12.25307902615119	4.23546078209005	4.91650653264192
C	11.49263780994454	6.60651030704394	5.95249437116531
H	11.30307263212015	5.74764760425546	6.58491678559839
H	10.80562694286338	7.38771423130025	6.23886994514798
H	12.49654745475862	6.95714553434940	6.16118062548390
H	8.18805393295742	8.00028513754680	5.43528995777504
H	8.45981195226212	8.49331923306556	3.76739944962540
H	9.81754940191523	8.31145009700471	4.86647021039845
H	11.75474238824617	6.99737183495673	2.48253871808487
H	5.43876394066846	5.13602193125071	0.45263890473340
H	8.07443810302118	5.59324772164010	0.19155161367107
H	5.20470538445805	2.88583183664677	1.91741500723936
H	7.71330778814771	2.08148088924650	2.47177774010776
H	12.23815549361624	0.29346912338382	0.08090832333659
H	10.24569106166047	2.10452400941371	0.17403151714718
H	13.25673931598457	0.18483121258842	2.57589661371314
H	11.89823552836658	1.97831204826888	4.03773236965930
Cl	9.61127618374967	3.97955427945866	5.04735325001004

43

Coordinates from ORCA-job INT1_tbu_aaac_sn2_pyrr2_cmp_Compound_1

Sn	9.41792604027149	3.36950824121035	3.41467073690874
C	9.90782422121533	5.46752871285777	4.06710072950908
N	8.89524213959730	6.23731100765130	4.27348223943902
N	7.91402795164717	3.68477614728607	2.08977590688332
N	10.78408478500575	2.23946124010688	2.45803846013721
C	11.34433294145795	2.76178841151821	1.29653981131423
C	7.91563476330870	4.77028403983445	1.23411805855902
C	6.60373612251474	3.30864479666733	2.28895991112927
C	11.76613997403459	1.52501036905061	3.11190477877322
C	6.62752129377453	5.04202933454803	0.86742164568147
C	12.63115319243907	2.32335268895023	1.20075919636256
C	5.79599570645957	4.11394113874046	1.53868074659572
C	12.89719404575533	1.53716082286918	2.34999184945234
C	7.51194983459374	5.75122303744720	4.37352132683156
H	7.48241365196080	4.72738713725866	4.71023245796515
H	7.01600432452239	5.85651431317440	3.41495667502173
H	7.00759517383611	6.35972676804125	5.11161601071925
C	11.73795362957214	6.51995046839979	2.77369427555663
H	12.79302781091586	6.76966826124485	2.80283017177149

H	11.18793929922134	7.42385222569472	2.54105820456475
C	8.93790824682560	7.70314964045914	4.38177579620265
C	11.35120269418888	5.90426708713269	4.12484473655414
C	12.21399998976871	4.65678001746881	4.33368858165405
H	13.24507862528866	4.95614789397907	4.47232909435525
H	12.20187515523212	3.99745818406453	3.47468435631412
H	11.91924969112076	4.10402814082155	5.22178545676396
C	11.64680716449899	6.85394764445937	5.29512976320025
H	11.17996048522534	6.51100742184220	6.21298115002405
H	11.35612522125663	7.87869287762130	5.12358541562600
H	12.71656639354853	6.85796865027038	5.46285609483479
H	8.91206537247737	7.99741308670573	5.42309386127034
H	8.05175736264458	8.07817478642922	3.88801249035014
H	9.80842039529706	8.10196660300208	3.89810285594166
H	11.59543527232560	5.81227684370627	1.96293588124117
H	6.31753575660736	5.78994295062908	0.16521763608621
H	8.83650822570808	5.21850233217828	0.91254593966774
H	4.73161639330660	4.02749135889859	1.45121480917273
H	6.36229603697943	2.48396340572097	2.92944561888475
H	13.29387966224184	2.49370773231173	0.37607230065186
H	10.73807170551985	3.30665733837981	0.59896106035915
H	13.80155013211082	1.00237905360864	2.56106605115096
H	11.55582692043218	1.03796198761879	4.04305111680792
Cl	8.67251619528942	2.19842580013909	5.24969673970973

28

Coordinates from ORCA-job sn2_pyrr3_cmp_Compound_1

Sn	-0.52343693653375	0.31058019494107	0.81735807849579
N	1.61182854809325	0.00380628100016	0.77914649120206
C	2.31228423083803	-0.32102181755188	-0.34623835919716
C	3.65943777509971	-0.33054555056153	-0.07154256433152
C	3.78918189064107	0.00335257345216	1.29529176643316
C	2.51703416818387	0.20158106596975	1.77979292881808
H	4.44973909364650	-0.55228202090005	-0.76465118384267
H	4.70058841260552	0.08811856432277	1.85773938613368
H	2.18604632694379	0.47439012447474	2.76257860509160
N	-0.45290946192854	0.65166435877584	2.94563346460458
C	-0.13413658974411	1.79612842753669	3.61503768028003
C	-0.09980901830571	1.54391968792593	4.96696195812472
C	-0.41093689136156	0.17603134943474	5.13649006547957
C	-0.62176630008233	-0.33203683446366	3.87646861391655
H	0.05055432454906	2.70482335650986	3.07641227318540
H	0.12135112158864	2.25781118307025	5.73870845418479
H	-0.47579721601581	-0.36683263336599	6.06127954729043
H	-0.87144945583710	-1.33247763796668	3.57345827388152
N	-0.24648628343793	2.41742460124667	0.44864131852319
C	0.91282802044672	3.13542555376190	0.43773044472205
C	0.62569099890136	4.46987656552212	0.26631591700036
C	-0.77989836577390	4.57733980303606	0.16924824754849
C	-1.27455399819055	3.29967810983713	0.28350358167587

H	1.85682475310041	2.64111481021735	0.55827070515172
H	1.34127333181925	5.26968955579426	0.21654608889482
H	-1.35606196577928	5.47350125605598	0.03104288136835
H	-2.29234191017036	2.95480777487478	0.26837185671348
H	1.80027339670372	-0.51443670295051	-1.27116152134900

52

Coordinates from ORCA-job TS1_sn2_pyrr3_attack_optTS

Sn	9.73977149852692	3.19200238718476	5.22968952470572
C	10.76735838602693	6.87504410260869	4.49404307092168
N	8.13192933421459	1.89929961661790	5.71552284391326
C	7.36424191895360	2.16681416278787	6.82102463318259
C	7.40292479649813	1.07530043548849	4.90876760216625
C	6.16609056376313	1.50480476037209	6.72313519212877
H	5.37817170443798	1.50542049927263	7.45157693982988
C	6.19306310713821	0.80406583772292	5.49722641131651
H	5.42346435822718	0.17145125216711	5.09838427503948
N	9.47912726281508	7.00433304014429	4.52896349255061
N	8.47268239609198	4.03046377593599	3.62976678605967
N	10.76320941862177	2.00559501627059	3.79081516907288
C	10.34410050436201	1.36757454978557	2.65671450396430
C	8.73153858580426	4.21102287405879	2.30669160654113
C	7.16154172375294	4.35781338099235	3.83128621444220
C	12.11932512839839	1.81946963813246	3.87939235034902
C	7.59187658928032	4.65607580365314	1.66112487307891
C	11.41767298305904	0.78621166754841	2.03046190974073
C	6.58514338374424	4.74828123559687	2.64363557695357
C	12.55723393001158	1.07541110821266	2.81393632722623
C	8.64485102323840	7.35736812554382	3.37460874554371
H	8.47629778085375	6.49123899161616	2.74334016538634
H	9.10132288227259	8.15612812832899	2.81770276857213
H	7.69739236222439	7.69095966787528	3.76219650081665
C	11.12794069001682	6.98709514966732	1.92778803975575
H	11.92802220079457	6.78491323637304	1.22557219878109
H	10.78341258473156	7.99372436702462	1.72953199622511
C	8.72736003784667	6.83343265205841	5.78024791181153
C	11.72724882864572	6.82827381809068	3.32251702406469
C	12.40522647656628	5.44535275426396	3.36210049875737
H	13.15638292344997	5.42607254441366	2.58056664209369
H	11.70107161672526	4.64671615183935	3.16423764593691
H	12.89393779979222	5.24538501630533	4.30511495635813
C	12.78432485350218	7.92375997726767	3.50883007412210
H	13.37423977851599	7.78039429745656	4.40320584109651
H	12.33287256427801	8.91044329549512	3.54307759983903
H	13.45340321885679	7.89293437155713	2.65677929852628
H	9.09591421584905	5.97067555314506	6.31625481440237
H	7.69664652808203	6.66929323707885	5.51552018276971
H	8.83156123317239	7.72091847410010	6.39408331459962
H	10.33536428398070	6.28058878113953	1.72589636418954
H	7.80060276289227	0.73935580820638	3.97233683330745

H	7.74422666235726	2.78767599344741	7.61137929374978
H	7.49534389669904	4.85274027971833	0.61011008897568
H	9.68558954404253	3.94520002552344	1.89497290297598
H	5.56104422976085	5.03326471751277	2.49799421369919
H	6.70878534719796	4.21288622284465	4.79531080668970
H	11.38555783929873	0.21837717773398	1.12043134946152
H	9.31303342557125	1.38904327035783	2.36655114075782
H	13.56748692795989	0.76614945619056	2.62674486981889
H	12.67132449266290	2.22260150063673	4.70836628587153
Cl	11.53548141443337	6.74961281263357	6.01931232786071

52

Coordinates from ORCA-job INT1_tbu_aaac_sn2_pyrr3_cmp_Compound_1

Sn	9.52363362405825	3.70548335625150	3.88777119926177
C	10.35209815300216	5.60762926552854	4.61417745222725
N	8.26634048509283	2.96850049656706	5.30478223272682
C	7.88723969034329	3.55580583220861	6.48923712528320
C	7.53874461666042	1.81019917925405	5.15391280059845
C	6.93441362927611	2.77587677575282	7.08092581933373
H	6.45904263050516	2.97198000856533	8.02169465364205
C	6.71125621621857	1.66658865582599	6.23129296517749
H	6.03238640926210	0.85361833183377	6.39645194760321
N	9.35663469299321	6.35398768143162	5.24841708555260
N	8.32660426734218	3.76558575650886	2.21762102085311
N	10.79754084256087	2.19653345606934	3.39395924721595
C	10.82380630116191	1.59364282332815	2.15431996556444
C	8.71423401625932	4.15309691943834	0.95634845137795
C	6.95182541894266	3.79439272359314	2.25851953388168
C	11.90252068289556	1.77256462977391	4.09312063225541
C	7.60041209394768	4.39666108543151	0.20151403551585
C	11.92292742450003	0.78560438418416	2.08320040732480
C	6.47885913356206	4.16867875997856	1.03127956379082
C	12.60839060684680	0.89914519131140	3.31487183671509
C	8.03420305695069	6.48804408891295	4.68920450135116
H	7.77901633334265	5.66544372254005	4.03392563109269
H	7.92522042641140	7.40002004982752	4.09939380445377
H	7.29978229238708	6.50995369292336	5.48986601629025
C	10.47023359121721	7.07166791916423	2.65024968420209
H	11.09827959438613	7.48126462202380	1.86592099808127
H	9.96033444066893	7.89862874419415	3.13208571385144
C	9.69392989722623	7.43484233105667	6.14422808454037
C	11.33562368459559	6.29297355549375	3.63892467255936
C	12.15804027710732	5.26359789256332	2.87696810162154
H	12.85839260540063	5.77043204964259	2.22224068194833
H	11.54449782230152	4.63295044888617	2.23653677813465
H	12.72211421047677	4.61750047697763	3.53880891204849
C	12.30037642636512	7.26077267414357	4.31932751418402
H	12.92888702928256	6.75719862895647	5.04268436626588
H	11.79005705961359	8.07595684237043	4.81286228126629
H	12.94562871134830	7.69442225739294	3.56169520844789

H	8.91120271672741	7.51875855686079	6.89328053047636
H	9.77062982746721	8.39912803405550	5.63702566922931
H	10.62553623528971	7.22903027443092	6.65090653661710
H	9.72165182213551	6.44385808396404	2.17477336333898
H	7.67883548193448	1.18405340906899	4.29482133948862
H	8.35283625183745	4.46291364695795	6.81600855655014
H	7.59093517920811	4.68709139169861	-0.83045328566949
H	9.75201440970833	4.19578693231374	0.68979094071035
H	5.44637259270964	4.24832436761855	0.75399574261275
H	6.42859819990308	3.51878841228364	3.15280377732122
H	12.19372186722117	0.16856709623032	1.24936440662175
H	10.04309345262920	1.77171207467305	1.44346480465300
H	13.50574681860811	0.38802324001047	3.60289637713177
H	12.08675118020276	2.12198457221707	5.08770262055262
Cl	11.39228556990444	4.75976459770982	5.99011769412421

37

Coordinates from ORCA-job sn2_pyrr4_cmp_Compound_1

Sn	-0.45433500714875	-0.08121151895117	1.01314614342084
N	1.72792150236855	0.02984408305863	0.68648862666217
C	2.41282053863523	1.09128878725167	0.17048005111889
C	3.74396813968270	0.76568010528487	0.02688365387589
C	3.88144864895882	-0.56820202324324	0.47444875138166
C	2.62642473756116	-0.98122105794330	0.86563283535407
H	4.51857090713435	1.41465843423572	-0.34432237196894
H	4.78350150765032	-1.15398691290829	0.52055311838434
H	2.31373111777871	-1.91980355999172	1.27702269995800
N	-0.20785944848914	0.61231405570740	3.08426644607009
C	0.95175375998021	0.91614406876627	3.72065059675250
C	0.68676879191628	1.30676546088250	5.01794289003388
C	-0.71463961305275	1.23671938717848	5.17987264562314
C	-1.21783004978961	0.80647987495350	3.96927692365747
H	1.88796873673138	0.83003619585880	3.20442693936836
H	1.41363071053433	1.60416759028857	5.75351933573337
H	-1.28312216821693	1.46848952012861	6.06379848649060
H	-2.23753339122994	0.62859105479491	3.67873684813109
N	-0.44810277694441	2.27429193983653	0.61078478636736
C	-0.12210407685647	3.34097622979502	1.38237056632777
C	-0.20533331979594	4.51291934718249	0.65106757226074
C	-0.60817752971602	4.13854171718650	-0.65069470606473
C	-0.74521089227180	2.76233368054435	-0.62015834187387
H	0.15728979100291	3.19823654444316	2.40962032580602
H	-0.00621483005376	5.50914786089726	1.01054975720456
H	-0.77739426146066	4.78575968015362	-1.49549968493464
H	-1.02904520866815	2.09135897477689	-1.41384299361705
N	-0.00245317692494	-2.19005067082001	2.04754162276380
C	0.45414764410096	-2.53729784036926	3.27661633673059
C	0.63739845246464	-3.90670963972304	3.35770808889761
C	0.26909388746289	-4.42974786352000	2.09769727252291
C	-0.11638664043706	-3.34052202667570	1.33702061659918

H	0.62760397836582	-1.78201767588082	4.02030458800314
H	0.98845352042905	-4.45766843517388	4.21477280197792
H	0.28182771490660	-5.46178632451021	1.78789661930988
H	-0.45758034902897	-3.31339279425393	0.31545416120056
H	1.90695965242036	2.01157675075883	-0.04205200952930

61

Coordinates from ORCA-job TS1_sn2_pyrr4_attack_optTS

Sn	9.80625363907294	2.60612022280248	4.07396247845533
C	10.46864198913759	7.83749402596184	4.57000674054240
N	11.69248090060087	2.71969421300637	5.17345311972904
N	8.93747830922497	1.18647947779623	5.34073123723623
C	9.54183117437933	0.56821501231193	6.40350696635542
C	11.79958823727530	3.50236898731835	6.29759868343095
C	12.88121824937422	2.80943054490659	4.50344310218614
C	7.62264583883195	0.80497277100631	5.32591792068082
C	13.05858064721277	4.03583932443546	6.37214545120354
C	8.62177155161890	-0.21733911026018	7.04893545913871
H	8.81006764921960	-0.83253874971694	7.90844147894576
C	13.75346529698053	3.59153226149809	5.21961905679136
C	7.39512265538325	-0.06539623469148	6.36035211862810
H	6.46097770018509	-0.54242696549638	6.58890779781365
N	9.78062732796222	9.02562415194940	4.52751798729654
N	8.07373674642820	2.90152033468769	2.79678534681926
N	10.66856180352262	1.31871305451830	2.65942246817485
C	11.02268434597513	1.68346141221955	1.38968423359344
C	7.20836685952627	3.95014690558535	2.90730634473721
C	7.53846408080866	2.00549526185452	1.91598720447356
C	11.30372491295668	0.14468295845758	2.94537256367663
C	6.12225477996674	3.73262753584918	2.09497412523334
C	11.86183954792233	0.73563310637304	0.86021930831405
C	6.33376260513384	2.48685438923596	1.46221946614541
C	12.04142249139657	-0.25078704937642	1.85711613783318
C	8.73183982987873	9.17357964214347	5.51197758952561
H	8.15536703483023	8.25913121256275	5.55907947792376
H	8.08022711000434	9.99302882650818	5.21910080714942
H	9.12305476274759	9.38548090554059	6.51056178104867
C	10.58997597789778	7.82038912638750	2.10866441038241
H	11.03506582883548	7.30218861996885	1.26425645446092
H	10.75310327256285	8.88395644970530	1.97110740792083
C	10.56624446410790	10.24950098344686	4.40936849731354
C	11.20816678752926	7.29451222940100	3.39998468314868
C	11.09337521169781	5.75110452799101	3.38204257678268
H	11.72357574298785	5.33340230702030	2.59977286276831
H	10.06473352921322	5.47496680035747	3.19174406091668
H	11.40875691029806	5.33894987157953	4.33197381853155
C	12.71178281296603	7.61559521715514	3.42402136773504
H	13.18647553983709	7.17516623625244	4.29227952337899
H	12.88674981282747	8.68715974748248	3.44368549736124
H	13.19040678794445	7.20992143165145	2.53683134055841

H	11.12375673045772	10.45340978354043	5.32918608458651
H	9.90638050329378	11.08960422981191	4.21035069900076
H	11.27140359899568	10.16830979936539	3.59417220986448
H	9.52104635295279	7.64003325374604	2.09178734515750
H	6.95998619868020	1.17497625906387	4.56866496252934
H	10.58057543656021	0.73536253194308	6.60676733353346
H	5.28227656232059	4.38954982881123	1.96933705048578
H	7.43134175926456	4.77497366968620	3.55830449191914
H	5.69000227288865	2.00376628217647	0.75066046915271
H	8.06011153500688	1.10034795025591	1.67745090308255
H	12.28307651314380	0.74328098315214	-0.12707040216320
H	10.62901929278914	2.58076604697896	0.95244470601343
H	12.62363272657258	-1.14940655009172	1.78001348200285
H	11.17540742155278	-0.32149727426097	3.90282531270642
H	13.02395457975395	2.28237489289778	3.57994702489856
H	14.77936874491667	3.78714591248754	4.96921249163896
H	10.96459624877116	3.61134370876596	6.96294341740182
H	13.43815292727462	4.66328960941527	7.15605645117386
Cl	11.17609883854096	7.41530910486712	6.16567801267215

61

Coordinates from ORCA-job INT1_tbu_aaac_sn2_pyrr4_cmp_Compound_1

Sn	10.22557097110696	3.83456963970499	4.14603804336064
C	10.61590407332500	6.12090940514703	4.21120284462660
N	11.85634850769159	3.29456061199267	5.43980290250762
N	8.93818865217338	2.75140533238483	5.41210981896970
C	9.27554737533211	1.70688308306186	6.23551321503511
C	11.87521223407441	3.42647814601861	6.80034471250920
C	13.14926160255056	3.09144139012383	5.04023360959219
C	7.57340188305928	2.88570508394609	5.46023761790713
C	13.15573230171412	3.28334629654786	7.26657466547867
C	8.14177515084938	1.19339146467477	6.80699737910745
H	8.10313183543617	0.36800793479324	7.49256414198416
C	13.97537754772231	3.06943111322588	6.13467853610024
C	7.05409201511986	1.95104939655135	6.31500552145503
H	6.01348845859732	1.81979010387672	6.54383673630968
N	9.38153628568843	6.75393486170376	4.42722646478786
N	8.51806611477887	3.98856806176125	2.78770537403107
N	11.01994368858405	2.48478237232379	2.74448382579068
C	11.06488297601231	2.60597331692099	1.38312845023648
C	7.56651331959453	4.96220011514981	2.62190205459287
C	7.99252849743038	2.83367801832438	2.27320204532320
C	11.39728710004218	1.20673140814341	3.05574627669665
C	6.46516676398303	4.43679112702450	1.99300367553394
C	11.48254973265203	1.42308355079138	0.83188643399871
C	6.73883463209066	3.06930759800790	1.77153638981678
C	11.69171301659420	0.52501233796338	1.90337940762972
C	8.64332563097667	6.29822458414349	5.58650835234070
H	8.69084083124422	5.22520749153268	5.70345585608837
H	7.59753033088009	6.56237696628807	5.47067374085392

H	9.02632370366804	6.74106362488559	6.50728884272586
C	10.54048783352782	6.55345318664491	1.74076264024543
H	11.14680396535683	6.73988225872795	0.85832204068281
H	9.76075762649528	7.30504650449342	1.77433617735390
C	9.28980287330958	8.19995721170382	4.35805173257259
C	11.43816633958626	6.58311844115935	2.97584031380406
C	12.59586722402705	5.61303208486756	2.75169836524046
H	13.22198279048926	5.98187854800982	1.94432854498302
H	12.26690594339364	4.62531391171395	2.45342587465924
H	13.20654585493931	5.51311820020892	3.63977118640605
C	12.10164538399941	7.96391266882379	3.08640032474166
H	12.82983559563197	7.97842392788892	3.88612722879739
H	11.41909536943900	8.78493311761958	3.24059569966000
H	12.62543353547826	8.15231095420803	2.15266504101991
H	9.95889002272670	8.68940111360980	5.06918347852290
H	8.27168872810184	8.48297499054351	4.60013045802120
H	9.49920690556706	8.56366219528710	3.36468494922403
H	10.04825307681773	5.59739060743667	1.61573367180514
H	7.07038018515506	3.60845862541099	4.84923028902524
H	10.29725285295299	1.41673244655801	6.35785811977176
H	5.57860274703182	4.97706044915525	1.71663075762246
H	7.75594241859473	5.96394296821791	2.94208196278576
H	6.10317154197685	2.34522234703660	1.29799009130442
H	8.54632472637237	1.91742448358391	2.30928067683058
H	11.61486641062321	1.22790119616494	-0.21529098653531
H	10.76025143161772	3.51337362253376	0.90226866939130
H	12.02019984016669	-0.49479145566952	1.84073845252629
H	11.44389327639853	0.88861526858030	4.07716411464306
H	13.38293834946985	2.94079284438675	4.00599767886979
H	15.03492383478294	2.89476205902403	6.12236326727184
H	10.97039316959350	3.61739092570366	7.34157827806896
H	13.46340439008367	3.32339926709539	8.29449953973015
Cl	11.74067052331980	6.44739059225627	5.73809442556323

10 Literature

(1) Ruppert, H.; Greb, L. Calix[4]Pyrrolato Stannate(II): A Tetraamido Tin(II) Dianion and Strong Metal-Centered σ-Donor. *Angew. Chem. Int. Ed.* **2022**, *61* (13), e202116615. https://doi.org/10.1002/anie.202116615.

(2) Ebenbeck, W. D.; Hilgers, P. D.; Marhold, A. D.; Barten, J. A. D.; Kolomeitsev, A. D.; Röschenthaler, G.-V. P. D. Fluorierungsreagenzien Und Verfahren Zu Deren Herstellung. DE10300112A1, July 15, 2004. https://patents.google.com/patent/DE10300112A1/de (accessed 2022-11-09).

(3) Wang, J.; Li, S.; Zhang, S. Novel Hydroxide-Conducting Polyelectrolyte Composed of an Poly(Arylene Ether Sulfone) Containing Pendant Quaternary Guanidinium Groups for Alkaline Fuel Cell Applications. *Macromolecules* **2010**, *43* (8), 3890–3896. https://doi.org/10.1021/ma100260a.

(4) Schrempp, D. F.; Kaifer, E.; Wadepohl, H.; Himmel, H.-J. Copper Complexes of New Redox-Active 4,5-Bisguanidino-Substituted Benzodioxole Ligands: Control of the Electronic Structure by Counter-Ligands, Solvent, and Temperature. *Chem. – Eur. J.* **2016**, *22* (45), 16187–16199. https://doi.org/10.1002/chem.201602402.

(5) Sheldrick, G. Crystal Structure Solution with ShelXT. *Acta Crystallogr A* **2015**, *71*, 3–8.

(6) Sheldrick, G. Crystal Structure Refinement with SHELXL. *Acta Crystallogr. Sect. C* **2015**, *71* (1), 3–8. https://doi.org/doi:10.1107/S2053229614024218.

(7) Hübschle, C. B.; Sheldrick, G. M.; Dittrich, B. ShelXle: A Qt Graphical User Interface for SHELXL. *J. Appl. Crystallogr.* **2011**, *44* (6), 1281–1284. https://doi.org/10.1107/S0021889811043202.

(8) Sheldrick, G. A Short History of SHELX. *Acta Crystallogr. Sect. A* **2008**, *64* (1), 112–122. https://doi.org/doi:10.1107/S0108767307043930.

(9) Neese, F. Software Update: The ORCA Program System—Version 5.0. *WIREs Comput. Mol. Sci.* **2022**, e1606. https://doi.org/10.1002/wcms.1606.

(10) Rüger, R.; Franchini, M.; Trnka, T.; Yakovlev, A.; van Lenthe, E.; Philipsen, P.; van Vuren, T.; Klumpers, B.; Soini, T. AMS 2021.102, SCM. *AMS 2021102 SCM* **2021**.

(11) te Velde, G.; Bickelhaupt, F. M.; Baerends, E. J.; Fonseca Guerra, C.; van Gisbergen, S. J. A.; Snijders, J. G.; Ziegler, T. Chemistry with ADF. *J. Comput. Chem.* **2001**, *22* (9), 931–967. https://doi.org/10.1002/jcc.1056.

(12) Mardirossian, N.; Head-Gordon, M. Mapping the Genome of Meta-Generalized Gradient Approximation Density Functionals: The Search for B97M-V. *J. Chem. Phys.* **2015**, *142* (7), 074111. https://doi.org/10.1063/1.4907719.

(13) Caldeweyher, E.; Bannwarth, C.; Grimme, S. Extension of the D3 Dispersion Coefficient Model. *J. Chem. Phys.* **2017**, *147* (3), 034112. https://doi.org/10.1063/1.4993215.

(14) Weigend, F.; Ahlrichs, R. Balanced Basis Sets of Split Valence, Triple Zeta Valence and Quadruple Zeta Valence Quality for H to Rn: Design and Assessment of Accuracy. *Phys. Chem. Chem. Phys.* **2005**, *7* (18), 3297–3305. https://doi.org/10.1039/B508541A.

(15) Weigend, F. Accurate Coulomb-Fitting Basis Sets for H to Rn. *Phys. Chem. Chem. Phys.* **2006**, *8* (9), 1057–1065. https://doi.org/10.1039/B515623H.

(16) Pracht, P.; Bohle, F.; Grimme, S. Automated Exploration of the Low-Energy Chemical Space with Fast Quantum Chemical Methods. *Phys. Chem. Chem. Phys.* **2020**, *22* (14), 7169–7192. https://doi.org/10.1039/C9CP06869D.

(17) Bannwarth, C.; Caldeweyher, E.; Ehlert, S.; Hansen, A.; Pracht, P.; Seibert, J.; Spicher, S.; Grimme, S. Extended Tight-Binding Quantum Chemistry Methods. *WIREs Comput. Mol. Sci.* **2021**, *11* (2), e1493. https://doi.org/10.1002/wcms.1493.

(18) Marenich, A. V.; Cramer, C. J.; Truhlar, D. G. Universal Solvation Model Based on Solute Electron Density and on a Continuum Model of the Solvent Defined by the

Bulk Dielectric Constant and Atomic Surface Tensions. *J. Phys. Chem. B* **2009**, *113* (18), 6378–6396. https://doi.org/10.1021/jp810292n.
(19) Kozuch, S.; Gruzman, D.; Martin, J. M. L. DSD-BLYP: A General Purpose Double Hybrid Density Functional Including Spin Component Scaling and Dispersion Correction. *J. Phys. Chem. C* **2010**, *114* (48), 20801–20808. https://doi.org/10.1021/jp1070852.
(20) Grimme, S.; Antony, J.; Ehrlich, S.; Krieg, H. A Consistent and Accurate Ab Initio Parametrization of Density Functional Dispersion Correction (DFT-D) for the 94 Elements H-Pu. *J. Chem. Phys.* **2010**, *132* (15), 154104. https://doi.org/10.1063/1.3382344.
(21) Ren, X.; Rinke, P.; Blum, V.; Wieferink, J.; Tkatchenko, A.; Sanfilippo, A.; Reuter, K.; Scheffler, M. Resolution-of-Identity Approach to Hartree–Fock, Hybrid Density Functionals, RPA, MP2 and GW with Numeric Atom-Centered Orbital Basis Functions. *New J. Phys.* **2012**, *14* (5), 053020. https://doi.org/10.1088/1367-2630/14/5/053020.
(22) Stoychev, G. L.; Auer, A. A.; Neese, F. Automatic Generation of Auxiliary Basis Sets. *J. Chem. Theory Comput.* **2017**, *13* (2), 554–562. https://doi.org/10.1021/acs.jctc.6b01041.
(23) Zhurko, G. Chemcraft, 2005. https://chemcraftprog.com.
(24) Adamo, C.; Barone, V. Toward Reliable Density Functional Methods without Adjustable Parameters: The PBE0 Model. *J. Chem. Phys.* **1999**, *110* (13), 6158–6170. https://doi.org/10.1063/1.478522.
(25) Glendening, E. D.; Badenhoop, J. K.; Reed, A. E.; Carpenter, J. E.; Bohmann, J. A.; Morales, C. M.; Landis, C. R.; Weinhold, F. *NBO 6.0*. Google Scholar There is no corresponding record for this reference.
(26) Ziegler, T.; Rauk, A. On the Calculation of Bonding Energies by the Hartree Fock Slater Method. *Theor. Chim. Acta* **1977**, *46* (1), 1–10. https://doi.org/10.1007/BF00551648.
(27) Ziegler, T.; Rauk, A. Carbon Monoxide, Carbon Monosulfide, Molecular Nitrogen, Phosphorus Trifluoride, and Methyl Isocyanide as .Sigma. Donors and .Pi. Acceptors. A Theoretical Study by the Hartree-Fock-Slater Transition-State Method. *Inorg. Chem.* **1979**, *18* (7), 1755–1759. https://doi.org/10.1021/ic50197a006.
(28) Ziegler, T.; Rauk, A. A Theoretical Study of the Ethylene-Metal Bond in Complexes between Copper(1+), Silver(1+), Gold(1+), Platinum(0) or Platinum(2+) and Ethylene, Based on the Hartree-Fock-Slater Transition-State Method. *Inorg. Chem.* **1979**, *18* (6), 1558–1565. https://doi.org/10.1021/ic50196a034.
(29) Mitoraj, M. P.; Michalak, A.; Ziegler, T. A Combined Charge and Energy Decomposition Scheme for Bond Analysis. *J. Chem. Theory Comput.* **2009**, *5* (4), 962–975. https://doi.org/10.1021/ct800503d.
(30) Grimme, S.; Ehrlich, S.; Goerigk, L. Effect of the Damping Function in Dispersion Corrected Density Functional Theory. *J. Comput. Chem.* **2011**, *32* (7), 1456–1465. https://doi.org/10.1002/jcc.21759.
(31) Becke, A. D. Density-Functional Exchange-Energy Approximation with Correct Asymptotic Behavior. *Phys. Rev. A* **1988**, *38* (6), 3098–3100. https://doi.org/10.1103/PhysRevA.38.3098.
(32) Perdew, J. P. Density-Functional Approximation for the Correlation Energy of the Inhomogeneous Electron Gas. *Phys. Rev. B* **1986**, *33* (12), 8822–8824. https://doi.org/10.1103/PhysRevB.33.8822.
(33) Knizia, G.; Klein, J. E. M. N. Electron Flow in Reaction Mechanisms—Revealed from First Principles. *Angew. Chem. Int. Ed.* **2015**, *54* (18), 5518–5522. https://doi.org/10.1002/anie.201410637.
(34) Xie, L.-G.; Dixon, D. J. Tertiary Amine Synthesis via Reductive Coupling of Amides with Grignard Reagents. *Chem. Sci.* **2017**, *8* (11), 7492–7497.

https://doi.org/10.1039/C7SC03613B.
(35) Erdmann, P.; Leitner, J.; Schwarz, J.; Greb, L. An Extensive Set of Accurate Fluoride Ion Affinities for P-Block Element Lewis Acids and Basic Design Principles for Strong Fluoride Ion Acceptors. *ChemPhysChem* **2020**, *21* (10), 987–994. https://doi.org/10.1002/cphc.202000244.

3.5 Chemistry of Anti-van't Hoff-Le Bel Calix[4]pyrrolato Stannanes

The following section describes the chemistry of *meso*-substituted calix[4]pyrrolato stannanes $\mathbf{2^R}$ featuring a square-planar anti-van't Hoff-Le Bel structure. First, preliminary computational studies on the planarization of tetrapyrrolato stannane **12** and the comparison of $\mathbf{2^{Me}}$ with its lighter homologs $\mathbf{8^{Me}}$ and $\mathbf{9^{Me}}$ will highlight the reactivity differences expected for stannanes $\mathbf{2^R}$ (**Section 3.5.1**). Subsequently, the experimental chemistry of $\mathbf{2^R}$ featuring methyl and ethyl *meso*-substituents (R = Me, Et, **Section 3.5.2**) and the synthesis of a new, sterically demanding calix[4]pyrrole (R = *o*Phen, *ortho*-phenylene) ligand $\mathbf{H_4[1^{oPhen}]}$ and its application in Sn(IV) chemistry will be described (**Section 3.5.3**).

3.5.1 *In Silico* Comparison of Silicon, Germanium, and Tin Calix[4]pyrroles

As covered in **Section 1.5** and shown experimentally in the work in **Section 3.4**,[272] planarization of the tetrakis(pyrrolato) stannane system **12** through the application of calix[4]pyrrolato ligands significantly increases the Lewis acidity of these Sn(IV) compounds. Figure 26 summarizes a series of computed parameters showcasing the effect of planarization on Lewis acidity and the electronic structure of tetrakis(pyrrolato) stannanes: i) $\mathbf{2^R}$ (R = Me, Et) possess energetically stabilized LUMOs and reduced HOMO-LUMO gaps, ii) the FIA_{solv} values increase by 73 and 56 kJ mol^{-1} for $\mathbf{2^{Me}}$ and $\mathbf{2^{Et}}$, respectively, iii) the partial charge at the tin center δ(Sn) increases slightly for $\mathbf{2^{Me}}$, and iv) $\mathbf{2^R}$ show significantly decreased *Wiberg bond indices* (WBI) for the Sn-N bonds indicating a less covalent bonding character. As reported for the related *meso*-octaalkylcalix[4]pyrrolato stannates(II) $\mathbf{[2^R]^{2-}}$ in **Section 3.2**, the inductive effect of the *meso*-ethyl substituents increases the electron-richness of the calix[4]pyrrole ligand backbone. For $\mathbf{2^{Et}}$ this effect results in a decreased Lewis acidity when compared to $\mathbf{2^{Me}}$.

In silico comparison with its silicon and germanium analogs $\mathbf{8^{Me}}$ and $\mathbf{9^{Me}}$ revealed particularities for the Lewis acid and element-ligand cooperative chemistry of $\mathbf{2^{Me}}$. In accordance with PEARSON'S theory of *Hard and Soft Lewis Acids and Bases* (HSAB),[273–275] the affinity towards the hard fluoride anion (FIA_{solv}) decreases while the affinity towards the soft chloride anion (CIA_{solv}) increases within the series Si, Ge, Sn (Figure 26 A). The HIA_{solv} values for *meso*-octamethylcalix[4]pyrrolato silane, germane, and stannane all lie in a close range between 457 and 467 kJ mol^{-1}. These observations are in good agreement with

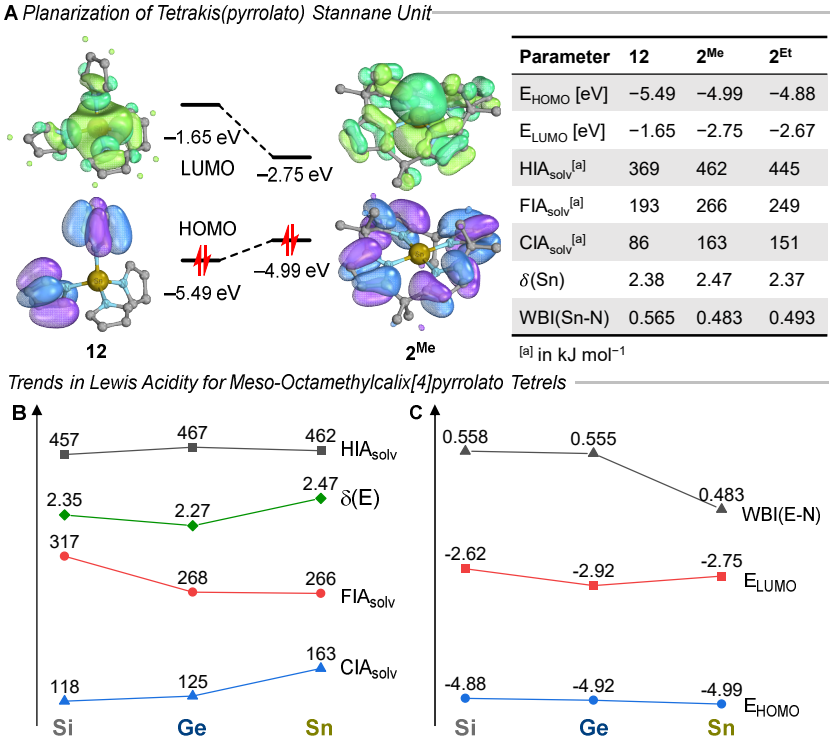


Figure 26. A) Comparison of computed parameters for unconstrained stannane **12** with methyl- and ethyl-substituted calix[4]pyrrolato stannanes **2^{R}** (R = Me, Et) and trends in Lewis acidity within group 14 *meso*-octamethylcalix[4]pyrrolato compounds featuring Si (**8^{Me}**), Ge (**9^{Me}**), and Sn (**2^{Me}**). **B)** Solvation-corrected ion affinities for hydride (HIA_{solv}), fluoride (FIA_{solv}), and chloride (CIA_{solv}) in kJ mol^{-1} and partial charge of the central atom E δ(E). **C)** FMO energies in eV and WBI of the E-N bond. All orbital energies were computed on the B97M-D3(BJ)/def2-TZVPP CPCM SMD(DCM)//B97M-D3(BJ)/def2-TZVPP level of theory. Solvation-corrected ion affinities were calculated on the DSD-BLYP-D3(BJ)/def2-QZVPP//BP86/TZP COSMO-RS(DCM)//B97M-D3(BJ)/def2-TZVPP level of theory. δ(E) and WBI were obtained *via* NBO calculations on the PBE0 def2-TZVPP//B97M-D3(BJ)/def2-TZVPP level of theory.

the significant decrease in E-H bond energy for heavier tetrel atoms E which counteracts their increased soft Lewis acidity.[140,141,276]

In a first approximation the partial charge at the central element E δ(E) aligns with the electronegativity trend within group 14 according to PAULING.[138] However, even though tin is slightly more electronegative than silicon (1.96 *vs* 1.90), the partial charge at Sn in **2^{Me}** is significantly more positive (Figure 26 B). This effect can be explained by the decreased covalency of the Sn-N bonds in **2^{Me}** resulting in a reduced transfer of

electron density from N to the Sn center compared to the respective Si-N and Ge-N bonds in $\mathbf{8}^{Me}$ and $\mathbf{9}^{Me}$ (see WBI in Figure 26 A and C and E-N bond lengths in Table S18). No clear-cut trend could be identified for the FMO energies and the obtained values are probably caused by an interplay of electronegativity and orbital interaction effects. In summary, based on these computed parameters stannane $\mathbf{2}^{Me}$ can be expected to be a strong, soft Lewis acid.

Silicon and germanium calix[4]pyrrolato compounds react with a variety of unsaturated carbon-hetero atom and carbon-carbon multiple bonds forming so-called 1,2-adducts by means of element-ligand cooperativity (Figure 27).[113,122] For Lewis basic substrates such as carbonyls and nitriles the initial step is the formation of a σ-adduct *via* TS1.[115,122] The subsequent nucleophilic attack of the α-carbon atom in the calix[4]pyrrole ligand backbone at the polarized substrate forms the respective 1,2-adducts *via* TS2. For weakly-donating substrates such as phenylacetylene and styrene, a concerted mechanism involving a single transition structure was found.

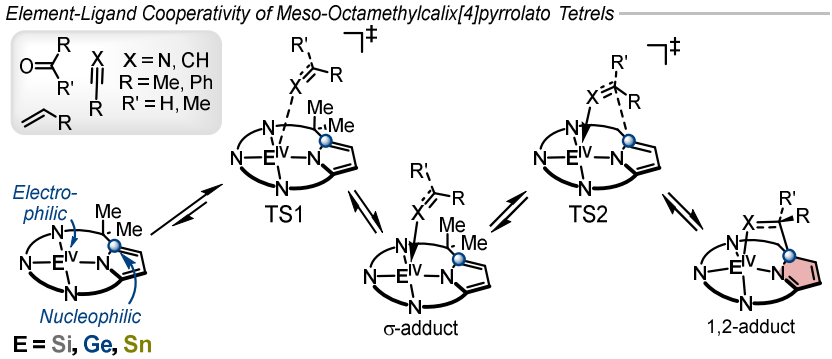


Figure 27. General reaction scheme for the cooperative binding of carbonyl, nitriles, alkenes, and alkynes by calix[4]pyrrolato tetrels. In the absence of strong donor functionalities such as oxygen or nitrogen atoms (phenylacetylene and styrene), concerted mechanisms going from TS1 directly to the 1,2-adduct were obtained.

Comparison of the computed thermodynamics (PW6B95-D3(BJ)/def2-QZVPP//BP86/TZP COSMO-RS(DCM)) for these substrate activation reactions revealed marked differences between the tin-containing $\mathbf{2}^{Me}$ and its silicon and germanium analogs $\mathbf{8}^{Me}$ and $\mathbf{9}^{Me}$ (Figure 28). In general, $\mathbf{2}^{Me}$ yields more stable σ-adducts with carbonyls and MeCN and prefers this binding mode over the cooperative binding as 1,2-adducts. The inverse can be observed for $\mathbf{8}^{Me}$ and $\mathbf{9}^{Me}$ with the silane $\mathbf{8}^{Me}$ forming the most stable 1,2-adducts. For the exergonic formation of an 1,2-adduct the energy gain through the

newly formed bonds between substrate and calix[4]pyrrole tetrel have to compensate the loss of energy caused by the dearomatization of one pyrrole unit (red). Thus, the observed trends align well with the bond dissociation energies of E-O and E-N single bonds which decrease within the sequence E = Si > Ge > Sn, thereby destabilizing the respective 1,2-adducts.[141] As described for $\mathbf{9^{Et}}$ in **Section 1.4.2**, calix[4]pyrrolato germanes activate MeCN *via* a 1,2-adduct followed by cleavage and rearrangement of the calix[4]pyrrole ligand backbone. In contrast, the computational results in Figure 28 predict the formation of a stable σ-adduct of acetonitrile with $\mathbf{2^{Me}}$. The pronounced Lewis acidity of stannane $\mathbf{2^{Me}}$ can further be rationalized by the absence of a transition structure TS1 for the entry of a Lewis basic substrate. Relaxed surface scans showed an essentially barrierless formation of a Lewis σ-adduct and transition structure optimizations always led to the

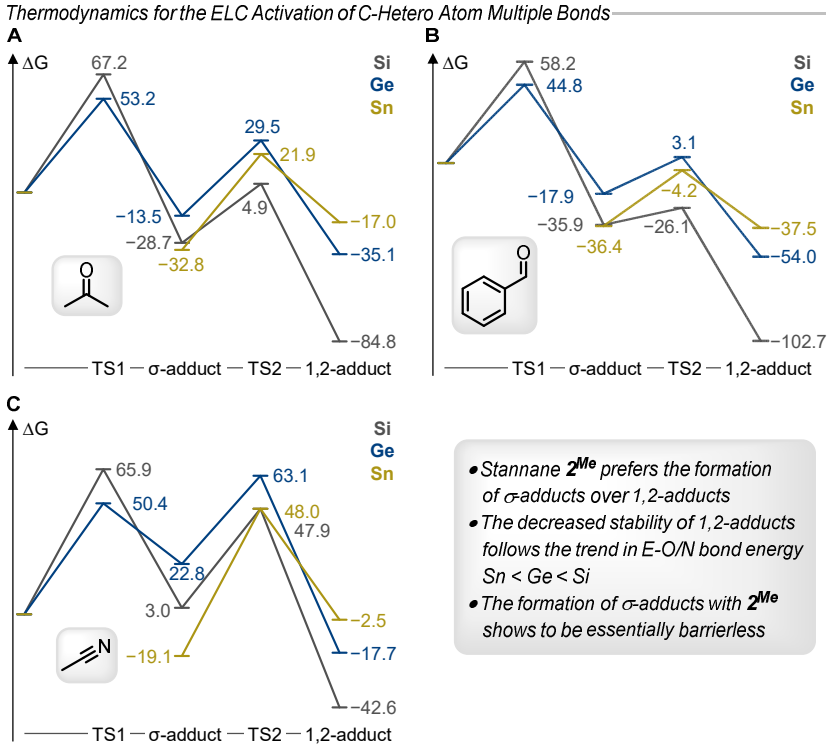


Figure 28. Gibbs free enthalpies computed at the PW6B95-D3(BJ)/def2-QZVPP//BP86/TZP COSMO-RS(DCM)//B97M-D3(BJ)/def2-TZVPP level of theory for the cooperative activation of **A)** acetone, **B)** benzaldehyde, and **C)** acetonitrile according to the general reaction mechanism shown in Figure 27.

relaxation into the σ-adduct ground state structure. Thus, the Lewis acidic center in **2**^{Me}, seems to be more accessible than the respective Si and Ge centers in **8**^{Me} and **9**^{Me} indicating a reduced deformation energy *i.e.,* an increased flexibility for the tin calix[4]pyrrole system.

For the activation of carbon-carbon multiple bonds only minor differences in the overall free reaction enthalpy could be observed. However, for both phenylacetylene and styrene, **2**^{Me} shows significantly lowered activation barriers relative to **8**^{Me} and **9**^{Me}. This effect is most pronounced for the activation of styrene (Figure 29 A and B). Energy decomposition analysis (EDA) of styrene 1,2-adducts using the extended transition state method (ETS) in combination with the natural orbitals for chemical valence (NOCV) theory revealed key differences between the group 14 central atoms (Table S19). The exemplary plot of the ETS-NOCV difference density for the 1,2-adduct of styrene and **2**^{Me} shows the depletion (red) and accumulation (blue) of electron density upon adduct formation and aligns well with the cooperative binding between an electrophilic Sn(IV) center and a nucleophilic calix[4]pyrrole α-carbon atom (Figure 29 C). Both the total orbital interaction ($\Delta E_{oi,tot}$) between the calix[4]pyrrole tetrel and styrene fragment and the total bonding energy (ΔE) become less exergonic in the order Si > Ge > Sn in line with decreased E-C bond energies. However, this trend is not represented in the computed ΔG values shown in Figure 29 B. The standard EDA scheme does not include the preorganization/deformation of the substrates prior to the adduct formation. To account for the deformation energies (DE) of calix[4]pyrrole tetrels, the single point energies of their preorganized structures were compared to the respective energies of their minimum energy structures. Plotting of ΔE, DE, and their sum ΔE+DE revealed how the decreased deformation energies of heavier group 14 calix[4]pyrroles compensate for their weaker bonding interactions with the respective styrene fragments (Figure 29 D). With the lowest DE of 146.1 kJ mol^{-1}, **2**^{Me} again possessed an increased flexibility. These findings also align with the reduced covalency of the E-N bonds in **2**^{Me} when compared to **8**^{Me} and **9**^{Me} (see WBI in Figure 26 C). The increased flexibility of **2**^{Me} further allow a low-energy preorganization of **2**^{Me} during its encounter with styrene in TS1 resulting in the drastically reduced energy barriers for this reaction.

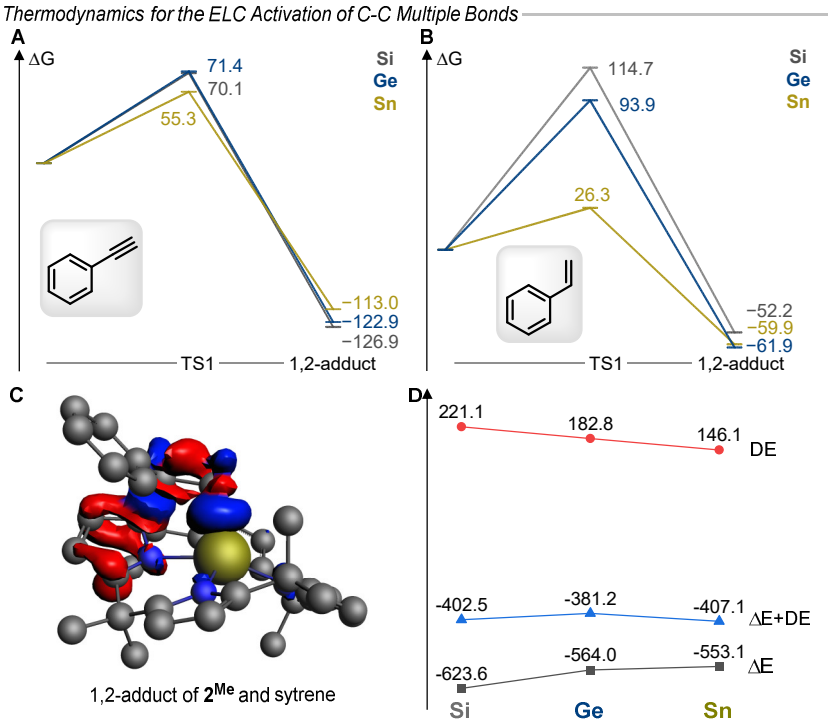


Figure 29. Gibbs free enthalpies in kJ mol^{-1} computed at the PW6B95-D3(BJ)/def2-QZVPP//BP86/TZP COSMO-RS(DCM)//B97M-D3(BJ)/def2-TZVPP level of theory for the cooperative activation of **A)** phenylacetylene and **B)** styrene according to the general reaction mechanism shown in Figure 27. For phenylacetylene and styrene no σ-adduct could be optimized and a concerted reaction mechanism showing only one transition structure TS1 was found. **C)** Exemplary ETS-NOCV difference density plot of the 1st NOCV-channel for the 1,2-adduct of **2^{Me}** and styrene computed on the BP86-D3/TZ2P//B97M-D3(BJ)/def2-TVZPP level of theory. NOCV deformation densities sampled at a value of 0.004. The color code of the charge flow is red to blue. **D)** Plots of the total bonding energy (ΔE), deformation energy of the calix[4]pyrrole tetrel (DE), and their sum for the 1,2-adducts with styrene computed on the BP86-D3/TZ2P//B97M-D3(BJ)/def2-TVZPP level of theory. All values are given in in kJ mol^{-1}.

In conclusion, compared to the respective silanes and germanes, calix[4]pyrrolato stannanes are expected to be strong, soft Lewis acids with an increased molecular flexibility, reduced energy barriers for the ELC activations of C-C multiple bonds, and a reduced tendency to form 1,2-adducts with carbonyl and nitrile substrates. The following sections will focus on the experimental realization of these *in silico* predicted properties.

3.5.2 Chemistry of *Meso*-octaalkylcalix[4]pyrrolato Stannanes

In 1999 FLORIANI and coworkers reported the synthesis of the bis(thf) adduct of *meso*-octaethylcalix[4]pyrrolato stannane **2^{Et}-(thf)$_2$** and described its application for the modification of the ligand backbone by oxidative dealkylation (see **Section 0**).[112] The following section will describe the synthesis of formerly unknown methyl-substituted **2^{Me}-(thf)$_2$**, and explore the chemistry of **2^{Me}** and **2^{Et}** towards their isolation as free, square-planar Sn(IV) Lewis acids.

In analogy to the procedure reported for the synthesis of **2^{Et}-(thf)$_2$**, reaction of a suspension of **[Li$_4$(thf)$_x$][1^{Me}]** in toluene with one equivalent of bis(thf)-tin(IV) tetrachloride $SnCl_4(thf)_2$ yielded **2^{Me}-(thf)$_2$** already at room temperature in an acceptable yield of 67% at multigram scale (Figure 30 A). ^{1}H NMR spectroscopy in CD_2Cl_2 showed only one set of resonances for the pyrrole C-H, the *meso*-methyl groups, and the THF donors, being in line with the expected D_{4h} symmetry of **2^{Me}-(thf)$_2$**. For both adducts **2^{R}-(thf)$_2$** (R = Me, Et), $^{117/119}$Sn satellites and cross signals in ^{1}H,^{119}Sn-HMBC NMR experiments disclosed the incorporation of a tin center into the calix[4]pyrrolato ligand backbone and its coordination by THF donors (Figure 30 B). The ^{119}Sn chemical shifts of −553.6 (R = Me) and −561.1 ppm (R = Et) are in the range of literature known, highly coordinated Sn centers.[277] In contrast to the broad THF resonances reported for the germane bis(thf) adduct **9^{Et}-(thf)$_2$**,[122] the ^{1}H NMR spectra of **2^{R}-(thf)$_2$** showed narrow signals which even enabled the resolution of the multiplet structure for the THF units (Figures S1 and S1 in the Appendix). These observations align well with the computed dissociation free enthalpies of THF bound to the Sn(IV) centers (ΔG_{diss}(THF)) being 55.2 and 63.3 kJ mol^{-1} for the 1st and 2nd THF dissociation from **2^{Me}-(thf)$_2$** and 69.0 and 88.9 kJ mol^{-1} for **2^{Et}-(thf)$_2$**, respectively (DSD-BLYP-D3(BJ)/ def2-QZVPP // BP86 / TZP COSMO-RS(DCM) // B97M-D4/ def2-TZVPP // CREST /GFN2-xTB level of theory). These values lie between 40 and 70 kJ mol^{-1} above the values computed for germane **9^{Et}**, indicating increased Lewis acidity against THF for stannanes **2^{R}**.[122] Furthermore, the increased THF binding strength for R = Et is in line with the results obtained for differently substituted *meso*-octaalkylcalix[4]pyrrolato aluminates **[5^{R}]$^-$** (R = Me, Et, C6), which showed an increased dispersion interaction between the *meso*-ethyl substituents and coordinated THF (see **Section 1.4.1**).

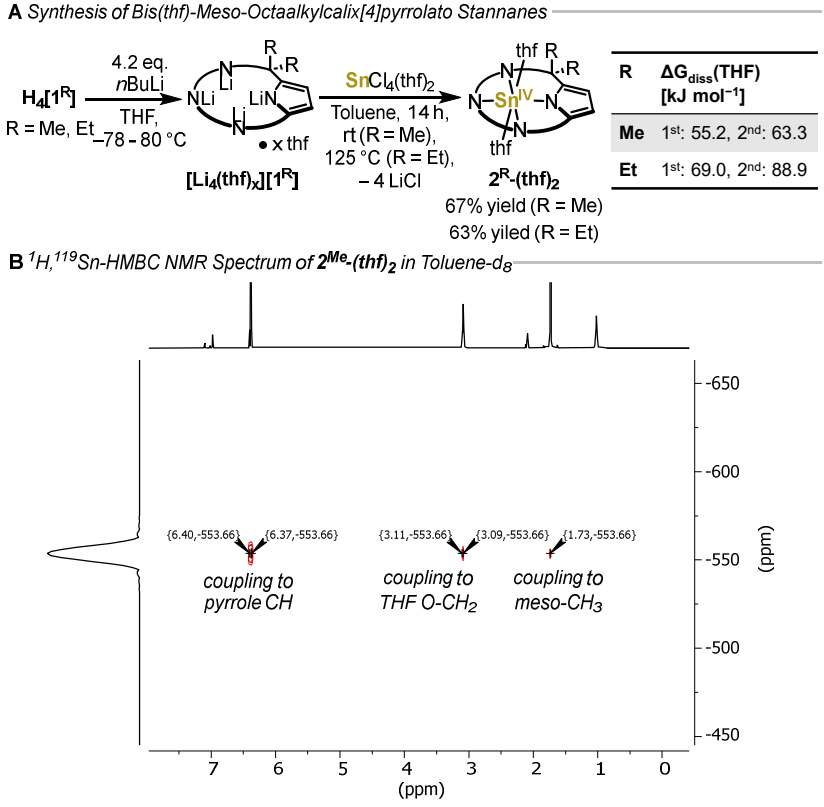


Figure 30. A) Synthesis of the bis(thf) adducts of *meso*-octaalkylcalix[4]pyrrolato stannanes $\mathbf{2^R}$ (R = Me, Et) and dissociation free enthalpies ΔG_{diss} for the 1st and 2nd THF bound to $\mathbf{2^R}$ in kJ mol^{-1} computed at the DSD-BLYP-D3(BJ)/def2-QZVPP//BP86/TZP COSMO-RS(DCM)//B97M-D4/def2-TZVPP//CREST/GFN2-xTB level of theory. **B)** Exemplary ^{1}H,^{119}Sn-HMBC NMR spectrum of $\mathbf{2^{Me}\text{-}(thf)_2}$ in toluene-d_8 recorded at 295 K.

Even though FLORIANI and coworkers reported that single crystals of $\mathbf{2^{Et}\text{-}(thf)_2}$ could be grown from THF and *n*-hexane, no discussion of its solid-state molecular structure was reported and no structural data for $\mathbf{2^{Et}\text{-}(thf)_2}$ could be found in the *Cambridge Structural Database* (CSD) of the *Cambridge Crystallographic Data Center* (CCDC). Cooling of a concentrated solution of $\mathbf{2^{Et}\text{-}(thf)_2}$ in toluene to −30°C yielded single crystals suitable for X-ray diffraction. However, multiple attempts to obtain high-quality single crystals for $\mathbf{2^{Me}\text{-}(thf)_2}$ remained unsuccessful. The solid-state molecular structure of $\mathbf{2^{Et}\text{-}(thf)_2}$ is shown in Figure 31 A. Compared to the free, square planar silane $\mathbf{8^{Et}}$ ($d_{Si\text{-}N} \approx 179.4$ pm)[113] and the germane bis(thf) adduct $\mathbf{9^{Et}\text{-}(thf)_2}$ ($d_{Ge\text{-}N} \approx 196.5$ pm),[122] $\mathbf{2^{Et}\text{-}(thf)_2}$ exhibits elongated Sn-

N bonds ($d_{Sn-N} \approx 209.0$ pm) in line with an increased nuclear radius and the reduced covalency of the Sn-N bonds described in the previous section. For **9^{Et}-(thf)$_2$** and **2^{Et}-(thf)$_2$**, the pyrrolato units are tilted out of the N_4 coordination plane. This increases the cavity size of the calix[4]pyrrole macrocycle and arranges the *meso*-ethyl substituents away from the axial coordination sites opening up space to accommodate the THF ligands. For the free *meso*-octaethylcalix[4]pyrrolato silane **8^{Et}** the tilting of pyrrole units cannot be observed and the ethyl substituents point inward showing agostic-type interaction of the CH_2 groups with the Lewis acidic Si(IV) center. These observations further underline the structural flexibility of the *meso*-octaalkylcalix[4]pyrrolato ligand backbone in these complexes.

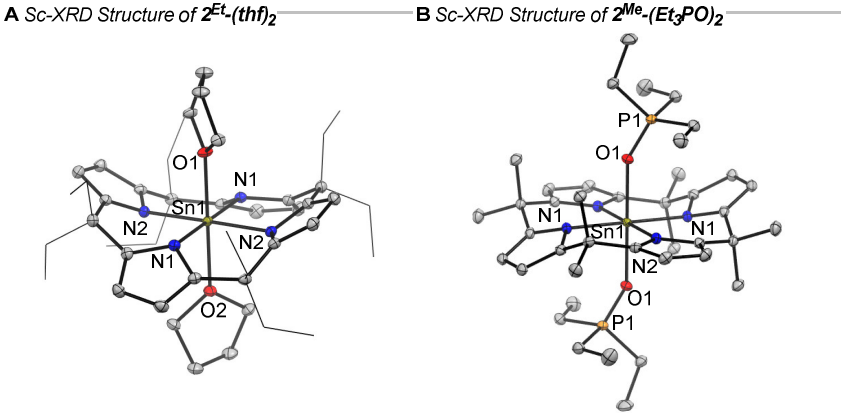


Figure 31. Solid-state molecular structure of **A) 2^{Et}-(thf)$_2$** and **B) 2^{Me}-(Et$_3$PO)$_2$**. Ellipsoids are drawn with a probability of 50%. Hydrogen atoms are omitted for clarity. *Meso*-ethyl substituents are drawn as wireframe for clarity. **2^{Et}-(thf)$_2$** co-crystallized with two toluene molecules per formula unit which are omitted for clarity. Selected bond lengths [pm] and angles [deg] for **2^{Et}-(thf)$_2$**: Sn1-N1 = 209.51(11), Sn1-N2 = 208.46(11), Sn1-O1 = 219.61(13), Sn1-O2 = 221.94(13), N1-Sn1-N2 = 89.78(4), N1-Sn1-N1 = 179.58(6), N2-Sn1-N2 = 179.18(6); and **2^{Me}-(Et$_3$PO)$_2$**: Sn1-N1 = 212.22(14), Sn1-N2 = 211.77(12), Sn1-O1 = 212.38(13), P1-O1 = 151.65(11), N1-Sn1-N2 = 89.75(5), N1-Sn1-N1 = 180.0, N2-Sn1-N2 = 180.00(2).

To probe the exchange of ligands at the Sn(IV) centers and obtain a first experimental value for the effective Lewis acidities of **2^{R}** *via* the *Gutmann-Beckett* method, **2^{R}-(thf)$_2$** (R = Me, Et) were reacted with two equivalents of triethylphosphine oxide (Et_3PO) in CD_2Cl_2.[43] For R = Me the immediate, clean formation of **2^{Me}-(Et$_3$PO)$_2$** accompanied by the releases of THF (two multiplets at 3.67 and 1.81 ppm)[278] could be observed *via* ^{1}H NMR spectroscopy (Figure 32 A and Figure S3 in the Appendix). The $^{31}P\{^1H\}$ NMR spectrum showed one resonance at 66.8 ppm exhibiting $^{117/119}$Sn satellites with a $^2J_{Sn-P}$ coupling of

217.8 Hz. In contrast, for R = Et the stepwise exchange of THF with Et_3PO could be observed. ^1H and $^{31}P\{^1H\}$ NMR spectroscopy after the addition of one equivalent of Et_3PO showed the formation of two new species ($\delta(^{31}P)$ = 69.4 (major species) and 65.2 ppm (minor species)) and broad signals for free THF at 3.30 and 1.59 ppm, while the majority of the starting material **2^{Et}-(thf)$_2$** remained unconsumed (Figure S5 in the Appendix). The broadened, highfield-shifted resonances indicated the exchange of THF with Et_3PO. Addition of a second equivalent of phosphine oxide increased the resonances for the newly formed species and free THF, and changed their relative signal intensities ($\delta(^{31}P)$ = 69.4 (minor) and 65.2 ppm (major)). Furthermore, no resonance for free Et_3PO could be observed at 51.2 ppm (Figure S6). These observations allowed us to assign the ^{31}P shift at 69.4 ppm to the mono(Et_3PO)-mono(thf) adduct **2^{Et}-(Et_3PO)(thf)** and at 65.2 ppm to the bis(Et_3PO) adduct **2^{Et}-(Et_3PO)$_2$** (Figure 32 B). The *Gutmann-Beckett* shifts $\Delta\delta(^{31}P)$ for the bis adducts **2^{R}-(Et_3PO)$_2$** are in a comparable range and agree with the slightly increased Lewis acidity of **2^{Me}** ($\Delta\delta(^{31}P)$ = 15.7 ppm) compared to **2^{Et}** ($\Delta\delta(^{31}P)$ = 14.0 ppm). However, $\Delta\delta(^{31}P)$ is heavily influenced by the coordination of Et_3PO to the given Lewis acid.[44] At least for **2^{Et}**, the presence of free THF and the increased THF dissociation free enthalpies ΔG_{diss}(THF) seem to influence this equilibrium. Owing to the formation of bis(Et_3PO) adducts, the recorded shifts more correctly represent the Lewis acidity of the pentacoordinated **2^{R}-(Et_3PO)** mono adducts rather than the free Lewis acids **2^{R}**. Thus, comparison with *Gutmann-Beckett* parameters of other Lewis acids should be avoided. However, a marked difference to the related calix[4]pyrrolato germane **9^{Et}** can be observed. While **9^{Et}-(thf)$_2$** reacted with Et_3PO in an undesired ELC activation of the P-O double bond, **2^{R}** formed stable σ-adducts. This represents the first experimental validation of the predictions made in previous **Section 3.5.1** (*vide supra*).

Eventually, keeping the CD_2Cl_2 reaction solutions at room temperature overnight caused the formation of single crystals suitable for X-ray diffraction confirming the formation of bis(Et_3PO) adducts. The solid-state molecular structure of **2^{Me}-(Et_3PO)$_2$** allowed the first characterization of the new Lewis acid **2^{Me}** in the solid state (Figure 31 B). The Sn-N, Sn-O, and P-O bond lengths can be related to the values obtained for **2^{Et}-(Et_3PO)$_2$** (Figure S34). Both adducts show slightly elongated P-O bonds (151.65(11) for R = Me, 150.62(10) for R = Et) when compared to the solid-state structure of Et_3PO (149.4(2) pm),[279] agreeing with a weakened π-backbonding from oxygen to phosphorus caused by the coordination to the Sn(IV) centers.

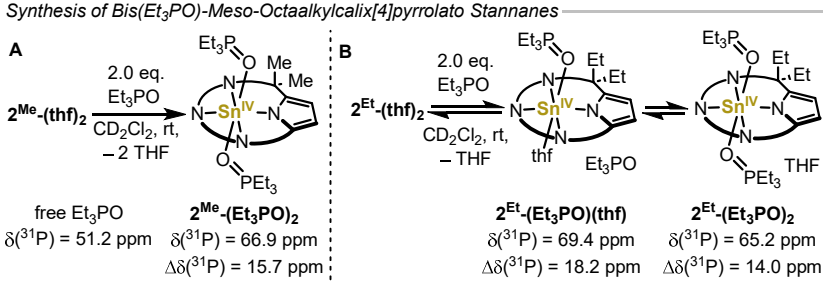


Figure 32. Synthesis of the bis(Et$_3$PO) adducts of **A) 2^{Me}** and **B) 2^{Et}** and their ^{31}P NMR δ(^{31}P) and *Gutmann-Beckett* shifts Δδ(^{31}P).

For calix[4]pyrrolato silane **8^{Et}** abstraction of chloride anions from the parent chloridosilicate **[Cl-8^{Et}]$^-$** yielded the free, square-planar silane (see **Section 1.4.2**). Following a similar synthetic route, **2^{R}-(thf)$_2$** (R = Me, Et) were reacted with different halide anion sources to yield the respective fluorido- and chloridostannate(IV) salts **[NBu$_4$][F-2^{R}]** and **[PPh$_4$][Cl-2^{R}]**. Reaction of **2^{R}-(thf)$_2$** with 1.0 eq. of tetrabutylammonium difluorotriphenylsilicate (TBAT) [NBu$_4$][F$_2$SiPh$_3$] in CH_2Cl_2 at 50 °C caused the complete consumption of the starting material and formation of clear solutions (Figure 33 A). Precipitation *via* the addition of excess *n*-pentane and drying of the isolated solids at reduced pressure and 100 °C allowed the removal of residue THF yielding **[NBu$_4$][F-2^{R}]** in 65% (R = Me) and 84% yield (R = Et). ^{1}H and ^{13}C NMR spectra of **[NBu$_4$][F-2^{R}]** in CD_2Cl_2 indicated the presence of a C_{4v} symmetric calix[4]pyrrole unit with two diastereotopic sets of *meso*-alkyl substituents in line with pentacoordinated fluoridostannate(IV) centers. ^{1}H,^{119}Sn-HMBC NMR spectroscopy showed doublets at −466.7 ppm (R = Me) and −481.1 ppm (R = Et) in the ^{119}Sn domain with large $^1J_{Sn\text{-}F}$ coupling constants of around 2300 Hz (Figures S7 and S8).[280] Respectively, ^{19}F NMR spectra showed resonances with $^{117/119}$Sn satellites at −152.45 ppm (R = Me) and −154.42 ppm (R = Et). Reaction of **2^{Me}-(thf)$_2$** with one equivalent of tetraphenylphosphonium chloride PPh_4Cl in CH_2Cl_2 at room temperature proceeded within minutes. In contrast to the respective fluoridostannate(IV), the removal of residual THF required drying under reduced pressure at 120 °C for an elongated time period of four days and delivered **[PPh$_4$][Cl-2^{Me}]** at a multigram scale in 88% yield (Figure 33 B). As observed for the synthesis of bis(Et$_3$PO) adducts **2^{R}-(Et$_3$PO)$_2$**, the strengthened THF binding in **2^{Et}-(thf)$_2$** hampered the ligand exchange with other Lewis bases in CH_2Cl_2. An NMR-scale reaction of **2^{Et}-(thf)$_2$** with one equivalent of PPh_4Cl in CD_2Cl_2 indicated an equilibrium between **2^{Et}-(thf)$_2$** and a new C_{4v} symmetric species which could be shifted to the product side *via* the addition of a second equivalent of PPh_4Cl

(Figure S9). However, evaporation of the reaction solution did not allow the isolation of a discrete product. Owing to its low boiling point, CH_2Cl_2 was evaporated before the released THF, thereby gradually increasing the THF concentration in the reaction solution and shifting the equilibrium towards the starting material. The absence of such an equilibrium for the synthesis of **[NBu$_4$][F-2^{Et}]** could be explained by the 100 kJ mol^{-1} more exothermic binding of fluoride anions than chloride anions to **2^R** (see FIA_{solv} and CIA_{solv} values in **Section 3.5.1**). Surprisingly, changing the reaction medium to THF resolved this problem. Even though, excess THF as a solvent hinders the initial dissociation of THF from **2^{Et}-(thf)$_2$**, its reduced polarity seemed to disfavor the dissociation of the chloride anion from **[Cl-2^{Et}]$^-$** after the formation of the chloridostannate(IV). Stirring a suspension of **2^{Et}-(thf)$_2$** and PPh_4Cl in THF at 75 °C for 14 hours resulted in the complete consumption of PPh_4Cl and the formation of a clear reaction solution. As for **[PPh$_4$][Cl-2^{Me}]**, evaporation of the solvent and drying under reduced pressure and 120 °C for four days delivered chloridostannate(IV) **[PPh$_4$][Cl-2^{Et}]** at multigram scale in 97% yield. The **[PPh$_4$][Cl-2^R]** salts show NMR characteristics similar to their fluoridostannate(IV) counterparts in line with the formation of pentacoordinated chloridostannate(IV) centers. Replacing F^- with Cl^- resulted in slightly downfield-shifted ^{119}Sn resonances at −432.3 ppm **[PPh$_4$][Cl-2^{Me}]** and −463.3 ppm for **[PPh$_4$][Cl-2^{Et}]**. The requirement of a more rigorous drying procedure to quantitatively remove THF residues from **[PPh$_4$][Cl-2^R]** indicated the increased Lewis acidity of the Sn(IV) center coordinated by Cl^- in comparison to F^-. As described in the original work in **Section 3.4**, the steric demand of a ligand on one side of the Lewis acid **2^{Et}** can influence the structure of the calix[4]pyrrole ligand backbone and thereby the accessibility of the second *trans*-coordination site. In addition, both axial donors in the bis adducts of **2^R** compete for the interaction with the same vacant p_z-type LUMO orbital localized at tin. Based on the structural parameters found for the four halidostannates(IV) (*vide infra*) and their computed FIA_{solv} and CIA_{solv} values (*vide supra*), most likely the

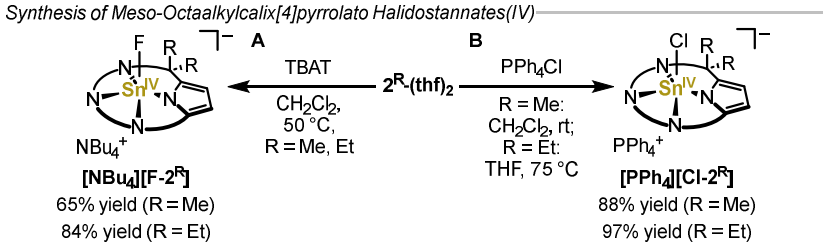


Figure 33. Synthesis of **A)** tetrabutylammonium *meso*-octaalkylcalix[4]pyrrolato fluoridostannates(IV) **[NBu$_4$][F-2^R]** and **B)** the respective tetraphenylphosphonium chloridostannates(IV) **[PPh$_4$][Cl-2^R]**.

competition for the vacant p_z-type LUMO orbital is the driving force for the strengthened coordination of THF *trans* to Cl.

Eventually, the anions **[X-2^{R}]$^{-}$** (X = F, Cl; R = Me, Et) could be identified *via* high-resolution mass spectrometry (HR-MS) employing the electrospray ionization (ESI) technique. Storing concentrated solutions in CH_2Cl_2 and *n*-pentane at −30 °C yielded single crystals suitable for X-ray diffraction for all halidostannate(IV) salts. The solid-state molecular structures of the respective anions are depicted in Figure 34. They all possess comparable Sn-N bond lengths between 206 and 210 pm. Comparison with literature known, hypercoordinated tin(IV) porphyrin fluorides and chlorides showed slightly shortened Sn-X bond lengths for the calix[4]pyrrolato halidostannates(IV) **[X-2^{R}]$^{-}$** indicating a strong halide binding (~5-7 pm shorter Sn-X bonds in **[X-2^{R}]$^{-}$**).[281,282] Marked differences were observed between the symmetry of the sc-XRD structures and their symmetry based on NMR spectra in solution. For **[X-2^{Me}]$^{-}$** the calix[4]pyrrole backbone adopts a clear C_{2v}

Sc-XRD Structures of Meso-Octaalkylcalix[4]pyrrolato Halidostannates(IV)

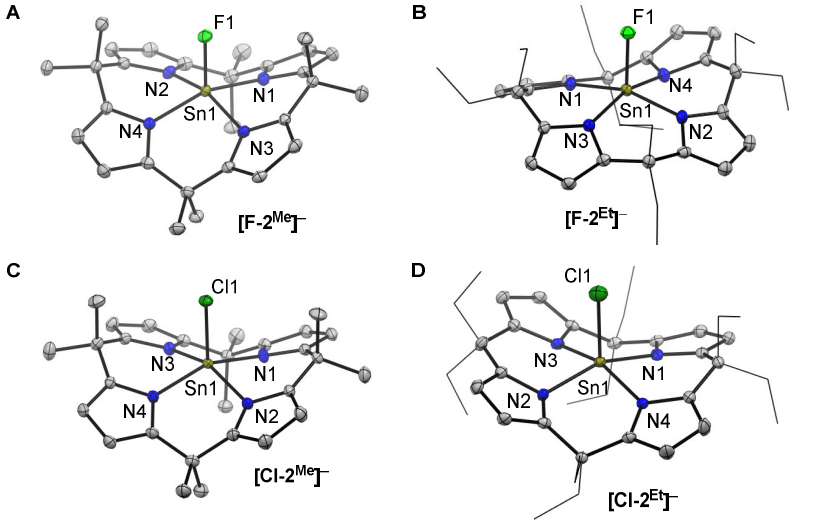


Figure 34. Solid-state molecular structures of **A) [NBu$_4$][F-2^{Me}]**,and **B) [NBu$_4$][F-2^{Et}]**, **C) [PPh$_4$][Cl-2^{Me}]**, and **D) [PPh$_4$][Cl-2^{Et}]**. Ellipsoids are drawn with a probability of 50%. Hydrogen atoms, counter-cations, and co-crystallized solvent molecules are omitted for clarity. *Meso*-ethyl substituents are drawn as wireframe for clarity. Selected bond lengths [pm] and angles [deg] for **[NBu$_4$][F-2^{Me}]**: avg. Sn1-N = 206.94(20), Sn1-F1 = 194.06(12), N1-Sn1-N4 = 159.23(7), N2-Sn1-N3 = 157.02(7); **[NBu$_4$][F-2^{Et}]**: avg. Sn1-N = 210.71(21), Sn1-F1 = 194.74(13), N1-Sn1-N2 = 159.46(7), N3-Sn1-N4 = 160.48(7); **[PPh$_4$][Cl-2^{Me}]**: avg. Sn1-N = 208.20(16), Sn1-Cl1 =235.40(5), N1-Sn1-N4 = 154.49(6), N2-Sn1-N3 = 154.20(6); and **[PPh$_4$][Cl-2^{Et}]**: avg. Sn1-N = 210.05(23), Sn1-Cl1 =234.66(9)), N1-Sn1-N2 = 156.16(8), N3-Sn1-N4 = 158.16(8).

symmetric orientation, while **[X-2^{Et}]$^-$** shows a less symmetric orientation of the pyrrolato units (X = F, Cl) in their solid states. However, owing to the C(sp^3)-tethered, highly flexible ligand backbone, fast conformational changes yielded higher C_{4v} symmetries at room temperature in solution. Similar effects could be observed for the dianionic calix[4]pyrrolato stannates(II) **[2^{R}]$^{2-}$** discussed in the original work in **Sections 3.1** and **3.2**.

First attempts to abstract halide anions from the halidostannates(IV) **[X-2^{Et}]$^-$** focused on the reaction of **[NBu$_4$][F-2^{Et}]** with lithium alkoxyaluminate Li[Al(O*t*Bu^F)$_4$], and **[PPh$_4$][Cl-2^{Et}]** with sodium and thallium(I) tetrakis(pentafluorophenyl)borate Na[BAr^{F20}] and Tl[BAr^{F20}] in CH_2Cl_2 (Figure 35). These salts were chosen as abstraction agents since the formation of only ionic byproducts would allow their straight forward separation from the neutral calix[4]pyrrolato stannanes **2^{R}**. Despite the high lattice energy of lithium fluoride,[283] Li[Al(O*t*Bu^F)$_4$] did not effect the fluoride abstraction from **[F-2^{Et}]$^-$** (Figure 35 A). The high solvation enthalpy of Li^+, its strong interaction with the pyrrole units in the calix[4]pyrrole ligand backbone (see ref. [115,284]), and the pronounced FIA_{solv} of stannane **2^{Et}** result in a strong stabilization of the lithium salt **Li[F-2^{Et}]**. Therefore, subsequent experiments focused on the abstraction of Cl^-(Figure 35 B). Reaction with Na[BAr^{F20}] and Tl[BAr^{F20}] both caused the slow precipitation of **M[Cl-2^{Et}]** (M = Na, Tl) as off-white solids accompanied by the disappearance of the ^{1}H NMR signals for the chloridostannate(IV) **[Cl-2^{Et}]$^-$** (Figures S10 and S11). Keeping these suspensions at room temperature for up to seven days did not lead to the elimination of MCl and the release of the free Lewis acid **2^{Et}**. Furthermore, ^{1}H NMR measurements after slight heating at 50 °C indicated the decomposition of **[Cl-2^{Et}]$^-$** accompanied by the formation of red reaction solutions. These observations are in line with the instability of free, planar silane **8^{Et}** even at slightly elevated temperature and highlight the necessity of room temperature reaction protocols for the synthesis of **2^{R}**.[113] Reaction of **[PPh$_4$][Cl-2^{Et}]** with M[BAr^{F20}] (M = Na, Tl) in CD_3CN improved the solubility of the **M[Cl-2^{Et}]** salt confirming the existence of a C_{4v} symmetric chloridostannate(IV) complex (Figure 36). In conclusion, the increased CIA_{solv} for **2^{Et}** relative to the respective silane **8^{Et}** made the abstraction of Cl^- unfeasible under these conditions. Thus, the synthesis of halidostannates(IV) containing more weakly bound iodide anions was targeted next.

Abstraction of Halide Anions from Meso-Octaalkylcalix[4]pyrrolato Halidostannates(IV)

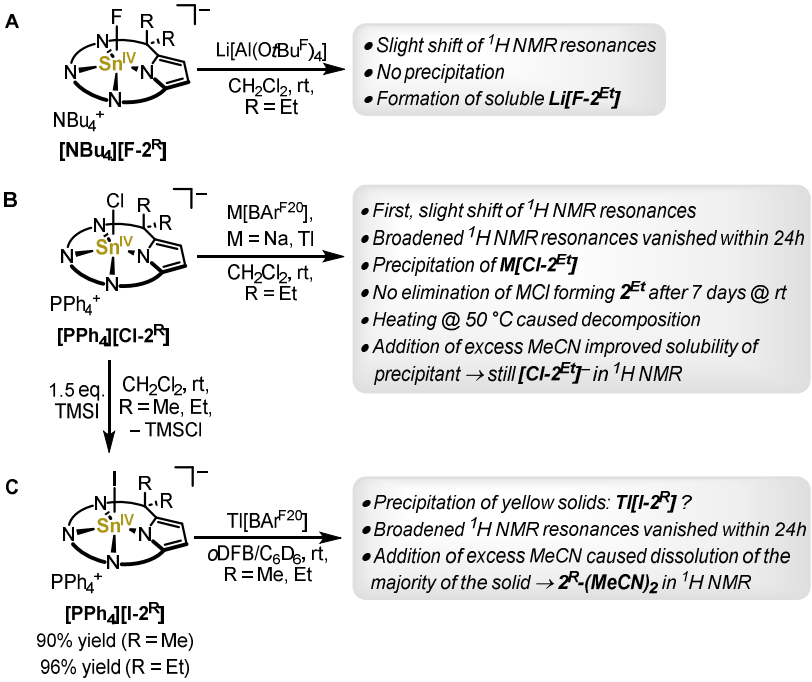


Figure 35. Attempts to synthesize the free, square-planar stannanes $\mathbf{2^R}$ *via* the abstraction of halide anions from halidostannates(IV) $\mathbf{[X\text{-}2^R]^-}$ (X = F, Cl, I; R = Me, Et) and the synthesis protocol to access $\mathbf{[PPh_4][I\text{-}2^R]}$ from the respective chloridostannates(IV) $\mathbf{[PPh_4][Cl\text{-}2^R]}$.

Calculation of the solvation-corrected iodide ion affinities (IIA_{solv}) clearly indicated the reduced strength of the Sn-I bond in $\mathbf{[I\text{-}2^R]^-}$ (IIA_{solv} of 130 and 141 kJ mol^{-1} for R = Me and Et, respectively). A first NMR-scale test reaction of $\mathbf{2^{Et}\text{-}(thf)_2}$ with tetraphenylphosphonium iodide PPh_4I in CD_2Cl_2 showed the incomplete consumption of the starting material (Figure S12). Based on the magnitude of IIA_{solv} in comparison to the THF dissociation free enthalpies ΔG_{diss}(THF) for $\mathbf{2^{Et}}$, direct synthesis of $\mathbf{[PPh_4][I\text{-}2^{Et}]}$ from the respective bis(thf) adduct appeared to be unlikely. Eventually, both methyl- and ethyl-substituted *meso*-octaalkylcalix[4]pyrrolato iodidostannate(IV) salts $\mathbf{[PPh_4][I\text{-}2^R]}$ could be accessed *via* the halide exchange from $\mathbf{[PPh_4][Cl\text{-}2^R]}$ with trimethylsilyl iodide (TMSI) in CH_2Cl_2 (Figure 35 C). In the absence of donor solvents such as THF and driven by the formation of TMSCl, this reaction delivered $\mathbf{[PPh_4][I\text{-}2^R]}$ in excellent yields above 90% within minutes at room temperature. The iodidostannate(IV) salts possess comparable ^1H and ^{13}C NMR properties to their respective fluorido and chlorido counterparts. However,

significantly highfield-shifted ^{119}Sn resonances at −618.3 and −632.1 ppm for R = Me and Et, respectively, and ESI mass spectrometry clearly evidenced the quantitative formation of **[I-2^{R}]$^{-}$**. Multiple attempts to grow single crystals of **[PPh$_4$][I-2^{R}]** suitable for X-ray diffraction remained unsuccessful.

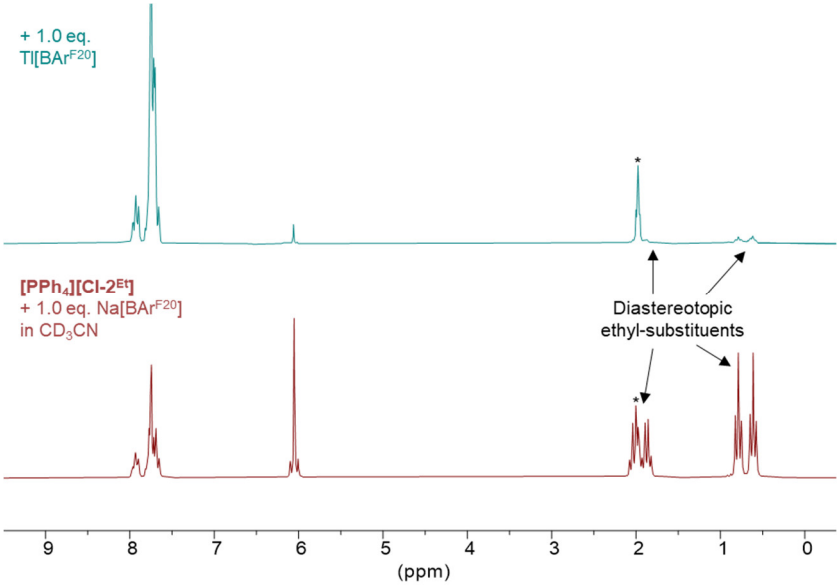


Figure 36. ^{1}H NMR spectra of **[PPh$_4$][Cl-2^{Et}]** after the addition 1.0 eq. Na[BAr^{F20}] (bottom) and Tl[BAr^{F20}] (top) (200 MHz, CD_3CN, 298 K). Solvent signals are indicated by an asterisk symbol (*).

To prevent possible side reactivity of the free stannanes **2^{R}** with CH_2Cl_2, the following abstraction reactions were performed in fluorobenzene (PhF) or 1,2-difluorobenzene (*o*DFB). Addition of one equivalent of Tl[BAr^{F20}] to a solution of **[PPh$_4$][I-2^{R}]** in *o*DFB spiked with C_6D_6 caused the immediate precipitation of yellow solids accompanied by the vanishing of ^{1}H NMR resonances for the calix[4]pyrrole complexes within minutes (Figure 35 C). The yellow color of the precipitates marked a clear difference to the Cl^{-} abstraction attempts using Tl[BAr^{F20}] (Figure 35 B). Repeating this reaction with **[PPh$_4$][I-2^{Me}]** in CD_3CN resulted in the precipitation of only a small amount of a yellow solid (TlI) and the presence of a D_{4h} symmetric calix[4]pyrrole complex in ^{1}H NMR spectroscopy (Figure 37). These observations are in line with the formation of the bis adduct **2^{Me}-(MeCN)$_2$** and precipitation of TlI. An explanation could be either i) the precipitation of **Tl[I-2^{R}]** in non-donor solvents and its decomposition into TlI and **2^{R}-(MeCN)$_2$** driven by the coordination of MeCN to the Lewis acid **2^{R}**, or ii) the precipitation of both TlI and **2^{R}** owing to the

oligomerization of the free Lewis acid in the absence of donor solvents. To investigate the possible oligomerization of the free Lewis acids $\mathbf{2^R}$, we switched to soluble abstraction agents which would remain in solution after the generation of the free Lewis acids and should allow their separation from the precipitated oligomers.

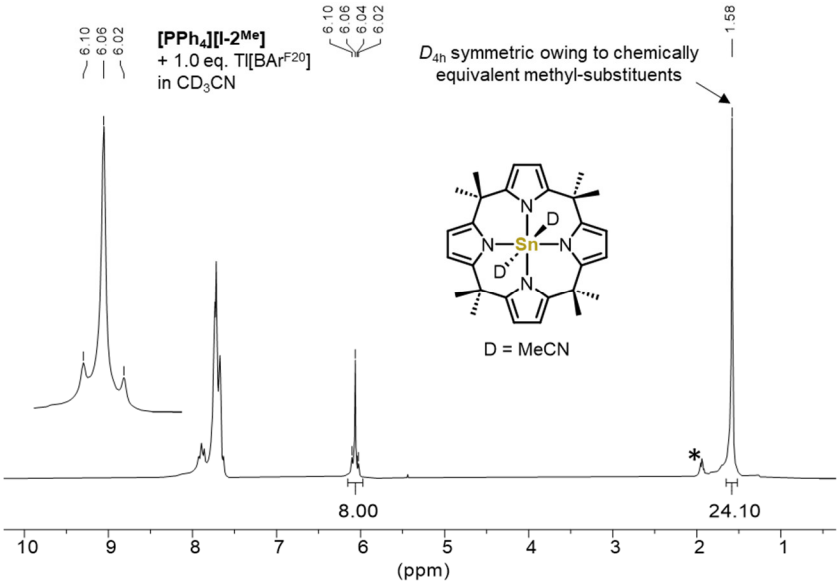


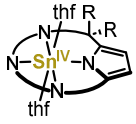
Figure 37. ^{1}H NMR spectra of **[PPh$_4$][I-2^{Me}]** after the addition 1.0 eq. Tl[BAr^{F20}] (200 MHz, CD_3CN, 298 K). Solvent signals are indicated by an asterisk (*).

Computations of the THF dissociation free enthalpies were performed to identify suitable molecular Lewis acids as THF abstraction agents for the generation of $\mathbf{2^R}$ from $\mathbf{2^R}$**-(thf)$_2$**. Tris(pentafluorophenyl)borane (BCF) represents one of the most prominent molecular Lewis acids with a wide area of applications and straight forward synthetic accessibility.[285] However, with a computed ΔG_{diss}(THF) of only 12.8 kJ mol^{-1} BCF proved to be unsuitable for the above mentioned task. Exchange of the boron center in BCF with aluminum *via* its transmetalation reaction with $AlMe_3$ significantly increases the Lewis acidity of these systems.[286,287] Indeed, with a computed ΔG_{diss}(THF) of 98.4 kJ mol^{-1} tris(pentafluorophenyl)alane (AlCF) surpasses the 1st and 2nd ΔG_{diss}(THF) of both methyl- and ethyl-substituted $\mathbf{2^R}$**-(thf)$_2$,** rendering it a promising THF abstraction agent. Reaction of $\mathbf{2^R}$**-(thf)$_2$** with 2.0 eq. AlCF in PhF or *o*DFB at room temperature caused the immediate precipitation of yellow (R = Me) or bright orange (R = Et) solids. Workup yielded both compounds in yields around 60% showing elemental compositions consistent with the

free Lewis acids **2^{R}** (Figure 38 A). The isolated compounds were badly soluble in standard organic solvents including benzene, toluene, CH_2Cl_2, *o*DFB, and halobenzenes such as PhF, PhCl, and PhBr. However, addition of an around 16-fold excess of MeCN to suspensions in CD_2Cl_2 led to clear, yellow solutions within minutes. ^{1}H and ^{13}C NMR spectra are consistent with D_{4h} symmetric bis(MeCN) adducts and comparable to the spectra obtained for the abstraction of iodide anions in CD_3CN (*vide supra*). $^{117/119}Sn$ satellites in ^{1}H NMR and $^{1}H,^{119}Sn$-HMBC NMR experiments disclosed the intact coordination of tin showing ^{119}Sn NMR shifts in the range of hexacoordinated Sn(IV) compounds (−610.1 for R = Me and −629.1 ppm for R = Et). The solutions were stable at room temperature for several days with no signs of degradation in the presence of MeCN. Thus, confirming the reactivity predicted in **Section 3.5.1**. In summary, these findings are consistent with the formation of di- or oligomeric aggregates of **2^{R}** in the absence of donor solvents rather than the initial precipitation of **Tl[I-2^{R}]** salts for the abstraction attempts discussed above (Figure 35 C). Resting the respective reaction solutions after the addition of AlCF instead of stirring them vigorously resulted in the deposition of single crystals suitable for X-ray diffraction.

Sc-XRD analysis gave definite proof of the chemical structures of the isolated solids confirming the dimerization of donor-free calix[4]pyrrolato stannanes **2^{R}**. For R = Me the pronounced ambiphilicity of the square-planar, anti-van't Hoff-Le Bel stannane resulted in the formation of a hexacycle involving the nucleophilic α-carbon atoms C_α and electrophilic Sn(IV) centers of two molecules (Figure 38 B). With bond lengths of 226.1(3) pm, the Sn1-C_α bonds are in the range of literature known hypercoordinated organotin compounds.[288] The bond lengths in the cooperatively bound pyrrole unit indicated its dearomatization and the formation of an imine double bond between N1 and C4 and a C-C double bond between C_β and C3. This change in electronic structure was further aided by an elongated Sn-N1 bond of 222.5(2) pm in comparison to the remaining Sn-N bonds lying in a close range between 210.6(2) and 212.1(2) pm. In general, this bonding situation is well-known for the cooperative substrate binding of other *p*-block calix[4]pyrroles containing Al(III), Ga(III), Si(IV), and Ge(IV) centers (see **Section 1.5**). Comparison with the sc-XRD structure of **(2^{Et})$_2$** revealed a significant influence of the *meso*-substituents R on the dimerization (Figure 38 C). Instead of involving the α-carbon atoms C_α, **2^{Et}** dimerized

A *Synthesis of Meso-Octaalkylcalix[4]pyrrolato Stannane Dimers* $(2^R)_2$



2^R-(thf)$_2$

2.0 eq. AlCF

PhF *or* oDFB,
30 min.,
– 2 AlCF(thf)

$(2^R)_2$
60% yield (R = Me)
66% yiled (R = Et)

LA	ΔG_{diss}(THF) [kJ mol^{-1}]
BCF	12.8
2^{Me}	1st: 55.2, 2nd: 63.3
2^{Et}	1st: 69.0, 2nd: 88.9
AlCF	98.4

Solid-state Molecular Structures of $(2^R)_2$

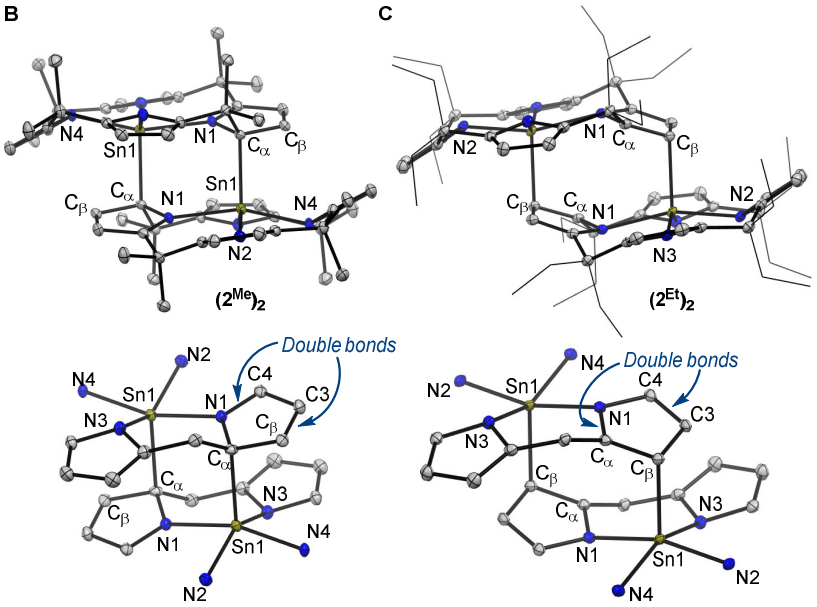


Figure 38. A) Synthesis of donor-free *meso*-octaalkylcalix[4]pyrrolato stannanes $(2^R)_2$ (R = Me, Et) and THF dissociation free enthalpies ΔG_{diss}(THF) for different Lewis acids (LA) in kJ mol^{-1} computed at the DSD-BLYP-D3(BJ) / def2-QZVPP // BP86 / TZP COSMO-RS(DCM) // B97M-D4 / def2-TZVPP // CREST/GFN2-xTB level of theory. Solid-state molecular structure of **B)** $(2^{Me})_2$ and **C)** $(2^{Et})_2$. Ellipsoids are drawn with a probability of 50%. Hydrogen atoms are omitted for clarity. *Meso*-ethyl substituents are drawn as wireframe for clarity. For the bottom structures the peripheral pyrrole units and all *meso*-substituents are omitted to clarify the connectivity of the dimers . Selected bond lengths [pm] and angles [deg] for $(2^{Me})_2$: Sn1-N1 = 222.5(2), Sn1-N2 = 210.6(2), Sn1-N3 = 211.9(2), Sn1-N4 = 212.1(2), Sn1-C_α = 226.1(3), C_α-C_β = 147.8(3), C_β-C3 = 133.5(4), C3-C4 = 144.6(4), N1-C_α =146.7(3), N1-C4 = 131.7(3), N1-Sn1-N4 = 160.81(8), N2-Sn1-N3 = 143.87(9); and $(2^{Et})_2$: Sn1-N1 =221.30(18), Sn1-N2 =209.73(18), Sn1-N3 = 211.95(17), Sn1-N4 = 211.60(17), Sn1-C_β = 228.7(2), C_α-C_β = 144.9(3), N1-C_α = 134.5(3), C_β-C3 = 146.4(3), C3-C4 = 135.0(3), N1-C4 = 142.4(3), N1-Sn1-N2 = 161.90(7), N3-Sn1-N4 = 152.27(7).

via the nucleophilic attack of the β-carbon atoms C_β at intermolecular Sn(IV) centers forming octacyclic structures. The Sn-N bonds in $(2^{Et})_2$ show the same elongation for

Sn1-N1 and are all close to the values observed for **(2^{Me})$_2$**. The Sn1-C_β bond is only slightly elongated by around 2.6 pm compared to the Sn1-C_α bond in **(2^{Me})$_2$**. More significant differences were presented in the conformation of the calix[4]pyrrole backbone. Increased N-Sn-N *trans*-valence angles in **(2^{Et})$_2$** indicate a smaller degree of distortion from the structure of the parent square-planar Lewis acid **2^{Et}**. Owing to the involvement of C_β atoms, the dearomatized pyrrole units in **(2^{Et})$_2$** exhibit different bond length alternations. Thus, the double bonds are located between N1-C_α and C3-C4 and not N1-C4 and C_β-C4 as in **(2^{Me})$_2$**. The nucleophilic attack of C_β atoms has already been observed for the reaction of dianionic *meso*-octamethylcalix[4]pyrrolato nickelates(II) with a range of electrophiles.[289] However, no case for *p*-block calix[4]pyrrolato compounds had been reported so far.

Quantum mechanical calculations including energy decomposition analysis (ETS-NOCV, BP86-D3/TZ2P//B97M-D3(BJ)/def2-TVZPP) delivered deeper insights into the dimerization of these ambiphilic stannanes. The exergonic dimerization free enthalpies ΔG_{dim} for **(2^{Me})$_2$** (B97M-D4/def2-TZVPP//BP86/TZP COSMO-RS(DCM)) revealed significant stabilization of the α-dimer **α-(2^{Me})$_2$** (−115.5 kJ mol^{-1}) over a theoretical β-dimer **β-(2^{Me})$_2$** (−65.2 kJ mol^{-1}). These observations agree with the nucleophilic character of the C_α atom which is mainly involved in the ligand cooperative activation of substrates. In contrast, no structure for the α-dimer **α-(2^{Et})$_2$** could be optimized at the given computational level indicating the significant influence of the increased steric demand around the ethyl-substituted calix[4]pyrrole stannane. Furthermore, a slight decrease in the stability of the β-dimer **β-(2^{Et})$_2$** (−56.1 kJ mol^{-1}) compared to **β-(2^{Me})$_2$** could be observed (Figure 39 A). ETS-NOCV difference density plots for the two most important interactions in **α-(2^{Me})$_2$** and **β-(2^{Me})$_2$** showed similar bonding interactions for both dimers with electron density flowing from the electron-rich pyrrole units of one **2^{Me}** to the electrophilic Sn(IV) centers of the second **2^{Me}** unit and *vice versa* (Figure 39 B). Detailed comparison of the ETS-NOCV results (see Table S20) revealed increased total orbital interaction energies $\Delta E_{oi,tot}$ and total bonding energies ΔE between the **2^{Me}** units in the α-dimer in line with the increased donor strength of the C_α atoms which form stronger dative Sn-C bonds than their neighboring C_β atoms. For the β-dimer **β-(2^{Et})$_2$**, $\Delta E_{oi,tot}$ and ΔE values comparable to the respective dimer **β-(2^{Me})$_2$** could be obtained (Table S21) agreeing with the respective magnitudes of the computed ΔG_{dim} values for **β-(2^{Me})$_2$** and **β-(2^{Et})$_2$**. However, a significant increase in stabilization *via* dispersion interactions was observed for the ethyl-substituted β-dimer **β-(2^{Et})$_2$** (ΔE_{disp} = −240.11 kJ mol^{-1} for R = Et and −182.06 kJ mol^{-1} for R = Me).

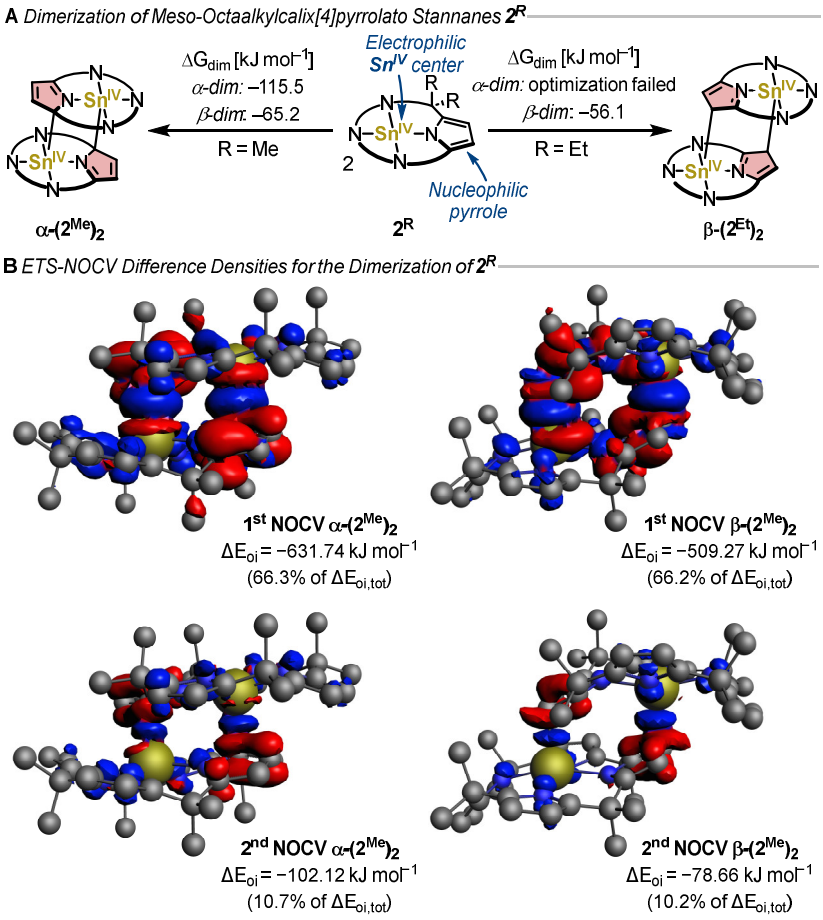


Figure 39. A) Dimerization free enthalpies ΔG_{dim} for $\mathbf{2^R}$ (R = Me, Et) computed at the B97M-D4/def2-TZVPP//BP86/TZP COSMO-RS(DCM) level of theory. **B)** Exemplary ETS-NOCV difference density plot of the 1st and 2nd NOCV-channel for the dimers **α-(2^{Me})$_2$** and **β-(2^{Me})$_2$** computed on the BP86-D3/TZ2P//B97M-D3(BJ)/def2-TVZPP level of theory. NOCV deformation densities sampled at a value of 0.001. The color code of the charge flow is red to blue.

Thus, even though the increased steric bulk of the ethyl substituents in $\mathbf{2^{Et}}$ did not allow the more-stable α-dimerization mode, increased dispersion interactions resulted in a stabilized β-dimer **β-(2^{Et})$_2$** with ΔG_{dim} values comparable to **β-(2^{Me})$_2$**.

Both the free, square-planar silane $\mathbf{8^{Et}}$ and the germane $\mathbf{9^{Et}}$ (after the abstraction of both THF from germane **9^{Et}-(thf)$_2$** with two equivalents of AlCF) showed no sign of

dimerization. To elucidate the unique properties of stannanes $\mathbf{2^R}$ enabling their isolation as $\mathbf{(2^R)_2}$, EDA computations on the hypothetical α-dimers $\mathbf{\alpha\text{-}(8^{Me})_2}$ and $\mathbf{\alpha\text{-}(9^{Me})_2}$ and β-dimers $\mathbf{\beta\text{-}(8^{Et})_2}$ and $\mathbf{\beta\text{-}(9^{Et})_2}$ have been conducted and compared to the results of the respective stannanes (Table S20 and S21, Figure 40). For both methyl- and ethyl-substituted calix[4]pyrroles change of the central atom E in the sequence Sn < Ge < Si caused an increase in the total orbital interaction energies $\Delta E_{oi,tot}$ and total bonding energies ΔE in the dimeric structures. These trends contradict the computed free dimerization energies ΔG_{dim} but can be reasoned by the decrease in bond strengths for the newly formed E-C bonds in the same sequence E = Si > Ge > Sn.[140,141,276] Good correlation with the trend observed for ΔG_{dim} was obtained by taking into account the deformation energy (DE) of the monomeric

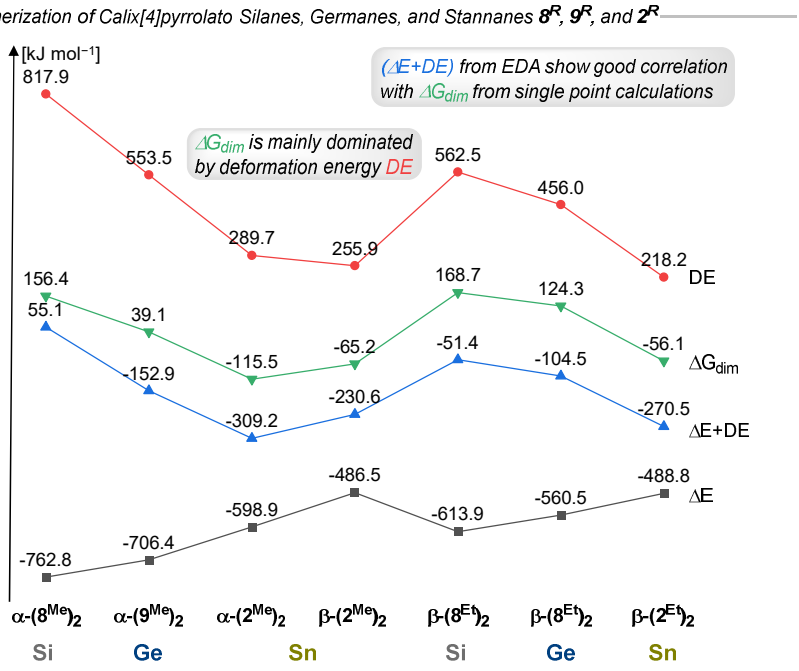


Figure 40. *In silico* comparison of the theoretical dimerization for calix[4]pyrrolato silanes, germanes, and stannanes $\mathbf{8^R}$, $\mathbf{9^R}$, and $\mathbf{2^R}$. Total bonding energies ΔE an deformations energies DE were obtained *via* ETS-NOCV calculations at the BP86-D3/TZ2P//B97M-D3(BJ)/def2-TVZPP level of theory. Dimerization free enthalpies ΔG_{dim} were computed at the B97M-D4/def2-TZVPP//BP86/TZP COSMO-RS(DCM) level of theory.

calix[4]pyrrolato group 14 compounds before the formation of dimeric structures (see plot of (ΔE+DE) in Figure 40). Previous computational studies for the ligand cooperative activation of styrene by **8**^{Me}, **9**^{Me}, and **2**^{Me} already highlighted the increased flexibility of the molecular framework in stannane **2**^{Me} owing to a reduced covalency of the respective E-N bonds (**Section 3.51**). Additionally, the shortening of the E-C bonds within the order E = Sn > Ge > Si causes a closer contact between both monomeric units and demands a more severe deformations of the calix[4]pyrrole ligand backbone in the dimers of **8**^{R} and **9**^{R} than for the stannanes **2**^{R}. In conclusion, decreased deformation energies for **2**^{R} and elongated Sn-C bonds can be seen as the main driving forces for the dimerization of these calix[4]pyrrole stannanes and the absence of dimerization for **8**^{Et} and **9**^{Et}.

To probe the potential of **(2**^{R}**)**$_2$ (R = Me, Et) for element-ligand cooperativity, suspensions of the respective dimer in CD_2Cl_2 were treated with a selection of substrates known to show ELC reactivity with previously reported calix[4]pyrrolato *p*-block compounds. For R = Me and Et no reaction with 1.5 bar of CO_2 gas could be observed even at elevated temperatures of 50 °C over 24 hours (Figure 41 A). CO_2 is known to form only weak, endergonic σ-adducts with *e.g.* aluminate **[5**^{Me}**]**$^-$ which subsequently react towards the cooperative 1,2-adduct **[CO$_2$-5**^{Me}**]**$^-$ (**Section 1.5.1)**.[115] A similar case could be computed for the σ-adduct of CO_2 and **2**^{Me} showing a free σ-adduct formation enthalpy of 37.1 kJ mol^{-1} (PW6B95-D3(BJ)/def2-QZVPP//BP86/ TZP COSMO-RS(DCM)). As discussed in the previous section, the low donor strength of phenylacetylene and styrene result in the formation of endergonic encounter complexes with **2**^{Me} before the overall exergonic binding as 1,2-adducts. Therefore, no reaction could be observed with **(2**^{Me}**)**$_2$ under the same conditions described for CO_2 (Figure 41 B). In conclusion, more Lewis basic substrates are required to compensate the dimerization free enthalpy ΔG_{dim} of **(2**^{Me}**)**$_2$ thereby hindering the activation of weak donors such as CO_2 and C-C multiple bonds.

(2^{Me}**)**$_2$ readily reacted with two equivalents of *i*PrOH forming a clear, yellow reaction solution within minutes (Figure 4 C). Characteristic signals for the dearomatized pyrrole unit (red) and coupling of the *iso*-propyl signal to a tin resonance at −466.3 ppm in ^{1}H,^{119}Sn-HMBC NMR spectroscopy clearly evidenced the cooperative splitting of the alcohol O-H bond and the quantitative formation of the product ***i*PrOH-2**^{Me}. Eventually, sc-XRD analysis of single crystals grown from the reaction solution confirmed the structure of the activation product (Figure 42 A). The bonding parameters in ***i*PrOH-2**^{Me} can be compared to the respective activation products with calix[4]pyrrole aluminate **[*i*PrOH-5**^{Me}**]**$^-$[118] and germane ***i*PrOH-9**^{Et}[122] and show the characteristic bond lengths alternations

for the dearomatized pyrrole unit. Addition of two equivalents of benzaldehyde (BA) caused the dissolution of both $(\mathbf{2^{Me}})_2$ and $(\mathbf{2^{Et}})_2$ within minutes (Figure 41 D). Broad signals in the ^{1}H NMR spectra indicated the formation of symmetric σ-adducts and dynamic coordination behavior in solution at room temperature. For R = Me additional signals showed the partial formation of the 1,2-adduct **BA-2^{Me}** with sharp signals for a dearomatized pyrrole unit and eight chemically inequivalent methyl substituents (Figure S20). While ^{1}H,^{119}Sn-HMBC NMR spectroscopy delivered no ^{119}Sn resonances for the σ-adducts owing to the severe line broadening in the ^{1}H NMR domain, a ^{119}Sn NMR shift of −487.5 ppm and characteristic cross signals clearly evidenced the cooperative binding of benzaldehyde in **BA-2^{Me}** (Figure S21). Integration of ^{1}H resonances yielded an approximate ratio of 3:2 σ-adduct to 1,2-adduct for **BA-2^{Me}** in agreement with the energetic similarity of both isomers discussed in the previous section. Furthermore, the absence of signs for the respective 1,2-adduct **BA-2^{Et}** again highlight the subtle influence of the *meso*-substituents on the equilibrium of substrate binding. Similar observations were made for the cooperative binding of CO_2 by the anionic gallates $\mathbf{[7^R]^-}$ (R = Me, Et) as described in **Section 1.5.1**.[120]

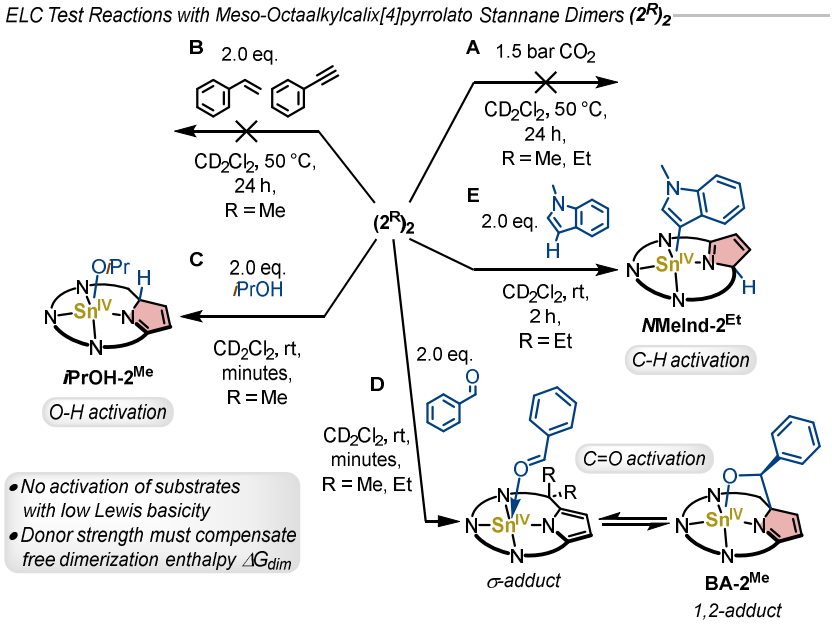


Figure 41. Test reactions of the isolated dimers $(\mathbf{2^R})_2$ with different substrates know to show an ELC reactivity with calix[4]pyrrole *p*-block compounds.

Activation of aromatic C-H bonds with neutral stannanes represents an essentially unexplored field. ROTHWELL and coworkers reported on the intramolecular activation of aromatic C-H bonds in phenoxy stannanes in the presence of Brønsted basic leaving groups taking up the proton.[290,291] However, no activation of intermolecular substrates has been reported so far. The strong electron-donor properties of *N*-methyl indole (*N*MeInd) could compensate the dimerization free enthalpy of $\mathbf{(2^{Et})_2}$ yielding a clear, orange CD_2Cl_2 reaction solution within two hours at room temperature (Figure 41 E). After the presumed formation of a Wheland-intermediate-type σ-adduct, the intramolecular deprotonation of the C3 position furnished the activation product ***N*MeInd-2^{Et}** as evidenced by ^{1}H and ^{119}Sn NMR spectroscopy ($\delta(^{119}Sn)$ = −402.6 ppm, Figure S23 and S24).[292] Single crystals grown from the crude reaction solution facilitated the analysis of the solid-state molecular structure of ***N*MeInd-2^{Et}** (Figure 42 B). With 209.44(19) pm, the newly formed Sn1-C8 bond is significantly shortened compared to the Sn-C bonds in the dimeric structure of $\mathbf{(2^{Et})_2}$ (Sn1-C_β = 228.7(2) pm). The large thermal ellipsoids for the atoms of the dearomatized pyrrole unit indicate the slight population of a second domain with the indole hydrogen atom bound to C25 instead of C22. However, describing this disorder did not improve the quality of the structure model. Interestingly, the hydrogen atom H22 is oriented *anti* relative to the *N*-methyl indol-3-yl residue bound to the Sn(IV) center. This unusual orientation causes a decreased N2-Sn1-N5 valence angle of 135.54(7)° and has never been reported for the cooperative activation of O-H bonds by calix[4]pyrrolato *p*-block compounds. For aluminate $\mathbf{[5^{Me}]^-}$ the deuteration of up to 75% of the β-positions in the calix[4]pyrrole backbone could be achieved *via* a series of low-energy [1,5]H/D sigmatropic rearrangements using EtOD as the solvent. Similar sigmatropic rearrangements could explain the *anti*-orientation of H22 after the initial formation of a *syn*-activation product. Additionally, free *N*-methyl indole could act as an auxiliary base in the activation of the aromatic C-H bond and deliver the *anti*-arranged proton in ***N*MeInd-2^{Et}**.[293,294] However, detailed investigations on the mechanism of C-H activation for *N*-methyl indole are still pending and have not been conducted as a part of this work.

Solid-state Molecular Structures of ELC Activation Products with $(2^{R})_2$

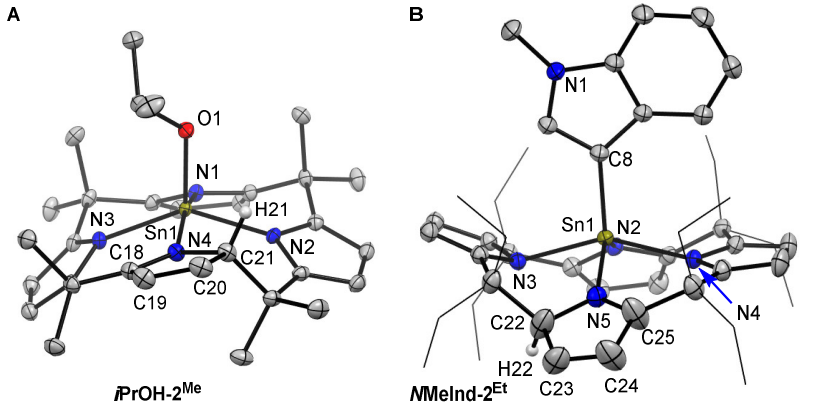


Figure 42. Solid-state molecular structure of **B)** ***i*PrOH-2^{Me}** and **C)** ***N*MeInd-2^{Et}**. Ellipsoids are drawn with a probability of 50%. Hydrogen atoms and co-crystallized DCM molecules are omitted for clarity. *Meso*-ethyl substituents are drawn as wireframe for clarity. Selected bond lengths [pm] and angles [deg] for ***i*PrOH-2^{Me}**: Sn1-O1 = 195.30(10) Sn1-N1 = 209.31(11), Sn1-N2 = 210.77(11), Sn1-N3 = 210.79(11), Sn1-N4 = 218.65(11), N4-C18 = 130.07(16), N4-C21 = 147.03(16), C18-C19 = 146.40(18), C19-C20 = 133.4(2), C20-C21 = 148.98(18), N1-Sn1-N4 = 163.34(4), N2-Sn1-N3 = 143.28(4); and ***N*MeInd-2^{Et}**: Sn1-N2 =208.42(16), Sn1-N3 =212.14(16), Sn1-N4 = 212.44(16), Sn1-N5 = 219.26(18), Sn1-C8 = 209.44(19), N5-C22 = 145.3(3), N5-C25 = 130.4(3), C22-C23 = 148.8(3), C23-C24 = 130.2(4), C24-C25 = 146.2(4), N2-Sn1-N5 = 135.54(7), N3-Sn1-N4 = 151.53(6).

As indicated by the computational and experimental comparison of **2^{Me}** and **2^{Et}** discussed above, already small changes of the *meso*-substituents can have a significant influence on the dimerization of these ambiphilic systems. Thus, the following section will focus on the design of calix[4]pyrrolato stannane complexes bearing sterically more demanding *meso*-substituents thereby preventing the dimerization of **2^{R}**.

3.5.3 Sterically Demanding *Meso*-octa(*ortho*-phenylene)calix[4] pyrrolato Stannane

As described in **Section 1.4**, the acid-catalyzed condensation of pyrroles and ketones accessed a large variety of *meso*-substituted calix[4]pyrroles. However, no reliable procedure for the synthesis of *meso*-octaarylcalix[4]pyrroles or systems with eight sterically crowded substituents has been reported so far.[295] With the aim to exchange some of the *meso*-substituents in **H$_4$[1^{Me}]** for rigid, sterically demanding groups, the literature known synthetic route shown in Figure 43 A was followed.[95] Condensation of pyrrole and fluorenone in a 2:1 ratio in dry ethanol at room temperature and an equimolar amount of BF_3●Et_2O as catalyst afforded the precipitation of a colorless solid within seven days. According to the reported procedure, the 9,9'-fluorendiyl dipyrromethane **42** could be isolated after washing the crude product with aqueous ammonia and extraction with CH_2Cl_2. **42** was subsequently employed in the synthesis of calix[4]pyrrole **H$_4$[1$^{Me/o Phen}$]** carrying four methyl- and four *ortho*-phenylene-*meso*-substituents. Surprisingly, ^{1}H NMR spectroscopy of the crude precipitant in $CDCl_3$ delivered an intense singlet at 9.38 ppm and a doublet at 5.43 ppm being characteristic for the pyrrole NH and CH of the symmetrically *meso*-octasubstituted calix[4]pyrrole **H$_4$[1$^{o Phen}$]**. Additionally, only minor signals referring to the expected dipyrromethane **42** could be observed (Figure S25). Further proof for the successful formation of **H$_4$[1$^{o Phen}$]** was obtained from matrix-assisted laser desorption/ionization (MALDI) HR-MS measurements which evidenced the presence of the $[M+H]^+$ ion at an *m/z* ratio of 917.365. Subsequent attempts to purify **H$_4$[1$^{o Phen}$]** *via* the workup with aqueous ammonia reported by TURNER *et al.* led to the decomposition of the calix[4]pyrrole thereby explaining the different reaction outcome reported in their publication from 1998. Since water can influence the equilibrium of the condensation reaction between pyrrole and carbonyl compounds, the synthetic procedure for **H$_4$[1$^{o Phen}$]** was optimized under rigorously anhydrous and inert conditions.[96] Storing HPLC-grade ethanol over activated 3Å molecular sieve for one week assured a water content below 15 ppm.[296] Employing this dry ethanol as the reaction medium for freshly distilled pyrrole and freshly sublimed fluorenone in a 1:1 ratio with 1.5 equivalents of BF_3●Et_2O as a Lewis acid catalyst allowed the multi-gram scale synthesis of **H$_4$[1$^{o Phen}$]** as a crude material. In standard organic solvents including chloroform and CH_2Cl_2 under ambient conditions the crude material showed first signs of degradation within hours accompanied by the formation of purple reaction solutions. Thus, a fast purification *via* flash column chromatography was required. Using a *puriFlash XS420Plus* flash column automat, silica gel with an average particle size between 40 and 63 µm, and a petrol ether (PE)/CH_2Cl_2 solvent system allowed

the isolation of **$H_4[1^{oPhen}]$ • CH_2Cl_2** containing one equivalent of CH_2Cl_2 pre formula unit in a moderate yield of 22% (Figure 43 B). Eventually, storing a concentrated solution of **$H_4[1^{oPhen}]$ • CH_2Cl_2** in MeCN at −30 °C yielded single crystals suitable for X-ray diffraction. The macrocyclic core of **$H_4[1^{oPhen}]$** shows the alternating up-down orientation of the pyrrole units also known for methyl- and ethyl-substituted systems (Figure 43 C). Comparison with the solid-state molecular structures of *meso*-octaethylcalix[4]pyrrole **$H_4[1^{Et}]$**[297] and **$H_4[1^{C5}]$**[298] containing spiro-cyclopentyl substituents, revealed no significant differences in bond lengths. However, tethering of the aryl *meso*-substituents into the conjugated fluorenediyl units in **$H_4[1^{oPhen}]$** resulted in a slight widening of the C_α-C- C_α valence bond angles (114.6(2)° *vs*. 111.1(3)° for **$H_4[1^{Et}]$** and 110.8(2) for **$H_4[1^{C5}]$**) and a concomitant decrease of the R-C-R bond angles. Owing to its reduced stability under ambient conditions, **$H_4[1^{oPhen}]$ • CH_2Cl_2** was stored under inert N_2 or argon atmosphere and all further reactions were carried out in dry, degassed solvents.

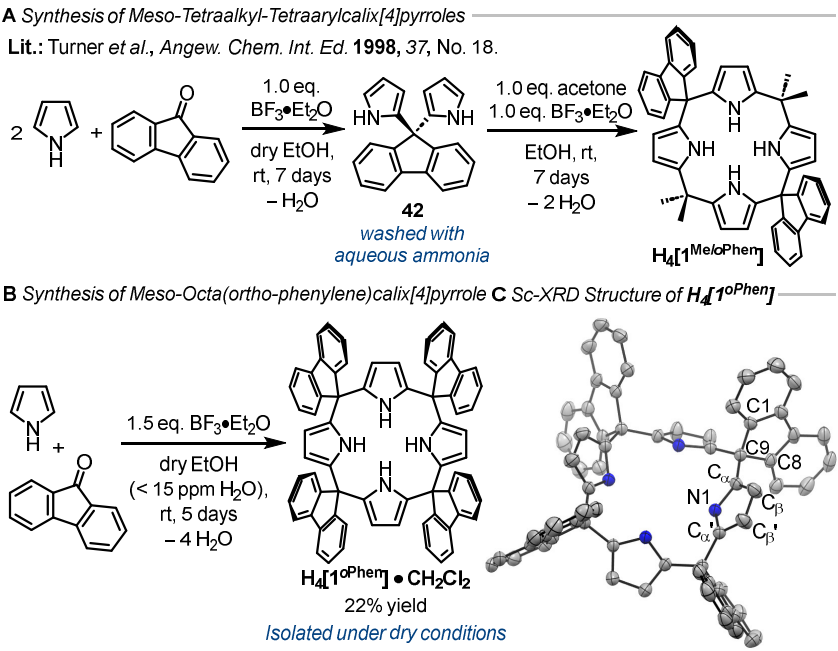


Figure 43. A) Literature known synthesis of **$H_4[1^{Me/oPhen}]$** and **B)** synthetic procedure for the synthesis of **$H_4[1^{oPhen}]$**. **C)** Solid-state molecular structure of **$H_4[1^{oPhen}]$**. Ellipsoids are drawn with a probability of 50%. Hydrogen atoms and co-crystallized MeCN molecules are omitted for clarity. Selected bond lengths [pm] and angles [deg]: N1-C_α = 137.6(3), N1-C_α' = 138.1(3), C_α-C_β = 135.6(4), C_α'-C_β' = 136.3(4), C_β-C_β' = 140.8(4), C_α-C9 = 151.0(3), C_α-C9-C_α' = 114.6(2), C1-C9-C8 = 101.1(2).

In analogy to the synthetic protocols starting from alkyl-substituted calix[4]pyrroles **H$_4$[1^R]** (R = Me, Et), **H$_4$[1$^{o\text{Phen}}$]** was deprotonated with *n*-butyl lithium at −75 to 60 °C in THF to afford the respective lithium salt [**Li$_4$(thf)$_x$][1$^{o\text{Phen}}$]**. The complete deprotonation could be observed *via* ^{1}H NMR spectroscopy. However, **H$_4$[1$^{o\text{Phen}}$]** showed to undergo side reactions with *n*-butyl lithium delivering **[Li$_4$(thf)$_x$][1$^{o\text{Phen}}$]** in low yield below 50% and poor purity (Figure 44 A). In contrast to **[Li$_4$(thf)$_x$][1^R]** (R = Me, Et), **[Li$_4$(thf)$_x$][1$^{o\text{Phen}}$]** and the side products formed during the deprotonation possessed a decreased solubility in standard organic solvents such as THF, toluene, and aliphatics excluding a purification *via* washing or preparative recrystallization. Additionally, the low solubility required the deprotonation at slightly elevated temperature to achieve a quantitative lithiation of all NH groups. Subsequent cooling of the THF reaction solution to room temperature afforded single crystals suitable for X-ray diffraction and delivered a possible explanation for the decreased solubility of the lithium salt (Figure 44 B). In the solid-state molecular structure of **[Li$_4$(thf)$_3$][1^{Et}]** one lithium cation is coordinated in the central cavity of the calix[4]pyrrolato tetraanion while the remaining cations are η^1- and η^2-coordinated by nitrogen atoms, the pyrrole π-system, and one THF molecule each forming an overall neutral compound.[299] In contrast, the sc-XRD structure of **[Li$_4$(thf)$_{10}$][1$^{o\text{Phen}}$]** revealed the bidentate coordination of two Li^+ in the calix[4]pyrrole core while two Li^+ reside as THF-solvated countercations $[Li(thf)_4]^+$. This ionic nature of **[Li$_4$(thf)$_{10}$][1$^{o\text{Phen}}$]** combined with the extended fluorenediyl π-systems in the ligand backbone most likely cause the limited solubility of the lithium salt. As described in the previous section, the reaction of $SnCl_4(thf)_2$ with the respective lithium calix[4]pyrrole salts in toluene effectively delivered **2^R-(thf)$_2$** (R = Me, Et). However, to enable the reaction of **[Li$_4$(thf)$_{10}$][1$^{o\text{Phen}}$]** the solvent medium had to be changed from toluene to mixtures of CH_2Cl_2 and THF (Figure 44 A). Even though, the combination of **[Li$_4$(thf)$_{10}$][1$^{o\text{Phen}}$]** and $SnCl_4(thf)_2$ enabled the successful incorporation of the Sn(IV) center into the calix[4]pyrrole ligand as evidenced by $^{117/119}$Sn satellites in ^{1}H NMR ($^4J_{H,Sn}$ = 12 Hz) and a δ(^{119}Sn) of −572.3 ppm (Figures S26 and S27), **2$^{o\text{Phen}}$-(thf)$_2$** could only be isolated in low yield and purity. Single crystals collected from the reaction solution showed to be suitable for X-ray diffraction. Eventually, the solid-state molecular structure shown in Figure 44 C gave definite proof of the incorporation of Sn(IV) and the formation of the bis(thf) adduct **2$^{o\text{Phen}}$-(thf)$_2$**. Despite a disorder in the calix[4]pyrrole and THF ligands and a reduced bond length precision, the Sn-N and Sn-O bond lengths in **2$^{o\text{Phen}}$-(thf)$_2$** are comparable to the respective parameters in **2^{Et}-(thf)$_2$**.

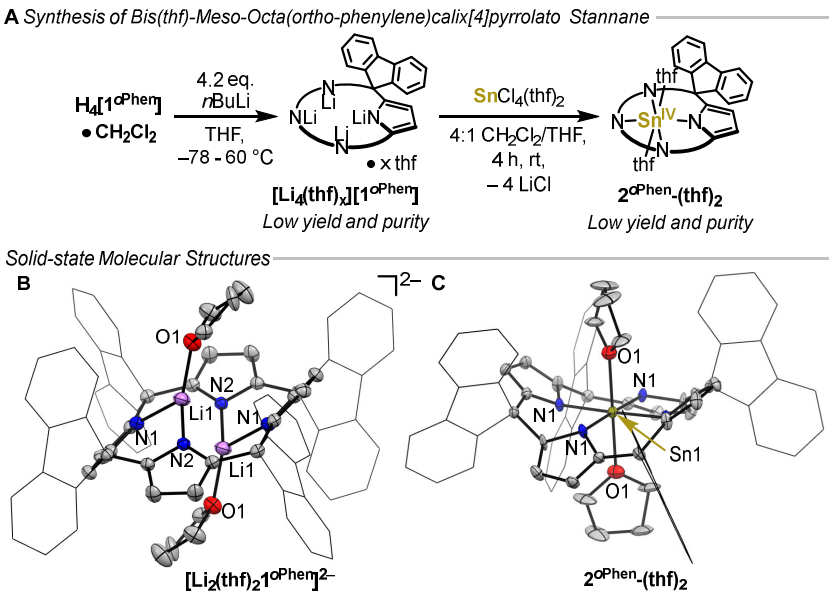


Figure 44. A) Deprotonation of **$H_4[1^{oPhen}]$** and synthesis of bis(thf)-*meso*-octa(*ortho*-phenylene)calix[4]pyrrolato stannane **2^{oPhen}-(thf)$_2$**. Solid-state molecular structure of **B) $[Li_4(thf)_{10}][1^{oPhen}]$** and **C) 2^{oPhen}-(thf)$_2$**. Ellipsoids are drawn with a probability of 50%. Hydrogen atoms are omitted for clarity. *Meso-ortho*-phenylene substituents are drawn as wireframe for clarity. For **B)** the two $[Li(thf)_4]^+$ counter cations and two co-crystallized THF molecules and for **C)** four co-crystallized CH_2Cl_2 molecules are omitted for clarity. Selected bond lengths [pm] and angles [deg] for **$[Li_4(thf)_{10}][1^{oPhen}]$**: N1-Li1 = 200.3(6), N2-Li1 =201.9(6), Li1-Li1 = 240.4(11), O1-Li1 = 196.4(17), N1-Li1-N2 = 96.5(2); and **2^{oPhen}-(thf)$_2$**: Sn1-N1 =214.0(15), Sn1-O1 = 223.1(10), N1-Sn1-N1 = 177.8(13).

After observing the degradation of **$H_4[1^{oPhen}]$** during the workup with aqueous ammonia solution and the increased amount of side products formed during the deprotonation with *n*-butyl lithium, **$H_4[1^{oPhen}]$** was suspected to decompose in the presence of Brønsted bases and especially under aqueous conditions. The dimethylamido-substituents in tetrakis(dimethylamido)tin(IV) ($Sn(NMe_2)_4$) can act as internal bases in the reaction with substrates containing OH and NH groups and enabled the synthesis of various tin(IV) compounds without the application of strong, external bases.[290,291,300] While NMR-scale test reactions of **$H_4[1^{oPhen}] \bullet CH_2Cl_2$** with one equivalent of $Sn(NMe_2)_4$ at 75 °C showed no reactivity in standard organic solvents including toluene, benzene, CH_2Cl_2, THF, MeCN, or *o*DFB, a solution in pyridine yielded the complete consumption of the starting material under the same conditions within 12 hours (Figure 45 A). NMR spectroscopy indicated the formation of a symmetric, hexacoordinated calix[4]pyrrole stannane complex with a ^{119}Sn NMR chemical shift of −590.8 ppm and the communication between pyridine and the

Sn(IV) center based on $^{1}H,^{119}Sn$-HMBC NMR experiments. Repeating this reaction on a preparative scale allowed the isolation of **2$^{o\text{Phen}}$-(py)$_2$** as a colorless solid in 75% yield. Pyridine presumably fulfilled two roles to enable the reaction of $Sn(NMe_2)_4$ with **H$_4$[1$^{o\text{Phen}}$]**. Based on the decreased intensity of the NH proton resonance in the ^{1}H NMR spectrum of a suspension of **H$_4$[1$^{o\text{Phen}}$]** in pyridine, pyridine can be expected to act as an auxiliary base activating the parent calix[4]pyrrole. Additionally, the high pyridine dissociation free enthalpies ΔG_{diss}(py) computed for **2$^{o\text{Phen}}$** (Figure 45 A), revealed its role as a strong donor and thermodynamic driving force for the formation of **2$^{o\text{Phen}}$-(py)$_2$** and the complete substitution of $HNMe_2$ from the Sn(IV) center. **2$^{o\text{Phen}}$-(py)$_2$** possesses a reduced solubility in CH_2Cl_2 but is readily soluble in heavy halobenzenes including PhCl and PhBr.

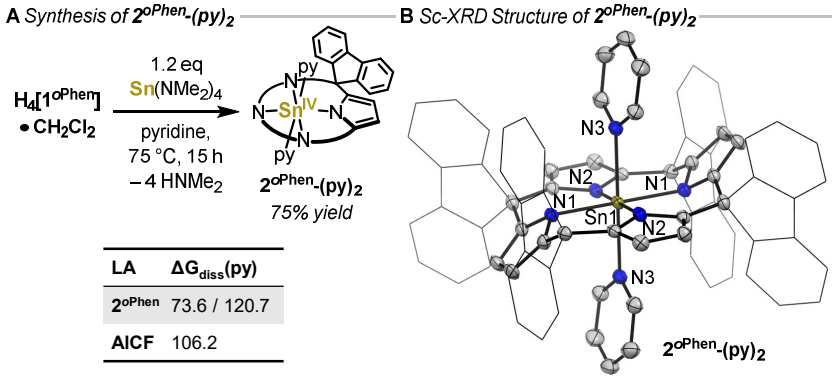


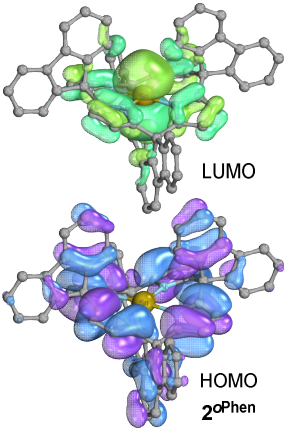
Figure 45. A) Synthesis of bis(pyridine)-*meso*-octa(*ortho*-phenylene)calix[4]pyrrolato stannane **2$^{o\text{Phen}}$-(py)$_2$** and pyridine dissociation free enthalpies ΔG_{diss}(py) for different Lewis acids (LA) in kJ mol^{-1} computed on the B97M-D4/def2-TZVPP//BP86/TZP COSMO-RS(DCM) level of theory. **B)** Solid-state molecular structure of **2$^{o\text{Phen}}$-(py)$_2$**. Ellipsoids are drawn with a probability of 50%. Hydrogen atoms and two co-crystallized *n*-pentane molecules are omitted for clarity. *Meso*-*ortho*-phenylene substituents are drawn as wireframe for clarity. Selected bond lengths [pm] and angles [deg]: Sn1-N1 = 213.2(2), Sn1-N2 = 212.1(3), Sn1-N3 = 229.4(2), N1-Sn1-N1 = 180.0, N2-Sn1-N2 = 180.0, N1-Sn1-N3 = 83.76(9), N2-Sn1-N3 = 88.18(9).

Gas phase diffusion of *n*-pentane into a concentrated solution of **2$^{o\text{Phen}}$-(py)$_2$** in CH_2Cl_2 yielded single crystals suitable for X-ray diffraction. The solid-state molecular structure shown in Figure 45 B confirmed the coordination of pyridine to the Sn(IV) center. The Sn-N bond lengths in **2$^{o\text{Phen}}$-(py)$_2$** are comparable to the respective bonds in bis(thf) adduct **2$^{o\text{Phen}}$-(thf)$_2$**. However, **2$^{o\text{Phen}}$-(py)$_2$** shows a different orientation of the pyrrolato units. **2$^{o\text{Phen}}$-(thf)$_2$** exhibits a saddle-shaped conformation whereas a waving orientation of the pyrroles can be observed in **2$^{o\text{Phen}}$-(py)$_2$**. Combined with their overall D_{4h} symmetry in solution at room temperature these findings attested the *meso*-

octa(*ortho*-phenylene)calix[4]-pyrrolato ligand backbone a similar conformational flexibility as observed for its methyl- and ethyl-substituted pendants. The pyridine co-ligands in $\mathbf{2}^{o\text{Phen}}\text{-}\mathbf{(py)}_2$ possess a slight inclination with N-Sn1-N3 valence angles below 90° which most likely are caused by crystal packing effects.

Comparison of computed parameters for $\mathbf{2}^{\mathbf{R}}$ with R = Me, Et, and *o*Phen allowed the first Lewis acidity scaling of the new *meso*-octa(*ortho*-phenylene)calix[4]pyrrolato stannane unit $\mathbf{2}^{o\text{Phen}}$ (Figure 46). The ligand-centered HOMO and tin-centered LUMO of $\mathbf{2}^{o\text{Phen}}$ show similar localizations as observed for $\mathbf{2}^{\mathbf{Me}}$ and $\mathbf{2}^{\mathbf{Et}}$. However, the HOMO in $\mathbf{2}^{o\text{Phen}}$ is significantly delocalized onto the *ortho*-phenylene substituents. As discussed in the original work in **Section 3.2**, the inductive effect of *meso*-substituents has a direct influence on the FMO energies of *meso*-octaalkylcalix[4]pyrrolato stannates(II) $[\mathbf{2}^{\mathbf{R}}]^{2-}$ (R = Me, Et).[301] A comparable trend was observed for the square-planar stannanes $\mathbf{2}^{\mathbf{R}}$. While the +I effect of ethyl substituents increase the FMO energies of $\mathbf{2}^{\mathbf{Et}}$ in comparison to $\mathbf{2}^{\mathbf{Me}}$, the -I effect of the aryl substituents in $\mathbf{2}^{o\text{Phen}}$ cause decreased FMO energies. Thus, based on its LUMO energy $\mathbf{2}^{o\text{Phen}}$ possesses an elevated intrinsic Lewis acidity (*cf.* **Section 1.2**). Employing

Comparison of Computed Parameters for $\mathbf{2}^{R}$ with R = Me, Et, and oPhen



Parameter	$\mathbf{2}^{\mathbf{Me}}$	$\mathbf{2}^{\mathbf{Et}}$	$\mathbf{2}^{o\text{Phen}}$	
E_{HOMO} [eV]	−4.99	−4.88	−5.06	
E_{LUMO} [eV]	**−2.75**	**−2.67**	**−2.87**	→ *Intrinsic Lewis acidity*
HIA_{solv}[a]	462	445	423	
FIA_{solv}[a]	**266**	**249**	**265**	→ *Global Lewis acidity*
CIA_{solv}[a]	163	151	158	
IIA_{solv}[a]	130	141	147	
δ(Sn)	2.47	2.37	2.39	
WBI(Sn-N)	0.483	0.493	0.485	

[a] in kJ mol^{-1}

Figure 46. Isosurface plots of the FMOs for $\mathbf{2}^{o\text{Phen}}$ and comparison of computed parameters for methyl-, ethyl- and (*ortho*-phenylene)-substituted calix[4]pyrrolato stannanes $\mathbf{2}^{\mathbf{R}}$ (R = Me, Et, *o*Phen). Solvation-corrected ion affinities for hydride (HIA_{solv}), fluoride (FIA_{solv}), and chloride (CIA_{solv}) in kJ mol^{-1} and partial charges of the central atom E δ(E). FMO energies in eV and WBI of the E-N bond. All orbital energies were computed on the B97M-D3(BJ)/def2-TZVPP CPCM SMD(DCM)//B97M-D3(BJ)/def2-TZVPP level of theory. Solvation-corrected ion affinities were calculated on the DSD-BLYP-D3(BJ)/def2-QZVPP//BP86/TZP COSMO-RS(DCM)//B97M-D3(BJ)/def2-TZVPP level of theory. δ(E)

and WBI were obtained *via* NBO calculations on the PBE0 def2-TZVPP//B97M-D3(BJ)/def2-TZVPP level of theory.

the global FIA_{solv} Lewis acidity scale rearranges this order and puts $\mathbf{2}^{o\mathbf{Phen}}$ (FIA_{solv} = 265 kJ mol^{-1}) on the same level as $\mathbf{2}^{\mathbf{Me}}$ (266 kJ mol^{-1}). However, combined with the resulting ion affinity values no universal trend could be identified. These findings again indicate the significant influence of secondary interactions such as attractive dispersion, steric repulsion, or the deformation energy (DE) on the binding of a given Lewis base. The expected increase in steric repulsion between two stannanes $\mathbf{2}^{o\mathbf{Phen}}$ could potentially hinder their dimerization under donor-free conditions. Indeed, DFT calculations of hypothetical α- and β-dimer structures **α-(2$^{o\mathbf{Phen}}$)$_2$** and **β-(2$^{o\mathbf{Phen}}$)$_2$** derived from **(2$^{\mathbf{Me}}$)$_2$** on the same computational level (B97M-D4/def2-TZVPP//BP86/TZP COSMO-RS(DCM)) did not allow the optimization of minimum energy structures.

The following paragraph will focus on first experimental attempts towards the synthesis of donor-free stannane $\mathbf{2}^{o\mathbf{Phen}}$. The tight binding of pyridine in **2$^{o\mathbf{Phen}}$-(py)$_2$** (ΔG_{diss}(py) of 73.6 and 120.7 kJ mol^{-1}) did not allow its complete abstraction with two equivalents of AlCF (ΔG_{diss}(py) of 106.2 kJ mol^{-1}) in *o*DFB. NMR spectroscopy evidenced the partial abstraction of pyridine and formation of a pentacoordinated Sn(IV) center with a $\delta(^{119}Sn)$ of −436.1 ppm in line with the computed ΔG_{diss}(py) values. However, attempts to isolate a pentacoordinated **2$^{o\mathbf{Phen}}$-(py)** *via* precipitation with *n*-pentane only led to the isolation of the starting material **2$^{o\mathbf{Phen}}$-(py)$_2$**. As described in the previous section, the abstraction of iodide anions from anionic iodidostannates(IV) **[I-2$^{\mathbf{R}}$]$^-$** (R = Me, Et) with thallium(I) salts led to the precipitation of all calix[4]pyrrole compounds most likely caused by the dimerization of the free Lewis acids $\mathbf{2}^{\mathbf{R}}$. To investigate this route for the potential synthesis of donor-free $\mathbf{2}^{o\mathbf{Phen}}$, **2$^{o\mathbf{Phen}}$-(py)$_2$** was first reacted with one equivalent of PPh_4Cl in CH_2Cl_2 at room temperature causing the complete dissolution of the starting material within minutes. Precipitation of the product with excess *n*-pentane and washing with PhCl to remove residual **2$^{o\mathbf{Phen}}$-(py)$_2$** delivered an off-white solid. As for the chloridostannates(IV) **[Cl-2$^{\mathbf{R}}$]$^-$** (R = Me, Et), the formation of a hexacoordinated complex bearing an additional solvent donor was observed. Prolonged drying of **[PPh$_4$][Cl-2$^{o\mathbf{Phen}}$-(py)]** at reduced pressure and 80 °C did not allow removal of the pyridine co-ligand. Additionally, degradation was observed at higher temperatures. To enable the complete removal of pyridine at room temperature, **[PPh$_4$][Cl-2$^{o\mathbf{Phen}}$-(py)]** was reacted with one equivalent of BCF acting as a neutral abstraction reagent. Eventually, a second purification step *via* precipitation with excess *n*-pentane delivered **[PPh$_4$][Cl-2$^{o\mathbf{Phen}}$]** in 55% yield showing a $\delta(^{119}Sn)$ of −452.8 ppm in line with the previously described chloridostannates(IV) (Figure

47 A). Gas phase diffusion of *n*-pentane into a concentrated solution of **[PPh$_4$][Cl-2^{oPhen}]** yielded single crystals. Despite their low quality, XRD analysis delivered the connectivity of **[PPh$_4$][Cl-2^{oPhen}]** and evidenced the successful removal of pyridine and formation of a pentacoordinated Sn(IV) center (Figure 47 B). Eventually, reaction of **[PPh$_4$][Cl-2^{oPhen}]** with a slight excess of TMSI in CH_2Cl_2 accessed the respective iodidostannate(IV) salt **[PPh$_4$][I-2^{oPhen}]**. First abstraction attempts *via* the reaction of **[PPh$_4$][I-2^{oPhen}]** with 1.2 equivalents of Tl[BAr^{F20}] in *o*DFB at room temperature showed marked differences to the

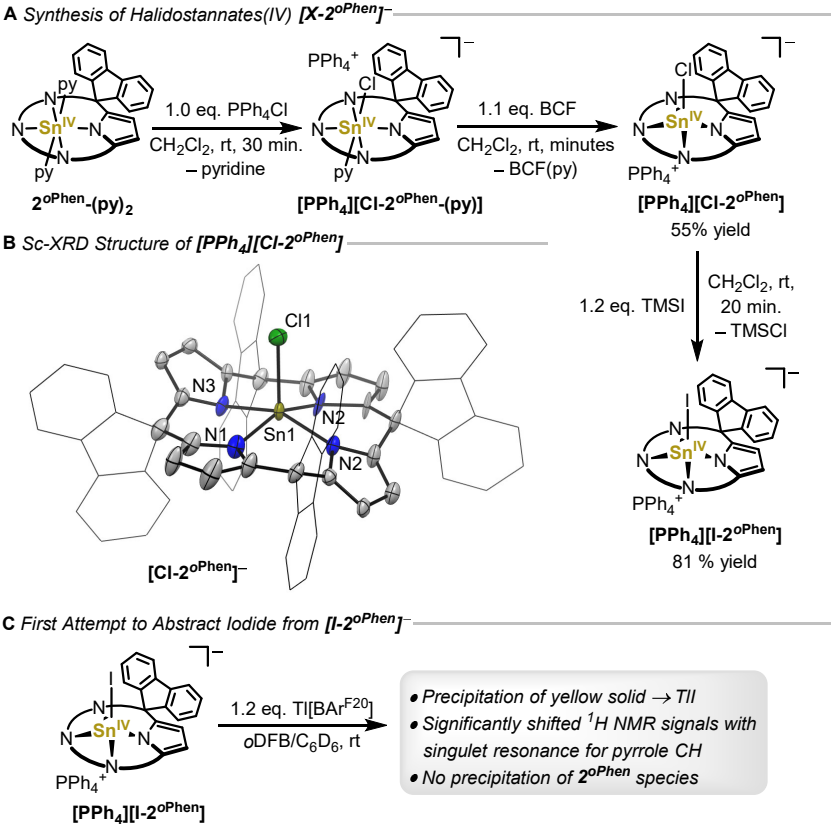


Figure 47. A) Synthesis of tetraphenylphosphonium *meso*-octa(*ortho*-phenylene)calix[4]pyrrolato halidostannates(IV) **[PPh$_4$][X-2^{oPhen}]** (X = Cl, I). **B)** Solid-state molecular structure of **[PPh$_4$][Cl-2^{oPhen}]**. Ellipsoids are drawn with a probability of 50%. Hydrogen atoms, PPh_4^+ countercation, and two co-crystallized CH_2Cl_2 molecules are omitted for clarity. *Meso-ortho*-phenylene substituents are drawn as wireframe for clarity. Owing to the low quality of the single crystal no bond lengths and angles were listed. **C)** First attempt to abstract iodide from **[I-2^{oPhen}]$^-$** using Tl[BAr^{F20}].

reactivity observed for the alkyl-substituted pendants (Figure 47 C). While the precipitation of a yellow solid indicated the formation of TlI, ^{1}H NMR spectroscopy still evidenced the presence of a $\mathbf{2}^{o\mathbf{Phen}}$ species with significantly shifted resonances in solution (Figure S28). Even though no further experimental work regarding the isolation and characterization of this new species has been conducted within the framework of this dissertation, these first results highlight the promising application of the sterically crowded *meso*-octa(*ortho*-phenylene)calix[4]pyrrolato ligand backbone to hinder the dimerization of the respective stannane $\mathbf{2}^{o\mathbf{Phen}}$ and enable its isolation as a donor-free, square-planar anti-van't Hoff-Le Bel stannane.

4 Reflection and Summary

This cumulative dissertation comprises various published and unpublished contributions to the field of structurally constrained tin compounds. In particular, it describes how structural constraint in *meso*-substituted calix[4]pyrrolato complexes can influence the nucleophilicity and donor strength of Sn(II), and the Lewis acidity of Sn(IV) centers. The following paragraph will summarize these contributions and connect the results of the publications in **Sections 3.1** – **3.4** and the unpublished work in **Section 3.5**.

The content of **Section 3.1** and **3.2** focused on the chemistry of *meso*-octaalkylcalix[4]pyrrolato stannates(II) $\mathbf{[2^R]^{2-}}$ bearing methyl- and ethyl-substituents at the *meso*-positions of the ligand backbone. After the initial report of $\mathbf{[2^{Et}]^{2-}}$ and its investigation as a strong σ-donor, nucleophile, reducing agent, and ligand in transition metal chemistry,[284] the following work disclosed a detailed discussion of the effects of ligand substitution on the electronic structure and reactivity of $\mathbf{[2^R]^{2-}}$ (Figure 48 A).[301] The macrocyclic effect of *meso*-octaalkylcalix[4]pyrrolato ligands $\mathbf{[1^R]^{4-}}$ (R = Me, Et) allowed to overcome the columbic repulsion associated with the formation of dianionic Sn(II) complexes. $\mathbf{[2^R]^{2-}}$ represented the first tetraamido tetrylene dianions and were isolated with Li^+, PPh_4^+, or NBu_4^+ countercations. Coordination of four anionic σ- and π-donating nitrogen atoms and their distortion into a constrained, square-pyramidal environment pushed the energetically buried electron lone pair at the Sn(II) center to extreme σ-donor capacities. The comparison between different *meso*-substituents R represented the first investigation of this kind in calix[4]pyrrole chemistry and the key findings of **Section 3.2** can be summarized as followed: i) inductive effects of R increase the electron-richness of the calix[4]pyrrolato ligand backbone in the series Me < Et, making $\mathbf{[2^{Et}]^{2-}}$ a stronger σ-donor and reducing agent on several experimental and theoretical scales; ii) the flexibility of the ligand backbone enabled *ruffling* and *doming* conformations of $\mathbf{[2^R]^{2-}}$ in the solid state and a fast equilibrium between both states at room temperature in solution; iii) the increased transfer of π-electron density from the calix[4]pyrrolato ligand to the Sn(II) center in *ruffling* $\mathbf{[2^R]^{2-}}$ make these conformers stronger σ-donors and weaker reducing agents based on quantum mechanical calculations; and iv) the *meso*-substituents R have a subtle influence on the preferred conformation of these calix[4]pyrrolato tin(II) complexes, thereby introducing an additional handle to control their electronics beyond pure

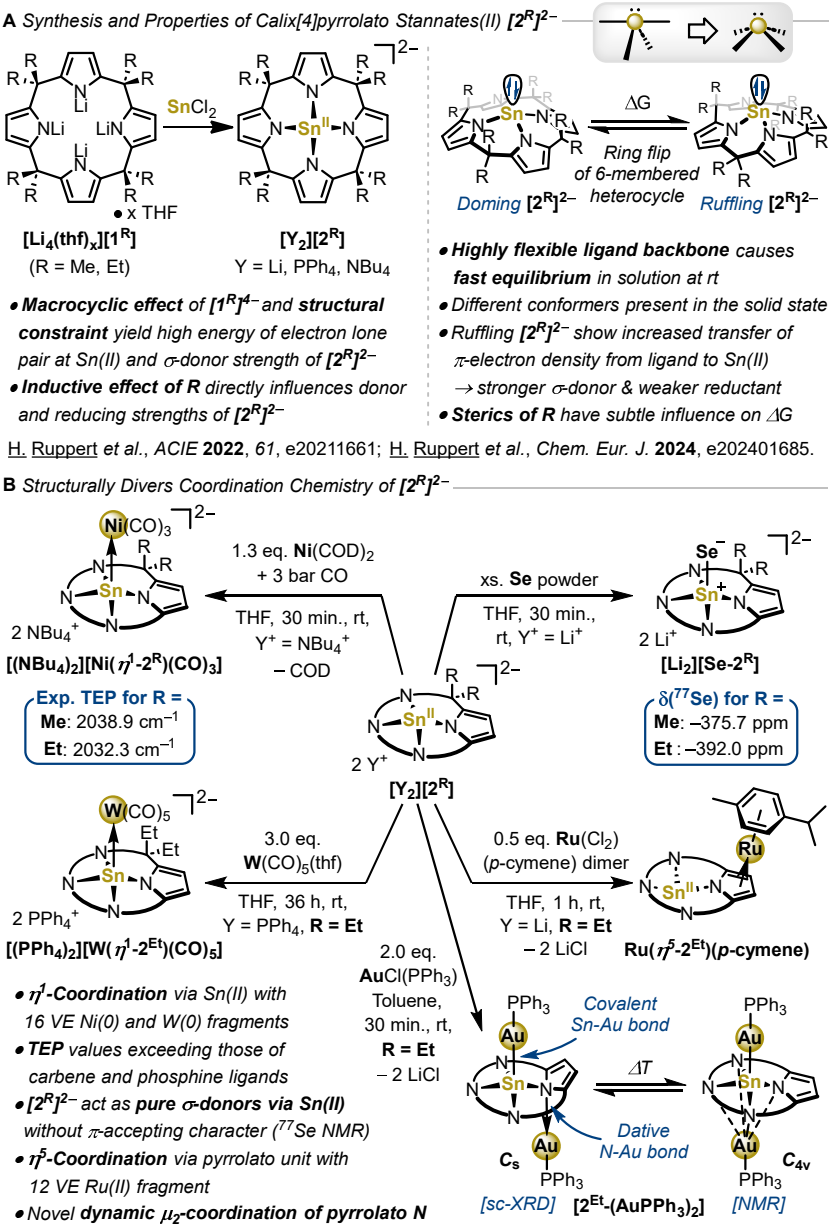


Figure 48. A) Synthesis, properties, and **B)** coordination chemistry of $[2^{R}]^{2-}$.

induction. Latter findings also highlighted the strong influence of pyrrole-out-of-plane displacements in calix[4]pyrrole chemistry and revealed a formerly unknown relationship with metalloporphyrins.

The coordination chemistry of dianions $\mathbf{[2^R]^{2-}}$ was described in **Section 3.1** for R = Et and **Section 3.2** for R = Me (Figure 48 B). Synthesis of the $Ni(CO)_3$ complexes for both $\mathbf{[2^R]^{2-}}$ delivered experimental TEP values of 2039 and 2032 cm^{-1} for R = Me and Et, respectively, and attested $\mathbf{[2^R]^{2-}}$ donor strengths exceeding those of previously described electron-rich carbene or phosphine ligands. ^{77}Se NMR chemical shifts of −392.0 and −375.7 ppm for the respective tin(II) selenides $\mathbf{[Se\text{-}2^R]^{2-}}$ confirmed the trend in donor strength rendered by the TEP values. In conjunction with computational bond analysis, they allowed to characterize the Sn(II) centers in $\mathbf{[2^R]^{2-}}$ as purely σ-donating without significant π-accepting character. Subsequently, the coordinative properties of $\mathbf{[2^{Et}]^{2-}}$ were exemplified in structurally diverse bimetallic complexes with nickel(0), tungsten(0), ruthenium(II), and gold centers. With the 16 valence electron (VE) fragments $[Ni(CO)_3]$ and $[W(CO)_5]$, $\mathbf{[2^{Et}]^{2-}}$ acted as a η^1-coordinating $2e^-$ donor ligand *via* the Sn(II) center. In contrast, with the 12 VE fragment [Ru(*p*-cymene)]$^{2+}$ the pyrrolato units in $\mathbf{[2^{Et}]^{2-}}$ also served as η^5-coordinating $6e^-$ donor ligands and formed the ruthenium(II) sandwich complex **Ru(η^5-2^{Et})(*p*-cymene)**. With $AuCl(PPh_3)$ two bimetallic complexes with one or two gold centers could be obtained (**Section 3.3**).[302] For the anionic complex $\mathbf{[2^{Et}\text{-}AuPPh_3]^-}$, sc-XRD and quantum mechanical bond analysis tools revealed the formation of a covalent Sn-Au bond owing to a significant charge transfer from tin(II) to gold(I) upon coordination. In the dinuclear complex $\mathbf{[2^{Et}\text{-}(AuPPh_3)_2]}$, the dynamic μ_2-coordination of all four pyrrole nitrogen atoms to the second $[AuPPh_3]^+$ fragment resulted in a C_{4v} symmetric complex in solution at room temperature – a coordination mode formerly unknown to calix[4]pyrrole chemistry. Combination of sc-XRD structure, variable temperature NMR measurements, and DFT simulations led to the migration mechanism for the second $[AuPPh_3]^+$ between the pyrrole units which heavily relies on the flexibility of the calix[4]pyrrolato ligand backbone.

The literature in **Section 3.1** and **3.2** described the application of $\mathbf{[2^R]^{2-}}$ as electron-rich reagents in chemical transformations with electrophiles (Figure 49 A). In this context, the augmented nucleophilicity and reducing strength of $\mathbf{[2^{Et}]^{2-}}$ enabled spontaneous substitution reactions at C(sp^2) or C(sp^3) centers in alkyl, and acyl chlorides. While literature-known, monoanionic Sn(II) nucleophiles such as $\mathbf{[\textit{n}Bu_3Sn]^-}$ require special oxidants as hydride acceptors, the dianionic nature of $\mathbf{[2^{Et}]^{2-}}$ and the concomitant formation of LiH

enabled the direct substitution of hydride at benzaldehydes.[284] Cyclic voltammetry of **[(NBu$_4$)$_2$][2^R]** salts revealed two ligand-centered, irreversible one-electron oxidations at potentials E_{ox} of −0.85 and −0.36 V (R = Me) and −0.95 and −0.49 V (R = Et, *vs.* fc$^+$/fc), respectively, in line with the increased electron-richness of **[2^{Et}]$^{2-}$**. For both complexes a third, irreversible two-electron oxidation wave could be observed at the same potential of 0.02 V which was attributed to the de-electronation of the Sn(II) centers. Interestingly, even though the reducing potential of **[2^{Et}]$^{2-}$** should not allow the direct reduction of iodobenzene (PhI), the reaction completed at room temperature within 24 hours. In THF, the oxidation of **[2^{Et}]$^{2-}$** yielded the bis(thf)-adduct **2^{Et}-(thf)$_2$**. While the lithium salt of **[2^{Et}]$^{2-}$** produced phenyl lithium which could be scavenged with benzophenone,

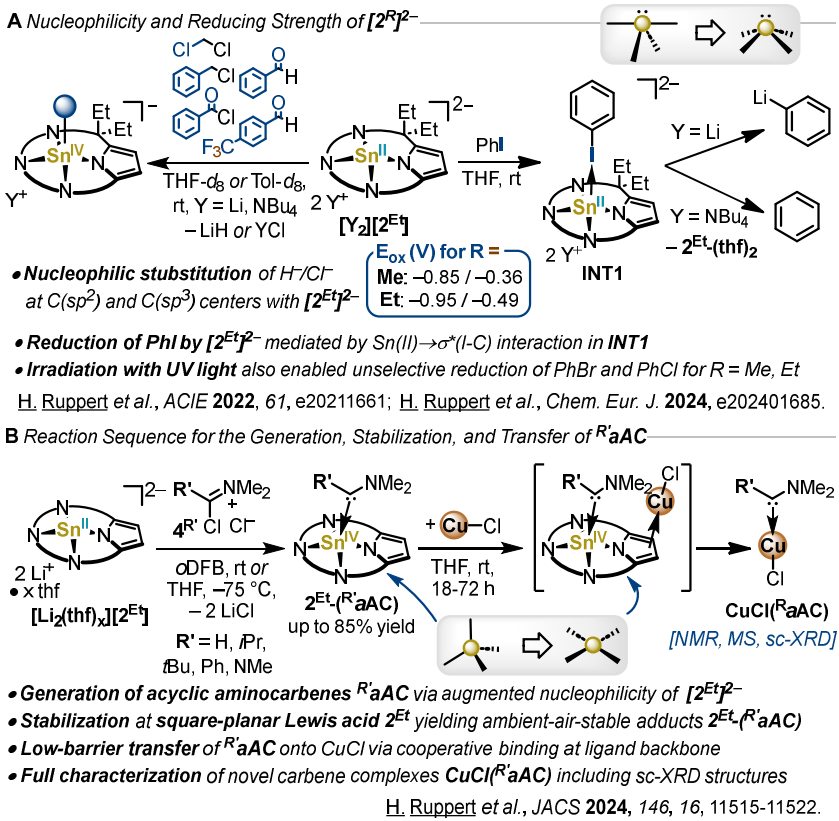


Figure 49. A) Applications of **[2^R]$^{2-}$** as nucleophiles and reducing agents and **B)** the umpolung reaction sequence for the generation, stabilization, and transfer of acyclic aminocarbenes.

ammonium countercations acted as a proton source and delivered benzene within 24 hours.[284,301] Computations suggested the intermediate formation of an encounter complex **INT1** between $[\mathbf{2^{Et}}]^{2-}$ and PhI *via* a Sn(II)→σ*(I-C) interaction which effectively lowered the barrier for an electron transfer (Figure 49 A). Thus, even though the reducing strength of $[\mathbf{2^{R}}]^{2-}$ is mainly influenced by the electronic structure of the ligand backbone, the Sn(II) center can act as a nucleophilic mediator for the reduction of electrophilic substrates. The absence of any signs of reduction for $[\mathbf{2^{Me}}]^{2-}$ further underlined the scaling of reactivity by *meso*-substitution. Eventually, preliminary experiments showed that the reducing strengths of $[\mathbf{2^{R}}]^{2-}$ can be boosted by photoexcitation with UV light and even enabled the reduction of bromo- and chlorobenzene.[301]

The work in **Section 3.4** covered the application of $[\mathbf{2^{Et}}]^{2-}$ as a nucleophilic reducing agent for the generation, stabilization, and transfer of various low-substituted acyclic aminocarbenes (Figure 49 B). Reaction of $\mathbf{[Li_2(thf)_x][2^{Et}]}$ with easily accessible chloroiminium salts $\mathbf{4^{R'}}$ resulted in an umpolung reaction, granting access to the acyclic aminocarbenes $^{\mathbf{R'}}\boldsymbol{a}\mathbf{AC}$ (R' = H, *i*Pr, *t*Bu, Ph, NMe_2). The newly formed carbenes were isolated as adducts with the *in situ*-generated, square-planar Sn(IV) Lewis acid $\mathbf{2^{Et}}$. Owed to its anti-van't-Hoff-Le-Bel configuration, $\mathbf{2^{Et}}$ possesses a marked Lewis acidity which enabled a strong binding and electronic stabilization of carbenes $^{\mathbf{R'}}\boldsymbol{a}\mathbf{AC}$ and led to the formation of ambient-air-stable adducts $\mathbf{2^{Et}}$**-(**$^{\mathbf{R'}}\boldsymbol{a}$**AC)**. While the thermodynamic stability of these adducts quenched the ambiphilic reactivity of the coordinated carbenes $^{\mathbf{R'}}\boldsymbol{a}\mathbf{AC}$, $\mathbf{2^{Et}}$**-(**$^{\mathbf{R'}}\boldsymbol{a}$**AC)** could effectively be used as transfer agents for the selective transmetalation of $^{\mathbf{R'}}\boldsymbol{a}\mathbf{AC}$ onto copper(I) halides. Quantum mechanical simulation of the transmetalation mechanism revealed the cooperative binding of copper(I) halide fragments *via* the calix[4]pyrrolato ligand backbone as a key step in the low-barrier synthesis of previously elusive carbene complexes **CuCl(**$^{\mathbf{R'}}\boldsymbol{a}$**AC)** at room temperature. Preceding studies on structurally constrained *p*-block elements have been restricted to specific, isolated attributes such as enhanced nucleophilicity, reducing strength, or Lewis acidity. In contrast, this carbene generation – stabilization – transfer series exploited the concatenation of these structural constraint aspects in a complex reaction sequence for the first time.

Eventually, computational and experimental work on the Lewis acidic and ambiphilic properties of anti-van't-Hoff-Le-Bel calix[4]pyrrolato stannanes $\mathbf{2^{R}}$ (R = Me, Et) revealed marked differences in comparison to their silicon and germanium pedants $\mathbf{8^{R}}$ (E = Si) and $\mathbf{9^{R}}$ (E = Ge, Figure 50 A). Comparison of computational results in **Section 3.5.1**

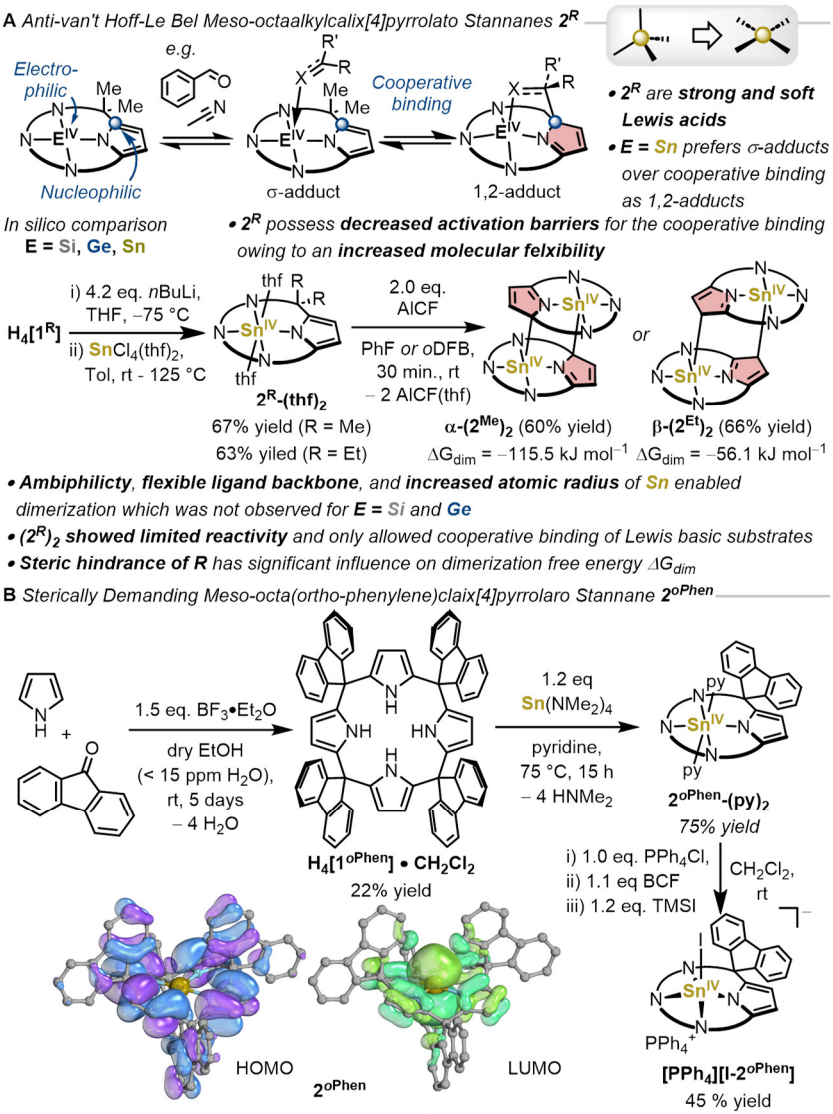


Figure 50. A) Chemistry of anti-van't Hoff-Le Bel *meso*-octaalkylcalix[4]pyrrolato stannanes 2^{R} (R = Me, Et) and **B)** first steps towards a monomeric, square-planar stannane 2^{oPhen} *via* the novel, sterically demanding ligand $H_4[1^{oPhen}]$.

characterized $\mathbf{2^R}$ as strong, soft Lewis acids with an increased molecular flexibility caused by less-covalent E-N bonds with the calix[4]pyrrolato macrocycle. Reduced E-O/N bond strengths for E = Sn also resulted in their lowered tendency to cooperatively bind carbonyls and acetonitrile as 1,2-adducts. In contrast, the increased atomic radius of tin allowed the essentially barrierless formation of σ-adducts with such substrates. As described in **Section 3.5.2**, after prior characterization of various mono- and bis-adducts of $\mathbf{2^R}$ with anionic (F^-, Cl^-, I^-) and neutral (THF, Et_3PO) donors, the isolation of the donor-free anti-van't Hoff-Le Bel stannanes was eventually achieved *via* the abstraction of THF from $\mathbf{2^R\text{-}(thf)_2}$ with *tris*(pentafluorophenyl)alane (AlCF). Caused by the pronounced ambiphilicity of $\mathbf{2^R}$, their flexible ligand backbone, and the increased atomic radius of Sn, compared to Si and Ge, the donor-free stannanes could only be isolated as dimers $\mathbf{(2^R)_2}$. Sc-XRD analysis revealed different dimerization modes depending on the steric demand of the *meso*-substituent. While $\mathbf{2^{Me}}$ forms the α-dimer $\mathbf{\alpha\text{-}(2^{Me})_2}$ involving the nucleophilic α-carbon atoms of the pyrrolato units, $\mathbf{2^{Et}}$ achieves a reduced steric repulsion *via* the β-dimer $\mathbf{\beta\text{-}(2^{Et})_2}$ (Figure 50 A). Notably, only a few cases for the cooperativity of the β-carbon atoms in calix[4]pyrrole complexes are known and no case has been reported in the context of *p*-block chemistry so far. The dimeric forms still allowed the cooperative activation of electron-rich and Lewis basic substrates, *i.e.* the O-H bond in *i*PrOH, the C-O double bond in benzaldehyde, and even the C3-H bond in *N*-methyl indole.

As evidenced by the computed dimerization free energies ΔG_{dim}, the steric demand of the *meso*-substituents R has a significant effect on the stability of the dimers $\mathbf{(2^R)_2}$. In an aim to increase the steric hindrance of R and eventually enable the isolation of a monomeric, square-planar stannane $\mathbf{2^R}$, a novel calix[4]pyrrole ligand was realized and its first application in Sn(IV) chemistry investigated (Figure 50 B, **Section 3.5.3**). Rigorously anhydrous conditions allowed the condensation reaction between fluorenone and pyrrole and delivered *meso*-octa(*ortho*-phenylene)calix[4]pyrrole $\mathbf{H_4[1^{oPhen}]}$. Even though *meso*-octaarylcalix[4]pyrroles have been mentioned in the literature, no synthetic method for their synthesis on a preparative scale has been reported so far. In contrast to alkyl-substituted $\mathbf{H_4[1^{Me}]}$ and $\mathbf{H_4[1^{Et}]}$, this new ligand showed to be sensitive towards moisture and strong bases and required an alternative synthetic pathway for the quantitative incorporation of a Sn(IV) center. After accessing the bis(pyridine) adduct $\mathbf{2^{oPhen}\text{-}(py)_2}$ on a preparative scale, reaction with PPh_4Cl followed by the halogenide exchange with trimethylsilyl iodide (TMSI) enabled the successful synthesis of the respective chlorido and iodidostannate(IV) salts $\mathbf{[PPh_4][X\text{-}2^{oPhen}]}$ (X = Cl, I) and the complete removal of the strongly donating pyridine co-ligands. Eventually, first test reactions for the iodide

abstraction from **[I-2$^{o\text{Phen}}$]**$^-$ with thallium(I) *tetrakis*(pentafluorophenylborate) (Tl[BAr^{F20}]) revealed marked differences to the behavior observed for its alky-substituted pendants **[I-2^{R}]**$^-$ (R = Me, Et). Thus, this synthetic pathway could be a promising route for the future isolation of a monomeric, anti-van't Hoff-Le Bel stannane **2**$^{o\text{Phen}}$. With a computed FIA$_{solv}$ of 265 kJ mol^{-1}, **2**$^{o\text{Phen}}$ possesses a Lewis acidity comparable to **2**^{Me} (FIA$_{solv}$ of 266 kJ mol^{-1}) and shows the characteristic p_z-type LUMO at tin and ligand-centered HOMO expected for a square-planar calix[4]pyrrole *p*-block compound.

To conclude, this dissertation described the synthesis of and reactivity studies on novel calix[4]pyrrolato complexes bearing Sn(II) and Sn(IV) centers. For the first time, structural constraint has been investigated as a tool to augment their reactivity and enabled chemical transformations formerly unknown for their unconstrained pendants. Besides structural constraint, key features of these compounds were recurringly based on the flexibility of the calix[4]pyrrolato ligand backbone and its cooperativity.

5 METHODS

5.1 General Remarks on Experimental Work

Experimental details

All reagents, solvents, and further materials were purchased from commercial sources and used as received if not stated differently. Solvents were degassed prior to use with three freeze-pump-thaw cycles and were stored in sealed Schlenk ampulla over activated molecular sieve (3 or 4 Å, respectively) under a dry argon atmosphere. Acetonitrile and liquid reagents were degassed by purging with dry argon gas. Pyrrole was distilled and fluorenone sublimed and both stored under dry argon atmosphere.

All reactions on preparative scale were carried out in flame-dried standard laboratory glassware under a dry argon or nitrogen atmosphere using Schlenk line techniques and were permanently magnetically stirred, if not stated differently. Syringes, magnetic stirring bars, and needles were dried and/or flushed with argon prior to use. Reactions on the NMR sample scale were done in dry J. Young NMR tubes.

Compounds sensitive to ambient conditions were handled and stored in a Sylatech glovebox filled with dry nitrogen gas. Removal of solvents *in vacuo* was performed using a Heidolph VV2000 rotary evaporator or a Schlenk line.

Literature known compounds were synthesized following published procedures. The respective publications are cited below. Analytical data of known compounds were compared to reference data and were found to be consistent. New compounds were characterized to the reported structures to the best of knowledge.

NMR spectroscopy

NMR spectra were collected with a Bruker BZH 200/52, a Bruker DPX200, a Bruker Avance II 400, a Bruker Avance III 400, or Bruker Avance III 600 spectrometers at geiven temperature. The measurements with the Bruker Avance II 400, Avance III 400, and the Bruker Avance III 600 spectrometers were done by the staff of the NMR spectroscopy facilities of the organic and inorganic chemistry department of Heidelberg University. The 600 MHz spectrometers were equipped with a 5-mm $^{1}H\{^{13}C/^{15}N/^{31}P\}$ or a 5-mm BBFO z-

axis gradient helium-cooled cryogenic probe. Spectra were acquired with field-frequency lock on the ^{2}H signal of the used solvent prior to data collection. Chemical shifts δ are reported in parts per million (ppm). Shifts of ^{1}H and ^{13}C nuclei are given relative to the tetramethylsilane resonance, ^{77}Se nuclei shifts relative to the dimethyl selenide, and ^{119}Sn shifts relative to the tetramethylstannane reference system. If not stated otherwise, ^{1}H and ^{13}C chemical shifts were taken from one-dimensional NMR spectra. To assist the correct peak assignment additional two-dimensional NMR spectra such as $^{1}H,^{1}H$-COSY, $^{1}H,^{13}C$-HSQC and -HMBC, and broadband ^{1}H-decoupled ^{13}C-DEPT135 were recorded (only selected spectra were depicted in the supplementary information). ^{1}H and ^{13}C NMR spectra were calibrated on appropriate solvent signals before data extraction.[278] ^{119}Sn chemical shifts were obtained from two-dimensional $^{1}H,^{119}Sn$-HMBC measurements. ^{77}Se chemical shifts were obtained from two-dimensional $^{1}H,^{77}Se$-HMBC measurements. ^{19}F and ^{31}P chemical shifts are reported relative to the trichlorofluoromethane and the H_3PO_4 (85% aq) reference system, respectively. ^{19}F and ^{31}P NMR spectra were not manually calibrated after processing. NMR signal coupling constants *J* are given in hertz (Hz). Peak multiplicities are given as singlet (*s*), doublet (*d*), triplet (*t*), quartet (*q*), quintet (*quint*), sextet (*sext*), septet (*sept*), and multiplet (*m*). NMR spectra were processed and plotted with *MestReNova* (version 15.0.1).[303]

Mass spectrometry

High resolution mass spectrometry (HR-MS) was done with a Bruker ApexQe FT-ICR instrument coupled to an electrospray ionization (ESI) source operating in positive or negative ion mode. Measurements were carried out by the staff of the mass spectrometry facilities of the department of inorganic chemistry of Heidelberg University. Samples were prepared with dry solvents under inert conditions with an approximate analyte concentration of $c = 10^{-5}$ mol L^{-1}. They were immediately analyzed after being brought in contact with air.

IR spectroscopy

Fourier-transform attenuated total reflection infrared spectroscopy (FT-ATR-IR) was done with an *Agilent Cary 630* spectrometer in solution or with solid material at room temperature inside a dry nitrogen-filled glovebox. The obtained spectra were manually baseline-corrected. The data is reported as: maximum wavenumber $\tilde{\nu}_{max}$ [cm^{-1}] of the respective absorption band, intensity (*s* = strong, *m* = medium, *w* = weak).

Cyclic voltammetry

Cyclic voltammetry was done inside a dry nitrogen-filled glove box at room temperature with a EmStat3+blue device from *PalmSens*, which was operated with the *PSTrace 5.7* software. A glassy carbon electrode (working area of 0.07 cm^2) was used as a working electrode, a platinum wire as a counter electrode, and a silver wire as a quasi-reference electrode. The scan rate was set to 0.05 V s^{-1}. *1,2*-Difluorobezene (*o*DFB) was used as the solvent and [NBu4][PF6] as the supporting electrolyte. The analyte concentration was approximately c = 10^{-3} mol L^{-1}, the supporting electrolyte concentration c_{supp} = 0.1 mol L^{-1}. The acquired data was externally referenced against the decamethylferrocene/decamethylferrocenium ($dmfc^+$/dmfc) redox couple and then transferred to the fc^+/fc reference. Under the same conditions as described fc+/fc has a redox potential of 532 mV and $dmfc^+$/dmfc a redox potential of 30 mV against the AgCl/Ag/KCl redox couple.[304] The $dmfc^+$/dmfc reference measurement was carried out under the same conditions as described.

Elemental analysis

Elemental analyses for the determination of C, H, and N contents were done with a *vario EL* or *vario MICRO cube* elemental analyzer. They were carried out by the staff of the microanalytical laboratory of the chemical institutes of Heidelberg University.

Single crystal X-ray diffraction

After removal from the crystallization sample, crystals were immersed in perfluorinated polyether oil (purchased from ABCR). A suitable crystal was picked and fixed on top of a CryoLoop. A *Bruker D8 Venture* dual wavelength Mo/Cu four-circle diffractometer with mirror optics as monochromator and an *Oxford Cryostream 700* low-temperature device was used for φ and ω-scans. Data collection was performed at 100 K using Mo-K_α radiation (λ = 0.71073 Å). A strategy for data acquisition was calculated with Bruker's *APEX3* or *APEX4* software.[305,306] The data were integrated with the *SAINT* program[307] and *SADABS-2016/2* was used for multi-scan absorption correction.[308] Structures were solved with direct methods as implemented in the [307]*SHELXT* 2018 structure solution program.[309] Structure refinement was carried out by full matrix least squares minimization on F^2 using the 2018/3 or 2019/3 version of *SHELXL*.[310–312] All non-hydrogen atoms were refined anisotropically. Hydrogen atom positions were calculated geometrically and refined using a riding model. Handling of the structural data during refinement was performed with the ShelXle graphical interface.[313] Data finalization was done with

FinalCif.[314] Crystallographic data for the structures reported here have been partly deposited with the Cambridge Crystallographic Data Centre (CCDC). Copies of the data can be obtained free of charge from: www.ccdc.cam.ac.uk/structures.

For data visualization, *Mercury* was used.[315,316] The thermal displacement ellipsoids were shown at a probability level of 50%.

5.2 Supplementary Details on Quantum Chemical Simulations

Programs and computational resources

All computations were carried out with the computational resources provided by the Baden-Württemberg High Performance Computing (bwHPC) program through the bwForCluster JUSTUS2 at Ulm University. The support of the state of Baden-Württemberg through bwHPC and the German Research Foundation is acknowledged. DFT calculations were carried out with ORCA 5.0.3.[317,318] The NBO6 program was used for NBO calculations through ORCA.[319] The Amsterdam Modelling Suite AMS2021.201 software package[8,9] was used for energy decomposition analysis (EDA),[320–322] BADER's quantum theory of atoms in molecules (QTAIM),[323–326] and NMR shift calculations. Input geometries were generated using Avogadro.[327] Optimized geometries were visualized *via* Chemcraft version 1.8.[328] Isosurface plots were created using the IboView software v20150427.[329]

Structure optimizations and frequency calculations

Throughout the presented research projects, various DFT-based levels of theory were applied which are mentioned respectively. In general, molecular structures were optimized toward minimum or transition structures. The obtained structures were verified as stationary points on the respective PES by the calculation of harmonic frequencies, either numerically or analytically. It was ensured that for minimum structures zero and for transition structures one negative force constant was present. In the case of transition states, the correct first-order saddle point on the potential energy surface was confirmed by animation of the imaginary frequency.

Where necessary, prior to the structure optimizations with DFT, conformational searching was done with CREST[330] using GFN2-xTB[331] within xTB using the following command line.[332]

```
crest [file_name].xyz --alpb solvent_name --chrg [charge] --
noreftopo > [file_name].out
```

The lowest energy conformer according to GFN2-xTB was subjected to a DFT structure optimization. Structure optimizations and frequency calculations were performed either at the PBEh-3c[333–336] level of theory including the respective basis sets[337,338] or B97M[339]-D4[340]/def2-TVZPP[341] level of theory employing a def2/J auxiliary basis set.[337] Minima structures were obtained with the following ORCA input lines:

```
! PBEh-3c RIJCOSX AutoAux TightSCF Opt Freq
```

```
! RKS B97M-D4 def2-TZVPP defGrid2 Opt NumFreq TightSCF
```

Single point energy calculations and thermochemistry

In cases where additional single point calculations were carried out after structure optimization, the final data which is reported was obtained by combination of the electronic energy from the higher-level single point computation with the thermal corrections from the frequency calculations on the lower computational level. Enthalpies were calculated at 298.15 K if not stated differently. For Gibbs free energies, the enthalpy values were merged with the vibrational entropy terms according to the rigid-rotor-harmonic-oscillator approximation (QRRHO) of GRIMME.[342]

For the calculation of implicit solvation influences on the thermochemical data, the conductor like screening model for real solvents (COSMO-RS)[343–345] as implemented in AMS was used. The default program settings were applied (BP86/TZP). Only the maximum number of structure optimization iterations was set to zero. COSMO-RS correction for enthalpies was achieved by the calculation of ΔG-corrections at five different temperatures (278.15, 288.15, 298.15, 308.15, 318.15 K). Following $\Delta G = \Delta H - T\Delta S$, the plot of the obtained Gibbs free energy corrections against the temperature allows to fit a straight line from which the corrections for ΔH were obtained.

Subsequent single point calculations employing the conductor-like polarizable continuum model based on solute electron density (C-PCM SMD)[346] were performed with the following ORCA input line:

```
! RKS B97M-D4 def2-TZVPP defGrid2 TightSCF
CPCM SMD TRUE
        SMDSOLVENT "solvent_name"
END
```

High-level thermodynamic data was obtained by subsequent single point calculations employing the double-hybrid density functional DSD-BLYP[347] and def2-QZVPP basis set[341] combined with the D3(BJ) dispersion correction[334] and the resolution-of-identity approximation[348] with automatically generated auxiliary basis sets[338] according to the following input line:

```
! RI-DSD-BLYP D3BJ def2-QZVPP RIJCOSX AutoAux defGrid3 TightSCF
```

NBO calculations were conducted on the PBE0[349]/def2-TZVP[341] level of theory (def2-TZVPP basis set for Au atoms) using NBO6.0.18a[319] as included in Orca 5.0.3 *via* the following ORCA input line:

```
! RKS PBE0 def2-TZVP NBO TightSCF defGrid2

%basis

   newgto Au "def2-TZVPP" end

end
```

Furthermore the $CHOOSE key list was used to specify meaningful Lewis structures for the NBO search.

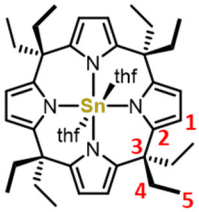
Calculations employing the Extended Transition State (ETS) method for energy decomposition analysis (EDA)[320–322] combined with the natural orbitals for chemical valence (NOCV)[350] calculations were performed on the BP86-D3(BJ)[336,351,352]/TZ2P level of theory with COSMO(THF) solvation correction.

QTAIM analyses were performed on PBE0-D3(BJ)/ZORA-TZ2P/COSMO(*solvent_name*) electron densities.[353–355] QTAIM charges of atoms were calculated using the grid-based method implemented in AMS.[356,357] The Numerical *Quality Good* keyword was used in the calculations to increase the numerical quality of the results in order to avoid numerical artefacts in the atomic charges.

5.3 Synthetic Procedures and Characterization Data

Synthesis of **H_4[1^R]**,[120] **[Li_4(thf)$_x$][1^R]** (R = Me, Et),[299] $SnCl_4(thf)_2$,[358] Na[BAr^{F20}],[359] Tl[BAr^{F20}],[360,361] BCF,[362] and AlCF[363] were performed according to literature known procedures and their purity confirmed by NMR spectroscopy prior to usage.

5.3.1 Bis(thf)-*meso*-octaethylcalix[4]pyrrolato stannane 2^{Et}-(thf)$_2$



2^{Et}-(thf)$_2$ was prepared according to a literature known procedure.[112] In a 250 mL Schlenk tube *tetra*-lithium *meso*-octaethylcalix[4]pyrrolate **[Li_4(thf)$_x$][1^{Et}]** (x = 3.5, 1.0 eq, 3.06 mmol, 2.50 g) was dissolved in 40 mL dry toluene. While stirring at room temperature *bis*-(thf) tin(IV) chloride $SnCl_4(thf)_2$ (1.0 eq., 3.06 mmol, 1.24 g) was added in portions. The reaction solution turned pink, and a precipitant formed. After stirring at 135 °C for 14 hours the reaction solution was allowed to reach room temperature and filtered over a POR4 sintered glass filter frit to remove lithium chloride formed during the reaction. The solvent of the filtrate was removed at reduced pressure and the residue washed with 8 mL *n*-hexane to afford **2^{Et}-(thf)$_2$** as a pink solid (1.54 g, 1.93 mol, 63% yield). Cooling of a concentrated solution of **2^{Et}-(thf)$_2$** in toluene to −30 °C yielded single crystals suitable for X-ray diffraction.

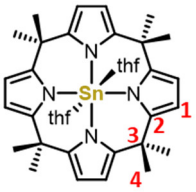
^{1}H NMR [^{1}H, ^{1}H,^{1}H-COSY] (399.89 MHz, CD_2Cl_2, 295 K): δ [ppm] = 6.11 (*s*, $^{117/119}$Sn satellites $^4J_{Sn,H}$ = 16 Hz, H_1, 8H), 3.10 – 2.99 (*m*, H_{thf}, 8H), 1.81 (*q*, $^3J_{H,H}$ = 7.3 Hz, H_4, 16H), 1.67 – 1.58 (*m*, H_{thf}, 8H), 0.63 (t, $^3J_{H,H}$ = 7.3 Hz, 24H).

^{13}C NMR [^{13}C{^{1}H}, ^{13}C-DEPT135, ^{1}H,^{13}C-HSQC, ^{1}H,^{13}C-HMBC] (100.56 MHz, CD_2Cl_2, 295 K): δ [ppm] = 142.60 (*s*, $^{117/119}$Sn satellites $^2J_{Sn,C}$ = 8 Hz, C_2), 108.34 (*s*, $^{117/119}$Sn satellites $^3J_{Sn,C}$ = 43 Hz, C_1H), 70.27 (*s*, $C_{thf}H_2$), 46.03 (*s*, C_3), 37.33 (*s*, $^{117/119}$Sn satellites $^4J_{Sn,C}$ = 12 Hz, C_4H_2), 25.90 (*s*, $C_{thf}H_2$), 9.81 (*s*, C_5H_3).

^{119}Sn NMR [^{119}Sn-INVGATE] (149.08 MHz, CD_2Cl_2, 295 K): δ [ppm] = −561.31.

488

5.3.2 Bis(thf)-*meso*-octamethylcalix[4]pyrrolato stannane 2^{Me}-(thf)$_2$



2^{Me}-(thf)$_2$ was prepared in analogy to the literature known procedure for **2^{Et}-(thf)$_2$**.[112] In a 250 mL Schlenk tube *tetra*-lithium *meso*-octamethylcalix[4]pyrrolate **[Li$_4$(thf)$_x$][1^{Me}]** (x = 3.4, 1.0 eq., 4.30 mmol, 3.00 g) was dissolved in 50 mL dry toluene. While stirring at room temperature bis(thf)-tin(IV) chloride $SnCl_4(thf)_2$ (1.0 eq., 4.30 mmol, 1.74 g) was added in portions. The reaction solution turned pink, and a precipitant formed. After stirring at room temperature for 14 hours the reaction solution was filtered over a POR4 sintered glass filter frit to remove lithium chloride formed during the reaction. The solvent of the filtrate was removed at reduced pressure and the residue washed with 30 mL *n*-hexane to afford **2^{Me}-(thf)$_2$** as a beige solid (1.89 g, 2.75 mol, 67% yield). Repeated attempts to generate single crystals suitable for X-ray diffraction remained unsuccessful.

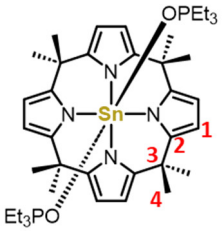
^{1}H NMR [^{1}H, ^{1}H,^{1}H-COSY] (600.13 MHz, Toluene-d_8, 295 K): δ [ppm] = 6.38 (*s*, $^{117/119}$Sn satellites $^4J_{Sn,H}$ = 18 Hz, H_1, 8H), 3.02 – 3.16 (*m*, H_{thf}, 8H), 1.73 (*s*, H_4, 24H), 0.97 - 1.07 (*m*, H_{thf}, 8H).

^{13}C NMR [^{13}C{^{1}H}, ^{13}C-DEPT135, ^{1}H,^{13}C-HSQC, ^{1}H,^{13}C-HMBC] (101.15 MHz, Toluene-d_8, 295 K): δ [ppm] = 147.28 (*s*, C_2), 106.00 (*s*, $^{117/119}$Sn satellites $^3J_{Sn,C}$ = 20 Hz, C_1H), 70.03 (*s*, $C_{thf}H_2$), 37.00 (*s*, C_3), 34.51 (*s*, C_4H_3), 25.30 (*s*, $C_{thf}H_2$).

^{119}Sn NMR [^{119}Sn,^{1}H-HMBC] (223.81 MHz, Toluene-d_8, 295 K): δ [ppm] = −553.6.

EA: calcd. for $C_{36}H_{48}N_4O_2Sn$: C, 62.89; H, 7.04; N, 8.15. Found: C, 62.77; H, 7.09; N, 7.94.

5.3.3 Bis(triethylphosphine oxide)-*meso*-octamethylcalix[4]pyrrolato stannane 2^{Me}-$(Et_3PO)_2$

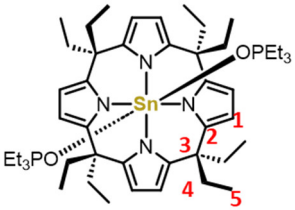


In a nitrogen-filled glovebox **2^{Me}-(thf)$_2$** (2.0 eq., 25 mg, 36.35 µmol) and triethylphosphine oxide (Et_3PO, 12.45 mg, 72.7 µmol) were dissolved in CD_2Cl_2 (0.45 ml) in a Young NMR tube. Formation of the product was confirmed by NMR spectroscopy and **2^{Me}-(Et_3PO)$_2$** was not isolated as a bulk material. Keeping the reaction solution at room temperature overnight facilitated the formation of single crystals suitable for X-ray diffraction.

^{1}H NMR (200 MHz, 298 K, CD_2Cl_2):): δ [ppm] = 6.04 (*s*, $^{117/119}$Sn satellites $^4J_{Sn,H}$ = 20 Hz, H_1, 8H), 1.54 (*s*, H_4, 24H), 1.46 – 1.24 (*m*, PCH_2, 12H), 0.62 (*m*, CH_2CH_3).

^{31}P{^{1}H} NMR (121 MHz, 298 K, CD_2Cl_2): δ = 66.8 ppm (*s*, $^{117/119}$Sn satellites $^2J_{P\text{-}Sn}$ = 217.8 Hz).

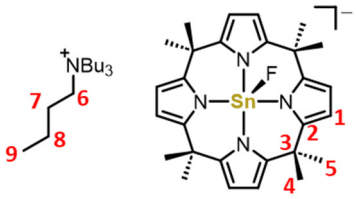
5.3.4 Bis(triethylphosphine oxide)-*meso*-octaethylcalix[4]pyrrolato stannane 2^{Et}-$(Et_3PO)_2$



In a nitrogen-filled glovebox **2^{Et}-(thf)$_2$** (8.0 mg, 10.0 µmol) and triethylphosphine oxide (Et_3PO, 1.0 eq., 1.4 mg, 10.0 µmol) were dissolved in CD_2Cl_2 (0.45 ml) in a Young NMR tube. After measuring ^1H and $^{31}P\{^1H\}$ NMR spectra a second eq. of Et_3PO was added to the reaction mixture and NMR measurements were repeated directly after the addition and after 12 hours at room temperature. Formation of the product was confirmed by NMR spectroscopy and **2^{Et}-$(Et_3PO)_2$** was not isolated as a bulk material. Keeping the reaction solution at room temperature overnight facilitated the formation of single crystals suitable for X-ray diffraction.

$^{31}P\{^1H\}$ NMR (121 MHz, 298 K, CD_2Cl_2): δ = 65.4 ppm (*s*, $^{117/119}$Sn satellites could not be resolved).

5.3.5 Tetrabutylammonium *meso*-octamethylcalix[4]pyrrolato fluoridostannate(IV) [NBu$_4$][F-2^{Me}]



3.0 mL CH_2Cl_2 were added to **2^{Me}-(thf)$_2$** (1.0 eq., 300 mg, 435.9 µmol) and TBAT (1.0 eq, 235.3 mg, 435.9 µmol) in a Schlenk tube. Stirring the reaction mixture at 50 °C for 13 hours caused the formation of a clear reaction solution. Addition of excess *n*-pentane caused the precipitation of a sticky/oily solid. After removal of the supernatant the precipitant was again treated with excess *n*-pentane causing the product to solidify. The product was isolated *via* filtration over a POR4 sintered glass filter frit and dried at reduced pressure at room temperature for one hour and subsequently at 100 °C for 12 hours yielding **[NBu$_4$][F-2^{Me}]** as a colorless solid (228.2 mg, 279.0 µmol, 65% yield). Keeping the supernatant from the precipitation with *n*-pentane at −30 °C overnight yielded single crystals suitable for X-ray diffraction.

^{1}H NMR [^{1}H, ^{1}H,^{1}H-COSY] (600 MHz, 298 K, CD_2Cl_2): δ [ppm] = 6.03 (s, $^4J(^1H\text{-}Sn)$ = 6 Hz, 8H, C*H*), 2.93 (t, $^3J(^1H\text{-}^1H)$ = 6 Hz, 8H, N-CH_2), 1.72 (s, 12H, β-CH_3), 1.56 (s, 12H, α-CH_3), 1.49 (qi, $^3J(^1H\text{-}^1H)$ = 6 Hz, 8H, N-CH$_2$-CH_2-), 1.33 (sext, $^3J(^1H\text{-}^1H)$ = 6 Hz, 8H, CH_2-CH$_3$), 0.97 (t, $^3J(^1H\text{-}^1H)$ = 6 Hz, 12H, CH$_2$-CH_3).

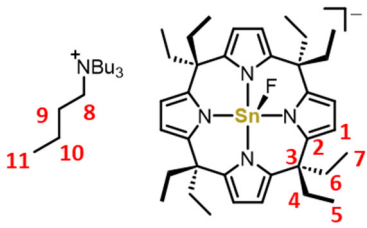
^{13}C NMR [^{13}C{^{1}H}, ^{13}C-DEPT135, ^{1}H,^{13}C-HSQC, ^{1}H,^{13}C-HMBC] (101 MHz, 298 K, CD_2Cl_2): δ [ppm] = 146.5 (CH*C*), 103.6 (*C*H), 59.2 (N-*C*H$_2$.), 36.5 (*C*(CH$_3$)$_2$), 35.7 (α-*C*H$_3$), 31.8 (β-*C*H$_3$), 24.2 (N-CH$_2$-*C*H$_2$-), 20.0 (*C*H$_2$-CH$_3$), 13.8 (CH$_2$-*C*H$_3$).

^{19}F NMR (565 MHz, 298 K, CD_2Cl_2): δ [ppm] = −152.45 (*s*, $^{117/119}$Sn satellites $^1J_{Sn,F}$ = 2266 Hz).

^{119}Sn NMR [^{119}Sn,^{1}H-HMBC] (223.81 MHz, 298 K, CD_2Cl_2): δ [ppm] = −466.7 (*d*, $^1J_{Sn,F}$ = 2308 Hz).

HR-MS (ESI, negative, CH_2Cl_2): calcd. for $[C_{28}H_{32}FN_4Sn]^-$ *m/z* = 563.1642, found *m/z* = 563.1633.

5.3.6 Tetrabutylammonium *meso*-octaethylcalix[4]pyrrolato fluoridostannate(IV) [NBu$_4$][F-2^{Et}]



3.0 mL CH_2Cl_2 were added to **2^{Et}-(thf)$_2$** (1.0 eq., 150 mg, 187.4 µmol) and TBAT (1.0 eq, 104.3 mg, 187.4 µmol) in a Schlenk tube. Stirring the reaction mixture at 50 °C for 13 hours caused the formation of a clear reaction solution. Addition of excess *n*-pentane caused the precipitation of a sticky/oily solid. After removal of the supernatant the precipitant was again treated with excess *n*-pentane causing the product to solidify. The product was isolated *via* filtration over a POR4 sintered glass filter frit and dried at reduced pressure at room temperature for one hour and subsequently at 100 °C for 12 hours yielding **[NBu$_4$][F-2^{Me}]** as a colorless solid (145 mg, 158.0 µmol, 84% yield). Keeping the supernatant from the precipitation with *n*-pentane at −30 °C overnight yielded single crystals suitable for X-ray diffraction.

^{1}H NMR [^{1}H, ^{1}H,^{1}H-COSY] (600 MHz, 298 K, CD_2Cl_2): δ [ppm] = 5.99 (*s*, $^{117/119}$Sn satellites $^4J_{Sn,H}$ = 24 Hz, H_1, 8H), 3.05 – 2.96 (*m*, H_8, 8H), 2.04 (*q*, $^3J_{H,H}$ = 7.3 Hz, H_4, 8H), 1.84 (*q*, $^3J_{H,H}$ = 7.2 Hz, H_6, 8H), 1.59 – 1.49 (*m*, H_9, 8H), 1.42 – 1.33 (*m*, H_{10}, 8H), 0.99 (*t*, $^3J_{H,H}$ = 7.3 Hz, H_{11}, 12H), 0.84 (*t*, $^3J_{H,H}$ = 7.3 Hz, H_5, 12H), 0.67 (*t*, $^3J_{H,H}$ = 7.2 Hz, H_7, 12H).

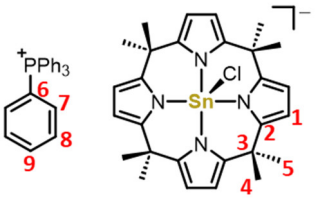
^{13}C NMR [^{13}C{^{1}H}, ^{13}C-DEPT135, ^{1}H,^{13}C-HSQC, ^{1}H,^{13}C-HMBC] (151 MHz, 298 K, CD_2Cl_2): δ [ppm] = 143.20 (*s*, $^{117/119}$Sn satellites $^2J_{Sn,C}$ = 14 Hz, C_2), 105.41 (*s*, $^{117/119}$Sn satellites $^3J_{Sn,C}$ = 44 Hz, C_1H), 59.28 (*s*, C_8H_2), 45.06 (*s*, $^{117/119}$Sn satellites $^3J_{Sn,C}$ = 14 Hz, C_3), 37.60 (*s*, C_6H_2), 35.33 (*s*, C_4H_2), 24.19 (*s*, C_9H_2), 20.04 (*s*, $C_{10}H_2$), 13.72 (*s*, $C_{11}H_3$), 10.27 (*s*, C_7H_3), 10.15 (*s*, C_5H_3).

^{19}F NMR (565 MHz, 298 K, CD_2Cl_2): δ [ppm] = −154.42 (*s*, $^{117/119}$Sn satellites $^1J_{Sn,F}$ = 2294 Hz).

^{119}Sn NMR [^{119}Sn,^{1}H-HMBC] (223.81 MHz, 298 K, CD_2Cl_2): δ [ppm] = −481.1 (*d*, $^1J_{Sn,F}$ = 2311 Hz).

HR-MS (ESI, negative, THF): calcd. for $[C_{36}H_{48}FN_4Sn]^-$ *m/z* = 675.2885, found *m/z* = 675.2916.

5.3.7 Tetraphenylphosphonium *meso*-octamethylcalix[4]pyrrolato chloridostannate(IV) [PPh_4][Cl-2^{Me}]



In a nitrogen-filled glovebox **2^{Me}-(thf)$_2$** (1.0 eq., 1.1 g, 1.598 mmol) and tetraphenylphosphonium chloride (1.0 eq., 596 mg, 1.598 mmol) were dissolved in 20 mL DCM and stirred at room temperature for one hour. The solvent of the reaction mixture was removed at reduced pressure and the residue dried at reduced pressure and 120 °C for three days to remove residue THF coordinated to the Sn(IV) center. **[PPh_4][Cl-2^{Me}]** was collected as a colorless solid (1.292 g, 1.407 mmol, 88% yield). Gas phase diffusion of *n*-pentane into a concentrated solution of **[PPh_4][Cl-2^{Me}]** in CH_2Cl_2 at −30 °C yielded single crystals suitable for X-ray diffraction.

^{1}H NMR [^{1}H, ^{1}H,^{1}H-COSY] (600 MHz, 298 K, CD_2Cl_2): δ = 7.85 - 7.83 (m, 4H, *p*-*H*(PPh_4)), 7.69 - 7.66 (m, 8H, *m*-*H*(PPh_4)), 7.57 - 7.54 (m, 8H, *o*-*H*(PPh_4)), 6.03 (s, ^{4}J(^{1}H-Sn) = 12 Hz, 8H, C*H*), 1.70 (s, 12H, CH_3), 1.54 (s, 12H, CH_3) ppm.

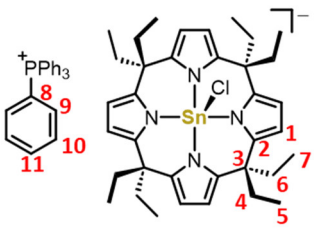
^{13}C NMR [^{13}C{^{1}H}, ^{13}C-DEPT135, ^{1}H,^{13}C-HSQC, ^{1}H,^{13}C-HMBC] (101 MHz, 298 K, CD_2Cl_2): δ = 147.3 (CH*C*), 136.1 (d, ^{4}J(^{31}P-^{13}C) = 2.0 Hz, *p*-*C*(PPh_4)), 134.8 (d, ^{3}J(^{31}P-^{13}C) = 7.1 Hz, *m*-*C*(PPh_4)), 131.0 (d, ^{2}J(^{31}P-^{13}C) = 8.1 Hz, *o*-*C*(PPh_4)), 117.8 (d, ^{1}J(^{31}P-^{13}C) = 59.6 Hz, C_q(PPh_4)), 104.1 (*C*H), 36.5 (*C*(CH_3)$_2$), 36.0 (*C*H_3), 32.8 (*C*H_3) ppm.

^{31}P{^{1}H} NMR (243 MHz, 298 K, CD_2Cl_2): δ = 23.22 (*s*, ^{13}C satellites $^1J_{P,C}$ = 90 Hz, PPh_4^+).

^{119}Sn NMR [^{119}Sn,^{1}H-HMBC] (223 MHz, 298 K, CD_2Cl_2): δ = −432.3 ppm.

HR-MS (ESI, negative, CH_2Cl_2): calcd. for $[C_{28}H_{32}ClN_4Sn]^-$ *m*/*z* = 579.1337, found *m*/*z* = 579.1384.

5.3.8 Tetraphenylphosphonium *meso*-octaethylcalix[4]pyrrolato chloridostannate(IV) [PPh$_4$][Cl-2^{Et}]



In a Schlenk tube **2^{Et}-(thf)$_2$** (1.0 eq., 1.4 g, 1.749 mmol) and tetraphenylphosphonium chloride (1.0 eq., 656 mg, 1.749 mmol) were dissolved in 20 mL THF and stirred at 75 °C for 16 hours. A clear, pinkish reaction solution was formed. The solvent of the reaction mixture was removed at reduced pressure and the residue dried at reduced pressure and 120 °C for three days to remove residue THF coordinated to the Sn(IV) center. **[PPh$_4$][Cl-2^{Et}]** was collected as a pinkish solid (1.740 g, 1.690 mmol, 97% yield). Gas-phase diffusion of *n*-pentane into a concentrated solution of **[PPh$_4$][Cl-2^{Et}]** in CH_2Cl_2 at −30 °C yielded single crystals suitable for X-ray diffraction.

^{1}H NMR [^{1}H, ^{1}H,^{1}H-COSY] (600 MHz, 298 K, CD_2Cl_2): δ = 7.90 – 7.85 (*m*, H_{11}, 4H), 7.73 – 7.69 (*m*, H_{10}, 8H), 7.59 – 7.55 (*m*, H_9, 8H), 6.04 (*s*, $^{117/119}$Sn satellites $^4J_{Sn,H}$ = 18 Hz, H_1, 8H), 1.90 (*q*, $^3J_{H,H}$ = 8 Hz, H_4, 8H), 1.87 (*q*, $^3J_{H,H}$ = 8 Hz, H_6, 8H), 0.63 (*t*, $^3J_{H,H}$ = 9 Hz, H_5, 12H), 0.62 (*t*, $^3J_{H,H}$ = 9 Hz, H_7, 12H).

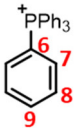
^{13}C NMR [^{13}C{^{1}H}, ^{13}C-DEPT135, ^{1}H,^{13}C-HSQC, ^{1}H,^{13}C-HMBC] (151 MHz, 298 K, CD_2Cl_2): δ = 143.63, (*s*, $^{117/119}$Sn satellites $^2J_{Sn,C}$ = 8 Hz, C_2), 136.17 (*d*, $^4J_{P,C}$ = 5.0 Hz, $C_{11}H$), 134.74 (*d*, $^2J_{P,C}$ = 11.0 Hz, C_9H), 131.02 (*d*, $^3J_{P,C}$ = 14.0 Hz, $C_{10}H$), 117.82 (*d*, $^1J_{P,C}$ = 89.0 Hz, C_8), 106.74 (*s*, $^{117/119}$Sn satellites $^3J_{Sn,C}$ = 39 Hz, C_1H), 45.98 (*s*, $^{117/119}$Sn satellites $^3J_{Sn,C}$ = 11 Hz, C_3), 39.53 (*s*, C_4H_2), 37.58 (*s*, C_6H_2), 10.12 (*s*, $C_{5,7}H_3$).

^{31}P{^{1}H} NMR (243 MHz, 298 K, CD_2Cl_2): δ = 23.26 (*s*, ^{13}C satellites $^1J_{P,C}$ = 90 Hz, PPh_4^+).

^{119}Sn NMR [^{119}Sn,^{1}H-HMBC] (223 MHz, 298 K, CD_2Cl_2): δ = −463.3 ppm.

HR-MS (ESI, negative, CH_2Cl_2): calcd. for $[C_{36}H_{48}ClN_4Sn]^-$ *m/z* = 691.2616, found *m/z* = 691.2668.

5.3.9 Tetraphenylphosphonium *meso*-octamethylcalix[4]pyrrolato iodidostannate(IV) [PPh_4][I-2^{Me}]





In a Schlenk tube **[PPh_4][Cl-2^{Me}]** (1.0 eq., 1.25 g, 1.361 mmol) was dissolved in 30 mL CH_2Cl_2. While stirring at room temperature, dropwise addition of trimethylsilyl iodide (1.6 eq., 319 µL, 2.178 mmol) caused a slight color change in the pale orange solution. After continued stirring for 30 minutes, addition of excess *n*-pentane caused the precipitation of the product as a pale brownish solid. Filtration over a POR4 sintered glass filter frit and drying at reduced pressure yielded **[PPh_4][I-2^{Me}]** as a pale brownish powder (1.237 g, 1.361 mmol, 90% yield). Various attempts to grow single crystals suitable for X-ray diffraction remained unsuccessful.

^{1}H NMR [^{1}H, ^{1}H,^{1}H-COSY] (600 MHz, 298 K, CD_2Cl_2): δ = 7.91 – 7.89 (*m*, H_{11}, 4H), 7.78 – 7.70 (*m*, H_{10}, 8H), 7.64 – 7.56 (*m*, H_9, 8H), 6.01 (*s*, H_1, 8H), 1.68 (s, H_4, 12H), 1.54 (s, H_5, 12H).

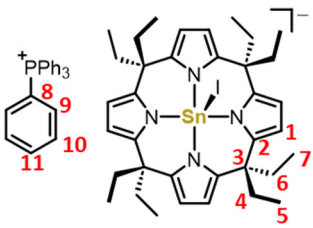
^{13}C NMR [^{13}C{^{1}H}, ^{13}C-DEPT135, ^{1}H,^{13}C-HSQC, ^{1}H,^{13}C-HMBC] (151 MHz, 298 K, CD_2Cl_2): δ = 147.21 (*s*, C_2), 136.11 (*d*, $^4J_{P,C}$ = 3.0 Hz, C_{11}H), 134.79 (*d*, $^2J_{P,C}$ = 11.0 Hz, C_9H), 131.00 (*d*, $^3J_{P,C}$ = 14.0 Hz, C_{10}H), 117.82 (*d*, $^1J_{P,C}$ = 89.0 Hz, C_8), 104.02 (*s*, C_1H), 36.40 (*s*, C_3), 36.00 (*s*, C_4H_3), 32.73 (*s*, C_5H_3).

^{31}P{^{1}H} NMR (243 MHz, 298 K, CD_2Cl_2): δ = 23.23 (*s*, ^{13}C satellites $^1J_{P,C}$ = 90 Hz, PPh_4^+).

^{119}Sn NMR [^{119}Sn,^{1}H-HMBC] (223 MHz, 298 K, CD_2Cl_2): δ = −618.3 ppm.

HR-MS (ESI, negative, CH_2Cl_2): calcd. for $[C_{28}H_{32}IN_4Sn]^-$ *m/z* = 671.0618, found m/z = 671.0699.

5.3.10 Tetraphenylphosphonium *meso*-octaethylcalix[4]pyrrolato iodidostannate(IV) [PPh_4][I-2^{Et}]



In a Schlenk tube **[PPh_4][Cl-2^{Et}]** (1.0 eq., 1.724 g, 1.697 mmol) was dissolved in 25 mL CH_2Cl_2. While stirring at room temperature, dropwise addition of trimethylsilyl iodide (1.5 eq., 373 µL, 2.546 mmol) caused a slight color change forming a pale orange solution. After continued stirring for 30 minutes, addition of excess *n*-pentane caused the precipitation of the product as a pale brownish solid. Filtration over a POR4 sintered glass filter frit and drying at reduced pressure yielded **[PPh_4][I-2^{Et}]** as a pale brownish powder (1.85 g, 1.648 mmol, 96% yield). Various attempts to grow single crystals suitable for X-ray diffraction remained unsuccessful.

^{1}H NMR [^{1}H, ^{1}H,^{1}H-COSY] (600 MHz, 298 K, CD_2Cl_2): δ = 7.90 – 7.86 (*m*, H_{11}, 4H), 7.76 – 7.68 (*m*, H_{10}, 8H), 7.61 – 7.53 (*m*, H_9, 8H), 6.07 (*s*, $^{117/119}$Sn satellites $^4J_{Sn,H}$ = 18 Hz, H_1, 8H), 1.84 (*q*, $^3J_{H,H}$ = 8 Hz, H_4 overlapped with H_6, 8H), 1.83 (*q*, $^3J_{H,H}$ = 8 Hz, H_6 overlapped with H_4, 8H), 0.57 (*t*, $^3J_{H,H}$ = 9 Hz, H_5 overlapped with H_7, 12H), 0.56 (*t*, $^3J_{H,H}$ = 9 Hz, H_7 overlapped with H_5, 12H).

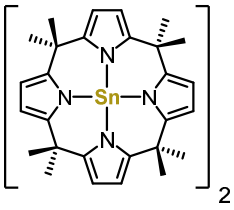
^{13}C NMR [^{13}C{^{1}H}, ^{13}C-DEPT135, ^{1}H,^{13}C-HSQC, ^{1}H,^{13}C-HMBC] (151 MHz, 298 K, CD_2Cl_2): δ = 143.54 (*s*, C_2), 136.15 (*d*, $^4J_{P,C}$ = 3.0 Hz, C_{11}H), 134.76 (*d*, $^2J_{P,C}$ = 11.0 Hz, C_9H), 131.02 (*d*, $^3J_{P,C}$ = 14.0 Hz, C_{10}H), 117.81 (*d*, $^1J_{P,C}$ = 89.0 Hz, C_8), 107.71 (*s*, $^{117/119}$Sn satellites $^3J_{Sn,C}$ = 33 Hz, C_1H), 46.61 (*s*, $^{117/119}$Sn satellites $^3J_{Sn,C}$ = 9.0 Hz, C_3), 41.08 (*s*, C_4H_2), 37.58 (*s*, C_6H_2), 10.43 (*s*, C_5H_3), 10.08 (*s*, C_7H_3).

^{31}P{^{1}H} NMR (243 MHz, 298 K, CD_2Cl_2): δ = 23.26 (*s*, ^{13}C satellites $^1J_{P,C}$ = 90 Hz, PPh_4^+).

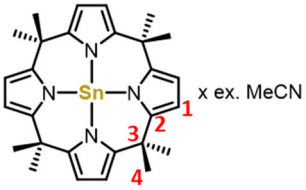
^{119}Sn NMR [^{119}Sn,^{1}H-HMBC] (223 MHz, 298 K, CD_2Cl_2): δ = −632.1 ppm.

MS (ESI, negative, CH_2Cl_2): calcd. for $[C_{36}H_{48}IN_4Sn]^-$ *m/z* = 783.1972, found *m/z* = 7831611.

5.3.11 *Meso*-octamethylcalix[4]pyrrolato stannane dimer $(2^{Me})_2$



Dropwise addition of a solution of tris(pentafluorophenyl)alane (AlCF) (2.0 eq, 872 µmol, 500.6 mg) in 2 mL fluorobenzene (PhF) to a solution of $\mathbf{2^{Me}\text{-}(thf)_2}$ (1.0 eq, 436 µmol, 300.0 mg) in 3 mL PhF while stirring at room temperature caused the formation of a yellow precipitation. After stirring at room temperature for five hours, the precipitant was isolated *via* filtration over a POR4 sintered glass filter frit and subsequently washed with PhF until the washing solution became colorless. Drying of the solid at vacuum afforded $\mathbf{2^{Me}}$ as a bright yellow powder (142 mg, 261 µmol, 60% yield). Resting the reaction solution after the addition of AlCF instead of stirring yielded single crystals suitable for X-ray diffraction. The poor solubility of $\mathbf{2^{Me}}$ in standard organic solvents hindered its characterization *via* NMR spectroscopy. However, addition of a 16-fold excess of MeCN to a suspension of $\mathbf{2^{Me}}$ in CD_2Cl_2 caused its complete dissolution under the formation of bis(acetonitrile)-*meso*-octamethylcalix[4]pyrrolato stannane $\mathbf{2^{Me}\text{-}(MeCN)_2}$ which could subsequently be characterized in solution.



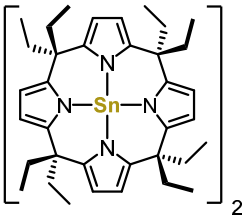
^{1}H NMR [^{1}H, ^{1}H,^{1}H-COSY] (600.18 MHz, CD_2Cl_2, 295 K): δ [ppm] = 6.06 (*s*, $^{117/119}$Sn satellites $^4J_{Sn,H}$ = 18 Hz, H_1, 8H), 1.57 (*s*, H_4, 24H).

^{13}C NMR [^{13}C{^{1}H}, ^{13}C-DEPT135, ^{1}H,^{13}C-HSQC, ^{1}H,^{13}C-HMBC] (150.93 MHz, CD_2Cl_2, 295 K): δ [ppm] = 147.76 (*s*, $^{117/119}$Sn satellites $^2J_{Sn,C}$ = 8 Hz, C_2), 105.20 (*s*, $^{117/119}$Sn satellites $^3J_{Sn,C}$ = 44 Hz, C_1H), 36.88 (*s*, $^{117/119}$Sn satellites $^4J_{Sn,C}$ = 11 Hz, C_3), 33.32 (*s*, C_4H_3).

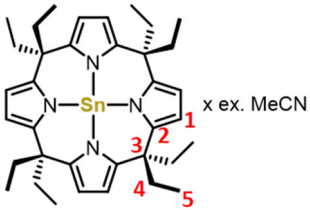
^{119}Sn NMR [^{119}Sn,^{1}H-HMBC] (223.69 MHz, CD_2Cl_2, 295 K): δ [ppm] = −610.1.

EA: calcd. for $C_{28}H_{32}N_4Sn$: C, 61.75; H, 5.93; N, 10.29. Found: C, 62.10; H, 6.02; N, 10.29.

5.3.12 *Meso*-octaethylcalix[4]pyrrolato stannane dimer $(2^{Et})_2$



Dropwise addition of a solution of tris(pentafluorophenyl)alane (AlCF) (2.0 eq, 696 µmol, 399.7 mg) in 2 mL toluene to a solution of $\mathbf{2^{Et}\text{-}(thf)_2}$ (1.0 eq, 348 µmol, 279.0 mg) in 3 mL toluene while stirring at room temperature caused the formation of an orange precipitation. After stirring at room temperature for five hours, the precipitant was isolated *via* filtration over a POR4 sintered glass filter frit and subsequently washed with toluene until the washing solution became colorless. Drying of the solid at vacuum afforded $\mathbf{2^{Et}}$ as a bright orange powder (150 mg, 230 µmol, 66% yield). Resting the reaction solution after the addition of AlCF instead of stirring yielded single crystals suitable for X-ray diffraction. The poor solubility of $\mathbf{2^{Et}}$ in standard organic solvents hindered its characterization *via* NMR spectroscopy. However, addition of a 16-fold excess of MeCN to a suspension of $\mathbf{2^{Et}}$ in CD_2Cl_2 caused its complete dissolution under the formation of *bis*-acetonitrile-*meso*-octaethylcalix[4]pyrrolato stannane $\mathbf{2^{Et}\text{-}(MeCN)_2}$ which could subsequently be characterized in solution.



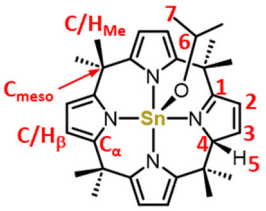
^{1}H NMR [^{1}H, ^{1}H,^{1}H-COSY] (600 MHz, CD_2Cl_2, 295 K): δ [ppm] = 6.15 (s, 8H), 6.15 (*s*, $^{117/119}$Sn satellites $^4J_{Sn,H}$ = 12 Hz, H_1, 8H), 1.86 (*q*, $^3J_{H,H}$ = 7.3 Hz, H_4, 16H), 0.59 (t, $^3J_{H,H}$ = 7.2 Hz, 24H).

^{13}C NMR [^{13}C{^{1}H}, ^{13}C-DEPT135, ^{1}H,^{13}C-HSQC, ^{1}H,^{13}C-HMBC] (150.93 MHz, CD_2Cl_2, 295 K): δ [ppm] = 142.90 (*s*, $^{117/119}$Sn satellites $^2J_{Sn,C}$ = 6 Hz, C_2), 108.48 (*s*, $^{117/119}$Sn satellites $^3J_{Sn,C}$ = 42 Hz, C_1H), 47.20 (*s*, C_3), 40.03 (*s*, C_4H_2), 10.03 (*s*, C_5H_3).

^{119}Sn NMR [^{119}Sn,^{1}H-HMBC] (223.7 MHz, CD_2Cl_2, 295 K): δ [ppm] = −629.1.

EA: calcd. for $C_{36}H_{48}N_4Sn$: C, 65.82; H, 7.37; N, 8.53. Found: C, 66.13; H, 7.39; N, 8.19.

5.3.13 Cooperative activation of *i*PrOH with $(2^{Me})_2$ forming *i*PrOH-2^{Me}



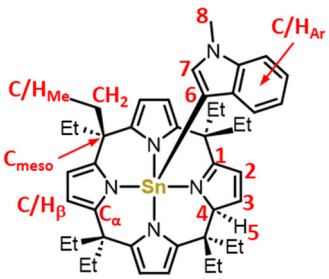
In a Young NMR tube **$(2^{Me})_2$** (1.0 eq., 5.8 µmol, 6.3 mg) was suspended in 0.45 mL CD_2Cl_2 and *i*PrOH was added in one portion (2.0 eq., 11.6 µmol, 0.89 µL). All starting material dissolved within minutes at room temperature forming a clear, yellow reaction solution. The cooperative addition of *i*PrOH was confirmed *in situ* by ^{1}H, ^{13}C, and ^{119}Sn NMR spectroscopy and no isolation of the product was attempted. Layering the NMR solution with *n*-pentane and storing it at −30 °C overnight yielded single crystals suitable for X-ray diffraction.

^{1}H NMR [^{1}H, ^{1}H,^{1}H-COSY] (600 MHz, CD_2Cl_2, 295 K): δ [ppm] = 7.85 (*d*, $^3J_{H,H}$ = 5.4 Hz, H_2, 1H), 7.12 (*dd*, $^3J_{H,H}$ = 5.4, 1.4 Hz, H_5, 1H), 6.30 – 6.24 (*m*, H_β, 1H), 6.20 (*d*, $^3J_{H,H}$ = 3.3 Hz, H_β, 1H), 6.15 – 6.13 (*m*, H_β, 1H), 6.12 (*d*, $^3J_{H,H}$ = 3.4 Hz, H_β, 1H), 6.02 – 5.97 (*m*, H_β, 2H), 5.39 (*s*, H_5, 1H), 3.74 (*hept*, $^3J_{H,H}$ = 5.8 Hz, H_6, 1H), 1.79 (*s*, H_{Me}, 3H), 1.77 (*s*, H_{Me}, 3H), 1.73 (*s*, H_{Me}, 3H), 1.69 (*s*, H_{Me}, 3H), 1.64 (*s*, H_{Me}, 3H), 1.62 (*s*, H_{Me}, 3H), 1.61 (*s*, H_{Me}, 3H), 0.91 (*d*, $^3J_{H,H}$ = 6.2 Hz, $H_{7'}$ 3H), 0.89 (*d*, $^3J_{H,H}$ = 6.1 Hz, $H_{7'}$ 3H), 0.77 (*s*, H_{Me}, 3H).

^{13}C NMR [^{13}C{^{1}H}, ^{13}C-DEPT135, ^{1}H,^{13}C-HSQC, ^{1}H,^{13}C-HMBC] (150.93 MHz, CD_2Cl_2, 295 K): δ [ppm] = 191.92 (*s*, C_1), 158.13 (*s*, C_2H), 150.18 (*s*, C_α), 148.48 (*s*, C_α), 147.56 (*s*, C_α), 145.62 (*s*, C_α), 145.36 (*s*, C_α), 142.27 (*s*, C_α), 129.50 (*s*, C_3H), 108.76 (*s*, C_βH), 106.51 (*s*, C_βH), 106.24 (*s*, C_βH), 105.56 (*s*, C_βH), 103.75 (*s*, C_βH), 103.63 (*s*, C_βH), 85.73 (*s*, C_4H), 67.16 (*s*, C_6H), 40.55 (*s*, C_{meso}), 39.91 (*s*, C_{meso}), 36.56 (*s*, C_{meso}), 36.53 (*s*, C_{meso}), 34.84 (*s*, $C_{Me}H_3$), 33.17 (*s*, $C_{Me}H_3$), 31.95 (*s*, $C_{Me}H_3$), 31.71 (*s*, $C_{Me}H_3$), 30.52 (*s*, $C_{Me}H_3$), 30.34 (*s*, $C_{Me}H_3$), 29.76 (*s*, $C_{Me}H_3$), 26.74 (*s*, C_7H_3), 26.66 (*s*, $C_{Me}H_3$), 24.72 (*s*, C_7H_3).

^{119}Sn NMR [^{119}Sn,^{1}H-HMBC] (223.7 MHz, CD_2Cl_2, 295 K): δ [ppm] = −466.3.

5.3.14 Cooperative activation of *N*-methyl indole with $(2^{Et})_2$ forming *N*MeInd -2^{Et}

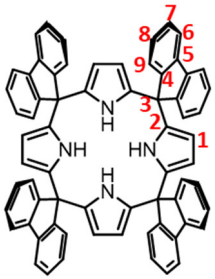


In a Young NMR tube $(\mathbf{2^{Et}})_2$ (1.0 eq., 5.8 µmol, 7.6 mg) was suspended in 0.45 mL CD_2Cl_2 and *N*-methyl indole (*N*MeInd) was added in one portion (2.0 eq., 11.6 µmol, 1.6 mg). After mixing for two hours at room temperature all starting material dissolved and a clear, orange reaction solution was formed. The cooperative addition of *N*MeInd was confirmed *in situ* by ^{1}H and ^{119}Sn NMR spectroscopy and no isolation of the product was attempted. Layering the NMR solution with *n*-pentane and storing it at −30 °C overnight yielded single crystals suitable for X-ray diffraction.

^{1}H NMR [^{1}H, ^{1}H,^{1}H-COSY] (600 MHz, CD_2Cl_2, 295 K): δ [ppm] = 7.61 (*d*, $^{3}J_{H,H}$ = 5.4 Hz, H_2, 1H), 7.10 – 7.04 (*m*, $H_{Ar,}$ 2H), 6.89 (*dd*, $^{3}J_{H,H}$ = 5.4, 1.4 Hz, H_5, 1H), 6.86 – 6.81 (*m*, $H_{Ar,}$ 1H), 6.57 (*d*, $^{3}J_{H,H}$ = 8.0 Hz, $H_{Ar,}$ 1H), 6.34 (*s*, H_7, 1H), 6.33 (*d*, $^{3}J_{H,H}$ = 7.8 Hz, H_β, 1H), 6.30 (*d*, $^{3}J_{H,H}$ = 3.5 Hz, H_β, 1H), 6.27 – 6.21 (*m*, H_β, 2H), 6.12 – 6.08 (*m*, H_β, 1H), 6.08 – 6.04 (*m*, H_β, 1H), 5.10 (*s*, H_5, 1H), 3.60 (*s*, H_8, 3H), 2.44 (*dq*, $^{3}J_{H,H}$ = 15.0, 7.5 Hz, CH_2, 1H), 2.06 – 1.75 (*m*, CH_2, 12H), 1.69 (*dq*, $^{3}J_{H,H}$ = 14.2, 7.2 Hz, CH_2, 1H), 1.35 (*ddq*, $^{3}J_{H,H}$ = 15.1, 9.7, 7.5 Hz, CH_2, 2H), 1.07 (*t*, $^{3}J_{H,H}$ = 7.3 Hz, H_{Me}, 3H), 0.84 – 0.78 (*m*, H_{Me}, 9H), 0.57 (*t*, $^{3}J_{H,H}$ = 7.2 Hz, H_{Me}, 3H), 0.55 (*t*, $^{3}J_{H,H}$ = 7.4 Hz, H_{Me}, 3H), 0.52 (*t*, $^{3}J_{H,H}$ = 7.4 Hz, H_{Me}, 3H), 0.48 (*t*, $^{3}J_{H,H}$ = 7.2 Hz, H_{Me}, 3H).

^{119}Sn NMR [^{119}Sn,^{1}H-HMBC] (223.7 MHz, CD_2Cl_2, 295 K): δ [ppm] = −402.6.

5.3.15 *Meso*-octa(*ortho*-phenylene)calix[4]pyrrole $H_4[1^{oPhen}]$



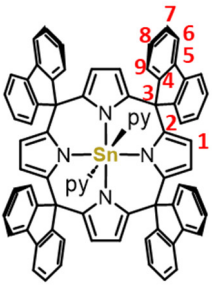
In a 1 L round bottom Schlenk flask freshly sublimed fluorenone (1.0 eq., 39.170 mmol, 7.2 g) and freshly distilled pyrrole (1.1 eq., 43.080 mmol, 3.0 mL) were dissolved in 250 mL dry ethanol which was dried over activated 3Å molecular sieve for more than seven days (< 15 ppm water). $BF_3{\bullet}OEt_2$ (1.5 eq., 58.760 mmol, 7.3 mL) was added dropwise and the reaction was stirred at room temperature. Within the first four hours the neon yellow, clear solution became dark purple and a colorless solid started to precipitate. After five days the solid was isolated *via* filtration over a POR4 sintered glass filter frit under inert atmosphere and washed with small amounts dry ethanol until the washing solution was only slightly purple. Drying at reduced pressure over night facilitated around 10 g of the crude product as an off-white solid. The subsequent purification *via* flash column chromatography (*puriFlash XS420Plus* flash column automat, 330 mL column, silica gel (40-63 µm), flow rate: 50 mL min^{-1}, gradient from 100:0 to 60:40 PE/DCM over 11 column volumes) was performed in two steps of ~5 g crude adsorbed on equal volumes of celite each to avoid overloading of the stationary phase and delivered **$H_4[1^{oPhen}] \bullet CH_2Cl_2$** as a colorless powder containing one equivalent CH_2Cl_2 pre formula unit (2.622 g, 2.203 mmol, 22% yield).

^{1}H NMR [^{1}H, ^{1}H,^{1}H-COSY] (600 MHz, CD_2Cl_2, 295 K): δ [ppm] = 9.26 (*s*, N*H*, 4H), 7.73 – 7.64 (*m*, $H_{6,9}$ 16H), 7.40 – 7.33 (*m*, $H_{7,8}$, 16H), 5.40 (*d*, $^4J_{H,H}$ = 2.6 Hz, H_1, 8H).

^{13}C NMR [^{13}C{^{1}H}, ^{13}C-DEPT135, ^{1}H,^{13}C-HSQC, ^{1}H,^{13}C-HMBC] (150.93 MHz, CD_2Cl_2, 295 K): δ [ppm] = 149.17 (*s*, C_{oPhen}), 139.84 (*s*, C_{oPhen}), 134.93 (*s*, C_2), 128.30 (*s*, $C_{oPhen}H$), 127.87 (*s*, $C_{oPhen}H$), 125.01 (*s*, $C_{oPhen}H$), 120.82 (*s*, $C_{oPhen}H$), 106.90 (*s*, C_1H), 56.48 (*s*, C_3).

HR-MS (MALDI, positive, in DCTB): calcd. for $[M+H]^+$: $C_{68}H_{45}N_4$ *m/z* = 917.364, found *m/z* = 917.365.

5.3.16 Bis(pyridine)-*meso*-octa(*ortho*-phenylene)calix[4]pyrrolato stannane $2^{o\text{Phen}}$-$(py)_2$



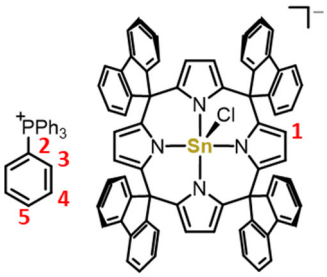
In a 50 mL Schlenk tube 10 mL pyridine were added to **$H_4[1^{o\text{Phen}}]$ • CH_2Cl_2** (1.0 eq., 490.2 µmol, 500 mg) causing the formation of a bright greenish suspension. While stirring at room temperature tetrakis(dimethylamido) tin(IV) (1.2 eq., 588.3 µmol, 148.4 µL) was added in portions causing the formation of a yellowish-green suspension. Stirring the reaction solution at 75 °C caused the dissolution of all starting material within the first 30 minutes followed by the precipitation of a colorless solid after one hour. After 15 hours a dark green suspension was formed. 50 % of the solvent was removed at reduce pressure and the precipitation isolated *via* filtration over a POR4 sintered glass filter frit, rinsed with *n*-pentane, and dried at reduced pressure. Subsequent washing with small amounts of CH_2Cl_2 and drying at reduced pressure afforded **$2^{o\text{Phen}}$-$(py)_2$** as a colorless solid. A second fraction could be isolated storing the washing solution at −30 °C overnight (437.5 mg, 367.6 µmol, 75% yield). Gas-phase diffusion of *n*-pentane into a concentrated solution of **$2^{o\text{Phen}}$-$(py)_2$** in CH_2Cl_2 yielded single crystals suitable for X-ray diffraction.

^{1}H NMR [^{1}H, ^{1}H,^{1}H-COSY] (600 MHz, CD_2Cl_2, 295 K): δ [ppm] = 8.23 – 8.19 (*m*, *para*-H_{py}, 2H), 7.68 – 7.65 (*m*, *meta*-H_{py}, 4H), 7.63 (*d*, $^3J_{H,H}$ = 7.5 Hz, H_9, 8H), 7.49 – 7.43 (*m*, *ortho*-H_{py}, 4H), 7.18 (*dd*, $^3J_{H,H}$ = 7.5, 9H), 6.90 (*dd*, $^3J_{H,H}$ = 7.5, 8H), 6.25 (*d*, $^3J_{H,H}$ = 7.7 Hz, 8H), 5.33 (*s*, H_1, 8H).

^{13}C NMR [^{13}C{^{1}H}, ^{13}C-DEPT135, ^{1}H,^{13}C-HSQC, ^{1}H,^{13}C-HMBC] (151 MHz, CD_2Cl_2, 295 K): δ [ppm] = 156.34, 148.85 (*s*, $^{117/119}$Sn satellites $^2J_{C,Sn}$ = 8.0 Hz, *ortho*-$C_{py}H$), 141.94 (*s*, *para*-$C_{py}H$), 140.97 (*s*, C_{oPhen}), 139.17 (*s*, C_{oPhen}), 134.46 (*s*, C_2), 127.97 (*s*, $C_{oPhen}H$), 127.05 (*s*, $C_{oPhen}H$), 126.80 (*s*, $^{117/119}$Sn satellites $^2J_{C,Sn}$ = 12.0 Hz, *meta*-$C_{py}H$), 123.79 (*s*, $C_{oPhen}H$), 120.28 (*s*, $C_{oPhen}H$), 111.00 (*s*, $^{117/119}$Sn satellites $^3J_{C,Sn}$ = 34.7 Hz, C_1H), 58.51 (*s*, $^{117/119}$Sn satellites $^3J_{C,Sn}$ = 12.1 Hz, C_3).

^{119}Sn NMR [^{119}Sn,^{1}H-HMBC] (223.7 MHz, CD_2Cl_2, 295 K): δ [ppm] = −590.8.

5.3.17 Tetraphenylphosphonium *meso*-octa(*ortho*-phenylene)calix[4]pyrrolato chloridostannate(IV) [PPh_4][Cl-2^{oPhen}]



In a 14 mL glass vial 10 mL CH_2Cl_2 were added to **2^{oPhen}-(py)$_2$** (1.0 eq., 84.0 µmol, 100 mg) and PPh_4Cl (1.0 eq., 84.0 µmol, 31.5 mg) and stirred for 30 minutes at room temperature yielding a clear orange solution. Addition of excess *n*-pentane caused the precipitation of an off-white solid which was isolated *via* filtration over a POR4 sintered glass filter frit. Subsequent washing with small amounts of PhCl and *n*-pentane followed by drying at reduced pressure for one hour yielded the intermediate adduct **[PPh_4][Cl-2^{oPhen}-(py)]**. Addition of 10 mL CH_2Cl_2 and BCF (1.1 eq., 92.4 µmol, 47.3 mg) yielded a clear orange solution within minutes. A second addition of excess *n*-pentane caused the precipitation of an off-white solid which was again isolated *via* filtration over a POR4 sintered glass filter frit. Washing with small amounts of *n*-pentane and drying at reduced pressure overnight delivered the pyridine-free product **[PPh_4][Cl-2^{oPhen}]** as a pale orange solid (65.0 mg, 46.2 µmol, 55% yield). Gas-phase diffusion of *n*-pentane into a concentrated solution of **[PPh_4][Cl-2^{oPhen}]** in CH_2Cl_2 yielded single crystals good enough to disclose the connectivity of the compounds *via* X-ray diffraction.

^{1}H NMR [^{1}H, ^{1}H,^{1}H-COSY] (400 MHz, CD_2Cl_2, 295 K): δ [ppm] = 7.96 – 7.89 (*m*, H_{oPhen}, 4H), 7.84 – 7.74 (*m*, H_5, 4H), 7.67 – 7.55 (*m*, H_4 overlayed with H_{oPhen}, 20H), 7.52 – 7.43 (*m*, H_3, 8H), 7.24 – 7.15 (*m*, H_{oPhen}, 16H), 5.18 (*s*, $^{117/119}$Sn satellites $^4J_{Sn,H}$ = 12 Hz, H_1, 8H).

^{31}P{^{1}H} NMR (162 MHz, 298 K, CD_2Cl_2): δ = 23.19 (*s*, ^{13}C satellites $^1J_{P,C}$ = 92 Hz, PPh_4^+).

^{119}Sn NMR [^{119}Sn,^{1}H-HMBC] (149.4 MHz, CD_2Cl_2, 295 K): δ [ppm] = −452.8.

6 References

[1] R. L. Melen, *Science* **2019**, *363*, 479–484.
[2] P. P. Power, *Nature* **2010**, *463*, 171–177.
[3] C. Weetman, S. Inoue, *ChemCatChem* **2018**, *10*, 4213–4228.
[4] D. Seyferth, *Organometallics* **2001**, *20*, 1488–1498.
[5] W. B. Jensen, *J. Chem. Educ.* **2003**, *80*, 952.
[6] D. Seyferth, *Organometallics* **2001**, *20*, 2940–2955.
[7] E. Frankland, B. C. Brodie, *Philos. Trans. R. Soc. Lond.* **1852**, *142*, 417–444.
[8] W. Caseri, *J. Organomet. Chem.* **2014**, *751*, 20–24.
[9] R. Abegg, *Z. Für Anorg. Chem.* **1904**, *39*, 330–380.
[10] I. Langmuir, *J. Am. Chem. Soc.* **1919**, *41*, 868–934.
[11] W. Kossel, *Ann. Phys.* **1916**, *354*, 229–362.
[12] G. N. Lewis, *J. Am. Chem. Soc.* **1916**, *38*, 762–785.
[13] W. Kutzelnigg, *Angew. Chem. Int. Ed. Engl.* **1984**, *23*, 272–295.
[14] A. Walsh, G. W. Watson, *J. Solid State Chem.* **2005**, *178*, 1422–1428.
[15] P. Schwerdtfeger, G. A. Heath, M. Dolg, M. A. Bennett, *J. Am. Chem. Soc.* **1992**, *114*, 7518–7527.
[16] T. Chu, G. I. Nikonov, *Chem. Rev.* **2018**, *118*, 3608–3680.
[17] J. H. van't Hoff, *Bull. Soc. Chim. Fr.* **1874**, *22*, 337.
[18] J. A. Le Bel, *Bull Soc Chim Fr* **1874**, *22*, 337–347.
[19] R. J. Gillespie, R. S. Nyholm, *Q. Rev. Chem. Soc.* **1957**, *11*, 339–380.
[20] R. J. Gillespie, *Coord. Chem. Rev.* **2008**, *252*, 1315–1327.
[21] H. J. Reich, N. H. Phillips, *J. Am. Chem. Soc.* **1986**, *108*, 2102–2103.
[22] H. J. Reich, N. H. Phillips, *Pure Appl. Chem.* **1987**, *59*, 1021–1026.
[23] L. Greb, *Chem. – Eur. J.* **2018**, *24*, 17881–17896.
[24] A. Maiti, R. Yadav, L. Greb, in *Adv. Inorg. Chem.*, Academic Press, **2023**, pp. 261–299.
[25] G. Bouhadir, D. Bourissou, *Chem. Soc. Rev.* **2004**, *33*, 210–217.
[26] T. J. Hannah, S. S. Chitnis, *Chem. Soc. Rev.* **2024**, *53*, 764–792.
[27] L. M. Sigmund, R. Maier, L. Greb, *Chem. Sci.* **2022**, *13*, 510–521.
[28] L. M. Sigmund, C. Ehlert, G. Gryn'ova, L. Greb, *J. Chem. Phys.* **2022**, *156*, 194113.
[29] H. Ruppert, L. M. Sigmund, L. Greb, *Chem. Commun.* **2021**, *57*, 11751–11763.
[30] J. R. Khusnutdinova, D. Milstein, *Angew. Chem. Int. Ed.* **2015**, *54*, 12236–12273.
[31] L. Greb, F. Ebner, Y. Ginzburg, L. M. Sigmund, *Eur. J. Inorg. Chem.* **2020**, *2020*, 3030–3047.
[32] M. K. Friedel, B. F. Hoskins, R. L. Martin, S. A. Mason, *J. Chem. Soc. Chem. Commun.* **1970**, 400–401.
[33] G. N. Lewis, *Valence and the Structure of Atoms and Molecules*, American Chemical Monograph Series, The Chemical Catalog Co., Inc., New York, **1923**.
[34] 'Lewis acid' in *IUPAC Compendium of Chemical Terminology*, 3rd ed. International Union of Pure and Applied Chemistry; **2006**. Online version 3.0.1, **2019**. https://doi.org/10.1351/goldbook.L03508.

[35] H. Fleischer, *Eur. J. Inorg. Chem.* **2001**, *2001*, 393–404.
[36] 'Lewis acidity' in *IUPAC Compendium of Chemical Terminology*, 3rd ed. International Union of Pure and Applied Chemistry; **2006**. Online version 3.0.1, **2019**. https://doi.org/10.1351/goldbook.L03509.
[37] A. R. Jupp, T. C. Johnstone, D. W. Stephan, *Dalton Trans.* **2018**, *47*, 7029–7035.
[38] A. R. Jupp, T. C. Johnstone, D. W. Stephan, *Inorg. Chem.* **2018**, *57*, 14764–14771.
[39] K. Müther, P. Hrobárik, V. Hrobáriková, M. Kaupp, M. Oestreich, *Chem. – Eur. J.* **2013**, *19*, 16579–16594.
[40] A. E. Ashley, T. J. Herrington, G. G. Wildgoose, H. Zaher, A. L. Thompson, N. H. Rees, T. Krämer, D. O'Hare, *J. Am. Chem. Soc.* **2011**, *133*, 14727–14740.
[41] D. Rodrigues Silva, L. de Azevedo Santos, M. P. Freitas, C. F. Guerra, T. A. Hamlin, *Chem. – Asian J.* **2020**, *15*, 4043–4054.
[42] A. Ben Saida, A. Chardon, A. Osi, N. Tumanov, J. Wouters, A. I. Adjieufack, B. Champagne, G. Berionni, *Angew. Chem.* **2019**, *131*, 17045–17049.
[43] M. A. Beckett, G. C. Strickland, J. R. Holland, K. Sukumar Varma, *Polymer* **1996**, *37*, 4629–4631.
[44] P. Erdmann, L. Greb, *Angew. Chem. Int. Ed.* **2022**, *61*, e202114550.
[45] R. F. Childs, D. L. Mulholland, A. Nixon, *Can. J. Chem.* **1982**, *60*, 809–812.
[46] K. F. Purcell, R. S. Drago, *J. Am. Chem. Soc.* **1966**, *88*, 919–924.
[47] J. R. Gaffen, J. N. Bentley, L. C. Torres, C. Chu, T. Baumgartner, C. B. Caputo, *Chem* **2019**, *5*, 1567–1583.
[48] P. Erdmann, L. Greb, *ChemPhysChem* **2021**, *22*, 935–943.
[49] H. Böhrer, N. Trapp, D. Himmel, M. Schleep, I. Krossing, *Dalton Trans.* **2015**, *44*, 7489–7499.
[50] K. O. Christe, D. A. Dixon, D. McLemore, W. W. Wilson, J. A. Sheehy, J. A. Boatz, *J. Fluor. Chem.* **2000**, *101*, 151–153.
[51] J. C. Haartz, D. H. McDaniel, *J. Am. Chem. Soc.* **1973**, *95*, 8562–8565.
[52] L. M. Sigmund, S. S. S. V., A. Albers, P. Erdmann, R. S. Paton, L. Greb, *Angew. Chem. Int. Ed.* **2024**, *63*, e202401084.
[53] Ng, W. *What Drives Computational Chemistry Forward: Theory or Computational Power?*, *Preprints* **2020**, 2020010189.
[54] P. Erdmann, J. Leitner, J. Schwarz, L. Greb, *ChemPhysChem* **2020**, *21*, 987–994.
[55] P. Erdmann, M. Schmitt, L. M. Sigmund, F. Krämer, F. Breher, L. Greb, *Angew. Chem. Int. Ed.* **2024**, e202403356.
[56] Minkin, V. I.. "Glossary of terms used in theoretical organic chemistry" *Pure and Applied Chemistry*, Vol. 71, no. 10, **1999**, pp. 1919-1981.
[57] N. V. Sidgwick, H. M. Powell, *Proc. R. Soc. Lond. Ser. Math. Phys. Sci.* **1997**, *176*, 153–180.
[58] M. B. Kindervater, K. M. Marczenko, U. Werner-Zwanziger, S. S. Chitnis, *Angew. Chem.* **2019**, *131*, 7932–7937.
[59] A. Hentschel, A. Brand, P. Wegener, W. Uhl, *Angew. Chem. Int. Ed.* **2018**, *57*, 832–835.
[60] S. Volodarsky, R. Dobrovetsky, *Chem. Commun.* **2018**, *54*, 6931–6934.
[61] F. Wang, O. Planas, J. Cornella, *J. Am. Chem. Soc.* **2019**, *141*, 4235–4240.
[62] T. P. Robinson, D. M. De Rosa, S. Aldridge, J. M. Goicoechea, *Angew. Chem.* **2015**, *127*, 13962–13967.

[63] N. L. Dunn, M. Ha, A. T. Radosevich, *J. Am. Chem. Soc.* **2012**, *134*, 11330–11333.
[64] J. Cui, Y. Li, R. Ganguly, A. Inthirarajah, H. Hirao, R. Kinjo, *J. Am. Chem. Soc.* **2014**, *136*, 16764–16767.
[65] T. P. Robinson, S.-K. Lo, D. De Rosa, S. Aldridge, J. M. Goicoechea, *Chem. – Eur. J.* **2016**, *22*, 15712–15724.
[66] D. Roth, A. T. Radosevich, L. Greb, *J. Am. Chem. Soc.* **2023**, *145*, 24184–24190.
[67] S. A. Culley, A. J. I. Arduengo, *J. Am. Chem. Soc.* **1984**, *106*, 1164–1165.
[68] H. Zhu, E. Y.-X. Chen, *Inorg. Chem.* **2007**, *46*, 1481–1487.
[69] D. Tanaka, Y. Kadonaga, Y. Manabe, K. Fukase, S. Sasaya, H. Maruyama, S. Nishimura, M. Yanagihara, A. Konishi, M. Yasuda, *J. Am. Chem. Soc.* **2019**, *141*, 17466–17471.
[70] A. Chardon, A. Osi, D. Mahaut, T.-H. Doan, N. Tumanov, J. Wouters, L. Fusaro, B. Champagne, G. Berionni, *Angew. Chem. Int. Ed.* **2020**, *59*, 12402–12406.
[71] C. Präsang, M. Hofmann, G. Geiseler, W. Massa, A. Berndt, *Angew. Chem. Int. Ed.* **2002**, *41*, 1526–1529.
[72] E. J. Thompson, T. W. Myers, L. A. Berben, *Angew. Chem. Int. Ed.* **2014**, *53*, 14132–14134.
[73] M. Driess, J. Aust, K. Merz, C. van Wüllen, *Angew. Chem. Int. Ed.* **1999**, *38*, 3677–3680.
[74] M. B. Krogh-Jespersen, J. Chandrasekhar, E. U. Wuerthwein, J. B. Collins, P. Von Rague Schleyer, *J. Am. Chem. Soc.* **1980**, *102*, 2263–2268.
[75] 'porphyrinogens' in *IUPAC Compendium of Chemical Terminology*, 3rd ed. International Union of Pure and Applied Chemistry; **2006**. Online version 3.0.1, **2019**. https://doi.org/10.1351/goldbook.P04764
[76] Floriani C, R. Floriani-Moro, in *Porphyr. Handb.*, **2000**.
[77] A. Baeyer, *Berichte Dtsch. Chem. Ges.* **1886**, *19*, 2184–2185.
[78] V. V. Chelintzev, B. V. Tronov, *J Russ Phys Chem Soc* **1916**, 105–155.
[79] P. A. Gale, J. L. Sessler, V. Král, V. Lynch, *J. Am. Chem. Soc.* **1996**, *118*, 5140–5141.
[80] P. A. Gale, J. L. Sessler, V. Král, *Chem. Commun.* **1998**, 1–8.
[81] Q. He, G. I. Vargas-Zúñiga, S. H. Kim, S. K. Kim, J. L. Sessler, *Chem. Rev.* **2019**, *119*, 9753–9835.
[82] S. A. Wagay, L. Khan, R. Ali, *Chem. – Asian J.* **2023**, *18*, e202201080.
[83] I. A. Rather, R. Ali, A. Ali, *Org. Chem. Front.* **2022**, *9*, 6416–6440.
[84] G. Cafeo, G. Carbotti, A. Cuzzola, M. Fabbi, S. Ferrini, F. H. Kohnke, G. Papanikolaou, M. R. Plutino, C. Rosano, A. J. P. White, *J. Am. Chem. Soc.* **2013**, *135*, 2544–2551.
[85] F. H. Kohnke, *Eur. J. Org. Chem.* **2020**, *2020*, 4261–4272.
[86] I. B. Toumia, M. Ponassi, P. Barboro, E. Iervasi, G. C. Vargas, B. Banelli, S. Fiordoro, L. C. Ghedira, F. H. Kohnke, A. Izzotti, C. Rosano, *Invest. New Drugs* **2022**, *40*, 1185–1193.
[87] S.-K. Ko, S. K. Kim, A. Share, V. M. Lynch, J. Park, W. Namkung, W. Van Rossom, N. Busschaert, P. A. Gale, J. L. Sessler, I. Shin, *Nat. Chem.* **2014**, *6*, 885–892.
[88] R. Lappano, C. Rosano, A. Pisano, M. F. Santolla, E. M. De Francesco, P. De Marco, V. Dolce, M. Ponassi, L. Felli, G. Cafeo, F. H. Kohnke, S. Abonante, M. Maggiolini, *Dis. Model. Mech.* **2015**, *8*, 1237–1246.

[89] Y. Inaba, Y. Nomata, Y. Ide, J. Pirillo, Y. Hijikata, T. Yoneda, A. Osuka, J. L. Sessler, Y. Inokuma, *J. Am. Chem. Soc.* **2021**, *143*, 12355–12360.
[90] B. S. Kumar, N. N. Pati, K. V. J. Jose, P. K. Panda, *Chem. Commun.* **2020**, *56*, 5637–5640.
[91] G. Cafeo, F. H. Kohnke, M. F. Parisi, R. Pistone Nascone, G. L. La Torre, D. J. Williams, *Org. Lett.* **2002**, *4*, 2695–2697.
[92] G. Cafeo, F. H. Kohnke, G. L. La Torre, M. F. Parisi, R. Pistone Nascone, A. J. P. White, D. J. Williams, *Chem. – Eur. J.* **2002**, *8*, 3148–3156.
[93] J. L. Sessler, J. A. Shriver, K. Jursíková, V. M. Lynch, M. Marquez, *J. Am. Chem. Soc.* **2000**, *122*, 12061–12062.
[94] B. Turner, A. Shterenberg, M. Kapon, K. Suwinska, Y. Eichen, *Chem. Commun.* **2002**, 404–405.
[95] B. Turner, M. Botoshansky, Y. Eichen, *Angew. Chem. Int. Ed.* **1998**, *37*, 2475–2478.
[96] J. S. Lindsey, I. C. Schreiman, H. C. Hsu, P. C. Kearney, A. M. Marguerettaz, *J. Org. Chem.* **1987**, *52*, 827–836.
[97] D. Jacoby, C. Floriani, A. Chiesi-Villa, C. Rizzoli, *J. Chem. Soc. Chem. Commun.* **1991**, 220–222.
[98] D. Jacoby, C. Floriani, A. Chiesi-Villa, C. Rizzoli, *J. Chem. Soc. Chem. Commun.* **1991**, 790–792.
[99] C. Floriani, R. Floriani-Moro, in *The Porphyrin Handbook Vol. 3.* (Ed.: K. M. Kadish, K. M. Smith, R. Guilard), Academic: San Diego, Calif.; London, **2000**, pp. 385-403.
[100] C. Floriani, R. Floriani-Moro, in *The Porphyrin Handbook Vol. 3.* (Ed.: K. M. Kadish, K. M. Smith, R. Guilard), Academic: San Diego, Calif.; London, **2000**, pp. 405-420.
[101] G. B. Deacon, M. G. Gardiner, P. C. Junk, J. P. Townley, J. Wang, *Organometallics* **2012**, *31*, 3857–3864.
[102] D. Jacoby, C. Floriani, A. Chiesi-Villa, C. Rizzoli, *J. Am. Chem. Soc.* **1993**, *115*, 3595–3602.
[103] L. Cuesta, J. L. Sessler, *Chem. Soc. Rev.* **2009**, *38*, 2716–2729.
[104] L. Bonomo, O. Dandin, E. Solari, C. Floriani, R. Scopelliti, *Angew. Chem. Int. Ed.* **1999**, *38*, 913–915.
[105] L. Bonomo, E. Solari, R. Scopelliti, C. Floriani, *Chem. – Eur. J.* **2001**, *7*, 1322–1332.
[106] W. Chen, Z.-R. Li, D. Wu, Y. Li, C.-C. Sun, F. L. Gu, *J. Am. Chem. Soc.* **2005**, *127*, 10977–10981.
[107] S. De Angelis, E. Solari, C. Floriani, A. Chiesi-Villa, C. Rizzoli, *J. Am. Chem. Soc.* **1994**, *116*, 5691–5701.
[108] J. Bachmann, D. G. Nocera, *J. Am. Chem. Soc.* **2005**, *127*, 4730–4743.
[109] J. Bachmann, D. G. Nocera, *J. Am. Chem. Soc.* **2004**, *126*, 2829–2837.
[110] L. Fabbrizzi, A. Poggi, *Transition Metals in Supramolecular Chemistry*, Springer Science & Business Media, **2013**.
[111] J. Jubb, C. Floriani, A. Chiesi-Villa, C. Rizzoli, *J. Am. Chem. Soc.* **1992**, *114*, 6571–6573.
[112] J.-M. Benech, L. Bonomo, E. Solari, R. Scopelliti, C. Floriani, *Angew. Chem. Int. Ed.* **1999**, *38*, 1957–1959.
[113] F. Ebner, L. Greb, *Chem* **2021**, *7*, 2151–2159.
[114] F. Ebner, L. Greb, *J. Am. Chem. Soc.* **2018**, *140*, 17409–17412.
[115] F. Ebner, L. M. Sigmund, L. Greb, *Angew. Chem. Int. Ed.* **2020**, *59*, 17118–17124.

[116] F. Ebner, H. Wadepohl, L. Greb, *J. Am. Chem. Soc.* **2019**, *141*, 18009–18012.
[117] F. Ebner, P. Mainik, L. Greb, *Chem. – Eur. J.* **2021**, *27*, 5120–5124.
[118] L. M. Sigmund, L. Greb, *Chem. Sci.* **2020**, *11*, 9611–9616.
[119] L. M. Sigmund, C. Ehlert, M. Enders, J. Graf, G. Gryn'ova, L. Greb, *Angew. Chem. Int. Ed.* **2021**, *60*, 15632–15640.
[120] L. M. Sigmund, E. Engels, N. Richert, L. Greb, *Chem. Sci.* **2022**, *13*, 11215–11220.
[121] M. Schorpp, R. Yadav, D. Roth, L. Greb, *Angew. Chem.* **2022**, *134*, e202207963.
[122] R. Yadav, P. Janßen, M. Schorpp, L. Greb, *J. Am. Chem. Soc.* **2023**, *145*, 17746–17754.
[123] F. Schön, L. M. Sigmund, F. Schneider, D. Hartmann, M. A. Wiebe, I. Manners, L. Greb, *Angew. Chem. Int. Ed.* **2022**, *61*, e202202176.
[124] J. M. Lipshultz, G. Li, A. T. Radosevich, *J. Am. Chem. Soc.* **2021**, *143*, 1699–1721.
[125] M. G. Chegerev, A. A. Starikova, A. V. Piskunov, V. K. Cherkasov, *Eur. J. Inorg. Chem.* **2016**, *2016*, 252–258.
[126] L. Greb, *Eur. J. Inorg. Chem.* **2022**, *2022*, e202100871.
[127] M. G. Chegerev, A. V. Piskunov, A. A. Starikova, S. P. Kubrin, G. K. Fukin, V. K. Cherkasov, G. A. Abakumov, *Eur. J. Inorg. Chem.* **2018**, *2018*, 1087–1092.
[128] Y. Xiong, D. Chen, S. Yao, J. Zhu, A. Ruzicka, M. Driess, *J. Am. Chem. Soc.* **2021**, *143*, 6229–6237.
[129] S. Yao, A. Kostenko, Y. Xiong, C. Lorent, A. Ruzicka, M. Driess, *Angew. Chem. Int. Ed.* **2021**, *60*, 14864–14868.
[130] R. Yadav, X. Sun, R. Köppe, M. T. Gamer, F. Weigend, P. W. Roesky, *Angew. Chem. Int. Ed.* **2022**, *61*, e202211115.
[131] A. G. Davies, M. Gielen, K. H. Pannell, E. R. T. Tiekink, Eds. , *Tin Chemistry: Fundamentals, Frontiers, and Applications*, John Wiley & Sons, Ltd, **2008**.
[132] J. K. Stille, *Angew. Chem. Int. Ed. Engl.* **1986**, *25*, 508–524.
[133] T. B. Grindley, D. R. Williams, P. P. Nag, P. Espinet, M. Genov, S. Pascual, A. M. Echavarren, J.-M. Chrétien, J. D. Kilburn, F. Zammattio, E. Le Grognec, J.-P. Quintard, R. Grigg, V. Sridharan, E. Shirakawa, D. Young, in *Tin Chem.*, John Wiley & Sons, Ltd, **2008**, pp. 497–665.
[134] S. Hanessian, in *Preparative. Carbohydrate Chemistry (1st ed.)*, CRC Press, **1997**.
[135] C. J. Evans, in *Chem. Tin* (Ed.: P.J. Smith), Springer Netherlands, Dordrecht, **1998**, pp. 442–479.
[136] J. Otera, M. Biesemans, V. Pinoie, K. Poelmans, R. Willem, W. J. Blank, E. T. Hessell, W. J. Kinart, C. M. Kinart, in *Tin Chem.*, John Wiley & Sons, Ltd, **2008**, pp. 667–720.
[137] S. K. Mandal, H. W. Roesky, in *Adv. Catal.* (Eds.: B.C. Gates, H. Knözinger), Academic Press, **2011**, pp. 1–61.
[138] L. Pauling, *J. Am. Chem. Soc.* **1932**, *54*, 3570–3582.
[139] A. Y. Timoshkin, *Chem. – Eur. J.* **2024**, *30*, e202302457.
[140] S. W. Benson, *J. Chem. Educ.* **1965**, *42*, 502.
[141] B. B. Darwent, *Bond Dissociation Energies in Simple Molecules*, U.S. National Bureau Of Standards, **1970**.
[142] C. Housecroft, A. Sharpe, *Inorganic Chemistry*, Pearson Deutschland, **2018**.
[143] E. I. Davydova, G. Balázs, M. Bodensteiner, M. Scheer, A. Y. Timoshkin, *J. Organomet. Chem.* **2023**, *983*, 122551.

[144] K. M. Stridsberg, M. Ryner, A.-C. Albertsson, in *Degradable Aliphatic Polyest.*, Springer, Berlin, Heidelberg, **2002**, pp. 41–65.
[145] A. Södergård, M. Stolt, in *PolyLactic Acid*, John Wiley & Sons, Ltd, **2010**, pp. 27–41.
[146] M. Janssen, S. Mebs, J. Beckmann, *Chem. Commun.* **2023**, *59*, 7267–7270.
[147] A. Thayyil, P. C. Parambil, *ChemPhysChem* **2023**, *24*, e202200761.
[148] L. J. Duarte, W. E. Richter, R. E. Bruns, P. L. A. Popelier, *J. Phys. Chem. A* **2021**, *125*, 8615–8625.
[149] J. B. Lambert, L. Lin, S. Keinan, T. Müller, *J. Am. Chem. Soc.* **2003**, *125*, 6022–6023.
[150] A. Sekiguchi, T. Fukawa, V. Ya. Lee, M. Nakamoto, *J. Am. Chem. Soc.* **2003**, *125*, 9250–9251.
[151] F. Diab, F. S. W. Aicher, C. P. Sindlinger, K. Eichele, H. Schubert, L. Wesemann, *Chem. – Eur. J.* **2019**, *25*, 4426–4434.
[152] M. Auer, F. Diab, K. Eichele, H. Schubert, L. Wesemann, *Dalton Trans.* **2022**, *51*, 5950–5961.
[153] J. S. Sapsford, D. Csókás, D. J. Scott, R. C. Turnell-Ritson, A. D. Piascik, I. Pápai, A. E. Ashley, *ACS Catal.* **2020**, *10*, 7573–7583.
[154] J. S. Sapsford, D. Csókás, R. C. Turnell-Ritson, L. A. Parkin, A. D. Crawford, I. Pápai, A. E. Ashley, *ACS Catal.* **2021**, *11*, 9143–9150.
[155] J. Li, C. Schenk, F. Winter, H. Scherer, N. Trapp, A. Higelin, S. Keller, R. Pöttgen, I. Krossing, C. Jones, *Angew. Chem.* **2012**, *124*, 9695–9699.
[156] K. M. Marczenko, S. Jee, S. S. Chitnis, *Organometallics* **2020**, *39*, 4287–4296.
[157] M. Yang, D. Tofan, C.-H. Chen, K. M. Jack, F. P. Gabbaï, *Angew. Chem. Int. Ed.* **2018**, *57*, 13868–13872.
[158] J. C. Gilhula, A. T. Radosevich, *Chem. Sci.* **2019**, *10*, 7177–7182.
[159] W. Lv, Y. Dai, R. Guo, Y. Su, D. A. Ruiz, L. L. Liu, C.-H. Tung, L. Kong, *Angew. Chem.* **2023**, *135*, e202308467.
[160] H. Schmidt, C. Lensink, S. K. Xi, J. G. Verkade, *Z. Für Anorg. Allg. Chem.* **1989**, *578*, 75–80.
[161] R. Schwesinger, H. Schlemper, *Angew. Chem. Int. Ed. Engl.* **1987**, *26*, 1167–1169.
[162] X. Liu, Y. Dai, M. Bao, W. Wang, Q. Li, C. Liu, X. Wang, Y. Su, *Chem. Sci.* **2023**, *14*, 5722–5727.
[163] X. Liu, Y. Dai, Q. Bao, Q. Li, N. Chen, Y. Su, X. Wang, *Angew. Chem. Int. Ed.* **2024**, e202406089.
[164] S. Tretiakov, L. Witteman, M. Lutz, M.-E. Moret, *Angew. Chem.* **2021**, *133*, 9704–9712.
[165] S. Volodarsky, I. Malahov, D. Bawari, M. Diab, N. Malik, B. Tumanskii, R. Dobrovetsky, *Chem. Sci.* **2022**, *13*, 5957–5963.
[166] T. A. N. Nguyen, G. Frenking, *Chem. – Eur. J.* **2012**, *18*, 12733–12748.
[167] H. Arp, J. Baumgartner, C. Marschner, P. Zark, T. Müller, *J. Am. Chem. Soc.* **2012**, *134*, 10864–10875.
[168] N. Parvin, S. Pal, V. C. Rojisha, S. De, P. Parameswaran, S. Khan, *ChemistrySelect* **2016**, *1*, 1991–1995.
[169] L. Álvarez-Rodríguez, J. A. Cabeza, P. García-Álvarez, D. Polo, *Coord. Chem. Rev.* **2015**, *300*, 1–28.

[170] F. E. Hahn, A. V. Zabula, T. Pape, A. Hepp, R. Tonner, R. Haunschild, G. Frenking, *Chem. – Eur. J.* **2008**, *14*, 10716–10721.
[171] M. Wagner, K. Dorogov, M. Schürmann, K. Jurkschat, *Dalton Trans.* **2011**, *40*, 8839–8848.
[172] C. Drost, P. B. Hitchcock, M. F. Lappert, *Angew. Chem. Int. Ed.* **1999**, *38*, 1113–1116.
[173] C. Mohapatra, L. T. Scharf, T. Scherpf, B. Mallick, K.-S. Feichtner, C. Schwarz, V. H. Gessner, *Angew. Chem. Int. Ed.* **2019**, *58*, 7459–7463.
[174] S. Takahashi, J. Sekiguchi, A. Ishii, N. Nakata, *Angew. Chem. Int. Ed.* **2021**, *60*, 4055–4059.
[175] C. Hu, L. L. Liu, *Inorg. Chem.* **2023**, *62*, 3592-3600.
[176] In *Organotin Chem.*, John Wiley & Sons, Ltd, **2004**, pp. 311–332.
[177] D.-Y. Wang, C. Wang, M. Uchiyama, *J. Am. Chem. Soc.* **2015**, *137*, 10488–10491.
[178] A. Capperucci, A. Degl'Innocenti, C. Faggi, G. Reginato, A. Ricci, P. Dembech, G. Seconi, *J. Org. Chem.* **1989**, *54*, 2966–2968.
[179] J. A. Marshall, G. S. Welmaker, B. W. Gung, *J. Am. Chem. Soc.* **1991**, *113*, 647–656.
[180] M. Contel, K. W. Hellmann, L. H. Gade, I. J. Scowen, M. McPartlin, M. Laguna, *Inorg. Chem.* **1996**, *35*, 3713–3715.
[181] L. H. Gade, *Eur. J. Inorg. Chem.* **2002**, *2002*, 1257–1268.
[182] M. Lutz, M. Haukka, T. A. Pakkanen, L. H. Gade, *Inorg. Chem.* **2003**, *42*, 2798–2804.
[183] B. Findeis, M. Contel, L. H. Gade, M. Laguna, M. C. Gimeno, I. J. Scowen, M. McPartlin, *Inorg. Chem.* **1997**, *36*, 2386–2390.
[184] M. Kilian, H. Wadepohl, L. H. Gade, *Organometallics* **2007**, *26*, 3076–3078.
[185] M. Kilian, H. Wadepohl, L. H. Gade, *Dalton Trans.* **2008**, 582–584.
[186] M. Kilian, H. Wadepohl, L. H. Gade, *Eur. J. Inorg. Chem.* **2008**, *2008*, 1892–1900.
[187] M. Kilian, H. Wadepohl, L. H. Gade, *Organometallics* **2008**, *27*, 524–533.
[188] S. Hagen, I. Pantenburg, F. Weigend, C. Wickleder, L. Wesemann, *Angew. Chem. Int. Ed.* **2003**, *42*, 1501–1505.
[189] L. Wesemann, S. Hagen, T. Marx, I. Pantenburg, M. Nobis, B. Drießen-Hölscher, *Eur. J. Inorg. Chem.* **2002**, *2002*, 2261–2265.
[190] L. Wesemann, T. Marx, U. Englert, M. Ruck, *Eur. J. Inorg. Chem.* **1999**, *1999*, 1563–1566.
[191] T. Marx, L. Wesemann, S. Dehnen, I. Pantenburg, *Chem. – Eur. J.* **2001**, *7*, 3025–3032.
[192] R. W. Chapman, J. G. Kester, K. Folting, W. E. Streib, L. J. Todd, *Inorg. Chem.* **1992**, *31*, 979–983.
[193] D. Joosten, I. Weissinger, M. Kirchmann, C. Maichle-Mössmer, F. M. Schappacher, R. Pöttgen, L. Wesemann, *Organometallics* **2007**, *26*, 5696–5701.
[194] T. Vollgraff, N. Michel, J. Sundermeyer, *Eur. J. Inorg. Chem.* **2021**, *2021*, 3852–3860.
[195] W. J. Belcher, P. J. Brothers, A. P. Meredith, C. E. F. Rickard, D. C. Ware, *J. Chem. Soc. Dalton Trans.* **1999**, 2833–2836.
[196] S. Onaka, Y. Kondo, M. Yamashita, Y. Tatematsu, Y. Kato, M. Goto, T. Ito, *Inorg. Chem.* **1985**, *24*, 1070–1076.
[197] J.-M. Barbe, R. Guilard, C. Lecomte, R. Gerardin, *Polyhedron* **1984**, *3*, 889–894.
[198] J. M. Barbe, C. Ratti, P. Richard, C. Lecomte, R. Gerardin, R. Guilard, *Inorg. Chem.* **1990**, *29*, 4126–4130.

[199] D. V. Konarev, A. V. Kuzmin, Y. Nakano, M. A. Faraonov, S. S. Khasanov, A. Otsuka, H. Yamochi, G. Saito, R. N. Lyubovskaya, *Inorg. Chem.* **2016**, *55*, 1390–1402.
[200] L. Yun, H. Vazquez-Lima, H. Fang, Z. Yao, G. Geisberger, C. Dietl, A. Ghosh, P. J. Brothers, X. Fu, *Inorg. Chem.* **2014**, *53*, 7047–7054.
[201] E. O. Fischer, A. Maasböl, *Angew. Chem. Int. Ed. Engl.* **1964**, *3*, 580–581.
[202] E. O. Fischer, *Angew. Chem.* **1974**, *86*, 651–663.
[203] K. Öfele, *J. Organomet. Chem.* **1968**, *12*, P42–P43.
[204] H.-W. Wanzlick, H.-J. Schönherr, *Angew. Chem. Int. Ed. Engl.* **1968**, *7*, 141–142.
[205] A. J. I. Arduengo, R. L. Harlow, M. Kline, *J. Am. Chem. Soc.* **1991**, *113*, 361–363.
[206] V. Lavallo, Y. Canac, C. Präsang, B. Donnadieu, G. Bertrand, *Angew. Chem. Int. Ed.* **2005**, *44*, 5705–5709.
[207] V. M. Marx, A. H. Sullivan, M. Melaimi, S. C. Virgil, B. K. Keitz, D. S. Weinberger, G. Bertrand, R. H. Grubbs, *Angew. Chem. Int. Ed.* **2015**, *54*, 1919–1923.
[208] U. S. D. Paul, U. Radius, *Eur. J. Inorg. Chem.* **2017**, *2017*, 3362–3375.
[209] S. P. Nolan, *Acc. Chem. Res.* **2011**, *44*, 91–100.
[210] P. Bellotti, M. Koy, M. N. Hopkinson, F. Glorius, *Nat. Rev. Chem.* **2021**, *5*, 711–725.
[211] Y. Wang, G. H. Robinson, *J. Am. Chem. Soc.* **2023**, *145*, 5592-5612.
[212] V. Lavallo, Y. Canac, B. Donnadieu, W. W. Schoeller, G. Bertrand, *Angew. Chem.* **2006**, *118*, 3568–3571.
[213] G. D. Frey, V. Lavallo, B. Donnadieu, W. W. Schoeller, G. Bertrand, *Science* **2007**, *316*, 439–441.
[214] O. Back, G. Kuchenbeiser, B. Donnadieu, G. Bertrand, *Angew. Chem.* **2009**, *121*, 5638–5641.
[215] D. Enders, O. Niemeier, A. Henseler, *Chem. Rev.* **2007**, *107*, 5606–5655.
[216] K. M. Hindi, M. J. Panzner, C. A. Tessier, C. L. Cannon, W. J. Youngs, *Chem. Rev.* **2009**, *109*, 3859–3884.
[217] J. W. Kamplain, C. W. Bielawski, *Chem. Commun.* **2006**, 1727–1729.
[218] A. V. Zhukhovitskiy, M. J. MacLeod, J. A. Johnson, *Chem. Rev.* **2015**, *115*, 11503–11532.
[219] A. J. Boydston, C. W. Bielawski, *Dalton Trans.* **2006**, 4073–4077.
[220] A. J. Boydston, K. A. Williams, C. W. Bielawski, *J. Am. Chem. Soc.* **2005**, *127*, 12496–12497.
[221] R. W. Alder, M. E. Blake, L. Chaker, J. N. Harvey, F. Paolini, J. Schütz, *Angew. Chem. Int. Ed.* **2004**, *43*, 5896–5911.
[222] Y. Canac, M. Soleilhavoup, S. Conejero, G. Bertrand, *J. Organomet. Chem.* **2004**, *689*, 3857–3865.
[223] L. M. Slaughter, *ACS Catal.* **2012**, *2*, 1802–1816.
[224] L. M. Slaughter, in *N-Heterocyclic Carbenes*, John Wiley & Sons, Ltd, **2014**, pp. 499–524.
[225] X. Cattoën, H. Gornitzka, D. Bourissou, G. Bertrand, *J. Am. Chem. Soc.* **2004**, *126*, 1342–1343.
[226] B. Rao, H. Tang, X. Zeng, L. L. Liu, M. Melaimi, G. Bertrand, *Angew. Chem. Int. Ed.* **2015**, *54*, 14915–14919.
[227] S. Solé, H. Gornitzka, W. W. Schoeller, D. Bourissou, G. Bertrand, *Science* **2001**, *292*, 1901–1903.

[228] M. Melaimi, R. Jazzar, M. Soleilhavoup, G. Bertrand, *Angew. Chem. Int. Ed.* **2017**, *56*, 10046–10068.
[229] H. Seo, D. R. Snead, K. A. Abboud, S. Hong, *Organometallics* **2011**, *30*, 5725–5730.
[230] T. Schulz, D. Weismann, L. Wallbaum, R. Guthardt, C. Thie, M. Leibold, C. Bruhn, U. Siemeling, *Chem. – Eur. J.* **2015**, *21*, 14107–14121.
[231] K. Denk, P. Sirsch, W. A. Herrmann, *J. Organomet. Chem.* **2002**, *649*, 219–224.
[232] A. J. Hartshorn, M. F. Lappert, K. Turner, *J. Chem. Soc. Dalton Trans.* **1978**, 348–356.
[233] M. F. Lappert, *J. Organomet. Chem.* **1975**, *100*, 139–159.
[234] B. Cetinkaya, M. F. Lappert, K. Turner, *J. Chem. Soc. Chem. Commun.* **1972**, 851–852.
[235] K. J. Hawkes, D. S. McGuinness, K. J. Cavell, B. F. Yates, *Dalton Trans.* **2004**, 2505–2513.
[236] D. R. Snead, I. Ghiviriga, K. A. Abboud, S. Hong, *Org. Lett.* **2009**, *11*, 3274–3277.
[237] D. R. Snead, S. Inagaki, K. A. Abboud, S. Hong, *Organometallics* **2010**, *29*, 1729–1739.
[238] M. Otto, S. Conejero, Y. Canac, V. D. Romanenko, V. Rudzevitch, G. Bertrand, *J. Am. Chem. Soc.* **2004**, *126*, 1016–1017.
[239] E. M. Badley, J. Chatt, R. L. Richards, G. A. Sim, *J. Chem. Soc. Chem. Commun.* **1969**, 1322–1323.
[240] F. Bonati, G. Minghetti, T. Boschi, B. Crociani, *J. Organomet. Chem.* **1970**, *25*, 255–260.
[241] E. O. Fischer, U. Schubert, W. Kleine, H. Fischer, K. P. Darst, C. M. Lukehart, L. T. Warfielo, D. J. Darensbourg, R. R. Burch Jr., J. A. Froelich, in *Inorg. Synth.*, John Wiley & Sons, Ltd, **1979**, pp. 164–172.
[242] I. Fernández, M. J. Mancheño, R. Vicente, L. A. López, M. A. Sierra, *Chem. – Eur. J.* **2008**, *14*, 11222–11230.
[243] A. Toledo, V. Salamanca, T. Pérez-Moro, A. C. Albéniz, *Organometallics* **2021**, *40*, 38–47.
[244] L. M. Slaughter, *Comments Inorg. Chem.* **2008**, *29*, 46–72.
[245] Y. A. Wanniarachchi, S. S. Subramanium, L. M. Slaughter, *J. Organomet. Chem.* **2009**, *694*, 3297–3305.
[246] M. O. Owusu, S. Handa, L. M. Slaughter, *Appl. Organomet. Chem.* **2012**, *26*, 712–717.
[247] C. Singh, A. Kumar, H. V. Huynh, *Inorg. Chem.* **2020**, *59*, 8451–8460.
[248] G. Bittner, H. Witte, G. Hesse, *Justus Liebigs Ann. Chem.* **1968**, *713*, 1–11.
[249] M. Gimferrer, S. Danés, E. Vos, C. B. Yildiz, I. Corral, A. Jana, P. Salvador, D. M. Andrada, *Chem. Sci.* **2022**, *13*, 6583–6591.
[250] D. Jędrzkiewicz, J. Mai, J. Langer, Z. Mathe, N. Patel, S. DeBeer, S. Harder, *Angew. Chem. Int. Ed.* **2022**, *61*, e202200511.
[251] C. Jones, A. Sidiropoulos, N. Holzmann, G. Frenking, A. Stasch, *Chem. Commun.* **2012**, *48*, 9855–9857.
[252] K. C. Mondal, H. W. Roesky, M. C. Schwarzer, G. Frenking, B. Niepötter, H. Wolf, R. Herbst-Irmer, D. Stalke, *Angew. Chem. Int. Ed.* **2013**, *52*, 2963–2967.
[253] S. Kundu, S. Sinhababu, V. Chandrasekhar, H. W. Roesky, *Chem. Sci.* **2019**, *10*, 4727–4741.

[254] E. Haldón, Á. Kozma, H. Tinnermann, L. Gu, R. Goddard, M. Alcarazo, *Dalton Trans.* **2016**, *45*, 1872–1876.
[255] J. W. Dube, Y. Zheng, W. Thiel, M. Alcarazo, *J. Am. Chem. Soc.* **2016**, *138*, 6869–6877.
[256] T. Johannsen, C. Golz, M. Alcarazo, *Angew. Chem. Int. Ed.* **2020**, *59*, 22779–22784.
[257] K. Dimroth, N. Grief, A. Klapproth, *Justus Liebigs Ann. Chem.* **1975**, *1975*, 373–386.
[258] M. D. Böhme, T. Eder, M. B. Röthel, P. D. Dutschke, L. F. B. Wilm, F. E. Hahn, F. Dielmann, *Angew. Chem. Int. Ed.* **2022**, *61*, e202202190.
[259] T. Böttcher, B. S. Bassil, L. Zhechkov, T. Heine, G.-V. Röschenthaler, *Chem. Sci.* **2012**, *4*, 77–83.
[260] T. Böttcher, B. S. Bassil, G.-V. Röschenthaler, *Inorg. Chem.* **2012**, *51*, 763–765.
[261] T. Böttcher, B. S. Bassil, L. Zhechkov, G.-V. Röschenthaler, *Inorg. Chem.* **2013**, *52*, 5651–5653.
[262] T. Böttcher, G.-V. Röschenthaler, *J. Fluor. Chem.* **2015**, *171*, 4–11.
[263] D. J. Scott, N. A. Phillips, J. S. Sapsford, A. C. Deacy, M. J. Fuchter, A. E. Ashley, *Angew. Chem.* **2016**, *128*, 14958–14962.
[264] T. W. Myers, L. A. Berben, *J. Am. Chem. Soc.* **2013**, *135*, 9988–9990.
[265] C. L. Shaves, N. Villegas-Escobar, E. R. Clark, I. M. Riddlestone, *Chem. – Eur. J.* **2023**, *29*, e202203806.
[266] T. M. Bass, C. R. Carr, T. J. Sherbow, J. C. Fettinger, L. A. Berben, *Inorg. Chem.* **2020**, *59*, 13517–13523.
[267] S. Volodarsky, D. Bawari, R. Dobrovetsky, *Angew. Chem. Int. Ed.* **2022**, *61*, e202208401.
[268] J. Abbenseth, O. P. E. Townrow, J. M. Goicoechea, *Angew. Chem. Int. Ed.* **2021**, *60*, 23625–23629.
[269] S. Lim, A. T. Radosevich, *J. Am. Chem. Soc.* **2020**, *142*, 16188–16193.
[270] J. Abbenseth, J. M. Goicoechea, *Chem. Sci.* **2020**, *11*, 9728–9740.
[271] *CRediT*, https://credit.niso.org/, (accessed July 1, **2024**).
[272] H. Ruppert, A. Meister, R. Pfretzschner, A. F. Vieira, L. Greb, *J. Am. Chem. Soc.* **2024**, *146*, 11515-11522.
[273] R. G. Pearson, *J. Chem. Educ.* **1968**, *45*, 643.
[274] R. G. Pearson, *J. Chem. Educ.* **1968**, *45*, 581.
[275] R. G. Pearson, *J. Am. Chem. Soc.* **1963**, *85*, 3533–3539.
[276] T. L. Cottrell, *The Strengths of Chemical Bonds*, Butterworth's Scientific Publications, London, **1954.**
[277] D. Agustin, M. Ehses, *Comptes Rendus Chim.* **2009**, *12*, 1189–1227.
[278] G. R. Fulmer, A. J. M. Miller, N. H. Sherden, H. E. Gottlieb, A. Nudelman, B. M. Stoltz, J. E. Bercaw, K. I. Goldberg, *Organometallics* **2010**, *29*, 2176–2179.
[279] Steffen Pospiech, Michael Bolte, Matthias Wagner, *CCDC 2159029*: Experimental Crystal Structure Determination, **2022**, https://dx.doi.org/10.5517/ccdc.csd.cc2bgn3l.
[280] R. J. Errington, in *Adv. Inorg. Chem.* (Eds.: R. van Eldik, L. Cronin), Academic Press, **2017**, pp. 287–336.
[281] A. Guenet, E. Graf, N. Kyritsakas, M. W. Hosseini, *Inorg. Chem.* **2010**, *49*, 1872–1883.

[282] R. Soman, D. Raghav, S. Sujatha, K. Rathinasamy, C. Arunkumar, *RSC Adv.* **2015**, *5*, 61103–61117.
[283] *Lithium Fluoride*. https://www.ucl.ac.uk/~ucapahh/research/crystal/lif.htm (accessed July 1, **2024**).
[284] H. Ruppert, L. Greb, *Angew. Chem. Int. Ed.* **2022**, *61*, e202116615.
[285] J. R. Lawson, R. L. Melen, *Inorg. Chem.* **2017**, *56*, 8627–8643.
[286] D. M. C. Ould, J. L. Carden, R. Page, R. L. Melen, *Inorg. Chem.* **2020**, *59*, 14891–14898.
[287] L. A. Mück, A. Y. Timoshkin, G. Frenking, *Inorg. Chem.* **2012**, *51*, 640–646.
[288] M. Saito, S. Imaizumi, T. Tajima, K. Ishimura, S. Nagase, *J. Am. Chem. Soc.* **2007**, *129*, 10974–10975.
[289] L. Bonomo, E. Solari, C. Floriani, A. Chiesi-Villa, C. Rizzoli, *J. Am. Chem. Soc.* **1998**, *120*, 12972–12973.
[290] G. D. Smith, P. E. Fanwick, I. P. Rothwell, *J. Am. Chem. Soc.* **1989**, *111*, 750–751.
[291] G. D. Smith, V. M. Visciglio, P. E. Fanwick, I. P. Rothwell, *Organometallics* **1992**, *11*, 1064–1071.
[292] K. Yamamoto, S. Kimura, T. Murahashi, *Angew. Chem. Int. Ed.* **2016**, *55*, 5322–5326.
[293] R. L. Hinman, E. B. Whipple, *J. Am. Chem. Soc.* **1962**, *84*, 2534–2539.
[294] F. J. Hoyuelos, B. García, S. Ibeas, M. S. Muñoz, A. M. Navarro, I. Peñacoba, J. M. Leal, *Eur. J. Org. Chem.* **2005**, *2005*, 1161–1171.
[295] Q. Tong, Z. Zhao, Y. Wang, *Beilstein J. Org. Chem.* **2022**, *18*, 325–330.
[296] D. B. G. Williams, M. Lawton, *J. Org. Chem.* **2010**, *75*, 8351–8354.
[297] Y. Furusho, T. Aida, *Chem. Commun.* **1997**, 2205–2206.
[298] S. Dey, K. Pal, S. Sarkar, *Tetrahedron Lett.* **2006**, *47*, 5851–5854.
[299] S. De Angelis, E. Solari, C. Floriani, A. Chiesi-Villa, C. Rizzoli, *J. Chem. Soc. Dalton Trans.* **1994**, 2467–2469.
[300] W. Plass, J. G. Verkade, *Inorg. Chem.* **1993**, *32*, 5145–5152.
[301] H. Ruppert, A. Meister, P. Janßen, L. Greb, *Chem. – Eur. J.* **2024**, e202401685.
[302] H. Ruppert, T. Schreyer, M. C. Dietl, M. Rudolph, S. K. Hashmi, L. Greb, *Z. Für Anorg. Allg. Chem.* **2024**, e202400081.
[303] *Mestrelab Research S.L.*, *Mnova*. https://mestrelab.com/download/mnova/ (accessed July 1, **2024**).
[304] D. Geiß, M. I. Arz, M. Straßmann, G. Schnakenburg, A. C. Filippou, *Angew. Chem.* **2015**, *127*, 2777–2782.
[305] *Bruker corp.*, *Apex Software*. https://www.bruker.com/de/products-and-solutions/diffractometers-and-x-ray-microscopes/single-crystal-x-ray-diffractometers/sc-xrd-software/apex.html (accessed July 1, **2024**).
[306] Z. Otwinowski, W. Minor, in *Methods Enzymol.*, Academic Press, **1997**, pp. 307–326.
[307] **2016**.
[308] G. M. Sheldrick, *J Appl Crystallogr* **2015**, *48*, 3–10.
[309] G. M. Sheldrick, *Acta Crystallogr. Sect. Found. Adv.* **2015**, *71*, 3–8.
[310] D. Kratzert, J. J. Holstein, I. Krossing, *J. Appl. Crystallogr.* **2015**, *48*, 933–938.
[311] P. Muller, R. Herbst-Irmer, A. Spek, T. Schneider, M. Sawaya, *Crystal Structure Refinement: A Crystallographer's Guide to SHELXL*, OUP Oxford, **2006**.

[312] G. Sheldrick, *Acta Crystallogr. Sect. C* **2015**, *71*, 3–8.
[313] C. B. Hübschle, G. M. Sheldrick, B. Dittrich, *J. Appl. Crystallogr.* **2011**, *44*, 1281–1284.
[314] D. Kratzert, *FinalCif*. https://dkratzert.de/finalcif.html (accessed July 1, **2024**).
[315] I. J. Bruno, J. C. Cole, P. R. Edgington, M. Kessler, C. F. Macrae, P. McCabe, J. Pearson, R. Taylor, *Acta Crystallogr. B* **2002**, *58*, 389–397.
[316] C. F. Macrae, P. R. Edgington, P. McCabe, E. Pidcock, G. P. Shields, R. Taylor, M. Towler, J. van de Streek, *J. Appl. Crystallogr.* **2006**, *39*, 453–457.
[317] F. Neese, *WIREs Comput. Mol. Sci.* **2022**, e1606.
[318] F. Neese, *WIREs Comput. Mol. Sci.* **2012**, *2*, 73–78.
[319] E. D. Glendening, J. K. Badenhoop, A. E. Reed, J. E. Carpenter, J. A. Bohmann, C. M. Morales, C. R. Landis, F. Weinhold, "NBO 6.0," **2013**.
[320] T. Ziegler, A. Rauk, *Theor. Chim. Acta* **1977**, *46*, 1–10.
[321] T. Ziegler, A. Rauk, *Inorg. Chem.* **1979**, *18*, 1755–1759.
[322] T. Ziegler, A. Rauk, *Inorg. Chem.* **1979**, *18*, 1558–1565.
[323] D. Stalke, *Chem. – Eur. J.* **2011**, *17*, 9264–9278.
[324] R. F. W. Bader, *Chem. Rev.* **1991**, *91*, 893–928.
[325] R. F. W. Bader, H. Essén, *J. Chem. Phys.* **1984**, *80*, 1943–1960.
[326] F. Cortesguzman, R. Bader, *Coord. Chem. Rev.* **2005**, *249*, 633–662.
[327] M. D. Hanwell, D. E. Curtis, D. C. Lonie, T. Vandermeersch, E. Zurek, G. R. Hutchison, *Avogadro: An Advanced Semantic Chemical Editor, Visualization, and Analysis Platform. J Cheminform 4: 17*, **2012**.
[328] G. A. Andrienko, *Chemcraft 1.8*. https://www.chemcraftprog.com (accessed July 1, **2024**).
[329] G. Knizia, J. E. M. N. Klein, *Angew. Chem. Int. Ed.* **2015**, *54*, 5518–5522.
[330] P. Pracht, F. Bohle, S. Grimme, *Phys. Chem. Chem. Phys.* **2020**, *22*, 7169–7192.
[331] C. Bannwarth, S. Ehlert, S. Grimme, *J. Chem. Theory Comput.* **2019**, *15*, 1652–1671.
[332] C. Bannwarth, E. Caldeweyher, S. Ehlert, A. Hansen, P. Pracht, J. Seibert, S. Spicher, S. Grimme, *WIREs Comput. Mol. Sci.* **2021**, *11*, e1493.
[333] S. Grimme, J. G. Brandenburg, C. Bannwarth, A. Hansen, *J. Chem. Phys.* **2015**, *143*, 054107.
[334] S. Grimme, J. Antony, S. Ehrlich, H. Krieg, *J. Chem. Phys.* **2010**, *132*, 154104.
[335] H. Kruse, S. Grimme, *J. Chem. Phys.* **2012**, *136*, 154101.
[336] S. Grimme, S. Ehrlich, L. Goerigk, *J. Comput. Chem.* **2011**, *32*, 1456–1465.
[337] F. Weigend, *Phys. Chem. Chem. Phys.* **2006**, *8*, 1057–1065.
[338] G. L. Stoychev, A. A. Auer, F. Neese, *J. Chem. Theory Comput.* **2017**, *13*, 554–562.
[339] N. Mardirossian, M. Head-Gordon, *J. Chem. Phys.* **2015**, *142*, 074111.
[340] E. Caldeweyher, C. Bannwarth, S. Grimme, *J. Chem. Phys.* **2017**, *147*, 034112.
[341] F. Weigend, R. Ahlrichs, *Phys. Chem. Chem. Phys.* **2005**, *7*, 3297–3305.
[342] S. Grimme, *Chem. – Eur. J.* **2012**, *18*, 9955–9964.
[343] A. Klamt, V. Jonas, T. Bürger, J. C. W. Lohrenz, *J. Phys. Chem. A* **1998**, *102*, 5074–5085.
[344] A. Klamt, *J. Phys. Chem.* **1995**, *99*, 2224–2235.
[345] A. Klamt, *COSMO-RS: From Quantum Chemistry to Fluid Phase Thermodynamics and Drug Design*, Elsevier, **2005**.
[346] A. V. Marenich, C. J. Cramer, D. G. Truhlar, *J. Phys. Chem. B* **2009**, *113*, 6378–6396.

[347] S. Kozuch, D. Gruzman, J. M. L. Martin, *J. Phys. Chem. C* **2010**, *114*, 20801–20808.
[348] X. Ren, P. Rinke, V. Blum, J. Wieferink, A. Tkatchenko, A. Sanfilippo, K. Reuter, M. Scheffler, *New J. Phys.* **2012**, *14*, 053020.
[349] C. Adamo, V. Barone, *J. Chem. Phys.* **1999**, *110*, 6158–6170.
[350] M. P. Mitoraj, A. Michalak, T. Ziegler, *J. Chem. Theory Comput.* **2009**, *5*, 962–975.
[351] A. D. Becke, *Phys. Rev. A* **1988**, *38*, 3098–3100.
[352] J. P. Perdew, *Phys. Rev. B* **1986**, *33*, 8822–8824.
[353] J. D. Rolfes, F. Neese, D. A. Pantazis, *J. Comput. Chem.* **2020**, *41*, 1842–1849.
[354] S. Grimme, *J. Comput. Chem.* **2004**, *25*, 1463–1473.
[355] M. Ernzerhof, G. E. Scuseria, *J. Chem. Phys.* **1999**, *110*, 5029–5036.
[356] J. I. Rodríguez, R. F. W. Bader, P. W. Ayers, C. Michel, A. W. Götz, C. Bo, *Chem. Phys. Lett.* **2009**, *472*, 149–152.
[357] J. I. Rodríguez, A. M. Köster, P. W. Ayers, A. Santos-Valle, A. Vela, G. Merino, *J. Comput. Chem.* **2009**, *30*, 1082–1092.
[358] Gerald R. Willey, Timothy J. Woodman, Robert J. Deeth, William Errington, *Main Group Met. Chem.* **1998**, *21*, 583–592.
[359] L. Omann, M. Oestreich, *Organometallics* **2017**, *36*, 767–776.
[360] J. Cullinane, A. Jolleys, F. S. Mair, *Dalton Trans.* **2013**, *42*, 11971–11975.
[361] J. S. Mohar, A. Reinholdt, T. M. Keller, P. J. Carroll, J. Telser, D. J. Mindiola, *Chem. Commun.* **2023**, *59*, 10101–10104.
[362] K. Bläsing, J. Bresien, R. Labbow, D. Michalik, A. Schulz, M. Thomas, A. Villinger, *Angew. Chem. Int. Ed.* **2019**, *58*, 6540–6544.
[363] S. Feng, G. R. Roof, E. Y.-X. Chen, *Organometallics* **2002**, *21*, 832–839.

7 APPENDIX

7.1 List of Abbreviations

A

***a*AAC** *Acyclic alkyl(amino)carbene*

***a*ArAC** *Acyclic aryl(amino)carbene*

ADC *Acyclic diaminocarbene*

AE ·*Association energy*

AlCF *Tris(pentafluorophenyl)alane*

B

BA *Benzaldehyde*

$[BAr^{F20}]^-$ *Tetrakis(pentafluorophenyl)-borate*

BCF *Tris(pentafluorophenyl)borane*

Bn *Benzyl residue*

C

***c*AAC** *Cyclic alkyl(amino)carbene*

CCDC *Cambridge Crystallographic Data Centre*

CD_2Cl_2 · *Dichloromethane-d_2*

CH_2Cl_2 · *Dichloromethane*

CIA · *Chloride ion affinity in the gas phase*

CIA_{solv} · *Solution phase chloride ion affinity (dichloromethane)*

CO_2 · *Carbon dioxide*

COSMO-RS · *Conductor-like screening model for real solvents*

COSY · *Correlation (NMR) spectroscopy*

CPCM *Conductor-like polarizable continuum model*

CREST · *Conformer-rotamer ensemble sampling tool*

CSD · *Cambridge Structural Database*

CT *Charge transfer*

D

d *Doublet*

DBTL *Dibutyltin dilaurate*

DBTO *Dibutyltin oxide*

DCM *Dichloromethane, synonym for methylene chloride CH_2Cl_2*

DE · *Deformation energy*

DEPT · *Distortionless enhancement by polarization transfer*

DFT · *Density functional theory*

Dip *2,6-Diisopropylphenyl*

dme · *1,2-Dimethoxyethane (ligand)*

DME · *1,2-Dimethoxyethane (solvent)*

dmfc *Decamethylferrocene*

dmfc$^+$ *Decamethylferrocenium*

E

ΔE *Total bonding energy (EDA)*

$\Delta E_{oi,tot}$ *Total orbital interaction energy (EDA)*

ECP · *Effective core potential*

EDA *Energy decomposition analysis*

EDG *Electron donating group*

ELC · *Element-ligand cooperativity*

eq. · *Equivalent*

ESI · *Electrospray ionization*

Et · *Ethyl (group)*

Et_2O *Diethyl ether*

ETS *Extended transition state (method)*

EWG *Electron withdrawing group*

F

fc · *Ferrocene*

fc$^+$ *Ferrocenium*

FIA · *Fluoride ion affinity in the gas phase*

FIA_{solv} · *Solution phase fluoride ion affinity (dichloromethane)*

FLP · *Frustrated Lewis pair*

FMO · *Frontier molecular orbital*

FT-ATR-IR · *Fourier-transform attenuated total reflection infrared (spectroscopy)*

G

GEI · *Global electrophilicity index*

H

HIA · *Hydride ion affinity in the gas phase*

HIA_{solv} · *Solution phase hydride ion affinity (dichloromethane)*

HMBC · *Heteronuclear multiple-bond correlation (NMR) spectroscopy*

HMDS *Hexamethyldisilazane or hexamethyldisilazide anion*

$HNTf_2$ · *Bis(trifluoromethyl)sulfonimide*

HOMO · *Highest occupied molecular orbital*

HR-MS · *High resolution mass spectrometry*

HSAB · *(Theory of) hard and soft Lewis acids and bases*

HSQC · *Heteronuclear single-quantum correlation (NMR) spectroscopy*

I

IIA · *Iodide ion affinity in the gas phase*

IIA_{solv} · *Solution phase iodide ion affinity (dichloromethane)*

INT · *Intermediate*

INVGATE *Inverse gated (NMR)*

***i*Pr** · *iso-Propyl (group)*

IUPAC · *International Union of Pure and Applied Chemistry*

IR · *Infrared*

ISC *Intersystem crossing*

L

LA *Lewis acid*

LUMO · *Lowest unoccupied molecular orbital*

M

m/z · *Mass-to-charge ratio*

Me · *Methyl (group)*

MeCN *Acetonitrile*

MeI *Methyl iodide*

MLC · *Metal-ligand cooperativity*

MO · *Molecular orbital*

N

NBO · *Natural bond orbital*

***n*Bu** · *n-Butyl (group)*

NBu_4 or NBu_4^+ · *Tetrabutylammonium*

NHC *N-Heterocylcic carbene*

***N*MeInd** *N-Methyl indole*

NMR · *Nuclear magnetic resonance*

NOCV *Natural orbitals for chemical valance (theory)*

NOESY · *Nuclear Overhauser effect (NMR) spectroscopy*

O

o/n · *over night*

***o*DFB** · *ortho-Difluorobenzene*

***o*Phen** *ortho-Phenylene (group)*

P

PCET *Proton-coupled electron transfer*

PES *Potential energy surface*

Ph · *Phenyl (group)*

PPh_4 or PPh_4^+ · *Tetraphenylphosphonium*

ppm · *Parts per million*

py *Pyridine (ligand)*

R

ROP *Ring-opening polymerization*

rt · *Room temperature*

S

sc-XRD · *Single crystal X-ray diffraction*

SOJTE *Second-order Jahn-Teller effect*

T

t · *Triplet*

TBAT · *Tetrabutylammonium difluoro-triphenylsilicate*

***t*Bu** · *tert-Butyl (group)*

TD-DFT · *Time-dependent density functional theory*

TEP · *Tolman electronic parameter*

thf · *Tetrahydrofuran (ligand)*

THF · *Tetrahydrofuran (solvent)*

TMS of TMS^+ *Trimethylsilyl or trimethylsilylium*

TS · *Transition state/structure*

U

UV · *Ultraviolet*

V

VE *Valence electron*

Vis · *Visible region of the electromagnetic spectrum*

VSEPR *Valence shell electron pair repulsion*

W

WBI · *Wiberg bond index*

X

XIA *General ion affinity towards anion X^- in the gas phase*

XIA_{solv} · *Solution phase affinity towards anion X^- (dichloromethane)*

xs · *excess*

7.2 NMR Spectra

7.2.1 2^{R}-(thf)$_2$

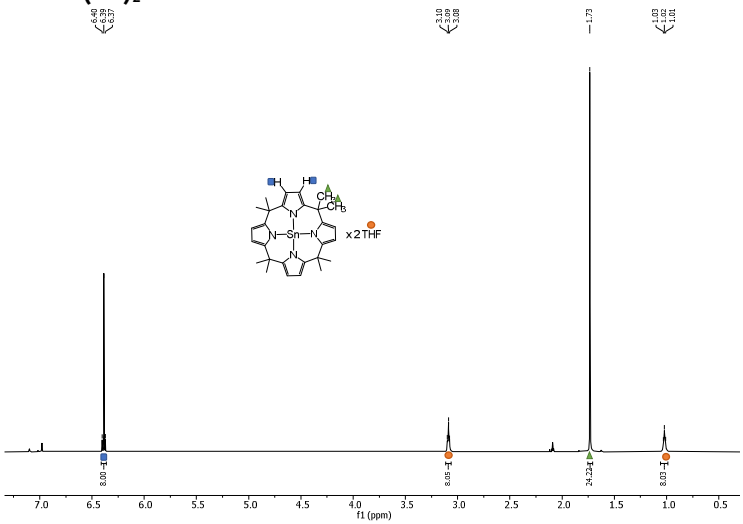


Figure S1. ^{1}H NMR spectrum of **2^{Me}-(thf)$_2$** (600.18 MHz, Toluene-d_8, 295 K).

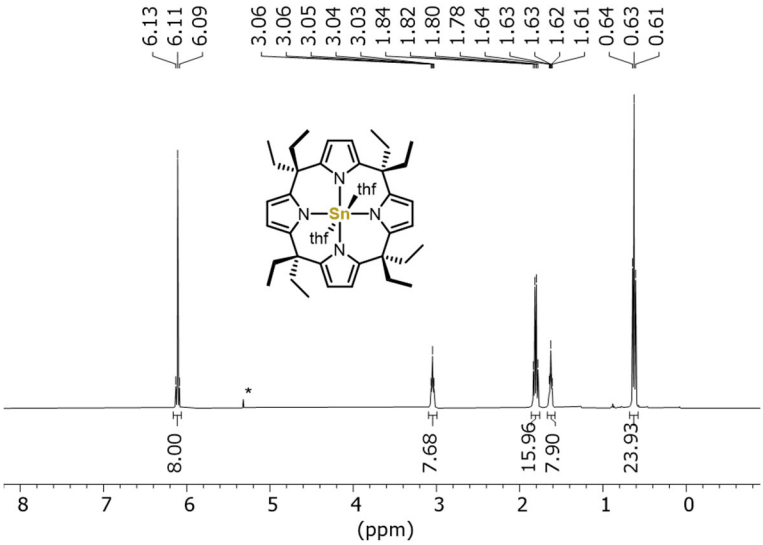


Figure S2. ^{1}H NMR spectrum of **2^{Et}-(thf)$_2$** (399.98 MHz, CD_2Cl_2, 295 K). Solvent signals are indicated by an asterisk (*).

7.2.2 2^{R}-$(Et_3PO)_2$

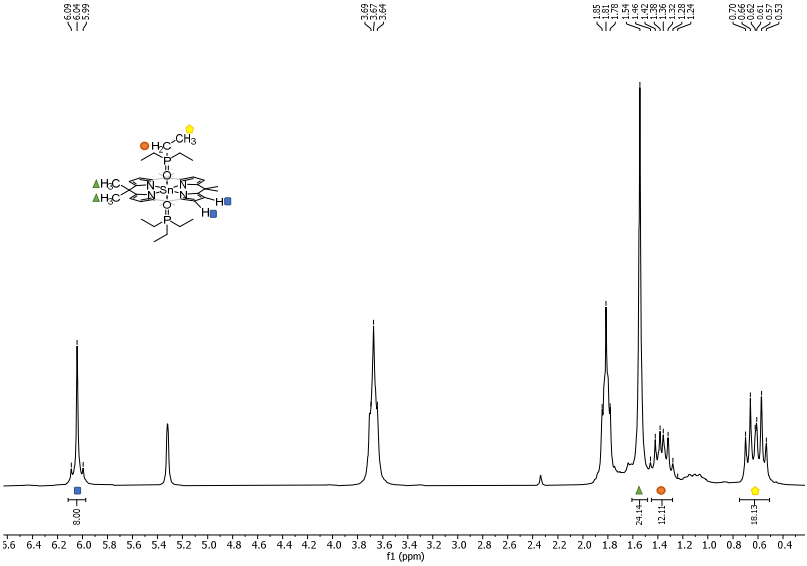


Figure S3: ^{1}H NMR spectrum (200 MHz, 298 K, CD_2Cl_2) of $\mathbf{2^{Me}}$-$\mathbf{(Et_3PO)_2}$.

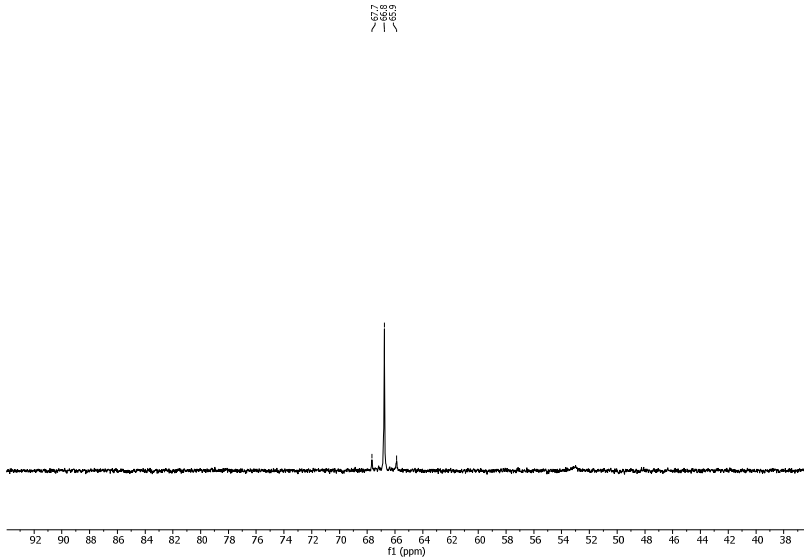


Figure S4: ^{31}P NMR spectrum (121 MHz, 298 K, CD_2Cl_2) of $\mathbf{2^{Me}}$-$\mathbf{(Et_3PO)_2}$.

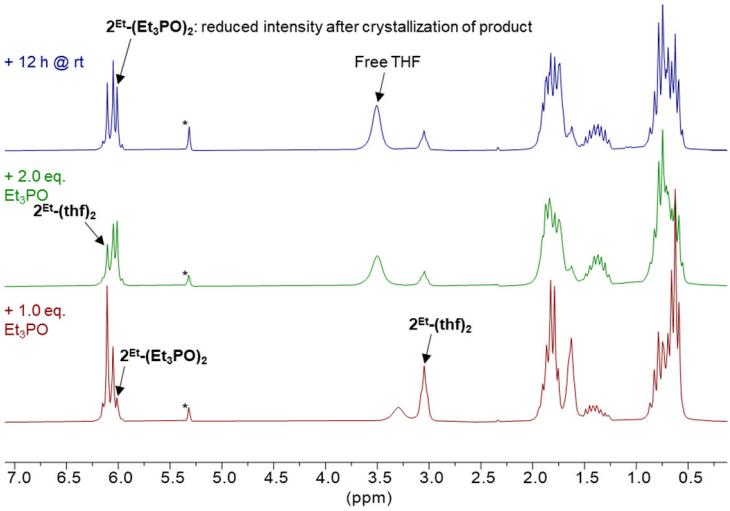


Figure S5: ^{1}H NMR spectra of $\mathbf{2^{Et}\text{-}(thf)_2}$ after the addition of 1.0 eq. and 2.0 eq. Et_3PO (200 MHz, 298 K, CD_2Cl_2). Solvent signals are indicated by an asterisk (*).

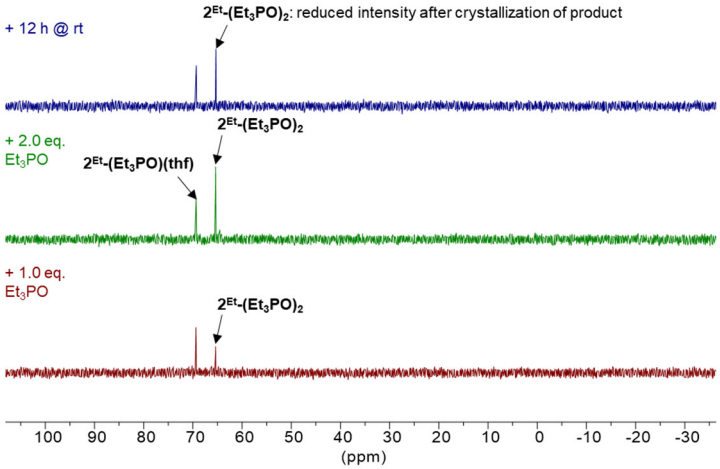


Figure S6: ^{31}P NMR spectrum of $\mathbf{2^{Et}\text{-}(thf)_2}$ after the addition of 1.0 eq. and 2.0 eq. Et_3PO (121 MHz, 298 K, CD_2Cl_2).

7.2.3 [NBu$_4$][F-2^R]

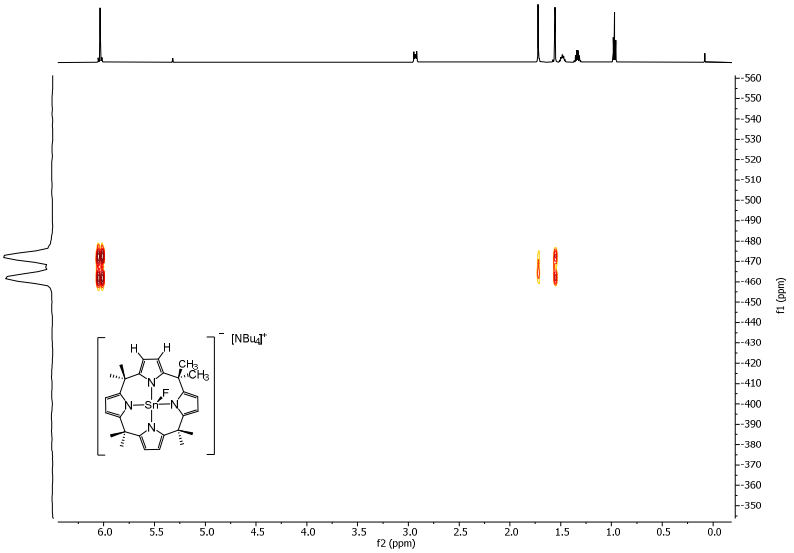


Figure S7. ^{1}H,^{119}Sn-HMBC NMR spectrum of **[NBu$_4$][F-2^{Me}]** (CD_2Cl_2, 298 K).

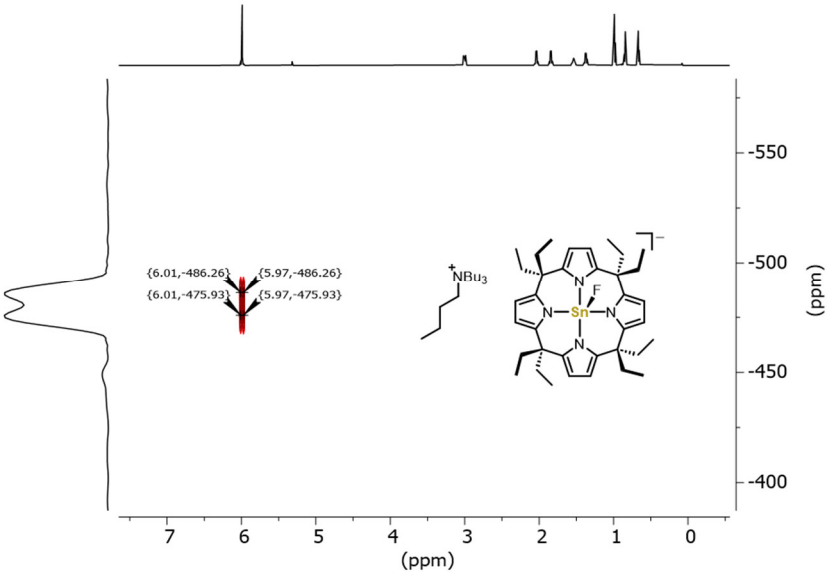


Figure S8. ^{1}H,^{119}Sn-HMBC NMR spectrum of **[NBu$_4$][F-2^{Et}]** (CD_2Cl_2, 298 K).

7.2.4 [PPh$_4$][Cl-2^{Et}]

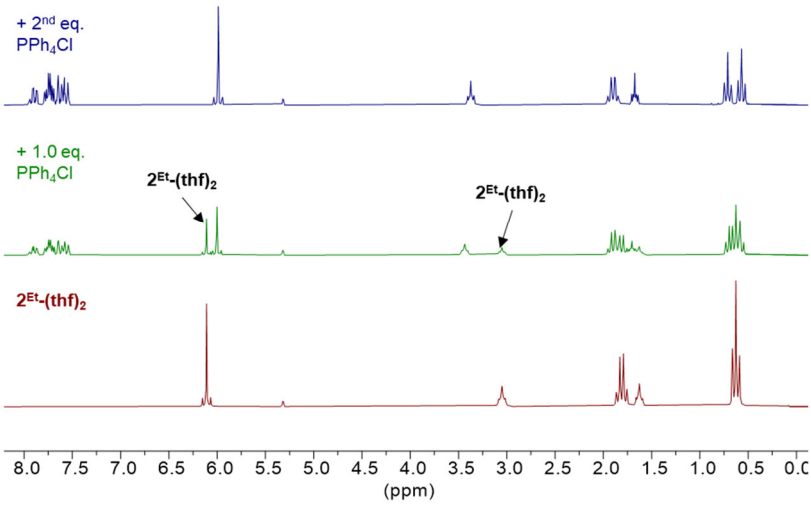


Figure S9. ^{1}H NMR spectrum of **2^{Et}-(thf)$_2$** after the addition of one and two eq. PPh$_4$Cl (200 MHz, CD_2Cl_2, 298 K).

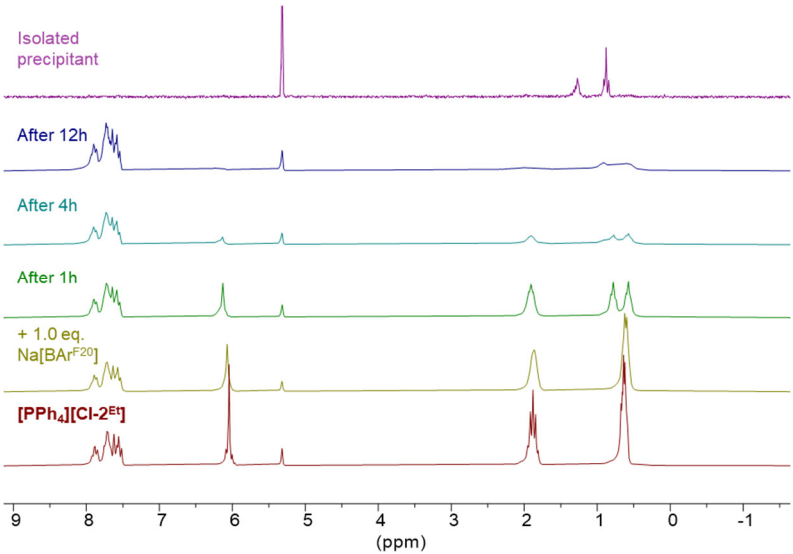


Figure S10. ^{1}H NMR spectrum of **[PPh$_4$][Cl-2^{Et}]** followed over time after the addition of one eq. Na[BAr^{F20}] (200 MHz, CD_2Cl_2, 298 K).

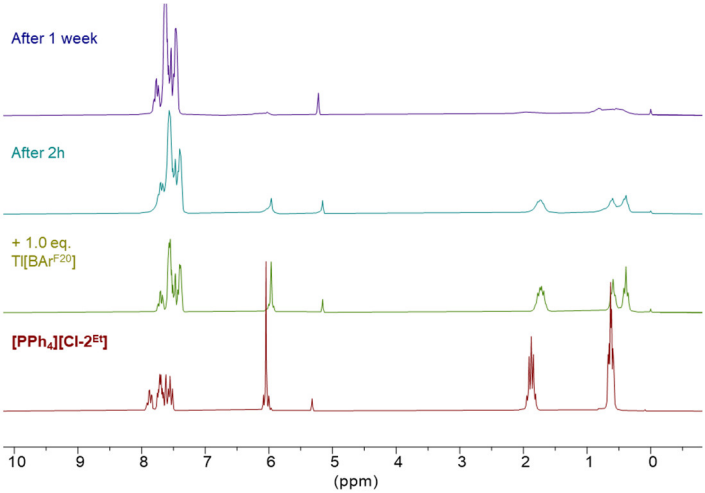


Figure S11. ^{1}H NMR spectrum of **[PPh$_4$][Cl-2^{Et}]** followed over time after the addition of one eq. Tl[BAr^{F20}] (200 MHz, CD_2Cl_2, 298 K).

7.2.5 [PPh$_4$][I-2^{Et}]

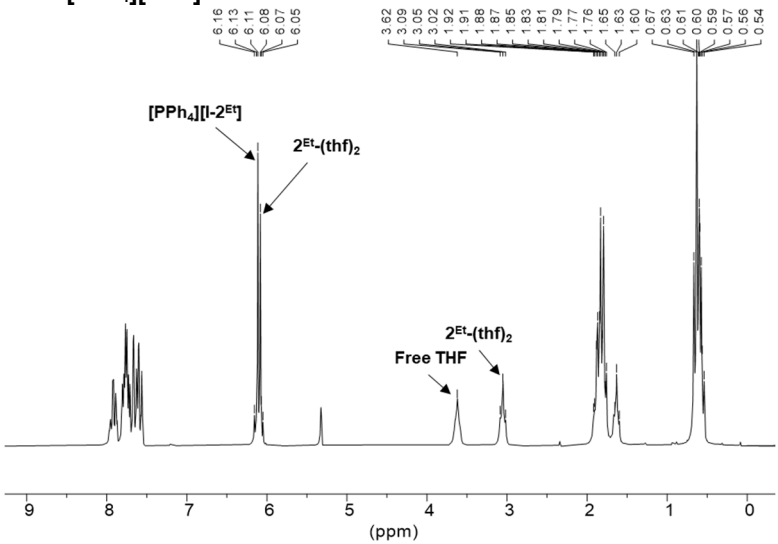


Figure S12. ^{1}H NMR spectrum of **2^{Et}-(thf)$_2$** after the addition of one eq. PPh_4I (200 MHz, CD_2Cl_2, 298 K).

7.2.6 $(2^{Me})_2$

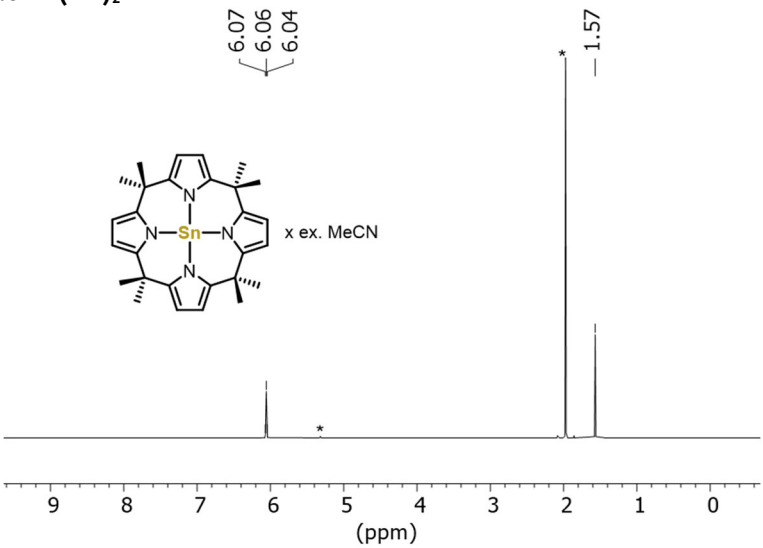


Figure S13. ^{1}H NMR spectrum of $\mathbf{2^{Me}}$ with an excess MeCN (600.18 MHz, CD_2Cl_2, 295 K). Solvent signals are indicated by an asterisk (*).

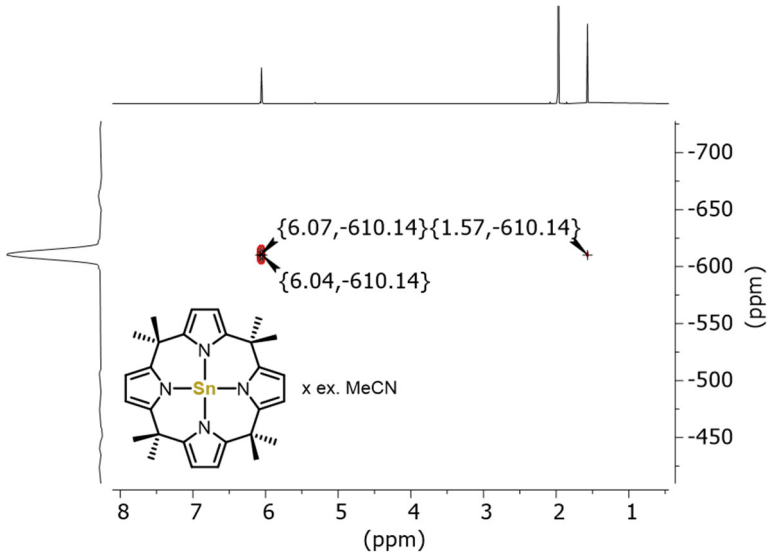


Figure S14. ^{1}H,^{119}Sn-HMBC NMR spectrum of $\mathbf{2^{Me}}$ with an excess MeCN (CD_2Cl_2, 295 K).

7.2.7 $(2^{Et})_2$

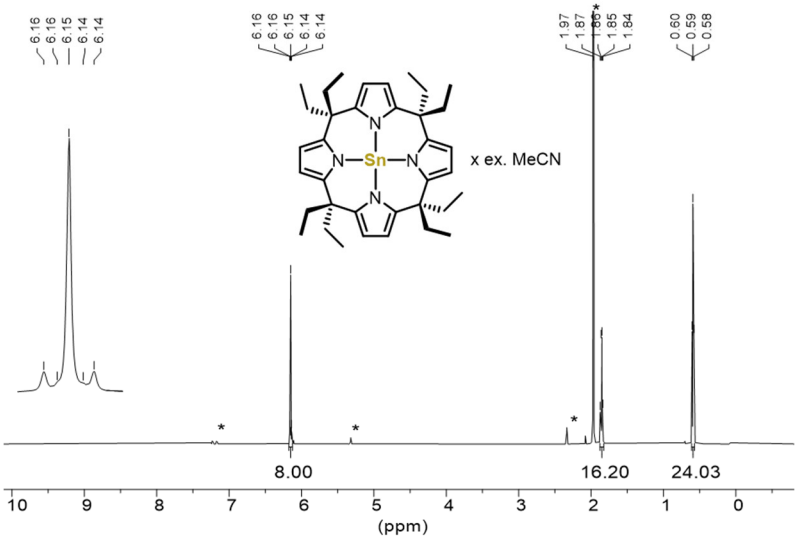


Figure S15. ^{1}H NMR spectrum of $\mathbf{2^{Et}}$ with an excess MeCN (600.18 MHz, CD_2Cl_2, 295 K). Solvent signals of CD_2Cl_2, MeCN, and small toluene residues are indicated by an asterisk (*).

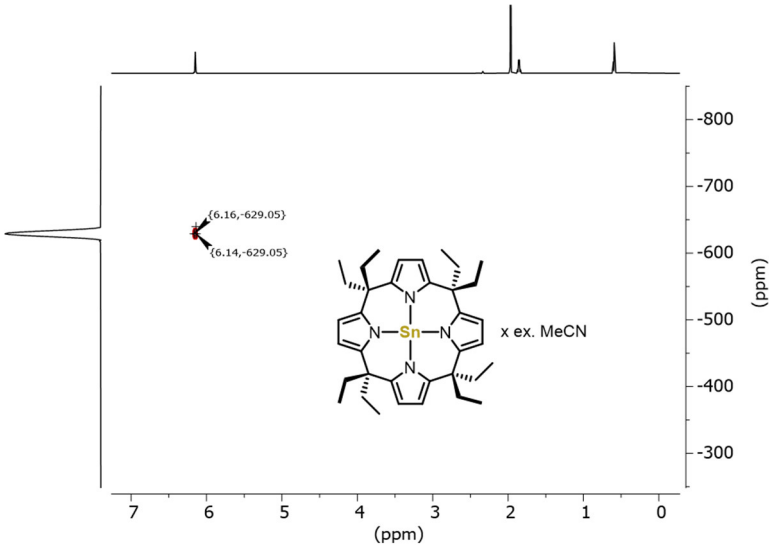


Figure S16. ^{1}H,^{119}Sn-HMBC NMR spectrum of $\mathbf{2^{Et}}$ with an excess MeCN (CD_2Cl_2, 295 K).

7.2.8 *i*PrOH-2^{Me}

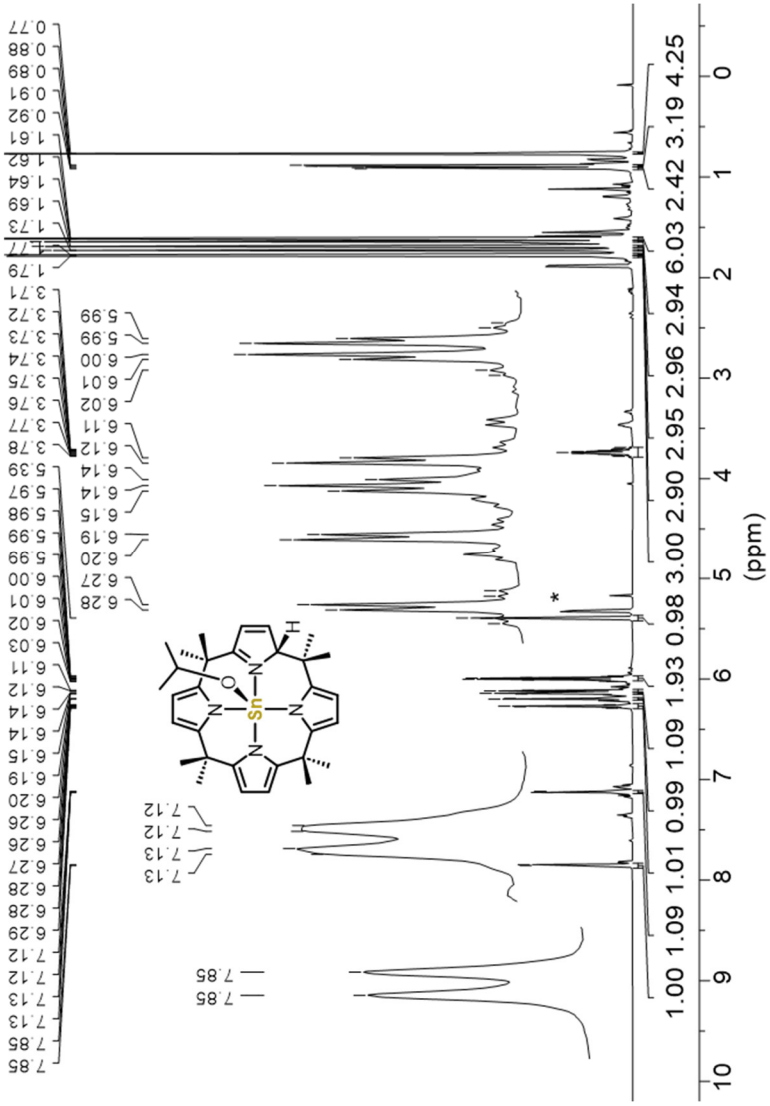


Figure S17. ^{1}H NMR spectrum of the reaction of **(2^{Me})$_2$** with *i*PrOH (600 MHz, CD_2Cl_2, 298 K). Solvent signals are indicated by an asterisk (*).

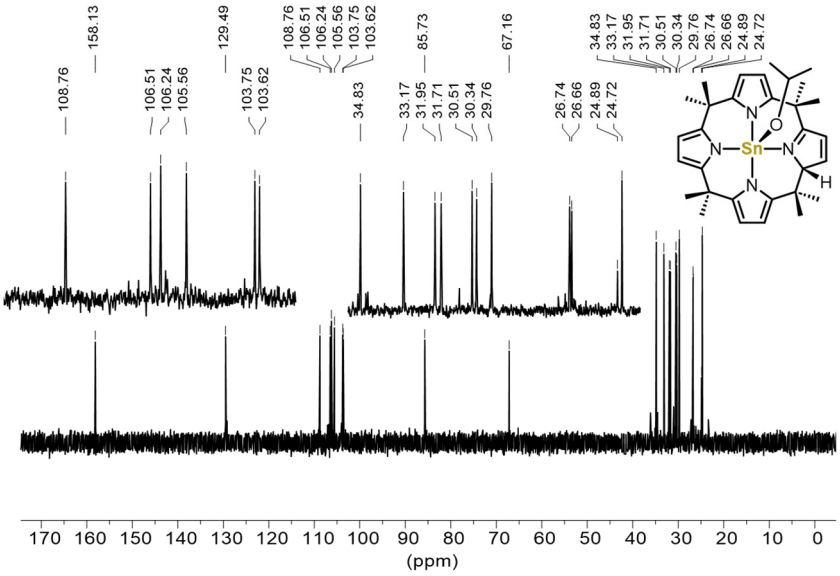


Figure S18. ^{13}C NMR spectrum of the reaction of $(\mathbf{2^{Me}})_2$ with *i*PrOH (150.93 MHz, CD_2Cl_2, 295 K). Solvent signals of CD_2Cl_2, MeCN, and small toluene residues are indicated by an asterisk (*).

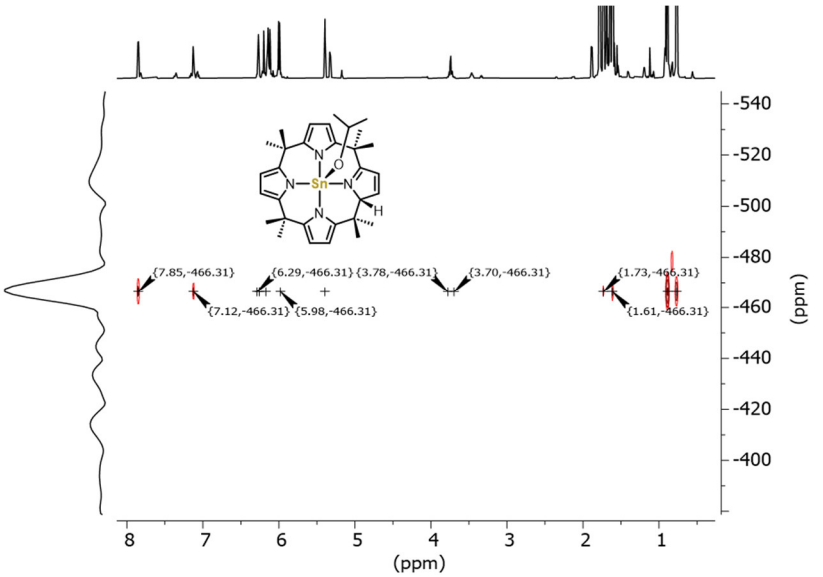


Figure S19. $^{1}H,^{119}Sn$-HMBC NMR spectrum of the reaction of $(\mathbf{2^{Me}})_2$ with *i*PrOH (CD_2Cl_2, 298 K).

7.2.9 BA-2^{R}

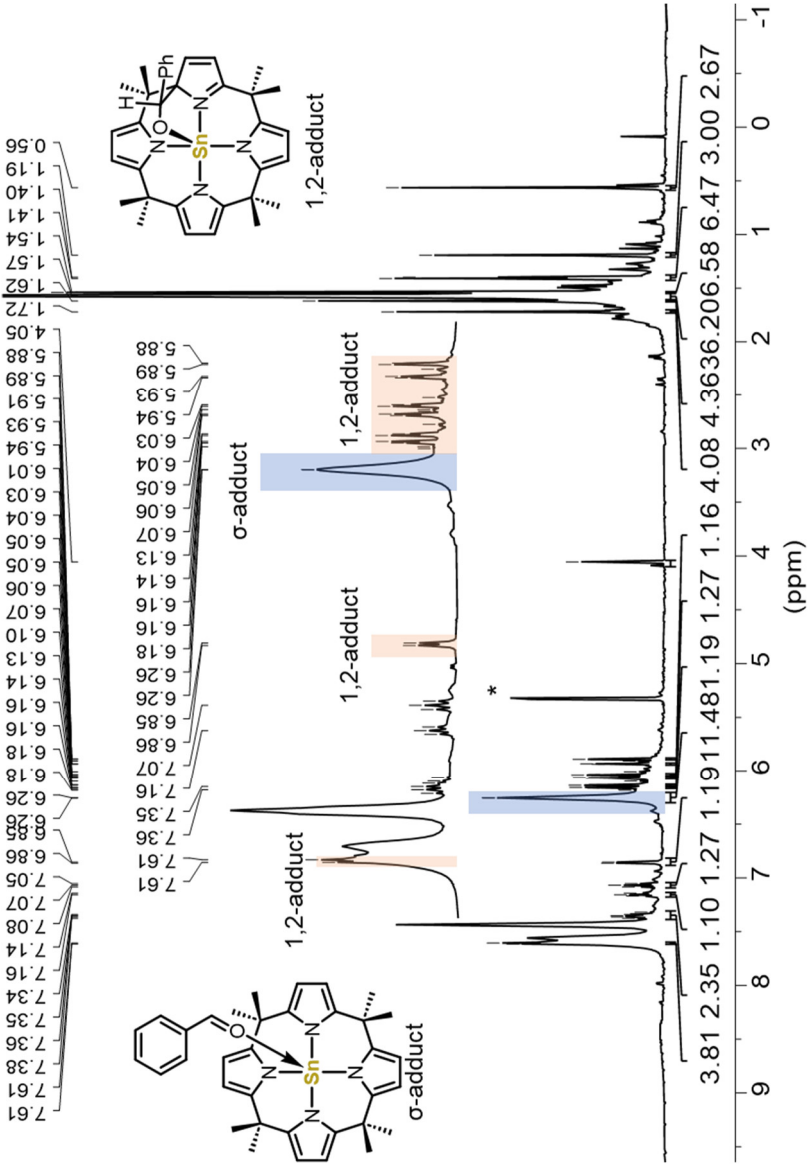


Figure S20. ^{1}H NMR spectrum of the reaction of **(2^{Me})$_2$** with benzaldehyde (600 MHz, CD_2Cl_2, 298 K). Solvent signals are indicated by an asterisk (*).

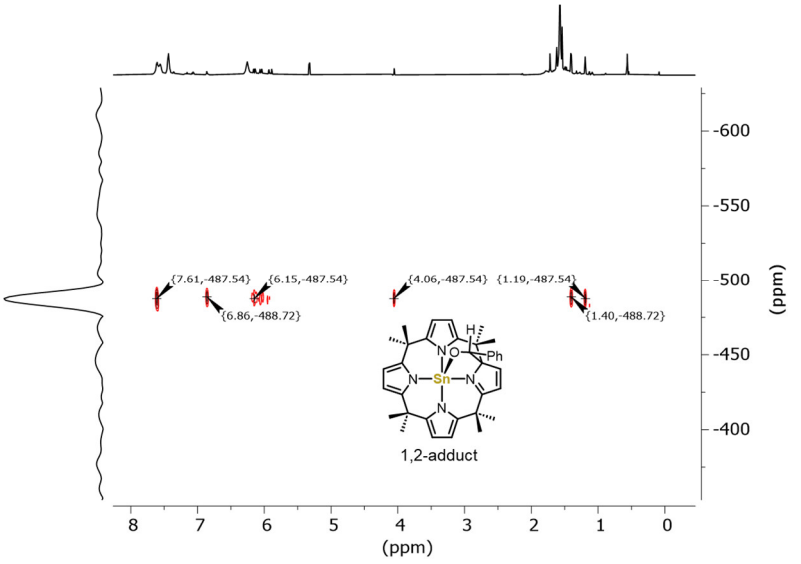


Figure S21. $^{1}H,^{119}Sn$-HMBC NMR spectrum of the reaction of $(\mathbf{2^{Me}})_2$ with benzaldehyde (CD_2Cl_2, 298 K).

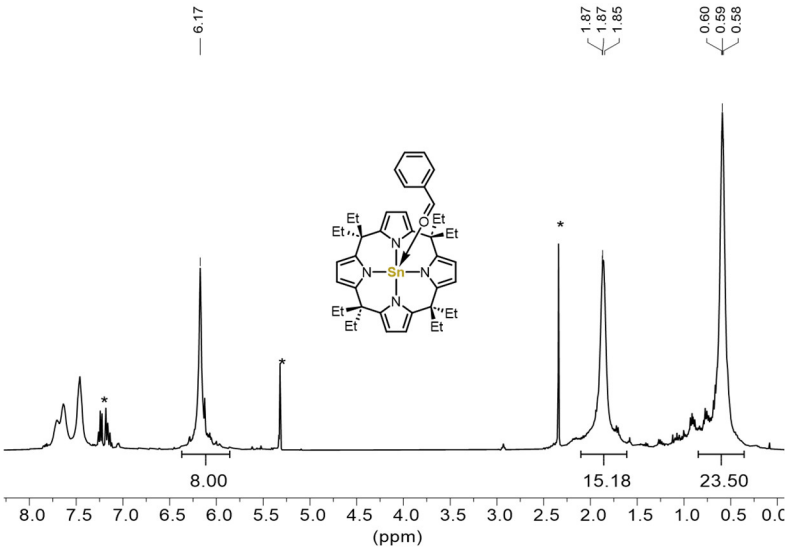


Figure S22. ^{1}H NMR spectrum of the reaction of $(\mathbf{2^{Et}})_2$ with benzaldehyde (600 MHz, CD_2Cl_2, 298 K). Signals of $CHDCl_2$ and residue toluene from the starting material are indicated by an asterisk (*).

7.2.10 NMeInd-2^{Et}

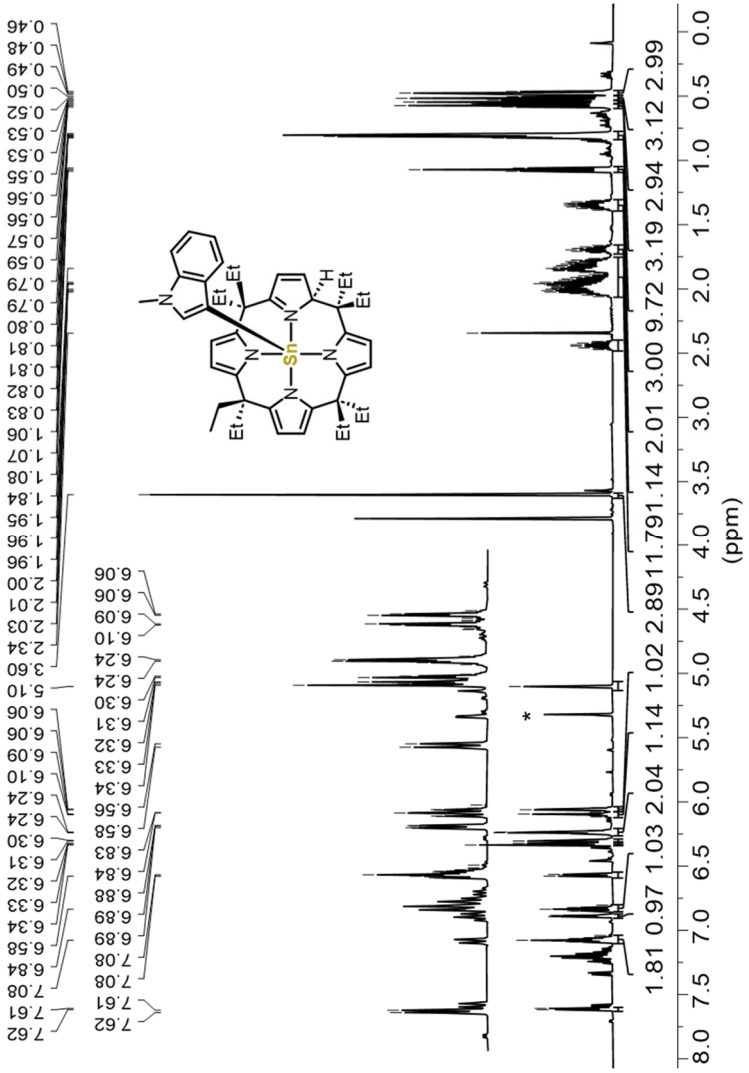


Figure S23. ^{1}H NMR spectrum of the reaction of **(2^{Et})$_2$** with *N*-methyl indole (600 MHz, CD_2Cl_2, 298 K). Solvent signals are indicated by an asterisk (*).

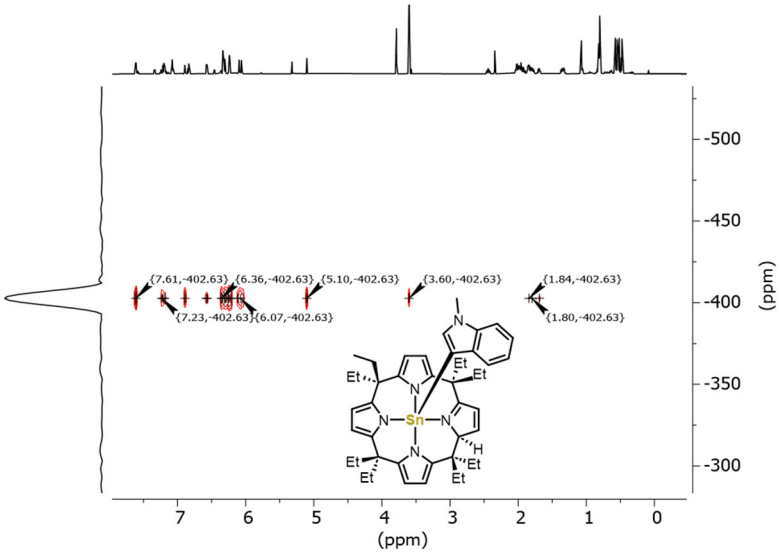


Figure S24. $^{1}H,^{119}Sn$-HMBC NMR spectrum of the reaction of $(\mathbf{2^{Et}})_2$ with *N*-methyl indole (CD_2Cl_2, 298 K).

7.2.11 $H_4[1^{oPhen}]$

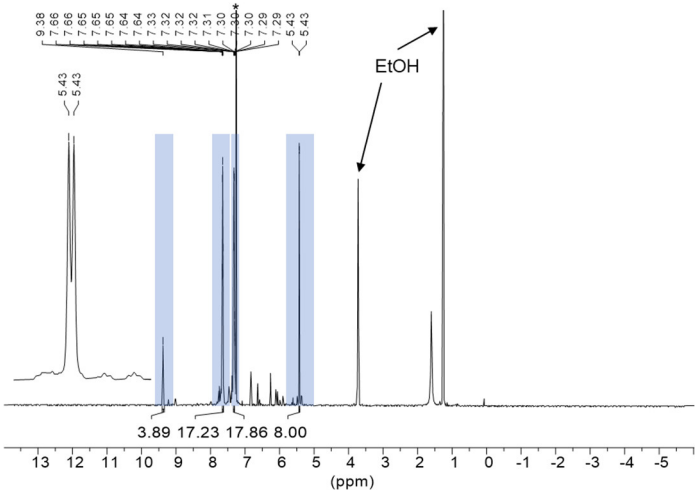


Figure S25. ^{1}H NMR spectrum of the crude precipitant from the reaction of pyrrole with (600 MHz, $CDCl_3$, 298 K). Resonances belonging to the calix[4]pyrrole $\mathbf{H_4[1^{oPhen}]}$ are indicated by a blue box. Solvent signals are indicated by an asterisk (*).

7.2.12 2^{oPhen}-$(thf)_2$

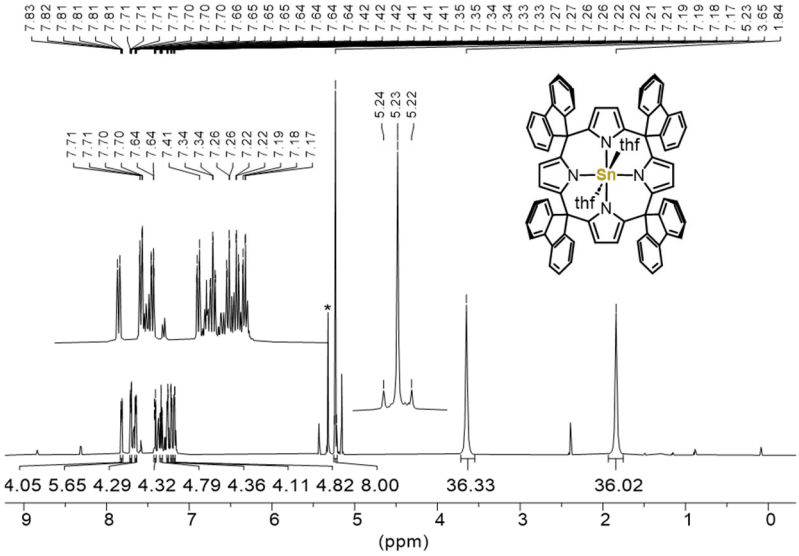


Figure S26. ^{1}H NMR spectrum of the reaction of **[Li$_4$(thf)x][1^{oPhen}]** with $SnCl_4(thf)_2$ in a CD_2Cl_2/THF mixture (600 MHz, $CDCl_3$, 298 K). Solvent signals are indicated by an asterisk (*).

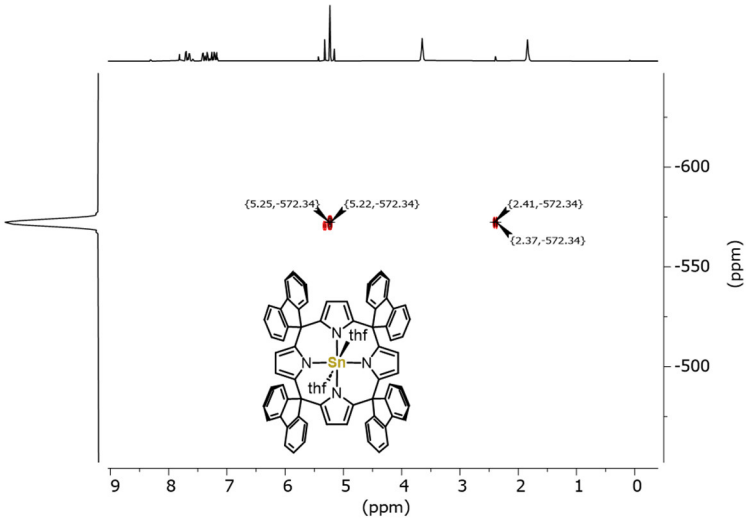


Figure S27. ^{1}H,^{119}Sn-HMBC NMR spectrum of the reaction of **[Li$_4$(thf)x][1^{oPhen}]** with $SnCl_4(thf)_2$ in a CD_2Cl_2/THF mixture (CD_2Cl_2, 298 K).

7.2.13 [PPh$_4$][I-2^{oPhen}]

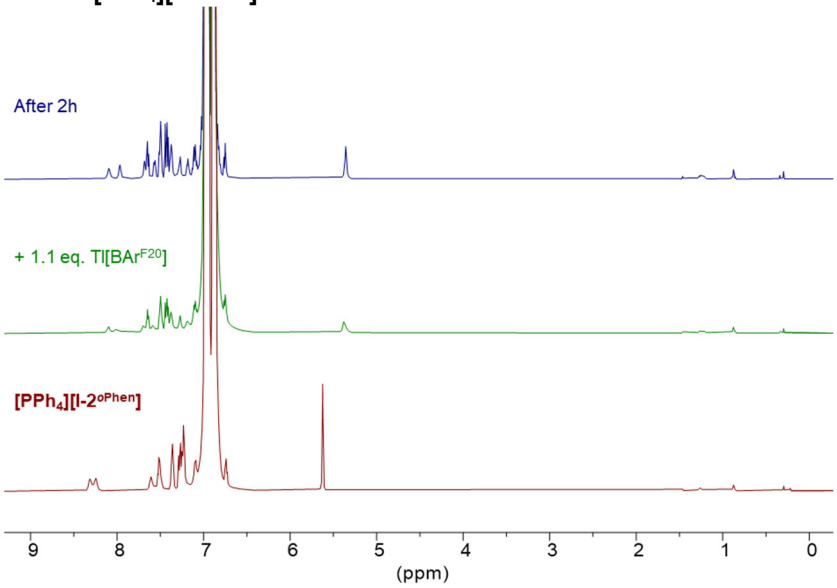


Figure S28. ^{1}H NMR spectrum of **[PPh$_4$][I-2^{oPhen}]** after the addition of 1.2 eq. Tl[BAr^{F20}] in *o*DFB (200 MHz, C_6D_6, 298 K).

7.3 Crystallographic Data

7.3.1 2^{Me}-$(Et_3PO)_2$

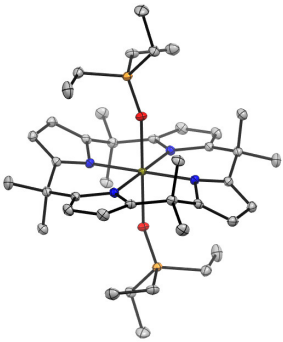


Figure S29. Solid state molecular structure of $\mathbf{2^{Me}\text{-}(Et_3PO)_2}$. Ellipsoids are drawn with a probability of 50%. Hydrogen atoms are omitted for clarity.

Table S1. Crystal data for $\mathbf{2^{Me}\text{-}(Et_3PO)_2}$.

Identification code	mo_hrpj34_a
Empirical formula	$C_{40}H_{62}N_4O_2P_2Sn$
Formula weight	811.56
Temperature [K]	100(2)
Crystal system	monoclinic
Space group (number)	$P2_1/n$ (14)
a [Å]	11.013(5)
b [Å]	16.596(7)
c [Å]	11.284(3)
α [°]	90
β [°]	108.721(18)
γ [°]	90
Volume [Å^3]	1953.3(13)
Z	2
ρ_{calc} [gcm^{-3}]	1.380
μ [mm^{-1}]	0.775
F(000)	852
Crystal size [mm^3]	0.324×0.304×0.205
Crystal colour	colourless
Crystal shape	block
Radiation	MoK_α (λ=0.71073 Å)
2θ range [°]	5.12 to 57.40 (0.74 Å)
Index ranges	−14 ≤ h ≤ 14, −22 ≤ k ≤ 18, −15 ≤ l ≤ 15
Reflections collected	19665
Independent reflections	5025, R_{int} = 0.0312, R_{sigma} = 0.0282
Completeness to θ = 25.242°	99.5 %
Data / Restraints / Parameters	5025/0/230
Absorption correction Tmin/Tmax (method)	0.6382/0.7462 (multi-scan)
Goodness-of-fit on F^2	1.040
Final *R* indexes, [I≥2σ(I)]	R_1 = 0.0213, wR_2 = 0.0516
Final *R* indexes, [all data]	R_1 = 0.0255, wR_2 = 0.0531
Largest peak/hole [eÅ^{-3}]	0.37/−0.60

7.3.2 [NBu$_4$][F-2^{Me}]

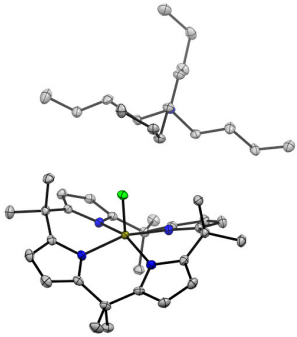


Figure S30. Solid state molecular structure of **[NBu$_4$][F-2^{Me}]**. Ellipsoids are drawn with a probability of 50%. Hydrogen atoms are omitted for clarity.

Table S2. Crystal data for **[NBu$_4$][F-2^{Me}]**.

Identification code	mo_hr499_0ma_a
Empirical formula	$C_{44}H_{68}FN_5Sn$
Formula weight	804.72
Temperature [K]	100(2)
Crystal system	orthorhombic
Space group (number)	$Pca2_1$ (29)
a [Å]	21.204(3)
b [Å]	11.2141(14)
c [Å]	17.278(3)
α [°]	90
β [°]	90
γ [°]	90
Volume [Å^3]	4108.5(10)
Z	4
ρ_{calc} [gcm^{-3}]	1.301
μ [mm^{-1}]	0.663
F(000)	1704
Crystal size [mm^3]	0.253×0.227×0.122
Crystal colour	colourless
Crystal shape	block
Radiation	MoK_α (λ=0.71073 Å)
2θ range [°]	3.84 to 57.45 (0.74 Å)
Index ranges	−28 ≤ h ≤ 28, −15 ≤ k ≤ 15, −23 ≤ l ≤ 23
Reflections collected	264545
Independent reflections	10604, R_{int} = 0.0632, R_{sigma} = 0.0193
Completeness to θ = 25.242°	100.0 %
Data / Restraints / Parameters	10604/1/472
Absorption correction Tmin/Tmax (method)	0.6841/0.7458 (multi-scan)
Goodness-of-fit on F^2	1.067
Final *R* indexes, [$I \geq 2\sigma(I)$]	R_1 = 0.0179, wR_2 = 0.0426
Final *R* indexes, [all data]	R_1 = 0.0187, wR_2 = 0.0433
Largest peak/hole [eÅ^{-3}]	0.26/−0.79

7.3.3 [PPh$_4$][Cl-2^{Me}]

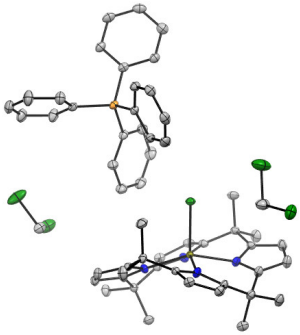


Figure S31. Solid state molecular structure of **[PPh$_4$][Cl-2^{Me}]**. Ellipsoids are drawn with a probability of 50%. Hydrogen atoms are omitted for clarity. The molecule co-crystallized with two CH_2Cl_2 molecules per formula unit.

Table S3. Crystal data for **[PPh$_4$][Cl-2^{Me}]**.

Identification code	mo_hrpj33_0m_a
Empirical formula	$C_{54}H_{56}Cl_5N_4PSn$
Formula weight	1087.93
Temperature [K]	100(2)
Crystal system	monoclinic
Space group (number)	$P2_1/c$ (14)
a [Å]	11.8784(15)
b [Å]	16.167(2)
c [Å]	25.913(5)
α [°]	90
β [°]	95.983(8)
γ [°]	90
Volume [Å^3]	4949.2(13)
Z	4
ρ_{calc} [gcm^{-3}]	1.460
μ [mm^{-1}]	0.860
F(000)	2232
Crystal size [mm^3]	0.308×0.159×0.128
Crystal colour	yellow
Crystal shape	block
Radiation	MoK_α (λ=0.71073 Å)
2θ range [°]	4.04 to 57.49 (0.74 Å)
Index ranges	−16 ≤ h ≤ 16, −21 ≤ k ≤ 21, −35 ≤ l ≤ 35
Reflections collected	256600
Independent reflections	12794, R_{int} = 0.0456, R_{sigma} = 0.0142
Completeness to θ = 25.242°	99.9 %
Data / Restraints / Parameters	12794/136/663
Absorption correction Tmin/Tmax (method)	0.6882/0.7458 (multi-scan)
Goodness-of-fit on F^2	1.157
Final *R* indexes, [$I \geq 2\sigma(I)$]	R_1 = 0.0285, wR_2 = 0.0647
Final *R* indexes, [all data]	R_1 = 0.0298, wR_2 = 0.0653
Largest peak/hole [eÅ^{-3}]	0.98/−0.60

7.3.4 $(2^{Me})_2$

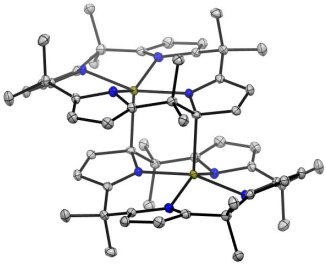


Figure S32. Solid state molecular structure of $(2^{Me})_2$. Ellipsoids are drawn with a probability of 50%. Hydrogen atoms are omitted for clarity.

Table S4. Crystal data for $(2^{Me})_2$.

Identification code	mo_hr432_a
Empirical formula	$C_{56}H_{64}N_8Sn_2$
Formula weight	1086.53
Temperature [K]	100(2)
Crystal system	monoclinic
Space group (number)	$P2_1/c$ (14)
a [Å]	11.308(4)
b [Å]	20.209(10)
c [Å]	10.006(3)
α [°]	90
β [°]	92.782(12)
γ [°]	90
Volume [Å^3]	2283.8(15)
Z	2
ρ_{calc} [gcm^{-3}]	1.580
μ [mm^{-1}]	1.144
F(000)	1112
Crystal size [mm^3]	0.161×0.104×0.027
Crystal colour	yellow
Crystal shape	flake
Radiation	MoK_α (λ=0.71073 Å)
2θ range [°]	4.03 to 54.00 (0.78 Å)
Index ranges	−14 ≤ h ≤ 14, −25 ≤ k ≤ 25, −12 ≤ l ≤ 12
Reflections collected	73726
Independent reflections	4993, R_{int} = 0.0598, R_{sigma} = 0.0226
Completeness to θ = 25.242°	100.0 %
Data / Restraints / Parameters	4993/0/306
Absorption correction Tmin/Tmax (method)	0.6712/0.7461 (multi-scan)
Goodness-of-fit on F^2	1.083
Final *R* indexes, [$I \geq 2\sigma(I)$]	R_1 = 0.0270, wR_2 = 0.0565
Final *R* indexes, [all data]	R_1 = 0.0403, wR_2 = 0.0618
Largest peak/hole [eÅ^{-3}]	0.46/−0.54

7.3.5 2^{Et}-$(thf)_2$

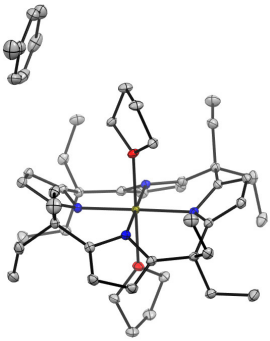


Figure S33. Solid state molecular structure of 2^{Et}-$(thf)_2$. Ellipsoids are drawn with a probability of 50%. Hydrogen atoms are omitted for clarity. The molecule co-crystallized with two toluene molecules per formula unit.

Table S5. Crystal data for 2^{Et}-$(thf)_2$.

Identification code	mo_hr225_1_0m_a
Empirical formula	$C_{58}H_{80}N_4O_2Sn$
Formula weight	983.95
Temperature [K]	100(2)
Crystal system	monoclinic
Space group (number)	$C2/c$ (15)
a [Å]	25.430(4)
b [Å]	12.5626(15)
c [Å]	18.079(2)
α [°]	90
β [°]	120.171(7)
γ [°]	90
Volume [Å^3]	4993.4(12)
Z	4
ρ_{calc} [gcm^{-3}]	1.309
μ [mm^{-1}]	0.558
F(000)	2088
Crystal size [mm^3]	0.564×0.551×0.286
Crystal colour	pink
Crystal shape	block
Radiation	MoK_α (λ=0.71073 Å)
2θ range [°]	5.60 to 54.00 (0.78 Å)
Index ranges	−32 ≤ h ≤ 32, −16 ≤ k ≤ 16, −23 ≤ l ≤ 23
Reflections collected	57255
Independent reflections	5420, R_{int} = 0.0480, R_{sigma} = 0.0220
Completeness to θ = 25.242°	99.7 %
Data / Restraints / Parameters	5420/137/313
Absorption correction Tmin/Tmax (method)	0.6579/0.746 (multi-scan)
Goodness-of-fit on F^2	1.067
Final *R* indexes, [$I \geq 2\sigma(I)$]	R_1 = 0.0198, wR_2 = 0.0497
Final *R* indexes, [all data]	R_1 = 0.0213, wR_2 = 0.0504
Largest peak/hole [eÅ^{-3}]	0.38/−0.44

7.3.6 2^{Et}-$(Et_3PO)_2$

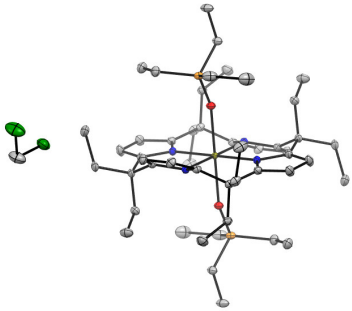


Figure S34. Solid state molecular structure of 2^{Et}-$(Et_3PO)_2$. Ellipsoids are drawn with a probability of 50%. Hydrogen atoms are omitted for clarity. The molecule co-crystallized with two CH_2Cl_2 molecules per formula unit. Selected bond lengths [pm] and angles [deg]: Sn1-N1 = 212.06(11), Sn1-N2 = 210.43(11), Sn1-O1 = 212.26(10), P1-O1 = 150.62(10), N1-Sn1-N2 = 89.84(4), N1-Sn1-N1 = 180.0, N2-Sn1-N2 = 179.999(17).

Table S6. Crystal data for 2^{Et}-$(Et_3PO)_2$.

Identification code	mo_hr226_1_a
Empirical formula	$C_{50}H_{82}Cl_4N_4O_2P_2Sn$
Formula weight	1093.62
Temperature [K]	100(2)
Crystal system	triclinic
Space group (number)	$P\bar{1}$ (2)
a [Å]	10.996(3)
b [Å]	11.132(2)
c [Å]	12.141(3)
α [°]	109.138(7)
β [°]	110.141(9)
γ [°]	92.359(10)
Volume [Å^3]	1298.1(6)
Z	1
ρ_{calc} [gcm^{-3}]	1.399
μ [mm^{-1}]	0.802
F(000)	574
Crystal size [mm^3]	0.252×0.158×0.124
Crystal colour	colourless
Crystal shape	block
Radiation	MoK_α (λ=0.71073 Å)
2θ range [°]	4.01 to 59.23 (0.72 Å)
Index ranges	−15 ≤ h ≤ 15, −15 ≤ k ≤ 15, −16 ≤ l ≤ 16
Reflections collected	74957
Independent reflections	7311, R_{int} = 0.0685, R_{sigma} = 0.0312
Completeness to θ = 25.242°	99.9 %
Data / Restraints / Parameters	7311/112/350
Absorption correction Tmin/Tmax (method)	0.6931/0.7424 (multi-scan)
Goodness-of-fit on F^2	1.048
Final *R* indexes, [$I \geq 2\sigma(I)$]	R_1 = 0.0226, wR_2 = 0.0536
Final *R* indexes, [all data]	R_1 = 0.0252, wR_2 = 0.0546
Largest peak/hole [eÅ^{-3}]	0.44/−0.37

7.3.7 [NBu$_4$][F-2^{Et}]

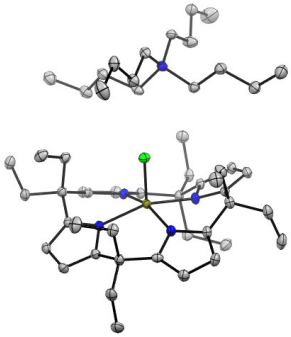


Figure S35. Solid state molecular structure of **[NBu$_4$][F-2^{Et}]**. Ellipsoids are drawn with a probability of 50%. Hydrogen atoms are omitted for clarity.

Table S7. Crystal data for **[NBu$_4$][F-2^{Et}]**.

Identification code	mo_hr491_a
Empirical formula	$C_{52}H_{84}FN_5Sn$
Formula weight	916.93
Temperature [K]	103(2)
Crystal system	monoclinic
Space group (number)	$P2_1/n$ (14)
a [Å]	11.641(3)
b [Å]	22.979(7)
c [Å]	18.253(5)
α [°]	90
β [°]	97.064(13)
γ [°]	90
Volume [Å^3]	4846(2)
Z	4
ρ_{calc} [gcm^{-3}]	1.257
μ [mm^{-1}]	0.570
F(000)	1960
Crystal size [mm^3]	0.262×0.079×0.059
Crystal colour	colourless
Crystal shape	block
Radiation	MoK_α (λ=0.71073 Å)
2θ range [°]	3.95 to 53.47 (0.79 Å)
Index ranges	−14 ≤ h ≤ 14, −29 ≤ k ≤ 29, −23 ≤ l ≤ 23
Reflections collected	106148
Independent reflections	10272, R_{int} = 0.0706, R_{sigma} = 0.0342
Completeness to θ = 25.242°	99.9 %
Data / Restraints / Parameters	10272/0/544
Absorption correction Tmin/Tmax (method)	0.6657/0.7455 (multi-scan)
Goodness-of-fit on F^2	1.048
Final *R* indexes, [I≥2σ(I)]	R_1 = 0.0310, wR_2 = 0.0612
Final *R* indexes, [all data]	R_1 = 0.0433, wR_2 = 0.0657
Largest peak/hole [eÅ^{-3}]	0.47/−0.65

7.3.8 [PPh$_4$][Cl-2^{Et}]

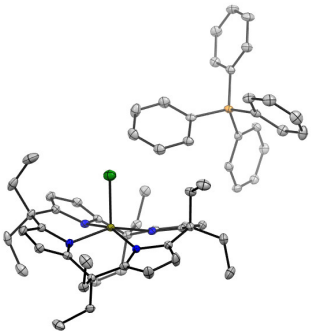


Figure S36. Solid state molecular structure of **[PPh$_4$][Cl-2^{Et}]**. Ellipsoids are drawn with a probability of 50%. Hydrogen atoms are omitted for clarity. The molecule co-crystallized with one highly disordered CH_2Cl_2 molecule per formula unit which has been squeezed during structure refinement.

Table S8. Crystal data for **[PPh$_4$][Cl-2^{Et}]**.

Identification code	mo_hr250_a_sq
Empirical formula	$C_{60}H_{68}ClN_4PSn$
Formula weight	1030.29
Temperature [K]	100(2)
Crystal system	triclinic
Space group (number)	$P\overline{1}$ (2)
a [Å]	11.568(3)
b [Å]	14.655(5)
c [Å]	16.519(8)
α [°]	80.807(13)
β [°]	84.966(12)
γ [°]	79.128(12)
Volume [Å^3]	2710.0(17)
Z	2
ρ_{calc} [gcm^{-3}]	1.263
μ [mm^{-1}]	0.591
F(000)	1076
Crystal size [mm^3]	0.178×0.133×0.061
Crystal colour	colorless
Crystal shape	block
Radiation	MoK_α (λ=0.71073 Å)
2θ range [°]	4.07 to 50.05 (0.84 Å)
Index ranges	−13 ≤ h ≤ 13, −17 ≤ k ≤ 17, −19 ≤ l ≤ 19
Reflections collected	44713
Independent reflections	9571, R_{int} = 0.0745, R_{sigma} = 0.0570
Completeness to θ = 25.242°	99.9 %
Data / Restraints / Parameters	9571/6/623
Absorption correction Tmin/Tmax (method)	0.6287/0.7458 (multi-scan)
Goodness-of-fit on F^2	1.032
Final *R* indexes, [$I \geq 2\sigma(I)$]	R_1 = 0.0331, wR_2 = 0.0754
Final *R* indexes, [all data]	R_1 = 0.0428, wR_2 = 0.0787
Largest peak/hole [eÅ^{-3}]	0.99/−0.70

7.3.9 $(2^{Et})_2$

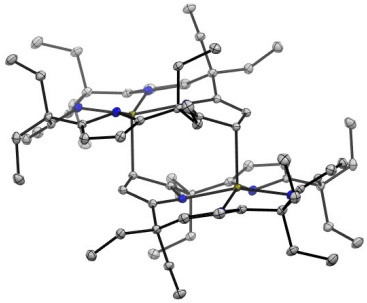


Figure S37. Solid state molecular structure of $(2^{Et})_2$. Ellipsoids are drawn with a probability of 50%. Hydrogen atoms are omitted for clarity.

Table S9. Crystal data for $(2^{Et})_2$.

Identification code	mo_hr532_a
Empirical formula	$C_{72}H_{96}N_8Sn_2$
Formula weight	1310.94
Temperature [K]	100(2)
Crystal system	triclinic
Space group (number)	$P\bar{1}$ (2)
a [Å]	10.6079(12)
b [Å]	11.5329(13)
c [Å]	12.6287(12)
α [°]	73.803(4)
β [°]	85.172(4)
γ [°]	83.666(5)
Volume [Å^3]	1472.3(3)
Z	1
ρ_{calc} [gcm^{-3}]	1.479
μ [mm^{-1}]	0.901
F(000)	684
Crystal size [mm^3]	0.136×0.062×0.033
Crystal colour	yellow
Crystal shape	block
Radiation	MoK_α (λ=0.71073 Å)
2θ range [°]	3.87 to 57.58 (0.74 Å)
Index ranges	−14 ≤ h ≤ 14, −15 ≤ k ≤ 15, −17 ≤ l ≤ 17
Reflections collected	59762
Independent reflections	7662, R_{int} = 0.0663, R_{sigma} = 0.0353
Completeness to θ = 25.242°	100.0 %
Data / Restraints / Parameters	7662/0/378
Absorption correction Tmin/Tmax (method)	0.6909/0.7458 (multi-scan)
Goodness-of-fit on F^2	1.084
Final *R* indexes, [I≥2σ(I)]	R_1 = 0.0291, wR_2 = 0.0620
Final *R* indexes, [all data]	R_1 = 0.0352, wR_2 = 0.0652
Largest peak/hole [eÅ^{-3}]	1.03/−0.62

7.3.10 *i*PrOH-2^{Me}

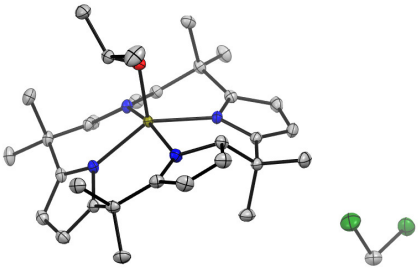


Figure S38. Solid state molecular structure of ***i*PrOH-2^{Me}**. Ellipsoids are drawn with a probability of 50%. Hydrogen atoms are omitted for clarity. The molecule co-crystallized with one CH_2Cl_2 molecules per formula unit.

Table S10. Crystal data for ***i*PrOH-2^{Me}**.

Identification code	mo_hr566a
Empirical formula	$C_{32}H_{42}Cl_2N_4OSn$
Formula weight	688.28
Temperature [K]	100(2)
Crystal system	monoclinic
Space group (number)	$P2_1/c$ (14)
a [Å]	11.581(4)
b [Å]	11.131(2)
c [Å]	23.776(7)
α [°]	90
β [°]	93.955(13)
γ [°]	90
Volume [Å^3]	3057.5(15)
Z	4
ρ_{calc} [gcm^{-3}]	1.495
μ [mm^{-1}]	1.043
F(000)	1416
Crystal size [mm^3]	0.281×0.172×0.116
Crystal colour	yellow
Crystal shape	block
Radiation	MoK_α (λ=0.71073 Å)
2θ range [°]	4.04 to 57.59 (0.74 Å)
Index ranges	−15 ≤ h ≤ 15, −15 ≤ k ≤ 15, −32 ≤ l ≤ 32
Reflections collected	207903
Independent reflections	7933, R_{int} = 0.0615, R_{sigma} = 0.0173
Completeness to θ = 25.242°	99.9 %
Data / Restraints / Parameters	7933/65/393
Absorption correction Tmin/Tmax (method)	0.6853/0.7458 (multi-scan)
Goodness-of-fit on F^2	1.024
Final *R* indexes, [I≥2σ(I)]	R_1 = 0.0181, wR_2 = 0.0428
Final *R* indexes, [all data]	R_1 = 0.0197, wR_2 = 0.0438
Largest peak/hole [eÅ^{-3}]	0.42/−0.46

7.3.11 *N*MeInd-2^{Et}

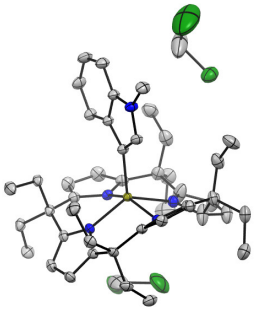


Figure S39. Solid state molecular structure of ***N*MeInd-2^{Et}**. Ellipsoids are drawn with a probability of 50%. Hydrogen atoms are omitted for clarity. The molecule co-crystallized with 1.5 CH_2Cl_2 molecules per formula unit.

Table S11. Crystal data for ***N*MeInd-2^{Et}**.

Identification code	mo_hr606a_2
Empirical formula	$C_{93}H_{120}Cl_6N_{10}Sn_2$
Formula weight	1828.06
Temperature [K]	100(2)
Crystal system	triclinic
Space group (number)	$P\bar{1}$ (2)
a [Å]	11.163(3)
b [Å]	11.847(3)
c [Å]	17.060(4)
α [°]	95.619(6)
β [°]	91.335(11)
γ [°]	102.849(17)
Volume [Å^3]	2186.8(10)
Z	1
ρ_{calc} [gcm^{-3}]	1.388
μ [mm^{-1}]	0.806
F(000)	950
Crystal size [mm^3]	0.267×0.218×0.202
Crystal colour	yellow
Crystal shape	block
Radiation	MoK_α (λ=0.71073 Å)
2θ range [°]	4.07 to 57.64 (0.74 Å)
Index ranges	−15 ≤ h ≤ 15, −16 ≤ k ≤ 16, −23 ≤ l ≤ 23
Reflections collected	139130
Independent reflections	11385, R_{int} = 0.0600, R_{sigma} = 0.0267
Completeness to θ = 25.242°	99.9 %
Data / Restraints / Parameters	11385/99/565
Absorption correction Tmin/Tmax (method)	0.6937/0.7458(multi-scan)
Goodness-of-fit on F^2	1.048
Final *R* indexes, [$I \geq 2\sigma(I)$]	R_1 = 0.0322, wR_2 = 0.0783
Final *R* indexes, [all data]	R_1 = 0.0339, wR_2 = 0.0794
Largest peak/hole [eÅ^{-3}]	1.28/−1.14

7.3.12 $H_4[1^{oPhen}]$

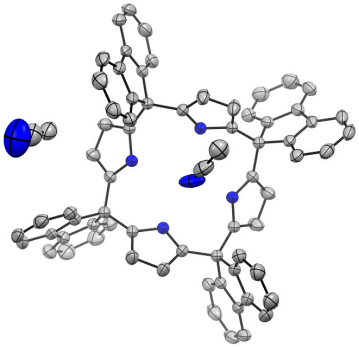


Figure S40. Solid state molecular structure of $H_4[1^{oPhen}]$. Ellipsoids are drawn with a probability of 50%. Hydrogen atoms are omitted for clarity. The molecule co-crystallized with six MeCN molecules per formula unit.

Table S12. Crystal data for $H_4[1^{oPhen}]$.

Identification code	mo_hr616a
Empirical formula	$C_{80}H_{62}N_{10}$
Formula weight	1163.39
Temperature [K]	100(2)
Crystal system	tetragonal
Space group (number)	$I4_1/a$ (88)
a [Å]	23.308(8)
b [Å]	23.308(8)
c [Å]	12.179(8)
α [°]	90
β [°]	90
γ [°]	90
Volume [Å^3]	6617(6)
Z	4
ρ_{calc} [gcm^{-3}]	1.168
μ [mm^{-1}]	0.070
F(000)	2448
Crystal size [mm^3]	0.182×0.162×0.095
Crystal colour	colourless
Crystal shape	block
Radiation	MoK_α (λ=0.71073 Å)
2θ range [°]	5.14 to 50.15 (0.84 Å)
Index ranges	−27 ≤ h ≤ 27, −27 ≤ k ≤ 27, −14 ≤ l ≤ 14
Reflections collected	131617
Independent reflections	2937, R_{int} = 0.1179, R_{sigma} = 0.0279
Completeness to θ = 25.242°	99.8 %
Data / Restraints / Parameters	2937/51/219
Absorption correction Tmin/Tmax (method)	0.6542/0.7452 (multi-scan)
Goodness-of-fit on F^2	1.039
Final *R* indexes, [I≥2σ(I)]	R_1 = 0.0726, wR_2 = 0.2223
Final *R* indexes, [all data]	R_1 = 0.0946, wR_2 = 0.2549
Largest peak/hole [eÅ^{-3}]	0.64/−0.32

7.3.13 $[Li_4(thf)_{12}][1^{oPhen}]$

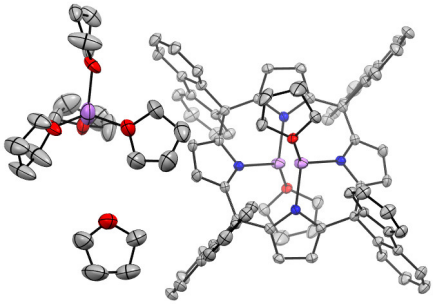


Figure S41. Solid state molecular structure of **$[Li_4(thf)_{12}][1^{oPhen}]$**. Ellipsoids are drawn with a probability of 50%. Hydrogen atoms are omitted for clarity. The molecule co-crystallized with two THF molecules not coordinated to lithium cations per formula unit.

Table S13. Crystal data for **$[Li_4(thf)_{10}][1^{oPhen}]$**.

Identification code	mo_hr660c_2_a
Empirical formula	$C_{116}H_{136}Li_4N_4O_{12}$
Formula weight	1806.04
Temperature [K]	108(2)
Crystal system	monoclinic
Space group (number)	$P2_1/n$ (14)
a [Å]	13.815(7)
b [Å]	20.467(7)
c [Å]	17.443(7)
α [°]	90
β [°]	92.919(13)
γ [°]	90
Volume [Å^3]	4926(4)
Z	2
ρ_{calc} [gcm^{-3}]	1.218
μ [mm^{-1}]	0.077
F(000)	1936
Crystal size [mm^3]	0.237×0.118×0.106
Crystal colour	yellow
Crystal shape	block
Radiation	MoK_α (λ=0.71073 Å)
2θ range [°]	3.98 to 56.56 (0.75 Å)
Index ranges	−18 ≤ h ≤ 18, −27 ≤ k ≤ 27, −23 ≤ l ≤ 23
Reflections collected	133874
Independent reflections	12211, R_{int} = 0.0922, R_{sigma} = 0.0497
Completeness to θ = 25.242°	99.8 %
Data / Restraints / Parameters	12211/1470/751
Absorption correction Tmin/Tmax (method)	0.6672/0.7458 (multi-scan)
Goodness-of-fit on F^2	1.050
Final *R* indexes, [*I*≥2σ(*I*)]	R_1 = 0.0964, wR_2 = 0.2537
Final *R* indexes, [all data]	R_1 = 0.1157, wR_2 = 0.2659
Largest peak/hole [eÅ^{-3}]	0.67/−0.52

7.3.14 2^{oPhen}-(thf)$_2$

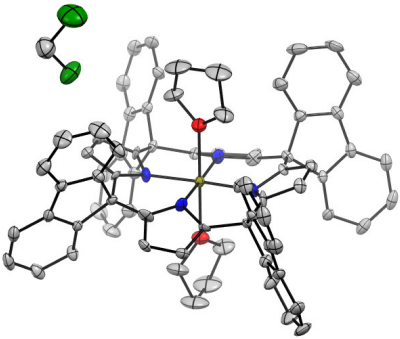


Figure S42. Solid state molecular structure of 2^{oPhen}-(thf)$_2$. Ellipsoids are drawn with a probability of 50%. Hydrogen atoms are omitted for clarity. The molecule co-crystallized with four CH_2Cl_2 molecules per formula unit.

Table S14. Crystal data for 2^{oPhen}-(thf)$_2$.

Identification code	mo_hr642x2_0m_a
Empirical formula	$C_{80}H_{64}Cl_8N_4O_2Sn$
Formula weight	1515.64
Temperature [K]	100(2)
Crystal system	tetragonal
Space group (number)	$I4_1/a$ (88)
a [Å]	23.4465(16)
b [Å]	23.4465(16)
c [Å]	12.2211(12)
α [°]	90
β [°]	90
γ [°]	90
Volume [Å^3]	6718.4(11)
Z	4
ρ_{calc} [gcm^{-3}]	1.498
μ [mm^{-1}]	0.752
F(000)	3096
Crystal size [mm^3]	0.296×0.154×0.074
Crystal colour	yellow
Crystal shape	block
Radiation	MoK_α (λ=0.71073 Å)
2θ range [°]	4.91 to 61.17 (0.70 Å)
Index ranges	−33 ≤ h ≤ 33, −33 ≤ k ≤ 33, −17 ≤ l ≤ 17
Reflections collected	187471
Independent reflections	5167, R_{int} = 0.0675, R_{sigma} = 0.0155
Completeness to θ = 25.242°	99.8 %
Data / Restraints / Parameters	5167/657/455
Absorption correction Tmin/Tmax (method)	0.6897/0.7461 (multi-scan)
Goodness-of-fit on F^2	1.154
Final *R* indexes, [I≥2σ(I)]	R_1 = 0.0359, wR_2 = 0.0924
Final *R* indexes, [all data]	R_1 = 0.0394, wR_2 = 0.0949
Largest peak/hole [eÅ^{-3}]	1.02/−0.59

7.3.15 $2^{o\text{Phen}}$-(py)$_2$

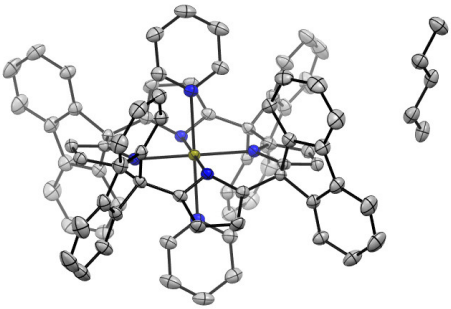


Figure S43. Solid state molecular structure of $2^{o\text{Phen}}$-(py)$_2$. Ellipsoids are drawn with a probability of 50%. Hydrogen atoms are omitted for clarity. The molecule co-crystallized with two *n*-pentane molecules per formula unit.

Table S15. Crystal data for $2^{o\text{Phen}}$-(py)$_2$.

Identification code	mo_hr717_1_a
Empirical formula	$C_{83}H_{62}N_6Sn$
Formula weight	1262.07
Temperature [K]	120(2)
Crystal system	monoclinic
Space group (number)	$P2_1/c$ (14)
a [Å]	12.727(7)
b [Å]	14.396(5)
c [Å]	17.836(6)
α [°]	90
β [°]	95.51(2)
γ [°]	90
Volume [Å^3]	3253(2)
Z	2
ρ_{calc} [gcm^{-3}]	1.289
μ [mm^{-1}]	0.444
F(000)	1304
Crystal size [mm^3]	0.129×0.117×0.085
Crystal colour	colourless
Crystal shape	block
Radiation	MoK_α (λ=0.71073 Å)
2θ range [°]	4.28 to 51.36 (0.82 Å)
Index ranges	−15 ≤ h ≤ 15, −17 ≤ k ≤ 17, −21 ≤ l ≤ 21
Reflections collected	64272
Independent reflections	6163, R_{int} = 0.0765, R_{sigma} = 0.0350
Completeness to θ = 25.242°	99.7 %
Data / Restraints / Parameters	6163/54/432
Absorption correction Tmin/Tmax (method)	0.628/0.7452 (multi-scan)
Goodness-of-fit on F^2	1.074
Final *R* indexes, [I≥2σ(I)]	R_1 = 0.0371, wR_2 = 0.1055
Final *R* indexes, [all data]	R_1 = 0.0485, wR_2 = 0.1130
Largest peak/hole [eÅ^{-3}]	0.86/−0.55

7.4 Quantum Chemical Data

7.4.1 Ion Affinities

Table S16. Computed reference values for the calculation of isodesmic ion affinities at the DSD-BLYP-D3(BJ)/def2-QZVPP//B97M-D4/def2-TZVPP//CREST/GFN2-xTB level of theory with COSMO-RS (DCM) solvent correction.[54]

Compound	DSD-BLYP-D3(BJ)/def2-QZVPP electronic energy [kJ mol^{-1}]	DSD-BLYP-D3(BJ)/def2-QZVPP Enthalpy with B97M-D4/def2-TZVPP thermal correction [kJ mol^{-1}]	COSMO-RS(DCM) enthalpy correction [kJ mol^{-1}]
$SiMe_3^+$	-1073011.45	-1072696.73	-243.0424
$HSiMe_3$	-1075327.40	-1074991.30	-18.0537
$FSiMe_3$	-1336053.07	-1335728.47	-24.6139
$ClSiMe_3$	-2281687.13	-2281364.08	-28.2197
H^-	-1335.46	-1332.98	-204.9089
F^-	-262071.30	-262068.82	-339.9314447
Cl^-	-1207915.21	-1207912.74	-304.7023
I^-	-781351.69	-781349.21	-260.1272101

Table S17. Computed isodesmic ion affinities computed at the DSD-BLYP-D3(BJ)/def2-QZVPP//B97M-D4/def2-TZVPP//CREST/GFN2-xTB level of theory with COSMO-RS (DCM) solvent correction.[54] The iodide ion affinities (IIA) were computed based on the direct reaction between Lewis acid and the iodide anion instead of an isodesmic reaction pathway (indicated with an asterisk *).

Compound	DSD-BLYP-D3(BJ)/def2-QZVPP electronic energy [Hartree]	DSD-BLYP-D3(BJ)/def2-QZVPP Enthalpy with B97M-D4/def2-TZVPP thermal correction [kJ mol^{-1}]	COSMO-RS(DCM) enthalpy correction [kJ mol^{-1}]	Isodesmic ion affinity in the gas phase [kJ mol^{-1}]	Isodesmic ion affinity in solution COSMO-RS(DCM) [kJ mol^{-1}]
12	-1051.795089	-2760669.62	-67.7328	**-**	**-**
$[12\text{-}H]^-$ (HIA)	-1052.47774	-2762444.83	-201.7585	**440**	**369**
$[12\text{-}F]^-$ (FIA)	-1151.768274	-3023140.86	-205.7735	**398**	**193**
$[12\text{-}Cl]^-$ (CIA)	-1511.96233	-3968831.55	-204.8109	**254**	**86**
2^{Me}	-1518.36375	-3984943.438	-81.87795744	**-**	**-**
$[2^{Me}\text{-}H]^-$ (HIA)	-1519.08316587098	-3986813.252	-210.0314762	**537**	**462**
$[2^{Me}\text{-}F]^-$ (FIA)	-1618.36503374004	-4247487.298	-214.2110033	**473**	**266**
$[2^{Me}\text{-}Cl]^-$ (CIA)	-1978.5566002756	-5193173.796	-213.092291	**325**	**163**

[2^{Me}-I]$^-$ (IIA)	-1816.064654	-4766552.10	-215.2577	**258***	**130***
2^{Et}	-1832.592908	-4809317.82	-88.0228	**-**	**-**
[2^{Et}-H]$^-$ (HIA)	-1833.314711	-4811193.84	-197.0115	**541**	**445**
[2^{Et}-F]$^-$ (FIA)	-1932.5948	-5071866.26	-205.1864	**475**	**249**
[2^{Et}-Cl]$^-$ (CIA)	-2292.792671	-6017567.29	-202.0575	**342**	**151**
[2^{Et}-I]$^-$ (IIA)	-2130.304396	-5590955.27	-200.9229	**288***	**141***
2^{oPhen}	-3046.330811	-7995675.13	-141.3964	**-**	**-**
[2^{oPhen}-H]$^-$ (HIA)	-3047.058078	-7997569.55	-266.5386	**502**	**423**
[2^{oPhen}-F]$^-$ (FIA)	-3146.339831	-8258242.93	-267.9313	**479**	**265**
[2^{oPhen}-Cl]$^-$ (CIA)	-3506.535142	-9203936.22	-273.7685	**330**	**158**
[2^{oPhen}-I]$^-$ (IIA)	-3344.04898	-8777330.57	-272.5956	**306***	**147***
8^{Me}	-1593.6531620	-4182607.1583573	-74.32554531	**-**	**-**
[8^{Me}-H]$^-$ (HIA)	-1594.36781159681	-4184461.5432805	-213.6390197	**522**	**457**
[8^{Me}-F]$^-$ (FIA)	-1693.67095331358	-4445194.4292002	-214.5188127	**517**	**317**
[8^{Me}-Cl]$^-$ (CIA)	-2053.82493379591	-5390781.5494921	-216.889596	**269**	**118**
8^{Et}	-1907.879517	-5006974.11	-82.8557	**-**	**-**
[8^{Et}-H]$^-$ (HIA)	-1908.593366	-5008826.58	-209.569	**517**	**439**
[8^{Et}-F]$^-$ (FIA)	-2007.897171	-5269562.17	-209.9329	**515**	**299**
[8^{Et}-Cl]$^-$ (CIA)	-2368.0555	-6215160.63	-208.5889	**279**	**100**
9^{Me}	-3380.81688999029	-8874809.4102206	-75.69476509	**-**	**-**
[9^{Me}-H]$^-$ (HIA)	-3381.53596341449	-8876676.3823336	-212.2396892	**535**	**467**
[9^{Me}-F]$^-$ (FIA)	-3480.81639904033	-9137348.9087755	-215.0881361	**469**	**268**
[9^{Me}-Cl]$^-$ (CIA)	-3840.99245077837	-10082993.0590068	-215.7600858	**278**	**125**

9^{Et}	-3695.044223	-9699179.28	-83.1395	**-**	**-**
$[9^{Et}\text{-H}]^-$ (HIA)	-3695.762413	-9701043.70	-205.2691	**529**	**447**
$[9^{Et}\text{-F}]^-$ (FIA)	-3795.04344	-9961717.45	-212.3126	**465**	**251**
$[9^{Et}\text{-Cl}]^-$ (CIA)	-4155.222511	-10907370.08	-211.7573	**283**	**107**
BCF	-2207.398689	-5795036.70	-45.7261	**-**	**-**
$[BCF\text{-H}]^-$ (HIA)	-2208.108117	-5796878.29	-159.6816	**507**	**416**
SbF_5	-739.2406776	-1940824.96	-27.6674	**-**	**-**
$[SbF_6]^-$ (FIA)	-839.2517859	-2203395.97	-215.8511	**498**	**343**

7.4.2 NBO Analysis Results

Table S18: NBO analysis results for $\mathbf{2^{R}}$ and $\mathbf{8^{Me}}$ and $\mathbf{9^{Me}}$ calculated on PBE0/def2-TZVPP//B97M-D4/def2-TVZPP//CREST/GFN2-xTB level of theory. NBO and second order perturbation theory stabilization energies $\Delta E^{(2)}$ for selected bonding interactions are given in kJ mol^{-1}. Additionally, Lewis density parameters $\%\rho_L$ and single point energies are given for each system.

12 (single point energy = −1051.951643526803 Eh, $\%\rho_L$ = 97.66)	
Averaged WBI for Sn-N bonds	0.565
Average Sn-N bond length	201.5 pm
Partial charge at Sn	2.375
Averaged partial charge at N	−0.721
Averaged partial charge at α-C	0.094
$\mathbf{2^{Me}}$ (single point energy = −1518.527738098259 Eh, $\%\rho_L$ = 98.16)	
Averaged WBI for Sn-N bonds	0.483
Average Sn-N bond length	203.0 pm
Partial charge at Sn	2.465
Averaged partial charge at N	−0.736
Averaged partial charge at α-C	0.137
$\mathbf{2^{Et}}$ (single point energy = −1832.695050922000 Eh, $\%\rho_L$ = 98.40)	
Averaged WBI for Sn-N bonds	0.493
Average Sn-N bond length	203.4
Partial charge at Sn	2.376
Averaged partial charge at N	−0.737
Averaged partial charge at α-C	0.141
$\mathbf{2^{oPhen}}$ (single point energy = −3046.335437309643 Eh, $\%\rho_L$ = 96.61)	
Averaged WBI for Sn-N bonds	0.485
Partial charge at Sn	2.388
Averaged partial charge at N	−0.735
Averaged partial charge at α-C	0.145
$\mathbf{8^{Me}}$ (single point energy = −1593.657573846916 Eh, $\%\rho_L$ = 98.07)	
Averaged WBI for Si-N bonds	0.558
Average Si-N bond length	178.1 pm
Partial charge at Si	2.348
Averaged partial charge at N	−0.777
Averaged partial charge at α-C	0.161
$\mathbf{9^{Me}}$ (single point energy = −3380.974184269192 Eh, $\%\rho_L$ = 98.12)	
Averaged WBI for Ge-N bonds	0.555
Average Ge-N bond length	188.0 pm
Partial charge at Ge	2.271
Averaged partial charge at N	−0.729
Averaged partial charge at α-C	0.149

7.4.3 ETS-NOCV Analysis Results

Table S19. ETS-NOCV bond analysis results for the 1,2-adducts of $\mathbf{2^{Me}}$, $\mathbf{8^{Me}}$, and $\mathbf{9^{Me}}$ with styrene computed on the BP86-D3/TZ2P//B97M-D3(BJ)/def2-TVZPP level of theory. All values given in kJ mol^{-1}.

Compound	**8^{Me} (Si)**	Styrene 1,2-adduct of $\mathbf{8^{Me}}$	**9^{Me} (Ge)**	Styrene 1,2-adduct of $\mathbf{9^{Me}}$	**2^{Me} (Sn)**	Styrene 1,2-adduct of $\mathbf{2^{Me}}$
Total Pauli Repulsion (ΔE_{Pauli})	166328.30	2749.91	165102.69	2669.03	163589.70	2466.34
Total Electrostatic Interaction (ΔV_{elst})	-34029.22	-1220.82	-33772.90	-1201.21	-33557.58	-1139.19
Total Orbital Interaction ($\Delta E_{oi,tot}$)	-171055.02	-2043.69	-169820.32	-1924.77	-168407.76	-1774.80
Total Dispersion Energy (ΔE_{disp})	-463.45	-108.99	-459.79	-107.04	-466.99	-105.47
Residue	-0.06	0.00	-0.06	-0.03	-0.05	-0.00
Total Bonding Energy (ΔE)	-39219.45	-623.59	-38950.38	-564.02	-38842.68	-553.12
Deformation Energy (DE)	-	**221.12**	-	**182.78**	-	**146.07**
NOCV 1	-	-1691.67	-	-1575.07	-	-1452.43
NOCV 2	-	-152.30	-	-146.65	-	-124.52

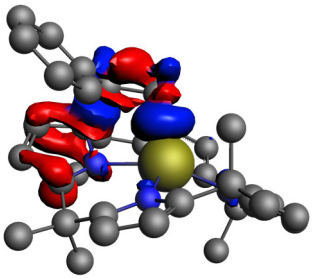


Figure S44. Exemplary ETS-NOCV difference density plot for the 1,2-adduct of styrene with $\mathbf{2^{Me}}$ computed on the BP86-D3/TZ2P//B97M-D3(BJ)/def2-TVZPP level of theory. NOCV deformation densities sampled at a value of 0.004. The color code of the charge flow is red to blue.

Table S20. ETS-NOCV bond analysis results for the dimers of $\mathbf{2^{Me}}$, $\mathbf{8^{Me}}$, and $\mathbf{9^{Me}}$ computed on the BP86-D3/TZ2P//B97M-D3(BJ)/def2-TVZPP COSMO-RS(DCM) level of theory. All values given in kJ mol^{-1}.

Compound	**8^{Me} (Si)**	**$(8^{Me})_2$ α-dimer**	**9^{Me} (Ge)**	**$(9^{Me})_2$ α-dimer**	**2^{Me} (Sn)**	**$(2^{Me})_2$ α-dimer**	**$(2^{Me})_2$ β-dimer**
Total Pauli Repulsion (ΔE_{Pauli})	166844.18	1991.10	165528.10	1841.88	163847.99	1495.34	1129.24
Total Electrostatic Interaction (ΔV_{elst})	-34145.17	-1154.83	-33863.02	-1111.06	-33595.51	-906.81	-642.38
Total Orbital Interaction ($\Delta E_{oi,tot}$)	-171448.70	-1358.56	-170151.01	-1193.38	-168625.55	-952.42	-769.72
Total Dispersion Energy (ΔE_{disp})	-271.89	-226.58	-269.57	-228.95	-265.14	-219.27	-182.06
Solvation Energy (ΔE_{solv})	-16.88	-13.93	-9.90	-14.90	-18.35	-15.72	-21.53
Residue	-0.06	-0.00	-0.05	0.00	-0.05	-0.00	-0.00
Total Bonding Energy (ΔE)	-39038.52	-762.79	-38765.45	-706.41	-38656.60	-598.89	-486.45
Deformation Energy (DE)	-	**817.86**	-	**553.46**	-	**289.70**	**255.86**
NOCV 1	-	-836.88	-	-637.77	-	-631.74	-509.27
NOCV 2	-	-239.03	-	-289.78	-	-102.12	-78.66
NOCV 3	-	-67.88	-	-64.48	-	-63.75	-48.73

Table S21. ETS-NOCV bond analysis results for the dimers of $\mathbf{2}^{Et}$, $\mathbf{8}^{Et}$, and $\mathbf{9}^{Et}$ computed on the BP86-D3/TZ2P//B97M-D3(BJ)/def2-TVZPP COSMO-RS(DCM) level of theory. All values given in kJ mol^{-1}.

Compound	**8^{Et} (Si)**	**$(8^{Et})_2$ β-dimer**	**9^{Et} (Ge)**	**$(9^{Et})_2$ β-dimer**	**2^{Et} (Sn)**	**$(2^{Et})_2$ β-dimer**
Total Pauli Repulsion (ΔE_{Pauli})	211513.19	1566.76	210147.94	1511.27	208491.03	1128.05
Total Electrostatic Interaction (ΔV_{elst})	-42805.15	-834.23	-42508.98	-792.00	-42262.35	-652.82
Total Orbital Interaction ($\Delta E_{oi,tot}$)	-219938.12	-1081.95	-218607.87	-1028.74	-217088.41	-719.66
Total Dispersion Energy (ΔE_{disp})	-407.66	-256.44	-401.64	-246.66	-398.14	-240.11
Solvation Energy (ΔE_{solv})	-10.62	-8.02	-10.49	-4.34	-10.80	-4.22
Residue	-0.05	-0.00	-0.06	-0.00	-0.06	-0.00
Total Bonding Energy (ΔE)	-51648.41	-613.89	-51381.11	-560.48	-51268.73	-488.76
Deformation Energy (DE)	-	**562.48**	-	**455.96**	-	**218.24**
NOCV 1	-	-604.98	-	-677.82	-	-439.02
NOCV 2	-	-218.00	-	-118.21	-	-90.50
NOCV 3	-	-46.36	-	-69.66	-	-45.03

8 Acknowledgements

Nach Vollendung dieser Arbeit möchte ich diese Stelle nutzen um mich bei allen zu bedanken welche mich in jedmöglicher Form dabei unterstützt haben.

Zuallererst danke ich *Prof. Dr. Lutz Greb* für die jahrelange Zusammenarbeit und die Möglichkeit meine Doktorarbeit in seinem Arbeitskreis anfertigen zu können. Lieber Lutz, vielen Dank für deine Hilfe und Beratung auf fachlicher Seite, deinen Einsatz für eine ideale Arbeitsumgebung und die Menschen in deiner Forschungsgruppe, sowie deine verständnisvolle Art, gerade in schwierigen Zeiten. Diese Werte habe ich in Bachelor- und Masterarbeit als auch meiner Promotion sehr zu schätzen gewusst und es war mir eine Freude diese Zeit als ein Teil deiner Gruppe zu verbringen.

Prof. Dr. Lutz H. Gade danke ich für die Übernahme des Koreferats für diese Dissertation.

Prof. Dr. Dr. Hans-Jörg Himmel und dem *AK Himmel* danke ich für die Diskussionen zu Teilen dieser Arbeit im entsprechenden Gruppenseminar sowie die Aufnahme in ihre Forschungsgruppe zu Beginn meiner Promotion und die darüber hinaus andauernde Zusammenarbeit.

Ohne die Infrastruktur der chemischen Institute der Universität Heidelberg wäre diese Arbeit nicht möglich gewesen. Dazu zählen die Mitarbeiterinnen und Mitarbeiter der analytischen Einrichtungen, wie den NMR-Laboren des ACI und OCI und der Massenanalytik, genauso wie die der Werkstätten und Verwaltungen. Namentlich möchte ich hier vor allem *Karin Gießmann*, *Silke Dussel* und *Ute Eisendick* nennen, welche bei bürokratischen Angelegenheiten stets zur Hilfe standen.

Für ihre direkten Beiträge zu Teilen dieser Arbeit als Forschungspraktikantinnen und Forschungspraktikanten möchte ich mich herzlich bei *Eva Steinmann*, *Juliette Schleicher*, *Paul Janßen*, *Sebastian Pauly*, *Arne Meister (2x)*, *André Faria Vieira*, *Ronja Pfretzschner* und *Till Schreyer* bedanken.

Der *Stiftung der Deutschen Wirtschaft (sdw)* danke ich für ein Promotionsstipendium des Studienförderwerks Klaus Murmann sowie die herzliche Aufnahme in die Regionalgruppe Mannheim-Heidelberg.

Vielen Dank an *Senta Kohl*, *Christoph Bendel*, *Nils, Ansmann*, *Paul Janßen*, *Arne Meister*, *Philipp Erdmann*, *Thaddäus Thorwart* und *Daniel Roth* für das Korrekturlesen dieser Arbeit.

Ohne Frage gibt es neben den genannten Personen noch eine Vielzahl weiterer, welche mich direkt oder indirekt während meines Studiums und der Promotion unterstützt haben. Dazu zählen natürlich der gesamte *AK Greb*, Kommilitoninnen und Kommilitonen sowie Freunde aus dem Studienumfeld und meiner Heimat. Diesen möchte ich an dieser Stelle gesammelt danken und weiter auf die angehängte, ausführlichere Danksagung verweisen.

Abschließend danke ich meiner Familie für ihre bedingungslose Unterstützung während meiner Studien- als auch Promotionszeit. Ganz besonders gilt dies für meine Eltern *Silvia* und *Georg*, welche mir alles ermöglichten, mir immer zur Seite standen, und leider den Abschluss dieser Arbeit nicht mehr miterleben konnten.

GESAMTFAKULTÄT FÜR MATHEMTIK, INGENIEUR- UND NATURWISSENSCHAFTEN

COMBINED FACULTY OF MATHEMATICS, ENGINEERING AND NATURAL SCIENCES

Eidesstattliche Versicherung gemäß § 8 der Promotionsordnung für die Gesamtfakultät für Mathematik, Ingenieur- und Naturwissenschaften der Universität Heidelberg / Sworn Affidavit according to § 8 of the doctoral degree regulations of the Combined Faculty of Mathematics, Engineering and Natural Sciences at Heidelberg University

1. Bei der eingereichten Dissertation zu dem Thema / The thesis I have submitted entitled

   Calix[4]pyrrolato Tin Complexes: Augmented Reactivity of Structurally Constrained Sn(II) and Sn(IV) Centers

   handelt es sich um meine eigenständig erbrachte Leistung / is my own work.

2. Ich habe nur die angegebenen Quellen und Hilfsmittel benutzt und mich keiner unzulässigen Hilfe Dritter bedient. Insbesondere habe ich wörtlich oder sinngemäß aus anderen Werken übernommeneInhalte als solche kenntlich gemacht. / I have only used the sources indicated and have not made unauthorized use of services of a third party. Where the work of others has been quoted or reproduced, the source is always given.

3. Die Arbeit oder Teile davon habe ich wie folgt/bislang nicht[1)] an einer Hochschule des ~~In- oder~~ Auslands als Bestandteil einer Prüfungs- oder Qualifikationsleistung ~~vorgelegt~~. / I have not yet/havealready[1)] presented this thesis or parts thereof to a university as part of an examination or degree.

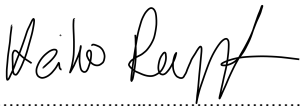
   Titel der Arbeit / Title of the thesis: ……
   Hochschule und Jahr / University and year: ……
   Art der Prüfungs- oder Qualifikationsleistung / Type of examination or degree: ……

4. Die Richtigkeit der vorstehenden Erklärungen bestätige ich. / I confirm that the declarations made above are correct.

5. Die Bedeutung der eidesstattlichen Versicherung und die strafrechtlichen Folgen einer unrichtigen oderunvollständigen eidesstattlichen Versicherung sind mir bekannt. / I am aware of the importance of a sworn affidavit and the criminal prosecution in case of a false or incomplete affidavit.

Ich versichere an Eides statt, dass ich nach bestem Wissen die reine Wahrheit erklärt und nichts verschwiegen habe. / I affirm that the above is the absolute truth to the best of my knowledge and that I have not concealed anything.

Heidelberg, 04.07.24
……
Ort und Datum / Place and date


……
Unterschrift / Signature

[1)] Nicht Zutreffendes streichen. Bei Bejahung sind anzugeben: der Titel der andernorts vorgelegten Arbeit, die Hochschule, das Jahr der Vorlage und die Art der Prüfungs- oder Qualifikationsleistung. / Please cross out what is not applicable. If applicable, please provide: the title of the thesis that was presented elsewhere, the name of the university,

The German text is legally binding.

Formblatt Kumulative Dissertation

1. Publikation/*Publication*:
Vollständige bibliographische Referenz/*Complete bibliographic reference:*

H. Ruppert, L. Greb, Angew. Chem. Int. Ed. 2022, 61, e20211661, https://doi.org/10.1002/anie.202116615.

2. Erst- oder gleichberechtigte Autorenschaft/*First or equal authorship*: Ja/*Yes* ☑ **Nein/*No*** ☐

Veröffentlicht/*Published* ☑
Zur Veröffentlichung angenommen/*Accepted* ☐
Eingereicht/*Submitted* ☐
Noch nicht eingereicht/*Not yet submitted* ☐

4.* Beteiligungen/*Contributions**

Contributor Role	**Doktorand/in/ *Doctoral Student***	**Co-Autor/in 1/ *Co-author 1***	**Co-Autor/in 2/ *Co-author 2***
Name, first name	Ruppert, Heiko	Greb, Lutz	
Methodology	lead	-	
Software	-	-	
Validation	lead	-	
Formal analysis	lead	-	
Investigation	lead	-	
Resources	-	lead	
Data Curation	lead	-	
Writing-Original Draft	lead	-	
Writing-Review&Editing	equal	equal	
Visualization	lead	-	
Supervision	equal	equal	
Project administration	equal	equal	
Funding acquisition	equal	equal	

Kategorien des CRediT (Contributor Roles Taxonomy, https://credit.niso.org/)

Hiermit bestätige ich, dass alle obigen Angaben korrekt sind/*I confirm that all declarations made above are correct.*

Unterschrift/*Signature* Heiko Ruppert _____ _____ _____
Doktorand/in/*Doctoral Student* | Co-Autor/in 1/*Co-author 1* | Co-Autor/in 2/*Co-author*

Betreuungsperson/Supervisor:
Hiermit bestätige ich, dass alle obigen Angaben korrekt sind und dass die selbstständigen Arbeitsanteile des/der Doktoranden/in an der aufgeführten Publikation hinreichend und signifikant sind/*I confirm that all declarations made above are correct and that the doctoral student's independent contribution to this publication is significant and sufficient to be considered for the cumulative dissertation.*

Prof. Lutz Greb _____ 02.07.2024
Name/*Name* | Unterschrift/*Signature* | Datum/*date*

Formblatt Kumulative Dissertation

1. Publikation/*Publication*:
Vollständige bibliographische Referenz/*Complete bibliographic reference:*

H. Ruppert, A. Meister, P. Janßen, L. Greb, Chem. Eur. J. 2024, e202401685, https://doi.org/10.1002/chem.202401685.

2. Erst- oder gleichberechtigte Autorenschaft/*First or equal authorship*: Ja/*Yes* ☑ **Nein/*No*** ☐

Veröffentlicht/*Published*	☐
Zur Veröffentlichung angenommen/*Accepted*	☑
Eingereicht/*Submitted*	☐
Noch nicht eingereicht/*Not yet submitted*	☐

4.* Beteiligungen/*Contributions**

Contributor Role	**Doktorand/in/ *Doctoral Student***	**Co-Autor/in 1/ *Co-author 1***	**Co-Autor/in 2/ *Co-author 2***
Name, first name	Ruppert, Heiko	Meister, Arne	Janßen, Paul
Methodology	lead	-	-
Software	-	-	-
Validation	lead	-	-
Formal analysis	lead	supporting	supporting
Investigation	lead	supporting	supporting
Resources	-	-	-
Data Curation	lead	supporting	supporting
Writing-Original Draft	lead	-	-
Writing-Review&Editing	equal	-	-
Visualization	lead	-	-
Supervision	equal	-	-
Project administration	equal	-	-
Funding acquisition	equal	-	-

****Kategorien des CRediT (Contributor Roles Taxonomy, https://credit.niso.org/)***

Hiermit bestätige ich, dass alle obigen Angaben korrekt sind/*I confirm that all declarations made above are correct.*

Unterschrift/*Signature* Heiko Ruppert (Doktorand/in/*Doctoral student*) Arne Meister (Co-Autor/in 1/*Co-author 1*) Paul Janßen (Co-Autor/in 2/*Co-author*)

Betreuungsperson/Supervisor:
Hiermit bestätige ich, dass alle obigen Angaben korrekt sind und dass die selbstständigen Arbeitsanteile des/der Doktoranden/in an der aufgeführten Publikation hinreichend und signifikant sind/*I confirm that all declarations made above are correct and that the doctoral student's independent contribution to this publication is significant and sufficient to be considered for the cumulative dissertation.*

Prof. Lutz Greb (Name/*Name*) (Unterschrift/*Signature*) 02.07.24 (Datum/*date*)

1. Publikation/*Publication*:
Vollständige bibliographische Referenz/*Complete bibliographic reference:*

H. Ruppert, T. Schreyer, M. C. Dietl, M. Rudolph, A. S. K. Hashmi, L. Greb, Z. Anorg. Allg. Chem. 2024, e202400081, https://doi.org/10.1002/zaac.202400081.

2. Erst- oder gleichberechtigte Autorenschaft/*First or equal authorship*: Ja/*Yes* ☑ Nein/*No* ☐

Veröffentlicht/*Published*
Zur Veröffentlichung angenommen/*Accepted* ☑
Eingereicht/*Submitted*
Noch nicht eingereicht/*Not yet submitted*

4.* Beteiligungen/*Contributions**

Contributor Role	**Doktorand/in/ *Doctoral Student***	**Co-Autor/in 1/ *Co-author* 1**	**Co-Autor/in 2/ *Co-author 2***
Name, first name	Ruppert, Heiko	Schreyer, Till	Dietl, Martin C.
Methodology	lead	-	-
Software	-	-	-
Validation	lead	-	-
Formal analysis	lead	supporting	-
Investigation	lead	supporting	supporting
Resources	-	-	-
Data Curation	lead	supporting	-
Writing-Original Draft	lead	-	-
Writing-Review&Editing	equal	-	-
Visualization	lead	-	-
Supervision	equal	-	-
Project administration	equal	-	-
Funding acquisition	equal	-	-

*****Kategorien des CRediT (Contributor Roles Taxonomy, https://credit.niso.org/)***

Hiermit bestätige ich, dass alle obigen Angaben korrekt sind/*I confirm that all declarations made above are correct.*

Unterschrift/*Signature* Heiko Ruppert (Doktorand/in/*Doctoral student*) T. Schreyer (Co-Autor/in 1/*Co-author 1*) M. Dietl (Co-Autor/in 2/*Co-author*)

Betreuungsperson/Supervisor:
Hiermit bestätige ich, dass alle obigen Angaben korrekt sind und dass die selbstständigen Arbeitsanteile des/der Doktoranden/in an der aufgeführten Publikation hinreichend und signifikant sind/*I confirm that all declarations made above are correct and that the doctoral student's independent contribution to this publication is significant and sufficient to be considered for the cumulative dissertation.*

Prof. Lutz Greb (Name/*Name*) Unterschrift/*Signature* 02.07.24 Datum/*date*

Formblatt Kumulative Dissertation

1. Publikation/*Publication*:
Vollständige bibliographische Referenz/*Complete bibliographic reference:*

H. Ruppert, A. Meister, R. Pfretzschner, A. F. Vieira, L. Greb, J. Am. Chem. Soc. 2024, 146, 16, 11515-11522, https://doi.org/10.1021/jacs.4c02446.

2. Erst- oder gleichberechtigte Autorenschaft/*First or equal authorship*: Ja/*Yes* ☑ Nein/*No* ☐

Veröffentlicht/*Published*	☑
Zur Veröffentlichung angenommen/*Accepted*	☐
Eingereicht/*Submitted*	☐
Noch nicht eingereicht/*Not yet submitted*	☐

4.* Beteiligungen/*Contributions**

Contributor Role	**Doktorand/in/ *Doctoral Student***	**Co-Autor/in 1/ *Co-author* 1**	**Co-Autor/in 2/ *Co-author 2***
Name, first name	Ruppert, Heiko	Meister, Arne	Pfretzschner, Ronja
Methodology	lead	-	-
Software	-	-	-
Validation	lead	-	-
Formal analysis	lead	supporting	supporting
Investigation	lead	supporting	supporting
Resources	-	-	-
Data Curation	lead	supporting	supporting
Writing-Original Draft	lead	-	-
Writing-Review&Editing	equal	-	-
Visualization	lead	-	-
Supervision	equal	-	-
Project administration	equal	-	-
Funding acquisition	equal	-	-

Kategorien des CRediT (Contributor Roles Taxonomy, https://credit.niso.org/)

Hiermit bestätige ich, dass alle obigen Angaben korrekt sind/*I confirm that all declarations made above are correct.*

Unterschrift/*Signature* Heiko Ruppert (Doktorand/in/*Doctoral student*) Arne Meister (Co-Autor/in 1/*Co-author 1*) R Pf (Co-Autor/in 2/*Co-author*)

Betreuungsperson/Supervisor:
Hiermit bestätige ich, dass alle obigen Angaben korrekt sind und dass die selbstständigen Arbeitsanteile des/der Doktoranden/in an der aufgeführten Publikation hinreichend und signifikant sind/*I confirm that all declarations made above are correct and that the doctoral student's independent contribution to this publication is significant and sufficient to be considered for the cumulative dissertation.*

Prof. Lutz Greb (Name/*Name*) (Unterschrift/*Signature*) 02.07.24 (Datum/*date*)